Chemical Reactor Analysis and Design

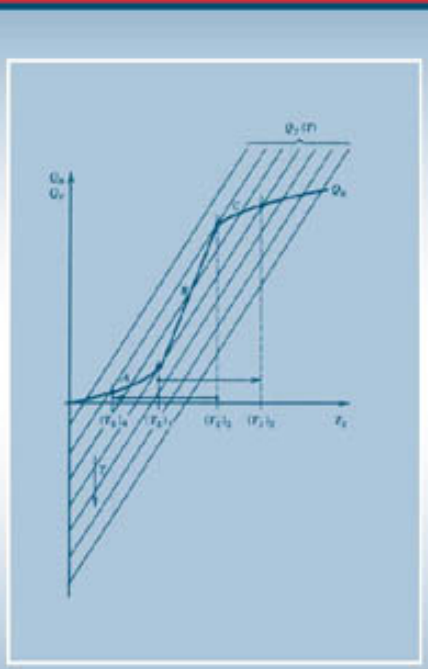

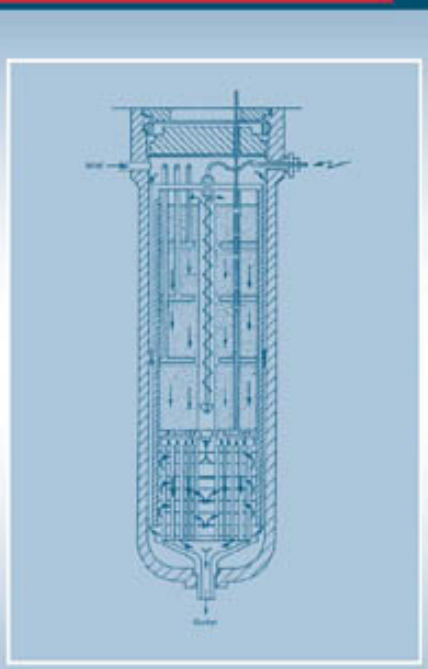

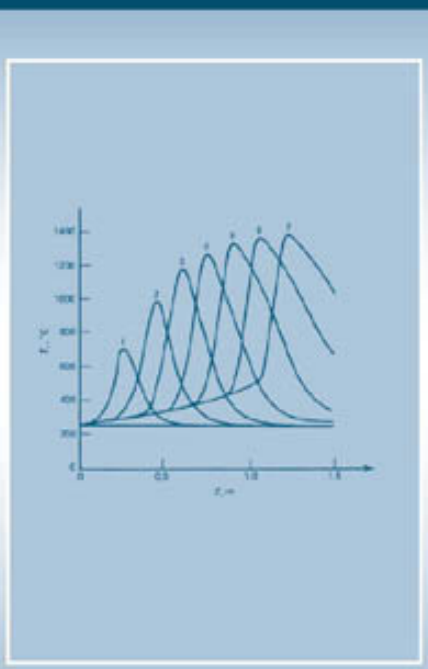

Froment | Bischoff | De Wilde

3rd Edition

This page intentionally left blank

Chemical Reactor Analysis and Design

3rd Edition

Gilbert F. Froment
Texas A&M University

Kenneth B. Bischoff[†]
University of Delaware

Juray De Wilde
Université Catholique de Louvain, Belgium

JOHN WILEY & SONS, INC.

ACQUISITIONS EDITOR Jennifer Welter
MARKETING MANAGER Christopher Ruel
EDITORIAL ASSISTANT Alexandra Spicehandler
SENIOR DESIGNER Kevin Murphy
EXECUTIVE MEDIA EDITOR Thomas Kulesa
PRODUCTION MANAGER Micheline Frederick
PRODUCTION EDITOR Amy Weintraub

This book was printed and bound by Hamilton Printing Company. The cover was printed by Phoenix Color.

This book is printed on acid free paper. ∞

Library of Congress Cataloging-in-Publication Data

Froment, Gilbert F.
Chemical reactor analysis and design. -- 3rd ed. / Gilbert Froment, Juray DeWilde, and Kenneth Bischoff.
p. cm.
Includes bibliographical references and index.
ISBN 978-0-470-56541-4 (cloth)
1. Chemical reactors. 2. Chemical reactions. 3. Chemical engineering. I. DeWilde, Juray. II. Bischoff, Kenneth B. III. Title.
TP157.F76 2011
660'.2832--dc22

2010014481

Printed in the United States of America

10 9 8 7 6 5 4 3 2 1

From Gilbert to Mia.
From Juray, to my brother Tibor, to Junior and Mathieu.

Chemical Reactor Analysis and Design

Gilbert F. Froment, Texas A&M University; K.B. Bischoff†, University of Delaware; Juray De Wilde, Université Catholique de Louvain.

This is the Third Edition of *Chemical Reactor Analysis and Design*. The first was published by Wiley in 1979 and the second, after a substantial revision, in 1990. When we undertook the third edition in 2008, eighteen years had elapsed since the second edition. This is a significant period of time during which chemical reaction engineering has considerably evolved. The tremendous growth of computer power and the easy access to it has significantly contributed to a more comprehensive description of phenomena, operations and equipment, thus enabling the development and application of more fundamental and presumably more accurate models. Modern chemical reaction engineering courses should reflect this evolution towards a more scientific approach. We have been permanently aware of these trends during the elaboration of the present edition and have largely rewritten the complete text. The more fundamental approach has not distracted us, however, from the emphasis on the real world of chemical reaction engineering, one of the main objectives and strengths of the first edition already, widely recognized all over the world.

We have maintained the structure of the previous editions, dividing the content into two parts. The first part deals with the kinetics of phenomena that are important in reaction engineering: reaction kinetics, both “homogeneous” — in a single phase — and “heterogeneous,” involving a gas- and a liquid- or solid phase. The mechanism of the reactions has been accounted for in greater detail than previously, in an effort to be more realistic, but also more reliable in their kinetic modeling e.g., in thermal cracking, polymerization, hydrocarbon processing and bio-processes. The field of reaction kinetics has substantially progressed by the growing availability through commercial software of quantum chemical methods. Students of chemical reaction engineering can no longer ignore their potential and they should be taught how to apply them meaningfully to real processes. Chapters 1, 2 and 3 attempt to do that. In the heterogeneous reaction case, heat and mass transfer phenomena at the interface and inside the reaction phase have to be considered. In modeling these the internal structure of the catalyst has been given more emphasis, starting from insight provided from well developed characterization tools and using advanced techniques like Monte Carlo simulation, Percolation theory and Effective Medium Approximation. This approach is further applied in Chapter 4 on gas-solid reactions and Chapter 5 on catalyst deactivation. The insertion of more realistic kinetics into structure models of the catalyst has also allowed accounting for the role of catalyst deactivation by coke formation in important commercial hydrocarbon conversion

processes, like butene dehydrogenation, steam reforming of natural gas and the catalytic cracking of vacuum gas oil. Chapter 6 on gas-liquid kinetics has retained its previous structure.

Part II addresses the chemical reactor itself, inserting the kinetic aspects of Part I into the modeling and simulation of the reactor operation. Chapter 7 introduces the fundamental mass-, energy- and momentum balances. The Chapters 8, 9, 10 and 11, dealing with the basic types, like the batch, semi-batch, continuous flow reactor with complete mixing and the tubular reactor, filled or not with solid catalyst, have been maintained, of course, and also their strong ties to industrial processes. Deviations of what was previously called "ideal " models and behavior are dealt with along entirely new lines, made possible by the progress of CFD — computational fluid dynamics — also made available by commercial software. This approach is introduced already in Chapter 11 on fixed bed reactors and consistently applied in Chapter 12, leading to a unified and structured approach of flow, residence time and conversion in the variety of reactors encountered in industrial practice. This is another field that has not yet received sufficient attention in chemical engineering curricula. Substantial progress and a growing number of applications can be expected in the coming years. It is illustrated also in Chapter 13 on fluidized- and transport bed reactors, that enters into greater details than before on the catalytic cracking of heavy oil fractions and reports on simulations based upon computational fluid dynamics.

A book like this has to show the path and prepare the future. We should not look down, however, upon the correlations derived from experimentation and collected by the profession over the years, be they limited in their range of application. There is no way that these could be refined or completely replaced yet by CFD application only. Unfortunately, the computational effort involved in the use of CFD in combination with reaction and transport phenomena throughout the entire reactor is overwhelming and its routine-like application to real, practical cases not for the immediate future. Chapter 14 on multiphase reactors is evidence for this and illustrates sound and proved engineering practice.

Finally, we want to remember Ken Bischoff, who deceased in July 2007 and could not participate in this third edition.

Gilbert F. Froment
Texas A & M University

Juray De Wilde
Université Catholique de Louvain

December 2009

About the Authors

G.F. Froment

Gilbert F. Froment received his Ph.D. in Chemical Engineering from the University of Gent, Belgium, in 1957. He did post-doctoral work at the University of Darmstadt in Germany and the University of Wisconsin. In 1968 he became a full professor of Chemical Engineering in Gent and launched the "Laboratorium voor Petrochemische Techniek" that became world famous. His scientific work centered on fixed bed reactor modeling, kinetic modeling, catalyst deactivation and thermal cracking for olefins production. In 1998 he joined the Chemical Engineering Department of Texas A & M University as a Research Professor. He has directed the work of 68 Ph.D students and published 350 scientific papers in international journals. He presented more than 320 seminars in universities and at international symposia all over the world. The book *Chemical Reactor Analysis and Design* (with K.B. Bischoff) is used worldwide in graduate courses and industrial research groups and was translated into Chinese. He has been on the editorial board of the major chemical engineering journals. In his present position, at Texas A & M University, Dr. Froment directs the research of a group of Ph.D students and post-docs on Chemical Reaction Engineering aspects of Hydrocarbon Processing in the Petroleum and Petrochemical Industry, more particularly on the kinetic modeling of complex processes like hydrocracking and hydrotreatment, catalytic cracking, catalytic reforming, methanol-to-olefins, solid acid alkylation, thermal cracking, using single event kinetics, a concept that he launched in the eighties. He received the prestigious R.H. Wilhelm Award for Chemical Reaction Engineering from the A.I.Ch.E. in 1978, the first Villermaux-Medal from the European Federation of Chemical Engineering in 1999 and the 3-yearly Amundson Award of ISCRE in 2007.

G.F. Froment is a Doctor Honoris Causa of the Technion, Haifa, Israel (1985), of the University of Nancy, France (2001) and an Honorary Professor of the Universidad Nacional de Salta (Argentina). He is a member of the Belgian Academy of Science (1984), the Belgian Academy of Overseas Science (1977), a Foreign Associate of the United States National Academy of Engineering (1999) and a member of the Texas Academy of Medicine, Science and Engineering (2003). He was a member of the Scientific Council of the French Petroleum Institute (1989-1997), of the Technological Council of Rhône-Poulenc (1988-1997) and has intensively consulted for the world's major petroleum and (petro)chemical companies.

K.B. Bischoff †

Kenneth B. Bischoff was the Unidel Professor of Biomedical and Chemical Engineering and past Chairman, Department of Chemical Engineering at the University of Delaware. Previously he was Acting Director for the Center for Catalytic Science and Technology. He was the Walter R. Read Professor of Engineering and Director of the School of Chemical Engineering at Cornell University and had been on the faculties of the Universities of Maryland and Texas (Austin), as well as a Postdoctoral Fellow at the University of Gent, Belgium. He had served as a consultant for Exxon Research and Engineering Company, General Foods Company, the National Institutes of Health, W. R. Grace company, Koppers Company, E. I. du Pont de Nemours & Co., Inc., and Westvaco Co., and was a registered professional engineer in the State of Texas. His research interests were in the areas of chemical reaction engineering and applications to pharmacology and toxicology, resulting in more than 100 journal articles and two textbooks: *Process Analysis and Simulation* (with D.M. Himmelblau) (1968); and *Chemical Reactor Analysis and Design*, (with G.F. Froment) (1979). He was elected to the National Academy of Engineering in 1988, and he received the 1972 Ebert Prize of the Academy of Pharmaceutical Sciences, the 1976 Professional Progress Award, the 1982 Institute Lecture Award, the 1982 Food, Pharmaceutical and Bioengineering Division Award, and the 1987 R. H. Wilhelm Award. In 1987 he was named a Fellow of the American Institute of Chemical Engineers. He was a Fellow of AAAS since 1980. Editorial boards on which he had served include *J. Pharmacokinetics and Biopharmaceutics*, from 1972 on; and *ACS Advances in Chemistry Series*, 1974 to 1981. In 1981 he became an Associate Editor of *Advances in Chemical Engineering*,
Dr. Bischoff passed away in 2007.

J. De Wilde

Juray De Wilde received his Ph.D in Chemical Engineering from the Ghent University, Belgium, in 2001. He did post-doctoral work at the Ghent University and was post-doc research associate at the Chemical Engineering Department of Princeton University, NJ. In 2005 he became professor of Chemical Engineering at the Université catholique de Louvain, Belgium, where he received his tenure in 2008. Dr. De Wilde published more than 30 papers in international journals and served as a member of scientific committees and as a consultant for numerous companies, including Total Petrochemicals, Tribute Creations, Dow

Corning, PVS Chemicals, The Catalyst Group, Nanotech-Nanopole, Certech, etc.. His research interests and expertise include dynamic methods for catalytic kinetics, the modeling and simulation of gas-solid flows, and process intensification, in particular for fluidized bed processes. With A. de Broqueville, he developed the rotating fluidized bed in a static geometry and the rotating chimney technologies.

Contents — Chemical Reactor Analysis and Design, Third edition

G.F. Froment, K.B. Bischoff, J. De Wilde

Chapter 1: Elements of Reaction Kinetics

Chapter 2: Kinetics of Heterogeneous Catalytic Reactions

Chapter 3: Transport Processes with Reactions Catalyzed by Solids

Chapter 4: Noncatalytic Gas-Solid Reactions

Chapter 5: Catalyst Deactivation

Chapter 6: Gas-Liquid Reactions

Chapter 7: The Modeling of Chemical Reactors

Chapter 8: The Batch and Semibatch Reactors

Chapter 9: The Plug Flow Reactor

Chapter 10: The Perfectly Mixed Flow Reactor

Chapter 11: Fixed Bed Catalytic Reactors

Chapter 12: Complex Flow Patterns

Chapter 13: Fluidized Bed and Transport Reactors

Chapter 14: Multiphase Flow Reactors

This page intentionally left blank

Notation

Great attention has been given to the detailed definition of the units of the different quantities: for example, when a dimension of length is used, it is always clarified as to whether this length concerns the catalyst or the reactor. We have found that this greatly promotes insight into the mathematical modeling of a phenomenon and avoids errors.

A	reaction component	
A_b	heat exchange surface, packed bed side	m^2
A_j	reacting species	
A_k	heat exchange surface in a batch reactor, on the side of the reaction mixture	m^2
A_m	logarithmic mean of A_k and A_r or of A_b and A_r	m^2
A_r	heat exchange surface for a batch reactor, on the side of the heat transfer medium	m^2
A_t	total heat exchange surface	m^2
A_v	gas-liquid interfacial area per unit liquid volume	m_i^2/m_L^3
A_o	frequency factor, for 1st order, e.g.	s^{-1}
A_v'	gas-liquid interfacial area per unit gas + liquid volume	m_i^2/m_{L+G}^3
$\tilde{A}$	single event frequency factor	s^{-1}
a	stoichiometric coefficient	
a_g	surface to volume ratio of a particle	m_p^2/m_p^3
a_m	external particle surface area per unit catalyst mass	$m_p^2/kg\,cat.$
a_v	external particle surface area per unit reactor volume	m_p^2/m_r^3
a', a_j'	order of reaction with respect to A, A_j	
a_v'	gas-liquid interfacial area per unit packed volume	m_i^2/m_r^3
a_v''	liquid-solid interfacial area per unit packed volume	m_i^2/m_r^3
B	reaction component	
B_m	fictitious component in Wei-Prater analysis	
$\mathbf{B}$	vector of fictitious components	
b	stoichiometric coefficient	
b'	order of reaction with respect to B	

b	vector of parameter estimates	
C_A, C_B, C_j	molar concentration of species *A, B, j*	kmol/m_f^3
$C_{Ab}, C_{Bb}, ...$	molar concentrations of species *A, B,* … in the bulk fluid	kmol/m_f^3
C_{A1}, C_{B1}	molar concentrations of adsorbed *A, B,* …	kmol/kg cat.
C_C	coke content of catalyst	kg coke/kg cat.
C_D	drag coefficient for spheres	
C_l	molar concentration of vacant active sites of catalyst	kmol/kg cat.
C_t	total molar concentration of active sites	kmol/kg cat.
C_o	inlet concentration	kmol/m_f^3
C	vector of molar concentrations	kmol/m_f^3
C_{Aeq}	molar concentration of *A* at equilibrium	kmol/m_f^3
C_{Ai}	molar concentration of *A* in front of the interface	kmol/m_f^3
C_{As}, C_s	molar concentration of fluid reactant inside the solid	kmol/m_f^3
C_{As}^s	molar concentration of fluid reactant at surface of solid	kmol/m_f^3
C'_{As}	molar concentration of *A* inside completely reacted zone of solid	kmol/m_f^3
$\overline{C}_A$	Laplace transform of C_A	
C_{pl}	concentration of sites covered with poison	kmol/kg cat.
C_{P1^∞}	equilibrium molar concentration of sorbed poison inside catalyst	kmol/kg cat.
C_{Ps}, C_{Ps}^c	molar concentration of poison in gas phase inside catalyst and at core boundary	kmol/m_f^3
C_S	solid (reactant) concentration	kmol/m_p^3
c_p	specific heat of fluid at constant pressure	kJ/kg K
c_{ps}	specific heat of solid	kJ/kg K
Da	Damköhler number; also Damköhler number for poisoning, $k_{sP}R/D_{eP}$	
D_A, D_B	molecular diffusivities of *A, B* in liquid film	m_L^3/m_L s
D_{AB}	molecular diffusivity for *A* in a binary mixture of *A* and *B*	m_f^3/m_f s
D_{Am}	molecular diffusivity for *A* in a multicomponent mixture	m_f^3/m_f s
D_K	Knudsen diffusivity	m_f^3/m_f s

D_e, D_{eA}, D_{eB}	effective diffusivities for transport in a (pseudo-) continuum, or in emulsion phase	$m_f^3/m\,cat.\ s$
D_{eG}	gas phase effective diffusivity in axial direction in a multiphase packed bed	$m_G^3/m_r\ s$
D_{eL}	liquid phase effective diffusivity in axial direction in a multiphase packed bed	$m_L^3/m_r\ s$
D_{eP}	effective pore diffusivity for poison	$m_f^3/m\,cat.\ s$
D_{ea}, D_{er}	effective diffusivities in axial, respectively radial directions in a packed bed	$m_f^3/m_r\ s$
D_{eg}	effective diffusivity for transport of *A* through a grain (Chapter 4)	$m_f^3/m_p\ s$
D_{ep}	effective diffusivity for transport of *A* in the pores between the grains (Chapter 4)	$m_f^3/m_p\ s$
$D_{j,l}$	eddy diffusivity for species *j* in the *l* direction	$m_f^3/m\,s$
D_l	eddy diffusivity in the *l* direction	$m_f^3/m\,s$
$D_e^{'}$	effective diffusivity for transport through completely reacted solid (Chapter 4)	$m_f^3/m_p\ s$
D_{jm}	effective molecular diffusivity of *j* in a multicomponent mixture	$m_f^3/m_f\ s$
D_{eff}	effective diffusivity, a combination of molecular and turbulent diffusivities in a fluid	$m_f^3/m_f\ s$
D_t	turbulent diffusivity in a fluid	$m_f^3/m_f\ s$
$D(x_u)$	divergence used in sequential model discrimination	
d	wall thickness	m
d_b	bubble diameter	m
d_c	coil diameter	m
d_p	particle diameter	m_p
d_r	reactor diameter	m_r
d_s	stirrer diameter	m
d_t	internal tube diameter; also tower diameter (Chapter 14)	m_r
E	activation energy; also internal energy; also energy of the particle, consisting of potential and kinetic contributions; also total energy, consisting of internal and kinetic energy (Chapter 12)	kJ/kmol kJ/kg

$E(\theta)d\theta$	residence time distribution function	
E_a	activation energy	kJ/kmol
$E_i(x)$	exponential integral function	
E^o	intrinsic activation barrier of a reference step of a given type of elementary step	kJ/kmol
Eö_b	Eötvös number, based on bubble diameter, $d_b \rho_L g/\sigma$	
$\hat{E}(r)$	number of pore mouths per network on a sphere at a distance r from the center of the particle	
e_{kin}	specific kinetic energy	kJ/kg
$\text{erf}(\eta)$	error function	
$\text{erfc}(\eta)$	complementary error function, 1 - $\text{erf}(\eta)$	
F	total molar flow rate	kmol/s
F_A	enhancement factor	
F_{Ao}, F_{jo}	molar feed rate of reactants A and j	kmol/s
F_c	ratio of variances, used to test model adequacy or used to select the best out of a number of competing models (Chapter 2)	
F_k	force exerted per unit cross section	N/m²
F'	volumetric gas flow rate	m_f^3/s
$F_o^{'}$	volumetric gas feed rate of feed	m_f^3/s
F''	volumetric gas flow rate (Chapter 14)	m_f^3/m_r^2 s
f	friction factor; also single-particle- or one-point joint micro-probability density function	
f_b	fraction of total fluidized bed volume occupied by bubble gas	m_b^3/m_r^3
f_e	fraction of total fluidized bed volume occupied by emulsion gas	m_{eg}^3/m_r^3
f_N	N-particle- or N-point joint micro-probability density function	
G	superficial mass flow velocity;	kg/m_r^2 s
	also standard Gibbs free energy	kJ
g	acceleration of gravity	m/s^2
H	Henry's law coefficient;	Nm/kmol or m³ bar/kmol
	also enthalpy;	kJ
H_L	liquid height	m
$H_{L,n}$	enthalpy of liquid on plate n	kJ/kmol

H_{fj}	heat of formation of species *j*	kJ/kmol
H_i	height of stirrer above bottom	m
$\overline{H}_j$	molar enthalpy of species *j*	kJ/kmol
$-\Delta H$	heat of reaction	kJ/kmol
$-\Delta H_a^\circ$	standard enthalpy of adsorption	kJ/kmol
Ha	Hatta number, γ	
h	Planck constant	kJ s
h_f	heat transfer coefficient for film surrounding a particle	$kJ/m_p^2\,s\,K$
h_F	froth height	m
$I(\alpha)d\alpha$	internal age distribution function	
I	internal distribution function	
I	initiator; also intermediate species; inert;	
I	unit matrix	
J	matrix of partial derivatives of function with respect to parameters (Chapter 2); Jacobian matrix	
$J_{j,l}$	molar flux of species *j* in *l* direction, with respect to mass average velocity	$kmol/m^2s$
j_D	*j*-factor for mass transfer, $\frac{k_g M_m p_{fA}}{G}\mathrm{Sc}^{2/3}$	
j_H	*j*-factor for heat transfer, $\frac{h_f}{c_p G}(\mathrm{Pr})^{2/3}$	
$K, K_A,$	equilibrium constants	m^2/N or $m^3/kmol$ or bar^{-1}
$K_1 \ldots$		
K	matrix of rate coefficients	s^{-1}
$\hat{K}$	kinetic energy per unit mass	m^2/s^2
$\hat{K}_1$	flow averaged kinetic energy per unit mass	m^2/s^2
k, k_{rA}	rate coefficient for a catalytic reaction; for 1st order, e.g.	$m_f^3/kg\,cat.\ s$
k	rate coefficient for a reaction between a fluid reactant *A* (order *n*) and a solid or solid component *S* (order *m*)	$m_f^{3n}(kmol\,A)^{1-n}$ $(kmol\ S)^{-m}\ m_p^{3m}$ $(kg.\ part)^{-1}\ s^{-1}$
k	turbulent kinetic energy	kJ/kg
k_B	Boltzmann constant	kJ/K
k_C	coking rate coefficient for 1st order coking, e.g.	s^{-1}

k_G	mass transfer coefficient from gas to liquid interface, based upon partial pressure driving force	kmol/m^2 bar s
k_I	bubble-emulsion phase interchange coefficient	m_f^3/m_r^3 s
k_L	mass transfer coefficient from interface to liquid bulk, based on concentration driving force	$m_L^3/m_i^2 \cdot s$
k_T	mass transfer coefficient (including interfacial area) between flowing and stagnant liquid in a multiphase reactor	m_L^3/m_r^3 s
k_{T1}, k_{T2}	mass transfer coefficient (including interfacial area) between regions 1 and 2 of flow model (Chapter 12)	m_L^3/m_r^3 s
k_c	rate coefficient based on concentrations	$s^{-1}\{kmol/m^3\}^{1-(a'+b'...)}$
k_g	mass transfer coefficient from gas to solid interface	
	when based on concentration driving force	m_f^3/m_i^2 s
	when based upon partial pressure driving force	kmol/m_i^2 bar s
k_{gP}	interfacial mass transfer coefficient for catalyst poison	m_f^3/m_p^2 s
k_l	mass transfer coefficient between liquid and catalyst surface, referred to unit interfacial area	m_L^3/m_i^2 s
k_p	reaction rate coefficient based on partial pressures	s^{-1} kmol/m_f^3 $(N/m^2)^{-(a'+b'...)}$
k_{pr}	rate coefficient for propagation reaction in addition polymerization	m³/kmol · s
k_{rP}	rate coefficient for first-order poisoning reaction at core boundary	m_f^3/m² cat.s
k_t, k_{tr}	rate coefficients for termination reactions	m³/kmol · s or s^{-1}
k_y	rate coefficient based on mole fractions	kmol/m_f^3 s
k_1	elutriation rate coefficient (Chapter 13)	kg/m² s
$k_1, k_2 \ldots$	reaction rate coefficients	
k_A°	rate coefficient of catalytic reaction in absence of coke	
k_g°	mass transfer coefficient in case of equimolar counterdiffusion, $k_g Y_{fA}$	m_f^3/m_is
k_l'	mass transfer coefficient between stagnant liquid and catalyst surface in a multiphase reactor	m_L^3/m_r^3 s

$(k_{bi})_b$	mass transfer coefficient from bubble to interchange zone, referred to unit bubble volume	m_f^3/m_b^3 s
$(k_{be})_b$	overall mass transfer coefficient from bubble to emulsion, referred to unit bubble volume	m_f^3/m_b^3 s
$(k_{ie})_b$	mass transfer coefficient from interchange zone to emulsion, referred to unit bubble volume	m_f^3/m_b^3 s
$(k_{ce})_c$	mass transfer coefficient from bubble + interchange zone to emulsion, referred to unit bubble + interchange zone volume	m_G^3/m_c^3 s
$\tilde{k}$	single event rate coefficient	see k, k_{rA}
L	volumetric liquid flow rate	m_L^3/s
	also distance from center to surface of catalyst pellet (Chapter 3)	m_p
L	pore length	m
L_f	total height of fluidized bed	m_r
L_{mf}	height of a fluidized bed at minimum fluidization	m_r
L'	molar liquid flow rate	kmol/s
Lw'	modified Lewis number, $\lambda_e / \rho_s c_{ps} D_e$	
l	vacant active site	
M	ratio of initial concentrations C_{Bo} / C_{Ao}	
M_j	molecular mass of species j	kg/kmol
M_m	mean molecular mass	kg/kmol
M_1	monomer (Chapter 1)	
m	Henry's coefficient based on mole fractions; also mass fraction	kg/kg total
m_t	total mass	kg
$\dot{m}$	total mass flow rate	kg/s
$\dot{m}_j$	mass flow rate of component j	kg/s
N	stirrer revolution speed; also runaway number, $2U / R_t \rho c_p k_v$ (Chapter 11); also total number of particles in the sample space	s^{-1}
$\dot{N}_A$	molar rate of absorption per unit gas-liquid interfacial area also molar flux of A with respect to fixed coordinates	$kmol/m_i^2$ s $kmol/m^2$ s
$\dot{N}_A(t)$	instantaneous molar absorption rate in element of age t per unit gas-liquid interfacial area	$kmol/m_i^2$ s

$N_A, N_B,$	number of kmoles of reacting components	kmol
$N_j ...$	of *A, B, j* … in reactor	
N_n	number of pore networks in a particle	
N_s	dimensionless group, $\frac{3D_{ep}t_{ref}C_{p,ref}}{R^2\rho_s C_{P1^\infty}}$ (Chapter 5)	
N_t	total number of kmoles in reactor	kmol
N_o	minimum stirrer speed for efficient dispersion	s^{-1}
N_o^*	characteristic speed for bubble aspiration and dispersion	s^{-1}
n	order of reaction; number of experiments	
n_C	carbon number	
n_e	number of single events; also number of replicated experiments	
P	total pressure; also probability that a site is accessible (Chapter 5); also power input; also reaction product	N/m^2 Nm/s
Pr	Prandtl number, $c_p \mu / \lambda$	
Pr_t	turbulent Prandtl number, $Pr_t = \mu_t c_P / \lambda_t$	
P_i	probability that a molecule is in the *i*-th quantum state with energy level E_i	
P_N	profit over *N* adiabatic fixed beds	
$P_1, P_2 ...$	active polymer	
Pe_a	Peclet number based on particle diameter, $u_i d_p / D_{ea}$	
Pe_a'	Peclet number based on reactor length, $u_i L / D_{ea}$	
$\overline{P}_N$	number averaged degree of polymerization	
$\overline{P}_W$	mass averaged degree of polymerization	
p	probability of adding another monomer unit to a chain; also number of parameters	
$P_A, P_B,$	partial pressures of components *A, B, j* …	N/m^2, also bar
$P_j ...$		
P_c	critical pressure	N/m^2, also bar
P_{fA}	film pressure factor	N/m^2, also bar
P_k	production of turbulent kinetic energy	$kg/(m \cdot s^3)$
P_s	solid phase pressure	N/m_r^2
p_t	total pressure	N/m^2, also bar

Q	reaction component;	
	also (total) partition function	
Q_{ox}, Q_a, Q_{abs}	heats of oxidation	kJ/kmol
	adsorption, absorption	
q	stoichiometric coefficient;	
	also heat flux;	kJ/m² s
q'	order of reaction with respect to Q	
q_j'	order of reaction with respect to Q_j	
q_t, q_r, q_v, q_{el}	translational, rotational, vibrational and electronic contributions to the total partition function Q	
R	gas constant;	kJ/kmol K
	also radius of a spherical particle (Chapters 4 and 5);	m_p
	also reaction component	
Re	Reynolds number, $d_p G/\mu$ or $d_t G/\mu$	
R_j	total rate of change of the amount of component j	kmol/m_f^3 s
R_t	tube radius	m_r
R_1, R_2	free radicals	
r	pore radius (Chapter 3)	m
	also radial position in spherical particle;	m_p
	also stoichiometric coefficient;	
	also space vector (Chapter 1)	
r_A	rate of reaction of component A per unit volume for homogeneous reaction	kmol/m_f^3 s
	or per unit catalyst mass for heterogeneous reaction	kmol/kg cat. s
r_C	rate of coke deposition	kg coke/kg cat. s
r_P	rate of poison deposition	kmol/kg cat. s
r_S	rate of reaction of S, reactive component of solid, in gas-solid reactions or rate of reaction of solid itself	kmol/kg part. s
r_{Ai}	rate of reaction of A at interface	kmol/m_i^2 s
r_b	radius of bend of coil	m
r_c	radial position of unpoisoned or unreacted core in sphere	m_p
$\bar{r}$	mean pore radius	m
$\tilde{r}_A$	rate of reaction of component A in terms of the variation of its mass fraction	kg A/(kg total·s)
S	reaction component also dimensionless group, $\beta\gamma$;	
	also entropy;	kJ/K
Sc	Schmidt number, $\mu/\rho D$	

S_g	internal surface area per unit mass of catalyst	m² cat./kg cat.
S	external surface area of a pellet	m_p^2
Sh_m	modified Sherwood number for liquid film, $k_L / A_v D_A$	
Sh'	modified Sherwood number, $k_g L/D_e$ (Chapter 3)	
Sh_p'	modified Sherwood number for poisoning $k_{gP}R/D_{ep}$	
$S(\beta)$	objective function also joint confidence region (Chapter 2)	
$-\Delta S_a^o$	standard entropy of adsorption of a component	kJ/kmol K
s	stoichiometric coefficient; also parameter in Danckwerts' age distribution function; also Laplace transform variable	s^{-1}
s_e^2	pure error variance	
s_i^2	estimate of experimental error variance of model i	
s'	order of reaction with respect to S	
$\bar{s}^2$	pooled estimate of variance	
T	temperature; also kinetic energy functional	K
T_R	bed temperature at radius R_t	K
T_c	critical temperature	K
T_m	maximum temperature	K
T_r	temperature of surroundings	K
T_s, T_s^s	temperature inside solid, resp. at solid surface	K
t	clock time;	s
	also age of surface element (Chapter 6)	s
$t(n-p, 1-\alpha/2)$	tabulated $\alpha/2$ percentage point of the t-distribution with n-p degrees of freedom	
t_{ref}	reference time	s
t'	reduced time	
$t*$	time required for complete conversion (Chapter 4)	s
$\bar{t}$	contact time	s
$\Im(s, \alpha)$	transfer function of flow model (Chapter 12)	
U	overall heat transfer coefficient; also functional expressing the interaction between electrons	kJ/m² s K
u	linear velocity	m_r/s
u_b	bubble rise velocity, absolute	m_r/s
u_{br}	bubble rise velocity, with respect to emulsion phase	m_f^3/m_r^2 s

u_e	emulsion gas velocity, interstitial	m_r/s
u_i	interstitial velocity	m_r/s
u_{iG}, u_{iL}	interstitial velocity of gas, resp. liquid	m_r/s
u_l	fluid velocity in direction l	m/s
u_s	superficial velocity	m_f^3/m_r^2 s
u_{sG}	superficial gas velocity	m_G^3/m_r^2 s
u_t	terminal velocity of particle	m_r/s
V	reactor volume or volume of considered "point"	m_r^3
V	volume of particle	m_p^3
V_R	equivalent reactor volume	m_r^3
V_b	bubble volume	m_b^3
V_c	critical volume; also volume of bubble	
	+ interchange zone	m_f^3
V_{iz}	volume of interchange zone	m^3
V_s	product molar volume	m^3/kmol
V_b'	bubble volume corrected for the wake	m_b^3
V_c'	corrected volume of bubble + interchange zone	m_c^3
V_{iz}'	volume of interchange zone, corrected for wake	m^3
$\mathbf{V}(b)$	variance-covariance matrix of estimates b	
$\mathbf{V}(\varepsilon)$	matrix of error variance	
v^{il}	elements of inverse of matrix $\mathbf{V}(\varepsilon)$	
W	total catalyst mass	kg cat.
$W(d_p)$	mass of amount of catalyst with diameter d_p	kg
$W(\theta)$	increase in value of reacting mixture	\$
We	Weber number, $\rho_L L^2 d_p / \Omega^2 \rho_L$	
W_j	amount of catalyst in bed j of a multibed	
	adiabatic reactor	kg
$W_o, W_p,$	cost of reactor idle time, reactor charging time	\$/s
W_Q, W_R	reactor discharging time and of reaction time	
w_{ij}	weighting factor in objective function (Chapters 1 and 2)	
w_j	price per kmole of chemical species A_j	\$/kmol
x	fractional conversion	

$x_A, x_B,$ $x_j \ldots$	fractional conversion of *A, B, j* …	
x_{Aeq}	fractional conversion of *A* at equilibrium	
x_{aK}	conversion of acetone into ketene (Chapter 9)	
x_{at}	total conversion of acetone (Chapter 9)	
x_n	mole fraction in liquid phase on plate *n*	
$\mathbf{x}_m$	eigenvector of rate coefficient matrix **K**	
$x'_A, x'_B \ldots$	conversion of *A, B* …	kmol
$x''_A, x''_B \ldots$	conversion of *A, B* … for constant density	kmol/m³
$\boldsymbol{X}$	matrix of settings of independent variables	
$\boldsymbol{X}^T$	transpose matrix of $\boldsymbol{X}$	
$\mathbf{Y}$	vector of species mass fractions	
Y_A	species mass fraction	kg *A*/kg total
y	radius of grain in grain model of Sohn and Szekely (Chapter 4)	m
$\hat{y}$	estimated value of dependent variable	
y	coordinate perpendicular to gas-liquid interface; also radial position inside a grain in grain model of Sohn and Szekely (Chapter 4)	m
$\underline{\mathbf{y}}$	vector of mole fractions	
$\bar{y}$	arithmetic mean of n_e replicate observations	
y	vector of observations of dependent variable	
$y_A, y_B,$ $y_j \ldots$	mole fraction of species *A, B, j* …	
y_G	gas film thickness	m
y_L	liquid film thickness for mass transfer	m
y_h	liquid film thickness for heat transfer	m
y_n	mole fraction in gas phase leaving plate *n*	
y_1, y_2	weight fractions of gas oil, gasoline (Chapter 5)	
Z	compressibility factor; also total reactor or column length	m_r
Z_c	critical compressibility factor	
z	distance inside a slab of catalyst also axial coordinate in reactor	m_p m_r
$\boldsymbol{z}$	spatial coordinate vector	
z_j	distance coordinate in *j* direction	m
z_l	distance coordinate in *l* direction	m

Greek Symbols

α	convective heat transfer coefficient;	kJ/m² s K
	also transfer coefficient;	
	also profit resulting from the conversion of 1 kmole of *A* into desired product	$/kmol
$\boldsymbol{\alpha}$	vector of flow model parameters	
α, α_c	deactivation constants	kg cat./kg coke
α_i	convective heat transfer coefficient, packed bed side	kJ/m² s K
α_{ij}	stoichiometric coefficient of component *j* in the *i*th reaction	
α_k	convective heat transfer coefficient on the side of the reaction mixture	kJ/m²sK
α_r	convective heat transfer coefficient on the side of the heat transfer medium	kJ/m²sK
α_u	convective heat transfer coefficient for a packed bed on the side of the heat transfer medium	kJ/m²sK
α_w	convective heat transfer coefficient in the vicinity of the wall	kJ/m²sK
α_w^s	wall heat transfer coefficient for solid phase	kJ/m²sK
α_w^f	wall heat transfer coefficient for fluid	kJ/m²sK
β	parameter;	
	also radical involved in a bimolecular propagation step;	
	also $1/k_B T$;	
	also weighting factor in objective function (Chapter 2);	
	also stoichiometric coefficient (Chapter 5);	
	also cost of 1 kg of catalyst (Chapter 11);	
	also dimensionless adiabatic temperature rise, $(T_{ad} - T_o)/ T_o$;	
	also thermal expansion coefficient;	
	also interphase momentum transfer coefficient;	kg/(m_r^3 s)
	also Prater number = $(-\Delta H) D_e C_s^s / \lambda_e T_s^s$ (Chapter 3)	
Γ_e	locus of equilibrium conditions in $x - T$ diagram	
Γ_m	locus of the points in $x - T$ diagram where the rate is maximum	
$\Gamma_{\lambda m}$	locus of maximum rate along adiabatic reaction path in $x - T$ diagram	
γ	Hatta number, for first order reaction $\sqrt{kD_A} / k_{L,A}$;	
	for reaction with order *m* with respect to *A*	

	and n with respect to B: $\sqrt{\frac{2}{m+1} k C_{Ai}^{m-1} C_{Bi}^{n} D_A} \,/\, k_{L,A}$	
	also dimensionless activation energy, E/RT (Chapters 3 and 11);	
	also dissipation of pseudo-thermal energy (solid phase) by inelastic particle-particle collisions	$kg/(m_r s^3)$
δ	molar ratio steam / hydrocarbon	
δ_A	expansion per mole of reference component A, $(q+s-a-b)/a$	
ε	void fraction of packing;	m_f^3/m_r^3
ε	turbulence dissipation rate	m_r^2/s^3
$\boldsymbol{\varepsilon}$	column vector of n experimental errors	
ε_A	expansion factor, $y_{Ao}\,\delta_A$	
ε_G	gas hold up	m_G^3/m_r^3
ε_L	liquid holdup	m_L^3/m_r^3
ε_{LF}	liquid holdup in flowing fluid zone in packed bed	m_L^3/m_r^3
ε_c	void fraction of cloud, that is, bubble	
	+ interchange zone	m^3/m_c^3
ε_g	gas phase volume fraction	m_g^3/m_r^3
ε_m	pore volume of macropores	m_f^3/m_p^3
ε_{mf}	void fraction at minimum fluidization	m_f^3/m_r^3
ε_s or ε_g^s	internal void fraction or porosity;	m_f^3/m_p^3
	also solid phase volume fraction	m_s^3/m_r^3
ε_Y	scalar dissipation rate	1/s
ε_μ	pore volume of micropores	m_f^3/m_p^3
$\varepsilon_L^{'}$	dynamic holdup	m_f^3/m_r^3
	factor used in pressure drop equation for the bends in pipes	
ζ_m	quantity of fictitious component	
η	effectiveness factor for solid particle	
η_o	effectiveness factor for reaction in an unpoisoned catalyst	
η_L	utilization factor, liquid side	
η_G	global utilization factor; also effectiveness factor for particle + film	
Θ	granular temperature	J/kg

θ	fractional coverage of catalyst surface; also dimensionless time, $D_e t/L^2$ (Chapter 3), $ak'C_A t$ (Chapter 4); residence time; angle between pore and radial at distance r from center of spherical particle	rad
θ_P	reactor charging time	s
θ_R	reaction time	s
θ_Q	reactor discharging time	s
θ_f	reaction time corresponding to final conversion	s
θ_o	reactor idle time	s
κ	conductivity pseudo-thermal energy (solid phase)	kg/m s
Λ	angle described by bend of coil	rad
$\mathbf{\Lambda}$	matrix of eigenvalues	
λ	thermal conductivity	kJ/m s K
λ_e	effective thermal conductivity in a solid particle	kJ/m s K
λ_{eff}	effective thermal conductivity, a combination of molecular and turbulent conductivities	kJ/m s K
$\lambda_{ea}, \lambda_{er}$	effective thermal conductivity in a packed bed in axial, respectively radial direction	kJ/m$_r$ s K
λ_l	effective thermal conductivity in l direction	kJ/m s K
λ_m	negative of eigenvalue of rate coefficient matrix **K**; also molecular conductivity	kJ/m s K
λ_s	thermal conductivity of solid	kJ/m$_p$ s K
λ_t	turbulent conductivity	kJ/m s K
$\lambda_{er}^f, \lambda_{er}^s$	effective thermal conductivity for the fluid phase, respectively solid phase in a packed bed	kJ/m$_r$ sK
$\lambda(L)$	probability density function of pore length	
μ	dynamic viscosity; also type of radical in a unimolecular propagation step	kg/m s, also Pa·s
μ_s	viscosity at the temperature of the heating coil surface; also solid phase shear viscosity	kg/m s kg/m s
μ_w	viscosity at the temperature of the wall	kg/m s
ν	vibration frequency	
ξ	extent of reaction; also reduced length, z/L or reduced radial position inside a particle, r/R	kmol

ξ_c	reduced radial position of core boundary	
ξ_i	extent of *i*th reaction	kmol
ζ_s	solid phase bulk viscosity	kg/m s^2
ξ'	radial coordinate inside particle	m $_p$
ξ_i'	extent of *i*th reaction per unit mass of reaction mixture	kmol kg^{-1}
ρ	density	kg/m^3
ρ_B	catalyst bulk density	kg cat./m^3_r
ρ_L	liquid density	kg/m^3_L
ρ_b	bulk density of bubble phase	kg/m^3_b
ρ_e	bulk density of emulsion phase	kg/m^3_e
ρ_f	fluid density	kg/m^3_f
ρ_g	gas density	kg/m^3_G
ρ_{mf}	bulk density of fluidized bed at minimum fluidization	kg/m^3_r
ρ_s	density of catalyst	kg cat./m^3_p
σ	standard deviation; also active alumina site (Chapter 2); also symmetry number	kg cat/m^3 cat.
σ^2	variance of experimental error	
σ_L	surface tension of liquid	N/m
$\sigma_{L,c}$	critical surface tension of liquid	N/m
σ_P	sorption distribution coefficient (Chapter 5)	
τ	tortuosity factor for catalyst;	
	also mean residence time;	s
	also time scale or decay time (Chapter 12);	s
τ_Y	micro-mixing time	s
τ_{ji}	shear stress tensor, *ji*th component	kg/(m s^2)
ϕ	Thiele modulus for 1st order	
	$V / S\sqrt{k\rho_s / D_{eA}}$ (Chapters 3 and 5)	
	$V / S\sqrt{k\left(T_s^s\right) C_s / D_e}$ (Chapter 11)	
$\boldsymbol{\varphi}$	internal coordinate vector	
φ_A, φ_C	deactivation functions for main and coking reactions (site coverage)	
$\hat{\varphi}_A, \hat{\varphi}_C$	deactivation functions (at particle level)	
ϕ_A, ϕ_C	deactivation functions (observed)	

χ^2	distribution used in model discrimination	
ψ	sphericity of a particle	
$\Psi(r)$	spatial amplitude of the matter wave as a function of its position in space, defined with respect to the nucleus	
$\Psi(t)$	age distribution function	
Ω	cross section of reactor or column	m_r^2

Subscripts

$A, B...$	with respect to *A, B* …
B	Batchelor scale
C	coke
G	gas; also global or regenerator
I	integral scale
K	Kolmogorov scale
L	liquid
P	poison
R	reactor
T	at actual temperature
T_1	at reference temperature
a	adsorption; also in axial direction
ad	adiabatic
b	bulk; also bubble phase
c	bubble + interchange zone; also critical value; based on concentration
d	desorption
e	emulsion phase; also effective or exit stream from reactor
eq	at chemical equilibrium
f	fluid; also film; also at final conversion
g	average; also grain or gas; also gas phase
gl	global
i	interface; also *i*th reaction; also in *i*th direction
j	with respect to *j*th component; also in *j*th direction
l	liquid; also in *l* direction
m	maximum; also measurement point; also molecular; also mixture
n	tray number
o	overall
p	pellet, particle; also based on partial pressures
r	reactor dimension; also surrounding; also in radial direction;

	also rotational;
	also reactant
rad	radiation
s	inside solid; also surface based or superficial velocity;
	also solid phase
sr	surface reaction
t	total; also tube; also translational;
	also turbulent
u	velocity field
v	vibrational
w	at the wall
y	based on mole fractions
0	initial or inlet condition; also overall value
‡	activated complex

Superscripts

L	of the large scale structures
S	of the small scale structures
T	transpose
d	stagnant fraction of fluid
f	flowing fraction of fluid
g	gas phase
r	reactant
s	condition at external surface; also at solid surface;
	also solid phase
0	in absence of poison or coke
'	fluctuating
•	radical
∧	calculated or estimated value
‡	activated complex

Other

|	conditional
$\langle\ \rangle$	on the macro-scale; macro-scale- or
	Reynolds-averaged
$\langle\tilde{\ }\rangle$	Favre-averaged
$\{\ \}$	on the reactor scale; reactor-scale averaged

Chapter 1

Elements of Reaction Kinetics

In this chapter attention is focused on a representative volume of the reactor. This volume contains one single fluid phase only. It is uniform in composition and temperature. If the reactor is spatially uniform, the representative volume is the total volume; if not, the representative volume is limited to a differential element — a "point".

1.1 DEFINITIONS OF CHEMICAL RATES

1.1.1 Rates of Disappearance of Reactants and of Formation of Products

The rate of a homogeneous reaction is determined by the composition of the reaction mixture, the temperature, and the pressure. An equation of state links the pressure with the temperature and composition. Therefore, the following developments focus on the influence of the latter variables.

Consider the reaction

$$aA + bB \ldots \rightarrow qQ + sS \ldots \qquad (1.1.1\text{-}1)$$

Rates can be deduced from the change with time of the composition of the representative volume. The components *A* and *B* react with rates

$$r_A' = -\frac{dN_A}{dt} \qquad r_B' = -\frac{dN_B}{dt}$$

while *Q* and *S* are formed with rates

$$r_S' = \frac{dN_S}{dt} \qquad r_Q' = \frac{dN_Q}{dt}$$

N_j represents the molar amount of one of the chemical species in the reaction and *t* represents time.

1.1.2 The Rate of a Reaction

The following equalities exist between the different rates:

$$-\frac{1}{a}\frac{dN_A}{dt} = -\frac{1}{b}\frac{dN_B}{dt} = \frac{1}{q}\frac{dN_Q}{dt} = \frac{1}{s}\frac{dN_S}{dt} \qquad (1.1.2\text{-}1)$$

Each term of these equalities may be considered as *the* rate of the reaction.

In the case of N chemical species participating in M independent chemical reactions,

$$\alpha_{i1}A_1 + \alpha_{i2}A_2 + \ldots + \alpha_{iN}A_N = 0$$

or

$$\sum_{j=1}^{N} \alpha_{ij} A_j = 0 \qquad i = 1, 2, \ldots, M \qquad (1.1.2\text{-}2)$$

with the convention that the stoichiometric coefficients α_{ij} are taken positive for products and negative for reactants. A comparison with (1.1.1-1) would give $A_1 \equiv A$, $\alpha_1 \equiv -a$ (for only one reaction the subscript i is redundant, and $\alpha_{ij} \rightarrow \alpha_j$), $A_2 \equiv B$, $\alpha_2 \equiv -b$, $A_3 \equiv Q$, $\alpha_3 \equiv q$, $A_4 \equiv S$, $\alpha_4 \equiv s$.

By independent it is meant that no one of the stoichiometric equations can be derived from the others by a linear combination. For further discussion see Prigogine and Defay [1954], Denbigh [1955], and Aris [1965].

The rate of reaction is generally expressed on an intensive basis, say, reaction volume, so that, when V represents the volume occupied by a spatially uniform reaction mixture,

$$r_i \equiv \frac{1}{V}\frac{1}{\alpha_{ij}}\left(\frac{dN_j}{dt}\right)_i \qquad (1.1.2\text{-}3)$$

For the simpler case,

$$r = \frac{-1}{aV}\frac{dN_A}{dt} = \frac{-1}{aV}\frac{d}{dt}(C_A V) = \frac{-1}{aV}\left(V\frac{dC_A}{dt} + C_A\frac{dV}{dt}\right) \qquad (1.1.2\text{-}4)$$

where C_A represents the molar concentration of A (kmol/m^3_f). When the density remains constant, that is, when the reaction volume does not vary, (1.1.2-4) reduces to

$$r = \frac{-1}{a}\frac{dC_A}{dt} \qquad (1.1.2\text{-}5)$$

In this case it suffices to measure the change in concentration to obtain the rate of reaction.

Conversions, rather than concentrations, are often used in the rate expressions. They are defined as follows:

$$x_A' = N_{A_0} - N_A \qquad x_B' = N_{B_0} - N_B \tag{1.1.2-6}$$

For constant density,

$$x_A'' = C_{A_0} - C_A \qquad x_B'' = C_{B_0} - C_B \tag{1.1.2-7}$$

Fractional conversions that show immediately how far the reaction has progressed are frequently used:

$$x_A = \frac{N_{A_0} - N_A}{N_{A_0}} \qquad x_B = \frac{N_{B_0} - N_B}{N_{B_0}} \tag{1.1.2-8}$$

Which conversion is used should always be clearly defined.

The following relations may be easily derived from equations (1.1.2-6) through (1.1.2-8):

$$x_j' = N_{j_0} x_j \tag{1.1.2-9}$$

$$\frac{x_A'}{a} = \frac{x_B'}{b} = \ldots = \frac{x_Q'}{q} \ldots \tag{1.1.2-10}$$

$$x_B = \frac{b}{a} \frac{N_{A_0}}{N_{B_0}} x_A \tag{1.1.2-11}$$

An alternate but related concept to the conversion is the extent or degree of advancement of the general reaction (1.1.2-2), which is defined as

$$\xi = \frac{N_j - N_{j0}}{\alpha_j} \tag{1.1.2-12a}$$

a quantity that is the same for any species. Also,

$$N_j = N_{j0} + \alpha_j \xi \tag{1.1.2-12b}$$

where N_{j0} is the initial amount of A_j present in the reaction mixture. For multiple reactions,

$$N_j = N_{j0} + \sum_{i=1}^{M} \alpha_{ij} \xi_i \tag{1.1.2-13}$$

Equations (1.1.2-8) and (1.1.2-12) can be combined to give

$$N_j = N_{j0} + \alpha_j \frac{N_{A_0}}{a} x_A$$

If species A is the limiting reactant (present in least amount), the maximum extent of reaction is found from

$$0 = N_{A_0} + \alpha_A \xi_{\max}$$

and the fractional conversion defined by (1.1.2-8) becomes

$$x_A = \frac{\xi}{\xi_{\max}} \tag{1.1.2-14}$$

Either conversion or extent of reaction can be used to characterize the amount of reaction that has occurred. For industrial applications, the conversion of a feed is usually of interest, while for scientific applications, such as irreversible thermodynamics [Prigogine, 1967], the extent is often more useful. Further details are given by Boudart [1968] and Aris [1969].

In terms of the extent of reaction, the reaction rate (1.1.2-3) can be written

$$r_i = \frac{1}{V}\frac{1}{\alpha_{ij}}\left(\frac{dN_j}{dt}\right)_i = \frac{1}{V}\frac{d\xi_i}{dt} \tag{1.1.2-15}$$

With this rate, the change in moles of any species is, for a single reaction,

$$\frac{dN_j}{dt} = \alpha_j V r \tag{1.1.2-16}$$

and for multiple reactions,

$$\frac{dN_j}{dt} = \sum_{i=1}^{M} \alpha_{ij} V r_i = V R_j \tag{1.1.2-17}$$

R_j is used as a definition of the “net” rate of change of species j.

1.2 RATE EQUATIONS

1.2.1 General Structure

According to the law of mass action, the rate of reaction, (1.1.1-1), is written

$$r = k_c C_A^{a'} C_B^{b'} \tag{1.2.1-1}$$

The proportionality factor k_c is called the rate coefficient, or rate constant. By definition, this rate coefficient is independent of the quantities of the reacting species, but dependent on the other variables that influence the rate. When the reaction mixture is thermodynamically nonideal, k_c will often depend on the concentrations because the latter do not completely take into account the interactions between molecules. In such cases thermodynamic activities need to be used in (1.2.1-1).When r is expressed in kmol/m^3. h, the rate coefficient k_c, based on (1.2.1-1) has dimensions

$$\mathrm{h}^{-1}(\mathrm{kmol/m}^3)^{[1-(a'+b'+\ldots)]}$$

It can also be verified that the dimensions of the rate coefficients used with conversions are the same as those given for use with concentrations. Partial pressures may also be used as a measure of the quantities of the reacting species,

$$r = k_p\, p_A^{a'}\, p_B^{b'} \qquad (1.2.1\text{-}2)$$

In this case the dimensions of the rate coefficient are

$$\mathrm{h}^{-1}(\mathrm{kmol/m}^3)\mathrm{bar}^{-(a'+b'+\ldots)}$$

With thermodynamically nonideal conditions (e.g., high pressures), partial pressures may have to be replaced by fugacities. When use is made of mole fractions, the corresponding rate coefficient has dimensions $\mathrm{h}^{-1}(\mathrm{kmol/m}^3)$. According to the ideal gas law,

$$C_i = \frac{p_i}{RT} = \frac{p_t}{RT}\, y_i$$

so that

$$k_c = (RT)^{a'+b'+\ldots} \cdot k_p = \left(\frac{RT}{p_t}\right)^{a'+b'+\ldots} \cdot k_y \qquad (1.2.1\text{-}3)$$

In the following, the subscript is often dropped. The powers *a'*, *b'*, ... are called "partial orders" of the reaction with respect to *A*, *B*, ... The sum *a'* + *b'* + ... may be called the "global order", or generally just "order" of the reaction.

Rate equations like (1.2.1-1) or (1.2.1-2) are strictly valid only for elementary reactions or steps. Some reactions consist of a number of elementary steps between intermediates with a short lifetime, less readily observable than the reactants and products. Then the orders in (1.2.1-1) do not necessarily correspond to the stoichiometric coefficients of the overall reaction. This is why it is recommended to verify the orders experimentally.

1.2.2 Influence of Temperature

The rate of a reaction depends on the temperature, through the variation of its rate coefficient. According to Arrhenius:

$$\ln k = -\frac{E}{R}\frac{1}{T} + \ln A_0 \qquad (1.2.2\text{-}1)$$

where

T = temperature (K)
R = gas constant = 8.314 (kJ/kmol K)
E = activation energy (kJ/kmol)
A_0 = a constant called the frequency factor

Consequently, when ln k is plotted versus $1/T$, a straight line with slope $-E/R$ is obtained.

Arrhenius came to this formula by thermodynamic considerations. Indeed, for the reversible reaction,

$$A \underset{2}{\overset{1}{\rightleftarrows}} Q$$

the van't Hoff relation is as follows:

$$\frac{d}{dT}\ln K_C = \frac{\Delta H}{RT^2} \qquad (1.2.2\text{-}2)$$

Since

$$K_c = \left(\frac{C_R}{C_A}\right)_{eq} = \frac{k_1}{k_2}$$

equation (1.2.2-2) may be written

$$\frac{d}{dT}\ln k_1 - \frac{d}{dT}\ln k_2 = \frac{\Delta H}{RT^2}$$

This led Arrhenius to the conclusion that the temperature dependence of k_1 and k_2 must be analogous to (1.2.2-2):

$$\frac{d}{dT}\ln k_1 = \frac{E_1}{RT^2} \qquad \frac{d}{dT}\ln k_2 = \frac{E_2}{RT^2}$$

with

$$E_1 - E_2 = \Delta H \qquad (1.2.2\text{-}3)$$

which is (1.2.2-1). Note that $E_2 > E_1$ for an exothermic and conversely for an endothermic reaction. Since then, this hypothesis has been confirmed many times experimentally, although, according to the collision theory, k should be

proportional to $T^{1/2}\exp[-E/RT]$ and, from the theory of the activated complex, to $T\exp[-E/RT]$. (Note that these forms also satisfy the van't Hoff relation.) The influence of $T^{1/2}$ or even T in the product with $e^{-E/RT}$ is very small, however, and to observe this influence requires extremely precise data.

The Arrhenius equation is only strictly valid for single reactions. If a reaction is accompanied by a parallel or consecutive side reaction which is not accounted for in detail, deviations from the straight line may be experienced in the Arrhenius plot for the overall rate. If there is an influence of transport phenomena on the measured rate, deviations from the Arrhenius law may also be observed. This is illustrated in Chapter 3.

From the practical standpoint, the Arrhenius equation is of great importance for interpolating and extrapolating the rate coefficient to temperatures that have not been investigated. With extrapolation, take care that the mechanism is the same as in the range investigated.

EXAMPLE 1.2.2.A

DETERMINATION OF THE ACTIVATION ENERGY

For a first-order reaction, the following rate coefficients were found:

Temperature, °C	**k**, h^{-1}
38.5	0.044
53.1	0.301
77.9	1.665

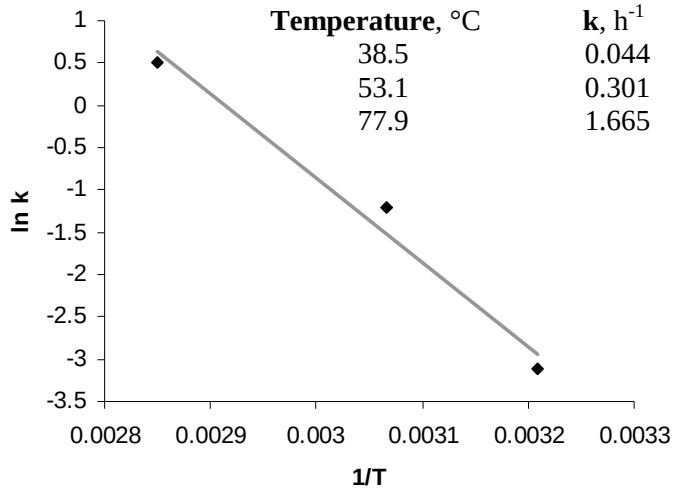

When these values are plotted in a diagram of ln *k* versus 1/*T*, with *T* in degrees Kelvin, a straight line is obtained with slope –*E*/*R*, leading to an *E* value of 83.8 kJ/mol. ■

1.2.3 Typical Rate Equations for Simple Reactions

1.2.3.1 Reversible First-Order Reactions

The rate of the reaction

$$A \underset{2}{\overset{1}{\rightleftarrows}} Q$$

can be written

$$r_A = -\frac{dC_A}{dt} = k_1 C_A - k_2 C_Q \qquad (1.2.3.1\text{-}1)$$

Accounting for the stoichiometry,

$$C_A + C_Q = C_{A_0} + C_{Q_0} \qquad (1.2.3.1\text{-}2)$$

leads to

$$\begin{aligned} -\frac{dC_A}{dt} &= k_1 C_A - k_2 \left(C_{A_0} + C_{Q_0} - C_A\right) \\ &= \left(k_1 + k_2\right) C_A - k_2 \left(C_{A_0} + C_{Q_0}\right) \end{aligned} \qquad (1.2.3.1\text{-}3)$$

The solution to this simple differential equation is

$$C_A = \left(C_{A_0} + C_{Q_0}\right) \frac{k_2}{k_1 + k_2} + \frac{k_1 C_{A_0} - k_2 C_{Q_0}}{k_1 + k_2} e^{-\left(k_1 + k_2\right)t} \qquad (1.2.3.1\text{-}4)$$

Introducing the equilibrium concentration of A (C_A when $t \rightarrow \infty$)

$$C_{Aeq} = \frac{k_2}{k_1 + k_2} \left(C_{A_0} + C_{Q_0}\right) \qquad (1.2.3.1\text{-}5)$$

yields

$$\left(C_A - C_{Aeq}\right) = \left(C_{A_0} - C_{Aeq}\right) e^{-\left(k_1 + k_2\right)t} \qquad (1.2.3.1\text{-}6)$$

or

$$\ln \frac{C_A - C_{Aeq}}{C_{A_0} - C_{Aeq}} = -\left(k_1 + k_2\right)t \qquad (1.2.3.1\text{-}7)$$

This equation can also be written in terms of conversion to give

$$\ln\left(1 - \frac{x_A}{x_{Aeq}}\right) = -\left(k_1 + k_2\right)t \qquad (1.2.3.1\text{-}8)$$

This result can also be found more simply by first introducing the conversion into the rate expression and then integrating. Also, the rate expression can be alternately written as

$$r_A = (k_1 + k_2)\left(C_A - C_{Aeq}\right) = (k_1 + k_2)C_{A_0}\left(x_{Aeq} - x_A\right) \quad (1.2.3.1\text{-}9)$$

1.2.3.2 Second-Order Reversible Reactions

For a second-order reversible reaction,

$$A + B \underset{2}{\overset{1}{\rightleftarrows}} Q + S$$

the net rate, made up of forward and reverse rates, is given by

$$r_A = k_1 C_A^{a'} C_B^{b'} - k_2 C_Q^{q'} C_S^{s'} \quad (1.2.3.2\text{-}1)$$

or

$$r_A = k_1\left(C_A^{a'} C_B^{b'} - \frac{1}{K_C} C_Q^{q'} C_S^{s'}\right) \quad (1.2.3.2\text{-}2)$$

where

$$K_C = \frac{k_1}{k_2} = \left(\frac{C_Q^{q'} C_S^{s'}}{C_A^{a'} C_B^{b'}}\right)_{eq} \quad (1.2.3.2\text{-}3)$$

represents the equilibrium constant.

Equation (1.2.3.2-2) can be written in terms of conversions to simply find the integrated form (for $a' = 1 = b' = q' = s'$):

$$C_{A_0}\frac{dx_A}{dt} = k_1\left[\begin{array}{l}\left(C_{A_0} - C_{A_0}x_A\right)\left(C_{B_0} - C_{A_0}x_A\right) \\ -\frac{1}{K}\left(C_{Q_0} + C_{A_0}x_A\right)\left(C_{S_0} + C_{A_0}x_A\right)\end{array}\right] \quad (1.2.3.2\text{-}4)$$

or

$$\frac{dx_A}{dt} = \frac{k_1}{K}\left\{\begin{array}{l}C_{A_0}(K-1)x_A^2 - \left[K\left(C_{A_0} + C_{B_0}\right) + C_{Q0} + C_{S_0}\right]x_A \\ + KC_{B_0} - \left(\frac{C_{Q_0}C_{S_0}}{C_{A_0}}\right)\end{array}\right\} \quad (1.2.3.2\text{-}5a)$$

$$= \frac{k_1}{K}\left(\alpha x_A^2 + \beta x_A + \gamma\right) \quad (1.2.3.2\text{-}5b)$$

and after integration:

$$\frac{k_1 t}{K} = \frac{1}{q}\ln\frac{1 + 2\alpha x_A/(\beta - q)}{1 + 2\alpha x_A/(\beta + q)} \quad (1.2.3.2\text{-}6)$$

where

$$\alpha = C_{A_0}\left(K-1\right) \tag{1.2.3.2-7}$$

$$\beta = -\left[K(C_{A_0}+C_{B_0})+C_{Q_0}+C_{S_0}\right] \tag{1.2.3.2-8}$$

$$\gamma = KC_{B_0} - \frac{C_{Q_0}C_{S_0}}{C_{A_0}} \tag{1.2.3.2-9}$$

$$q^2 = \beta^2 - 4\alpha\gamma \geq 0 \tag{1.2.3.2-10}$$

1.2.3.3 Autocatalytic Reactions

An autocatalytic reaction is catalyzed by its products and has the form

$$A + Q \overset{1}{\underset{2}{\rightleftarrows}} Q + Q$$

Here,

$$-\frac{dC_A}{dt} = k_1 C_A C_Q - k_2 C_Q^2 \tag{1.2.3.3-1}$$

$$\frac{dC_Q}{dt} = k_1 C_A C_Q - k_2 C_Q^2 \tag{1.2.3.3-2}$$

so that

$$\frac{d}{dt}\left(C_A + C_Q\right) = 0 \tag{1.2.3.3-3}$$

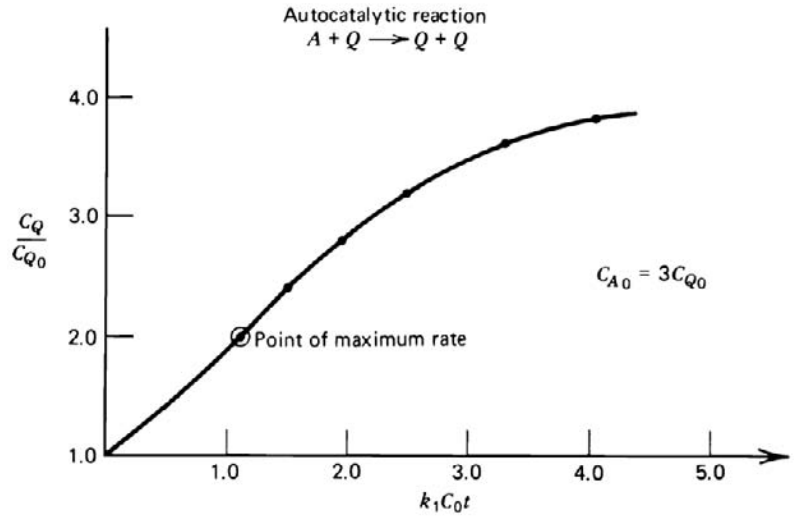

Figure 1.2.3.3-1
C_Q / C_{Q_0} versus dimensionless time.

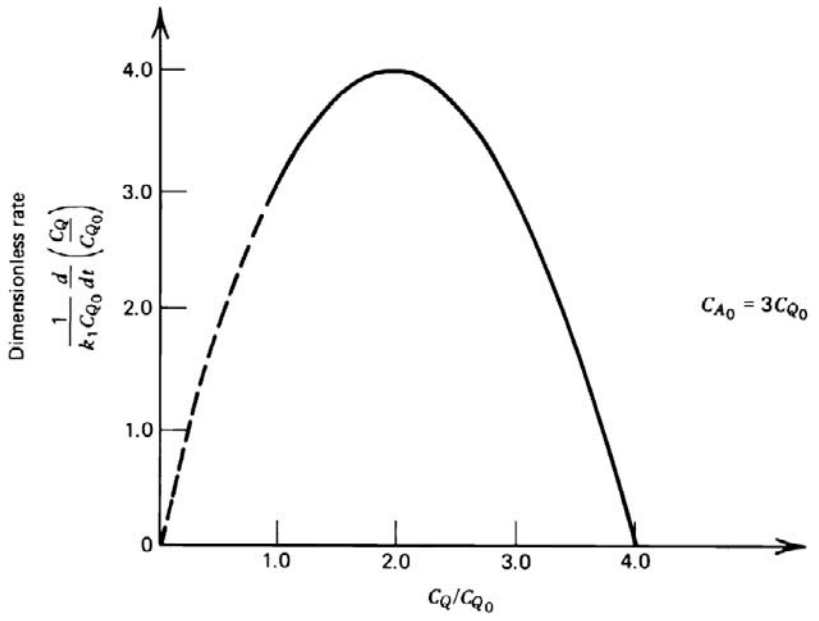

Figure 1.2.3.3-2
Dimensionless rate versus C_Q/C_{Q0}.

or

$$C_A + C_Q = \text{constant} = C_{A_0} + C_{Q_0} \equiv C_0 \qquad (1.2.3.3\text{-}4)$$

In this case it is most convenient to solve for C_Q:

$$\frac{dC_Q}{dt} = k_1(C_0 - C_Q)C_Q - k_2 C_Q^2 \qquad (1.2.3.3\text{-}5)$$

or

$$k_1 C_0 t = \ln\left|\left(\frac{C_Q}{C_{Q_0}}\right)\frac{C_0 - (1 - k_2/k_1)C_{Q_0}}{C_0 - (1 - k_2/k_1)C_Q}\right| \qquad (1.2.3.3\text{-}6)$$

C_A is found from

$$C_A(t) = C_0 - C_Q(t) \qquad (1.2.3.3\text{-}7)$$

Note that initially some Q must be present for any reaction to occur, but A could be formed by the reverse reaction. For the irreversible case, $k_2 = 0$,

$$k_1 C_0 t = \ln\left|\frac{C_Q \cdot C_{A_0}}{(C_0 - C_Q)C_{Q_0}}\right| \qquad (1.2.3.3\text{-}8)$$

Here, both A and Q must be present initially for the reaction to proceed. A plot of $C_Q(t)$ gives an "S-shaped" curve, starting at $C_Q(0) = C_{Q0}$ and ending at $C_Q(\infty) =$

$C_0 = C_{A0} + C_{Q0}$. This is sometimes called a “growth curve”, since it represents a build-up followed by a depletion of the reacting species. Figures 1.2.3.3-1 and 1.2.3.3-2 illustrate this.

Autocatalytic reactions can occur in homogeneous catalytic and enzyme processes, although usually with different specific kinetics.

1.2.4 Kinetic Analysis

With kinetics assumed to be of the mass action type, two main characteristics remain to be determined by the kinetic analysis: 1) the rate coefficient, *k*; 2) the reaction order, global *a’ + b’* or partial *a’* with respect to *A*, *b’* with respect to *B*. The order of a reaction is preferably determined from experimental data. It only coincides with the molecularity for elementary processes that actually occur as described by the stoichiometric equation (1.1.1-1). When the latter is only an "overall" equation for a process that really consists of several steps, the order cannot be predicted on the basis of this equation. Only for elementary reactions does the order have to be 1, 2, or 3. The order may be a fraction or even a negative number. In Section 1.6 examples will be given of reactions whose rate cannot be expressed as a simple product like (1.2.1-1).

The kinetic analysis can proceed along two methods: the differential and the integral.

1.2.4.1 The Differential Method of Kinetic Analysis

Consider a volume element of the reaction mixture in which the concentrations have unique values. For an irreversible first-order reaction with constant density transforming *A* into *B*, (1.1.2-5) and (1.2.1-1) reduce to

$$r_A = -\frac{dC_A}{dt} = kC_A \qquad (1.2.4.1\text{-}1)$$

When the rate coefficient k (h^{-1}) is known, (1.2.4.1-1) permits the calculation of the rate r_A for any concentration of the reacting component. Conversely, when the change in concentration is measured as a function of time, (1.2.4.1-1) permits the calculation of the rate coefficient. This method for obtaining k is known as the "differential" method. In principle, with (1.2.4.1-1), one set (C_A ; t) suffices to calculate k when C_{A0} is known. In practice, it is necessary to check the value of k for a set of values of (C_A ; t) or rather (r_A ; t).

To determine the order, n, of the reaction $A \rightarrow B$ for which a value of 1 was taken in (1.2.4.1-1), a number of values of n is chosen and the rate coefficient k is calculated for the sets (r_A ; t). The order leading to a unique value

for k, i.e., independent of C_A or t will be retained. This iterative procedure may be avoided by taking the logarithm of the rate equation. For the first order kinetics of (1.2.4.1-1) a plot of log r versus log C_A yields k.
For the more general form (1.2.1-1)

$$\log r = \log k + a' \log C_A + b' \log C_B \qquad (1.2.4.1\text{-}2)$$

three sets of values of r, C_A and C_B suffice in principle to determine k, a' and b', were it not for experimental errors inherent to experimental data of this type. Equation (1.2.4.1-2) is of the type

$$y = a_0 + a x_1 + b x_2 \qquad (1.2.4.1\text{-}3)$$

and, therefore, it is preferable to determine the best values of the parameters by linear regression, a procedure that will be discussed in detail in Chapter 2.

Another way of determining partial orders is to carry out a number of experiments in which all but one of the reactants are present in large excess. The partial order with respect to A e.g., is then obtained from

$$r = k' C_A^{a'} \qquad \text{where} \qquad k' = k C_B^{b'} C_C^{c'} \qquad (1.2.4.1\text{-}4)$$

By taking logarithms,

$$\log r = \log k' + a' \log C_A \qquad (1.2.4.1\text{-}5)$$

The slope of the straight line in a log r versus log C_A plot is a'. The same procedure is then applied to determine the other orders.

In a batch reactor with uniform concentration, sets of data of the type used here are easily obtained. A well mixed reactor with constant feed and effluent is generally operated at steady state and only one conversion is measured for A. To get a set of conversion values the feed conditions have to be varied. In a tubular reactor the conversion evolves along the reactor, but sampling is generally limited to the exit. Again, with steady state conditions only one exit conversion is obtained for A and the feed rate has to be varied to obtain the desired evolution of this conversion. These principles will be discussed in detail in Chapters 9 and 10, dealing with the characteristics of these reactors.

1.2.4.2 The Integral Method of Kinetic Analysis

Integration of (1.2.4.1-1) leads to

$$kt = \ln\left(C_{A0} / C_A\right) \qquad (1.2.4.2\text{-}1)$$

where k is obtained from a semi-log plot of C_A/C_{A0} versus time. When the order of the reaction is unknown, several values for it can be tried. The stoichiometric

equation may be a guide for this. The value for which k, obtained from (1.2.4.1-2) or (1.2.4.1-5), is found to be independent of the concentration is considered to be the correct order.

For a simple order, the rate expression can be integrated and special plots utilized to determine the rate coefficient. A plot of $1/C_A$ versus t or $x_A/(1\text{-}x_A)$ versus t is used similarly for a second-order irreversible reaction. For reversible reactions with first order in both directions a plot of $\ln(C_A - C_{Aeq})/(C_{A0} - C_{Aeq})$ or $\ln(1 - x_A/x_{Aeq})$ versus t yields $(k_1 + k_2)$ from the slope of the straight line. Using the thermodynamic equilibrium constant $K = k_1/k_2$, both k_1 and k_2 are obtained. Certain more complicated reaction rate forms can be rearranged into such linear forms. These plots are useful for an estimate of the "quality" of the fit to the experimental data and can also provide initial estimates to formal regression techniques that will be systematically discussed in Chapter 2.

TABLE 1.2.4.2-1
INTEGRATED FORMS OF SIMPLE KINETIC EXPRESSIONS FOR REACTIONS WITH CONSTANT DENSITY

Zero order

$$kt = C_{A_0} - C_A \qquad kt = C_{A_0} x_A$$

$$A \xrightarrow{\text{First order}} Q$$

$$kt = \ln\frac{C_{A_0}}{C_A} \qquad kt = \ln\frac{1}{1-x_A}$$

$$2A \xrightarrow{\text{Second order}} Q + S$$

$$kt = \frac{1}{C_A} - \frac{1}{C_{A_0}} \qquad C_{A_0} kt = \frac{x_A}{1-x_A}$$

$$A + B \longrightarrow Q + S$$

$$kt = \frac{1}{C_{A_0} - C_{B_0}} \ln\frac{C_{B_0}}{C_{A_0}}\frac{C_A}{C_B} \qquad C_{A_0} kt = \frac{1}{1-M}\ln\frac{M(1-x_A)}{M - x_A}$$

$$M = \frac{C_{B_0}}{C_{A_0}}$$

$$3A \xrightarrow{\text{Third order}} Q$$

$$2kt = \frac{1}{C_A^2} - \frac{1}{C_{A_0}^2} \qquad 2kt = \frac{1}{C_{A_0}^2}\left[\frac{1}{(1-x_A)^2} - 1\right]$$

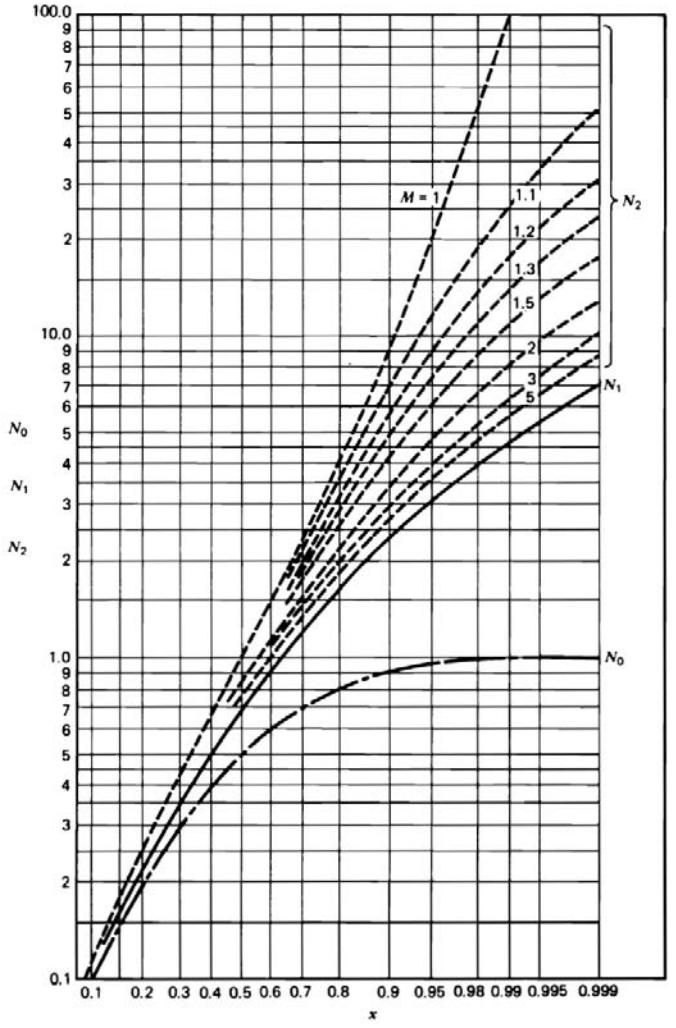

$$N_0 = \frac{kt}{C_{A_0}} = x \qquad N_1 = kt = \ln\frac{1}{1-x}$$

$$N_2 = C_{B_0} kt = \frac{M}{1-M}\ln\frac{M(1-x)}{M-x} \qquad \left(M = \frac{C_{B_0}}{C_{A_0}}\right)$$

Figure 1.2.4.2-1
Graphical representation of various integrated kinetic equations.
[Caddell and Hurt, 1951].

The integrated forms of several other simple-order kinetic expressions, obtained under the assumption of constant density, are listed in Table 1.2.4.2-1. Fig.1.2.4.2-1 graphically represents the various integrated kinetic equations of Table 1.2.4.2-1 [Caddell & Hurt, 1951]. Note that for a second order reaction with a large ratio of feed components, the reaction order degenerates into pseudo-first-order.

1.3 COUPLED REACTIONS

1.3.1 Parallel Reactions

The rate equations for simultaneous coupled reactions are constructed by combining terms of the type (1.2.1-1). For simple first order parallel reactions e.g.,

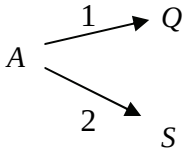

the rates can be written:

$$r_A = -\frac{dC_A}{dt} = k_1 C_A + k_2 C_A$$
$$r_Q = \frac{dC_Q}{dt} = k_1 C_A \qquad (1.3.1\text{-}1)$$
$$r_S = \frac{dC_S}{dt} = k_2 C_A$$

When $C_Q = C_S = 0$ at $t = 0$, integration yields:

$$C_A = C_{A0} \exp[-(k_1 + k_2)t]$$
$$C_Q = \frac{k_1}{k_1 + k_2} C_{A0} \left[1 - \exp[-(k_1 + k_2)t]\right] \qquad (1.3.1\text{-}2)$$

Fig.1.3.1-1 illustrates the behavior of the concentrations of *A*, *Q* and *S*.

With coupled reactions it is of interest to express how selective *A* has been converted into one of the products, e.g., *Q*. This is done by means of the selectivity, preferably defined in moles of *Q* produced per mole of *A* converted. The differential, point or instantaneous selectivity at a given time, t_1, can be written:

$$\frac{dC_Q}{dC_A} = \frac{k_1}{k_1 + k_2} \qquad (1.3.1\text{-}3)$$

The overall or global selectivity over the time span 0–*t* during which the reacting species were in contact is obtained after integration. It is generally different from the instantaneous value, but in the particular case of parallel reactions with the same order the two are identical:

$$\frac{C_Q}{C_{A0} - C_A} = \frac{k_1}{k_1 + k_2} \tag{1.3.1-4}$$

In terms of conversions the selectivity should be phrased as "the fraction of *A* converted into *Q* " — not "the conversion of *Q* " !

With complex processes like thermal cracking of a mixture of hydrocarbons to produce ethylene, use is often made of the "yield" of a component *Q*. This is usually defined in terms of weight: kg of *Q* produced per 100 kg of *A* fed (not *converted* !).

Selectivities or yields depend upon the type of reactor in which the reaction is carried out. The selection and design of a reactor optimizing the selectivity for a desired product is a rewarding task for the engineer and will be illustrated in Chapter 10.

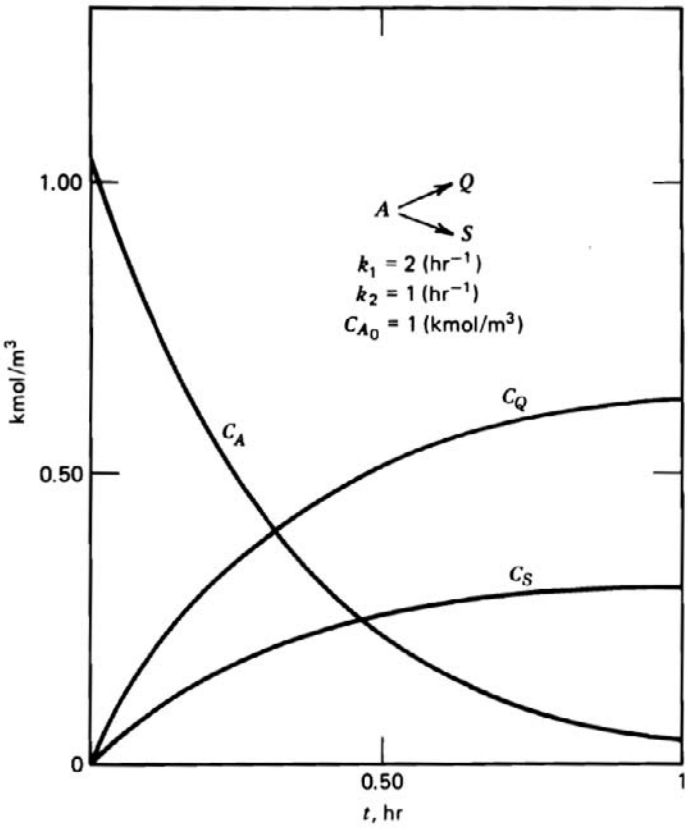

Figure 1.3.1-1
Parallel first order reactions. Concentration-time profiles.

1.3.2 Consecutive Reactions

Consider the consecutive reactions

$$A \xrightarrow{1} Q \xrightarrow{2} S$$

The rate of disappearance of *A* is written:

$$r_A = k_1 C_A^{a'} \tag{1.3.2-1}$$

and the net rate of formation of *Q*, involving formation and decomposition into *Q* is:

$$r_Q = k_1 C_A^{a'} - k_2 C_Q^{q'} \tag{1.3.2-2}$$

For the rate of formation of *S* out of *Q*:

$$r_S = k_2 C_Q^{q'} \tag{1.3.2-3}$$

For first-order reactions *a'* = *q'* = *s'* = 1 so that

$$r_A = -\frac{dC_A}{dt} = k_1 C_A \tag{1.3.2-4}$$

$$r_Q = \frac{dC_Q}{dt} = k_1 C_A - k_2 C_Q \tag{1.3.2-5}$$

Integrating with initial conditions $C_A = C_{A0}$; $C_Q = C_S = 0$ leads to

$$C_A = C_{A0} \exp[-k_1 t]$$

$$C_Q = \frac{k_1 C_{A0}}{k_2 - k_1} (\exp[-k_1 t] - \exp[-k_2 t]) \tag{1.3.2-6}$$

$$C_{A0} = C_A + C_Q + C_S$$

The results are illustrated in Fig.1.3.2-1.

If experimental data on C_A, C_Q and C_S versus time are available, the assumed orders can be checked and the values of k_1 and k_2 can be obtained by fitting the experimental curves.

The maximum in the C_Q versus *t* curve is found by differentiating the equation for C_Q with respect to *t* and setting the result equal to zero:

$$t_m = \ln \frac{k_2}{k_1} \Big/ k_2 - k_1 \tag{1.3.2-7}$$

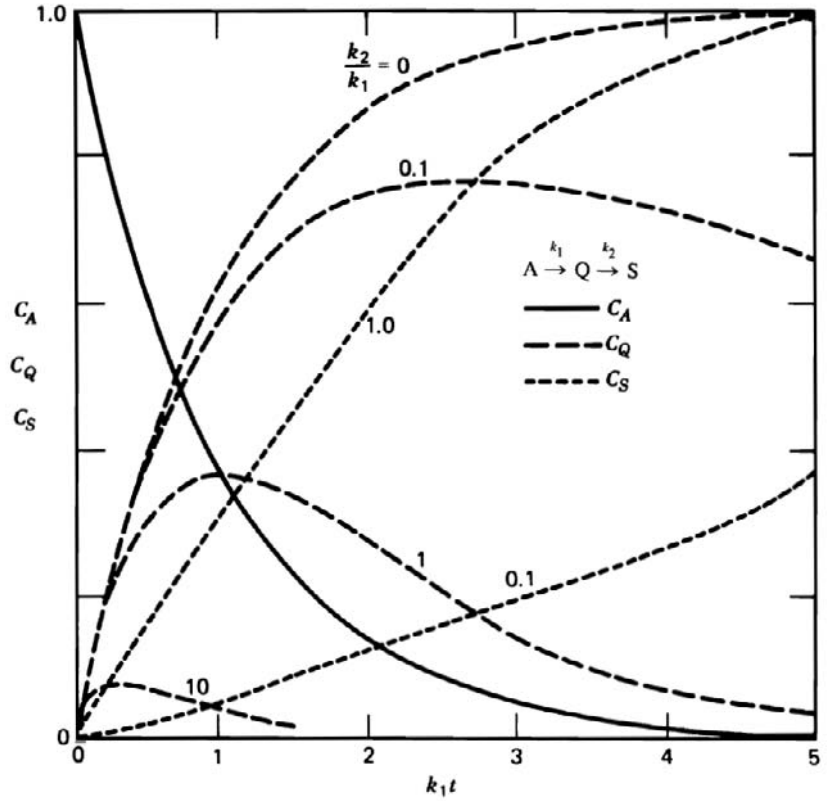

Figure 1.3.2-1

Consecutive first order reactions. Concentration versus time profiles for various ratios of k_2/k_1.

Dividing the rate equations by one another to find the point selectivity gives:

$$\frac{dC_Q}{dC_A} = \frac{k_2}{k_1}\frac{C_Q}{C_A} - 1 \qquad (1.3.2\text{-}8)$$

Integrating after switching to the conversion of *A* gives the integral selectivity:

$$\frac{C_Q}{C_{A0}} = (1 - x_A)\left(\frac{1 - (1 - x_A)^{k_2/k_1}}{k_2/k_1}\right) \qquad (1.3.2\text{-}9)$$

which is, unlike for parallel reactions, a function of the conversion of the reactant *A*. The higher this conversion, the lower the selectivity towards the intermediate *Q* will be. Again yields can be used, of course.

1.3.3 Mixed Parallel-Consecutive Reactions

Coupled reactions of the type

$$A + B \xrightarrow{1} Q$$

$$Q + B \xrightarrow{2} S$$

are also encountered, e.g., in the chlorination of benzene. The main feature is the presence of the common reactant *B*. The rate equations are:

$$-\frac{dC_A}{dt} = k_1 C_A C_B \qquad (1.3.3\text{-}1)$$

$$\frac{dC_Q}{dt} = k_1 C_A C_B - k_2 C_Q C_B \qquad (1.3.3\text{-}2)$$

There is no simple solution for this set of differential equations as a function of time. A useful approach consists of dividing (1.3.3-2) by (1.3.3-1), leading to the selectivity relation :

$$\frac{dC_Q}{dC_A} = \frac{k_2 C_Q}{k_1 C_A} - 1 \qquad (1.3.3\text{-}3)$$

This is precisely what was obtained for the simpler consecutive first order case. The common reactant, *B*, has no effect on the selectivities but causes a different time behavior.

1.4 REDUCING THE SIZE OF KINETIC MODELS

1.4.1 Steady State Approximation

When the intermediate *Q* in the consecutive reaction scheme of Section 1.3.2 is very reactive, meaning that $k_2 >> k_1$, the equations (1.3.2-6) reduce to

$$C_A = C_{A0} \exp[-k_1 t] \qquad (1.4.1\text{-}1)$$

$$C_Q = \frac{k_1 C_{A0}}{k_2} \exp(-k_1 t) \qquad (1.4.1\text{-}2)$$

and

$$k_2 C_Q = k_1 C_A \qquad (1.4.1\text{-}3)$$

reflecting that the intermediate Q is transformed practically as soon as it is formed. After a short induction time C_Q becomes constant at a very low value. It is as if the intermediate is at a steady state: $dC_Q / dt = 0$. This differential equation is the condition to be satisfied before the reaction scheme $A \rightarrow Q \rightarrow S$ may be reduced to $A \rightarrow S$, which is simpler and contains one rate coefficient less.

For (1.4.1-1)–(1.4.1-3) to be a useful approximation of the complete scheme, the induction time should be very short, meaning that the concentration of the intermediate must be very small. From (1.3.2-6) it is seen how the maximum in the curve C_Q versus t moves towards $t = 0$ as $k_2 >> k_1$. Quite frequently the existence of an intermediate is chemically logical, but it is difficult or impossible to measure its concentration. The pseudo steady state approximation is then a very useful tool. Examples will be encountered in Section 1.5 on bio-kinetics and Section 1.6 on complex reactions.

The concentrations are the solutions of two differential equations and one algebraic equation

$$r_A = -\frac{dC_A}{dt} = k_1 C_A \qquad (1.4.1\text{-}4)$$

$$k_1 C_A - k_2 C_Q = 0 \qquad (1.4.1\text{-}5)$$

$$r_S = \frac{dC_S}{dt} = k_2 C_Q \qquad (1.4.1\text{-}6)$$

1.4.2 Rate Determining Step of a Sequence of Reactions

A relatively long sequence of steps, frequently encountered in practice, evidently requires quite a number of rate equations. In many cases one of the steps is intrinsically much slower than the others. A steady state is established in which the rates of the other steps adapt to the rate of this step — it is the rate determining step. For steady state conditions only one rate equation will suffice to describe the process. All the other steps will be in quasi equilibrium. The rate determining step may change with the operating conditions so that care has to be taken when using this concept. The change will be revealed by shifts in the product distribution.

Examples of application of rate determining steps will be encountered in Section 1.5 and in the formulation of the kinetics of catalytic processes in Chapter 2. In Section 2.3.1 a single reaction $A \rightarrow R$, consisting of 3 steps: chemisorption of A, chemical reaction and desorption of R, proceeding sequentially, is dealt with. The introduction of a rate determining step reduces a complicated global rate equation to a much more tractable form. Of course, the three possible rate determining steps have to be considered and this leads to three

rate equations which have to be confronted with the experimental data to validate the assumption and to retain the most representative among them.

1.5 BIO-KINETICS

The kinetic equations of bio-processes are very similar, at least in a first approach, to those derived in the previous sections.

1.5.1 Enzymatic Kinetics

Enzymes are high molecular weight polypeptides i.e., proteins containing (-*C*-*N*-) bonds that can be remarkably efficient in catalyzing certain reactions. Examples are the production of glucose from starch, of the sweetener aspartame from phenylamine, and of acrylamide from acrylonitrile. Enzymes are also immobilized on a solid carrier to separate them more easily from the reaction mixture. In what follows, the basic kinetics of enzymatic processes will be derived using mass action kinetics and using procedures entirely analogous to those illustrated in the previous sections.

The reactant, *A* (called substrate in the bio field) and the enzyme, *E*, combine in a reversible way to form a complex *A*-*E* which decomposes into the product, *P*, thereby regenerating the enzyme:

$$A + E \underset{k_{-1}}{\overset{k_1}{\rightleftarrows}} A\text{-}E \xrightarrow{k_2} E + P \tag{1.5.1-1}$$

Using mass action kinetics, the net rate of disappearance of *A* can be written:

$$r_A = k_1 C_A C_E - k_{-1} C_{A-E} \tag{1.5.1-2}$$

and the rate of formation of *P* out of *A*-*E* :

$$r_P = k_2 C_{A-E} \tag{1.5.1-3}$$

whereby again use is made here of the convention that a rate is positive. It is in the mass balance that the formation or disappearance leads to a quantity that is negative or positive. The net rate of formation of *A*-*E* becomes:

$$r_{A-E} = k_1 C_A C_E - \left(k_{-1} + k_2\right) C_{A-E} \tag{1.5.1-4}$$

There are two ways of arriving at rate equations for this process that do not contain the generally inaccessible concentration of the complex, $C_{A\text{-}E}$, any more. The first one considers the decomposition of *A*-*E* to be the rate determining step, the second applies the pseudo steady state approximation.

If the decomposition of the complex *A-E* into the product *P* and the enzyme *E* is the rate determining step of the process, the first step, the formation of $C_{A\text{-}E}$, reaches equilibrium, so that

$$C_{A-E} = K C_A C_E \tag{1.5.1-5}$$

with $K = k_1/k_{-1}$ its equilibrium constant.
The rate of formation of *P* can then be written:

$$r_P = k_2 C_{A-E} = k_2 K C_A C_E \tag{1.5.1-6}$$

and accounting for $C_E = C_E^0 - C_{A-E}$ in the elimination of C_E , (1.5.1-6) becomes

$$r_P = \frac{k_2 K C_A C_E^0}{1 + K C_A} \tag{1.5.1-7}$$

$$\text{or} \quad r_A = r_P = \frac{k_2 C_A C_E^0}{K_M + C_A} \tag{1.5.1-8}$$

This is the Michaelis-Menten equation for the rate of a simple enzymatic reaction and $K_M = k_{-1}/k_1$ is known as the Michaelis-Menten constant. At high reactant concentration (C_A much larger than K_M), the rate levels off and becomes zero order with respect to the reactant, $r_A = k_1 C_E^0$. At low C_A (1.5.1-8) degenerates into a first order rate equation. This equation is entirely similar to the Hougen-Watson rate equations that will be derived in Chapter 2 for reactions catalyzed by solids.

In the second approach, formulated by Briggs and Haldane, the formation of the complex *A-E* does not necessarily reach equilibrium, but its concentration is eliminated by applying the pseudo steady state approximation

$$\frac{dC_{A-E}}{dt} = 0 \tag{1.5.1-9}$$

so that (1.5.1-4) becomes:

$$C_{A-E} = \frac{k_1 C_A C_E}{k_{-1} + k_2} \tag{1.5.1-10}$$

Substituting this concentration into (1.5.1-2):

$$r_A = k_1 C_A C_E \left(1 - \frac{k_{-1}}{k_{-1} + k_2}\right) \tag{1.5.1-11}$$

C_E can be related to C_A by $C_E = C_E^0 - C_{A-E}$ so that:

$$C_E = \frac{C_E^0}{1 + \dfrac{k_1 C_A}{k_{-1} + k_2}} \tag{1.5.1-12}$$

and

$$r_A = r_P = \frac{k_2 C_A C_E^0}{K_M + C_A} \tag{1.5.1-13}$$

which is exactly the form of the Michaelis-Menten equation with K_M now given by

$$K_M = \frac{k_{-1} + k_2}{k_1} \tag{1.5.1-14}$$

It may take some time for $C_{A\text{-}E}$ to reach steady state, in particular if the enzyme concentration is relatively large compared to that of the substrate, which is seldom the case, however. During that time span the solution (1.5.1-13) would be a poor approximation of the rigorous solution, which requires numerical methods, however. Equation (1.5.1-8) or (1.5.1-13) is often written in the form

$$r_A = \frac{r_m C_A}{K_M + C_A} \tag{1.5.1-15}$$

where $r_m = k_2 C_E^0$ is the maximum possible rate. The rate reaches half this maximum value when C_A equals K_M. This equation has been rearranged in various forms to determine the best possible values of r_m and K_M from linear plots of the usual steady state experimental data. One example is the Lineweaver-Burke plot of $1/r$ versus C_A. More general mathematical techniques for this parameter estimation will be discussed in Chapter 2. If, for more insight into the process, the rate coefficients k_1, k_{-1} and k_2 of the elementary steps themselves are required, only transient experimentation (stopped flow, or relaxation …) can help.

In many cases there is another component that competes with *A* for active sites of the enzyme or that interferes with *A-E*, even if it adsorbs on sites that are different in nature. In enzymatic kinetics such a component is called an inhibitor and represented by *I*.

In the case of competitive interaction with the enzyme

$$I + E \underset{k_{-3}}{\overset{k_3}{\rightleftarrows}} I\text{-}E \tag{1.5.1-16}$$

the total concentration of enzyme now equals

$$C_E^0 = C_{A-E} + C_{I-E} + C_E$$

$$= C_{A-E} + \left(\frac{k_3}{k_{-3}} C_I + 1 \right) C_E \qquad (1.5.1\text{-}17)$$

leading to

$$r_A = r_P = \frac{k_2 C_A C_E^0}{K_M \left(1 + \frac{C_I}{K_I} \right) + C_A} \qquad (1.5.1\text{-}18)$$

The opposite is also observed: the addition of a component may enhance the efficiency of the enzyme. Such a component is called a co-factor.

Enzymatic activity depends on temperature, but also on the pH and mechanical factors like shear stress and pressure.

1.5.2 Microbial Kinetics

Whereas an enzyme is a lifeless chemical substance, microbial transformations occur in living cells and are catalyzed by enzymes added or produced in the process.

These transformations are encountered on a large scale in fermentations, e.g., in the production of penicillin, a secondary metabolite of the fungus Pennicilium. Such a process can be represented by a kind of stoichiometric equation:

$$A + aNH_3 + bO_2 \rightarrow y_B \text{ cell biomass} + y_P \text{ product} + y_D\, CO_2 + cH_2O$$

A, called substrate, is the carbon-energy source and consists of nutrient sugars. Also added are *P*, *S*, *K*, *Na*, *Ca*, and *Mg*. The biomass and product mainly consist of *C*, *H*, *O* and *N*. y_B is the molar selectivity of biomass, based on 1 mol substrate converted. y_P is the selectivity for product, *P* and y_D is the selectivity for CO_2. Further, $y_B + y_P + y_D = 1$.

Consider again a closed volume with uniform composition and temperature — in practice a batch reactor, in which only changes with time occur. From its initial composition the medium evolves after seeding by an inoculum, which is a small amount of the living cell culture with optimized composition, through respectively a lag phase, an exponential growth of the number of cells, a stationary phase during which the increase in number of cells is compensated for by their destruction and a death phase with an (exponential) decrease in the number of cells.

The rate of biomass production, i.e., the increase in the number of cells during the exponential growth phase, is described by the empirical Monod-kinetics, which are shaped after the Michaelis-Menten kinetics for enzymatic reactions:

$$r = \frac{r_m C_A}{K_S + C_A} \tag{1.5.2-1}$$

In (1.5.2-1), r is a fractional or specific growth rate of biomass, in other words the growth of the concentration of biomass with respect to its total amount (kg/m^3). Further, r_m is the maximum specific rate of biomass growth, i.e., the rate when the substrate concentration is not limiting (C_A much larger than K_S) and K_S — the Monod– or saturation constant — is the concentration of substrate A at which the rate equals half of its maximum value, r_m. That means that the rate of change of the amount of biomass can be written:

$$r_B = \frac{dC_B}{dt} = rC_B = \frac{r_m C_B C_A}{K_S + C_A} \tag{1.5.2-2}$$

In the original Monod equation, r is represented by μ, r_m by μ_{max} and C_A by S. Also, μ is called the growth rate constant, with dimension h^{-1}.
The rate of substrate consumption is related to the rate of biomass production by:

$$-\frac{dC_A}{dt} = \frac{dC_B}{y_B dt} \tag{1.5.2-3}$$

where y_B is the molar selectivity of the biomass production (mol biomass produced / mol of substrate A converted).

Certain substances slow down the rates mentioned above. Even the substrate can exert a negative effect. At high concentrations it can react with the complex and yield a product which is of no interest and this competition slows down the production of P. The specific rate is then lower and becomes, e.g.,

$$r = \frac{r_m C_A}{K_S + C_A + \dfrac{C_A^2}{K_i}} \tag{1.5.2-4}$$

In this case r, when plotted versus the substrate concentration, exhibits a maximum, whereas with Monod-kinetics it tends to an asymptotic value. Equation (1.5.2-4) is a rate equation, named after Graef and Andrews [1973], that has been used, e.g., in the simulation of penicillin production.

The stationary phase is reached when the substrate *A* is exhausted, but the production of toxins may also play a role in this.

The rate of destruction of the cell is described by $r_d = k_d C_B$, expressing that at any time the number of cells which die is a fraction of those living, thus leading to an exponential decay.

Finally, it should be kept in mind that the rate of transport processes through the cell membrane may also contribute to the overall rate.

In the microbial field, the equations given above are called unstructured kinetic models. They assume that the biomass behaves as a chemical, retaining its identity as long as it is not converted. In reality the biomass, the living cells, continuously evolves. In structured models the biomass cell consists of a number of interacting units or components, thus leading to very complex reaction schemes. Williams [1967] considered the simplest possible structural model: a cell consisting of only 2 components, a synthetic one, *R*, representing RNA and a structural and genetic portion, *D*, representing a protein plus DNA. The total biomass concentration *M* is the sum of the concentrations of *D* and *R*. The component *R* is produced out of the external nutrient, *A*. The *D* component is fed from *R*. Cell division and growth of the biomass only start after the amount of *D* has doubled. *D* synthesis is autocatalytic. Translating this insight into mathematics leads to the following model equations:

For the consumption of nutrient *A* in the formation of *R*

$$r_A = -\frac{dC_A}{dt} = k_1 C_A C_M \qquad (1.5.2\text{-}5)$$

For the net rate of formation of *R*

$$r_R = \frac{dC_R}{dt} = k_1 C_A C_M - k_2 C_R C_D \qquad (1.5.2\text{-}6)$$

For the autocatalytic synthesis of *D*

$$r_D = \frac{dC_D}{dt} = k_2 C_R C_D \qquad (1.5.2\text{-}7)$$

For the rate of cell growth

$$r_M = \frac{dC_M}{dt} = k_1 C_A C_M \qquad (1.5.2\text{-}8)$$

The model does not include the death phase, but industrially the amount of nutrient is chosen to terminate the microbial growth before the onset of the death phase, anyway. The cell growth is initiated by inoculation with cells from a stationary nutrient exhausted culture, i.e., when $C_A = C_R = 0$ and $M = D$. Numerical integration of (15.2-5 to 15.2-8) leads to results for a batch culture given in Fig. 1.5.2-1. The model shows a lag phase, an exponential growth phase, a change in the cell composition and a stationary phase with a relatively small number of cells.

Evidently, the number of the components of the cell can be increased and refined to better approximate its real composition, but that leads to very complicated models. Even more, the population of the cells is not homogeneous, but consists of a collection of individuals at various stages of development. Accounting for their heterogeneity leads to what has been called “segregated” models. A parallel with Chemical Engineering process modeling may be worthwhile here. In this discipline also the complexity of real processes is being addressed to a growing extent. In petroleum refining, e.g., multicomponent, even very complicated feedstocks, derived from crude oil, are dealt with: vacuum gas oil in catalytic cracking, e.g. It consists of homolog series of hydrocarbon classes like *n* & *i*-paraffins, naphthenes, aromatics, etc. Until a number of years ago these classes were dealt with as single “pseudo-components”. Presently, the details of the homolog series are introduced into the kinetic models for improving the predictive capabilities. How to deal with this without developing overwhelming and unrealistic complexity is today’s challenge. The kinetic aspects of this problem will be discussed in detail in Chapter 2.

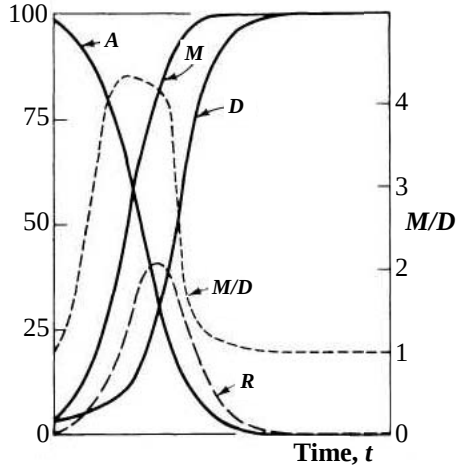

Figure 1.5.2-1
Evolution with time of various components of a batch culture [F.M. Williams, 1967] (for $k_1 = 0.0125\ s^{-1}$; $k_2 = 0.025\ s^{-1}$; $M_0/D_0 = 1$).

Further reading:
- J.E. Bailey & D.F. Ollis, *Biochemical Engineering Fundamentals*, McGraw-Hill, NY (1996).
- J.J. Dunn, E. Heinzle, J. Ingham, & J.E. Prenosil, *Biological Reaction Engineering Principles, Application and Modeling with PC Simulation*, VCH, NY (1992).
- M.L. Shuler & F. Kargi, *Bioprocess Engineering. Basic Concepts*, Prentice Hall, Englewood Cliffs, NJ (1992).

1.6 COMPLEX REACTIONS

Many processes of the chemical industry consist of extremely complex reaction schemes, often because the feedstock is a complicated mixture derived from natural resources, but in some cases even with a simple feed. Examples of non-catalytic processes will be dealt with here, of catalytic processes in Chapter 2. Important non-catalytic processes are thermal cracking (also called pyrolysis), polymerization, combustion, oxidation, and photochlorination. They proceed through radical steps. By way of example, the first two will be dealt with here.

1.6.1 Radical Reactions in the Thermal Cracking for Olefins Production

In the thirties, serious efforts were undertaken to elucidate the reactions taking place in the pyrolysis process and to formulate the kinetics. A cracking reaction, globally represented by $A_1 \rightarrow A_2 + A_3$, really proceeds through a sequence of elementary steps involving radicals:

1. Initiation or formation of free radicals
2. Propagation by reaction of the free radicals with reactants
3. Decomposition of the large produced radicals
4. Termination by reaction of free radicals to form stable products

Consider a simple example of a free radical reaction, which is represented by the following stoichiometric equation:

$$A_1 \rightarrow A_2 + A_3 \qquad (1.6.1\text{-}1)$$

but proceeds in reality by the following steps:

$$A_1 \xrightarrow{k_1} 2R_1^{\bullet} \qquad \text{Initiation} \qquad (1.6.1\text{-}2)$$

$$\left.\begin{array}{ll} R_1^{\bullet} + A_1 \xrightarrow{k_2} R_1H + R_2^{\bullet} & \text{Hydrogen abstraction} \\ R_2^{\bullet} \xrightarrow{k_3} A_2 + R_1^{\bullet} & \text{Radical decomposition} \end{array}\right\} \text{Propagation} \qquad \begin{array}{l}(1.6.1\text{-}3)\\(1.6.1\text{-}4)\end{array}$$

$$R_1^{\bullet} + R_2^{\bullet} \xrightarrow{k_4} A_3 \qquad \text{Termination} \qquad (1.6.1\text{-}5)$$

where $R_1^\bullet$ and $R_2^\bullet$ are radicals (e.g., when hydrocarbons are cracked, $CH_3^\bullet$, $C_2H_5^\bullet$, $H^\bullet$). The rate of consumption of A_1 may be written:

$$-\frac{dC_{A_1}}{dt} = k_1 C_{A_1} + k_2 C_{A_1} C_{R_1} \tag{1.6.1-6}$$

The rate of initiation is generally intrinsically much smaller than the rate of propagation so that in (1.6.1-6) the term $k_1 C_{A_1}$ may be neglected. The problem is now to express the C_{R_i}, which are difficult to measure, as a function of the concentrations of species that are readily measurable. For this purpose, use is made of the hypothesis of the steady-state approximation:

$$\frac{dC_{R_1}}{dt} \approx 0 \qquad \frac{dC_{R_2}}{dt} \approx 0 \tag{1.6.1-7}$$

or, in detail,

$$\frac{dC_{R_1}}{dt} = 0 = 2k_1 C_{A_1} - k_2 C_{R_1} C_{A_1} + k_3 C_{R_2} - k_4 C_{R_1} C_{R_2} \tag{1.6.1-8}$$

$$\frac{dC_{R_2}}{dt} = 0 = k_2 C_{R_1} C_{A_1} - k_3 C_{R_2} - k_4 C_{R_1} C_{R_2} \tag{1.6.1-9}$$

These conditions must be fulfilled simultaneously. By elimination of C_{R_2}, a quadratic equation for C_{R_1} is obtained

$$2k_1 C_{A_1} - k_2 C_{R_1} C_{A_1} + \frac{k_2 k_3 C_{R_1} C_{A_1}}{k_3 + k_4 C_{R_1}} - \frac{k_2 k_4 C_{R_1}^2 C_{A_1}}{k_3 + k_4 C_{R_1}} = 0 \tag{1.6.1-10}$$

the solution of which is

$$C_{R_1} = \left(\frac{k_1}{2k_2}\right) + \sqrt{\left(k_1 / 2k_2\right)^2 + \left(k_1 k_3 / k_2 k_4\right)} \tag{1.6.1-11}$$

Because k_1 is very small, this reduces to

$$C_{R_1} \approx \sqrt{\frac{k_1 k_3}{k_2 k_4}} \tag{1.6.1-12}$$

so that (1.6.1-6) becomes

$$-\frac{dC_{A_1}}{dt} = \sqrt{\frac{k_1 k_2 k_3}{k_4}} C_{A_1} \tag{1.6.1-13}$$

which means that the reaction is essentially first order.

There are other possibilities for termination. Suppose that

$$R_1^{\bullet} + R_1^{\bullet} \xrightarrow{k_5} A_1$$

is the fastest termination step. It can be shown by a procedure completely analogous to the one given above that the rate is given by

$$-\frac{dC_{A_1}}{dt} = k_2\sqrt{\frac{k_1}{k_5}}\left(C_{A_1}\right)^{3/2} \qquad (1.6.1\text{-}14)$$

meaning that the global reaction is of order 3/2.

In ethane pyrolysis, A_1 would be ethane, $R_1^{\bullet}$ the methyl radical, R_1H methane, and $R_2^{\bullet}$ the ethyl radical, but the latter decomposes into ethylene and a new radical, $R_3^{\bullet}$, which is the hydrogen radical. With first order initiation and a termination producing ethane from $C_2H_5^{\bullet}$ and $H^{\bullet}$, the overall rate equation would be of the first order in ethane.

EXAMPLE 1.6.1.A
ACTIVATION ENERGY OF A COMPLEX REACTION

The overall activation energy of the cracking, if globally expressed by (1.6.1-1), is really made up of the activation energy of the individual steps.
From $k_o = (k_1k_2k_3/k_4)^{1/2}$

$$\ln k_o = 1/2 \ln (k_1k_2k_3 / k_4) \qquad (1.6.1.A\text{-}1)$$

Expressing the individual k in terms of the Arrhenius equation $k = A \exp[-E/RT]$ leads to

$$E_o = 1/2 (E_1 + E_2 + E_3 - E_4) \qquad (1.6.1.A\text{-}2)$$

An estimate of the overall activation energy of the cracking is obtained by substituting typical values of E for initiation (356 kJ/mol), hydrogen abstraction (42 kJ/mol) radical decomposition (147 kJ/mol) and termination (0 kJ/mol) into (1.6.1.A-2). The result is 272.5 kJ/mol. For the specific case of ethane pyrolysis, values given by Benson [1960, p.354] lead to E_o of 282.5 kJ/mol. These E_o values are much lower than the E of initiation and the nominal values for breaking C-C-bonds. ■

Ethylene and propylene are the main building blocks for the petrochemical industry. In 2008 the world ethylene capacity was of the order of 80.10^6 tons/year, the propylene capacity of 40×10^6. They are produced at 800-850 °C in huge furnaces containing a number of parallel tubes in which the residence time of the gases is well below 0.5 s. The technical aspects of this

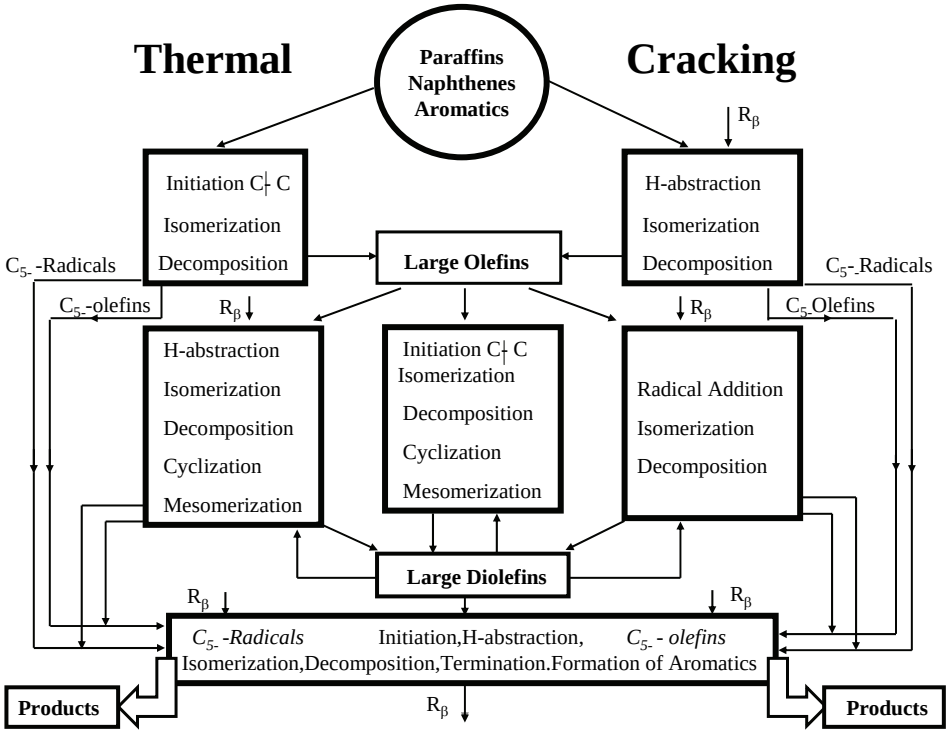

Figure 1.6.1-1
Thermal cracking pathways and types of elementary steps.

operation will be dealt with in Chapters 9 and 12. The feedstock used in industry for olefins production varies with the geographic location: ethane-propane mixtures where these are available or naphtha from the refineries in other areas. Naphtha is a mixture of paraffins, naphthenes and aromatics with *C*-numbers ranging from C_4 to C_{12}**.** What matters in such operation is not only the rate at which the feed is converted — that can be mastered by the operating conditions and the design of the reactor — but also the selectivities for the various products, i.e., the product slate. Overall kinetics are not adequate to predict or simulate this aspect, not even for ethane or propane feeds, let alone for naphtha. What is required in the first place is a detailed reaction scheme. Sundaram and Froment [1977, 1978] modeled the thermal cracking of ethane, propane, *n*- and *i*-butanes and their mixtures by means of a set of 133 elementary steps of radical chemistry. The steps to be considered extend well beyond those accounted for in the introductory part of this section. They are given in Fig. 1.6.1-1: initiation by scission of a *C*-*C* bond or by hydrogen abstraction, isomerization, decomposition of large radicals, cyclization, mesomerization, addition of radicals to double bonds and termination. As shown in Fig. 1.6.1-1 there are two main routes for the

conversion of the feed components and intermediate products: one starting with initiation through the thermal scission of a *C-C* bond, one by the scission of a *C-H* bond by means of small radicals like $H^{\bullet}$ or $CH_3^{\bullet}$, so called β-radicals which are involved in bi-molecular steps. These initiations are followed by isomerization of the produced radicals and by decomposition through scission of a *C-C* bond in β-position with respect to the carbon carrying the negative charge of the radical. The decomposition yields large so called μ-radicals, R_μ, which are unstable and further react in two ways: with β-radicals, R_β, or by initiation. The μ-radicals undergo monomolecular decompositions. One of the two pathways with β-radicals, the addition, is specific for unsaturates, of course. The olefins

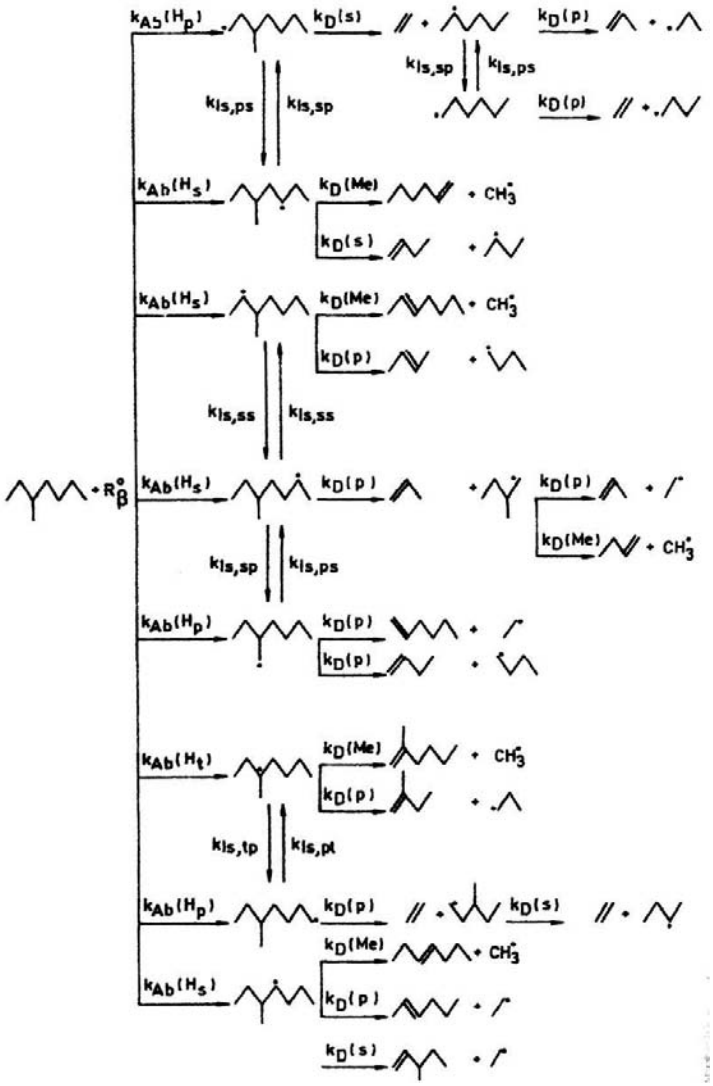

Figure 1.6.1-2

Cracking network of 3-Me-heptane. From Clymans and Froment [1984].

may also produce large diolefins. After a number of cycles only small radicals and di-radicals are left which then react in their specific ways among themselves.

Fig. 1.6.1-2 gives an example of the scheme of elementary steps occurring in the thermal cracking of 3-methylheptane, just one of the 200-300 feed components to be considered in the modeling of naphtha-cracking. It is initiated by a β-radical. Hydrogen atoms with different nature (primary, secondary) can be abstracted from such a molecule. The produced methyl-heptyl radicals can isomerize but also decompose by β-scission into hexyl–radicals. The large olefins will further react by *H*-abstraction or radical-addition.

Obviously, to describe the gigantic detailed reaction network of the thermal cracking of naphtha, computer generation is required. The structure of chemical components and the products of their transformation can be represented by means of binary vectors and matrices. This will be discussed in some more detail in Chapter 2. Generating the reaction network evidently requires knowledge of the properties of radical chemistry. The abstraction of a primary radical takes more energy than that of a secondary or tertiary radical. Rules for such events were derived by Rice & Herzfeld [1944] and by Kistiakowsky [1928]. A scrutiny of the 3-methyl heptane network represented in Fig. 1.6.1-2 reveals a very large number of rate coefficients for the elementary steps occurring in thermal cracking of a mixture like naphtha. There are hundreds of decomposition rate coefficients e.g., but it is clear that these really belong to a very small number of types, depending not so much on the length of the radical that is being decomposed, but rather on the configuration and therefore the stability of the moiety where the event occurs, on the nature of the resulting radical ($H^\bullet$, $CH_3^\bullet$, primary, secondary, …) and of the resulting olefin, e.g., on the presence of a conjugated double bond. A systematization of the elementary steps and of the rate coefficients permitted Van Damme et al. [1975; 1981] and Willems and Froment [1988a, 1988b] to reduce the total number of independent rate coefficients for naphtha cracking to 68.

The rate of disappearance of 3-methylheptane (3–*Me*–C7) through hydrogen abstraction by $R^\bullet_\beta$ (e.g., $H^\bullet$ or $CH_3^\bullet$), the rate of disappearance of the latter and the rate of formation of the $R_\beta H$ can be written:

$$r(3\text{–}Me\text{–}C7) = r(R^\bullet_\beta) = r(R_\beta H) = \sum_{i=1}^{8} k_{Ab}(H_p \text{ or } H_S)(3-Me-C_7)(R^*_\beta) \qquad (1.6.1\text{-}15)$$

The order of the various species in this and similar rate equations corresponds with the molecularity because they are transformed by truly elementary steps of radical chemistry.

The net rates of formation of the 1- and 5-heptyl radical are written:

$$r_{3-Me-1-C_7H_{15}^{\bullet}} = k_{Ab}\left(H_p\right)\left(3-Me-C_7H_{16}\right)\left(R_{\beta}^{\bullet}\right) + k_{Is,sp}\left(3-Me-5-C_7H_{15}^{\bullet}\right) - \left(k_{Is,ps}+k_D(s)\right)\left(3-Me-1-C_7H_{15}^{\bullet}\right) \quad (1.6.1\text{-}16)$$

$$r_{3-Me-5-C_7H_{15}^{\bullet}} = k_{Ab}\left(H_s\right)\left(3-Me-C_7H_{16}\right)\left(R_{\beta}^{\bullet}\right) + k_{Is,ps}\left(3-Me-1-C_7H_{15}^{\bullet}\right) - \left(k_{Is,sp}+k_D(Me)+k_D(s)\right)\left(3-Me-5-C_7H_{15}^{\bullet}\right) \quad (1.6.1\text{-}17)$$

To eliminate these inaccessible concentrations the pseudo steady state hypothesis is called upon. When that hypothesis is satisfied those two rates become zero. The set of equations can then be solved for the radical concentrations, yielding e.g., for $(3-Me-1-C_7H_{15}^{\bullet})$:

$$\left(3-Me-1-C_7H_{15}^{\bullet}\right) = \frac{\left(k_{Ab}(H_p)\left(k_{Is,sp}+k_D(Me)+k_D(s)\right)+k_{Ab}(H_s)k_{Is,sp}\right)\left(3-Me-C_7H_{16}\right)\left(R_{\beta}^{\bullet}\right)}{\left(k_{Is,sp}+k_D(s)\right)\left(k_{Is,sp}+k_D(Me)+k_D(s)\right)-k_{Is,ps}k_{Is,sp}} \quad (1.6.1\text{-}18)$$

The decomposition of these $R_{\mu}^{\bullet}$-radicals generates olefins, $R_{\beta}^{\bullet}$ and new $R_{\mu}^{\bullet}$-radicals. The rate of formation of ethylene and $2-C_6H_{13}^{\bullet}$ out of $3-Me-1-C_7H_{15}^{\bullet}$ is given by:

$$r_{C_2H_4} = k_D(s)\left(3-Me-1-C_7H_{15}^{\bullet}\right) \quad (1.6.1\text{-}19)$$

$$r_{2-C_6H_{13}^{\bullet}} = k_D(s)\left(3-Me-1-C_7H_{15}^{\bullet}\right) \quad (1.6.1\text{-}20)$$

with $(3-Me-1-C_7H_{15}^{\bullet})$ given by (1.6.1-18). For each partial network leading to ethylene and propylene, the rate of production of ethylene and propylene is of partial first order with respect to both the feed molecule and the abstracting β-radical. The rate coefficient is in reality a complicated expression containing sums and products of the rate coefficients of the various elementary steps. The temperature dependency of this "rate coefficient" evidently does not satisfy the Arrhenius law.

The μ-radical $2-C_6H_{13}^{\bullet}$ disappears through isomerization and decomposition with formation of ethylene and new radicals. The reaction path is developed until a stage at which only relatively stable olefins are obtained. Specific reactions of ethylene and propylene may have to be added, though.

The other steps shown in Fig. 1.6.1-2 are dealt with along the same lines and ultimately contribute to the ethylene and propylene yields by equations similar to (1.6.1-19). There is more. It can be seen from Fig. 1.6.1-1 that, next to *H*-abstraction by a β-radical, 3-*Me*-C_7H_{16} also disappears by initiation through β-scission leading to ethylene, propylene, and so on, by similar pathways.

In a naphtha, 200-300 components may lead to these olefins, so that all the networks have to be developed and their ethylene production summed up. It is clear that a realistic kinetic analysis of the cracking of a complex hydrocarbon mixture into olefins is not a simple task. The rate parameters of the elementary steps can only be accessed by an investigation of the kinetics of a number of specific feed components, preferably with increasing complexity. Even for the paraffin family, cracking ethane and propane will not suffice because they do not generate all the steps encountered with the higher members.

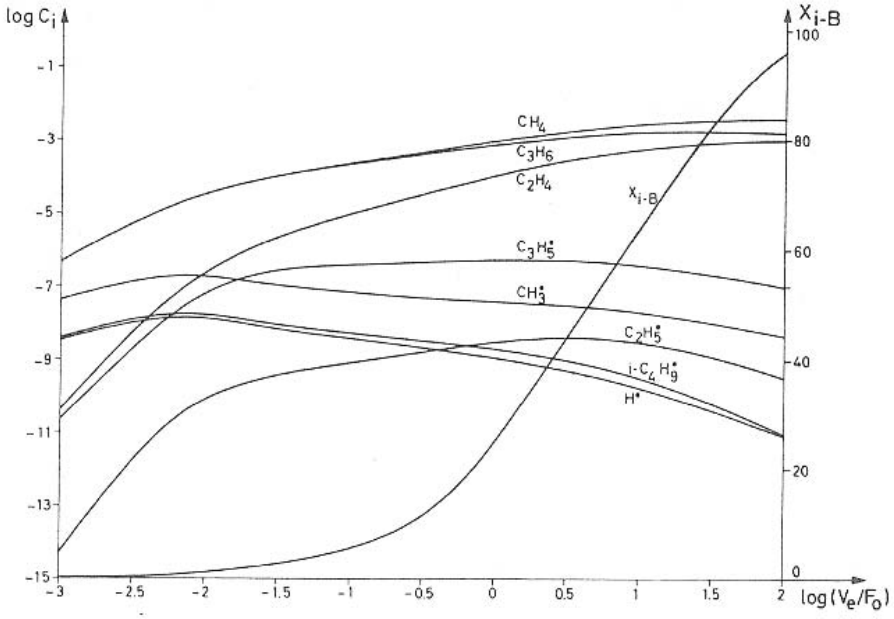

Figure 1.6.1-3

Calculated concentration of radicals, molecules, and conversion along an isothermal reactor for isobutane cracking: T = 775°C; P_0 = 1.4 atm abs; δ = 0.4 kg of steam/kg of butane. From Sundaram and Froment [1978].

Fig. 1.6.1-3 shows the evolution along the tubular reactor of molecular and radical species in an ethane thermal cracker. The radical concentration in such a process is orders of magnitude smaller than that of the molecular species.

1.6.2 Free Radical Polymerization

A substantially simplified scheme of radical polymerization, presented here to illustrate the kinetic modeling of such processes, can be written [Hamielec et al., 1967; Ray, 1972; Ray and Laurence, 1977]:

Initiation

$$I \xrightarrow{k_d} 2R_0$$

$$R_0 + M_1 \xrightarrow{k_i} R_1$$

Propagation

$$R_{n-1} + M_1 \xrightarrow{k_p} R_n$$

Termination

By combination

$$R_n + R_m \xrightarrow{k_{tc}} P_{n+m}$$

By disproportionation

$$R_n + R_m \xrightarrow{k_{td}} P_n + P_m$$

I is an initiator e.g., benzoylperoxide; M_1 the monomer; R_1, R_{n-1}, R_n, R_m are active chains i.e., macroradicals containing 1, n–1, n and m monomer units, P_n, P_m and P_{n+m} are "dead" polymers, i.e., macromolecules. In what follows these symbols will also represent concentrations.

In a homogeneous, uniform volume, as encountered in batch processing, the continuity equations for these components are:

For the initiator

$$-\frac{dI}{dt} = k_d I \tag{1.6.2-1}$$

For the radical formed out of the initiator

$$\frac{dR_0}{dt} = 2fk_d I - k_i R_0 M_1 \tag{1.6.2-2}$$

where f stands for the efficiency of the splitting of I.

For the growing polymer macroradical

$$\frac{dR_1}{dt} = k_i R_0 M_1 - k_p R_1 M_1 - \left(k_{tc} + k_{td}\right) R_1 R \qquad (1.6.2\text{-}3)$$

with $R = \sum_{n=1}^{\infty} R_n$ the total concentration of growing macroradical

$$\frac{dR_n}{dt} = k_p M_1 \left(R_{n-1} - R_n\right) - \left(k_{tc} + k_{td}\right) R_n R \qquad (1.6.2\text{-}4)$$

for n = 2, 3, ..., ∞

Summation of the equation (1.6.2-3) and of the set of equations (1.6.2-4) leads to

$$\frac{dR}{dt} = k_i R_0 M_1 - \left(k_{tc} + k_{td}\right) R^2 \qquad (1.6.2\text{-}5)$$

For the monomer

$$-\frac{dM_1}{dt} = k_i R_0 M_1 + k_p R M_1 \qquad (1.6.2\text{-}6)$$

For the concentration of "dead" polymer or macromolecule containing n monomers

$$\frac{dP_n}{dt} = k_{tc} \sum_{m=1}^{n-1} R_m R_{n-m} + k_{td} R_n R \qquad (1.6.2\text{-}7)$$

Assuming pseudo steady state for the (macro-)radicals, (1.6.2-2) becomes

$$k_i R_0 M_1 = 2 f k_d I \qquad (1.6.2\text{-}8a)$$

and (1.6.2-5)

$$2 f k_d I = \left(k_{tc} + k_{td}\right) R^2 \qquad (1.6.2\text{-}8b)$$

so that

$$R = \left(\frac{2 f k_d I}{k_{tc} + k_{td}} \right)^{1/2} \qquad (1.6.2\text{-}9)$$

The following relations between the concentrations of the macroradicals can then be derived:

From (1.6.2-4)

$$R_n = \alpha R_{n-1} \qquad (1.6.2\text{-}10)$$

with

$$\alpha = \frac{k_p M_1}{k_p M_1 + (k_{tc} + k_{td})R} \tag{1.6.2-11}$$

which is called the probability of propagation.

From (1.6.2-3) and (1.6.2-5)

$$R_1 = (1-\alpha)R \tag{1.6.2-12}$$

The relation between R_n, the concentration of the polymer macroradical containing n monomer units and the total concentration of active polymer or macroradicals, R, is conveniently obtained from the generating function

$$G(s) = \sum_{n=1}^{\infty} s^n R_n \tag{1.6.2-13}$$

$$G(s) = sR_1 + \sum_{n=1}^{\infty} s^n \alpha R_{n-1} \tag{1.6.2-14}$$

and based upon the right shifting property of the generating function and equation (1.6.2-12)

$$G(s) = s(1-\alpha)R + \alpha s G(s) \tag{1.6.2-15}$$

$$G(s) = \frac{(1-\alpha)}{1-\alpha s} sR \tag{1.6.2-16}$$

Expanding $(1-\alpha s)^{-1}$ in a series, (1.6.2-16) becomes

$$G(s) = (1-\alpha)R \sum_{n-1}^{\infty} \alpha^{n-1} s^n \tag{1.6.2-17}$$

Identification with the definition (1.6.2-13) leads to the relation

$$R_n = (1-\alpha)\alpha^{n-1} R \tag{1.6.2-18}$$

which is the concentration distribution of the macroradicals with respect to the chain length, made up of n monomer units.

Now the evolution with time of the various molecular components can be derived. Integration of (1.6.2-1) leads to

$$I = I_0 \exp(-k_d t) \tag{1.6.2-19}$$

and of (1.6.2-6) for the monomer concentration, accounting for (1.6.2-9), to

$$M_1 = M_{10} \exp\left\{\left(\frac{2k_p}{k_d}\cdot\frac{2fk_dI_0}{k_{tc}+k_{td}}\right)^{\frac{1}{2}}\left[\exp\left(-\frac{k_dt}{2}\right)-1\right]\right\} \quad (1.6.2\text{-}20)$$

The time evolution of the concentration of the macromolecules can be further explicited than in (1.6.2-7)

$$\frac{dP_n}{dt} = k_{td}R(1-\alpha)R\alpha^{n-1} + \frac{1}{2}k_{tc}R^2(1-\alpha)^2\alpha^{n-2}(n-1) \quad (1.6.2\text{-}21)$$

with initial value P_{n0} and for $n \geq 2$.
The integration has to be performed numerically.

In general, the complete detailed distribution of chain length or molecular weight of the growing polymer and of the dead polymer or macromolecules is not required. The knowledge of the mean, variance and skewness of these distributions provides sufficient insight into the polymerization process and its product. These characteristics are related to the moments of the distributions and these are conveniently calculated by means of generating functions [Ray, 1972; Mc Laughlin and Bertolucci, 1993]. For the growing macroradical, the generating function is $G(s)$. The *k* moments are obtained from

$$\lambda_k = \sum_{i=s}^{k} a_{ki}\left[\frac{\partial^i G(s)}{\partial s^i}\right]_{s=1} \quad \text{with } k = 0, 1, 2, \ldots \quad (1.6.2\text{-}22)$$

For the zero-th moment $a_{ki} = 1$; for the first $a_{ki} = 0$ and 1; for the second $a_{ki} = 0$, 1 and 1, so that

$$\lambda_0 = G(1,t)$$

$$\lambda_1 = \left.\frac{\partial G(s,t)}{\partial s}\right|_{s=1} \quad (1.6.2\text{-}23)$$

$$\lambda_2 = \left.\frac{\partial^2 G(s,t)}{\partial s^2}\right|_{s=1} + \left.\frac{\partial G(s,t)}{\partial s}\right|_{s=1}$$

Differentiating (1.6.2-16) gives:

$$\frac{\partial G}{\partial s} = \frac{(1-\alpha)R}{1-\alpha s} + \frac{\alpha G(s)}{1-\alpha s} \quad (1.6.2\text{-}24)$$

so that

$$\lambda_0 = (1-\alpha)R + \alpha\sum_{n=1}^{\infty} R_n = R \quad (1.6.2\text{-}25)$$

which is the total concentration of macroradicals or growing polymer and:

$$\lambda_1 = \frac{R}{1-\alpha} \tag{1.6.2-26}$$

which is the total number of monomer units in the growing polymer.
Then, the number average chain length (or degree of polymerization) is given by

$$\frac{\lambda_1}{\lambda_0} = \frac{\sum^{\infty} n R_n}{\sum^{\infty} R_n} = \frac{1}{1-\alpha} \tag{1.6.2-27}$$

and the weight average chain length of the growing polymer is

$$\frac{\lambda_2}{\lambda_1} = \frac{\sum^{\infty} n^2 R_n}{\sum^{\infty} n R_n} = \frac{1+\alpha}{1-\alpha} \tag{1.6.2-28}$$

The polydispersity is the ratio of the weight to the number average chain length and equals 1+α. For long chain polymers, the propagation probability α is close to 1 so that the polydispersity is close to 2.

For the derivation of these distributions for the dead polymer, i.e., the macromolecules, a generating function

$$F(s,t) = \sum_{n=2}^{\infty} s^n P_n(t) \tag{1.6.2-29}$$

is introduced.
Combining with (1.6.2-21) yields

$$\frac{dF(s,t)}{dt} = k_{td} R\left[G(s,t) - sR_1\right] + \frac{1}{2} k_{tc} G(s,t)^2 \tag{1.6.2-30}$$

where $G(s,t)$ is given by (1.6.2-17).
The zero-th moment of the numerical chain length distribution of the macromolecules is given by

$$\frac{d\lambda_0}{dt} = \frac{dF(1,t)}{dt} = \left(\alpha k_{td} + \frac{1}{2} k_{tc} \right) R^2 \tag{1.6.2-31}$$

The first and second moments are obtained in a way similar to that already encountered for the macroradicals.

The preceding conveys the approach to be used in the kinetic modeling of free radical polymerization encountered e.g., with styrene, vinylacetate, methylmetacrylate. For practical applications the reaction scheme should be completed with further elementary steps like chain transfer between the macroradicals and the monomer and the solvent. These add terms to the RHS of the continuity equations (1.6.2-3 to 1.6.2-5), but the development followed here is not affected. Also, diffusion control of propagation and termination (Tromsdorff effect) may have to be accounted for [Gerrens, 1976]. The kinetic modeling of the various types and techniques of polymerization and the application to the reactor modeling and process development were reviewed by Kiparissides [1996] and Villa [2007].

1.7 MODELING THE RATE COEFFICIENT

1.7.1 Transition State Theory

In the preceding sections, the rate coefficient, *k*, was considered as a parameter to be derived from experimental data. From the 1930s onwards, theoretical work was undertaken to model *k* and to calculate it from first principles. Today, progress in theoretical chemistry and computational power allows the calculation of *k* with a satisfactory accuracy, at least for elementary steps in homogeneous media. An elementary step does not have any detectable intermediate between the reactants and products. It corresponds to the least change in structure at the molecular level. There are various approaches for the modeling of *k*, like the collision theory and the transition state theory (TST), presently the favored one.

In TST the bimolecular reaction

$$A + B \rightarrow P \tag{1.7.1-1}$$

is considered to proceed over an activated complex, $AB^{\ddagger}$, which is in equilibrium with *A* and *B* and whose configuration corresponds to a maximum of the potential energy. The rate of dissociation of $AB^{\ddagger}$ into the product, *P*, is taken to be rate determining, so that the rate of (1.7.1-1) can be written:

$$r = k^{\ddagger} C_{AB^{\ddagger}} \tag{1.7.1-2}$$

and, given the equilibrium between *A*, *B* and $AB^{\ddagger}$,

$$r = k^{\ddagger} K_C^{\ddagger} C_A C_B \tag{1.7.1-3}$$

with $$K_C^{\ddagger}(T) = \frac{C_{AB^{\ddagger}} C_0}{C_A C_B} \tag{1.7.1-4}$$

where C_0 is the standard state concentration of A, B and $AB^{\ddagger}$, often taken to be 1.00 kmol/m^3. The k obtained from the experimental data is the product $k^{\ddagger}K_C^{\ddagger}$.

The rate will now be related to the change in energy of $AB^{\ddagger}$ as it passes the potential energy barrier towards the products. This passage is linked to the vibrational contribution to $E_{AB\ddagger}$.

From statistical thermodynamics the equilibrium constant can be expressed in terms of the partition functions per unit volume:

$$K_C^{\ddagger} = \frac{Q_{AB}^{\ddagger\ \ddagger} C_0}{Q_A Q_B} \exp\left[-\frac{E_0}{RT}\right] \tag{1.7.1-5}$$

The partition functions express the distribution of the energy states of an entity, be it the molecule A or B or the activated complex $AB^{\ddagger}$. They are referred to the selected zero-point energy-level. The exponential function in (1.7.1-5) takes care of the adaptation to the actual reaction temperature. E_0 represents the difference between the selected zero-point molar energy levels of the activated complex and the reactants. In practical terms: E_0 is the activation energy required by the reactants at 0°K.

The probability P_i that a molecule is in the i-th quantum state with energy level E_i, is given by

$$P_i = \frac{\exp\left[-\frac{E_i}{k_B T}\right]}{\sum_i \exp\left[-\frac{E_i}{k_B T}\right]} \tag{1.7.1-6}$$

where $\exp\left[-E_i/k_B T\right]$ is the Boltzmann distribution and k_B the Boltzmann constant, which is the gas constant R divided by the Avogadro number. The denominator is the sum of the probabilities over all E_i states of a molecule. It is the partition function Q:

$$Q = \Sigma \exp\left[-\frac{E_i}{k_B T}\right] \tag{1.7.1-7}$$

The total partition function Q of the reactants and of the activated complex consists of translational, rotational, vibrational and electronic contributions, respectively q_t, q_r, q_v, q_{el}. These contributions may be considered as independent of one another, so that from probability theory

$$Q = q_t\, q_r\, q_v\, q_{el} \tag{1.7.1-8}$$

The evolution of the configuration of the activated complex along the reaction pathway or reaction "coordinate" leading to the product is reflected in the evolution of its energy level, *E*, and can be expressed in terms of translation or vibration. The translation of a non linear molecule containing *N* atoms is described by the evolution of the coordinates of its center of mass. The same is true for rotation. Neglecting the electronic contribution, 3*N*–6 possibilities or "degrees of freedom" are left for vibration modes in the three dimensional *E*-space. Among these the one that leads to the dissociation of the activated complex is very loose and ultimately its frequency ν will tend to zero.

The contribution of this particular vibrational mode to the partition function of $AB^{\ddagger}$ can be calculated from quantum mechanics to be

$$q_\nu = \frac{1}{1 - \exp\left[-\dfrac{h\nu}{k_B T}\right]} \tag{1.7.1-9}$$

where *h* is the Planck constant and ν the vibration frequency.
The limit of q_ν for ν tending to zero is written $q_\nu^{'}$. Expanding the exponential in (1.7.1-9) and retaining only the first term leads to

$$q_\nu^{'} = \lim_{\nu \to 0} \frac{1}{1 - \exp\left[-\dfrac{h\nu}{k_B T}\right]} = \frac{k_B T}{h\nu} \tag{1.7.1-10}$$

The frequency ν expresses the passage of the vibrating complex over the top of the energy barrier towards the product. It yields a rate that can be written

$$r = \nu\, C_{AB}^{\ddagger} = \frac{k_B T}{h} \frac{Q_{AB}^{'\ddagger} C_0}{Q_A Q_B} \exp\left[-\frac{E_0}{RT}\right] C_A C_B \tag{1.7.1-11}$$

and the experimental rate constant of the reaction becomes

$$k = \frac{k_B T}{h} K_C^{'\ddagger} \tag{1.7.1-12}$$

$Q_{AB}^{'\ddagger}$ differs from $Q_{AB}^{\ddagger}$ because $\frac{k_B T}{h}$ was factored out.

Equation (1.7.1-11) was first derived by Eyring and by Glasstone et al. [1941], but by associating the decomposition of $AB^{\ddagger}$ into *P* to a particular translation, instead of vibration.

The rate is expressed in molecules per unit volume and time. To express it in moles per unit volume and time, the RHS of (1.7.1-11) has to be multiplied by the Avogadro number.
The group

$$\frac{k_B T}{h}\frac{Q'^{\ddagger}_{AB} C_0}{Q_A Q_B}$$

in (1.7.1-11) represents the frequency factor, *A*, encountered already in the rate equations given in Section 1.2.2.

The TST is viewed here mainly as a tool for the calculation of rate coefficients, an endeavor that has now become possible with dedicated software and powerful computers. Before that it has also been used to explain the observed behavior of reacting media, e.g., under thermodynamically non ideal conditions (high pressure, strong electrolyte solutions) and to correctly express the rate in terms of fugacities or activities [Boudart, 1968].

The equilibrium between the reactants and the activated complex can also be written in terms of thermodynamic functions. Introducing the standard Gibbs free energy and with $K_C^{\ddagger}$ in terms of activities

$$K_C^{\ddagger} = \exp[-\Delta G^{\circ\ddagger}/(RT)^{\Delta n}] \qquad (1.7.1\text{-}13)$$

with Δn = change in number of moles as the reactants are transformed into the activated complex. For the bimolecular reaction (1.7.1-1), (1.7.1-12) can be written (with $\Delta n = 1$)

$$k = \frac{k_B T}{h}\exp\left[-\frac{\Delta G'^{\circ\ddagger}}{RT}\right] \qquad (1.7.1\text{-}14)$$

where $\Delta G'^{\circ\ddagger}$ is the change of the Gibbs free energy upon conversion of the reactants into the activated complex. Equation (1.7.1-14) can be further explicited into

$$k = \frac{k_B T}{h}\exp\left[\frac{\Delta S'^{\circ\ddagger}}{R}\right]\exp\left[-\frac{\Delta H'^{\circ\ddagger}}{RT}\right] \qquad (1.7.1\text{-}15)$$

In (1.7.1-15) the frequency factor *A* is now given by

$$\frac{k_B T}{h}\exp\left[\frac{\Delta S'^{\circ\ddagger}}{R}\right]$$

The quantities $\Delta G'^{\circ\ddagger}$, $\Delta S'^{\circ\ddagger}$, and $\Delta H'^{\circ\ddagger}$ are not ordinary thermodynamic quantities because one of the degrees of freedom of the activated complex has been removed to impose the pathway leading to the product.

Through E_i, the partition function connects the mechanical properties of the system to the thermodynamic properties, hidden behind T. Introducing the total internal energy, E_t, which is a weighted sum of the potential and kinetic energies of all the particles of the system:

$$E_t = \sum_i P_i E_i \tag{1.7.1-16}$$

or, accounting for (1.7.1-6 and 1.7.1-7)

$$E_t = \sum_i E_i \frac{\exp\left[\frac{-E_i}{k_B T}\right]}{Q} \tag{1.7.1-17}$$

with $\beta = \frac{1}{k_B T}$, equation (1.7.1-17) can be written:

$$\sum_i E_i \frac{\exp[-\beta E_i]}{Q} = -\frac{1}{Q}\frac{\partial}{\partial \beta}\sum_i \exp[-\beta E_i] = -\frac{\partial \ln Q}{\partial \beta} \tag{1.7.1-18}$$

and finally, using $\frac{\partial T}{\partial \beta} = -\frac{1}{k_B \beta^2} = -k_B T^2$

$$E_t = k_B T^2 \frac{\partial \ln Q}{\partial T} \tag{1.7.1-19}$$

Given

$$c_V = \left(\frac{\partial E_t}{\partial T}\right)_V \quad \text{and} \quad S = \int_0^T \frac{c_V}{T'} dT'$$

the molar entropy can now be related to the partition function by

$$S(T) = k_B \ln Q + k_B T \frac{\partial \ln Q}{\partial T} \tag{1.7.1-20}$$

The entropy consists, like the partition function, of translational, rotational, vibrational and electronic contributions:

$$S = S_t + S_r + S_v + S_e \tag{1.7.1-21}$$

$\Delta H'^{\circ\ddagger}$, introduced in (1.7.1-15), is not necessarily identical to the activation energy E_a as encountered in the Arrhenius equation $k = A\exp[-E_a/RT]$, based

upon experimental data. A difference in number of moles between the activated complex and the reactants should be accounted for.

The Arrhenius equation can also be written

$$\frac{d \ln k}{dT} = \frac{E_a}{RT^2} \tag{1.7.1-22}$$

Consider the case in which n molecules of reactant lead to one molecule of activated complex. Taking the logarithm of k in (1.7.1-15), differentiating with respect to T, multiplying by RT^2 and equating with (1.7.1-22) leads to

$$E_a = \Delta H'^{\circ\ddagger} + (1-\Delta n)^{\ddagger} RT \tag{1.7.1-23}$$

For the bimolecular case dealt with here $\Delta n^{\ddagger} = 1$, so that

$$E_a = \Delta H'^{\circ\ddagger} + 2RT \tag{1.7.1-24}$$

The change in enthalpy that appears from (1.7.1-15) onwards is calculated by subtracting the heats of formation of the reactants from those of the products.

The text by Laidler [1969] is a recommended guide for acquiring insight into transition state theory. The texts by Benson [1960], Boudart [1968], Laidler [1973] and by McQuarrie and Simon [1997] are classic references for kinetics at the fundamental level considered here.

1.7.2 Quantum Mechanics. The Schrödinger Equation

The quantum mechanical state of a particle like an atom or a molecule, in particular the various contributions to the partition function Q, can be calculated from the solution of the Schrödinger equation for quantum wave mechanics or from approximations thereof. The Schrödinger equation reflects that a particle has both a corpuscular and a wave-like behavior. Classical mechanics, dealing with large objects, only considers the first property but at the atomic scale both characteristics have to be accounted for.

Consider an atom, a particle consisting of a nucleus and electrons. The former generates a potential energy field, $V(r)$, in which the electrons move and contribute with their kinetic energy to the total energy E of the particle. In three dimensional space and in the stationary state the equation for the wave motion of a single particle with mass m can be written

$$-\frac{h^2}{2m}\nabla^2\psi(r) + V(r)\psi(r) = E\psi(r) \tag{1.7.2-1}$$

$\Psi(r)$ describes the spatial amplitude of the matter wave as a function of its position in space, defined with respect to the nucleus. The symbol r represents a space vector, h is the Planck constant and E is the energy of the particle, consisting of potential and kinetic contributions. Mathematically (1.7.2-1) is an eigenvalue problem and ψ is the eigenfunction. It can be solved exactly for the hydrogen molecule, with one nucleus and one electron, but problems arise when the wave function of a particle with a number of electrons has to be calculated because of their interaction. The Hartree approach deals with an N-electron wave function as the product of N independent single orbital functions and does not explicitly account for the interaction between the electrons [Hartree, 1928; Levine, 1999].

The steady state of a molecule corresponds to a minimum energy. The minimization of the energy has to start from an approximation of the molecular structure by means of what is called basis functions. These represent an atomic orbital by a linear combination of Gaussian functions with different exponents. The number of Gaussian functions does not necessarily have to be the same for the inner shell and the valence shell electrons.

To improve the accuracy by including the interaction between electrons without running into excessive computational problems many approximate solutions of the wave equation have been proposed. Today the most commonly used approach is called “Density Functional Theory” (DFT).

1.7.3 Density Functional Theory

DFT uses the density of the electron distribution as a fundamental variable. The many body wave function depends on $3N$ spatial variables (3 per electron), the electron density only on 3 variables (the space coordinates).

In a “many body” case the nuclei interact among themselves through Coulomb forces and generate a static “external” potential V that determines the spatial distribution of the moving electrons. The stationary state of the electrons is characterized by the wave function $\Psi(r)$ and is described in DFT by:

$$H\Psi = (T + U + V)\Psi \qquad (1.7.3\text{-}1)$$

where H is the electronic molecular Hamiltonian operating on Ψ, T is the known kinetic energy functional and U is a functional expressing the interaction between electrons (a functional is a function of a function, in this case of the electron density). Whereas V is system dependent, both T and U are universal operators. U expresses the problem in greater detail than the Hartree approach and accounts for exchange- and correlation potentials. The first is a direct result of the introduction of the Pauli exclusion principle accounting for the spin of the

electrons and requiring the wave functions to be anti-symmetric. Secondly, electrons with opposite spin undergo electrostatic Coulomb interaction causing a "correlation" potential. The exchange and correlation potentials are both approximated in DFT by functionals of the electron density. In the local density approximation (LDA) the functional only depends on the electron density at the coordinate where the functional is evaluated. A further refinement, the generalized gradient approximation (GCA), also accounts for the gradient of the electron density in that location.

In quantum chemistry calculations, the Becke, Lee, Yang, Parr (BLYP) functional is often applied. Becke dealt with the exchange contribution [1993] and Lee, Yang and Parr with the correlation contribution to the potential energy [1988]. The B3LYP method uses a hybrid functional, combining Beck's exchange functional with the potential energy calculated according to the Hartree-Fock approach. The 3 refers to the presence of three parameters reflecting the weight of the Hartree-Fock exchange approach (Hartree + exchange potential) in this combination. Starting from this B3LYP level model the energy of the molecule is then minimized to yield the best possible structure of the molecule (bond length, bond angles, energy, etc.).

Determining the structure of the activated complex of an elementary reaction requires additional steps. This structure corresponds to a saddle point on the potential energy surface. The progress of the transition of the reactant(s) towards the activated complex along the reaction coordinate is followed in a stepwise manner. In each step of the progress — e.g., the extension of the bond length between 2 C-atoms in the case of a dissociation or the increase of the dihedral angle about the double bond in the case of cis-trans isomerization of an olefin — the energy of the ensemble is optimized, e.g., using the B3LYP-6-31G theory, until a configuration with the highest potential energy is reached. To check if the TST has really been reached the Intrinsic Reaction Coordinate (IRC) method is used. A saddle point connects two valleys on the potential energy surface. The forward descent along the reaction coordinate should yield the product, the backward descent the reactant(s).

Once the configuration of the transition state has been identified its energy E is available. The partition functions, entropies and enthalpies of the activated complex can then be calculated and substituted together with those of the reactants into the expression for the rate coefficient k.

The application of equations (1.7.1-11) and (1.7.3-1) will be illustrated in Section 2.6 of Chapter 2 dealing with the modeling of the rate of catalytic reactions.

PROBLEMS

1.1 For the thermal cracking of ethane in a tubular reactor, the following data were obtained for the rate coefficient at different reference temperatures:

T (°C)	702	725	734	754	773	789	803	810	827	837
k (s^{-1})	0.15	0.273	0.333	0.595	0.923	1.492	2.138	2.718	4.137	4.665

Determine the corresponding activation and frequency factor.

1.2 Derive the result given in Table 1.2.4.2-1 for the reaction

$$A + B \rightarrow Q + S$$

1.3 Derive the solutions to the rate equations for the first-order reversible reaction given in Section 1.2.3.

1.4 A convenient laboratory technique for measuring the kinetics of ideal gas-phase single reactions is to follow the change in total pressure in a constant volume and temperature container. The concentration of the various species can be calculated from the total pressure change. Consider the reaction

$$aA + bB + \ldots \rightarrow qQ + sS + \ldots$$

(a) Show that the extent can be found from

$$\xi = \frac{V}{RT}\frac{p_t - p_{t0}}{\Delta\alpha}$$

where $\Delta\alpha = q + s + \ldots - a - b - \ldots$
(Note that the method can only be used for $\Delta\alpha \neq 0$.)

(b) Next, show that the partial pressure for the jth species can be found from

$$p_j = p_{j0} + \frac{\alpha_j}{\Delta\alpha}\left(p_t - p_{t0}\right)$$

(c) Use the method to determine the rate coefficient for the first-order decomposition of di-*t*-butyl peroxide:

$$(CH_3)_3COOC(CH_3)_3 \rightarrow 2(CH_3)_2CO + C_2H_6$$

The data given below are provided by J.H. Raley, F.E. Rust, and W.E. Vaughn [*J. Am. Chem. Soc.*, 70, 98 (1948)].They were obtained at 154.6°C under a 4.2-mm Hg partial pressure of

nitrogen, which was used to feed the peroxide to the reactor. Determine the rate coefficient by means of the differential and integral method of kinetic analysis.

***t*, min**	**p_t , mm Hg**
0	173.5
2	187.3
3	193.4
5	205.3
6	211.3
8	222.9
9	228.6
11	239.8
12	244.4
14	254.5
15	259.2
17	268.7
18	273.9
20	282.0
21	286.8
∞	491.8

1.5 The results of Problem 1.4 can be generalized for the measurement of any property of the reaction mixture that is linear in the concentration of each species:

$$\lambda_j = K_j\, C_j$$

The λ_j could be partial pressures (as in Problem 1.4), various spectral properties, ionic conductivity in dilute solutions, and so on. Then, the total observed measurement for the mixture would be

$$\lambda = \sum_j \lambda_j = \sum_j K_j C_j$$

(a) For the general single reaction

$$\sum_j \alpha_j A_j = 0$$

show that the relation between the extent of reaction and λ is

$$\lambda = \lambda_0 + \left(\sum_j \alpha_j K_j \right) \frac{\xi}{V}$$

where

$$\lambda_0 = \sum_j K_j C_{j0}$$

(b) After a long ("infinite") time, the extent ξ_∞ can be evaluated for irreversible reactions from the limiting reagent, and for reversible reactions from thermodynamics. Use these values to formulate the desired relation containing only measured or determined variables [see Frost and Pearson, 1961]:

$$\frac{\lambda - \lambda_0}{\lambda_\infty - \lambda_0} = \frac{\xi}{\xi_\infty}$$

1.6 Show that the general expression for the concentration at which the autocatalytic reaction of Section 1.2.3.3 has a maximum rate is

$$\left(\frac{C_Q}{C_{Q0}}\right)_{\max} = \frac{1}{2}\left(1 + \frac{C_{A0}}{C_{Q0}}\right)$$

Note that this agrees with the specific results in the section.

1.7 Derive the concentration as a function of time for the general three-species first-order reactions

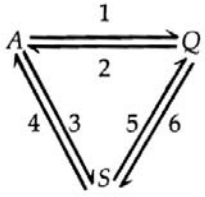

These relations should reduce to all the various results for first-order reactions given in Sections 1.2 and 1.3. Also determine the equilibrium concentrations C_{Aeq}, C_{Qeq}, C_{Seq} in terms of the equilibrium constants for the three reactions.

1.8 For the complex reactions

$$aA + bB \overset{1}{\rightarrow} qQ$$

$$q'Q + b'B \overset{2}{\rightarrow} sS$$

(a) Use Eqs. (1.1.2-15) and (1.1.2-17) to express the time rates of change of N_A, N_B, N_Q, and N_S in terms of the two extents of

reaction and the stoichiometric coefficients *a*, *b*, *b'*, *q*, *q'* and *s*; for example,

$$\frac{dN_A}{dt} = -a\frac{d\xi_1}{dt} + (0)\frac{d\xi_2}{dt}$$

(b) In practical situations it is often useful to express the changes in all the mole numbers in terms of the proper number of independent product mole number changes—in this case, two. Show that the extents in part (a) can be eliminated in terms of dN_Q/dt and dN_s/dt to give

$$\frac{dN_A}{dt} = -\frac{a}{q}\left(\frac{dN_Q}{dt}\right) - \frac{a}{s}\frac{q'}{q}\left(\frac{dN_S}{dt}\right)$$

$$\frac{dN_B}{dt} = -\frac{b}{q}\left(\frac{dN_Q}{dt}\right) - \left(\frac{b}{s}\frac{q'}{q} + \frac{b'}{s}\right)\left(\frac{dN_S}{dt}\right)$$

This alternate formulation will be often used in the practical problems to be considered later in the book.

(c) For the general reaction

$$\sum_{j=1}^{N} \alpha_{ij} A_j = 0 \qquad\qquad i = 1, 2, ..., M$$

the mole number changes in terms of the extents are

$$\frac{dN_j}{dt} = \sum_{j=1}^{M} \alpha_{ij} \frac{d\xi_i}{dt}$$

or

$$\frac{d\mathbf{N}}{dt} = \boldsymbol{\alpha}^T \frac{d\boldsymbol{\xi}}{dt}$$

where $\mathbf{N}$ is the N-vector of numbers of moles, $\boldsymbol{\xi}$ is the M-vector of extents, and $\boldsymbol{\alpha}^T$ is the transpose of the $M \times N$ stoichiometric coefficient matrix $\boldsymbol{\alpha}$. Show that, if an alternate basis of mole number changes is defined as an M-vector,

$$\frac{d\mathbf{N}^b}{dt}$$

the equivalent expressions for all the mole number changes are

$$\frac{d\mathbf{N}}{dt} = \boldsymbol{\alpha}^T \{[\boldsymbol{\alpha}^b]^T\}^{-1} \frac{d\mathbf{N}^b}{dt}$$

where $\boldsymbol{\alpha}^b$ is the $M \times M$ matrix of the basis species stoichiometric coefficients.

Finally, show that these matrix manipulations lead to the same result as in part (b) if the basis species are chosen to be Q and S.

1.9 Show that the overall orders for a free radical reaction mechanism with a first-order initiation step are 3/2 and 1/2 for ββ and μμ terminations, respectively.

1.10 The thermal decomposition of dimethyl ether

$$CH_3OCH_3 \rightarrow CH_4 + CO + H_2$$

or

$$CH_3OCH_3 \rightarrow CH_4 + HCHO$$

is postulated to occur by the following free radical chain mechanism:

$$CH_3OCH_3 \xrightarrow{k_1} CH_3^{\bullet} + OCH_3^{\bullet}$$

$$CH_3^{\bullet} + CH_3OCH_3 \xrightarrow{k_2} CH_4 + CH_2OCH_3^{\bullet}$$

$$CH_2OCH_3^{\bullet} \xrightarrow{k_3} CH_3^{\bullet} + HCHO$$

$$CH_3^{\bullet} + CH_2OCH_3^{\bullet} \xrightarrow{k_4} C_2H_5OCH_3$$

(a) For a first-order initiation step, use the Goldfinger-Letort-Niclause table [1948] to predict the overall order of reaction.

(b) With the help of the steady-state assumption and the usual approximations of small initiation and termination coefficients, derive the detailed kinetic expression for the overall rate

$$\frac{-d[CH_3OCH_3]}{dt} = k_0[CH_3OCH_3]^n$$

and verify that the overall order n is as predicted in part (a). Also find k_0 in terms of k_1, k_2, k_3, and k_4.

(c) If the activation energies of the individual steps are $E_1 = 325$, $E_2 = 62.8$, $E_3 = 159$, $E_4 = 33.5$ kJ/mol, show that the overall activation energy is $E_0 = 262$ kJ/mol.

1.11 Laidler and Wojciechowski [1961] provide the following table of individual rate constants for ethane pyrolysis:

Reaction	A_0^a	E, kJ/mol	
1	1.0×10^{17}	356	1st-order initiation
1a	$2(6.5) \times 10^{17}$	294	2nd-order initiation
2	2.0×10^{11}	44	hydrogen abstraction
3	3.0×10^{14}	165	radical decomposition
4	3.4×10^{12}	28	$H\cdot + C_2H_6 \rightarrow H_2 + C_2H_5$
5	1.6×10^{13}		$H\cdot + C_2H_5 \rightarrow$ termination
6	1.6×10^{13}		$C_2H_5 + C_2H_5 \rightarrow$ termination

[a] In s^{-1} or $cm^3\ mol^{-1}s^{-1}$.

(a) Derive the overall kinetic expressions for the four combinations of the two possible initiation steps (1 or 1a) and the termination steps (5 or 6).

(b) Compare the overall rate constants at $T = 873$ K with the experimental value of $8.4 \times 10^{-4}\ s^{-1}$.

(c) Show that the ratio of the rates of reaction 5 and 6 is given by

$$\frac{r_5}{r_6} = \frac{k_3 k_5}{k_4 k_6} \frac{1}{[C_2H_6]}$$

(d) Calculate the "transposition pressure level" where terminations 5 and 6 are equivalent ($r_5 = r_6$) at $T = 640°C$, and compare with the measured value of 60 mm Hg. At this point, the overall reaction is changing from 1 to 3/2 order.

1.12* The overall reaction for the decomposition of nitrogen pentoxide can be written as

$$2N_2O_5 \rightarrow 4NO_2 + O_2$$

The following reaction mechanism is proposed:

$$N_2O_5 \rightarrow NO_3 + NO_2$$

$$NO_2 + NO_3 \rightarrow N_2O_5$$

* These problems were contributed by Prof. W.J. Hatcher, Jr., University of Alabama.

$$NO_2 + NO_3 \rightarrow NO_2 + O_2 + NO$$

$$NO + NO_3 \rightarrow 2NO_2$$

If the steady-state approximation for the intermediates is assumed, prove that the decomposition of N_2O_5 is first order [see R.A. Ogg, *J. Chem. Phys.*, 15, 337 (1947)].

1.13[*] The previous reaction was carried out in a constant volume and constant temperature vessel to allow the application of the "total pressure method" outlined in Problem 1.4. There is one complication however: the dimerization reaction $2NO_2 \rightleftharpoons N_2O_4$ also occurs. It may be assumed that this additional reaction immediately reaches equilibrium, the dimerization constant being given by

$$\log K_p = \frac{2866}{T} - \log T - 9.132 \qquad (T \text{ in K}; K_p \text{ in mm}^{-1})$$

The following data were obtained by F. Daniels and E.H. Johnson [*J. Am. Chem. Soc.*, 43, 53 (1921)], at 35°C, with an initial pressure of 308.2 mm Hg:

t, min	p_t, mm Hg	t, min	p_t, mm Hg
40	400.2	140	492.3
50	414.0	160	503.2
60	426.5	180	512.0
70	438.0	200	519.4
80	448.1	240	531.4
90	457.2	280	539.5
100	465.2	320	545.2
120	480.0	360	549.9
		∞	565.3

Determine the first-order rate coefficient as a function of time. What is the conclusion?

1.14 Reconsider the data of Problem 1.13. Determine the order of reaction together with the rate coefficient that best fits the data. Now, recalculate the value of the rate coefficient as a function of time.

REFERENCES

Aris, R., *Introduction to the Analysis of Chemical Reactors*, Prentice-Hall, Englewood Cliffs, N.J. (1965).

Aris, R., *Arch. Ration. Mech. Anal.*, 27, 356 (1968).

Aris, R., *Elementary Chemical Reactor Analysis*, Prentice-Hall, Englewood Cliffs, N.J. (1969).

Becke, A.D., *J. Chem. Phys.*, 98, 5648 (1993).

Benson, S.W., *Foundations of Chemical Kinetics*, McGraw-Hill, New York (1960).

Benson, S.W., *Ind. Eng. Chem. Proc. Des. Dev.*, 56, 19 (1964).

Benson, S.W., *Thermochemical Kinetics*, Wiley, New York (1968).

Boudart, M., *Kinetics of Chemical Processes*, Prentice-Hall, Englewood Cliffs, N.J. (1968).

Caddell, J.R., Hurt, D.M., *Chem. Eng. Prog.*, 47, 333 (1951).

Clymans, P.J., and Froment, G.F., *Comp. Chem. Eng.*, 8, 137 (1984).

Denbigh, K.B., *The Principles of Chemical Equilibrium*, Cambridge University Press, Cambridge (1955).

Eckert, C.A., *Ind. Eng. Chem.*, 59, No. 9, 20 (1967).

Eckert, C.A., *Ann. Rev. Phys. Chem.*, 23, 239 (1972).

Eckert, C.A., and Boudart, M., *Chem. Eng. Sci.*, 18, 144 (1963).

Eckert, C.A., Hsieh, C.K., and McCabe, J.R., *AIChE J.*, 20 (1974).

Froment, G.F., *AIChE J.*, 21, 1041 (1975).

Frost, A.A., and Pearson, R.G., *Kinetics and Mechanisms*, 2nd ed., Wiley, New York (1961).

Gerrens, H., in *Proceedings 4th Int. Symp. Chem. React. Eng.* (*ISCRE-4*), Dechema, Frankfurt (1976).

Glasstone, S., Laidler, K.J., and Eyring, H., *The Theory of Rate Processes*, McGrawHill, New York (1941).

Goldfinger, P., Letort, M., and Niclause, M., *Contribution à l'étude de la structure moleculaire*, Victor Henri Commemorative Volume, Desoer, Liège (1948).

Graef, S.P., and Andrews, J.F., *AIChE Symp. Ser.*, 70, 101 (1973).

Hamielec, A.E., Hodgins, J.W., and Tebbens, K., *AIChE J.*, 13, 1087 (1967).

Hartree, D., *The Wave Mechanics of an Atom with a Non-Coulomb Central Field. Part I. Theory and Methods*, Proc. Camb. Phil. Soc., 24, 89-312 (1928).

Kiparissides, C., in *Chemical Reaction Engineering: From Fundamentals to Commercial Plants and Products*, Eds. G.F. Froment and G.B. Marin, *Chem. Eng. Sci.*, 51, 1637 (1996).

Kistiakowsky, G., *J. Am. Chem. Soc.*, 50, 2315 (1928).

Laidler, K.J., *Theories of Chemical Reaction Rates*, McGraw-Hill, New York (1969).

Laidler, K.J., *Chemical Kinetics*, 2nd Ed., TMH (1973).

Laidler, K.J., and Wojciechowski, B.W., *Proc. Roy. Soc. London*, A260, 91 (1961).

Lee, C., Yang, W., and Parr, R.G., *Phys. Rev. B*, 37, 785 (1988).

Levine, I.N., *Quantum Chemistry*, 5th ed., Prentice Hall (1999).

Luss, D., and Golikeri, S.V., *AIChE J.*, 21, 865 (1975).

Mc Laughlin, K.W., and Bertolucci, C.M., *J. Math. Chem.*, 14, 71 (1993).

McQuarrie, D.A., and Simon J.D., *Physical Chemistry. A Molecular Approach*, University Science Books, Sausalito, Cal. (1997).

Monod, J., *Annu. Rev. Microbiol.*, 3, 371 (1949).

Prigogine, I., Ed. *Advances in Chemical Physics*, Vol. II, Interscience, New York (1967).

Prigogine, I., and Defay, R.; transl. by Everett, D.H., *Chemical Thermodynamics*, Longman, London (1954).

Ray, W.H., *J. Macromolec. Sci. - Rev. Macromol. Chem.*, C8, 1, (1972).

Ray, W.H., and Laurence, R.L., in *Chemical Reactor Theory*, Eds. N.R. Amundson & L. Lapidus, Prentice Hall, Englewood Cliffs, NJ (1977).

Rice, F.O., and Herzfeld, K.F., *J. Am. Chem. Soc.*, 56, 284 (1944).

Sundaram, K.M., and Froment, G.F., *Chem. Eng. Sci.*, 32, 601 (1977).

Sundaram, K.M., and Froment, G.F., *Ind. Eng. Chem. Fundam.*, 17, 174 (1978).

Van Damme, P.S., Narayanan, S., and Froment, G.F., *AIChE J.*, 21, 1065 (1975).

Van Damme, P.S., Froment, G.F., and Balthasar, W.A., *Ind. Eng. Chem. Proc. Des. Dev.*, 1, 366 (1981).

Villa, C.M., Ind. Eng. Chem. Res., 46, No. 18, 5815 (2007).
Willems, P.A., and Froment, G.F., *Ind. Eng. Chem. Res.*, 27, 1959 (1988a).
Willems, P.A., and Froment, G.F., *Ind. Eng. Chem. Res.*, 22, 19 (1988b).
Williams, F.M., *J. Theoret. Biol.*, 15, 190 (1967).

Chapter 2

Kinetics of Heterogeneous Catalytic Reactions

2.1 INTRODUCTION

The principles of homogeneous reaction kinetics and the equations derived in Chapter 1 remain valid for the kinetics of heterogeneous catalytic reactions, provided the concentrations and temperatures substituted in the equations are really those prevailing at the point of reaction. The formation of a surface complex is an essential feature of reactions catalyzed by solids, and the kinetic equation must account for this. In addition, transport processes may influence the overall rate — heat and mass transfer between the fluid and the solid or inside the porous solid — so that the conditions over the local reaction site do not correspond to those in the bulk fluid around the catalyst particle. Figure 2.1-1 shows the seven steps involved when molecules move into the catalyst, react on active sites, and the products moves back to the bulk fluid stream. To simplify the notation, the index *s*, referring to concentrations inside the solid, will be dropped in this chapter.

The seven steps are:

1. Transport of reactants *A*, *B*, ... from the main stream to the catalyst pellet surface.
2. Transport of reactants in the catalyst pores.
3. Adsorption of reactants on the catalytic site.
4. Chemical reaction between adsorbed atoms or molecules.
5. Desorption of products *R*, *S*, ...
6. Transport of the products in the catalyst pores back to the particle surface.
7. Transport of products from the particle surface back to the main fluid stream.

Steps, 1, 3, 4, 5, and 7 are strictly consecutive processes and can be studied separately and then combined into an overall rate, somewhat analogous to a series of resistances in heat transfer through a wall. However, steps 2 and 6 cannot be entirely separated: active centers are spread all over the pore walls so that the distance the molecules have to travel, and therefore the resistance they encounter, is not the same for all of them. This chapter concentrates on steps 3, 4, and 5 and ignores the complications induced by the transport phenomena, discussed in detail in Chapter 3.

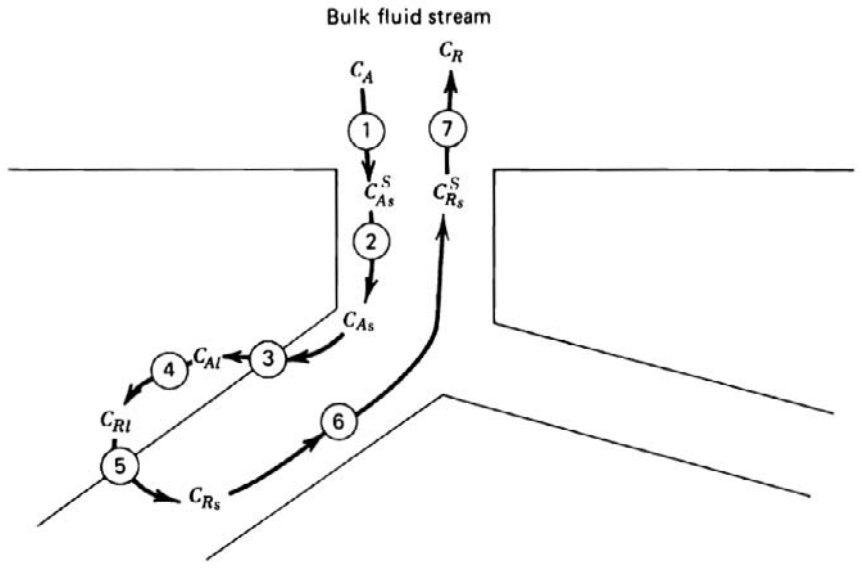

Figure 2.1-1
Steps involved in reactions on a solid catalyst.

In this chapter the main goal is to obtain suitable expressions to represent the kinetics of catalytic processes. An entry to this area is provided in books on chemical kinetics and catalysis. Some texts of interest for chemical engineers are by Thomas and Thomas [1967], Boudart [1968, 1984] and Dumesic et al. [1993]. A discussion of several important industrial catalytic processes is given in Gates, Katzer, and Schuit [1978] and Farrauto and Bartholomew [1997]. For further comprehensive surveys, see Emmett [1960], Anderson and Boudart [1987], and the series *Advances in Catalysis* [1949 and later].

Even though catalytic mechanisms won't be considered in detail, there are certain principles that are useful in developing rate expressions. The most obvious is that the catalytic reaction is often much more rapid than the corresponding homogeneous reaction. From the principle of microscopic reversibility, the reverse reaction will be similarly accelerated, and so the overall equilibrium will *not* be affected. As an example of this acceleration, Boudart [1958] compared the homogeneous versus catalytic rates of ethylene hydrogenation. The first route involves a chain mechanism, with the initiation step (Chapter 1) involving hydrogen and ethyl radicals — a usual difficult first step. The first step of the catalytic reaction, on the other hand, is the formation of a solid surface-ethylene complex, which is apparently energetically more favorable. Using the available data for both types of reactions, and knowing the surface area per volume of the CuO/MgO catalyst, Boudart showed that the two rates were

Homogeneous:

$$r = 10^{27} \exp\left(-\frac{43{,}000}{RT}\right) p_{H_2}$$

Catalytic:

$$r = 2.10^{27} \exp\left(-\frac{13{,}000}{RT}\right) p_{H_2}$$

For example, at 600 K the ratio of catalytic rate to homogeneous rate is 1.44×10^{11}.

The above equations show that the main reason for the much higher catalytic rate is the decrease in activation energy, which is the commonly accepted special feature of catalytic versus homogenous reactions.

There are various explanations for the ease of formation of the surface complex. One can visualize certain structural requirements of the underlying solid surface atoms to accommodate the reactants, and this had led to one important set of theories. Various electron transfer steps are involved in the formation of the complex bonds, so that the electronic nature of the catalyst is

undoubtedly also important. This had led to other considerations concerning the nature of catalysis. Surface science techniques and investigations have significantly contributed to the progress of the understanding of catalysis. Books by Ertl et al. [1997] and by Somorjai [1994] are revealing in this respect.

The present book does not intend to discuss properties of catalysts, but rather to present a systematic approach for developing the kinetics of processes catalyzed by solids as a tool for the design of the process. Nevertheless, to stress that kinetic studies cannot be dissociated from a thorough knowledge of the catalyst properties and function, two types of catalysts are briefly discussed: acid and metal catalysts. Acidic catalysts, such as silica/alumina, can apparently act as Lewis (electron acceptor) or Brønsted (proton donor) acids, and thus form some sort of carbonium/carbenium ion from hydrocarbons. There is some analogy between this hydrogen-deficient entity and a free radical, but their reaction behavior is different. Metal catalysts are primarily used in hydrogenations and dehydrogenations. The classical example of the difference in behavior of acid and metal catalysts is the ethanol decomposition:

$$C_2H_5OH \xrightarrow[catalyst]{acid} C_2H_4 + H_2O \quad \text{(dehydration)}$$

or

$$C_2H_5OH \xrightarrow[catalyst]{metal} C_2H_4O + H_2 \quad \text{(dehydrogenation)}$$

With hydrocarbons, the two types of catalysts cause cracking or isomerization versus hydrogenation or dehydrogenations.

An interesting and very practical example of these phenomena concerns catalysts composed of both types of materials — called “dual function,” or bifunctional catalysts [Mills et al., 1953]. A lucid discussion is provided by Weisz [1962] and by Oblad et al. [1955] who also present a few examples illustrating the importance of these concepts, not only to catalysis, but also to the kinetic behavior. Much of the reasoning is based on the concept of reaction sequences involving the surface intermediates. Consider the scheme below in which the species within the dashed box are the surface intermediates and *l* represents an active site of the catalyst:

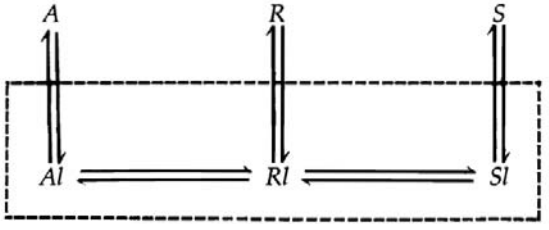

The amount of *R* in the fluid phase now depends not only on the relative rates between *Al, Rl, Sl,* as in homogeneous kinetics, but also on the relative rates of desorption and reaction. Here, *Al, Rl, Sl* represent the surface-bound species. For irreversible surface reactions, and very slow desorption rates, no fluid phase *R* will even be observed! A detailed experimental verification of this general type of behavior was provided by Dwyer, Eagleton, Wei and Zahner [1968] for the successive deuterium exchanges of neopentane. They obtained drastic changes in product distributions as the ratio (surface reaction rate)/(desorption rate) is increased.

In a bifunctional catalyst the above consecutive reactions can each be catalyzed by a different type of site (e.g., a metal and an acid):

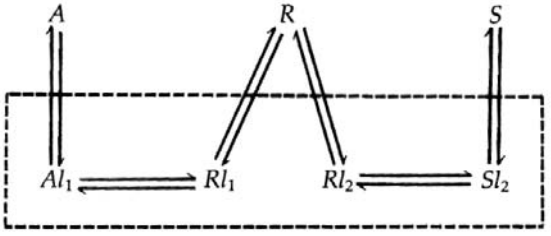

The essential difference between the two catalysts is that the true intermediate, *R*, must desorb, move through the fluid phase, and adsorb on the new site if any product *S* is to be formed.

Weisz defines a "nontrivial" polystep sequence as one where a unique conversion or selectivity can be achieved relative to the usual type of sequence. Thus,

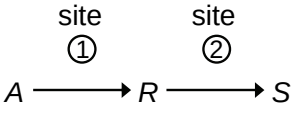

would be considered "trivial", because the results obtained from a bifunctional catalyst would be essentially similar to those from the two reactions carried out one after the other. For the sequence

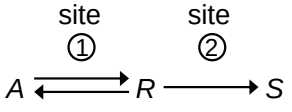

the maximum conversion into *S* would be limited by the equilibrium amount of *R* formed when the steps were successively performed. However, if the second site were intimately adjacent to the first, the Rl_1 intermediate would be continuously "bled off", thus shifting the equilibrium toward higher overall conversion. This is important for cases with very adverse equilibrium and appears to be the situation

for the industrially important isomerization of saturated hydrocarbons (encountered in "catalytic reforming"), which are generally believed to proceed by the following sequence:

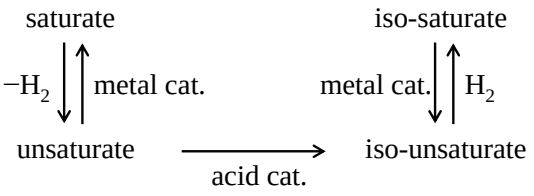

[See also Sinfelt, 1964, and Haensel, 1965]. The isomerization step is usually intrinsically very fast, and so the first part of the reaction has exactly the above sequence similar to an earlier qualitative study by Mills et al. [1953]. Weisz and co-workers performed experiments to prove this conjecture. They made small particles of acid catalyst and small particles containing platinum. These particles were then formed into an overall pellet. They found that a certain intimacy of the two catalysts was required for appreciable conversion of *n*-heptane into isoheptane. Particles larger than about 90 μm forced the two steps to proceed consecutively, since the intermediate unsaturates resulting from the metal site dehydrogenation step could not readily move to the acid sites for isomerization. This involves diffusion steps that will be discussed in Chapter 3. Further evidence that olefinic intermediates are involved was obtained from experiments showing that essentially similar product distributions occur with dodecane or dodecene feeds.

Another example presented dealt with cumene cracking, which is straightforward with an acidic silica/alumina catalyst:

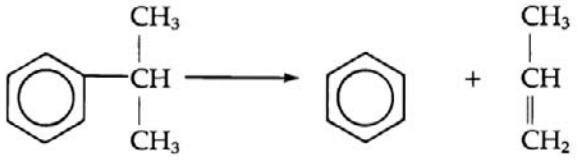

A different product distribution was observed with a Pt/Al_2O_3 catalyst, which mainly favors the reaction:

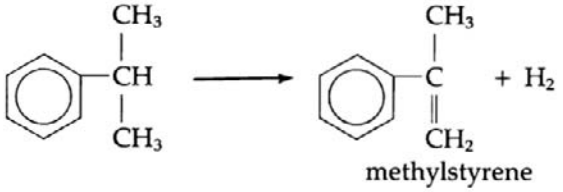

The presumed sequence was

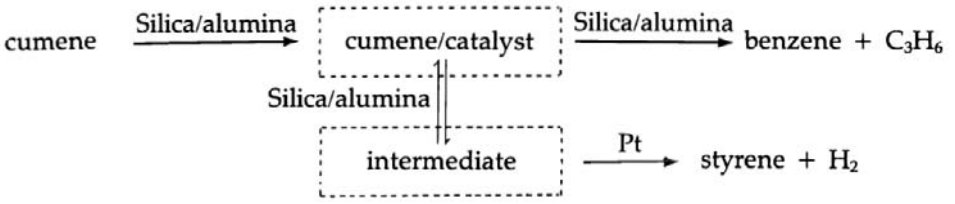

With only acid sites, the intermediate actually plays no role, but the metal sites permit the alternative, and then apparently dominant, reaction. Many further aspects of the behavior of polyfunctional catalysts on the conversion and selectivity of sets of reactions were also discussed by Weisz [1962].

2.2 ADSORPTION ON SOLID CATALYSTS

The above was rather qualitative as far as the surface intermediates are concerned. It is generally conceded that its formation involves an adsorption step. Before proceeding to the derivation of rate equations a brief discussion of this subject is useful. Further references are Brunauer [1945], de Boer [1968], Flood [1967], Gregg and Sing [1967], Clark [1970], and Hayward and Trapnell [1964].

There are two broad categories of adsorption:

Physisorption	**Chemisorption**
Through van der Waals forces	Involves covalent chemical bonds
Multilayer coverage possible	Only single layer coverage

For a surface-catalyzed reaction to occur, chemical bonds must be involved. The classical theory of Langmuir is based on the following hypotheses:

- The adsorption sites are energetically uniform.
- Monolayer coverage.
- No interaction between adsorbed molecules.

This theory is most suitable for describing chemisorption (except possibly for the first assumption) and low-coverage physisorption where a single layer is likely. For higher-coverage physisorption, a theory that accounts for multiple layers was introduced by Brunauer-Emmett-Teller (B-E-T) [Brunauer, 1945; Brunauer et al., 1940; de Boer, 1968; Flood, 1967; Gregg and Sing, 1967; and Clark, 1970].

Langmuir also assumed that the usual mass action laws could describe the individual steps. Calling *l* an adsorption site, and *Al* adsorbed *A*, adsorption and its reverse step — desorption — can be written:

$$A + l \rightleftarrows Al \tag{2.2-1}$$

The rates of adsorption and desorption are given by

$$r_a = k_a C_A C_l \qquad \text{with rate coefficient} \qquad k_a = A_a e^{-Ea/RT} \tag{2.2-2}$$

$$r_d = k_d C_{Al} \qquad \text{with rate coefficient} \qquad k_d = A_d e^{-Ed/RT} \tag{2.2-3}$$

where C_l and C_{Al} are surface concentrations, in kmol/kg catalyst, and the rates are in kmol/(kg catalyst · s). The sites are either vacant or covered by adsorbed *A*, so that the total concentration of sites consists of

$$C_t = C_l + C_{Al} \tag{2.2-4}$$

At equilibrium, the "adsorption isotherm" is obtained by equating the rates of adsorption and desorption:

$$k_d C_{Al} = k_a C_A C_l$$

$$= k_a C_A \left(C_t - C_{Al}\right)$$

The concentration of adsorbed *A* is given by

$$C_{Al} = \frac{C_t K_A C_A}{1 + K_A C_A} \tag{2.2-5a}$$

and the adsorption equilibrium constant is defined by

$$K_A = \frac{k_a}{k_d}$$

Equation (2.2-5a) is the mathematical expression of a hyperbola. An alternate way to write (2.2-5a) is in terms of the fractional coverage:

$$\theta = \frac{C_{Al}}{C_t} = \frac{K_A C_A}{1 + K_A C_A} \tag{2.2-5b}$$

Three forms of isotherm commonly observed are shown in Figure 2.2-1. Here, p_{sat} refers to the saturation pressure of the gas at the given temperature. Type I is the Langmuir isotherm, and Type II results from multilayer physisorption at higher coverages. Type IV is the same as Type II, but in a solid

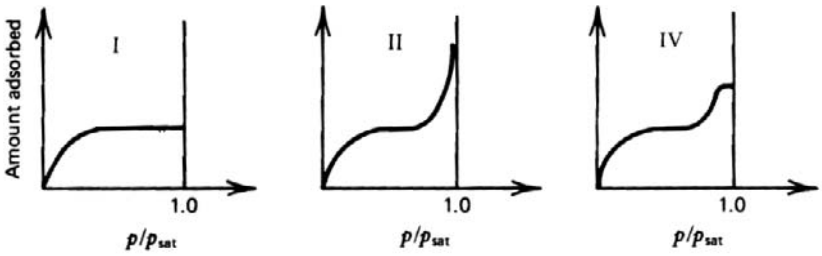

Figure 2.2-1
Types of adsorption isotherm. After Brunauer et al. [1940].

of finite porosity, giving the final level portion as $p \to p_{sat}$. The "heat of adsorption" is

$$Q_a = E_d - E_a \tag{2.2-6}$$

and for chemisorption, it can have a magnitude similar to that for chemical reactions — more than 42 kJ/mol.

The Langmuir treatment can be extended to other situations. For two species adsorbing on the same sites,

$$A + l \rightleftarrows Al$$

$$B + l \rightleftarrows Bl$$

$$\frac{dC_{Al}}{dt} = k_{aA} C_A C_l - k_{dA} C_{Al} \tag{2.2-7a}$$

$$\frac{dC_{Bl}}{dt} = k_{aB} C_B C_l - k_{dB} C_{Bl} \tag{2.2-7b}$$

$$C_t = C_t + C_{Al} + C_{Bl} \tag{2.2-7c}$$

At equilibrium,

$$C_{Al} = K_A C_A C_l \tag{2.2-8a}$$

$$C_{Bl} = K_B C_B C_l \tag{2.2-8b}$$

$$C_t = C_l + K_A C_A C_l + K_B C_B C_l \tag{2.2-8c}$$

and

$$C_l = \frac{C_t}{1 + K_A C_A + K_B C_B} \tag{2.2-9}$$

The concentrations of adsorbed species are given by

$$C_{il} = \frac{C_t K_i C_i}{1 + K_A C_A + K_B C_B} \tag{2.2-10}$$

If the molecule dissociates upon adsorption:

$$A_2 + 2l \rightleftarrows 2Al$$

and at equilibrium

$$C_{Al}^2 = K_A C_{A_2} C_l^2 \tag{2.2-11}$$

Then,

$$C_t = C_l + \sqrt{K_A C_{A_2}}\, C_l$$

and finally,

$$C_{Al} = \frac{C_t \sqrt{K_A C_{A_2}}}{1 + \sqrt{K_A C_{A_2}}} \tag{2.2-12}$$

Another way to state the assumptions of the classical Langmuir theory is that the heat of adsorption Q_a is independent of surface coverage θ. This is not always the case, and more general isotherms for nonuniform surfaces can be developed by integrating over the individual sites, θ_i, [e.g., see Clark, 1970 and Rudnitsky and Alexeyev, 1975]:

$$\theta = \int_0^1 \frac{(A_a / A_d)\exp[Q_a(\theta_i)/RT]C_A}{1 + (A_a / A_d)\exp[Q_a(\theta_i)/RT]C_A}\, d\theta_i$$

If Q_a depends logarithmically on θ over a range of surface coverages greater than zero,

$$Q_a = -Q_{am} \ln \theta$$

$$\theta = \exp\left(-\frac{Q_a}{Q_{am}}\right)$$

$$d\theta = \frac{d\theta}{dQ_a} dQ_a$$

$$= -\frac{1}{Q_{am}} \exp\left(-\frac{Q_a}{Q_{am}}\right) dQ_a$$

Then,

$$\theta = \frac{1}{Q_{am}} \int_0^\infty \frac{\exp(-Q_a / Q_{am})\, dQ_a}{1 + (A_d / A_a)\left(C_A^{-1} \exp(-Q_a / RT)\right)}$$

$$\approx \left(\frac{A_a}{A_d} C_A \right)^{RT/Q_{am}}, \qquad Q_{am} >> RT$$

$$\theta \equiv a C_A^m$$

This equation has the form of the Freundlich isotherm, which often empirically provides a good fit to adsorption data, especially in liquids, that cannot be adequately fit by a Langmuir isotherm. Using a linear dependence of Q_a on θ,

$$Q_a = Q_{a0}(1 - \alpha\theta)$$

approximately gives the Temkin-isotherm

$$\theta \approx \left(\frac{RT}{\alpha Q_{a0}} \right) \ln \left[\frac{A_a}{A_d} C_A \right]$$

that has been extensively used for ammonia synthesis kinetics.

Even though these isotherms presumably account for nonuniform surfaces, they have primarily been developed for single adsorbing components. Unlike with the Langmuir isotherm the rational extension to interactions in multicomponent systems are not yet possible. This latter point is important for further applications in the present book, and so only the Langmuir isotherms will be used in developing rate expressions. Not all adsorption data can be represented by a Langmuir isotherm, however. This problem will receive further attention in Section 2.3.3.

2.3 RATE EQUATIONS

Any attempt to formulate a rate equation for a solid-catalyzed reaction starts from the basic laws of chemical kinetics encountered in the treatment of homogeneous reactions, but care has to be taken to substitute in these laws the concentrations and temperatures at the locus of reaction itself. These do not necessarily correspond to those just above the surface or the active site, due to the adsorption characteristics. To develop the kinetics, an expression is required that relates the rate and amount of adsorption to the concentration of the component of the fluid in contact with the surface.

The application of Langmuir isotherms for the various reactants and products was begun by Hinshelwood, in terms of fractional coverage, and the more convenient use of surface concentrations for complex reactions by Hougen and Watson [1947]. Thus, the developments below are often termed Langmuir-

Hinshelwood or Hougen-Watson rate equations. For the sake of brevity in this text they will be referred to as Hougen-Watson rate equations.

2.3.1 Single Reactions

Consider the simple reaction

$$A \rightleftarrows R$$

The chemisorption step is written as

$$A + l \rightleftarrows Al$$

where l represents a vacant site.

Assuming a simple mass action law,

$$r_a = k_A \left(C_A C_l - \frac{C_{Al}}{K_A} \right) \qquad (2.3.1\text{-}1)$$

where

k_A	=	chemisorption rate coefficient
C_l	=	concentration of vacant site
C_{Al}	=	concentration of chemisorbed A
K_A	=	adsorption equilibrium constant

The chemical reaction step proper is written:

$$Al \rightleftarrows Rl$$

If both reaction steps are assumed to be of first order, the net rate of reaction of Al is

$$r_{sr} = k_{sr} \left(C_{Al} - \frac{C_{Rl}}{K_{sr}} \right) \qquad (2.3.1\text{-}2)$$

where

k_{sr}	=	surface reaction rate coefficient
K_{sr}	=	surface reaction equilibrium constant

Finally, the desorption step is

$$Rl \rightleftarrows R + l$$

with rate

$$r_d = k_R^{'} \left(C_{Rl} - \frac{C_R C_l}{K_d} \right)$$

or

$$r_d = k_R\left(\frac{C_{Rl}}{K_R} - C_R C_l\right) \qquad (2.3.1\text{-}3)$$

where

k'_R = rate constant for desorption step (Rl)
k_R = rate constant for adsorption R
K_R = adsorption equilibrium constant of $R = 1/K_d$

Rather than both adsorption and desorption constants, adsorption equilibrium constants are customarily used.

The overall reaction is the sum of the individual steps so that the thermodynamic equilibrium constant for the reaction is

$$K = K_A K_{sr} / K_R \qquad (2.3.1\text{-}4)$$

This relation can be used to eliminate one of the other equilibrium constants, often the unknown K_{sr} of the surface reaction between adsorbed species.

If the total concentration of sites, C_t, is assumed constant, it must consist of the vacant plus occupied sites, so that

$$C_t = C_l + C_{Al} + C_{Rl} \qquad (2.3.1\text{-}5)$$

The total sites concentration may not always remain constant during use. This will be discussed further in Chapter 5 on catalyst deactivation.

The rigorous combination of these three consecutive rate steps leads to a very complicated expression, but this needs to be done only in principle for transient conditions, although even then a sort of steady-state approximation is often used for the surface intermediates, assuming that conditions on the surface are stationary. The rate of change of the various species are

$$-\frac{dC_A}{dt} = r_A \frac{W}{V}$$

$$\frac{dC_{Al}}{dt} = r_A - r_{sr}$$

$$\frac{dC_{Rl}}{dt} = r_{sr} - r_d$$

$$\frac{dC_R}{dt} = r_d \frac{W}{V}$$

where W = mass of catalyst and V = volume of fluid.

A steady-state approximation on the middle two equations, as in Chapter 1, imposes that the three surface rates are equal:

$$r_a = r_{sr} = r_d = r_A \tag{2.3.1-6}$$

Combining (2.3.1-1)-(2.3.1-6) permits eliminating the unobservable variables C_l, C_{Al}, C_{Rl} in terms of the fluid phase compositions C_A and C_R and leads to [Aris, 1965]:

$$r_A = \frac{C_t\left[C_A - (C_R/K)\right]}{\left(\frac{1}{K_A k_{sr}} + \frac{1}{k_A} + \frac{1}{K k_R}\right) + \left(\frac{1}{K_A k_{sr}} + \frac{1+K_{sr}}{K k_R}\right)K_A C_A + \left(\frac{1}{K_A k_{sr}} + \frac{1+K_{sr}}{K_{sr} k_A}\right)K_R C_R} \tag{2.3.1-7}$$

Equation (2.3.1-7) gives the reaction rate in terms of fluid phase compositions and of the parameters of the various steps. Even for this very simple reaction, the result is rather complicated. Quite often it is found that one of the steps is intrinsically much slower than the others, and it is then termed the "rate controlling step". Suppose that, considered separately, the surface reaction were very slow compared to the adsorption or desorption steps:

$$k_A, k_R >> k_{sr}$$

Equation (2.3.1-7) then approximately reduces to

$$r_A = \frac{K_A k_{sr} C_t\left[C_A - (C_R/K)\right]}{1 + K_A C_A + K_R C_R} \tag{2.3.1-8}$$

which is much simpler than the more general steady state approximation case. Another example would be adsorption of *A* rate controlling:

$$k_R, k_{sr} >> k_A$$

which leads to

$$r_A = \frac{k_A C_t\left[C_A - (C_R/K)\right]}{1 + \left(1 + \frac{1}{K_{sr}}\right)K_R C_R} \tag{2.3.1-9a}$$

$$= \frac{k_A C_t\left[C_A - (C_R/K)\right]}{1 + \frac{K_A}{K} C_R + K_R C_R} \tag{2.3.1-9b}$$

For other than simple first-order reactions, the derivation of the general steady state approximation based expression similar to (2.3.1-7) is exceedingly tedious, or even impossible, so that a rate-controlling step is usually assumed right from the beginning. More than one rate-controlling step is certainly possible, however. For example, if one step is controlling in one region of the operating variables and another for a different region, there must obviously be a region between the two where both steps have roughly equal importance. The resulting kinetic equations are not as complicated as the general result, but still quite a bit more than those for one rate-controlling step. For further discussion, see Bischoff and Froment [1965] and Shah and Davidson [1965].

As an example of this procedure, the rate equation for $A \rightleftarrows R$ will now be derived for surface reaction rate controlling. This means that in (2.3.1-1), $k_A \to \infty$; and since from (2.3.1-6) the rate must remain finite

$$C_A C_l - \frac{C_{Al}}{K_A} \to 0$$

or

$$C_{Al} \cong K_A C_A C_l \tag{2.3.1-10}$$

Equation (2.3.1-10) does *not* mean that the adsorption step is in true equilibrium, for then the rate would be identically zero, in violation of (2.3.1-6). The proper interpretation is that for very large k_A, the surface concentration of A is very close to that given by (2.3.1-10). Similarly, from (2.3.1-3), for desorption

$$C_{Rl} \cong K_R C_R C_l \tag{2.3.1-11}$$

Substituting (2.3.1-10) and (2.3.1-11) into (2.3.1-5) gives:

$$C_t = C_l\left(1 + K_A C_A + K_R C_R\right)$$

or

$$C_l = \frac{C_t}{1 + K_A C_A + K_R C_R} \tag{2.3.1-12}$$

Substituting (2.3.1-10)-(2.3.1-12) into (2.3.1-2) and accounting for (2.3.1-4) finally yields:

$$r_A = k_{sr}\left(K_A C_A - \frac{K_R C_R}{K_{sr}}\right) C_l$$

$$= \frac{K_A k_{sr} C_t \left[C_A - \left(C_R / K\right)\right]}{1 + K_A C_A + K_R C_R}$$

This final result is exactly the same as (2.3.1-8) which was found by reducing the more general equation (2.3.1-7).

The total active sites concentration C_t is often not measurable. Note from (2.3.1-7), (2.3.1-8), and (2.3.1-9) and the other expressions that C_t always occurs in combination with the rate constants k_A, k_{sr}, and k_R. Therefore, it is customary to include C_t into these rate coefficients so that $k = k_i C_t$. If the number of active sites of a given catalyst is modified, e.g., in the manufacturing process or because of perturbations during its operation, the value of the rate coefficient has to be redetermined.

EXAMPLE 2.3.1.A

COMPETITIVE HYDROGENATION REACTIONS

This application of the foregoing concepts was discussed by Boudart [1962]. The following data on the liquid-phase catalytic cohydrogenation of *p*-xylene (*A)* and tetralin (*B*) were given by Wauquier and Jungers [1957]. As a simulation of a practical situation, a mixture of *A* and *B* was hydrogenated, giving the following experimental data:

Composition of Mixture			**Total Hydrogenation Rate**	
C_A	C_B	$C_A + C_B$	**Exp.**	**Calc.**
610	280	890	8.5	8.3
462	139	601	9.4	9.0
334	57	391	10.4	9.8
159	10	169	11.3	11.3

The common simple procedure of correlating total rate with total reactant concentration leads to the rate *increasing* with *decreasing* concentration (i.e., a negative order). This effect would be rather suspect as a basis for design. To investigate it closer, data on the hydrogenation rates of *A* and *B* alone were measured, and they appeared to be zero-order reactions with the following rates:

Hydrogenation rate of *A* alone:

$$(r_A)_1 = 12.9 \qquad \text{(2.3.1.A-a)}$$

Hydrogenation rate of *B* alone:

$$(r_B)_2 = 6.7 \qquad \text{(2.3.1.A-b)}$$

Also, *B* is more strongly adsorbed than *A*, and the ratio of equilibrium constants is

$$\frac{K_A}{K_B} = 0.18 \qquad \text{(2.3.1.A-c)}$$

How to explain all of these features by means of a consistent rate equation ?

Consider a simple chemisorption scheme with the surface reaction rate controlling:

$$A + l \rightleftarrows Al \qquad C_{Al} = K_A C_A C_l \qquad \text{(2.3.1.A-d)}$$

where concentrations have been used for the bulk liquid composition.

If the reaction product is weakly adsorbed, the equation for the total site concentration becomes

$$C_t \cong C_l + C_{Al} = C_l\left(1 + K_A C_A\right) \qquad \text{(2.3.1.A-e)}$$

For a simple first-order, irreversible surface reaction,

$$Al \rightarrow product \qquad \left(r_A\right)_1 = k_1^{'} C_{Al} \qquad \text{(2.3.1.A-f)}$$

From (2.3.1.A-d) and (2.3.1.A-e)

$$\left(r_A\right)_1 = \frac{k_1^{'} C_t K_A C_A}{1 + K_A C_A} \qquad \text{(2.3.1.A-g)}$$

In liquids, an approximately full coverage of adsorption sites is common (i.e., very large adsorbed concentrations), which means that $K_A C_A >> 1$, and equation (2.3.1.A-g) becomes

$$\left(r_A\right)_1 = k_1^{'} C_t = k_1 = 12.9 \qquad \text{(2.3.1.A-h)}$$

and the zero-order behavior of *A* alone is rationalized. Similarly, for *B* reacting alone,

$$\left(r_B\right)_1 = \frac{k_2^{'} C_t K_B C_B}{1 + K_B C_B} \approx k_2^{'} C_t = k_2 \qquad \text{(2.3.1.A-i)}$$

$$= 6.7 \qquad \text{[Eq. (2.3.1.A-b)]} \qquad \text{(2.3.1.A-j)}$$

When *A* and *B* react simultaneously,

$$C_t = C_l + C_{Al} + C_{Bl}$$

$$= C_l\left(1 + K_A C_A + K_B C_B\right)$$

$$\approx C_l\left(K_A C_A + K_B C_B\right) \qquad \text{(2.3.1.A-k)}$$

and

$$r_A = k_1' C_{Al} = \frac{k_1 K_A C_A}{K_A C_A + K_B C_B} \qquad \text{(2.3.1.A-l)}$$

$$r_B = k_2' C_{Bl} = \frac{k_2 K_B C_B}{K_A C_A + K_B C_B} \qquad \text{(2.3.1.A-m)}$$

The total rate is given by

$$r = r_A + r_B = \frac{k_1 K_A C_A + k_2 K_B C_B}{K_A C_A + K_B C_B} \qquad \text{(2.3.1.A-n)}$$

$$= \frac{\left(k_1\right)\dfrac{K_A}{K_B}\dfrac{C_A}{C_B} + \left(k_2\right)}{\dfrac{K_A}{K_B}\dfrac{C_A}{C_B} + 1}$$

$$= \frac{12.9(0.18)\dfrac{C_A}{C_B} + 6.7}{0.18\dfrac{C_A}{C_B} + 1} \qquad \text{(2.3.1.A-o)}$$

If the values of C_A and C_B given in the cohydrogenation data table are substituted into (2.3.1.A-o), it is found that the values of the total rate given in that table are predicted. In addition to illustrating an adsorption scheme for a real reaction, this example also shows that the observed phenomena can only be explained by accounting for the adsorption of the reacting species. ■

Consider now a slightly more complicated reaction. Dehydrogenation reactions are of the form

$$A \rightleftarrows R + S$$

The fluid phase composition will be expressed in partial pressures rather than concentrations, as is the custom for gases. Assume that the adsorption of A is rate controlling, so that for the chemisorption step:

$$A + l \rightleftarrows Al \qquad C_{Al} \neq C_l K_A p_A \qquad \text{(2.3.1-13)}$$

For the reaction step,

$$Al + l \rightleftarrows Rl + Sl \qquad K_{sr} = \frac{C_{Rl} C_{Sl}}{C_{Al} C_l} \tag{2.3.1-14}$$

and for the desorption steps,

$$Rl \rightleftarrows R + l \qquad C_{Rl} = C_l K_R p_R \tag{2.3.1-15}$$

$$Sl \rightleftarrows S + l \qquad C_{Sl} = C_l K_S p_S \tag{2.3.1-16}$$

The total concentration of active sites is

$$\begin{aligned} C_t &= C_l + C_{Al} + C_{Rl} + C_{Sl} \\ &= C_l + \frac{C_l K_R p_R C_l K_S p_S}{K_{sr} C_l} + C_l K_R p_R + C_l K_S p_S \\ &= C_l \left(1 + \frac{K_A}{K} p_R p_S + K_R p_R + K_S p_S \right) \end{aligned} \tag{2.3.1-17}$$

where the overall equilibrium relation $K = K_A K_{sr} / K_R K_S$ was used in the last step.

Equations (2.3.1-14) through (2.3.1-17) are now substituted into the rate equation for adsorption,

$$r_A = k_A' \left(p_A C_l - \frac{C_{Al}}{K_A} \right)$$

giving

$$r_A = \frac{k_A \left(p_A - p_R p_S / K \right)}{1 + \frac{K_A}{K} p_R p_S + K_R p_R + K_S p_s} \tag{2.3.1-18}$$

Equation (2.3.1-18) is the kinetic equation of the reaction $A \rightleftarrows R+S$ under the assumption that the adsorption is of the type $A+l \rightleftarrows Al$ (i.e., without dissociation of A), is of second order to the right, first order to the left, and is the rate-determining step of the process. The form of the kinetic equation would be different if it had been assumed that step 2 — the reaction itself — or step 3 — the desorption — were rate determining. The form would also have been different had the mechanism of adsorption been assumed different.

When the reaction on two adjacent sites is rate determining, the kinetic equation is as follows:

$$r_A = \frac{k_{sr} K_A \left[p_A - (p_R p_S / K) \right]}{\left(1 + K_A p_A + K_r p_R + K_S p_S \right)^2} \tag{2.3.1-19}$$

where $k_{sr} = k'_{sr} s C_t$ and s = number of nearest neighbor sites.
For a reaction $A + B \rightarrow$ products, the proper driving force is based on the adsorbed concentration of B that is *adjacent* to the adsorbed A:

$$C_{Bl|adj} = \text{(number of nearest neighbors) (probability of } B \text{ being adsorbed)}$$

$$= s\left(\frac{C_{Bl}}{C_t}\right) \text{ so that}$$

$$r_A = k'_{sr} C_{Al} C_{Bl|adj}$$

$$= \frac{k'_{sr}\left(C_t K_A p_A\right)\left[\left(s / C_t\right) C_t K_B p_B\right]}{\left(1 + K_A p_A + K_B p_B + \ldots\right)^2}$$

$$= \frac{k'_{sr} s C_t K_A K_B p_A p_B}{\left(1 + K_A p_A + K_B p_B + \ldots\right)^2}$$

In the above equations the factor s is included with C_t. See Hougen and Watson [1944] for further details. Similar reasoning leads to (2.3.1-19).

When the desorption of R is the rate-determining step,

$$r_A = \frac{k_R K\left(\frac{p_A}{p_S} - \frac{p_R}{K}\right)}{1 + K_A p_A + K K_R \frac{p_A}{p_S} + K_S p_S} \qquad (2.3.1\text{-}20)$$

$$k'_A C_t = k_A$$

Kinetic equations for reactions catalyzed by solids accounting for chemisorption may always be written as a combination of three groups:

A kinetic group [e.g., in (2.3.1-18)]: $k'_A C_t = k_A$

A driving-force group:

$$p_A - \left(p_R p_S / K\right)$$

An adsorption group:

$$1 + \frac{K_A}{K} p_R p_S + K_R p_R + K_S p_S$$

such that the overall rate is written as:

$$= \frac{(\text{kinetic factor})(\text{driving} - \text{force group})}{(\text{adsorption group})} \qquad (2.3.1\text{-}21)$$

Summaries of these groups for various kinetic schemes are given in Table 2.3.1-1 [see Yang and Hougen, 1950]. The various kinetic terms k and kK all contain the total number of active sites C_t. Some of them also contain the number of adjacent active sites s, or $s/2$, or $s(s-1)$. Both C_t and s are usually not known and therefore are not explicitly written in these groups. They are characteristic for a given catalyst system, however. For the bimolecular reaction

$$A + B \rightleftarrows R + S$$

the Yang-Hougen tables yield for surface reaction controlling:

$$r_A \frac{C_t k_{sr} K_A K_B \left[p_A p_B - \left(p_R p_S / K\right)\right]}{\left(1 + K_A p_A + K_B p_B + K_R p_R + K_S p_S + K_I p_I\right)^2}$$

where I is any adsorbable inert.

Finally, schemes alternate to the H-W mechanisms are the Rideal-Eley mechanisms, where one adsorbed species reacts with another species in the gas phase:

$$Al + B \rightarrow Rl$$

These yield similar kinetic expressions.

2.3.2 Coupled Reactions

For transformations consisting of sequences of reversible reactions, it is frequently possible to take advantage of the concept of the rate-determining step to simplify the kinetic equations. This is similar to the approach used above for single reactions consisting of a sequence of adsorption, reaction, and desorption steps. Boudart [1972] has discussed this approach and shown that catalytic sequences comprised of a large number of steps can frequently be treated as if they took place in at most two steps.

An example of this is provided by Hosten and Froment's study [1971] of the kinetics of *n*-pentane isomerization on a dual function Pt/Al_2O_3 reforming catalyst, carried out in the presence of hydrogen. As discussed earlier in Section 2.1 of this chapter, this reaction involves a three-step sequence consisting of dehydrogenation, isomerization, and hydrogenation. The dehydrogenation and hydrogenation steps occur on platinum sites, represented by l; the isomerization step occurs on the acidic alumina sites, represented by σ.

TABLE 2.3.1-1
GROUPS IN KINETIC EQUATIONS FOR REACTIONS ON SOLID CATALYSTS[a]

Driving-Force Groups

Reaction	$A \rightleftarrows R$	$A \rightleftarrows R + S$	$A + B \rightleftarrows R$	$A + B \rightleftarrows R + S$
Adsorption of *A* controlling	$p_A - \frac{p_R}{K}$	$p_A - \frac{p_R p_S}{K}$	$p_A - \frac{p_R}{K p_B}$	$p_A - \frac{p_R p_S}{K p_B}$
Adsorption of *B* controlling	0	0	$p_B - \frac{p_R}{K p_A}$	$p_B - \frac{p_R p_S}{K p_A}$
Desorption of *R* controlling	$p_A - \frac{p_R}{K}$	$\frac{p_A}{p_S} - \frac{p_R}{K}$	$p_A p_B - \frac{p_R}{K}$	$\frac{p_A p_B}{p_S} - \frac{p_R}{K}$
Surface reaction controlling	$p_A - \frac{p_R}{K}$	$p_A - \frac{p_R p_S}{K}$	$p_A p_B - \frac{p_R}{K}$	$p_A p_B - \frac{p_R p_S}{K}$
Impact of *A* controlling (*A* not adsorbed)	0	0	$p_A p_B - \frac{p_R}{K}$	$p_A p_B - \frac{p_R p_S}{K}$
Homogeneous reaction controlling	$p_A - \frac{p_R}{K}$	$p_A - \frac{p_R p_S}{K}$	$p_A p_B - \frac{p_R}{K}$	$p_A p_B - \frac{p_R p_S}{K}$

Replacements in the General Adsorption Groups

$$(1 + K_A p_A + K_B p_B + K_R p_R + K_S p_S + K_I p_I)^n$$

Reaction	$A \rightleftarrows R$	$A \rightleftarrows R + S$	$A + B \rightleftarrows R$	$A + B \rightleftarrows R + S$
When adsorption of *A* is rate controlling, replace $K_A p_A$ by	$\frac{K_A p_R}{K}$	$\frac{K_A p_R p_S}{K}$	$\frac{K_A p_R}{K p_B}$	$\frac{K_A p_R p_S}{K p_B}$
When adsorption of *B* is rate controlling, replace $K_B p_B$ by	0	0	$\frac{K_B p_R}{K p_A}$	$\frac{K_B p_R p_S}{K p_A}$
When desorption of *R* is rate controlling, replace $K_R p_R$ by	$K K_R p_A$	$K K_R \frac{p_A}{p_S}$	$K K_R p_A p_B$	$K K_R \frac{p_A p_B}{p_S}$
When adsorption of *A* is rate controlling with dissociation of *A*, replace $K_A p_A$ by	$\sqrt{\frac{K_A p_R}{K}}$	$\sqrt{\frac{K_A p_R p_S}{K}}$	$\sqrt{\frac{K_A p_R}{K p_B}}$	$\sqrt{\frac{K_A p_R p_S}{K p_B}}$
When equilibrium adsorption of *A* takes place with dissociation of *A*, replace $K_A p_A$ by (and similarly for other components adsorbed with dissociation)	$\sqrt{K_A p_A}$	$\sqrt{K_A p_A}$	$\sqrt{K_A p_A}$	$\sqrt{K_A p_A}$
When *A* is not adsorbed, replace $K_A p_A$ by (and similarly for other components that are not adsorbed)	0	0	0	0

Kinetic Groups	
Adsorption of *A* controlling	k_A
Adsorption of *B* controlling	k_B
Desorption of *R* controlling	$k_R K$
Adsorption of *A* controlling with dissociation	k_A
Impact of *A* controlling	$k_A K_B$
Homogeneous reaction controlling	k

	Surface Reaction Controlling			
	$A \rightleftarrows R$	$A \rightleftarrows R + S$	$A + B \rightleftarrows R$	$A + B \rightleftarrows R + S$
Without dissociation	$k_{sr}K_A$	$k_{sr}K_A$	$k_{sr}K_AK_B$	$k_{sr}K_AK_B$
With dissociation of *A*	$k_{sr}K_A$	$k_{sr}K_A$	$k_{sr}K_AK_B$	$k_{sr}K_AK_B$
B not adsorbed	$k_{sr}K_A$	$k_{sr}K_A$	$k_{sr}K_A$	$k_{sr}K_A$
B not adsorbed, *A* dissociated	$k_{sr}K_A$	$k_{sr}K_A$	$k_{sr}K_A$	$k_{sr}K_A$

Exponents of Adsorption Groups	
Adsorption of *A* controlling without dissociation	$n = 1$
Desorption of *R* controlling	$n = 1$
Adsorption of *A* controlling with dissociation	$n = 2$
Impact of *A* without dissociation $A + B \rightleftarrows R$	$n = 1$
Impact of *A* without dissociation $A + B \rightleftarrows R + S$	$n = 2$
Homogeneous reaction	$n = 0$

	Surface Reaction Controlling			
	$A \rightleftarrows R$	$A \rightleftarrows R + S$	$A + B \rightleftarrows R$	$A + B \rightleftarrows R + S$
No dissociation of *A*	1	2	2	2
Dissociation of *A*	2	2	3	3
Dissociation of *A* (*B* not adsorbed)	2	2	2	2
No dissociation of *A* (*B* not adsorbed)	1	2	1	2

[a]From Yang and Hougen [1950]

Each of these steps involves adsorption, surface reaction, and desorption so that the following mechanistic scheme can be written for the overall reaction:

Dehydrogenation:

$$A + l \rightleftarrows Al \qquad K_1 = c_{Al} / p_A \cdot c_l$$

$$Al + l \rightleftarrows Ml + H_2 l \qquad K_2 = c_{Ml} \cdot c_{H_2 l} / c_{Al} \cdot c_l$$

$$H_2 l \rightleftarrows H_2 + l \qquad K_3 = p_{H_2} \cdot c_l / c_{H_2 l}$$

$$Ml \rightleftarrows M + l \qquad K_4 = p_M \cdot c_l / c_{Ml}$$

Isomerization:

$$M + \sigma \rightleftarrows M\sigma \qquad K_5 = c_{M\sigma} / p_M \cdot c_\sigma$$
$$M\sigma \rightleftarrows N\sigma \qquad K_6 = c_{N\sigma} / c_{M\sigma}$$
$$N\sigma \rightleftarrows N + \sigma \qquad K_7 = p_N \cdot c_\sigma / c_{N\sigma}$$

Hydrogenation:

$$N + l \rightleftarrows Nl \qquad K_8 = c_{Nl} / p_N \cdot c_l$$
$$H_2 + l \rightleftarrows H_2 l \qquad K_9 = c_{H_2 l} / p_{H_2} \cdot c_l$$
$$Nl + H_2 l \rightleftarrows Bl + l \qquad K_{10} = c_{Bl} \cdot c_l / c_{Nl} \cdot c_{H_2 l}$$
$$Bl \rightleftarrows B + l \qquad K_{11} = p_B \cdot c_l / c_{Bl}$$

It was observed experimentally that the overall rate was independent of total pressure, and this provides a clue as to which step might be rate determining. When one of the steps of the dehydrogenation or hydrogenation reactions is considered to be rate determining, the corresponding overall rate equation is always pressure dependent. This results from the changing of the number of moles and was illustrated already by the treatment of dehydrogenation reactions given above. Since these pressure-dependent rate equations are incompatible with the experimental results, it may be concluded that the isomerization step proper determines the rate of the overall action. Additional evidence for this conclusion was based on the enhancement of the overall rate by addition of chlorine, which only affects the activity of the acid site.

When the surface reaction step in the isomerization is rate determining, the overall reaction rate is given by

$$r = \frac{kK_5\left(p_M - \dfrac{p_N}{K_5 K_6 K_7}\right)}{1 + K_5 p_M + \dfrac{1}{K_7} p_N}$$

The total pressure dependence of the rate is only apparent. Provided the isomerization is rate controlling, *n*-pentene is in equilibrium with *n*-pentane/hydrogen and isopentene with isopentane/hydrogen. When the equilibrium relations are used, the partial pressures of the pentenes can be expressed in terms of the partial pressures of the pentanes and hydrogen, leading to

$$r = \frac{kK_5K_D\left(p_A - \frac{p_B}{K}\right)}{p_{H_2} + K_5K_D p_A + \frac{1}{K_7K_H} p_B}$$

where $K_D = K_1K_2K_3K_4$ is the equilibrium constant for dehydrogenation, and $K_H = K_8K_9K_{10}K_{11}$ is the equilibrium constant for hydrogenation. The equation clearly shows that this rate is independent of total pressure.

When adsorption of *n*-pentene on the acid sites is the rate-determining step, a similar derivation leads to

$$r = \frac{kK_D\left(p_A - \frac{p_B}{K}\right)}{p_{H_2} + \frac{1}{K_7K_H}\left(\frac{1}{K_6} + 1\right)p_B}$$

and for desorption of isopentene rate controlling:

$$r = \frac{kK_5K_DK_6\left(p_A - \frac{p_B}{K}\right)}{p_{H_2} + K_5K_D(1 + K_6)p_A}$$

The latter two equations also lead to rates that are independent of total pressure. The discrimination between these three rate equations for pentane isomerization is illustrated in Section 2.6.2.

Several more complex reactions such as the catalytic reforming of heptanes on Pt/Re/alumina were dealt with in terms of sets of rate equations of the Hougen-Watson type by Van Trimpont et al. [1986]. The hydrogenolysis of thiophene and benzothiophene on Co/Mo/alumina was studied along the same lines by Van Parijs et al. [1986a, b] and is also discussed in Examples 2.6.4.A and 2.7.2.2.A.

Froment [1987a, 1987b] further extended the Hougen-Watson approach to complex reactions such as hydrocracking and illustrated the derivation of the rate equations not only reflecting the chemisorption of the reacting species, but also the effect of some of the species on the nature and properties of the actives sites, as encountered, for example, in Co/Mo catalysis.

Some reaction schemes can lead to multiplicity of steady states: the rate of reaction is not unique for one and the same gas-phase composition. This is a result of the interaction of the nonlinear dependence of the rate of reaction on adsorbed concentrations and the linear dependence of the rate of adsorption on

these concentrations. Bykov et al. [1976a, b], Bykov and Yablonskii [1981], Eigenberger [1978], and Hosten and Froment [1985] modeled this phenomenon. It turns out that, for reactions occurring on one type of site only, multiplicity of the rate requires more than one rate-determining step and more than three sites participating simultaneously in at least one of the elementary steps.

2.3.3 Some Further Thoughts on the Hougen-Watson Rate Equations

It should be pointed out here that the concept of a rate-determining step is not an essential characteristic or restriction of the Hougen-Watson rate equations. Note that Section 2.3 started out without introducing the notion of a rate-determining step. So far, however, very few kinetic studies exist in which it was thought to be necessary to apply the more general approach, except for non-steady-state behavior. An essential characteristic of the Hougen-Watson approach, on the other hand, is to account in an explicit way for the interaction of the reacting components with the catalytic surface.

There is still a strong belief that the Hougen-Watson approach is only a systematic, but still empirical, formalism leading to a better fit of the experimental data because of the increased number of parameters, but is incapable of reflecting the true mechanism. The assumptions behind Langmuir's equation have often been recalled, but not always on the basis of convincing data. A pragmatic attitude is probably more fruitful in this matter: The Langmuir theory as applied by Hougen and Watson permits a structured approach to catalytic kinetics and its basic restrictions generally lead to deviations which are minor with respect to the inaccuracies associated with kinetic experimentation [Froment, 1987b].

The validity of the approach is also discussed in a paper by Boudart [1986]. Certainly, the nonuniformity of catalytic surfaces, revealed by data on the heats of chemisorption, is a reality, but does this mean that a reaction necessarily senses this nonuniformity — that the reaction is structure sensitive? That depends on the reaction itself, but also on the operating conditions. It may be that the reaction requires only one (or perhaps two) metal atoms or actives sites to proceed, but also that the operating conditions lead to a surface which is almost completely covered by species, so that the nonuniformities are no longer felt. In such a case the use of Hougen-Watson rate equations, based on the Langmuir isotherm, is "… not only useful, but it is also correct. In all cases their use provides physical intuition, improvable rate equations and mechanistic insight unattainable through empirical rate laws" [Boudart, 1986]. Since then, further support for this point of view has been published.

Ammonia synthesis has been classically referred to as an example of a reaction in which the nonuniformity of the surface sites is felt in the kinetics. This is based upon the work of Temkin and Pyzhev [1940], who resorted to the Freundlich isotherm, instead of the Langmuir isotherm, in the derivation of their rate equation. It should be noted in the first place that this equation is close to the Hougen-Watson form, however [Boudart, 1986]. Stoltze and Nørskov [1985, 1987], using Ertl's reaction scheme for ammonia synthesis and the Langmuir assumptions, came to a very convincing agreement between high-pressure experimental results and the Hougen-Watson-type rate equation. [See also Bowker et al., 1988; and Stoltze and Nørskov, 1988].

Stoltze and Nørskov's work is significant in other aspects, too: the authors calculated sticking coefficients from ultrahigh vacuum work on single crystals and adsorption equilibrium constants from statistical thermodynamics. This is an example illustrating that it is possible to bridge the "pressure gap", that is, relate high-vacuum and high-pressure results—another controversial topic in catalysis.

The discussion about the need to account for nonuniformity of the active sites is still going on. Kiperman et al. [1989] mention a series of kinetic studies in which it was necessary to formulate the rate equations in terms of nonuniform surfaces. The correspondence on this matter with Boudart [1989] is well worth reading.

2.4 COMPLEX CATALYTIC REACTIONS

2.4.1 The Kinetic Modeling of Commercial Catalytic Processes

The feedstocks used in petroleum refining and in many petrochemical processes are generally very complex. They consist of homologous series of hydrocarbon families like paraffins, olefins, naphthenes and aromatics. These series each contain a large number of components, extending in a typical Vacuum Gas Oil (VGO) feedstock for a hydrocracker e.g., from C15 to C40 and each of these components leads to complicated reaction pathways, contributing in their own way to the product distribution. Conventional kinetic modeling would clearly lead to an unrealistic large number of rate coefficients. Because of this complexity, but also because of incomplete chemical analysis, the kinetic modeling of these processes has often been based upon reaction schemes consisting of a small number of reactions between pseudo-components or between "lumps" of species, sometimes defined more by physical properties, like boiling range, than by chemical characteristics. A typical example is the three lump model (Gas Oil, Gasoline, coke + dry gas), involving four reactions, used in

the sixties for the simulation of the catalytic cracking of gas oil [Nace et al., 1971]. The rate coefficients of such unrealistic models inevitably depend upon the feed composition, so that extensive and costly experimentation is required when the feedstock is changed. The second generation of models [Jacob et al., 1976], contains 10 lumps involved in 21 reactions. Even ten lumps or pseudo-components do not suffice to characterize in a satisfactory way the feed and effluent composition and properties. Consequently, the rate parameters can not be feed-invariant.

In recent years more detailed models were developed. Liguras and Allen [1989] described the conversion of Vacuum Gas Oil in terms of a relatively large number of pseudo-components, most of which are lumps in their own way. Klein et al. [1991] generated these pseudo-components from analytical characteristics using Monte-Carlo simulation. Instead, Quann and Jaffe [1992, 1996] and Christensen et al. [1999] in their "Structure Oriented Lumping" (SOL) expressed the chemical transformations by accounting for typical structures of the various types of molecules, without completely eliminating lumps and because of that, rate parameters that still depend upon the feedstock composition.

The approach to be presented here has been developed by Froment and co-workers [Baltanas et al., 1989; Vynckier and Froment, 1991; Froment, 2005]. The model retains the full detail of the reaction pathways of all the individual feed components and reaction intermediates. It is expressed in terms of elementary steps, like e.g., the shift of a methyl group along a paraffinic chain or the scission of a C-C-bond. These steps only involve moieties of the molecule and can occur in various positions of one and the same molecule. The isomerization of a normal paraffin into mono-branched paraffins e.g., is in fact a global transformation, called "reaction", but it consists in reality of a number of elementary steps. The number of types of elementary steps which are possible for hydrocarbons reacting on a given catalyst is much smaller than the number of molecules in the mixture. Assigning a unique rate coefficient to a certain type of elementary step would be an excessive simplification, however. The configuration of reactant and product, like their number of C-C-bonds and degree of branching also contributes to the value of this coefficient.

The reduction of the number of parameters of the kinetic model to a tractable level is possible only through a fundamental modeling of the rate coefficient itself, as already discussed in Section 1.7 of Chapter 1. Such an approach can be expected to lead to parameter values which are invariant with respect to the feedstock composition and has become possible through a better understanding of the underlying chemistry, growth in computational tools and advances in instrumental analysis. What follows deals with the fundamental kinetic modeling of processes catalyzed by acids, generally zeolites and

involving elementary steps of carbenium and carbonium ions, in one word: cations. Industrial examples are: catalytic reforming of naphtha for octane boosting, catalytic cracking and hydrocracking of VGO to produce lighter and more valuable fractions, alkylation of C_3 and C_4 components to produce high octane gasoline, isomerization of pentane and hexane into the corresponding iso-paraffins to be added to the gasoline fraction to increase their octane number and the conversion of methanol into olefins, the main building blocks of the petrochemical industry. In certain cases (catalytic reforming, hydrocracking, isomerization) the acid catalysts are loaded with metals that have a (de)hydrogenation function to produce (or remove) olefinic intermediates which are more reactive on the acid sites than the saturates. That does not affect the approach discussed here because the metal content is chosen sufficiently high to ensure that the rate determining step is still associated with steps occurring on the acid sites of the catalyst, producing a preferred product slate. This permits an entirely general kinetic approach, applicable to all the processes mentioned above.

The model development presented here is to be compared with the well accepted modeling of thermal cracking and of polymerization processes which both proceed through elementary steps of radical chemistry, as already outlined in Chapter 1 [Froment, 1992; Kiparissides, 1996].

2.4.2 Generation of the Network of Elementary Steps

For the model to be of real use the chemical steps of the process have to be accounted for with sufficient detail. Only then the product distribution, which is an important feature of complex commercial processes, can be reliably predicted. Typical elementary steps encountered in carbocation chemistry with various families of hydrocarbons are shown in Fig. 2.4.2-1. The species involved in charge-isomerization or hydride shift, in methyl shift, in branching isomerization via a protonated cyclopropane (PCP) intermediate or in the scission of a bond in β-position with respect to the C-atom carrying the positive charge are carbenium ions. The species with a pentavalent C-atom generated by hydride abstraction from a saturated component and which is subject to protolytic scission is a carbonium ion. This ion deserves special attention when the catalyst does not contain a dehydrogenating metal producing the intermediate olefins. It should be added here that different interpretations can not be excluded: Kazansky [1997] concluded from ab initio calculations and high resolution 13 MAS NMR that alkyl carbenium ions would really be intermediates which are rapidly converted into surface alkoxy ions that are covalently bonded to the surface oxygen ions.

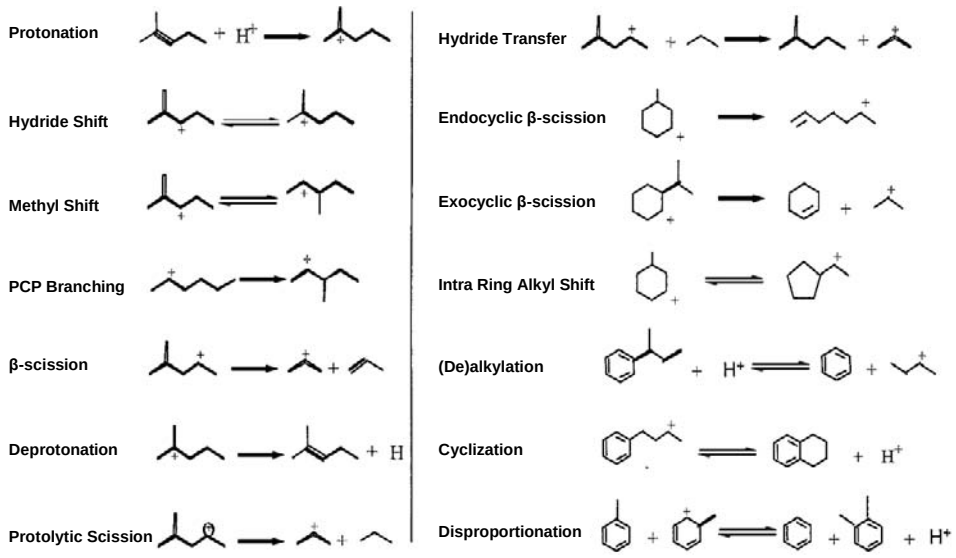

Figure 2.4.2-1

Elementary steps of cyclic and acyclic hydrocarbons and carbenium ions.

More recently alkoxide intermediates were given more importance and the carbenium ions formed out of intermediate olefins would really operate as the activated complex. The matter is not settled yet and an interesting discussion can be found in a paper by Boronat and Corma [2008].

With complex feedstocks this approach evidently leads to gigantic networks, whose generation needs to be automated by computer software. Such software was developed by Clymans and Froment [1984] for thermal cracking and radical based chemistry and by Baltanas and Froment [1985] for catalytic processes based upon carbocation chemistry. Further fundamental work and application to hydrocarbon pyrolysis, Fischer-Tropsch synthesis and amino acid biosynthesis was performed by Broadbelt and coworkers [2005].

Hydrocarbons can be represented either by a Boolean relation matrix or by a vector. The species is preferably characterized by a vector because the matrices, although sparse, take a large amount of computer memory. The matrices are required, however, to carry out operations reflecting the elementary steps. They are easily generated out of the vectors stored in the computer memory whenever required by the pathway development.

The elementary steps of carbocation chemistry shown in Fig. 2.4.2-1 can be computer-generated by applying a set of operations to the matrices. The algorithm is illustrated in Fig. 2.4.2-2 for the methyl-shift in the 2-methyl-3-heptyl carbenium ion, yielding the 3-methyl-2-heptyl carbenium ion. The program searches all the neighbors of the positively charged carbon atom and

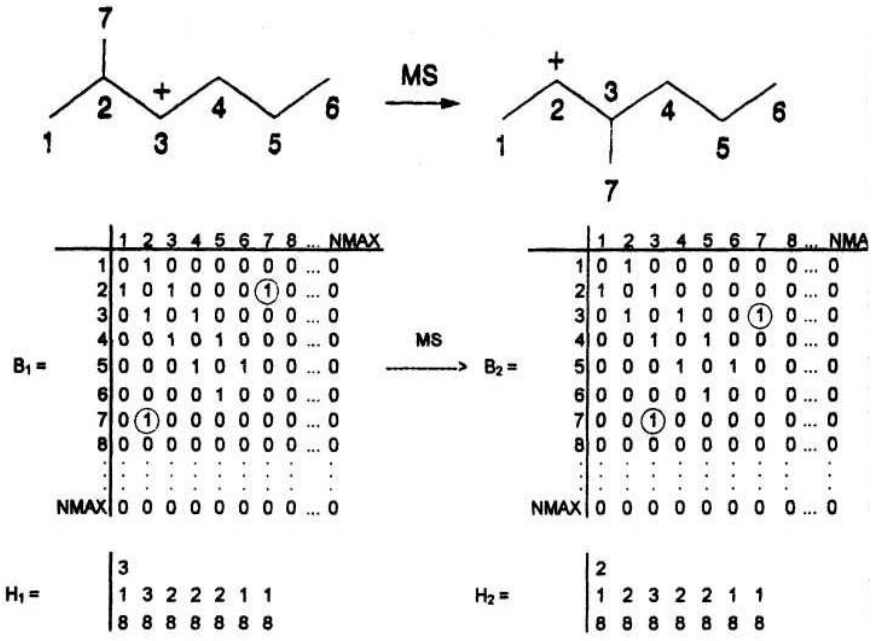

Figure 2.4.2-2

Matrix and vector representation of 2 Me-hexane and its isomer 3-Me-hexane [Froment, 1999].

checks if these are linked to any methyl group. If this is the case the bond between the neighbor and the methyl group is broken and the positively charged carbon atom is formed. The positive charge index is set to its new position. Notice that the sum of the 1's in a row reflects the nature of the carbon atom: primary, secondary, tertiary, a property that determines the behavior of that atom and that has to be accounted for in the reaction network development.

The vector representation always contains 3 rows. The first row contains one element only: zero for a molecule or the label of the C-atom carrying the positive charge for an ion. The elements of the second row indicate the degree of branching of the carbon atoms of the hydrocarbon, 1 for a primary, 2 for a secondary, 3 for a tertiary and 4 for a quaternary carbon atom. Information on the presence and position of a double bond or a positive charge is provided in arrays. Squaring the Boolean relation matrix and setting the elements on the diagonal to zero leads to the carbon atoms in β-position with respect to each other. These positions have to be detected for generating the cracking scheme of a carbenium ion through β-scission of a C-C-bond.

A simple aromatic hydrocarbon like *n*-hexyl-benzene yields 13 paraffins, 21 olefins, 53 aromatics, 80 aromatic olefins and 4 naphtheno-aromatics. The catalytic cracking of a C-20 *n*-paraffin generates 417 *i*-paraffins, 6417 olefins,

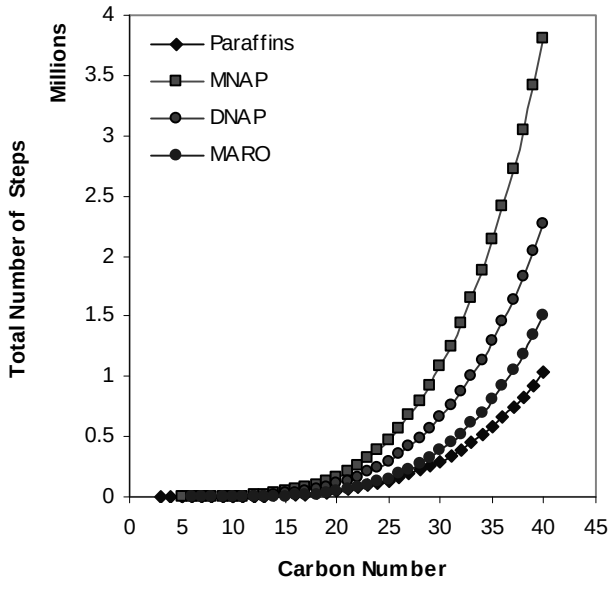

Figure 2.4.2-3

Number of elementary steps of some classes of the hydrocarbon families in hydrocracking: paraffins, P; mononaphthenes, MNAP; dinaphthenes, DNAP; monoaromatics, MARO. From Kumar and Froment [2007].

and 6938 acyclic carbenium ions; the cracking of a C-40 *n*-paraffin generates 4237 *i*-paraffins, 151057 olefins, and 155889 acyclic carbenium ions. Fig. 2.4.2-3 shows the number of elementary steps of a number of hydrocarbon (sub)classes in hydrocracking.

2.4.3 Modeling of the Rate Parameters

Beyond a number of assumptions and thermodynamic constraints a substantial reduction of the number of parameters to be determined from a set of experimental data is only possible by modeling the rate parameters. The modeling is based upon transition state theory. It makes use of the single event concept introduced by Froment and co-workers [Baltanas et al., 1989; Vynckier and Froment, 1991; Park and Froment, 2001; Feng et al., 1993; Svoboda et al., 1995; De Wachtere et al., 1999; Martinis and Froment, 2006; Kumar and Froment, 2007; Froment, 2005] and of the Evans-Polanyi relationship for the activation energy [1938].

2.4.3.1 The Single Event Concept

In Chapter 1 the transition state theory for the transformation of a reactant into a product via an intermediate, called activated complex, was introduced. That led to equation (1.7.1-15) [Eyring, 1935]:

$$k = \frac{k_B T}{h} \exp\left(\frac{\Delta S'^{\circ\ddagger}}{R}\right) \exp\left(-\frac{\Delta H'^{\circ\ddagger}}{RT}\right) \qquad (2.4.3.1\text{-}1)$$

The standard entropy that enters into the frequency factor of the rate coefficient contains electronic, translational, vibrational and rotational contributions:

$$\Delta S'^{\circ\ddagger} = \Delta S'^{\circ\ddagger}_{\text{trans}} + \Delta S'^{\circ\ddagger}_{\text{vib}} + \Delta S'^{\circ\ddagger}_{\text{elec}} + \Delta S'^{\circ\ddagger}_{\text{rot}}$$

The latter can be split into internal and external contributions, but both consist of an intrinsic term ($\hat{S}^{\circ\ddagger}$) and a term containing the symmetry number, σ, that reflects the structure of the species:

$$\Delta S'^{\circ\ddagger}_{\text{rot}} = \Delta \hat{S}^{\circ\ddagger} + R \ln(\sigma^r_{gl} / \sigma^{\ddagger}_{gl}) \qquad (2.4.3.1\text{-}2)$$

To account for the effect of n chiral centers, a "global" symmetry number, $\sigma_{gl} = \sigma_{ext}\sigma_{int} / 2^n$, is defined, so that the change in standard entropy due to symmetry changes associated with the transformation of the reactant into the activated complex is written:

$$\Delta S'^{\circ\ddagger}_{\text{sym}} = R \ln(\sigma^r_{gl} / \sigma^{\ddagger}_{gl}) \qquad (2.4.3.1\text{-}3)$$

where σ^{r}_{gl} and $\sigma^{\ddagger}_{gl}$ are the global symmetry numbers for the reactant and the transition state, respectively [Vynckier and Froment, 1991].

When the symmetry contribution (2.4.3.1-3) is factored out, equation (2.4.3.1-1) for the rate coefficient of a monomolecular elementary step e.g., becomes

$$k = \left(\frac{\sigma^r_{gl}}{\sigma^{\ddagger}_{gl}}\right)\left(\frac{k_B T}{h}\right) \exp\left(\frac{\Delta \hat{S}^{\circ\ddagger}}{R}\right) \exp\left(-\frac{\Delta H'^{\circ\ddagger}}{RT}\right) \qquad (2.4.3.1\text{-}4)$$

A "single event" frequency factor $\tilde{A}$ that does not depend upon the structure of the reactant and activated complex and is unique for a given type of elementary step can be defined as

$$\tilde{A} = \frac{k_B T}{h} \exp\left(\frac{\Delta \hat{S}^{\circ\ddagger}}{R}\right) \qquad (2.4.3.1\text{-}5)$$

It is advisable to consider $\tilde{A}$ as a parameter to be determined from the experimental data, although computer software now permits obtaining reasonably approximate values for TST parameters.

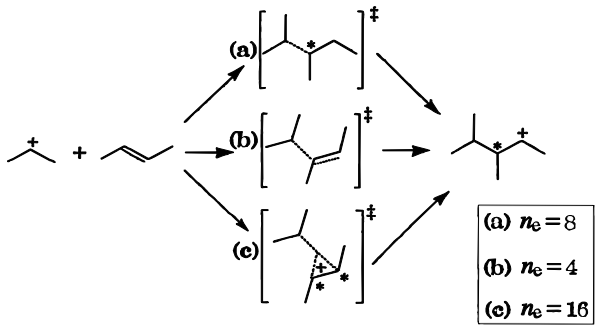

Figure 2.4.3.1-1

Number of single events in the elementary step propyl carbenium ion + butene as a function of the assumed activated complex. From Park and Froment [2001].

Equation (2.4.3.1-4) can also be written

$$A = n_e \tilde{A} \tag{2.4.3.1-6}$$

with

$$n_e = \sigma_{gl}^{r} / \sigma_{gl}^{\ddagger}$$

Hence, the frequency factor of an elementary step, A, is a multiple of that of a structure independent "single event" frequency factor, $\tilde{A}$.

The number of single events, n_e, is the ratio of the global symmetry numbers of the reactant and activated complex [Froment, 2005]. The calculation of the global symmetry numbers of the reacting and produced carbenium ion and of the activated complex requires their configuration, as already explained in Section 1.7. These can be determined by means of quantum chemical packages such as GAUSSIAN or GAMESS. The global symmetry numbers range from 6 for the methyl and ethyl carbenium ion to 9 for 3-octyl R^+ and 3-heptyl R^+ and much higher values for strongly branched R^+. When the carbenium ion has a bond with the zeolite the symmetry number differs from that of the free R^+ for which most of the numerical values available in the literature were obtained, but the effect of the link is the same for the activated complex, so that the number of single events is not affected [Park and Froment, 2001].

An example of how the configuration of the activated complex determines the number of single events of the elementary steps is shown in Fig. 2.4.3.1-1.

2.4.3.2 The Evans-Polanyi Relationship for the Activation Energy

Whereas the single event concept accounts for the effect of the structure on the frequency factor of an elementary step the linear free energy type relationship of

Evans and Polanyi [1938] accounts for the effect of structure and chain length upon the enthalpy contribution to the rate coefficient of a given type of elementary step through

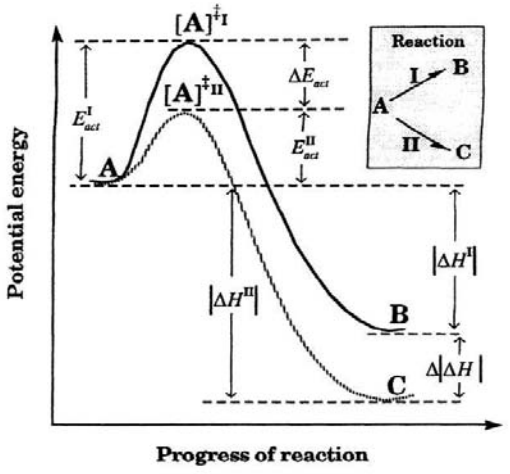

Figure 2.4.3.2-1

Relationship between the activation energies of two elementary steps belonging to the same type.

$$E_a = E° - \alpha \Delta H_r \qquad \text{(Exothermic reaction)} \qquad (2.4.3.2\text{-}1)$$

$$E_a = E° - (1 - \alpha)\Delta H_r \qquad \text{(Endothermic reaction)}$$

This relation permits the calculation of the activation energy, E_a, for any elementary step or single event pertaining to a certain type, provided α, the "transfer coefficient" and E°, the "intrinsic activation barrier" of a reference step of that type are available. They are the only 2 independent rate parameters for this type of step. Use of modern quantum chemical packages, such as GAUSSIAN, is essential for the calculation of ΔH_r, which is the difference between the heats of formation of reactant and product.

Written according to Arrhenius the temperature dependency of the single event rate coefficient becomes

$$\tilde{k} = \tilde{A} \exp\left(-\frac{E_a}{RT}\right) \qquad (2.4.3.2\text{-}2)$$

in which $\tilde{A}$ is a "single event" frequency factor, different from the usual one because the structure effect on the entropy change has been accounted for by factoring out the number of single events, n_e.

The single event concept and the Evans-Polanyi relationship drastically reduce the number of independent rate coefficients and thus enable addressing the complex problems encountered in industrial processes.

2.4.4 Application to Hydrocracking

The Hougen-Watson rate equations go further than the mass action kinetic equations in that they account explicitly for the interaction of the reacting species with the catalyst sites, but as to the mechanism they don't go very far beyond what is expressed by the stoichiometric equation. In Sections 2.4.2 and 2.4.3 on the other hand, the reaction was decomposed in elementary steps. This is now illustrated by means of an example.

Consider the hydrocracking of a long chain paraffin on a zeolite catalyst containing a metal (e.g., Pt). This is a type of reaction encountered in the Fischer-Tropsch route to gasoline and diesel and in which long chain paraffins are produced from CO and H_2 on a Fe or Co catalyst and subsequently cracked in the presence of hydrogen to the size corresponding to gasoline and diesel specifications. In this process the pressure is of the order of 150 bar so that the reacting hydrocarbons and their products are mainly in the liquid phase. In the following the species will be considered only inside the catalyst pore network, so as to focus only on the kinetic aspects.

After diffusion inside the zeolite the paraffin P is adsorbed on the metal (de)hydrogenation function. The concentration of the sorbed paraffin is given by the Langmuir isotherm

$$C_{Pi} = \frac{C_{sat} K_i P_i}{1 + \sum_i K_i P_i} \qquad (2.4.4\text{-}1)$$

The adsorbed P is dehydrogenated into several olefins:

$$P_i \rightleftarrows O_{ij} + H_2 \qquad (2.4.4\text{-}2)$$

The dehydrogenation step is assumed to be intrinsically much faster than the elementary steps of the olefins on the acid sites of the catalyst, so that it reaches quasi-equilibrium and

$$C_{Oij} = \frac{K_{DHij}}{p_{H2}} C_{Pi} \qquad (2.4.4\text{-}3)$$

The olefins are protonated on Bronstedt sites and produce carbenium ions

$$O_{ij} + H^+ \rightleftarrows R_{ik}^+ \qquad (2.4.4\text{-}4)$$

which in turn undergo isomerization and β-scission cracking steps on the acid sites:

$$R_{ik}^+ \rightleftarrows R_{lo}^+ \qquad (2.4.4\text{-}5)$$

$$R_{lo}^{+} \rightarrow R_{qr}^{+} + O_{uv} \tag{2.4.4-6}$$

After deprotonation of the carbenium ions and hydrogenation of the olefins the isoparaffins and the smaller paraffins resulting from the cracking desorb from the zeolite sites and diffuse back through the pore network.

The acid catalyzed steps are assumed to be rate determining so that the composite reaction rates of the paraffins are identical to those of the olefins on the acid sites:

$$R_{Pi} = \sum_{j} R_{Oij} \tag{2.4.4-7}$$

The rates of formation of the olefins on the acid sites can be expressed in terms of carbenium ion concentrations:

$$\begin{aligned} R_{O_{ij}} &= \sum_{k} n_e \tilde{k}_{De}(m_{ik};O_{ij}) C_{R_{ik}^{+}} - \sum_{k} n_e \tilde{k}_{\mathrm{Pr}}(m_{ik}) C_{O_{ij}} C_{H^{+}} \\ &+ \sum_{l}\sum_{o} n_e \tilde{k}_{Cr}(m_{lo};m_{qr},O_{ij}) C_{R_{lo}^{+}} \end{aligned} \tag{2.4.4-8}$$

n_e is specific for each type of elementary step and m_{ik} is the type (*s* or *t*) of carbenium ion R_{ik}^{+}. The concentrations of the carbenium ions are not directly accessible but can be calculated from the pseudo-steady-state approximation for the carbenium ions:

$$\begin{aligned} R_{R_{ik}^{+}} &= \sum_{j} n_e \tilde{k}_{\mathrm{Pr}}(m_{ik}) C_{O_{ij}} C_{H^{+}} - \sum_{j} n_e \tilde{k}_{De}(m_{ik};O_{ij}) C_{R_{ik}^{+}} \\ &- \sum_{l}\sum_{o} n_e \tilde{k}_{isom}(m_{ik};m_{lo}) C_{R_{ik}^{+}} + \sum_{l}\sum_{o} n_e \tilde{k}_{isom}(m_{lo};m_{ik}) C_{R_{lo}^{+}} \\ &- \sum_{l}\sum_{o} n_e \tilde{k}_{Cr}(m_{ik};m_{lo},O_{uv}) C_{R_{ik}^{+}} + \sum_{l}\sum_{o} n_e \tilde{k}_{Cr}(m_{lo};m_{ik},O_{uv}) C_{R_{lo}^{+}} = 0 \end{aligned} \tag{2.4.4-9}$$

and a balance on the Brønsted sites:

$$C_t = C_{H^{+}} + \sum_{i}\sum_{k} C_{R_{ik}^{+}} \tag{2.4.4-10}$$

Notice that the rate equations for the steps on the acid sites do not differ in structure from that dealt with in Chapter 1. They do not have the shape of the Hougen-Watson equations dealt with in the present Chapter 2 because the rate equations are written in terms of carbenium ions linked to the catalyst sites, so as to take advantage of the single event approach. As shown here they are not explicitly related to the fluid phase around the site, be it gaseous or liquid.

Equations (2.4.4-8) and (2.4.4-9) form a set of linear equations that can be solved to yield the unknown $C_{R^{+}ik}$ and C_{H}^{+}, which can in turn be used to

calculate the net rates of formation of the paraffins from (2.4.4-7) and (2.4.4-8). Similar equations to the above can be derived for naphthenes and aromatics.

Experimental data lead to parameter estimates revealing that the (de)protonation steps are in quasi-equilibrium and also that the concentration of R^+ on the active sites of the zeolite is extremely low compared to the total concentration of sites, so that (2.4.4-10) reduces to $C_t = C_H^+$. The consequence is that in this type of data collection the protonation equilibrium constant cannot be determined independently from the single event isomerization and cracking rate coefficients, leading to "composite" parameters for the latter.

The carbon number of the paraffin feed can extend up to 100. The reaction network has to be generated by computer as indicated in Sections 2.4.1 and 2.4.2. The reduction of the number of kinetic parameters is performed using the single event concept and the Evans-Polanyi relationship.

In later work on the hydrocracking of long chain paraffins on a Pt/US-Y zeolite Kumar and Froment [2007] derived the 14 independent rate parameters required to describe the rate processes on both the metal and the acid sites from experimental data on hexadecane. Of the total of 14 only 5 were required to describe the rate processes on the acid sites. The other 9 relate to the steps on the metal sites. It is worthwhile to have a kinetic model that considers the steps on either type or both of the catalyst functions to be rate determining. The equations can then be applied not only to predict the rates but beyond that also to evaluate the catalyst upon its aptitude to deliver the desired product distribution.

It is not possible, of course, to deal with a set of rate equations of the order of hundred thousands in the design of reactors or simply in the derivation of the rate parameters from experimental data. In the particular case of the hydrocracking of paraffins advantage can be taken from the experimental observations that permit to deduce that the hydride- and methyl-shift type isomerizations are very fast, intrinsically much faster than the branching isomerization through a protonated cyclo propane mechanism. That means that for a certain carbon-number the isomers with the same degree of branching can be considered to be at equilibrium among themselves. They can then be considered together, not as a "lump" or a pseudo-component, but as a Group of Isomers, GOI. Each member of such a group is allowed to react according to the rules of carbocation chemistry. For paraffins there are 4 such GOI: the *n*-paraffins, obviously a set of pure components, the GOI of respectively single-, di- and tri-branched isomers. The same is true for the olefins. The algebraic manipulations of this strict or thermodynamic grouping [Kuo and Wei, 1969] are described in detail by Kumar and Froment [2007].

An application of the above approach to the hydrocracking of VGO will be illustrated in Chapter 13 within the context of the simulation of three phase

reactors. It also draws the attention upon the need for more detailed analysis of the complex oil fractions, making use of high pressure liquid chromatography, the combination of gas chromatography and mass spectrometry and high resolution mass spectrometry, rather than the usual characterization methods.

2.5 EXPERIMENTAL REACTORS

The selection of the equipment for a kinetic study is a task that requires considerable expertise and attention. The success or failure of the study depends to a large extent on the judicious selection of the type of reactor and on the specific aspects of its design. The wrong selection of reactor type or an inadequate design will be revealed only after months of construction and months of operation, often too late to permit correction within the timing set for the process development. It should be kept in mind that there is no such thing as a "universal" reactor for bench scale studies of catalytic processes, but neither should the bench scale reactor be a reduced scale replica of the industrial reactor. In the very first place, the bench scale reactor has to provide the kinetic data that are required for the further development of the process. Specific aspects and effects of the industrial reactor have to be introduced through modelling and simulation, which is discussed extensively in Chapters 7 to 14 of this book.

Kinetic experiments on heterogeneous catalytic reactions are generally carried out in flow reactors. The flow reactor may be of the tubular type illustrated schematically in Fig. 2.5-1 and generally operated in single pass. To keep the interpretation as simple as possible the flow is considered to be perfectly ordered with uniform velocity (of the "plug flow" type, to be discussed in Chapter 9). This requires a sufficiently high velocity and a tube-to-particle diameter ratio of at least 10, to avoid too much short-circuiting along the wall, where the void fraction is higher than in the core of the bed. The tube diameter should not be too large either, however, to avoid radial gradients of temperature and concentration, which again lead to complications in the interpretation, as will be shown in Chapter 11. For this reason, temperature gradients in the longitudinal (i.e., in the flow direction) should also be avoided. Although adequate models, numerical methods and fast computers can handle non-isothermal situations, determining the functional form of the rate equation is realistic only on the basis of isothermal data. Isothermal conditions are not easily achieved with reactions having important heat effects. Care should be taken to minimize heat transfer resistance at the outside wall (for very exothermic reactions, for example, through the use of molten salts). Ultimately, however, no further gain can be realized because the most important resistance then becomes that at the inside wall, and this cannot be decreased at will, tied as it is to the

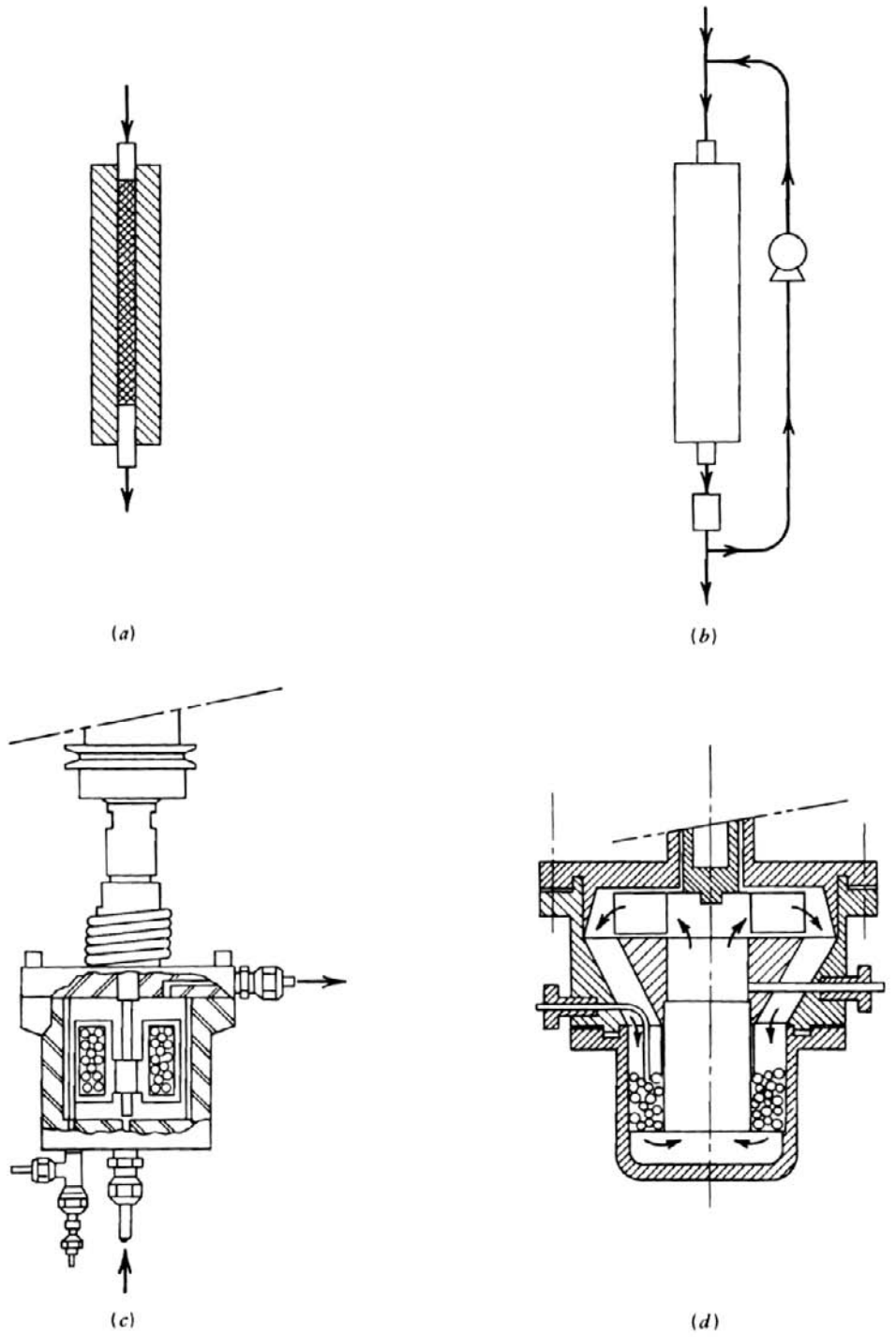

Figure 2.5-1

Various types of experimental reactors. (a) tubular reactor, (b) tubular reactor with recycle, (c) spinning basket reactor, and (d) reactor with internal recycle.

process conditions. If isothermicity is still not achieved, the only remaining possibility is to dilute the catalyst bed. Excessive dilution has to be avoided as well: all the fluid streamlines should hit the same number of catalyst particles.

Plug flow tubular reactors are generally operated in an integral way, that is, with relatively large conversion. This is achieved by choosing an amount of catalyst, W (kg), that is rather large with respect to the flow rate of the reference component A at the inlet, F_{A0} (kmol/h). By varying the ratio W/F_{A0}, a wide range of conversions (x) may be obtained. To determine the reaction rate, the conversion versus W/F_{A0} data pertaining to the same temperature have to be differentiated, as can be seen from the continuity equation for the reference component A in this type of reactor (see Chapter 9):

$$F_{A0}dx_A = r_A dW$$

Over the whole reactor,

$$\frac{W}{F_{A0}} = \int_{x_{A1}}^{x_{A2}} \frac{dx_A}{r_A}$$

Plug flow reactors can also be operated in a differential way. In that case the amount of catalyst is relatively small so that the conversion is limited and may be considered to occur at a nearly constant concentration of A. The continuity equation for A then becomes an algebraic equation:

$$F_{A0}\Delta x_A = r_A W \tag{2.5-1}$$

and r_A follows directly from the measured conversion.

Very accurate analytical methods are required in this case, of course. Furthermore, it is always a matter of debate how small the conversion has to be to fulfil the requirements. Figure 2.5-1 also shows a reactor with recycle. In kinetic investigations such a reactor is applied to come to a differential way of operation without excessive consumption of reactants. The recirculation may be internal, too, also shown in Fig. 2.5-1. It is clear that in both cases it is possible to come to a constant concentration of the reactant over the catalyst bed. These conditions correspond to those of complete mixing, a concept that will be discussed in Chapter 10 and whereby the rate is also derived from (2.5-1). Another way of achieving complete mixing of the fluid is also shown in Fig. 2.5-1. In this reactor the catalyst is inserted into a basket which spins inside a vessel. Recycle reactors or spinning basket reactors present serious challenges of mechanical nature when they have to operate at high temperatures and pressures, as is often required with petrochemical and petroleum refining processes. An

excellent review of laboratory reactors and their limitations has been presented by Weekman [1974].

Collecting reliable kinetics for multiphase processes (gas, solid, liquid) requires a reactor achieving intimate contact between the phases and ensuring a simple flow pattern so that the equations describing the operation remain simple and contain no parameters beyong those of the kinetic equations. This is practically impossible with the tubular bench scale reactor. Equipment that satisfies these requirements is the Robinson-Mahoney reactor — an extension of the gas/solid phase Berty reactor. It operates with complete mixing of the fluid phases which are intimately mixed and in excellent contact with all of the solid. What is measured in this way is a point conversion. To span a sufficient range of conversions the feed rates have to be varied. Vanrysselberghe and Froment [1998] and Froment et al. [2008] made extensive use of this type of reactor in their kinetic studies of hydrodesulfurization of Light Cycle Oil, a product fraction of catalytic cracking of vacuum gas oil and key components thereof.

In recent years the nonsteady state mode has been used to an increasing extent because it permits accessing intermediate steps of the overall reaction. Very complete reviews of this topic are presented by Mills and Lerou [1993] and by Keil [2001]. Specific reactors have been developed for transient studies of catalytic reaction schemes and kinetics. One example is the TAP-reactor ("Transient Analysis of Products") that is linked to a quadrupole mass spectrometer for on line analysis of the response to an inlet pulse of the reactants. The TAP reactor was introduced by Gleaves et al. in 1968 and commercialized in the early nineties. An example of application to the oxidation of o.xylene into phthalic anhydride was published by Creten et al. [1997], to the oxidation of methanol into formaldehyde by Lafyatis et al. [1994], to the oxidation of propylene into acroleine by Creten et al. [1995] and to the catalytic cracking of methylcyclohexane by Fierro et al. [2001]. "Stopped flow" experimentation is another efficient technique for the study of very fast reactions completed in the microsecond range, encountered in protein chemistry, e.g., in relaxation techniques an equilibrium state is perturbed and its recovery is followed on line. Sophisticated commercial equipment has been developed for these techniques.

Transport phenomena can seriously interfere with the reaction itself, and great care should be taken to eliminate these as much as possible in kinetic investigations.

Transfer resistances between the fluid and the solid, which is discussed more quantitatively in Chapter 3, may be minimized by sufficient turbulence. With the tubular reactor this requires a sufficiently high flow velocity. This is not so simple to realize in laboratory equipment, since the catalyst weight is often

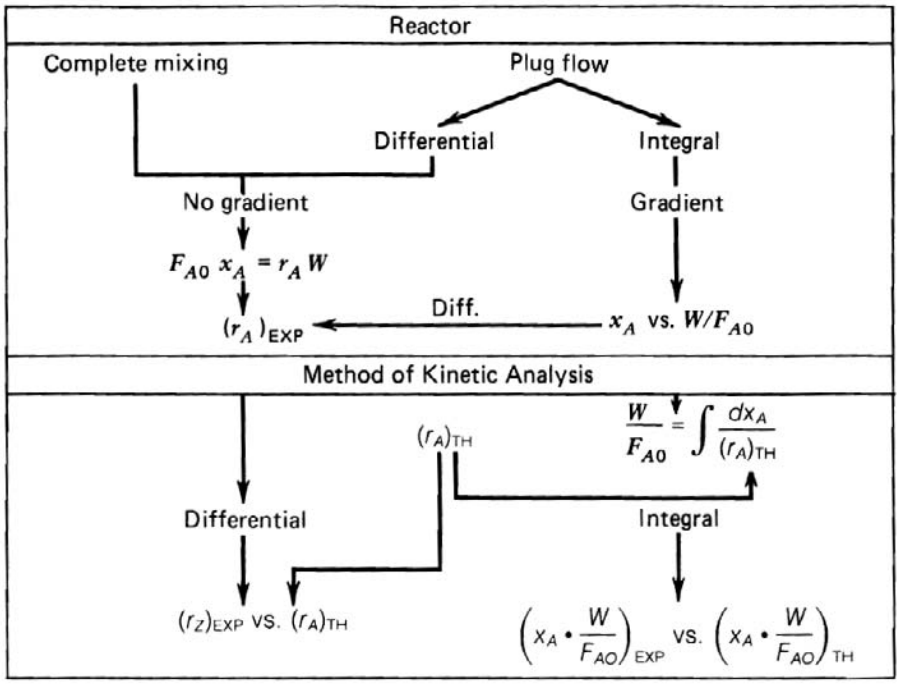

Figure 2.5-2

Relationship between differential and integral methods of kinetic analysis and differential and integral reactors.

restricted to avoid a too high consumption of reactant or to permit isothermal operation. With the spinning basket reactor, the speed of rotation has to be high.

Transport resistances inside the particle, also discussed in detail in Chapter 3, can also obscure the true rate of reaction. It is very difficult to determine the true reaction kinetic equation in the presence of this effect. Suffice it to say here that internal resistance can be decreased, for a given catalyst, by crushing the catalyst to reduce its dimensions. If the industrial reactor is to operate with a catalyst with which internal resistances are of importance, the laboratory investigation will involve experiments at several particle diameters.

The experimental results may be analyzed in two ways, as mentioned already in Chapter 1—by the differential method of kinetic analysis or by the integral method, which uses the x versus W/F_{A0} data. The results obtained in an integral reactor may be analyzed by the differential method provided the x versus W/F_{A0} curves are differentiated to get the rate, as illustrated by Fig. 2.5-2. Both methods are discussed in the following section.

2.6 MODEL DISCRIMINATION AND PARAMETER ESTIMATION

2.6.1 The Differential Method of Kinetic Analysis

A classical example of this method is the study of the dehydrogenation of isooctenes of Hougen and Watson [1947]. By considering all possible mechanisms and the rate-determining steps, they set up 18 possible rate equations. Each equation was confronted with the experimental data, and the criterion for acceptance of the model was that the parameters, k_1, K_A, K_R, … had to be positive. In this way 16 out of the18 possible models could be rejected. The choice between the seventeenth and the eighteenth model was based on the goodness of fit. The way Hougen and Watson determined the parameters deserves further discussion. Let us take the reaction $A \rightleftarrows R + S$, with the surface reaction on dual sites as the rate-controlling step, as an example. Equation (2.3.1-19) may be transformed into

$$y = a + bp_A + cp_R + dp_S \tag{2.6.1-1}$$

where

$$y = \sqrt{\frac{p_A - \dfrac{p_R p_S}{K}}{r_A}}$$

$$a = \frac{1}{\sqrt{kK_A}} \qquad b = \frac{K_A}{\sqrt{kK_A}}$$

$$c = \frac{K_R}{\sqrt{kK_A}} \qquad d = \frac{K_S}{\sqrt{kK_A}}$$

Equation (2.6.1-1) lends itself particularly well for determining *a*, *b*, *c* and *d*, which are combinations of the parameters of (2.3.1-19), by linear regression. This method has been criticized on the grounds that it is not sufficient to estimate the parameters but it also has to be shown that they are statistically significant. Furthermore, before rejecting a model because one or more parameters are negative, it has to be shown that they are significantly negative. This leads to statistical calculations (e.g., of the confidence intervals).

Later, Yang and Hougen [1950] proposed to discriminate on the basis of the total pressure dependence of the initial rate. Initial rates are measured, for example, with a feed consisting of only *A* when no products have yet been formed (i.e., when $p_R = p_S = 0$). Nowadays, this method is only one of the so-

called "intrinsic parameter methods" [see Kittrell and Mezaki, 1967]. Equations (2.3.1-19), (2.3.1-18), and (2.3.1-20) are then simplified into:

$$r_{A0} = \frac{k_{sr} K_A p_t}{(1 + k_A p_t)^2} \tag{2.6.1-2}$$

$$r_{A0} = k_A p_t \tag{2.6.1-3}$$

$$r_{A0} = \frac{k_R K p_t}{K K_R p_t} = \frac{k_R}{K_R} \tag{2.6.1-4}$$

Clearly, these relations reveal by mere inspection which one is the rate-determining step (see Fig. 2.6.1-1). A more complete set of curves encountered when r_{A0} is plotted versus the total pressure or versus the feed composition can be found in Yang and Hougen [1950].

These methods are illustrated in what follows on the basis of the data of Franckaerts and Froment [1964]. They studied the dehydrogenation of ethanol into acetaldehyde in an integral-type flow reactor over a Cu/Co on asbestos catalyst. In most of the experiments, the binary azeotropic mixture ethanol-water containing 13.5 mole percent water was used. This was called "pure feed." A certain number of experiments were also carried out with so-called "mixed feed", containing ethanol, water, and one of the reaction products, acetaldehyde, for reasons which will become obvious from what follows. Figure 2.6.1-2 shows an example of a conversion versus W/F_{A0} diagram at 1 bar with pure feed. Analogous diagrams were established at 3, 4, 7, and 10 bar, with both pure and mixed feed. From these results the initial rates were obtained by numerically differentiating the data at $x = 0$ and $W/F_{A0} = 0$. The temperature and total pressure

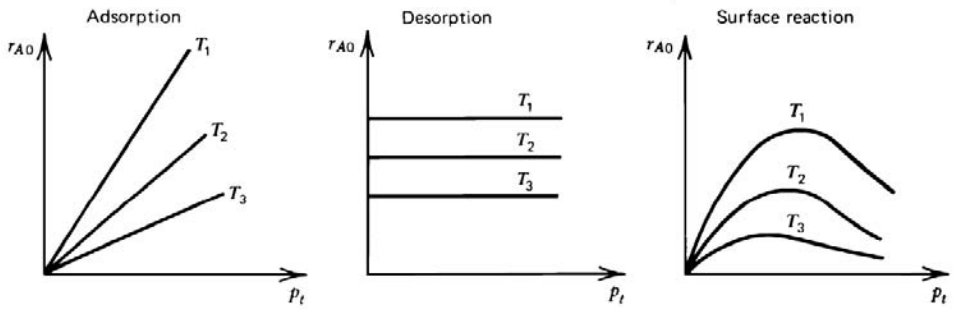

Figure 2.6.1-1

Initial rate versus total pressure for various rate-controlling steps.

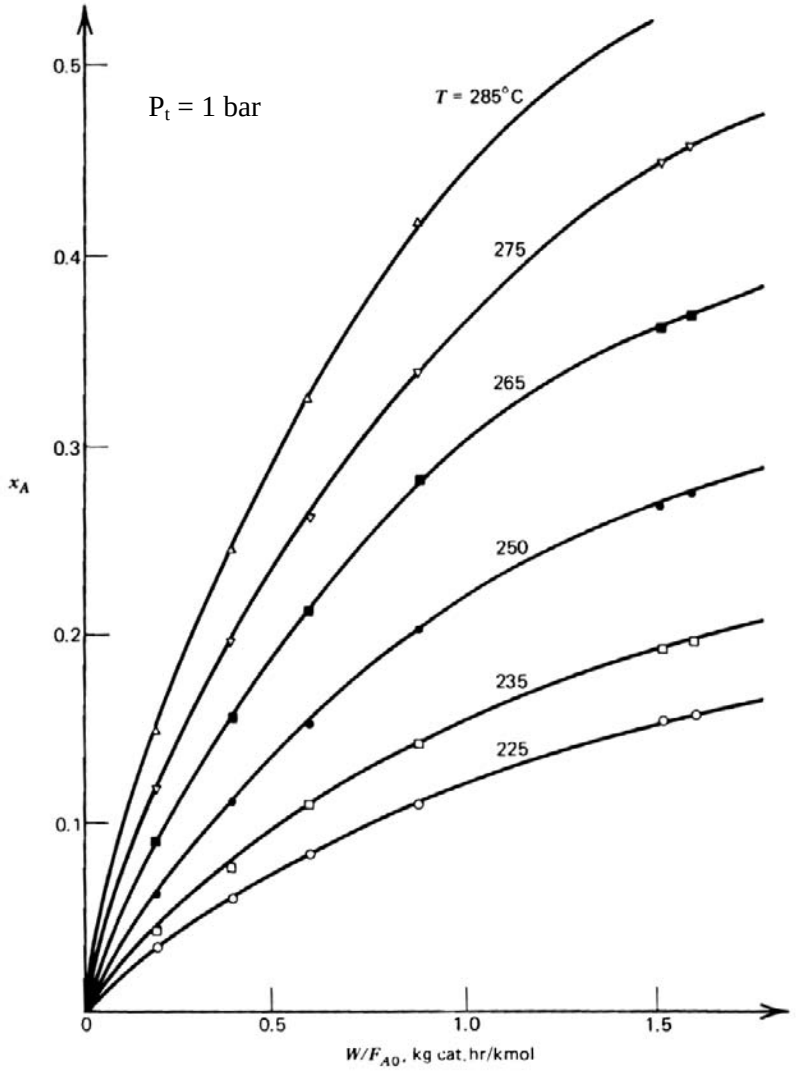

Figure 2.6.1-2

Ethanol dehydrogenation. Conversion versus space-time at various temperatures (W/F_{A0}, kg cat. hr/kmol). From Franckaerts and Froment [1964].

dependence of this initial rate is shown in Fig. 2.6.1-3. This clearly shows that the surface reaction on dual sites is the rate-determining step. An even more critical test results from rearranging (2.6.1-2):

$$\sqrt{\frac{p_t}{r_{A0}}} = \frac{1}{\sqrt{kK_A}} + \frac{K_A}{\sqrt{kK_A}}\, p_t \qquad (2.6.1\text{-}5)$$

which leads to the plot shown in Fig. 2.6.1-4. The parameters k and K_A may be calculated from the intercept and the slope. Of course, it is even better to use

linear regression methods. It is evident that the other parameters K_R and K_S can only be determined from the complete data, making use of the full (2.3.1-19):

$$r = \frac{kK_A(p_A - \frac{p_R p_S}{K})}{(1 + K_A p_A + K_R p_R + K_S p_S + K_W p_W)^2} \qquad (2.6.1\text{-}6)$$

where the additional term $K_W p_W$ takes into account the presence of water in the feed and its possible adsorption. To determine all the parameters of (2.6.1-6) the equation is transformed into

$$y = a + bp_A + cp_R + dp_S + ep_W \qquad (2.6.1\text{-}7)$$

where y, a, b, c and d have the form given in (2.6.1-1) and where

$$e = \frac{K_W}{\sqrt{kK_A}}$$

Note that for pure feed of A, the reaction stoichiometry dictates that $p_R = p_S$, and so from this type of data only the sum of $c + d = (K_R + K_S)/\sqrt{kK_A}$ can

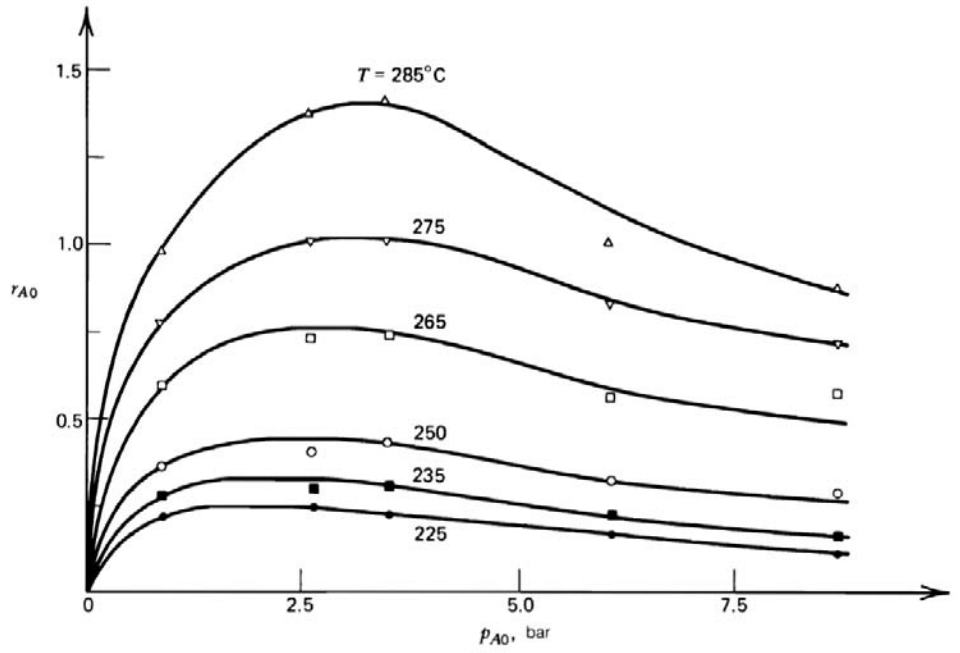

Figure 2.6.1-3

Ethanol dehydrogenation. Initial rate versus total pressure at various temperatures. From Franckaerts and Froment [1964].

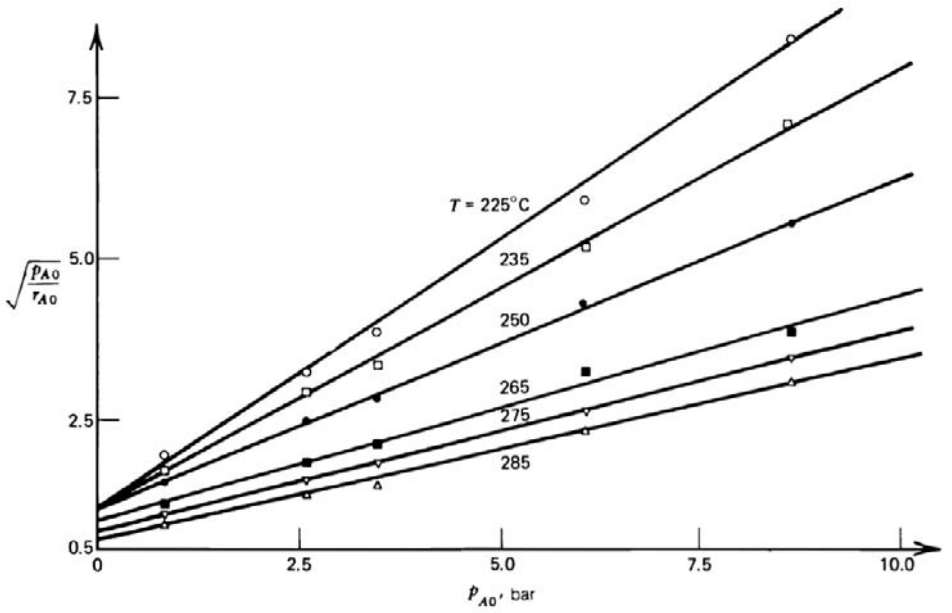

Figure 2.6.1-4

Ethanol dehydrogenation. Rearranged initial rate data. From Franckaerts and Froment [1964].

be determined. K_R and K_S can only be obtained individually when experimental results are available for which $p_R \neq p_S$. This requires mixed feeds containing *A* and either *R* or *S* or both in unequal amounts. The equilibrium constant *K* was obtained from thermodynamic data, and the partial pressure and rates were derived directly from the data. The groups, *a*, *b*, *c*, *d* and *e* may then be estimated by linear regression. Further calculations lead to the 95 percent confidence limits; the *t*-test, which tests for the significance of a regression coefficient; and an *F*-test, which determines if the regression is adequate. Franckaerts and Froment [1964] performed these estimations and the statistical calculations for different sets of experimental data as shown in Fig. 2.6.1-5 to illustrate which kind of experiments should be performed to determine all the parameters significantly. They also found K_W to be nonsignificant and deleted it from the equations without affecting the values of the other parameters. The final results are shown in the Arrhenius and Van't Hoff plot of Fig. 2.6.1-6.

From the standpoint of statistics, the rearrangement of (2.3.1-19) into (2.6.1-1) and the determination of the parameters from this equation may be criticized. What is minimized by linear regression are the $\sum$(residuals)^2 between experimental and calculated *y*-values. The theory requires the error to be normally distributed. This may be true for r_A, but not necessarily for the group $\sqrt{(p_A - p_R p_S / K)/r_A}$; and this may, in principle, affect the values of *k*, K_A, K_R,

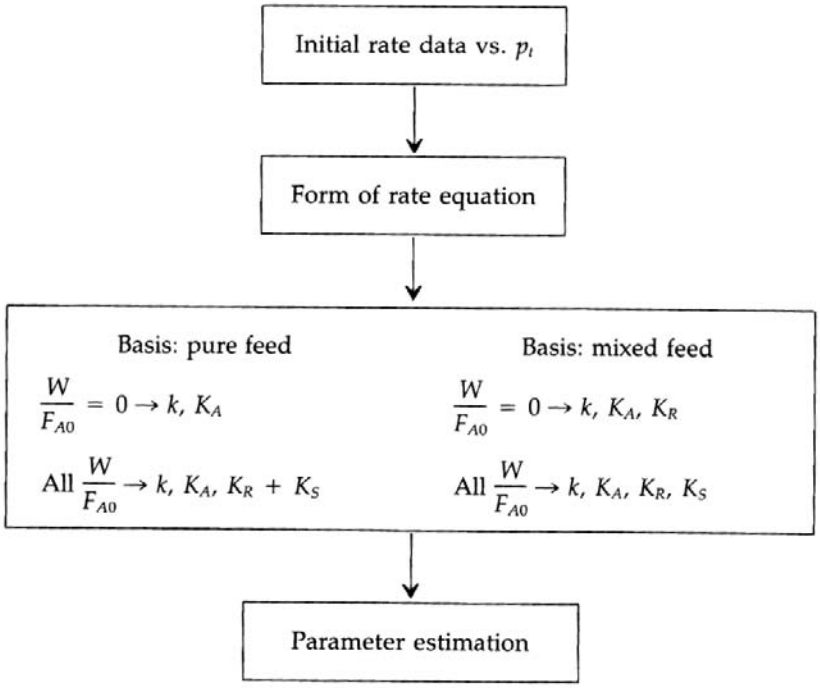

Figure 2.6.1-5

Strategy of experimentation for model discrimination and parameter estimation. From Franckaerts and Froment [1964].

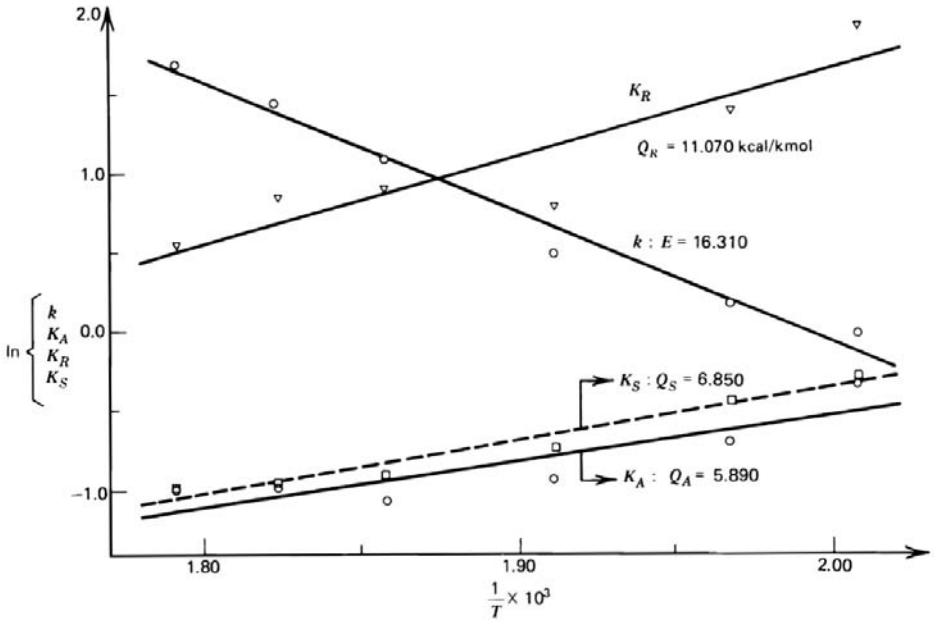

Figure 2.6.1-6

Ethanol dehydrogenation. Arrhenius plot for rate coefficient and Van't Hoff plot for adsorption coefficients. From Franckaerts and Froment [1964].

K_S, … However, when the rate equation is not rearranged, the regression is no longer linear, in general, and the minimization of the sum of squares of residuals becomes iterative. Search procedures are recommended for this [see Marquardt, 1963]. It is even possible to consider the data at all temperatures simultaneously. The Arrhenius law for the temperature dependence then enters explicitly into the equations and increases their nonlinear character.

2.6.2 The Integral Method of Kinetic Analysis

The integration of the rate equation leads to

$$\frac{W}{F_{A0}} = f(x, k, K_A, ...)$$

What can be minimized in this case is either $\sum[(W / F_{A0}) - (W \hat{/} F_{A0})]^2$ or $\sum(x - \hat{x})^2$.

The regression is generally nonlinear, and in the second case the computations are even more complicated because the equation is implicit in *x*. Peterson and Lapidus [1965] used the integral method with nonlinear regression on Franckaerts and Froment's data and found excellent agreement, as shown by Table 2.6.2-1. A further illustration of such agreement is based on Hosten and Froment's data on the isomerization of *n*-pentane [1971] as analyzed by Froment and Mezaki [1970].

The data indicated that the overall rate was independent of total pressure, supporting the conclusion that the isomerization step was rate controlling. Within this step, three partial steps may be distinguished: surface reaction, adsorption, or desorption, which could be rate controlling. The first was rejected because of (significant) negative parameter values. The adsorption and desorption rate expressions each contained two parameters—with values given in Table 2.6.2-2. Note here that discrimination based on the Yang-Hougen total pressure criterion is impossible in this case, since both rate equations are independent of total pressure.

TABLE 2.6.2-1
COMPARISON OF THE DIFFERENTIAL AND INTEGRAL METHODS AT 285°C

	k (kmol/kg cat. hr)	K_A (atm^{-1})	K_R (atm^{-1})	K_S (atm^{-1})
Differential method with linear regression	1.66	0.40	2.23	0.49
Integral method with nonlinear regression	2.00	0.39	3.17	0.47

In this case the expression W/F_{A0} versus $f(x)$ was linear in two groups containing the parameters, so that linear regression was possible when the sum of squares on W/F_{A0} was minimized. When the objective function was based on the conversion itself, an implicit equation had to be solved and the regression was nonlinear. Only approximate confidence intervals can then be calculated from a linearization of the model equation in the vicinity of the minimum of the objective function.

TABLE 2.6.2-2
ISOMERIZATION OF *N*-PENTANE
COMPARISON OF METHODS FOR PARAMETER ESTIMATION[a]

$$n\text{-pentane} \overset{\text{Pt}}{\rightleftharpoons} n\text{-pentene} \overset{Al_2O_3 + Cl_2}{\rightleftharpoons} \text{isopentene} \overset{\text{Pt}}{\rightleftharpoons} \text{isopentane}$$

Integral Method

Desorption rate controlling: $r = \dfrac{k\left(p_A - \dfrac{p_B}{K}\right)}{p_{H_2} + K_A p_A} \rightarrow \dfrac{W}{F_{A0}} = \dfrac{1}{k}(\alpha_1 + \alpha_2 K_A)$

Regression	Linear	Nonlinear
k (kmol/kg cat. bar h)	0.93 ± 0.21	0.92 ± 0.09[b]
K_A (bar^{-1})	2.20 ± 1.94	2.28 ± 0.95[b]

Sum of squares of residuals: 1.05 $\left(\text{on } \dfrac{W}{F_{A0}}\right)$ 2.82×10^{-3} (on x)

Adsorption rate controlling: $r = \dfrac{k\left(p_A - \dfrac{p_B}{K}\right)}{p_{H_2} + K_B p_B} \rightarrow \dfrac{W}{F_{A0}} = \dfrac{1}{k}(\alpha_1 + \alpha_3 K_B)$

Regression	Linear	Nonlinear
k (kmol/kg cat. bar h)	0.89 ± 0.10	0.89 ± 0.07[b]
K_B (bar^{-1})	6.57 ± 3.47	8.50 ± 2.78[b]

Sum of squares of residuals: 0.70 $\left(\text{on } \dfrac{W}{F_{A0}}\right)$ 1.25×10^{-3} (on x)

[a] Subscript A represents *n*-pentane; subscript B is isopentane; α_1, α_2, and α_3 are functions of the feed composition, and of K, x and η, given in the original paper of Hosten and Froment [1971]. K is the equilibrium constant, x is the conversion, and η the selectivity for the isomerization, accounting for a small fraction of the pentane converted by hydrocracking.
[b] Approximate 95 percent confidence interval.

Again the agreement between the linear and nonlinear regressions is excellent, which is probably due to the precision of the data. Poor data may give differences, but they probably do not deserve such a refined treatment, in any event. They should be revised experimentally in the first place.

2.6.3 Parameter Estimation and Statistical Testing of Models and Parameters in Single Reactions

In the examples given above, reference was made to parameter estimation using regression methods and to the statistical testing of models and parameters. In the present section this topic will be presented in a systematic way.

2.6.3.1 Models That Are Linear in the Parameters

Let the kinetic model of the reaction relating the dependent variable y, the settings of the independent variables x, and the p parameters β, be an algebraic equation. For n observations of y (which can be conversion or rate)

$$\mathbf{y} = \boldsymbol{X}\boldsymbol{\beta} + \boldsymbol{\varepsilon} \qquad (2.6.3.1\text{-}1)$$

in which $\boldsymbol{\varepsilon}$ is the column vector of n experimental errors associated with the n observations.

In Section 2.6.1, dealing with the differential method of kinetic analysis, y represents

$$\sqrt{\frac{p_A - \dfrac{p_R p_S}{K}}{r_A}}$$

and x represents the various partial pressures p_A, p_R, and p_S. With the integral method of kinetic analysis, y represents W/F_{A0} and x groups containing the conversion, total pressure and eventually a dilution ratio, as will be illustrated in Example 2.7.1.1.B.

Estimates $\mathbf{b}$ for the parameters $\boldsymbol{\beta}$ are determined by minimization of the objective function — the sum of squares of residuals:

$$\boldsymbol{\varepsilon}^T \boldsymbol{\varepsilon} \xrightarrow{\boldsymbol{\beta}} \text{Min} \qquad (2.6.3.1\text{-}2)$$

where $\boldsymbol{\varepsilon}^T$ is the transpose of $\boldsymbol{\varepsilon}$. The minimization yields the vector of parameter estimates

$$\mathbf{b} = (\boldsymbol{X}^T \boldsymbol{X})^{-1} \boldsymbol{X}^T \mathbf{y} \qquad (2.6.3.1\text{-}3)$$

Testing hypotheses, in other words, testing models and their parameters, requires information on the experimental error. When the errors are normally or Gauss-distributed, have zero mean, constant variance σ^2, and are uncorrelated, the error covariance matrix is simply

$$\mathbf{V}(\boldsymbol{\varepsilon}) = \mathbf{I}\sigma^2 \tag{2.6.3.1-4}$$

where **I** is the identity matrix.
In that case, **b** is an unbiased estimate of **β**, and the $(p \times p)$-variance-covariance matrix of the estimates **b** is given by

$$\mathbf{V}(\mathbf{b}) = (\boldsymbol{X}^T \boldsymbol{X})^{-1}\sigma^2 \tag{2.6.3.1-5}$$

When the model is adequate, that is, when there is no lack of fit, an unbiased estimate of the experimental error variance σ^2 is given by

$$s^2 = \frac{\sum_{i=1}^{n}(y_i - \hat{y}_i)^2}{n - p} \tag{2.6.3.1-6}$$

n being the number of experiments.

When the errors are normally distributed with zero mean but the error variance is not constant, and the errors are interdependent, **I** in (2.6.3.1-4) becomes a full $(n \times n)$ matrix **V**, and the unweighted least squares method as applied in (2.6.3.1-2 and 3) is not appropriate any longer to determine **b**. The objective function then becomes

$$S(\boldsymbol{\beta}) = \sum_{i=1}^{n}\sum_{l=1}^{n} v^{il}(y_i - \hat{y}_i)(y_l - \hat{y}_l) \overset{\boldsymbol{\beta}}{\rightarrow} \text{Min} \tag{2.6.3.1-7}$$

in which v^{il} are the elements of the inverse of the matrix **V**. The parameter estimates are then obtained from

$$\mathbf{b} = (\boldsymbol{X}^T \mathbf{V}^{-1} \boldsymbol{X})^{-1} \boldsymbol{X}^T \mathbf{V}^{-1} \mathbf{y} \tag{2.6.3.1-8}$$

and the covariance matrix of these estimates is obtained from

$$\mathbf{V}(\mathbf{b}) = (\boldsymbol{X}^T \mathbf{V}^{-1} \boldsymbol{X})^{-1} \sigma^2 \tag{2.6.3.1-9}$$

An estimate s^2 of what is now an unknown proportionality factor σ^2 is calculated from

$$s^2 = \frac{(\mathbf{y} - \boldsymbol{X}\mathbf{b})^T \mathbf{V}^{-1} (\mathbf{y} - \boldsymbol{X}\mathbf{b})}{n - p} \tag{2.6.3.1-10}$$

instead of (2.6.3.1-6).

Various sums of square are used to test models. Figure 2.6.3.1-1 shows the partitioning of the total sum of square into its components. The model adequacy can be tested when the "lack of fit" sum of squares and the "pure error" sum of squares are available. The latter can be calculated when n_e replicated experiments have been performed. An estimate of the "pure error" variance is obtained from

$$s_e^2 = \frac{\text{pure error sum of squares}}{\text{number of degrees of freedom}} = \frac{\sum_{j=1}^{n_e} (y_j - \bar{y})^2}{n_e - 1} \qquad (2.6.3.1\text{-}11)$$

where $\bar{y}$ represents the arithmetic mean of the n_e replicate observations. The *F*-test on model adequacy is based upon the following ratio F_c, which is compared with the corresponding tabulated value

$$F_c = \frac{\dfrac{\text{lack of fit sum of squares}}{n - p - n_e + 1}}{\dfrac{\text{pure error sum of squares}}{n_e - 1}} \begin{matrix} ? \\ > \\ < \end{matrix} F(n - p - n_e + 1, n_e - 1; 1 - \alpha) \quad (2.6.3.1\text{-}12)$$

$F(n–p–n_e+1, n_e–1; 1–\alpha)$ is the tabulated α-percentage point of the *F*-distribution with $n–p–n_e+1$ and $n_e–1$ degrees of freedom. If the calculated value exceeds the tabulated value, there is a probability of $1–\alpha$ (e.g., 95%) that the model is inadequate. The model is rejected because of lack of fit.

When replicates are not available and the pure error sum of squares is not known, a different *F*-test can be applied. It is based upon the regression sum of squares and the residual sum of squares:

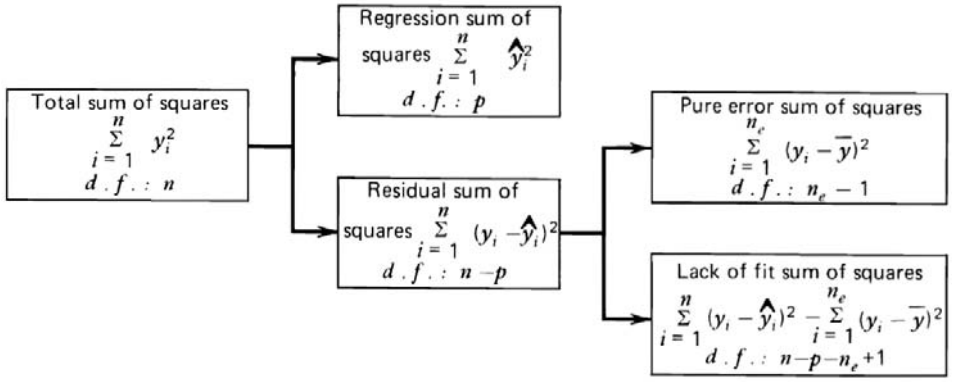

Figure 2.6.3.1-1
Partitioning of the sums of squares. After Draper and Smith [1966].

$$F_c = \frac{\sum_{i=1}^{n} \frac{\hat{y}_i^2}{p}}{\sum_{i=1}^{n} \frac{(y_i - \hat{y}_i)^2}{n-p}} \begin{matrix} ? \\ > \\ < \end{matrix} F(p, n-p; 1-\alpha) \qquad (2.6.3.1\text{-}13)$$

The calculated ratio is distributed like $F(p, n–p)$. If F_c is larger than $F(p, n–p; 1–\alpha)$, the regression is considered to be meaningful. Among a set of rival models, the one with the highest F_c would be considered the "best", without guarantee, however, that it would be statistically "adequate".

The estimates of the model parameters can also be tested. When the errors are normally distributed with zero mean and constant variance, the random variable

$$\frac{|b_j - \beta_j|}{\sigma(b_j)} = n \qquad (2.6.3.1\text{-}14)$$

is distributed like the normal (Gaussian) distribution. At the 95% probability level, the calculated n values have to exceed 1.96 for b_j to be significantly different from a reference value of β_j, generally zero. When the error variance $\sigma^2(b_j)$ or the standard deviation $\sigma(b_j)$ is not known, an unbiased estimate $s(b_j)$ is used instead. The random variable

$$\frac{|b_j - \beta_j|}{s(b_j)} \text{ with } s(b_j) = \sqrt{[\mathbf{V}(b)]_{jj}} \qquad (2.6.3.1\text{-}15)$$

is distributed like $t(n–p)$. This property is used in a two-sided t-test to verify if the estimate b_j differs from a reference value, generally zero, when the other parameters are kept constant at their optimal estimated value. When

$$t_c = \frac{|b_j - 0|}{s(b_j)} > t\left(n-p; 1-\frac{\alpha}{2}\right) \qquad (2.6.3.1\text{-}16)$$

the hypothesis that b_j would be zero can be rejected. The quantity $t(n–p; 1–(\alpha/2))$ is the tabulated $\alpha/2$ percentage point of the t distribution with $n–p$ degrees of freedom. With α generally taken to be 0.05, the probability of having rejected a correct hypothesis (namely, $b_j = 0$) is 0.05 only. Of greater importance than this test against a single reference value are the confidence limits. These are limits on the complete collection of reference values which are not significantly different from the optimal estimates b_j at the selected probability level $1–\alpha$, provided that

the other estimates are kept constant upon their optimal estimate. The confidence intervals are defined by

$$b_j - t\left(n-p;1-\frac{\alpha}{2}\right)s(b_j) \le \beta_j \le b_j + t\left(n-p;1-\frac{\alpha}{2}\right)s(b_j) \qquad (2.6.3.1\text{-}17)$$

They are symmetrical with respect to the optimal point estimate b_j.

The joint confidence region defines the region of joint parameter uncertainty, and it is obtained when all the parameters vary simultaneously. All parameter sets $\boldsymbol{\beta}$ that satisfy the relation

$$S(\boldsymbol{\beta}) = S(\mathbf{b})\left[1+\frac{p}{n-p}F(p,n-p,1-\alpha)\right] \qquad (2.6.3.1\text{-}18)$$

form the surface enclosing all the parameter combinations that do not significantly differ from the optimal estimates **b** at the probability level 1–α. $S(\boldsymbol{\beta})$ represents the numerical value of the objective function $(\mathbf{y}-\boldsymbol{X}\boldsymbol{\beta})^T(\mathbf{y}-\boldsymbol{X}\boldsymbol{\beta})$ evaluated at a set of values $\boldsymbol{\beta}$ for the parameters, whereas $S(\mathbf{b})$ is the value at the optimal parameter estimates, namely, the minimum residual sum of squares.

This contour can be shown to be also given by

$$(\mathbf{b}-\boldsymbol{\beta})^T\boldsymbol{X}^T\boldsymbol{X}(\mathbf{b}-\boldsymbol{\beta}) = ps^2F(p,n-p;1-\alpha) \qquad (2.6.3.1\text{-}19)$$

Equation (2.6.3.1-19) represents a p-dimensional hyperellipsoid in parameter space, centered at **b** (Fig. 2.6.3.1-2).

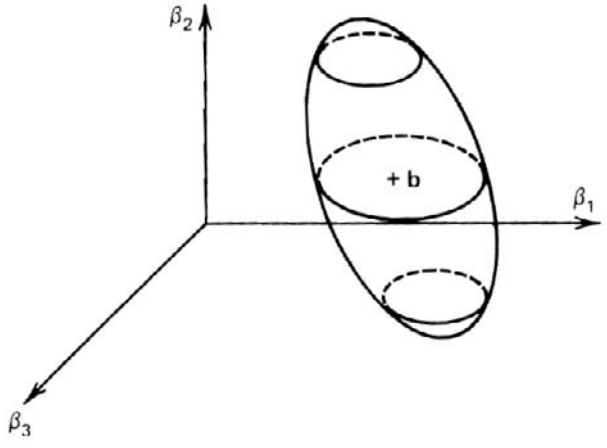

Figure 2.6.3.1-2
Joint confidence region in three dimensional space.

2.6.3.2 Models That Are Nonlinear in the Parameters

Let such a model be represented by

$$y_i = f(\mathbf{x}_i, \boldsymbol{\beta}) + \varepsilon_i \tag{2.6.3.2-1}$$

The minimization of the least squares criterion

$$S(\boldsymbol{\beta}) = \sum_{i=1}^{n} \left[y_i - f(\mathbf{x}_i, \boldsymbol{\beta}) \right]^2 \xrightarrow{\boldsymbol{\beta}} \text{Min} \tag{2.6.3.2-2}$$

by the Newton-Gauss technique or variants thereof leads to an iterative cycle. These methods are based upon a linearization of the model equation with respect to the parameters by a Taylor series development around an initial guess $\mathbf{b}_0$ for $\boldsymbol{\beta}$, neglecting all partial derivatives of second and higher order. The resulting set of observation equations is linear in the Δb_j :

$$f(\mathbf{x}_i, \boldsymbol{\beta}) \cong f(\mathbf{x}_i, \mathbf{b}_0) + \sum_{j=1}^{p} \left. \frac{\partial f(\mathbf{x}_i, \boldsymbol{\beta})}{\partial \beta_j} \right|_{\boldsymbol{\beta}=\mathbf{b}_0} \Delta b_j \tag{2.6.3.2-3}$$

With models that are nonlinear in the parameters, the derivatives in (2.6.3.2-3) do not lead to the settings $\mathbf{x}$ of the independent variables, as in (2.6.3.1-3), but to

$$\Delta \mathbf{b}_{s+1} = (\mathbf{J}_s^T \mathbf{J}_s)^{-1} \mathbf{J}_s^T \mathbf{r}_s \tag{2.6.3.2-4}$$

where

$$\mathbf{J}_s = \left[J_{s_{ij}} \right] = \left[\left. \frac{\partial f(\mathbf{x}_i, \boldsymbol{\beta})}{\partial \beta_j} \right|_{\boldsymbol{\beta}=\mathbf{b}_s} \right] \tag{2.6.3.2-5}$$

and

$$\mathbf{r}_s = \mathbf{y} - \mathbf{f}(\mathbf{x}, \mathbf{b}_s) \tag{2.6.3.2-6}$$

This value will not lead in one step to the minimum of (2.6.3.1-2). The value $\Delta \mathbf{b}_{s+1}$ is then added to $\mathbf{b}_s$ and so on, until convergence is achieved. The method converges rapidly close to the minimum of $S(\boldsymbol{\beta})$ but with poor initial values of $\mathbf{b}_0$ it may not. To avoid divergence in this region, Marquardt [1963] worked out a "compromise" between the method of steepest descent and that of Newton-Gauss. The steepest descent method is most efficient far from the minimum, whereas it is the other way around close to the minimum. The compromise has the ability to change the size and the direction of the optimization step by means of a scalar parameter λ, which is a Lagrangian multiplier, so that (2.6.3.2-4) becomes

$$\Delta \mathbf{b}_{s+1} = (\mathbf{J}_s^T \mathbf{J}_s + \lambda_s \mathbf{I})^{-1} \mathbf{J}_s^T \mathbf{r}_s \tag{2.6.3.2-7}$$

where **I** is a $p \times p$ identity matrix. λ is adapted during the minimization. When λ is infinite, the direction is that of the steepest gradient, but the step size would be zero. When λ is set to zero, the direction is that of the Newton-Gauss method, but the step size is maximum. A constraint is used to ensure that $S(\mathbf{b}_{s+1}) \leq S(\mathbf{b}_s)$ to avoid step sizes reaching into a zone where the Taylor series approximation becomes deficient.

Significance tests (*t*-values) for the individual parameter estimates can be performed, as well as an overall significance test (*F*-value) of the regression. Provided that replicate experiments have been performed, the model adequacy (*F*-value) can be tested.

The minimization routines mentioned above are very sensitive to the selected set of initial values for the unknown parameters. If that set is too far away from the optimal set, divergence is possible or convergence to some local minimum, yielding erroneous values for the parameters. Methods that do not use first and second derivatives but only the function value itself, like Rosenbrock's method, may require less expertise but they are extremely slow in reaching the minimum. One method that only uses function values and has been successfully applied in recent years is the "evolutionary" algorithm called "Genetic Algorithm" (GA) [Mitchell, 1996; Moros et al., 1996; Falkenhauer, 1997]. It starts from a relatively large number n_{sog} (100; … 500), of sets of randomly chosen values of the parameters, spread out over that part of the parameter hyperspace that comprises the possible ranges of parameter values and, therefore, the optimal set. Each set is encoded as a string of bits. The objective function is calculated for each set. The parameter sets are then ranked according to the value of their corresponding objective function. If the selected convergence test is not satisfied, another step, i.e., another iteration on the parameter sets is required. The best sets of the previous iteration may be retained into the next, but a number of others will be adapted. Strings of higher quality are combined two by two to produce sets for the next GA iteration. Each combination consists of an exchange of portions of the strings, an operation called crossover. The new sets of parameters are further adapted by so called mutation, whereby randomly chosen bits of an encoded set may switch between 0 and 1. A balance should be kept between diversity of the sets and their convergence so as to avoid premature convergence and limitation of the search to a part of the hyperspace perhaps containing only a local minimum. That imposes restrictions on the number or "rate" or "probability" of crossover and mutation and it is advised to apply the GA with different values of these probabilities. A new generation of sets of parameters is thus created and the values of the corresponding objective function are calculated again until a GA-criterion is satisfied and final values for the parameters are obtained. In general the GA is good at finding a promising region

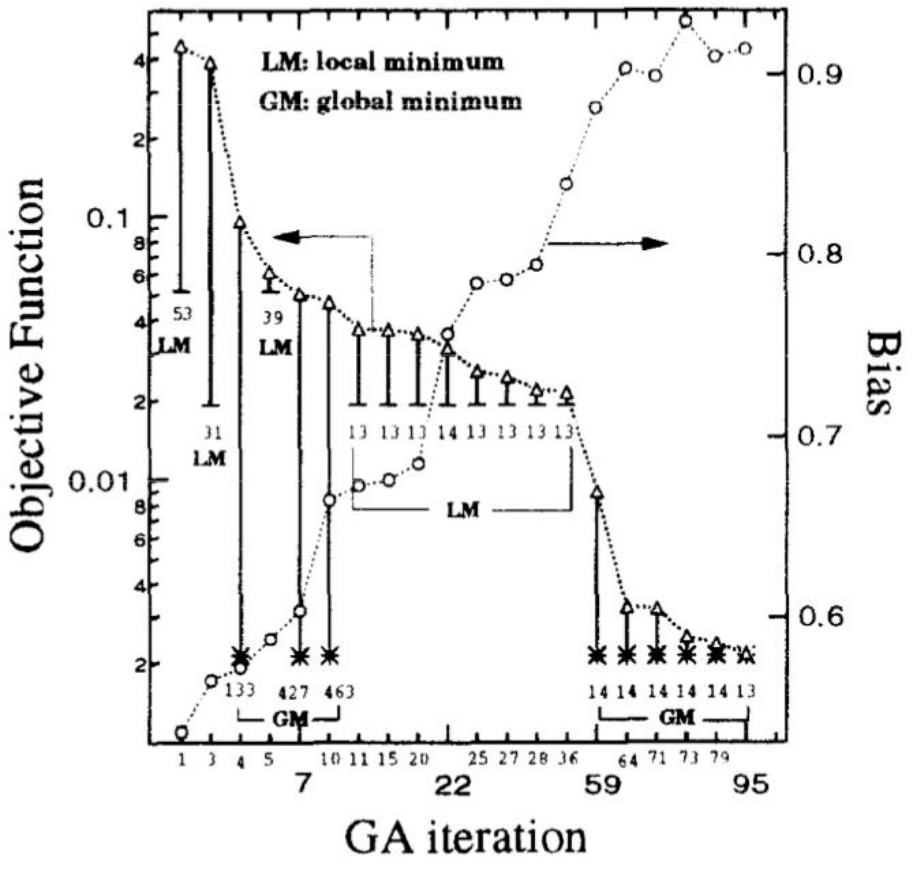

Figure 2.6.3.2-1
Performance of a hybrid GA. From Park and Froment [1998].

of parameter space but, because of the discretization, not as good at fine tuning as the optimizers mentioned above. This is why Park and Froment [1998] combined the GA with Marquardt's approach into a "Hybrid Genetic Algorithm" and applied it to the estimation of the kinetic parameters of the dehydrogenation of ethanol, already dealt with under Section 2.6.1. Fig. 2.6.3.2-1 illustrates the performance of such a hybrid GA. A recent example of application was published by Saha and Ghoshal [2007].

2.6.4 Parameter Estimation and Statistical Testing of Models and Parameters in Multiple Reactions

There are only a few examples of the application of the Hougen-Watson formalism to more than a single reaction. De Deken et al. [1982] developed Hougen-Watson rate equations for steam reforming, described in terms of two parallel reactions. Marin and Froment [1982] developed a set of rate equations

for hexane reforming on Pt/Al_2O_3 catalysts, and Van Trimpont et al. [1986] for heptane reforming. Van Parijs and Froment [1986a and b] and Van Parijs et al. [1986] investigated hydrodesulfurization on Co/Mo catalysts by means of model components like thiophene and benzothiophene. They used two or three simultaneous rate equations to describe the kinetic behavior. This work considered both a constant and a varying concentration of active sites and will be used here as a case history to illustrate various important features.

The formulas are relatively straightforward extensions of those presented above in Section 2.6.3 and will be briefly mentioned here. Let the kinetic model consist of v linear algebraic equations relating the v dependent and observed variables y to the independent variables x and containing p parameters, represented by $\boldsymbol{\beta}$:

$$\begin{aligned} \mathbf{y}_1 &= \boldsymbol{X}_1\boldsymbol{\beta} + \boldsymbol{\varepsilon}_1 \\ \mathbf{y}_2 &= \boldsymbol{X}_2\boldsymbol{\beta} + \boldsymbol{\varepsilon}_2 \\ &\vdots \\ \mathbf{y}_h &= \boldsymbol{X}_h\boldsymbol{\beta} + \boldsymbol{\varepsilon}_h \\ &\vdots \\ \mathbf{y}_v &= \boldsymbol{X}_v\boldsymbol{\beta} + \boldsymbol{\varepsilon}_v \end{aligned} \qquad \text{where} \qquad \boldsymbol{\varepsilon}_h = \begin{vmatrix} \varepsilon_{h1} \\ \varepsilon_{h2} \\ . \\ . \\ . \\ \varepsilon_{hn} \end{vmatrix} \tag{2.6.4-1}$$

When the v experimental errors are normally distributed with zero mean and those associated with the hth and kth responses (e.g., in the differential method of kinetic analysis r_h and r_k) are statistically correlated, the parameters are estimated from the minimization of the following multiresponse objective criterion:

$$S(\boldsymbol{\beta}) = \sum_{h=1}^{v}\sum_{k=1}^{v}\sigma^{hk}\sum_{i=1}^{n}\left[y_{ih} - \hat{y}_{ih}\right]\left[y_{ik} - \hat{y}_{ik}\right] \xrightarrow{\boldsymbol{\beta}} \text{Min} \tag{2.6.4-2}$$

where σ^{hk} are the elements of the inverse of the $(v \times v)$ error covariance matrix, n represents the number of experiments, and $\hat{y}_{ih}$ is the model value of the hth response for the ith experiment.

The parameter estimates are given by

$$\mathbf{b} = \left(\sum_{h=1}^{v}\sum_{k=1}^{v}\sigma^{hk}\boldsymbol{X}_h^T\boldsymbol{X}_k\right)^{-1}\sum_{h=1}^{v}\sum_{k=1}^{v}\sigma^{hk}\boldsymbol{X}_h^T\mathbf{y}_k \tag{2.6.4-3}$$

The covariance matrix of the estimates is given by

$$\mathbf{V}(\mathbf{b}) = \left(\sum_{h=1}^{v}\sum_{k=1}^{v}\sigma^{hk}\boldsymbol{X}_h^T\boldsymbol{X}_k\right)^{-1} \tag{2.6.4-4}$$

and the joint confidence region is given by

$$(\mathbf{b}-\boldsymbol{\beta})^T\left(\sum_{h=1}^{v}\sum_{k=1}^{v}\sigma^{hk}\boldsymbol{X}_h^T\boldsymbol{X}_k\right)(\mathbf{b}-\boldsymbol{\beta})=\frac{p}{nv-p}S(\mathbf{b})F(p,nv-p;1-\alpha) \quad (2.6.4\text{-}5)$$

When the equations are nonlinear in the parameters, the parameter estimates are obtained by minimizing the objective function by methods like that of Newton-Raphson or that of Newton-Gauss or an adaptation of the latter such as the Marquardt algorithm [1963]. In the latter case parameters are iteratively improved by the following formula:

$$\Delta\mathbf{b}_{s+1}=\left(\sum_{h=1}^{v}\sum_{k=1}^{v}\sigma^{hk}\mathbf{J}_{hs}^T\mathbf{J}_{ks}+\lambda_s\mathbf{I}\right)^{-1}\sum_{h=1}^{v}\sum_{k=1}^{v}\sigma^{hk}\mathbf{J}_{hs}^T\mathbf{r}_{ks} \quad (2.6.4\text{-}6)$$

The matrix $\mathbf{J}_h$ is defined by

$$\mathbf{J}_h=\left[J_{h_{ij}}\right]=\left[\left.\frac{\partial f_h(\mathbf{x}_i,\boldsymbol{\beta})}{\partial\boldsymbol{\beta}_j}\right|_{\boldsymbol{\beta}=\mathbf{b}}\right] \quad (2.6.4\text{-}7)$$

and the index s refers to the iteration number.

The σ^{hk} are generally unknown, but they can be estimated from replicated experiments. The matrix **S**, which is an estimate of the covariance matrix of experimental errors $\sum$, is given by

$$\mathbf{S}=\left[s_{hk}\right]=\left[\frac{\sum_{i=1}^{n_e}(y_{ih}-\bar{y}_h)(y_{ik}-\bar{y}_k)}{n_e-1}\right] \quad (2.6.4\text{-}8)$$

where $\bar{y}_h$ represents the average value of the response h over the n_e replicate experiments.

If no replicate experiments were carried out and the error covariance matrix is completely unknown, the determinant criterion of Box and Draper [1965] can be used:

$$\det\begin{vmatrix}\sum[y_{i1}-f_1(\mathbf{x}_i,\boldsymbol{\beta})]^2 & \cdots & \sum[y_{i1}-f_1(\mathbf{x}_i,\boldsymbol{\beta})][y_{iv}-f_v(\mathbf{x}_i,\boldsymbol{\beta})]\\ \sum[y_{i1}-f_1(\mathbf{x}_i,\boldsymbol{\beta})][y_{i2}-f_2(\mathbf{x}_i,\boldsymbol{\beta})] & \cdots & \sum[y_{i2}-f_2(\mathbf{x}_i,\boldsymbol{\beta})][y_{iv}-f_v(\mathbf{x}_i,\boldsymbol{\beta})]\\ \vdots & & \vdots\\ \sum[y_{i1}-f_1(\mathbf{x}_i,\boldsymbol{\beta})][y_{iv}-f_v(\mathbf{x}_i,\boldsymbol{\beta})] & \cdots & \sum[y_{iv}-f_v(\mathbf{x}_i,\boldsymbol{\beta})]^2\end{vmatrix}$$

$$\boldsymbol{\beta}\downarrow$$

Min

(2.6.4-9)

where all summations relate to n.

In minimizing the multiresponse objective functions given above, advantage is taken of the complete information collected on all the dependent variables.

After the parameters have been estimated, the significance of the overall regression for each of the rival models should be tested. This can be done by means of an F-test, of the type given in (2.6.3.1-13), essentially comparing the regression sum of squares and the residual sum of squares. The ratio

$$F_c = \frac{\sum_{h=1}^{v}\sum_{k=1}^{v}\sigma^{hk}\sum_{i=1}^{n}\hat{y}_{ih}\hat{y}_{ik} / p}{\sum_{h=1}^{v}\sum_{k=1}^{v}\sigma^{hk}\sum_{i=1}^{n}(y_{ih}-\hat{y}_{ih})(y_{ik}-\hat{y}_{ik})/(nv-p)} \qquad (2.6.4\text{-}10)$$

is distributed like F with p and $nv - p$ degrees of freedom. If the calculated F value exceeds the tabulated α percentage point (with $\alpha = 0.05$, e.g.) of the F distribution with degrees of freedom (p, $nv - p$), the regression is considered to be meaningful. Among the rival models, the one with the highest F value is to be preferred, provided the model is statistically adequate and provided its parameters satisfy the physicochemical constraints and are positive and statistically significantly different from zero.

The significance of the individual parameters is tested by comparing b_j with its standard deviation, which is a measure of its scatter. If the estimate b_j were zero, the ratio

$$\frac{b_j}{\sqrt{\left(\sum_{h=1}^{v}\sum_{k=1}^{v}\sigma^{hk}\mathbf{J}_h^T\mathbf{J}_k\right)^{-1}_{jj}}} \qquad (2.6.4\text{-}11)$$

would be distributed like the standard normal distribution provided that $\sum$ is known. An unbiased estimate **S** can be obtained from replicated experiments. Therefore, if the above ratio exceeds the corresponding tabulated α percentage point of this distribution ($\alpha = 0.05$, e.g.) which amounts to 1.96, the assumption $b_j = 0$ is rejected. The estimate is then significantly different from zero and effectively contributes to the model. The index jj refers to the element on the jth row and jth column of the matrix between brackets. In the opposite case, the parameter may be deleted from the model or further experimentation should be performed to determine it more significantly.

When the model cannot be written in algebraic form, the differential equations have to be numerically integrated for each data set in each iteration cycle of the parameter estimation.

When the integral method of kinetic analysis is applied, numerical integration of the continuity equations containing the rate equations is generally necessary for the comparison of the predicted and experimental responses for each experiment in each iteration cycle of the parameter estimation. Examples can be found in the work of De Pauw and Froment [1975] on *n*-pentane reforming in the presence of coke formation, in the work of Emig, Hofmann, and Friedrich [1972] on methanol oxidation, and in Example 2.6.4.A on benzothiophene hydrogenolysis.

Mention should be made of an approach using selectivity relationships rather than concentration versus space-time relationships. The selectivity relationships lend themselves more to analytical integration. The method is of fairly general application when the feed consists of a single component and the Hougen-Watson-type rate equations all have the same denominator. Froment [1975] discussed the application of the method to *o*-xylene oxidation.

EXAMPLE 2.6.4.A
BENZOTHIOPHENE HYDROGENOLYSIS

In hydrodesulfurization on Co/Mo catalysts, benzothiophene (*B*) yields ethylbenzene (*E*) and hydrogen sulfide according to two routes. The first is a direct hydrogenolysis route leading to styrene, which is practically instantaneously hydrogenated to ethylbenzene. The second route consists of a hydrogenation to dihydrobenzothiophene (*D*), which is subsequently hydrogenolyzed. There is evidence, based on kinetic and surface science experimentation, that two types of sites are involved: so-called σ sites in the hydrogenolysis and τ sites in the hydrogenation. Van Parijs and Froment [1986a and b] and Van Parijs, Hosten, and Froment [1986] studied benzothiophene hydrogenolysis and hydrogenation on an industrial Co/Mo catalyst in an integral tubular reactor at total pressures ranging from 1 to 30 bar, temperatures between 513 and 578 K, and ratios of hydrogen to hydrocarbon in the feed between 4 and 9. The integral method of kinetic analysis was adopted, and the objective function was based upon the exit conversions. To obtain these from postulated rate equations required numerical integration of the continuity equations for the reaction components, assuming plug flow in the reactor.

Three independent rate equations are necessary: one for the direct hydrogenolysis of benzothiophene on σ sites, $r_{B,\sigma} = f(\mathbf{x},\boldsymbol{\beta})$; one for its hydrogenation to dihydrobenzothiophene on τ sites, $r_{B,\tau} = f(\mathbf{x},\boldsymbol{\beta})$; and one for the hydrogenolysis of the latter to ethylbenzene on σ sites, $r_{D,\sigma} = f(\mathbf{x},\boldsymbol{\beta})$, where $\mathbf{x}$ represents the vector of partial pressures and $\boldsymbol{\beta}$ the parameter vector.

A larger number of reaction schemes can be written for the three reactions mentioned above, depending upon whether hydrogen is competitively adsorbed or not, atomically or molecularly, and upon which step (adsorption, surface reaction, or desorption) is rate determining. Using a sequential experimental design procedure, to be discussed in Section 2.7, led to the conclusion that the surface reactions are the rate-determining steps (r. d. s.) in the three reactions and that hydrogen is competitively and atomically adsorbed. Therefore, the following reaction scheme was retained among those postulated:

Direct hydrogenolysis of benzothiophene into styrene on σ sites:

$H_2 + 2\sigma \rightleftarrows 2H\sigma$		$K_{H,\sigma} = c_{H,\sigma}^2 \big/ p_H c_\sigma^2$
$B + \sigma \rightleftarrows B\sigma$		$K_{B,\sigma} = c_{B,\sigma} \big/ p_B c_\sigma$
$B\sigma + 2H\sigma \rightarrow S\sigma + Y\sigma + \sigma$	(r.d.s.)	$r_{B,\sigma} = k_{b,\sigma}^* c_{B,\sigma} c_{H,\sigma}^2$
$S\sigma + H_2 \rightleftarrows H_2S + \sigma$		$K_{S,\sigma} = c_{S,\sigma} p_H \big/ c_\sigma p_S$
$Y\sigma \rightleftarrows Y + \sigma$		$K_{Y,\sigma} = c_{Y,\sigma} \big/ p_Y c_\sigma$

Hydrogenation of benzothiophene into dihydrobenzothiophene on τ sites:

$H_2 + 2\tau \rightleftarrows 2H\tau$		$K_{H,\tau} = c_{H,\tau}^2 \big/ p_H c_\tau^2$
$B + \tau \rightleftarrows B\tau$		$K_{B,\tau} = c_{B,\tau} \big/ p_B c_\tau$
$B\tau + 2H\tau \rightleftarrows D\tau + 2\tau$	(r.d.s.)	$r_{B,\tau} = k_{B,\tau}^* (c_{B,\tau} c_{H,\tau}^2 - c_{D,\tau} c_\tau^2 / K^*)$
$D\tau \rightleftarrows D + \tau$		$K_{D,\tau} = c_{D,\tau} \big/ p_D c_\tau$

Hydrogenolysis of dihydrobenzothiophene on σ sites:

$H_2 + 2\sigma \rightleftarrows 2H\sigma$		$K_{H,\sigma} = c_{H,\sigma}^2 \big/ p_H c_\sigma^2$
$D + \sigma \rightleftarrows D\sigma$		$K_{D,\sigma} = c_{D,\sigma} \big/ p_D c_\sigma$
$D\sigma + 2H\sigma \rightarrow S\sigma + E\sigma + \sigma$	(r.d.s.)	$r_{D,\sigma} = k_{D,\sigma}^* c_{D,\sigma} c_{H,\sigma}^2$
$S\sigma + H_2 \rightleftarrows H_2S + \sigma$		$K_{S,\sigma} = c_{S,\sigma} p_H \big/ c_\sigma p_S$
$E\sigma \rightleftarrows E + \sigma$		$K_{E,\sigma} = c_{E,\sigma} \big/ p_E c_\sigma$

The unknown concentrations of σ and τ sites are eliminated by means of the balances

$$c_{\sigma,t} = c_{\sigma} + c_{H,\sigma} + c_{S,\sigma} + c_{B,\sigma} + c_{D,\sigma} + c_{E,\sigma} + c_{Y,\sigma}$$

$$c_{\tau,t} = c_{\tau} + c_{H,\tau} + c_{B,\tau} + c_{D,\tau} + c_{E,\tau} + c_{Y,\tau}$$

The corresponding rate equations are

$$r_{B,\sigma} = \frac{k_{B,\sigma} K_{B,\sigma} K_{H,\sigma} p_B p_H}{\left(1 + \sqrt{K_{H,\sigma} p_H} + K_{B,\sigma} p_B + K_{D,\sigma} p_D + K_{S,\sigma} \frac{p_S}{p_H} + K_{E,\sigma} p_E + K_Y \frac{p_E}{p_H}\right)^3} \tag{2.6.4.A-a}$$

$$r_{B,\tau} = \frac{k_{B,\tau} K_{B,\tau} K_{H,\tau} (p_B p_H - p_D / K_1)}{\left(1 + \sqrt{K_{H,\tau} p_H} + K_{B,\tau} p_B + K_{D,\tau} p_D + K_{E,\tau} p_E + K_Y' \frac{p_E}{p_H}\right)^3} \tag{2.6.4.A-b}$$

$$r_{D,\sigma} = \frac{k_{D,\sigma} K_{D,\sigma} K_{H,\sigma} p_D p_H}{\left(1 + \sqrt{K_{H,\sigma} p_H} + K_{B,\sigma} p_B + K_{D,\sigma} p_D + K_{S,\sigma} \frac{p_S}{p_H} + K_{E,\sigma} p_E + K_Y \frac{p_E}{p_H}\right)^3} \tag{2.6.4.A-c}$$

The parameters were estimated by means of (2.6.4-2). Replicated experiments allowed the calculation of $\sum$, according to (2.6.4-8). The fit of the models and the significance of the parameters were tested by means of the statistical criteria (2.6.4-10) and (2.6.4-11). The parameters were also tested for their physicochemical consistence using rules to be described in Section 2.6.5. In all three equations the estimation led to equality of the adsorption coefficients for *B* and *D*: in (2.6.4.A-a) and (2.6.4.A-c) $K_{B,\sigma} = K_{D,\sigma}$, in (2.6.4.A-b) $K_{B,\tau} = K_{D,\tau}$. For lack of statistical significance of K_Y and K'_Y, the terms $K_Y(p_E/p_H)$ in (2.6.4.A-a) and (2.6.4.A-c) and $K'_Y(p_E/p_H)$ in (2.6.4.A-b) were deleted. Finally, the term $K_{E,\sigma}p_E$ was also deleted in (2.6.4.A-a) and (2.6.4.A-c). Additional and more specific experiments would be required to significantly determine these parameters and terms. ■

In the above example it has been assumed that the total concentration of the σ and τ sites is completely determined by the composition and preparation of the catalyst and is independent of the gas-phase conditions. In the remote control model for hydrodesulfurization proposed by Delmon [1979], spillover hydrogen, generated on Co_9S_8 in amounts depending upon the partial pressures of H_2 and H_2S reacts with MoS_2 to produce slightly reduced centers active in hydrogenation, or strongly reduced centers active in hydrogenolysis. In that case

$c_{\sigma,t}$ and $c_{\tau,t}$ would no longer be constant but would vary with p_H and p_S. In their study of the hydrogenolysis of thiophene, Van Parijs et al. [1984] derived Hougen-Watson-type models reflecting the interconversion of sites, implied in the remote control model. The equations led to an excellent fit of the data at higher sulfur contents, but the fit was not conclusively better than that of the classical Hougen-Watson model with fixed concentration of sites. More specific experiments than those of Van Parijs et al. [1984] would be required to unambiguously discriminate between the two types of models, but it is clear that the approach can go a long way in accounting for detailed aspects of the reaction, qualitatively revealed, for example, by surface science techniques.

2.6.5 Physicochemical Tests on the Parameters

Testing the fit of the rate equation to the experimental data and calculating the confidence interval of the parameters should be part of any kinetic modeling study but it is not sufficient yet. With the mechanistic insight incorporated to a maximum extent into the models, the parameters of the latter should satisfy well-established physicochemical laws. As mentioned already, the rate coefficients have to obey the Arrhenius temperature dependence. Boudart et al. [1967] also derived constraints on the adsorption enthalpies and entropies which are too often overlooked.

Since adsorption is exothermic, the adsorption enthalpy has to satisfy the inequality

$$-\Delta H_a^0 > 0 \tag{2.6.5-1}$$

while the adsorption entropy has to satisfy

$$0 < -\Delta S_a^0 < S_g^0 \tag{2.6.5-2}$$

As a rule, the following limits for the adsorption entropy are observed:

$$41.8 < -\Delta S_a^0 < (51.04 + 1.4 \cdot 10^{-3} T)(-\Delta S_a^0) \tag{2.6.5-3}$$

An example of application of these rules to the testing of rate parameters in the dehydrogenation of methylcyclohexane on Pt and Pt/Re catalysts was published by Van Trimpont et al. [1986] and to the dehydrogenation of ethylbenzene into styrene by Won Jae Lee and Froment [2008].

2.7 SEQUENTIAL DESIGN OF EXPERIMENTS

Too frequently, kinetic studies are deficient in their design. There is no fitting technique that can compensate for a poor experimental design. In the design of

experiments a lot can be achieved with just common sense. The variables should cover a sufficient range, and the structure of the proposed rate equations may point toward areas of optimal experimentation. With complex multivariable models, however, a rigorous, systematic approach may be required to achieve maximum efficiency. Until recently, most designs were of the factorial type (i.e., the variables are set a priori for a number of experiments), but sequential methods seem to be increasingly applied [Lazic, 2004; Taguchi et al., 2004]. The sequential methods take advantage of the information and insight obtained from the previous experiments to select the settings of the independent variables for the next experiment in an optimal way. Two types of sequential methods for optimal design have been developed: (1) for optimal discrimination between rival models with known structure [Box and Hill, 1967; Box and Henson, 1969; Hosten and Froment, 1976] and (2) for optimal parameter estimation in an existing model [Box and Lucas, 1959; Froment and Mezaki, 1970].

2.7.1 Sequential Design for Optimal Discrimination between Rival Models

2.7.1.1 Single Response Case

Suppose one has to discriminate between two models $y^{(1)} = ax + b$ and $y^{(2)} = ax$, where y is a dependent variable that can be conversion or rate. It is logical to design an experiment where a maximum difference or "divergence" can be expected between the two models. From Fig. 2.7.1.1-1, this would be for values of the independent variable x close to zero and x_j, but surely not in the vicinity of x_3.

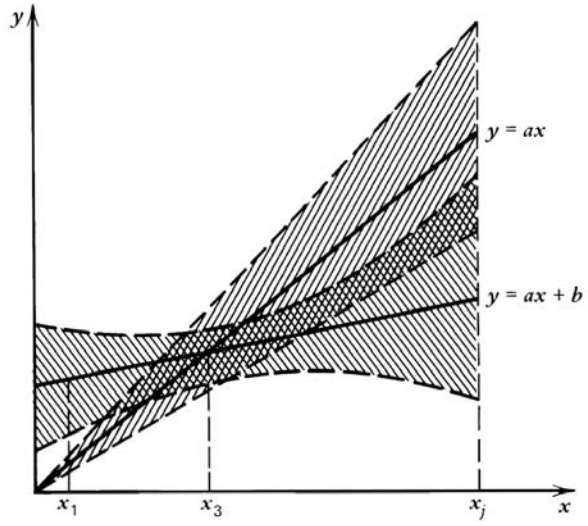

Figure 2.7.1.1-1
Discrimination between two linear models.

Suppose $n - 1$ experiments have been performed at $n - 1$ settings of x, so that estimates for a and b can be obtained. These are the preliminary experiments, carried out at values of the independent variable that are chosen with common sense or by making use of an a priori method. To select the setting of x for the first sequentially designed experiment, the operability region on the x axis is divided into a certain number of intervals.

Design Criterion. The design criterion is based upon the divergence defined, for example, as follows:

$$D(\mathbf{x}_u) = \sum_{r=1}^{m-1} \sum_{s=r+1}^{m} \left| \hat{y}^{(r)}(\mathbf{x}_u) - \hat{y}^{(s)}(\mathbf{x}_u) \right| \qquad (2.7.1.1\text{-}1)$$

where m is the number of rival models and the grid points are numbered u. The divergence is calculated in each grid point, and the setting of the operating variable(s) $\mathbf{x}$ for the nth experiment is that value which maximizes $D(\mathbf{x}_u)$. It is clear now that a number of preliminary experiments are required, since the calculation of $\hat{y}^{(r)}(\mathbf{x}_u)$ requires estimates for the model parameters $\boldsymbol{\beta}$.

A design criterion of the type given in (2.7.1.1-1) was used by Hunter and Reiner [1965]. It may occur that the confidence intervals on the responses $\hat{y}^{(r)}(\mathbf{x}_u)$ and $\hat{y}^{(s)}(\mathbf{x}_u)$ overlap as shown in Fig. 2.7.1.1-1 for large $\mathbf{x}_u$. Therefore, Box and Hill [1967] proposed a criterion that accounts for the variances of the predicted response values. It has been experienced, however, that the optimal settings predicted by this formula frequently agree with the simpler expression (2.7.1.1-1).

After the nth experiment has been designed, the models are tested for their adequacy. In other words: did the experiment provide sufficient information for discrimination between the rival models ?

Test on model of adequacy. The type of test depends on the information available on the experimental error variance σ^2.

1. σ^2 known: It can be shown that

$$\chi_c^2 = \frac{(n - p_r)s_r^2}{\sigma^2} \approx \chi^2(n - p_r) \qquad (2.7.1.1\text{-}2)$$

provided that s_r^2 is an unbiased estimate of σ^2. Models whose $\chi_c^2 > \chi^2(n - p_r; 1 - \alpha)$ are discarded; s_r^2 = estimate of σ^2 + lack of fit, obtained through model r.

2. σ^2 unknown, but s_e^2 is available from $n_e + 1$ replicates:

$$F_c = \frac{s_r^2}{s_e^2} \sim F(n - p_r, n_e) \qquad (2.7.1.1\text{-}3)$$

provided s_r^2 is an unbiased estimate of σ^2, that is, calculated for the correct model. Models whose $F_c > F(n-p_r, n_e; 1-\alpha)$ are discarded.

3. No information on σ^2: Bartlett's test can be applied:

$$\chi_c^2 = \frac{\ln \bar{s}^2 \sum_{r=1}^{m} (\text{d.f.})_r - \sum_{r=1}^{m} (\text{d.f.})_r s_r^2}{1 + \frac{1}{3(m-1)} \left[\sum_{r=1}^{m} \frac{1}{(\text{d.f.})_r} - \frac{1}{\sum_{r=1}^{m} (\text{d.f.})_r} \right]} \sim \chi^2(m-1) \quad (2.7.1.1\text{-}4)$$

where $\bar{s}^2$ is a pooled estimate of σ^2 + lack of fit, based on all competing models, and m is the number of models:

$$\bar{s}^2 = \frac{\sum_{r=1}^{m} (\text{d.f.})_r s_r^2}{\sum_{r=1}^{m} (\text{d.f.})_r} \quad (2.7.1.1\text{-}5)$$

Whenever χ_c^2 exceeds $\chi^2(m-1; 1-\alpha)$, the model with the largest s_r^2 is discarded and χ_c^2 is recalculated, based upon the remaining models. Models are discarded as long as χ_c^2 exceeds the appropriate tabulated value.

Tests 1 and 2 determine the true model adequacy; test 3 can only yield the "best" model. Applying the above statistics to models that are nonlinear in the parameters requires the model to be locally linear. For the particular application considered here, this means that the residual mean square distribution is approximated to a reasonable extent by the χ^2 distribution. Furthermore, care has to be taken for outliers, since χ^2 appears to be rather sensitive to departures of the data from normality. In Example 2.7.1.1.A, given below, this was taken care of by starting the elimination from scratch again after each experiment. Finally, the theory requires the variance estimates that are tested on homogeneity to be statistically independent. It is hard to say to what extent this restriction is fulfilled. From the examples given, which have a widely different character, it would seem that the procedure is efficient and reliable.

Box and Hill [1967] and Box and Henson [1969] tested the model adequacy on the basis of Bayesian probabilities.

EXAMPLE 2.7.1.1.A

MODEL DISCRIMINATION IN THE DEHYDROGENATION OF 1-BUTENE INTO BUTADIENE

Dumez and Froment [1976] studied the dehydrogenation of 1-butene into butadiene on a chromium oxide/aluminum oxide catalyst in a differential reactor. This work is probably the first in which the experimental program was actually and uniquely based on a sequential discrimination procedure. The reader is also referred to a more detailed treatment of Dumez, Hosten, and Froment [1977]. The following mechanisms were considered to be plausible:

a) Atomic Dehydrogenation; Surface Recombination of Hydrogen

1.	$B + l \rightleftarrows Bl$	a_1
2.	$Bl + l \rightleftarrows Ml + Hl$	a_2
3.	$Ml + l \rightleftarrows Dl + Hl$	a_3
4.	$Dl \rightleftarrows D + L$	a_4
5.	$2Hl \rightleftarrows H_2l + l$	
6.	$H_2l \rightleftarrows H_2 + l$	

where B = *n*-butene, D = butadiene, H_2 = hydrogen and M = an intermediate complex.

b) Atomic Dehydrogenation; Gas-Phase Hydrogen Recombination

1.	$B + l \rightleftarrows Bl$	b_1
2.	$Bl + l \rightleftarrows Ml + Hl$	b_2
3.	$Ml + l \rightleftarrows Dl + Hl$	b_3
4.	$Dl \rightleftarrows D + l$	b_4
5.	$2Hl \rightleftarrows H_2 + 2l$	

c) Molecular Dehydrogenation

1.	$B + l \rightleftarrows Bl$	c_1
2.	$Bl + l \rightleftarrows Dl + H_2l$	c_2
3.	$Dl \rightleftarrows D + l$	c_3
4.	$H_2l \rightleftarrows H_2 + l$	

d) Atomic Dehydrogenation; Intermediate Complex with Short Lifetime; Surface Recombination of Hydrogen

1.	$B + l \rightleftarrows Bl$	d_1
2.	$Bl + 2l \rightleftarrows Dl + 2Hl$	d_2
3.	$Dl \rightleftarrows D + l$	
4.	$2Hl \rightleftarrows H_2l + l$	
5.	$H_2l \rightleftarrows H_2 + l$	

e) As in (d) but with Gas-Phase Hydrogen Recombination

1. $B + l \rightleftarrows Bl$ e_1

2. $Bl + 2l \rightleftarrows Dl + 2Hl$ e_2

3. $Dl \rightleftarrows D + l$

4. $2Hl \rightleftarrows H_2 + 2l$

For each of these mechanisms several rate equations may be deduced, depending on the rate-determining step that is postulated. Fifteen possible rate equations were retained, corresponding to the rate-determining steps a_1 ... a_4, b_1 ... b_4, c_1 ... c_3, d_1, d_2, e_1 and e_2, respectively. These equations will not be given here, except the finally retrained one, by way of example:

$$r = \frac{k_1 K_1 s C_t \left(p_B - \frac{p_{H_2} p_D}{K} \right)}{\left(1 + K_1 p_B + \frac{p_D}{K_3} + \frac{p_{H_2}}{K_4} \right)^2}$$

The discrimination was based on the divergence criterion of (2.7.1.1-1) in which y is replaced by r and model adequacy criterion (2.7.1.1-4) is utilized. Since the experiments were performed in a differential reactor, the independent variables were the partial pressures of butene p_B, butadiene p_D, and hydrogen p_{H2}. The operability region for the experiments at 525°C is shown in Fig. 2.7.1.1.A-1. The equilibrium surface is also represented in this figure by means of hyperbola parallel to the $p_D p_{H2}$ plane and straight lines parallel to the $p_B p_{H2}$ and $p_B p_D$ planes, respectively. Possible experiments are marked with a small circle. Experimental settings too close to the equilibrium were avoided, for obvious reasons. The maximum number of parameters in the possible models is six, so that at least seven preliminary experiments are required to estimate the parameters and start the discrimination procedure with (2.7.1.1-1). As can be seen from Table 2.7.1.1.A-1, after these seven preliminary experiments already the models a_3, b_3, a_4, b_4 and c_3 may be eliminated. The eighth experiment, which is the first of the designed ones, is carried out at the conditions represented by (8) in Fig. 2.7.1.1.A-1. The model adequacies are then recalculated. Note that after each experiment the elimination was started from scratch again to avoid discarding a model on the basis of one or more experiments with a biased error, especially in the early stages of discrimination.

After seven designed experiments or after a total of 14 experiments, no further discrimination was possible between the dual-site rate-determining

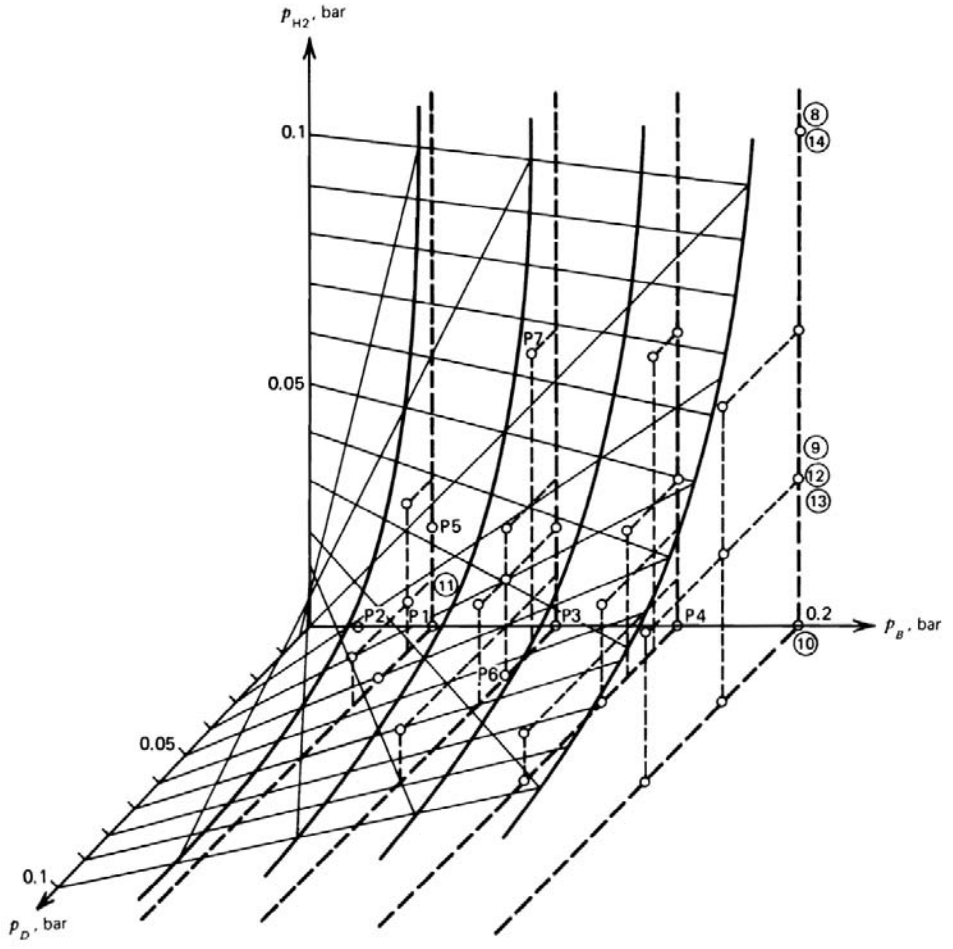

Figure 2.7.1.1.A-1

Model discrimination in butene dehydrogenation. Operability region, equilibrium surface, location of preliminary and designed experiments at 525°C. From Dumez, Hosten and Froment [1977].

models a_2, b_2, c_2, d_2 and e_2, because the differences between these models were smaller than the experimental error. The models a_2, b_2, and d_2 were then eliminated because they contained at least one parameter that was not significantly different from zero at the 95% confidence level. It is interesting to note that none of the designed feed compositions contains butadiene. From the preliminary experiments it follows already that butadiene is strongly adsorbed. Consequently, it strongly reduces the rate of reaction and therefore the divergence. The design is based upon maximum divergence. Finally, it should be stressed how efficient sequential design procedures are for model discrimination. A classical experimental program, less conscious of the ultimate goal, would no doubt have involved a much more extensive experimental program. It is true that,

TABLE 2.7.1.1.A-1
DEHYDROGENATION OF 1-BUTENE EVOLUTION OF SEQUENTIAL MODEL DISCRIMINATION

Number of Designed Experiments	0	1	2	3	4	5	6	7
Total Number of Experiments	**7**	**8**	**9**	**10**	**11**	**12**	**13**	**14**
$(\chi^2)_t$	χ_c^2							
23.68	50.59	68.80	85.31	84.80	98.38	114.14	129.44	139.13
Eliminated model (EM)	a_3	a_3	a_3	a_3	a_3	a_3	a_3	a_3
22.36	43.66	58.78	72.61	69.55	80.84	93.82	106.40	113.60
EM	b_3	b_3	b_3	b_3	b_3	b_3	b_3	b_3
21.03	32.50	42.19	50.55	43.37	50.86	58.81	66.39	69.17
EM	a_4	a_4	a_4	a_4	a_4	a_4	a_4	a_4
19.68	27.36	35.44	42.47	36.67	43.81	50.87	57.58	59.70
EM	b_4	b_4	b_4	b_4	b_4	b_4		b_4
18.31	20.18	25.82	30.72	28.03	34.75	40.40	45.75	46.92
EM	c_3	c_3	c_3	c_3	c_3	c_3	c_3	c_3
16.92	1.91	3.37	4.56	14.04	20.59	23.74	26.66	26.39
EM					a_1	a_1	a_1	a_1
15.51					18.83	21.79	24.53	24.39
EM					b_1	b_1	b_1	b_1
14.07					16.59	19.20	21.78	21.45
EM					d_1	d_1	d_1	d_1
12.59					13.95	16.23	18.32	18.18
EM					e_1	e_1	e_1	e_1
11.07					9.38	10.97	12.42	12.06
EM							c_1	c_1
9.49							0.44	1.28

at first sight, the limited number of experiments provides less feeling for the influence of the process variables on the rate or conversion, which is, of course, of great importance for practical application. Such information is easily obtained a posteriori, however: the detailed response surface can be generated from the retained model. ■

EXAMPLE 2.7.1.1.B
ETHANOL DEHYDROGENATION: SEQUENTIAL DISCRIMINATION USING THE INTEGRAL METHOD OF KINETIC ANALYSIS

The above example dealt with the design of an experimental program carried out in a differential reactor. When the data are obtained in an integral reactor, it is more convenient to deal with the integrated form of the rate equation. This is

illustrated in the present example, which also deals with real data, although the design is only applied a posteriori.

In the work of Franckaerts and Froment on ethanol dehydrogenation [1964], three rate equations were retained. They were already referred to in (2.3.1-18), (2.3.1-19), and (2.3.1-20). The authors discriminated between these models on the basis of a classical experimental program. This allowed the calculation of the initial rates, and these were then plotted versus the total pressure.

Assuming the tubular reactor to be ideal and isothermal, the continuity equation for ethanol may be written

$$F_{A0}dx = r_A dW \qquad \text{(2.7.1.1.B-a)}$$

where r_A may be given by either (2.3.1-18), (2.3.1-19), or (2.3.1-20), in which the partial pressures are expressed in terms of the conversion of ethanol. Equation (2.3.1-19) then takes the form

$$r_A = \frac{kK_A\left[\frac{1-x}{a+x}p_t - \frac{x^2}{(a+x)^2K}p_t^2\right]}{\left[1+K_A\frac{1-x}{a+x}p_t+(K_R+K_S)\frac{x}{a+x}p_t\right]^2}$$

where a = 1 + 0.155 and 0.155 is the molar ratio of water to ethanol in the feed. What is measured in an integral reactor is the exit conversion, so that Eq. (2.7.1.1.B-a) has to be integrated for the three rival rate equations to give an expression of the form

$$\frac{W}{F_{A0}} = f(k, K_A, K_R, K_S, p_t, x) \qquad \text{(2.7.1.1.B-b)}$$

which is implicit in the dependent variable, the conversion x. The independent variables are W/F_{A0} and p_t. Equations like (2.7.1.1.B-b) are generally rather complex. By way of example, for the rate equation (2.3.1-19), the integrated continuity equation becomes

$$\frac{W}{F_{A0}} = \frac{1}{kK_A}(D_1 + D_2 + D_3)$$

where

$$D_1 = \frac{2A_1}{\sqrt{4A_2C_2 - B_2^2}}\left[\arctan\left(\frac{2C_2x + B_2}{\sqrt{4A_2C_2 - B_2^2}}\right) - \arctan\left(\frac{B_2}{\sqrt{4A_2C_2 - B_2^2}}\right)\right]$$

$$D_2 = \frac{B_1}{2C_2}\left[\log\left(\frac{A_2 + B_2 x + C_2 x^2}{A_2}\right) - \frac{B_2 D_1}{A_1}\right]$$

$$D_3 = C_1\left[\frac{x}{C_2} - \frac{B_2}{2C_2^2}\log\left(\frac{A_2 + B_2 x + C_2 x^2}{A_2}\right) + \left(\frac{B_2^2 - 2A_2 C_2}{2C_2^2}\right)\frac{D_1}{A_1}\right] \quad \text{(2.7.1.1.B-c)}$$

when $4A_2C_2 - B_2^2$ is positive.

The other symbols are

$$A_1 = (1.155 + K_A p_t)^2$$

$$B_1 = 2.31 - 2K_A^2 p_t^2 - 0.31 K_A p_t + 2K_A(K_R + K_S) p_t^2$$

$$C_1 = \left[1 - K_A p_t + (K_R + K_S) p_t\right]^2$$

$$A_2 = 1.155 p_t \ , \quad B_2 = -0.155 p_t \ , \quad C_2 = -p_t\left(1 + \frac{p_t}{K}\right)$$

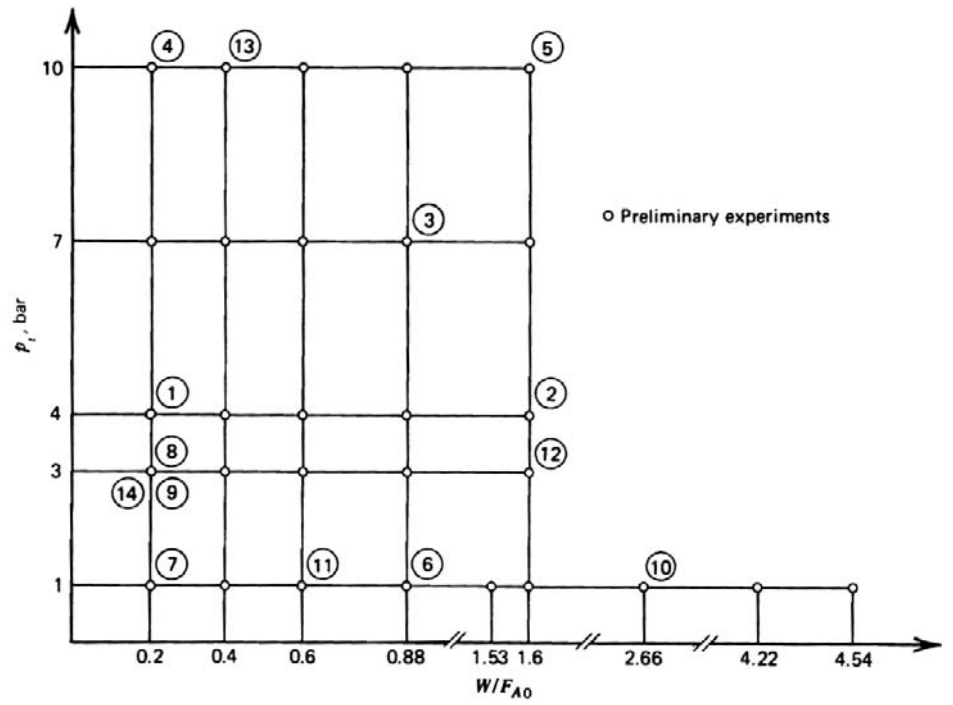

Figure 2.7.1.1.B-1

Ethanol dehydrogenation. Operability region, location of preliminary and of designed experiments for optimal discrimination. Preliminary experiments 1, 2, 3, 4, and 5.

TABLE 2.7.1.1.B-1
SEQUENTIAL DESIGN FOR OPTIMUM DICSRIMINATION IN THE DEHYDROGENATION OF ETHANOL INTO ACETALDEHYDE, USING INTEGRAL REACTOR DATA

Experiment Number	W/F_{A0}	p_t	x	χ_c^2	χ_{tab}^2	Delete Model
1	0.2	4	0.14			
2	1.6	4	0.32			
3	0.88	7	0.214			
4	0.2	10	0.1			
5	1.6	10	0.229	2.81	5.99	
6	0.88	1	0.339	5.83		
7	0.2	1	0.118	2.0		
8	0.2	3	0.14	3.75		
9	0.2	3	0.14	5.40		
10	2.66	1	0.524	7.59	5.99	Adsorption
				2.01	3.84	
11	0.6	1	0.262	3.07		
12	1.6	3	0.352	3.42		
13	0.4	10	0.148	3.64		
14	0.2	3	0.14	4.60	3.84	Desorption

Figure 2.7.1.1.B-1 shows the operability region in the $p_t - (W/F_{A0})$ plane at 275°C. Since (2.7.1.1.B-b) contains four parameters, at least five preliminary runs have to be performed. Then, the parameters are calculated by means of nonlinear regression, minimizing the sum of squares of residuals of the true dependent variable x—preferably not of W/F_{A0}, as mentioned already. This requires a routine for solving the implicit equation for x, of course.

Next, the first experiment is designed using the criterion (2.7.1.1-1) in which y now stands for the conversion x. Then, the adequacy criterion (2.7.1.1-4) is applied. The design is given in Table 2.7.1.1.B-1. Here, too, the adsorption and desorption models are rejected and the model with surface reaction as rate-determining step is retained. Again the designed experiments, encircled on the figure, are located on the borderline of the operability region. Note that the design procedure for sequential discrimination is applicable even when the continuity equation (2.7.1.1.B-a) cannot be integrated analytically, but only numerically. This problem is encountered quite often when dealing with complex reactions.

■

2.7.1.2 Multiresponse Case

Design Criterion. The divergence now becomes

$$D(\mathbf{x}_u) = \sum_{h=1}^{v} \sigma^{hh} \sum_{r=1}^{m-1} \sum_{s=r+1}^{m} \left| \hat{y}_{uh}^{(r)} - \hat{y}_{uh}^{(s)} \right| \qquad (2.7.1.2\text{-}1)$$

where v is the number of responses.

Test on Model Adequacy. Minimize the objective function $S(\boldsymbol{\beta})^{(r)}$:

$$S(\boldsymbol{\beta})^{(r)} = \sum_{h=1}^{v} \sum_{k=1}^{v} \sigma^{hk} \sum_{i=1}^{n} (y_{ih} - \hat{y}_{ih}^{(r)})(y_{ik} - \hat{y}_{ik}^{(r)}) \xrightarrow{\boldsymbol{\beta}} \text{Min} \qquad (2.7.1.2\text{-}2)$$

where r is one of the models [see (2.7.1.1-1)].

In the minimum, $S(\boldsymbol{\beta})^{(r)}$ becomes $S(\mathbf{b})^{(r)}$:

$$S(\mathbf{b})^{(r)} \sim \chi^2(nv - p_r, 1-\alpha) \qquad (2.7.1.2\text{-}3)$$

provided there is no lack of fit. This comparison is made for all models 1, ..., r, ..., m.

If

$$S(\mathbf{b})^{(r)} < \chi^2(nv - p_r, 1-\alpha) \qquad (2.7.1.2\text{-}4)$$

then there is no bias and no lack of fit, and the model is adequate.

If

$$S(\mathbf{b})^{(r)} > \chi^2(nv - p_r, 1-\alpha)$$

then model r is discarded.

Van Parijs et al. [1986] applied sequential discrimination in their experimental study of benzothiophene hydrogenolysis. The final rate equations were already given in Example 2.6.4.A. The efficiency of the sequential discrimination was remarkable. At 533 K, a total of seven experiments (four preliminary, three designed) were sufficient to reject 14 out of 16 rivals. Only one of the two remaining models was consistently the best at 513, 553, and 573 K also, after four, five and nine designed experiments, respectively. A total of 41 experiments sufficed to select the best among the postulated rate equations. The location of the settings of these experiments is shown in Fig. 2.7.2.2.A-1 of Example 2.7.2.2.A.

2.7.2 Sequential Design for Optimal Parameter Estimation

2.7.2.1 Single Response Models

The joint confidence region is given by

$$(\boldsymbol{\beta} - \mathbf{b})^T \boldsymbol{X}^T \boldsymbol{X} (\boldsymbol{\beta} - \mathbf{b}) = \delta \qquad (2.7.2.1\text{-}1)$$

with δ depending upon the probability level and the number of degrees of freedom (see 2.6.3.1-19). This formula represents a closed hyperellipsoidal surface centered at **b**, as can be shown by reduction to its canonical form (Fig. 2.6.3.1-2). A translation of coordinates

$$\mathbf{Z} = \boldsymbol{\beta} - \mathbf{b}$$

leads to

$$\mathbf{Z}^T \boldsymbol{X}^T \boldsymbol{X} \mathbf{Z} = \delta$$

and the axes are rotated by an orthogonal transformation

$$\mathbf{Z} = \mathbf{U}\mathbf{v}$$

yielding

$$\mathbf{v}^T (\mathbf{U}^T \boldsymbol{X}^T \boldsymbol{X} \mathbf{U}) \mathbf{v} = \delta \qquad (2.7.2.1\text{-}2)$$

with **U** an orthogonal matrix with columns that are the eigenvectors of $\boldsymbol{X}^T\boldsymbol{X}$. The matrix $\mathbf{U}^T\boldsymbol{X}^T\boldsymbol{X}\mathbf{U}$ is a diagonal matrix with the eigenvalues λ_j of $\boldsymbol{X}^T\boldsymbol{X}$ on its main diagonal. In scalar notation,

$$\left(\frac{v_1}{\sqrt{\frac{\delta}{\lambda_1}}} \right)^2 + \left(\frac{v_2}{\sqrt{\frac{\delta}{\lambda_2}}} \right)^2 + \cdots \left(\frac{v_p}{\sqrt{\frac{\delta}{\lambda_p}}} \right)^2 = 1 \qquad (2.7.2.1\text{-}3)$$

This is the standard equation of a *p*-dimensional ellipsoid.

Minimum Volume Design. The volume of the hyperellipsoid is given by

$$\text{volume} = C \prod_{j=1}^{p} \sqrt{\frac{\delta}{\lambda_j}} = C \frac{(\sqrt{\delta})^p}{\sqrt{\det \boldsymbol{X}^T \boldsymbol{X}}} \qquad (2.7.2.1\text{-}4)$$

where *C* is a constant depending upon the dimension *p* of the parameter space. To minimize the volume, the determinant $\boldsymbol{X}^T\boldsymbol{X}$ is maximized. The next

experiment is designed in the grid point where the determinant is maximum [Box and Lucas, 1959].

Spherical Shape Design. The next experiment is designed at those settings which maximize the smallest eigenvalue of $\boldsymbol{X}^T\boldsymbol{X}$, which leads to the maximum contraction of the largest principal axis of the ellipsoid [Hosten, 1974]. When the models are nonlinear, $\boldsymbol{X}$ is replaced by **J**.

2.7.2.2 Multiresponse Models

The models considered are algebraic and linear in the parameters. The joint confidence region is given by

$$(\mathbf{b}-\boldsymbol{\beta})^T\left(\sum_{h=1}^{v}\sum_{k=1}^{v}\sigma^{hk}\boldsymbol{X}_h^T\boldsymbol{X}_k\right)(\mathbf{b}-\boldsymbol{\beta})=\frac{p}{nv-p}S(\mathbf{b})F(p,nv-p;1-\alpha) \tag{2.7.2.2-1}$$

Therefore, the objective function to be maximized is

$$\det\left(\sum_{h=1}^{v}\sum_{k=1}^{v}\sigma^{hk}\boldsymbol{X}_h^T\boldsymbol{X}_k\right) \tag{2.7.2.2-2}$$

when the minimum volume criterion of Box and Hunter is used. When Hosten's shape criterion is adopted, the smallest eigenvalue of

$$\sum_{h=1}^{v}\sum_{k=1}^{v}\sigma^{hk}\boldsymbol{X}_h^T\boldsymbol{X}_k \tag{2.7.2.2-3}$$

has to be maximized.

When the models are nonlinear in the parameters, $\boldsymbol{X}$ is replaced by **J**. An example of application of sequential design for optimal estimation is given by Van Parijs et al. [1986] in their study of benzothiophene hydrogenolysis. At 533 K the desired accuracy of the parameters of the equations given in Example 2.6.4.A was reached after four more experiments beyond the seven required for discriminating between the 16 rival models. In total, no more than 16 experiments were required for the four temperature levels that were investigated.

EXAMPLE 2.7.2.2.A
SEQUENTIAL DESIGN FOR OPTIMAL PARAMETER ESTIMATION IN BENZOTHIOPHENE HYDROGENOLYSIS

The benzothiophene hydrogenolysis, accompanied by hydrogenation was already dealt with in Example 2.6.4.A in which the rate equations (a) through (c) were

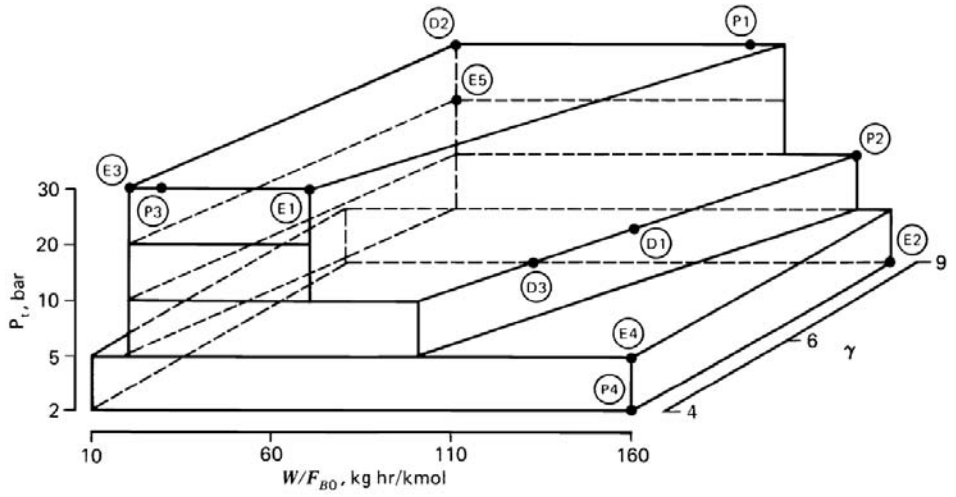

Figure 2.7.2.2.A-1

Settings of the experimental conditions. From Van Parijs et al. [1986].

derived and in Section 2.7.1 to illustrate the power of sequential methods in model discrimination. In this example the application of the determinant criterion (2.7.2.2-2) and the shape criterion (2.7.2.2-3) is illustrated. The σ^{ij} which enter into these criteria were estimated from replicated experiments and are given by (2.6.4-8).

Table 2.7.2.2.A-1 illustrates the sequential design for optimal estimation at 533 K. First, D_3 recalls the values of the parameter estimates arrived at after the last sequential discrimination experiment. The addition of one single experiment, E_1, designed according to the determinant criterion, suffices to make $K_{E,\tau}$ also statistically significant. Three more experiments designed according to the determinant criteria E_2 through E_4 sufficed to stabilize the determinant and the parameter values. Therefore, E_5 was designed according to the shape criterion, but no further improvement of the parameter values was obtained. Figure 2.7.2.2.A-1 shows the location of the settings, not only for the experiments dealt with here, but also of the sequentially designed experiments for optimal discrimination dealt with in Section 2.7.1 and of the four preliminary experiments required to start the optimal discrimination.

Note that all the designed experiments are located on the borders of the experimental space, a typical feature of sequential design.

TABLE 2.7.2.2.A-1

ESTIMATION AT 533 K OF THE PARAMETERS IN THE RATE EQUATIONS (a) THROUGH (c) OF EXAMPLE 2.6.4.A

	k_B^*, τ × 10^2	K_B, τ	K_E, τ × 10^{-2}	k_D, σ × 10	$K_{H.\sigma}^{1/2}$ × 10	K_B, σ × 10^{-1}	K_S, σ × 10^{-2}	k_B, σ × 10	$\det_{max}$ or $\lambda_{max}(E_5)$	p_t	γ	$\frac{W}{F_B^0}$
D_3	4.193 (4.3)	1.940 (2.0)	2.620 (1.7)	1.192 (3.1)	6.461 (4.6)	1.869 (5.6)	4.074 (2.6)	2.353 (7.6)	1.27×10^8	30	4	60
E_1	4.117 (4.9)	1.987 (2.3)	2.545 (2.0)	1.251 (3.7)	6.548 (5.2)	1.873 (8.0)	4.115 (3.5)	2.331 (8.5)	4.99×10^8	2	9	160
E_2	4.120 (5.4)	2.005 (3.4)	2.612 (2.7)	1.251 (4.1)	6.254 (7.0)	1.816 (11.)	3.842 (4.7)	2.358 (9.4)	2.12×10^9	30	4	24
E_3	4.346 (6.0)	1.961 (3.6)	2.748 (2.4)	1.264 (4.3)	5.881 (6.9)	1.927 (12.)	3.342 (4.3)	2.231 (8.7)	1.11×10^{10}	5	4	160
E_4	4.011 (4.3)	2.028 (3.4)	2.493 (2.2)	1.157 (3.8)	6.338 (6.2)	1.909 (10.)	1.956 (3.3)	1.880 (9.0)	1.81×10^{11}	20	9	40
E_5	4.123 (5.2)	2.023 (3.0)	2.905 (2.3)	1.042 (3.8)	5.940 (6.4)	1.909 (11.)	2.078 (4.0)	2.035 (10.)	1.83×10^{-4}	2	9	100

[a]The corresponding calculated n-values are mentioned in parenthesis.

2.8 EXPERT SYSTEMS IN KINETICS STUDIES

The steps involved in sequential experimental design for optimal discrimination and estimation can be represented in a simplified flow diagram as shown in Fig. 2.8-1. The loops can even be closed so that the settings of the independent variables are implemented on the experimental setup directly by the computer.

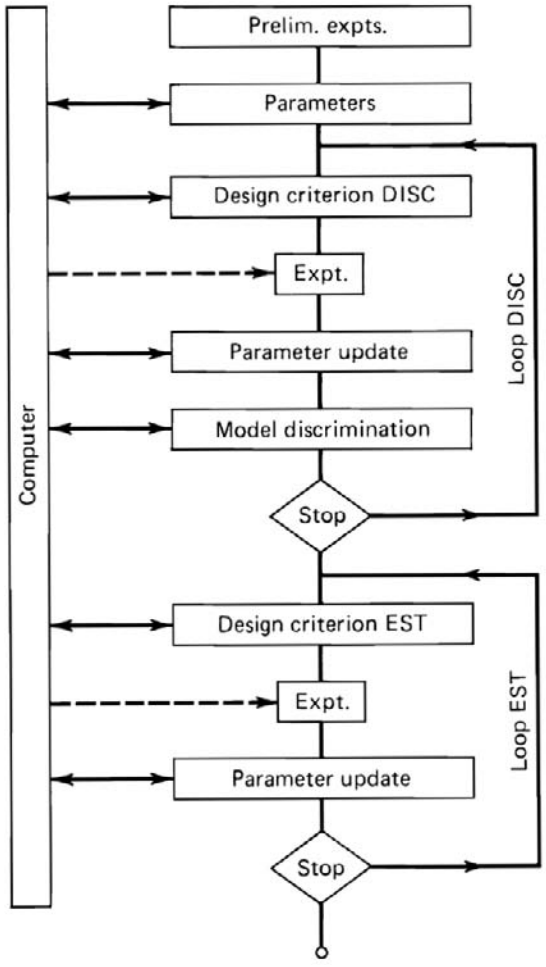

Figure 2.8-1
Sequential optimal design of experiments.

PROBLEMS

2.1 Derive the basic equation (2.3.1-7) for a single reversible catalytic reaction.

2.2 Consider the catalytic reaction

$$A + B \rightleftarrows R + S$$

(a) Derive the Hougen-Watson rate equation, assuming that adsorption is rate controlling.

(b) Compare the result of part (a) with that found from Yang and Hougen, Table 2.3.1-1.

2.3 In a study of the dehydrogenation over a brass catalyst of *sec*-butyl alcohol to methyl ethyl ketone,

$$CH_3CHOHC_2H_5 \rightarrow CH_3COC_2H_5 + H_2$$

L.H. Thaller and G. Thodos [*AIChE J.*, 6, 369 (1960)] obtained data that appeared to show two different rate-controlling steps, depending on the temperature level. At low temperatures, surface reaction was controlling, while at high temperatures desorption of (perhaps) hydrogen seemed rate controlling. A selection of their initial rate data is given in the table below.

(a) Using the data at T = 371°C, determine the parameters of the appropriate initial rate expression.

(b) Using the data at T = 288°C and 302°C, again determine the parameters.

T (°C)	P_t (bar.)	r_{A0} (kmol/kg cat. hr)
371	1.0	0.195
371	2.0	0.189
371	4.0	0.188
371	9.0	0.198
371	12.0	0.190
315.5	1.0	0.0392
315.5	7.0	0.0416
315.5	4.0	0.0416
315.5	10.0	0.0326
315.5	14.6	0.0247
315.5	5.5	0.0415
315.5	8.5	0.0376
315.5	3.0	0.0420
315.5	0.22	0.0295
315.5	1.0	0.0410
302	1.0	0.0227
302	3.0	0.0277
302	5.0	0.0255
302	7.0	0.0217
302	9.6	0.0183
288	1.0	0.0115
288	3.0	0.0161
288	2.0	0.0146

Note that the intermediate temperature level results should presumably depend upon both surface reaction and desorption steps, since at some point both steps will have equal rates (see Problem 2.5).

2.4 The Michaelis-Menten (Briggs-Haldane) mechanism in enzyme kinetics is based upon the following reaction scheme between the reactant (substrate *S*), and the catalyst (enzyme *E*) to give the product *P*:

$$S + E \rightleftarrows ES \rightarrow P + E$$

(a) Use the steady-state hypothesis for the enzyme-substrate complex *ES* to derive the Michaelis-Menten kinetic expression:

$$-\frac{d[S]}{dt} = \frac{(k_3[E_0])([S]-[P]/K)}{K_m + [S] + (k_4/k_1)[P]} = \frac{d[P]}{dt}$$

where $[E_0] = [E] + [ES]$ represents the measurable total enzyme concentration, $K_m = (k_2 + k_3) / k_1$ is the "Michaelis constant" and $K = k_1k_3/k_2k_4$.

(b) Show that the maximum initial rate is given by:

$$\left| -\frac{d[S]}{dt} \right|_{\max} = k_3[E_0]$$

2.5 **(a)** For the reaction in Problem 2.3, show that the initial rate expression, assuming that *both* surface reaction and desorption of *R* are rate controlling, is:

$$r_{AO} = \left[k_R + \frac{k_R^2}{2k_{sr}} \frac{(1+k_A p_A)^2}{K_A P_A} \right] - \left\{ \left[K_R + \frac{k_R^2}{2k_{sr}} \frac{(1+K_A P_A)^2}{K_A P_A} \right]^2 - k_R^2 \right\}^{1/2}$$

Replace K_R by k_R.

See Bischoff and Froment [1965].

(b) Show that the result reduces to the proper Yang and Hougen Table 2.3.1-1 results for each of the special cases $(K_R/K_{sr}) \rightarrow \infty$ and $(K_{sr}/K_R) \rightarrow \infty$.

(c) Using the combined results of Problem 2.3 and the above results, compare the model with the data at the intermediate temperature level, $T = 315.5°C$. [See also Shah and Davidson (1965) and R. W. Bradshaw and B. Davidson, *Chem. Eng. Sci.*, 24, 1519 (1969).]

2.6 Consider the reaction $A \rightleftarrows R + S$, occurring on dual sites. Determine the rate equation in the case that all four elementary steps are simultaneously rate determining.

2.7 The following data were obtained by Sinfelt and co-workers [Sinfelt, J. H. et al., *J. Phys. Chem.*, 64, 1559 (1960)] for the dehydrogenation of methylcyclohexane to toluene. In addition, they found that the product toluene had essentially no effect on the rate.

T (°C)	P_M (bar.)	p_{H_2} (bar.)	R_D (kmol/kg cat. h)
315	0.36	1.1	0.012
315	0.36	3.0	0.012
315	0.07	1.4	0.0086
315	0.24	1.4	0.011
315	0.72	1.4	0.013
344	0.36	1.1	0.030
344	0.36	3.1	0.032
344	0.08	1.4	0.020
344	0.24	1.4	0.034
344	0.68	1.4	0.034
372	0.36	1.1	0.076
372	0.36	4.1	0.080
372	1.1	4.1	0124
372	2.2	4.1	0.131

(a) Discuss which of the steps — adsorption, surface reaction, or desorption — might be rate controlling given the data in the above table.

(b) Show that a rate expression based on the mechanism

$$A + l \rightleftarrows Al$$

$$Al \rightleftarrows Rl$$

$$Rl \rightarrow Q + S + l$$

fits the data; also estimate the activation energies.

(c) Discuss the results of (b) in the light of (a).

2.8 The isomerization of *n*-pentane was considered in the text, where several rate expressions were stated. Derive the final result for desorption of isopentene controlling:

$$r = \frac{kK_5K_DK_6(p_A - p_B/K)}{p_{H2} + K_5K_D(1+K_6)p_A}$$

2.9 For the isomerization of *n*-pentane, derive the rate expression when the surface reaction step of the dehydrogenation reaction is rate controlling. Compare this rate with the correct rate of Problem 2.8, especially regarding variations with total pressure.

2.10 For the isomerization of *n*-pentane, the following experimental data were collected by Hosten and Froment [1971]:

x	y	W/F_{A0} (*kg cat. hr/kmol*)
0.4025	4.853	5.92
0.35	5.253	3.84
0.2784	5.29	2.84
0.2001	5.199	1.75
0.3529	6.833	5.74
0.2728	7.33	3.84
0.2038	7.344	2.66
0.3248	7.638	5.28
0.2571	8.514	3.9
0.2011	8.135	2.65
0.3017	10.598	5.73
0.2413	11.957	4.37
0.1734	10.227	2.65

where γ is the molar ratio H_2/hydrocarbon. The pentane feed contained 92.65 mole-% iso-C_5. The overall equilibrium constant is 2.07, while the selectivity for isomerization is nearly constant and equal to 0.91. Estimate the parameters in the adsorption model by means of the integral method of kinetic analysis. Both W/F_{A0} and x can be used as dependent variables. Comment on this choice. Compare the results and the computational effort for both cases.

2.11 A catalytic reaction $A \rightleftarrows B$ is carried out in a fixed bed reactor. Show the concentration profiles of adsorbed species as a function of bed depth for various rate-determining steps.

2.12 The dehydrogenation of ethanol was carried out in an integral reactor at 275°C with the following results:

x	p_t	W/F_{A0}
0.118	1	0.2
0.196	1	0.4
0.292	1	0.6
0.339	1	0.88
0.446	1	1.53
0.454	1	1.6
0.524	1	2.66
0.59	1	4.22
0.60	1	4.54
0.14	3	0.2
0.2	3	0.4
0.25	3	0.6
0.286	3	0.88
0.352	3	1.6
0.14	4	0.2
0.196	4	0.4
0.235	4	0.6
0.271	4	0.88
0.32	4	1.6
0.112	7	0.2
0.163	7	0.4
0.194	7	0.6
0.214	7	0.88
0.254	7	1.6
0.1	10	0.2
0.148	10	0.4
0.175	10	0.6
0.188	10	0.88
0.229	10	1.6

with p_t in bar and W/F_{A0} in kg cat. hr/kmol.

The overall equilibrium constant is 0.589. The feed consisted of the azeotropic mixture ethanol-water, containing 13.5 mole-% water. Water is not adsorbed on the catalyst. Estimate the parameters of the adsorption, surface reaction, and desorption models, using conversion as the regression variable. Comment on the feasibility for the estimation of the parameters. Which model is the best? On what basis?

2.13 Boolean Relation Matrix and Label Representation of Molecules and Ions.

(a) Write the Boolean relation matrix and the label representation of

(i) 3-Me-pentane -2+ carbenium ion

(ii) Naphthalene

(iii) Cumene (i-Propylbenzene)

(b) What are the Me-shift isomerizations and the β-scissions that the 3-Me-pentane -2+ ion can undergo? What are the products? Hint: For the β-scissions first construct the matrix M^2–1 in order to determine the 3 -carbon atoms.

REFERENCES

Advances in Catalysis, Academic Press, New York (1949-).
Alwahabi, S.M., and Froment, G.F., *Ind. Eng. Chem. Res.*, 43, 5098 (2004).
Alwahabi, S.M., and Froment, G.F., *Ind. Eng. Chem. Res.*, 43, 5112 (2004).
Anderson, J.R., and Boudart, M., Eds., *Catalysis. Science and Technology*, Springer Verlag, Berlin (1987).
Aris, R., *Introduction to the Analysis of Chemical Reactors*, Prentice-Hall, Englewood Cliffs, N.J. (1965).
Baltanas, M., and Froment, G.F., *Comp. Chem. Eng.*, 9, 71 (1985).
Ba1tanas, M., Van Raemdonck, K., Froment, G.F., and Mohedas, R.S., *Ind. Eng. Chem. Res.*, 28, 899 (1989).
Benson, S.W., Cruickshank, R.F., Golden, D.M., Haugen, G.R., O'Neal, H., Rodgers, A.S., Shaw, R., and Walsh, R., *Chem. Rev.*, 69, 279 (1969).
Beveridge, G.S.G., and Schechter, R.S., *Optimization Theory and Practice*, McGraw-Hill, New York (1970).
Bischoff, K.B., and Froment, G.F., *Ind. Eng. Chem. Fundam.*, 1, 195 (1965).
Bishop, D.M., and Laidler, K.J.J., *Chem. Phys.*, 42, 1688 (1965).
Boronat, M., and Corma, A., *Appl. Cat., A General*, 336, 2-10 (2008).
Boudart, M., *Ind. Chim. Belg.*, 23, 383 (1958).
Boudart, M., *Chem. Eng. Prog.*, 58, No. 73 (1962).
Boudart, M., *Kinetics of ChemicalProcesses*, Prentice-Hall, Englewood Cliffs, N.J. (1968).
Boudart, M., *AIChE J.*, 18, 465 (1972).
Boudart, M., *Ind. Eng. Chem. Fundam.*, 25, 656 (1986).
Boudart, M., *Ind. Eng. Chem. Res.*, 28, 379 (1989).
Boudart, M., and Djéga-Mariadassou, *Kinetics of Heterogeneous Catalytic Reactions*, Princeton University Press, Princeton, N.J. (1984).
Boudart, M., Mears, D., and Vannice, M.A., in Congrès International Chimie Industrielle, *Ind. Chim. Belge*, 32, 281 (1967).
Bowker, M., Parker, I., and Waugh, K.C., *Surface Science*, 197, L223 (1988).
Box, G.E.P., and Draper, N.R., *Biometrika*, 52, 355 (1965).
Box, G.E.P., and Henson, T.L., M.B.R. Tech. Rept. No. 51, University of Wisconsin, Madison, Wisconsin (January 1969).
Box, G.E.P., and Hill, W.J., *Technometrics*, 9, 57 (1967).
Box, G.E.P., and Lucas, H.L., *Biometrika*, 46, 77 (1959).
Broadbelt, L.J., and Pfaendtner, J., *AIChE J.*, 51, 2112 (2005).
Brunauer, S., *The Adsorption of Gases and Vapors*, Princeton University Press, Princeton, N.J. (1945).
Brunauer, S., Deming, L.S., Deming, W.E., and Teller, E.J., *J. Am. Chem. Soc.*, 62, 1723 (1940).
Bykov, V.I., Elokhin, V.I., and Yablonskii, G.S., *React. Kinet. Catal. Lett.*, 4, 191 (1976a).
Bykov, V.I., Chumakov, G.A., Elokhin, V.I., and Yablonskii, G.S., *React. Kinet. Catal. Lett.*, 5, 397 (1976b).
Bykov, V.I., and Yablonskii, G.S., *Int. Chem. Eng.*, 21, 142 (1981).
Christensen, G., Apelia, M.R., Hickey, K.J., and Jaffe, S.B., *Chem. Eng. Sci.*, 54, 2753 (1999).
Clark, A., *The Theory of Adsorption and Catalysis*, Academic Press, New York (1970).
Clymans, P.J., and Froment, G.F., *Comp. Chem. Eng.*, 8(2), 71 (1984).

Creten, G.L., Lafyatis, D.S., and Froment G.F., *J. Catal.*, 154, 151-162 (1995).
Creten, G., Kopinke, F.D., and Froment, G.F., *Can. J. Chem. Eng.*, 75, 882 (1997).
de Boer, J.H., *The Dynamical Character of Adsorption*, 2nd ed., Oxford University Press, Oxford (1968).
De Deken, J.C., Devos, E.F., and Froment, G.F., in "Chemical Reaction Engineering, Boston", A.C.S. Symp. Ser., 196, ed. by J. Wei and Ch. Georgakis, A.C.S., Washington, D.C. (1982).
Delmon, B., *C.R. Acad. Sci. Paris*, T289, Serie C, 173 (1979).
De Pauw, R.P., and Froment, G.F., *Chem. Eng. Sci.*, 30, 789 (1975).
De Wachtere, N.V., Santaella, F., and Froment, G.F., *Chem. Eng. Sci.*, 54, 3653 (1999).
Draper, N.R., and Smith, H., *Applied Regression Analysis*, Wiley, New York (1966).
Dumesic J.A., Rudd, D.F., Aparicio, L.M., Rekoske, J.E., and Trevino, A.A., "The Microkinetics of Heterogeneous Catalysis", A.C.S., Washington D.C. (1993).
Dumez, F.J., and Froment, G.F., *Ind. Eng. Chem. Proc. Des. Dev.*, 15, 291 (1976).
Dumez, F.J., Hosten, L.H., and Froment, G.F., *Ind. Eng. Chem. Fundam.*, 16, 298 (1977).
Dwyer, F.G., Eagleton, L.C., Wei, J., and Zahner, J.C., *Proc. Roy. Soc. London*, A302, 253 (1968).
Eigenberger, G., *Chem. Eng. Sci.*, 33, 1255 (1978).
Emig, G., Hofmann, H., and Friedrich, F., *Proc. 2nd Int. Symp. Chem. React. Eng.*, Amsterdam, 1972, Elsevier, B5-23 (1972).
Emmett, P.H., Ed., *Catalysis*, Vols. 1-7, Reinhold, New York (1954-1960).
Ertl, G., Knözinger, H., and Weitkamp, J., "Handbook of Heterogeneous Catalysis", Vol. 1-5, Wiley-VCH, Weinheim (1997).
Evans, M.G., and Polanyi, J.C., *Trans. Faraday Soc.*, 34(1), 0011 (1938).
Eyring, H., *Chem. Rev.*, 17, 65 (1935).
Falkenhauer, E., "Genetic Algorithms and Grouping Problems", J. Wiley & Sons, Chichester, England (1997).
Farrauto, R.J., and Bartholomew, C.H., "Fundamentals of Industrial Catalytic Processes", Blackie Academic and Professional, London (1997).
Feng, W., Vynckier, E., and Froment, G.F., *Ind. Eng. Chem. Res.*, 32, 2997 (1993).
Fierro, V., Duplan, J.L., Verstraete, J., Schuurman, Y., and Mirodatos, C., in *Studies in Surface Science and Catalysis*, Eds.: G.F. Froment and K.C. Waugh, 133, pp. 341-348, Elsevier Science B.V. (2001).
Flood, E.A., Ed., The Solid-Gas Interface, 2 Vols., Marcel Dekker, New York (1967).
Franckaerts, J., and Froment, G.F., *Chem. Eng. Sci.*, 19, 807 (1964).
Froment, G.F., in *Proc. 7th Eur. Symp.*, "Computer Application in Process Development", Erlangen, Dechema (April 1974).
Froment, G.F., *AIChE J.*, 21, 1041 (1975).
Froment, G.F., in *Proc. 4th Int. Symp. Chem. React. Eng.*, Heidelberg, 1976, Dechema (1976).
Froment, G.F., *Catalysis Today*, 1, 455 (1987a).
Froment, G.F., *Chem. Eng. Sci.*, 42, 1073 (1987b).
Froment, G.F., *Chem. Eng. Sci.*, 47, 2163 (1992).
Froment, G.F., *Cat. Today*, 52, 153 (1999).
Froment, G.F., *Cat. Rev.*, 1, 83 (2005).
Froment, G.F., and Mezaki, R., *Chem. Eng. Sci.*, 25, 293 (1970).
Froment, G.F., and Hosten, L.H., in *Catalysis. Science and Technology*, ed. by Anderson, J.R. and Boudart, M., Springer-Verlag, Berlin (1987).
Froment, G.F., Castaneda, L.C., and Marin Rosas, C., *Cat. Today*, 130, 446 (2008).
Gates, B.C., Katzer, J.R., and Schuit, G.C.A., *Chemistry of Catalytic Processes*, McGraw-Hill, New York (1978).
Germain, J.E., *Catalytic Conversion of Hydrocarbons*, Academic Press, New York (1969).
Gleaves, J., Ebner, J.R., and Kuechler, T.C., *Cat. Rev. Sc. Eng.*, 30(1), 498 (1968).
Greensfelder, B.S., Voge, G.M., and Good, H.H., *Ind. Eng. Chem.*, 41, 2573 (1949).
Gregg, S.J., and Sing, K.S.W., *Adsorption, Surface Area, and Porosity*, Academic Press, New York (1967).
Haensel, V., *Ind. Eng. Chem.*, 57, No. 6, 18 (1965).
Hayward, D.O., and Trapnell, B.M.W., *Chemisorption*, Butterworths, London (1964).
Himmelblau, D.M., *Applied Non-Linear Programming*, McGraw-Hill, New York (1972).

Hoffmann, U., and Hofmann, H., *Einfuhrung in die Optimierung*, Verlag Chemie, Weinheim, BRD (1971).
Hosten, L.H., *Chem. Eng. Sci.*, 29, 2247 (1974).
Hosten, L.H., and Froment, G.F., *Ind. Eng. Chem. Proc. Des. Dev.*, 10, 280 (1971).
Hosten, L.H., and Froment, G.F., in *Proc. 4th Int. Symp. Chem. React. Eng.*, Heidelberg 1976, Dechema (1976).
Hosten, L.H., and Froment, G.F., *Chem. Eng. Sci.*, 40, 1273 (1985).
Hougen, O.A., and Watson, K.M., *Chemical Process Principles*, Vol. III, Wiley, New York (1947).
Hunter, W.G., and Reiner, A.M., *Technometrics*, 7, 307 (1965).
Jacob, S.M., Gross, B., Voltz, S.E., and Weeckman, V.W., *AIChE J.*, 22, 701 (1976).
Jacobs, P.A., *Carboniogenic Activity of Zeolites*, Elsevier, Amsterdam (1977).
Juusola, J.A., Bacon, D.W., and Downie, J., *Can. J. Chem. Eng.*, 50, 796 (1972).
Kazansky, V.B., Memorial Boreskov Conference, Abstracts, Part 1, Institute of Catalysis, Novosibirsk, Russia, July 7-11 (1997).
Keil, F.J., in *Studies in Surface Science and Catalysis*, Eds.: G.F. Froment and K.C. Waugh, 133, pp. 41-55, Elsevier Science B.V. (2001).
Kiperman, S.L., Kumbilieva, K.E., and Petrov, L.A., *Ind. Eng. Chem. Res.*, 28, 376 (1989).
Kittrell, J.R., *Adv. Chem. Eng.*, 8, 97 (1970).
Kittrell, J.R., and Mezaki, R., *AIChE J.*, 13, 389 (1967).
Kiparissides, C., *Chem. Eng. Sci.*, 51, 1637 (1996).
Klein, M.T., Neurock, M., Nigam, A., and Libanati, C., in "Chemical Reactions in Complex Mixtures –The Mobil Workshop", Sapre, A.V. and Krambeck, F.J., Eds., 126-142, Van Nostrand Reinhold, New York (1991).
Kumar, H., and Froment, G.F., *Ind. Eng. Chem. Res.*, 46(18), 5881 (2007).
Kuo, J.C.W., and Wei, J., *I. & E.C. Fund.*, 8, 124 (1969).
Lafyatis, D.S., Creten, G.L., and Froment, G.F., *Appl. Cat., General*, 180, 85-103 (1994).
Lazic, Z.R., *Design of Experiments in Chemical Engineering: A Practical Guide*, Wiley-VCH (2004).
Lee, W.J., Froment, G.F., *Ind. Eng. Chem. Res.*, 47, 9183 (2008).
Liguras, D.K., and Allen, D.T., *Ind. Eng. Chem. Res.*, 28, 674 (1989).
Marin, G.B., and Froment, G.F., *Chem. Eng. Sci.*, 37, 754 (1982).
Marquardt, D.W., *J. Soc. Ind. Appl. Math.*, 2, 431 (1963).
Martens, J.A., Jacobs, P.A., "Conceptual Background for the Conversion of Hydrocarbons on Heterogeneous Acid Catalysts", in *Theoretical Aspects of Heterogeneous Catalysis*, Moffat J.B., Van Nostrand Reinhold, New York, p. 52 (1990).
Martinis, J.M., and Froment, G.F., *Ind. Eng. Chem. Res.*, 45, 940 (2006).
Mills, G.A., Heinemann, H., Milliken, T.H., and Oblad, A.G., *Ind. Eng. Chem.*, 45, 134 (1953).
Mills, P.L., and Lerou, J.J., *Rev. in Chem. Engng.*, 9(1-2), 3-97 (1993).
Mitchell, M., "An Introduction to Genetic Algorithms", MIT Press, Cambridge, MA (1996).
Moros, R., Kalies, H., Rex, H.G., and Schaffarczyck, S.T., *Chem. Eng. Sci.*, 20, 1257 (1996).
Nace, D.M., Voltz, S.E., and Weekman, V.W., *Ind. Eng. Chem. Proc. Des. Dev.*, 10, 530 (1971).
Oblad, A.G., Milliken, T.H., and Mills, G.A., *The Chemistry of Petroleum Hydrocarbons*, Reinhold, New York (1955).
Park, T.Y., and Froment, G.F., *Comput. Chem. Eng.*, 22, Suppl., S103 (1998).
Park, T.Y., and Froment, G.F., *Ind. Eng. Chem. Res.*, 40, 4172 (2001).
Park, T.Y., and Froment, G.F., *Ind. Eng. Chem. Res.*, 40, 4187 (2001).
Park, T.Y., and Froment, G.F., *Ind. Eng. Chem. Res.*, 43(3), 682 (2004).
Peterson, T.I., and Lapidus, L., *Chem. Eng. Sci.*, 21, 655 (1965).
Pollak, E., and Pechukas, P., *J. Am. Chem. Soc.*, 100, 2984 (1978).
Quann, R.J., and Jaffe, S.B., *Chem. Eng. Sci.*, 31, 1615 (1996).
Quann, R.J., and Jaffe, S.B., *Ind. Eng. Chem. Res.*, 31, 2483 (1992).
Rosenbrock, H.H., and Storey, C., *Computational Techniques for Chemical Engineers*, Pergamon Press, New York (1966).

Rudnitsky, L.A., and Alexeyev, A.M., *J. Catal.*, 37, 232 (1975).
Saha, B., and Ghoshal, A.K., *Ind. Eng. Chem. Res.*, 46(17), 5485-5492 (2007).
Shah, M.J., and Davidson, B., *Ind. Eng. Chem.*, 57, No. 10, 18 (1965).
Sinfelt, J.H., *Adv. Chem. Eng.*, 5, 37 (1964).
Somorjai, G.A., "Introduction to Surface Chemistry and Catalysis", J. Wiley and Sons, New York (1994).
Stoltze, P., and Nørskov, J.K., *Phys. Rev. Lett.*, 55, 2502 (1985).
Stoltze, P., and Nørskov, J.K., *J. Vacuum Sci. Technol.*, 5, 581 (1987).
Stoltze, P., and Nørskov, J.K., *Surface Science*, 197, L230 (1988).
Svoboda, G.D., Vynckier, E., Debrabandere, B., and Froment, G.F., *Ind. Eng. Chem. Res.*, 34, 3793 (1995).
Taguchi, G., Jugulum, R., and Taguchi, S., *Computer-Based Robust Engineering: Essential for DFSS*, ASQ Quality Press (2004).
Temkin, M.I., and Pyzhev, V., *Acta. Phys. Clin. USSR*, 12, 327 (1940).
Thomas, C.L., *Catalytic Processes and Proven Catalysts*, Academic Press, New York (1970).
Thomas, J.M., and Thomas, W.J., *Introduction to the Principles of Heterogeneous Catalysis*, Academic Press, New York (1967).
Thomson, S.J., and Webb, G., *Heterogeneous Catalysis*, Wiley, New York (1968).
Van Parijs, I.A., and Froment, G.F., *Ind. Eng. Chem. Prod. Res. Rev.*, 25, 431 (1986a).
Van Parijs, I.A., and Froment, G.F., *Appl. Catal.*, 21, 273 (1986b).
Van Parijs, I.A., Froment, G.F., and Delmon, B., *Bull. Soc. Chim. Belge*, 93, 823 (1984).
Van Parijs, I.A., Hosten, L.H., and Froment, G.F., *Ind. Eng. Chem. Prod. Res. Dev.*, 25, 437 (1986).
Vanrysselberghe, V., and Froment, G.F., *Ind. Eng. Chem. Res.*, 37, 4231 (1998).
Van Trimpont, P.A., Marin, G.B., and Delmon, B., *Appl. Catal.*, 24, 53 (1986).
Van Trimpont, P.A., Marin, G.B., and Froment, G.F., *Ind. Eng. Chem. Fundam.*, 25, 544 (1986).
Venuto, P.B., *Chem. Tech.*, April (1971).
Voge, G.M., *Catalysis*, ed. by Emmett, P.H., Vol. VI, Reinhold, New York (1958).
Vynckier, E., and Froment, G.F., in *Kinetic and Thermodynamic Lumping of Multicomponent Mixtures*, Astarita G., Sandler, S.L., Eds., 131, Elsevier Science Publishers BV, Amsterdam, The Netherlands (1991).
Wauquier, J.P., and Jungers, J.C., *Bull. Soc. Chim., France*, 1280 (1957).
Weekman, V.W., *AIChE J.*, 20, 833 (1974).
Weisz, P.B., *Adv. Catal.*, 13, 137 (1962).
Wilde, D.G., and Beightler, C.S., *Foundations of Optimization*, Prentice-Hall, Englewood Cliffs, N.J. (1967).
Yang, K.H., and Hougen, O.A, *Chem. Eng. Prog.*, 46, 146 (1950).

Chapter 3

Transport Processes with Reactions Catalyzed by Solids

In Chapter 2, rates were derived for reactions confined to an elementary volume of a catalyst particle, uniform in temperature and concentration. In the present chapter the complete particle and its immediate fluid-phase environment will be considered. The conditions in this system are not necessarily uniform, so that the various transport phenomena mentioned in the Introduction to Chapter 2 now have to be accounted for. Accordingly, the particle will be considered either as a pseudocontinuum or as a truly heterogeneous medium.

PART ONE
INTERFACIAL GRADIENT EFFECTS

3.1 REACTION OF A COMPONENT OF A FLUID AT THE SURFACE OF A SOLID

Let a component *A* of a fluid react on active centers at the surface of a solid. It is convenient for the present to define a rate based on the interfacial surface area, and if it is first order:

$$r_{Ai} = k_r C_{Ai} \tag{3.1-1}$$

where

r_{Ai} = rate of reaction of *A* at surface, $\text{kmol}/\text{m}_\text{p}^2\text{s}$

k_r = rate coefficient for the reaction, $\text{m}_\text{f}^3/\text{m}_\text{p}^2\text{s}$

C_{Ai} = concentration of *A* at the interface, $\text{kmol}/\text{m}_\text{f}^3$

The consumption of *A* at the interface has to be compensated for by transport from the bulk fluid, the flux of which can be written:

$$N_A = k_g\left(C_A - C_{Ai}\right) \tag{3.1-2}$$

where

N_A = mass flux with respect to the fixed solid surface, $\text{kmol}/\text{m}_\text{p}^2\text{s}$

k_g = mass transfer coefficient, $\text{m}_\text{f}^3/\text{m}_\text{p}^2\text{s}$

C_A = concentration of *A* in bulk stream, $\text{kmol}/\text{m}_\text{f}^3$

For steady state, the two rates must be equal, and this permits eliminating the unmeasured surface concentration C_{Ai}:

$$r_{Ai} = N_A = r_A$$

Thus,

$$C_{Ai} = \frac{k_g}{k_r + k_g} C_A$$

and

$$\begin{aligned} r_A &= \left(\frac{1}{k_g} + \frac{1}{k_r} \right)^{-1} C_A \\ &= k_0 C_A \end{aligned} \tag{3.1-3}$$

where an "overall" rate coefficient can be defined as

$$\frac{1}{k_0} = \frac{1}{k_g} + \frac{1}{k_r} \tag{3.1-4}$$

There are two limiting cases: When the mass transfer step is much faster than the surface reaction step, $k_g >> k_r$, and (3.1-4) gives $k_0 \cong k_r$. Also, $C_{Ai} \cong C_A$, and so the reactant concentration at the surface is the same as that measured in the bulk. The observed rate corresponds to the actual reaction—this is termed "reaction controlling". The other limit is that of almost instantaneous reaction, $k_r >> k_g$, and (3.1-4) gives $k_0 \cong k_g$. Also, $C_{Ai} \cong 0$, and the observed rate corresponds to the fluid-phase mass transfer step, not to the reaction—this is termed "diffusion controlling".

The same procedure may be followed for a second-order reaction:

$$r_{Ai} = k_r C_{Ai}^2 \tag{3.1-5}$$

which, with (3.1-2) leads to

$$r_A = k_g \left\{ \left[1 + \left(\frac{1}{2} \right) \frac{k_g}{k_r C_A} \right] - \sqrt{\left[1 + \left(\frac{1}{2} \right) \frac{k_g}{k_r C_A} \right]^2 - 1} \right\} C_A \tag{3.1-6}$$

A totally different form of concentration dependence is found, which is neither first order or second order (or one could state that the "overall" coefficient is not constant). Equation 3.1-6 reduces to the proper form in the two limiting situations:

$$r_A \cong k_r C_A^2 \qquad k_g >> k_r$$

$$r_A \cong k_g C_A \qquad k_r >> k_g$$

For an *n*th-order reaction, one finds

$$r_A = k_r\left(C_A - \frac{r_A}{k_g}\right)^n \tag{3.1-7}$$

r_A cannot be solved explicitly from (3.1-7) for arbitrary n, so that no equation equivalent to (3.1-3) or (3.1-6) is obtained. r_A may be obtained by iterative methods [see Frank-Kamenetskii, 1969]. Thus, in general, consecutive rate processes of different order cannot easily be combined into an overall expression, but can be handled by numerical techniques.

The occurrence of consecutive steps does not lead to serious complications when the rate is to be predicted, provided, of course, the rate coefficients and the order of the reaction are given. The reverse problem, namely the determination of the order and the rate coefficients is much more complicated. Sometimes, transport coefficients may be found in the literature for the case at hand so that it becomes possible to calculate the mass transfer effect. Generally, however, it will be necessary to derive the mass transfer coefficients from specific experiments. The experiments have to be performed under conditions for which the global rate is entirely determined by the mass transfer rate. This is generally achieved by operating at higher temperatures since the reaction rate coefficient is enhanced much more by a temperature increase than the mass transfer coefficient — the activation energy of the reaction is much higher than that of the transport phenomenon. The other extreme situation, whereby the global rate is entirely determined by the rate of reaction, may be reached by increasing the turbulence or by operating at a lower temperature. Finally, it is evident that these experiments should be performed under isothermal conditions to avoid further complications such as the need to include a heat transfer rate equation in the treatment.

3.2 MASS AND HEAT TRANSFER RESISTANCES

3.2.1 Mass Transfer Coefficients

Section 3.1 described how the mass transfer coefficient can be combined with the rate coefficient for simple reactions. This section gives more detailed discussion of how to obtain values for the mass transfer coefficients.

As mentioned previously, the mass transfer coefficient is defined as in transport processes [e.g., Bird, Stewart, and Lightfoot (1960)] and several driving force units are in common use:

$$N_A = k_g\left(y_A - y_{As}^s\right)$$

$$= k_g \left(C_A - C_{As}^s \right) \qquad (3.2.1\text{-}1)$$

$$= k_g \left(p_A - p_{As}^s \right)$$

The units and numerical values of k_g are different for each of these equations, but to avoid complicating the notation, only one symbol is used here, as was already done for the rate coefficient in Chapter 1.

As will be recalled from transport phenomena texts, it is most useful to define a mass transfer coefficient to describe only the diffusive transport and not the total, comprising diffusive plus convective contributions. The coefficients are identical only for the special case of equimolar counterdiffusion, and this is the value of the coefficient k^0_g that is actually correlated in handbooks.

Consider the diffusion of species *A* through a stagnant film of *B*, a phenomenon commonly encountered in unit operations. When the driving force is expressed in mole fractions the film theory, together with the proper solution of the diffusion equations, leads to:

$$k_g = \frac{k_g^0}{(y_b)_{\log mean}}$$

An analogous treatment can be followed in the case of reaction:

$$aA + bB + ... \rightleftarrows rR + sS + ...$$

and yields for the transport of species *A*, when the fluxes of *B*, *R* and *S* are related to that of *A* through the reaction stoichiometry :

$$k_g = \frac{k_g^0}{y_{fA}} \qquad (3.2.1\text{-}2)$$

where

$$y_{fA} = \frac{\left(1 + \delta_A y_A\right) - \left(1 + \delta_A y_{As}^s\right)}{\ln \dfrac{1 + \delta_A y_A}{1 + \delta_A y_{As}^s}} \qquad (3.2.1\text{-}3)$$

with

$$\delta_A = \frac{\left(r + s + ...\right) - \left(a + b + ...\right)}{a} \qquad (3.2.1\text{-}4)$$

This expression is often written in terms of partial and total pressures and is then called the “film pressure factor p_{fA}”. The basis for (3.2.1-2) to (3.2.1-4) is considered in Example 3.2.3.A. Correlations for the mass transfer coefficients can be presented in terms of the j_D factor, for example:

$$k_g^0 = \frac{j_D G}{M_m} Sc^{-2/3}$$

$$\text{or} \quad k_g = \frac{j_D G}{M_m y_{fA}} Sc^{-2/3} \qquad (3.2.1\text{-}5)$$

$$= \frac{j_D G}{M_m p_{fA}} Sc^{-2/3} \quad \text{(gases)}$$

$$\text{and} \quad j_D = f(\text{Re})$$

where Sc = Schmidt number = $\mu/\rho_f D$, and the k_g differ in numerical value, depending on the driving force.

Of particular interest for the following chapters is the mass transfer coefficient between a fluid and the particles of a packed bed. Figure 3.2.1-1 shows some of the most significant experimental results for this situation. For use in calculations it is convenient to have a numerical expression for the relation j_D versus Re. The following relations are fairly representative for the results shown in Fig. 3.2.1-1. The intersection of the lines at Re = 190 has no physical meaning, merely representing the correlation of Hougen [1961] and Yoshida et al. [1962]. For packed beds of spheres with $\varepsilon = 0.37$,

for Re = $d_p G/\mu < 190$,

$$j_D = 1.66(\text{Re})^{-0.51} \qquad (3.2.1\text{-}6a)$$

and for Re > 190,

$$j_D = 0.983(\text{Re})^{-0.41} \qquad (3.2.1\text{-}6b)$$

The use of these correlations for calculating values for k_g is illustrated below.

3.2.2 Heat Transfer Coefficients

Fluid-to-particle interfacial heat transfer resistances also need to be considered. These are described by

$$(-\Delta H) r_A = h_f a_m (T_s^s - T) \qquad (3.2.2\text{-}1)$$

where r_A is expressed in kmol/(kg_{solid} s) and a_m is the external surface per weight of solid (m^2_p/kg_{solid}). The heat transfer coefficient h_f is also correlated with respect to the Reynolds number by means of a j-factor expression:

$$h_f = j_H c_P G \,\text{Pr}^{-2/3} \quad \text{and} \quad j_H = f(\text{Re}) \qquad (3.2.2\text{-}2)$$

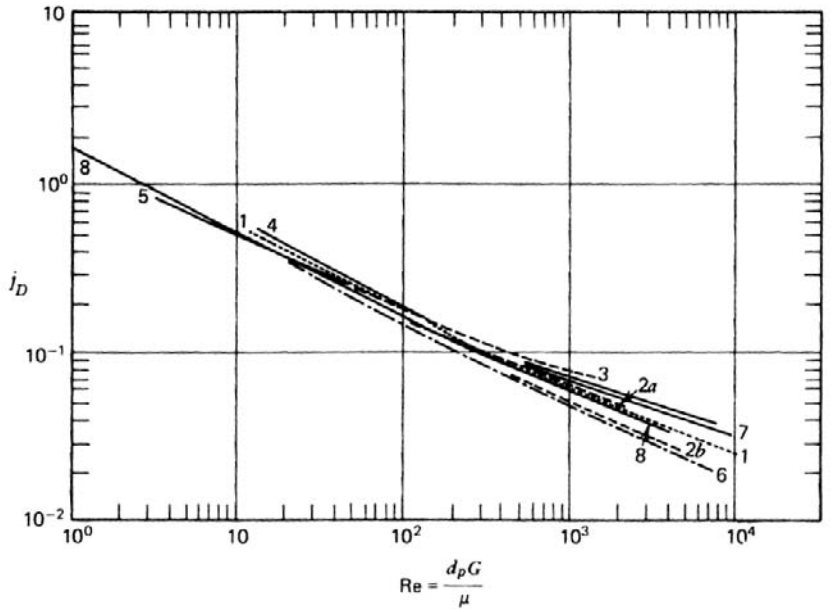

Figure 3.2.1-1

Mass transfer between a fluid and a bed of particles (spheres; ε = 0.37). Curve 1: Gamson et al. [1943]; Wilke and Hougen [1945]. Curve 2: Taecker and Hougen [1949]. Curve 3: McCune and Wilhelm [1949]. Curve 4: Ishino and Otake [1951]. Curve 5: Bar Ilan and Resnick [1957]. Curve 6: de Acetis and Thodos [1960]. Curve 7: Bradshaw and Bennett [1961]. Curve 8: Hougen [1961]; Yoshida, Ramaswami, and Hougen [1962].

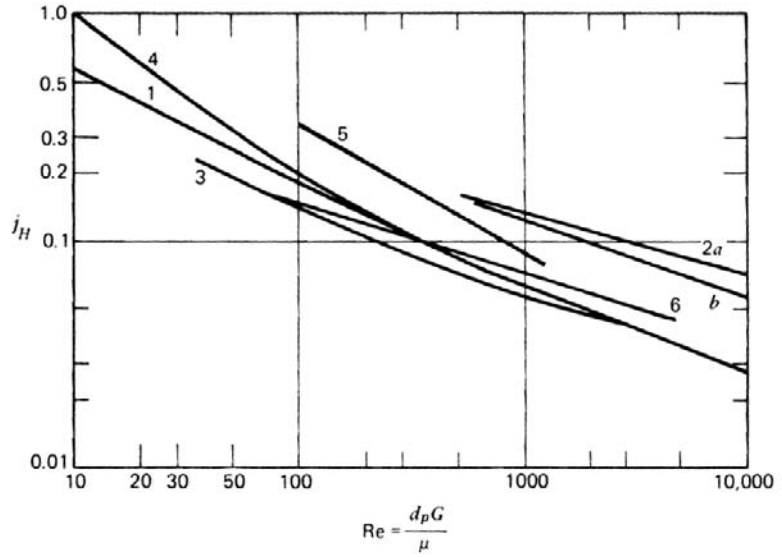

Figure 3.2.2-1

Heat transfer between a fluid and a bed of particles (spheres; ε = 0.37). Curve 1: Gamson et al. [1943]; Wilke and Hougen [1945]. Curve 2: Baumeister and Bennett (a) for d_t/d_p > 20, (b) mean correlation [1958]. Curve 3: Glaser and Thodos [1958]. Curve 4: de Acetis and Thodos [1960]. Curve 5: Sen Gupta and Thodos [1963]. Curve 6: Handley and Heggs [1968].

The most representative experimental results for the case of interfacial heat transfer between a fluid and the particles of a packed bed are shown in Fig. 3.2.2-1. A comprehensive discussion of j_D and j_H correlations was published by Schlünder [1978].

3.2.3 Multicomponent Diffusion in a Fluid

For a binary mixture, the single diffusivity D_{AB} is used in the Schmidt number. Most practical problems involve multicomponent mixtures, whose rigorous treatment is much more complicated, however.

In general, the flux of a given chemical species can be driven not only by its own concentration gradient, but also by those of all the other species [see Toor (1964), for example]:

$$\boldsymbol{N}_j = -\sum_{k=1}^{N-1} C_t D_{jk} \nabla y_k + y_j \sum_{k=1}^{N} \boldsymbol{N}_k \qquad j = 1, 2, ..., N-1 \qquad (3.2.3\text{-}1)$$

The second term accounts for bulk flow of the mixture. The exact form of the D_{jk} depends on the system under study. For ideal gases, the kinetic theory leads to the Stefan-Maxwell equations, that can be rearranged into the form of (3.2.3-1). A treatment using matrix methods is given by Stewart and Prober [1964]. For liquids, there is no complete theory yet — for a discussion of corrections for thermodynamic nonidealities see Bird, Stewart, and Lightfoot [1960]. A comprehensive review of available information on gas diffusion is given by Mason and Marrero [1970]. Diffusion in liquids was reviewed by Dullien, Ghai, and Ertl [1973, 1974].

The form of (3.2.3-1) is often judged to be too complex for many engineering calculations. A common approach is to define a mean binary diffusivity for species *j* diffusing through the mixture:

$$\boldsymbol{N}_j = -C_t D_{jm} \nabla y_j + y_j \sum_{k=1}^{N} \boldsymbol{N}_k \qquad (3.2.3\text{-}2)$$

Using (3.2.3-1), Toor [1964] and Stewart and Prober [1964] showed that the matrix of the D_{jk} could be diagonalized, which then gives the form of (3.2.3-2), and the many solutions available for binary mixtures can be adapted to multicomponent mixtures.

The Stefan-Maxwell equations for ideal gases are given in Bird, Stewart, and Lightfoot [1960] as:

$$-C_t \nabla y_j = \sum_{\substack{k=1 \\ k \neq j}}^{N} \frac{1}{D_{jk}} \left(y_k \boldsymbol{N}_j - y_j \boldsymbol{N}_k \right) \tag{3.2.3-3}$$

where the D_{jk} are the usual binary diffusivities. For a binary mixture,

$$-C_t \nabla y_1 = \frac{1}{D_{12}} \left[\boldsymbol{N}_1 - y_1 \left(\boldsymbol{N}_1 + \boldsymbol{N}_2 \right) \right] \tag{3.2.3-4}$$

where $y_1 + y_2 = 1$ was utilized. Solving for the flux,

$$\boldsymbol{N}_1 = -C_t D_{12} \nabla y_1 + y_1 \left(\boldsymbol{N}_1 + \boldsymbol{N}_2 \right) \tag{3.2.3-5}$$

For equimolar counter diffusion, $\boldsymbol{N}_2 = -\boldsymbol{N}_1$ and

$$\boldsymbol{N}_1 = -C_t D_{12} \nabla y_1 \tag{3.2.3-6}$$

For a multicomponent gas mixture, a binary diffusivity for species j diffusing through the mixture is found by equating the driving force ∇y_j in (3.2.3-2) and (3.2.3-3), with the result

$$\frac{1}{D_{jm}} = \frac{\displaystyle\sum_{k=1}^{N} \frac{1}{D_{jk}} \left(y_k - y_j \frac{N_k}{N_j} \right)}{1 - y_j \displaystyle\sum_{k=1}^{N} N_k / N_j} \tag{3.2.3-7}$$

The classical use of (3.2.3-7) in unit operations is the so-called “Wilke equation” for diffusion of species 1 through stagnant 2, 3, …. Here, all the flux ratios are zero for $k = 2, 3, \ldots$, and (3.2.3-7) reduces to

$$\frac{1}{D_{1m}} = \frac{1}{1 - y_1} \sum_{k=2,3,\ldots}^{N} \frac{y_k}{D_{1k}} \tag{3.2.3-8}$$

Even though (3.2.3-8) is often recommended for computing a diffusivity in reacting media, it is not really the appropriate equation, except for very dilute solutions. In other cases, the other species are not necessarily stagnant.The steady-state flux ratios of the various components are determined by the reaction stoichiometry. For a general chemical reaction,

$$\frac{N_j}{\alpha_j} = \text{constant}$$

and (3.2.3-7) becomes

$$\frac{1}{D_{jm}} = \frac{\sum_{k\neq j}^{N} \frac{1}{D_{jk}} \left(y_k - y_j \frac{\alpha_k}{\alpha_j} \right)}{1 - y_j \sum_{k=1}^{N} \left(\alpha_k / \alpha_j \right)} \tag{3.2.3-9a}$$

$$= \frac{1}{1+\delta_j y_j} \sum_{k\neq j}^{N} \frac{1}{D_{jk}} \left(y_k + y_j \frac{\alpha_k}{|\alpha_j|} \right) \tag{3.2.3-9b}$$

The last equation is written for species *j*, a reactant. In a theoretical study, Hsu and Bird [1960] have compared various uses of (3.2.3-9) in a ternary mixture with surface reaction versus the exact solution of the Stefan-Maxwell equations. The most straightforward is to use merely some mean composition $\bar{y}_j$ to compute an average value of D_{jm}.

It is also useful for certain applications, to define an alternate binary diffusivity with the flux relative to the fixed solid—any bulk flow is then included in the values for D''_{jm}:

$$\boldsymbol{N}_j = -C_t D''_{jm} \nabla y_j \tag{3.2.3-10}$$

leading to:

$$\frac{1}{D''_{jm}} = \sum_{k\neq j}^{N} \frac{1}{D_{jk}} \left(y_k - \frac{N_k}{N_j} y_j \right) \tag{3.2.3-11}$$

which is essentially just the numerator of (3.2.3-7). Kubota et al. [1969] solved the same problem as Hsu and Bird, and stated that the results indicated that, using constant mean compositions, (3.2.3-11) provided somewhat more accurate representation of the exact Stefan-Maxwell results than did (3.2.3-7).

EXAMPLE 3.2.3.A

USE OF A MEAN BINARY DIFFUSIVITY

For a chemical reaction

$$aA + bB + \ldots \rightleftarrows rR + sS + \ldots \tag{3.2.3.A-a}$$

(3.2.3-9) gives for the mean binary diffusivity

$$\frac{1}{D_{Am}} = \frac{1}{1+\delta_A y_A} \left[\begin{array}{l} \frac{1}{D_{AB}} \left(y_B - \frac{b}{a} y_A \right) + \frac{1}{D_{AR}} \left(y_R + \frac{r}{a} y_A \right) \\ + \frac{1}{D_{AS}} \left(y_S + \frac{s}{a} y_A \right) \ldots \end{array} \right] \tag{3.2.3.A-b}$$

with

$$\delta_A = \frac{r + s + ... - a - b - ...}{a}$$

The flux expression (3.2.3-2) can be written for one-dimensional diffusion as

$$N_A = -C_t D_{Am} \frac{dy_A}{dz} + y_A\left(N_A + N_B + N_R + N_S + ...\right) \quad \text{(3.2.3.A-c)}$$

$$= -C_t D_{Am} \frac{dy_A}{dz} + y_A N_A\left(1 + \frac{b}{a} - \frac{r}{a} - \frac{s}{a} - ...\right) \quad \text{(3.2.3.A-d)}$$

or

$$N_A = \frac{-C_t D_{Am}}{1 + \delta_A y_A} \frac{dy_A}{dz} \quad \text{(3.2.3.A-e)}$$

When integrated over the film thickness L for steady-state diffusion, with N_A = constant, and with an average constant value for D_{Am}, (3.2.3.A-e) gives

$$N_A = \frac{C_t D_{Am}}{L\delta_A} \ln \frac{1 + \delta_A y_{A0}}{1 + \delta_A y_A(L)} = \left(\frac{C_t D_{Am}}{L}\right) \frac{y_{A0} - y_A(L)}{y_{fA}} \quad \text{(3.2.3.A-f)}$$

where L depends on Re and y_{fA} is the "film factor" of (3.2.1-3), which is defined relative to the equimolar counterdiffusion case with $\delta_A = 0$, $y_{fA} = 1$. ■

3.3 CONCENTRATION OR PARTIAL PRESSURE AND TEMPERATURE DIFFERENCES BETWEEN BULK FLUID AND SURFACE OF A CATALYST PARTICLE

One of the most important uses of the above mass and heat transfer relationships is in determining external mass and heat transfer resistances for catalyst particles. Here, the rate is usually expressed in terms of catalyst mass (kmol / kg cat. s), and using a_m = external surface per weight of catalyst (m^2_p / kg cat.) gives

$$r_A = a_m k_g \left(C_A - C_{As}^s\right) \qquad (k_g \text{ in } \mathrm{m_f^3/m_p^2 s})$$

$$= a_m k_g \left(p_A - p_{As}^s\right) \qquad (k_g \text{ in kmol / m}_\mathrm{p}^2 \text{ s bar}) \quad \text{(3.3-1)}$$

In experimental kinetic studies in particular, the question often arises if the partial pressure drop Δp_A over the so-called external film may be neglected. One has to check whether or not it is allowed to substitute p_A, the partial pressure of A in the bulk fluid stream, into the rate equation for the reaction. The value of k_g is determined from a correlation, such as (3.2.1-5) with (3.2.1-2) and (3.2.1-3).

The calculation of Δp_A is not straightforward, since the calculation of the film pressure factor p_{fA} requires the knowledge of p_{As}^s. Iteration is required. Start with the assumption that $p_{As}^s = p_A$ or $\Delta p_A = 0$. It can be shown by L'Hopital's rule that in this case $p_{fA} = p_t + \delta_A p_A$. With this value of p_{fA}, the mass transfer coefficient k_g is calculated by means of (3.2.1-5), and with this k_g the partial pressure drop Δp_A is obtained from relationship (3.3-1). Substitution of Δp_A in (3.2.1-3) gives a better estimate for p_{fA} with which a new value for k_g and Δp_A is computed. The cycle is continued until convergence of the Δp_A values is obtained.

It is usually, but not always, found that Δp_A is rather small. It is more common to find fairly large ΔT. Significant ΔT, or Δp_A, are especially likely in laboratory reactors, which operate with low flow rates, whereas commercial reactors commonly have very high flow rates and Reynolds numbers and therefore small external film resistance.

A simple estimate of the temperature difference in terms of the concentration drop is provided by dividing (3.2.2-1) by (3.3-1), as shown by Smith [1970]:

$$\left(T_s^s - T\right) = \frac{k_g}{h_f}\left(-\Delta H\right)\left(C_A - C_{As}^s\right) \tag{3.3-2a}$$

$$= \left[\frac{j_D}{j_H}\left(\frac{\mathrm{Pr}}{Sc}\right)^{2/3}\right]\left[\frac{\left(-\Delta H\right)}{\rho_f c_p}\right]\frac{\Delta C_A}{y_{fA}} \tag{3.3-2b}$$

For gases flowing in packed beds, the values of the groups are such that

$$\left(T_s^s - T\right) \cong 0.7\left[\frac{\left(-\Delta H\right)}{M_m c_p}\right]\frac{\Delta p_A}{p_{fA}} \tag{3.3-2c}$$

The maximum possible actual temperature difference would occur for complete conversion and very rapid reaction and heat release, so that $p_{As}^s \cong 0$:

$$\left(\Delta T\right)_{\max} \cong 0.7\left[\frac{\left(-\Delta H\right)}{M_m c_p}\right]\left[\frac{\ln\left(1 + \delta_A p_A / p_t\right)}{\delta_A}\right] \tag{3.3-3}$$

When the physical properties, the reaction stoichiometry, and the bulk fluid-phase composition are available, a quick estimate of $(\Delta T)_{max}$ is possible.

EXAMPLE 3.3.A

INTERFACIAL GRADIENTS IN ETHANOL DEHYDROGENATION EXPERIMENTS

The dehydrogenation of ethanol into acetaldehyde,

$$C_2H_5OH \rightleftarrows CH_3CHO + H_2$$

$$A \rightleftarrows R + S$$

is studied in a tubular reactor with fixed catalytic bed at 275°C and 1 bar. The molar feed rate of ethanol, F_{A0}, is 0.01 kmol/h; the weight of catalyst, W, is 0.01 kg. At this value of W/F_{A0} the measured conversion is 0.362 and the reaction rate r_A is 0.193 kmol/kg cat. h. The inside diameter of the reactor is 0.035m. The catalyst particles are of cylindrical shape with diameter = height = d = 0.002 m. The bulk density of the bed, ρ_B, amounts to 1500 kg/m^3 and the void fraction ε is 0.37. From these, a_m = 1.26 m^2/kg. Estimate the partial pressure and temperature difference between the bulk gas stream and catalyst surface.

In a calculation of this type, it is frequently encountered that physicochemical data concerning the reacting components are lacking. Excellent estimates may then be obtained through the use of general correlations for the transport properties. In this example, only correlations that can be found in Reid, Prausnitz, and Sherwood [1977] are used. The background of these correlations is also explained in that book.

ESTIMATION OF THE PARTIAL PRESSURE DROP OVER THE FILM

ESTIMATION OF VISCOSITIES

H_2: Use the Lennard-Jones potential, with

$$\sigma = 2.827 \text{ Å}, \qquad \frac{\varepsilon_0}{k} = 59.7 \text{ K}, \qquad \Omega_v = 0.8379$$

$$\mu_{H_2} = \frac{0.002669\sqrt{2 \times 548}}{(2.827)^2 \times 0.8379} = 0.013195 \text{ cp} = 0.0475 \text{ kg/m h}$$

$$= 1.32 \times 10^{-5} \text{ kg/m s, or Pa s}$$

C_2H_5OH: Use the Stockmayer potential, with

$$\sigma = 4.31 \text{ Å}, \qquad \frac{\varepsilon_0}{k} = 431 \text{ K}, \qquad \delta = 0.3, \qquad \Omega_v = 1.422$$

$$\mu_{Eth} = \frac{0.002669\sqrt{46 \times 548}}{(4.31)^2 \times 1.422} = 0.01604 \text{ cp} = 0.05775 \text{ kg/m h}$$

$$= 1.604 \times 10^{-5} \text{ kg/m s, or Pa s}$$

CH_3CHO: Use the method of corresponding states, since the potential parameters are not available:

$T_c = 461$ K, $p_c = 55.4$ bar, $Z_c = 0.257$

$$\mu_{Ac}\xi = (1.9T_r - 0.29) \times 10^{-4} Z_c^{-2/3}$$

with

$$\xi = \frac{T_c^{1/6}}{M^{1/2} p_c^{2/3}} = \frac{461^{1/6}}{\sqrt{44}(54.7)^{2/3}} = 0.029078$$

$$\mu_{Ac} = \frac{1}{0.029078}\left(1.9 \times \frac{548}{461} - 0.29\right) \times 10^{-4} \frac{1}{(0.257)^{2/3}}$$

$$= 0.016748 \text{ cp} = 0.060293 \text{ kg/m h} = 1.675 \times 10^{-5} \text{ kg/m s, or Pa s}$$

VISCOSITY OF THE GAS MIXTURE

Composition of the reaction mixture:

$$p_A = \frac{1 - x_A}{1 + x_A} p_t = 0.4684 \text{ bar}, \qquad y_A = 0.4684$$

$$p_R = p_S = \frac{x_A}{1 + x_A} p_t = 0.2658 \text{ bar}, \qquad y_R = y_S = 0.2658$$

Since the hydrogen content cannot be neglected, Wilke's method may yield too high a value for the viscosity of the mixture. Therefore, the viscosity is computed from

$$\mu_m = \Sigma\, y_j \mu_j$$

or

$$\mu_m = 0.4684 \times 0.05775 + 0.2658 \times (0.0475 + 0.060293)$$

$$= 0.0557 \text{ kg/m h} = 1.547 \times 10^{-5} \text{ kg/m s}$$

From Wilke's method, a value of 0.06133 kg/m h is obtained.

$$M_m = \Sigma\, y_j M_j = 0.4684 \times 46 + 0.2658 \times (44 + 2)$$

$= 33.77$ kg/kmol

$$\rho_m = \frac{M_{m0}}{V_0}\frac{T_0}{T} = \frac{33.77}{22.4}\times\frac{273}{548} = 0.7510 \text{ kg/m}^3$$

DIFFUSION COEFFICIENTS

Since some of the required potential parameters are not known, the semiempirical relation of Fuller-Schettler-Giddings will be applied:

$(\Sigma v)_{H_2} = 7.07 \text{ cm}^3/\text{mol}$

$(\Sigma v)_{C_2H_5OH} = 2v_C + 6v_H + v_0 = 2 \times 16.5 + 6 \times 1.98 + 5.48 = 50.4 \text{ cm}^3/\text{mol}$

$(\Sigma v)_{CH_3CHO} = 2v_C + 4v_H + v_0 = 2 \times 16.5 + 4 \times 1.98 + 5.48 = 46.4 \text{ cm}^3/\text{mol}$

$$D_{Eth-H_2} = D_{AS} = \frac{0.00101\times(548)^{1.75}\sqrt{\frac{1}{46}+\frac{1}{2}}}{1.0133\left[(50.36)^{1/3}+(7.07)^{1/3}\right]^2}$$

$= 1.4235 \text{ cm}^2/\text{s} = 1.4235 \times 10^{-4} \text{ m}^2/\text{s}$

Note: D_{AS} has been experimentally measured at 340 K as 0.578 cm^2/s. The Fuller-Schettler-Giddings formula yields for D_{AS} at 340 K

$$D_{AS} = 1.4235\times\left(\frac{340}{548}\right)^{1.75} = 0.6174 \text{ cm}^2/\text{s} = 0.6174 \times 10^{-4} \text{ m}^2/\text{s}$$

Percentage error:

$$\frac{0.61742 - 0.578}{0.578}\times 100 = 6.82\%$$

$$D_{Eth\text{-}Ac} = D_{AR} = \frac{0.00101\times(548)^{1.75}\times\sqrt{\frac{1}{44}+\frac{1}{46}}}{1.0133\left[(46.4)^{1/3}+(50.36)^{1/3}\right]^2}$$

$= 0.2466 \text{ cm}^2/\text{s} = 0.2466 \times 10^{-2} \text{ m}^2/\text{s}$

From (3.2.3-9),

$$D_{am} = \left(\frac{\frac{y_R + y_A}{D_{AR}} + \frac{y_S + y_A}{D_{AS}}}{1 + y_A}\right)^{-1} = \left(\frac{\frac{0.2658 + 0.4684}{0.2466\times10^{-4}} + \frac{0.2658 + 0.4684}{1.4235\times10^{-4}}}{1 + 0.4684}\right)^{-1}$$

$= 0.4203 \times 10^{-4}$ m^2/s

Now the Schmidt and Reynolds numbers may be calculated:

$$Sc = \frac{\mu_m}{\rho_m D_{Am}} = \frac{1.547 \times 10^{-5}}{0.751 \times 0.4203 \times 10^{-4}} = 0.490, \text{ from which } (Sc)^{2/3} = 0.622$$

$$G = \frac{0.01 \times 46}{\frac{\pi}{4}(0.035)^2 \times 3600} = 0.1328 \text{ kg/m}^2 \text{ s}$$

$$\text{Re} = \frac{d_p G}{\mu_m} = \frac{2.289.10^{-3} \times 0.1328}{1.547 \times 10^{-5}} = 19.65$$

Since Re < 190, the following j_D correlation should be used:

$$j_D = 1.66(\text{Re})^{-0.51} \quad \text{and} \quad j_D = 0.3635$$

Now the partial pressure drop can be calculated. Assuming that $\Delta p_A = 0$ and with $\delta_A = 1$, the film pressure factor for a reaction $A \rightleftarrows R + S$ becomes

$$p_{fA} = p_t + \delta_A p_A = 1 + 0.4684 = 1.4684 \text{ bar}$$

$$\Delta p_A = \frac{r_A M_m p_{fA}}{a_m G j_D}(Sc)^{2/3} = \frac{0.193 \times 33.77 \times 1.4684}{3600 \times 1.26 \times 0.1328 \times 0.3635} \times 0.622$$

$$\Delta p_A = 0.0272 \text{ bar}$$

Substitution of this estimate for Δp_A in (3.2.1-3), written in terms of partial pressures, leads to a better estimate for p_{fA}:

$$p_{fA} = \frac{0.0272}{\ln(1.4684/1.4412)} = 1.4547$$

This new estimate for the film pressure factor may be considered sufficiently close to the starting value 1.4684, so that no further iterations on Δp_A need to be performed.

ESTIMATION OF THE TEMPERATURE DROP OVER THE FILM

The calculation of ΔT requires two further properties of the reaction mixture to be calculated: the specific heat c_p and the thermal conductivity λ. The c_p values for the pure components can be found in the literature or can be estimated accurately from the correlation of Rihani and Doraiswamy [1965]. The c_p values are given in the table below.

	Ethanol	Acetaldehyde	Hydrogen
T_b (K)	351.7	294	20.4
T_c (K)	516.3	461	33.3
ΔH_v (kJ/kmol)	38604	27006	-
ΔS_v (kJ/kmol K)	109.8	91.86	
ρ_b (kmol/m^3)	$\frac{1000}{63}$	$\frac{783}{44}$	
C_p (kJ/kmol K)	106.5	81.2	29.3
λ (kJ/m s K)	4.61×10^{-5}	3.977×10^{-5}	27.2×10^{-5}

The heat capacity of the mixture may be computed accurately by means of

$$c_{pm} = \Sigma y_j c_{Pj}$$

$$= 0.4684 \times 106.5 + 0.2658 \times (81.2 + 29.3) = 79.25 \text{ kJ/kmol K}$$

The thermal conductivities of the pure components are estimated by Bromley's method.

The following details provide the basis for the numbers in the table:

C_2H_5OH (polar nonlinear molecule): From Perry and Chilton [1984],

$$\Delta H_{vb} = 38604 \text{ kJ/kmol}$$

Consequently,

$$\Delta S_{vb} = \frac{\Delta H_{vb}}{T_b} = \frac{38604}{351.7} = 109.78 \text{ kJ/kmol K}$$

ρ_b, the density of liquid ethanol at the normal boiling point, is estimated using Schroeders' rule:

$$V_b = 9 \times 7 = 63 \text{ cm}^3\text{/mol}$$

$$\rho_b = \frac{1000}{63} \text{ kmol/m}^3$$

$$\alpha = 3\rho_b\left(\Delta S_{vb} - 36.63 - R\ln T_b\right)$$

$$\alpha = 3 \times \frac{1}{63}\left(109.8 - 36.63 - 8.315 \times \ln 351.7\right) = 1.16$$

$$c_{int\,rot} = 4.98 + 8.50 = 13.48 \text{ kJ/kmol K}$$

$$\downarrow \qquad \downarrow$$

$$\text{—}CH_2\text{—}OH \qquad CH_3CH_2\text{—}$$

$$c_v = c_p - 8.37 = 106.47 - 8.37 = 98.1 \text{ kJ/kmol K}$$

$$\frac{M\lambda}{\mu} = 1.3c_v + 15.07 - 0.3c_{int\,rot} - 0.69\frac{T_c}{T} - 3\alpha$$

$$\frac{46\times\lambda}{1.604\times10^{-5}} = 1.3 \times 98.1 + 15.07 - 0.3 \times 13.48 - 2.89 \times \frac{516.3}{548}$$

$$- 3 \times 1.16 = 132.35 \text{ kJ/kmol K}$$

$$\lambda = 4.61 \times 10^{-5} \text{ kJ/m s K}$$

CH_3CHO (polar nonlinear molecule): ΔH_{vb} has to be estimated, Giacalone's method is used:

$$\Delta H_{vb} = \frac{RT_bT_C \ln p_c}{T_c - T_b} = \frac{8.315\times294\times461\times\ln 54.7}{461-294}$$

$$\Delta H_{vb} = 27006 \text{ kJ/kmol}$$

$$\Delta S_{vb} = \frac{\Delta H_{vb}}{T_b} = \frac{27006}{294} = 91.86 \text{ kJ/kmol K}$$

ρ_b is found in the literature: $\frac{783}{44}$ kmol/m^3;

$$\alpha = 3\times\frac{0.783}{44}(91.86 - 36.63 - 8.315\times\ln 294) = 0.426$$

$$c_{int\,rot} = 5.07 \text{ kJ/kmol K}$$

$$c_v = c_p - 8.37 = 81.17 - 8.37 = 72.80 \text{ kJ/kmol K}$$

$$\frac{44\times\lambda}{1.675\times10^{-5}} = 1.3\times72.8 + 15.07 - 0.3\times5.07 - 2.89\times\frac{461}{548}$$

$$- 3 \times 0.426 = 104.48 \text{ kJ/kmol K}$$

$$\lambda = 3.977 \times 10^{-5} \text{ kJ/m s K}$$

H_2 (nonpolar linear molecule):

$$\frac{M\lambda}{\mu} = 1.3c_v + 14.23 - 2.93\frac{T_c}{T}$$

$$\frac{2\times\lambda}{1.3195\times10^{-5}} = 1.3\times20.91 + 14.23 - 2.93\times\frac{33.3}{548}$$

$$= 41.235 \text{ kJ/kmol K}$$

$$\lambda = 27.20 \times 10^{-5} \text{ kJ/m s K}$$

THERMAL CONDUCTIVITY OF THE GAS MIXTURE

To estimate the factors A_{ij} the Lindsay-Bromley equation is appropriate and will be applied here.

The required Sutherland constants are

$S_{Eth} = 1.5 \times 351.7 = 527.55$ K $S_{Eth\text{-}Ac} = 482.34$ K

$S_{Ac} = 1.5 \times 294 = 441$ K $S_{Ethh-H_2} = 204.15$ K

$S_{H_2} = 79$ K $S_{Ac-H_2} = 186.65$ K

The Lindsay-Bromley formula yields

$A_{12} = 0.9615$ $A_{21} = 1.038$

$A_{13} = 0.3653$ $A_{31} = 3.1565$

$A_{23} = 0.3872$ $A_{32} = 3.0988$

$$\lambda_m = \frac{4.61\times10^{-5}}{1+0.9615\times\frac{0.2658}{0.4684}+0.3654\times\frac{0.2658}{0.4684}} + \frac{3.977\times10^{-5}}{1+1.038\times\frac{0.4684}{0.2658}+0.387\times1}$$

$$+\frac{27.20\times10^{-5}}{1+3.156\times\frac{0.4684}{0.2658}+3.0988\times1}$$

$$\lambda_m = 6.682\times10^{-5} \text{ kJ/m s K}$$

Note: If the thermal conductivity of the mixture had been considered as linear in the composition, λ_m would be given by

$$\lambda_m = \Sigma\, y_j \lambda_j$$

or

$$\lambda_m = \left[0.4684\times4.61+0.2658\times(3.977+27.2)\right]\times10^{-5}$$

$$= 10.446\times10^{-5} \text{ kJ/m s K}$$

This value is 50 percent higher than the more correct estimate. Then, the Prandtl number is

$$\mathrm{Pr} = \frac{c_{pm}\mu_m / M_m}{\lambda_m} = \frac{(79.25/33.8)\times 1.547\times 10^{-5}}{6.682\times 10^{-5}} = 0.5428$$

$$(\mathrm{Pr})^{2/3} = 0.665$$

From Fig. 3.2.2-1, a value of 0.60 may be chosen for j_H at Re = 19.65. The heat of reaction is calculated as follows:

$$-\Delta H = (\Delta H)_{Eth} - (\Delta H)_{Ac} - (\Delta H)_{H_2} = 70338 \text{ kJ/kmol}$$

so that

$$\Delta T = \frac{r_A(-\Delta H)(\mathrm{Pr})^{2/3}}{a_m j_H c_p G} = \frac{0.193\times 70338\times 0.665}{3600\times 1.26\times 0.6\times \dfrac{79.25}{33.77}\times 0.1328} = 10.6 \text{ K}$$

This is a difference between bulk and surface temperatures that has to be accounted for. ■

PART TWO
INTRAPARTICLE GRADIENT EFFECTS

After discussing various aspects of external mass transfer and surface reactions, transport and reaction inside a porous catalyst will now be dealt with.

3.4 MOLECULAR, KNUDSEN, AND SURFACE DIFFUSION IN PORES

Fig. 3.4-1 presents ranges of pore sizes in which molecular, Knudsen, and configurational diffusion occur. Values of the corresponding diffusivities are also shown.

Molecular and Knudsen diffusion will be discussed first. Configurational diffusion, mainly encountered with zeolite catalysts, will be discussed separately in Section 3.5.4.

Molecular diffusion of a component is driven by a composition gradient. In a mixture of n components, the partial pressure gradient of component i is given by the Stefan-Maxwell equation:

$$\nabla p_i = -RT\sum_{j\neq i}^{M}\frac{y_j \boldsymbol{N}_{D,i} - y_i \boldsymbol{N}_{D,j}}{D'_{D,ij}} \qquad (3.4\text{-}1)$$

where y_i is the mol fraction of i and $\boldsymbol{N}_{D,i}$ its flux. The molecular diffusivities are independent of the composition, inversely proportional to the total pressure in a

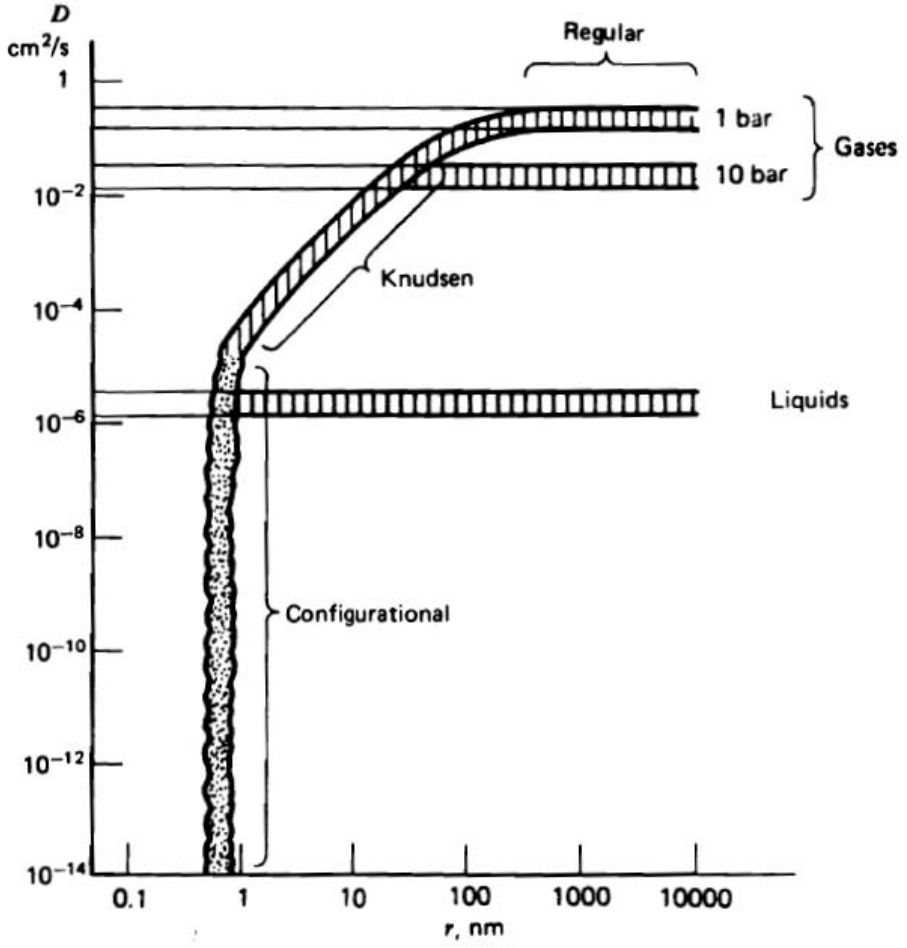

Figure 3.4-1

Diffusivity and size of pore radius. Regions of molecular, Knudsen and configurational diffusion. [Adapted from Weisz, 1973.]

gaseous mixture and proportional to $T^{3/2}$. The momentum transfer occurs by collisions between the atoms or molecules of the mixture. The fluxes are expressed per unit external surface of the catalyst particle, so that the homogeneous phase diffusivity D_{ij} has to be reduced by a factor ε_s:

$$D_{ij}^{'} = \varepsilon_s D_{ij} \tag{3.4-2}$$

where ε_s is the void fraction of the catalyst particle (m^3_f / m^3_{cat}). According to Dupuit's theorem, this is also the fraction of the particle surface taken by the pore mouths.

When the mean free path of the components is much larger than the pore dimensions, the momentum transfer mainly results from collisions with the pore walls. This is the Knudsen diffusion regime, encountered at pressures below 5 bar and with pore sizes between 3 and 200 nm. The flux of *i* is then written as:

$$\boldsymbol{N}_{K,i} = -\frac{D_{K,i}}{RT}\frac{\nabla p_i}{l} \tag{3.4-3}$$

with $\boldsymbol{N}_{K,i}$ in kmol *i* / m^2_S h and $D_{K,I}$ in m^3_f / m_S h. The Knudsen diffusion flux of *i* is independent of the fluxes of the other components. The diffusivity is given by

$$D_{K,i} = \frac{2r}{3}\sqrt{\frac{8RT}{\pi M_i}} \tag{3.4-4}$$

M_i is the molecular weight of *i*, in kg/kmol. $D_{K,i}$ is a function of the pore radius, is independent of the total pressure and varies with $T^{1/2}$.

The ratio of D_K for components *i* and *j* is given by Graham's law:

$$\frac{D_{K,i}}{D_{K,j}} = \sqrt{\frac{M_j}{M_i}} \tag{3.4-5}$$

Like the molecular diffusion flux the Knudsen diffusion flux (3.4-3) is referred to the total particle surface area, so that:

$$D'_{K,i} = \varepsilon_b D_{K,i} \tag{3.4-6}$$

When both types of diffusion occur simultaneously and there is a flux from viscous or laminar flow, the partial pressure gradient of component *i* is given by:

$$\nabla p_i = -RT\left[\frac{\boldsymbol{N}_{K,i}}{D'_{K,i}} + \sum_{j\neq i}\frac{y_j\boldsymbol{N}_{D,i} - y_i\boldsymbol{N}_{D,j}}{D'_{D,ij}}\right] - \frac{y_i B_o p_t}{\mu D'_{K,i}}\nabla p_t \tag{3.4-7}$$

where B_o is Darcy's permeability constant. This equation corresponds to the dusty gas model equation, rigorously derived from the kinetic gas theory [Mason et al., 1961; 1962; 1969; 1970]. The viscous flow term is generally negligible, except when $B_o p_t / \mu D_{K,i} > 10 - 20$, i.e., for micron-size pores.

In a binary mixture of *A* and *B* for which $y_B = 1 - y_A$ and neglecting the viscous flow:

$$\frac{1}{D_A'} = \frac{1 - y_A\left(1 + \dfrac{\boldsymbol{N}_B}{\boldsymbol{N}_A}\right)}{D_{D,AB}'} + \frac{1}{D_{K,A}'} \tag{3.4-8}$$

and for equimolar counterdiffusion $(\boldsymbol{N}_B = -\boldsymbol{N}_A)$:

$$\frac{1}{D_A'} = \frac{1}{D_{D,AB}'} + \frac{1}{D_{K,A}'} \tag{3.4-9}$$

This additive resistance relation is the Bosanquet formula.

For diffusion in a multicomponent mixture, the more complicated Stefan-Maxwell equation for D_D is sometimes replaced by the equation for an equivalent binary mixture:

$$\frac{1}{D_{jm}'} = \sum_{k=1}^{m} \frac{1}{D_{jk}'}\left(y_k - \frac{\boldsymbol{N}_k}{\boldsymbol{N}_j} y_j\right) + \frac{1}{D_{K,j}'} \tag{3.4-10}$$

A third mode of transport inside pores is surface diffusion. This proceeds by hopping of the molecules from one adsorption site to another. In recent years it has been studied experimentally using sophisticated surface science techniques like field ion microscopy and scanning tunnelling microscopy (STM). If this diffusion is modeled as a random walk, the diffusivity is given by:

$$D_s = \frac{k\lambda^2}{\tau'} \tag{3.4-11}$$

where λ is the jump length, τ' is the correlation time for the motion and k is a numerical proportionality factor. The correlation time τ can be measured separately by deuteron NMR. The parameters λ and τ each vary with temperature according to the van't Hoff exponential law. The pre-exponential factor of the D_s is then $D_{s,a} = k\lambda_0^2 / \tau_0'$ and the energy factor $E_D = 2E_\lambda - E_\tau$. The pre-exponential factor τ_0 is inversely proportional to the number of available sites to which a molecule could jump [Rigby, 2003]. This number is known for structured surfaces like zeolites, but much less for amorphous surfaces where the sites belong more to patches, whose sizes depend on the roughness of the solid.

Surface diffusivity has been shown to depend on the surface coverage and to be more important in micro- than in macroporous material. In the past, its flux has been expressed in terms of a Fickian law, but the driving force can not be the fluid phase concentration gradient.

It is not clear yet if this mode of transport significantly contributes to the diffusivity in industrial processes. It should be mentioned that recent work of the

catalyst producing company Haldor Topsoe investigated surface diffusion in the steam reforming process on a Ni/alumina catalyst and in methanol synthesis on Cu-ZnO/alumina [Clausen, 2007].

In the preceding the walls of the pores were assumed to be smooth, whereas in reality they have a certain roughness. Small angle X-ray scattering e.g., shows that a frequently used catalyst support like γ-alumina is fractal on a molecular scale. The fractal morphology of a surface influences the Knudsen diffusivity of gases [Coppens and Froment, 1995]. The effect of this was illustrated by Coppens and Froment [1996] in their simulation of the catalytic reforming of naphtha, an industrial process for boosting the octane number of the product gasoline. A Pt-Re/alumina catalyst with smooth pore surface yielded e.g., 18.9 wt% iso-paraffins and 70.1 wt% of aromatics. For the same intrinsic reaction rates per unit mass of catalyst accounting for the fractal nature of the surface led to values of respectively 21.7 and 66.2 wt%.

3.5 DIFFUSION IN A CATALYST PARTICLE

3.5.1 A Pseudo-Continuum Model

3.5.1.1 Effective Diffusivities

Catalyst particles have a very complicated pore structure and describing diffusion from the external surface to the active sites where the reactions take place is not a simple task. In practical applications the catalyst particle is generally considered as a continuum through which the molecules move by “effective” diffusion. In terms of Fick’s law for diffusion the molar flux of a component *A*, expressed per total unit pellet surface, is written

$$N_A = -D_{eA}\frac{dC_A}{dz} \qquad (3.5.1.1\text{-}1)$$

or in a sphere

$$N_A = -D_{eA}\left(\frac{\partial^2 C_A}{\partial r^2} + \frac{2}{r}\frac{\partial C_A}{\partial r}\right) \qquad (3.5.1.1\text{-}2)$$

with the diffusion flux oriented along the radius of the continuum.

In Section 3.4 already the homogeneous medium diffusivity was corrected for the ratio of surface holes to total surface area of the catalyst. For a random pore network this ratio is, according to Dupuit’s law, equal to the internal void fraction, ε_s. Another adaptation is required because of the tortuous nature of the pores and eventual pore constrictions. The diffusion path length along the

pores from the external particle surface to the center is not necessarily oriented along the normal from the surface to the center and therefore it is longer than the particle radius. This is why the concentration gradient based on the particle radial coordinate, must be corrected by a "tortuosity" factor, τ, which is larger than l, leading to an effective diffusivity

$$D_{eA} = \frac{D_A^{'}}{\tau} = \frac{\varepsilon_s}{\tau} D_A \quad \text{with units} \quad \frac{\mathrm{m}_\mathrm{f}^3}{\mathrm{m}_\mathrm{p}\mathrm{s}} \qquad (3.5.1.1\text{-}3)$$

3.5.1.2 Experimental Determination of Effective Diffusivities of a Component and of the Tortuosity

Two types of techniques are commonly used for the determination of the internal void fraction and the tortuosity. The first uses a column packed with the catalyst and having a d_t/d_p ratio such that the flow approximates the ideal plug flow pattern. It is conveniently inserted in the furnace of a gas chromatograph that has all the parts for detecting the feed and response signals, besides temperature- and flow controls and six way valves. A narrow tracer pulse is injected in the carrier gas flow and the response is measured at the exit of the column. The pulse widens as a consequence of the dispersion in the bed, adsorption on the catalyst surface and effective diffusion inside the catalyst particle. The tracer does not have to be the component *A* itself. The injected pulse should have an adequate residence time in the column and sufficient widening. Preference is given to transient measurements because steady state operation would not measure the effect of the dead end pores.

The data treatment of the transient experiments in a packed column is based on the early Van Deemter model [1956], later refined by Pazdernik and Schneider [1981] and by Kubin [1965] and Kucera [1965a, b]. The latter model consists of a transient continuity equation for the tracer flowing through the packed column and a transient equation for the effective diffusion in the pores of the catalyst, also accounting for the adsorption of tracer on the active sites of the catalyst. Such equations will be developed in Chapter 11 on fixed bed reactors. The model contains three parameters: the effective diffusivity, the adsorption equilibrium coefficient K_A and D_{ax}, the axial dispersion coefficient accounting for deviation from the plug flow pattern in the bed. They should be fitted simultaneously. That can be done by characterizing the response to the pulse (which is a distribution function) by means of moments, or in the time domain, making use of Laplace or Fourier transforms of the pulse-response.

The second technique is based upon the Wicke-Kallenbach cell. Originally, this cell was used in the steady state mode, but presently transient

operation is preferred. A single catalyst particle is used as a membrane. Above the membrane, a steady flow of a convenient carrier gas is maintained. The tracer is injected into this gas in the form of a very narrow pulse. It diffuses through the catalyst membrane and is swept in the compartment underneath by a carrier gas that takes it to a detector, e.g., a TCD of a gas chromatograph.The problem with the single particle cell is the small amount of tracer that diffuses through the membrane, requiring a very sensitive detector. Van Melckebeke and Froment [1995] constructed a cell containing 12 catalyst pellets distant from each other by 30° and located on a circle at a certain radial distance from the center. The measurement technique was also transient.

The modeling of the phenomena in the (adapted) Wicke–Kallenbach cell is less complicated: the equation for the tracer is limited to the catalyst pellet itself. It contains only 2 parameters: the effective diffusivity, D_{eA}, and the adsorption equilibrium coefficient, K_A.

The model equations for the catalyst pellet also contain the tortuosities τ_D, τ_K or a combination of both τ and ε_s. Their determination requires specific equipment. Well instrumented catalyst characterization equipment, including computerized data treatment, is commercially available, in particular for mercury porosimetry and nitrogen–sorption and –desorption.

EXAMPLE 3.5.1.2.A

EXPERIMENTAL DETERMINATION OF THE EFFECTIVE DIFFUSIVITY OF A COMPONENT AND OF THE CATALYST TORTUOSITY BY MEANS OF THE PACKED COLUMN TECHNIQUE

Catalyst: Pt-Sn-*y*-alumina catalyst for the catalytic reforming of naphtha.
Column internal diameter: 10^{-2} m; column length: 0.805 m; particle radius: 0.975×10^{-3} m; void fraction of the packing: 0.429 m^3_f / m^3_r; density of the catalyst, ρ_{cat}: 1080 kg cat/m^3_{cat}.

Further information concerning the catalyst is required to derive D_e from the measuments by means of the model. That is derived, as already mentioned, from Hg-porosimetry, N_2-adsorption and -desorption.

Hg-porosimetry determines the pore volume as a function of the amount of intruded mercury. The pore radius is calculated from the Washburn equation for cylindrical pores. At 2000 bar all pores larger than 3.3 nm are filled with Hg. The total pore volume amounts to 0.6169 cm^3/g cat (Fig. 3.5.1.2.A-1a). The curves also show that at low pressure no Hg intrudes in the macropores, meaning that with this catalyst the macropores would only be accessible at higher pressures, i.e., through the mesopores.

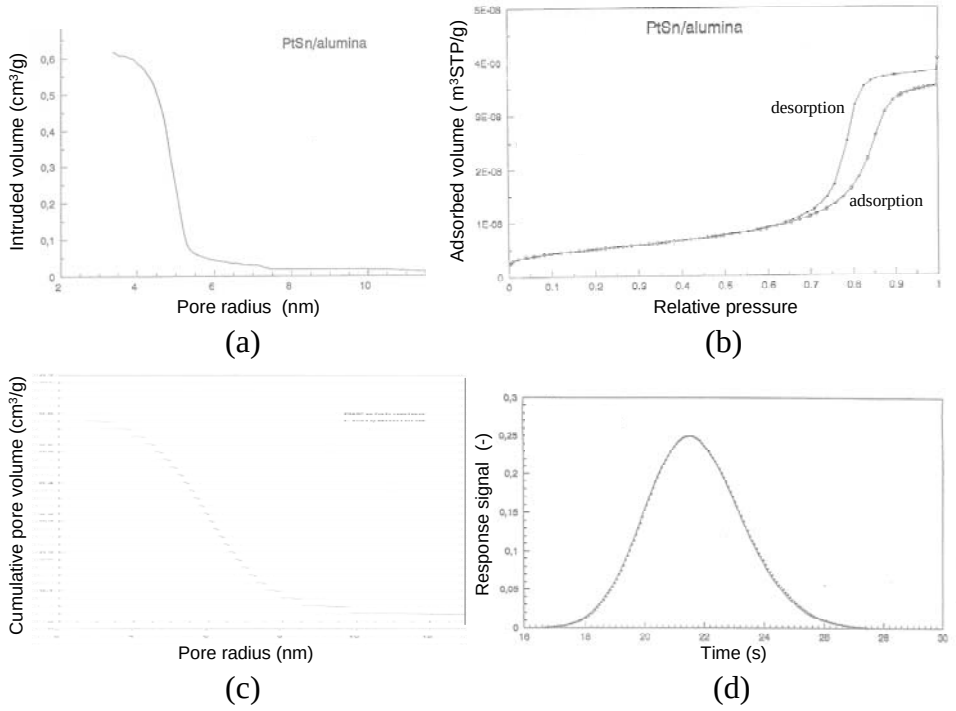

Figure 3.5.1.2.A-1

From Van Melkebeke and Froment [1995].

(a) Determination of total pore volume by mercury-porosimetry.

(b) Nitrogen -adsorption and -desorption isotherms at 77 K.

(c) Cumulative pore volume, calculated from the nitrogen adsorption data.

(d) Determination of D_e and τ. Transient packed column technique. Experimental (....) and fitted (——) response signals. Tracer gas: Methane; Carrier gas: Helium; Interstitial velocity: 0.068533 m/s; Re = 0.26197; 150°C.

The nitrogen sorption (Fig. 3.5.1.2.A-1b) shows a steep increase of the amount adsorbed at a relative pressure of 0.9999. At that pressure the macropores are filled by nitrogen through capillary condensation. From the Washburn equation a total volume of adsorbed N_2 of 0.6269 cm^3/g cat is calculated, in excellent agreement with that derived from Hg-porosimetry. The volume of N_2 adsorbed until that sharp rise, 0.5453 cm^3/g cat, is the meso pore volume. Consequently, the macropores occupy 0.08165 cm^3/g cat, which is 13% of the total.

The cumulative pore volume distribution (Fig. 3.5.1.2.A-1c) is derived from the nitrogen adsorption curve by means of the Broekhoff-De Boer equation for cylindrical pores. The inflection point in that curve translates into the differential pore volume distribution by a peak at 5.953 nm, which is the mean pore radius.

The density of the solid, ρ_s, measured by a He-pycnometer was 3324 kg/m^3_{sol}, that of the particle 1082 kg/m^3_{cat}. The void fraction of the particle follows from $\varepsilon_s = 1 - \rho_p/\rho_s$ and amounts to 0.676 m^3_f / m^3_p.

Fig. 3.5.1.2.A-1d shows the exit response signal of the tracer pulse injected into the packed column. Fitting of this data by means of the Kubin and Kucera-model leads to the parameter values: $D_e = 0.8474 \times 10^{-6} \pm 0.0085$ (m^3_f / m_s s) at 422.80 K and for an approximate 95% confidence-interval; $K_A = 1.8067 \times 10^{-4} \pm 0.0010$ (m^3_f / kg cat); $D_{ax} = 0.7619$ m^2_r / s ± 0.0074.

The diffusion is mainly of the Knudsen type. The tortuosity factor τ_K amounts to 2.36 when CH_4 is used as a tracer gas and to 2.27 with Ar.

■

EXAMPLE 3.5.1.2.B
APPLICATION OF THE PELLET TECHNIQUE

Catalyst: Fe-Cr catalyst for ethylbenzene dehydrogenation into styrene.
Particle diameter: 3×10^{-3} m; $\varepsilon_s = 0.477$; $\rho_s = 4140$ kg cat / m^3_s; $\rho_p = 2167$ kg cat / m^3_p.

Experimental figures very similar to that of Fig. 3.5.1.2.A-1d for the packed column technique are obtained. At a total pressure of 2.41 bar the effective diffusivity was calculated to amount to 3.665×10^{-6} m^3_f / m^2 s. The diffusion covered both the Knudsen and molecular regime. By performing experiments at various total pressures, ranging from 1.51 to 3.01 bar, it became possible to distinguish between τ_K and τ_D. The values found were 3.19 and 2.52, respectively.

It is also possible to measure D_e and τ in the presence of reaction. This requires model equations of the type to be presented in Chapter 11. Examples of this approach are given by Dumez and Froment [1976] and by Xu and Froment [1989].

■

3.5.2 Structure Models

The continuum model with global characteristics (the void fraction, ε_s, and tortuosity factor, τ) may be a convenient representation of the catalyst internal structure, but it is definitely not the most accurate. It may lead to unsatisfactory prediction of the performance of the catalyst in a reactor and can not serve as a guide for improving its morphology in the manufacturing process. Taking advantage of the growing possibilities of computers, more realistic models were developed over the years. These will now be discussed in some detail.

3.5.2.1 The random pore model

The "random pore" model, or macro- micro-pore model, of Wakao and Smith [1962, 1964] is intended for application to pellets manufactured by compression of small particles. The void fraction and pore radius distributions are each replaced by two averaged values: ε_M , r_M for the macro and ε_μ , r_μ for the micro distribution (often a pore radius of ~100 Å is used as the dividing point between macro and micro). The particles which contain the micro-pores are randomly positioned in the pellet space. The interstices are the macro-pores of the pellet (see Fig. 3.5.2.1-1). The diffusion flux consists of three parallel contributions: the first through the macro-pores, the second through the micro-pores and the third through interconnected macro-micro-pores in which the dominant resistance lies in the latter. The contributions to the diffusivity are added up to yield:

$$D_e = \varepsilon_M^2 D_M + (1-\varepsilon_M)^2 \frac{\varepsilon_\mu^2}{(1-\varepsilon_M)^2} D_\mu + 2[2\varepsilon_M(1-\varepsilon_M)]\frac{\varepsilon_\mu^2}{(1-\varepsilon_M)^2} D_\mu \qquad (3.5.2.1\text{-}1)$$

$$= \varepsilon_M^2 D_M + \frac{\varepsilon_\mu^2(1+3\varepsilon_M)}{1-\varepsilon_M} D_\mu$$

In the second and third terms D_μ is based on the microvoid area, so that the value of the ratio of microvoid to total particle area is required. In (3.5.2.1-1), D_M and D_μ are obtained from (3.4-9), but without correcting for porosity and tortuosity, which are already accounted for in (3.5.2.1-1):

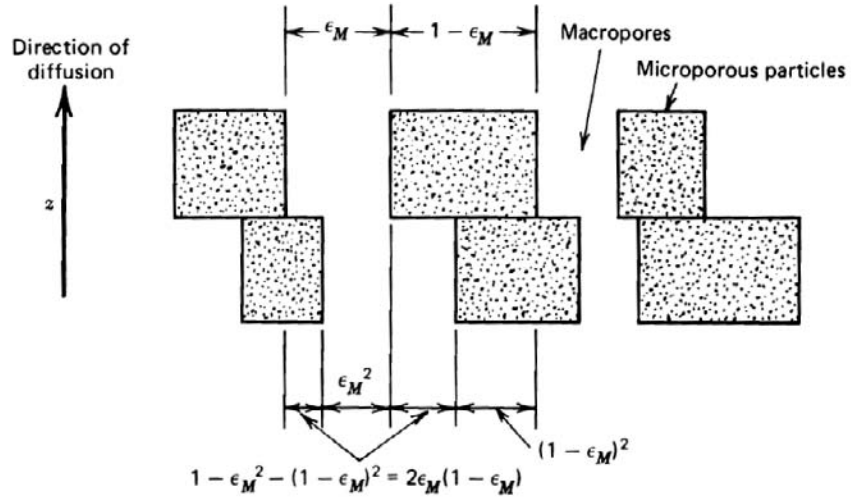

Figure 3.5.2.1-1

Diffusion areas in random pore model. Adapted from Smith [1970].

$$\frac{1}{D_{M\ or\ \mu}} = \frac{1}{D_{AB}} + \frac{1}{D_{KM}\ or\ D_{K\mu}} \qquad (3.5.2.1\text{-}2)$$

Note that the tortuosity factor, τ, does not appear in (3.5.2.1-1). For either $\varepsilon_\mu = 0$ or $\varepsilon_M = 0$, this equation reduces to

$$D_e = \left(\varepsilon_s^2 D\right)_{M\ or\ \mu} \qquad (3.5.2.1\text{-}3)$$

which implies that $\tau = 1 / \varepsilon_s$. This is often a reasonable approximation [see Weisz and Schwartz, 1962; Satterfield, 1970].

For catalysts without clear distinction between micro- and macro-pores, a different approach is required.

3.5.2.2 The Parallel Cross-Linked Pore Model

The parallel cross-linked pore model has been developed by Johnson and Stewart [1965] and Feng and Stewart [1973]. Equation (3.4-7) is considered to apply to a single pore of radius r in the solid, and the diffusivities are interpreted as the actual values, rather than effective diffusivities corrected for porosity and tortuosity. A pore size and orientation distribution function $f(r, \Omega)$ is defined. Then, $f(r, \Omega)dr d\Omega$ is the fraction open area of pores with radius r and a direction that forms an angle Ω with the pellet axis. The total porosity is then

$$\varepsilon_s = \iint f(r,\Omega)\, dr\, d\Omega \qquad (3.5.2.2\text{-}1)$$

and the total internal surface area

$$\rho_s S_g = \iint \frac{2}{r} f(r,\Omega) dr\, d\Omega \qquad (3.5.2.2\text{-}2)$$

The pellet flux is obtained by integrating the flux in a single pore with orientation l and by accounting for the distribution function:

$$\boldsymbol{N}_j = \iint \boldsymbol{\delta}_l N_{j,l} f(r,\Omega)\, dr\, d\Omega \qquad (3.5.2.2\text{-}3)$$

where $\boldsymbol{\delta}_l$ represents a unit vector or direction cosine between the l direction and the coordinate axes. Feng et al. [1974] utilized the complete Stefan-Maxwell formulation, (3.4-7), but only the results for the simpler mean binary diffusivity are dealt with here. Applied to a single pore and therefore excluding the porosity and tortuosity corrections, (3.5.1.1-1) may be written:

$$N_{j,l} = -D_{jm}\frac{dC_j}{dl}$$

$$= -D_{jm}\boldsymbol{\delta}_l . \nabla C_j \qquad (3.5.2.2\text{-}4)$$

where

$$\frac{1}{D_{jm}} = \sum_{k=1}^{N}\frac{1}{D_{jk}}\left(y_k - \frac{N_k}{N_j}y_j\right) + \frac{1}{D_{Kj}} \qquad (3.5.2.2\text{-}5)$$

Then, (3.5.2.2-3) becomes

$$\boldsymbol{N}_j = -\iint D_{jm}\boldsymbol{\delta}_l\boldsymbol{\delta}_l . \nabla C_j\, f(r,\Omega)\, dr\, d\Omega \qquad (3.5.2.2\text{-}6)$$

where $\boldsymbol{\delta}_l\,\boldsymbol{\delta}_l$ is the tortuosity tensor.

Two limiting cases can be considered:

Perfectly communicating pores. The concentrations are identical at a given position z, that is, $C_j(z; r, \Omega) = C_j(z)$.

Noncommunicating pores. The complete profile $C_j(z; r, \Omega)$ is first derived for a given pore and then averaged.

For pure diffusion at steady state, $dN_j/dz = 0$ or N_j = constant, and (3.5.2.2-6) can be directly integrated:

$$N_{jz}\int_0^L dz = \iint dr\, d\Omega\left[-\int_{C_{j0}}^{C_{jL}} D_{jm}\, dC_j\right]\delta_l\delta_l\, f(r,\Omega) \qquad (3.5.2.2\text{-}7)$$

For that case, no assumption need to be made about the communication of the pores, and (3.5.2.2-7) can be applied. For other situations the two extremes give different results, as will be discussed later.

In the usual types of catalyst particles with random pore structure, the connectivity is high and the situation would be closest to the communicating pore case. Then, since C_j is now independent of r and Ω, (3.5.2.2-6) can be written

$$\boldsymbol{N}_j = -\left[\int D_{jm}(r)\,\kappa(r)\, d\varepsilon_s(r)\right]\nabla C_j \qquad (3.5.2.2\text{-}8)$$

where $\kappa(r)$ is a reciprocal tortuosity that results from the integration over Ω, and also the differential form of (3.5.2.2-1) was used. From (3.5.2.2-8) it follows that the proper diffusivity to use is the one weighted with respect to the measured pore size distribution.

Finally, if the pore size and orientation effects are uncorrelated,

$$f(r,\Omega) = f(r)\, f_{\Omega}(\Omega)$$

where $f(r)$ is the pore size distribution function and

$$\int f_{\Omega}(\Omega) d\Omega = 1$$

(3.5.2.2-8) becomes

$$N_j = -\left[\int D_{jm}(r)\, d\varepsilon_s(r) \right] \left[\int f_{\Omega} \kappa\, d\Omega \right] \nabla C_j \qquad (3.5.2.2\text{-}9)$$

For completely random pore orientations, the tortuosity depends only on the vector component cos Ω, and

$$\int f_{\Omega} \kappa\, d\Omega = \int f_{\Omega} \cos^2 \Omega\, d\Omega = \frac{1}{3}$$

so that, in the notation of (3.5.1.1-3), $\tau = 3$.

Satterfield and Cadle [1968a; b] and Brown et al. [1969] have tested the various models against experimental data for several types of solids and pressures. Both the macro-micro and the parallel path models are often superior to the simple mean pore size model, as might be expected. The former two are more or less equivalent, where applicable, but the parallel path model seems to be slightly more general in its predictive abilities.

3.5.3 Network Models

3.5.3.1 A Bethe Tree Model

The Bethe tree shown in Fig. 3.5.3.1-1 is a branching network of pores with a coordination number of 3 and no closed loops. Three pores merge in each node. From this node 2 pores emerge. Higher coordination numbers can also be considered and the pores can have a variable diameter. The main advantage of the Bethe tree shown here is that it can yield analytical solutions for the fluxes, but the absence of closed loops is not entirely realistic. Its use will be illustrated in Chapter 5 on catalyst deactivation. What will be illustrated here is how to derive a tortuosity factor from this type of geometry.

Beeckman and Froment [1982] represent the catalyst texture by a network of pores structured as a tree with a degree of branching equal to 2 and connectivity Z = 3. The bonds of the tree correspond to the pores of the catalyst; the nodes correspond to their intersection. Each pore is characterized by two stochastic variables: the pore length L and the pore diameter. The probability density function of the former, $\lambda(L)$, is derived from the assumption that the

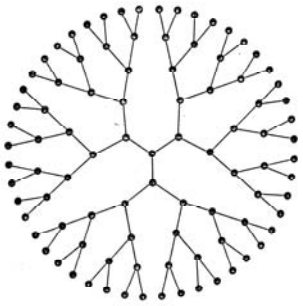

Figure 3.5.3.1-1
Bethe tree.

branching probability $v\,dL$ is independent of the pore length and, hence, is of the Poisson type:

$$\lambda(L) = ve^{-vL} \tag{3.5.3.1-1}$$

with v^{-1} the average pore length. The probability density function of the pore diameter can be obtained from nitrogen desorption and mercury penetration measurements. In this way a heterogeneous model is developed for a particle. The equations for the fluxes and for the effectiveness factor take on a much more complicated form than those derived above, which start from a homogeneous or continuum model. Such a heterogeneous model is a valuable tool for dealing with situations in which the prediction of surface fluxes only yields insufficient information. This is the case when site coverage and pore blockage by coke and metal deposition lead to catalyst deactivation, as in resid hydrodesulfurization, for example.

The flux of a component A toward the center and through a sphere at a distance r, measured from the center onwards, may be written

$$N_A(r) = \frac{D_A \hat{E}(r) N_n \pi d'^2}{4\rho} \left.\frac{dC_A}{dr}\right|_r \tag{3.5.3.1-2}$$

where D_A is the true molecular or Knudsen diffusivity or a combination of both according to (3.4-9); $\hat{E}(r)$ is the number of pore mouths per network on the sphere located at a distance r from the center; N_n is the number of networks; d' is the pore diameter; and ρ represents the ratio of $d\bar{x}$, the average pore length between concentric spheres at (r, $r + dr$) and of dr, the distance between the spheres, measured along a radial.

The product $\hat{E}(r)\,N_n$ can be expressed in terms of the basic parameters involved in the characterization of the network structure. This is not required for

the calculation of the tortuosity factor corresponding to the network model outlined here. To achieve this goal, the product $\hat{E}(r)\ N_n$ is eliminated from (3.5.3.1-2) in favor of a measurable quantity, the porosity $\varepsilon(r)$. According to Dupuit's theorem, the latter is the fraction of the surface of the sphere at a distance r from the center which is taken by pore cross mouths, so that

$$\varepsilon(r) = \hat{E}(r) N_n \frac{\pi d'^2}{4} \frac{\rho\tau}{4\pi r^2} \tag{3.5.3.1-3}$$

Elimination of $\hat{E}(r)\ N_n$ between (3.5.3.1-2) and (3.5.3.1-3) yields

$$N_A(r) = \frac{D_A \varepsilon(r)}{\rho^2} 4\pi r^2 \left.\frac{dC_A}{dr}\right|_r \tag{3.5.3.1-4}$$

which can also be written in the conventional form already encountered in Section 3.5.1:

$$N_A(r) = \frac{D_A \varepsilon(r)}{\tau} 4\pi r^2 \left.\frac{dC_A}{dr}\right|_r \tag{3.5.3.1-5}$$

so that $\tau = \rho^2$.

What remains to be done is to find an expression for ρ. From Fig. 3.5.3.1-2, the relation between dr, the distance along the radial, and dx, the distance along a pore making an angle θ with the radial at a distance r from the center of the spherical particle, is easily derived:

$$dx = \sqrt{r^2 \cos^2\theta + 2r\,dr} - r\cos\theta \tag{3.5.3.1-6}$$

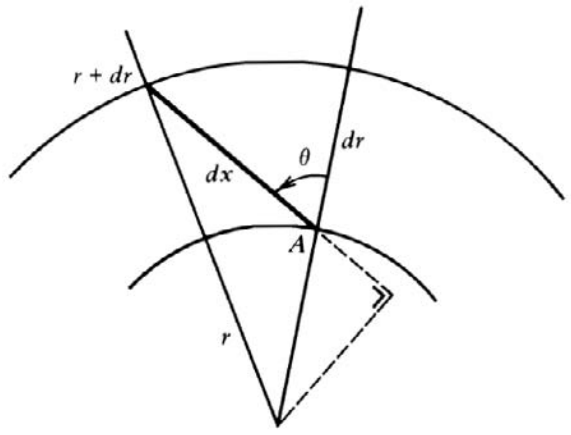

Figure 3.5.3.1-2

Pore making an angle θ with respect to radial at a distance r from the center of a spherical particle.

Since various orientations θ are possible for the pores between spheres (r, $r + dr$), the distance dx is variable and has to be weighted. To do so, a surface element dS is chosen on a unit sphere centered in A. Since all orientations θ have the same probability, the density of intersection of the pores with the surface, represented by δ, is uniform, but the location of dS determines the length dx. The sum of the surfaces dS corresponding to the same dx is a ring cut on the surface of the unit sphere by two cones with their top in A and forming angles θ and $\theta + d\theta$ with the radial through A. The weighting of dx with respect to the surface area is given by

$$\bar{dx} = \frac{\iint dx\,\delta\,dS}{\iint \delta\,dS} \tag{3.5.3.1-7}$$

The larger θ, the larger is the number of pore intersections with the ring. The surface of the ring is proportional to sin θ, and (3.5.3.1-7) can now be expressed in terms of r and θ:

$$\bar{dx} = \frac{\int_0^{\pi/2} dx \sin\theta\, d\theta}{\int_0^{\pi/2} \sin\theta\, d\theta} \tag{3.5.3.1-8}$$

The denominator of (3.5.3.1-8) equals 1, so that

$$\rho = \frac{\bar{dx}}{dr} = \frac{\int_0^{\pi/2} \left[\ \sqrt{r^2\cos^2\theta + 2r\,dr} - r\cos\theta\ \right] \sin\theta\, d\theta}{dr} \tag{3.5.3.1-9}$$

Evaluating the integral and taking limits for $dr \rightarrow 0$ leads to a value $\rho = 2$, so that $\tau = 4$, which is close to the experimental values.

A less detailed model led Wheeler [1955] to a value of 2. Wakao and Smith [1962] obtained values between 2.5 and 3.5 for macro-micro pore networks. Feng and Stewart [1973] and also Dullien [1975] obtained a value of 3 for perfectly interconnecting pores with completely random orientation. Experimental values reported by Feng and Stewart [1973] for alumina pellets are 4.6; by Dumez and Froment [1976] for a chromia/alumina catalyst, 5; by De Deken et al. [1982] for a Ni/Al_2O_3 steam reforming catalyst, 4.4 to 5.0; by Satterfield and Caddle [1968], from 2.8 to 7.3; and by Patel and Butt [1974] from 4 to 7 for a nickel/molbydate catalyst. Note that the above calculation does not account for dead end pores and that the pores are considered to be strictly

cylindrical. The equations are easily extended to the case of a distribution of pore diameters.

3.5.3.2 Disordered Pore Media

Amorphous catalysts do not have the regular or structured morphology dealt with above. Yet, a more representative model of the structure is required for an accurate prediction of their performance, in particular when the structure is modified during its application, e.g., through pore blockage by poisons carried by the feed or by coke formed by the process itself. A pore medium can evidently be considered as a network of channels — preferably 3-dimensional — with a size distribution, but the disorder also has to be included. The problem is two-fold: a structure has to be generated and the operation and performance of such a structure has to be described. Two frequently used methods are briefly described here: the Monte-Carlo generation and simulation and the Effective Medium Approximation.

MONTE-CARLO SIMULATION

Disordered pore media, like amorphous catalysts, are often modeled by finite networks consisting of channels intersecting in nodes. These networks can be square or cubic. Because of the computational effort, the number of nodes in a cubic network has to be limited: a 20 × 20 × 20 grid is often seen as an optimal choice. Measurements mentioned under Section 3.5.1.2 provide the particle internal void fraction and the pore size distribution or its average. A certain pore diameter distribution is generated for the network by means of a random number generator. Also by means of this tool, a certain fraction of pores are blocked to create a certain disorder. The experimental results set the concentrations at the boundary of the network (see Example 3.5.1.2.B). The diffusion equations are then integrated for each pore and the net flux is set equal to zero in each node. Knowing these permits the calculation of the diffusivities.

The calculations are repeated a large number of times for the same overall blockage probability and average pore size and the calculated set of values of D_e is averaged. Both Knudsen diffusivities and molecular diffusivities can be obtained in this way. They can be compared with values derived from a continuum model.

EFFECTIVE MEDIUM APPROXIMATION (EMA)

The objective of EMA is to construct a small size network that permits the derivation of the relation between diffusivity and blockage without considering the complete network.

Let a catalyst particle be represented by a cubic network that is partially disordered by blocking a certain amount of bonds (pores) or nodes. That sets a blockage probability and is achieved by using a random number generator. The original network is then replaced by a hypothetical uniform (or "homogeneous") medium, called the "equivalent network", with the same topology, i.e., connectivity, but no blockage, therefore with a single D_{eq}, lower than that in the open pores of the original network, of course. Then an ensemble of pores of the equivalent network is replaced by a stochastically blocked cluster of pores and nodes taken from the original network. The resulting network is called "composite network". Except in what is called the "stochastic cluster", the diffusivity in the composite network has to be the same as D_{eq} of the equivalent network. The stochastic cluster can be very small, i.e., contain only a few pores and nodes and yet, when judiciously chosen, provide accurate values for the diffusivity, which would otherwise require a much more demanding Monte-Carlo simulation of the complete original network. The quality of the approximation achieved by the composite network with its stochastic cluster can be evaluated by pushing the blockage probability to its critical value. It is a property of networks that not all pores or nodes of a network have to be blocked to completely prevent accessibility of one pore or node to a diffusing molecule. There are several methods to calculate this critical blockage probability, q_c, called percolation threshold. In a cubic network, this q_c is 0.75. The selected EMA configuration has to lead to this value to be representative.

More information on percolation theory and EMA can be found in Kirkpatrick [1973]; Burganos and Sotirchos [1987]; Zhang and Seaton [1992]; Sahimi [1994]; Keil [1996]; Beyne and Froment [2001].

EXAMPLE 3.5.A

OPTIMIZATION OF CATALYST PORE STRUCTURE

The preceding paragraphs dealt with the modeling of the morphology and topology of catalyst particles and their effect on the diffusion flux of the reacting species, ultimately on the catalyst performance. The application of these models is not limited to the description of the operation of the catalyst in a given process, but can also be of value as a guideline for the manufacture of the catalyst.

An early example is the work of Pereira and Beeckman [1989] and of Hegedus and Pereira [1990] who optimized the porous structure, more particularly the micropore diameter and the mean porosity of a titania-supported vanadia catalyst for the reduction of NO_x by a mixture of NH_3 and O_2. Another example is given for hydrodemetallation by Keil and Rieckmann [1994]. The support of such a catalyst is manufactured by pelletizing powder of the support

and active material into a shape, size and strength required by the specific process technology: fixed bed reactor, fluidized bed reactor, and so on. That leads to a catalyst with meso-pores in between volumes of solid material containing micro-or nanopores. The large pores are channels through which the reacting species and their products diffuse to and from the nanopores which represent by far the main fraction of the internal surface and contain the majority of active sites. The current manufacturing processes produce random configurations of meso- and nanopores and it is not likely that the connection of the "feed channels" or "distributors" to the nanopores is optimal. Recently Coppens and co-workers [Johanessen et al., 2007; Wang et al., 2007] spent considerable attention on hierarchically structured catalysts that would optimize the function of the distributor channels by designing their connection with the nanopores. To achieve a gain in activity and selectivity of the catalyst by improving the diffusivity, the volume taken by the distributor channels has to be relatively large, but that implies a reduction of the volume fraction taken by the active solid that can only be compensated for by a gain in connectivity. It was found that a large number of parallel straight channels with a position-dependent channel diameter and no branches leads to a global optimum. For a single reaction and any type of rate equation the η vs. generalized modulus relationship discussed in Section 3.6.2 was applicable, but with the effective diffusivity replaced by the molecular diffusivity, reflecting that with the optimized structure and connectivity the main resistance to diffusion is located in the large channels. They also showed that the performance of the catalyst layer deposited in the monolith reactor of the NO_x reduction process, studied by Pereira and Beeckman [1989], could be further improved by hierarchically structuring the layer consisting of parallel channel and active zones in a bimodal way [Wang and Coppens, 2008]. ■

3.5.4 Diffusion in Zeolites. Configurational Diffusion

Zeolites are an important family of catalysts consisting of AlO_4 and SiO_4 tetrahedra which are three-dimensionally connected, forming cavities and pores. Y-zeolites e.g., are used in catalytic cracking and hydrocracking, ZSM-5 in xylene isomerization, and in MTO — the Methanol-to-Olefins process. Synthetic zeolites have a very regular structure and their pores and cages have sizes which are of the same order of magnitude as those of the reacting molecules. In the diffusion process, the latter are in contact with the zeolite walls, thereby undergoing the influence of the atoms of the wall. This type of diffusion is called configurational.

The macroscopic experimental techniques for determining *D*, like the Wicke-Kallenbach membrane cell or the packed bed column operate in a transient mode and with a concentration gradient. They yield transport diffusivities. Instead, microscopic experimental techniques like NMR or quasi elastic neutron reflection operated under equilibrium conditions yield self-diffusivities. The latter mechanism leads to spatial uniformization of labeled and unlabeled molecules even without external concentration gradient. The self-diffusion can also be described by the macroscopic Fickian law or at the microscopic level by a mean square displacement, as applied by Einstein to describe Brownian motion and leading to

$$D_s = \frac{1}{N}\sum_{i=1}^{N}\lim_{t\to\infty}\frac{\left[\vec{r}^{\,i}(t)-\vec{r}^{\,i}(0)\right]^2}{t} \qquad (3.5.4\text{-}1)$$

where N is the number of particles and $r^i(t)$ the position of particle i at time t. Transport- and self-diffusivities may differ substantially and only agree at zero coverage.

The simulation of diffusion through zeolite structures uses techniques like molecular dynamics and Monte-Carlo simulation.

3.5.4.1 Molecular Dynamics Simulation

The molecular dynamics technique simulates the trajectory of a molecule in a zeolite pore or cage by integrating Newton's classical equations of motion for N atoms interacting through a potential energy V, consisting of kinetic and potential contributions. The interaction between the N atoms generates forces F_i causing the atoms to move:

$$F_i = m_i \frac{d^2 r_i}{dt^2} \qquad (3.5.4.1\text{-}1)$$

The result is a trajectory that specifies how the positions and velocities of the particles vary with time. In general the time increment is set to a few femtoseconds, in some cases even less.

The kinetic energy is given by

$$\frac{1}{2}\sum_{i}^{N} m_i\left[v_i(t)\right]^2 \qquad (3.5.4.1\text{-}2)$$

The potential energy of a single atom has to account for all the interaction energies with the atoms of the molecule, with those of the zeolite wall, and also for the internal bond bending, vibration, etc. Dual interactions are calculated

from the Lennard-Jones potential, but presently many-body interactions are more used than the two body interactions:

$$\varphi(r) = \sum_{i=1}^{N} \sum_{i'=1}^{N} 4\varepsilon \left[\left(\frac{\sigma}{r} \right)^{12} - \left(\frac{\sigma}{r} \right)^{6} \right] \qquad (3.5.4.1\text{-}3)$$

The self diffusivity is obtained from the trajectory by means of the Einstein relation (3.5.4-1).

Runnebaum and Maginn [1997] studied the diffusion of *n*-Parrafins with 8C to 20C in a silicalite with straight pores and sinusoidal interconnections by means of Molecular Dynamics (Fig. 3.5.4.1-1). The values for *D* are close to the experimental results obtained by microscopic techniques. *D* depends on the chain length but also on the pore geometry (straight or zig zag). At 390 K the transfer of molecules from one type of pore to the other is slow and the zeolite behaves as if it was made up of one dimensional pores. Molecules hop from one potential hole to the next after reorientation with respect to the pore contour. The variation of *D* with the chain length is not monotonic: paraffins in C8 and C16 are favored. Their length coincides with that of a pore or a multiple of it. They are said to be in resonance with the pore. These results confirm work of Gorring, that was

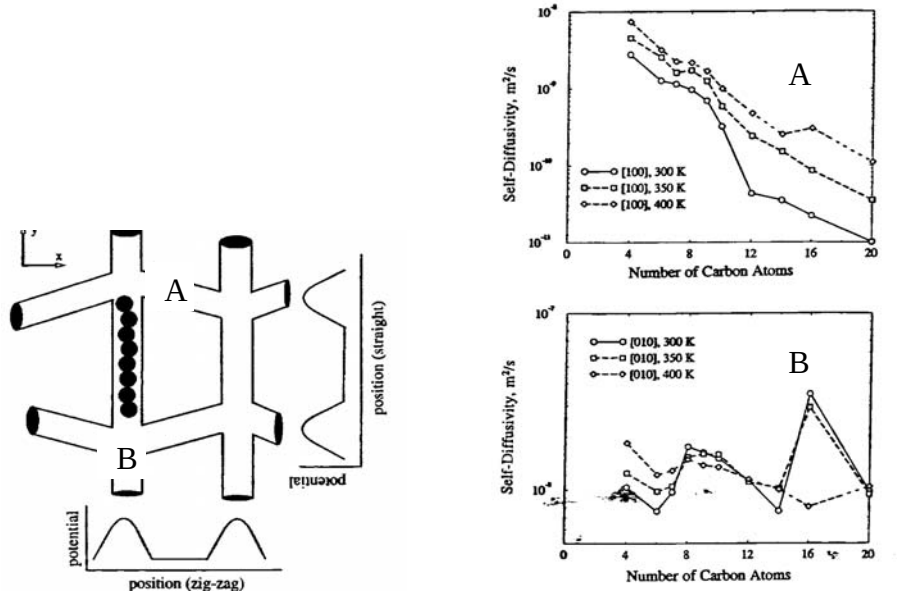

Figure 3.5.4.1-1

Molecular Dynamics simulation of the diffusion of *n*-paraffins in the Silicalite (a zeolite). A: zig-zag pores; B: straight pores. From Runnebaum and Maginn [1997].

controversial at the time it was published [1973]. The resonance disappears above 400 K, i.e. at temperatures at wich zeolites are generally applied in chemical processes.

3.5.4.2 Dynamic Monte-Carlo Simulation

The pore space of the zeolite is simplified to a lattice consisting of a grid of active sites connected by bonds. Molecules occupy a fraction θ of the sites and hop from site to site along bonds connecting neighboring free sites. A large number of stochastic occupation patterns is laid out and the trajectories are calculated so as to come to a meaningful average value of the diffusivity.

A comprehensive discussion of diffusion in zeolites and its simulation is presented in Keil et al. [2000] and Smit and Krishna [2003] have illustrated the potential of molecular simulations in zeolitic process design.

3.6 DIFFUSION AND REACTION IN A CATALYST PARTICLE. A CONTINUUM MODEL

3.6.1 First-Order Reactions. The Concept of Effectiveness Factor

When reaction occurs on the pore walls simultaneously with diffusion, the process is not a strictly consecutive one and both phenomena must be considered together. For a first-order reaction, equimolar counterdiffusion and isothermal conditions the steady-state continuity equation for *A* can be written when the *y* coordinate is oriented from the center line to the surface of the slab:

$$D_{eA}\frac{d^2C_s}{dy^2} - k\rho_s C_s = 0 \qquad (3.6.1\text{-}1)$$

where k = reaction rate coefficient (m^3_g / kg cat. s).
The boundary conditions are

$$C_s(L) = C_s^s \quad \text{at the surface} \qquad (3.6.1\text{-}2)$$

$$\frac{dC_s(0)}{dy} = 0 \quad \text{at the center line}$$

and the solution is

$$\frac{C_s(y)}{C_s^s} = \frac{\cosh\sqrt{\frac{k\rho_s}{D_{eA}}}y}{\cosh\sqrt{\frac{k\rho_s}{D_{eA}}}L} \qquad (3.6.1\text{-}3)$$

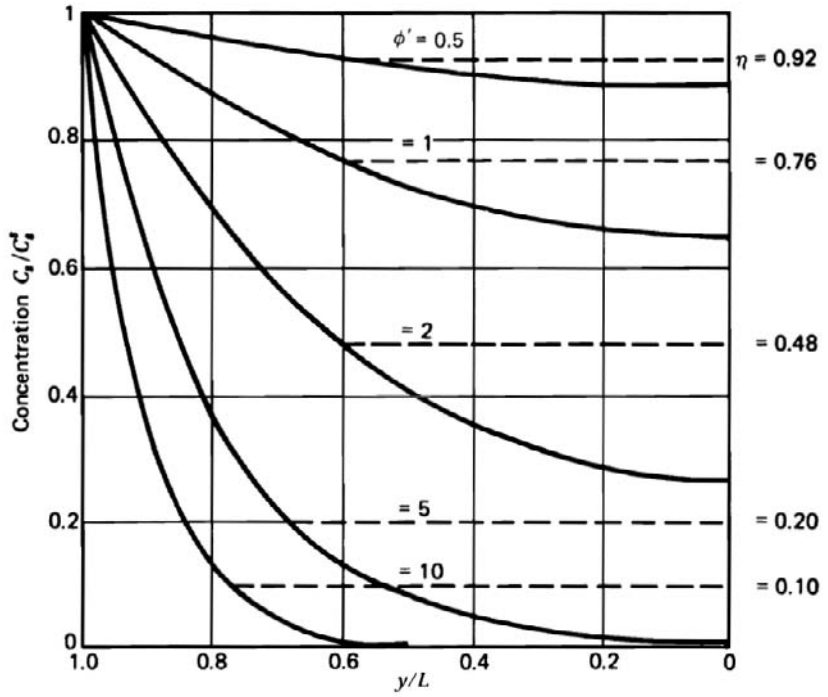

Figure 3.6.1-1

Distribution and average value of reactant concentration within a catalyst slab as a function of the parameter ϕ'. Adapted from Levenspiel [1962].

The concentration profiles are as shown in Fig. 3.6.1-1. The diffusion resistance causes a concentration profile in the pellet because reactants cannot diffuse in from the bulk at a sufficient rate. A small diffusion resistance (say, large D_{eA}) gives a rather flat profile, whereas a steep curve is obtained for a large diffusion resistance. As the rate of reaction at any point in the slab equals $k\rho_s C_s(y)$, this profile causes an average rate which is lower than that obtained at the surface concentration C_s^s. The ratio of available area between a porous and an impervious catalyst is so large that this penalty is minimal when compared to the gain in productivity associated with the porosity.

The curves in Fig. 3.6.1-1 could be used to directly characterize the diffusion limitations, but it is more convenient to have a "rating factor" for the effect. This was provided by Thiele [1939] and Zeldowich [1939], who defined the effectiveness factor:

$$\eta = \frac{\text{rate of reaction with pore diffusion resistance}}{\text{rate of reaction at surface conditions}}$$

$$\eta = \frac{\dfrac{1}{W_c}\int r_A(C_s)\,dW_c}{r_A(C_s^s)} \tag{3.6.1-4}$$

The observed reaction rate is

$$(r_A)_{obs} = \eta\, r_A(C_s^s) \tag{3.6.1-5}$$

When the concentration profile (3.6.1-3) is substituted into the numerator of (3.6.1-4) this equation becomes, for a first-order reaction,

$$\eta = \frac{\tanh \phi'}{\phi'} \tag{3.6.1-6}$$

where for a slab of thickness L

$$\phi' = \text{ modulus } = L\sqrt{k\rho_s / D_{eA}} \tag{3.6.1-7}$$

A plot of (3.6.1-6) is shown in Fig. 3.6.1-2. For $\phi' \to 0$, the effectiveness factor $\eta \to 1$, which means no appreciable resistance, and conversely for $\phi' \to \infty$. Note that the latter can occur for low diffusivity, large pellet size L, or very rapid reaction rate. From the mathematical properties of tanh ϕ', the asymptotic relation as $\phi' \to \infty$ (i.e., exceeds 3) is

$$\eta_\infty \sim \frac{1}{\phi'} \tag{3.6.1-8}$$

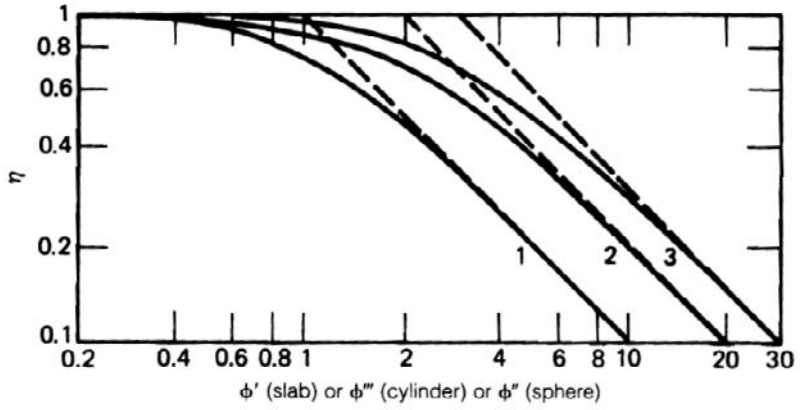

Figure 3.6.1-2

Effectiveness factors for slab (1), cylinder (2), and sphere (3). From Aris [1969a, b].

These results can be extended to more practical pellet geometries, such as cylinders or spheres, by solving the continuity equation for *A* in these geometries. For a sphere,

$$D_{eA}\frac{1}{r^2}\frac{d}{dr}\left(r^2\frac{dC_{As}}{dr}\right)=r_A\rho_s \tag{3.6.1-9}$$

and for the same boundary conditions, the result is

$$\eta=\frac{3}{\phi''}\frac{\phi''\coth\phi''-1}{\phi''} \tag{3.6.1-10}$$

where

$$\phi''=R\sqrt{k\rho_s/D_{eA}} \tag{3.6.1-11}$$

and *R* is the sphere radius.

The (ϕ'', η) plot has roughly the same shape as the result from (3.6.1-6), but the asymptote for $\phi'' \to \infty$ is

$$\eta_\infty \sim \frac{3}{\phi''} \tag{3.6.1-12}$$

In other words, the curve has shifted on a log-log plot by a factor of 3 (see Fig. 3.6.1-2). Therefore, if a new modulus were defined with a characteristic length of *R*/3, the following would result:

$$\phi=\frac{R}{3}\sqrt{k\rho_s/D_{eA}}=\frac{\phi''}{3} \tag{3.6.1-13}$$

$$\eta=\frac{1}{\phi}\frac{(3\phi)\coth(3\phi)-1}{(3\phi)} \tag{3.6.1-14}$$

$$\eta_\infty \sim \frac{1}{\phi} \qquad \phi \to \infty \tag{3.6.1-15}$$

Now the curve for spheres exactly coincides with that for slabs when $\phi \to \infty$ (and $\phi \to 0$, of course), and almost coincides (~10 to 15 percent) for the whole range of ϕ.

Aris [1957] noted this, and from similar results for cylinders and other geometries proposed a modulus leading for all shapes to $\phi-\eta$ curves that are practically superimposed:

$$\phi=\frac{V}{S}\sqrt{\frac{k\rho_s}{D_{eA}}} \tag{3.6.1-16}$$

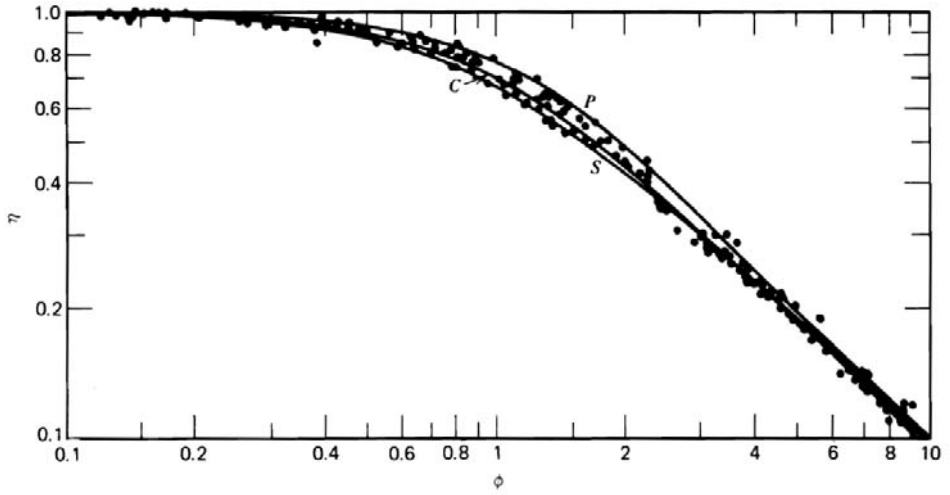

Figure 3.6.1-3

Effectiveness factors for slab (*P*), cylinder (*C*), and sphere (*S*) as functions of the Thiele modulus. Dots represent calculations by Amundson and Luss [1967] and Gunn and Thomas [1965]. From Aris [1965a, b].

where S is the external surface area of the pellet. Note that for spheres,

$$L = \frac{V}{S} = \frac{\frac{4}{3}\pi R^3}{4\pi R^2} = \frac{R}{3} \tag{3.6.1-17}$$

as found above. Thus, Fig. 3.6.1-1 is approximately true for first-order reaction and any shape of catalyst pellet, even irregular ones, if the proper modulus defined by (3.6.1-16) is used.

3.6.2 More General Rate Equations. The Generalized Modulus

The analytical integration of the continuity equation for the diffusing and reacting component A in a catalyst particle is possible only for a first-order reaction. A catalytic reaction generally has a more complicated rate equation, however, as shown in Chapter 2. It is attractive to extend the application of the simple relation (3.6.1-6 or 3.6.1-14) to any type of rate equation, be it only approximately. This is what led Aris [1965a, b], Bischoff [1965], and Petersen [1965a, b] to the introduction of a "generalized" modulus.

Again, to simplify the mathematical treatment somewhat, slab geometry is dealt with first. The extension to any geometry is straightforward and was already explained in the derivation of (3.6.1-16).

The continuity equation for *A* diffusing and reacting inside an elementary volume of a porous catalyst can be written

$$\frac{d}{dy}\left[D_{eA} \frac{dC_s}{dy} \right] = r_A \rho_s \tag{3.6.2-1}$$

with boundary conditions:

at the centerline of the slab:

$$\frac{dC_s(0)}{dy} = 0 \tag{3.6.2-2a}$$

at the surface:

$$C_s(L) = C_s^s \tag{3.6.2-2b}$$

Note that D_{eA} is a function of C_s. A first integration leads to

$$D_{eA} \frac{dC_s}{dy} = \left[2 \int_{C_s^0}^{C_s} D_{eA} r_A \rho_s dc' \right]^{1/2} \tag{3.6.2-3}$$

In this equation C_s^0, the concentration of *A* in the centerline, is not known, but it can be calculated from the following implicit equation, obtained from the integration of (3.6.2-3):

$$L = \int_{C_s^0}^{C_s^s} \frac{D_{eA} dc''}{\left[2 \int_{C_s^0}^{C''} D_{eA} r_A \rho_s dc' \right]^{1/2}} \tag{3.6.2-4}$$

In (3.6.1-4) the effectiveness factor was defined as the ratio of the actual amount of *A* reacting in a particle to the amount that would react if the concentration of *A* inside the particle would be uniform and equal to the surface value C_s^s. Clearly, the actual amount of *A* that reacts can also be derived from the flux of *A* at the surface, so that an alternate way of calculating the effectiveness factor is

$$\eta = \frac{D_{eA} \dfrac{dC_s(L)}{dy}}{L r_A(C_s^s) \rho_s} \tag{3.6.2-5}$$

Combining (3.6.2-3) and (3.6.2-5) leads to

$$\eta = \frac{\sqrt{2}}{Lr_A(C_s^s)\rho_s}\left[\int_{C_s^0}^{C_s^s} D_{eA}(C_s^{'})\, r_A(C_s^{'})\, \rho_s\, dC'_s\right]^{1/2} \qquad (3.6.2\text{-}6)$$

with C_s^0 calculated from (3.6.2-4). It is easily seen that for a first-order reaction this equation reduces to (3.6.1-6).

The next step is to define a modulus which would generalize (3.6.1-6) to any type of rate equation. It is evident that (3.6.2-6) satisfies the condition that η = 1 when $C_s = C_s^s$. Further, it is seen from the graphical representation of the latter equation in Fig. 3.6.1-3 that, for large values of the modulus, η becomes proportional to $1/\phi$. If (3.6.2-6) is to fit (3.6.1-6), it has to behave in the same way. For strong diffusion limitations:

$$\eta_\infty = \frac{\sqrt{2}}{Lr_A(C_s^s)\rho_s}\left[\int_{C_{s,eq}}^{C_s^s} D_{eA}(C_s^{'})\, r_A(C_s^{'})\, \rho_s\, dC'_s\right]^{1/2} \equiv \frac{1}{\phi} \qquad (3.6.2\text{-}7)$$

In this equation the lower bound of the integral of (3.6.2-6) has been replaced by $C_{s,eq}$, the equilibrium concentration of *A* for a reversible reaction or by zero for an irreversible reaction. Indeed, when the diffusional limitations are very pronounced, very little reactant would be able to diffuse to the center of the pellet, and any that did would be in equilibrium with the products. It is clear that this assumption may not be fulfilled for intermediate values of the modulus, where, rigorously, C_s^0 would have to be calculated from (3.6.2-4), adding complexity to the computations.

Equation (3.6.2-7) defines a generalized modulus:

$$\phi = \frac{V}{S}\frac{r_A(C_s^s)\rho_s}{\sqrt{2}}\left[\int_{C_{s,eq}}^{C_s^s} D_{eA}(C_s^{'})\, r_A(C_s^{'})\, \rho_s\, dC_s^{'}\right]^{1/2} \qquad (3.6.2\text{-}8)$$

which extends (3.6.1-14) and, therefore, Fig. 3.6.1-3, at least approximately, to any rate equation and to concentration-dependent diffusivity — see equation (3.4-8) or (3.4-10).

Specific applications have been provided by Dumez and Froment [1976], Frouws et al. [1976], and Xu and Froment [1989]. It is clear from this work that the generalized modulus approach, as defined by (3.6.2-8), over-estimates η in the intermediate ranges by some 10 to 15 percent, because of the assumption C_s^0 = $C_{s,eq}$ or zero.

EXAMPLE 3.6.2.A

APPLICATION OF GENERALIZED MODULUS FOR SIMPLE RATE EQUATIONS

First-Order Reversible Reaction, $A \rightleftarrows P$

For this case the rate equation for the net disappearance of reactant *A* can be written

$$r_A = \frac{k}{K}\left[(1+K)C_s - \Sigma C_s^s\right]$$

where *K* is the equilibrium constant and ΣC_s^s is the sum of the surface concentrations of reactant and product.

Also,

$$C_{s,eq} = \frac{\Sigma C_s^s}{1+K}$$

and with constant D_{eA} ,

$$\int_{C_{s,eq}}^{C_s^s} D_{eA}\, r_A(C_s')\, \rho_s\, dC_s' = \frac{k\rho_s D_{eA}}{K} \int_{C_{s,eq}}^{C_s^s} \left[(1+K)C' - \Sigma C_s^s\right] dC_s'$$

$$= \frac{k\rho_s D_{eA}}{K}\left[\frac{1+K}{2}\left(C_s^{s^2} - C_{s,eq}^2\right) - \Sigma C_s^s\left(C_s^s - C_{s,eq}\right)\right]$$

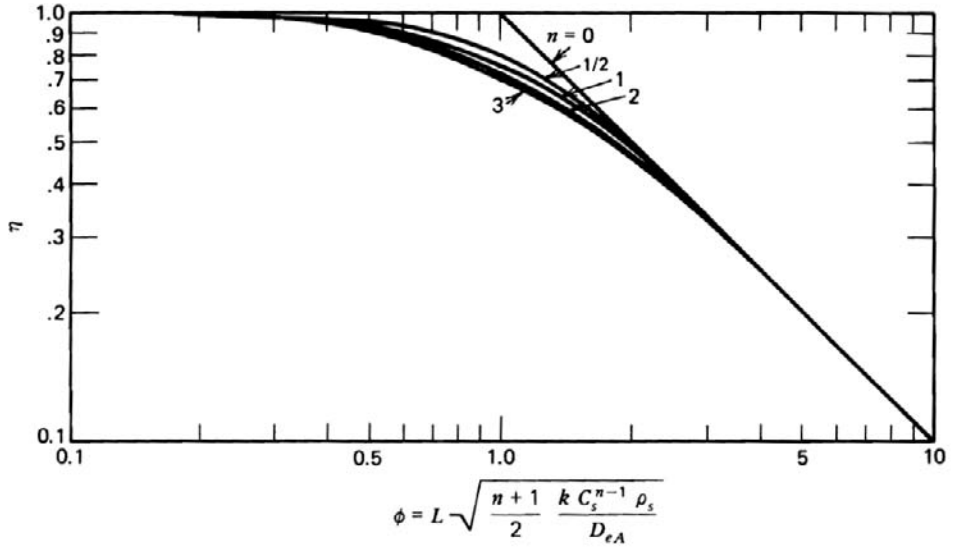

Figure 3.6.2.A-1

Relationship of η versus generalized modulus for simple-order reactions.

so that

$$\phi = \frac{V}{S}\sqrt{\frac{k\rho_s}{D_{eA}}}\frac{(1+K)C_s^s - \Sigma C_s^s}{\sqrt{2K}\left[\frac{1+K}{2}\left[\left(C_s^s\right)^2 - C_{s,eq}^2\right] - \Sigma C_s^s\left(C_s^s - C_{s,eq}\right)\right]^{1/2}}$$

$$= \frac{V}{S}\sqrt{\frac{k\rho_s}{D_{eA}}\frac{1+K}{K}}$$

For an irreversible reaction ($K \to \infty$), the last equation reduces to (3.6.1-16) [Carberry, 1962a, b].

Irreversible Reaction with Order *n*

The generalized modulus becomes

$$\phi = \frac{V}{S}\sqrt{\frac{n+1}{2}\frac{k\left(C_s^s\right)^{n-1}\rho_s}{D_{eA}}} \qquad n > -1$$

The corresponding η versus ϕ plot with n as a parameter is shown in Fig. 3.6.2.A-1. A single curve is obtained for values of the generalized modulus exceeding 2.5. Between 0.4 and 2.5 a set of curves, depending on the order is obtained. ■

3.6.3 Multiple Reactions

It should be emphasized that even the generalized modulus approach is limited to a single rate equation. For processes involving coupled multiple reactions there is no other possibility than to rigorously integrate the set of continuity equations for the key components. A very efficient method that has been preferred to a number of numerical integration techniques for the 2-point boundary value problem discussed here is orthogonal collocation [Finlayson, 1972; Villadsen and Michelsen, 1978]. The technique can handle large sets of differential equations and was applied by Coppens and Froment [1996] and by Sotelo-Boyas and Froment [2009] in their simulation of the catalytic reforming of naphtha on a PtRe/alumina catalyst. The feed contains 29 components and equilibrated Groups of Isomers, GOI, involved in 86 reactions. The approach is briefly outlined and illustrated in what follows.

The interparticle profiles of the M components and GOI are obtained from their continuity equations:

$$\nabla \cdot N_j = \rho_s R_j^e \qquad j = 1 \ldots M \tag{3.6.3-1}$$

where N_j is the flux of component j and

$$R_j^e = \sum_{i=1}^{Q} \alpha_{ij} r_i^e \tag{3.6.3-2}$$

are the effective rates of the Q reactions in which j is involved. These rates are of the Hougen-Watson type, dealt with in Chapter 2. The set (3.6.3-1) has to be combined with the Stefan-Maxwell equations for multicomponent diffusion relating the fluxes to the partial pressure gradients

$$-\nabla p_j = R_g T \sum_{\substack{k=1 \\ k \neq j}}^{M} \frac{p_k N_j - p_j N_k}{p_t D_{e,jk}} + \frac{N_j}{D_{e,Kj}} \tag{3.6.3-3}$$

Equation (3.6.3-3) can be written more concisely as

$$-\nabla p_j = \sum_{k=1}^{M} \kappa_{j,k} N_k \tag{3.6.3-4}$$

The elements of the matrix κ are:

$$\kappa_{jk} = -\frac{p_j}{p_t D_{e,jk}} \qquad k \neq j$$

$$\kappa_{jj} = \frac{1}{D_{e,Kj}} + \sum_{\substack{k=1 \\ k \neq j}} \frac{p_k}{p_t D_{e,jk}} \tag{3.6.3-5}$$

For a spherical particle with isotropic diffusion and reaction, the p_j are only a function of the radial position. To improve the convergence of the solution procedure each p_j is normalized by dividing it by the partial pressure at the surface, p^s_j. In the following, this ratio is represented by y_j. The boundary conditions (B.C.) can now be written, for a spherical particle:

at the surface	$\bar{y} = \bar{y}^s$	
at the center	$\bar{y}$ finite	(3.6.3-6)

From the latter B.C. it follows that any polynomial expansion of the dimensionless partial pressure profiles, $\bar{y}$, as applied in the collocation approach, will only contain even powers of the radial position, r. Replacing, therefore, r by $\xi = (2r / d_p)^2$ in the equations derived by the substitution of equation (3.6.3-3) into equation (3.6.3-1) leads to:

$$4\xi\frac{d^2\bar{y}}{d\xi^2}-4\xi\left(\frac{d\kappa'}{d\xi}\right)\kappa'^{-1}\frac{d\bar{y}}{d\xi}+6\frac{d\bar{y}}{d\xi}+R_gT\frac{d_p^2}{4}\kappa' R=0 \qquad (3.6.3\text{-}7)$$

where $\kappa'_{jk}=\dfrac{\kappa_{jk}}{p_j^0}$ and with B.C. (3.6.3-6).

The orthogonal collocation approach transforms the set of *M* nonlinear differential equations (3.6.3-7) into a set of *M·N* nonlinear algebraic equations in *N* internal collocation points ξ which are the roots of the two parameter Jacobi polynomial $P_N^{(\alpha,\beta)}(\xi)$ of degree *N* and with α and β chosen according to the specifics of the problem. These roots can be obtained using e.g., the Newton-Raphson method.

The first and second derivatives of $\bar{y}$ in the collocation points ξ_i are calculated from

$$\frac{d\bar{y}(\xi_i)}{d\xi}=\sum_{k=1}^{N+1}\bar{y}^{(k)}A_{ki} \qquad \frac{d^2\bar{y}(\xi_i)}{d\xi^2}=\sum_{k=1}^{N+1}\bar{y}^{(k)}B_{ki} \qquad (3.6.3\text{-}8)$$

where *A* and *B* are matrices whose elements follow directly from the theory of orthogonal collocation [see Villadsen and Michelsen, 1978, for *A* and *B* or their transpose]. Equation (3.6.3-7) becomes

$$\sum_{k=1}^{N+1}4\xi_i B_{ij}y_j-\left(\frac{d\kappa'}{d\xi}\right)\kappa'^{-1}\sum_{k=1}^{N+1}4\xi_i A_{ij}y_j+6\sum_{k=1}^{N+1}A_{ij}y_j+\frac{d_p^2}{4}\rho_s R_g T\kappa' R=0 \qquad (3.6.3\text{-}9a)$$

The B.C.

$$\bar{y}^{(N+1)}=\bar{y}^s$$

are already included, but the equations in the external collocation point $\xi_{N+1}=1$ for which $i=N+1$ are redundant. This set of *M·N* nonlinear algebraic equations can be solved by the Powell hybrid method or modifications thereof.

Once the partial pressures in the *N*+1 collocation points ξ_k are known the effective reaction rates can be calculated by approximating the integral in

$$r_i^e=\frac{24}{d_p^3}\int_0^{\frac{d_p}{2}}r_i(p)r^2dr=\frac{3}{2}\int_0^1 R_j^s(p)\sqrt{\xi}d\xi \qquad i=1\ldots Q \qquad (3.6.3\text{-}9b)$$

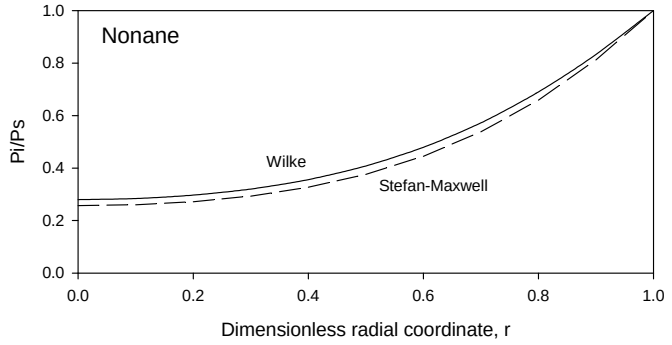

Figure 3.6.3-1

Catalytic reforming of naphtha on Pt-Sn/alumina. Dimensionless partial pressure profile inside the particle for the reactant nonane. Total pressure: 7 bar, T = 510 °C, molar ratio H_2/Hydrocarbons = 5. From Sotelo-Boyas and Froment [2009].

by a weighted sum of the reaction rates in ξ_k and ξ_{N+1}, i.e., at the surface

$$r^e = \sum_{k=1}^{N+1} w_N^{(k)} r(p^{(k)}) \qquad (3.6.3\text{-}10)$$

This is a Radon quadrature. With the known partial pressures at the surface included, the collocation points are the roots of a Jacobi polynomial of degree N and parameters $\alpha = 1$ and $\beta = 1/2$, as can be seen from (3.6.3-9a and 3.6.3-9b). These collocation points and quadrature weights are used in (3.6.3-10).

Fig. (3.6.3-1) shows an internal dimensionless partial pressure profile for one of the naphtha feed components, nonane, taken at the inlet of bed 1. The profile is obtained using $N = 4$. It leads to an effectiveness factor for nonane at this position of 0.56. The profile is decreasing towards the center.

In the catalytic reforming of methane for synthesis gas production, Xu and Froment [1989] also applied collocation. The reactions are very fast in that case and the partial pressures of the reacting molecules drop to zero in a very shallow surface layer of the particle. In that case, spline collocation has to be used. Xu and Froment [1989] used 2 subintervals with collocation used as above. Extra equations have to be added to impose continuity of the first derivative in the spline point $y(\xi)$.

3.7 FALSIFICATION OF RATE COEFFICIENTS AND ACTIVATION ENERGIES BY DIFFUSION LIMITATIONS

The generalized modulus for an *n*th-order reaction derived in Example 3.6.2.A can be used to show how observed kinetic parameters are related to the intrinsic

kinetic parameters when strong pore diffusion limitations occur. For an *n*th order reaction, for example,

$$\left(r_A\right)_{obs} = \eta k\left(C_s^s\right)^n \tag{3.7-1}$$

$$\sim \frac{1}{\phi} k\left(C_s^s\right)^n$$

$$\left(r_A\right)_{obs} = \frac{S}{V}\sqrt{\frac{2}{n+1} D_{eA} k}\left(C_s^s\right)^{(n+1)/2} \tag{3.7-2}$$

and the concentration dependence of the observed rate leads to an order $(n+1)/2$. Only for a first-order reaction would the true order be observed. Also,

$$k_{obs} = \eta k$$

$$= \frac{S}{V}\sqrt{\frac{2}{n+1}}\left[A_D e^{-E_D/RT} A_0 e^{-E/RT}\right]^{1/2} \tag{3.7-3}$$

so that

$$E_{obs} = -\frac{d\ln\left(k_{obs}\right)}{d\left(1/T\right)} = \frac{E + E_D}{2} \approx \frac{E}{2} \tag{3.7-4}$$

where A_D and E_D are the frequency factor and the activation energy for effective diffusion, respectively. With strong pore diffusion limitations, the observed activation energy is one half the true one [Wheeler, 1955].

Weisz and Prater [1954] showed that over the entire range of ϕ, the falsified activation energy is given by

$$\frac{E_{obs}}{E} = 1 + \frac{1}{2}\frac{d\ln\eta}{d\ln\phi} \tag{3.7-5}$$

or considering the diffusivity:

$$E_{obs} = E + \frac{1}{2}\left(E - E_D\right)\frac{d\ln\eta}{d\ln\phi} \tag{3.7-6}$$

Languasco, Cunningham, and Calvelo [1972] derived a similar relation for the falsified order:

$$n_{obs} = n + \frac{n-1}{2}\frac{d\ln\eta}{d\ln\phi} \tag{3.7-7}$$

From the shape of the effectiveness factor curves it is seen that the logarithmic slopes vary from 0 to –1, which yields the simple limits given above.

Reviews and books on intraparticle diffusion in multicomponent catalytic reactions were written by Schneider [1975], Cussler [1976], and Jackson [1977].

EXAMPLE 3.7.A

EFFECTIVENESS FACTORS FOR SUCROSE INVERSION IN ION EXCHANGE RESINS

The first-order reaction,

$$C_{12}H_{22}O_{11} + H_2O \xrightarrow{H^+} C_6H_{12}O_6 + C_6H_{12}O_6$$

(sucrose) (glucose) (fructose)

was studied in particles with different size by Gilliland, Bixler, and O'Connell [1971]. Pellets of Dowex resin with diameters of $d_p = 0.77 \times 10^{-3}$ m, 0.55×10^{-3} m, and 0.27×10^{-3} m were used, and in addition crushed Dowex with $d_p \approx 0.04$ mm, all at 50°C. By techniques to be discussed later in this chapter, the crushed resin was shown not to have any diffusion limitations so that the rate coefficient thus obtained was the instrinsic rate coefficient. The results were as follows:

d_p (mm)	$k\rho_s\,(s^{-1})^a$	$k/k_{0.04}$	$\phi = R\sqrt{k\rho_s / D_{eA}}$	η
0.04	0.0193	1.0	0.53	1.0
0.27	0.0110	0.570	3.60	0.600
0.55	0.00664	0.344	7.35	0.352
0.77	0.00487	0.252	10.3	0.263

[a] Calculated on the basis of approximate normality of acid resin = 3*N*.

The diffusivity of sucrose inside the pellet was also separately measured, in the Na^+ resin form: $D_{eA} = 2.69 \times 10^{-7}$ cm^2/s. More exact values for the H^+ resin form were also computed from the reaction data; but as an example of the estimation of an effectiveness factor, the Na^+ value will be used here.

The Thiele modulus for spheres can be computed from

$$\phi'' = R\sqrt{k\rho_s / D_e}$$

The values are shown in the above table. It is seen that the effectiveness factor values thus determined give a good estimation for the decrease in the observed rate coefficients.

Gilliland et al. [1971] also determined rate coefficient values at 60° and 70°C. The observed activation energies were:

d_p (mm)	E (kJ/mol)
0.04	105
0.27	84
0.55	75
0.77	75
Homogeneous acid solution	105

The activation energy for diffusion was about 34 kJ/mol, so that in the region of strong pore diffusion limitation with $d_p = 0.77 \times 10^{-3}$ m, the predicted falsified activation energy is

$$E_{obs} = \frac{105 + 34}{2} = 70 \text{ kJ/mol}$$

which is close to the experimental value of 75 kJ/mol.

■

3.8 INFLUENCE OF DIFFUSION LIMITATIONS ON THE SELECTIVITIES OF COUPLED REACTIONS

The question of diffusional effects on the selectivity of multiple reactions is of particular importance for industrial processes. The basic concepts were provided by Wheeler [1951] through consideration of three categories of processes.

The simplest is that of parallel, independent reactions (Wheeler Type I):

$$A \xrightarrow{1} R, \text{ with order } a_1$$

$$B \xrightarrow{2} S, \text{ with order } a_2$$

In the absence of diffusion limitations, the selectivity ratio was already given in Chapter 1:

$$\left(\frac{r_R}{r_S}\right) = \frac{k_1}{k_2}\frac{(C_{As})^{a_1}}{(C_{Bs})^{a_2}} \tag{3.8-1}$$

With pore diffusion limitations, the two independent rates are each merely multiplied by the effectiveness factor to give

$$\left(\frac{r_R}{r_S}\right)_{obs} = \frac{\eta_1 k_1}{\eta_2 k_2}\frac{(C_{As})^{a_1}}{(C_{Bs})^{a_2}} \tag{3.8-2}$$

For strong pore diffusion limitations, when $\eta_i \sim 1/\phi_i$,

$$r_i \sim \left(\frac{2}{a_i + 1} \frac{k_i D_{ei}}{L^2} \right)^{1/2} \left(C_{is}^s \right)^{(a_i+1)/2}$$

and (3.8-2) becomes

$$\left(\frac{r_R}{r_S} \right)_{obs} \sim \left[\frac{a_2 + 1}{a_1 + 1} \frac{k_1}{k_2} \frac{D_{eA}}{D_{eB}} \frac{\left(C_{As}^s \right)^{a_1+1}}{\left(C_{Bs}^s \right)^{a_2+1}} \right]^{1/2} \tag{3.8-3a}$$

For first-order reactions and $D_{eA} = D_{eB}$

$$\left(\frac{r_R}{r_s} \right)_{obs} = \sqrt{\frac{k_1}{k_2}} \frac{C_{As}^s}{C_{Bs}^s} \tag{3.8-3b}$$

Comparison of (3.8-3b) with (3.8-1) shows that the effect of strong pore diffusion limitations is to change the ratio of rate constants, k_1/k_2, to the square root of the ratio. When k_1 exceeds k_2, other conditions being equal, the selectivity ratio will be reduced by the diffusional resistance.

The next case to be considered is that of consecutive first-order reactions (Wheeler Type III):

$$A \xrightarrow{1} R \xrightarrow{2} S$$

Here, the selectivity for *R* in the absence of pore diffusion limitation is

$$\frac{r_R}{r_A} = 1 - \frac{k_2}{k_1} \frac{C_{Rs}}{C_{As}} \tag{3.8-4}$$

The continuity equations for *A* and *R* accounting for diffusion limitations are, for slab geometry,

$$D_{eA} \frac{d^2 C_{As}}{dz^2} = k_1 \rho_s C_{As}$$

$$D_{eR} \frac{d^2 C_{Rs}}{dz^2} = -k_1 \rho_s C_{As} + k_2 \rho_s C_{Rs}$$

The first equation leads to the well known solution which is then substituted into the second equation. The results for the selectivity of *R* are

$$\left(\frac{r_R}{r_A}\right)_{obs} = \frac{\int_0^L r_R dz}{\int_0^L r_A dz} = \frac{\int_0^L (k_1 C_{As} - k_2 C_{Rs}) dz}{\int_0^L k_1 C_{As} dz}$$

$$= \frac{1-(\sigma\eta_2/\eta_1)}{1-\sigma} - \left(\frac{\eta_2}{\eta_1}\right)\frac{k_2}{k_1}\frac{C_{Rs}^s}{C_{As}^s} \qquad (3.8\text{-}5)$$

where

$$\eta_i = \frac{\tanh\phi_i}{\phi_i} \qquad \phi_i = L\sqrt{k_i \rho_s / D_{ei}} \qquad \text{with } i = 1, 2$$

$$\sigma = \left(\frac{\phi_2}{\phi_1}\right)^2 = \frac{k_2 D_{eA}}{k_1 D_{eR}}$$

Again, it is most instructive to look at the asymptotic region of strong pore diffusion limitation. For $D_{eA} = D_{eR}$:

$$\left(\frac{r_R}{r_A}\right)_{obs} \sim \frac{1}{1+\sqrt{\sigma}} - \frac{1}{\sqrt{\sigma}}\frac{k_2}{k_1}\frac{C_{Rs}^s}{C_{As}^s} \qquad (3.8\text{-}6a)$$

$$= \frac{1}{1+\sqrt{k_2/k_1}} - \sqrt{\frac{k_2}{k_1}}\frac{C_{Rs}^s}{C_{As}^s} \qquad (3.8\text{-}6b)$$

The main difference between (3.8-6b) and (3.8-4) is that the ratio of rate constants, k_2/k_1, is effectively reduced to its square root, although there are now also several other complications. Comparing these results with those given in Chapter 1 clearly shows the reduction in selectivity caused by the diffusion limitations.

The third case of parallel reactions with a common reactant (Wheeler Type II) is mathematically more complicated. The only situation of interest occurs when the reaction orders are different; otherwise, the selectivity ratio is simply a function of the ratio of rate constants:

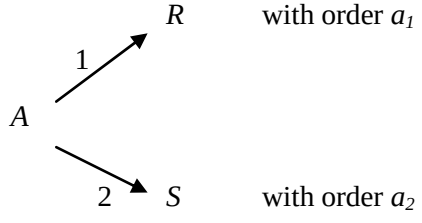

In the absence of diffusion limitations,

$$\frac{r_R}{r_s} = \frac{k_1}{k_2}\left(C_{As}^s\right)^{a_1-a_2} \tag{3.8-7}$$

The selectivity ratio in the presence of pore diffusion limitations is found by integrating the continuity equation for *A* accounting for diffusion and reaction:

$$D_{eA}\frac{d^2C_{As}}{dz^2} - (k_1\rho_s C_{As}^{a_2} + k_2\rho_s C_{As}^{a_1}) = 0$$

The selectivity ratio is obtained from

$$\left(\frac{r_R}{r_s}\right)_{obs} = \frac{\int_0^L r_R dz}{\int_0^L r_s dz} \tag{3.8-8a}$$

$$= \frac{k_1\int_0^L C_{As}^{a_1} dz}{k_2\int_0^L C_{As}^{a_2} dz} \tag{3.8-8b}$$

The mathematical solutions of interest are quite involved, but Roberts [1972] has presented several useful results. In the asymptotic region of strong diffusion limitation an approximate solution is:

$$\frac{\left(r_R / r_A\right)_{obs}}{\left(r_R / r_A\right)} \sim \frac{a_2 + 1}{2a_1 - a_2 - 1} \tag{3.8-9}$$

for

$$\frac{r_R}{r_S} = \frac{k_1\left(C_{As}^s\right)^{a_1-a_2}}{k_2} << 1$$

also with

$$\frac{r_R}{r_A} = \frac{r_R}{r_R + r_S} \tag{3.8-10}$$

$$= \left\{\left[\frac{k_2}{k_1}\left(C_{As}^s\right)^{a_2-a_1}\right] + 1\right\}^{-1}$$

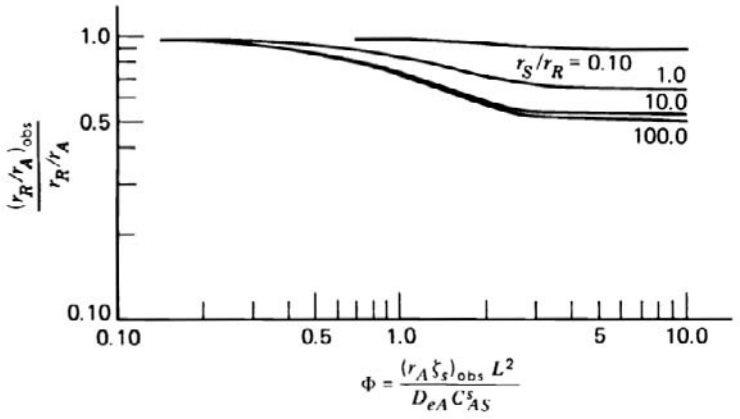

Figure 3.8-1

Relative yield ratio versus modulus Φ for various values of r_S/r_R — second- and first-order reactions. From Roberts [1972].

The selectivity is

$$\left(\frac{r_R}{r_S}\right)_{obs} = \left[\left(\frac{r_R}{r_A}\right)^{-1}_{obs} - 1\right]^{-1} \tag{3.8-11}$$

This case does not result in a simple square root alteration of the rate constant as derived for the other two cases. For $a_1 = 2$, $a_2 = 1$, the largest deviation from the ratio with no diffusion effects in (3.8-9) is = 1/2. For $a_1 = 2$, $a_2 = 0$, this becomes 1/5. Fig. 3.8-1 shows the results for the (2, 1) case.

Carberry [1962a, b] extended the results of Wheeler on consecutive first-order reactions (Wheeler Type III) to pellets containing macro- and micropores. Such a situation is quite common when the pellet has been shaped from microparticles by compression. The micropores were considered to be in series with the macropores, and only the latter communicate with the pellet surface [Mingle and Smith, 1961].

Solving the continuity equation for *A* in a microporous particle with slab geometry (see Section 3.6.1) for a first-order reaction leads to

$$r'_A = k_1 C_{As} \eta' \tag{3.8-12}$$

with

$$\eta_\mu = \frac{\tanh \Phi_\mu}{\Phi_\mu} \qquad \text{and} \qquad \Phi_\mu = \sqrt{\frac{k\rho_s}{D'_{eA}}} L_\mu$$

The concentration C_{As} in (3.8-12) is the surface concentration for the microporous particle, which is also the concentration in the macropores.

The continuity equation for *A* in the pellet as a whole has the same form as in (3.8-12). The concentration C_{As} at any position in the macropores is determined also by the reaction in the micropores, which are visualized as branching at right angles from the macropores. The rate averaged over the pellet may then be written:

$$r_A = k_1 C_{As}^s \eta_\mu \eta_\mu \qquad (3.8\text{-}13)$$

$$= k_1 C_{As}^s \eta$$

where

$$\eta_M = \frac{\tanh \Phi}{\Phi} \quad \text{with} \quad \Phi = \sqrt{\frac{k_1 \rho_s \eta_\mu}{D_{eA}}} L$$

is the effectiveness factor for the macropores and $\eta_0 = \eta_M \eta_\mu$ is the pellet effectiveness factor.

Often, micropores are so short that $\eta' = 1$. Significant micropore diffusion limitations only occur when the resistance in the macropores is pronounced.

The net rate of production of the intermediate *R* is derived along the same lines. Simplifying Carberry's equations by neglecting external transport limitations, the following equation for the selectivity for *R* is obtained:

$$\left(\frac{r_R}{r_A}\right)_{obs} = \frac{1 - \sigma\left(\frac{\eta_2}{\eta_1}\right)\left(\frac{\eta_2'}{\eta_1'}\right)}{1-\sigma} - \left(\frac{\eta_2}{\eta_1}\right)\left(\frac{\eta_2'}{\eta_1'}\right)\frac{k_2}{k_1}\frac{C_{Rs}^s}{C_{As}^s} \qquad (3.8\text{-}14)$$

where

$$\sigma = \left(\frac{k_2}{k_1}\frac{D_{eR}}{D_{eA}}\right) = \left(\frac{k_2}{k_1}\frac{D_{er}'}{D_{eA}'}\right)$$

Again, it is easiest to visualize the results in the asymptotic region, that is, for large ϕ and ϕ_μ. With $D_{eA} = D_{eR}$:

$$\left(\frac{r_R}{r_A}\right)_{obs} = \frac{1-(k_2/k_1)^{1/4}}{1-(k_2/k_1)} - \left(\frac{k_2}{k_1}\right)^{1/4}\frac{C_{Rs}^s}{C_{As}^s} \qquad (3.8\text{-}15)$$

A comparison of (3.8-15) with (3.8-6b) reveals a further decrease of the selectivity.

3.9 CRITERIA FOR THE IMPORTANCE OF INTRAPARTICLE DIFFUSION LIMITATIONS

Possible pore diffusion limitations can be evaluated by computing the generalized modulus and use of Fig. 3.6.1-3 to see if the value of η is less than unity. In the design situation this procedure can be used because $k\rho_s$ is known, but at the stage of determining kinetic parameters from experimental data, this is not applicable because $k\rho_s$ is not available yet. Therefore, criteria for the importance of pore diffusion that do not explicitly contain $k\rho_s$ are also needed. Two main types are in use.

The first involves performing experiments with two different sizes of catalyst. Then, from (3.6.2-8), if it is assumed that $k\rho_s$ and D_{eA} are the same for both sizes,

$$\frac{\phi_1}{\phi_2} = \frac{L_1}{L_2} \tag{3.9-1}$$

$$\text{with } L = \frac{V}{S}.$$

Also,

$$\frac{(r_{obs})_1}{(r_{obs})_2} = \frac{\eta_1}{\eta_2} \tag{3.9-2}$$

The two sizes will give different values for the moduli [only the ratio can be determined from (3.9-1)]. If the two observed rates are the same, $\eta_1 = \eta_2$ and the operation must be on the horizontal part of the $\phi - \eta$ curve (i.e., no pore diffusion limitations). At the other extreme, $\eta = 1/\phi$, and

$$\frac{(r_{obs})_1}{(r_{obs})_2} = \frac{\phi_2}{\phi_1} = \frac{L_2}{L_1} \tag{3.9-3}$$

Therefore, in this case the observed rates are inversely proportional to the two pellet sizes. For intermediate degrees of pore diffusion limitation, the ratio of rates will be less than proportional to L_2/L_1.

The second method is based upon the Weisz-Prater criterion [1954]. It is arrived at by rewriting the Thiele modulus (3.6.1-16):

$$k\rho_s = \frac{\phi^2}{L^2} D_{eA}$$

Substituting this into the rate equation of a first-order reaction in the presence of diffusion limitations gives:

$$r_A \rho_s = \eta k \rho_s C_s^s$$

so that

$$r_A \rho_s = \eta \frac{\phi^2}{L^2} D_{eA} C_s^s$$

When all the directly *observable* quantities are brought on one side of the equation,

$$\frac{\left(r_A \rho_s\right)_{\text{obs}} L^2}{D_{eA} C_s^s} = \eta \phi^2 \equiv \Phi \tag{3.9-4}$$

From the two limiting areas of Fig. 3.6.1-3, it follows that:

1. For ϕ << 1, η = 1, (no pore diffusion limitation), and so $\eta\phi^2$ becomes << 1;
2. For ϕ >> 1, $\eta = 1/\phi$ (strong pore diffusion limitation), and $\Phi = \eta\phi^2$ >> 1.

The criterion for the absence of diffusion limitations for a first-order reaction then becomes:

$$\Phi = \frac{\left(r_A \rho_s\right)_{\text{obs}} L^2}{D_{eA} C_s^s} << 1 \tag{3.9-5}$$

Using the generalized modulus, the Weisz-Prater criterion (3.7-5) was extended by Petersen [1965a, b] and Bischoff [1967] to the case where the reaction rate is not first order and may be written as

$$r_A(C_b) \rho_s = k \rho_s g(C) \tag{3.9-6}$$

where $g(C)$ contains the concentration dependence. Following the same procedure, the extended criterion is

$$\Phi = \frac{\left(r_A \rho_s\right)_{\text{obs}} L^2 g(C_s^s)}{2 \int_{C_{s,eq}}^{C_s^s} D_{eA}(C)\, g(C)\, dC} << 1 \tag{3.9.7}$$

This can also be accomplished by replotting the effectiveness factor curve of Fig. 3.6.2.A-1 in Example 3.6.2.A as η versus $\Phi \equiv \eta\phi^2$, so that the abcissa contains only directly observed quantities. Equation (3.7-7) can also be written:

$$\Phi = \frac{\left(r_A \rho_s\right)_{\text{obs}} L^2}{\overline{D}_{eA} C_s^s} << \frac{2 \int_{C_{s,eq}}^{C_s^s} \left(D_{eA} / \overline{D}_{eA}\right) g(C)\, dC}{C_s^s g(C_s^s)} \tag{3.9-8}$$

where $\overline{D}_{eA}$ is an average value of D_{eA}. This criterion should be compared with Weisz and Prater's criterion for first-order reactions.

Alternate but similar criteria have been derived using perturbation techniques about the surface concentration by Hudgins [1968] and using collocation methods by Stewart and Villadsen [1969]. Their results are essentially given by:

$$\Phi = \frac{(r_A \rho_s)_{\text{obs}} L^2}{D_{eA} C_s^s} << \frac{g(C_s^s)}{C_s^s g'(C_s^s)} \tag{3.9-9}$$

where $g' \equiv dg/dC$. Gonzo and Gottifredi [1983] premised that diffusion limitations could be neglected when $\eta > 0.95$ or

$$|1 - \eta| \leq 0.05 \tag{3.9-10}$$

Writing the continuity equation for the key component A in terms of the dimensionless concentration $C = C_A/C_{As}$ the following equation is obtained for a spherical particle with uniform activity:

$$\frac{d^2 C}{dr^2} + \frac{2}{r}\frac{dC}{dr} = \Phi F(C) \tag{3.9-11}$$

with B.C. $dC/dr = 0$ at the center ($r = 0$) and $C = 1$ at the surface ($r = 1$) with r the characteristic dimension, V/S i.e. $R/3$ for a sphere with radius R, and $F(C)$ the rate of reaction. To satisfy the condition (3.9-10) Φ must be very small, suggesting an approximate series solution:

$$C \approx 1 + \Phi A(r) + O(\Phi^2) \tag{3.9-12}$$

Substituting (3.9-12) into (3.9-11) and collecting terms of equal powers of Φ leads to the following equation for $A(r)$:

$$\frac{d^2 A}{dr^2} + \frac{2}{r}\frac{dA}{dr} = 1 \tag{3.9-13}$$

The effectiveness factor can be written:

$$\eta = \int_0^1 3F(C) r^2 dr \tag{3.9-14}$$

Expanding $F(C)$ in Taylor series leads to:

$$\eta = 1 + \Phi \alpha F'(1) + O(\Phi^2) \tag{3.9-15}$$

where $F'(1)$ is the first derivative of F with respect to C, evaluated at the surface where $C = 1$, and

$$\alpha = -\int_0^1 3A(r)r^2 dr \tag{3.9-16}$$

Substituting (3.9-14) into (3.9-10) gives the criterion

$$\left|\alpha\Phi F'(1)\right| \le 0.05 \tag{3.9-17}$$

α for a sphere with uniform activity equals 1/15.

For a Hougen-Watson type rate equation

$$r_A = \frac{k\,C_A}{1 + K_A C_A + \sum_j K_j C_j} \tag{3.9-18}$$

The rate of this single reaction has to be expressed in terms of the concentration of the key reactant A.

Because of the difference between the D_j the concentration of the species j can not be obtained simply from the stoichiometry, but the diffusion has to be explicitly accounted for:

$$D_{eA}\left(\frac{d^2C_A}{dr^2} + \frac{2}{r}\frac{dC_A}{dr}\right) = \alpha_j D_{ej}\left(\frac{d^2C_j}{dr^2} + \frac{2}{r}\frac{dC_j}{dr}\right) \tag{3.9-19}$$

Integrating twice and accounting for the boundary conditions at the surface leads to the algebraic equation:

$$C_j = \lambda_j (C - 1) + 1 \tag{3.9-20}$$

where

$$\lambda_j = -\frac{C_{As} D_{eA}}{\alpha_j C_{js} D_{ej}}$$

and α_j is the stoichiometric coefficient of j in the reaction $A \rightarrow \sum_{j=1}^{N} \alpha_j J$.

For the rate equation (3.9-18):

$$F(C) = \frac{C_A(1 + K_1)}{1 + K_1 C_A} \quad \text{with} \quad K_1 = \frac{K_A C_{As} + \sum_j \lambda_j K_j C_{js}}{1 + \sum_j (1 - \lambda_j) K_j C_{js}} \tag{3.9-21}$$

and consequently $F'(1) = \dfrac{1}{1+K_1}$

so that the criterion becomes, in terms of observables:

$$\frac{L^2 r_{obs}\rho_s}{D_{eA}C_{As}} \leq 0.75(1+K_1) \tag{3.9-22}$$

with $L = V/S = R/3$ for a sphere.

Gonzo and Gottifredi [1983] applied (3.9-17) and extensions accounting also for interfacial gradients to experimental data of Wu and Nobe [1977] on the reduction of NO with ammonia and of Kehoe and Butt [1970] on benzene hydrogenation.

EXAMPLE 3.9.A

APPLICATION OF THE EXTENDED WEISZ-PRATER CRITERION

The use of the general criterion, (3.9-7) is illustrated by applying it to the case of the carbon-carbon dioxide reaction

$$C + CO_2 \rightarrow 2CO \tag{3.9.A-a}$$

Peterson [1965a, b] used some of the data of Austin and Walker [1963] to show how the application of a first-order criterion would not be correct. Here, the data are recalculated on the basis of (3.9-7). This reaction appears to be very strongly inhibited by adsorption of the product, carbon monoxide, which leads to large deviations from first-order behavior. The rate equation was of the Hougen-Watson type:

$$r_{CO_2} = \frac{kC_{co_2}}{1+K_2C_{co}+K_3C_{co_2}} \tag{3.9.A-b}$$

From the reaction stoichiometry, and assuming equal diffusivities and zero carbon monoxide concentration at the particle surface, (3.9.A-b) becomes

$$r_{CO_2} = \frac{kC_{CO_2}}{\left(1+2K_2C^s_{CO_2}\right)+\left(K_3-2K_2\right)C_{CO_2}} \tag{3.9.A-c}$$

where

$C^s_{co_2} = C_{obs} =$ concentration of CO_2 at the particle surface.

If (3.9.A-c) is substituted into the general criterion, (3.9-7) one obtains

$$\Phi = \frac{\left(r_{CO_2}\rho_s\right)_{obs} L^2}{2D_{eCO_2}} \left\{ \frac{1+K_3 C^s_{CO_2}}{K_3 - 2K_2} \left[1 - \frac{1+2K_2 C^s_{CO_2}}{C^s_{CO_2}\left(K_3 - 2K_2\right)} \ln \frac{1+K_3 C^s_{CO_2}}{1+2K_2 C^s_{CO_2}} \right] \right\}^{-1}$$

$$<< 1 \qquad (3.9.A\text{-}d)$$

At 1000 K, the following data were used:

$C^s_{CO_2}$ (1 bar) = 1.22×10^{-5} mol/cm^3; $K_2 = 4.15 \times 10^9$ cm^3/mol;

$K_3 = 3.38 \times 10^5$ cm^3/mol; $D_{eCO_2} = 0.1$ cm^2/s;

$L = 0.7$ cm; $\left(r_{CO_2}\rho_s\right)_{obs} = 4.67 \times 10^{-9}$ mol/cm^3 s.

If these data are substituted into the general criterion (3.9-7) and (3.9.A-d), a value of $\Phi = 2.5$ is obtained. This value exceeds one, meaning that diffusion limitations were occurring. This is effectively what Austin and Walker concluded from observation of cross-sections of the coke particles. If the above values were substituted into the first-order Weisz-Prater criterion, (3.9-5), Φ would be 2.28×10^{-3}, indicating the absence of diffusion limitations.

This example clearly illustrates the necessity of using the correct rate equation and criteria for diffusion limitation.

■

3.10 MULTIPLICITY OF STEADY STATES IN CATALYST PARTICLES

Theoretical studies have shown that one and the same external condition can lead to more than one steady-state concentration profile inside a catalyst particle. Satterfield et al. [1966; 1967], for example, have shown that rate equations of the form:

$$r_A = \frac{kC(C+E)}{(1+KC_s)^2} \qquad (3.10\text{-}1)$$

lead to multiple solutions for the steady-state continuity equation for *A*, (3.6.2-1), for certain ranges of the parameters, primarily large values of *K*.

Carbon monoxide oxidation on Pt catalysts is an example of a reaction of practical importance that can lead to multiplicity of steady states when the resistance to diffusion leads to significant concentration gradients. Typical for multiple steady states is a sudden jump from a relatively low rate of reaction or conversion to relatively high values upon an increase of the catalyst temperature. Upon decreasing the temperature, the jump back to the low reaction rate occurs

at a different value, leading to a hysteresis [Hegedus et al., 1977]. This phenomenon, which is not favorable for smooth industrial operation, is discussed further in Chapter 11.

Complex reaction mechanisms and catalytic surface effects can also lead to multiplicity. Only multiplicity resulting from the combined effect of diffusion, adsorption, and reaction in an isothermal particle will be briefly dealt with here. Luss [1968] derived the following necessary and sufficient condition for uniqueness:

$$\left(C_s - C_s^s\right)\frac{d1\mathrm{n}\, r_A(C_s)\rho_s}{dC_s} \le 1 \tag{3.10-2}$$

For an *n*th-order reaction, this condition requires that

$$n \ge (n-1)\frac{C_s}{C_s^s} \tag{3.10-3}$$

from which it can be seen that only reactions that behave as if they had a negative order can lead to multiplicity for a certain range of values of C_s / C_s^s. Luss also showed that for rate equations of the form

$$r_A = \frac{kC_s}{\left[\ 1 + \left(KC_s^s\right)\left(C_s / C_s^s\right)^2\ \right]} \tag{3.10-4}$$

uniqueness is guaranteed when

$$KC_s^s \le 8 \tag{3.10-5}$$

Interfacial concentration and temperature gradients as well as temperature gradients inside the particle widen the range of operating conditions which may lead to the occurrence of multiple steady states. For further discussion of this pathological behavior, the reader is referred to Lee and Luss [1969, 1970, 1971], Luss [1971, 1976], and Varma and Aris [1977].

3.11 COMBINATION OF EXTERNAL AND INTERNAL DIFFUSION LIMITATIONS

The addition of fluid-phase resistance to internal resistance is relatively easy for a first-order reaction. It has to be accounted for that C_s^s is not known and must be related to the fluid field value *C* by

$$k_g\left(C - C_s^s\right) = D_{eA}\left(\frac{dC_s}{dz}\right)_s \tag{3.11-1}$$

which leads to the solution in terms of C :

$$C_s = C\frac{\cosh(\phi\, z/L)}{\cosh\phi + \dfrac{D_{eA}\phi}{Lk_g}\sinh\phi} \tag{3.11-2}$$

Equation (3.11-2), when used in defining the effectiveness factor based on the bulk fluid concentration C, gives

$$\eta_G = \frac{D_{eA}C\dfrac{(\phi/L)\sinh\phi}{\cosh\phi + (D_{eA}\phi/Lk_g)\sinh\phi}}{Lk\rho_s C}$$

$$= \frac{(\tanh\phi)/\phi}{1 + (D_{eA}\phi/Lk_g)\tanh\phi} \tag{3.11-3}$$

The subscript G refers to a "global" (particle + film) effectiveness factor, which includes *both* resistances, and which reduces to (3.6.1-6) for $k_g \to \infty$. Equation (3.11-3) is more conveniently written as [Aris 1969]:

$$\frac{1}{\eta_G} = \frac{1}{\eta} + \frac{\phi^2}{\text{Sh'}} \tag{3.11-4}$$

$$= \frac{\phi}{\tanh\phi} + \frac{k\rho_s}{k_g}\left(\frac{V}{S}\right) \tag{3.11-5}$$

where Sh' = $k_g L / D_{eA}$ = modified Sherwood number (note that the particle half-width and the effective diffusivity are used rather than the usual parameters). This number is also called the Biot number for mass transfer (Bi_m).

Again, (3.11-4) clearly shows the additivity of resistances for first-order reaction. Note that in the asymptotic region, where ϕ is large,

$$\frac{1}{\eta_G} \sim \phi + \frac{\phi^2}{\text{Sh'}} \tag{3.11-6}$$

and for sufficiently large ϕ and finite Sh',

$$\frac{1}{\eta_G} \approx \frac{\phi^2}{\text{Sh'}}$$

In this situation, the ultimate log slope would be –2 rather than –1 for only internal diffusion.

Petersen [1965a, b] has demonstrated that with realistic values of the mass transfer and diffusion parameters, external transport limitations will never exist unless internal diffusion limitations are also present.

A comprehensive study by Mehta and Aris [1971] provides graphs for *n*th-order reactions. A brief summary of their results follows:

$$\phi_G = \phi\left[1+\frac{2}{n+1}\frac{\eta\phi^2}{\mathrm{Sh'}}\right]^{(n-1)/2}$$

$$\frac{1}{\eta_G} = \frac{1}{\eta}\left[1+\frac{2}{n+1}\frac{\eta\phi^2}{\mathrm{Sh'}}\right]^{n}$$

where

$$\phi = L\sqrt{\frac{n+1}{2}k\rho_s\left(C_s^s\right)^{n-1}/D_{eA}} \qquad \eta = \eta(\phi) - \text{ as usual}$$

$$\phi_G = L\sqrt{\frac{n+1}{2}k\rho_s C^{n-1}/D_{eA}} \qquad \eta_G = \eta_G(\phi_G)$$

For a given situation, ϕ_G and Sh' can be computed. An iterative solution is required to find ϕ and η, and thus η_G.

3.12 DIAGNOSTIC EXPERIMENTAL CRITERIA FOR THE ABSENCE OF INTERNAL AND EXTERNAL MASS TRANSFER LIMITATIONS

In kinetic studies it is advised to avoid experimentation in which external transport limitations are experienced. These can be easily avoided by adapting the flow rates. Yet, Koros and Nowak [1967] and Madon and Boudart [1982] have drawn attention to the lack of generality of the usual diagnostic test for external mass and heat transfer limitations. In this experimental test, the conversion (or the rate) is measured at constant space-time, W/F_{A0}, but the flow velocity is varied by adapting simultaneously W and F_{A0}. If the conversion (or the rate) is not affected, the conclusion is drawn that there are no external transport limitations. At the low Reynolds numbers encountered in laboratory reactors, the mass and heat transfer coefficients are quite insensitive to changes in flow rates, so that these have to be varied over a very wide range.

The experimental test for the effect of internal mass transfer that compares rates at various particle sizes has to be interpreted with skill, because changes in the flow velocity may affect the heat transfer between the bed and the wall and, therefore, the temperature field. What Koros and Nowak [1967]

proposed instead can be interpreted as follows: a particle of the catalyst to be studied is crushed and the fines are mixed in various ratios, *f*, with inert fines of the same size and having the same porous structure. The various mixtures are compressed into particles with the same size as the original undiluted catalyst particle. The rate of the process is then measured, under identical conditions, with the various types of particles. When the observed rate is plotted versus *f*, a straight line can be expected for the region of low *f*, that is, for the kinetic regime. If the linearity extends up to $f = 1$, that is, to the undiluted, original particle, then the latter can be safely used to study the intrinsic kinetics, at least, for the same operating conditions. If the curve rate versus *f* deviates from linearity, mass transfer (and/or heat transfer) limitations occur. Clearly, the recommendations made in Section 2.4.1 should be kept in mind in this experimentation.

The above reasoning can be formulated, for example, for a first-order rate equation

$$\left(r_A\right)_{obs} = \eta_G k C_A \tag{3.12-1}$$

so that from (3.11-4)

$$\left(r_A\right)_{obs} = \frac{1}{\dfrac{1}{\eta} + \dfrac{k\rho_s}{k_g a_g}} k C_A \tag{3.12-2}$$

When there are no mass transfer limitations, $\eta_G = 1$, so that

$$\left(r_A\right)_{obs} = k C_A \tag{3.12-3}$$

and the observed rate varies linearly with the amount of active material, which determines the activity and, therefore, k or $k\rho_s$. When external mass transfer is rate limiting,

$$\left(r_A\right)_{obs} = k_g a_g C_A / \rho_s \tag{3.12-4}$$

and the observed rate is independent of the fraction of active material.

When internal mass transfer is rate limiting η is inversely proportional to ϕ, so that

$$\left(r_A\right)_{obs} \sim a_g \sqrt{D_{eA} k / \rho_s}\, C_A \tag{3.12-5}$$

and the relation is nonlinear.

Madon and Boudart [1982] have applied this approach by varying the metal loading of Pt/SiO_2 catalysts. In this approach care has to be taken to maintain the dispersion of the metal constant, however.

3.13 NONISOTHERMAL PARTICLES

3.13.1 Thermal Gradients Inside Catalyst Particles

Thus far, only concentration gradients inside the pellet were considered. Are temperature gradients also possible? Using magnetic crystallite thermometry, Calo [1984] showed that in the steady state, the average Ni crystalline temperature in ethane hydrogenolysis is not measurably different from that of the support. This was also shown by Kehoe and Butt in their experimental study of benzene hydrogenation [1972]. Nevertheless, the question has generated a considerable amount of theoretical work that will be briefly reviewed in what follows. To start with, continuity equations for the independent reacting species and the energy equation are coupled through the rate terms and now have to be solved simultaneously. For slab geometry, these can be written

$$\frac{d}{dz}\left[D_{eA}\frac{dC_s}{dz}\right] = r_A(C_s, T_s)\rho_s \tag{3.13.1-1}$$

$$-\frac{d}{dz}\left[\lambda_e \frac{dT_s}{dz}\right] = (-\Delta H) r_A(C_s, T_s)\rho_s \tag{3.13.1-2}$$

where λ_e is the effective thermal conductivity of the pellet [see Satterfield, 1970; Smith, 1970, for further details]; an order of magnitude values is $\lambda_e \approx 4 \times 10^{-3}$ J/s cm K.

Some information can be obtained without the full solution. If (3.13.1-2) is divided by $-\Delta H$ and subtracted from (3.13.1-1), the following equation results:

$$\frac{d}{dz}\left[D_{eA}\frac{dC_s}{dz} + \frac{\lambda_e}{(-\Delta H)}\frac{dT_s}{dz}\right] = 0 \tag{3.13.1-3}$$

which, when integrated from the center to a point z, gives

$$D_{eA}\frac{dC_s}{dz} + \frac{\lambda_e}{(-\Delta H)}\frac{dT_s}{dz} = \text{constant} = 0 \tag{3.13.1-4}$$

Another integration gives, for constant D_{eA} and λ_e,

$$D_{eA}C_s + \frac{\lambda_e}{(-\Delta H)}T_s = \text{constant} = D_{eA}C_s^s + \frac{\lambda_e}{(-\Delta H)}T_s^s$$

or

$$T_s - T_s^s = \frac{D_{eA}(-\Delta H)}{\lambda_e}\left(C_s^s - C_s\right) \tag{3.13.1-5}$$

Equation (3.13.1-4) can be used to eliminate either C_s or T_s from one of the differential equations, with the result that, in general, only one (nonlinear) equation with one dependent variable must be solved.

The maximum temperature difference in a particle is obtained at complete conversion ($C_s = 0$) [Prater, 1958]:

$$\frac{(\Delta T_s)_{\max}}{T_s^s} = \frac{(-\Delta H) D_{eA} C_s^s}{\lambda_e T_s^s} \equiv \beta \tag{3.13.1-6}$$

This result is actually true for any particle geometry, under steady-state conditions. For industrial processes β is very small, so that the temperature difference between the surface and the inside of the particle is negligible, at least for steady-state conditions [Hlavacek et al., 1969].

Theoretical work has been done on the effectiveness factor for nonisothermal particles. Fig. 3.13.1-1 shows the results of the computations by Weisz and Hicks [1962] for $\gamma = E/RT_s^s = 20$. For $\beta > 0.1$, that is, for sufficiently exothermic reactions, the effectiveness factor can exceed the value of 1. In such a case the temperature rise, which increases the value of the rate constant, would more than offset the decrease in reactant concentration C_{As}, so that r_A averaged over the particle exceeds that at surface conditions. The converse is true for endothermic reactions.

Figure 3.13.1-1 also shows that for large β and for a narrow range of ϕ" values, three possible values of η could be obtained. This multiplicity of steady states is a consequence of the strong nonlinearity of the heat generation term in the right-hand side of (3.13.1-2). This multiplicity will be discussed in a later section. Detailed study shows that only the upper and lower values of η are actually attained, depending upon the direction of approach. The center value represents an unstable state.

The set of plots of the type of Fig. 3.13.1-1 for various γ may be reduced to a single diagram with similar curves but with $\beta\gamma$ as a parameter instead of β only [Tinkler and Metzner, 1961; Carberry, 1961; Aris, 1965a, b; and Petersen, 1965a, b]. Liu [1969] expressed these curves by means of the simple formula

$$\eta \cong \frac{1}{\phi_s} \exp\left(\frac{\beta\gamma}{5}\right) \tag{3.13.1-7}$$

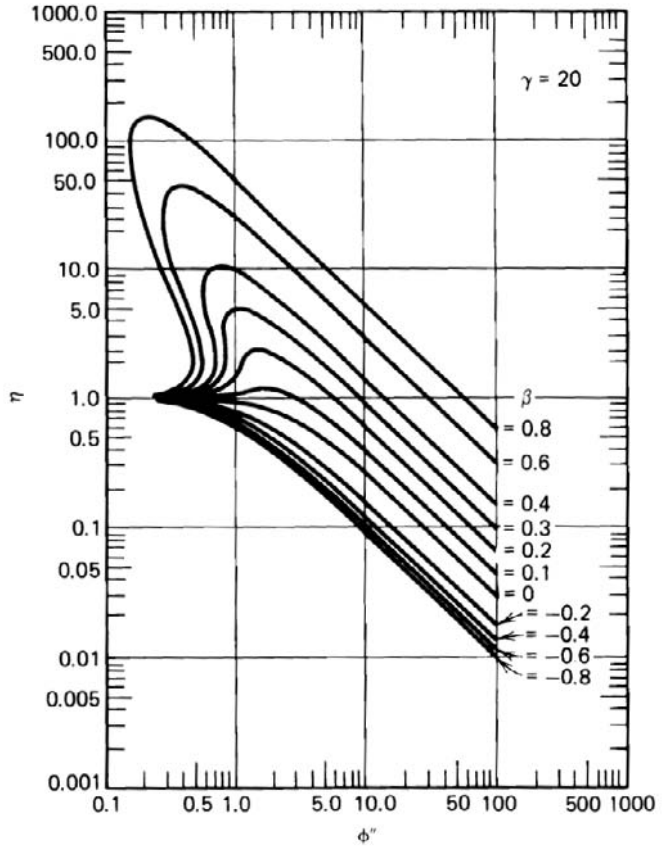

Figure 3.13.1-1

Effectiveness factor with first-order reaction in spherical nonisothermal catalyst pellet. From Weisz and Hicks [1962].

A thorough computational study of Drott and Aris [1969] indicated that the uniqueness criterion of Luss [1968],

$$\beta\gamma < 4(1+\beta) \tag{3.13.1-8}$$

provided a good estimate of conditions for stability. Also, the ranges of the Thiele modulus, for which multiple steady states could conceivably occur, were quite narrow — for rather drastic parameter values, only between ϕ = 0.47 and 0.49. Therefore, it may be concluded that in practical situations, internal gradients are unlikely to cause particle instability.

3.13.2 External and Internal Temperature Gradients

External temperature gradients are much more likely. In transient situations, temperatures exceeding the steady-state maximum temperature of (3.13.1-5) could exist [Wei, 1966; Georgakis and Aris, 1974].

Lee and Luss [1969] derived formulas for the maximum temperature differences between bulk fluid, catalyst surface, and catalyst interior in terms of directly observable quantities: the Weisz modulus and the effective Sherwood and Nusselt numbers based on external values. The steady-state mass and heat balances for an arbitrary reaction, using slab geometry, are

$$D_{eA}\frac{d^2C_s}{dz^2} = r_A(C_s,T_s)\,\rho_s \tag{3.13.2-1}$$

$$-\lambda_e\frac{d^2T_s}{dz^2} = (-\Delta H)r_A(C_s,T_s)\,\rho_s \tag{3.13.2-2}$$

The particle surface boundary conditions are

$$D_{eA}\frac{dC_s}{dz} = k_g\left(C - C_s^s\right) \tag{3.13.2-3}$$

at $z = L$

$$\lambda_e\frac{dT_s}{dz} = h_f\left(T - T_s^s\right) \tag{3.13.2-4}$$

Following Prater's [1958] procedure, (3.13.2-1) and (3.13.2-2) can be combined to give:

$$\frac{d^2}{dz^2}\left[D_{eA}C_s + \frac{\lambda_e}{(-\Delta H)}T_s\right] = 0 \tag{3.13.2-5}$$

Integrating once from the pellet center to the surface, and utilizing (3.13.2-3) and (3.13.2-4), leads to:

$$D_{eA}\left.\frac{dC_s}{dz}\right|_L + \frac{\lambda_e}{(-\Delta H)}\left.\frac{dT_s}{dz}\right|_L = 0 = k_g\left(C - C_s^s\right) - \frac{h_f}{(-\Delta H)}\left(T_s^s - T\right) \tag{3.13.2-6}$$

A second integration and rearrangement gives the overall temperature difference

$$T_s - T = \left(T_s^s - T\right) - \frac{D_{eA}(-\Delta H)}{\lambda_e}\left(C_s - C_s^s\right)$$

$$= (-\Delta H)\frac{k_g}{h_f}\left(C - C_s^s\right) + (-\Delta H)\frac{D_{eA}}{\lambda_e}\left(C_s^s - C_s\right) \tag{3.13.2-7}$$

The right-hand side of (3.13.2-7) is the sum of the external and internal temperature differences, as pointed out by Hlavacek and Marek [1970]. The

maximum temperature difference corresponds to complete conversion when C_s = 0:

$$\frac{T_{s,\max} - T}{T} = \beta_G \frac{\text{Sh'}}{\text{Nu'}}\left(1 - \frac{C_s^s}{C}\right) + \beta_G \frac{C_s^s}{C} \tag{3.13.2-8}$$

where $\beta_G \equiv (-\Delta H) D_{eA} C / (\lambda_e T)$, at *bulk fluid* conditions.

In the final step C_s^s / C is expressed in terms of an observable rate, the volume-averaged rate in the pellet:

$$(r_A \rho_s)_{\text{obs}} = \frac{1}{L}\int_0^L r_A \rho_s \, dz = + \frac{D_{eA}}{L} \left.\frac{dC_s}{dz}\right|_L$$

$$= \frac{k_g}{L}\left(C - C_s^s\right) \tag{3.13.2-9}$$

Using the observable (Weisz) modulus,

$$\Phi_G \equiv \frac{L^2 (r_A \rho_s)_{\text{obs}}}{D_{eA} C} = \text{Sh'}\left(1 - \frac{C_s^s}{C}\right) \tag{3.13.2-10}$$

Substituting (3.13.2-10) into (3.13.2-8) gives the result of Lee and Luss [1969] [their Eq. 11, which was in spherical geometry]:

$$\frac{T_{s,\max} - T}{T} = \beta_G \left[1 + \Phi_G \left(\frac{1}{\text{Nu'}} - \frac{1}{\text{Sh'}}\right)\right] \tag{3.13.2-11}$$

Lee and Luss also presented results for the maximum surface-to-interior temperature difference. Recall from (3.9-4) that the observable modulus can also be written in terms of the usual modulus and the effectiveness factor:

$$\Phi_G = \eta_G \phi^2$$

where $\phi = L\sqrt{k\rho_s / D_{eA}}$ for a first-order reaction, and, from (3.11-4)

$$\frac{1}{\eta_G} = \frac{1}{\eta} + \frac{\phi^2}{\text{Sh'}}$$

Either type of modulus can be used in the analysis.

Carberry [1975] presented an analysis showing that the fraction of the total temperature difference external to the pellet can be found in terms of a new observable quantity and the ratio of the effective Sherwood to Nusselt numbers,

thus obviating the need to have precise values for both of them. Bischoff [1976] defined a new dimensionless observable group:

$$Ca \equiv \frac{L(r_A \rho_s)_{\text{obs}}}{k_g C} = \frac{\Phi_G}{\text{Sh}'} \tag{3.13.2-12}$$

Then, (3.13.2-11) can be written in terms of *Ca* and only the ration Sh'/Nu':

$$\frac{T_{s,\max} - T}{T} = \beta_G \left[1 + Ca\left(\frac{\text{Sh}'}{\text{Nu}'} - 1 \right) \right] \tag{3.13.2-13}$$

Similarly, the interior temperature difference is

$$\frac{T_{s,\max} - T_s^s}{T} = \beta_G \left(1 - \Phi_G \frac{1}{\text{Sh}'} \right) \tag{3.13.2-14}$$

$$= \beta_G (1 - Ca) \tag{3.13.2-15}$$

and the external temperature difference

$$\frac{T_s^s - T}{T} = \beta_G \Phi_G \frac{1}{\text{Nu}'} \tag{3.13.2-16}$$

$$= \beta_G Ca \left(\frac{\text{Sh}'}{\text{Nu}'} \right) \tag{3.13.2-17}$$

Finally, the fractional external temperature difference is the ratio of (3.13.2-17) to (3.13.2-13):

$$\frac{T_s^s - T}{T_{s,\max} - T} = \frac{Ca(\text{Sh}'/\text{Nu}')}{1 + Ca[(\text{Sh}'/\text{Nu}') - 1]} \tag{3.13.2-18}$$

Equations (3.13.2-10) through (3.13.2-18) are a summary of the various temperature differences in terms of two possible observable groups.

EXAMPLE 3.13.2.A

TEMPERATURE GRADIENTS INSIDE THE CATALYST PARTICLES IN BENZENE HYDROGENATION

Equations (3.13.2-10) through (3.13.2-18) can be applied in the analysis of Kehoe and Butt's data on benzene hydrogenation [1972], a sample of which is given in Fig. 3.13.2.A-1. Pellet 2 is a 25 percent Ni, 25 percent graphite, 50 percent γ-alumina Harshaw catalyst with radius 0.69 cm, length 6.10 cm,

density 1.57 g/cm³, heat capacity 0.783 J/g K, effective 0.035 cm^3_f / cm_p s, and characteristic length = $(R/2)/(1 + R/L)$ = 0.296 cm.

For run 212 the measured external temperature difference is about 11°C for a bulk fluid temperature of 139°C. The observed rate r_A is 22.4 × 10^{-6} mol/g cat. s.

The dimensionless parameters are

$$\beta_G = (-\Delta H) D_{eA} C / \lambda_e T$$

$$= \frac{(209000)(0.035)(2.9\times10^{-5})(0.195)}{(14.65\times10^{-3})(412)}$$

$$= 0.0070$$

$$\Phi_G = \frac{L^2 r_A \rho_s}{D_{eA} C} = \frac{(0.31)^2 (22.4\times10^{-6})(1.57)}{(0.035)(2.96\times10^{-5})(0.195)}$$

$$= 16.7$$

The maximum external temperature difference is then estimated from (3.13.2-16):

$$T_s^s - T = T\beta_G \Phi_G \frac{1}{\text{Nu}'}$$

$$= 412(0.0070)(16.7)\left(\frac{1}{1.35}\right) = 412(0.0866) = 36 \text{ K}$$

The actual value of 11°C indicates that at the high reactant concentration of y_B = 0.195, the internal pellet concentration was not quite zero.

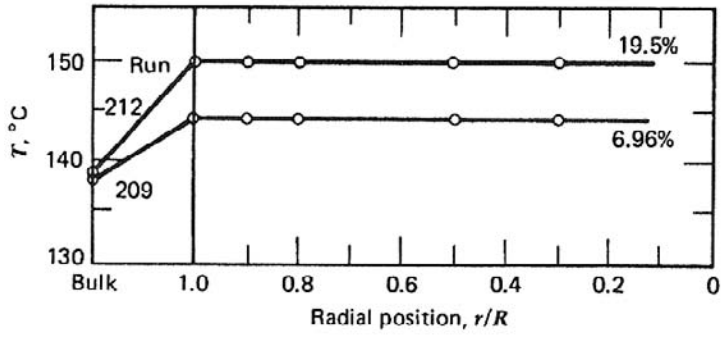

Figure 3.13.2.A-1

Measured internal and external profiles for pellet 2, as a function of feed composition. From Kehoe and Butt [1972].

The maximum overall temperature difference is estimated from (3.13.2-11):

$$T_{s,\max} - T = T\beta_G\left[1+\Phi_G\left(\frac{1}{\text{Nu}'}-\frac{1}{\text{Sh}'}\right)\right]$$

$$= (412)(0.0070)\left[1+16.7\left(\frac{1}{1.35}-\frac{1}{401}\right)\right] = (412)(0.0933) = 38 \text{ K}$$

Finally, the internal temperature difference should be 38 – 36 = 2 K. The value can also be estimated from (3.13.2-14) or (3.13.1-6), the latter using the measured surface temperature. Thus,

$$T_{s,\max} - T_s^s = T\beta_G\left(1-\phi_G\frac{1}{\text{Sh}'}\right)$$

$$= (412)(0.0070)\left(1-\frac{16.7}{401}\right) = (412)(0.00671) = 2.8 \text{ K}$$

Again, this maximum value bounds the actual results. The interior temperature differences are very small, even for this highly exothermic reaction. This conclusion is general. ■

Mears [1971a] showed that (3.13.2-11) (in spherical coordinates) could be combined with a perturbation expansion of the rate about $T_s = T$, to yield an experimental criterion for a 5 percent deviation from the rate at bulk temperature:

$$\frac{(-\Delta H)(r_A\rho_s)_{\text{obs}}(R/3)}{h_f T} < 0.05\frac{RT}{E} \qquad (3.13.2\text{-}19)$$

Mears [1971b] compares these and other criteria for diffusional effects.

Combining external and internal gradients also has an effect on the possible unstable behavior of the catalyst pellet. This could be studied by solving the complete transient balances together with the boundary conditions (3.13.2-3 and 3.13.2-4). However, because of the mathematical complexity, most information concerns the steady-state situation.

McGreavy and Cresswell [1969] and Kehoe and Butt [1970] have presented computations for the effectiveness factor that illustrate the complicated behavior that can occur. Criteria for multiplicity to occur, similar to (3.13.1-8), have been derived by several investigators. Luss [1976], for example, concludes

that for first-order reactions, the proper sufficient criterion for uniqueness of the steady state, for all values of Sh', is

$$\beta_{G\gamma G} < 4\left(\frac{\text{Nu}'}{\text{Sh}'} + \beta_G\right) \tag{3.13.2-20}$$

where $\beta_G = \dfrac{D_{eA}(-\Delta H)C}{\lambda_e T}$ $\gamma_G = \dfrac{E}{RT}$

are evaluated at bulk fluid conditions. The sufficient condition for existence of multiple steady states, for certain value of Sh', is

$$\beta_{G\gamma G} > 8\left(\frac{\text{Nu}'}{\text{Sh}'} + \beta_G\right) \tag{3.13.2-21}$$

The intermediate region is complicated by various internal concentration gradient effects. Comparison of (3.13.2-20) with (3.13.1-8) for typical values of Nu'/Sh' ≈ 0.1 – 0.2 shows that multiple steady states are more likely to be caused by external transport resistances.

The situation is more complicated for other orders of reaction. Luss [1976] shows that for order $n > 1$, there is less likelihood of multiplicity, and the converse is true for $n < 1$. As might be expected, the situation for reaction orders approaching zero- or negative-order behavior could combine possible concentration and thermal instabilities; for example, see Smith et al. [1975].

Solutions of the complete transient equations, containing an additional dimensionless parameter, the Lewis number Lw' = $\lambda_e/\rho_s C_{ps} D_{eA}$, are much more complex. Lee and Luss [1971] have shown for some cases that Lw' > 1 (an author's definition of the Lewis number must be carefully checked, because sometimes the reciprocal of Lw' is used) can lead to limit cycles and other complex behavior. However, Ray [1972] estimates that for this to occur, considering reasonable values of β and λ, the critical value for Lw' would have to exceed 5, if not 10. Such high values are not likely at all. For NH_3-synthesis Lw' = 2.6×10^{-4}, and for ethylene hydrogenation Lw' = 0.11.

To conclude, an overall summary of calculations based on the above results indicates that the usual order of events is to have first chemical reaction control throughout the pellet. Next, with higher intrinsic rates of reaction, internal pore diffusion begins to have an effect, followed by external heat transfer resistance. Finally, for extremely rapid reactions there is the possibility of external mass transfer resistance and temperature gradients of some significance. Only for unrealistic situations is it likely that particle instabilities might occur, and even then only for narrow ranges of temperature.

PROBLEMS

3.1 The cracking of cumene into benzene and propylene was carried out in a fixed bed of zeolite particles at 362°C and atmospheric pressure, in the presence of a large excess of nitrogen. At a point in the reactor where the cumene partial pressure was 0.0689 bar, a reaction rate of 0.153 kmol/kg cat. h was observed. Further data are:

$$M_m = 34.37\,\text{kg/kmol}; \qquad \rho_g = 0.66\,\text{kg/m}^3;$$

$$\mu = 0.094\,\text{kg/m h}; \qquad \lambda_g = 0.155\,\text{kJ/m h °C};$$

$$c_p = 0.33\,\text{kcal/kg °C}; \qquad \text{Re} = 0.052;$$

$$\text{Pr} = 0.846; \qquad D_{Am} = 0.096\,\text{m}^2\text{/h};$$

$$a_m = 45\,\text{m}^2\text{cat./kg cat.}; \qquad G = 56.47\,\text{kg/m}^2\text{h};$$

$$-\Delta H = -175.084\,\text{kJ/kmol}.$$

Under these conditions, show that the partial pressure and temperature drops over the external film surrounding the particles are negligible.

3.2 The solid density of an alumina particle is 3.8 g/cm^3, the pellet density is 1.5 g/cm^3, and the internal surface is 200 m^2/g. Compute the pore volume per gram, the porosity, and the mean pore radius.

3.3 Turning to a general description of pore diffusion, the "dusty gas" theory of Mason et al. [1961, 1962] utilizes the results from the formal kinetic theory of gases, with one "species", the "dust", having a very large "molecular weight". Their final results can be clearly visualized in the form utilized by Feng and Stewart [1973]:

$$\begin{aligned}\mathbf{N}_j = &\,(\text{diffusive flux}) \;+\; (\text{viscous flow flux}) \\ &+\; (\text{fluxes caused by other driving forces}) \qquad (1)\\ = &\,\mathbf{N}_j^{(D)} + \mathbf{N}_j^{(v)} + \ldots\end{aligned}$$

where the viscous flow flux is found from

$$\mathbf{N}_j^{(v)} = -y_j \left(\frac{B_0 p_t}{RT\,\mu} \right) \nabla p_t \qquad (2)$$

with B_0 = D'Arcy constant, a function of porous media geometry, = $r^2/8$ for a long cylinder of radius r, and the diffusive flux is found from the extended Stefan-Maxwell form

$$\frac{-1}{RT}\nabla p_j = \sum_{k=1}^{N}\frac{1}{D_{e,jk}}(y_k\mathbf{N}_j^{(D)} - y_j\mathbf{N}_k^{(D)}) + \frac{\mathbf{N}_j^{(D)}}{D_{e,Kj}} \tag{3}$$

Equations (1) to (3) can also be combined to give a single equation containing only the total flux resulting from both diffusive and viscous flow mechanisms:

$$\frac{-1}{RT}\nabla p_j = \sum_{k=1}^{N}\frac{1}{D_{e,jk}}(y_k\mathbf{N}_j - y_j\mathbf{N}_k) + \frac{\mathbf{N}_j}{D_{e,Kj}} + \frac{y_j}{D_{e,Kj}}\left(\frac{B_0 p_t}{RT\mu}\right)\nabla p_t \tag{4}$$

Carefully watching how the various fluxes combine, derive (4) for the molar flux in a porous medium.

3.4 A catalyst considered by Satterfield [1970] has a void fraction of 0.40, and internal surface area of 180 m^2/g, and a pellet density of 1.40 g/cm^3. Estimate the effective diffusivity of thiophene with hydrogen at T = 660 K.

3.5 Calculate the diffusion flux for ethylene diffusing in hydrogen at 298 K in porous medium with the following properties: thickness = 1 cm, ε_s = 0.40, ρ_s = 1.4 g/cm^3, S_g = 105 m^2/g. The conditions are steady pressure p of ethylene on one side and hydrogen on the other, for $0.1 < p < 40$ bar.

3.6 The data given below, on diffusion of nitrogen (A) and helium (B) in porous catalyst pellets, have been provided by Henry, Cunningham, and Geankoplis [1967], who utilized the steady-state Wicke-Kallenback-Wesz technique. An alumina pellet with the following properties was used:

p_t (mm Hg)	y_{AL}	y_{A0}	$N_A \times 10^8$ (mol/cm^2s)	$-N_B/N_A$
0.500	0.0407	0.911	0.449	2.52
1.506	0.0358	0.900	0.881	3.06
3.25	0.0888	0.863	2.62	2.22
8.00	0.1760	0.735	4.78	2.65
30.72	0.2140	0.658	11.3	2.78
100.6	0.1640	0.708	22.2	2.62
299.7	0.1340	0.769	42.1	2.37
600.1	0.1460	0.723	43.9	2.86

Length = 1.244 cm; pore volume = 0.5950 cm^3/g;
Porosity = 0.233 (macro); 0.492 (micro);
Pore radius = 20.000 Å (macro); 37 Å (micro);
Internal surface = 202 m^2/g.

(a) Compare the flux ratios with the theoretical prediction.

(b) Compute the experimental diffusivities, and plot $D_e p_t$ versus p_t. At what pressure is there a transition between Knudsen and bulk diffusion?

(c) Use the dusty-gas model, assuming one dominant pore size, to predict the changes of D_e with pressure up to 2 bar. What value of tortuosity is required?

(d) Repeat the calculations of part (c) with the random pore model.

(e) Repeat the calculations of part (c) with the parallel cross-linked pores model.

3.7 Derive (3.6.1-10) for the effectiveness factor for a first-order reaction in a spherical catalyst pellet.

3.8 A series of experiments were performed using various sizes of crushed catalyst to determine the importance of pore diffusion. The reaction may be assumed to be first order and irreversible. The surface concentration of reactant was $C_s^s = 2 \times 10^{-4}$ mol/cm^3.
Data:

Diameter of sphere (cm):	0.25	0.075	0.025	0.0075
$r_{\text{obs}}\,(\text{mol/h cm}^3)$:	0.22	0.70	1.60	2.40

(a) Determine the "true" rate constant k_v and the effective diffusivity D_e from the above data.

(b) Predict the effectiveness factor and the expected rate of reaction r_{obs} for a commercial *cylindrical* catalyst pellet of dimensions 0.5 cm × 0.5 cm.

3.9 The following rates were observed for a first-order irreversible reaction, carried out on a spherical catalyst:

$$\text{for } d_p = 0.6\,\text{cm}; r_{\text{obs}} = 0.09\,\text{mol/g cat.h}$$

$$\text{for } d_p = 0.3\,\text{cm}; r_{\text{obs}} = 0.162\,\text{mol/g cat.h}$$

Strong diffusional limitations were observed in both cases. Determine the true rate of reaction. Is diffusional resistance still important with d_p = 0.1 cm?

3.10 A second-order gas phase reaction, $A \rightarrow R$, occurs in a catalyst pellet, and has a rate coefficient

$$k\rho_s = 3.86 \text{ m}^3/\text{kmol s}$$

The reactant pressure is 1 bar, the temperature is 600 K, the molecular diffusivity is D_{AR} = 0.10 cm^2/s, and the reactant molecular weight is M_A = 60.

The catalyst pellets have the following properties:

radius of sphere R = 9 mm;
pellet density ρ_s = 1.2 g/cm^3;
internal surface area S_g = 100 m^2/g;
internal void fraction ε_s = 0.60.

(a) Estimate the effective diffusivity.

(b) Determine if there may be pore diffusion limitations.

(c) If part (b) results in pore diffusion limitation, what might be done to eliminate them? Justify your answer(s) with quantitative calculations.

3.11 A gas oil is cracked at 630°C and 1 bar by passing vaporized feed through a packed bed of spheres of silica alumina catalyst with radius = 0.088 cm. For a feed rate of 60 cm^3 liquid/cm^3, h, a 50 percent conversion is found. The following data are also known

liquid density = 0.869 g/cm^3;
feed molecular weight = 225 g/mol;
bulk density of packed bed = 0.7 g cat./ cm_r^3;
solid density of catalyst = 0.95 g cat./cm^3 cat.;
effective diffusivity in catalyst = 8×10^{-4} cm^2/s;
average reactant concentration = 0.6×10^{-5} mol/cm^3.

Assume a first-order reaction and treat data as being average data of a differential reactor.

(a) Show that the *average* reaction rate is 3.9×10^{-5} mol/cm^3 cat. s.

(b) Determine from the data whether or not pore diffusion was important.

(c) Find the value of the effectiveness factor.

(d) Determine the value of the rate coefficient.

REFERENCES

Abed, R., and Rinker, R.G., *J. Catal.*, 34, 246 (1974).
Amundson, N.R., and Luss, D., *AIChE J.*, 13, 759 (1967).
Anderson, J.L., and Quinn, J., *Biophys. J.*, 14, 130 (1974).
Aris, R., *Chem. Eng. Sci.*, 6, 262 (1957).
Aris, R., *Ind. Eng. Chem. Fundam.*, 4, 227 (1965a).
Aris, R., *Introduction to the Analysis of Chemical Reactors*, Prentice-Hall, Englewood Cliffs, N.J. (1965b).
Aris, R., *Chem. Eng. Sci.*, 24, 149 (1969a).
Aris, R., *Elementary Chemical Reactor Analysis*, Prentice-Hall, Englewood Cliffs, N.J. (1969b).
Aris, R., *The Mathematical Theory of Diffusion and Reaction in Permeable Catalysts*, Vols. I and II, Oxford University Press, London (1975).
Austin, L.G., and Walker, P.L., *AIChE J.*, 9, 303 (1963).
Balder, J.R., and Petersen, E.E., *J. Catal.*, 11, 195, 202 (1968).
Bar Ilan, M.I., and Resnick, W., *Ind. Eng. Chem.*, 49, 313 (1957).
Barrer, R.M., *Adv. Chem.*, 102 (1971).
Baumeister, E.B., and Bennett, C.O., *AIChE J.*, 4, 70 (1958).
Beeckman, J.W., and Froment, G.F., *Ind. Eng. Chem. Fundam.*, 21, 243 (1982).
Beyne, A.O.E., and Froment, G.F., *Chem. Eng. J.*, 82, 281 (2001).
Bird, R.B., Stewart, W.E., and Lightfoot, E.N., *Notes on Transport Phenomena*, Wiley, New York (1958).
Bird, R.B., Stewart, W.E., and Lightfoot, E.N., *Transport Phenomena*, Wiley, New York (1960).
Bischoff, K.B., *AIChE J.*, 11, 351 (1965).
Bischoff, K.B., *Chem. Eng. Sci.*, 22, 525 (1967).
Bischoff, K.B., *Ind. Eng. Chem. Fundam.*, 15, 229 (1976).
Bradshaw, R.D., and Bennett, C.O., *AIChE J.*, 7, 50 (1961).
Brown, L.F., *Chem. Eng. Sci.*, 27, 213 (1972).
Brown, L.F., Haynes, H.W., and Manogue, W.H., *J. Catal.*, 14, 220 (1969).
Brown, L.M., Sherry, H.S., and Krambeck, F.J., *J. Phys. Chem.*, 75, 3846, 3855 (1971).
Brunauer, S., Mikhail, R.Sh., and Bodor, E.E., *J. Coll. Interface Sci.*, 25, 353 (1967).
Burganos, V.N., and Sotirchos, S.V., AIChE J., 33(40), 1678 (1987).
Butt, J.B., *AIChE J.*, 9, 707 (1963).
Cadle, P.J., and Satterfield, C.N., *Ind. Eng. Chem. Proc. Des. Dev.*, 7, 189, 192 (1968).
Calo, T.S., *J. Catal.*, 90(1), 40 (1984).
Carberry, J.J., *AIChE J.*, 7, 350 (1961).
Carberry, J.J., *AIChE J.*, 8, 557 (1962a).
Carberry, J.J., *Chem. Eng. Sci.*, 17, 675 (1962b).
Carberry, J.J., *Ind. Eng. Chem. Fundam.*, 14, 129 (1975).
Chang-Tai Wang, and Smith, J.M., *AIChE J.*, 29, 132 (1983).
Chen, N.Y., Lucki, S.J., and Mower, E.B., *J. Catal.*, 13, 329 (1969).
Clausen, B.S., "Advanced Materials in Catalysis"-Nanomat Conference, Bergen, Norway, June 6-7 (2007).
Colton, C.K., Satterfield, C.N., and Lai, C.J., *AIChE J.*, 21, 289 (1975).
Coppens, M.O., and Froment, G.F., *Fractals*, 3, 807-820 (1995).
Coppens, M.O., and Froment, G.F., *Chem. Eng. Sci.*, 51, 10, 2283 (1996).
Cussler, E.L., *Multicomponent Diffusion*, Chemical Engineering Monographs, 3, Elsevier Scientific Publ. Comp., Amsterdam (1976).
de Acetis, J., and Thodos, G., *Ind. Eng. Chem.*, 52, 1003 (1960).
De Deken, J.C., Devos, E.F., and Froment, G.F., in A.C.S. Symp. Series, "Chemical Reaction Engineering", 196 (1982).
Dedrick, R.L., and Beckmann, R.B., *Chem. Eng. Prog. Symp. Ser.*, No. 74, 63, 68 (1967).
Di Napoli, N.M., Williams, R.J.J., and Cunningham, R.E., *Lat. Am. J. Chem. Eng. Appl. Chem.*, 5, 101 (1975).
Dogu, G., and Smith, J.M., *AIChE J.*, 21, 58 (1975).
Drott, D.W., and Aris, R., *Chem. Eng. Sci.*, 24, 541 (1969).
Dullien, F.A.L., *AIChE J.*, 21, 299 (1975).
Dullien, F.A.L., Ghai, R.K., and Ertl, H., *AIChE J.*, 19, 881 (1973).

Dullien, F.A.L., Ghai, R.K., and Ertl, H., *AIChE J.*, 20, 1 (1974).
Dumez, F.J., and Froment, G.F., *Ind. Eng. Chem. Des. Dev.*, 15, 297 (1976).
Feng, C.F., Kostrov, V.V., and Stewart, W.E., *Ind. Eng. Chem. Fundam.*, 13, 5 (1974).
Feng, C.F., and Stewart, W.E., *Ind. Eng. Chem. Fundam.*, 12, 143 (1973).
Finlayson, B.A., *The Method of Weighted Residuals and Variational Principles*, Academic Press, N.Y. (1972).
Frank-Kamenetskii, D., *Diffusion and Heat Exchange in Chemical Kinetics*, 2nd ed. Plenum Press, New York (1969).
Frouws, M.J., Vellenga, K., and De Wilt, H.G.J., *Biotech. Bioeng.*, 18, 53 (1976).
Gamson, B.W., Thodos, G., and Hougen, O.A., *Trans. AIChE*, 39, 1 (1943).
Georgakis, C., and Aris, R., *Chem. Eng. Sci.*, 29, 291 (1974).
Gilliland, E.R., Bixler, H.L., and O'Connell, J.E., *Ind. Eng. Chem. Fundam.*, 10, 185 (1971).
Glaser, M.B., and Thodos, G., *AIChE J.*, 4, 63 (1958).
Gonzo, E.E., and Gottifredi, J.C., *Cat. Rev. Sci. Eng.*, 25, 119 (1983).
Gorring, R.L., *J. Catal.*, 31, 13 (1973).
Gregg, S.J., and Sing, K.S.W., *Adsorption, Surface Area, and Porosity*, Academic Press, New York (1967).
Gumbleton, J.J., *Chemtech.*, 10, 630 (1980).
Gunn, R.D., and King, C.J., *AIChE J.*, 15, 507 (1969).
Gunn, D.J., and Thomas, W.J., *Chem. Eng. Sci.*, 20, 89 (1965).
Handley, D., and Heggs, P.J., *Trans. Inst. Chem. Eng.*, 46, 251 (1968).
Hegedus, L.L., and Gumbleton, J.J., *Chemtech.*, 10, 630 (1980).
Hegedus, L.L., Oh, S.H., and Baron, K., *AIChE J.*, 23, 632 (1977).
Hegedus, L.L., and Petersen, E.E., *Catal. Rev.*, 9, 245 (1974).
Hegedus, L.L., and Pereira, C.J., *Chem. Eng. Sci.*, 45, 2027 (1990).
Henry, J.P., Cunningham, R.S., and Geankoplis, C.J., *Chem. Eng. Sci.*, 22, 11 (1967).
Hlavacek, V., Kubicek, M., and Marek, M., *J. Catal.*, 15, 17, 31 (1969).
Hlavacek, V., and Marek, M., *Chem. Eng. Sci.*, 25, 1537 (1970).
Hougen, O.A., *Ind. Eng. Chem.*, 53, 509 (1961).
Hougen, O.A., and Watson, K.M., *Chemical Process Principles*, Wiley, New York (1947).
Hsu, H.W., and Bird, R.B., *AIChE J.*, 6, 516 (1960).
Hudgins, R.R., *Chem. Eng. Sci.*, 23, 93 (1968).
Ishino, T., and Otake, T., *Chem. Eng.* (Tokyo), 15, 258 (1951).
Jackson, R., *Transport in Porous Catalysts*, Chemical Engineering Monographs, 4, Elsevier Scientific Publ. Comp., Amsterdam (1977).
Jacobs, P.A., *Carboniorgenic Activity of Zeolites*, Elsevier Scientific Publ. Company, Amsterdam (1977).
Johannessen, E., Wang, G., and Coppens, M.-O., *Ind. Eng. Chem. Res.*, 46, 4245 (2007).
Johnson, M.L.F., and Stewart, W.E., *J. Catal.*, 4, 248 (1965).
Kehoe, J.P.G., and Butt, J.B., *Chem. Eng. Sci.*, 24, 345 (1970).
Kehoe, J.P.G., and Butt, J.B., *AIChE J.*, 18, 347 (1972).
Keil, F.J., *Chem. Eng. Sci.*, 51, 1543 (1996).
Keil, F.J., and Rieckmann, C., *Chem. Eng. Sci.*, 49, 4811 (1994).
Keil, F.J., Krishna, R., and Coppens, M.-O., *Reviews in Chemical Engineering*, 16, 71-197 (2000).
Kirkpatrick, S., *Rev. Mod. Phys.*, 45(4), 574 (1973).
Knudsen, C.W., Roberts, G.W., and Satterfield, C.N., *Ind. Eng. Chem. Fundam.*, 5, 325 (1966).
Koros, R.M., and Nowak, E.J., *Chem. Eng. Sci.*, 22, 470 (1967).
Kubin, M., *Collec. Czech. Commun.*, 30, 1104 (1965); ibid. 30, 2900 (1965).
Kubota, H., Yamanaka, Y., and Dalla Lana, I.G., *J. Chem. Eng. Japan*, 2, 71 (1969).
Kucera, E.J., *Chromatog.*, 19, 237 (1965).
Languasco, J.M., Cunningham, R.E., and Calvelo, A., *Chem. Eng. Sci.*, 27, 1459 (1972).
Lee, J.C.M., and Luss, D., *Ind. Eng. Chem. Fundam.*, 8, 597 (1969).
Lee, J.C.M., and Luss, D., *AIChE J.*, 16, 620 (1970).
Lee, J.C.M., and Luss, D., *Chem. Eng. Sci.*, 26, 1433 (1971).
Levenspiel, O., *Chemical Reaction Engineering*, Wiley, New York (1962).
Liu, S.L., *AIChE J.*, 15, 337 (1969).

Luss, D., *Chem. Eng. Sci.*, 23, 1249 (1968).
Luss, D., *Chem. Eng. Sci.*, 26, 1713 (1971).
Luss, D., *Proc. 4th Int. Symp. Chem. React. Eng.*, Heidelberg (April 1976).
Madon, R.J., and Boudart, M., *Ind. Eng. Chem. Fundam.*, 21, 438 (1982).
Mason, E.A., Evans, R.B.III, and Watson, G.M., *J. Chem. Phys.*, 35, 2076 (1961); 36, 1894 (1962).
Mason, E.A., and Evans, R.B., *J. Chem. Educ.*, 46, 358 (1969).
Mason, E.A., and Marrero, T.R., *Advances in Atomic Molec. Physics*, Vol. 6, Academic Press, New York (1970).
McCune, L.K., and Wilhelm, R.H., *Ind. Eng. Chem.*, 41, 1124 (1949).
McGreavy, C., and Cresswell, D., *Chem. Eng. Sci.*, 24, 608 (1969).
Mears, D.E., *J. Catal.*, 20, 127 (1971a).
Mears, D.E., *Ind. Eng. Chem. Proc. Des. Dev.*, 10, 541 (1971b).
Mehta, B.N., and Aris, R., *Chem. Eng. Sci.*, 26, 1699 (1971).
Mingle, J.O., and Smith, J.M., *AIChE J.*, 7, 243 (1961).
Patel, P.V., and Butt, J.B., *Ind. Eng. Chem. Proc. Des. Dev.*, 14, 298 (1974).
Pazdernik, O., and Schneider, P., *J. Chromatogr.*, 207, 181 (1981).
Pereira, C.J., and Beeckman, J.W., *Ind. Eng. Chem.*, 28, 422 (1989).
Perry, R.H., and Chilton, C.H., *Chemical Engineers Handbook*, 6th ed., McGrawHill, New York (1984).
Petersen, E.E., *Chem. Eng. Sci.*, 20, 587 (1965a).
Petersen, E.E., *Chemical Reaction Analysis*, Prentice-Hall, Englewood Cliffs, N.J. (1965b).
Prater, C.D., *Chem. Eng. Sci.*, 8, 284 (1958).
Ray, W.H., *Proc. 2nd Int. Symp. Chem. React. Eng.*, Amsterdam (1972).
Ray, W.H., *Proc. 5th Int. Symp. Chem. React. Eng.*, Amsterdam, A-8 (1972).
Reid, R.C., Prausnitz, J., and Sherwood, T.K., *The Properties of Gases and Liquids*, 3rd ed., McGraw-Hill, New York (1977).
Rester, S., and Aris, R., *Chem. Eng. Sci.*, 24, 793 (1969).
Reyes, S., and Jensen, K.F., *Chem. Eng. Sci.*, 40, 1723 (1985).
Riekert, L., *Adv. Catal.*, 21, 281 (1970).
Rigby, S.P., *Langmuir*, 19, 364 (2003).
Rihani, D.N., and Doraiswamy, L.K., *Ing. Eng. Chem. Fundam.*, 4, 17 (1965).
Roberts, G., *Chem. Eng. Sci.*, 27, 1409 (1972).
Rothfeld, L.B., *AIChE J.*, 9, 19 (1963).
Runnebaum, R.C., and Maginn, E.J., *J. Phys. Chem.*, B, 6394 (1997).
Sahimi, M., *Journal de Physique I*, 4, 1263 (1994).
Satterfield, C.N., *Mass Transfer in Heterogeneous Catalysis*, MIT Press, Cambridge, Mass. (1970).
Satterfield, C.N., and Cadle, P.J., *Ind. Eng. Chem. Fundam.*, 7, 202 (1968a).
Satterfield, C.N., and Cadle, P.J., *Ind. Eng. Chem. Proc. Des. Dev.*, 7, 256 (1968b).
Satterfield, C.N., Colton, C.K., and Pitcher, W.H., Jr., *AIChE J.*, 19, 628 (1973).
Satterfield, C.N., Roberts, C.W., and Hartman, J., *Ind. Eng. Chem. Fundam.*, 5, 317 (1966).
Satterfield, C.N., Roberts, C.W., and Hartman, J., *Ind. Eng. Chem. Fundam.*, 6, 80 (1967).
Schlünder, E.U., in *Chemical Reaction Engineering Reviews-Houston*, ed. by D. Luss and V.W. Weekman, A.C.S. Symp. Series, 72, Washington, D.C. (1978).
Schmidt, A.D., Clinch, A.B., and Ray, W.H., *Chem. Eng. Sci.*, 39, 419 (1984).
Schneider, P., *Catal. Rev.*, 12, 201 (1975).
Schneider, P., and Smith, J.M., *AIChE J.*, 14, 886 (1968).
Scott, D.S., and Dullien, F.A.L., *AIChE J.*, 8, 29 (1962).
Sen Gupta, A., and Thodos, G., *AIChE J.*, 9, 751 (1963).
Sheintuch, M., and Brandon, S., *Chem. Eng. Sci.*, 44, 69 (1989).
Sladek, K.J., Gilliland, E.R., and Baddour, R.F., *Ind. Eng. Chem. Fundam.*, 13, 100 (1974).
Smit, B., and Krishna, R., *Chem. Eng. Sci.*, 58, 557-568 (2003).
Smith, J.M., *Chemical Engineering Kinetics*, 2nd ed., McGraw-Hill, New York (1970).
Smith, J.M., *Chem. Eng. Sci.*, 17, 825 (1962).
Smith, T.G., Zahradnik, J., and Carberry, J.J., *Chem. Eng. Sci.*, 30, 763 (1975).

Sotelo-Boyas, R., and Froment, G.F., *Ind. Eng. Chem. Res.*, 48(3), 1107 (2009).
Steisel, N., and Butt, J.B., *Chem. Eng. Sci.*, 22, 469 (1967).
Stewart, W.E., and Prober, R., *Ind. Eng. Chem. Fundam.*, 3, 224 (1964).
Stewart, W.E., and Villadsen, J., *AIChE J.*, 15, 28 (1969).
Storvick, T.S., and Mason, E.A., *J. Chem Phys.*, 46, 3199 (1967).
Strider, W., and Aris, R., *Variational Methods Applied to Problems of Diffusion and Reaction*, Springer-Verlag, New York (1973).
Taecker, R.G., and Hougen, O.A., *Chem. Eng. Prog.*, 45, 188 (1949).
Thiele, E.W., *Ind. Eng. Chem.*, 31, 916 (1939).
Tinkler, J.D., and Metzner, A.B., *Ind. Eng. Chem.*, 53, 663 (1961).
Toor, H.L., *AIChE J.*, 10, 448, 460 (1964).
Van Brakel, J., and Heertjes, P.M., *Int. J. Heat Mass Trans.*, 17, 1093 (1974).
Van Deemter, J.J., Zuiderweg, F.J., and Klinkenberg, A., *Chem. Eng. Sci.*, 5, 271 (1956).
Van Melkebeke, J., and Froment, G.F., unpublished (1995).
Varma, A., and Aris, R., in *Chemical Reactor Theory. A Review*, ed. by L. Lapidus and N.R., Amundson, Prentice-Hall, Englewood Cliffs, N.J. (1977).
Villadsen, J., and Michelsen, M.L., "Solution of Differential Equation Models by Polynomial Approximation", Prentice Hall, Englewood Cliffs, N.J. (1978).
Wakao, N., and Smith, J.M., *Chem. Eng. Sci.*, 17, 825 (1962).
Wakao, N., and Smith, J.M., *Ind. Eng. Chem. Fundam.*, 3, 123 (1964).
Wang, G., Johannessen, E., Kleijn, C.R., de Leeuw, S.W., and Coppens, M.-O., *Chem. Eng. Sci.*, 62, 5110 (2007).
Wang, G., and Coppens, M.O., *Ind. Eng. Chem. Res.*, 47(11), 3847 (2008).
Wei, J., *Chem. Eng. Sci.*, 21, 1171 (1966).
Weisz, P.B., *Adv. Catal.*, 13, 148 (1962).
Weisz, P.B., *Chem. Technol.*, 504 (1973).
Weisz, P.B., *Z. Physik Chem.* (Frankfurt), 11, 1 (1957).
Weisz, P.B., and Hicks, J.S., *Chem. Eng. Sci.*, 17, 265 (1962).
Weisz, P.B., and Prater, C.D., *Adv. Catal.*, 6, 143 (1954).
Weisz, P.B., and Schwartz, A.B., *J. Catal.*, 1, 399 (1962).
Wheeler, A., *Adv. Catal.*, 3, 313 (1951).
Wheeler, A., in *Catalysis*, Vol II, Ed.: Emmett P.H., Rheinhold Publishers, New York (1955).
Wicke, E., and Kallenbach, R., *Kolloid Z.*, 97, 135 (1941).
Wilke, C.R, and Hougen, O.A., *Trans. AIChE J.*, 41, 445 (1945).
Wu, S.C., and Nobe, K., *Ind. Eng. Chem. Prod. Res. Dev.*, 16, 136 (1977).
Xu, J., and Froment, G. F., *AIChE J.*, 35, 88, 97 (1989).
Yang, R.T., Fenn, J.B., and Haller, G.L., *AIChE J.*, 19, 1052 (1973).
Yoshida, F., Ramaswami, D., and Hougen, O.A., *AIChE J.*, 8, 5 (1962).
Zeldowich, Ia. B., *Zhur. Fiz. Khim.*, 13, 163 (1939).
Zhang, L., and Seaton, N.A., *AIChE J.*, 38(11), 1816 (1992).

Chapter 4

Noncatalytic Gas-Solid Reactions

4.1 A QUALITATIVE DISCUSSION OF GAS-SOLID REACTIONS

In this Chapter the reaction between a fluid and a solid or a component of a solid is discussed in quantitative terms. Such a reaction is frequently encountered in the process industry (e.g., in coal gasification, ore processing, iron production in the blast furnace, and roasting of pyrites). There are no true gas-solid production processes in the petrochemical industry, but gas-solid reactions are encountered (e.g., in the regeneration of coked catalysts by means of oxygen-containing gases or in the reduction or reoxidation of nickel-reforming or iron-ammonia-synthesis catalysts prior to or after their use in the production proper). For all these examples the knowledge of the rate of reaction is a prerequisite to the analysis of an existing process, to the design of a new reactor, or to the safe conduct of the regeneration or reoxidation.

Gas-solid reactions have several aspects in common with reactions catalyzed by a porous solid, discussed already in Chapter 3. In the present case, too, transport effects and reaction have to be considered simultaneously. Again, it depends on the relative magnitudes of the rate of transport and the rate of

reaction whether or not important gradients inside and around the particle are built up or not. There is one essential difference, however: with gas-solid reactions the conditions inside the particle change with time, since the solid itself is involved in the reaction. The process is therefore essentially of a non-steady-state nature.

In this chapter rate equations are set up for fluid-solid reactions. In Chapter 11 an example of such a reaction carried out in a fixed bed of particles is worked out and illustrates the difference in behavior of the reactor as compared with a fixed bed catalytic reactor.

Concentrating now on the phenomena inside a particle, an easily visualized situation is that of a gas reacting with a solid of low porosity to yield a porous reacted layer, often called “ash” layer. The reaction then takes place in a narrow zone that moves progressively from the outer surface to the center of the particle. Such a situation is described by the so-called heterogeneous shrinking-core model:

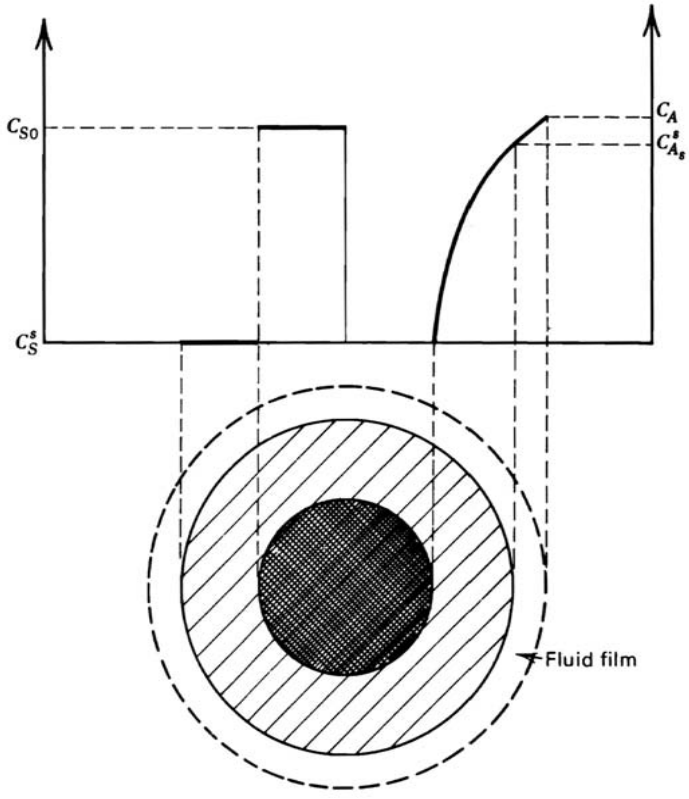

Figure 4.1-1

Heterogeneous shrinking core model with sharp interface. Concentration profiles of gas and solid reactants. From Wen [1968].

heterogeneous because there are two distinct layers inside the particle, with clearly distinct properties. Figure 4.1-1 illustrates such a situation. When the transport rates through the two layers are not too different and the true rate of reaction is not infinitely fast, the situation is no longer as clear-cut, and the sharp boundary between reacted and unreacted zone no longer exists. Such a case is illustrated in Fig. 4.1-2. In the extreme, with very porous material, when the transport through both reacted and unreacted structures is usually fast compared with the true reaction rate, the latter is governing the rate of the overall phenomenon. Then, there are no gradients whatever inside the particle and the situation could be called truly homogeneous. Such a situation is represented in Fig. 4.1-3. Thus, it is clear that the transport inside the particle plays an important role. Again, as in the case of transport inside a catalyst particle (dealt with in Chapter 3), the transport is evidently not a true diffusion, but rather an effective diffusion. In Chapter 3 it was also pointed out that a considerable effort has been made to relate the effective diffusivity to a detailed picture of the catalyst structure. The goal is to avoid having to determine the effective diffusivity for each reacting system and each catalyst and to rely on easily determined catalyst properties. With an effective diffusion (and an effective conduction) concept, the particle is then considered as a continuum. This alters the problem to one of accounting for the detailed solid structure only through the effective diffusivity

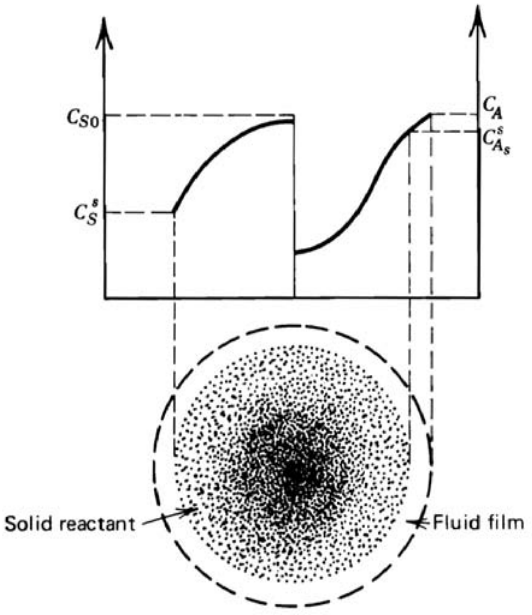

Figure 4.1-2
General model. From Wen [1968].

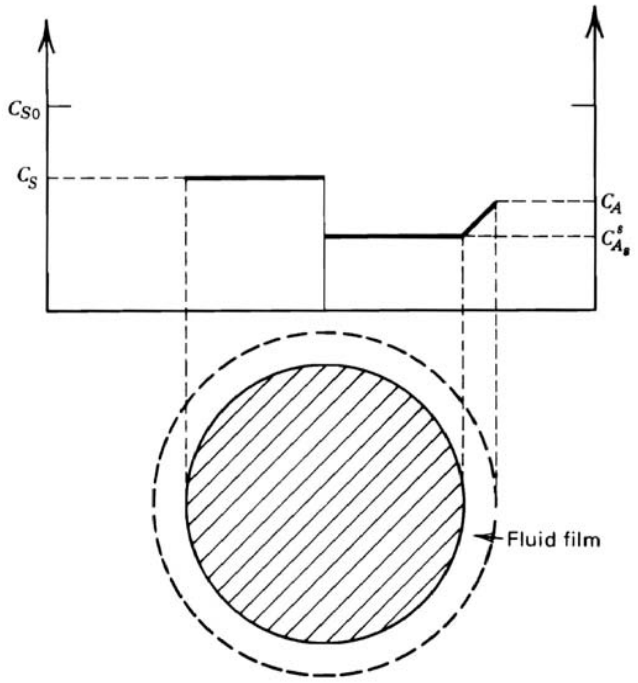

Figure 4.1-3
Truly homogeneous model. Concentration profiles. From Wen [1968].

and not through the model equations proper. The same approach is used for gas-solid reactions, too, although probably with considerably less accuracy, since the solid structure is modified by the reaction. Models have been proposed that do account explicitly for the solid structure through the mathematical model, albeit in a rather simplified way.

In some cases, particularly at relatively low temperatures, the curves of conversion versus time have a sigmoidal shape. When the rate is plotted as a function of conversion, the curve shows a maximum. This behavior has been explained in terms of nucleation. In a first stage, nuclei are being formed and the rate is low. In a second stage, a reaction front develops starting from the nuclei and growing into the surrounding solid. Such an approach has been developed in great detail by Delmon [1969].

4.2 GENERAL MODEL WITH INTERFACIAL AND INTRAPARTICLE GRADIENTS

When the particle is assumed to be isothermal, only differential material balances have to be written. The differential balance on the reacting gaseous component *A*—the continuity equation for *A*—contains an accumulation term accounting for

the transient nature of the process, a term arising from the transport by effective diffusion and a reaction term:

$$\frac{\partial}{\partial t}(\varepsilon_s C_{As}) = \frac{1}{r^2}\frac{\partial}{\partial r}\left(D_{eA} r^2 \frac{\partial C_{As}}{\partial r} \right) - r_A \rho_s \tag{4.2-1}$$

and the continuity equation for the reacting component of the solid is

$$\frac{\partial C_S}{\partial t} = -r_S \rho_s \tag{4.2-2}$$

The rates are based on weight of the particle, as in the preceding chapters on catalytic reactions. The dimensions of r_A are kmol *A*/kg part. s_i; of r_S, kmol *S*/kg part. s when only a component *S* of the solid reacts or kmol solid/kg part. s when all the solid reacts. The concentration C_{As} is expressed in kmol A/m^3_f and C_S is expressed in kmol S/m^3_p when only a component of the solid reacts or in kmol solid/m^3_p when all the solid reacts. The initial and boundary conditions are

At $t = 0$:

$$C_{As} = C_{As_0} \qquad \text{and} \qquad C_S = C_{S0} \tag{4.2-3}$$

In the center of the sphere, $r = 0$:

$$\frac{\partial C_{As}}{\partial r} = 0 \tag{4.2-4}$$

for reasons of symmetry;

and at the surface, $r = R$:

$$D_{eA}\left(\frac{\partial C_{As}}{\partial r} \right)_{r=R} = k_g \left(C_A - C^s_{As} \right) \tag{4.2-5}$$

where C^s_{As} is the concentration of *A* at the particle surface. The effective diffusivity of *A*, represented by D_{eA}, is considered to vary with position if there is a change in porosity resulting from the reaction.

If it is assumed that the porosity depends linearly on the solid reactant conversion:

$$\varepsilon_s = \varepsilon_{s0} + C_{S0}(v_s - v_P)\left(1 - \frac{C_S}{C_{S0}} \right) \tag{4.2-6}$$

where ε_{s0} is the initial porosity, C_{s0} is the initial concentration of the reacting component of the solid, v_s and v_P are the reactant and product molar volumes,

respectively (see Problem 4.1). It can be seen from (4.2-6) that the porosity increases if the reaction product has a lower molar volume than the reactant, that is, it is more dense. Wen [1968] related the effective diffusivity to ε_s by means of the relation

$$\frac{D_{eA}}{D_{eA0}} = \left(\frac{\varepsilon_s}{\varepsilon_{s0}} \right)^{\beta} \tag{4.2-7}$$

where β lies between 2 and 3, the value of 2 corresponding to the random pore model. Alterations in the porous structure itself (e.g., through sintering) can also affect the diffusivity. An example is given by Kim and Smith [1974].

Equation (4.2-1) may often be simplified. Indeed, it is justified to neglect $\varepsilon_s(\partial C_{As}/\partial t)$ when

$$\frac{C_{As}}{C_S} \leq 10^{-3}$$

as was shown by Bischoff [1963, 1965], Luss [1968], and Theofanous and Lim [1971], and extensions have been given by Yoshida, Kunii, and Shimizu [1975]. This condition is always satisfied for gas-solid reactions, but not necessarily for liquid-solid reactions. Physically, neglecting the transient term in (4.2-1) means that the rate at which the reaction layer moves is small with respect to the rate of transport of *A*. This assumption has frequently been referred to as the pseudo-steady-state approximation.

In (4.2-1) the rates of reaction r_A and r_S may be of the type encountered in Chapter 1 or Chapter 2. In general, the system of (4.2-1) and (4.2-2) cannot be integrated analytically.

A transformation of the dependent variables C_{As} and C_S allowed DelBorghi, Dunn, and Bischoff [1976] and Duduković [1976] to reduce the coupled set of partial differential equations for reactions first order in the fluid concentration and, with constant porosity and diffusivity, into a single partial differential equation. With the pseudo-steady-state approximation, this latter equation is further reduced to an ordinary differential equation of the form considered in Chapter 3 on diffusion and reaction (see Problem 4.2). An extensive collection of solutions of such equations has been presented by Aris [1974].

Wen [1968] integrated (4.2-1) and (4.2-2) numerically for the following rate equations:

$$r_A = kC_{As}^n C_S^m \tag{4.2-8a}$$

$$r_S = \frac{k}{a} C_{As}^n C_S^m \tag{4.2-8b}$$

where a is the number of moles of A reacting with one mole of S.
Note that k in (4.2-8) has the dimensions

$$\mathrm{m}_f^{3n}\ (\text{kmol } A)^{1-\mathrm{n}}\ (\text{kmol } S)^{-\mathrm{m}}\ \mathrm{m}_p^{3m}\ (\text{kg part.})^{-1}\ \mathrm{s}^{-1}$$

The results are represented in Figs. 4.2-1 and 4.2-2 for $n = 2$ and $m = 1$. Figure 4.2-1 shows C_A and C_S profiles at various reduced times

$$\theta = \frac{k\rho_s}{a} C_{As_0}^2 t$$

in the absence of interfacial gradients (Sh' = ∞) and for

$$\frac{C_{s0}(\nu_s - \nu_p)}{\varepsilon_{s0}} = 9 \qquad \beta = 2 \qquad \text{and} \qquad \phi'' = R\sqrt{\frac{k\rho_s C_{As}^s C_{s0}}{D_{eA0}}} = 1$$

x is the fractional conversion of S. The latter group is the Thiele modulus already encountered in Chapter 3. One is a low value for ϕ'' so that the chemical reaction is rate controlling and there are practically no gradients inside the particle. This is a situation that could be described satisfactorily by the homogeneous model and is encountered at low temperatures. Figure 4.2-2 corresponds to a case for

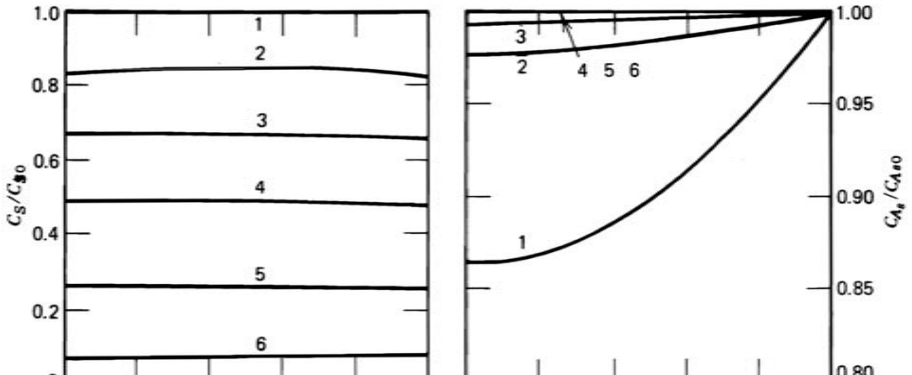

Curve	θ	x
1	0	0
2	0.189	0.165
3	0.429	0.341

Curve	θ	x
4	0.749	0.521
5	1.389	0.748
6	2.669	0.930

Figure 4.2-1
General model. Concentration profiles for ϕ'' = 1. From Wen [1968].

which the modulus ϕ'' is high and for which the diffusion of A through the solid is rate controlling. This is a situation that could be described by the heterogeneous model with shrinking core.

When the form of the kinetic equation is such that the concentration of the reacting solid component, C_S, drops to zero in a finite time, two stages have to be considered in solving (4.2-1) and (4.2-2). In the first stage, which extends until the time at which C_S becomes zero at the surface of the particle, the complete equations (4.2-1) and (4.2-2) are solved directly. The second stage involves only diffusion through the region with completely exhausted solid reactant, up to the front where reaction is occurring, from which location onward the complete equations are used again. This is illustrated below for the useful special case of a zero-order reaction with respect to the reacting solid concentration, a good approximation for the situation when all of the solid is reactive.

Wen also has simplified (4.2-1) somewhat by allowing only two values for D_{eA}, instead of letting it vary according to (4.2-7): a value D_{eA} for diffusion through unreacted or partially reacted solid and a value D'_{eA} for diffusion of A through completely reacted solid [Wen, 1968]. This scheme is most useful, of course, only for those kinetic forms leading to complete conversion in a finite time. As mentioned already, this then means that two stages must be considered.

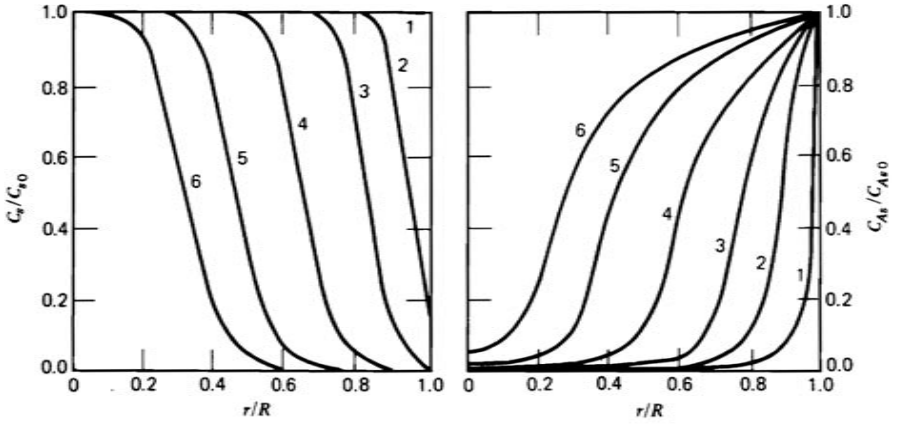

Curve	θ	x
1	0	0
2	1.84	0.151
3	4.88	0.417
4	10.16	0.708
5	16.40	0.892
6	20.56	0.957

Figure 4.2-2
General model. Concentration profiles for ϕ'' = 70. From Wen [1968].

In the first stage, (4.2-1) reduces to

$$\varepsilon_s \frac{\partial C_{As}}{\partial t} = D_{eA}\left(\frac{\partial^2 C_{As}}{\partial r^2} + \frac{2}{r}\frac{\partial C_{As}}{\partial r} \right) - r_A \rho_s \tag{4.2-9}$$

with (4.2-2) and the boundary conditions (4.2-3), (4.2-4), and (4.2-5) unchanged and with $\partial C_{As}/\partial t = 0$ when the pseudo-steady-state hypothesis is valid. For an isothermal particle and a single reaction with simple kinetics, at least, the location where C_S drops to zero is obviously the surface where C_A is the highest. The second stage begins when C_S has reached zero at the surface. In the outer zone, which is originally very thin and gradually moves to extend to the center of the particle, there is no reaction any longer, only transport, and equations (4.2-1) and (4.2-2) reduce to

$$D'_{eA}\left(\frac{\partial^2 C'_{As}}{\partial r^2} + \frac{2}{r}\frac{\partial C'_{As}}{\partial r} \right) = 0 \tag{4.2-10}$$

where the prime denotes conditions and properties related to the completely reacted zone. The boundary condition at the surface is unchanged. The boundary condition on the side of the inner zone, at some distance r_m from the center, expresses the continuity in the C_A profile and the equality of fluxes on both sides of that boundary at $r = r_m$:

$$C'_{As} = C_{As}$$

$$D'_{eA}\frac{\partial C'_{As}}{\partial r} = D_{eA}\frac{\partial C_{As}}{\partial r} \tag{4.2-11}$$

For the inner zone, in which both transport and reaction occur, the differential equations are those of the first stage, but the boundary conditions are $\partial C_{As}/\partial r = 0$ at $r = 0$ and (4.2-11) at the boundary with the outer zone. This model corresponds to that set up by Ausman and Watson to describe the rate of burning of carbon deposited inside a catalyst particle [1962]. Analytical integration of this fairly general two-stage model is only possible for a zero-order, first-order, or pseudo-first-order rate law. For the last two cases (4.2-8) reduces to

$$r_A = kC_{As} \qquad \text{or} \qquad kC_{As}C_{S0} \tag{4.2-12}$$

The equations are developed in the paper by Ishida and Wen [1968]. The gas concentration profile during the first stage is found by solving (4.2-9)

accounting for (4.2-12) and for the boundary condition (4.2-5). This leads to, for a pseudo-first-order reaction,

$$\frac{C_{As}}{C} = \frac{1}{\theta_e}\frac{\sinh(\phi'' \xi)}{\xi \sinh \phi''} \tag{4.2-13}$$

with

$$\xi = \frac{r}{R} \qquad \text{and} \qquad \phi'' = R\sqrt{\frac{k\rho_s C_{s0}}{D_{eA}}}$$

$$\theta_e = 1 + \left(\frac{D_{eA}}{k_g R}\right)(\phi'' \coth \phi'' - 1)$$

and dimensions for $k\rho_s$ of m^3_g/kmol S s.

The solid concentration profile is found by integrating (4.2-2) with r_S following from (4.2-12):

$$\frac{C_s}{C_{s0}} = 1 - \frac{\sinh(\phi'' \xi)}{\xi \sinh \phi''}\frac{\theta}{\theta_e} \tag{4.2-14}$$

with

$$\theta = \frac{k}{a}\rho_s C_A t$$

Finally, the solid conversion is found as follows:

$$x = 1 - 3\int_0^1 \frac{C_s}{C_{s0}}\xi^2 d\xi$$

$$= \frac{3}{\phi''^2}(\phi'' \coth \phi'' - 1)\frac{\theta}{\theta_c} \tag{4.2-15}$$

The second stage begins when $C_S(R, t) = 0$, which from (4.2-14) is, at time,

$$t_e = \frac{a\theta_e}{k\rho_s C_A} = \frac{a}{k\rho_s C_A}\left[1 + \left(\frac{D_{eA}}{k_g R}\right)(\phi'' \coth \phi'' - 1)\right]$$

Then, the concentrations during the second stage are found from (4.2-10) and (4.2-11), and the solid conversion is given by

$$x = 1 - \xi_m^3 + \frac{3\xi_m}{\phi''^2}\left[(\phi''\xi_m)\coth(\phi''\xi_m) - 1\right] \tag{4.2-16}$$

where the position of the moving boundary of completely exhausted solid, ξ_m = $\xi_m(\theta)$, is found from the implicit equation:

$$\theta = 1 + \left(1 - \frac{D_{eA}}{D'_{eA}}\right)\ln\left[\frac{\xi_m \sinh\phi''}{\sinh(\phi''\xi_m)}\right] + \frac{\phi''^2_2}{6}(1-\xi_m)^2(1+2\xi_m)$$

$$+\left[\left(\frac{D_{eA}}{D'_{eA}}\right)(1-\xi_m) + \left(\frac{D_{eA}}{k_g R}\right)\xi_m\right]\left[(\phi''\xi_m)\coth(\phi''\xi_m) - 1\right]$$

$$+\frac{D'_{eA}\phi''^2_2}{k_g R 3}(1-\xi_m^3)$$

where ϕ''_2 is the Thiele modulus for the second stage, containing D'_{eA}.

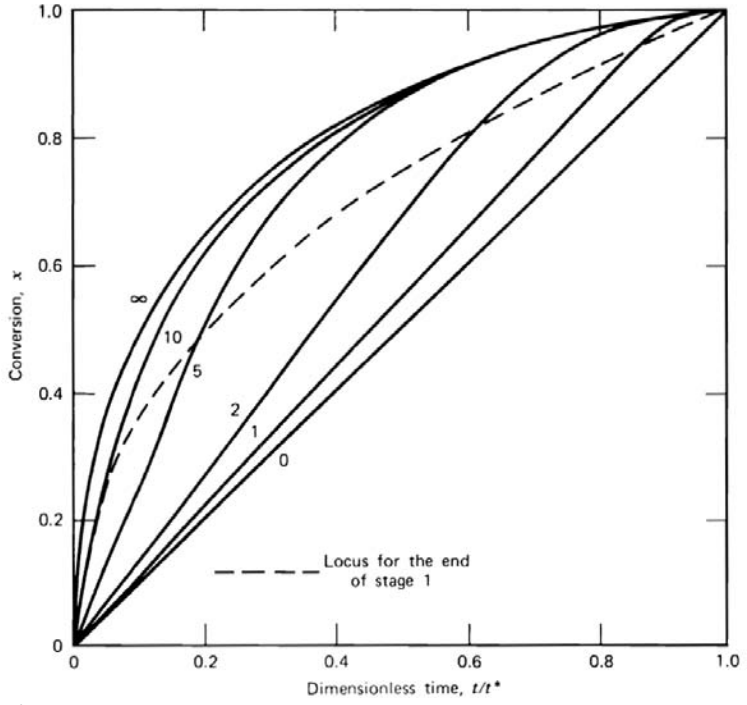

Figure 4.2-3

Fractional conversion of solid reactant as a function of dimensionless time for homogeneous model with zero-order solid kinetics (sphere).

$$\frac{k_g R}{D_{eA}} = \infty = D_{eA} = D'_{eA};\ \phi'' = R\sqrt{\frac{k\xi C_{S0}}{D_{eA}}} = 0, 1, 2, 5, 10, \infty$$

t^* = time for complete conversion. From Ishida and Wen [1968].

Figure 4.2-3 illustrates how the conversion progresses with time, and also indicates the boundary between the first and second stages [see Ishida and Wen, 1968]. Note that with strong diffusional limitations, say, $\phi'' > 5$, the first stage ends at less than 50 percent conversion of solid, and so the rather complicated second-stage description is used over a considerable range of final reaction. The homogeneous and heterogeneous models mentioned above may be considered as special cases of the two-stage model.

A homogeneous model *latu sensu* (i.e., with intraparticle concentration gradients but without distinct zones) requires $D_{eA} = D'_{eA}$. A truly homogeneous model, strictly speaking, requires $D_{eA} = D'_{eA}$ and the reaction to be rate controlling. The truly homogeneous model utilizes (4.2-2), with $C_{As} = C^s_{As}$:

$$\frac{\partial C_S}{\partial t} = -r_S \rho_s = f(C_S)$$

This relation can then be directly integrated:

$$\int_0^{C_S} \frac{dC_S}{(-r_S \rho_s)} = t \tag{4.2-17}$$

yielding expressions identical to those given in Table 1.2.4.2-1. For example, the result when the order with respect to the fluid concentration of *A* is 1 and with respect to the solid concentration is zero, is

$$C_S - C_{S0} = -\frac{k}{a} \rho_s C^s_{As} C_{S0} t$$

or

$$x = \frac{k}{a} \rho_s C^s_{As} t \tag{4.2-18}$$

The heterogeneous model is obtained when $D_{eA} << D'_{eA}$ (i.e., when the effective diffusivity of *A* in the unreacted solid is much smaller than in the reacted layer, so that the reaction is confined to a very narrow zone). When $D_{eA} = D'_{eA}$ a narrow reaction zone will, of course, also be obtained when $D_{eA} = D'_{eA} << k$ (i.e., when $\phi'' << 1$). The equations are easily directly derived, as is shown in Section 4.3.

4.3 HETEROGENEOUS MODEL WITH SHRINKING UNREACTED CORE

The model equation is again (4.2-1) in which the time derivative is set equal to zero, as implied by the pseudo-steady-state approximation:

$$\frac{1}{r^2}\frac{\partial}{\partial r}\left(D'_{eA}r^2\frac{\partial C'_{As}}{\partial r}\right)=0 \tag{4.3-1}$$

whereas the continuity equation for the reacting component of the solid is exactly (4.2-2). A prime is used in (4.3-1), in accordance with the notation in Section 4.2, to denote conditions in a completely reacted zone. Also, since the reaction is confined to a front — which supposes that the true reaction rate is relatively large — the reaction rate term does not appear in the right-hand side, but only in the boundary condition at the reaction front:

At $r = r_c$:

$$D'_{eA}\left(\frac{\partial C'_{As}}{\partial r}\right)=ak_sC'_{As}C_{S0} \tag{4.3-2}$$

The boundary condition at the surface is unchanged:

At $r = R$:

$$D'_{eA}\left(\frac{\partial C'_{As}}{\partial r}\right)=k_g(C_A-C^s_{As}) \tag{4.3-3}$$

The rate coefficient k_s, with dimensions $s^{-1}m_p$ (kmol A)$^{-1}$ m^3_f is based on the reacting surface. It can be related to the weight-based k or to $k\rho_s$ used in Section 4.2 through the boundary condition (4.3-2), which is valid also at $t = 0$, when the reaction plane is at the surface (i.e., when $r = r_c = R$). The concentration gradient $\partial C'_{As}/\partial r$ at $t = 0$ can be obtained from the general model with two stages. For the first stage the concentration profile of A is given by (4.2-13), which may be rewritten as

$$C_{As}=C^s_{As}\frac{\sinh(\phi''\xi)}{\xi\sinh\phi''} \tag{4.3-4}$$

since for $r = R$ (i.e., $\xi = 1$)

$$\frac{C^s_{As}}{C_A}=\frac{1}{\theta_e}$$

Differentiating (4.3-4) with respect to r at $r = R$ and multiplying by D_{eA} leads to

$$D_{eA}\left.\frac{\partial C_{As}}{\partial r}\right|_R = \frac{D_{eA}C_{As}^s}{R}\left(\phi''\coth\phi'' - 1\right) \tag{4.3-5}$$

Substituting (4.3-5) into (4.3-2) taken at $r = R$ and considering that for large ϕ'' the expression ϕ'' coth ϕ'' – 1 reduces to ϕ'' yields

$$k_s = \sqrt{\frac{D_{eA}k\rho_s}{a^2 C_{S0}}} \tag{4.3-6}$$

The continuity equation for A, (4.3-1), can be integrated twice to yield the following expression for the concentration profile of A:

$$C_{As}^{'} = (C_{As}^{'})_{r=r_c} + B\left(\frac{1}{r_c} - \frac{1}{r}\right)$$

where B is an integration constant and the subscript c refers to conditions at the reaction front. Accounting for the boundary conditions easily leads to

$$\frac{C_{As}^{'}}{C_A} = \frac{\left(1 + \dfrac{D_{eA}^{'}}{k_s C_{S0} r_c}\right)\dfrac{1}{r_c} - \dfrac{1}{r}}{\left(1 + \dfrac{D_{eA}^{'}}{a k_s C_{S0} r_c}\right)\dfrac{1}{r_c} - \left(1 - \dfrac{D_{eA}^{'}}{k_g R}\right)\dfrac{1}{R}} \tag{4.3-7}$$

The concentration of A at the reaction front is obtained by setting $r = r_c$ in equation (4.3-7).

The time required for the reaction front to move from the surface to a distance r_c from the center of a spherical particle is obtained from (4.2-2) combined with (4.2-11):

$$a r_s^{'} = D_{eA}^{'}\left(\frac{\partial C_{As}^{'}}{\partial r}\right)_{r=r_c} \tag{4.3-8}$$

The transition from the surface-based rate to the change with time of the volume-based solid concentration requires a slight adaptation of (4.3-8) and yields

$$-a\frac{d\left(C_{S0}\dfrac{4\pi r_c^3}{3}\right)}{dt} = D_{eA}^{'}\left.\left(\frac{\partial C_{As}^{'}}{\partial r}\right)\right|_{r=r_c} 4\pi r_c^2$$

and, with $\partial C_{eS}^{'}/\partial r$ derived from (4.3-7),

$$aC_{S0}\frac{dr_c}{dt} = -\frac{D_{eA}^{'}C_A\dfrac{1}{r_c^2}}{\left(1+\dfrac{D_{eA}^{'}}{ak_sC_{S0}r_c}\right)\dfrac{1}{r_c}-\left(1-\dfrac{D_{eA}^{'}}{k_gR}\right)\dfrac{1}{R}}$$

and, finally,

$$t = \frac{aRC_{S0}}{C_A}\left[\frac{1}{3}\left(\frac{1}{k_g}-\frac{R}{D_e^{'}}\right)\left(1-\frac{r_c^3}{R^3}\right)+\frac{R}{2D_{eA}^{'}}\left(1-\frac{r_c^2}{R^2}\right)+\frac{1}{ak_sC_{S0}}\left(1-\frac{r_c}{R}\right)\right] \tag{4.3-9}$$

The time t^* required for complete conversion is found by setting $r_c = 0$ in this formula, so that

$$t^* = \frac{aRC_{S0}}{C_A}\left(\frac{1}{3k_g}+\frac{R}{6D_{eA}^{'}}+\frac{1}{ak_sC_{S0}}\right) \tag{4.3-10}$$

The three terms inside the parentheses of (4.3-10) represent the three resistances involved in the process. They are purely in series in this case. When the mass transfer through the external film is rate controlling, $3k_g >> ak_s\,C_{S0}$ and $k_g << 2\,D_{eA}^{'}/R$ so that (4.3-9) becomes

$$t = \frac{aRC_{S0}}{3C_Ak_g}x \tag{4.3-11}$$

where x is the conversion, defined by

$$x = 1-\frac{\left(\dfrac{4}{3}\right)\pi r_c^3}{\left(\dfrac{4}{3}\right)\pi R^3} = 1-\left(\frac{r_c}{R}\right)^3$$

When the effective diffusion through the reacted core is rate controlling, $2D_{eA}/R \gtrless k_g$ and $6D_{eA}/R << a\,k_s^{'}C_{S0}$ so that (4.3-9) in that case becomes

$$t = \frac{aR^2C_{S0}}{6D_{eA}^{'}C_A}\left[1-3(1-x)^{2/3}+2(1-x)\right] \tag{4.3-12}$$

The third limiting case of chemical reaction rate controlling is not consistent with the concept of a shrinking core model with a *single* diffusivity throughout the particle: the existence of a sharp boundary implies transport by effective diffusion that is potentially slow with respect to the reaction.

From plots of x versus time it is possible to find out which is the rate-determining step. Also, from experiments with particles having different radii a comparison of the time required to reach the same conversion will reveal a dependence on the ratio of the particle sizes that is different for each rate-controlling step, as is clear from a scrutiny of (4.3-11) and (4.3-12). Evidently, both (4.3-11) and (4.3-12) could have been obtained directly from specific models considering only one step rate controlling, in contrast with the more general approach outlined in this section. White and Carberry [1965] have considered situations where the particle size changes with reaction.

Park and Levenspiel [1975] have proposed an extension of the basic shrinking core model, called the crackling core model. This arose from the observation that the initial state of many reacting solids is essentially nonporous and that a first step, either physical or chemical, is required to form a porous and reactive intermediate. The model essentially makes use of various combinations of the models discussed above.

EXAMPLE 4.3.A

COMBUSTION OF COKE WITHIN POROUS CATALYST PARTICLES

An examination of this problem was provided by Weisz and Goodwin [1963, 1966]. The pellets were silica/alumina cracking catalyst, and the coke resulted from the cracking of light gas oil and naphtha. Measurements of the burning rate were followed by oxygen consumption rates, as shown in Fig. 4.3.A-1.

It is evident that the pellets must have had significant diffusional resistance at the higher (> 450°C) temperatures. Using the Weisz-Prater criterion discussed in Chapter 3, with values of $C_A = 3 \times 10^{-6}$ mol/cm^3 and $D_{eA} \approx 5 \times 10^{-3}$ cm^2/s (for oxygen under combustion conditions), one can determine the rate below which diffusional limitations should be absent:

$$(r_A)_{obs} < \frac{C_A D_{eA}}{R^2} = 4 \times 10^{-7} \quad \text{mol/cm}^3\text{s}$$

This agrees very well with results in the figure.

By submerging the silica/alumina pellets in a high-refractive-index liquid (carbon tetrachloride), they are rendered transparent, and the coke profiles for various temperature levels can be observed, as shown in Fig. 4.3.A-2. These

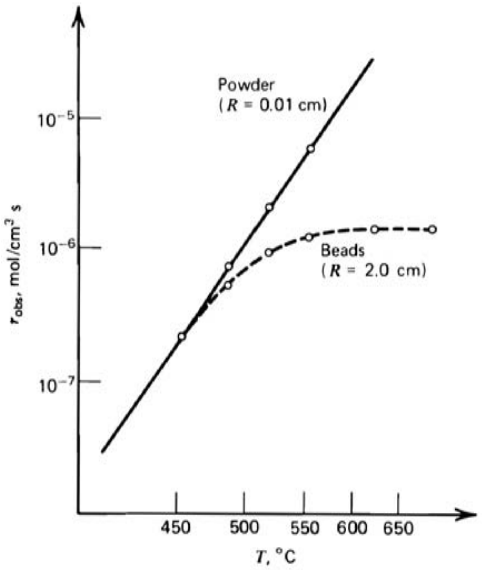

Figure 4.3.A-1

Average observed burning rates of conventional silica alumina cracking catalyst. Initial carbon content 3.4 wt-%. Beads (dashed line), and ground-up catalyst (full curve). From Weisz and Goodwin [1963].

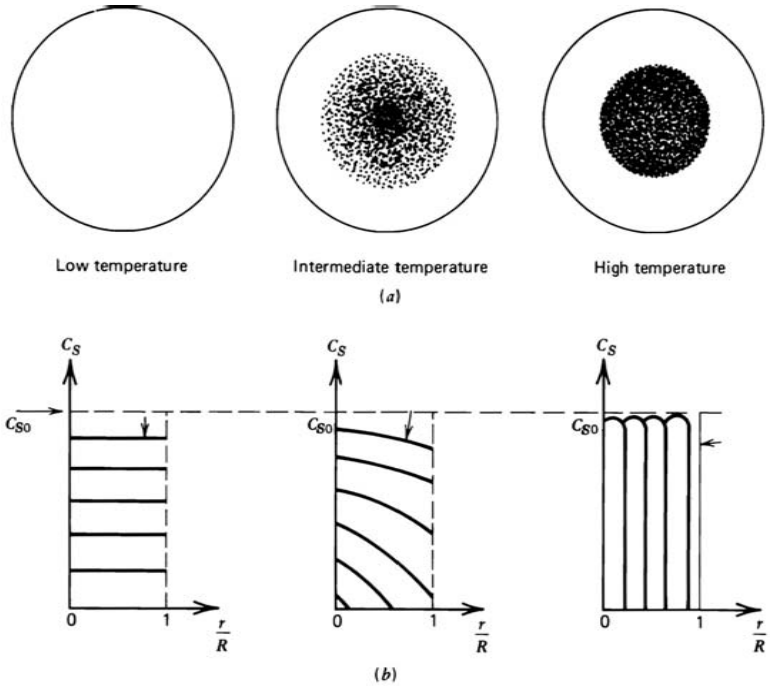

Figure 4.3.A-2

Appearance after partial burnoff (a) and coke concentration versus radius in beads for successive stages of burnoff (b), for three temperature levels. From Weisz and Goodwin [1963].

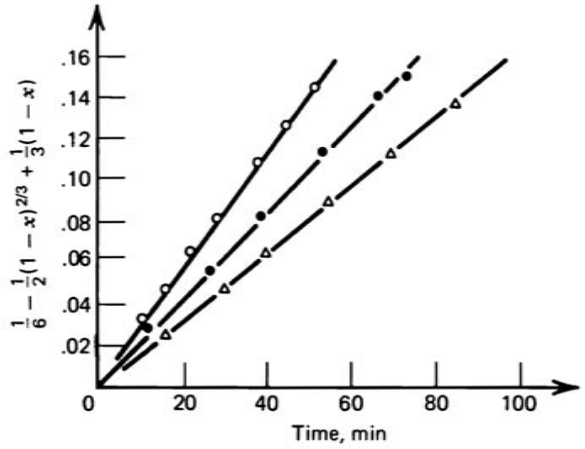

Figure 4.3.A-3

Burnoff function versus time for three different diameter beads. From Weisz and Goodwin [1963].

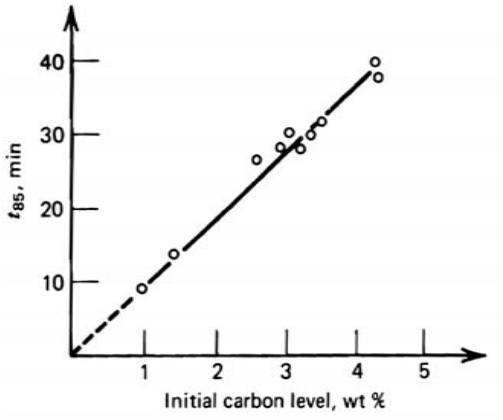

Figure 4.3.A-4

Dependence of burnoff time on initial carbon level for diffusion-controlled combustion (silica alumina cracking catalyst, 700°C). From Weisz and Goodwin [1963].

range from almost a homogeneous situation (as defined above) to the sharp-boundary shell-progressive situation. For the latter, (4.3-12) can be used:

$$\frac{1}{6} - \frac{1}{2}(1-x)^{2/3} + \frac{1}{3}(1-x) = \left(\frac{D_{eA}}{aR^2}\frac{C_A}{C_{S0}}\right)t \qquad (4.3.\text{A-a})$$

Figure 4.3.A-3 illustrates the agreement of the data with the form of (4.3.A-a) at 700°C. The slopes of the lines provide values of $D_{eA}C_A/aR^2C_{S0}$. Alternatively, the time for complete combustion can be obtained for $x = 1$:

$$t^* = \frac{1}{6}\frac{aR^2 C_{S0}}{D_{eA} C_A} \qquad (4.3.A\text{-b})$$

Actually, this complete combustion time is often hard to determine unambiguously from (scattered) experimental data, and so the 85 percent completion time was more convenient:

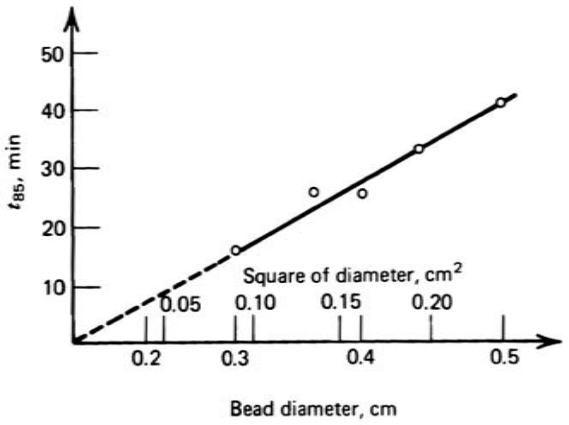

Figure 4.3.A-5

Dependence of burnoff time on bed size for diffusion-controlled combustion. From Weisz and Goodwin [1963].

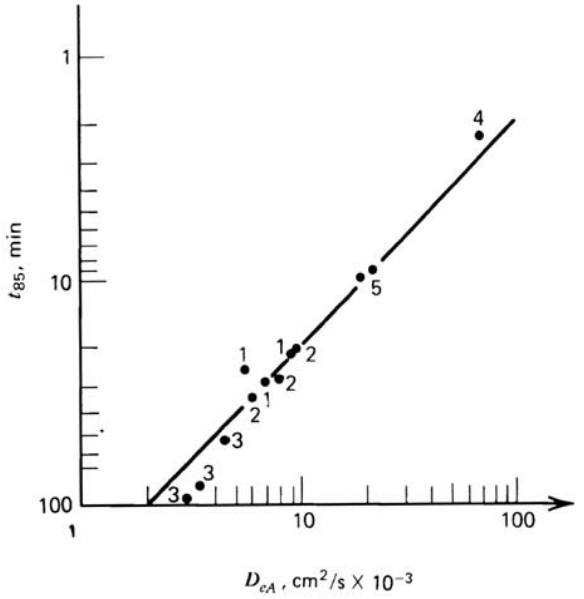

Figure 4.3.A-6

Dependence of burnoff time on structural diffusivity of various types of spherical particles for diffusion-controlled combustion region. From Weisz and Goodwin [1963].

TABLE 4.3.A-1
COMPARISON OF BURNOFF TIMES IN AIR AND OXYGEN[a]

	Air			Oxygen			
Catalyst	C_{S0} (%)	t_{85} (min)	t_{85} corr. (min)	C_{S0} (%)	t_{85} (min)	t_{85} corr. (min)	Ratio t_λ/t_{air}
Silica alumina (lab. prep.)							
R = 0.24cm ; temp. 630°C	4.0	45	45	4.6	10.5	9.1	---
t_{85} corrected to							
C_{S0} = 4.8% wt	3.7	48	52	4.1	10.6	10.3	---
Average			48.5			9.7	0.20
Silica alumina (0.15% Cr_2O_3, commercial)							
R = 0.19 cm ; temp. 690°C	3.0	30	29.7	3.35	6.3	5.55	---
t_{85} corrected to	3.4	29	25.6	---	---	---	---
C_{S0} = 3% wt	3.2	27	25.2	---	---	---	---
Average			26.6			5.55	0.21

[a]From Weisz and Goodwin [1963].

$$t_{85} = 0.0755 \frac{aR^2 C_{S0}}{D_{eA} C_A} \tag{4.3.A-c}$$

If all the bases of the model are correct, this 85 percent time should vary (1) linearly with initial coke level, (2) with the square of the particle size, (3) inversely with the effective diffusivity, and (4) inversely with oxygen partial pressure. Figures 4.3.A-4, 4.3.A-5, and 4.3.A-6 and Table 4.3.A-1 indicate that all of these are verified by the data. Thus, for high temperatures, the shrinking-core model provides a good description. At lower temperatures, the more general models would be required, however.

■

4.4 MODELS ACCOUNTING EXPLICITLY FOR THE STRUCTURE OF THE SOLID

Sohn and Szekely [1972] developed a model in which the particle is considered to consist of a matrix of very small grains between which the fluid has easy access through the pores. Figure 4.4-1 illustrates how the reactive component of the grains is converted throughout the particle, which has a fluid reactant concentration gradient caused by the resistance to diffusion in the particle. This situation can be described on the basis of the models developed in Sections 4.2 and 4.3.

The fluid reactant concentration in the particle is obtained from

$$\varepsilon_s \frac{\partial C_{As}}{\partial t} = D_{ep} \frac{\partial^2 C_{As}}{\partial r^2} - D_{eg} \left. \frac{\partial C_{Ag}}{\partial y} \right|_Y (1 - \varepsilon_s) a_g \tag{4.4-1}$$

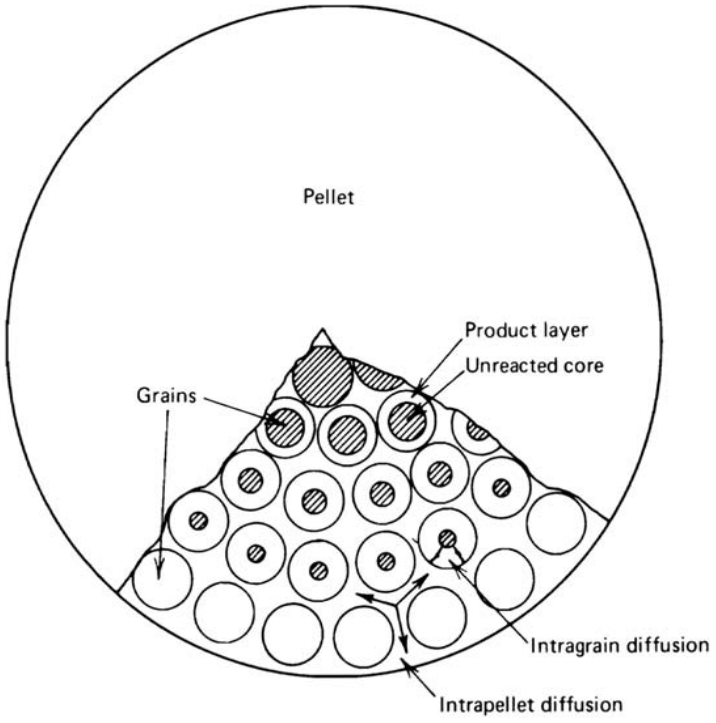

Figure 4.4-1
Schematic representation of grain model. From Sohn and Szekely [1972].

with boundary conditions analogous to (4.2-3), (4.2-4), and (4.2-5), where r is a coordinate inside the particle and y a coordinate in the grain; Y is the radius of the grain, or the half-width of the equivalent slab, oriented from the center to the surface for transport of A inside the grain; D_{eg} is the grain effective diffusivity of A; D_{ep} is an effective diffusivity for transport through the pores between the grains and is, therefore, different from the D_{eA} and D'_{eA} used in the models described above, which do not distinguish between pores and solid (i.e., consider the particle as a pseudohomogeneous solid); C_{Ag} is the fluid reactant concentration in the grain; and a_g is the surface-to-volume ratio of the grain. The factor $(1 - \varepsilon_s)a_g$ arises from the fact that (4.4-1) is written per unit particle volume, whereas the flux $D_{eg}(\partial C_{Ag}/\partial y)|_Y$ is per unit grain surface area. Equation (4.4-1) is a particular form of (4.2-1) expressing the fact that A reacts only in the grains. Slab geometry is used for simplicity.

To obtain the concentration profile in the grain, the general model of Section 4.2 can be used. For slab geometry, the model equations are

$$\varepsilon_g \frac{\partial C_{Ag}}{\partial t} = D_{eg} \frac{\partial^2 C_{Ag}}{\partial y^2} - r_A \rho_{sg} \tag{4.4-2}$$

$$\frac{\partial C_{Sg}}{\partial t} = -r_S \rho_{sg} \tag{4.4-3}$$

with boundary conditions

At $t = 0$:

$$C_{Ag} = C_{Ag0} \qquad \text{and} \qquad C_{Sg} = C_{Sg0}$$

At $y = 0$:

$$\frac{\partial C_{Ag}}{\partial y} = 0$$

At $y = Y$:

$$C_{Ag} = C_{As}(r)$$

As before, various rate laws could be substituted into these equations. Numerical integration would normally be required to solve the system (4.4-1), (4.4-2), and (4.4-3).

For the special case where the phenomena in the grain can be represented by the shrinking-core model, which is plausible since the grains are often very dense, (4.2-2) and (4.2-3) lead to the same types of solutions as given in Section 4.3. Note that the shrinking-core models permit the concentration of the reactive solid component in the grains to become zero in a finite time, so that the solution of the particle equation (4.4-1) may involve two stages. For example, for grains with slab geometry and pseudo-steady state, (4.4-2) without the rate term can be integrated twice, using the boundary conditions across the completely reacted shell, to give

$$\frac{C_{Ag}}{C_{As}} = 1 - \frac{\dfrac{Y - y}{Y - y_c}}{1 + \left(\dfrac{D_{eg}}{k \rho_s C_{Sg0} y_c} \right) \dfrac{1}{Y - y_c}} \tag{4.4-4}$$

from which

$$\left.\frac{\partial C_{Ag}}{\partial y}\right|_{Y} = \frac{C_{As}}{\left(\dfrac{D_{eg}}{k\rho_s C_{Sg0} y_c}\right) + (Y - y_c)} \tag{4.4-5}$$

Substituting (4.4-5) into the pseudo-steady-state from of (4.4-1) for particle slab geometry leads to

$$D_{ep}\frac{\partial^2 C_{As}}{\partial r^2} - \frac{k\rho_s C_{Sg0}(1-\varepsilon_s)a_g C_{As}}{1 + \dfrac{k\rho_s C_{Sg0} y_c}{D_{eg}}(Y - y_c)} = 0 \tag{4.4-6}$$

with

$$\frac{\partial\left(\dfrac{y_c}{Y}\right)}{\partial t} = \frac{-\left(\dfrac{k\rho_s}{a}\right)C_{As}}{1 + \dfrac{k\rho_s C_{Sg0} y_c}{D_{eg}}(Y - y_c)} \tag{4.4-7}$$

Even these equations are not amenable to a complete analytical solution.

Sohn and Szekely [1974] developed a very useful approximate solution, valid for various geometries of grain and particle, based on the additivity of times to reach a given conversion for different limiting processes — a concept analogous to that discussed after (4.3-10). The concept states that the time required to attain a given conversion is the sum of the times required to attain the same conversion (1) in the absence of any diffusion resistance, (2) with intraparticle diffusion controlling, and (3) with intragrain diffusion controlling. In mathematical terms,

$$\frac{k\rho_s}{a}\frac{C_A a_g t}{F_g} \approx g_{Fg}(x) + \left[\frac{(1-\varepsilon_s)k\rho_s C_{Sg0} F_p}{2D_{ep}a_p^2}\left(\frac{a_g}{F_g}\right)\right] p_{Fp}(x) + \frac{k\rho_s C_{Sg0}}{2D_{eg}a_g}\, p_{Fg}(x) \tag{4.4-8}$$

where F_g and F_p are geometric factors for grain and particle, respectively, and have the values: 1 for slabs, 2 for cylinders, and 3 for spheres. The conversion x in the grain attained by a shrinking-core mechanism is written

$$x = 1 - \left(\frac{a_g y_c}{F_g}\right)^{Fg}$$

where g_{Fg}, p_{Fp}, and p_{Fg} are functions corresponding to the limiting situations mentioned above and are defined as follows:

$$g_{fg} = 1 - (1-x)^{1/Fg}$$

$$p_{Fp} = p_{Fg} = x^2 \qquad \text{for } F_p \text{ or } F_g = 1$$

$$= x + (1-x)\ln(1-x) \qquad \text{for } F_p \text{ or } F_g = 2$$

$$= 1 - 3(1-x)^{2/3} + 2(1-x) \qquad \text{for } F_p \text{ or } F_g = 3$$

Comparing the last expression with (4.3-7), obtained for the shrinking-core model with diffusion rate controlling, shows that $p_{Fp} = p_{Fg}$ is nothing but the ratio of the time required to reach a given conversion to the time required to reach complete conversion. Sohn and Szekely showed that (4.4-8) leads to a remarkably accurate approximation to the results obtained by numerical integration.

An analysis of experimental results on the reaction of SO_2 with limestone using a grain model similar to the one discussed in this section was published by Pigford and Sliger [1973]. Another structural model, accounting for parallel pores, was developed by Szekely and Evans [1970].

The grain model offers only a very elementary picture of the pore system in a particle. The effective diffusivity D_{eg} in (4.4-2) is based on the tortuosity, which reflects the network structure in a rather loose way. The tortuosity factor concept usually does not consider detailed aspects such as the possibility of making originally closed pores accessible to the reacting gas by structure modifications resulting from the reaction. Nor does it normally account for pore plugging caused by the expansion of the solid volume fraction that may result from the reaction, thereby slowing down the reaction and leading to incomplete conversion of the solid.

Clearly, only a heterogeneous model with a detailed description of the pore network and the resulting mass transfer can account for the above effects. The model of Beeckman and Froment [1982], described in Chapter 3, Section 3.5.3.1, is one possibility. More complex models have been considered, but analytical solution then becomes impossible.

Reyes and Jensen [1987] modeled the sulfation of calcined limestone by SO_2, accounting for the pore size distribution and the possibility of pore plugging by expansion of the solid volume fraction. The continuity equations were of the type (4.4-2) and (4.4-7). The evolution of the pore size distribution with time was obtained through the simultaneous solution of a population balance equation (see Froment and Bischoff [1990], Chapter 12, Example 12.7.2). The evolution of the

accessible surface area with the pore radius restriction and plugging was modeled through percolation theory. The network was of the Bethe type with a coordination number 6, so that Monte-Carlo simulation was required to derive percolation results.

4.5 ON THE USE OF MORE COMPLEX KINETIC EQUATIONS

The developments given above were mainly focused on the model equations. Less attention was paid to the kinetic equations. There is no reason to limit kinetic equations for gas-solid reactions to those of the power law type. Gas phase reactants may adsorb on the solid or on components of the solid before reacting. In such a case the kinetic equation takes on the form of the Hougen-Watson equations discussed in Chapter 2. In their study of the reoxidation of a Ni/alumina catalyst used in a secondary reformer of an ammonia plant Hatcher et al. [1978] considered the oxygen to be adsorbed on the nickel. The rate equation is given in Example 11.8.2.A, in which this process is modeled and simulated. Chida and Tadaki [1982] further developed rate equations for noncatalytic gas-solid reactions accounting for the adsorption of the gas-phase reactant in the shrinking-core model. Cases can arise for dual-site adsorption, encountered in the reduction of zinc oxide by hydrogen, where multiplicity of steady-state concentration profiles becomes possible, namely, when the adsorption coefficient of hydrogen is large.

PROBLEMS

4.1 Derive (4.2-6) by using simple geometric arguments (see also Kim and Smith [1974] and Wen [1968]).

4.2 Consider the general model with the reaction first order in fluid-phase concentration:

$$\varepsilon_s \frac{\partial C_{As}}{\partial t} = D_{eA}\nabla^2 C_{As} - k\rho_s C_{As} f(C_S)$$

$$\frac{\partial C_S}{\partial t} = -k\rho_s C_{As} f(C_S)$$

where $f(C_S)$ is the rate dependence on the solid reactant concentration (e.g., a grain model or mass action form). The simplest boundary conditions would be

$$C_{As} = 0$$
$$C_S = C_{S0} \qquad \text{at } t = 0$$

and

$$C_{As} = C_{As}^s \qquad \text{on the pellet surface}$$

(a) Show that the new variable

$$\psi(\mathbf{x},t) \equiv k\int_0^t C_{As}(\mathbf{x},t')dt' \quad \text{(cumulative concentration)}$$

is also defined by the formal integral

$$\psi = -\int_{C_{S0}}^{C_S} \frac{dC_s'}{f(C_s')}$$

This result can be solved, in principle, for

$$C_S = H_S\left[\psi(\mathbf{x},t); C_{S0}\right]$$

(b) Then, the new variable can be differentiated in space (∇) and these results combined with the original mass balance differential equation to yield

$$\varepsilon_s \frac{\partial \psi}{\partial t} = D_{eA}\nabla^2\psi - k\left[C_{S0} - H_S(\psi; C_{S0})\right]$$

Prove this result.

(c) The boundary conditions can similarly be transformed to

$$\psi = 0 \qquad \text{at } t = 0$$

$$\psi = C_{As}^s kt \qquad \text{on the surface}$$

Prove these additional results.

(d) The results of parts (b) and (c) show that the original two coupled partial differential equations can be reduced to solving one diffusion-type equation, with a time-dependent boundary condition — a much simpler problem. For the special case of rectangular (slab) geometry, and where the pseudo-steady-state approximation is valid (gas-solid reaction), show that the mathematical problem is reduced to

$$D_{eA}\frac{\partial^2\psi}{\partial z^2} = k\left[C_{S0} - H_s(\psi; C_{S0})\right]$$

with

$$\psi = kC_{As}^s t \qquad \text{on the surface } (z = L)$$

and

$$\frac{\partial\psi}{\partial z} = 0 \qquad \text{at the center, } z = 0 \text{ (symmetry)}$$

Thus, note that the results of Chapter 3 can be utilized to solve the transformed problem.

For a zero-order solid concentration dependence $(f(C_S) = C_{S0})$, show that the following results are obtained:

$$C_{As} = C_{As}^s \frac{\cosh(\phi' z/L)}{\cosh\phi'} \qquad \phi' = L\sqrt{kC_{S0}/D_{eA}}$$

$$C_S = C_{S0}\left[1 - \frac{\cosh(\phi' z/L)}{\cosh\phi'}(kC_{As}^s t)\right]$$

which are the type of results obtained by Ishida and Wen [1968] in (4.2-13) and (4.2-14).

(e) Finally, for the slab geometry of part (d), show that the conversion is given by

$$x_A(t) = \frac{1}{\phi'}\left\{2\int_{\psi_c}^{kC_{As}^s t}\frac{\left[C_{S0} - H(\psi)\right]d\psi}{C_{S0}}\right\}^{1/2}$$

which is based on the generalized modulus concept of Chapter 3. Thus, it is seen that the complicated gas-solid reaction problem can be reduced to an analogy with the simpler effectiveness factor problem of Chapter 3. For more general results, see DelBorghi, Dunn, and Bischoff [1976] and for extensive results for first-order solid reactions, $f(C_S) = C_S$, see Duduković [1976].

4.3 **(a)** Derive the results of (4.2-13) to (4.2-15) by directly solving appropriate differential mass balances.

(b) Compute the conversion-time results of Fig. 4.2-3 for $\phi = 2.0$ (first stage only).

4.4 The secondary steam reformer of an ammonia plant has to be opened to replace the Ni/alumina catalyst. This requires the prior careful reoxidation of the pyrophoric Ni-catalyst. Simulate the reoxidation by means of an oxygen/nitrogen mixture containing 5 volume % oxygen. Use the general model of Section 4.2 to calculate the evolution with time of the concentration profiles of oxygen (A) and Ni (S) in the catalyst particle for various values of the rate parameters and for conversions based on S of up to 50 %. The initial Ni content of the catalyst (C_{S0}) is 0.00624 kmol/kg cat.

The rate equation for ½ O_2 + Ni into NiO is

$$r_{Ni} = kK_A p_A C_S^2 / 1+K_A P_A \qquad [\text{mol Ni/cm}^3 \text{ cat. s}]$$

with

$$k = 21.7 \exp(-3520/T)$$

$$K_A = 0.305 \exp(3070/T) \quad [1/\text{bar}]$$

The particle is isothermal at 300°C and suspended in a gaseous atmosphere at a total pressure of 1.52 bar. Is there a transition between uniform and shrinking core situations ?

The porosity of the particle, ε_{s0}, is 0.45. Neglect the change caused by the oxidation. Calculate the effective diffusivity of oxygen for a random pore model with only macropores.

(In Chapter 11 this operation will be dealt with at the reactor level.)

REFERENCES

Aris, R., *The Mathematical Theory of Diffusion and Reaction in Permeable Catalysts*, Oxford University Press, London (1974).
Ausman, J.M., and Watson, C.C., *Chem. Eng. Sci.*, 17, 323 (1962).
Beeckman, J.W., and Froment, G.F., *Ind. Eng. Chem. Fundam.*, 21, 243 (1982).
Bischoff, K.B., *Chem. Eng. Sci.*, 18, 711 (1963).
Bischoff, K.B., *Chem. Eng. Sci.*, 20, 783 (1965).
Chida, T., and Tadaki, T., *Int. Chem. Eng.*, 22, 503 (1982).
Costa, E.C., and Smith, J.M., *AIChE J.*, 17, 947 (1971).
DelBorghi, M., Dunn, J.C., and Bischoff, K.B., *Chem. Eng. Sci.*, 31, 1065 (1976).
Delmon, B., *Introduction à la cinétique hétérogène*, Technip, Paris (1969).
Duduković, M.P., *AIChE J.*, 22, 945 (1976).
Froment, G.F., and Bischoff, K.B., *Chemical Reactor Analysis and Design*, 2nd Ed., Wiley (1990).
Hatcher, W., Viville, L., and Froment, G.F., *Ind. Eng. Chem. Proc. Des. Dev.*, 17, 491 (1978).
Ishida, M., and Wen, C.Y., *AIChE J.*, 14, 311 (1968).
Kim, K.K., and Smith, J.M., *AIChE J.*, 20, 670 (1974).
Luss, D., *Can. J. Chem. Eng.*, 46, 154 (1968).

Luss, D., and Amundson, N.R., *AIChE J.*, 15, 194 (1969).
Park, J.Y., and Levenspiel, O., *Chem. Eng. Sci.*, 30, 1207 (1975).
Pigford, R.L., and Sliger, G., *Ind. Eng. Chem. Proc. Des. Dev.*, 12, 85 (1973).
Reyes, S., and Jensen, K.F., *Chem. Eng. Sci.*, 42, 565 (1987).
Sampath, B.S., and Hughes, R., *The Chemical Engineer*, No. 278, 485 (1973).
Sohn, H.Y., *AIChE J.*, 19, 191 (1973).
Sohn, H.Y., and Szekely, J., *Chem. Eng. Sci.*, 27, 763 (1972).
Sohn, H.Y., and Szekely, J., *Chem. Eng. Sci.*, 29, 630 (1974).
Szekely, J., and Evans, J.W., *Chem. Eng. Sci.*, 25, 1091 (1970).
Theofanous, T.G., and Lim, H.C., *Chem. Eng. Sci.*, 26, 1297 (1971).
Wang, S.C., and Wen, C.Y., *AIChE J.*, 18, 1231 (1972).
Weisz, P.B., and Goodwin, R.D., *J. Catal.*, 2, 397 (1963).
Weisz, P.B., and Goodwin, R.D., *J. Catal.*, 6, 227, 425 (1966).
Wen, C.Y., *Ind. Eng. Chem.*, 60, No. 9, 34 (1968).
White, D.E., and Carberry, J.J., *Can. J. Chem. Eng.*, 43, 334 (1965).
Yoshida, K., Kunii, D., and Shimizu, F.J., *Chem. Eng. Japan*, 8, 417 (1975).

Chapter 5

Catalyst Deactivation

5.1 TYPES OF CATALYST DEACTIVATION

Catalysts frequently lose an important fraction of their activity while in operation. There are primarily three causes for deactivation.

5.1.1 Solid-State Transformations

There are many types of transformations that can occur in the wide variety of catalysts used today in industry. Only a few examples will be given here.

Alumina is frequently used as a carrier for metals, preferably in the γ-modification. Under the prolonged effect of temperature, a transition into the α-modification is possible. Likewise, amorphous silica carrier can evolve into the crystalline form by the effect of temperature or of foreign substances such as gases, or the presence of impurities, such as sodium ions which catalyze nucleation.

The texture of catalysts is often modified during operation, as revealed by shifts in the pore size distribution. In chromia/alumina catalysts segregation of the components has been shown to occur, but deactivation has also been shown to occur through the formation of a solid solution.

When a V_2O_5/MoO_3 catalyst is used for the oxidation of benzene into maleic anhydride in a fixed bed reactor, the MoO_3 has been shown to migrate downstream from the hot spot.

Sintering of metals loaded on a support also leads to deactivation, for example, with Pt/alumina catalysts used in the reforming of hydrocarbons. The phenomenon has been modeled in mathematical terms by Flynn and Wanke [1974, 1975] and by Rückenstein and Pulvermacher [1973] and reviewed by Dadyburjor [1987]. The whole field of solid-state transformations was

thoroughly discussed by Delmon and Grange [1980] and Delmon [1997]. Sintering involves the migration of crystallites and their coalescence, a mechanism modeled by Rückenstein and Pulvermacher [1973] or that of single atoms from small to larger crystallites, called ripening and modeled by Flynn and Wanke [1974, 1975]. The combination of both was modeled by Rückenstein and Dadyburjor [1978]. Ripening is said to be of the Ostwald type or "global" when the atoms move from a small to a larger crystallite through an intermediate surface phase or "direct" when there is no such phase. The migration has to do with differences in degree of saturation between the various entities. In more recent work Rückenstein has also given attention to the thermodynamic aspects of wetting and spreading and to the influence of the gas phase atmosphere [1991; 1994; 1997].

5.1.2 Poisoning

This is the result of an essentially irreversible chemisorption of some impurity in the feed stream.

5.1.3 Coking

This is the term used when the deactivation is the result of the deposition of carbonaceous residues from reactants, products or intermediates.

This chapter discusses the local (i.e., up to the particle size) effects of deactivation by poisoning and by coking. The effect on the reactor scale is dealt with in Chapter 11.

5.2 KINETICS OF CATALYST POISONING

5.2.1 Introduction

Metal catalysts are poisoned by a wide variety of compounds. The sensitivity of Pt-reforming catalysts and of Ni-steam-reforming catalysts is well known. To protect the catalyst, "guard" reactors are installed in industrial operation. They contain Co/Mo catalysts that transform the sulfur compounds into easily removable components. The poisoning of a Pt hydrogenation catalyst by sulfur coverage is illustrated in Fig. 5.2.1-1. Acid catalysts can be readily poisoned by basic compounds, as shown in Fig.5.2.1-2. Poisoning by metals in the feed is also encountered. For example, in hydrotreating petroleum residuum fractions, parts per million iron, nickel, and vanadium compounds in the feed suffice to completely deactivate the catalyst after a few months of operation. A review paper by Maxted [1951] is still useful for a rapid introduction to this area. The

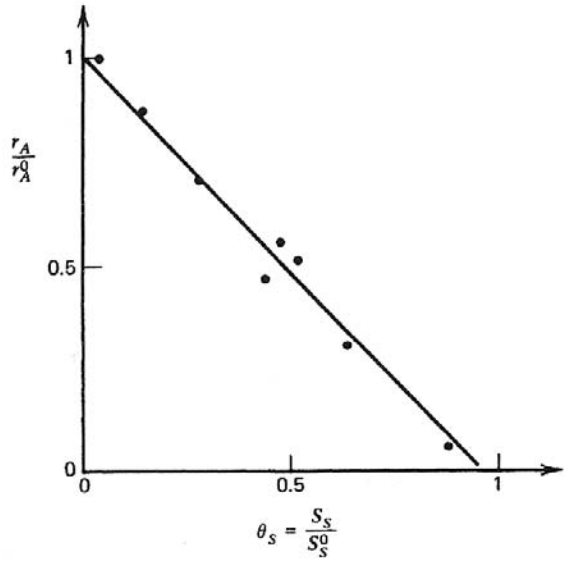

Figure 5.2.1-1

Liquid-phase hydrogenation of maleic acid (concentration 2.5×10^{-2} mol) on a platinum catalyst. Variation of relative rate of hydrogenation, r_A/r^0_A, with degree of coverage by sulfur. After Lamy Pitara et al. [1985].

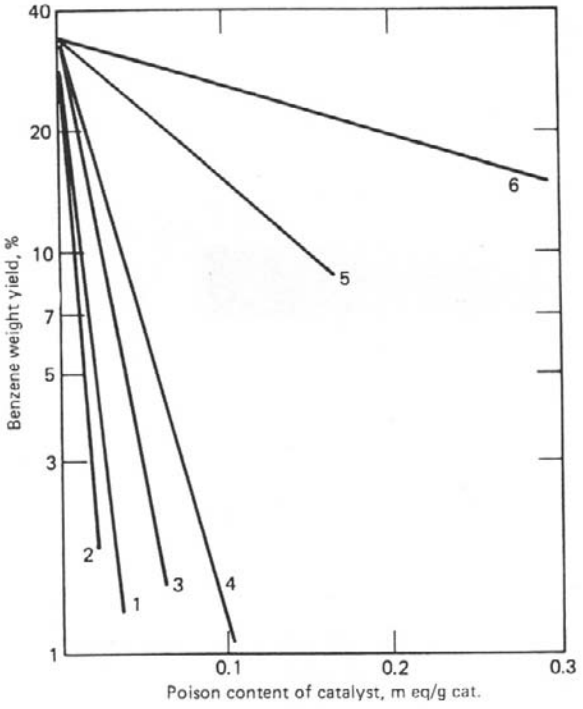

Figure. 5.2.1-2

Cumene dealkylation. Poisoning effect of (1) quinoline, (2) quinaldine, (3) pyrrole, (4) piperidine , (5) decyclamine, and (6) aniline. After Mills et al. [1950].

comprehensive review of Butt on deactivation [1972] also deals with several aspects of poisoning. An extensive review was published by Hegedus and McCabe [1980].

When an impurity in the feed is irreversibly chemisorbed on the catalyst, the latter acts very similarly to an adsorbent or an ion-exchange resin in an adsorption or ion exchange process.The impurity naturally does not necessarily act like the reactants (or products) and could be deposited into the solid independently of the main chemical reaction and have no effect on it. More often, however, the actives sites for the main reaction are also active for the poison chemisorption, and the interactions need to be considered. The chemisorption of the poison can be treated by the mathematical methods used in adsorption, ion exchange, or chromatography. Several results based on various assumptions concerning the chemisorption, diffusion, and deactivation or poisoning effects on the main catalytic reaction will be described. Within the context of the assumptions, these results give a rational form for the function expressing the deactivation in the case of poisoning, and also valuable clues for possible functions to use for coking, about which less is known quantitatively.

5.2.2 Kinetics of Uniform Poisoning

An early analysis by Wheeler [1955] treated poisoning in an idealized pore, and this analysis can be generalized to a catalyst particle as is shown in Chapter 3. Fundamental to this development, and the others of this section, is the assumption that the catalytic site that has adsorbed poison on it is completely inactive. If C_{Pl} is the concentration of sites covered with poison, the fraction of sites remaining active, called the deactivation or activity function, is represented by

$$\Phi = \frac{C_t - C_{Pl}}{C_t} \tag{5.2.2-1}$$

This deactivation function is based on the presumed chemical events occurring on the active sites, and can be related to various chemisorption theories. The overall observed activity changes of a catalyst pellet can also be influenced by diffusional effects, but the deactivation function utilized here will refer only to the deactivation chemistry, to which these other effects can then be added.

C_{Pl} is not normally measured, so that it must be expressed in terms of the poison concentration C_{Ps} in the gas phase inside the catalyst. Wheeler used a linear relation,

$$C_{Pl} = \sigma_P C_{Ps} \tag{5.2.2-2}$$

that can be a reasonable approximation over an appreciable fraction of the total saturation level. Since the rate coefficient of the reaction, k_{rA}, is proportional to the number of available active sites, its value at the poison level C_{Ps} is given by

$$k_{rA} = k_{rA}^0\left(1-\sigma_P\frac{C_{Ps}}{C_t}\right) = k_{rA}^0\left(1-\sigma C_{Ps}\right) = \Phi k_{rA}^0 \qquad (5.2.2\text{-}3)$$

and the activity decreases linearly with the poison concentration.

Consider now the case whereby diffusion limitations are influencing the main reaction inside the pore and let the reaction be of first order. At the uniform poison level C_{Ps},

$$r_A = \eta k_{rA} C_A \qquad (5.2.2\text{-}4)$$

$$= \frac{1}{\phi}[\coth(3\phi) - \frac{1}{3\phi}]k_{rA}C_A \qquad (5.2.2\text{-}5)$$

where, as usual,

$$\phi = \frac{R}{3}\sqrt{\frac{k_{rA}\rho_s}{D_{eA}}} \qquad (5.2.2\text{-}6)$$

Substituting k_{rA} in (5.2.2-5) and (5.2.2-6) by its value given by (5.2.2-3), so as to account for the effect of the poison, yields the rate in the form

$$r_A = \frac{\coth(3\phi^0\sqrt{1-\sigma C_{Ps}}) - \dfrac{1}{3\phi^0\sqrt{1-\sigma C_{Ps}}}}{\phi^0\sqrt{1-\sigma C_{Ps}}}(1-\sigma C_{Ps})k_{rA}^0 C_A \qquad (5.2.2\text{-}7)$$

The ratio of this rate to that at zero poison level, taken at identical C_A values, can be written

$$\frac{r_A}{r_A^0} = \frac{3\phi^0\sqrt{1-\sigma C_{Ps}}\coth(3\phi^0\sqrt{1-\sigma C_{Ps}}) - 1}{3\phi^0\coth(3\phi^0) - 1} \qquad (5.2.2\text{-}8)$$

Two limiting cases are of interest. For virtually no diffusion limitations to the main reaction, $\phi^0 \to 0$ and

$$\frac{r_A}{r_A^0} \to 1-\sigma C_{Ps} \qquad (5.2.2\text{-}9)$$

so that this ratio is just the deactivation function as defined by (5.2.2-3). The opposite extreme of strong diffusion limitation, $\phi^0 \to \infty$, leads to a distorted version of the true deactivation function:

$$\frac{r_A}{r_A^0} \rightarrow \sqrt{1-\sigma C_{Ps}} \qquad (5.2.2\text{-}10)$$

Notice also that in this case r_A / r_A^0 decreases less rapidly with C_{Ps}, owing to a better utilization of the catalyst surface as the reaction is more poisoned.

5.2.3 Shell-Progressive Poisoning

A similar model that specifically considers the poison deposition in a catalyst pellet was presented by Olson [1968] and by Carberry and Gorring [1966]. Here, the poison deposition leads to a moving boundary of a poisoned shell surrounding an unpoisoned core. Models of this type are also often used for non catalytic heterogeneous reactions, as discussed in detail in Chapter 4. The pseudo steady-state assumption is made that the boundary moves rather slowly compared to the poison diffusion or reaction rates. Then, steady-state diffusion results can be used for the shell, and the total mass transfer resistance consists of the usual external interfacial, pore diffusion, and boundary chemical reaction steps in series.

The mathematical statement of the rate of poison deposition is as follows:

$$\frac{4}{3}\pi R^3 r_P \rho_s = \frac{d}{dt}[C_{Pl\infty}\frac{4}{3}\pi(R^3 - r_c^3)]\rho_s \qquad (5.2.3\text{-}1)$$

$$= 4\pi R^2 k_{gP}(C_p - C_{Ps}^s)\rho_s / \varepsilon_s \qquad \text{(external interfacial step)} \qquad (5.2.3\text{-}2)$$

$$= \frac{4\pi D_{eP}}{\left(\frac{1}{r_c} - \frac{1}{R}\right)}(C_{Ps}^s - C_{Ps}^c)\frac{\rho_s}{\varepsilon_s} \qquad \text{(steady diffusion through a spherical shell)} \qquad (5.2.3\text{-}3)$$

$$= 4\pi r_c^2 k'_{sP}\sigma_P C_{Ps}^c / S_c$$
$$= 4\pi r_c^2 k_{sP} C_{Ps}^c / S_c \qquad \text{(deposition rate at boundary)} \qquad (5.2.3\text{-}4)$$

where R = radius of particle; r_c = radius of unpoisoned core; C_P, C_{Ps}^s, C_{Ps}^c = bulk fluid, solid surface, core boundary concentrations, respectively, of poison; $C_{Pl\infty}$ = solid concentration of poison at saturation; k_{gP} = external interfacial mass transfer coefficient; k'_{sP} = core surface reaction rate coefficient for poison; D_{eP} = effective pore diffusivity of poison; σ_P = sorption distribution coefficient;

and S_c = surface area of core per unit particle volume. The pellet average poison concentration can be represented by $\langle C_{Pl} \rangle$, and is related to the unpoisoned core radius by

$$\frac{\langle C_{Pl} \rangle}{C_{Pl\infty}} = 1 - \left(\frac{r_c}{R} \right)^3 = 1 - \xi^3 \tag{5.2.3-5}$$

If the intermediate concentrations C_{Ps}^s and C_{Ps}^c are eliminated in the usual way from (5.2.3-1) through (5.2.3-4), one obtains

$$\frac{d}{dt'} \left(\frac{\langle C_{Pl} \rangle}{C_{Pl\infty}} \right) = \frac{N_s C_P / C_{P,ref}}{\frac{1}{Sh_P'} + \frac{1-\xi}{\xi} + \frac{1}{Da\,\xi^2}} \tag{5.2.3-6}$$

where the dimensionless groups are

$Sh'_P = k_{gP} R/D_{eP}$ = modified Sherwood number for poison;

$Da = k_{sP} R/D_{eP}$ = Damköhler number;

$N_s = 3D_{eP} t_{ref} C_{P,ref} / R^2 \rho_s C_{Pl\infty}$;

$t' = t/t_{ref}$.

The reference time t_{ref} and the concentration $C_{P,ref}$ are chosen for a specific application (e.g., in a flow reactor, the mean residence time and feed concentration, respectively). Equation (5.2.3-6) now permits a solution for the amount of poison, $\langle C_{Pl} \rangle / C_{Pl\infty}$, to be obtained as a function of the bulk concentration C_P and the physicochemical parameters. In a packed bed tubular reactor, C_P varies along the longitudinal direction. Equation (5.2.3-6) would then be a partial differential equation coupled to the flowing fluid-phase mass balance equation—these applications are considered in Chapter 11.

Equation (5.2.3-6) can easily be solved for the case of C_P = constant:

$$N_s \frac{C_P}{C_{P,ref}} t' = \int_0^{(\langle C_{Pl} \rangle / C_{Pl\infty})} \left[\frac{1}{Sh_P'} + \frac{1-(1-x)^{1/3}}{(1-x)^{1/3}} + \frac{1}{Da(1-x)^{2/3}} \right] dx$$

$$= \left(\frac{1}{Sh_P'} - 1 \right) \left(\frac{\langle C_{Pl} \rangle}{C_{Pl\infty}} \right) - \frac{3}{2} \left[1 - \left(\frac{\langle C_{Pl} \rangle}{C_{Pl\infty}} \right)^{2/3} \right]$$

$$+\frac{3}{2}-\frac{3}{Da}\left[1-\left(\frac{\langle C_{Pl}\rangle}{C_{Pl\infty}}\right)\right]^{1/3}+\frac{3}{Da} \qquad (5.2.3\text{-}7)$$

This is an implicit equation for $\langle C_{Pl}\rangle / C_{Pl\infty}$, which is represented in Fig. 5.2.3-1. These results can be used to predict the poison deposition as a function of time and the physiochemical parameters.

Now that the poison concentration is known, its effect on the chemical reaction must be derived. Again, this is based on the assumption that the poisoned shell is completely inactive so that, for a first-order reaction occurring only in the unpoisoned core of the catalyst, the mathematical model becomes:

$$D'_{eA}\frac{1}{r^2}\frac{d}{dr}\left(r^2\frac{dC'_{As}}{dr}\right)=0 \qquad r_c < r \le R \qquad (5.2.3\text{-}8)$$

$$D_{eA}\frac{1}{r^2}\frac{d}{dr}\left(r^2\frac{dC_{As}}{dr}\right)=k_{rA}\rho_s C_{As} \qquad 0 < r < r_c \qquad (5.2.3\text{-}9)$$

where

D'_{eA} = effective diffusivity of A in poisoned shell;
D_{eA} = effective diffusivity of A in unpoisoned core;
k_{rA} = rate coefficient for the chemical reaction.

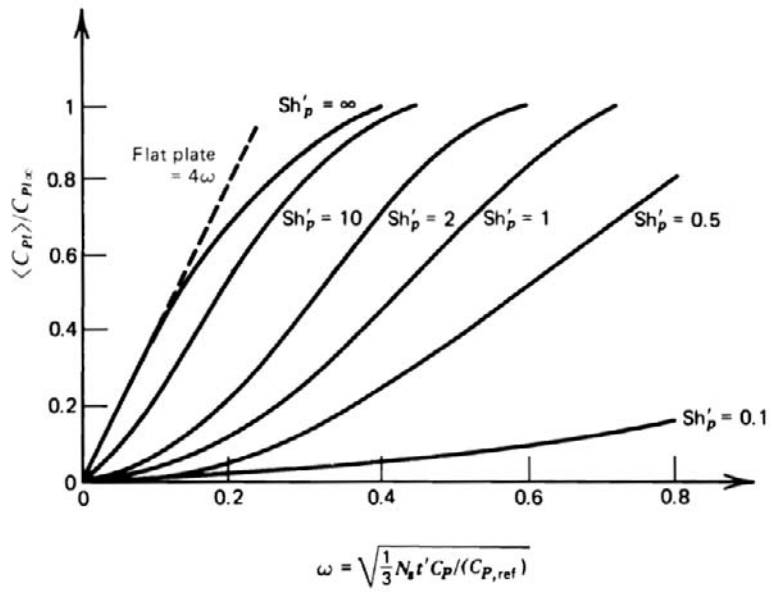

Figure 5.2.3-1

Fraction of spherical catalyst pellet poisoned versus dimensionless time. Da = ∞, meaning infinite interfacial mass transfer coefficient for the poison. After Carberry and Gorring [1966].

The boundary conditions are

$$D'_{eA}\frac{dC'_{As}}{dr} = k_{gA}(C_A - C^s_{As}) \qquad r = R \qquad (5.2.3\text{-}10a)$$

$$C_{As} = C'_{As} \text{ and } D_{eA}\frac{dC_{As}}{dr} = D'_{eA}\frac{dC'_{As}}{dr} \qquad r = r_c \qquad (5.2.3\text{-}10b)$$

$$C_{As} = \text{finite value} \qquad r = 0 \qquad (5.2.3\text{-}10c)$$

These equations are again based on a pseudo steady-state approximation so that intrinsically the deactivation rate must be much slower than the diffusion or chemical reaction rates. The equations can be easily solved, as in Chapter 3, and the result substituted into the definition of the effectiveness factor, with the following results:

$$\eta\left(\frac{\langle C_{Pl}\rangle}{C_{Pl\infty}}\right) = \frac{4\pi R^2 D'_{eA}\left.\frac{dC'_{As}}{dr}\right|_{r=R}}{\frac{4}{3}\pi R^3 k_{rA}\rho_s C_A}$$

$$\eta\left(\frac{\langle C_{Pl}\rangle}{C_{Pl\infty}}\right) = \frac{1/3(\phi''_2)^2}{\frac{1}{Sh'_A} + \frac{1-\xi}{\xi} + \left(\frac{\phi''}{\phi''_2}\right)^2 \frac{1}{\xi[(3\phi''\xi)\coth(3\phi''\xi) - 1]}} \qquad (5.2.3\text{-}11)$$

$$= \frac{1/3\phi''^2}{\frac{1}{Sh'_A} + \frac{1-\xi}{\xi} + \frac{1}{\xi[(3\phi''\xi)\coth(3\phi''\xi) - 1]}} \qquad (5.2.3\text{-}12)$$

The latter result is true for $D'_{eA} = D_{eA}$, and so $\phi''_2 = \phi''$. Also, the dimensionless parameters are

$$\xi = \frac{r_c}{R} = \left[1 - \left(\frac{\langle C_{Pl}\rangle}{C_{Pl\infty}}\right)\right]^{1/3}$$

$$Sh'_A = \frac{k_{gA}R}{D'_{eA}} \quad = \text{modified Sherwood number for component } A$$

$$\phi'' = \frac{R}{3}\sqrt{k_{rA}\rho_s / D_{eA}} \quad = \text{modulus}$$

$$\phi_2'' = \frac{R}{3}\sqrt{k_{rA}\rho_s / D_{eA}'} \quad = \text{modulus}$$

Finally, the ratio of the rate at a poison level $\langle C_{Pl} \rangle$ to that at zero poison content, taken at identical C_A values, is given by:

$$\frac{r_A}{r_A^0} = \frac{\mu\left(\dfrac{\langle C_{Pl} \rangle}{C_{Pl\infty}}\right)}{\eta(0)} \tag{5.2.3-13}$$

where $\eta(0)$ is the effectiveness factor for the unpoisoned catalyst. It can be obtained from (5.2.3.-11) or (5.2.3-12) with $\langle C_{Pl} \rangle$ = 0. The limiting form of r_A / r_A^0 for $\phi \to 0$ is

$$\frac{r_A}{r_A^0} = \xi^3 = 1 - \left[\frac{\langle C_{Pl} \rangle}{C_{Pl\infty}}\right]$$

This is the deactivation function for the shell-progressive model.

To summarize, (5.2.3-13) is an equation for the ratio of the rate in the presence of poisoning to that without poisoning, in terms of the physicochemical parameters of the reaction and of the amount of poison ($\langle C_{Pl} \rangle / C_{Pl\infty}$). The latter is found from (5.2.3-6) with the poisoning physicochemical parameters and the fluid-phase bulk concentration C_P taken at a point in the reactor.

The ratios of rates, r_A / r_A^0, from Sections 5.2.2 and 5.2.3 are illustrated in Fig 5.2.3-2. The pore mouth poisoning model gives a very rapid decline, especially for strong diffusion limitations. Balder and Petersen [1968] presented an interesting experimental technique which permits both the decrease in overall reaction rate and the center line reactant concentration in a single particle to be measured. The results of the above models can be re-plotted as r_A / r_A^0 versus the center line concentration by algebraically eliminating the $\langle C_{Pl} \rangle / C_{Pl\infty}$. Thus, the poisoning phenomena can be studied without detailed knowledge of the poison concentrations.

Ray [1972] has considered the case of a nonisothermal particle, which could show instability in a certain narrow range of conditions.

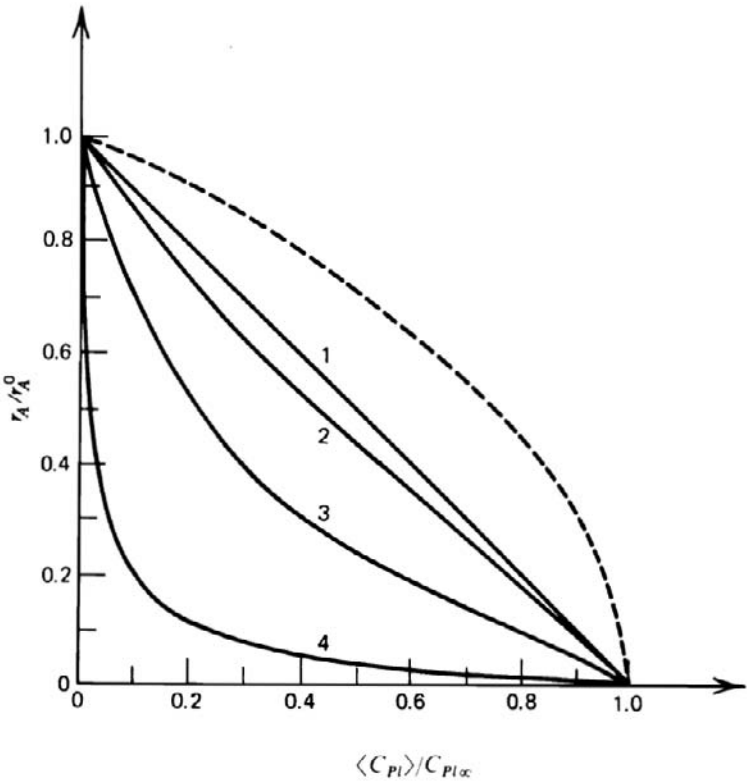

Figure 5.2.3-2

r_A/r^0_A in terms of amount of poison for uniform [Eq. (5.2.2-10)] and shell-progressive [Eq. (5.2.3-13)] models. $Sh'_A \rightarrow \infty$.

---- : uniform poisoning with diffusional limitations on main reaction;

—— : shell progressive;

curve 1 : $\phi'' = 0$, $\eta(0) = 1$;

curve 2 : $\phi'' = 3$, $\eta(0) = 0.67$;

curve 3 : $\phi'' = 10$, $\eta(0) = 0.27$;

curve 4 : $\phi'' = 100$, $\eta(0) = 0.03$.

5.2.4 Effect of Shell-Progressive Poisoning on the Selectivity of Simultaneous Reactions

Sada and Wen [1967] extended these catalyst poisoning models to sets of simultaneous reactions. The poison deposition was described as in (5.2.3-7), but for very rapid poisoning, $D_a \rightarrow \infty$. The results were expressed in terms of the dimensionless position of the poison boundary, $\xi = r_c / R$. The profiles are described by

$$N_s \frac{C_P}{C_{P,ref}} t' = 3(1-\xi)\left(\frac{1-\xi}{2} + \frac{1}{Sh'_P}\right) \qquad \text{(slab)} \qquad (5.2.4\text{-}1)$$

$$= \frac{1}{2}(1-\xi)^2(1+2\xi) + \frac{1-\xi^3}{Sh'_p} \quad \text{(sphere)} \qquad (5.2.4\text{-}2)$$

The three basic selectivity problems were solved for various cases of one or both reactions poisoned. Only a brief selection of results will be presented here.

For independent simultaneous first-order reactions,

$$A \xrightarrow{1} R$$

$$B \xrightarrow{2} S$$

The model equations for diffusion and reaction are

In the poisoned shell:

$$D_{eA}\nabla^2 C'_{As} = 0$$

$$D_{eB}\nabla^2 C'_{Bs} = k_2 \rho_s C'_{Bs} \quad \text{(when reaction 2 is not poisoned)}$$

$$= 0 \qquad \text{(when reaction 2 is poisoned)}$$

In the reactive core:

$$D_{eA}\nabla^2 C_{As} = k_1 \rho_s C_{As} = -D_{eR}\nabla^2 C_{Rs}$$

$$D_{eB}\nabla^2 C_{Bs} = -D_{eS}\nabla^2 C_{Ss}$$

At the poison boundary

$$C_{is} = C'_{is} \qquad \nabla C_{is} = \nabla C'_{is}$$

These conditions are used together with the usual ones for the external surface and center of the pellet. The effective diffusivities have been assumed to be constant and also equal in both the shell and core regions. The solutions of these equations are then substituted into the definition of the selectivity, with the following results:

$$\left(\frac{r_R}{r_S}\right)_{bulk} = \left.\frac{D_{eR}\nabla C'_{Rs}}{D_{eS}\nabla C'_{Ss}}\right|_{surface}$$

$$= \left(\frac{C_A D_{eA}}{C_B D_{eB}}\right) \frac{\dfrac{1}{\phi_2 \tanh \phi_2} + \dfrac{1}{Sh'_B}}{\dfrac{1}{\phi_1 \tanh(\phi_1 \xi)} + (1-\xi) + \dfrac{1}{Sh'_A}} \qquad (5.2.4\text{-}3)$$

for an infinite slab and for only reaction 1 being poisoned, and

$$\left(\frac{r_R}{r_S}\right)_{bulk} = \left(\frac{C_A D_{eA}}{C_B D_{eB}}\right) \frac{\dfrac{1}{\phi_2 \tanh(\phi_2 \xi)} + (1-\xi)\dfrac{1}{Sh_B'}}{\dfrac{1}{\phi_1 \tanh(\phi_1 \xi)} + (1-\xi) + \dfrac{1}{Sh_A'}} \qquad (5.2.4\text{-}4)$$

when both reactions are poisoned. (Sada and Wen also present solutions for infinite cylinders and for spheres.) In (5.2-4-3) and (5.2.4-4)

$$\phi_1 = L\sqrt{k_1 \rho_s / D_{eA}} \qquad \phi_2 = L\sqrt{k_2 \rho_s / D_{eB}}$$

An example of the results from (5.2.4-3) is shown in Fig. 5.2.4-1.

From (5.2.4-3), for $\phi \to 0$ (and $Sh' \to \infty$),

$$\left(\frac{r_R}{r_S}\right)_{bulk} \approx \left(\frac{C_A k_1}{C_B k_2}\right)\xi$$

which shows that the selectivity is proportional to the unpoisoned fraction of the

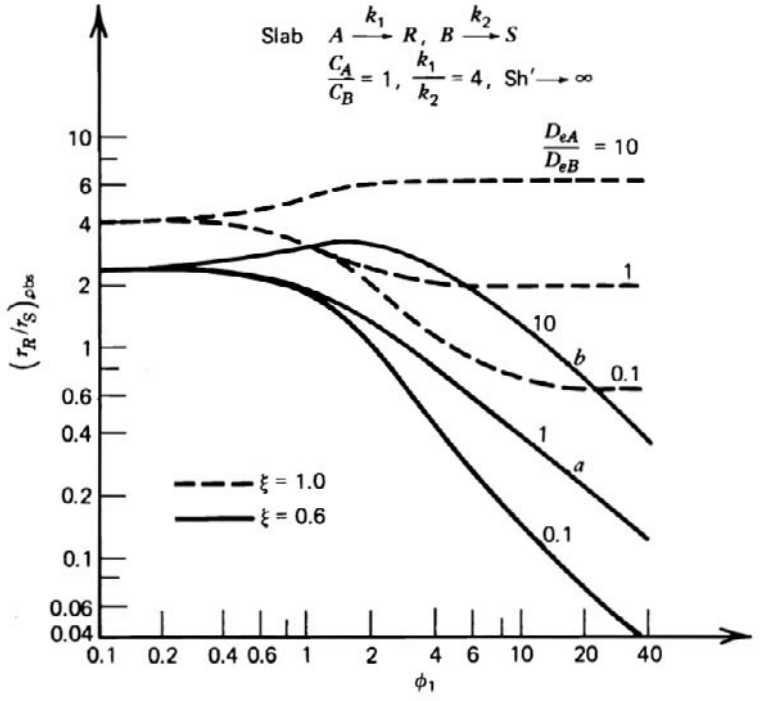

Figure 5.2.4-1

Selectivity as a function of the Thiele modulus ϕ, for independent reactions indicating two types of variations (*a* and *b*). From Sada and Wen [1967].

catalyst volume. Whether the selectivity curve has a maximum or not depends on the values of ξ, ϕ, and $\sqrt{k_{rB}D_{eA}/k_{rA}D_{eB}}$. In the asymptotic region, where $\phi \to \infty$,

$$\left(\frac{r_R}{r_S}\right)_{bulk} \approx \frac{C_A}{C_B}\sqrt{\frac{k_1 D_{eA}}{k_2 D_{eB}}}\frac{1}{1+\phi_1(1-\xi)} \qquad \phi_1 >> 1$$

Again a square root dependency is the dominant factor, as discussed in Chapter 3, but the catalyst poisoning is an additional effect.

For consecutive first-order reactions,

$$A \xrightarrow{1} R \xrightarrow{2} S$$

the solutions of the appropriate equations for diffusion and reaction are used to obtain the selectivity:

$$\left(\frac{r_R}{r_S}\right)_{bulk} = \left.\frac{D_{eR}\nabla C_R}{D_{eS}\nabla C_S}\right|_{surface}$$

$$= \left[\xi\left(\frac{\phi_2}{\phi_1} - \frac{\phi_1}{\phi_2}\right) - 1\right]^{-1} \tag{5.2.4-5}$$

where

$$\varepsilon = \frac{\left[1 - \frac{1}{Sh_B'}\phi_2 \tanh\phi_2\right]\tanh(\phi_1\xi)\cosh\phi_2}{\tanh(\phi_2\xi) - \frac{\phi_1}{\phi_2}\tanh(\phi_1\xi) - \theta} \tag{5.2.4-6}$$

$$\theta = \frac{C_R}{C_A}\frac{\frac{k_1\rho_s}{D_{eA}} - \frac{k_2\rho_s}{D_{eR}}}{\frac{k_1\rho_s}{D_{eR}}}\sinh\phi_2\left\{1 + \phi_1\left[(1-\xi) + \frac{1}{Sh_A'}\right]\tanh(\phi_1\xi)\right\}$$

for only reaction 1 poisoned, and

$$\varepsilon = \frac{\left\{1 + \left[1 - \xi + \frac{1}{Sh_B'}\right]\phi_2 \tanh(\phi_2\xi)\right\}\tanh(\phi_1\xi)}{\tanh(\phi_2\xi) - \frac{\phi_1}{\phi_2}\tanh(\phi_1\xi) + \theta} \tag{5.2.4-7}$$

$$\theta = \frac{C_R}{C_A} \frac{\dfrac{k_1}{D_{eA}} - \dfrac{k_2}{D_{eR}}}{\dfrac{k_1}{D_{eR}}} \tanh(\phi_2 \xi) \left\{ 1 + \left[(1-\xi) + \frac{1}{Sh_A^{'}} \right] \phi_1 \tanh(\phi_1 \xi) \right\}$$

for both reactions poisoned.

Finally, the case of first-order parallel reactions was considered:

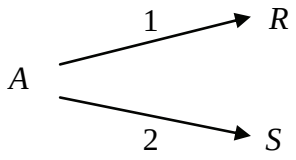

The results were:

$$\left(\frac{r_R}{r_S} \right)_{bulk} = \left. \frac{D_{eR} \nabla C_R}{D_{eS} \nabla C_S} \right|_{surface}$$

$$= \left[\left(1 + \frac{k_2}{k_1} \right) \varepsilon' - 1 \right]^{-1} \qquad (5.2.4\text{-}8)$$

where

$$\varepsilon' = \cosh \phi_1 (1-\xi) + \frac{\phi_2^{'} \sinh \phi_2^{'} (1-\xi)}{\phi_{12} \tanh(\phi_{12} \xi)} \qquad (5.2.4\text{-}9)$$

when only reaction 1 is poisoned, and

$$\varepsilon' = 1 \qquad (5.2.4\text{-}10)$$

when both reactions are poisoned. In (5.2.4-9)

$$\phi_2^{'} = L \sqrt{k_2 \rho_s / D_{eA}} \qquad \phi_{12} = L \sqrt{(k_2 + k_1) \rho_s / D_{eA}}$$

The results of (5.2.4-10) illustrate the obvious result that when both first-order parallel reactions are equally poisoned, the selectivity is not affected, although the conversion of *A* would be. The more interesting case of non-first-order parallel reactions would be much more difficult to solve.

Figure 5.2.4-2 illustrates the results for several types of poisoning. Many other combinations are possible, but the method of analyzing these problems should now be clear.

Sahimi and Tsotsis [1985] have simulated catalyst deactivation by poisoning in structure models of catalysts, discussed in Chapter 3.

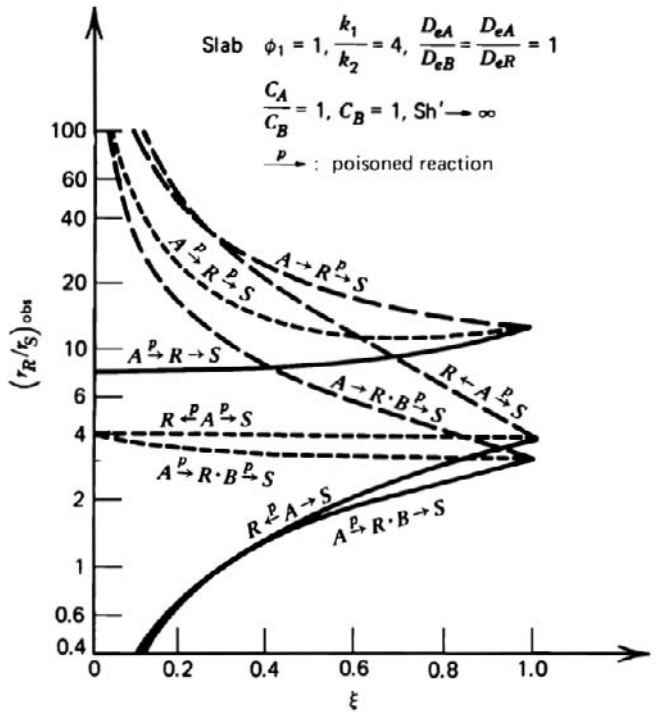

Figure 5.2.4-2

Selectivities in multiple reactions for three types of poisoning. From Sada and Wen [1967].

5.3 KINETICS OF CATALYST DEACTIVATION BY COKE FORMATION

5.3.1 Introduction

Many petroleum refining and petrochemical processes, such as the catalytic cracking of gasoil, catalytic reforming of naphtha, and dehydrogenation of ethylbenzene and butene are accompanied by undesired side reactions leading to the formation of carbonaceous deposits, which are strongly or irreversibly adsorbed on the active sites. These deposits can be high molecular weight species produced e.g., by the polymerization of olefins or by alkylation steps leading to multiring aromatics.They are commonly — but not quite appropriately — called “coke” because their amount is generally determined at higher temperatures by controlled combustion. Appleby, Gibson, and Good [1962] made a detailed study of the coking tendency of various aromatics on silica/alumina catalysts. Figure 5.3.1-1 shows some of their results. The roles of acidity and pore structure of zeolite catalysts is discussed by Guisnet et al. [1997]. The “coke”, or rather the deactivating agent, causes a decrease in activity of the catalyst, which is reflected

in a drop of conversion to the product(s) of interest. To maintain the production rates within the desired limits, the catalyst has to be regenerated, intermittently or, preferably, continuously. Around 1940, entirely new techniques, such as fluidized or moving bed operation, were developed for the purpose of continuous catalyst regeneration.

In what follows, the effect of coking on the rates of reaction is expressed quantitatively. Generally only empirical correlations have been used for this purpose. What is needed, however, for a rational design accounting for the effect of the catalyst deactivating agent on the reactor behavior, is a quantitative formulation of its rate of formation. Such a kinetic equation is by no means easy to develop.

The empirical Voorhies correlation [1945] for coking in the catalytic cracking of gasoil,

$$C_C = At^n \qquad \text{with} \qquad 0.5 < n < 1 \tag{5.3.1-1}$$

has been widely accepted and generalized beyond the scope of the original

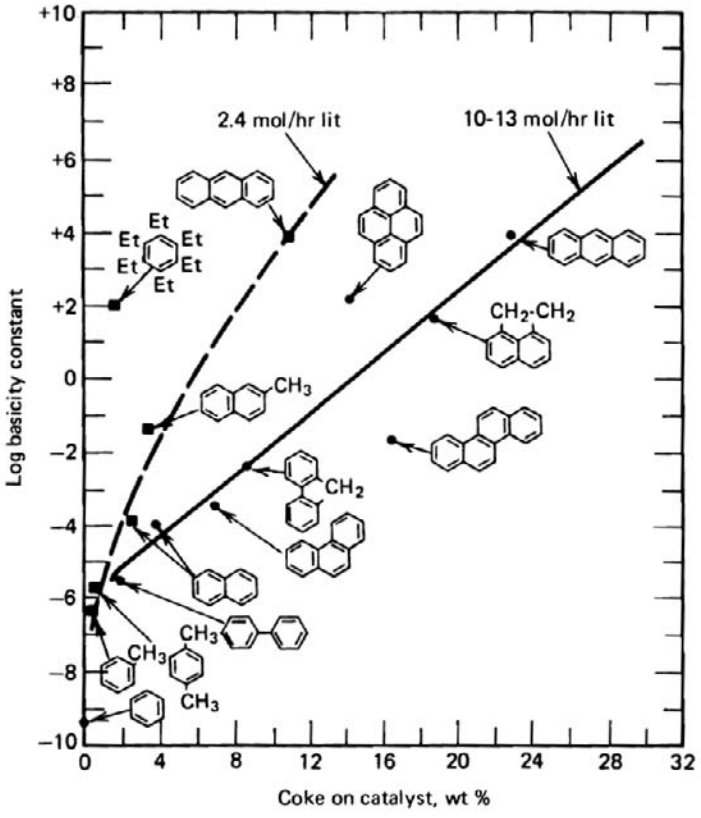

Figure 5.3.1-1

Coke formation in catalytic cracking from hydrocarbons with different basicity. From Appleby et al. [1962].

contribution. Yet, such an equation completely ignores the origin of the deactivating agent called coke. Obviously, coke is formed from the reaction mixture itself, so that it must result in some way or other from the reactants, the products or some intermediates. Therefore, the rate of coking must depend on the composition of the reaction mixture, the temperature, and the catalyst activity and it is not justified to treat its rate of formation separately from that of the main reaction. Froment and Bischoff [1961, 1962] were the first to relate these variables quantitatively to the rate of coking and to draw the conclusions from it as far as kinetics and reactor behavior are concerned. They considered the coke to be formed either by a reaction path parallel to the main reaction

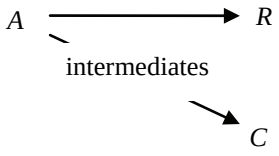

(5.3.1-2)

or by a reaction path consecutive to the main:

$$A \rightarrow R\text{—intermediates} \rightarrow C \qquad (5.3.1\text{-}3)$$

In certain more complex processes the coke formation may also belong to the above basic schemes. Consider the isomerization of *n*-pentane on a dual function catalyst:

$$nC_5 \overset{Pt}{\rightleftarrows} nC_5^{=} \overset{Al_2O_3}{\rightleftarrows} iC_5^{=} \overset{Pt}{\rightleftarrows} iC_5$$

Hosten and Froment [1971] and De Pauw and Froment [1975] showed that the rate-determining step for this reaction carried out on a catalyst with a high platinum content is the adsorption of *n*-pentene. In this case, any carbon formation starting from a component situated in this scheme before the rate-determining step would give rise to a characteristic behavior analogous to the parallel scheme given above, even if this component is not the feed component itself. Any coking originating from a component situated in the reaction sequence after the rate-determining step could be considered to occur according to the consecutive scheme given above, as if the coke were formed from the reaction product. Indeed, in this case all the components formed after the rate-determining step are in quasi-equilibrium with the final product.

5.3.2 Kinetics of Coke Formation

5.3.2.1 Deactivation Functions

An obvious way of expressing the deactivation of a catalyst by coke formation in a constant environment is the ratio of fluxes of the reactant *A*

$$\frac{N_A(t \text{ or } C_C)}{N_A(t \text{ or } C_C = 0)}$$

Only when there are no diffusion limitations will this ratio of fluxes equal the ratio of chemical reaction rates r_A / r_A^0, represented in what follows by Φ_A, the deactivation (or activity) function. The coke formation itself may also be subject to deactivation, expressed as

$$\frac{\frac{dC_C}{dt}(t \text{ or } C_C)}{\frac{dC_C}{dt}(t \text{ or } C_C = 0)}$$

The deactivation function for the coking reaction in the absence of diffusion limitations can be written

$$\Phi_C = \frac{r_C}{r_C^0}$$

Only recently has a rather general and rigorous approach been developed relating these observations to the characteristic features of the reactions and of the catalyst. These developments are reviewed in the following sections, without entering into the mathematical details. Situations with increasing complexity will be dealt with: coke formation on sites only, and on sites located in pores or in networks of pores, with or without diffusion limitations. When only sites are considered, the deactivation functions will be written φ, for a number of sites in a pore $\hat{\varphi}$, and for a particle Φ. Experimental values, deduced from measurements on particles or beds of particles, will be represented by Φ.

5.3.2.2 Catalyst Deactivation by Site Coverage Only

Consider a simple reaction $A \rightleftarrows B$ with the conversion of adsorbed *A* into adsorbed *B* on a single site as the rate-determining step. The steps may be written

$$A + l \rightleftarrows Al \quad \text{with} \quad C_{Al} = K_A C_A C_l \qquad (5.3.2.2\text{-}1)$$

$$Al \rightarrow Bl \qquad (5.3.2.2\text{-}2)$$

$$Bl \rightleftarrows B + l \quad \text{with} \quad C_{Bl} = K_B C_B C_l \tag{5.3.2.2-3}$$

With (5.3.2.2-2) as the rate-determining step the rate on a given site can be written:

$$r_A = k_{sr}\left(C_{Al} - \frac{C_{Bl}}{K_{sr}}\right)$$

or, accounting for (5.3.2.2-1) and (5.3.2.2-3)

$$r_A = -\frac{dC_A}{dt} = k_{sr} K_A C_l \left(C_A - \frac{C_B}{K}\right) \tag{5.3.2.2-4}$$

It was shown in Chapter 2 that C_l can be eliminated by means of a site balance and (5.3.2.2-1) and (5.3.2.2-3).

Suppose now some species C is irreversibly adsorbed on the active site and competes with A and B for their occupation:

$$C + l \rightleftarrows Cl \tag{5.3.2.2-5}$$

so that the site balance now includes C_l :

$$C_t = C_l + C_{Al} + C_{Bl} + C_{Cl} \tag{5.3.2.2-6}$$

Let the deactivating agent C be formed out of Al by a reaction parallel to the main reaction. For first order kinetics its rate of formation can be written

$$r_C = \frac{dC_{Cl}}{dt} = k_C C_{Al} \tag{5.3.2.2-7}$$

Integrating (5.3.2.2-4) and (5.3.2.2-7) simultaneously for a given C_A, while accounting for (5.3.2.2-6), leads to equations for C_B and C_C as a function of time that reflect the deactivation. The problem is the rate equation (5.3.2.2-7) for the formation of the deactivating agent. The latter is normally not really identified and its concentration on the catalyst is measured as coke by means of combustion. This implies there is no unambiguous measure of the site coverage.

There is one very recent example of application of the rigorous approach outlined here. It deals with the deactivation in the solid acid alkylation process for the production of high octane gasoline [Martinis and Froment, 2006]. The kinetic modeling of the reaction between 1-butene and *i*-butane on a Y-zeolite catalyst was expressed in terms of elementary steps and the kinetics were written in terms of single events, discussed in Chapters 1 and 2. It was found that the

deactivation was caused by the irreversible adsorption of product carbenium ions with nC higher than 8. The concentrations of these species covering the sites could not be measured, but they were obtained using the properties of the single event rate coefficients, mentioned in Chapter 2, namely the uniqueness of the single event frequency factor for a given type of elementary step and the possibility of calculating the activation energy by means of the Evans-Polanyi relationship. The number of single events is derived from the symmetry numbers of the reactant and the activated complex.

What has been done until now, however, is to take a less rigorous approach. Starting from (5.3.2.2-6) there are two possibilities to eliminate the inaccessible C_l from (5.3.2.2-4) and write the rate equations in terms of observables only. The first is to write (5.3.2.2-6) as follows

$$C_t = C_l\left(1 + K_A C_A + K_B C_B + \frac{C_{Cl}}{C_l}\right) \qquad (5.3.2.2\text{-}8)$$

where C_{Al} and C_{Bl} were eliminated by means of (5.3.2.2-1) and (5.3.2.2-3). Now (5.3.2.2-4) becomes

$$r_A = \frac{k_{sr} C_t K_A \left(C_A - \frac{C_B}{K}\right)}{1 + K_A C_A + K_B C_B + \frac{C_{Cl}}{C_l}} \qquad (5.3.2.2\text{-}9)$$

Since neither C_{Cl} nor C_l can be measured, some empirical relation for C_{Cl}/C_l has to be substituted into (5.3.2.2-8) to express the decline of r_A. The ratio C_{Cl}/C_l could be replaced by some function of a measurable quantity (e.g., coke) or of less direct factors such as the ratio of total amount of *A* fed to the amount of catalyst or even process time. This approach was followed in the early work of Johanson and Watson [1946] and Rudershausen and Watson [1954]. In the terminology of Szepe and Levenspiel [1971] it corresponds to “non separable deactivation”.

The second possibility is to write (5.3.2.2-6) as

$$C_t - C_{Cl} = C_l(1 + K_A C_A + K_B C_B) \qquad (5.3.2.2\text{-}10)$$

Substitution of C_l into (5.3.2.2-4) leads to

$$r_A = \frac{k_{sr} C_t K_A \varphi_A \left(C_A - \frac{C_B}{K}\right)}{1 + K_A C_A + K_B C_B} \qquad (5.3.2.2\text{-}11)$$

where $\varphi_A = (C_t - C_{Cl})/C_t$ is the fraction of active sites remaining active. In what follows it will be called the deactivation function. $k_{sr}C_t\varphi_A$ can be written as $k = k^0\varphi_A$ with k^0 the value of the rate coefficient of the main reaction in the absence of deactivation. Equation (5.3.2.2-11) is a more convenient equation to work with than (5.3.2.2-9). In Szepe and Levenspiel's terminology it corresponds to "separable deactivation". To date, there is no convincing experimental evidence for non separable deactivation by coke formation. Only strongly nonuniform surfaces lead to a true non separability, as calculated by Butt et al. [1978].

In the absence of insight into the chemistry of formation of the carbonaceous deposits and into the way and rate at which active sites are covered by the deactivating agent there is no other possibility than to relate φ_A empirically to the deactivation. The most direct measure of C_{Cl} and, therefore, of φ_A is the coke content of the catalyst, also written C_C. On the basis of experimental observations, Froment and Bischoff [1961, 1962] proposed the following forms:

$$\varphi_A = \exp(-\alpha C_C) \tag{5.3.2.2-12}$$

$$\varphi_A = \frac{1}{1+\alpha C_C}$$

The rate equation for the parallel coke formation (5.3.2.2-7) can be written:

$$r_C = \frac{dC_C}{dt} = k_C K_A C_A C_l \tag{5.3.2.2-13}$$

and, after elimination of C_{Al} using (5.3.2.2-1)

$$r_C = \frac{k_C^0 C_t K_A \varphi_C C_A}{1 + K_A C_A + K_B C_B} \tag{5.3.2.2-14}$$

with $\varphi_C = (C_t - C_{Cl})/C_t$ now a deactivation function for the coke formation, e.g., again an exponential or hyperbolic function of the coke content, but not necessarily identical to those for the main reaction, even when only one and the same type of active site is involved in the main and coking reactions. A different φ_C would result if the rate-determining step in the coking sequence would involve a number of active sites different from that in the main reaction or if the coking sequence would comprise more than one rate-determining step. If the coking would occur exclusively on completely different sites, it would only deactivate itself, of course. A unique deactivation function for both the main and the coking side reaction was experimentally observed by Dumez and Froment [1976] in butene dehydrogenation on chromia/alumina, to be discussed in Examples

5.3.3.A and 5.3.3.B. An example of a complex reaction, the catalytic cracking of gasoil, with more than one deactivation function will be discussed later in Example 5.3.3.C.

Note also that when the main reaction involves n_A sites, the deactivation function φ_A becomes

$$\varphi_A = \left(\frac{C_t - C_{Cl}}{C_t} \right)^{n_A} \tag{5.3.2.2-15}$$

and when the coking reaction involves n_C sites φ_C becomes

$$\varphi_C = \left(\frac{C_t - C_{Cl}}{C_t} \right)^{n_C} \tag{5.3.2.2-16}$$

at least if there is no limit on the available number of sites [for this restriction, see Nam and Froment, 1987].

If the deactivating agent would be formed from a reaction product (i.e., by a consecutive reaction),

$$Bl \rightleftarrows Cl$$

its rate of formation would be written

$$r_C = \frac{k_C^0 C_t K_B \varphi_C C_B}{1 + K_A C_A + K_B C_B} \tag{5.3.2.2-17}$$

Equations (5.3.2.2-9) or (5.3.2.2-11) for r_A and (5.3.2.2-14) or (5.3.2.2-17) for r_C form a set of simultaneous equations reflecting that the coking depends on the mechanism of coking and on the composition of the reaction mixture. Consequently, even under isothermal conditions, the coke is not uniformly deposited in a reactor or inside a catalyst particle whenever there are gradients in concentration of reactants and products. If the deactivation occurs by site coverage only, the coke profile will be descending in the pore or in the reactor from the inlet onward for parallel coking, but ascending for consecutive coking.

The approach followed in deactivation studies is often different from the one outlined here. The alternate approach does not consider a coking rate equation and uses an empirical time-related deactivation function for the particle or bed $\Phi = f(t)$ called "activity" [Szepe and Levenspiel, 1971; Wojchiechowski, 1968]. Linear, hyperbolic or exponential functions of time were used. Deriving the activity Φ with respect to time gives the corresponding rates of change of the activity and defines a so-called order of deactivation, from which it has been attempted to get some insight into the mechanism of deactivation—an attempt

doomed to fail if not coupled with direct information on the deactivating agent itself.

At first sight, using $\Phi = f(t)$ instead of $\Phi_C = f(C_C)$ would present a definite advantage. An equation like

$$r_A = \frac{k^0 K_A e^{-\alpha t}\left(C_A - \frac{C_B}{K}\right)}{1 + K_A C_A + K_B C_B}$$

which has to be compared with (5.3.2.2-9), expresses r_A directly in terms of time and therefore suffices in itself to predict the deactivation at any process time. The approach favored here introduces a separate Φ_C based on the coke content of the catalyst and leads to an equation for r_A containing the coke content, not time. Consequently, the latter approach requires an additional rate equation for the coke formation to introduce process time. Furthermore, the deactivation function with respect to time is definitively easier to arrive at than the one with respect to coke. However, using only one deactivation function and relating it directly to time is far more restricted and presents several drawbacks.

First, it follows from the definition of φ_C and (5.3.2.2-11) that

$$-\frac{1}{C_t}\frac{dC_{Cl}}{dt} = \frac{d\varphi_C}{dt} = -\frac{k_C^0 K_A \varphi_C C_A}{1 + K_A C_A + K_B C_B}$$

so that

$$\varphi_C = \exp\left[-\int_0^t \frac{k_C K_A C_A}{1 + K_A C_A + K_B C_B} dt\right] \qquad (5.3.2.2\text{-}18)$$

It is obvious that φ_C cannot be a simple function of time, as generally assumed, except if the coke formation does not depend on the concentrations of the reacting species. Also, in $\Phi = f(\alpha, t)$, the "constant" α is really a function of the operating conditions determining the coke deposition, so that the application of $\Phi = f(t)$ is strictly limited to the conditions prevailing during its determination. With the approach favored here, α is a true constant related to the deactivating event itself, because the effect of the operating variables on the deactivation is explicitly accounted for through the coking rate equation.

Furthermore, when the coke content of the catalyst is not determined, only one deactivation function can be derived, from the decay with time of the main reaction. The model may then be biased. There is more, however. Since $\Phi = f(t)$ does not contain the coke content, which is related to the local concentration of the reacting species, it predicts a deactivation independent of concentration, that is, the approach predicts a uniform deactivation in a pellet or a

tubular reactor (for isothermal conditions, at least). In reality, non uniformity in deactivation, because of coke profiles, does occur in pellets (or tubular reactors), as will be shown in the next section. The consequences of neglecting coke profiles in kinetic studies, in catalyst regeneration, or in design calculations may be serious [Froment and Bischoff, 1961; 1962].

In real situations nonlinear relations are observed when φ_A and φ_C are plotted versus the coke content. A first explanation would be that more than one site is involved in the reactions, as is obvious from (5.3.2.2-12) and (5.3.2.2-13). For single-site mechanisms, other explanations than just site coverage have to be provided. One possible explanation is simultaneous site coverage and growth of coke, eventually leading to pore blockage. Also, when the coke grows on the sites that are already covered, $\varphi_A \neq \varphi_C$, except if all coke would have the same size.

5.3.2.3 Catalyst Deactivation by Site Coverage and Pore Blockage

Active sites are located in pores, and under certain circumstances the coke may grow to a size such that the pore is blocked. Sites between a blockage and the pore end or between two locations of blockage in a double-ended pore are no longer accessible and have to be considered as being deactivated. Because there is no preferential location for the coverage of a site and for the subsequent blockage of the pore, Beeckman and Froment [1979] used a probabilistic approach to formulate the rates of the phenomena. In these terms the deactivation function φ_A becomes the probability that a site is still active, *S*. But when blockage occurs, the probability that a site is accessible, *P*, has to be accounted for, so that the deactivation function now becomes

$$\varphi_A = PS$$

The deactivation function now depends upon structural aspects of the pores, for example, their diameter and also on their site densities. Beeckman and Froment [1979] first developed the theory for a rate of growth, $r_P^0 \geq \beta C_t M r_S^0$, where r_S^0 is the initial rate of fractional site coverage and β is the degree of polymerization of coke. In other words, the rate-determining step is the rate of site coverage. They assumed that the size of the coke in a pore depends in the first place upon the operating conditions, but also that it cannot exceed the pore diameter. Therefore, if the operating conditions are appropriate, all the coke has the same size—corresponding to the pore diameter—and φ_C is a measure of the site coverage. A single-ended pore gets blocked as soon as a coke precursor is formed on a site.

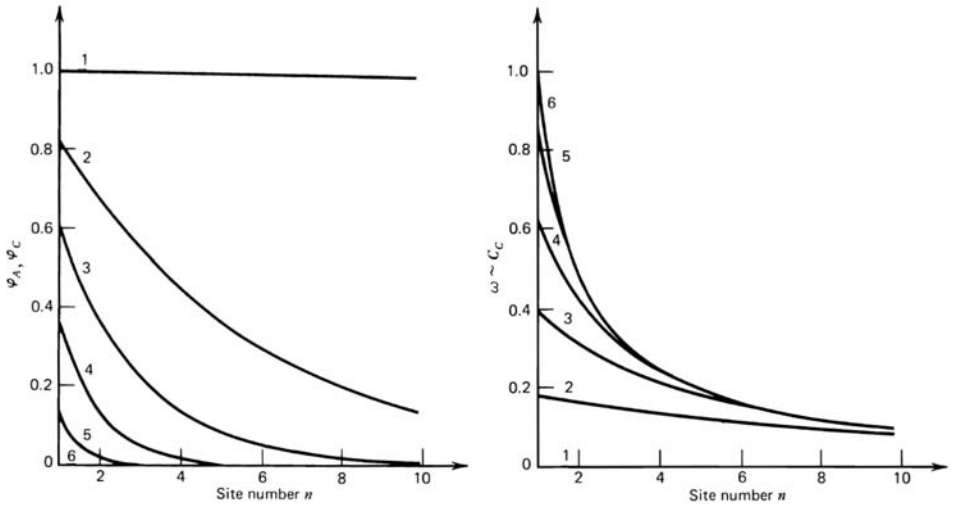

Figure 5.3.2.3-1a

Local value of deactivation function versus site number for a single-ended pore with a deterministic distribution of sites. Parameter $r^0_s t$: curve 1, 0; curve 2, 0.02; curve 3, 0.50; curve 4, 1.00; curve 5, 2.00; curve 6, ∞. From Beeckman and Froment [1979].

Figure 5.3.2.3-1b

Local value of coke content versus site number for a single-ended pore with a deterministic distribution of sites. Parameter $r^0_s t$ as in Fig. 5.3.2.3-1a.

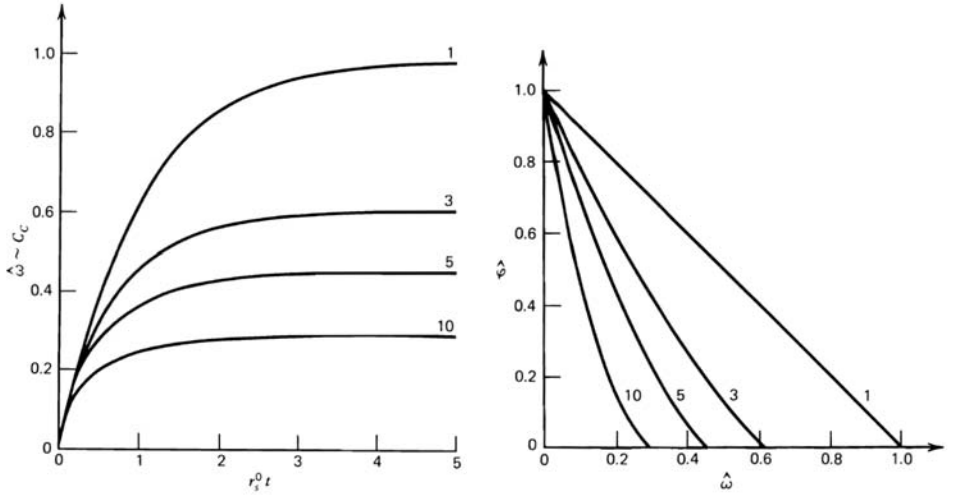

Figure 5.3.2.3-1c

Average coke content in the pore versus reduced time $r^0_s t$ for a single-ended pore with a deterministic distribution of sites. Parameter: Ns, number of sites in the pore.

Figure 5.3.2.3-1d

Global deactivation function versus global degree of coverage for a single-ended pore with a deterministic distribution of sites. Parameter, Ns as in Fig. 5.3.2.3-1c. From Beeckman and Froment [1979].

Blockage of the pore causes coke profiles, even when there are no concentration gradients of *A* and *B* in the pore, that is, when there are no diffusional limitations, as shown in Fig. 5.3.2.3-1.

The highest coke content is always located close to the pore mouth, as observed, for example, in the hydrodesulfurization of heavy oil fractions. When the main reaction and the coking occur on the same, single sites, $\varphi_A = \varphi_C$. When blockage occurs, φ is no longer a simple exponential function of time and concentrations, of the type shown in (5.3.2.2-18) for φ_C. An example of a curve $\hat{\varphi}$ versus $\hat{\omega}$ (or C_C) is shown in Fig. 5.3.2.3-1d.

In a more general theory [Beeckman and Froment, 1980], the potential rate of polymerization is considered to be of the same order of magnitude as the potential rate of site coverage. Two periods have to be distinguished: a first, ranging from $t = 0$ to $t = t_b$, the time required to reach a size sufficient to block the pore and during which only site coverage and growth occurs; and second, for $t > t_b$, during which blockage occurs and the site density determines the deactivation. This is illustrated in Fig. 5.3.2.3-2.

Now the fraction of sites covered is no longer a direct measure of the coke content, because there is no unique size for the coke. Blockage can cause deactivation of the main reaction, even when it occurs on sites different from those involved in coking. The formulas for such a situation were also reported [Froment, 1984].

5.3.2.4 Deactivation by Site Coverage and Pore Blockage in the Presence of Diffusion Limitations

For single pores the model equations closely resemble the classical second-order differential equations encountered in Chapter 3 to express transport resulting from concentration gradients by means of “effective” diffusion. But they also contain the probabilities *S* and *P* encountered earlier in this section, in the form of differential equations.

The equation for *S* contains r_s^0, which is not a constant any longer over the pore, because of the concentration gradients. Consequently, the mechanism of formation of the coke precursor covering a site now enters into the picture, through equations such as (5.3.2.2-11) and (5.3.2.2-14). Also, through the blockage, the distance available to diffusion is affected. Finally, since with practical catalysts the rate of coking is small compared with the rate of the main reaction, pseudo steady state may be assumed in deriving the continuity equation for *A*. With parallel coking ($Al \rightarrow Cl$), the coke profile is not significantly different in aspect from that predicted in the absence of diffusion limitations because the concentration gradient simply emphasizes the effect of blockage.

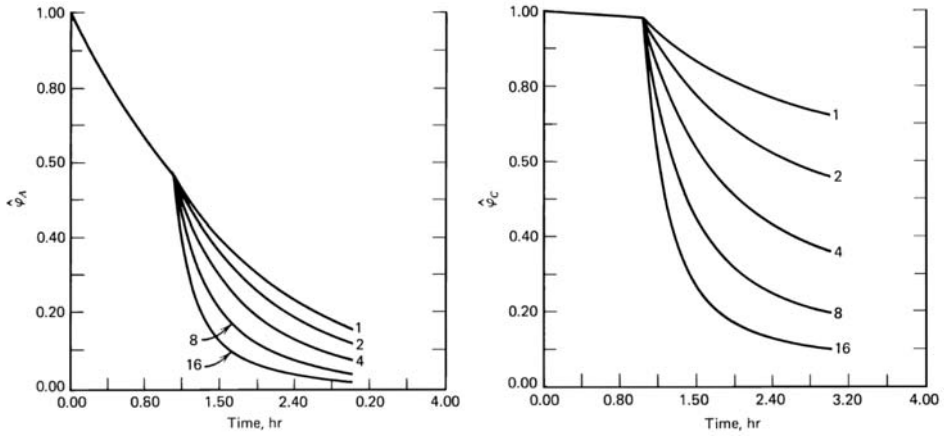

Figure 5.3.2.3-2a

Pore-averaged deactivation function for main reaction versus time. Parameter σL, number of sites per pore. From Beeckman and Froment [1982].

Figure 5.3.2.3-2b

Pore-averaged deactivation function for coking versus time. Parameter σL. From Beeckman and Froment [1982].

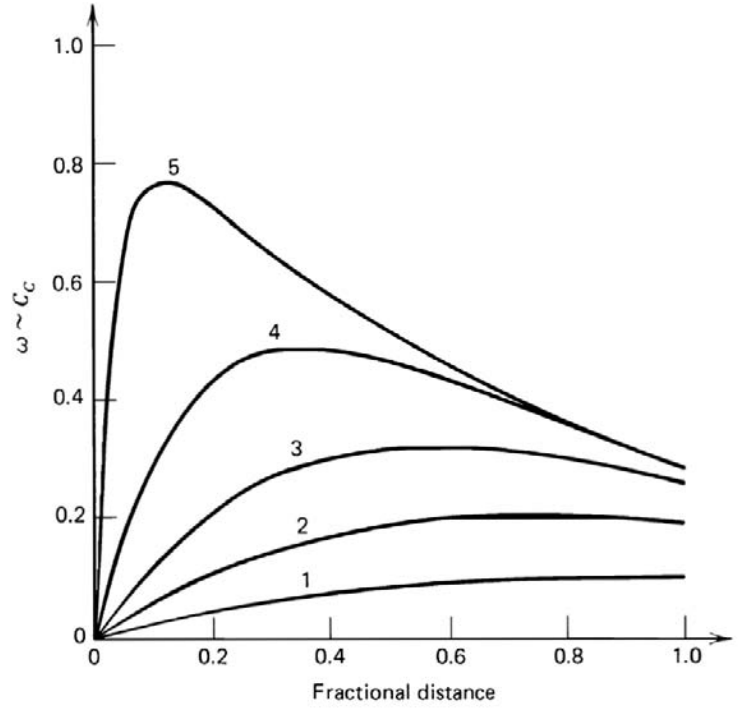

Figure 5.3.2.4-1

Site coverage in a simple-ended pore in the presence of diffusion limitations and blockage. Consecutive coking. Curve 1, 0.122 h; curve 2, 0.0356 h; curve 3, 0.0931 h; curve 4, 0.4453 h; curve 5, 8.42 h. From Beeckman and Froment [1980].

With consecutive coking, however, ($Bl \rightarrow Cl$), the concentration gradient and the probability of blockage are opposite, so that an interesting coke profile is obtained, as shown in Fig. 5.3.2.4-1 for a single-ended pore.

In a pore open on both sides, a saddle-like coke content profile may develop. This has been observed in acetylene hydrogenation in ethylene streams from olefin-producing units [Wright et al., 1979] and was explained by Froment [1984] in terms of the above theory. In this very fast reaction on a Pd/alumina catalyst, diffusion limitations are known to occur. Parallel coking from acetylene and ethylene is possible, but the strongest contribution to coking comes from the "green oil"—a reaction product. The latter mechanism leads to a saddle-like coke profile. The observed coke content at the surface is not zero, as would be the case with purely consecutive coking—see Fig. 5.3.2.4-1. This is explained in terms of parallel contributions from acetylene and ethylene.

5.3.2.5 Deactivation by Site Coverage, Growth of Coke, and Blockage in Networks of Pores

It may be questioned how representative a pore really is for a catalyst particle. No doubt in the future, with growing attention for the more detailed characterization of catalyst particle structures, more elaborate representations of the particle will be used. Beeckman and Froment [1982] developed the theory for reaction and deactivation by coke formation in random networks of pores. The deactivation was considered to occur through site coverage and pore blockage. Diffusion limitations were also included, but only for deactivation by site coverage.

The main difficulty with networks is the formulation of the probability that a site is accessible, P. The latter is obtained from

$$P = 1 - q^2(D)$$

where $q(D)$ is the probability of not reaching the boundary of the network, starting from a point in a randomly chosen pore and moving toward one end of the pore; $q(D)$ has to be expressed in terms of the structure of the pores and the network. The network considered by Beeckman and Froment, already discussed in Chapter 3, is a special case of a β-tree, used in percolation theory and in which each pore branches only into two others. The probability that a pore branches in a distance dx is $\nu(D)dx$; the probability that it changes diameter in the distance dx is $\beta(D)dx$; the probability of having an active site in dx is $\sigma(D)dx$. The probability $q(D)$ contains these structural parameters. Beeckman and Froment worked out the relationship Φ versus essentially the coke content for a Wheeler network with

80 percent of the sites in micropores with a diameter D_1, which can be blocked, and 20 percent of the sites in macropores with a diameter D_2, too large to be blocked and in which $P = 1$. The curve Φ versus C_C now becomes a function of the number of sites per pore, the ratio σ/ν, and deviates from a straight line.

Beyne and Froment [1993] applied percolation theory to a US-Y zeolite catalyzing a process $A \rightleftarrows B$ subject to diffusion limitations and to consecutive coking leading to site coverage and to pore blockage. After a certain process time, the percolation threshold was reached at some radial position of the particle and blockage of the volume behind it occurred.

5.3.3 Kinetic Analysis of Deactivation by Coke Formation

The data required for a kinetic formulation of the deactivation of the main reaction are probably best collected in a differential reactor. Some extrapolation to zero time is required when the reaction rate of the main reaction cannot be observed at zero coke content. The procedure can be hazardous with very fast coking, of course. In their study of butene dehydrogenation, Dumez and Froment [1976] were able to take samples of the exit stream of stabilized operation of the fixed bed reactor after 2 minutes, while the observations extended over more than 30 minutes.

In some cases decoupling of the main and the coking reactions is possible. In *n*-pentane isomerization on a Pt-reforming catalyst, De Pauw and Froment [1975] determined the kinetics of the main reaction by operating at high ratios of hydrogen to hydrocarbon. The coking kinetics were subsequently obtained from experiments at low hydrogen partial pressure, taking advantage of the knowledge gained on the kinetics of the main reaction.

Levenspiel [1972] has presented a conceptual discussion of the derivation of the rate equations for deactivation from experiments in appropriate equipment. Weekman [1974] has rated various types of laboratory equipment for their adequacy with respect to coking studies. Hegedus and Petersen [1973 a; b] used a single-pellet reactor in the hydrogenation of cyclopropane on a Pt/Al_2O_3 catalyst. They showed how a plot of the ratio of the main reaction rate at any time to that at zero time versus the normalized center plane concentration of the reactant A permits discrimination between coking mechanisms. The success of this method strongly depends on the accuracy with which the center plane concentration can be measured. Thiele moduli in the range of 1 to 5 are required.

A specific and very useful equipment for coking rate studies is the electrobalance, used by Takeuchi et al. [1966] in their study of the dehydrogenation of isobutene, by Ozawa and Bischoff [1968] in their investigation of coking associated with ethylene cracking, by De Pauw and

Froment [1975], Dumez and Froment [1976], Snoeck and Froment [1997] and Devoldere and Froment [1999]. The equipment consists of a heated reactor tube in which a basket suspended at the arm of a micro-balance contains the catalysts. The amount of coke deposited on the catalyst is continuously monitored by the balance. Only differential operation, i.e., with very low conversion, can yield the correct result: only then there is no coke profile in the basket. The point conditions are also required because the fraction of gaseous reactant flowing through the basket is unknown. With differential operation the difference in composition of the two fractions is negligible and the correct space time is accessible. The general problem with differential operation is the need for accurate analysis of feed and exit. The problem can be circumvented by allowing higher conversions through operation with complete mixing, also ensuring point conditions. This is why Beirnaert et al. [1994] developed a recycle electro-microbalance. Its application was illustrated in a study of deactivation in the catalytic cracking of paraffins. The set up is shown in Fig. 5.3.3-1.

A convenient type of equipment for studies of this type is the tapered element oscillating microbalance (TEOM), developed by Patashnick and Rupprecht [1980] and shown in Fig. 5.3.3-2. The advantage of this equipment is that the full amount of gas is flowing through the element containing the catalyst bed, which is brought to oscillation. The evolution of the amount of

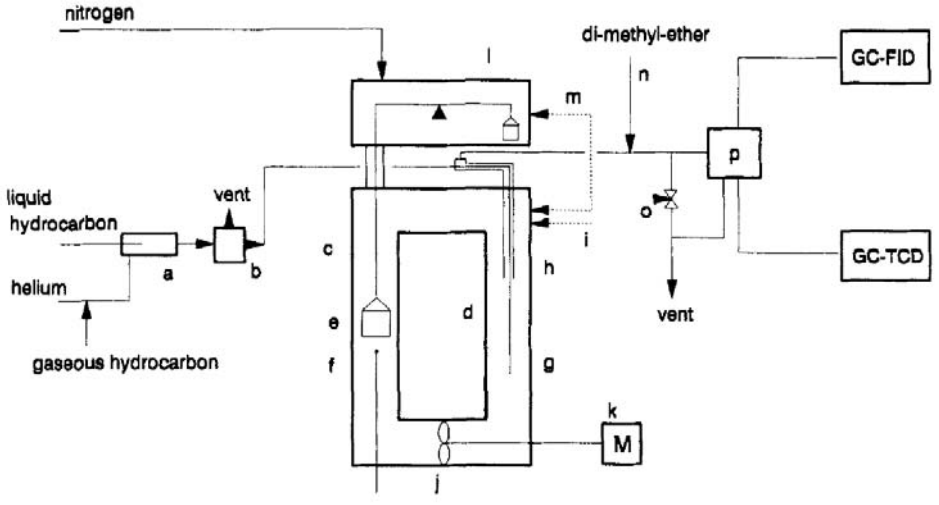

Figure 5.3.3-1

Recycle micro-electrobalance for catalyst deactivation studies [Beirnaert et al., 1994].

a-evaporator; b-bypass valves; c-reactor tube; d-recycle tube; e-catalyst basket; f-thermocouple; g-inlet; h-exit; i-pressure gauge; j-gas ventilator; k-electromotor; l-microbalance; m-differential pressure meter; n-internal standard for analysis; o-needle valve for pressure control; p-six way valve.

carbonaceous deposit on the catalyst is monitored by means of the variation of the oscillation amplitude of the element, measured by an electronic feedback amplifier operating with an infra-red emitter and detector. For an unambiguous and accurate kinetic analysis differential operation is still required, however. An example of application to the deactivation of a Pt-Re/alumina catalyst was published by Liu et al. [1997].

As in any kinetic analysis, care has to be taken with diffusion influences, as already mentioned in Section 5.3.2.1. Assuming that these have been eliminated in the experimentation, a modern approach for the experimental work and data analysis could be as represented in Fig. 5.3.3-3.

Both φ_A and C_C contain the rate of fractional site coverage r_s^0 and the structural parameters, σ, ν, γ. The latter are evidently preferably determined by independent physicochemical measurements, to limit the number of parameters to be determined in the estimation. Obtaining r_s^0 from observations on both the

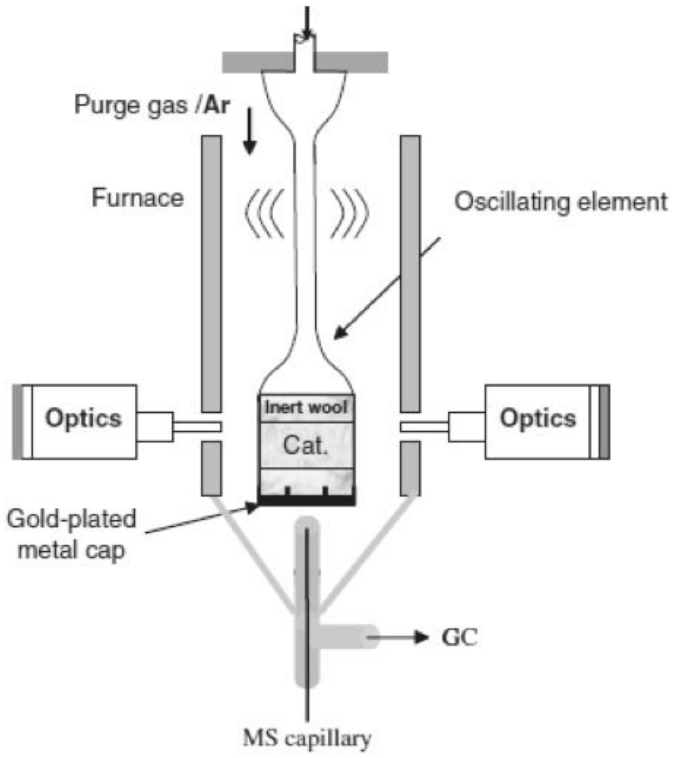

Figure 5.3.3-2

Tapered element oscillating microbalance reactor [Patashnick and Rupprecht (TEOM Series 1500 PMA Reaction Kinetics Analyzer) Thermo Electron Corporation. Environmental Instruments Division, East Greenbush, N.Y. 12061].

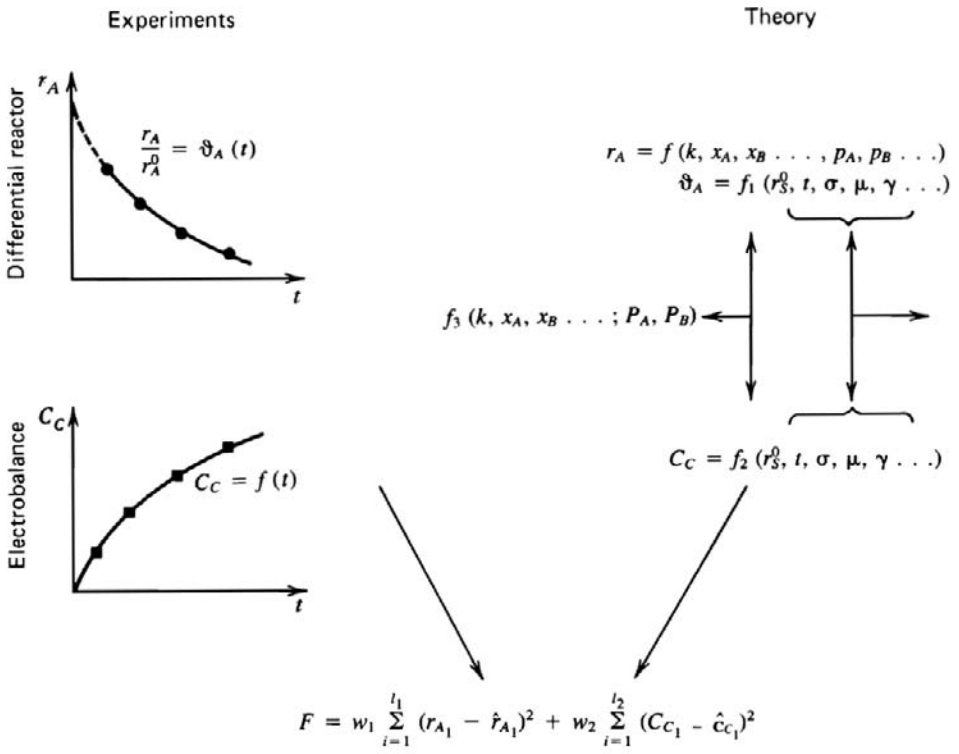

Figure 5.3.3-3
Kinetic analysis of main and coking reaction. [Froment, 1982].

deactivation of the main reaction and on the coke content is evidently to be preferred to obtaining it from the main reaction only. A multiresponse nonlinear regression will avoid producing different values of r_s^0 from both types of experimentation, which would otherwise have to be weighted a posteriori in a non optimal way. The objective function F contains weighting factors w_1 and w_2, whereas l_1 and l_2 are the number of data points on r_A and C_C , respectively. The symbols $\hat{r}_{Ai}$ and $\hat{C}_{Ci}$ represent estimates for r_{Ai} and C_{Ci} based on the kinetic models to be tested. The discrimination between rival kinetic models then proceeds along classical ways.

The data can also be obtained in an integral fixed reactor, of course. Information on the coke content profile in a tubular reactor may yield valuable information as to the mechanism of coking—parallel or consecutive—and, therefore, as to the form of r_C^0 , as will be shown in the next section. If the integral method of kinetic analysis is applied to the data, as was done by De Pauw and Froment [1975], the conversion x_A replaces the rate r_A in the objective function, requiring integration of the rate equation.

EXAMPLES OF APPLICATION TO INDUSTRIAL PROCESSES

EXAMPLE 5.3.3.A
COKE FORMATION IN THE DEHYDROGENATION OF 1-BUTENE INTO BUTADIENE

Dumez and Froment [1976] studied the dehydrogenation of 1-butene into butadiene in the temperature range of 480° to 630°C on a chromia/alumina catalyst containing 20 wt-% Cr_2O_3 and having a surface area of 57 m²/g. The investigation dealt with the kinetics of both the main reaction and the coke formation.

The kinetics of the main reaction was determined in a differential reactor. The rates in the absence of coke deposition, r_H^0, were obtained by extrapolation to zero time. Accurate extrapolation was possible: the reactor was stabilized in less than 2 minutes after introduction of the butene, whereas the measurements of the rates r_H extended to on stream times of more than 30 minutes.

Fifteen possible rate equations of the Hougen-Watson type were derived from various dehydrogenation schemes and rate-determining steps. The discrimination between these models was achieved by means of sequentially designed experiments, according to the method outlined in Chapter 2. At 525°C, for example, 14 experiments, 7 of which were preliminary, sufficed for the discrimination. The following rate equation, corresponding to molecular dehydrogenation and surface reaction on dual sites as a rate-determining step, was retained:

$$r_H^0 = \frac{k_H^0 K_B \left(p_B - \frac{p_H p_D}{K} \right)}{\left(1 + K_B p_B + K_H p_H + K_D p_D\right)^2} \qquad (5.3.3.\text{A-a})$$

where K_B, K_H, and K_D, and p_B, p_H, and p_D are adsorption equilibrium constants and partial pressures of butene, hydrogen, and butadiene, respectively.

The kinetics of the coking and the deactivation functions for coking were determined by means of a microbalance. The catalyst was placed in a stainless steel basket suspended at one balance arm. The temperature was measured in two positions by thermocouples placed just below the basket and between the basket and the quartz tube surrounding it. The temperature in the coking experiments ranged from 480°C to 630°C, the butene pressure from 0.02 to 0.25 bar, the butadiene pressure from 0.02 to 0.15 bar. Individual components as well as mixtures of butene and butadiene, butene and hydrogen, and butadiene and

hydrogen were fed. The hydrogen pressure ranged from 0 to 0.15 atm. Coke deposition on the basket itself was always negligible.

The deactivation function for coking was determined from the experimental coke-versus-time curves as described below. Coke was shown to be deposited from both butene and butadiene, while hydrogen exerted an inhibiting effect. An example of the evolution of the coke content of the catalyst with time is given in Fig. 5.3.3.A-1. Since the microbalance is a differential reactor, operating at point values of the partial pressures and the temperature, the decrease in the rate of coking observed with increasing coke content reflects the deactivating effect of coke. The rate equation for coke formation therefore has to include a deactivation function, multiplying the rate in the absence of coke:

$$\frac{dC_C}{dt} = r_C^0 \Phi_C \qquad \text{(5.3.3.A-b)}$$

where r_C^0 is the initial coking rate, a function of the partial pressures and temperature that reduces to a constant for a given experiment in the microbalance. Several expressions were tried for Φ_C:

$$\Phi_C = \exp(-\alpha C_C)$$

$$\Phi_C = 1 - \alpha C_C$$

$$\Phi_C = (1 - \alpha C_C)^2$$

$$\Phi_C = \frac{1}{1 + \alpha C_C}$$

$$\Phi_C = \frac{1}{(1 + \alpha C_C)^2}$$

The deactivation function is expressed in terms of the coke content of the catalyst, not in terms of time as has been done frequently. Indeed, time is not the true variable for the deactivation, as discussed earlier. The deactivation functions for the coking used here are still empirical in the sense that they do not explicit the mechanism of the deactivation-site coverage or blocking or both, as will be attempted in Example 5.3.3.B.

Substitution of the deactivation function into (5.3.3.A-b) and integration with respect to time yields, respectively,

$$C_C = \frac{1}{\alpha} \ln(1 + \alpha r_C^0 t)$$

$$C_C = \frac{1}{\alpha}[1 - \exp(-\alpha r_C^0 t)]$$

$$C_C = \frac{1}{\alpha}\left(1 - \frac{1}{1 + \alpha r_C^0 t}\right) \qquad \text{(5.3.3.A-c)}$$

$$C_C = \frac{1}{\alpha}(\sqrt{2\alpha r_C^0 t + 1} - 1)$$

$$C_C = \frac{1}{\alpha}(\sqrt[3]{3\alpha r_C^0 t + 1} - 1)$$

where α and r_C^0 were determined by fitting the experimental data by means of a least squares criterion.

For the majority of the 50 experiments $\Phi_C = \exp(-\alpha C_C)$ turned out to give the best fit. An explanation based on a pore blocking mechanism has been attempted [Beeckman and Froment, 1979; 1980; see also Example 5.3.3.B]. The parameter α was found to be identical for coking from either butene or butadiene and independent of the operating variables, as was concluded from the partial correlation coefficients between α and T, p_B, p_H, and p_D, respectively, and the t-test values for the zero hypothesis for the partial correlation coefficient.

The determination of the complete rate equation for coke deposition required the simultaneous treatment of all experiments, so that p_B, p_H, p_D, and T were varied. The exponential deactivation function was substituted into the rate

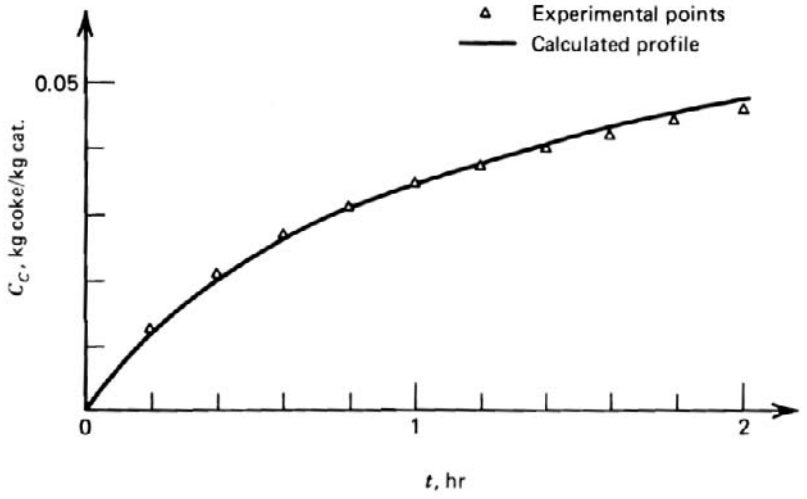

Figure 5.3.3.A-1

Butene dehydrogenation. Coke content of catalyst as a function of time in thermobalance experiment. From Dumez and Froment [1976].

equation for coking. After integration of the latter the parameters were determined by minimization of

$$\Im = \sum_{i=1}^{n} (C_C - \hat{C}_C)_i^2 \qquad (5.3.3.A\text{-d})$$

where n is the total number of experiments. Several rate equations, either empirical or based upon the Hougen-Watson concept, were tested. The best global fit was obtained with the following equation:

$$\frac{dC_C}{dt} = \frac{k_{CB}^0 p_B^{nCB} + k_{CD}^0 p_D^{nCD}}{(1 + K_{CH}\sqrt{p_H})^2} \exp(-\alpha C_C) \qquad (5.3.3.A\text{-e})$$

with

$$k_{CB}^0 = A_{CB}^0 \exp\left(\frac{-E_{CB}}{RT}\right)$$

$$k_{CD}^0 = A_{CD}^0 \exp\left(\frac{-E_{CD}}{RT}\right) \qquad (5.3.3.A\text{-f})$$

and K_{CH} independent of temperature.

The terms in the numerator of the right hand side express the rates of coke formation out of butene and butadiene, the numerator the inhibiting effect of hydrogen. The integrated equation used in the objective function (5.3.3.A-d) was

$$C_C = \frac{1}{\alpha} \ln\left\{1 + \alpha\left[\frac{k_{CB}^0 p_B^{nCB} + k_{CD}^0 p_D^{nCD}}{(1 + K_{CH}\sqrt{p_H})^2}\right] t\right\} \qquad (5.3.3.A\text{-g})$$

The deactivation function for the dehydrogenation was also determined by means of the microbalance, by measuring simultaneously the coke content and the composition of the exit gases as functions of time. To eliminate the effect of bypassing, the conversions were all referred to the first value measured. Fig. 5.3.3.A-2 shows the relation $r_H / r_H^0 = \Phi_H$ versus the coke content, easily derived from the measurements $r_H / r_H^0 = \Phi_H$ versus time and coke content versus time. Although there is a certain spread of the data, no systematic trend with respect to the temperature or the partial pressures could be detected. The temperature ranged from 520° to 616°C, the butene pressure from 0.036 to 0.16 bar. Again, the best fit was obtained with an exponential function: $\Phi_H = \exp(-\alpha C_C)$. A value of 32.12 was determined for α. The agreement with the value found for the

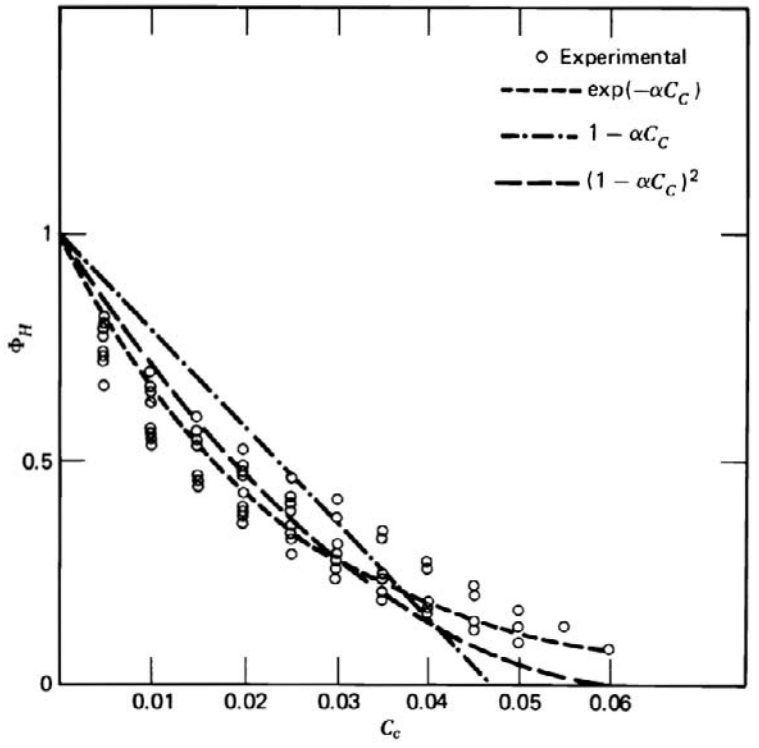

Figure 5.3.3.A-2

Butene dehydrogenation. Deactivation function for the main reaction, Φ_H, versus time. Experimental data at various temperatures and partial pressures. From Dumez and Froment [1976].

deactivation parameter for the two coking reactions is remarkable [compare Eq. (5.3.3.A-i)]. It may be concluded that the main reaction and the coking reactions occur on the same sites.

The set of rate equations may now be written

$$r_H = \frac{1.826\times10^7 \exp(-29236/RT)\left(p_B - \dfrac{p_N p_D}{K}\right)}{(1+1.727\,p_B + 3.593\,p_H + 38.028\,p_D)^2}\exp(-42.12C_C) \qquad \text{(5.3.3.A-h)}$$

$$r_C = \frac{1.5588\times10^8 \exp(-32860/RT)\,p_B^{0.743} + 5.108\times10^5 \exp(-21042/RT)\,p_D^{0.853}}{(1+1.695\sqrt{p_H})^2} \times \exp(-45.53C_C) \qquad \text{(5.3.3.A-i)}$$

The process is also subject to diffusion limitations, causing concentration profiles inside the catalyst particle. To generate these profiles requires continuity equations for the reaction components. Assuming pseudo-steady state for the

main reaction and taking hydrogen as the key component, the continuity equation for the latter is of the form discussed in Chapter 3. Since the rate equation (5.3.3.A-h) contains the coke content an additional continuity equation containing the rate equation (5.3.3.A-i) has to be written to express the evolution of the coke content profiles inside the catalyst with time. The results of the integration of this set of equations are shown in Fig. 5.3.3.A-3 for a particle at the inlet of the reactor.

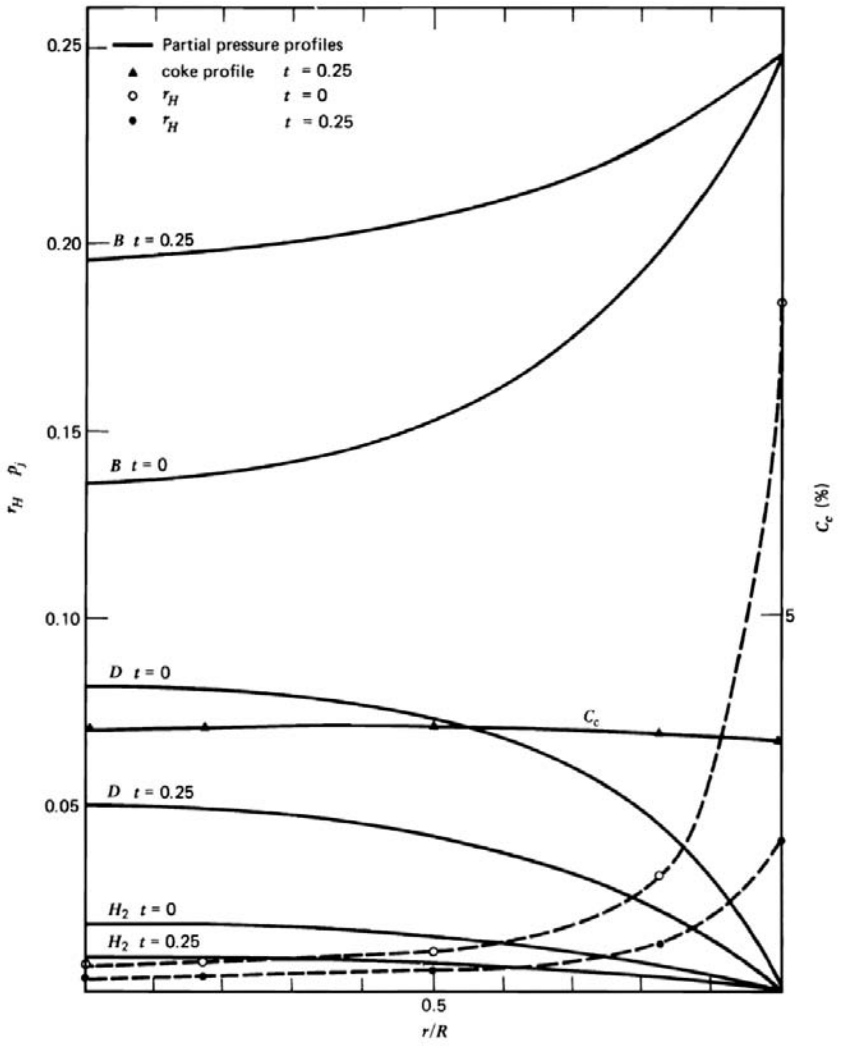

Figure 5.3.3.A-3

Butene dehydrogenation. Partial pressure, rate, and coke profiles inside a catalyst particle located at the reactor inlet for zero process time and after 0.25 h. Parallel-consecutive coking mechanism and inhibition by hydrogen. From Dumez and Froment [1976].

The deactivation function does not explicitly express the cause of deactivation: site coverage or pore blockage. Therefore, the profiles inside the particle only result from the diffusion limitations. The rather uniform coke content is a result of the parallel-consecutive nature of the coke formation, combined with the inhibiting effect of hydrogen.

Gottifredi and Froment [1997] presented a straightforward and accurate semi-analytical solution for the concentration profiles inside a catalyst particle in the presence of coke formation. They applied the solution to the butene dehydrogenation dealt with here and obtained an excellent agreement with the profiles shown in Fig. 5.3.3.A-3. The method significantly simplifies and reduces the computational effort involved in reactor simulation and kinetic analysis.

■

EXAMPLE 5.3.3.B

RIGOROUS KINETIC EQUATIONS FOR CATALYST DEACTIVATION BY COKE DEPOSITION IN THE DEHYDROGENATION OF 1-BUTENE INTO BUTADIENE

Marin et al. [1986] fitted the rate of site coverage in butene dehydrogenation by means of a single-site equation:

$$r_s^0 = \frac{A_A^0 \exp(-E_A/RT)\, p_A + A_D^0 \exp(-E_D/RT)\, p_D}{1 + K_A p_A + K_D p_D + K_H p_H} \qquad (5.3.3.\text{B-a})$$

In this equation the concentrations of adsorbed intermediates between butene and butadiene and the corresponding coke precursors are neglected.

Instantaneous growth of coke was assumed, that is, the rate-determining step is the rate of site coverage by coke precursor. The molecular mass of coke, M_C, is unique and determined by the reaction conditions. It is independent of time.

For a network of macro-and micropores with a distribution in size, the following average coke content in the pores that can be blocked was obtained from the approach of Beeckman and Froment [1979], described in Chapter 3:

$$\hat{C}_C(D,1) = C_t \frac{\nu}{\sigma(D)}\, pV(D) \qquad (5.3.3.\text{B-b})$$

$$\left\{ 2\ln\left[1 + \frac{\sigma(D)}{\nu}\left(1 - \exp(-r_s^0 t)\right)\right] + \left[1 + \frac{\sigma(D)}{\nu}\left(1 - \exp(-r_s^0 t)\right)\right]^{-1} - 1 \right\}$$

where $v\,dx$ is the probability that a pore branches in an interval dx; $\sigma(D)dx$ is the probability that a site is located in an interval dx of a pore with diameter D; ρ is the density of coke and coke precursor (kg/m^3); and $V(D)$ is the molar volume of coke which blocks a pore with diameter D (m^3/kmol coke). For a coke content in the macropores with diameter $D > D_C$, which cannot be blocked, the following expression was derived:

$$C_C(D > D_C, t) = (1-\gamma)C_t M_C(1-\exp(-r_s^0 t)) \qquad (5.3.3.B\text{-c})$$

In (5.3.3.B-b) and (5.3.3.B-c)

$$D_C = \left(\frac{6M_C}{\pi\, p\, N_A}\right)^{1/3} \qquad (5.3.3.B\text{-d})$$

$$V(D) = \frac{\pi D^3 N_A}{6} \qquad (5.3.3.B\text{-e})$$

$$\sigma(D) = \frac{\pi D C_1 N_A}{A_S} \qquad (5.3.3.B\text{-f})$$

The total coke content of the catalyst follows from

$$C_C(t) = \int_0^{D_C} g^S(D)\hat{C}_C(D,l)dD + C_C(D > D_C, t) \qquad (5.3.3.B\text{-g})$$

The coke diameter D_C is derived from the molecular mass, assuming a spherical shape of the coke molecule. In the fraction γ of pores with a diameter smaller than D_C, the coke diameter equals the pore diameter. Values for the textural parameters were obtained from physical measurements: electron microscopy, nitrogen desorption, and mercury porosimetry.

The density of the coke was taken to be 1800 kg/m^3. A value of 3.8×10^{-6} kmol/kg cat. based upon O_2 uptake data was assigned to the total concentration of active sites. The number of parameters in (5.3.3.B-a) through (5.3.3.B-g) amounts to eight. Their value was determined by means of nonlinear regression of coking data covering a wide range of temperatures and feed compositions. Table 5.3.3.B-1 lists the estimates for the parameters with their corresponding approximate individual *t*-values. The significance of the global regression is expressed by the ratio of the mean regression sum of squares to the mean residual sum of squares, *F*.

The *F* value is high, indicating an excellent fit, while the *t* values associated with the parameters lead to significant estimates for the latter. The

TABLE 5.3.3.B-1
INSTANTANEOUS COKE GROWTH: RESULTS OF REGRESSION OF THE COMPLETE SET OF COKING CURVES WITH MODEL EQUATIONS (5.3.3.B-a) THROUGH (5.3.3.B-g)[a]

Parameter	Value	*t* Value
M_C (kg coke/kmol coke)	1.892×10^4	71.5
A_A^0 (1/bar)	6.855×10^8	15.2[b]
E_A (kJ/kmol)	1.256×10^5	30.2
A_D^0 (1/bar)	3.980×10^6	21.8[b]
E_D (kJ/kmol)	8.105×10^4	30.0
K_A (1/bar)	2.801	4.6
K_D (1/bar)	7.785	6.1
K_H (1/bar)	18.61	15.1
F value	4408	

[a] $\rho = 1.8 \times 10^3$ kg coke/kg cat.; $C_1 = 3.8 \times 10^{-6}$ kmol sites/kg cat.; $\eta^{-1} = 5 \times 10^3$ nm.

[b] On the reparametrized preexponential factors.

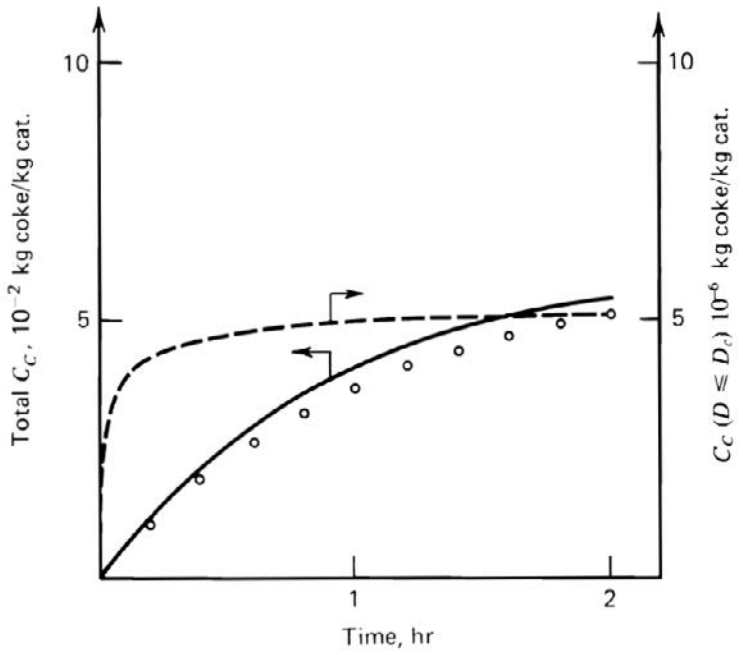

Figure 5.3.3.B-1

Coke content versus time at 823 K, $p_A = 0.240$ bar, $p_B = p_H = 0.0$ bar. Points: experimental. Solid line: total coke content calculated with instantaneous growth equations. Dashed line: coke content in pores which can be blocked, calculated from Eq. (5.3.3.B-b). Parameter values from Table 5.3.3.B-1. From Marin, Beeckman and Froment [1986].

highest binary correlation coefficient between the parameter estimates amounts to 0.44. Fig. 5.3.3.B-1 compares experimental and calculated coke contents for a typical set of reaction conditions.

The coke diameter derived from (5.3.3.B-d) and from the molecular mass listed in Table 5.3.3.B-1, amounts to 3.22 nm. This is sufficiently large to render 13.1 percent of the catalyst surface area inaccessible by pore blockage. The average site density in the pores that can be blocked equals 2.81×10^8 m^{-1} and corresponds to 1.41×10^3 active sites per pore. Because of this high number of active sites per pore and the absence of connectivity between the mesopores, blockage occurs within a few seconds. Hence, little coke is deposited in these pores, as shown in Fig. 5.3.3.B-1. At infinite time, a value for the coke content of 5.10×10^{-6} kg coke/kg cat. is obtained from the first term in (5.3.3.B-g). This value can be neglected with respect to the value of 6.26×10^{-2} kg coke/kg cat. at infinite time for the coke content in the pores that cannot be blocked. The contributions to the coke content by the two terms in (5.3.3.B-g) are comparable during the first seconds of the deactivation only. A significant separate determination of C_t and M_C can only be expected from kinetic data collected during this initial time period, since the second term of (5.3.3.B-g) contains the product $C_t M_C$, whereas the first term is proportional to C_t only.

Finally it should be noted that expressions for the rate of fractional site coverage other than those leading to (5.3.3.B-a) were tested. This led to only marginal changes of the significance of the global regression.

The model described above assumes that the rate constants of all the elementary steps following the coke precursor formation are much larger than the rate constant of the formation of the coke precursor itself. If this is not so, the rate of growth of the coke becomes finite. This rate may be considered to be independent of coke size or it may decrease as the coke grows. The second possibility was further developed and led to a fit of the data superior to that shown in Fig. 5.3.3.B-1. ■

EXAMPLE 5.3.3.C

COKE FORMATION AND CATALYST DEACTIVATION IN STEAM REFORMING OF NATURAL GAS

Steam reforming of natural gas on Ni-alumina catalysts is a major operation of the chemical industry. It produces a mixture of CO, CO_2 and hydrogen, the synthesis gas, for methanol production, for the Fischer-Tropsch synthesis of higher hydrocarbon and, after removal of CO and CO_2, for ammonia synthesis. The process is very endothermic and is carried out above 750°C at 20-30 bar in large furnaces containing e.g., 300 reactor tubes in parallel. Xu and Froment

[1989] studied the kinetics of the process in a bench scale tubular flow reactor. The reaction scheme retained after discrimination between 21 possible sets of rate equations is shown in Fig. 5.3.3.C-1 for a mixture of propane, ethane and methane. It starts with a sequence of progressive abstraction of hydrogen. At the appropriate step in the sequence, oxygen from the dissociation of water is inserted and CO and CO_2 are formed in parallel. They also further interact through the water gas shift reaction. The rate determining steps in the steam reforming steps proper are the parallel surface reaction CHO + l $\rightleftarrows$ CO–l and CHO + l $\rightleftarrows$ CO_2–l and in the water gas shift CO–l + O–l $\rightleftarrows$ CO_2–l. Writing these steps in terms of the accessible gas phase concentrations leads to the rate equations given in Fig. 5.3.3.C-2 for steam reforming of pure methane. All the steps mentioned here take place on the same sites so that the rate equations all have the same denominator.

If the oxygen is not introduced as indicated in Fig. 5.3.3.C-2 the H-abstraction continues and leads to a component CH_x that does not desorb any more from the Ni-catalyst and causes deactivation. An additional phenomenon has to be accounted for in the modeling: the carbon diffuses through the Ni particle and exerts such a pressure at the rear side of it that the particle is lifted from the alumina support. The carbon continues to grow in the form of a "whisker" that carries the Ni at the top of its stem. When the potential for growth is used up the growth stops and the carbon or coke simply settles at the Ni surface, covering it progressively. The "coke" is mainly formed by methane cracking. The coking scheme is shown in Fig. 5.3.3.C-3. The coke is also gasified by hydrogen and water. Coking and gasification were studied by Snoeck, Froment and Fowles [1997] in an electrobalance, operated in the differential mode. The net rate of coking is also given in Fig. 5.3.3.C-3. The term $\alpha_{O\text{-}1}$ in the denominator is a complex function of the concentrations, but need not be further specified here. The rate equation is of particular importance to locate operating conditions for which coke formation may occur. Fig. 5.3.3.C-4 shows results of Snoeck, Froment and Fowles [1997] who used these equations to investigate zones in an industrial natural gas reformer where coke formation could occur. For a given temperature and total pressure profile in the reactor tube, the ratios of steam to methane and of CO_2 to methane are determining. For a ratio H_2O/CH_4 in the feed of 1.0 and no recycle CO_2 the net coking rate, i.e., the difference between the rate of formation and the rate of gasification, is pronounced from 5.0 m in the tube onwards; for a H_2O/CH_4 ratio of 1.3 and $CO_2/CH_4 = 0.7$ the zone of coke formation extends from 4 to 9.0 m, but the rate is low. For the other ratios there will be no coke deposition. It should be noted that these coking limits used to be determined by means of thermodynamic calculations. The coke formation

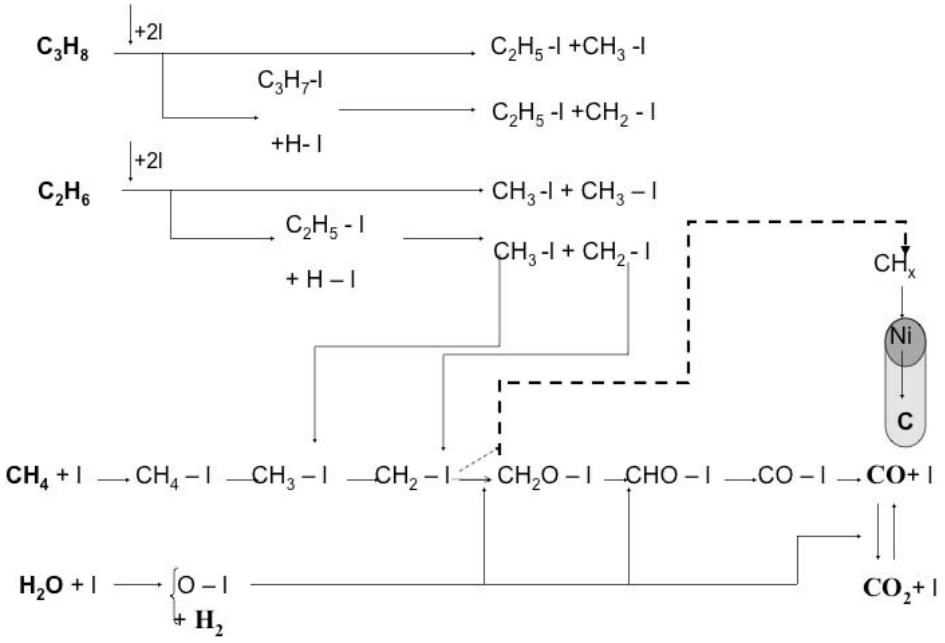

Figure 5.3.3.C-1

Reaction scheme for the reforming of a mixture of propane, ethane and methane written in terms of elementary steps.

$$r_{sr,CO} = \frac{\frac{k_3}{p_{H_2}^{2.5}}\left(p_{CH_4}p_{H_2O} - \frac{p_{H_2}^3 p_{CO}}{K_3}\right)}{\left(1 + K_{CO}p_{CO} + K_{H_2}p_{H_2} + K_{CH_4}p_{CH_4} + K_O\frac{p_{H_2O}}{p_{H_2}}\right)^2}$$

$$r_{sr,CO_2} = \frac{\frac{k_4}{p_{H_2}^{3.5}}\left(p_{CH_4}p_{H_2O}^2 - \frac{p_{H_2}^4 p_{CO_2}}{K_4}\right)}{\left(1 + K_{CO}p_{CO} + K_{H_2}p_{H_2} + K_{CH_4}p_{CH_4} + K_O\frac{p_{H_2O}}{p_{H_2}}\right)^2}$$

$$r_{wgs} = \frac{\frac{k_5}{p_{H_2}}\left(p_{CO}p_{H_2O} - \frac{p_{H_2}p_{CO_2}}{K_5}\right)}{\left(1 + K_{CO}p_{CO} + K_{H_2}p_{H_2} + K_{CH_4}p_{CH_4} + K_O\frac{p_{H_2O}}{p_{H_2}}\right)^2}$$

Figure 5.3.3.C-2

Set of rate equations for the steam reforming of methane.

Methane cracking

$$CH_4 + l \rightleftarrows CH_4\text{–}l \qquad K_{CH_4}$$

$$CH_4\text{–}l + l \rightleftarrows CH_3\text{–}l + H\text{–}l \qquad \text{rds } 1/k_M^+ \text{ and } k_M^-$$

$$CH_3\text{–}l + 3l \rightleftarrows C\text{–}l + 3H\text{–}l \qquad K_r$$

$$H_2 + 2l \rightleftarrows 2H\text{–}l \qquad K_H$$

$$C\text{–}l \rightleftarrows C_{Ni,f} + l \qquad 1/K_C$$

Boudouard

$$CO_2 + 2l \rightleftarrows O\text{–}l + CO\text{–}l \qquad 1/K_{O,CO_2};\ k_{O,CO_2}^+ \text{ and } k_{O,CO_2}^-$$

$$CO\text{–}l \rightleftarrows CO + l \qquad 1/K_{CO}$$

$$H_2O + l \rightleftarrows O\text{–}l + H_2 \qquad 1/K_{O,H_2O},\ k_{O,H_2O}^+, \text{ and } k_{O,H_2O}^-$$

$$C\text{–}l + O\text{–}l \rightleftarrows CO\text{–}l + l \qquad \text{rds } 2/k_O^+ \text{ and } k_O^-$$

$$\frac{D_{C,Ni}}{d_a}(c_{C,\{Ni,f\}} - c_{C,\{Ni,sat\}})a_{Ni} \longleftarrow \textbf{Diffusion through Ni}$$

$$r_{C,net} = \frac{\left[k_M^+ K_{CH_4}\left(p_{CH_4} - \frac{1}{K_{M,av}^*}p_{H_2}^{\ 2}\right) + \left(k_O^- K_{CO} p_{CO} - k_O^{+\prime}\frac{c_{O\text{–}l}}{c_l}\right)\right]}{\left[1 + K_{CH_4}p_{CH_4} + K_{CO}p_{CO} + \frac{1}{K_r''}p_{H_2}^{\ 3/2} + \frac{c_{O\text{–}l}}{c_l}\right]^2}$$

Figure 5.3.3.C-3

Elementary steps of coke formation from methane cracking and of the gasification of coke by H_2O and H_2. Net rate equation for coke formation accounting also for diffusion of carbon through the Ni particles of catalyst.

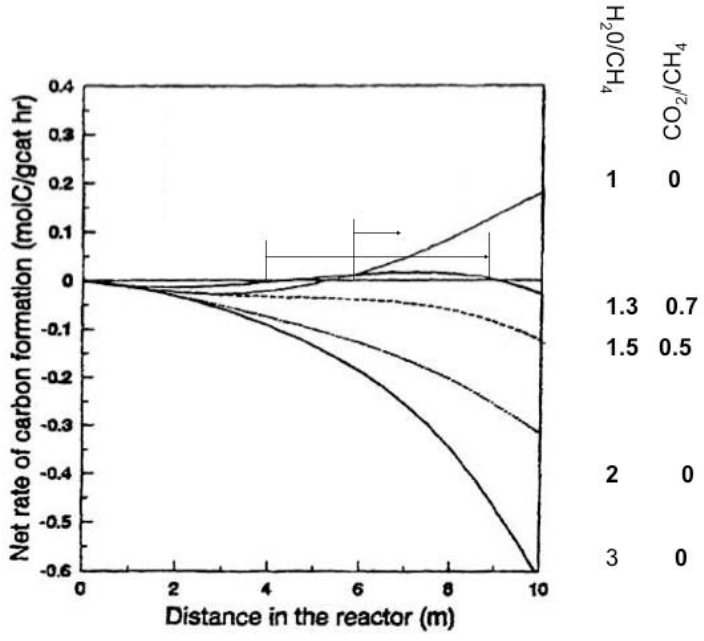

Figure 5.3.3.C-4

Net rate of coke formation along the reactor for various compositions of the feed and a fixed temperature and total pressure profile. From Snoeck et al. [1997].

is a kinetic problem, however, so that the approach illustrated here is more accurate and more specific for the catalyst.

It is of particular importance to predict zones of coke accumulation because the associated deactivation of the catalyst reduces the local endothermic effect leading to overheating of the reactor tube under the effect of the heat flux from the furnace to the reacting mixture. The formation of whisker coke is particularly detrimental because it can be blown off the catalyst under the high flow rates encountered in steam reformers. The dust is then blown out of the reactor into downstream equipment, like heat exchangers or compressors, where it can be particularly damaging.

■

EXAMPLE 5.3.3.D

COKE FORMATION IN THE CATALYTIC CRACKING OF VACUUM GAS OIL

Catalyst deactivation is an essential aspect of the catalytic cracking of Vacuum Gas Oil (VGO). It led to the fluidized bed process and later, with the advent of more active catalysts to the transport bed or riser process. Also, the process is conceived in such a way that the regeneration of the catalyst by burning off the coke produces the heat required to perform the endothermic catalytic cracking, as will be illustrated in Chapter 13.

The kinetics of the catalytic cracking of vacuum gas oil for gasoline production were modeled in terms of elementary steps of carbocation chemistry, as discussed in Chapter 2 and the number of independent parameters was reduced using the single event concept [Moustafa and Froment, 2003]. The next step was to define the nature of the deactivating agent, commonly called “coke” and whose quantity is determined by combustion of the carbonaceous deposits on the catalyst. In line with the mechanistic approach for the modeling of the process the deactivating agent was defined as a carbenium ion with a size and structure preventing its desorption, thus permanently covering the actives sites of the catalyst. The literature agrees that coke mainly consists of polyaromatic molecules [Appleby et al., 1962; Mignard et al., 1989; Guisnet et al., 1997; see also Fig. 5.3.1-1]. Therefore, the deactivating agent was defined to consist of at least 5-ring aromatic rings and to contain a number of C-atoms of at least 40, i.e., exceeding that of the VGO-feed. Also, their basic character results in a strong adsorption on the acid zeolite catalyst used in catalytic cracking.

Instead of dealing with coke formation as a black box, as is usually done, it was written in terms of elementary steps of carbenium- and carbonium-ion chemistry, just like the “main reactions”. In this way, advantage can be taken of

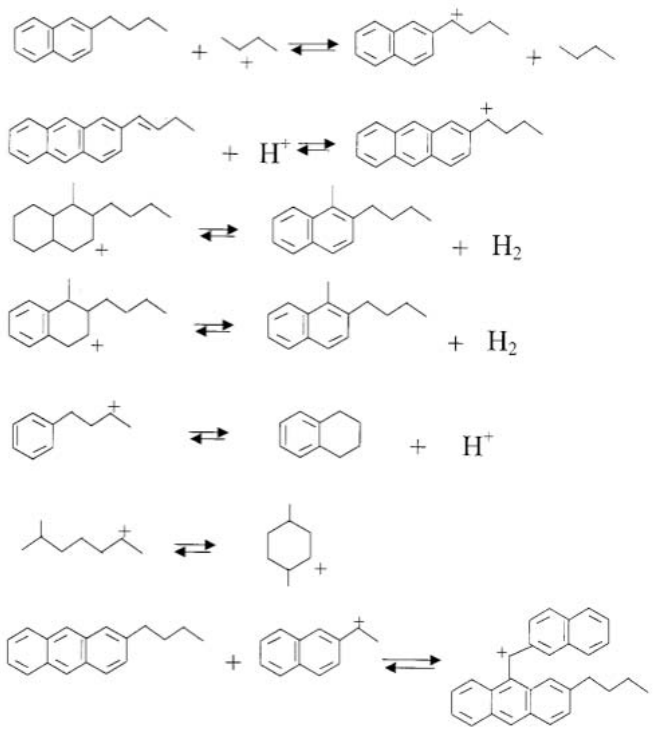

Figure 5.3.3.D-1

Mechanistic scheme for coke formation in the catalytic cracking of vacuum gas oil [Moustafa and Froment, 2003].

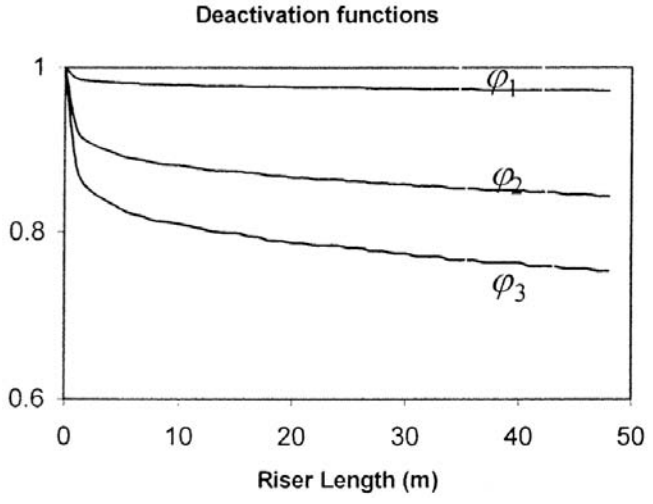

Figure 5.3.3.D-2

Deactivation functions used in the modeling of the deactivation of the US-Y-zeolite catalyst in the catalytic cracking of vacuum gas oil [Moustafa and Froment, 2003].

the identity or analogy of common types of steps. Consequently, when the single event approach is used, the number of rate parameters does not significantly increase. A simplified representation of the coking scheme is shown in Fig. 5.3.3.D-1. It should be clear from this scheme that "coke" is not a dead species and may interact with other species of the reacting mixture, a feature also deduced from commercial operation.

Next the activity of the catalyst has to be related to the amount of deactivating agent. This is done by means of exponential deactivation functions. Three deactivating functions were selected: one for the effect of alkylation, one for the monomolecular steps and one for the bimolecular steps, as illustrated in Fig. 5.3.3.D-2. The deactivation parameter in the exponentials was derived from the experimental data. The evolution of the deactivating functions with the "coke" content is also shown.

■

5.3.4 Conclusions

Catalyst deactivation by the formation of carbonaceous species is a phenomenon with far reaching and important consequences that justify substantial attention in the development of a process and its catalyst. In a recent review on coking in hydrocarbon processing Froment [2008] showed how the pathways to the deactivating agent(s) are often of the same type as those leading to the main products. Advantage was taken of these similarities to formulate more realistic rate equations for the phenomenon and thus establish a link with the composition of the reacting mixture. Such a kinetic model is necessary for the prediction of the accumulation of coke with process time and of the evolution of the catalyst deactivation and its effect on the reactor performance and product selectivities. Knowledge of the quantity and profile of the deactivating agent in the reactor is important also for the in situ regeneration of the catalyst, an operation that needs to be conducted with care to avoid damaging the catalyst by temperature excursions, in particular if it is to be frequently repeated. A better insight in the chemistry of the formation of the deactivating agents will also contribute to the development of more adequate catalysts for the process.

PROBLEMS

5.1 For shell-progressive poisoning, the "shrinking core" model of Chapter 4 was utilized to derive the time rate of change of poison deposition, (5.2.3-6.) Complete the steps leading to this result.

5.2 The effect on the reaction rate for shell-progressive poisoning is based on equations (5.2.3-8), (5.2.3-9), and (5.2.3-10). Use these to derive the effectiveness factor relationship (5.2.3-11).

5.3 The amount of poison deposited is given as a function of the dimensionless process time by Fig. 5.2.3-1. Also, the deactivation function for given poison levels is in Fig. 5.2.3-2. Combine these in a figure for the deactivation function as a function of dimensionless time for the shell-progressive mechanism.

5.4 Derive (5.2.4-5) and (5.2.4-7) for poisoning effects with consecutive reactions.

5.5 Derive (5.2.4-8) and (5.2.4-9) for poisoning effects with parallel reactions.

5.6 Coke profiles in catalyst pellets have been measured by Richardson [1972], as shown in Fig. 1. Use these to determine the parameters in an appropriate deactivation model:

(a) Which coking mechanism prevailed?

(b) Utilizing reasonable assumptions, which should be stated, complete the analysis with a deactivation model.

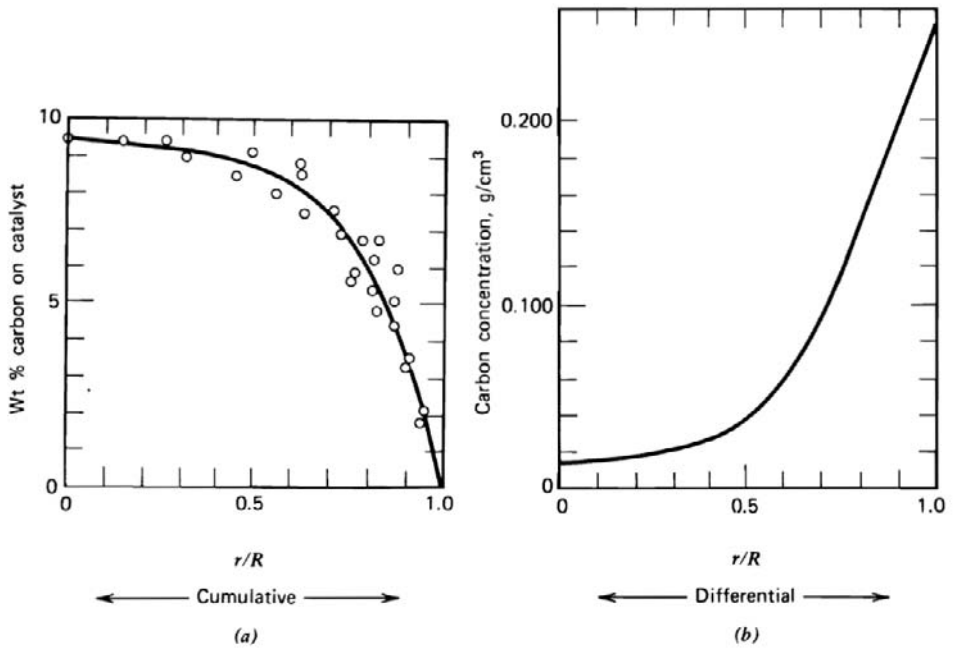

Figure 1

Measurement of carbon profiles. (a) Experimental data. (b) Calculated profile. Parallel fouling mechanism. From Richardson [1972].

REFERENCES

Appleby, W.G., Gibson, J.W., and Good, G.M., *Ind. Eng. Chem. Proc. Des. Dev.*, 1, 102 (1962).
Balder, J., and Petersen, E.E., *Chem. Eng. Sci.*, 23, 1287 (1968).
Beeckman, J.W., and Froment, G.F., *Ind. Eng. Chem. Fundam.*, 18, 245 (1979).
Beeckman, J.W., and Froment, G.F., *Chem. Eng. Sci.*, 35, 805 (1980).
Beeckman, J.W., and Froment, G.F., *Ind. Eng. Chem. Fundam.*, 21, 243 (1982).
Beeckman, J.W., In-Sik Nam, and Froment, G.F., in *Catalyst Deactivation 1987*, Eds. B. Delmon and G.F. Froment, Elsevier Science Publishers B.V., 365-379 (1987).
Beirnaert, H.C., Vermeulen, R., and Froment, G.F., *Stud. Surf. Sci. Catal.*, 88, 97 (1994).
Beyne, A.O.E., and Froment, G.F., *Chem. Eng. Sci.*, 48, 503 (1993).
Butt, J.B., *Adv. in Chem. Ser.*, 108, 259, A.C.S., Washington, D.C. (1972).
Butt, J.B., *J. Catal.*, 41, 190 (1976).
Butt, J.B., Wachter, C.K., and Billimoria, R.M., *Chem. Eng. Sci.*, 33, 1321 (1978).
Campbell, D.R., and Wojciechowski, B.W., *Can. J. Chem. Eng.*, 47, 413 (1969).
Carberry, J.J., and Gorring, R.L., *J. Catal.*, 5, 529 (1966).
Dadyburjor, D.B., in *Catalyst Deactivation 1987*, ed. by B. Delmon and G.F. Froment, Elsevier, Amsterdam (1987).
Delmon, B., and Grange, P., in *Catalyst Deactivation*, ed. by B. Delmon and G.F. Froment, Elsevier, Amsterdam (1980).
Delmon, B., in *Catalyst Deactivation*, C.H. Bartholomew, G.A. Fuentes (Eds.), Vol. 111, Studies in Surface Science and Catalysis, Elsevier, Amsterdam, p. 39 (1997).
De Pauw, R., and Froment, G.F., *Chem. Eng. Sci.*, 30, 789 (1975).
Devoldere, K.R., and Froment, G.F., *Ind. Eng. Chem. Res.*, 38, 2626 (1999).
Dumez, F.J., and Froment, G.F., *Ind. Eng. Chem. Proc. Des. Dev.*, 15, 291 (1976).
Flynn, P.C., and Wanke, S.F., *J. Catal.*, 34, 390 (1974); *ibid.*, 34, 400 (1975).
Froment, G.F., in *Progress in Catalyst Deactivation*, NATO Advanced Study Institute E54, ed. by J.L. Figeiredo, Nijhoff, The Hague (1982).
Froment, G.F., in *Actas do 9° Symposio Iberio-Americano de Catalyse*, Lisboa (July 1984).
Froment, G.F., *J. Mol. Catal. A-Chem*, 163, 147 (2000).
Froment, G.F., *Catalysis Reviews. Science and Engineering*, 50(1), 1 (2008).
Froment, G.F., and Bischoff, K.B., *Chem. Eng. Sci.*, 16, 189 (1961).
Froment, G.F., and Bischoff, K.B., *Chem. Eng. Sci.*, 17, 105 (1962).
Gottifredi, J.C., and Froment, G.F., *Chem. Eng. Sci.*, 52, 1883 (1997).
Guisnet, M., Magnaux, P., and Martin, D., in *Catalyst Deactivation 1997*, Eds. C.H. Bartholomeus and G.A. Fuentes, 1-19 (1997); *Studies in Surface Science and Catalysis*, 111, Elsevier (1997).
Hegedus, L., and McCabe, R.W., in *Catalyst Deactivation*, ed. by B. Delmon and G.F. Froment, Elsevier, Amsterdam (1980).
Hegedus, L., and Petersen, E.E., *J. Catal.*, 28, 150 (1973a).
Hegedus, L., and Petersen, E.E., *Chem. Eng. Sci.*, 28, 69 (1973b).
Hosten, L.H., and Froment, G.F., *Ind. Eng. Chem. Proc. Des. Dev.*, 10, 280 (1971).
Johanson, L.N., and Watson, K.M., *Natl. Petr. News-Technol. Sect.*, (August 1946).
Lamy-Pitara, E., Bencharif, L., and Barbier, J., *Appl. Catal.*, 18, 117 (1985).
Levenspiel, O., *J. Catal.*, 25, 265 (1972).
Liu, K., Fung, S.C., Ho, T.C., and Rumschitzki, D.S., in *Catalyst Deactivation 1997*, Eds. C.H. Bartholomeus and G.A. Fuentes, 625-638 (1997); *Studies in Surface Science and Catalysis*, 111, Elsevier (1997).
Marin, G.B., Beeckman, J.W., and Froment, G.F., *J. Catal.*, 97, 416 (1986).
Martinis, J.M., and Froment, G.F., *Ind. Eng. Chem. Res.*, 45, 940 (2006).
Martinis, J.M., and Froment, G.F., *Ind. Eng. Chem. Res.*, 45, 954 (2006).
Masamune, S., and Smith, J.M., *AIChE J.*, 12, 384 (1966).
Maxted, E.B., *Adv. in Catal.*, 3, 129 (1951).
Mignard, S., Cartraud, P., Magnoux, P., and Guisnet, M., *J. Catal.*, 117, 503 (1989).
Mills, G.A., Boedekker, E.R., and Oblad, A.G., *J. Am. Chem. Soc.*, 72, 1554 (1950).
Moustafa, T.M., and Froment, G.F., *Ind. Eng. Chem. Res.*, 42, 14 (2003).
Murakami, Y., Kobayashi, T., Hattori, T., and Masuda, M., *Ind. Eng. Chem. Fundam.*, 7, 599 (1968).

Nam, In-Sik, and Froment, G.F., *J. Catal.*, 108, 271 (1987).
Olson, J.H., *Ind. Eng. Chem. Fundam.*, 7, 185 (1968).
Ozawa, Y., and Bischoff, K.B., *Ind. Eng. Chem. Proc. Des. Dev.*, 7, 67 (1968).
Pachovsky, R.A., and Wojciechowski, B.W., *AIChE J.*, 19, 802 (1973).
Patashnick, and Rupprecht, TEOM Series 1500 PMA Reaction Kinetics Analyzer, Thermo Electron Corporation, Environmental Instruments Division, East Greenbush, NY 12061 (1980).
Ray, W.H., *Chem. Eng. Sci.*, 27, 489 (1972).
Richardson, J.T., *Ind. Eng. Chem. Proc. Des. Dev.*, 11, 8 (1972).
Rückenstein, E., and Pulvermacher, B., *AIChE J.*, 19, 456 (1973).
Rückenstein, E., and Dadyburjor, D.B., *Thin Solid Films*, 55, 89 (1978).
Rückenstein, E., in *Catalyst Deactivation*, Eds. C.H. Bartholomew and J.B. Butt, Studies in Surface Science and Catalysis, 585 (1991).
Rückenstein, E., *J. Colloid Interface Sci.*, 188, 218 (1997).
Rückenstein, E., in *Catalyst Deactivation 1994*, Eds. B. Delmon and G.F. Froment, 33-52 (1994); *Studies in Surface Science and Catalysis*, 88, Elsevier (1994).
Rudershausen, C.G., and Watson, C.C., *Chem. Eng. Sci.*, 3, 110 (1954).
Sada, E., and Wen, C.Y., *Chem. Eng. Sci.*, 22, 559 (1967).
Sahimi, M., and Tsotsis, T.T., *J. Catal.*, 96, 552-562 (1985).
Snoeck, J.W., Froment, G.F., and Fowles, M., *J. Catal.*, 169, 240 (1997).
Snoeck, J.W., Froment, G.F., and Fowles, M., *J. Catal.*, 169, 250 (1997).
Snoeck, J.W., Froment, G.F., and Fowles, M., *Ind. Eng. Chem. Res.*, 41, 3548 (2002).
Snoeck, J.W., Froment, G.F., and Fowles, M., *Ind. Eng. Chem. Res.*, 41, 4252 (2002).
Snoeck, J.W., Froment, G.F., and Fowles, M., *Int. J. Chem. Reactor Eng.*, 1, A7 (2003).
Suga, K., Morita, Y., Kunugita, E., and Otake, T., *Int. Chem. Eng.*, 7, 742 (1967).
Szepe, S., and Levenspiel, O., *Proc. 4th Eur. Symp. Chem. Reaction Eng.*, Brussels, 1968, Pergamon Press, London (1971).
Takeuchi, M., Ishige, T., Fukumuro, T., Kubota H., and Shindo, M., *Kag. Kog.* (Engl. Ed.), 4, 387 (1966).
Villadsen, J., *Selected Approximation Methods for Chemical Engineering Problems*, Danmarks Tekniske Hojskole (1970).
Voorhies, A., *Ind. Eng. Chem.*, 37, 318 (1945).
Weekman, V.W., *Ind. Eng. Chem. Proc. Des. Dev.*, 7, 90 (1968).
Weekman, V.W., *Ind. Eng. Chem. Proc. Des. Dev.*, 8, 385 (1969).
Weekman, V.W., *AIChE J.*, 20, 833 (1974).
Weekman, V.W., and Nace, D.M., *AIChE J.*, 16, 397 (1970).
Wheeler, A., in *Catalysis*, ed. by P.H. Emmett, Vol. II, Reinhold, New York (1955).
Wojchiechowski, B.W., *Can. J. Chem. Eng.*, 46, 48 (1968).
Wright, C.J., McMillan, J.W., and Cookson, J.A., *J. Chem. Comm.*, 968 (1979).
Xu, J., and Froment, G.F., *AIChE J.*, 35, 88 (1989).
Xu, J., and Froment, G.F., *AIChE J.*, 35, 97 (1989).

Chapter 6

Gas-Liquid Reactions

6.1 INTRODUCTION

There are many examples of reactions between gases and liquids in industry. They belong to two categories. The first category groups the gas purification processes such as removal of CO_2 from synthesis gas by means of aqueous solutions of hot potassium carbonate or ethanolamines, or the removal of H_2S

and CO_2 from hydrocarbon cracking gas by means of ethanolamines or sodium hydroxyde. The second category groups the production processes such as the reaction between a gaseous CO_2 stream and an aqueous ammonia solution to give ammonium carbonate, air oxidation of acetaldehyde and higher aldehydes to give the corresponding acids, or oxidation of cyclohexane to give adipic acid—one of the steps of nylon 66 synthesis. Other production processes are chlorination of benzene and other hydrocarbons, absorption of NO_2 in water to give nitric acid, absorption of SO_3 in H_2SO_4 to give oleum, air oxidation of cumene to cumenehydroperoxide—one of the steps of the Hercules-Distillers phenol process.

These processes are carried out in a variety of equipment ranging from a bubbling absorber to a packed tower or plate column. The design of the absorber itself requires models characterizing the operation of the process equipment, and this is discussed in Chapter 14. The present chapter is concerned only with the rate of reaction between a component of a gas and a component of a liquid—it considers only a point in the reactor where the partial pressure of the reactant A in the gas phase is p_A, the concentration of A in the liquid C_A, and the concentration of B is C_B. Setting up rate equations for such a heterogeneous reaction will again require consideration of mass and eventually heat transfer rates in addition to the true chemical kinetics. Therefore, models for transport from a gas to a liquid phase are discussed first.

6.2 MODELS FOR TRANSFER AT A GAS-LIQUID INTERFACE

Several models have been proposed to describe the phenomenon occurring when a gas phase is brought into contact with a liquid phase. The model that has been used most is the two-film theory proposed by Whitman [1923] and by Lewis and Whitman [1924]. In this theory a stagnant layer is supposed to exist in both phases along the interface. In the gas phase the component A experiences a resistance to its transfer to the interface which is entirely concentrated in the film. At the interface itself there is no resistance so that Henry's law is satisfied:

$$p_{Ai} = HC_{Ai} \tag{6.2-1}$$

where H has the dimension m³ bar/kmol.

The resistance to transfer of A from the interface to the bulk liquid is supposed to be entirely located in the liquid film. Beyond that film the turbulence is sufficient to eliminate concentration gradients. This concept is illustrated in Fig. 6.2-1. The two-film theory originated from the picture adopted for heat transfer between a fluid and a solid surface along which the fluid is flowing in turbulent motion. In that case it is also assumed that at each point along the

surface heat is transferred from the fluid to the solid through a laminar boundary layer only by conduction. The entire temperature gradient is limited to this film, since the turbulence is sufficient to eliminate any gradient outside the film. Applying Fourier's law to the conduction through the film in the direction perpendicular to the flow leads to

$$q = \frac{\lambda}{y_h}(T_b - T_s)$$

where y_h is the liquid film thickness for heat transfer; λ is the conductivity; and T_b and T_s are the bulk and surface temperatures, respectively. Since the film thickness is not measurable, a convection heat transfer coefficient α is introduced:

$$\alpha = \frac{\lambda}{y_h}$$

The same concept has been applied to mass transfer in the gas and liquid phases, for which one can write, in the absence of reaction,

$$N_{AG} = \frac{D_{AG}}{y_G}(p_A - p_{Ai}) \tag{6.2-2}$$

$$N_{AL} = \frac{D_{AL}}{y_L}(C_{Ai} - C_A) \tag{6.2-3}$$

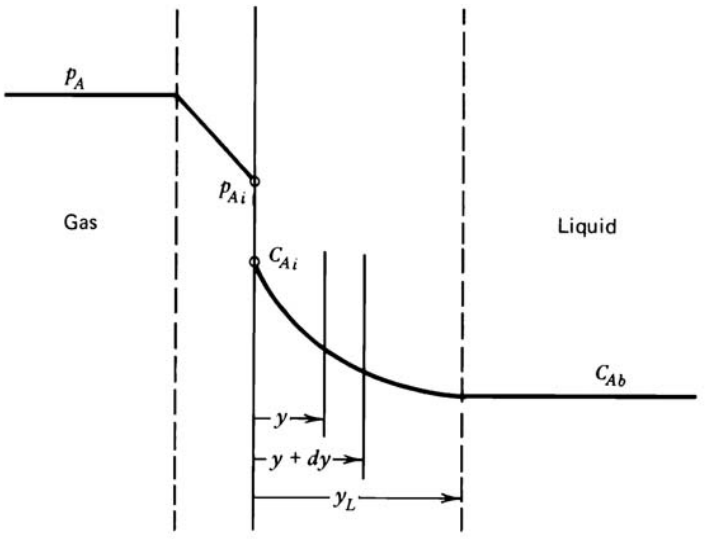

Figure 6.2-1
Two-film concept for mass transfer between a gas and a liquid.

Again, the absence of information on both y_G and y_L leads to the introduction of mass transfer coefficients for the transport of A in the gas and liquid phases, k_G and k_L, respectively:

$$k_G = \frac{D_{AG}}{y_G} \quad \text{and} \quad k_L = \frac{D_{AL}}{y_L} \tag{6.2-4}$$

The two-film theory is an essentially steady-state theory. It assumes that the steady-state profiles corresponding to the given p_A and C_A are instantaneously realized. This requires that the capacity of the films be negligible. The two-film theory certainly lacks reality in postulating the existence of films near the interface between the gas and liquid, yet it contains the essential features of the phenomenon, that is, the dissolution and the diffusion of the gas, prior to transfer to the turbulent bulk of the liquid. Nevertheless, the theory has enabled consistent correlation of data obtained in equipment in which the postulates are hard to accept completely.

These considerations have led to other models, called "penetration" or "surface renewal" models. In these models the surface at any point is considered to consist of a mosaic of elements with different ages at the surface. An element remains at the surface for a certain time and is exposed to the gas. The element has a volume capacity for mass, is quiescent during its stay at the surface, and is infinitely deep according to some investigators, or limited to a certain depth according to others. While at the surface each of the elements is absorbing at a different rate, depending on its age, and therefore also on the concentration profile that has been established. After a certain time of exposure, the element is replaced by an element coming from the bulk of the liquid. The mechanism of this replacement is not relevant at this point: it may be due to turbulence or to the flow characteristics in the equipment. For example, think of a packed bed absorber in which the liquid may flow over the particles in laminar flow but is mixed at contact points between particles and in voids, bringing fresh, unexposed elements to the liquid surface. The surface renewal models, in dropping the zero capacity restriction on the film, have to consider the establishment of the profiles with the age of the element at the surface. Consequently, they are essentially nonsteady in nature. Furthermore, they have to assume an age distribution function for the elements of the surface, $\Psi(t)$. The average rate of absorption of the surface at the point considered is then

$$N_A = \int_0^\infty N_A(t)\Psi(t)dt \tag{6.2-5}$$

where $N_A(t)$ is the rate of absorption in an element of the mosaic constituting the surface having an age t.

The models discussed above will not be applied to the situation of transfer accompanied by reaction. We first use the two-film theory, then the surface renewal theory. The literature on the subject is overwhelming, and no attempt is made to be complete. Instead, the general concepts are synthesized and illustrated. More extensive coverage can be found in several textbooks more oriented toward gas absorption [Sherwood, Pigford and Wilke, 1975; Ramm, 1953; Astarita, 1967; Danckwerts, 1970; and Astarita et al., 1983].

6.3 TWO-FILM THEORY

6.3.1 Single Irreversible Reaction with General Kinetics

First, consider the case of a chemical reaction that is very slow with respect to the mass transfer, so that the amount of A that reacts during its transfer through the liquid film is negligible. The rate of transfer of A from the liquid interface to the bulk may then be written

$$N_A A_v = k_L A_v \left(C_{Ai} - C_{Ab}\right)$$

where A_v represents the interfacial area per liquid volume $\left(\mathrm{m}_i^2 / \mathrm{m}_L^3\right)$. The reaction then occurs completely in the bulk at a rate $r_A = r_A\,(C_{Ab}, C_{Bb})$. When the two phenomena are purely in series, as assumed here, the resistances may be added, as was shown in Chapter 3 for the simple example of a reaction between a gas and a nonporous solid, to yield the resistance or the rate coefficient for the overall phenomenon. As mentioned previously, in this chapter only a "point" in a reactor will be considered, for instance, a volume dV at a certain height in a packed column, with uniform concentrations in a cross section. To arrive at C_{Ab} and C_{Bb} at that point in the reactor requires consideration of the complete reactor with its typical flow pattern and type of operation. This problem is discussed in Chapter 14.

When the rate of reaction cannot be neglected with respect to the mass transfer, the amount reacted in the film has to be accounted for in an explicit way. Let A be the component of the gas phase reacting with a nonvolatile component B in the liquid phase and let the film be isothermal. The reaction considered is

$$aA + bB \rightarrow qQ + pP$$

and is confined to the liquid phase. Consider only the liquid phase first. Since concentration gradients are limited to the film, a mass balance on A in a slice of

thickness *dy* and unit cross section in the liquid film is set up (Fig. 6.2-1). Since the two-film theory implies steady state, the balance may be written

$$D_A \frac{d^2 C_A}{dy^2} = r_A \tag{6.3.1-1}$$

and, of course,

$$D_B \frac{d^2 C_B}{dy^2} = \frac{b}{a} r_A \tag{6.3.1-2}$$

where

$$r_A = f(C_A, C_B; T)$$

and, with *BC*,

$$y = 0 \qquad C_A = C_{Ai} \qquad C_B = C_{Bi} \tag{6.3.1-3}$$

$$y = y_L \qquad C_A = C_{Ab} \qquad C_B = C_{Bb} \tag{6.3.1-4}$$

where C_{Ab} is the bulk concentration of unreacted species.

The bulk concentrations must be determined from an equation for the mass flux through the film-bulk boundary:

$$A_v N_A\big|_{y=y_L} = (1 - A_v y_L) r_{Ab} + \left(\begin{array}{l} \text{net amount of } A \text{ transported} \\ \text{into corresponding} \\ \text{differential bulk volume by} \\ \text{various mechanisms—for} \\ \text{example, flow} \end{array} \right) \tag{6.3.1-5}$$

The last term of (6.3.1-5) arises from the fact that the element of bulk fluid considered here is not isolated from its surroundings. When C_{Ab} is not zero, *A* is transported through liquid flow and diffusion mechanisms into and out of the element, as is discussed in detail in Chapter 14 on gas-liquid reactors. Some past work has ignored this term, presumably to obtain general results relating C_{Ab} to the reactor conditions at the given point but thereby introducing important errors in C_{Ab}. For very rapid reactions, for which C_A attains the bulk value (e.g., zero or an equilibrium value C_{Aeq} for a reversible reaction) at $y \le y_L$, (6.3.1-4) does not apply, of course. A different approach is given later for this situation.

Integrating (6.3.1-1) or (6.3.1-2) with the given boundary conditions and rate equation leads to the concentration profiles of *A* and *B* in the liquid film. The rate of the overall phenomenon, as seen from the interface, then follows from the application of Fick's law:

$$N_A = -D_A \left. \frac{dC_A}{dy} \right|_{y=0} \tag{6.3.1-6}$$

In general, (6.3.1-1) cannot be integrated analytically. This is only feasible for some special cases of rate equations. We limit ourselves first to those cases in order to illustrate the specific features of gas-liquid reactions.

6.3.2 First-Order and Pseudo-First-Order Irreversible Reactions

In this case (6.3.1-1) becomes

$$D_A \frac{d^2 C_A}{dy^2} = k C_A \tag{6.3.2-1}$$

where $k = ak'C_{Bb}$ for a pseudo-first-order reaction. The integral of (6.3.2-1) may be written as

$$C_A = A_1 \cosh\left(\gamma \frac{y}{y_L}\right) + A_2 \sinh\left(\gamma \frac{y}{y_L}\right)$$

where

$$\gamma = y_L \sqrt{\frac{k}{D_A}} = \frac{\sqrt{kD_A}}{k_L}$$

since $k_L = D_A/y_L$. The group γ is sometimes called the Hatta number and is very similar to the modulus used in the effectiveness factor approach of Chapter 3. Accounting for the *BC*, (6.3.1-3) and (6.3.1-4) permits the determination of the integration constants A_1 and A_2. The solution is

$$C_A = \frac{C_{Ai} \sinh\left(\gamma\left(1 - \frac{y}{y_L}\right)\right) + C_{Ab} \sinh\left(\gamma \frac{y}{y_L}\right)}{\sinh \gamma} \tag{6.3.2-2}$$

from which it is found, applying (6.3.1-6), that

$$N_A\big|_{y=0} = \frac{\gamma D_A}{y_L} \frac{C_{Ai} \cosh \gamma - C_{Ab}}{\sinh \gamma}$$

This equation is easily rewritten into

$$N_A = \frac{\gamma}{\tanh \gamma}\left(1 - \frac{C_{Ab}}{C_{Ai}} \frac{1}{\cosh \gamma}\right) k_L C_{Ai} \tag{6.3.2-3}$$

As mentioned already, this equation has to be combined with a mass balance in the bulk to define C_{Ab} and also C_{Bb}, which enters through γ. The concentration

C_{Bb} is constant in any one horizontal slice, but not necessarily over all heights of the equipment. The mass balances yielding C_{Ab} and C_{Bb} are given in Chapter 14.

Let this flux N_A now be compared with that obtained when there is no resistance to mass transfer in the liquid, that is, when the concentration of A in the liquid is C_{Ai} throughout. From the analogy with the effectiveness factor concept, a liquid utilization factor η_L will be defined as follows:

$$\eta_L = \frac{N_A A_v}{k C_{Ai}} = \frac{1}{\gamma \mathrm{Sh}_m \tanh \gamma} \left(1 - \frac{C_{Ab}}{C_{Ai}} \frac{1}{\cosh \gamma} \right) \tag{6.3.2-4}$$

where $\mathrm{Sh}_m = k_L / A_v D_A$ is a modified Sherwood number.

For very rapid reactions (i.e., when γ exceeds 3) cosh $\gamma > 10$, and since $C_{Ab} / C_{Ai} \leq 1$, (6.3.2-4) becomes

$$\eta_L = \frac{1}{\gamma \mathrm{Sh}_m \tanh \gamma}$$

For $\gamma > 5$, the only meaningful situation when $C_{Ab} = 0$, the utilization factor reduces to

$$\eta_L = \frac{1}{\gamma \mathrm{Sh}_m} = A_v \sqrt{\frac{D_A}{k}}$$

which means that in a plot of log η_L versus $\gamma \mathrm{Sh}_m$, a straight line with slope –1 is obtained.

So far, the gas film resistance has not been included. This is easily done by eliminating C_{Ai} from (6.3.2-3) by means of the gas film flux expression $N_A = k_G(p_{Ab} - p_{Ai})$, together with Henry's law and by accounting for the fact that the resistances to transport through the gas and liquid film are purely in series. The following result is obtained:

$$N_A = \frac{p_{Ab} - \dfrac{H C_{Ab}}{\cosh \gamma}}{\dfrac{1}{k_G} + \dfrac{H}{k_L} \dfrac{\tanh \gamma}{\gamma}} \tag{6.3.2-5}$$

Note that when $\gamma \to 0$, the equation for physical mass transfer is recovered. When $\gamma \to \infty \left(\gamma > 5 \right)$, (6.3.2-5) leads to

$$N_A = \frac{p_{Ab}}{\dfrac{1}{k_G} + \dfrac{H}{k_L \gamma}}$$

which is the equation derived when $C_{Ab} = 0$, through a simplified approach that can be found in the literature. Indeed, when γ is large, the reaction is completed in the film.

It is also possible to base a utilization factor on the bulk gas-phase composition, much in the same way as was done already with the η_G concept for reaction and transport around and inside a catalyst particle. Let this global utilization factor, based on the bulk gas phase composition, η_G, be defined as the ratio of the actual rate per unit volume of liquid to the rate that would occur at a liquid concentration equivalent to the bulk gas-phase partial pressure of the reactant *A*:

$$\eta_G = \frac{N_A A_v H}{k p_{Ab}} \tag{6.3.2-6}$$

Since $N_A A_v = \eta_L k C_{Ai}$ and $N_A = k_G (p_{Ab} - p_{Ai})$, using $p_{Ai} = HC_{Ai}$ leads to

$$N_A = \frac{p_{Ab}}{\frac{1}{k_G} + \frac{HA_v}{k\eta_L}} \tag{6.3.2-7}$$

Combining (6.3.2-6) and (6.3.2-7) leads to

$$\frac{1}{\eta_G} = \frac{1}{\eta_L} + \frac{k}{Hk_G A_v}$$

or, in terms of the modified Sherwood number for the liquid-phase mass transfer,

$$\frac{1}{\eta_G} = \frac{1}{\eta_L} + \left(\frac{k_L}{Hk_G}\right)\gamma^2 \mathrm{Sh}_m \tag{6.3.2-8}$$

For large γ,

$$\frac{1}{\eta_G} = \gamma \mathrm{Sh}_m + \left(\frac{k_L}{Hk_G}\right)\gamma^2 \mathrm{Sh}_m$$

In the region of extremely rapid reaction, the utilization factor approach, which refers the observed rate to the maximum possible chemical rate, has the drawback of requiring accurate values of the rate coefficient *k*. An alternate way is to refer to the physical liquid-phase mass transfer rate, which is increased by the chemical reaction. This then leads to the definition of an enhancement factor F_A:

$$F_A = \frac{N_A}{k_L (C_{Ai} - C_{Ab})} \tag{6.3.2-9}$$

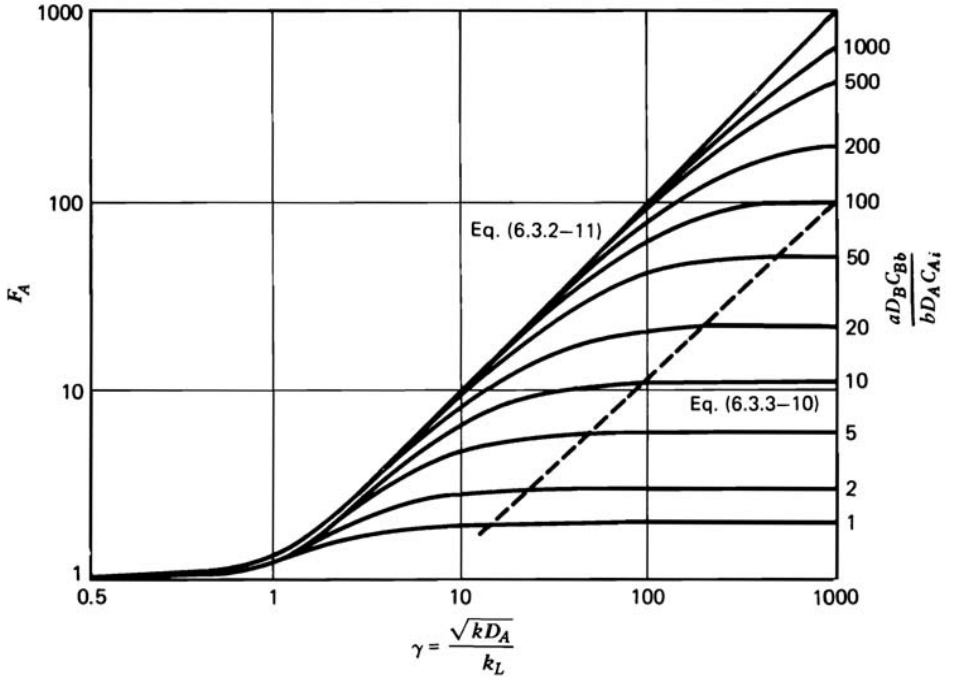

Figure 6.3.2-1
Enhancement factor diagram for $C_{Ab} = 0$.

and substituting N_A from (6.3.2-3) leads to

$$F_A = \frac{\gamma}{\tanh\gamma}\left(1 - \frac{C_{Ab}}{C_{Ai}}\frac{1}{\cosh\gamma}\right) \qquad (6.3.2\text{-}10)$$

In the literature it is often assumed that in the presence of chemical reaction the concentration of A in the bulk is essentially zero. Starting from (6.3.1-1) with the B.C. at $y = y_L$, $C_A = C_{Ab} = 0$. The solution for this situation is easily found:

$$N_A = F_A k_L C_{Ai}$$

where

$$F_A = \frac{\gamma}{\tanh\gamma} \qquad (6.3.2\text{-}11)$$

Note that F_A equals γ for very large γ. The reaction is essentially completed in the film when $\gamma > 3$, whereas it takes place mainly in the bulk when $\gamma < 0.3$.

At this point a diagram can be constructed showing F_A as a function of γ, as first given by Van Krevelen and Hoftijzer [1948], but only for the case of no reaction in the bulk (Fig. 6.3.2-1). The other curves in the diagram pertain to

second-order and instantaneous reactions, and their derivation and discussion are given in the next section.

The enhancement factor approach, like the utilization factor approach, permits accounting for gas-phase resistance. Again the gas-phase flux equation, Henry's law, the liquid-phase flux equation, and the equality of fluxes through both phases can be combined to eliminate C_{Ai}, with the result that

$$N_A = \frac{p_{Ab}}{\dfrac{1}{k_G} + \dfrac{H}{F_A k_L}} \tag{6.3.2-12}$$

where F_A is given by (6.3.2-11).

6.3.3 Single, Instantaneous, and Irreversible Reactions

When the reaction is infinitely fast, the thickness of the reaction zone will be reduced to that of a plane situated at a distance y_1 from the interface as illustrated in Fig. 6.3.3-1. In the zone of the liquid film between the interface and the reaction plane at y_1, C_A varies between C_{Ai} and zero, and there is no more B, as shown in Fig. 6.3.3-1. In the zone between y_1 and y_L, there is no more A, only B, which varies between zero and C_{Bb}. The location of the reaction plane is dictated by the concentrations C_{Ai} and C_{Bb}, but also by the diffusion rates.

The concentration profile for A in the zone $y = 0$ to $y = y_1$ is obtained from (6.3.1-1) in which r_A is set equal to zero, since there is no reaction in that zone. A first integration leads to

$$D_A \frac{dC_A}{dy} = \text{constant} = -N_A$$

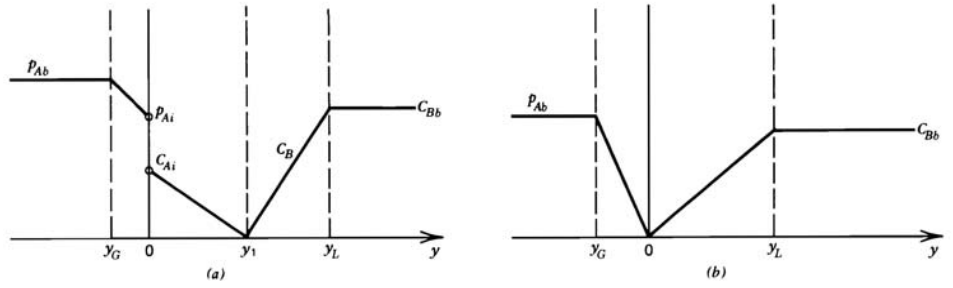

Figure 6.3.3-1

Absorption and infinitely fast reaction. Concentration profiles for A and B, when (a) $C_{Bb} < C'_{Bb}$ and (b) $C_{Bb} = C'_{Bb}$, respectively. See (6.3.3-7).

Note that in the absence of reaction the concentration profile is linear, as drawn in Fig. 6.3.3-1. A second integration leads to

$$N_A = \frac{D_A}{y}\left(C_{Ai} - C_A\right) \tag{6.3.3-1}$$

Applied to the zone $y = 0$ to y_1, where $C_A = 0$, (6.3.3-1) becomes

$$N_A = \frac{D_A}{y_1} C_{Ai}$$

The flux of B is obtained in a similar way, leading to

$$-N_B = \frac{D_B}{y_L - y_1} C_{Bb} \tag{6.3.3-2}$$

where

$$\frac{N_A}{a} = -\frac{N_B}{b}$$

Consequently,

$$y_1 N_A = D_A C_{Ai}$$

and, from (6.3.3-2),

$$\left(y_L - y_1\right) N_A = \frac{a}{b} D_B C_{Bb}$$

By summing up the two last expressions, one obtains

$$N_A = k_L C_{Ai}\left(1 + \frac{a}{b}\frac{D_B}{D_A}\frac{C_{Bb}}{C_{Ai}}\right) \tag{6.3.3-3}$$

where, as before,

$$k_L = \frac{D_A}{y_L}$$

Again, define a utilization factor as

$$\eta_L = \frac{N_A A_v}{k C_{Ai}} = \frac{k_L\left(1 + \frac{a}{b}\frac{D_B}{D_A}\frac{C_{Bb}}{C_{Ai}}\right) A_v}{k} \tag{6.3.3-4}$$

or, in terms of the modified Sherwood number,

$$\eta_L = \frac{1}{\gamma^2 \mathrm{Sh}_m}\left(1 + \frac{a}{b}\frac{D_B}{D_A}\frac{C_{Bb}}{C_{Ai}}\right) \tag{6.3.3-5}$$

This is a utilization factor that considers the liquid phase only and represents the slowing-down effect of the mass transfer on the maximum possible chemical rate, which would occur for the interfacial concentration of A, C_{Ai}, and the bulk concentration of B, C_{Bb}.

When the gas-phase resistance is important, an overall utilization factor η_G can be derived that is identical to that given in (6.3.2-8) for the pseudo-first-order case. The value of η_L is determined from (6.3.3-5), which could also be written in terms of the bulk gas-phase partial pressure of A as

$$\eta_L = \frac{1}{\gamma^2 \mathrm{Sh}_m}\frac{1 + \frac{a}{b}\frac{D_B}{D_A}\frac{C_{Bb}H}{p_{Ab}}}{1 - \frac{a}{b}\frac{D_B}{D_A}\frac{C_{Bb}}{p_{Ab}}\frac{k_L}{k_G}} \tag{6.3.3-6}$$

It can be seen from (6.3.3-5) or (6.3.3-6) that the utilization factor (therefore, the rate of the overall phenomenon) is increased by raising the concentration of the liquid-phase reactant $C_{Bb.}$ This is only true up to a certain point, however. Indeed, as C_{Bb} is increased, the plane of reaction, located at $y = y_1$, moves toward the interface. The reaction takes place at the interface itself when $y_1 = 0$, that is, when

$$y_L = \frac{a}{b}\frac{D_B C_{Bb}}{N_A}$$

The corresponding concentration of B is denoted C'_{Bb}

$$C'_{Bb} = \frac{b}{a}\frac{y_L N_A}{D_B} = \frac{b}{a}\frac{D_A}{D_B}\frac{N_A}{k_L} \tag{6.3.3-7}$$

For the value of C'_{Bb} given by (6.3.3-7), both C_{Ai} and C_{Bi} become zero at the interface, as shown in Fig. 6.3.3-1. Beyond that value no further acceleration of the overall rate is possible by increasing C_{Bb}, since the rate is determined completely by the transfer rate in the gas phase. In addition, p_A drops to zero at the interface and the overall rate equation reduces to

$$N_A = k_G p_{Ab} \tag{6.3.3-8}$$

so that

$$C'_{Bb} = \frac{b}{a}\frac{D_A}{D_B}\frac{k_G}{k_L} p_{Ab} \tag{6.3.3-9}$$

This relationship also shows that η_L as determined from (6.3.3-6) is always a positive quantity.

In the region of extremely rapid reaction, the utilization factor approach, which refers the observed rate to the maximum possible chemical rate, has the drawback of requiring accurate values of the rate coefficient *k*. An alternate approach is given by the enhancement factor concept. From the definition of F_A given in (6.3.2-9) and from (6.3.3-3), it follows that

$$F_A = \frac{k_L C_{Ai}\left(1 + \dfrac{a}{b}\dfrac{D_B}{D_A}\dfrac{C_{Bb}}{C_{Ai}}\right)}{k_L\left(C_{Ai} - 0\right)} = 1 + \frac{a}{b}\frac{D_B}{D_A}\frac{C_{Bb}}{C_{Ai}} \qquad (6.3.3\text{-}10)$$

Obviously, $F_A \geq 1$, so that the mass transfer rate is "enhanced" by the chemical reaction. As C_{Bb} is increased, (6.3.3-10) indicates that the enhancement factor F_A increases, but only until the critical value C'_{Bb} is attained, (6.3.3-9).

Equation (6.3.3-10) is also represented in Fig. 6.3.2-1. Since F_A is independent of γ in the present case, a set of horizontal lines with (a/b) (D_B/D_A) (C_{Bb}/C_{Ai}) as a parameter is obtained. The curves in the central part that connect the lines for infinitely fast reactions to the curve for a pseudo-first-order reaction correspond to moderately fast second-order reactions. They were calculated by Van Krevelen and Hoftijzer [1948] under the assumption that *B* is only weakly depleted near the interface. For moderately fast reactions, this assumption was reasonably confirmed by more rigorous computations.

When there is appreciable gas-phase resistance, again the gas-phase flux equation, Henry's law, the liquid-phase flux equation, and the equality of the fluxes through both phases can be combined to eliminate C_{Ai} with the result:

$$N_A = \frac{p_{Ab} + \dfrac{a}{b}\dfrac{D_B}{D_A} H C_{Bb}}{\dfrac{1}{k_G} + \dfrac{H}{k_L}} \qquad (6.3.3\text{-}11)$$

which again illustrates the rule of addition of resistances. This equation may also be written in terms of F_A and yields

$$N_A = \frac{p_{Ab}}{\dfrac{1}{k_G} + \dfrac{H}{F_A k_L}} \qquad (6.3.3\text{-}12)$$

This equation is inconvenient to use as such because F_A still contains the interfacial concentration C_{Ai}. The enhancement factor F_A can also be expressed explicitly in terms of observables to give

$$F_A = \frac{1 + \frac{a}{b}\frac{D_B}{D_A}\frac{HC_{Bb}}{p_{Ab}}}{1 - \frac{a}{b}\frac{D_B}{D_A}\frac{C_{Bb}}{p_{Ab}}\frac{k_L}{k_G}}$$

Thus far, no attention has been paid in this chapter to the effect of the diffusivities. Often, instantaneous reactions involve ionic species. Care has to be taken in such cases to account for the influence of ionic strength, not only on the rate coefficient but also on the mobility of the ions. An example is the absorption of HCl into NaOH, which can be represented by $H^+ + OH^- \rightarrow H_2O$. This is an instantaneous irreversible reaction. When the ionic diffusivities are equal the diffusivities may be calculated from Fick's law. But H^+ and OH^- have much greater mobilities than the other ionic species and the results may be greatly in error if based solely on molecular diffusivities. This is illustrated by Fig. 6.3.3-2, adapted from Sherwood and Wei's work [1955] on the absorption of HCl and NaOH [Danckwerts, 1970]. The enhancement factor may be low by a factor of 2 if only molecular diffusion is accounted for in the mobility of the species. Important differences would also occur in the system HAc – NaOH. When CO_2 is absorbed in dilute aqueous NaOH, the "effective" diffusivity of OH^- is about twice that of CO_2.

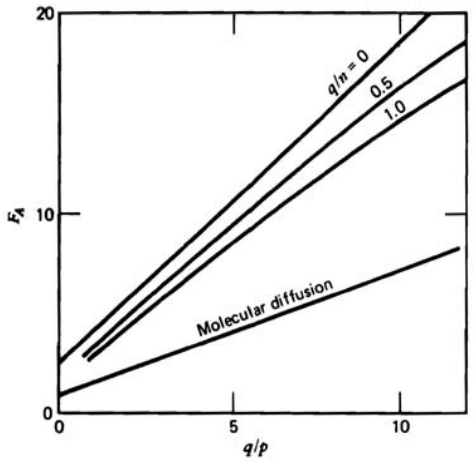

Figure 6.3.3-2

Enhancement factor for absorption of HCl in aqueous NaOH. q = concentration of OH^- in liquid bulk; p = concentration of H^+ at interface; n = concentration of Na^+ in liquid bulk. After Danckwerts [1970].

6.3.4 Some Remarks on Boundary Conditions and on Utilization and Enhancement Factors

The literature on gas-liquid reactions has mainly dealt with gas absorption processes in which the reaction is applied as a means of accelerating the absorption. The reactions used in these absorption processes are very fast, as can be seen from some typical k values, selected from a paper by Sharma and Danckwerts [1970], given in Table 6.3.4-1. With such fast reactions γ is large, and it is often justified to consider the reaction to be completed in the film. But from Table 6.3.4-2 [Barona, 1973], which gives characteristic parameters of important industrial gas-liquid reactions, it follows that quite often γ is much smaller than 1. Consequently, take care not to resort immediately to the mathematical solutions often encountered in the literature, which are mainly oriented toward fast processes.

The approach followed in the preceding sections started from the most general situation, retaining the possibility of reaction in the bulk. Two approaches have been used throughout to characterize the interaction between mass transfer and the slowing down of the reaction between components of a gas and a liquid: one expressing the slowing down of the reaction rate by the mass transfer and leading to the utilization factor, and a second expressing the enhancement effect of the reaction on the physical mass transfer and leading to the older concept of the enhancement factor. The much wider acceptance of the enhancement factor approach may be explained by the historical development of

TABLE 6.3.4-1
RATE COEFFICIENTS AT 25°C OF REACTIONS BETWEEN CO_2 OR COS AND VARIOUS SOLUTIONS[a]

	Solution	Ionic Strength (kg/m^3)	k ($m^3/kmol\ h$)
CO_2	Monoethanolamine	—	27×10^6
	Diethanolamine	—	5.4×10^6
	Carbonate buffer + arsenite	1-5	$3600\text{-}36\times10^6$
	Morpholine	—	65×10^6
	Aqueous NaOH or KOH	0.5-6	$18\times10^6\text{-}36\times10^6$
	Aqueous Na_2S	1.5-9	$18\times10^6\text{-}22\times10^6$
COS	Monoethanolamine	—	57,600
	Diethanolamine	—	39,600
	Diisopropylamine	—	21,600
	Morpholine	—	792,000
	NaOH (1*M*)		43,200

[a]After Sharma and Danckwerts [1970].

the field, mainly determined by gas absorption processes. What are the relative merits of the two concepts? It would seem that each approach has its well-defined optimum field of application, depending on the process and its rate of reaction. Of course, when the reaction rate is very slow and there is no conversion in the film, the simple series approach for mass transfer and reaction, outlined in Section 6.3.1, is logical and there is no need for either the η_L or the F_A concept.

For intermediate reaction rates, the use of the enhancement factor is not consistent with the standard approach of diffusional limitations in reactor design and may be somewhat confusing. Furthermore, there are cases where there simply is no purely physical mass transfer process to refer to, for example, the chlorination of decane, which is dealt with in the coming Section 6.3.6 on complex reactions or the oxidation of *o*-xylene in the liquid phase. Since those processes do not involve a diluent, there is no corresponding mass transfer process to be referred to. This contrasts with gas absorption processes like CO_2 absorption in aqueous alkaline solutions, for which a comparison with CO_2 absorption in water is possible. The utilization factor approach for pseudo-first-order reactions leads to $N_A A_v = \eta_L k C_{Ai}$ and, for these cases, refers to known concentrations C_{Ai} and C_{Bb}. For very fast reactions, however, the utilization factor approach is less convenient, because the reaction rate coefficient frequently is not accurately known. The enhancement factor is based on the readily determined k_L, and in this case there is no problem with the driving force, since $C_{Ab} = 0$. Note also that both factors η_L and F_A are closely related. Indeed, from (6.3.3-5) and (6.3.3-10) for instantaneous reactions,

$$\frac{\eta_L}{F_A} = \frac{1}{\gamma^2 \mathrm{Sh}_m}$$

From (6.3.2-4) and (6.3.2-10) for pseudo-first-order reactions the same relation is found.

Finally, the question may be raised if there is any advantage at all in the use of η_L and F_A. As for the effectiveness factor for solid-catalyzed gas-phase reactions, the advantage lies in the possibility of characterizing the interaction between mass transfer and reaction by means of a single number varying between zero and 1 for the utilization factor. The N_A equation in itself is much less explicit in this respect, of course. As will be evidenced in Chapter 14, there is no advantage or even no need for the explicit use of η_L or F_A in design calculations, since the mass flux equations can be directly used.

TABLE 6.3.4-2
CHARACTERISTIC PARAMETERS OF SOME INDUSTRIAL GAS-LIQUID REACTIONS[a]

[a]From Barona [1973]. B: Benzene; MCB: monochlorobenzene; TCE: 1,1,2-trichloroethane; 1 PB: 1-propylbenzene; EB: ethylbenzene; T: toluene; *o*-X: *o*-xylene; *p*-X: *p*-xylene; MC: monochloride of 1 PB, EB, T, *p*-X, and *o*-X; THF: tetrahydrofurane; HP: hydroperoxide; *o*-TA: *o*-toluic acid; ADBN: azodiisobutyronitrile.

Reactions	T (°C)	C_{A0} (kmol/m³)	C_{B0} (kmol/m³)	Catalyst	Cat. conc. (kmol/m³)	D_A (m³/m h)	k_L (m_L^3/m_i^2 h)	k	γ
Chlorinations									
$B + Cl_2 \rightarrow MCB + HCl$	80		10.45	$FeCl_3$		2.027×10^{-5}	1.303	4.143 m³/kmol h	0.0227
$B + Cl_2 \rightarrow MCB + HCl$	20	0.1245	11.22	$SnCl_4$	0.049	1.059×10^{-5}	0.716	43.09 m³/kmol h	0.0999
$TCE + Cl_2 \rightarrow C_2H_4Cl_4 + HCl$	70		10.26			8.856×10^{-6}	0.576	4.619 m³/kmol h	0.0357
$1PB + Cl_2 \rightarrow MC + HCl$	20	0.1750	7.183	$SnCl_4$	0.012	1.099×10^{-5}	0.734	850.6 m³/kmol h	0.353
$EB + Cl_2 \rightarrow MC + HCl$	20	0.1060	8.179	$SnCl_4$	0.00208	1.234×10^{-5}	0.828	2087 m³/kmol h	0.554
$T + Cl_2 \rightarrow MC + HCl$	20	0.1135	9.457	$SnCl_4$	0.00036	1.309×10^{-5}	0.828	3468 m³/kmol h	0.791
$p\text{-}X + Cl_2 \rightarrow MC + HCl$	20	0.0685	8.066	$SnCl_4$	0.00066	1.234×10^{-5}	0.698	14450 m³/kmol h	1.718
$o\text{-}X + Cl_2 \rightarrow MC + HCl$	20	0.1100	8.311	$SnCl_4$	0.00066	1.018×10^{-5}	0.796	16050 m³/kmol h	1.464
Oxidations									
$THF + O_2 \rightarrow HP$	65		12.35	ADBN	0.06	2.131×10^{-5}	1.145	0.0138 h^{-1}	0.00047
$EB + O_2 \rightarrow HP$	80			Cu^{II}-Stearate	1.62×10^{-5}	3.197×10^{-5}	1.498	0.000375 h^{-1}	0.00073
$EB + O_2 \rightarrow HP$	80		7.736	Cu^{II}-Stearate	0.056	3.197×10^{-5}	1.498	2.627 m³/kmol h	0.0170
$o\text{-}X + O_2 \rightarrow o\text{-}TA$	160					5.389×10^{-5}	0.929	0.1025 m³/kmol h	0.258

6.3.5 Extension to Reactions with Higher Orders

So far, only pseudo-first-order and instantaneous second-order reactions were discussed. In between, there is the range of truly second-order behavior for which the continuity equations for *A*, (6.3.1-1), or *B*, (6.3.1-2), cannot be solved analytically, only numerically. To obtain an approximate analytical solution, Van Krevelen and Hoftijzer [1948] dealt with this situation in a way analogous to that applied to pseudo-first-order kinetics, namely, by assuming that the concentration of *B* remains approximately constant close to the interface. They mainly considered very fast reactions encountered in gas absorption so that they could set $C_{Ab} = 0$, that is, the reaction is completed in the film. Their development is in terms of the enhancement factor F_A. The approximate equation for F_A is entirely analogous with that obtained for a pseudo-first-order reaction (6.3.2-11), but with γ replaced by γ', where

$$\gamma' = \gamma\sqrt{1-(F_A-1)\frac{b}{a}\frac{D_A}{D_B}\frac{C_{Ai}}{C_{Bb}}} \qquad (6.3.5\text{-}1)$$

This approximate solution is valid to within 10 percent of the numerical solution. Obviously, when $C_{Bb} >> C_{Ai}$, then $\gamma' = \gamma$ and the enhancement factor equals that for pseudo-first order. When this is not the case, F_A is obtained from an implicit equation. Van Krevelen and Hoftijzer solved (6.3.5-1) and plotted F_A versus γ in the diagram of Fig. 6.3.2-1 given in Section 6.3.2, connecting the results for pseudo-first-order and instantaneous second-order reactions.

Porter [1966] and also Kishinevskii et al. [1971] derived approximate equations for the enhancement factor that were found by Alper [1973] to be in excellent agreement with the Van Krevelen and Hoftijzer equation (for Porter's equation when $\gamma \geq 2$) and which are explicit. Porter's equation is

$$F_A = 1+\frac{a}{b}\frac{D_B}{D_A}\frac{C_{Bb}}{C_{Ai}}\left[1-\exp-\left(\frac{\gamma-1}{\frac{a}{b}\frac{D_B}{D_A}\frac{C_{Bb}}{C_{Ai}}}\right)\right]$$

Kishinevskii's equation is

$$F_A = 1+\frac{\gamma}{\alpha}\left[1-\exp\left(-0.65\gamma\sqrt{\alpha}\right)\right]$$

where

$$\alpha = \frac{\gamma}{\frac{a}{b}\frac{D_B}{D_A}\frac{C_{Bb}}{C_{Ai}}} + \exp\left(\frac{0.68}{\gamma} - \frac{0.45\gamma}{\frac{a}{b}\frac{D_B}{D_A}\frac{C_{Bb}}{C_{Ai}}}\right)$$

For an irreversible reaction of global order $m + n$ (m with respect to A, n with respect to B), the approach followed by Hikita and Asai [1964] was very similar to that of Van Krevelen and Hoftijzer. The rate of reaction was written as

$$r_A = kC_A^m C_B^n$$

Furthermore, C_B was considered to be nearly constant in the film, while C_{Ab} was set zero. Hikita and Asai again cast the results into the form of a physical absorption rate multiplied by an enhancement factor:

$$F_A = \frac{\gamma''}{\tanh \gamma''}$$

where

$$\gamma'' = \frac{\sqrt{\frac{2}{m+1} kC_{Ai}^{m-1} C_{Bi}^n D_A}}{k_L} = \gamma \sqrt{\frac{2}{m+1} C_{Ai}^{m-1} C_{Bi}^{n-1}}$$

γ'' evidently reduces to γ when $n = 1$ and $m = 1$. Reversible first-order reactions have been considered by Danckwerts and Kennedy [1954], and by Huang and Kuo [1963, 1965]. The latter found for the enhancement factor for the case of a rapid pseudo-first-order reversible reaction (i.e., equilibrium in the liquid bulk) the following expression:

$$F_A = \frac{1 + \frac{D_A}{KD_R}}{\frac{D_A}{KD_R} + \frac{\tanh\left(1 + \frac{D_A}{KD_R}\right)\gamma}{\left(1 + \frac{D_A}{KD_R}\right)\gamma}}$$

From this equation it can be seen that the reversibility of the reaction can have an important effect on the enhancement factor compared to the corresponding irreversible case with the same γ value. Instantaneous reversible reactions were studied by Olander [1960].

6.3.6 Coupled Reactions

Complex reactions have also been dealt with. To date, a fairly complete catalog of solutions is available for various reactions, both simple and coupled and with fairly general kinetics as long as no solid catalyst is involved. With coupled reactions the selectivity is, of course, crucial and an important question is whether or not the transport limitations alter the selectivities obtained when the chemical reaction is rate controlling.

The following types of coupled reactions are the most likely to be encountered:

Type 1:

$$A(g) + B(l) \rightarrow \text{product}$$
$$A(g) + C(l) \rightarrow \text{product}$$

Type 2:

$$A(g) + B(l) \rightarrow \text{product}$$
$$D(g) + B(l) \rightarrow \text{product}$$

Type 3:

$$A(g) + B(l) \xrightarrow{1} R(l)$$
$$A(g) + R(l) \xrightarrow{2} S(l)$$

With type 1 reaction schemes, the concentration profiles of B and C both decrease from the bulk to the interface, and no marked selectivity effects can be expected when the transport properties are not greatly dissimilar. The same is true for type 2 reaction schemes. The simultaneous absorption of two gases has been worked out and presented graphically by Goettler and Pigford [1964]. Astarita and Gioia [1965] analyzed the simultaneous absorption of H_2S and CO_2 in NaOH solutions.

For type 3 schemes, B and R have opposite trends, as shown in Fig. 6.3.6-1. In that case the ratio C_B/C_R could change markedly over the film even for moderate changes in the transport of each species, and the selectivity $r_1/r_2 = k_1C_b/k_2C_R$ could differ quite a bit from that obtained when the chemical reaction rate is controlling. Van de Vusse [1966a, b] has discussed the selectivities of type 3 schemes with rates $r_1 = k_1C_AC_B$ and $r_2 = k_2C_AC_R$, but for fast reactions completed in the film.

The continuity equations for A, B, and R, respectively, may be written, for steady state,

$$D_A \frac{d^2C_A}{dy^2} = r_1 + r_2$$

$$D_B \frac{d^2 C_B}{dy^2} = r_1$$

$$D_R \frac{d^2 C_R}{dy^2} = -r_1 + r_2$$

with B.C.,

$$C_A = C_{Ai}; \quad \frac{dC_B}{dy} = 0 \quad \text{and} \quad \frac{dC_R}{dy} = 0 \quad \text{at } y = 0$$

$$\frac{dC_A}{dy} = 0; \quad C_B = C_{Bb} \quad \text{and} \quad C_R = C_{Rb} \quad \text{at } y = y_L$$

The discussion is again in terms of the group $\gamma = \sqrt{k_1 C_{Bb} D}\,/_L$ and C_{Bb}/C_{Ai} (Van de Vusse assumed the diffusivities to be equal). When γ exceeds 2 (i.e., when the reaction is very fast), gradients of B and R occur in the film when $C_{Bb}/C_{Ai} < \gamma$. Then, an effect of mass transfer will be detected, not only on the rate of the global phenomenon, but also on the selectivity. When $\gamma < 0.5$ and $k_1 C_{Bb} < k_L A_v$, the rate of the global phenomenon corresponds to the true chemical reaction rate. When $k_1 C_{Bb} > k_L A_v$, the rate of the global phenomenon is $k_L A_v C_{Ai}$, which is the rate of mass transfer, and in that case there are no gradients of B and R. In both these cases there is no change in selectivity with respect to that observed in a homogeneous reaction and determined entirely by the chemical kinetics. Figure 6.3.6-2 illustrates these conclusions quantitatively for certain values of the determining groups.

The values of k_1 and k_2 are such that in the absence of diffusional limitations the maximum value of C_R/C_{Bb} would be 0.77. This value is found as

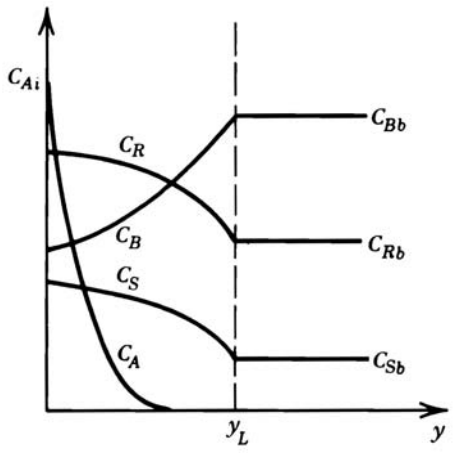

Figure 6.3.6-1

Type 3 reaction scheme. Typical B and R profiles in the film and bulk.

follows. In a semibatch the ultimate selectivity is an integral value of the instantaneous. For a given C_{Bb}, the latter is given by

$$\frac{dC_{Rb}}{dC_{Bb}} = \frac{k_2}{k_1}\frac{C_{Rb}}{C_{Bb}} - 1$$

with boundary conditions $C_{Rb} = 0$ and $C_{Bb} = C_{B0}$ at $t = 0$. Integration of this relationship leads to the integral or ultimate selectivity:

$$\left(1 - \frac{k_2}{k_1}\right)\frac{C_{Rb}}{C_{B0}} = \left(\frac{C_{Bb}}{C_{B0}}\right)^{k_2/k1} - \frac{C_{Bb}}{C_{B0}} \qquad (6.3.6\text{-}1)$$

When C_{Rb}/C_{B0} is plotted versus C_{B0}, a maximum is observed, as shown in Fig. 6.3.6-2. The value of C_{Rb}/C_{B0} at this maximum is 0.77. It is seen that for $\sqrt{kC_{Ai}D}/k_L = 6.3$, the ratio C_{Rb}/C_{B0} is substantially lower for all C_{B0}/C_{Ai} and exhibits a minimum. Only for $C_{B0}/C_{Ai} >> \gamma$ is the value of 0.77 approached. Extrapolation of the curve to extremely low values of C_{B0}/C_{Ai} is somewhat hazardous, because the boundary condition used by Van de Vusse, $C_{Ab} = 0$, no longer holds for these conditions.

Van de Vusse [1966 a, b] also performed experiments on the chlorination of *n*-decane, with a reaction scheme of the type considered here, in a semibatch reactor. In such a reactor the chlorine gas is bubbled continuously through a batch of *n*-decane. In some experiments the *n*-decane was pure, in others it was diluted with dichlorobenzene. In some experiments the batch was stirred, in others not.

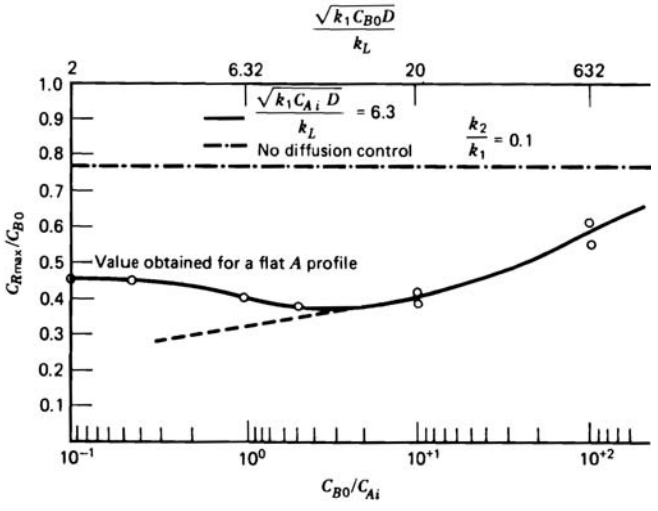

Figure 6.3.6-2

Type 3 reaction scheme. Influence of C_{B0}/C_{Ai} on selectivity. From Van de Vusse [1966a].

The experimental results could be explained in terms of the above considerations. In all experiments $\gamma \geq 1$ (from 150 to 500), hence the rate of the process was limited by diffusion, but the selectivity was only affected when $C_{B0}/C_{Ai} < \gamma$. This condition was only fulfilled for the experiments in which *n*-decane (*B*) was diluted. For only these experiments were the selectivities in nonstirred conditions found to differ from those with stirring.

Hashimoto et al. [1968] considered the same type of reaction, but also accounted for the possibility of reaction in the bulk by setting the boundary conditions at $y = y_L$ as follows: $C_A = C_{Ab}$; $C_B = C_{Bb}$ and $C_R = C_{Rb}$. The order with respect to *A*, the gaseous component, was taken to be zero, that with respect to *B* and *R*, 1. This could be encountered in high-pressure oxidation reactions, for example. From typical profiles shown in Fig. 6.3.6-1, it follows that when there are *B* and *R* profiles, the *R* selectivity in the film is lower than that in the bulk. In such a case, higher selectivity can be expected when the amount reacting in the bulk is large as compared to that reacting in the film.

The selectivity of *R* can be written as

$$\frac{dC_R}{dC_B} = \frac{N_{Rf} + N_{Rb}}{N_{Bf} + N_{Bb}}$$

and with the above boundary conditions this selectivity has to be calculated in two steps. The fluxes in the film are obtained from

$$N_{Bf} = -D_B \left.\frac{dC_B}{dy}\right|_{y=y_L}$$

$$N_{Rf} = -D_R \left.\frac{dC_R}{dy}\right|_{y=y_L}$$

and those in the bulk are obtained from

$$N_{Bb} A_v = r_1\big|_{y=y_L} \left(1 - A_v y_L\right)$$

$$N_{Rb} A_v = \left(-r_1 + r_2\right)\big|_{y=y_L} \left(1 - A_v y_L\right)$$

The values of C_{Bb} are obtained from the reactor mass balances, as will be shown in Chapter 14 on the design of gas-liquid reactors. Figure 6.3.6-3 shows the effect of the group $\left(D_A / k_L\right)\sqrt{k / D_B}$ on the *R* yield as a function of the conversion of *B* in a semibatch reactor. When this group is zero (i.e., $k_L >> k$), the

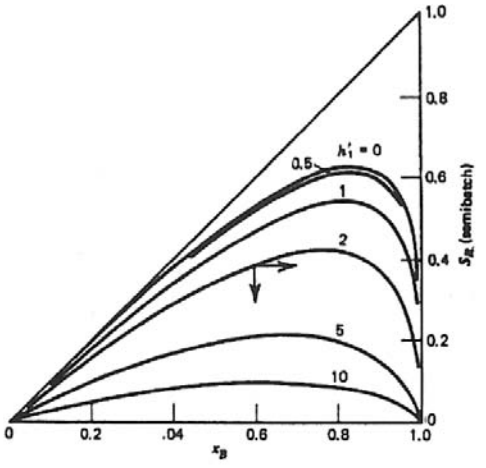

Figure 6.3.6-3
Selectivity for *R* as a function of conversion of *B*.
$S_R = C_{Rb}/C_{B0}$; h_i' = parameter group $D_A\sqrt{K / D_B / K_L}$. From Hashimoto et al. [1968].

purely chemical yield is obtained. Hashimoto et al. [1968] also presented their results in a diagram like that of Fig. 6.3.6-2. Since they accounted for reaction in the bulk, they could accurately determine the yield at very low values of C_{Bb}/C_{Ai}, in contrast with Van de Vusse.

Derivations were given for reversible, consecutive, and parallel reactions with any order by Onda et al. [1970a, b, c; 1972]. Onda et al. assumed that the concentrations at $y = y_L$ are the equilibrium values corresponding to the reversible reaction in the bulk. The development was analogous to that of Van Krevelen and Hoftijzer [1948] and Hikita and Asai [1964]. This led to approximate expressions for the enhancement factor giving values in close agreement with those obtained by numerical integration. Ouwerkerk [1978] and Cornelissen [1980] also derived approximate solutions for two parallel reactions that are in a different kinetic regime, namely, the absorption of CO_2 and H_2S in alkanolamine.

6.4 SURFACE RENEWAL THEORY

In surface renewal models, the liquid surface is assumed to consist of a mosaic of elements with different age at the surface. The rate of absorption at the surface is then an average of the rates of absorption in each element, weighted with respect to a distribution function $\psi(t)$— see (6.2.5). Under this heading of surface renewal theory, we shall also occasionally mention results of Higbie's [1935] so-called "penetration theory," which can be considered as a special case in which

every element is exposed to the gas for the same length of time before being replaced. The main emphasis of this section is on the Danckwerts [1951] approach using the distribution function for completely random replacement of surface elements:

$$\psi(t) = s\mathrm{e}^{-st} \tag{6.4-1}$$

By definition of a distribution function, it follows that the fraction of the surface having been exposed to the gas for a time between t and $t + dt$ is given by $\psi(t)dt = s\mathrm{e}^{-st}\,dt$. Also, since we are dealing with fractions, the distribution is normalized, so that

$$\int_0^\infty \psi(t)dt = 1 \tag{6.4-2}$$

Such an age distribution function would arise when the rate of replacement of the surface elements is proportional to the number of elements or fraction of the surfacing having that age, t:

$$-\frac{d\psi(t)}{dt} = s\psi(t) \tag{6.4-3}$$

Integration of (6.4-3), taking (6.4-2) into account, leads to (6.4-1), where s is a rate coefficient for surface element replacement and is the parameter of the model. Consequently, with this expression for $\psi(t)$, the average rate of absorption, becomes, from (6.2-5)

$$N_A = \int_0^\infty N_A(t)\psi(t)dt = s\int_0^\infty N_A(t)e^{-st}dt \tag{6.4-4}$$

Again, as for the two-film theory, analytical integration of the equations is only possible for a few particular cases, especially since the equations are now partial differential equations with respect to both position and time. In contrast with what was done for the film theory, the instantaneous reaction will be discussed prior to the pseudo-first-order reaction — a more logical sequence to introduce further developments.

6.4.1 Single Instantaneous Reactions

In contrast with the two-film model, the reaction plane is not fixed in space. Since the element at the surface is considered to have a finite capacity, transients have to be considered. In the zone between the interface at $y = 0$ and the location of the reaction plane at $y_1(t)$, a non-steady-state balance on A leads to

$$\frac{\partial C_A}{\partial t} = D_A \frac{\partial^2 C_A}{\partial y^2} \qquad (6.4.1\text{-}1)$$

In the zone between $y_1(t)$ and infinity,

$$\frac{\partial C_B}{dt} = D_B \frac{\partial^2 C_B}{\partial y^2} \qquad (6.4.1\text{-}2)$$

with boundary conditions

for *A*:

$$\begin{array}{llllll} t = 0 & y > 0 & C_A = C_{A0} & = 0 \text{ in the case considered here} & & \\ t > 0 & y = 0 & C_A = C_{Ai} & & & \\ & y = \infty & C_A = C_{Ab} & = C_{A0} & = 0 & (6.4.1\text{-}3) \end{array}$$

for *B*:

$$\begin{array}{llll} t = 0 & y \geq 0 & C_B = C_{B0} & \\ t > 0 & y = \infty & C_B = C_{Bb} & = C_{B0} \end{array}$$

The solution of these equations is well known. It may be obtained by the Laplace transform as

$$C_A = A_1 + A_2 \mathrm{erf}\left(\frac{y}{2\sqrt{D_A t}}\right) \qquad (6.4.1\text{-}4)$$

$$C_B = B_1 + B_2 \mathrm{erf}\left(\frac{y}{2\sqrt{D_B t}}\right) \qquad (6.4.1\text{-}5)$$

where

$$\mathrm{erf}(x) = \frac{2}{\sqrt{\pi}} \int_0^x e^{-\eta^2} d\eta$$

Before determining the integration constants by applying the boundary conditions; an inspection of (6.4.1-4) permits relating the position of the reaction plane y_1 to time. Indeed, in that place $C_A = 0$, so that necessarily

$$y_1(t) = 2\beta\sqrt{t} \qquad (6.4.1\text{-}6)$$

where β is a constant that remains to be determined. Accounting for the boundary conditions, together with (6.4.1-6), leads to the following expressions for C_A and C_B:

$$\frac{C_A}{C_{Ai}} = \frac{\operatorname{erfc}\left(\dfrac{y}{2\sqrt{D_A t}}\right) - \operatorname{erfc}\left(\dfrac{\beta}{\sqrt{D_A}}\right)}{\operatorname{erf}\left(\dfrac{\beta}{\sqrt{D_A}}\right)} \qquad (6.4.1\text{-}7)$$

where $\operatorname{erfc}(\eta) = 1 - \operatorname{erf}(\eta)$. For $0 < y < 2\beta\sqrt{t}$,

$$\frac{C_B}{C_{B0}} = \frac{\operatorname{erf}\left(\dfrac{y}{2\sqrt{D_B t}}\right) - \operatorname{erf}\left(\dfrac{\beta}{\sqrt{D_A}}\right)}{\operatorname{erfc}\left(\dfrac{\beta}{\sqrt{D_B}}\right)}$$

In the reaction plane $y_1(t) = 2\beta\sqrt{t}$, the stoichiometry requires that $N_A/a = -(N_B/b)$. Writing the fluxes in terms of Fick's law leads to an additional relation that enables β to be determined. The result is

$$e^{\beta^2/D_B}\operatorname{erfc}\left(\frac{\beta}{\sqrt{D_B}}\right) = \frac{a}{b}\frac{C_{Bb}}{C_{Ai}}\sqrt{\frac{D_B}{D_A}}e^{\beta^2/D_A}\operatorname{erf}\left(\frac{\beta}{\sqrt{D_A}}\right) \qquad (6.4.1\text{-}8)$$

An example of the evolution of the profiles with time is given in Fig. 6.4.1-1.

The flux of A at the interface at any time is obtained by differentiating (6.4.1-7), as indicated by (6.3.1-6):

$$N_A(t) = \frac{C_{Ai}}{\operatorname{erf}\left(\dfrac{\beta}{\sqrt{D_A}}\right)}\sqrt{\frac{D_A}{\pi t}} \qquad (6.4.1\text{-}9)$$

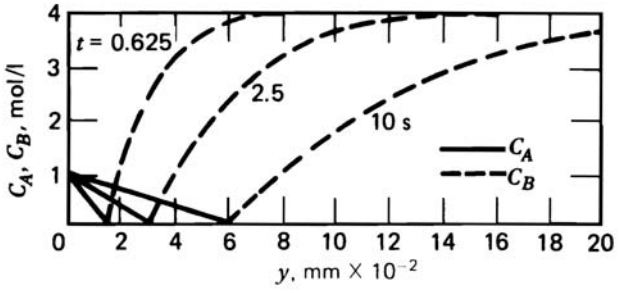

Figure 6.4.1-1
Location of the reaction plane with time. From Perry and Pigford [1953].

The average rate of absorption at the surface is, with Higbie's uniform age $\bar{t}$,

$$N_A = \frac{1}{\bar{t}}\int_0^{\bar{t}} N_A(t)dt = \frac{2C_{Ai}}{\operatorname{erf}\left(\dfrac{\beta}{\sqrt{D_A}}\right)}\sqrt{\frac{D_A}{\pi \bar{t}}} = \frac{k_L C_{Ai}}{\operatorname{erf}\left(\sqrt{\dfrac{\beta}{D_A}}\right)} \qquad (6.4.1\text{-}10)$$

since, for purely physical absorption, $N_A = 2C_{Ai}\sqrt{D_A/\pi\bar{t}}$, but also $N_A = k_L C_{Ai}$. With Danckwerts' age distribution function (6.4-1),

$$N_A = \int_0^{\infty} N_A(t)\,\psi(t)dt = \frac{\sqrt{D_A s}C_{Ai}}{\operatorname{erf}\left(\dfrac{\beta}{\sqrt{D_A}}\right)} = \frac{k_L C_{Ai}}{\operatorname{erf}\left(\dfrac{\beta}{\sqrt{D_A}}\right)} \qquad (6.4.1\text{-}11)$$

since, for purely physical absorption, $N_A = \sqrt{D_A s}C_{Ai} = k_L C_{Ai}$. In this case both results are identical.

Again, the results can be expressed in terms of a utilization factor η_L or an enhancement factor F_A. From (6.4.1-11) it follows immediately that

$$F_A = \frac{1}{\operatorname{erf}\left(\dfrac{\beta}{\sqrt{D_A}}\right)}$$

When $D_A = D_B$, the enhancement factor is of the same form for both the film and surface renewal models. Indeed, in the film model

$$F_A = 1 + \frac{a}{b}\frac{C_{Bb}}{C_{Ai}}$$

From (6.4.1-8) it can be shown that an identical result is obtained for the surface renewal model. The agreement is not surprising for this special case: when β is small the rate of displacement of the reaction plane is small, so that steady state is practically realized, as in the film theory. Even when $D_A \neq D_B$, the difference between the film and surface renewal models amounts to only a few percent.

From the definition (6.3.2-4),

$$\eta_L = \frac{N_A A_v}{kC_{Ai}} = \frac{\sqrt{D_A s}A_v}{\operatorname{erf}\left(\dfrac{\beta}{\sqrt{D_A}}\right)k} = \frac{k_L A_v}{\operatorname{erf}\left(\dfrac{\beta}{\sqrt{D_A}}\right)k} \qquad \left(D_A = D_B\right)$$

which can be reduced to the same form as (6.3.3-4). Finally, it should be noted that the calculation of N_A as carried out here required an expression for the concentration profile (6.4.1-7). With the surface age distribution adopted in the surface renewal model, a shortcut may be taken, as illustrated in the next section.

6.4.2 Single Irreversible (Pseudo)-First-Order Reactions

The equation governing diffusion, first-order reaction, and accumulation of A in a unit volume element of the liquid may be written

$$\frac{\partial C_A}{\partial t} = D_A \frac{\partial^2 C_A}{\partial y^2} - kC_A \qquad (6.4.2\text{-}1)$$

with boundary conditions

$t > 0$	$y = 0$	$C_A = C_{Ai}$
$t > 0$	$y = \infty$	$C_A = 0$
$y > 0$	$t = 0$	$C_A = 0$

The first condition expresses that, from a certain time onward, a gas, in which the component A has a partial pressure p_A, is brought into contact with the liquid, so that a concentration C_{Ai} is obtained at the interface. The initial concentration of A in the liquid is considered to be zero. Since the exposure time of the element at the surface is rather brief and since its capacity is not considered to be zero, the concentration front of A is not likely to extend to the inner edge of the element. This is expressed by the B.C.: for $t > 0$, $C_A = 0$ at $y = \infty$. In the case of a pseudo-first-order reaction, $k = ak'C_{Bb}$, of course.

The equation is conveniently integrated by means of Laplace transforms. Transforming with respect to time leads to

$$s\overline{C}_A - C_A(t=0) = D_A \frac{d^2\overline{C}_A}{dy^2} - k\overline{C}_A$$

or

$$\frac{d^2\overline{C}_A}{dy^2} - \left(\frac{k+s}{D_A}\right)\overline{C}_A = 0$$

The integral of this differential equation is

$$\overline{C}_A = A_1 \exp\left[\sqrt{\frac{k+s}{D_A}}y\right] + A_2 \exp\left[-\sqrt{\frac{k+s}{D_A}}y\right]$$

The boundary condition $C_A = 0$ for $y = \infty$ requires A_1 to be zero. A_2 is determined from the boundary condition at $y = 0$:

$$A_2 = \frac{C_{Ai}}{s}$$

so that

$$\overline{C}_A = \frac{C_{Ai}}{s} \exp\left[-\sqrt{\frac{k+s}{D_A}} y \right] \tag{6.4.2-2}$$

Finally, $C_A(y, t)$ is obtained by an inverse transformation of (6.4.2-2), leading to

$$\frac{C_A}{C_{Ai}} = \frac{1}{2} \exp\left(-y\sqrt{\frac{k}{D_A}} \right) \operatorname{erfc}\left(\frac{y}{2\sqrt{D_A t}} - \sqrt{kt} \right)$$

$$+ \frac{1}{2} \exp\left(y\sqrt{\frac{k}{D_A}} \right) \operatorname{erfc}\left(\frac{y}{2\sqrt{D_A t}} + \sqrt{kt} \right) \tag{6.4.2-3}$$

For this solution, see Carslaw and Jaeger [1959]. For large values of kt,

$$\frac{C_A}{C_{Ai}} = \exp\left[-y\sqrt{\frac{k}{D_A}} \right]$$

since erf x tends to 1 for large x and tends to zero with x. Consequently, for sufficiently large times, the concentration profiles do not change any more — they have attained the steady state.

At time t, the instantaneous rate of absorption $N_A(t)$ in an element having a surface age t is given by

$$N_A(t) = \sqrt{kD_A} C_{Ai} \left[\operatorname{erf}\left(\sqrt{kt}\right) + \frac{e^{-kt}}{\sqrt{\pi kt}} \right] \tag{6.4.2-4}$$

The elements have a distribution of residence times at the surface. The rate that would be observed, at any instant, over a unit surface would be an average:

$$N_A = \int_0^\infty N_A(t) \psi(t) dt$$

With Higbie's distribution function all elements of the surface have the same age. Such a situation could be encountered with a quiescent liquid or with completely laminar flow. In that case N_A is found from the average of (6.4.2-4) in which t

takes a definite value $\bar{t}$, the uniform time of exposure. With Danckwerts' age distribution function (6.4-1), the average rate of absorption per unit surface, N_A, is given by

$$N_A = \int_0^\infty N_A(t) s e^{-st} dt = \sqrt{D_A (k+s)} C_{Ai} \qquad (6.4.2\text{-}5)$$

Note that the rate of absorption is proportional to $\sqrt{D_A}$, whereas the film theory predicts $N_A \sim D_A$. Equations (6.4.2-5) and (6.4.1-11) for instantaneous reaction were first derived by Danckwerts [1950].

The parameter s can be related to the transfer coefficient k_L used in the film model and to the diffusivity in the following way:
In the absence of reaction, (6.4.2-5) reduces to

$$N_A = \sqrt{D_A s} C_{Ai}$$

In terms of a transfer coefficient, $N_A = k_L C_{Ai}$, so that

$$k_L^2 = D_A s$$

Equation (6.4.2-5) now becomes

$$N_A = \sqrt{D_A \left(k + \frac{k_L^2}{D_A} \right)} C_{Ai} = k_L C_{Ai} \sqrt{1 + D_A \frac{k}{k_L^2}} \qquad (6.4.2\text{-}6)$$

or

$$N_A = F_A k_L C_{Ai} \quad \text{where } F_A = \sqrt{1 + D_A \frac{k}{k_L^2}} = \sqrt{1+\gamma^2} \qquad (6.4.2\text{-}7)$$

Again, the rate of absorption has been expressed as the product of the physical absorption rate and an enhancement factor F_A. The enhancement factor derived from Higbie's approach is easily found to be

$$F_A = \gamma \left[\left(1 + \frac{\pi}{8\gamma^2} \right) \operatorname{erf}\left(\frac{2}{\sqrt{\pi}} \gamma \right) + \frac{1}{2\gamma} \exp\left(-\frac{4}{\pi} \gamma^2 \right) \right] \qquad (6.4.2\text{-}8)$$

The three expressions (6.4.2-7), (6.4.2-8), and the corresponding (6.3.2-11) for the film theory look quite different. Yet they lead to identical results when $\gamma \to 0$ and $\gamma \to \infty$, while they differ only by a few percent for intermediate values of γ. This is illustrated in Table 6.4.2-1 [see Beek, 1968] for the film and surface renewal theory of Danckwerts. The utilization factor is given by

$$\eta_L = \frac{A_v \sqrt{D_A (k+s)}}{k}$$

which is very similar to $\eta_L = A_v \sqrt{D_A / k}$ derived from the film theory when γ is large.

In general, for practical applications one is less interested in the concentration profiles near the interface and the rate of absorption in an element having a surface age t, $N_A(t)$. What matters primarily is the flux over the total surface, N_A. As mentioned already in Section 6.4.1, a shortcut can be taken to obtain N_A when the Danckwerts distribution is adopted, which avoids the difficult inversion of the transform. Indeed,

$$N_A = s\int_0^\infty N_A(t) e^{-st} dt = s\int_0^\infty \left[-D_A \frac{\partial C_A}{dy} \right]_{y=0} e^{-st} dt$$

$$= -D_A s \frac{d}{dy} \left[\int_0^\infty C_A e^{-st} dt \right]_{y=0} = -D_A s \frac{d\overline{C}_A}{dy}\bigg|_{y=0}$$

where $\overline{C}_A$ is the Laplace transform of C_A. Therefore, N_A can be obtained directly by differentiating the Laplace transform with respect to time of the original differential equation — in this case (6.4.2-1).

The surface renewal models only consider the liquid phase. In Section 6.3 on the film model, the resistances of both gas and liquid phases were

TABLE 6.4.2.1
COMPARISON OF MODEL PREDICTION FOR PSEUDO-FIRST-ORDER REACTION[a]

	F_A for C_{Ab} = 0		
γ	**Film** $\frac{\gamma}{\tanh \gamma}$	**Surface renewal** $\sqrt{1+\gamma^2}$	**Penetration** $\gamma\left[\left(1+\frac{\pi}{8\gamma^2}\right)\mathrm{erf}\left(\frac{2}{\sqrt{\pi}}\gamma\right)+\frac{1}{2\gamma}\exp\left(-\frac{4}{\pi}\gamma^2\right)\right]$
0.01	1.00	1.00	0.94
0.1	1.00	1.00	1.005
0.3	1.04	1.04	1.035
1	1.31	1.41	1.37
3	3.02	3.16	3.12
10	10.00	10.05	10.39

[a]After Beek [1968].

combined into one single expression like (6.3.2-5). The same can be done here; Danckwerts [1951] has shown that in most cases the surface renewal models combined with a gas side resistance lead to the same rules for the addition of resistances as the two-film theory.

6.4.3 Surface Renewal Models with Surface Elements of Limited Thickness

One feature of the surface renewal model that may not be realistic is that the elements at the surface extend inwards to infinity, as expressed by the boundary condition

$$t > 0 \qquad y = \infty \qquad C_A = 0 \qquad \text{or} \qquad \frac{\partial C_A}{\partial y} = 0$$

As previously mentioned, this arises from the consideration that the residence time of a surface element at the interface is very short, so that it is likely that A has never penetrated to the inner edge of the element before it is replaced. Models that limit the depth of the surface element have also been proposed and applied to purely physical mass transfer first — such as the surface rejuvenation model of Danckwerts [1955] and the film penetration model of Toor and Marchello [1958]. These were later extended to mass transfer with reaction. Harriott [1962] and Bullin and Dukler [1972] extended these models by assuming that eddies arriving at random times come to within random distances from the interface. This leads to a stochastic formulation of the surface renewal.

The price that is paid for the greater generality of the models is twofold, however. First, there is the need for two parameters: one expressing the surface renewal and one expressing the thickness of the element. Second, there is the mathematical complexity of the expression for the flux N_A. Is the price worth paying? This question can be partly answered by means of Huang and Kuo's application of the film penetration model to first-order reactions, both irreversible and reversible [1963, 1965].

The differential equation is that of (6.4.2-1), but the boundary condition at $y = y_L$ is now as follows:

$$t > 0 \qquad C_A = C_{Ab} \qquad C_B = C_{Bb}$$

For first-order irreversible reactions and Danckwerts' residence time distribution, Huang and Kuo derived two solutions: one for long exposure times that expresses the concentration gradients in trigonometric function series, and the following solution for rather short exposure times, obtained by Laplace transforms:

$$N_A = \sqrt{D_A(k+s)}C_{Ai}\left[\left(1-\frac{s\dfrac{C_{Ab}}{C_{Ai}}}{k+s}\right)\coth\sqrt{\frac{k+s}{D_A}}y_L - \frac{C_{Ab}}{C_{Ai}}\frac{k}{k+s}\operatorname{csch}\sqrt{\frac{k+s}{D_A}}y_L\right] \qquad (6.4.3\text{-}1)$$

The difference in the numerical values predicted from (6.4.3-1) and the film and the simple surface renewal model turns out to be negligible.

Huang and Kuo also solved two equations for a rapid first-order reversible reaction (i.e., equilibrium in the bulk liquid). The solutions are extremely lengthy and will not be given here. From a comparison of the film, surface renewal, and intermediate film penetration theories it was found that for irreversible and reversible reactions with equal diffusivities of reactant and product, the enhancement factor was insensitive to the mass transfer model. For reversible reactions with product diffusivity smaller than that of the reactant, the enhancement factor can differ by a factor of 2 between the extremes of film and surface renewal theory. To conclude, it would seem that the choice of the model matters little for design calculations: the predicted differences are negligible with respect to the uncertainties of prediction of some of the model or operating parameters.

6.5 EXPERIMENTAL DETERMINATION OF THE KINETICS OF GAS-LIQUID REACTIONS

6.5.1 Introduction

The approach to be followed in the determination of rates or detailed kinetics of the reaction in a liquid phase between a component of dissolved gas and a component of the liquid is, in principle, the same as that outlined in Chapter 2 for gas-phase reactions on a solid catalyst. In general, the experiments are carried out in flow reactors of the integral type. The data may be analyzed by the integral or the differential method of kinetic analysis. However, for a single reaction, two continuity equations, in general, are required: one for the absorbing component *A* in the gas phase and one for *A* in the liquid phase. In addition, a material balance is required, linking the consumption of *B*, the reactant of the liquid phase, to that of *A*. The continuity equations for *A*, which contain the rate equations derived in

this chapter, depend upon the type of reactor used in the experimental study. They are discussed in detail in Chapter 14.

From the preceding sections it follows that the global rate of consumption contains several parameters: k, k_L, k_G, and D_A. In many cases, A_v, which depends on the equipment and the operating conditions, also has to be determined. As advised already for gas-phase reactions catalyzed by solids, when the true chemical rate is to be measured, efforts should be undertaken to eliminate mass transfer limitations, and vice versa. If this turns out to be impossible, the dependence of the global rate on the factors determining the mass transfer — the liquid and gas flow rates, or the agitation — has to be investigated over a sufficient range, since these are the elements that will vary when extrapolating to other sizes or types of equipment. Except when reliable correlations are available or when use is made of special equipment, to be discussed below, special attention has to be given to the specific interfacial area. Physical absorption experiments only allow the products $k_L A_v$ and $k_G A_v$ to be measured. Adequately chosen experiments involving both mass transfer and reaction allow k_L, k_G, and A_v to be determined separately. These experiments do not necessarily involve the reactions of the process to be studied. In fact, model reactions with known kinetics are preferably used for this.

6.5.2 Determination of k_L and A_v

In the first place, the gas-phase resistance has to be eliminated. This requires high turbulence in the gas phase or the use of undiluted absorbing species A. With pure A or when a large excess of A is used with respect to B, the reacting component of the liquid, the bulk gas-phase composition is constant.

Of course, the product $k_L A_v$ need not necessarily be obtained from physical mass transfer. Experiments involving mass transfer and reaction eliminate the problems associated with approaching the gas-liquid equilibrium. The product $k_L A_v$ can be obtained, for example, from experiments involving instantaneous reaction in the liquid, so that, according to the film theory,

$$N_A A_v = k_L A_v C_{A_i} \left(1 + \frac{a}{b} \frac{D_b}{D_A} \frac{C_{Bb}}{C_{A_i}} \right)$$

Instantaneous reactions include the absorption of NH_3 in H_2SO_4, of SO_2 or Cl_2 or HCl in alkali solutions, and of H_2S and HCl in amine solutions. Again, gas-phase resistance is eliminated, generally by using undiluted gas.

To determine k_L and A_v separately, use can be made of a relatively fast (pseudo)-first-order reaction with known kinetics. For $\gamma > 3$, (6.3.2-5) becomes

$$N_A A_v = \frac{p_{Ab} A_v}{\dfrac{1}{k_G} + \dfrac{H \tanh \gamma}{k_L \gamma}} \tag{6.5.2-1}$$

But, since tanh γ tends to 1 when $\gamma > 3$,

$$N_A A_v = \frac{p_{Ab} A_v}{\dfrac{1}{k_G} + \dfrac{H}{k_L \gamma}} \tag{6.5.2-2}$$

Letting k_G approach infinity and substituting the details of γ leads to

$$N_A A_v = \frac{\sqrt{kD_A}}{H} p_{Ab} A_v \tag{6.5.2-3}$$

Equation (6.5.2-3) does not contain k_L, so that, when $N_A A_v$ and p_A are measured and k, D_A, and H are known, A_v can be calculated. To satisfy the above conditions, use is made of the reaction between CO_2 and a carbonate-bicarbonate buffer containing arsenite [Sharma and Danckwerts, 1963; Roberts and Danckwerts, 1962] or between CO_2 and aqueous amines [Sharma, 1965].

Another possibility is to use a pseudo-first-order reaction, rather slow, so that little A reacts in the film, yet sufficiently fast to make C_{Ab} zero. This approach has been used by Danckwerts et al. [1963], who interpreted their results in terms of the surface renewal theory. The system they investigated was CO_2 absorption in CO_3^{2-}/HCO_3^- buffers of different compositions. The reaction is of the pseudo-first-order and the surface renewal model leads to the rate of absorption given by (6.4.2-5), namely, $N_A A_v = A_v \sqrt{D_A (k + s)} C_{A_i}$. Danckwerts et al. plotted $(N_A A_v / C_{Ai})^2$ versus the values of k corresponding to the different compositions of the buffer. This led to a straight line with slope $D_A A_v^2$ and intercept $D_A s A_v^2$, from which A_v and s were obtained, or A_v and k_L, since $k_L = \sqrt{D_A s}$.

6.5.3 Determination of k_G and A_v

The product $k_G A_v$ can be obtained from purely physical experiments or from experiments in the presence of an instantaneous reaction. It was shown in Section 6.3.3 that when $C_{Bb} > C'_{Bb}$, the reaction is confined to the interface and $N_A A_v = k_G A_v p_A$. Measuring $N_A A_v$ for a given p_{Ab} leads to $k_G A_v$. Both unknowns can be determined separately when a rapid reaction ($\gamma > 5$) is carried out in the same equipment, and $C_{Ab} = 0$. Then, from (6.5.2-2) it follows that when $p_{Ab}/N_A A_v$ is plotted versus $H/\gamma k_L$ or $H/\sqrt{kD_A}$, the intercept is $1/k_G A_v$ and the slope is A_v.

Sharma and Danckwerts [1970] have discussed the above and other methods and provide valuable quantitative information on a variety of gas-liquid reactions.

6.5.4 Specific Equipment

As previously mentioned, when the rate coefficient of the reaction has to be determined, it is recommended to eliminate mass transfer effects as much as possible. Also, to get rid of the problem of the interfacial area, specific equipment with known A_v has been devised. The wetted wall column was used in early studies to determine the kinetics of the reaction itself. Care has to be taken to have a laminar film (Re < 250–400) and to avoid ripples that increase the interfacial area. In a film flowing down a vertical tube of a diameter d_t the velocity u at any depth y from the interface is given by

$$u = \frac{3}{2}\left(\frac{L}{\pi d_t}\right)^{2/3}\left(\frac{g\rho_L}{3\mu}\right)^{1/3}\left[1 - y^2\left(\frac{\pi g d_t \rho_L}{3\mu L}\right)^{2/3}\right] \qquad (6.5.4\text{-}1)$$

where L is the liquid flow rate (m³/hr). Since at the wall $u = 0$, the film thickness is $\delta = (3\mu L / \pi g d_t \rho_L)^{1/3}$ and the liquid velocity at the surface equals

$$\frac{3}{2}\left(\frac{L}{\pi d_t}\right)^{2/3}\left(\frac{g\rho_L}{3\mu}\right)^{1/3} \qquad (6.5.4\text{-}2)$$

In classical versions, both the gas and the liquid generally flow countercurrently. In more recent versions such as those shown in Fig. 6.5.4-1 only the liquid flows and the amount of gas absorbed as a function of time is followed by means of a gas buret and a soap film meter. From the lowering of the soap meniscus, the amount of A that is absorbed may be calculated. Dividing this amount by the elapsed time yields the rate of absorption. Looking now at the jet, with its known A_v and contact time between gas and liquid, $\bar{t}$, an amount is absorbed:

$$Q = \int_0^{\bar{t}} N_A(t)\,dt$$

The average rate of absorption is $Q/\bar{t}$. This is exactly the quantity measured by the gas buret and soap film meter, so that

$$N_A = (1/\bar{t})\int_0^{\bar{t}} N_A(t)\,dt$$

is known. The contact time is calculated from u_s and the height Z. This equipment was used by Roberts and Danckwerts [1962].

Another equipment frequently used for rapid reactions is the laminar jet in which the liquid velocity is uniform, so that the contact time is nothing but the height/velocity ratio. The contact time can be varied from 0.001 s to 0.1 s by varying the liquid rate from the jet. Such equipment, an example of which is shown in Fig. 6.5.4-2, has been used by Nysing et al. [1959] and Sharma and Danckwerts [1963].

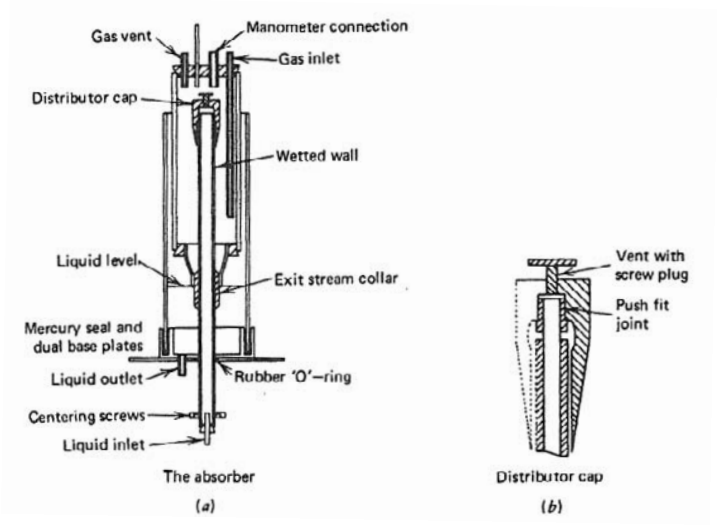

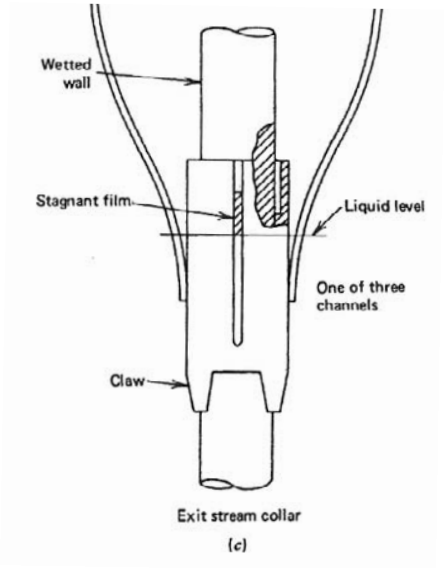

Figure 6.5.4-1
Wetted wall column. From Danckwerts [1970].

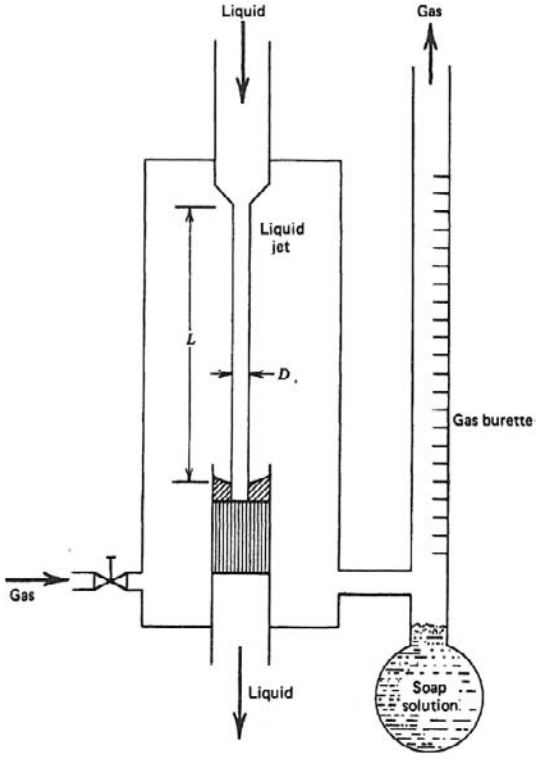

Figure 6.5.4-2
Laminar jet with soap–film gas flow meter. After Beek [1968].

Danckwerts and Kennedy [1954] have used the rotating drum shown schematically in Fig. 6.5.4-3. It has been devised to expose a liquid flowing over a known surface of the rotating drum for a given time to a gas. The contact times can be varied between 0.01 and 0.25 s. The construction is more complicated than that of the wetted wall and jet equipment.

Danckwerts and co-workers have interpreted the data in terms of contact or exposure time and Higbie's penetration theory as follows. For a pseudo-first-order reaction $N_A(t)$ is given by (6.4.2-4), and the amount absorbed during the contact time $\bar{t}$ per unit surface,

$$Q = \int_0^{\bar{t}} N_A(t)dt$$
$$= C_{Ai}\sqrt{\frac{D_A}{k'C_{Bb}}}\left[\left(k'C_{Bb}\bar{t}+\frac{1}{2}\right)\mathrm{erf}\left(\sqrt{k'C_{Bb}\bar{t}}\right)+\sqrt{\frac{k'C_{Bb}\bar{t}}{\pi}}\exp\left(-k'C_{Bb}\bar{t}\right)\right] \quad (6.5.4\text{-}3)$$

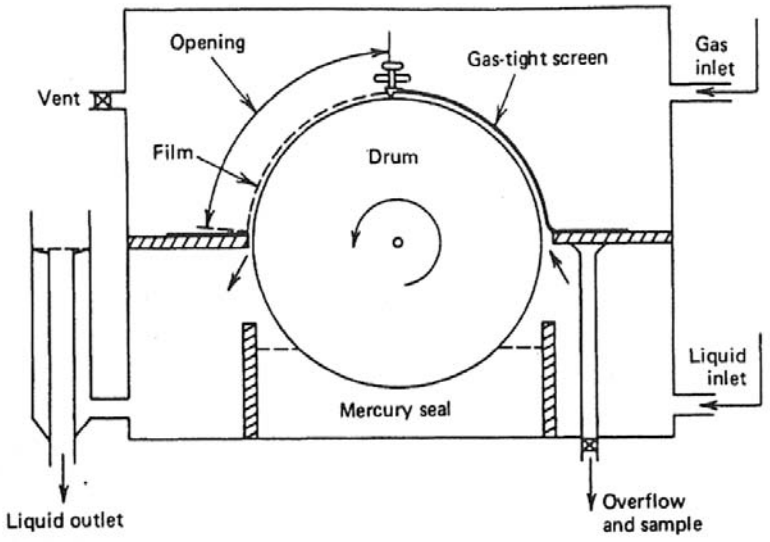

Figure 6.5.4-3
Rotating drum. After Danckwerts and Kennedy [1954], from Danckwerts [1970].

where the contact surface is known in this case. The average rate of absorption is

$$\frac{Q}{\bar{t}} = \int_0^{\bar{t}} N_A(t)\frac{dt}{\bar{t}}$$

For short contact times ($k'C_{Bb}\bar{t}$ < 0.5), expansion of erf and exp and neglecting higher orders of $k'\bar{t}$ leads to

$$N_A = \frac{Q}{\bar{t}} = 2C_{Ai}\sqrt{\frac{D_A}{\pi\bar{t}}}\left(1+\frac{k'C_{Bb}\bar{t}}{3}\right) \qquad (6.5.4\text{-}4)$$

For long times $k'C_{Bb}\bar{t}$ > 2, the error function goes to 1 so that

$$N_A = \frac{Q}{\bar{t}} = C_{Ai}\sqrt{D_A k'C_{Bb}}\left(1+\frac{1}{2k'C_{Bb}\bar{t}}\right) \qquad (6.5.4\text{-}5)$$

By plotting $N_A\sqrt{\bar{t}}$ versus $\bar{t}$, as is obvious from (6.5.4-4), $2C_{Ai}\sqrt{D_A/\pi}$ is obtained as intercept. Plotting N_A versus $1/2k'C_{Bb}\bar{t}$ yields $C_{Ai}\sqrt{D_A k'C_{Bb}}$ as an intercept, so that k' and C_{Ai} are obtained. An illustration of this method is given in Sharma and Danckwerts' study of CO_2 absorption in a liquid jet [1963]. An extensive discussion of more laboratory experiments and of their analysis is given in Astarita et al. [1983].

PROBLEMS

6.1 Derive the rate equation for a reversible first-order gas-liquid reaction

$$A \rightleftharpoons P$$

using the film theory ($D_A = D_P$).

$$\text{B.C.: } y = 0 \qquad C_A = C_{Ai}$$

$$\frac{dC_P}{dy} = 0$$

$$y = y_1 \qquad C_A = C_{Ab}$$

$$C_P = KC_{Ab}$$

Show that

$$N_A = \frac{k_L\left(C_{Ai} - C_{Ab}\right)\left(1+K\right)}{1 + K\dfrac{\tanh\gamma'}{\gamma'}}$$

where

$$\gamma' = \sqrt{\frac{k\left(1+K\right)D_A}{K\,k_L^2}}$$

6.2 Derive the integral selectivity equation, (6.3.6-1).

6.3 A gas is being absorbed into a liquid in which the concentration of the reactive component B is 0.1 M. The reaction between the gaseous component A and the component B is extremely fast. The conditions are such that C_{Ai} = 0.1 M. Furthermore, $D_A = 10^{-5}$ cm²/s. Compare the enhancement factors based on the film theory and the surface renewal theory for the cases when (a) $D_B = D_A$, (b) $D_B = \frac{1}{2} D_A$, and (c) $D_B = 2D_A$.

6.4 Consider the absorption of gaseous CO_2 by a NaOH solution. The stoichiometry is as follows:

$$CO_2 + 2NaOH \rightleftharpoons Na_2CO_3 + H_2O$$

Consider the solubility of CO_2 to be independent of the NaOH concentration and let the diffusivities of CO_2 and NaOH in the liquid be approximately equal.

(a) Can the reaction be considered as being of the pseudo-first order when the gas-liquid contact time is 0.01 s and when

(i) The partial pressure of CO_2 is 0.1 bar and the concentration of NaOH is 1 mol/l?

(ii) The partial pressure of CO_2 is 1 bar and the concentration of NaOH is 1 mol/l?

(b) When the gas-liquid contact time is 0.1 s and the NaOH concentration is 3 mol/l, what is the partial pressure of CO_2 above which the reaction is no longer pseudo-first order?
Take $k' = 10^7$ cm³/mol s and $H = 25 \times 10^{-3}$ cm³ bar/mol.

6.5 CO_2 is absorbed at 25°C into a 2.5-M monoethanolamine solution in a rotating drum type of absorber. The contacting surface is 188.5 cm² and the contact time is 0.2 s. The partial pressure of CO_2 in the gas phase is 0.1 bar. The reaction is as follows:

$$CO_2 + 2R_2NH \rightarrow R_2NCOO^- + R_2NH_2^+$$

The rate of absorption at these conditions is found to be 3.26×10^{-4} mol/s. What is the value of the rate coefficient neglecting the gas-phase resistance and considering the reaction to obey pseudo-first-order behavior?
Additional data are $D_A = 1.4 \times 10^{-5}$ cm²/s; $D_B = 0.77 \times 10^{-5}$ cm²/s;
Henry's constant $H = 30.2 \times 10^3$ bar cm³/mol.

REFERENCES

Alper, E., *Chem. Eng. Sci.*, 28, 2092 (1973).
Astarita, G., *Mass Transfer with Chemical Reaction*, Elsevier, Amsterdam (1967).
Astarita, G., and Gioia, F., *Ind. Eng. Chem. Fundam.*, 4, 317 (1965).
Astarita, G., Savage, D.W., and Bisio, A., *Gas Treating with Chemical Solvents*, Wiley-Interscience, New York (1983).
Barona, N., *Proc. 20th Anniv. Dept. Chem. Eng.*, University of Houston (1973).
Beek, W.J., *Stofoverdracht met en zonder Chemische Reaktie.* Notes, University of Delft (1968).
Bullin, J.A. and Dukler, A.E., *Chem. Eng. Sci.*, 27, 439 (1972).
Carslaw, H.S., and Jaeger, J.C., *Conduction of Heat in Solids*, 2nd ed., Oxford University Press, London (1959).
Cornelissen, A.E., *Trans. Inst. Chem. Eng.*, 58, 242 (1980).
Danckwerts, P.V., *Trans. Farad. Soc.*, 46, 300 (1950).
Danckwerts, P.V., *Ind. Eng. Chem.*, 43, 1460 (1951).
Danckwerts, P.V., *A.I.Ch.E. J.*, 1, 456 (1955).
Danckwerts, P.V., *Gas-Liquid Reactions*, McGraw-Hill, New York (1970).
Danckwerts, P.V., and Kennedy, A.M., *Trans. Inst. Chem. Eng.*, 32, S49 (1954a).
Danckwerts, P.V., and Kennedy, A.M., *Trans. Inst. Chem. Eng.*, 32, S53 (1954b).
Danckwerts, P.V., Kennedy, A.M., and Roberts, D., *Chem. Eng. Sci.*, 18, 63 (1963).
De Leye, L., and Froment, G.F., *Computers & Chem. Eng.*, 10(5), 505 (1986).
Goettler, L.A., and Pigford, R.L., Paper 25e, in *Proc. 57th Ann. Meeting of A.I.Ch.E.* (1964).
Harriott, P., *Chem. Eng. Sci.*, 17, 149 (1962).
Hashimoto, K., Teramoto, M., Nagayasu, T., and Nagata, S., *J. Chem. Eng. Japan*, 1, 132 (1968).
Higbie, R., *Trans. Am. Inst. Chem. Eng.*, 31, 365 (1935).
Hikita, H., and Asai, S., *Int. Chem. Eng.*, 4, 332 (1964).
Huang, C.J., and Kuo, C.H., *A.I.Ch.E. J.*, 9, 161 (1963).

Huang, C.J., and Kuo, CH.H., *A.I.Ch.E. J.*, 11, 901 (1965).
Kishinevskii, M.K., Kormenko, T.S., and Popat, T.M., *Theor. Found. Chem. Eng.*, 4, 641 (1971).
Kramers, H., and Westerterp, K.R., *Elements of ChemicalReactor Design and Operation*, Academic Press, New York (1963).
Lewis, W.K., and Whitman, W.G., *Ind. Eng. Chem.*, 16, 1215 (1924).
Nysing, R.A.T.O., Hendricksz, R.H., and Kramers, H., *Chem. Eng. Sci.*, 10, 88 (1959).
Olander, D.R., *A.I.Ch.E. J.*, 6, 233 (1960).
Onda, K., Sada, E., Kobayashi, T., and Fujine, M., *Chem. Eng. Sci.*, 25, 753 (1970a).
Onda, K., Sada, E., Kobayashi, T., and Fujine, M., *Chem. Eng. Sci.*, 25, 761 (1970b).
Onda, K., Sada, E., Kobayashi, T., and Fujine, M., *Chem. Eng. Sci.*, 25, 1023 (1970c).
Onda, K., Sada, E., Kobayashi, T., and Fujine, M., *Chem. Eng. Sci.*, 25, 247 (1972).
Ouwerkerk, C., *Hydrocarbon Process*, 57(4), 89 (1978).
Perry, R.H., and Pigford, R.L., *Ind. Eng. Chem.*, 45, 1247 (1953).
Porter, K.E., *Trans. Inst. Chem. Eng.*, 44, T25 (1966).
Ramm, T., *Absorptionsprozesse in der ChemischenTechnik*, VEB Verlag, Berlin (1953).
Roberts, D., and Danckwerts, P.V., *Chem. Eng. Sci.*, 17, 961 (1962).
Sharma, M.M., *Trans. Far. Soc.*, 61, 681 (1965).
Sharma, M.M., and Danckwerts, P.V., *Chem. Eng. Sci.*, 18, 729 (1963).
Sharma, M.M., and Danckwerts, P.V., *Brit. Chem. Eng.*, 15, 522 (1970).
Sherwood, T.K., Pigford, R.L., and Wilke, C.R., *Mass Transfer*, McGraw-Hill, New York (1975).
Sherwood, T.K., and Wei, J., *A.I.Ch.E. J.*, 1, 522 (1955).
Toor, H.L., and Marchello, J.N., *A.I.Ch.E. J.*, 4, 98 (1958).
Van de Vusse, J.G., *Chem. Eng. Sci.*, 21, 631 (1966a).
Van de Vusse, J.G., *Chem. Eng. Sci.*, 21, 645 (1966b).
Van Krevelen, D.W., and Hoftijzer, P.J., *Rec. Trav. Chim. Pays-Bas*, 67, 563 (1948).
Whitman, W.G., *Chem.* & *Met. Eng.*, 29, 147 (1923).

Chapter 7

The Modeling of Chemical Reactors

7.1 APPROACH

The number of types of reactors is very large in the chemical industry. Even for the same operation, such as nitration of toluene, different types are used: the batch reactor, the continuous stirred tank, and a cascade of stirred tanks. Flow reactors of the tubular type are used for such widely different processes as the nitration of glycerine, the sulfonation of aromatics, or gas-phase reactions such as thermal cracking or the nitration of paraffins. Flow reactors with fixed bed of catalyst particles are used in the ammonia or methanol syntheses and in the oxidation of xylene into phthalic anhydride. A series of such fixed bed reactors is used in SO_3 synthesis or in hydrocarbon reforming. Reactors with fluidized or moving beds are used for cracking hydrocarbons, for oxidizing naphthalene, or for oxychlorinating ethylene.

The modeling of chemical reactors, as it is conceived in the following chapters, is not based on the external form of the equipment nor on the reaction taking place in it, nor even on the nature of the medium — homogeneous or not.

Focusing on the *phenomena* taking place in the reactor reduces the apparent diversity into a small number of models or basic reactor types. The phenomena occurring in a reactor may be broken down into reaction, transfer of mass, heat, and momentum. The modeling and design of reactors is based on the equations describing these phenomena: the reaction rate equation and the continuity, energy, and momentum equations. The form and complexity of these equations will now be discussed, for introductory and orienting purposes, in qualitative terms. The equations themselves are derived in Section 7.3 of this chapter.

7.2 ASPECTS OF MASS, HEAT AND MOMENTUM BALANCES

The first step toward the calculation of the conversion of feed component *A* in the reactor consists of applying the law of conservation of mass on a volume element of the reactor, fixed in space:

$$\underset{\text{I}}{\begin{bmatrix}\text{amount of } A\\ \text{introduced}\\ \text{per unit time}\end{bmatrix}} - \underset{\text{II}}{\begin{bmatrix}\text{amount of } A\\ \text{leaving per}\\ \text{unit time}\end{bmatrix}} - \underset{\text{III}}{\begin{bmatrix}\text{amount of } A\\ \text{converted per}\\ \text{unit time}\end{bmatrix}} = \underset{\text{IV}}{\begin{bmatrix}\text{amount of } A\\ \text{accumulated}\\ \text{per unit time}\end{bmatrix}} \tag{7.2-1}$$

In mathematical terms (7.2-1) is nothing but the so-called continuity equation for *A*. If *A* reacts in more than one phase, such an equation is needed for each of these phases.

The mechanisms by which *A* can enter or leave the volume element are flow and — for those cases where the concentration is not uniform in the reactor — molecular diffusion, in practice generally of minor importance, however. The motion of a fluid, even through empty pipes, is not really ordered and difficult to describe. Even if the true detailed flow pattern were known, the continuity equation would be so complicated that its integration would be extremely complicated and tedious, if not impossible. The crossing of different streamlines, and mixing of fluid elements with different characteristics that result from this crossing, are difficult points in the design of chemical reactors. For a first approach, it is therefore natural to consider two extreme conceptual cases: first, where there is no mixing of the streamlines, and second, where the mixing is complete. These two extremes may be formulated with sufficient approximation by the tubular plug flow reactor and the continuous flow stirred tank with complete mixing.

In a plug flow reactor all fluid elements move with equal velocity along parallel streamlines. The plug flow is the only mechanism for mass transport, and there is no mixing between fluid elements. The reaction, therefore, leads to a

concentration gradient in the axial flow direction. For steady-state conditions, for which term IV is zero, the continuity equation is a first-order ordinary differential equation with the axial coordinate as variable. For non-steady-state conditions, the continuity equation is a partial differential equation with axial coordinate and time as variables. Narrow and long tubular reactors closely satisfy the conditions for plug flow when the viscosity of the fluid is low.

Reactors with complete mixing may be subdivided into batch and continuous types. In a batch-type reactor with complete mixing, the composition is uniform throughout the reactor. Consequently, the continuity equations may be written for the entire contents, not only over a volume element. The composition varies with time, however, so that a first-order ordinary differential equation is obtained, with time as variable. The form of this equation is analogous with that for the plug flow case. In the continuous flow type, an entering fluid element is instantaneously mixed with the contents of the reactor so that it loses its identity. This type also operates at a uniform concentration level. In the steady state, the continuity equations are algebraic equations.

Both types of continuous reactors considered here are conceptual idealized cases. They are important cases, because they are easy to calculate, and give the extreme values of the conversions between which those realized in a real reactor will occur — provided that there is no bypassing in this reactor. The design of a real reactor, with its intermediate level of mixing, requires information about this mixing. The mixing can be revealed at the outlet of the reactor by a spread or distribution in residence time (the length of time spent in the reactor) between fluid elements. Such a distribution is relatively easy to measure. The resulting information may then be used as such in the design or used with a model for the real behavior of the reactor. The design of nonideal cases along both lines of approach is discussed in Chapter 12.

In an energy balance over a volume element of a chemical reactor, kinetic, potential, and work terms may usually be neglected relative to the heat of reaction and other heat transfer terms, so that the balance reduces to

$$\underset{\text{I}}{\begin{bmatrix}\text{amount of}\\ \text{heat added}\\ \text{per unit time}\end{bmatrix}} - \underset{\text{II}}{\begin{bmatrix}\text{amount of heat}\\ \text{removed}\\ \text{per unit time}\end{bmatrix}} + \underset{\text{III}}{\begin{bmatrix}\text{heat effect of}\\ \text{the reaction}\\ \text{per unit time}\end{bmatrix}} = \underset{\text{IV}}{\begin{bmatrix}\text{variation of}\\ \text{heat content}\\ \text{per unit time}\end{bmatrix}} \tag{7.2-2}$$

The mathematical expression for (7.2-2) is generally called the energy equation, and its integrated form is called the heat balance. The form of these equations results from considerations closely related to those for the different types of continuity equations. When the mixing is so intense that the concentration is

uniform over the reactor, it may be accepted that the temperature is also uniform. When plug flow is postulated, it is natural to accept that heat is also only transferred by that mechanism. When molecular diffusion is neglected, the same may be done for heat conduction. When the concentration in a section perpendicular to flow is considered to be uniform, then it is natural to also consider the temperature to be uniform in this section. It follows that when heat is exchanged with the surroundings, the temperature gradient has to be situated entirely in a thin "film" along the wall. This also implies that the resistance to heat transfer in the central core is zero in a direction perpendicular to the flow. This condition is not always fulfilled, especially for fixed bed catalytic reactors: besides heat transfer by convective flow, other mechanisms often have to be accounted for. Even here it may be necessary, in order to keep the mathematics tractable, to use simplified models, to be discussed in later chapters.

The momentum balance can be obtained by application of Newton's second law on a moving fluid element. Over a volume element of a chemical reactor, the balance of momentum in direction *i* can be written as:

$$\begin{bmatrix}\text{amount of}\\ \text{momentum}\\ \text{in direction } i\\ \text{added}\\ \text{per unit time}\end{bmatrix} - \begin{bmatrix}\text{amount of}\\ \text{momentum}\\ \text{in direction } i\\ \text{removed}\\ \text{per unit time}\end{bmatrix} + \begin{bmatrix}\text{effect of pressure}\\ \text{and shear stress}\\ \text{forces on amount}\\ \text{of momentum}\\ \text{in direction } i\\ \text{per unit time}\end{bmatrix} = \begin{bmatrix}\text{variation of}\\ \text{amount of}\\ \text{momentum}\\ \text{in direction } i\\ \text{per unit time}\end{bmatrix}$$

I II III IV

with $i = 1, 2, 3.$ (7.2-3)

In chemical reactors, only pressure drop and friction forces have to be considered in most cases. A number of specific pressure drop equations are discussed in the chapters on tubular plug flow reactors and on fixed bed catalytic reactors.

7.3 THE FUNDAMENTAL MODEL EQUATIONS

7.3.1 The Species Continuity Equations

7.3.1.1 A General Formulation

The derivation of differential mass balances or continuity equations for the components of an element of fluid flowing in a reactor is considered in detail in texts on transport processes, for example, by Bird et al. [1960; 2007]. These authors showed that a fairly general form of the continuity equation for a chemical species *j* reacting in a flowing fluid with varying density, temperature, and composition is

$$\frac{\partial C_j}{\partial t} + \nabla \cdot (C_j \mathbf{u}) + \nabla \cdot \mathbf{J}_j = R_j \qquad (7.3.1.1\text{-}1)$$

If species *j* occurs in more than one phase, such a continuity equation has to be written for each phase. These equations are linked by the boundary conditions and generally also by a term expressing the transfer of *j* between the phases. Such a term is not included by (7.3.1.1-1), since the following discussion is centered on the various forms that the continuity equations can take in single-phase or "homogeneous" or, by extension, in "pseudohomogeneous" reactors as a consequence of the flow pattern. Specific modeling aspects resulting from the presence of more than one phase, solid, or fluid are illustrated in detail in Chapter 11 on fixed bed reactors, in Chapter 13 on fluidized bed reactors, and in Chapter 14 on multiphase reactors.

The terms and symbols used in this equation have the following meaning: C_j is the molar concentration of species *j* (kmol/m³ fluid), so that $\partial C_j / \partial t$ is the nonsteady-state term expressing accumulation or depletion; ∇ is the "nabla", or "del", operator. In a rectangular coordinate system, *x*, *y*, *z* with unit vectors $\boldsymbol{\delta}_x$, $\boldsymbol{\delta}_y$, and $\boldsymbol{\delta}_z$, the gradient of a scalar function *f* is represented by ∇f and the divergence of a vector function **v** by $\nabla \cdot \mathbf{v}$. More explicitly,

$$\nabla f = \frac{\partial f}{\partial x}\boldsymbol{\delta}_x + \frac{\partial f}{\partial y}\boldsymbol{\delta}_y + \frac{\partial f}{\partial z}\boldsymbol{\delta}_z$$

$$\nabla \cdot \mathbf{v} = \frac{\partial v_x}{\partial x} + \frac{\partial v_y}{\partial y} + \frac{\partial v_z}{\partial z}$$

Here, **u** is the three-dimensional mass-average velocity vector in (m/s) and defined by

$$\mathbf{u} = \sum_{j=1}^{N} \frac{M_j C_j}{\rho_f} \mathbf{u}_j$$

where ρ_f is the density of the mixture, and $\mathbf{u}_j$ represents the velocity of molecules of species *j*. The term $\nabla \cdot (C_j \mathbf{u})$ thus accounts for the transport of mass by convective flow.

The $\mathbf{J}_j$ term is the molar flux vector for species *j* with respect to the mass-average velocity (kmol/m² s). When the flow is laminar or perfectly ordered, the term $\nabla \cdot \mathbf{J}_j$ results from molecular diffusion only. It can be written more explicitly as an extension, already encountered in Chapter 3, of Fick's law for diffusion in binary systems, as

$$\mathbf{J}_j = -\rho_f D_{jm} \nabla \left(\frac{C_j}{\rho_f} \right) \qquad (7.3.1.1\text{-}2)$$

where D_{jm} is the effective binary diffusivity for the diffusion of j in the multicomponent mixture. Of course, appropriate multicomponent diffusion laws could also be used — for ideal gases the Stefan-Maxwell equation, as was done in Section 3.2.3 of Chapter 3. In (7.3.1.1-2) the driving force has been taken as moles of j per total mass of fluid, for the sake of generality [Bird et al., 1960; 2007]. The term $\nabla \cdot \mathbf{J}_j$ can also account for the flux resulting from deviations of perfectly ordered flow, as encountered with turbulent flow or with flow through a bed of solid particles, for example, but this will be discussed further below.

R_j is the total rate of change of amount of j because of reaction, as defined in Chapter 1, that is, $\alpha_j r$ for a single reaction and $\sum_{i=1}^{M} \alpha_{ij} r_i$ for multiple reactions. The α_{ij} are negative for reactants and positive for reaction products. The units of R_j depend on the nature of the reaction. If the reaction is homogeneous, the units could be kmol/m^3 s; but for a reaction catalyzed by a solid, preference would be given to kmol/kg cat. s, multiplied by the catalyst bulk density in the reactor.

From the definitions given it is clear that $\sum_j M_j \mathbf{J}_j = \sum_j M_j C_j (\mathbf{u}_j - \mathbf{u}) = 0$, while $\sum_j M_j R_j = 0$, due to the conservation of mass in a reacting system. If each term of (7.3.1.1-1) is multiplied by the molecular weight M_j, and the equation is then summed over the total number of species N, accounting for the relation $\rho_f = \sum_j M_j C_j$, the total continuity equation is obtained:

$$\frac{\partial \rho_f}{\partial t} + \nabla \cdot (\rho_f \mathbf{u}) = 0 \qquad (7.3.1.1\text{-}3)$$

Note that the usual continuity equation used in fluid mechanics is also true for a reacting mixture. Equation (7.3.1.1-3) can be used to rewrite (7.3.1.1-1) in a form that is sometimes more convenient for reactor calculations. The first two terms can be rearranged as follows:

$$\begin{aligned} \frac{\partial C_j}{\partial t} + \nabla \cdot (C_j \mathbf{u}) &= \frac{\partial}{\partial t}\left(\rho_f \frac{C_j}{\rho_f} \right) + \nabla \cdot \left(\rho_f \frac{C_j}{\rho_f} \mathbf{u} \right) \\ &= \rho_f \left[\frac{\partial}{\partial t}\left(\frac{C_j}{\rho_f} \right) + \mathbf{u} \cdot \nabla \left(\frac{C_j}{\rho_f} \right) \right] + 0 \end{aligned}$$

where the last zero term results from the total continuity equation (7.3.1.1-3). This result suggests that C_j/ρ_f (moles j per unit mass of mixture) is a convenient

and natural variable. This is indeed the case, since C_j/ρ_f is simply related to the conversion (or extent), a variable frequently used in reactor modeling:

$$\frac{C_j}{\rho_f} = \frac{\left(C_j/\rho_f\right)}{\left(C_j/\rho_f\right)_0}\left(\frac{C_j}{\rho_f}\right)_0 = \frac{N_j}{N_{j0}}\left(\frac{C_j}{\rho_f}\right)_0$$

$$= (1-x_j)\left(\frac{C_j}{\rho_f}\right)_0 \qquad (7.3.1.1\text{-}4)$$

where N_j is the total number of moles of j present in the reactor and the subscript zero refers to reactor inlet values.

Combining these latter results with (7.3.1.1-1) and (7.3.1.1-2) leads to an equation in terms of conversions:

$$\rho_f\left(\frac{\partial x_j}{\partial t} + \mathbf{u}\cdot\nabla x_j\right) - \nabla\cdot\left(\rho_f D_{jm}\nabla x_j\right) = -\left(\frac{\rho_f}{C_j}\right)_0 R_j \qquad (7.3.1.1\text{-}5)$$

Equations (7.3.1.1-1) and (7.3.1.1-5) are, in fact, extensions of the species continuity equations used in previous chapters, where the flow terms were normally not present. These somewhat detailed derivations have been used to carefully illustrate the development of the equations of transport processes into forms needed to describe chemical reactors. It is seldom that the full equations have to be utilized, and normally only the most important terms will be retained in practical situations. However, (7.2-1) or (7.3.1.1-5) are useful to have available as a fundamental basis.

Equation (7.3.1.1-5) implicitly assumes perfectly ordered flow in that $\nabla\cdot(\rho_f\ D_{jm}\nabla x_j)$ is specific for molecular diffusion. Deviations from perfectly ordered flow, as encountered with turbulent flow, lead to a flux that is also expressed as if it arose from a diffusion-like phenomenon, in order to avoid too complex mathematical equations. The proportionality factor between the flux and the concentration gradient is then called the turbulent, or "eddy", diffusivity. Since this transport mechanism is considered to have the same driving force as molecular diffusion, the two mechanisms are summed and the resulting proportionality factor is called "effective" diffusivity D_e. In highly turbulent flow, the contribution of molecular diffusion is usually negligible, so that D_e is then practically identical for all the species of the mixture. Through its turbulent contribution, the effective diffusion is not isotropic, however. For more details, refer to Hinze [1959].

Equation (7.3.1.1-5) now becomes

$$\rho_f\left(\frac{\partial x_j}{\partial t}+\mathbf{u}\cdot\nabla x_j\right)=\frac{\partial}{\partial x}\left(\rho_f D_{e,x}\frac{\partial x_j}{\partial x}\right)+\frac{\partial}{\partial y}\left(\rho_f D_{e,y}\frac{\partial x_j}{\partial y}\right)$$

$$+\frac{\partial}{\partial z}\left(\rho_f D_{e,z}\frac{\partial x_j}{\partial z}\right)-\left(\frac{\rho_f}{C_j}\right)_0 R_j \qquad (7.3.1.1\text{-}6)$$

When the reactor contains a solid catalyst, the flow pattern is strongly determined by the presence of the solid. Generally, the flux of *j* resulting from the mixing effect is expressed in the form of Fick's law. Consequently, the form of equation (7.3.1.1-6) is not altered, but the effective diffusivity now also contains the effect of the packing. This topic is dealt with extensively in Chapter 11 on fixed bed catalytic reactors. For further explanation of the effective transport coefficients, see Himmelblau and Bischoff [1968] and Slattery [1972].

7.3.1.2 Specific Forms

The form of the general continuity equations is usually too complex to be conveniently solved for practical application for reactor design or simulation. If one or more terms are dropped from (7.3.1.1-6) and/or integral averages over the spatial directions are considered, the continuity equation for each component reduces to that of an ideal, basic reactor type, as outlined in Section 7.2. In these cases it is often easier to apply (7.2-1) directly to a volume element of the reactor. This will be done in the next chapters, dealing with basic or specific reactor types, but in the present chapter, it will be shown how the simplified equations can be obtained from the fundamental ones.

It is very common in reactors to have flow predominantly in one direction, say, *z* (think of tubular reactors). The major gradients then occur in that direction, under isothermal conditions at least. For many cases, then, the cross-sectional average values of concentration (or conversion) and temperature might be used in the equations, instead of radially distributed values. The former are obtained from

$$\langle\zeta\rangle\equiv\frac{\mathbf{1}}{\boldsymbol{\Omega}}\iint_{\boldsymbol{\Omega}}\zeta\, d\boldsymbol{\Omega}$$

where ζ represents any variable, $\boldsymbol{\Omega}$ is the cross section inside the rigid boundary, and $d\boldsymbol{\Omega} = dx\, dy$. Virtually all the terms contain products of dependent variables, and the first approximation that must be made is that the average of the product is close to the product of the averages; for example,

$$\left\langle \rho_f u_z \frac{\partial x_j}{\partial z} \right\rangle \cong \left\langle \rho_f u_z \right\rangle \frac{\partial \left\langle x_j \right\rangle}{\partial z}$$

In this case, the approximation would clearly be best for highly turbulent flow, for which the velocity profiles are relatively flat. The discrepancies actually enter into the effective transport coefficients, which have to be empirically measured in any event. Another approximation concerns the reaction rate term:

$$\left\langle R_j(C_j, T) \right\rangle \cong R_j\left(\left\langle C_j \right\rangle, \left\langle T \right\rangle\right)$$

Thus, (7.3.1.1-6) becomes, after integration over the cross section,

$$\left\langle \rho_f \right\rangle \frac{\partial \left\langle x_j \right\rangle}{\partial t} + \left\langle \rho_f u \right\rangle \frac{\partial \left\langle x_j \right\rangle}{\partial z} = \left\langle \rho_f D_{e,z} \right\rangle \frac{\partial^2 \left\langle x_j \right\rangle}{\partial_z^2} - \left(\frac{\rho_f}{C_j} \right)_0 R_j \quad \text{(7.3.1.2-1)}$$

(1) (2) (3) (4)

where the velocity in the flow direction is represented by *u*. In the presence of packing, a distinction would have to be made between the true local fluid velocity, called the interstitial velocity (m/s), and the velocity considered over the whole cross section, as if there were no solid, called the superficial velocity (m^3 fluid/m^2 cross section s). A so-called "one-dimensional model" is now obtained. If the convective transport is completely dominant over any diffusive transport, in particular, that in the flow direction — that is, the fluid moves like a "plug" — term (3) may be neglected. Assuming steady-state conditions, term (1) also drops out, so that the simplified equation (7.3.1.2-1) becomes (leaving out the brackets for simplicity)

$$\rho_f u \frac{dx_j}{dz} = -\left(\frac{\rho_f}{C_j} \right)_0 R_j$$

while the continuity equation (7.3.1.1-3) reduces to

$$\frac{d}{dz}\left(\rho_f u\right) = 0$$

This last equation is simply integrated to give

$$(\rho_f u) = (\rho_f u)_0 = \text{constant} = G \ (\text{kg/m}^2\,\text{s})$$

where *G* is usually termed the mass flow velocity. This result is then combined with the continuity equation for species *j*, giving

$$u_0 \frac{dx_j}{dz} = -\frac{1}{C_{j0}} R_j(x_j) \qquad (7.3.1.2\text{-}2)$$

One modification is normally made before performing the final integration step:

$$\frac{dz}{u_0} = \frac{d(\Omega z)}{\Omega u_0} = \frac{dV}{F_0^{'}}$$

where $F_0^{'}$ is the volumetric flow rate of the feed (m^3/s) and dV is a differential element of reactor volume. Integration now gives

$$\frac{V}{F_0^{'}} = -C_{j0} \int \frac{dx_j}{R_j(x_j)} \qquad (7.3.1.2\text{-}3)$$

More often, this equation is written in the form

$$\frac{V}{F_{j0}} = -\int \frac{dx_j}{R_j(x_j)} \qquad (7.3.1.2\text{-}4)$$

whereby $F_{j0} = F_0^{'} C_{j0}$ is the molar feed rate of species j (kmol/s). The last equation is used to describe the *plug flow reactor*.

Other simplified forms result when the entire reactor may be considered to be uniform—operating under conditions of complete mixing, the idealized picture of a well-mixed vessel. Averaging over all the spatial directions equation (7.3.1.2-1) can be further integrated over z:

$$\bar{x}_f \equiv \frac{\Omega}{V} \int \langle x_j \rangle dz$$

$$= \frac{1}{V} \iiint x_j \, dx dy dz$$

For simplicity, again, the overlines, referring to mean values, will from now on be left out. Because of the assumption of complete uniformity, no effective transport terms need to be considered. Note that the final coordinate direction here refers to the fluid, which could be expanding, in contrast to the rigid boundary assumed for x and y. A more general and more rigorous derivation using the transport theorems of vector/tensor analysis has been given by Bird [1957]. In the batch case, when no fluid is entering or leaving the reactor except at the time of loading or unloading, (7.3.1.2-1), with terms (2) and (3) zero, can be integrated to yield

$$\frac{d}{dt}\left(V\rho_f x_j\right) = -\left(\frac{\rho_f}{C_j}\right)_0 R_j V \qquad (7.3.1.2\text{-}5)$$

or

$$\frac{d}{dt}(N_{j0} x_j) = -R_j V$$

since $V(\rho_f/\rho_{f0})C_{j0} = V_0 C_{j0} = N_{j0}$, the total number of moles of j initially present. N_j is related to N_{j0} by $N_j = N_{j0}(1 - x_j)$, so that finally

$$\frac{dN_j}{dt} = R_j V \qquad (7.3.1.2\text{-}6)$$

or, in integral form,

$$\theta = \int \frac{dN_j}{R_j V} \qquad (7.3.1.2\text{-}7)$$

This is the mass balance equation for the *batch reactor*. The symbol t for "clock time" is replaced here by the more usual symbol θ for "batch residence time".

For the continuous, completely mixed reactor, it is useful to start from the reduced continuity equation in terms of concentrations, analogous to equation (7.3.1.2-1) (but without diffusion term):

$$\frac{\partial\langle C_j\rangle}{\partial t} + \frac{\partial\langle uC_j\rangle}{\partial z} = R_j \qquad (7.3.1.2\text{-}8)$$

Since

$$\langle uC_j\rangle = \frac{\langle F_j\rangle}{\Omega} = \frac{\langle F'C_j\rangle}{\Omega}$$

where F' is the volumetric flow rate (m³/s), this yields, after integration over z and multiplication by Ω,

$$\frac{d}{dt}(VC_j) + \int \frac{d\langle F_j\rangle}{dz} dz = R_j V \qquad (7.3.1.2\text{-}9)$$

If $F_{j,0}$ and $F_{j,e}$ represent, respectively, the inlet and outlet flow rates of species j, the following equation is obtained:

$$\frac{dN_j}{dt} = F_{j,0} - F_{j,e} + R_j V \qquad (7.3.1.2\text{-}10)$$

Again, Bird [1957] presents a more rigorous derivation, with the identical result. Under steady-state conditions, (7.3.1.2-10) reduces to an algebraic equation:

$$F_{j,e} - F_{j,0} = R_j V \qquad (7.3.1.2\text{-}11)$$

which is the mass balance for the *continuous flow stirred tank reactor* (CSTR).

If (7.3.1.2-10) is multiplied by the molecular weight M_j and summed on j, a total mass balance is obtained:

$$\frac{dm_t}{dt} = F_0^{'}\rho_{f,0} - F_e^{'}\rho_{f,e} \qquad (7.3.1.2\text{-}12a)$$

$$= \dot{m}_0 - \dot{m}_e \qquad (7.3.1.2\text{-}12b)$$

where $m_t = \sum_j M_j N_j$ is the total mass, and $\dot{m}$ is the mass flow rate (kg/s). Equation (7.3.1.2-12) could also be obtained by integrating (7.3.1.1-3) over the volume. For liquids, the density is approximately constant, and if the volume is fixed, (7.3.1.2-12) shows that the inlet and exit flows must be the same.

7.3.2 The Energy Equation

7.3.2.1 A "General" Formulation

Again, reference is made to Bird et al. [1960; 2007] for the rigorous derivation, in various coordinate systems, of the fundamental energy equation. The following form contains the phenomena that are of importance in reactors:

$$\underbrace{\sum_j M_j C_j c_{pj}\left(\frac{\partial T}{\partial t} + \mathbf{u}\cdot\nabla T\right)}_{(1)\quad(2)} = \underbrace{\sum_i \left(-\Delta H_i\right) r_i}_{(3)} + \underbrace{\nabla\cdot(\lambda\nabla T)}_{(4)} - \underbrace{\sum_j \mathbf{J}_j \nabla H_j}_{(5)} + \underbrace{Q_{\text{rad}}}_{(6)} \qquad (7.3.2.1\text{-}1)$$

where c_{pj} is the specific heat of species j (kJ/kg K), λ is the thermal conductivity of the mixture (kJ/m s K), and the H_j are partial molar enthalpies (kJ/kmol). The respective terms arise from (1) change of heat content with time, (2) convective flow, (3) heat effect of the chemical reactions, (4) heat transport by conduction, (5) energy flux by molecular diffusion, and (6) radiation heat flux.

Other energy terms encountered with particular flow conditions are work of expansion or viscous dissipation terms, primarily important in high-speed flow; external field effects, mechanical or electrical, can also occur. Since they usually are of much less importance, they will not be considered here. Heat radiation in the reactor is often neglected, except in the case of fixed bed catalytic reactors operating at high temperatures, but then it is generally lumped with the heat conduction and a few more heat transport mechanisms into an "effective"

heat conduction having the form of term (4) in (7.3.2.1-1). When this is done in (7.3.2.1-1) and the diffusion term (5) is neglected the result is

$$\sum_j M_j C_j c_{pj}\left(\frac{\partial T}{\partial t}+\mathbf{u}\cdot\nabla T\right)=\sum_i\left(-\nabla H_i\right)r_i+\frac{\partial}{\partial x}\left(\lambda_{e,x}\frac{\partial T}{\partial x}\right)+\frac{\partial}{\partial y}\left(\lambda_{e,y}\frac{\partial T}{\partial y}\right)+\frac{\partial}{\partial z}\left(\lambda_{e,z}\frac{\partial T}{\partial z}\right) \tag{7.3.2.1-2}$$

where λ_e is an effective thermal conductivity. Again, when there is more than one phase, more than one energy equation has to be written and a transfer term has to be introduced. For the same reasons as mentioned in Section 7.3.1.1 this has not been done here. It will be delayed to the specific cases discussed in the following chapters.

7.3.2.2 Specific Forms

The "general" energy equation can be simplified in the same way as the continuity equation, since the approximations introduced there are assumed to be equally applicable here. But, whereas mass is generally not diffusing through the wall, heat frequently is. In deriving the one-dimensional model by averaging over the cross section, a boundary condition for heat transfer at the reactor wall has to be introduced for this reason. It is commonly written as

$$\left(\lambda_{e,n}\frac{\partial T}{\partial n}\right)_R=\alpha_w\left(T_w-T_R\right) \tag{7.3.2.2-1}$$

where n represents the direction normal to the wall, α_w is a convective heat transfer coefficient, T_w is the temperature of the wall, and T_R is the fluid temperature in the immediate vicinity of the wall. The right-hand side of equation (7.3.2.2-1) would be zero for an adiabatic reactor. Equation (7.3.2.1-2) then becomes, when averaged over cylindrical geometry with diameter d_r,

$$\sum_j\left\langle M_j C_j c_{pj}\right\rangle\left(\frac{\partial\langle T\rangle}{\partial t}+\langle u\rangle\frac{\partial\langle T\rangle}{\partial z}\right)=\sum_i\langle-\Delta H_i\rangle\langle r_i\rangle+\frac{\partial}{\partial z}\left(\langle\lambda_{e,z}\rangle\frac{\partial\langle T\rangle}{\partial z}\right)+\frac{4}{d_r}\left(\lambda_{e,n}\frac{\partial T}{\partial n}\right)_w \tag{7.3.2.2-2}$$

An important point is that the *z* component of the conduction term retains its identity, in terms of averaged variables, but the *x* and *y* components are integrated out with the wall boundary condition (7.3.2.2-1), which is now written

$$\frac{4}{d_r}\left(\lambda_{e,n}\frac{\partial T}{\partial n}\right)_R = \frac{4\alpha_w}{d_r}\left(T_w - T_R\right)$$

$$\equiv \frac{4U}{d_r}\left(T_r - \langle T\rangle\right)$$

where T_r is the temperature of the surroundings and U is an overall heat transfer coefficient. The latter approximation actually locates the heat transfer with the wall in a thin film. For the tubular reactor, the heat conduction in the *z* direction is usually much smaller than the heat transported by convection.

The resulting equation is

$$\sum_j \langle M_j C_j c_{pj}\rangle\left(\frac{\partial\langle T\rangle}{\partial t} + \langle u\rangle\frac{\partial\langle T\rangle}{\partial z}\right) = \sum_i \langle -\Delta H_i\rangle\langle r_i\rangle + \frac{4U}{d_r}(T_r - \langle T\rangle) \tag{7.3.2.2-3}$$

For steady-state conditions (7.3.2.2-3) becomes, after multiplying by $\Omega = \pi d_r^2/4$ (and omitting the brackets),

$$\sum_j \dot{m}_j c_{pj}\frac{dT}{dz} - \Omega\sum_i\left(-\Delta H_i\right)r_i - \pi d_r U(T_r - T) = 0 \tag{7.3.2.2-4}$$

This is the energy equation for a single-phase tubular reactor with plug flow. Note that (7.3.2.2-4) is coupled with the continuity equation, mainly by the reaction term, but also through the heat capacity term on the left-hand side. The latter is sometimes written in terms of a specific heat that is averaged with respect to temperature and composition, that is, $\sum_j \dot{m}_j c_{pj} \equiv \dot{m}\bar{c}_p$.

A rigorous macroscopic energy balance is obtained by integrating over the entire reactor volume:

$$\sum_j m_j c_{pj}\frac{dT}{dt} = \sum_j F_{j,0}(H_{j,0} - H_{j,e}) + V\sum_i\left(-\Delta H_i\right)r_i + \int \pi d_t U(T_r - T)\,dz \tag{7.3.2.2-5}$$

It can also be found by a careful integration of (7.3.2.2-3) over the reactor [see Bird, 1957]. Representing the heat exchange surface of the reactor by A_k, (7.3.2.2-5) reduces to

$$m_t c_p \frac{dT}{dt} = V\sum_i (-\Delta H_i) r_i + A_k U (T_r - T) \qquad (7.3.2.2\text{-}6)$$

for the batch reactor or, with $F_{j,e} = F_{j,0} + R_j V$, to

$$\sum_j F_{j,e} H_{j,e} - \sum_j F_{j,0} H_{j,0} = A_k U (T_r - T) \qquad (7.3.2.2\text{-}7)$$

for the continuous flow stirred tank reactor.

The following chapters deal in detail with reactor types such as the batch reactor (Chapter 8), the tubular reactor with plug flow (Chapter 9), and the continuous flow reactor with complete mixing (Chapter 10). Deviations from plug flow will be encountered in Chapter 11 on fixed bed catalytic reactors, and several degrees of sophistication will be considered there. The problem of modeling nonideal and multiphase reactors will be developed in Chapter 12, whereas the important specific cases of fluidized bed reactors and of gas–liquid–solid reactors will be discussed in Chapters 13 and 14, respectively. Each of these chapters starts from the basic equations developed here or from combinations of these. Correlations are given for the mass and heat transfer parameters for each specific case. The operational characteristics of the reactors are derived from the solution of basic equations; and the performance of reactors in several industrial processes will be simulated and investigated.

7.3.3 The Momentum Equations

The balance of momentum in directions z_i (i = 1, 2, 3) is described by the Navier-Stokes equations:

$$\frac{\partial}{\partial t}(\rho_f \mathbf{u}) + \nabla \cdot (\rho_f \mathbf{uu}) = -\nabla P - \nabla \cdot \boldsymbol{s} + \rho_f \mathbf{g} \qquad (7.3.3\text{-}1)$$

where

$$\boldsymbol{s} = -\left\{ -\frac{2}{3}\mu (\nabla \cdot \mathbf{u}) \boldsymbol{I} + \mu \left[(\nabla \mathbf{u}) + (\nabla \mathbf{u})^T \right] \right\} \qquad (7.3.3\text{-}2)$$

with μ the molecular viscosity in (Pa s) and **uu**, $\boldsymbol{s}$, $\boldsymbol{I}$, and $\nabla \mathbf{u}$ second-order tensors. $\boldsymbol{I}$ is the unit tensor and superscript T indicates transpose of.

In (7.3.3-1), the respective terms result from (1) change of momentum with time, (2) convection, (3) the pressure gradient, (4) the shear stress, and (5) gravity. The pressure field, required for the solution of (7.3.3-1), can be calculated from the total continuity equation (7.3.1.1-3) and a relation between pressure, density, temperature, and composition, for example the ideal gas law for gas flows.

Appropriate boundary conditions have to be used. At walls, the no-slip condition is applied, that is, a zero velocity is imposed. At inlets, a given velocity or velocity profile can be imposed.

The solution of (7.3.3-1)-(7.3.3-2) is not straightforward. A detailed treatment of the subject is given in Chapter 12 on complex flow patterns. In many cases, a given type of velocity field can be imposed and the corresponding pressure field is calculated from a specific pressure drop equation.

PROBLEMS

7.1 Write (7.3.1.1-6) in terms of ξ_i', the extent of the *i*th reaction per unit mass of the reaction mixture, in (kmol/kg) and defined by

$$\xi_i' = \frac{\xi_i}{N_{j0}}\left(\frac{C_j}{\rho_f}\right)_0$$

7.2 Derive the steady-state continuity and energy equations and appropriate boundary conditions for the tubular reactor with turbulent flow, corresponding to the various situations represented in the following figure, from Himmelblau and Bischoff [1968].

The continuity equation for the first case is given (in cylindrical coordinates) by

$$u(r)\frac{\partial C_j}{\partial z} = D_{e,z}(r)\frac{\partial^2 C_j}{\partial_z^2} + \frac{1}{r}\left[\frac{\partial}{\partial r} r D_{e,r}(r)\frac{\partial C_j}{\partial r}\right] + R_j$$

with boundary conditions

$$u(r)C_{j0} = u(r)C_j(0,r) - D_{e,z}(r)\frac{\partial C_j(0,r)}{\partial z}$$

$$z = L \qquad \frac{\partial C_j}{\partial z} = 0, \qquad \text{all } r$$

$$r = 0 \qquad \frac{\partial C_j}{\partial r} = 0, \qquad \text{all } z$$

$$r = R_t \qquad \frac{\partial C_j}{\partial r} = 0, \qquad \text{all } z$$

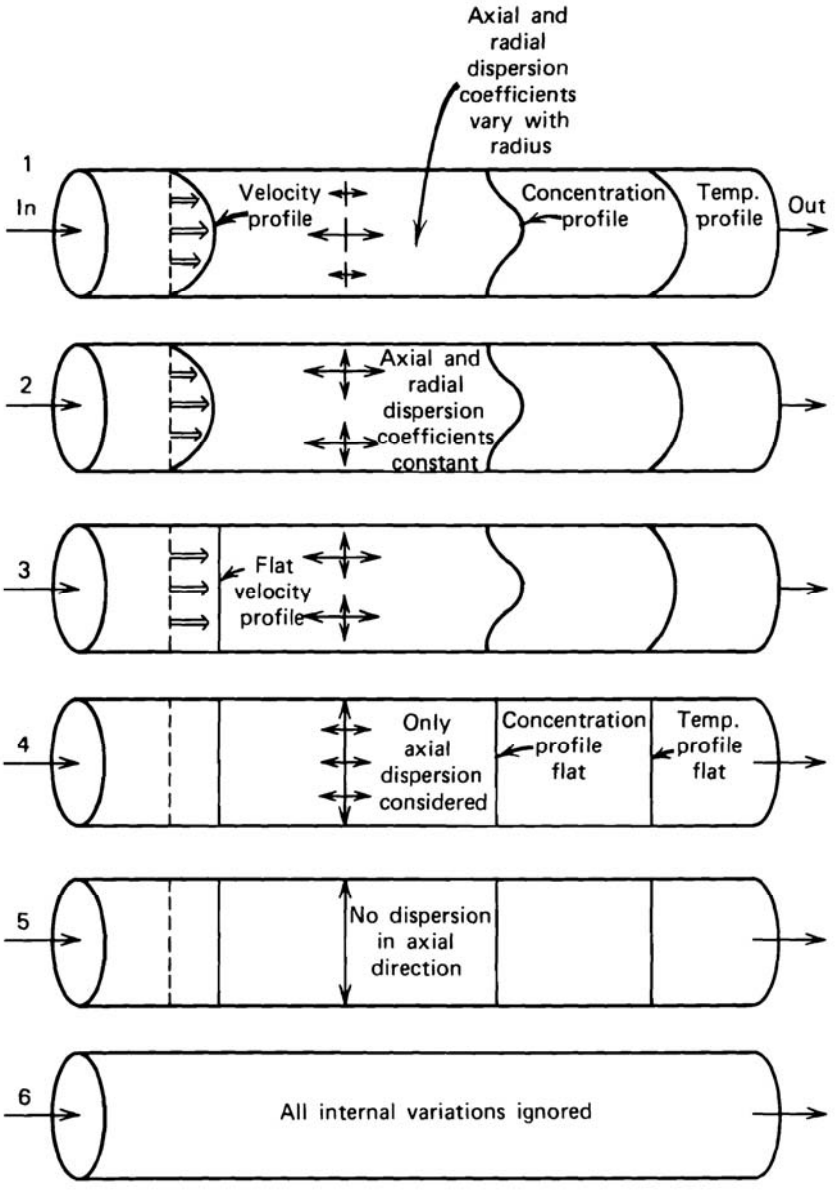

7.3 Write all the above equations in dimensionless form.

REFERENCES

Bird, R.B., *Chem. Eng. Sci.*, 6, 123 (1957).
Bird, R.B., Stewart, W.E., and Lightfoot, E.N., *Transport Phenomena*, Wiley, New York (1960); Revised 2nd Edition, Wiley (2007).
Himmelblau, D.M., and Bischoff, K.B., *Process Analysis and Simulation*, Wiley, New York (1968).
Hinze, J.O., *Turbulence*, McGraw-Hill, New York (1959).
Slaterry, J., *Momentum, Energy and Mass Transfer in Continua*, McGraw-Hill, New York (1972).

Chapter 8

The Batch and Semibatch Reactors

INTRODUCTION

Batch reactors are generally used for liquid phase reactions. When a solid catalyst has to be kept in suspension or when there are two liquid phases, as in the nitration of aromatics, for instance, an agitator is required. Agitation is also necessary to equalize the temperature in the reactor and to keep it at the desired level by efficient heat exchange through a jacket or an internal coil. Consequently, the batch reactor is generally considered to be spatially uniform in composition and temperature. The composition changes with time, however. Temperature sequencing may be favorable for the selectivity or for achieving complete conversion in a safe way.

In pure batch operation the reactants are completely fed into the reactor at the beginning. For better control of temperature this type of operation may not

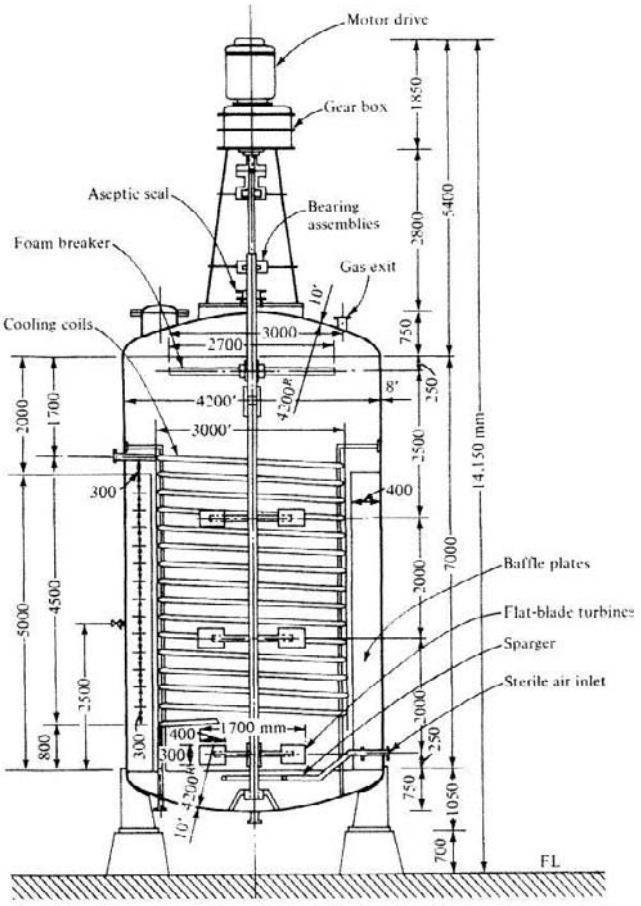

Figure 8-1

Batch reactor for the production of antibiotics by fermentation. Reprinted from S. Aiba, A.E. Humphrey and N.F. Milis, "Biochemical Engineering", 2nd Ed., University of Tokyo Press, Tokyo, 1973 and from J.E. Bailey and D.F. Ollis, "Biochemical Engineering Fundamentals", McGraw Hill, New York, 1986.

be advisable and the reactant(s) may have to be added progressively to the contents of the vessel. The reactor is then said to operate in the semibatch mode. Or, a product may be withdrawn, for instance, water in an esterification subject to equilibrium, to reach complete conversion of the reactant(s).

Batch and semibatch reactors are most often used for low production capacities, where the cost of labor and dead time are only a small fraction of the unit cost of the product. They are generally encountered in the area of specialty chemicals and polymers and in pharmaceuticals, in particular, in plants with a wide variety of products. Large batch reactors are used in fermentations for antibiotic production, an example of which is given in Fig. 8-1.

8.1 THE ISOTHERMAL BATCH REACTOR

Because of the uniformity of concentration, the continuity equation for the key reactant *A* may be written for the entire reactor volume:

$$-\frac{dN_A}{d\theta} = Vr_A(C_A) \tag{8.1-1}$$

where θ = residence time in the reactor. It is convenient to specifically represent this residence time in the reactor by a special symbol — for completely batch systems it is the same as "clock" time *t*, but in other applications the distinction will be useful. For a general set of reactions, (8.1-1) can be extended to

$$\frac{dN_j}{d\theta} = V\sum_{i=1}^{R}\alpha_{ij}r_i \equiv VR_j \tag{8.1-2}$$

These mass balances, for example (8.1-1), are often written in terms of conversions:

$$\frac{dx_A}{d\theta} = \frac{V}{N_{A0}}r_A \tag{8.1-3}$$

Then, (8.1-3) is readily put into integral form:

$$\theta = N_{A0}\int_{x_{A0}}^{x_{Af}}\frac{dx_A}{Vr_A} \tag{8.1-4}$$

Note that the batch residence time θ can be interpreted as the area from x_{A0} to x_{Af} under the curve of $N_{A0} / V\, r_A(x_A)$ versus x_A.

The above equations were already encountered in Section 1.1.2 of Chapter 1. The equations defining reaction rates were written there for a "point", a volume in which the composition is uniform. This is also assumed here for the ideal, well stirred batch reactor, whatever its volume.

The volume of the reaction mixture can change for two reasons: (1) external means (e.g., filling a reaction vessel or adding a second reactant) and (2) changes in densities of reactants or products (e.g., molar expansion of gases). The first possibility is often termed "semibatch" operation. The second is usually not very important for liquids, and is neglected. The proper formulation for gases will be derived below, although batch gas-phase reactors are not commonly used in industry because of the small mass capacity. A gas phase could be part of the reaction mixture, however. Also laboratory gas-phase reactors have been utilized.

With no expansion, as for liquids, (8.1-4) becomes

$$\theta = C_{A0}\int_{x_{A0}}^{x_{Af}} \frac{dx_A}{r_A(x_A)} \tag{8.1-5a}$$

$$= -\int_{C_{A0}}^{C_{Af}} \frac{dC_A}{r_A(C_A)} \tag{8.1-5b}$$

and for simple rate forms can be easily integrated analytically, as illustrated in Section 1.3.

For reactions with the stoichiometry

$$aA + bB \ldots \rightleftarrows qQ + sS + \ldots$$

the following mole balance can be made at a given extent of reaction based on conversion A:

$$\begin{aligned}
N_A &= N_{A0} - N_{A0}x_A \\
N_B &= N_{B0} - \frac{b}{a}N_{A0}x_A \\
N_Q &= N_{Q0} + \frac{q}{a}N_{A0}x_A \\
N_S &= N_{S0} + \frac{s}{a}N_{A0}x_A \\
N_I &= N_{I0} \quad \text{(inert)} \\
\hline
N_t &= N_{t0} + N_{A0}\frac{q+s\ldots-a-b\ldots}{a}x_A
\end{aligned}$$

Therefore, the total number of moles is given by

$$N_t = N_{t0} + N_{A0}\delta_A x_A$$

from which

$$\frac{N_t}{N_{t0}} = 1 + (y_{A0}\delta_A)x_A \equiv 1 + \varepsilon_A x_A \tag{8.1-6}$$

For gases and using the equation of state:

$$p_t V = ZN_t RT$$

$$\frac{V}{V_0} = \left(\frac{Z}{Z_0}\frac{T}{T_0}\frac{p_{t0}}{p_t}\right)\frac{N_t}{N_{t0}}$$

$$= \left(\frac{Z}{Z_0}\frac{T}{T_0}\frac{p_{t0}}{p_t}\right)(1 + \varepsilon_A x_A) \tag{8.1-7}$$

The concentrations to be substituted into the rate equation, can be expressed as

$$C_A = \frac{N_A}{V} = \frac{N_{A0}}{V_0}\frac{(1 - x_A)}{(1 + \varepsilon_A x_A)}\left(\frac{Z_0}{Z}\frac{T_0}{T}\frac{p_t}{p_{t0}}\right) \tag{8.1-8}$$

and the partial pressures,

$$p_A = p_t \frac{N_A}{N_t} = p_t \frac{N_{A0}}{N_{t0}}\frac{(1 - x_A)}{(1 + \varepsilon_A x_A)} \tag{8.1-9}$$

$$= p_{A0}\frac{(1 - x_A)}{(1 + \varepsilon_A x_A)}\left(\frac{p_t}{p_{t0}}\right)$$

For an *n*th-order reaction e.g.,

$$Vr_A = VkC_A^n = k\frac{N_{A0}^n}{V_0^{n-1}}\frac{(1 - x_A)^n}{(1 + \varepsilon_A x_A)^{n-1}} \qquad \text{(const. } T, p_t\text{)}$$

and (8.1-4) becomes

$$\theta = \frac{1}{kC_{A0}^{n-1}}\int_{x_{A0}}^{x_{Af}} \frac{(1 + \varepsilon_A x_A)^{n-1}}{(1 - x_A)^n}\,dx_A \qquad \text{(const. } T, p_t\text{)}$$

which in the absence of molar expansion, $\varepsilon_A = 0$, is the same as (8.1-5a), of course.

EXAMPLE 8.1.A

EXAMPLE OF DERIVATION OF A KINETIC EQUATION FROM BATCH DATA

The reaction $A + B \rightarrow Q + S$ is carried out in the liquid phase at constant temperature. It is believed the reaction is elementary and, since it is bimolecular, it is natural to first try second-order kinetics. The density may be considered constant.

Let *B* be the component with highest concentration, while the most convenient way to follow reaction is by titration of *A*. A batch-type experiment led to the data given in Table 8.1.A-1.

If the hypothesis of second order is correct, the following relation between the rate and the concentration of *A* and *B* will be valid for any time, and therefore for any composition:

$$r_A = r_B = kC_AC_B \tag{8.1.A-a}$$

and *k* has to have the same value for all levels of C_A and C_B. When the differential method is used, equation (8.1.A-a) is the starting point. By substituting the rate equation (8.1.A-a) in the material balances, (8.1-1) with $C_A = N_A / V$,

$$r_A = -\frac{dC_A}{d\theta} = kC_AC_B \tag{8.1.A-b}$$

This means r_A may be obtained as tangent to the curve C_A versus θ.

Substituting the corresponding C_A and C_B leads to *k*. The values of C_B follow from $C_B = C_{B0} - (C_{A0} - C_A)$. Table 8.1.A-2 gives the values of *k* obtained in this way. The variation of *k* is small and does not invalidate the second-order hypothesis, especially as the precision of the method is getting smaller as the reaction proceeds. A value of 61×10^{-2} m^3/h kmol may be used for *k*.

TABLE 8.1.A-1
CONCENTRATION-VERSUS-TIME DATA

$\mathbf{C_{B0} = 0.585\,kmol/m^3}$ $\mathbf{C_{A0} = 0.307\,kmol/m^3}$	
Time (h)	**C_A (kmol/m^3)**
0	0.307
1.15	0.211
2.90	0.130
5.35	0.073
8.70	0.038

TABLE 8.1.A-2
COMPARISON OF k DETERMINED BY INTEGRAL AND DIFFERENTIAL METHOD

				k (m^3/kmol h)	
Time (h)	C_A	C_B (kmol/m^3)	r_A (kmol/m^3 h)	**From (b)**	**From (e)**
1.15	0.211	0.489	6.52×10^{-2}	63.1×10^{-2}	61.2×10^{-2}
2.90	0.130	0.408	3.32×10^{-2}	62.5×10^{-2}	61.9×10^{-2}
5.35	0.073	0.351	1.49×10^{-2}	58.4×10^{-2}	62.0×10^{-2}
8.70	0.038	0.316	0.72×10^{-2}	59.6×10^{-2}	60.8×10^{-2}

The integral method is based on (8.1-5a). Before integration is possible, C_A and C_B must be expressed as a function of one variable, the fractional conversion x_A. In this case

$$C_A = C_{A0}(1 - x_A)$$

$$C_B = C_{B0}\left(1 - \frac{x_A}{M}\right)$$

where

$$M = \frac{C_{B0}}{C_{A0}}$$

Equation (8.1-5a) becomes

$$\theta = \frac{C_{A0}}{kC_{A0}C_{B0}} \int_0^{x_A} \frac{dx_A}{(1 - x_A)(1 - x_A / M)} \tag{8.1.A-c}$$

or

$$C_{B0}k\theta = \frac{M}{1 - M} \ln \frac{M(1 - x_A)}{M - x_A} \tag{8.1.A-d}$$

or, with concentrations,

$$k\theta = \frac{1}{C_{A0} - C_{B0}} \ln \frac{C_{B0}C_A}{C_{A0}C_B} \tag{8.1.A-e}$$

These equations also lead to a constant value for k, which confirms that the reaction has second-order kinetics. Peterson [1962] has discussed further aspects of differential versus integral fitting of data from batch reactor experiments.

■

EXAMPLE 8.1.B
STYRENE POLYMERIZATION IN A BATCH REACTOR

The kinetics of free radical polymerization and the molecular weight distribution of the polymer were already discussed in Section 1.6.2 of Chapter 1. To improve the chemical and mechanical properties of the polymer great efforts were undertaken a number of years ago to achieve narrow distributions. This is possible with anionic or cationic — so-called living — polymerization, in which chains can not terminate or transfer and grow at a rather uniform rate, thus yielding a polymer with a polydispersity close to one. This type of polymerization requires very special operating conditions and high purity of the feed, however.

More recently it has become possible to achieve this goal also in free radical polymerization by stabilizing propagating macroradical chains and make them "dormant". This has been called "living" free radical polymerization (LFRP). It involves reducing the concentrations of the active chains, thus making bimolecular terminations almost negligible. One way of doing this is by scavenging the active chain by means of a nitroxide chemical that will simply be called here TEMPO:

$$R_n + TEMPO \rightleftarrows R_n - T$$

The process is called NMLP (from nitroxide mediated "living" polymerization).
A second possibility is to regulate the equilibrium between active and dormant chains by means of an exchange or redox reaction, involving a metal ion like Cu, Mn, Fe and a halogen like Br:

$$R_n + Br - Cu^{II} \rightleftarrows R_n - Br + Cu^{I}$$

This is called "atom transfer radical polymerization" (ATRP).
In the following developments R_n-T and R_n-Br, the dormant chains and their concentrations, will be represented by D_n.

Butté et al. [1999] applied a comprehensive mechanistic scheme covering both NMLP and ATRP to the simulation of the polymerization of styrene. The scheme is given in Table 8.1.B-1, together with the rate equations. The nomenclature in Table 8.1.B-1 is completely in line with that of Section 1.6.2. The symbols represent both the species and their concentration. The initiation by thermal decomposition of the monomer, not included in the scheme of Section 1.6.2, was observed by Hui and Hamielec [1972].

TABLE 8.1.B-1
REACTION SCHEME AND RATE EQUATIONS FOR LFRP
(BOTH NMLP AND ATRP)

REACTION STEPS		RATE EQUATIONS
Initiation		
by monomer decomposition		
	$3M_1 \rightarrow 2R_0$	$r_0 = k_{it} M_1^3$
by initiator decomposition		
	$I \rightarrow 2R_0$	$r_{id} = k_{id} I$
Propagation		
	$R_n + M_1 \rightarrow R_{n+1}$	$r_p = k_p M_1 \lambda_0$
Exchange steps		
Scavenging		
in NMLP	$R_n + T \rightarrow D_n$	$r_{s1} = k_{s1} T \lambda_0$
in ATRP	$R_n + X \rightarrow D_n + Y$	$r_{s2} = k_{s2} X \lambda_0$
Reactivation		
in NMLP	$D_n \rightarrow R_n$	$r_{a1} = k_{a1} \mu_0$
in ATRP	$D_n + Y \rightarrow R_n + X$	$r_{a2} = k_{a2} Y \mu_0$
Termination		
by combination		
	$R_n + R_m \rightarrow P_{n+m}$	$r_{tc} = k_{tc} \lambda_0^2$
Transfer		
with monomer		
	$R_n + M_1 \rightarrow R_0 + P_n$	$r_{fm} = k_{fm} M_1 \lambda_0$
Dormant species decomposition		
in NMLP	$D_n \rightarrow P_n$	$r_{dc_1} = k_{dc_1} \mu_0$
in ATRP	$D_n + X \rightarrow P_n + 2$	$r_{dc_2} = k_{dc_2} X \mu_0$

All the rate coefficients are assumed to be independent of the chain length. The rates of the various steps are directly related to the moments of the polymeric species, taken to be sufficiently representative of the complete distribution of the species. λ_0, μ_0, and η_0 are the zero-th moments of the active, dormant and dead chain distributions and also their total concentration. The moments λ_1, μ_1, and η_1 represent the total number of monomer units in the active, dormant and dead chains, i.e., their degree of polymerization. The

moments λ_2, μ_2, and η_2 can be related to the variance around the mean of the distributions and provide information on their width. $\lambda_1 / \lambda_0, \mu_1 / \mu_0$, and η_1 / η_0 are the number average chain lengths of the various chains.

For the ATRP type of LFRP the continuity equations for the various species can be written:

Initiator:

$$-\frac{dI}{dt} = r_{id}$$

Monomer:

$$-\frac{dM_1}{dt} = (3r_{it} + r_p + r_{fm})$$

For *X*, *Y* and *Z*:

$$-\frac{dX}{dt} = r_{s2} - r_{a2} + r_{dc_2}$$

$$-\frac{dY}{dt} = r_{s2} - r_{a2}$$

$$\frac{dZ}{dt} = r_{dc_2}$$

Active chains:

These are radicals, for which pseudo-steady state may be assumed, so that

$$\frac{d\lambda_0}{dt} = 0 = 2(r_0 + r_{id}) - r_{s_2} + r_{a_2} - r_{tc}$$

$$\frac{d\lambda_1}{dt} = 0 = r_{a_2}\frac{\mu_1}{\mu_0} - (r_{a_2} + r_{tc} + r_{fm})\frac{\lambda_1}{\lambda_0} + r_p$$

$$\frac{d\lambda_2}{dt} = 0 = r_{a_2}\frac{\mu_2}{\mu_0} - (r_{s_2} + r_{tc} + r_{fm})\frac{\lambda_2}{\lambda_0} + r_p\left(1 + 2\frac{\lambda_1}{\lambda_0}\right)$$

Dormant chains:

$$\frac{d\mu_i}{dt} = r_{s_2}\frac{\lambda_i}{\lambda_0} - (r_{a_2} + r_{dc})\frac{\mu_i}{\mu_0} \qquad i = 0,1,2$$

Dead chains (macromolecules):

$$\frac{d\eta_0}{dt} = r_{dc} + r_{fm} + \frac{1}{2}r_{tc}$$

$$\frac{d\eta_1}{dt} = r_{dc}\frac{\mu_1}{\mu_0} + \left(r_{fm} + r_{tc}\right)\frac{\lambda_1}{\lambda_0}$$

$$\frac{d\eta_2}{dt} = r_{dc}\frac{\mu_2}{\mu_0} + \left(r_{fm} + r_{tc}\right)\frac{\lambda_2}{\lambda_0} + r_{tc}\left(\frac{\lambda_1}{\lambda_0}\right)^2$$

The model consists of 11 ordinary differential equations and three algebraic equations (the pseudo steady state equations for $\lambda_0, \lambda_1, \lambda_2$). The unknowns are the concentrations of *M*, *X*, *Y*, *S*, I_2 and the moments λ_i, μ_i, η_i (i = 0, 1, 2).

Butté et al. [1999] carried out experiments for both types of free radical polymerization of styrene and simulated the results using kinetic parameters obtained from the literature after adaptation accounting for their own observations.

Only the results for ATRP are shown here. Figure 8.1.B-1 deals with the polymerization of styrene at 110 °C with 1-phenlylethylbromide as an initiator and addition of a Cu-complex. The model prediction and experimental results are in reasonable agreement. The number average molecular weight increases with the conversion of the monomer and the polydispersity P_w/P_n drops to a value close to one from a relativity low conversion onwards. The evolution of the Cu-concentration is also shown.

Also in LFRP of styrene, Matyaszewski et al. [1997] obtained values of P_w/P_n of 1.1.

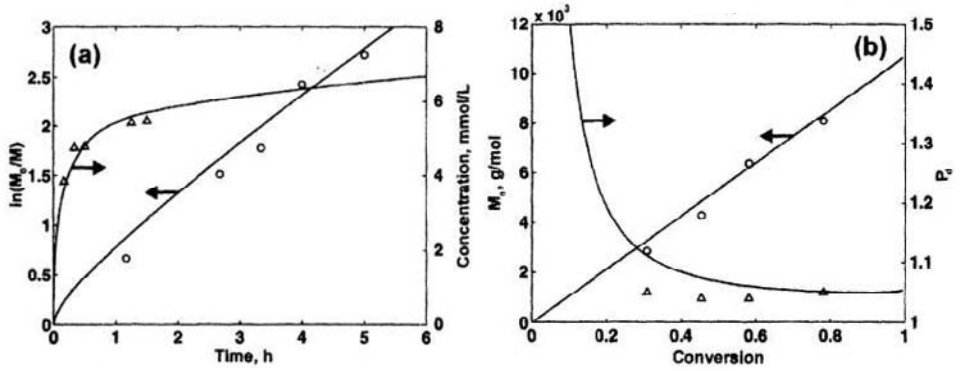

Figure 8.1.B-1

Atom transfer radical polymerization of styrene at 110°C [Butté et al., 1999].

■

EXAMPLE 8.1.C
PRODUCTION OF GLUCONIC ACID BY AEROBIC FERMENTATION OF GLUCOSE

Gluconic acid is produced on an industrial scale by aerobic fermentation of glucose with the enzymes Aspergillus niger and catalase. The stoichiometry is simple: glucose + ½ O_2 yields gluconic acid. The fermentation is carried out at 30°C in a batch reactor and consists of three stages with different loadings of concentrated solutions of the substrate, glucose. The charge also contains corn steep liquor, $MgSO_4$, K- and ammonium phosphate, urea, anti-foam and the enzymes. The rate depends on the pH, controlled by the addition of NaOH, except in the third stage, so that the product is really a mixture of gluconic acid and Na-gluconate.

Reuss et al. [1986] modeled this process on the basis of a careful experimental program. The kinetics of gluconic acid production were described by means of the Michaelis-Menten equation (Section 1.5.1 of Chapter 1). At a pH of 5.6 the constant K_M in that equation amounted to 0.36 mmol/h and the specific oxygen uptake rate (half of the specific production rate, γ_P) 65 mol oxygen per kg dry weight and per hour.

The production rate is intrinsically very fast but limited by the oxygen uptake of the liquid. The volumetric oxygen transfer coefficient $k_L a_v$ was also affected by the increasing viscosity of the medium as the amount of biomass increased.

Using the definitions and symbols of microbial kinetics the model equations can be written:

$$\frac{dX}{dt} = \mu X$$

$$\frac{dP}{dt} = \gamma_P X$$

$$-\frac{dS}{dt} = \frac{\mu X}{y_{\chi/S}} + \frac{\gamma_P X}{y_{P/S}} + m_S X$$

$$\frac{dC_L}{dt} = k_L a_v (C_L^* - C_L) - \frac{\mu X}{y_{\chi/O}} - \frac{\gamma_P X}{y_{P/O}} - m_O X$$

X represents the biomass, P the product, and S the glucose (or substrate) concentration (kg/m^3). For a clear insight into the first equation in particular it is useful to remember that μ is the *specific* biomass growth rate in h^{-1} (see Section

1.5.2). γ_P is the specific production rate of P in kg P per hour and kg biomass; $y_{X/S}$ is the biomass weight selectivity (kg biomasss produced per kg glucose converted); $y_{P/S}$ is the product wt selectivity (kg gluconic acid/kg glucose converted); m_S is the glucose consumption per hour and referred to 1 kg dry biomass. In the fermentation jargon it is called "maintenance coefficient for glucose" (0.048 kg glucose/kg dry weight·h). The last equation describes the evolution with time of C_L, the concentration of dissolved oxygen, with saturation concentration C^*_L. The weight of biomass produced per mol oxygen converted is represented by $y_{X/O}$ and $y_{P/O}$ is the weight of P produced per mol of oxygen converted. m_O is the oxygen consumption per hour, again referred to 1 kg of dry biomass and called "maintenance coefficient for oxygen" (1.61 mol O_2/kg dry weight·h).

Figure 8.1.C-1 shows the computed and experimental time histories for biomass, glucose and product.

Reuss et al. [1986] applied this model to investigate optimal operating policies, e.g., controlled continuous feeding of the glucose, or operating at a higher pressure so as to increase the oxygen concentration and enhance the global rate.

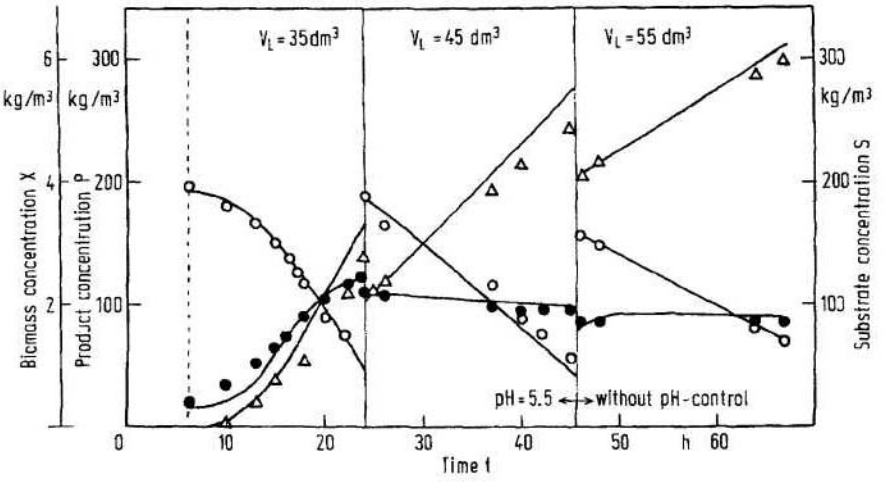

Comparison between on-line computer estimations (solid lines) and laboratory mesurements (● – biomass, ○ – substrate, △ – product)

Figure 8.1.C-1

Batch fermentation of glucose into gluconic acid [Reuss et al., 1986].

■

8.2 THE NONISOTHERMAL BATCH REACTOR

In practice it is not always possible, or even desirable, to carry out a reaction under isothermal conditions. In this situation both the energy and mass balances must be solved simultaneously:

$$\frac{dx_A}{d\theta} = \frac{V}{N_{A0}} r_A(x_A, T) \tag{8.1-3}$$

$$m_t c_p \frac{dT}{d\theta} = V(-\Delta H) r_A(x_A, T) + qA_k \tag{8.2-1}$$

where (8.2-1) is the appropriate simplified heat balance and A_k is the heat exchange surface from Section 7.2.4. The term qA_k represents any addition or removal of heat from the reactor. For adiabatic operation, $q = 0$, while for a heat exchange coil it would have the form

$$q = U(T_r - T) \tag{8.2-2}$$

where T_r = temperature of heating or cooling medium. Equation (8.2-1) can be combined with (8.1-3) to yield

$$m_t c_p \frac{dT}{d\theta} - (-\Delta H) N_{A0} \frac{dx_A}{d\theta} = qA_k = 0 \qquad \text{adiabatic} \tag{8.2-3}$$

Thus,

$$m_t c_p (T - T_0) - (-\Delta H) N_{A0} (x_A - x_{A0}) = \int_0^\theta qA_k \, d\theta \tag{8.2-4a}$$

$$= qA_k \theta, \quad q = \text{const.} \tag{8.2-4b}$$

$$= 0, \qquad \text{adiabatic} \tag{8.2-4c}$$

For the latter situation, the adiabatic temperature change, for a certain conversion level, is

$$T - T_0 = \frac{(-\Delta H) N_{A0}}{m_t c_p} (x_A - x_{A0}) = \frac{1}{\lambda} (x_A - x_{A0}) \tag{8.2-5}$$

Therefore, in this case T can be substituted from (8.2-5) into (8.1-3), which then becomes a single differential equation in x_A [or x_A can be substituted into (8.2-1)]. This is done by utilizing (8.1-4), where the integral is evaluated by choosing increments of x_A and the corresponding $T(x_A)$ from (8.2-5). Again, the reaction

time θ can be represented by the area under the curve $N_{A0} / V\, r_A(x_A, T(x_A))$ versus x_A.

Some analytical solutions are possible for simple-order rate forms — they are given for the analogous situation for plug flow reactors in Chapter 9.

Finally, the maximum adiabatic temperature change occurs for $x_A = 1.0$, and then (for $x_{A0} = 0$):

$$(\Delta T)_{ad} = T_{ad} - T_0 = \frac{(-\Delta H)N_{A0}}{m_t c_p} \tag{8.2-6}$$

Equation (8.2-4c) can be written in the alternate form

$$T = T_0 + (\Delta T)_{ad}\, x_A \tag{8.2-7}$$

More general situations require numerical solutions of the combined mass and heat balances. Several situations can occur:

The temperature is constant or a prescribed function of time, $T(\theta)$ — here, the differential equation (8.1-3) can be solved alone as

$$\frac{dx_A}{d\theta} = \frac{V}{N_{A0}} r_A(x_A, T(\theta))$$

Also, (8.2-1) or (8.2-3) can then be solved to find the heating requirements:

$$q(\theta)A_k = m_t c_p \frac{dT(\theta)}{d\theta} - (-\Delta H)V\, r_A(x_A(\theta), T(\theta))$$

Heat exchange is zero, constant, or a prescribed function of time. First, (8.2-4) is used to compute $T = T(x_A, \theta)$ and then substituted into the continuity equation for A, (8.1-3), which can then be integrated:

$$\frac{dx_A}{d\theta} = \frac{V}{N_{A0}} r_A(x_A, T(x_A, \theta))$$

The temperature variation can be found by using the computed values of $x_A(\theta)$:

$$T(\theta) = T(x_A(\theta), \theta)$$

Alternatively, the combined equations (8.1-3) and (8.2-1) can be solved simultaneously as coupled differential equations.

Heat exchange is given by $q = U(T_r - T)$. Direct numerical solution of the coupled mass and heat balances is performed.

If convergence problems arise in the numerical solutions, it is often useful to use conversion as the independent variable. The mass balance links

increments of conversion to increments of time and through the heat balance these yield increments of temperature. Iterations on the evaluations of the rates are also often required.

For case 3 above, values of the heat transfer coefficient are required. The factor U, appearing in (8.2-2), is a heat transfer coefficient, defined as follows:

$$\frac{1}{U} = \frac{1}{\alpha_k} + \frac{d}{\lambda}\frac{A_k}{A_m} + \frac{1}{\alpha_r} \cdot \frac{A_k}{A_r} \tag{8.2-8}$$

where:

α_k, A_k = heat transfer coefficient (kJ/m^2 h °C) and heat transfer surface (m^2) on the side of the reaction mixture, respectively
α_r, A_r = the same, but on the side of the heat transfer medium
A_m = logarithmic mean of A_k and A_r
λ = conductivity of the wall through which heat is transferred (kJ/m h °C)
d = wall thickness (m)

The literature data concerning α_k and α_r are not always in accordance. As a guide the following relations are given.

For reactors in which heat is transferred through a wall, α_k may be obtained from the following dimensionless equation for stirred vessels:

$$\frac{\alpha_k d_r}{\lambda}\left(\frac{\mu_w}{\mu}\right)^{0.14} = 0.36\left(\frac{d_s^2 N \rho_L}{\mu}\right)^{0.66}\left(\frac{c_p \mu}{\lambda}\right)^{0.33} \tag{8.2-9}$$

where:

d_r = reactor diameter (m)
d_s = propeller diameter (m)
μ_w = viscosity of the reaction mixture at the temperature of the wall (kg/m h)
μ = viscosity of the reaction mixture at the temperature of the reaction mixture
λ = thermal conductivity of the reaction mixture (kJ/m h °C)
N = revolutions per hour (h^{-1})
ρ_L = density of reaction mixture (kg/m^3)

[From Chilton, Drew, and Jebens, 1944].

More extensive work by Chapman, Dallenbach, and Holland [1964] on a batch reactor with baffles and taking into account the liquid height H_L and the propeller position H_s led to the following equation:

$$\frac{\alpha_k d_r}{\lambda}\left(\frac{\mu_w}{\mu}\right)^{0.24} = 1.15\left(\frac{d_s^2 N\rho_L}{\mu}\right)^{0.65}\left(\frac{c_p\mu}{\lambda}\right)^{0.33}\left(\frac{H_s}{d_s}\right)^{0.4}\left(\frac{H_L}{d_s}\right)^{-0.56} \qquad (8.2\text{-}10)$$

Further work on this subject has been done by Strek [1963].

For α_r several cases are possible. When the reaction vessel is heated (e.g., with steam), the Nusselt equation may be applied, provided film condensation is prevailing.

For heat transfer through a coil, α_k may be calculated from an equation such as (8.2-9), but with a larger coefficient, due to the effect of the coil on the turbulence. According to Chilton et al. [1944], this coefficient would be 0.87. It is likely to depend also on the mixing intensity. Other literature sources also mention a value of 1.01.

Values of α_r may be obtained from the following equation, valid for turbulent conditions:

$$\frac{\alpha_r d_t}{\lambda} = 0.023\left(\frac{d_t G}{\mu}\right)^{0.8}\left(\frac{c_p\mu_s}{\lambda}\right)^{0.4}\Phi \qquad (8.2\text{-}11)$$

where:

Φ = $1 + 3.5(d_t / d_c)$
d_t = inner diameter of the pipe (m)
d_c = coil diameter (m)
μ_s = viscosity of the heat transfer medium at the surface of the coil (kg/m h)

Equation (8.2-11) is an adaptation of the classical Dittus and Boelter equation for straight pipes. Further information on this topic can be found in Holland and Chapman [1966]. Various aspects of agitator selection are dealt with by Gates et al. [1975].

EXAMPLE 8.2.A

DECOMPOSITION OF ACETYLATED CASTOR OIL ESTER

This example has been adapted from Smith [1970] and Cooper and Jeffreys [1971]. The overall reaction for the manufacture of drying oil is

$$\begin{pmatrix}\text{acetylated}\\ \text{castor oil}\\ \text{ester}\end{pmatrix}(l) \rightarrow \begin{pmatrix}\text{drying}\\ \text{oil}\end{pmatrix}(l) + \text{CH}_3\text{COOH}(g)$$

The charge of oil to the batch reactor is 227 kg and has a composition such that complete hydrolysis gives 0.156 kg acid/kg ester. The initial temperature is T_0 =

613 K. The physiochemical properties are as follows: c_p = 2.51 kJ/kg K, molecular weight of the acid = 60 kg/kmol, $(-\Delta H) = -62.8 \times 10^3$ kJ/kmol. The rate of acid production is first order with respect to the ester concentration, expressed in kmol/m^3 [Grummitt and Fleming, 1945].

$$r_A = \left(\frac{1}{60}\right) C_A \exp\left(35.2 - \frac{22450}{T}\right) \quad \text{kg acid/m}^3\,\text{s} \qquad (8.2.\text{A-a})$$

A constant heat supply is provided by an electrical heater and a final conversion of 70 percent is desired.

This is an example of case 2 discussed above, and so (8.2-4) is utilized. First, the adiabatic situation is computed using (8.2-5). The adiabatic curve is linear in conversion and has a slope which is the adiabatic temperature change

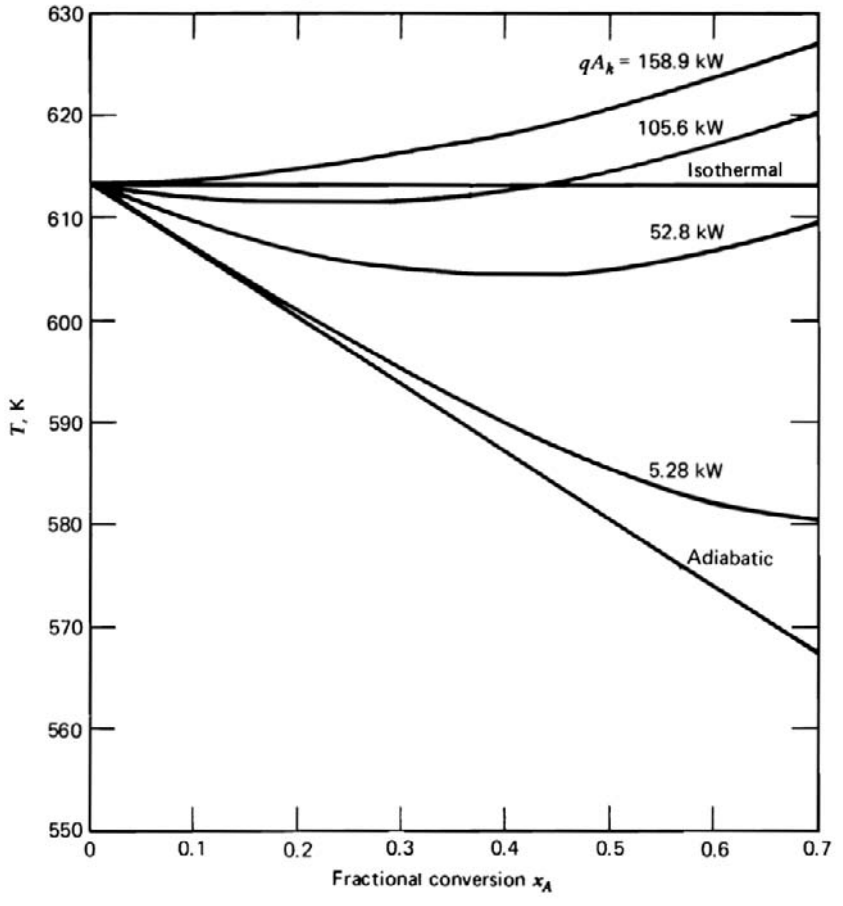

Figure 8.2.A-1

Temperature-conversion progress for various rates of heat input. From Cooper and Jeffreys [1971].

from (8.2-6):

$$(\Delta T)_{ad} = \frac{(-62.8\times10^3\,\text{kJ/kmol})(0.156\,\text{kg/kg})(227\,\text{kg})}{(227\,\text{kg})(2.51\,\text{kJ/kg K})(60\,\text{kg/kmol})} \qquad \text{(8.2.A-b)}$$

$$= -65\ \text{K}$$

Thus,

$$T = 613 - 65x_A \quad \text{K} \qquad \text{(8.2.A-c)}$$

as shown in Fig. 8.2.A-1. For this endothermic reaction the temperature drops drastically with adiabatic operation, and heating needs to be considered.

Temperature-conversion curves for various heat inputs were calculated by Cooper and Jeffreys, using (8.2-4b) to obtain $T = T(x_A, \theta)$:

$$T = 613 - 65x_A + \frac{qA_k}{m_t c_p}\theta \qquad \text{(8.2.A-d)}$$

For qA_k = 52.8 kW,

$$\frac{qA_k}{m_t c_p} = \frac{52.8\,\text{kW}}{(227\,\text{kg})(2.51\,\text{kJ/kg K})} = 0.0927\,\text{K/s}$$

Substitution into (8.1-3) leads to:

$$\frac{dx_A}{d\theta} = \frac{1}{60C_{A0}}C_{A0}(1-x_A)\exp\left(35.2 - \frac{22450}{T}\right) \qquad \text{(8.2.A-e)}$$

$$= \frac{(1-x_A)}{60}\exp\left(35.2 - \frac{22450}{613 - 65x_A + 0.0927\theta}\right) \qquad \text{(8.2.A-f)}$$

Fig. 8.2.A-1 shows the evolution of temperature with conversion for various heat inputs. For a heat input of 105.6 kW, e.g., the temperature drops until a conversion of 40 percent is reached.

It is also instructive to look at the conversion-time profile (Fig. 8.2.A-2). For $qA_k = 52.8$ kW the first half of the final conversion of 70 % is reached in about 2.5 min, while the second half takes 5 min. This is even more pronounced for the adiabatic case with its rapid temperature drop. The total reaction time required for 70 percent conversion depends upon the heat input rate, as shown in the table below.

One could also select the proper heater size to achieve 70 % conversion in a given time — say, 20 min. In such a case equations (8.2.A-d) and (8.2.A-e)

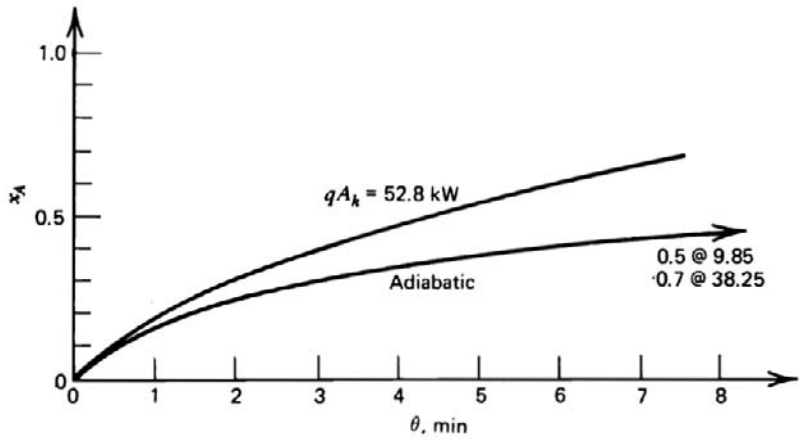

Figure 8.2.A-2
Conversion versus time curve for adiabatic operation and a heat input rate of 52.8 kW.

Heat input rate (kW)	θ_f for 70% conversion (min)
(Adiabatic, $q = 0$)	(38.25)
5.28	23.64
52.8	7.48
105.6	4.72
158.9	3.55

would have to be solved iteratively for the unknown value of q. Alternatively, the simulation results presented here yield by means of a simple interpolation $qA_k = 8$ kW. ■

8.3 SEMIBATCH REACTOR MODELING

When addition of reactants, together with removal of liquid and vapor, is also considered, the equations become:

Continuity equation for species j:

$$\frac{d(C_j V)}{dt} = F_1' C_{j,0} - F_2' C_j - F_{3,v}' C_{j,v} - V\sum_{i=1}^{N} \alpha_{ij} r_i \qquad (8.3\text{-}1)$$

in which F_1' is the liquid feed rate and F_2' is the liquid withdrawal rate (both in m^3/h), and $F_{3,v}'$ is the vapor withdrawal rate (m^3 vapor/h).

Energy equation:

$$\rho c_p V \frac{dT}{dt} = F_1' c_p \rho T_1 - F_2' c_p \rho T - F_{3,v}' \sum C_{j,v} \Delta H_v + Q + V\sum_{i=1}^{N} r_i(-\Delta H_i) \qquad (8.3\text{-}2)$$

Accounting for the change in volume:

$$\frac{dV}{dt} = F_1^{'} - F_2^{'} - F_{3,1}^{'}$$

with

$$F_{3,1}^{'} = F_{3,v}^{'} \frac{273}{273+T} p_t \frac{1}{22.4} \frac{1}{C_{t,1}} \tag{8.3-3}$$

where T is in degrees C and $C_{t,1}$ is the total liquid concentration. Equation (8.3-3) has to be substituted into (8.3-1) and (8.3-2).

EXAMPLE 8.3.A

SIMULATION OF SEMIBATCH REACTOR OPERATION (WITH L.H. HOSTEN†)

Consider the following set of reactions:

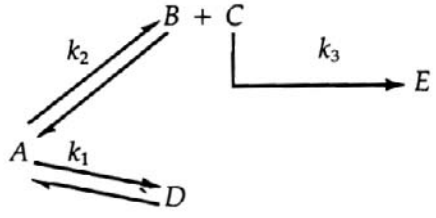

with rate equations

for $A \rightleftarrows D$:

$$r_1 = k_1\left(C_A - \frac{C_D}{K_1}\right) \qquad \text{with } (-\Delta H_1) = 62805 \text{ kJ/kmol}$$

for $A \rightleftarrows B + C$:

$$r_2 = k_2\left(C_A - \frac{C_B C_C}{K_2}\right) \quad \text{with } (-\Delta H_2) = -83740 \text{ kJ/kmol}$$

for $C \rightarrow E$:

$$r_3 = k_3 C_C \qquad \text{with } (-\Delta H_3) = (-\Delta H_2).$$

The rate coefficients are given by

$$k_1 = k_3 = 10 \exp\left(23.25 - \frac{5033}{T}\right) \text{ h}^{-1}$$

$$k_2 = 60\exp\left(23.25 - \frac{5033}{T}\right) \text{ h}^{-1}$$

and the equilibrium constants by

$$K_1 = 0.5; \qquad K_2 = 2.92 \text{ kmol/m}^3$$

The reactor is a cylindrical vessel with a diameter of 0.8 m and is operated in a semibatch mode. The initial load is 0.1826 m^3 of pure *A* at a concentration of 17.48 kmol/m^3 and an initial temperature of 25°C. The copper coil for heat exchange has an internal diameter of 0.015m, an external diameter of 0.019 m, a length of 14 m, and an exchange surface of 0.748 m^2. The thermal conductivity of the copper is 1.402 kJ/m h K. The diameter of the coil is 0.35 m. The paddle agitator has a diameter of 0.3 m and revolves at 150 rpm.

A mixture of *A* and *D*, containing respectively 7.1 and 31.89 kmol/m^3, is fed at 25°C during 3 hours at a rate of 0.1068 m^3/h. Then, the reaction is continued for another 3 hours. There is no liquid withdrawal. The operating pressure is 1 bar.

Integration of the set of equations (8.3-1) to (8.3-3), for example by means of a Runge-Kutta-Gill routine, yields concentrations, temperature, volume of the reactor contents, and vapor flow rate as functions of time. Determining the vapor flow rate requires an additional equation, expressing that, when the reactor content is boiling, the sum of the partial pressures must equal the total pressure above the liquid. When the liquid behaves in an ideal way, the vapor pressures satisfy Raoult's law:

$$p_i = x_i p_i^*$$

where the equilibrium pressures p_i^* are calculated from Riedel's equation. The flow rate $F_{3,v}^{'}$ is then calculated by means of a one-dimensional search procedure.

TABLE 8.3.A-1
DATA FOR RIEDEL'S VAPOR PRESSURE EQUATION

Component	T_b (K)	T_c (K)	P_c (bar)
A	454.1	594.4	57.1
B	351.5	516.2	63.0
C	340.3	523.2	37.8
D	373.	647.3	217.6
E	420.	520.	60.

TABLE 8.3.A-2
PHYSICAL PROPERTIES OF THE VESSEL CONTENTS AND HEATING MEDIUM

	Vessel Contents	**Heating Medium**
Thermal conductivity (kJ/m h K)	1.0429	0.979
Viscosity (kg/m h)	1.287	5.4
Specific heat (kJ/kg K)	2.805	2.847
Density (kg/m^3)	1000	
Heat of vaporization (kJ/kmol)	35493	

The boiling points under normal conditions and the critical properties of the five components, required in the calculation of their vapor pressure according to Riedel's equation, are given in Table 8.3.A-1.

The Q in (8.3-2) is the heat exchanged through the coil (kJ/h):

$$Q = UA\frac{\left(T_{in}^{'} - T\right) - \left(T_{ex}^{'} - T\right)}{\ln\dfrac{T_{in}^{'} - T}{T_{ex}^{'} - T}} = Wc_{ph}\left(T_{in}^{'} - T_{ex}^{'}\right)$$

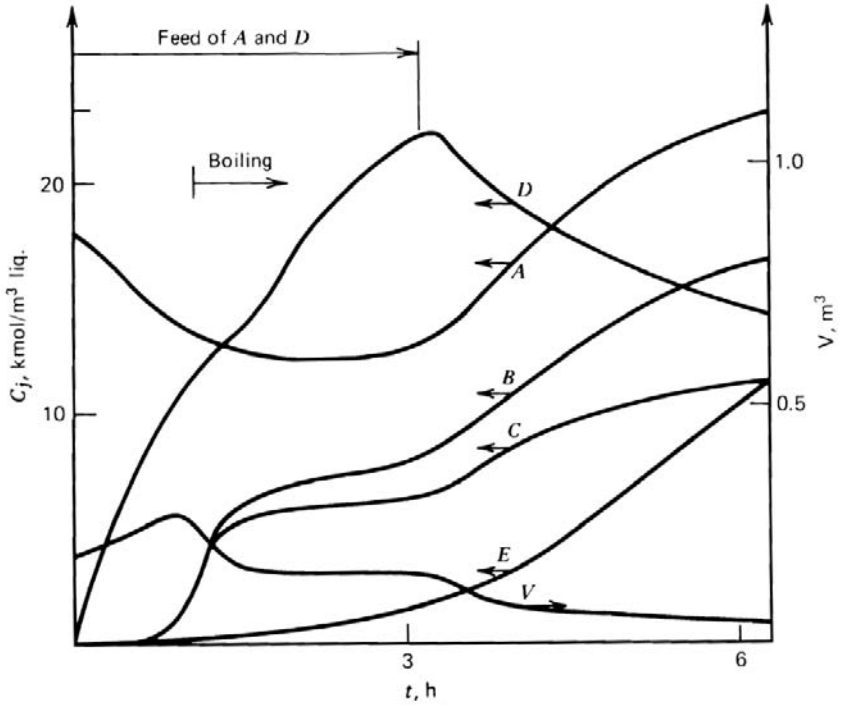

Figure 8.3.A-1
Evolution of liquid volume and product concentrations.

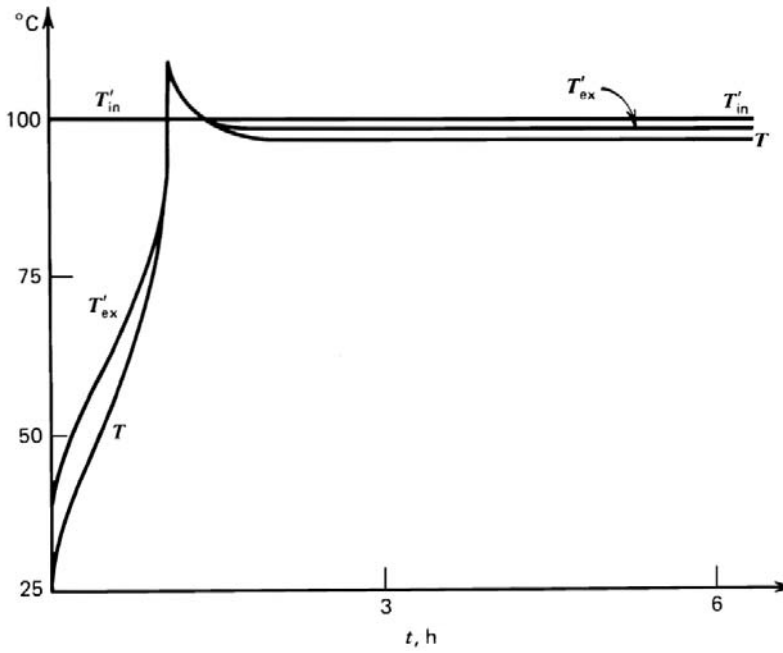

Figure 8.3.A-2

Evolution of reactor temperature and of inlet and exit temperatures of the heat exchanging medium.

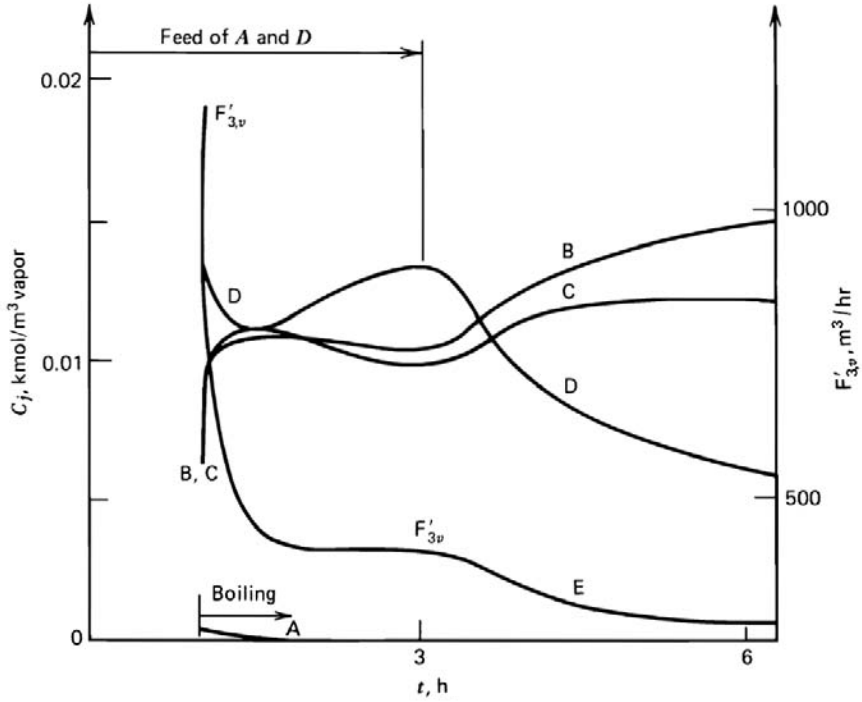

Figure 8.3.A-3

Evolution of vapor-phase composition.

where $T_{in}^{'}$ and $T_{ex}^{'}$ represent the temperature of the heating medium at the inlet and exit of the coil, respectively; W is the mass flow rate (kg/h) and c_{ph} is the specific heat. The overall heat transfer coefficient U includes scale formation on both sides of the coil surface.

The flow rate of the heating medium is 250 kg/h, and its inlet temperature is 100°C.

Average physical properties of the reacting components and of the heating medium are given in Table 8.3.A-2. The average heat of vaporization of the reacting fluid is 35493 kJ//kmol.

Fig. 8.3.A-1 shows the concentrations in the liquid and the volume of the latter as a function of time; Fig. 8.3.A-2 shows the temperature of the reactor contents, T, and the inlet and exit temperatures of the heat exchanging medium, $T_{in}^{'}$ and $T_{ex}^{'}$ respectively and Fig. 8.3.A-3 the vapor-phase composition and vapor withdrawal rate, $F_{3v}^{'}$. ■

8.4 OPTIMAL OPERATION POLICIES AND CONTROL STRATEGIES

Two main types of situations are considered:

1. Optimal batch operation time for the sequence of operations in a given reactor.

2. Optimal temperature (or other variable) variations during the course of the reaction, aiming at minimizing the reactor size.

Only the main features will be discussed here — more extensive details are given in Aris [1961]. To simplify the mathematical details only constant volume reactors are considered, but for most practical situations this is not a serious restriction.

8.4.1 Optimal Batch Operation Time

The discussion follows that of Aris [1961, 1965, 1969]. The price per kilomole of chemical species A_j is w_j, so that the net increase in value of the reacting mixture is

$$W(\theta) = \sum_{j=1}^{N} w_j \left(N_j - N_{j0}\right) \qquad (8.4.1\text{-}1)$$

$$= \sum_{j=1}^{N} w_j \sum_{i=1}^{M} \alpha_{ij} \xi_i$$

$$= \sum_{i=1}^{M} (\Delta W)_i \xi_i$$

where

$$(\Delta W)_i \equiv \sum_{j=1}^{N} \alpha_{ij} w_j \tag{8.4.1-2}$$

which is constant for a given stoichiometry and chemical costs. For a single reaction, it is more common to introduce the conversion of the key species, *A*, into (8.3.A-1):

$$W(\theta) = (\Delta W) \frac{N_{A0} x_A}{|\alpha_A|} \tag{8.4.1-3}$$

The cost of operation is usually based on four steps:

1. Preparation and reactor charging time θ_P, with cost per unit time, of W_P.
2. Reaction time θ_R, with W_R.
3. Reactor discharge time θ_Q, with W_Q.
4. Idle or "down" time θ_0, with W_0.

The total operation cost, then, is

$$W_T = \theta_0 W_0 + \theta_P W_P + \theta_Q W_Q + \theta_R W_R \tag{8.4.1-4}$$

Since the reactor operation is the main point of interest here, all the other times will be taken to be constant, and the main question is to determine the optimal reaction time, with its corresponding conversion. The net profit is

$$W(\theta_R) - W_T \tag{8.4-1-5}$$

and the optimum value of θ_R is found from

$$\frac{d}{d\theta_R}[W(\theta_R) - W_T] = 0 \tag{8.4.1-6}$$

or

$$\frac{dW(\theta_R)}{d\theta_R} = W_R \tag{8.4.1-7}$$

From (8.4.1-3),

$$\frac{dW(\theta_R)}{d\theta_R} = (\Delta W) \frac{N_{A0}}{|\alpha_A|} \frac{dx_A}{d\theta_R}$$

and combined with (8.1-3):

$$= (\Delta W) V \left. \frac{r_A}{|\alpha_A|} \right|_{\theta_R} \tag{8.4.1-8}$$

At the optimum

$$\frac{V}{|\alpha_A|} r_A(x_A)\Big|_{\theta_R} = \frac{W_R}{\Delta W} \tag{8.4.1-9}$$

The actual optimum reaction time θ_R is calculated from (8.1-4), evaluated at $x_{AR} = x_A(\theta_R)$ given by (8.4.1-9):

$$\theta_R = \frac{N_{A0}}{V} \int_0^{x_{AR}} \frac{dx_A}{r(x_A)} \tag{8.4.1-10}$$

Instead of the maximum net profit (8.4.1-5), the maximum of the net profit per unit time may be desired:

$$\frac{W(\theta_R) - W_T}{\theta_T} \tag{8.4.1-11}$$

where $\theta_T \equiv \theta_0 + \theta_P + \theta_Q + \theta_R$. Then, the optimum θ_R is found from

$$\frac{d}{d\theta_R}\left[\frac{W(\theta_R) - W_T}{\theta_T}\right] = 0 \tag{8.4.1-12}$$

or

$$\frac{dW(\theta_R)}{d\theta_R} - W_R = \frac{W(\theta_R) - W_T}{\theta_T} \tag{8.4.1-13}$$

Aris [1965] has provided a convenient graphical procedure for solving (8.4.1-13) for the optimal value of θ_R. Fig. 8.4.1-1 illustrates a typical curve for net profit. It is recognized that the right-hand side of (8.4.1-13) is precisely the slope of the tangent line $\overline{OL}$. From (8.4.1-13),

$$\frac{W(\theta_R) - W_T}{\theta_T} = \frac{d}{d\theta_R}\left[W(\theta_R) - W_T\right]$$

it is seen that the θ_R indicated in the figure is the time that satisfies (8.4.1-13), and is the optimum value for maximum net profit per unit time. The point *M* and corresponding θ_R' give the optimum for maximum net profit, from (8.4.1-6).

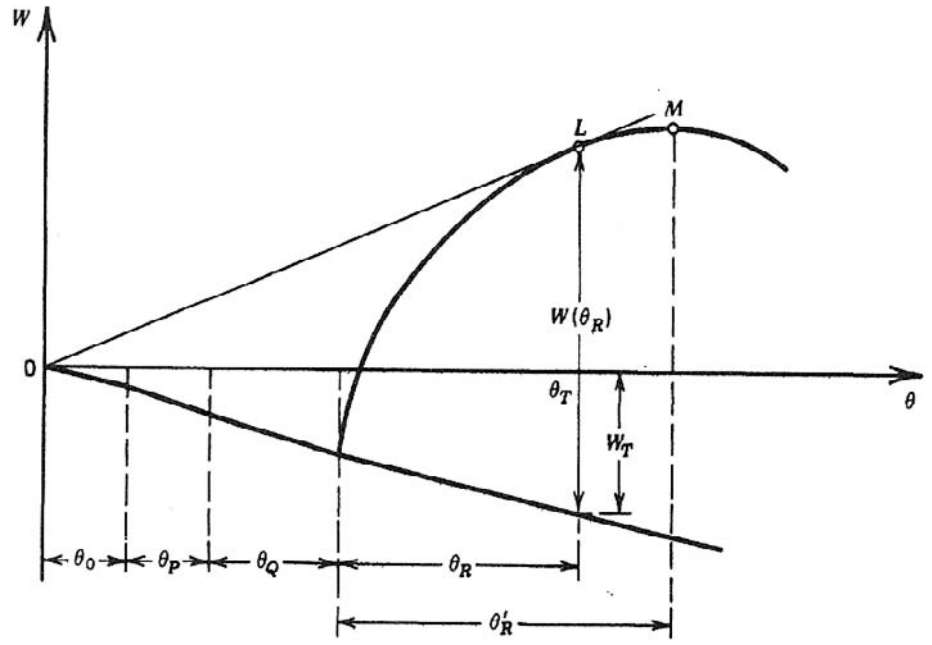

Figure 8.4.1-1
Net profit curve. From Aris [1965].

EXAMPLE 8.4.1.A
OPTIMUM CONVERSION AND MAXIMUM PROFIT FOR A FIRST-ORDER REACTION

For a simple first-order reaction, (8.1-4) gives

$$\theta = C_{A0}\int_0^{x_A}\frac{dx}{kC_{A0}(1-x)} = \frac{-1}{k}\ln(1-x_A) \qquad (8.4.1.A\text{-a})$$

or

$$x_A = 1-e^{-k\theta} \qquad (8.4.1.A\text{-b})$$

Thus, from (8.4.1-3),

$$W(\theta_R) = (\Delta W)N_{A0}\left(1-e^{-k\theta_R}\right) \qquad (8.4.1.A\text{-c})$$

and the value of θ_R for maximum profit is found from (8.4.1-7):

$$W_R = (\Delta W)N_{A0}\left(ke^{-k\theta_R}\right) \qquad (8.4.1.A\text{-d})$$

or

$$(\theta_R)_{opt} = \frac{1}{k}\ln\left[\frac{(\Delta W)k\,N_{A0}}{W_R}\right] \qquad (8.4.1.A\text{-e})$$

The optimum conversion is

$$\left(x_A\right)_{opt} = 1 - \frac{W_R}{\left(\Delta W\right) k\, N_{A0}} \qquad \text{(8.4.1.A-f)}$$

If the result (8.4.1.A-f) is substituted into the first-order rate form

$$V\left(r_A\right)_{opt,\theta_R} = V\, k\, C_{A0}\left(1 - x_A\right) = \frac{W_R}{\Delta W}$$

which is (8.4.1-9) for this situation. ■

8.4.2 Optimal Temperature Policies

This section considers two questions: (1) What is the best single temperature of operation? (2) What is the best temperature progression during the reaction time, or in other words the best trajectory? For single reactions, the results are relatively straightforward. If the reaction is *irreversible*, and if the rate increases with temperature the optimal temperature for either maximum conversion from a given reactor operation, or minimum time for a desired conversion, is the highest temperature possible. This highest temperature, T_{max}, is imposed by other considerations such as reactor materials and catalyst physical properties. Similarly, for reversible *endothermic* reactions where the equilibrium conversion increases with temperature ($E_{for.} > E_{rev.}$), the highest allowable temperature is the best policy.

The case of reversible *exothermic* reactions is more complicated, because even though the rate may increase with temperature, once the equilibrium conversion is reached, higher temperatures have an adverse effect on the equilibrium conversion. Thus, there is an optimum intermediate temperature where reasonably rapid rates are obtained together with a sufficiently high equilibrium conversion. The precise value of the optimal temperature is obtained from (8.1-4) at the final conversion x_{Af} :

$$\theta_f = C_{A0} \int_0^{x_{Af}} \frac{dx_A}{r\left(x_A, T\right)} \qquad \text{(8.4.2-1)}$$

This can always be integrated for a constant value of temperature, and then the best temperature found for a given conversion x_{Af}. It can be shown that this is exactly equivalent to the problem of choosing the optimal temperature for the maximum conversion for a given reaction time θ_f.

EXAMPLE 8.4.2.A
OPTIMAL TEMPERATURE TRAJECTORIES FOR FIRST-ORDER REVERSIBLE REACTIONS

For a first-order reversible reaction, the reaction rate is

$$A \underset{2}{\overset{1}{\rightleftarrows}} S$$

$$r_A = k_1 C_A - k_2 C_S \qquad \text{(8.4.2.A-a)}$$

$$= k_1 C_{A0}(1 - x_A) - k_2 C_{A0} x_A \quad (C_{S0} = 0)$$

It is convenient to use dimensionless variables [e.g., Millman and Katz, 1967] with

$$k_1 = A_1 e^{-E_1/RT} \rightarrow u = A_1 \theta_f e^{-E_1/RT} \qquad \text{(8.4.2.A-b)}$$

$$k_2 = A_2 e^{-E_2/RT} \rightarrow \beta u^{\alpha}$$

where

$$\beta = \frac{\theta_f A_2}{(\theta_f A_1)^{\alpha}} \qquad \text{(8.4.2.A-c)}$$

and

$$\alpha = \frac{E_2}{E_1}$$

$$\tau = \frac{\theta}{\theta_f}$$

Then, the mass balance (8.1-3) becomes

$$\frac{dx_A}{d\tau} = u(1 - x_A) - \beta u^{\alpha} x_A \qquad \text{(8.4.2.A-d)}$$

The optimum value of *u* leads to a temperature

$$T = \frac{E_1/R}{\ln(\theta_f A_1/u)} \qquad \text{(8.4.2.A-e)}$$

For a given *u*, (8.4.2.A-d) can be easily integrated to give:

$$\tau = \frac{x_{Aeq}}{u} \ln \frac{1 - (x_{A0}/x_{Aeq})}{1 - (x_A/x_{Aeq})} \qquad \text{(8.4.2.A-f)}$$

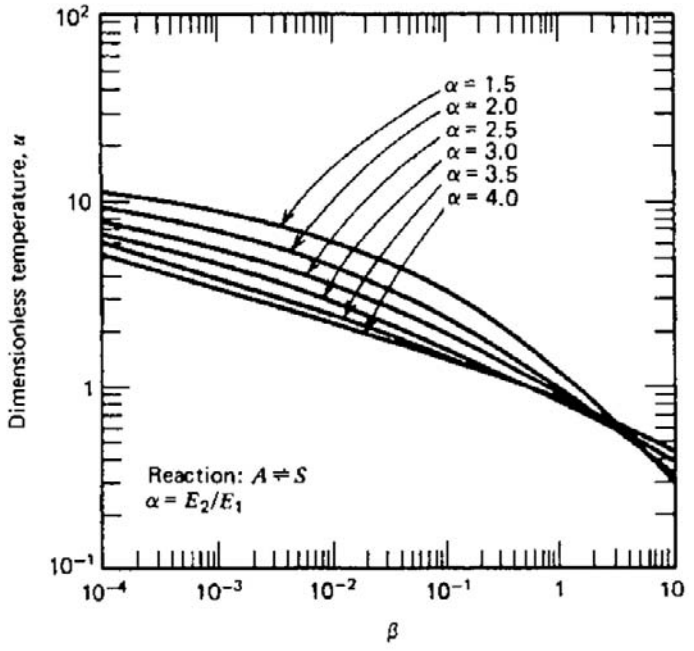

Figure 8.4.2.A-1

Dimensionless temperature versus parameter β. From Fournier and Groves [1970a].

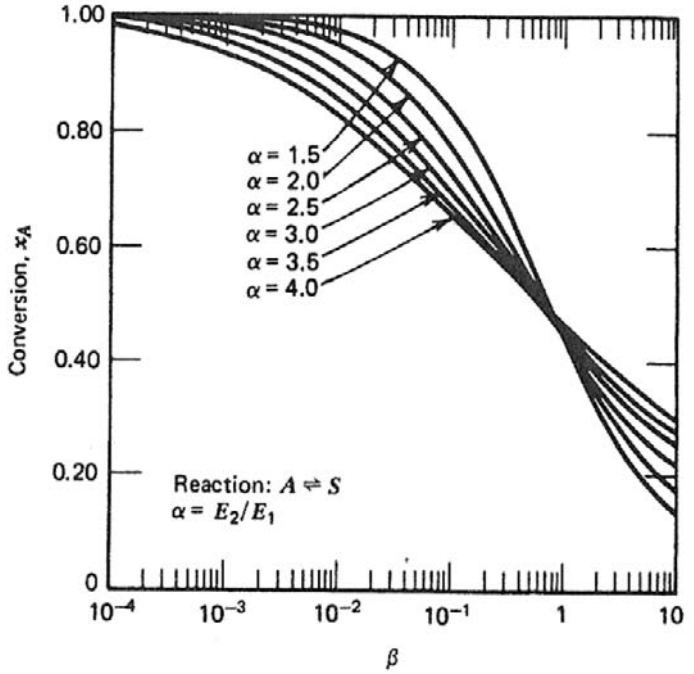

Figure 8.4.2.A-2

Conversion versus parameter β. From Fournier and Groves [1970a].

where the equilibrium conversion is given by

$$x_{Aeq}(u) = \left(1 + \beta u^{\alpha - 1}\right)^{-1} \qquad \text{(8.4.2.A-g)}$$

Equation (8.4.2.A-f) can be rearranged into

$$x_A = x_{Aeq}\left[1 - \left(1 - \left(\frac{x_{A0}}{x_{Aeq}}\right)\right)e^{-u\tau / x_{Aeq}}\right] \qquad \text{(8.4.2.A-h)}$$

The value of the optimum T, or equivalently u, for maximum x_{Af} with a given θ_f can now be readily calculated from

$$\left(\frac{\partial x_{Af}}{\partial u}\right)_{\tau=1} = 0 \qquad \text{(8.4.2.A-i)}$$

It can be shown that for a single reaction this result is equivalent to the problem of the optimum u for a minimum θ_f with a given x_{Af} [Aris, 1961]. Fournier and Groves [1970a] have provided useful charts based on equations (8.4.2.A-h) and (8.4.2.A-i). With Figs. 8.4.2.A-1 and 8.4.2.A-2, both equivalent problems can be readily solved by beginning with the known quantities: either α and $\beta(\theta_f)$ or α and x_{Af}. Other kinetic schemes have also been evaluated by Fournier and Groves [1970a].

Even better results for the reversible exothermic reaction can be obtained by choosing an optimal temperature variation with time. This type of operation is also feasible in practice, using automatic control techniques. Qualitative reasoning indicates that a high temperature at the beginning would be best, since this increases the rate constant, and the equilibrium limitations are usually not particularly important at this point. As the reaction progresses and approaches equilibrium, it is important to have lower temperatures that favor higher equilibrium conversions. Thus, the optimum temperature trajectory would be expected to decrease with time. Also, the maximum overall rate, made up of the sum of the instantaneous point rates, will be largest if each of the point rates is maximized. This reasoning cannot be extended to multiple reactions, however, since the overall optimum will be made up of the interactions of several rates.

■

For a single reaction, the condition of optimality to be fulfilled in each point is

$$\frac{\partial r_A}{\partial T} = 0 \qquad \text{(8.4.2-2)}$$

[A proof is given by Aris, 1965.] Only for simple cases analytical solutions are possible. For the reaction

$$A + B \underset{2}{\overset{1}{\rightleftarrows}} Q + S$$

the rate is

$$r_A = k_1 C_A C_B - k_2 C_Q C_S$$

$$= A_1 e^{-E_1/RT} C_{A0}^2 (1 - x_A)(M - x_A) - A_2 e^{-E_2/RT} C_{A0}^2 x_A^2 \quad (8.4.2\text{-}3)$$

where

$$M = \frac{C_{B0}}{C_{A0}} \qquad \text{and} \qquad C_{Q0} = 0 = C_{S0}$$

Then, the optimum temperature at each point is found from (8.4.2-2), with the results

$$T_{opt} = \left\{ \left(\frac{-R}{E_1 - E_2} \right) \ln \left[\left(\frac{A_2 E_2}{A_1 E_1} \right) \left(\frac{x_A^2}{(1 - x_A)(M - x_A)} \right) \right] \right\}^{-1}$$

$$\equiv \left\{ \frac{1}{(-B_1)} \ln [B_2 B_3] \right\}^{-1} \quad (8.4.2\text{-}4)$$

with

$$B_1 = \frac{E_1 - E_2}{R} \qquad \text{and} \qquad B_2 = \frac{A_2 E_2}{A_1 E_1}$$

Fournier and Groves [1970b] have provided solutions for several other reaction types. The definitions of B_1 and B_2 are the same for any single reversible reaction, but a parameter B_3 depends on the type of reaction:

Reaction	$\boldsymbol{B_3}$
$A \rightleftarrows S$	$\dfrac{x_A}{1 - x_A}$
$A \rightleftarrows Q + S$	$\dfrac{C_{A0} x_A^2}{1 - x_A}$
$A + B \rightleftarrows S$	$\dfrac{x_A}{C_{A0}(1 - x_A)(M - x_A)}$

Other kinetic forms can be similarly handled. The calculation procedure is then as follows. First, the result of utilizing (8.4.2-2), such as (8.4.2-4), is used

to determine $T_{opt}(x_A)$ which is then used in the integration of the mass balance (8.1-4) for $\theta(x_A)$:

$$\theta = C_{A0} \int_{x_{A0}}^{x_{Af}} \frac{dx_A}{r_A(x_A, T_{opt}(x_A))} \tag{8.4.2-5}$$

One complication that occurs can be seen from (8.4.2-4): for low conversions, B_3 may have a sufficiently small value to make $B_2B_3 \leq 1.0$. Then, (8.4.2-4) gives a value $T_{opt} \rightarrow \infty$ (or negative). In practice, of course, the temperature will have to be limited to some value $T_{max} < T_{opt}$ over a range of conversion going from zero to some critical value x_{Ac}. This critical conversion, $x_{Ac} > 0$, can be found by first using T_{max} in (8.4.2-5).

A more general consideration of these problems involves the optimization of some sort of objective function, like the equipment cost which usually depends on outlet conversions and total residence time. It is difficult to include all possible costs (e.g., safety), and so a simpler quantity, such as selectivity, is often used instead.

Denbigh and Turner [1971] consider two major categories:

1. Output problems. These are concerned with the attainment of the maximum output — the amount of reaction product(s) per unit time and reactor volume.
2. Selectivity problems. These are concerned with maximizing the selectivity — the fraction of reactant converted to the *desired* product.

The first type is most important for simple reactions with no side products and/or very expensive reactors and catalysts. The second type occurs with complex reactions, often producing harmful waste. Output problems are somewhat easier to solve in general, since their simpler reaction schemes involve less mathematical details.

The above case of single reversible exothermic reactions was an example of an output problem. Intuitive logic led to the qualitative conclusion that the optimum temperature profile was the one that maximized the rate at each point. This was also the quantitative solution and led to the design techniques presented. For selectivity problems, if the kinetics are not too complex, the proper qualitative trends of the optimal temperature profiles can also often be deduced by reasoning. However, the quantitative aspects must usually be determined by formal mathematical optimization methods. Simple policies, such as choosing the temperature for maximum local point selectivity, rarely lead to the maximum final overall selectivity because of the complex interactions between the various rates.

A few examples of this qualitative reasoning are worth discussing. Consider the scheme

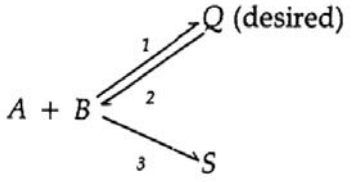

If $E_3 > E_1, E_2 > E_1$, the optimum temperature trajectory is *decreasing* in time, as for the simple reversible exothermic case, but not quite as high in the beginning, to avoid excessive side reaction. If $E_3 > E_1 > E_2$, the reversible reaction is endothermic, and so a high temperature level is desirable; but if too high, especially when C_A and C_B are large, too much side reaction occurs. The optimum trajectory here is *increasing*. If $E_2 > E_1 > E_3$, a decreasing trajectory is again to be preferred. Horn [see Denbigh and Turner, 1971, for references] has worked out the mathematical details of these cases.

Another example is the familiar

$$A + B \xrightarrow{1} Q \xrightarrow{2} S \quad (Q \text{ desired})$$

If $E_2 > E_1$, the initial temperature should be large for a rapid first reaction, but the temperature should be diminished as Q accumulates to preferentially slow down the degradation reaction 2. Again, a decreasing trajectory is preferable.

An example that has two answers depending on whether it is looked at from the output or yield viewpoint is the following:

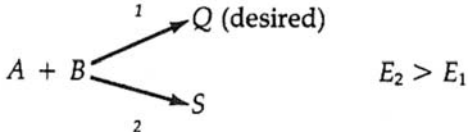

From the *output* point of view, the optimum trajectory is an *increasing* one. At the beginning of the reaction, the temperature should be low in order to promote formation of Q rather than S; but at the end of the reaction time, the temperature should be high to offset the otherwise low conversion rate — this gives more Q even though it also results in more S. If the reactor cost is not important, as in the selectivity problem, the temperature should be *as low as possible* throughout the reaction time. This gives, relatively, the highest Q but requires a very large reactor for significant conversion.

A final example is taken from Denbigh and Turner [1971]:

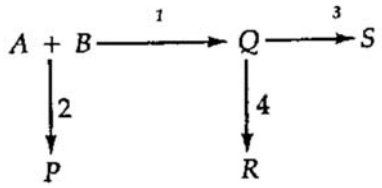

Here, the desired product *S* is formed through an intermediate, and both the feed reactants and the intermediates can undergo side reactions. The four possible cases from the point of view of yield are:

$E_1 > E_2, E_3 > E_4$	uniform high temperature
$E_1 < E_2, E_3 < E_4$	uniform low temperature
$E_1 < E_2, E_3 > E_4$	increasing temperature trajectory
$E_1 > E_2, E_3 < E_4$	decreasing trajectory.

Denbigh gave an example in which under isothermal conditions a yield of 25 percent was obtained, against 60 percent with an optimum temperature trajectory.

EXAMPLE 8.4.2.B

OPTIMUM TEMPERATURE POLICIES FOR CONSECUTIVE AND PARALLEL REACTIONS

The two basic coupled reaction schemes, consecutive and parallel, were considered in an interesting and useful simple way by Millman and Katz [1967], and illustrate the computation of optimum temperature trajectories. The details are expressed in dimensionless form, as above:

For consecutive reactions:

$$A \overset{1}{\rightarrow} Q \overset{2}{\rightarrow} S \qquad (Q \text{ desired})$$

$$\frac{dx_A}{d\tau} = u(1 - x_A) \qquad \text{and} \qquad \frac{dx_Q}{d\tau} = u(1 - x_A) - \beta u^{\alpha} x_Q$$

For parallel reactions:

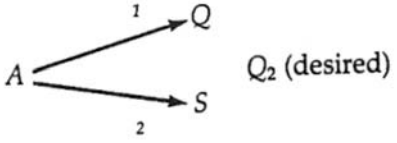

$$\frac{dx_A}{d\tau} = \left(u + \beta u^{\alpha}\right)(1 - x_A) \qquad \text{and} \qquad \frac{dx_Q}{d\tau} = u(1 - x_A)$$

where

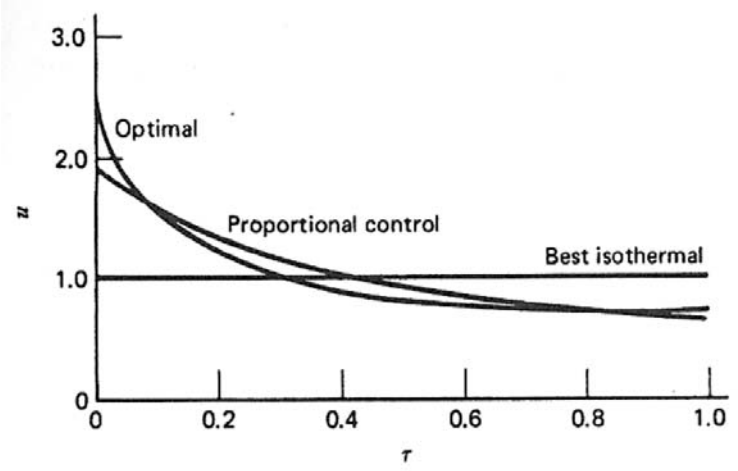

Figure 8.4.2.B-1

Temperature histories for consecutive reaction: $\alpha = 2$, $\beta = \frac{1}{2}$. Yields: best isothermal, 0.477; best proportional, 0.489; optimal, 0.491. From Millman and Katz [1967].

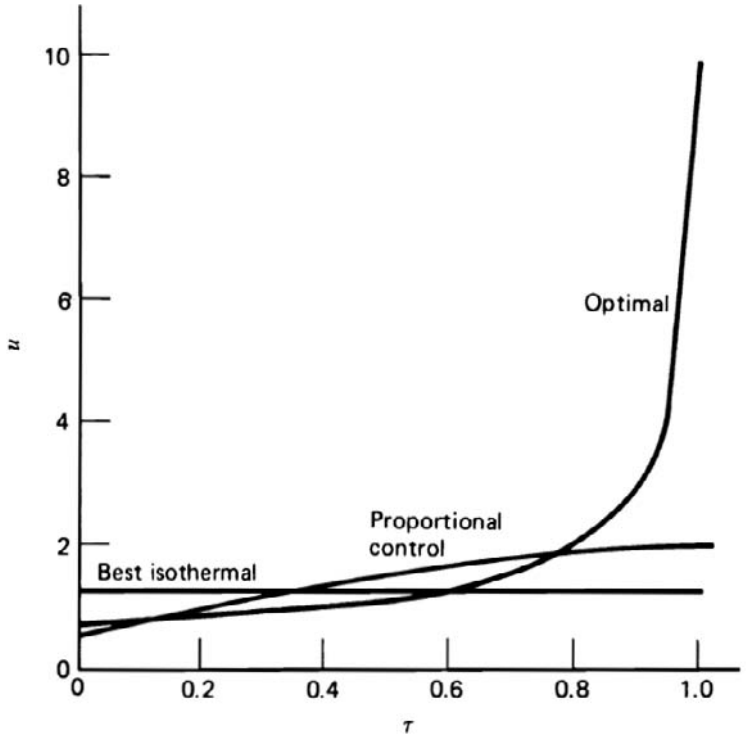

Figure 8.4.2.B-2

Temperature histories for parallel reaction: $\alpha = 2$, $\beta = \frac{1}{2}$. Yields: best isothermal, 0.535; best proportional, 0.559; optimal, 0.575. From Millman and Katz [1967].

$$x_A = \frac{C_{A0} - C_A}{C_{A0}} \qquad x_Q = \frac{C_Q}{C_{A0}} \qquad \tau = \frac{\theta}{\theta_f}$$

$$u = \theta_f A_1 e^{E_1/RT} \qquad \alpha = \frac{E_2}{E_1} \qquad \beta = \frac{\theta_f A_2}{(\theta_f A_1)^\alpha}$$

The rigorous optimization could be performed with several mathematical techniques — see Beveridge and Schechter [1970], and for a concise discussion of the Pontryagin maximum principle, see Ray and Szekely [1973]; also see Aris [1961] for specific chemical reactor examples.

The basic idea of a simple technique devised by Millman and Katz [1967] was to assume that the temperature trajectory to be determined could be approximated as a linear function of the desired product concentration to be maximized; specifically,

$$u(\tau) \approx c_0 + c_1 x_Q(\tau)$$

Then, the two parameters c_0 and c_1 are determined for the optimal condition $\max\{x_Q(\tau)\}$. This still requires a search technique to obtain the values of c_0 and c_1, but it was found that these computations were much simpler than the completely rigorous optimization. Actually, further terms in $dx_Q/d\tau$ and $\int x_Q d\tau$ gave better results than the linear function, and are based on standard three-mode process controller actions.

Two typical results are shown in Figs. 8.4.2.B-1 and 8.4.2.B-2, and it is seen that the best proportional (simple linear) results are close to the true optimal values. Note that this appears to be true, even though the temperature curves $u(\tau)$ have some differences between them — apparently the final yield is not particularly sensitive to all the details of the curves. ■

PROBLEMS

8.1 The esterification of butanol with acetic acid, using sulphuric acid as a catalyst, was studied in a batch reactor:

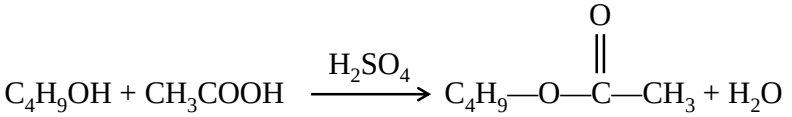

The reaction was carried out with an excess of butanol. The following data were collected [C.E. Lejes and D.F. Othmer, *I & E. C.*, 36, 968 (1945)]:

Time (h)	Acetic Acid Concentration (mol/l)
0	2.327
1	0.7749
2	0.4514
3	0.3151
4	0.2605

Set up a suitable kinetic model of the homogeneous type.

8.2 The following data on the conversion of hydroxyvaleric acid into valeroacetone were collected:

Time (min)	0	48	76	124	204	238	289
Acid Concentration (mol/l)	19.04	17.6	16.9	15.8	14.41	13.94	13.37

Derive a suitable kinetic model by means of both the differential and integral method of kinetic analysis.

8.3 The batch saponification of ethyl acetate,

$$CH_3COOC_2H_5 + NaOH \rightleftarrows CH_3COONa + C_2H_5OH$$

was carried out in a 200-ml reactor at 26°C. The initial concentrations of both reactants were 0.051 *N*.

(a) From the following time-versus-concentration data, determine the specific rate and tabulate as a function of composition of the reacting mixture:

Time (s)	NaOH (mol/l)
30	0.0429
90	0.0340
150	0.0282
210	0.0240
270	0.0209
390	0.0164
630	0.0118
1110	0.0067

(b) Determine a suitable reaction rate model for this reaction.

8.4 A daily production of 50,000 kg (50 tons metric) of ethyl acetate is to be produced in a batch reactor from ethanol and acetic acid:

$$\underset{(A)}{C_2H_5OH} + \underset{(B)}{CH_3COOH} \rightleftarrows \underset{(R)}{CH_3COOC_2H_5} + \underset{(S)}{H_2O}$$

The reaction rate in the liquid phase is given by

$$r_A = k\left(C_A C_B - C_R C_S / K\right)$$

At 100°C,

$$k = 7.23 \times 10^{-6}\ \text{m}^3 / \text{kmol s}$$
$$K = 2.93$$

A feed of 23 percent by weight of acid, 46 percent of alcohol, and no ester is to be used, with a 35 percent conversion of acid. The density is essentially constant at 1020 kg/m^3. The reactor will be operated 24h per day, and the time for filling, emptying, and the like, is 1 h total for reactors in the contemplated size range. What reactor volume is required?

8.5 A gas-phase decomposition $A \rightarrow R + S$ is carried out with initial conditions of T_0 = 300 K, p_t = 5 bar, and V_0 = 0.5 m^3. The heat of reaction is –6280 kJ/kmol, and the heat capacity of *A*, *R* and *S* are 125.6, 104.7, and 83.7 kJ/kmol K, respectively. The rate coefficient is

$$k = 10^{14} \exp\left(-\frac{10{,}000}{T}\right) \qquad \text{h}^{-1}$$

(a) Compute the conversion-time profile for isothermal conditions. Also, determine the heat exchange rates required to maintain isothermal conditions.

(b) Compute the conversion-time profile for adiabatic conditions.

8.6 A desired product *P* is made according to the following reactions scheme:

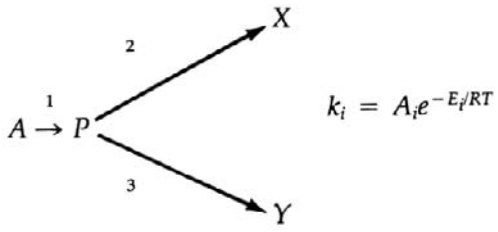

Discuss qualititatively the optimum temperature profile for the two cases:
(a) $E_2 > E_3 > E_1$; **(b)** $E_2 > E_1 > E_3$. Describe your reasoning *carefully*.

8.7 One method of decreasing the large initial heat release in a batch reaction is to utilize "semibatch" operation. Here, the reactor initially contains no reactant and is filled up with the reacting liquid — thus, there is an inflow but no outflow, and the reacting volume continuously changes. The mass balances are:
Total:

$$\frac{dV}{dt} = F_0'$$

Reactant *A*:

$$\frac{d}{dt}(VC_A) = F_0'C_{A0} - kVC_A$$

(a) Show that the reactant concentration at any time is, with isothermal operation,

$$\frac{C_A}{C_{A0}} = \frac{F_0'\left(1 - e^{-kt}\right)}{k\left(V_0 + F_0't\right)}$$

where V_0 = initial volume.

(b) Derive an expression for the rate of heat release and sketch the curve.

8.8 In a batch reactor with a volume $V = 5\ \text{m}^3$, an exothermic reaction $A \rightarrow P$ is carried out in the liquid phase. The rate equation is

$$r_A = kC_a$$

with

$$k = 4 \times 10^6 \exp\left(-\frac{7900}{T}\right) \qquad \text{s}^{-1}$$

The initial temperature T_0 of the reaction mixture is 20°C and the maximum allowable reaction temperature is 95°C. The reactor contains a heat exchanger with area $A_k = 3.3\ \text{m}^2$, and it can be operated with steam (T_r = 120°C, U = 1360 W/m^3°C) or with cooling water (T_r = 15°C, U = 1180 W/m^2°C). The times required for filling and emptying the reactor are 10 and 15 min, respectively. Other physicochemical data are:

$\Delta H = -1670$ kJ / kg;
$\rho c_p = 4.2 \times 10^6$ J / m^3 °C;
$M_A = 100$ kg / kmol;
$C_{A0} = 1$ kmol / m^3.

The desired conversion is $x_{Af} \geq 0.9$, and the batch reaction and complete reaction cycle times along the steam and water consumption rates are to be determined for the following policies of operation:

(a) Preheat to 55°C, let the reaction proceed adiabatically, start cooling when either $T = 95$°C or $x_A = 0.9$ occurs, and cool down to 45°C.

(b) Heat to 95°C, let the reaction proceed isothermally until $x_A = 0.9$ occurs, cool down to 45°C. [See H. Kramers and K.R. Westerterp, *Elements of Chemical Reactor Design and Operation*, Academic Press, New York (1963).]

8.9 The reversible reaction

$$A \underset{2}{\overset{1}{\rightleftarrows}} R$$

has the following rate parameters:

$A_1 = 7$ s^{-1} $\quad E_1 = 41{,}868$ kJ / kmol;
$A_2 = 5000$ s^{-1} $\quad E_2 = 83{,}736$ kJ / kmol.

The reaction is to be carried out in a batch reactor with a maximum allowable temperature of $T_{max} = 800$ K. For a conversion of $x_{Af} = 0.8$, determine the optimum isothermal operating temperature, and the resulting batch holding time. Also determine the heat exchange rate required.

If an optimum temperature profile is to be utilized, determine this as a function of conversion and a function of processing time. Determine the heat exchange rates required.

Additional data:

Density of liquid = 100 kg/m^3;
Heat capacity = 4.187 kJ/kg °C;
Initial mole fraction of reactant $A = 0.5$;
Molecular weights = 100 for A
= 20 for solvent.

8.10 In Example 8.4.2.B, the dimensionless equations for a parallel reaction were derived:

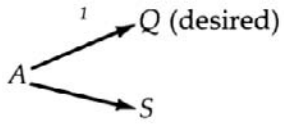

The initial conditions are $x_A = x_Q = 0$ at $\tau = 0$.

(a) Derive an expression for the optimal temperature for $max_u \{x_Q(\tau = 1)\}$.

(b) For the parameters $\alpha = 2$, $\beta = 1/2$, what is u_{opt}? If $E_1 = 83736$ kJ / kmol, what is T_{opt}?

8.11 An endothermic third-order reaction $3A \rightarrow 2B + C$ is carried out in a batch reactor. The reaction mixture is heated to 400°C. The reaction then proceeds adiabatically. During the heating period, 10 mol-% of A is converted. From this instant on, what is the time required to reach a conversion of 70 percent?

$(-\Delta H) = -104670$ kJ / kmol;
$V = 1$ m^3 = constant;
$c_{pm} = 2.47$ kJ / kg K;
$m_t = 950$ kg;
$N_{A0} = 10.2$ kmol;

$$\ln k = -\frac{10000}{RT} + 5 \quad [k \text{ in } (\text{m}^3 / \text{kmol } A)^2 / \text{s}].$$

REFERENCES

Aris, R., *The Optimal Design of Chemical Reactors*, Academic Press, New York (1961).
Aris, R., *Introduction to the Analysis of Chemical Reactors*, Prentice-Hall, Englewood Cliffs, N.J. (1965).
Aris, R., *Elementary Chemical Reactor Analysis*, Prentice-Hall, Inc., Englewood Cliffs, N.J. (1969).
Beveridge, G.S.G., and Schechter, R.S., *Optimization Theory and Practice*, McGraw-Hill, New York (1970).
Butté A., Storti G., and Morbidelli, M., *Chem. Eng. Sci.*, 54, 3225 (1999).
Chapman, F.S., Dallenbach, H., and Holland, F.A., *Trans. Inst. Chem. Eng.*, 42, T398 (1964).
Chilton, T.H., Drew, T.B., and Jebens, R.H., *Ind. Eng. Chem.*, 36, 510 (1944).
Cooper, A.R., and Jeffreys, G.V., *Chemical Kinetics and Reactor Design*, Prentice-Hall, Englewood Cliffs, N.J. (1971).
Denbigh, K.G., and Turner, J.C.R., *Chemical Reactor Theory*, 2nd ed., Cambridge University Press, London (1971).
Fournier, C.D., and Groves, F.R., *Chem. Eng.*, 77, No. 3, 121 (1970a).
Fournier, C.D., and Groves, F.R., *Chem. Eng.*, 77, No. 13, 157 (1970b).
Gates, L.E., Henley, T.L., and Fenic, J.G., *Chem. Eng.*, 110, No. 26, 110 (1975).
Grummitt, O., and Fleming, F., *Ind. Eng. Chem.*, 37, 4851 (1945).

Holland, F.A., and Chapman, F.S., *Liquid Mixing and Processing in Stirred Tanks*, Reinhold, New York (1966).
Hui, A.W., and Hamielec, A.E., *J. Appl. Pol. Sci.*, 16, 749 (1972).
Matyaszewski K., Patten, T.E., and Xia, J., *J. Am. Chem. Soc.*, 119, 674 (1997).
Millman, M.C., and Katz, S., *Ind. Eng. Chem. Proc. Des. Dev.*, 6, 447 (1967).
Peterson, T.I., *Chem. Eng. Sci.*, 17, 203 (1962).
Ray, W.H., and Szekely, J., *Process Optimization*, Wiley, New York (1973).
Reuss, M., Fröhlich, S., Kramer, B., Messerschmidt, K., and Pommerening, G., *Bioprocess Engineering*, 1, 79 (1986).
Reuss, M., Fröhlich, S., Kramer, B., Messerschmidt, K., and Pommerening, G., *Bioproc. Eng.*, 1, 79 (1986).
Smith, J.M., *Chemical Engineering Kinetics*, McGraw-Hill, New York (1970).
Strek, F., *Int. Chem. Eng.*, 3, 533 (1963).

Chapter 9

The Plug Flow Reactor

9.1 THE CONTINUITY, ENERGY, AND MOMENTUM EQUATIONS

Plug flow is a simplified and idealized picture of the motion of a fluid, whereby all the fluid elements move with a uniform velocity along parallel streamlines. This perfectly ordered flow is the only transport mechanism accounted for in the plug flow reactor model. Because of the uniformity of conditions in a cross section, the steady-state continuity equation is a very simple ordinary differential equation. Indeed, the mass balance over a differential volume element for a reactant *A* involved in a single reaction may be written

$$F_A - (F_A + dF_A) = r_A dV$$

By definition of the conversion,

$$F_A = F_{A0}(1 - x_A)$$

so that the continuity equation for *A* becomes

$$\frac{dx_A}{d\left(\frac{V}{F_{A0}}\right)} = r_A \tag{9.1-1}$$

or, in its integrated form,

$$\frac{V}{F_{A0}} = \int_{x_{A0}}^{x_A} \frac{dx_A}{r_A} \tag{9.1-2}$$

Equations (9.1-1) and (9.1-2) are, of course, easily derived also from (7.2.2-2) and (7.2.2-4) given in Chapter 7. For a single reaction and taking the reactant *A* as a reference component, $\alpha_A = -1$, so that $R_A = -r_A$. Equation (7.2.2-4) then directly yields (9.1-2).

When the volume of the reactor, *V*, and the molar flow rate of *A* at the inlet are given, (9.1-1) permits one to calculate the rate of reaction r_A at conversion x_A. For a set of values (r_A, x_A), a rate equation may then be worked out. This outlines how (9.1-1) or (9.1-2) may be used for a kinetic analysis, and will be discussed in more detail below.

When the rate of reaction is given and the feed component *A*, fed at a molar rate F_{A0} is to be converted to a value of, say, x_A, (9.1-2) permits the required reactor volume *V* to be determined. This is one of the design problems that can be solved by means of (9.1-2). Both aspects — kinetic analysis and design calculations — are illustrated further in this chapter. Note that (9.1-2) does not contain the residence time explicitly, in contrast with the corresponding equation for the batch reactor. The ratio V/F_{A0}, as expressed here in h m^3/kmol *A* — and called space time — is a true measure of the residence time only when there is no expansion or contraction due to a change in number of moles or other conditions. Using residence time as a variable offers no advantage since it is not directly measurable—in contrast with V/F_{A0}.

If there is expansion or contraction, the residence time θ has to be considered first over a differential volume element and is given by

$$d\theta = \frac{dV}{F_A / C_A} \tag{9.1-3}$$

where F_A is the (average) molar flow rate of *A* in that element. For constant temperature and pressure, C_A may be written, as explained already in (8.1-8) as

$$C_A = \frac{N_A}{V} = \frac{N_{A0}(1 - x_A)}{V_0(1 + \varepsilon_A x_A)} = C_{A0}\frac{1 - x_A}{1 + \varepsilon_A x_A}$$

where ε_A is the expansion factor, $\varepsilon_A = y_{A0}[(r+s+\cdots)-(a+b+\cdots)/a]$. Equation (9.1-3) becomes, after formal integration,

$$\theta = \int_0^V \frac{dV}{(F_{A0}/C_{A0})(1+\varepsilon_A x_A)} \tag{9.1-4}$$

What remains to be done before the integration is performed is to relate x_A and V. This is done by means of (9.1-1) so that finally

$$\theta = C_{A0} \int_{x_{A0}}^{x_A} \frac{dx_A}{(1+\varepsilon_A x_A) r_A} \tag{9.1-5}$$

Equation (9.1-5) shows that the calculation of θ requires the knowledge of the function $r_A = f(x_A)$. But, establishing such a relation is precisely the objective of a kinetic investigation. The use of θ is a superfluous intermediate step, since the test of a rate equation may be based directly on (9.1-2). Note also that when there is no change in number of moles due to the reaction — and only then — is there complete correspondence between (9.1-5) and the batch reactor equation, (8.1-5).

Thus, it is seen that the most direct measure of the reactor's capability for achieving the conversion is the space time V/F_{A0}, which is the result of a rigorous mass balance in the steady-state plug flow system. In industrial practice, the reciprocal is commonly used and termed "space velocity". Specifically, using

$$\frac{F_{A0}}{V} = \left(\frac{F_0'}{V}\right) C_{A0}$$

the group F_0'/V, with units volume of feed (measured at some reference conditions) per unit time per unit volume of reactor, is the space velocity. One must be careful concerning the choice of the reference conditions, since several customs are in use—see Hougen and Watson [1947]. For example, if a liquid feed is metered and then vaporized before entry into the reactor, it is common to use the liquid volumetric rate rather than the actual gas rate at reactor conditions, which is implied in F_0' corresponding to C_{A0}. Use of the molar flow rate F_{A0} obviates these difficulties, and it is the choice in this book. However, the space velocity customs need to be known to properly interpret existing literature data.

Take a first-order rate equation $r_A = kC_A$ or $kC_{A0}(1-x_A)$. Substitution of the latter expression in (9.1-2) leads to

$$k\frac{V}{F_{A0}/C_{A0}} = \ln\frac{1}{1-x_A}$$

or, in terms of the concentration of *A*,

$$k\frac{V}{F_{A0}/C_{A0}} = \ln\frac{C_{A0}}{C_A}$$

For constant temperature, pressure and total number of moles, $V/(F_{A0}/C_{A0})$ is nothing but the residence time so that these results are identical to the integrated forms given for a first-order reaction in Table 1.2.4.2-1, Chapter 1. All the other reactions considered in that table and those of more complex nature dealt with in the rest of that chapter will lead to the same integrated equations as those given here, provided θ is replaced by $V/(F_{A0}/C_{A0})$. This will not be so when these reactions are carried out in the flow reactor with complete mixing, as will be shown in Chapter 10.

Equation (9.1-1) or (9.1-2) can serve as the basic equation for the analysis or design of isothermal empty tubular reactors or of packed catalytic reactors of the tubular type. The applicability of these equations is limited only by the question of how well the concept "plug flow" is approximated in the real case. For empty tubular reactors, this is generally so with turbulent flow conditions and sufficiently high length/diameter ratio so that entrance effects can be neglected, such as in tubular reactors for thermal cracking. Deviations from the ideal, conceptual plug flow pattern are discussed in detail in Chapter 12.

For fixed bed catalytic reactors, the idealized flow pattern is generally well approximated when the packing diameter d_p is small enough with respect to the tube diameter d_t to have an essentially uniform void fraction over the cross section of the tube, at least up to the immediate vicinity of the wall. According to a rule of thumb, the ratio d_t / d_p should be at least 10. This may cause some problems when investigating a catalyst in small-size laboratory equipment. The application of the plug flow model to the design of fixed bed catalytic reactors is dealt with extensively in Chapter 11. For this reason the examples of this chapter deal exclusively with empty tubular reactors.

Tubular reactors do not necessarily operate under isothermal conditions in industry, for reasons of chemical equilibrium, of selectivity, or of profit optimization, or simply because it is not economically or technically feasible. It then becomes necessary to consider also the energy equation, that is, a heat balance on a differential volume element of the reactor. For reasons of analogy with the derivation of (9.1-1), it is assumed that convection is the only mechanism of heat transfer. Moreover, this convection is considered to occur by

plug flow and the temperature is completely uniform in a cross section. If heat is exchanged through the wall, the entire temperature difference with the wall is located in a very thin film close to the wall. The energy equation then becomes, in the steady state,

$$\sum_j \frac{\dot{m}_j}{\Omega} c_{pj} \frac{dT}{dz} + U \frac{\pi d_t}{\Omega}(T - T_r) - r_A(-\Delta H) = 0 \qquad (9.1\text{-}6)$$

where

$\dot{m}_j$ = mass flow rate of the component j (kg/h)
c_{pj} = specific heat of j (kJ/kg °C)
T, T_r = temperature of the fluid, respectively the surroundings (°C)
U = overall heat transfer coefficient (kJ/m^2 h K), based on the inside diameter of the tube. The formula for U and a correlation for the inside heat transfer coefficient have been given already in Chapter 8.
z = length coordinate of the reactor (m$_r$)
Ω = cross section of tube (m$_r^2$)

Note that (9.1-6) is nothing but (7.2.4-4) of Chapter 7, obtained by simplifying the "general" energy equation (7.2.3-1), provided that d_r, the reactor diameter, is replaced by d_t, the tube diameter. Using the general equations of Chapter 7 as a starting point clearly shows the assumptions used in the derivation of a specific form of the balance.

Equations (9.1-1) and (9.1-6) are coupled through the rate of reaction. The integration of this system of ordinary differential equations generally requires numerical techniques. Note that the group $\sum_j \dot{m}_j c_{pj}$ has to be adjusted for each increment. It is often justified to use a value of c_p averaged over the variations of temperature and compositions so that $\sum_j \dot{m}_j c_{pj}$ may be replaced by $\dot{m}\, c_p$, where $\dot{m}$ is the total mass flow rate; $(-\Delta H)$ is frequently also averaged over the temperature interval in the reactor.

Introducing (9.1-1) into (9.1-6) leads to

$$\frac{dT}{dz} = \frac{F_{A0}(-\Delta H)}{\sum_j \dot{m}_j c_{pj}} \frac{dx_A}{dz} - \frac{U\pi d_t}{\sum_j \dot{m}_j c_{pj}}(T - T_r) \qquad (9.1\text{-}7)$$

It follows that for an adiabatic reactor, for which the second term on the right-hand side is zero, there is a direct relation between Δx and ΔT.

Equations (9.1-1) and (9.1-6) or (9.1-7) are applicable to both empty tubular reactors or fixed bed tubular reactors, provided the assumptions involved

TABLE 9.1-1
VALUE OF α, CONVERSION FACTOR IN
THE FANNING PRESSURE DROP EQUATION

p_t	α	
	u (m/s)	u (m/h)
N/m^2 or Pa	1	7.72×10^{-8}
bar	10^{-5}	7.72×10^{-13}
atm	9.87×10^{-6}	7.62×10^{-13}
kgf/m^2	$\frac{1}{g_c} = \frac{1}{9.81} = 0.102$	7.87×10^{-9}

in the derivation are fulfilled. Again, the application to the latter case is discussed in detail in Chapter 11.

Sometimes the pressure drop in the reactor is sufficiently large to be accounted for, instead of using an average value. For an empty tube the Fanning equation may be used in the usual Bernoulli equation:

$$-\frac{dp_t}{dz} = 2f\alpha\frac{\rho_g u^2}{d_t} + \alpha\rho_g u\frac{du}{dz} \tag{9.1-8}$$

(assuming no significant effects of elevation changes). The value of the conversion factor α depends on the dimensions of the total pressure p_t and the flow velocity u. Some values are listed in Table 9.1-1. The Fanning friction factor f equals 16/Re for laminar flow in empty tubes. An expression that is satisfactory for Reynolds numbers between 5000 and 200,000 (i.e., for turbulent flow) is

$$f = 0.046\,\mathrm{Re}^{-0.2}$$

When the density of the reaction mixture varies with the conversion, ρ_g in equation (9.1-8) has to also account for this. This is illustrated in the example on the thermal cracking of ethane later in this chapter. Pressure drop equations for packed beds are discussed in Chapter 11.

9.2 KINETIC STUDIES USING A TUBULAR REACTOR WITH PLUG FLOW

9.2.1 Kinetic Analysis of Isothermal Data

The thermal cracking of propane was studied at atmospheric pressure and 800°C in a tubular reactor with plug flow and operated in the integral mode. The

TABLE 9.2.1-1
THERMAL CRACKING OF PROPANE.
CONVERSION VERSUS SPACE TIME DATA

V/F_{A0} (m^3 s/kmol)	$x_A = \frac{F_{A0} - F_A}{F_{A0}}$
32	0.488
50	0.630
59	0.685
64	0.714
75	0.760
82	0.782

experimental results are given in Table 9.2.1-1 [Buekens and Froment, 1968, 1971a, 1971b].

The global reaction, propane $\rightarrow$ products is considered to be irreversible. When first order is assumed, the rate equation may be written

$$r_A = kC_A$$

The kinetic analysis starts from either (9.1-1) or (9.1-2).

This reaction is carried out in the presence of a diluent, steam. The diluent ratio is κ (moles diluent/moles hydrocarbon). Furthermore, 1 mole of propane leads to 2 moles of products; in other words, the molar expansion $\delta_A = 1$. The relation between the propane concentration and the conversion has to account for the dilution and expansion and is obtained as follows. For a feed of F_{A0} moles propane per second, the flow rates in the reactor at a certain distance where a conversion x_A has been reached may be written

propane:	$F_{A0}(1 - x_A)$	(kmol/s)
products:	$F_{A0}(1 + \delta_A)x_A$	
diluents:	$F_{A0}\ \kappa$	
Total:	$F_{A0}[1 - x_A + (1 + \delta_A)x_A + \kappa]$	

so that, for the feed rate F_{A0},

$$F_t = F_{A0}(1 + \delta_A x_A + \kappa)$$

The mole fraction of propane consequently equals $(1 - x_A)/(1 + \delta_A x_A + \kappa)$ and the concentration $[(1 - x_A)/(1 + \delta_A x_A + \kappa)]C_t$. The diluent ratio κ is often used

in industrial practice, although exactly the same end results are found with the use of

$$\varepsilon_A = y_{A0}\delta_A = \frac{1}{1+\kappa}\delta_A$$

The rate equation that has to be introduced into (9.1-1) or (9.1-2) now becomes

$$r_A = k\frac{1-x_A}{1+\delta_A x_A+\kappa}C_t$$

Integral Method of Kinetic Analysis

Substituting the rate equation in (9.1-2) leads to

$$\frac{V}{F_{A0}} = \frac{1}{kC_t}\int_0^{x_A}\frac{1+\delta_A x_A+\kappa}{1-x_A}dx_A$$

from which, with $\delta_A = 1$,

$$k = -\frac{F_{A0}}{C_t V}[(2+\kappa)\ln(1-x_A)+x_A]$$

k can be calculated for a set of experimental conditions, remembering that $C_t = p_t/RT$. For $V/F_{A0} = 32$ and $x_A = 0.488$, a value of 4.14 s^{-1} is obtained for k. When k takes on the same value for all the sets of x_A versus V/F_{A0} data, the assumption of first order is correct. It can be seen from Table 9.2.1-2 that this condition is indeed fulfilled.

Differential Method of Kinetic Analysis

From (9.1-1) it follows that the slope of the tangent of the curve x_A versus V/F_{A0} is the rate of reaction of A at the conversion x_A. The rates are shown in Table 9.2.1-2. The k are calculated by both the integral and the differential method of kinetic analysis.

If the order of reaction were n, the rate equation would have to be written

$$r_A = kC_A^n$$

which becomes, after taking the logarithm,

$$\log r_A = \log k + n\log C_t + n\log\left(\frac{1-x_A}{1+\delta_A x_A+\kappa}\right)$$

TABLE 9.2.1-2
THERMAL CRACKING OF PROPANE. RATE VERSUS CONVERSION

		k (s^{-1})	
	r_A	Integral	Differential
x_A	($kmol/m^3$ s)		
0.488	0.00978	4.14	4.15
0.630	0.00663	4.11	4.11
0.685	0.00543	4.11	4.04
0.714	0.00492	4.15	4.08
0.760	0.00409	4.09	4.11
0.782	0.00354	4.03	3.94

A straight line is obtained in a log r_A versus $\log[(1-x_A)/(1+\delta_A x_A+\kappa)]$ plot. The slope is the order, while the intercept on the ordinate yields k.

If an order of 1 is assumed, the formula permits checking the constancy of k. For x_A = 0.488 and r_A = 0.00978 kmol/m^3 s, a k value of 4.15 s^{-1} is obtained; for x_A = 0.714 and r_A = 0.00492 kmol/m^3 s, a value 4.08 s^{-1} is obtained. The assumption of first order is verified.

9.2.2 Kinetic Analysis of Nonisothermal Data

The above example deals with a simple isothermal situation. In Chapters 1 and 2 it was suggested to operate reactors for kinetic studies, whenever possible, in an isothermal way. There are cases, however, in which isothermal operation is impossible, in spite of all precautions. The thermal cracking of hydrocarbons, a homogeneous reaction, is an example. In such a case it is inevitable that part of the reactor is used to bring the feed to the desired temperature. In contrast with catalytic reactors, there is no clear-cut separation between preheat and reaction section in this case. If the rate is to be determined at a reference temperature, say, T_1, and if the reaction volume is counted from the point where T_1 is reached, then the conversion in the preheat section, that cannot be avoided, is not accounted for. Similarly, at the outlet there is a section where the conversion continues to some extent while the reaction mixture is being cooled.

Such a situation can be dealt with in two ways. The first way is to analyze the data as such. The temperature dependence of the rate parameters is then directly included into the continuity equation, and the resulting equation is numerically integrated along the tube with estimates for the parameters. If the gas temperature profile itself is not available or insufficiently defined, the energy

equation has to be coupled to the continuity equation. To determine both the form of the rate equation and the temperature dependence of the parameters directly from nonisothermal data would require excessive computations.

Successful attempts of the derivation of rate parameters from the direct treatment of nonisothermal data, given the form of the rate equation, have been reported from the sixties onwards [Emig, Hofmann, and Friedrich, 1972; Lambrecht, Nussey and Froment, 1972; and Van Damme, Narayanan, and Froment, 1965]. The work of Van Damme et al. [1965] on the kinetic analysis of the cracking of propane is taken here as an example. In this work the gas temperature rose from 600°C at the inlet of the cracking section to 850°C at the exit, to simulate industrial operation. Since the gas temperature profile was given, the Arrhenius temperature dependence was directly accounted for in the continuity equation for propane, but no energy equation had to be coupled to it. The pressure profile was also directly accounted for. The resulting continuity equation was numerically integrated assuming a power law rate equation and with estimated values for the order *n*, with respect to propane, for the frequency factor A_0 and for the activation energy E. The calculated exit propane conversions were compared with the experimental. The sum of squares of deviations between calculated and experimental propane conversions was used as an objective function; the latter was minimized by nonlinear regression using Marquardt's routine.

The strong correlation between A_0 and E necessitated a reparameterization. Setting

$$A_0^{'} = A_0 \exp(-\frac{E}{R\overline{T}})$$

where $\overline{T}$ represents the average of all the measured temperatures, the continuity equation for propane,

$$F_{A0}dx = k\left(\frac{1-x}{1+\kappa+\delta x}\right)^n\left(\frac{p_t}{RT}\right)^n dV$$

became

$$F_{A0}dx = A_0^{'}\exp\left(\frac{E}{R\overline{T}}-\frac{E}{RT}\right)\left[\frac{1-x}{1+\kappa+\delta x}\right]^n\left(\frac{p_t}{RT}\right)^n dV$$

For 1.4 atm abs. (1.37 bar) and a steam dilution of 0.4 kg steam/kg propane, Van Damme et al. [1965] obtained n = 1.005, E = 214,226 kJ/kmol, and $A_0 = 1.7 \times 10^{11}$ as compared with n = 1, E = 213,500 kJ/kmol and $A_0 = 1.08 \times 10^{11}$ by a pseudoisothermal analysis using the equivalent reactor volume concept to be described next.

The equivalent reactor volume concept, introduced by Hougen and Watson [1947], allows for a second way of dealing with nonisothermal data. It first reduces the data to isothermality and determines the temperature dependence of the rate parameters in the second stage only. The equivalent reactor volume has been defined as that volume V_R which, at the reference temperature T_1 and the reference total pressure p_{t1}, would give the same conversion as the actual reactor, with its temperature and pressure profiles. It follows that

$$r_{T_1, p_{t1}} dV_R = r_{T, p_t} dV$$

so that, for a reaction with order n,

$$V_R = \int_0^V \left(\frac{p_t T_1}{p_{t1} T} \right)^n \exp\left[\frac{E}{R} \left(\frac{1}{T_1} - \frac{1}{T} \right) \right] dV$$

Once V_R has been derived, the calculation of the rate is straightforward, as for isothermal experiments, and is based solely on the continuity equation. Calculating V_R requires the knowledge of the temperature and pressure profiles along the tube and of the activation energy E. Note also that where several reactions are occurring simultaneously, the dependence of V_R on E leads to different V_R for each of the reactions considered.

In a kinetic study the activation energy is generally not known a priori, or only with insufficient accuracy. The use of the equivalent reactor volume concept therefore leads to a trial-and-error procedure: a value of E is guessed and with this value and the measured temperature profile V_R is calculated by numerical integration. Then, for the rate model chosen, the kinetic constant is derived. This procedure is carried out at several temperature levels and from the temperature dependence of the rate coefficient, expressed by Arrhenius' formula, a value of E is obtained. If this value does not agree with that used in the calculation of V_R, the whole procedure has to be repeated with a better approximation for E.

Froment et al. [1961a, b] proposed a short-cut method for the first estimate of E, which turned out to be extremely efficient. Consider two experiments carried out in an isobaric flow reactor, one at reference temperature T_1, the other at the reference temperature T_2, and let the conditions be such that the temperature difference $\Delta T = T_1 - T_2$ is the same over the whole length of the reactor. The reaction is homogeneous and of the type $A \rightarrow B$. If the feed rates are adjusted so that equal conversions are obtained, then the conversion x or the p_A-versus-V profiles are identical in both cases. Then, in all points,

$$\frac{dx_1}{dV} = \frac{dx_2}{dV}$$

$$(p_A)_1 = (p_A)_2$$

while ΔT is independent on V.

From the continuity equation

$$F_{A0}dx = A_0 \exp\left(-\frac{E}{RT}\right)(p_A)^n dV$$

applied to both experiments, it follows that

$$\frac{(F_{A0})_1}{(F_{A0})_2} = \exp\left[-\frac{E}{R}\left(\frac{1}{T_1} - \frac{1}{T_2}\right)\right] = \exp\left(\frac{E}{R}\frac{\Delta T}{T_1 T_2}\right)$$

from which

$$E = 2.3R\frac{T_1 T_2}{\Delta T}\log\frac{(F_{A0})_1}{(F_{A0})_2}$$

This means that the activation energies may be obtained from two experiments at different temperatures, without even knowing the rate constants, provided the conversions are the same and the temperature profiles, plotted versus V, are parallel.

The latter condition is not always fulfilled in practice. It requires that the heat effect of the reaction is negligible or entirely compensated for by the heat flux from or to the surroundings or (and) that the specific heat of the gases is very large. If the reactant A is consumed by more than one reaction, then, at equal conversion to the product of interest B, the partial pressure p_A is only equal in both experiments when the activation energies of the parallel reactions are equal. If not, the approximation is better the more the principal reaction prevails over the side reaction(s). Froment et al. [1961b] applied the V_R concept and the short-cut method for estimation of E to their data on the thermal cracking of acetone. It was also successfully applied by Buekens and Froment to the thermal cracking of propane and isobutane [1971a, b] and by Van Damme et al. [1965] to the thermal cracking of propane and propane-propylene mixtures.

9.3 DESIGN AND SIMULATION OF TUBULAR REACTORS WITH PLUG FLOW

It is clear from the preceding that the kinetic analysis of a process based upon nonisothermal data may be a demanding problem from the computational point of view. The reverse problem — designing or simulating a reactor when the

kinetics are known — is generally much more straightforward. Two examples of design equations of a nonisothermal tubular reactor with plug flow are given. The first case deals with a very simple situation allowing (semi) analytical integration. The second case deals with a reactor for the thermal cracking of hydrocarbons.

9.3.1 Adiabatic Reactor with Plug Flow

For simple irreversible reactions, a (semi) analytical solution of the continuity and energy equations is possible. Douglas and Eagleton [1962] published solutions for zero-, first-, and second-order reactions, both with a constant and varying number of moles. For a first-order reaction with constant density, the integration proceeds as follows:

Continuity equation for *A*:

$$F_{A0}\,dx = r_A\,dV \tag{9.3.1-1}$$

with $r_A = kp_{A0}(1-x)$, (9.3.1-1) may be written

$$dx = kp_{A0}(1-x)\frac{dV}{F_{A0}}$$

Energy equation:

$$F_{A0}\,dx(-\Delta H) = \dot{m}c_p\,dT \tag{9.3.1-2}$$

or

$$dx = \frac{\dot{m}c_p}{F_{A0}(-\Delta H)}\,dT$$

and, after integration:

$$x - x_0 = \frac{\dot{m}c_p}{F_{A0}(-\Delta H)}(T - T_0)$$

or

$$x = x_0 + \lambda(T - T_0) \tag{9.3.1-3}$$

where

$$\lambda = \frac{\dot{m}c_p}{F_{A0}(-\Delta H)}$$

Note the simple relation between the conversion and the temperature variation in adiabatic situations: the temperature variation is a measure of conversion, and vice versa.

Formal integration of (9.3.1-1) leads to

$$\frac{V}{F_{A0}} = \int_{x_0}^{x} \frac{dx}{kp_{A0}(1-x)}$$

After substituting *dx* by its expression based on (9.3.1-3) and of *k* by its Arrhenius epression, the following equation is obtained:

$$\frac{V}{F_{A0}} = \frac{1}{A_0}\int_{T_0}^{T} \frac{e^{E/RT}}{p_{A0}} \frac{\lambda dT}{\{1-[x_0+\lambda(T-T_0)]\}}$$

$$= \frac{\lambda}{A_0 p_{A0}} \int_{T_0}^{T} \frac{e^{E/RT}dT}{(1-x_0+\lambda T_0)-\tau T}$$

$$= \frac{\lambda}{A_0 p_{A0}} \int_{T_0}^{T} \frac{e^{E/RT}dT}{\lambda T\left[\frac{1-x_0+\lambda T_0}{\lambda T}-1\right]} \qquad (9.3.1\text{-}4)$$

Let

$$u = \frac{E}{RT}$$

Then,

$$T = \frac{E}{Ru} \qquad \text{and} \qquad dT = -\frac{E\,du}{Ru^2}$$

Equation (9.3.1-4) then becomes

$$\frac{V}{F_{A0}} = -\frac{1}{A_0 p_{A0}} \int_{E/RT_0}^{E/RT} \frac{e^u du}{u\left[\frac{R}{\lambda E}(1-x_0+\lambda T_0)u-1\right]}$$

$$= \frac{1}{A_0 p_{A0}} \int_{E/RT_0}^{E/RT} \frac{e^u du}{u} - \frac{1}{A_0 p_{A0}} \int_{E/RT_0}^{E/RT} \frac{e^u du}{u - \frac{\lambda E}{R(1-x_0+\lambda T_0)}}$$

Let

$$Z = u - \frac{E}{R(1-x_0+\lambda T_0)} \equiv u-\alpha, \quad dZ = du$$

$$Z_0 = \frac{E}{RT_0} - \frac{E}{R(1-x_0-\lambda T_0)}$$

Then,

$$\frac{V}{F_{A0}} = \frac{1}{A_0 p_{A0}} \int_{E/RT_0}^{E/RT} \frac{e^u du}{u} - \frac{e^\alpha}{A_0 p_{A0}} \int_{Z_0}^{Z} \frac{e^Z dZ}{Z}$$

$$\frac{V}{F_{A0}} = \frac{1}{A_0 p_{A0}} \left[Ei\left(\frac{E}{RT}\right) - Ei\left(\frac{E}{RT_0}\right) \right] - \frac{e^\alpha}{A_0 p_{A0}} \left[Ei(Z) - Ei(Z_0) \right] \quad (9.3.1\text{-}5)$$

For given feed conditions, (9.3.1-5) permits the calculation of V/F_{A0}, which limits the outlet temperature and therefore the outlet conversion to a set value. Obviously for a given V/F_{A0}, one can calculate the corresponding outlet conditions, but the expression is implicit with respect to T.

For more complicated rate equations, semianalytical integration is no longer possible.

9.3.2 Design and Simulation of Non-Isothermal Cracking Tubes for Olefins Production

The production of ethylene and propylene, the basic feedstocks of the petrochemical industry, by means of thermal cracking of hydrocarbons like ethane, propane or complex mixtures like naphtha, is one of the most important industrial operations of the chemical industry. Modern plants have a production capacity of 1 million tons of ethylene per year. The cracking is carried out in long coils, vertically suspended in large gas-fired furnaces. These consist of a convection section in which the hydrocarbon feed and the diluent steam are preheated up to 600–650°C by means of the flue gas exiting from the radiant or cracking section proper. In that section radiant burners are located on 2 opposing walls parallel with the tube row and long flame burners at the bottom of the furnace. Accounting for metallurgical constraints on the tube skin temperature the length of the cracking coil required to reach the desired conversion is typically of the order of 95 m for ethane cracking, 50 m for naphtha cracking. A coil consists of several straight tubes with an internal diameter of 0.1 m and a length of some 10 m and connected by bends. A typical furnace may contain 6 such coils, heated by some 200 burners. If the conversion is too low the product distribution may not meet the specifications, if it is too high the importance of reactions leading to coke formation on the tube walls is enhanced. The coke may accumulate to layers with a thickness of 0.01m causing an increased pressure drop and hampering the heat transfer to the reacting gases. It is periodically removed by controlled combustion, but that implies interrupting the cracking and a loss of production.

Simulating the furnace described above requires the following set of continuity equations for the components to be integrated, together with the energy equation and the pressure drop equation:

$$\frac{dF_j}{dz} = R_j \frac{\pi d_t^2}{4} = \left(\sum_i \alpha_{ij} r_i \right) \frac{\pi d_t^2}{4} \tag{9.3.2-1}$$

where j is the number of feed components and i the number of reactions.

$$\frac{dT}{dz} = \frac{1}{\sum_j F_j c_{pj}} \left[q(z) \pi d_t + \frac{\pi d_t^2}{4} \sum_i (-\Delta H_i) r_i \right] \tag{9.3.2-2}$$

$$-\frac{dp_t}{dz} = \alpha \left[\frac{2f}{d_t} + \frac{\zeta}{\pi r_b} \right] \rho_g u^2 + \alpha \rho_g u \frac{du}{dz} \tag{9.3.2-3}$$

with initial conditions $F_j = F_{j0}$, $T = T_0$, and $p_t = p_{t0}$ at $z = 0$. In (9.3.2-1), R_j is the total rate of change of the amount of the component j, and r_i is the rate of the ith reaction.

The pressure drop equation (9.3.2-3) accounts for friction losses in the straight part of the coil according to the Fanning equation and to the additional loss in the bends, according to Nekrasov's equation [1969]. Furthermore,

$$u = \frac{M_m F_t}{\rho_g \dfrac{\pi d_t^2}{4}} = \frac{G}{M_M} \frac{RT}{p_t} \tag{9.3.2-4}$$

$$\frac{du}{dz} = \frac{GR}{p_t} \left[T \frac{d\left(\dfrac{1}{M_m} \right)}{dz} + \frac{1}{M_m} \frac{dT}{dz} \right] - \frac{G}{M_m} \frac{RT}{p_t^2} \frac{dp_t}{dz} \tag{9.3.2-5}$$

so that (9.3.2-3) finally becomes

$$\frac{dp_t}{dz} = \frac{\dfrac{d}{dz}\left(\dfrac{1}{M_m} \right) + \dfrac{1}{M_m} \left[\dfrac{1}{T} \dfrac{dT}{dz} + \left(\dfrac{2f}{d_t} + \dfrac{\zeta}{\pi r_b} \right) \right]}{\dfrac{1}{M_m p_t} - \dfrac{p_t}{\alpha G^2 RT}} \tag{9.3.2.-6}$$

with

$$\frac{d}{dz}\left(\frac{1}{M_m}\right)=\frac{d}{dz}\left(\frac{\sum_j F_j}{G\Omega}\right)=\frac{\sum_j \frac{dF_j}{dz}}{G\Omega} \qquad (9.3.2\text{-}7)$$

The friction factor for straight tubes is taken from Knudsen and Katz [1958]:

$$f = 0.046\,\mathrm{Re}^{-0.2} \qquad \text{when} \qquad \mathrm{Re} = \frac{d_t G}{\mu}$$

The factor ζ used in the equation for the supplementary pressure drop in the bends is given by Nekrasov:

$$\zeta = \left(0.7 + \frac{\Lambda}{90°}0.35\right)\zeta'$$

where

$$\zeta' = \left(0.051 + 0.19\frac{d_t}{r_b}\right)$$

$\Lambda =$ angle described by the bend, here 180°

r_b = radius of the bend

Such a set of equations could be integrated by means of Runge-Kutta routines, were it not that with the elementary step and Single Event Kinetics approach described in Chapter 1, it becomes extremely stiff because of the orders of magnitude difference between the concentrations of molecular and radical species. The Gear routine [1971] was developed to cope with such problems.

Fig. 9.3.2-1 and Fig. 9.3.2-2 show results of the application of this plug flow reactor model to the thermal cracking of a naphtha, a complex mixture of hydrocarbons, leading to a reaction network generated by computer, as explained in Chapter 1. The feed flow rate per tube amounts to 2155 kg/h. The feed is diluted with steam (0.7 kg steam/kg naphtha) to lower the partial pressure of the hydrocarbons and suppress to a certain extent bimolecular reactions leading to higher molecular weight components and ultimately to coke formation on the Ni sites of the high-alloyed steel tubes. To achieve high production capacity, the space time in the cracking section has to be low, i.e., the residence time short — of the order of 0.45 s in the cracking section proper. Fig. 9.3.2-1 shows the profiles of conversion, gas temperature and pressure in the coil. The humps in the pressure profile result from the higher pressure drop in the bends. A conversion is chosen here to express the progress of the process. The definition of the conversion of a mixture like naphtha, containing more than 200 components in

measurable quantities and producing many thousands of intermediates, is not straightforward. Van Damme et al. [1981] used a weighted and normalized average of the conversion of 15 key components of the naphtha feed. To satisfy the definition of conversion, these components should only disappear in the process, without any formation. That excludes aromatics. By its very definition the conversion can not exceed 100 % but even when all the feed components are converted the products can further react among themselves, but in practice this is limited, to avoid a drop in the yield of ethylene. The use of the conversion requires a complete gas chromatographic analysis of the naphtha feed and the effluent, which is not common practice in industrial operation. The methane yield, defined as kg methane produced per 100 kg of naphtha fed, or the ratio of the weight yields of propylene and ethylene or of the yields of C_3- and propylene are used because of simpler on line analysis [Van Camp et al., 1985].

Fig. 9.3.2-2 shows the weight yield profiles of a number of the most important products. The ethylene yield monotonically increases in the range of operation of practical interest, but the propylene and butadiene yield exhibit a maximum.

The product distribution depends on the naphtha composition and, for a given furnace, on the operating conditions. The selection of the furnace and coil configuration and that of the operating conditions depends on a number of factors, one of which is the ratio of the ethylene to propylene yields. For a number of years a high value for this ratio, meaning “high severity” was favored. To achieve this, the heat flux from the furnace to the coil and, therefore, the tube skin temperature should be high. Fig. 9.3.2-3 illustrates the influence of residence time (and temperature profile) in the cracking section on the ethylene yield evolution with conversion for 2 dilution ratios. The gain in ethylene yield resulting from a reduction in residence time, coupled with the appropriate temperature profile, is very significant and the financial benefit substantial. The figure also illustrates how higher dilutions favor the ethylene selectivity. This is related to the complexity of the cracking reaction scheme. Simplifying in a drastic way it may be stated that the cracking reactions proper, leading to methane, ethylene and propylene are first-order reactions, whereas condensation reactions leading to aromatics and further also on the Ni-sites to coke, have a higher order and also a lower activation energy. Clearly, the partial pressure effect, which is of major importance in the coke formation and in the run length, leads to an optimization problem.

High severity operation led to the introduction of so-called split coils, i.e., a configuration 2-1, in which two tubes with smaller diameter, e.g., 0.05 m and, therefore, high surface to volume ratio, merge further in the furnace into a single tube with a diameter of 0.1 m and lower heat flux to the reacting gases. The

larger diameter of the single tube avoids overcracking and compensates for the narrowing of the tube caused by coke deposition, which is maximum in the high temperature zone towards the exit. It was experienced that optimal selectivities are tied to an optimal relation between the residence time and temperature level or profile, but there are various geometries to achieve this. This led to a reversed split coil with a totally different (1-2-4) configuration [Plehiers and Froment, 1987].

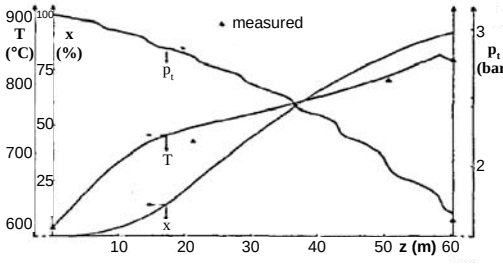

Figure 9.3.2-1

Profiles of conversion, process gas temperature and total pressure in a naphtha cracking coil. From Froment [1992].

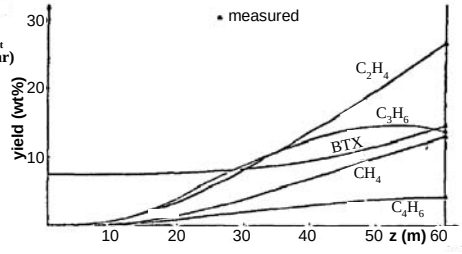

Figure 9.3.2-2

Yields of some important products of naphtha cracking as a function of reactor length. From Froment [1992].

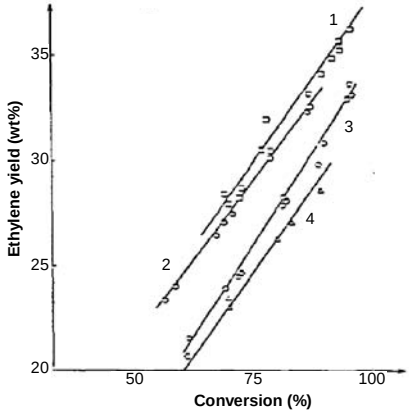

Figure 9.3.2-3

Ethylene wt % yield vs naphtha conversion [from Froment, 1992]:

θ=0.2 s 1- δ=0.7 θ=0.5 s 3- δ=0.7

2- δ=0.5 4- δ=0.5

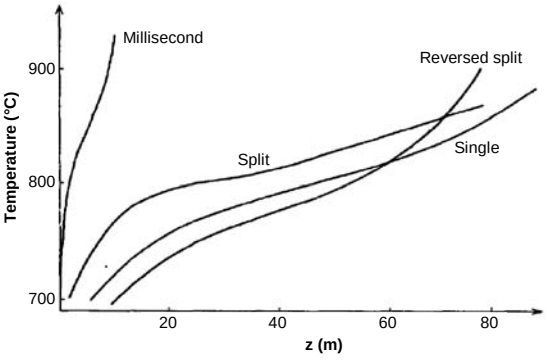

Figure 9.3.2-.4

Process gas temperature profiles in various types of reactors. From Plehiers and Froment [1987].

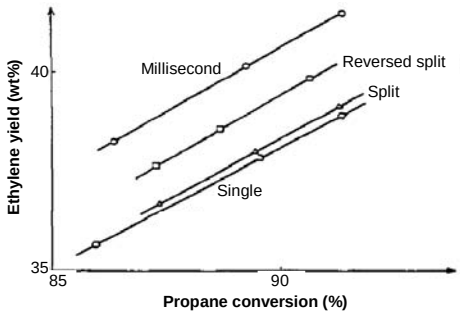

Figure 9.3.2-5

Ethylene wt % yields obtained in various types of reactors. From Plehiers and Froment [1987].

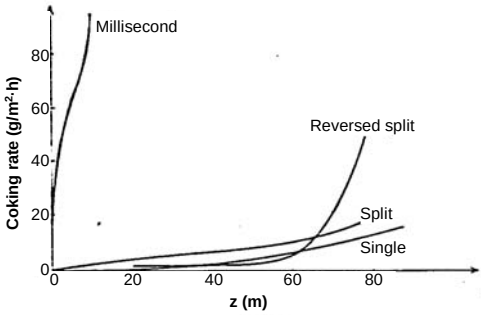

Figure 9.3.2-6

Profiles of initial coking rates in various types of reactors. From Plehiers and Froment [1987].

An extreme configuration that gained importance in the eighties is the millisecond cracker [Dluzniewski et al., 1981]. In this case the tubes are straight and have a total length of 10 to 12 m and a diameter of only 0.04 m. Reaching high conversions implies very high heat inputs, therefore high tube skin temperatures. The resulting ethylene yields are high but the negative aspect is the large number of parallel tubes and the large investment cost. The coking rates are high and the run lengths between decoking are short — of the order of 7 days compared with 50 days for classical furnaces.

Figs. 9.3.2-4, 9.3.2-5, and 9.3.2-6 report on the simulation of the cracking of a 15 wt% ethane – 85 wt% propane mixture with a steam dilution of 0.4 in various coil configurations: a millisecond tube, a reversed (1-2-4) split coil, a classical (2-1) split coil and a single coil. Fig. 9.3.2-4 illustrates the very different temperature profiles obtained with these configurations, Fig. 9.3.2-5 compares the ethylene yields and Fig. 9.3.2-6 the initial coking rate profiles [Plehiers and Froment, 1987]. For equal conversion, the ethylene yield obtained with the millisecond and reversed split coil are significantly higher than those obtained in a classical split coil or single coil. The penalty lies in the shorter run length resulting from the higher coking rates.

PROBLEMS

9.1 A gas-phase reaction, $A \rightarrow 2R$, is carried out in a tubular plug flow reactor at T = 60°C and p_t = 4.75 bar. The feed consists of 50 mol-% A and 50 mol-% inert at a rate of 4000 kg/h. The molecular weights of A and inert are 40 and 20, respectively, and the rate coefficient is k = 2000 h^{-1}. Determine the reactor size for 35 percent conversion of A.

9.2 The process

$$A \xrightarrow{k_1} B \xrightarrow{k_2} C$$

is carried out in a tubular reactor with plug flow. Both reactions are of first order. The feed consists of pure *A*. Given the following data,

$$C_{A0} = 0.05 \text{ kmol/m}^3$$
$$F_0' = 0.15 \text{ m}^3\text{/h}$$
$$\Omega = 2 \cdot 10^{-3} \text{ m}^2$$
$$k_1 = 172.5 \text{ h}^{-1}$$

calculate the length of the tube to maximize the yield of *B* in the cases **(a)** $k_2 = k_1/2$, **(b)** $k_2 = k_1$. What are the exit concentrations of *A*, *B*, and *C* in both cases?

9.3 **(a)** Repeat the derivations of Section 9.3-1, but for a zero-order reaction.
(b) Given the data

F_{A0}	= 20 kmol/h	T_0	= 300K
c_p	= 2.0935 kJ/kg°C	x_0	= 0; x = 0.9
$-\Delta H$	= 41,870 kJ/kmol	k_0	= 3.27×10^6 kmol/m^3 h
E	= 37,683 kJ/kmol	$\dot{m}$	= 1000 kg/h

calculate the reactor volume and exit temperature when the reaction is of zero order.
(c) Compare with the volume required when the reaction is carried out isothermally (1) at $T = T_0$, (2) at $T = (T_0 + T_e)/2$, where T_e is the exit temperature of the adiabatic reactor.

9.4 Prove that the curve x versus (V/F_{t0}), where x is the conversion, V the total reactor volume, and F_{t0} the total molar inlet flow rate of reactant plus inert diluent, is independent of the dilution ratio for a reversible reaction where both forward and reverse reactions are of first order only.

9.5 Derivation of a rate equation for the thermal cracking of acetone from nonisothermal data:
When submitted to thermal cracking conditions, acetone decomposes according to the overall reaction

$$CH_3COCH_3 \rightarrow CH_2{=}CO + CH_4$$

that may be considered irreversible in the range of practical interest (700° to 750°C). Ketene and methane are not the only products, however. In the range considered, ethylene, carbon monoxide and dioxide, hydrogen, and carbon are also obtained, probably according to the overall reactions

$$2CH_2{=}CO \rightarrow CH_2{=}CH_2 + 2CO$$

$$CH_3COCH_3 \rightarrow 3H_2 + CO + 2C$$

From isobaric experiments at atmospheric pressure in a laboratory flow reactor with 6 mm inside diameter and 1.20 m length, Froment et al. [1961a] obtained at 750°C the x-versus-V/F_{A0} diagram of Fig. 1, where

$$x_A = \frac{\text{moles of acetone decomposed}}{\text{moles of acetone fed}}$$

$$x_K = \frac{\text{moles of ketene formed}}{\text{moles of acetone fed}}$$

It can be seen how the curves do not extrapolate through the origin. This results from the fact that not all of the volume accounted for is at the reference temperature considered.

(a) Use the equivalent reactor volume concept to reduce the data to "isothermal" conditions. Use the short-cut method to estimate the

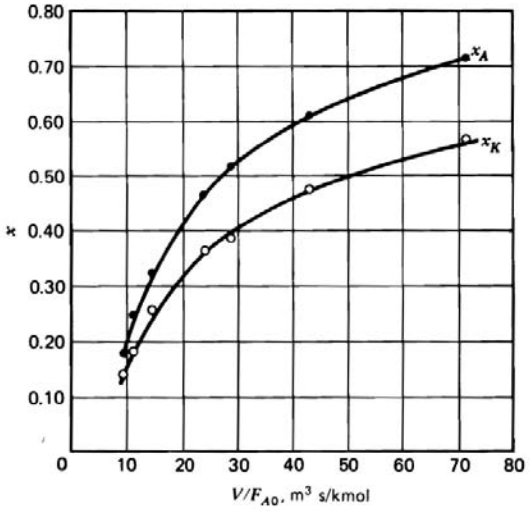

Figure 1

Acetone cracking. Conversion versus space-time diagram at 750°C. From Froment et al. [1961a, b].

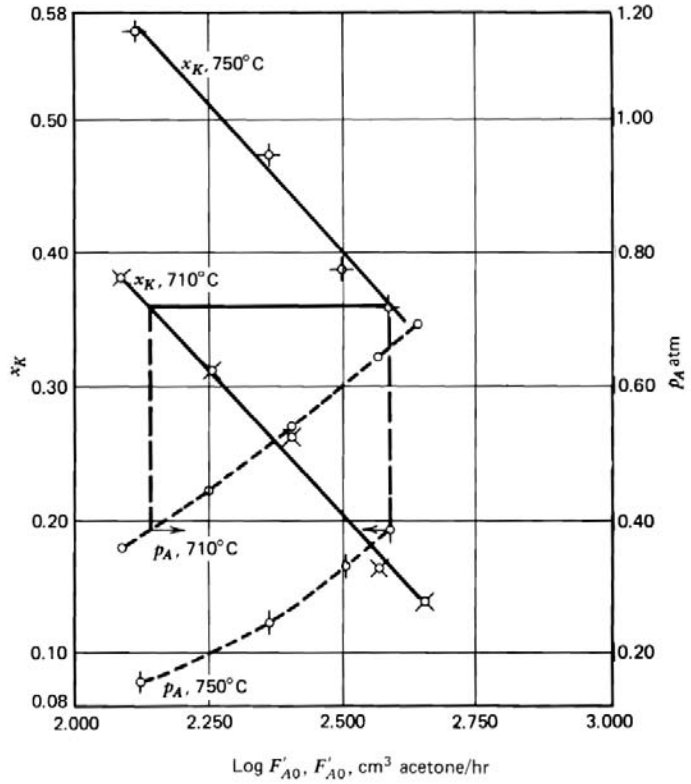

Figure 2

Acetone cracking. Short-cut method for estimation of activation energy. From Froment et al. [1961a, b].

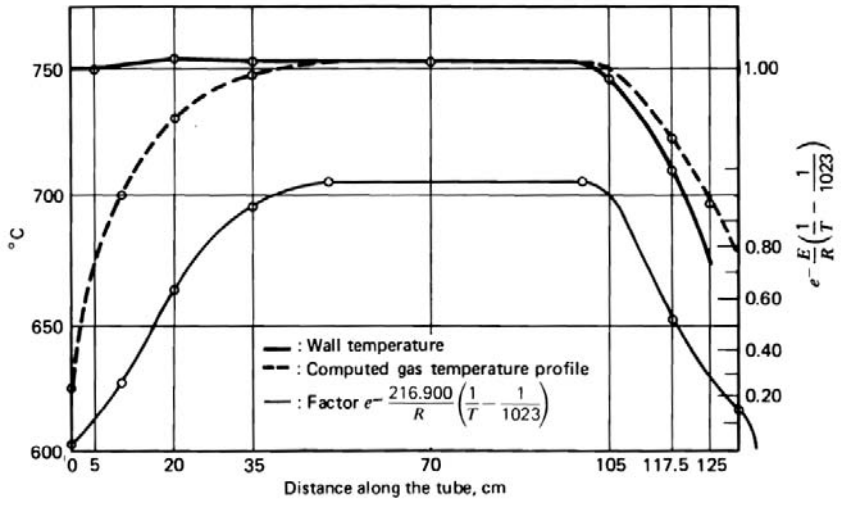

Figure 3

Acetone cracking. Temperature profiles for calculation of equivalent reactor volume. From Froment et al. [1961a, b].

activation energy. Figs. 2 and 3 are given. In Fig. 2 x_K and p_A are plotted versus log F'_{A0} for two series of experiments, one at 750°C, the other at 710°C. Verify if the conditions for a satisfactory estimate of E are fulfilled. Fig. 3 shows the temperature profiles, allowing obtaining the equivalent reactor volumes. Show that, after accounting for the equivalent reactor volumes, the curves x_K versus V_R/F_{A0} extrapolate through the origin.

(b) Use the corrected conversion versus space-time curves to derive a rate equation. Postulate the form

$$r_A = k\, p_A^n$$

Apply the differential and integral methods of kinetic analysis (see Chapter 2) to determine the rate coefficients and order at the different temperatures. To work out the integral method of kinetic analysis, it is necessary to express p_A as a function of x_k. A rigorous expression would only be possible if all reactions taking place were exactly known. Therefore, undertake an empirical fit of this function.

9.6 Thermal cracking of ethane:

The results given in Section 9.3.2 for the thermal cracking of naphtha and of a mixture of ethane-propane were obtained with very detailed radical kinetic schemes for these processes [Willems and Froment, 1988a, b]. The present problem formulates ethane cracking in terms of a drastically simplified molecular model containing 7 reactions. This reaction scheme and the corresponding kinetic model was derived from the radical scheme developed by Sundaram and Froment [1977]. Table 1 gives the kinetic parameters of these reactions. It should be mentioned that the kinetic parameters for the reverse reactions (2) and (5) were obtained from equilibrium data. Table 2 is the matrix of stoichiometric coefficients α_{ij} defined by

$$\sum_{j=1}^{N} \alpha_{ij} A_j = 0 \qquad i = 1, 2, \ldots, 7$$

The following heat flux profile was generated from uncoupled simulations of the heat transfer in the furnace firebox: first tube: 96

TABLE 1
MOLECULAR REACTION SCHEME AND KINETIC PARAMETERS FOR THE THERMAL CRACKING OF ETHANE[b]

Reaction	Order	A_0 (s^{-1})	E (kJ/mol)
1. $C_2H_6 \rightarrow C_2H_4 + H_2$	1	4.65×10^{13}	273,020
2. $C_2H_4 + H_2 \rightarrow C_2H_6$	2	8.75×10^{8a}	136,870
3. $2C_2H_6 \rightarrow C_3H_8 + CH_4$	1	3.85×10^{11}	273,190
4. $C_3H_6 \rightarrow C_2H_2 + CH_4$	1	9.81×10^{8}	154,580
5. $C_2H_2 + CH_4 \rightarrow C_3H_6$	2	5.87×10^{4a}	29,480
6. $C_2H_2 + C_2H_4 \rightarrow C_4H_6$	2	1.03×10^{12a}	172,750
7. $C_2H_4 + C_2H_6 \rightarrow C_3H_6 + CH_4$	2	7.08×10^{13a}	253,010

[a]Units m^3/kmol s; for first order s^{-1}. [b]From Sundaram and Froment [1977].

TABLE 2
MATRIX OF STOICHIOMETRIC COEFFICIENTS[a]

	CH_4	C_2H_2	C_2H_4	C_2H_6	C_3H_6	C_3H_8	C_4H_6	H_2	H_2O
$i \backslash j$	1	2	3	4	5	6	7	8	9
1			1	−1				1	
2			−1	1				−1	
3	1			−2		1			
4	1	1			−1				
5	−1	−1			1				
6		−1	−1				1		
7	1		−1	−1	1				

[a]From Sundaram and Froment [1977].

kJ/m^2s; second tube: 84; third: 80; fourth: 71; fifth: 63; seventh, eighth, ninth, and tenth tubes: 59.

Calculate the profiles of ethane conversion, temperature and pressure (smoothed) in the coil. The ethane conversion is limited to 60 % to limit the coke formation.

9.7 The following data for the enzymatic hydrolysis of *n*-benzoyl 1-arginine ethyl ester (BAEE) by tripsin bound to particles of porous glass were obtained in a fixed bed reactor for an initial concentration $C_{A0} = 0.5\ mM$.

X_A	V/F'_0, min
0.438	5.90×10^{-2}
0.590	8.03
0.670	9.58
0.687	9.46
0.910	14.72
0.972	18.00

a) For Michaelis-Menten kinetics and assuming plug flow operation, show that a plot of $(1/C_{A0}x_A)\ \ln(1 - x_A)^{-1}$ versus $V/F_{A0}x_A$ should give a straight line, from which the constants can be determined.

b) Compute values for the constants.

REFERENCES

Buekens, A.G., and Froment, G.F., *Ind. Eng. Chem. Proc. Des. Dev.*, 7, 435 (1968).

Buekens, A.G., and Froment, G.F., *Ind. Eng. Chem. Proc. Des. Dev.*, 10, 309 (1971a).

Buekens, A.G., and Froment, G.F., in *Proc. 4th Eur. Symp. Chem. React. Eng. 1968*, Pergamon Press, London (1971b).

Douglas, J.M., and Eagleton, L.C., *Ind. Eng. Chem. Fundam.*, 1, 116 (1962).

Dluzniewski J., Orriss R, and Wallace J., *Oil & Gas Journal*, April 6 (1981).

Emig, G., Hofmann, H., and Friedrich, H., *Proc. 2nd Int. Symp. Chem. React. Eng.*, p. B5-23, Elsevier, Amsterdam (1972).

Froment, G.F., Pijcke, H., and Goethals, G., *Chem. Eng. Sci.*, 13, 173 (1961a).

Froment, G.F., Pijcke, H., and Goethals, G., *Chem. Eng. Sci.*, 13, 180 (1961b).

Froment, G.F., *Chem. Eng. Sci.*, 47, 2163 (1992).

Gear, C.W., *Numerical Initial Value Problems in Ordinary Differential Equations*, Prentice-Hall, Englewood Cliffs, N.J. (1971).

Hougen, O.A., and Watson, K.M., *Chemical Process Principles*, Vol. III, Wiley, New York (1947).

Knudsen, J.G., and Katz, D.L., *Fluid Dynamics and Heat Transfer*, McGraw-Hill, New York (1958).

Lambrecht, G., Nussey, C., and Froment, G.F., in *Proc. 2nd Int. Symp. Chem. React. Eng.*, p. B2-19, Elsiever, Amsterdam (1972).

Nekrasov, B.B., *Hydraulics*, Peace Publishers, Moscow (1969).

Plehiers, P.M., and Froment, G.F., *Oil & Gas J.*, 41, Aug. 17 (1987).

Sundaram, K.M., and Froment, G.F., *Chem. Eng. Sci.*, 32, 601 (1977).

Van Camp, C.E., Van Damme, P.S., Willems, P.A., Clymans, P.J., and Froment, G.F., *Ind. Eng. Chem. Proc. Des. Dev.*, 24, 561 (1985).

Van Damme, P.S., Froment, G.F., and Balthasar, W.B., *Ind. Eng. Chem. Proc. Des. Dev.*, 20, 366 (1981).

Van Damme, P.S., Narayanan, S., and Froment, G.F., *A.I.Ch.E. J.*, 21, 1065 (1965).

Willems, P.A., and Froment, G.F., *Ind. Eng. Chem. Res.*, 27, 1959 (1988a).

Willems, P.A., and Froment, G.F., *Ind. Eng. Chem. Res.*, 27, 1966 (1988b).

Chapter 10

The Perfectly Mixed Flow Reactor

10.1 INTRODUCTION

This reactor type is the opposite extreme of the plug flow reactor dealt with in Chapter 9. The essential feature is the assumption of complete uniformity of concentration and temperature throughout the reactor, as contrasted with the assumption of no intermixing of successive fluid elements entering a plug flow vessel. Therefore, in the perfectly mixed flow reactor, the conversion takes place at a unique concentration (and temperature) level which, of course, is also the concentration of the effluent. To approach this ideal mixing pattern, it is necessary that the feed be intimately mixed with the contents of the reactor in a

time interval that is very small compared to the mean residence time of the fluid flowing through the vessel. Further discussions of deviations from these ideal flow patterns are given in Chapter 12. In this chapter, it is assumed that perfect mixing has been achieved.

The stirred flow reactor is frequently chosen when temperature control is a critical aspect, as in the nitration of aromatic hydrocarbons or glycerine (Biazzi process). The stirred flow reactor is also chosen when the conversion must take place at a constant composition, as in the copolymerization of butadiene and styrene, or when a reaction between two phases has to be carried out, or when a catalyst must be kept in suspension as in the polymerization of ethylene with Ziegler catalysts, the hydrogenation of α-methylstyrene to cumene, and the air oxidation of cumene to acetone and phenol (Hercules Distillers process).

Finally, several alternate names have been used for what is called here the *perfectly mixed flow reactor*. One of the earliest was "continuous stirred tank reactor," or CSTR, which some have modified to "continuous flow stirred tank reactor," or CFSTR. Other names are "backmix reactor," "mixed flow reactor," and "ideal stirred tank reactor."

10.2 MASS AND ENERGY BALANCES

10.2.1 Basic Equations

With complete mixing the volume is completely uniform in composition and temperature, the continuity equations for the various components and the energy equation may be integrated over the complete volume. From equations (7.1.1-1) and (7.2.2-10) it follows that, in molar units,

$$\frac{dN_j}{dt} = F_{j,0} - F_{j,e} + VR_j \qquad (10.2.1\text{-}1)$$

For single reactions it is useful to write this equation in terms of the conversion of the reactant *A*:

$$F_A = F_{A0}\left(1 - x_A\right)$$

so that

$$N_{A0}\frac{dx_A}{dt} = F_{A0}x_A + Vr_A \qquad (10.2.1\text{-}2)$$

Aris [1965] has discussed the reductions that are possible when the general set of reactions

$$\sum_j \alpha_{ij} A_j = 0$$

have to be considered. For arbitrary feed and/or initial compositions, which may not have stoichiometrically interrelated compositions, the mass balance can be written in terms of an extent for each independent reaction, plus variables related to the incompatibility of the feed and initial compositions. For constant feed, this single latter variable is related to the "washout" of the initial contents. In these general situations it is probably just as easy to directly integrate (10.2.1-1).

The energy balance is written [see (7.2.4-5)]:

$$m_t c_p \frac{dT}{dt} = \sum_j F_{j,0}\left(H_{j,0} - H_{j,e}\right) + V\sum_i \left(-\Delta H\right)_i r_i + Q(T) \qquad (10.2.1\text{-}3)$$

where $Q(T)$ represents external heat addition or removal from the reactor, for example, $A_k U(T_R - T)$. With mean specific heats the energy balance can be written

$$V\rho_f c_p \frac{dT}{dt} = F_0' \rho_f c_p \left(T_0 - T\right) + V\sum_i \left(-\Delta H_i\right) r_i + Q(T) \qquad (10.2.1\text{-}4)$$

10.2.2 Steady-State Reactor Design

As a consequence of the complete mixing, a continuous flow stirred tank reactor also operates isothermally. Therefore, in the steady state it is not necessary to consider the mass and energy balances simultaneously. Optimum conditions may be computed on the basis of the material balance alone, and afterwards the energy balance is used, in principle (see Section 10.4), to determine the external conditions required to maintain the desired temperature.

Thus, the design equation, from (10.2.1-2), is either

$$x_A = \frac{V}{F_{A0}} r_A \qquad (10.2.2\text{-}1)$$

or, for constant densitiy,

$$C_{A0} - C_A = \frac{V}{F'} r_A = \tau\, r_A \qquad (10.2.2\text{-}2)$$

where $\tau = V/F' = C_{A0}V/F_{A0}$ is called the mean residence (or holding) time. Given an expression for r_A, the above equations can then be readily solved for x_A as a function of the system parameters. For a first-order reaction,

$$r_A = kC_A = kC_{A0}\left(1 - x_A\right)$$

so that, with $x_{A0} = 0$,

$$x_A = \frac{kC_{A0}V / F_{A0}}{1+\left(kC_{A0}V / F_{A0}\right)} = 1 - \frac{1}{1+\left(kC_{A0}V / F_{A0}\right)} \qquad (10.2.2\text{-}3)$$

For constant density, the result is usually written as

$$\frac{C_A}{C_{A0}} = \frac{1}{1+(kV / F^{'})} = \frac{1}{1+k\tau} \qquad (10.2.2\text{-}4)$$

When two perfectly mixed reactors are connected in series, the mass balance for the second reactor is

$$x_{A2} - x_{A1} = \frac{V}{F_{A0}} r_A(x_{A2}) = \frac{V}{F_{A0}} kC_{A0}\left(1 - x_{A2}\right) \qquad (10.2.2\text{-}5)$$

When x_{A1} is eliminated by means of (10.2.2-3), so that the final conversion is written solely in terms of the conditions at the inlet (x_{A0} = 0), the following equation is obtained:

$$x_{A2} = 1 - \frac{1}{\left[1+\left(kC_{A0}V / F_{A0}\right)\right]^2} \qquad (10.2.2\text{-}6)$$

Note that V is the volume of *one* reactor. For n reactors in series,

$$x_{An} = 1 - \frac{1}{\left[1+\left(kC_{A0}V / F_{A0}\right)\right]^n} \qquad (10.2.2\text{-}7)$$

These formulas may be used for the study of the kinetics of a first-order reaction by measuring x_A, C_{A0}, F_{A0}, and V and then determining k. Alternatively, for a given reaction, they can be used for determining the volume required to achieve a certain production.

For second-order reactions, (10.2.2-1) becomes

$$F_{A0}x_A = VkC_AC_B \qquad (10.2.2\text{-}8)$$

With the irreversible reaction $A + B \rightarrow$ products, when equimolar quantities of A and B are fed to the reactor, the following equation is obtained:

$$x_A = 1 + \frac{F_{A0}}{2kC_{A0}^2V} - \left[\left(\frac{F_{A0}}{2kC_{A0}^2V}\right)^2 + \frac{F_{A0}}{kC_{A0}^2V}\right]^{1/2} \qquad (10.2.2\text{-}9)$$

The conversion at the exit of a second reactor of equal volume and placed in series with the first is

$$x_A = 1 + \frac{F_{A0}}{2kC_{A0}^2V} - \left\{ -\left(\frac{F_{A0}}{2kC_{A0}^2V}\right)^2 + \frac{F_{A0}}{kC_{A0}^2V}\left[\left(\frac{F_{A0}}{2kC_{A0}^2V}\right)^2 + \frac{F_{A0}}{kC_{A0}^2V}\right]^{1/2}\right\}^{1/2} \tag{10.2.2-10}$$

The results of (10.2.2-7) and (10.2.2-10) have been represented by Schoenemann and Hofmann [see Schoenemann, 1952] in convenient diagrams. Fig. 10.2.2-1 is the diagram for first-order reactions with constant density. The conversion for more complex kinetic forms must often be obtained numerically, by solving the algebraic equation (10.2.2-1) with the appropriate rate function on the right-hand side.

Note that (10.2.2-1), (10.2.2-7), and (10.2.2-10) do not explicitly contain the residence time, just as was the case for the continuity equations for the plug flow reactor in Chapter 9. They could be reformulated [Levenspiel, 1962], but, again as in Chapter 9, there is no advantage, and it is simpler to just use the directly manipulated variables F_{A0}, V, and C_{A0}. It is only for constant-density cases that the residence time V/F' directly appears, as illustrated by (10.2.2-4).

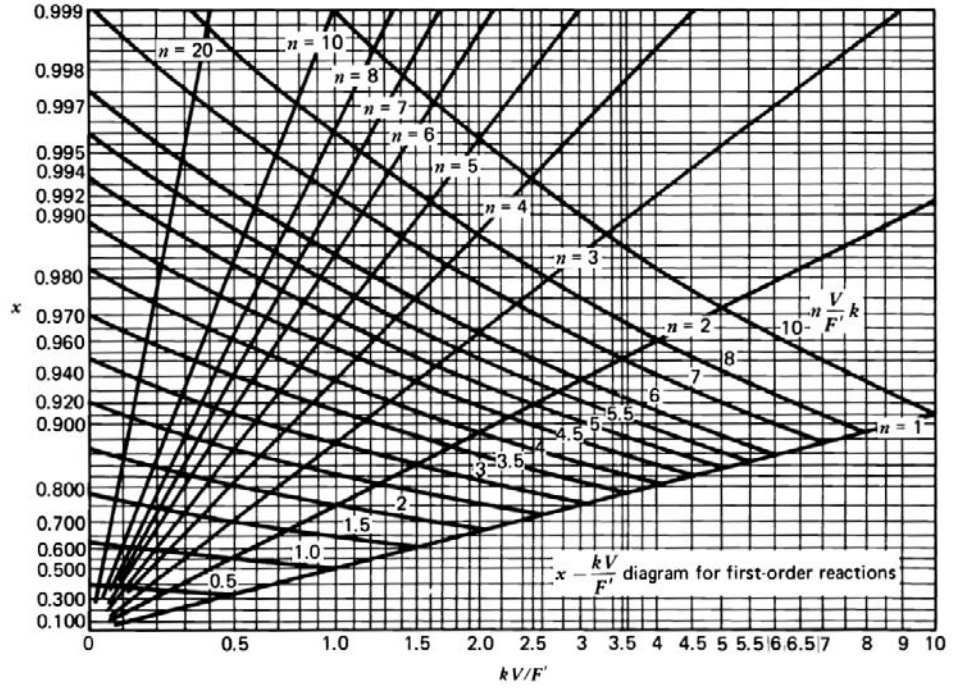

Figure 10.2.2-1

Plot of x versus kV/F' for first-order reactions. From Schoenemann [1952].

With the perfectly mixed flow reactor, the actual residence times of individual fluid elements are a continuous spectrum: by the completely random mixing, some fluid elements immediately reach the exit after their introduction, whereas some remain in the reactor for a very long time. The above results did not specifically consider this spread in residence time. The reason for this is that the assumption of perfect mixing implies that each fluid element instantaneously loses its identity. In principle, this means that the molecular environment is also completely uniform for the reacting species. By implicitly defining the molecular environment, the perfect mixing model only requires the conservation of mass to predict the overall conversion. If the intensity of actual mixing does not generate a uniform molecular environment before significant reaction occurs, then specific account must be taken of the spectrum, or distribution, of fluid residence times. These so-called "nonideal flow patterns" are considered in Chapter 12.

For a simple first-order irreversible reaction, with $kV/F' = 2.0$ it follows from (10.2.2-3) or (10.2.2-4) or Fig. 10.2.2-1 (the ordinate corresponding to the intersection of $kV/F' = 2.0$ and the $n = 1$ line) that the conversion will be $x_A = 0.667$). In a plug flow or batch reactor, the conversion would be:

$$x_A = 1 - \exp\left[-kV / F'\right] = 0.865$$

If this conversion were desired in a perfectly mixed flow reactor a value for $kV/F' = 6.5$ would be required (the abscissa of the intersection of the ordinate level of 0.865 and the $n = 1$ line in Fig 10.2.2-1). For the given k the reactor volume would have to be 6.5 times the flow rate, rather than only twice, as with plug flow. This example clearly illustrates that results obtained in a batch or plug flow tubular reactor cannot be directly extrapolated to a continuous flow stirred tank reactor — there may be large differences in conversion levels.

It also follows from the above discussion that it is difficult to obtain high conversions in a continuous flow stirred tank reactor (at least for first-order kinetics) without resorting to large volumes, in which perfect mixing may not be easily achieved. Therefore, it is often preferable to connect two or more smaller reactors in series, which will be shown to also reduce the total volume required to achieve a given conversion. Indeed, from Fig. 10.2.2-1, it is seen that a conversion of 0.865 can be obtained with $kV/F' = 1.75$. This means that the volume of each of the two tanks has to be 1.75 times the flow rate, for a total volume ratio of 3.5 instead of 6.5 — a savings of almost a factor of 2.

When the total volume ($= nV$) is kept constant, the subdivision of the reactor permits one to increase the overall conversion. Consider again the value $kV/F' = 2.0$ for a single-tank reactor, and determine the conversions when the total volume is such that $nVk/F' = 2.0$ while increasing n. The results can easily

be found from Fig. 10.2.2-1 by following the nVk/F' curve as it intersects the n = 1, 2, 3, ... curves, and reading the ordinate values:

n	nVk/F'	x_A
1	2	0.67
2	2	0.75
3	2	0.78
5	2	0.81
∞	2	0.87 (plug flow)

Alternatively, a given conversion may be reached with either a single large reactor volume or with a series of smaller reactors. The ultimate choice is based on economic factors, as illustrated in Fig. 10.2.2-2. The total reactor volume required decreases with more subdivision (large n), but with the cost per reactor proportional to $V^{0.6}$, the total cost proportional to $nV^{0.6}$ shows a definite minimum — in this case at about n = 4. Plant operational difficulties may also increase with n, and the optimum choice is usually a relatively small number of reactors in series, especially since most of the savings in total volume occur for $n < 5$. Exceptions are encountered in multistage contacting devices, but this is a more complicated situation.

For reaction orders other than 1, the best choice is not two equal-size tanks in series. Luss [1965] has provided a simple analytical procedure for determining the optimum size ratio. For second-order reactions in two tanks in series, this ratio is about 1:1 for low conversions and 1:2 for high conversion. The overall advantage of the variable-sized multistage reactor is rather small compared to that with equal sizes, so that usually equal-size tanks in series are chosen.

The result that for a given conversion the perfectly mixed flow reactor requires a larger volume than the plug flow reactor is only valid for reaction rate expressions for which the rate monotonically decreases with decreasing reactant concentration (e.g., simple orders greater than zero). For these reactions, it is clearly advantageous to operate a reactor at the highest possible average concentration level. In a perfectly mixed flow reactor, the conversion takes place at the concentration level of the effluent, which is low, whereas the plug flow reactor takes advantage of the higher concentrations in the inlet zone. The subdivision of the total volume by series of stirred tanks is an intermediate situation, which approaches the continuous concentration profile of the plug flow reactor, and therefore yields a higher conversion compared to that in a single tank.

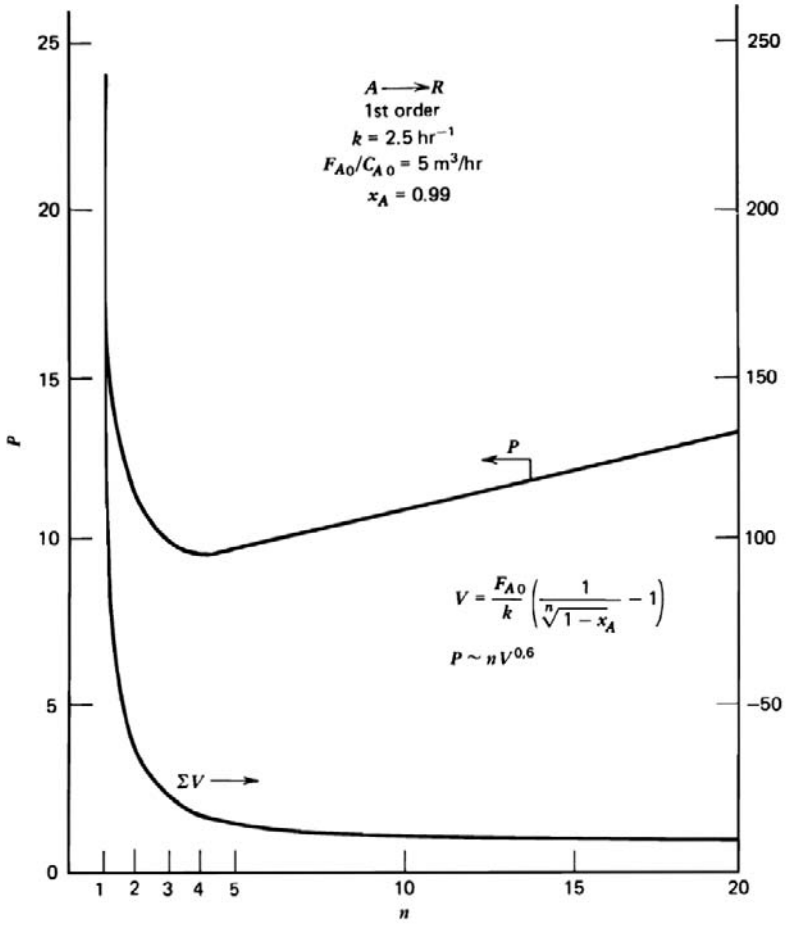

Figure 10.2.2-2
Economic optimum choice of number of perfectly mixed reactors in series.

These conclusions can be readily quantitatively visualized as shown in Fig. 10.2.2-3, which is based on the geometric nature of the plug flow or batch reactor design equation versus that for the perfectly mixed flow reactor.

For a plug flow or batch reactor,

$$\frac{V}{F_{A0}} = \int_{x_{A0}}^{x_{Ae}} \frac{dx_A}{r_A(x_A)}$$

For a perfectly mixed flow reactor,

$$\frac{V}{F_{A0}} = \frac{x_{Ae} - x_{A0}}{r_A(x_{Ae})}$$

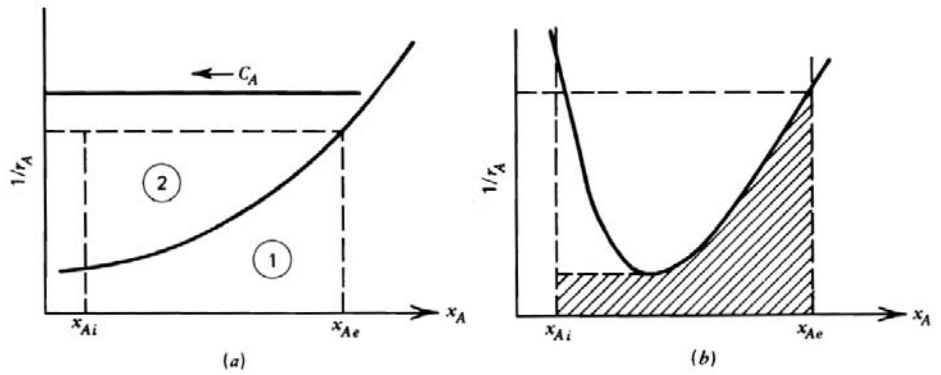

Figure 10.2.2-3

Comparison of plug flow and perfectly mixed flow reactor volumes.

The reactor size for plug flow is given by the area under the curve $1/r_A$ versus x_A (area 1 in Fig. 10.2.2-3a). For perfectly mixed flow, on the other hand, the size is given by the area of the rectangle with ordinate $1/r_A(x_{Ae})$ (i.e., evaluated at the exit conversion), which is the sum of areas 1 + 2. Clearly, for this case where the rate monotonically increases with concentration, the plug flow reactor will always have the smaller area, and thus a smaller size. However, Fig. 10.2.2-3b is a plot for another type of rate form, which could result from an autocatalytic reaction, a dual-site catalytic mechanism, "negative order", or any other form where the rate has a maximum in the concentration range. Here, the optimum arrangement is a perfectly mixed reactor followed by a plug flow reactor. The combined volume could be significantly smaller than that of either type of single reactor. Bischoff [1966] treated the case of Michaelis-Menten kinetics important in enzyme and fermentation reactions and showed for a typical case that the total volume is reduced by a factor of 2.77 with the optimal design.

In many cases the reactor volume is not the main factor in the choice of the reactor type. Most reactions of industrial importance are actually complex and the selectivity is far more important than the reactor size. Therefore, it is important that a judicious choice of reactor type permits one to influence the selectivity, which may depend on the concentration levels and, therefore, on the degree of mixing in the reactor. This is discussed in the next section.

10.3 DESIGN FOR OPTIMUM SELECTIVITY IN SIMULTANEOUS REACTIONS

10.3.1 General Considerations

The effect of the concentration levels on the selectivity of complex reactions can most readily be seen by considering a few examples. For parallel reactions

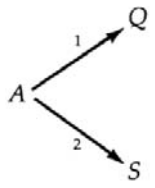

where Q is the desired product, the rate equations for the formation of Q and S are

$$r_Q = k_1 C_A^{a'_1}$$

$$r_S = k_2 C_A^{a'_2}$$

from which

$$\frac{r_Q}{r_S} = \frac{k_1}{k_2} C_A^{a'_1 - a'_2} \qquad (10.3.1\text{-}1)$$

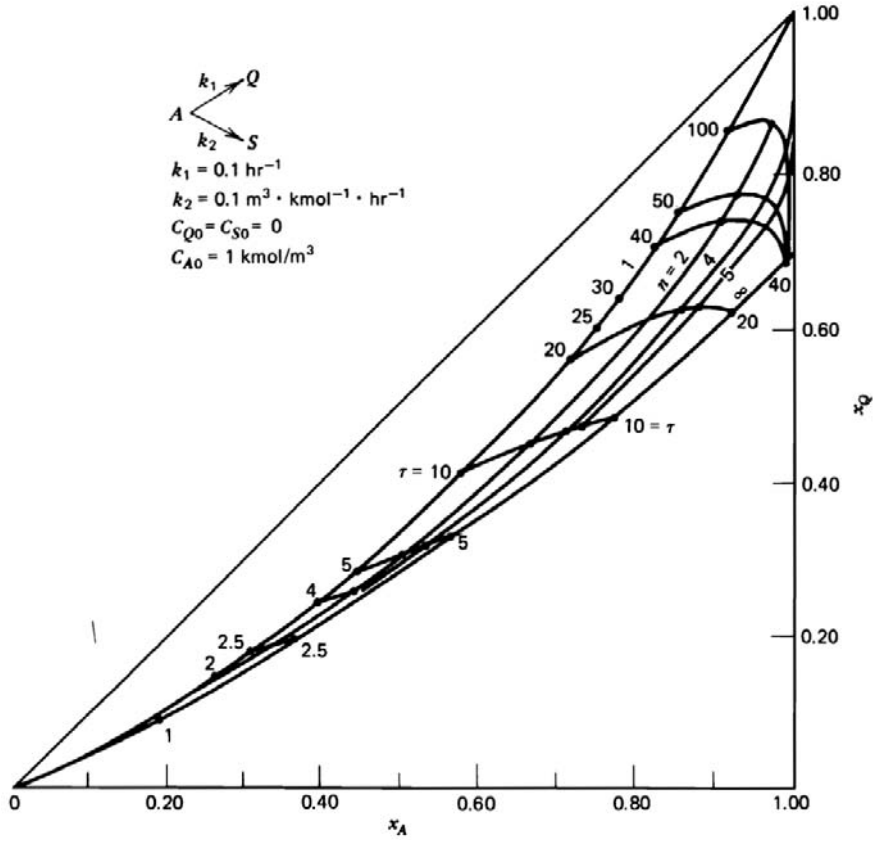

Figure 10.3.1-1

Conversions and selectivities for various degrees of mixing as a function of the mean residence time $\tau = V/F_A$.

The relative rates of formation depend on the ratio of the rate coefficients k_1/k_2, and on the difference in orders, $a_1' - a_2'$. When both rates have the same order, it is clear that the selectivity will not depend on the concentration level (although the conversion will). For given k_1/k_2 and $a_1' \neq a_2'$, the selectivity can be altered by the concentration environment, and this should then be chosen to maximize the desired product Q. When $a_1' < a_2'$, r_Q/r_S is small when C_A is large. In batch and plug flow reactors, part of the conversion is occurring at the high initial concentrations. In the perfectly mixed flow reactor, the feed concentration is immediately reduced to that of the outlet, which is low. Therefore, the selectivity (to Q) will be higher in the perfectly mixed flow reactor. Similar reasoning indicates that the opposite would be true for $a_1' > a_2'$. The former case is illustrated by the calculated results presented in Fig. 10.3.1-1, which compares the conversions to Q, $x_Q = C_Q/C_{A0}$, in batch or plug flow reactors with a cascade of perfectly mixed reactors. It is seen, as expected, that a single stirred tank would give the highest conversion to x_Q and thus the highest selectivity for Q.

Next, consider consecutive reactions:

$$A \xrightarrow{1} Q \xrightarrow{2} S$$

where Q is the desired product. For both reactions first order, the resulting rate equations have been integrated in Chapter 1 for the batch or plug flow reactors. A few curves are shown by way of example in Fig. 10.3.1-2. Also from Chapter 1, the maximum value of C_Q is

$$\left(\frac{C_Q}{C_{A0}}\right)_{\max} = \frac{k_1}{k_2 - k_1}\left(\exp\left[-k_1/k_{lm}\right] - \exp\left[-k_2/k_{lm}\right]\right) \quad (10.3.1\text{-}2)$$

which occurs at the particular holding time

$$\tau_{\max} = \left(C_{A0}\frac{V}{F_{A0}}\right)_{\max} = \frac{1}{k_{lm}} \equiv \frac{\ln\left(k_2/k_1\right)}{k_2 - k_1}$$

For the perfectly mixed flow reactor, the mass balances (10.2.2-2), lead to

$$C_A = \frac{C_{A0}}{1 + \left(k_1 C_{A0} V/F_{A0}\right)}$$

$$C_Q = \frac{k_1 C_{A0}^2 V/F_{A0}}{\left[1 + \left(k_1 C_{A0} V/F_{A0}\right)\right]\left[\left(1 + \left(k_2 C_{A0} V/F_{A0}\right)\right]\right.}$$

$$C_S = C_{A0} - C_A - C_Q$$

Then, it can easily be shown that the maximum value of C_Q is

$$\left(\frac{C_Q}{C_{A0}}\right)_{\max} = \left[\left(\frac{k_2}{k_1}\right)^{1/2} + 1\right]^{-2} \qquad (10.3.1\text{-}3)$$

which occurs at

$$\left(C_{A0}\frac{V}{F_{A0}}\right)_{\max} = (k_1 k_2)^{-1/2}$$

Comparison of (10.3.1-2) and (10.3.1-3) shows that again there are differences between the yields obtained in the reactor types discussed here. A specific example is shown in Fig. 10.3.1-2, where it is seen that the batch or plug flow reactor has greater selectivity for Q relative to the perfectly mixed flow reactor. For sets of first-order reactions, Wei [1966] has shown that the convexity of reaction paths is decreased from plug flow to mixed reactors because of the intermingling of fluid elements with different extents of reaction, and so the

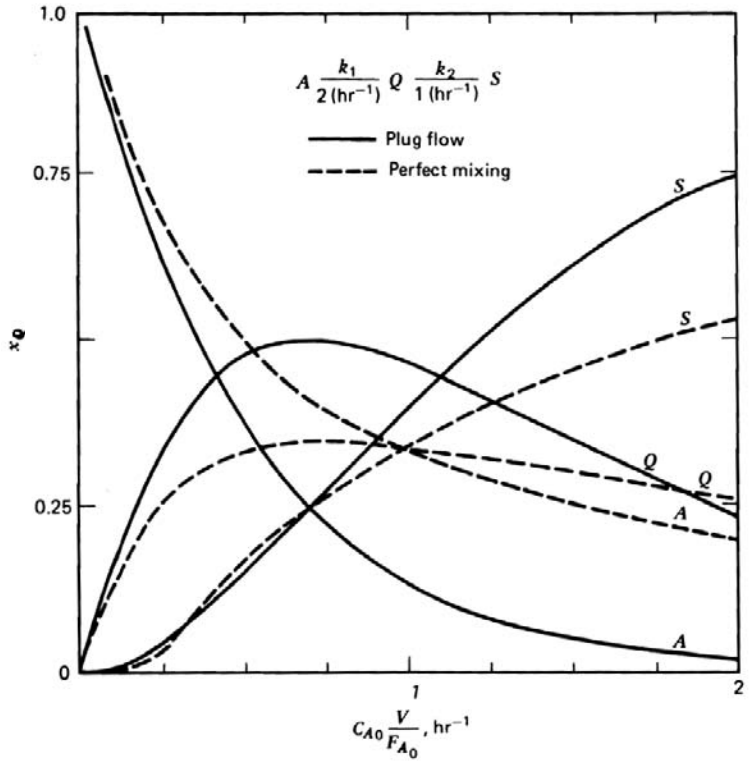

Figure 10.3.1-2

Consecutive reactions. Evolution of conversions with holding- or space time in batch or plug flow and perfectly mixed reactors.

relative selectivities will decrease. Also, if the orders of the two reactions are different, this can additionally affect the relative rates of the reactions in different reactor types. The broader distribution of residence times of the fluid elements in a perfectly mixed flow reactor will cause a broader maximum in the intermediate species concentrations.

For more complicated reaction networks, it is not always completely obvious how to apply the above concepts, as is seen from the example of van de Vusse [1964]:

$$A \xrightarrow{1} Q \xrightarrow{2} S$$

$$A + A \xrightarrow{3} R$$

where Q is the desired product. The rates of the reactions are

$$r_A = k_1 C_A + k_3 C_A^2 \tag{10.3.1-4}$$

$$r_Q = k_1 C_A - k_2 C_Q \tag{10.3.1-5}$$

and the yield C_Q/C_{A0}, or the selectivity $C_Q/(C_{A0} - C_A)$, can be found from the ratio of rates:

$$\frac{r_Q}{r_A} = \frac{k_1}{k_1 + k_3 C_A} - \frac{k_2 C_Q}{C_A(k_1 + k_3 C_A)} \tag{10.3.1-6}$$

$$= \frac{1}{1 + a_1(1 - x_A)} - \frac{a_2 x_Q}{(1 - x_A)[1 + a_1(1 - x_A)]}$$

The results depend on the two parameter groups

$$a_1 \equiv \frac{k_3 C_{A0}}{k_1} \qquad \text{and} \qquad a_2 \equiv \frac{k_2}{k_1} \tag{10.3.1-7}$$

For $k_3 C_{A0} >> k_2$, or $a_1 >> a_2$, it seems reasonable to expect that the parallel reaction is more critical than the consecutive step in decreasing the yield of Q, and based on the above paragraphs the optimum choice would be a perfectly mixed reactor rather than a plug flow reactor. Also, for $k_3 C_{A0} < k_2$, or $a_1 < a_2$, the consecutive reaction should dominate, and the plug flow reactor should be preferred. However, for $a_1 \cong a_2$, it is not so clear which is the optimum reactor type.

Van de Vusse [1964] performed computations to determine the proper choices. Using the ratio of the mass balances for a perfectly mixed reactor, (10.2.2-1) or (10.2.2-2), leads to:

$$\frac{r_Q}{r_A} = \frac{C_Q}{C_{A0} - C_A} = \frac{x_Q}{x_A}$$

which, accounting for (10.3.1-6), has the solution

$$x_Q = \frac{x_A(1-x_A)}{a_1(1-x_A)^2 + (1-a_2)(1-x_A) + a_2} \qquad (10.3.1\text{-}8)$$

For plug flow the relationship is

$$\frac{dx_Q}{dx_A} = \frac{r_Q}{r_A}$$

from which, given (10.3.1-6)

$$x_Q = \left[\frac{1-x_A}{1+a_1(1-x_A)}\right]^{a_2} \int_0^{x_A} \frac{[1+a_1(1-x)]^{a_2-1}}{(1-x)^{a_2}}\,dx \qquad (10.3.1\text{-}9a)$$

$$= \frac{(1-x_A)}{1+a_1(1-x_A)} \ln\left(\frac{1}{1-x_A}\right) \qquad \text{for } a_2 = 1 \qquad (10.3.1\text{-}9b)$$

From these results, the maximum yield and selectivity is found from

$$\frac{dx_Q}{dx_A} = 0 \qquad \text{or} \qquad \frac{d}{dx_A}\left(\frac{x_Q}{x_A}\right) = 0$$

Results of such computations were summarized by van de Vusse in Fig. 10.3.1-3. The conjectures concerning the optimum reactor type in the extreme regions of a_1 and a_2 are indeed verified, but also the more complicated middle region is clarified.

Further consideration of the van de Vusse reaction sequence leads to the conclusion that even better results might be obtained with a combination of reactor types or with a reactor of intermediate mixing level. At low conversion, when C_A is high, and very little Q has been formed, it is most important to suppress the parallel reaction, so that a perfectly mixed flow reactor is advantageous. At higher conversion, when C_A is relatively low, and an appreciable amount of Q has been formed, the loss of yield by the consecutive step dominates. To minimize this, plug flow is required. The optimum configuration is a perfectly mixed reactor followed by a plug flow reactor. Using a theoretical model of intermediate mixing levels, allowing for adjustment of the levels along the reactor length, Paynter and Haskins (1970) were able to formally

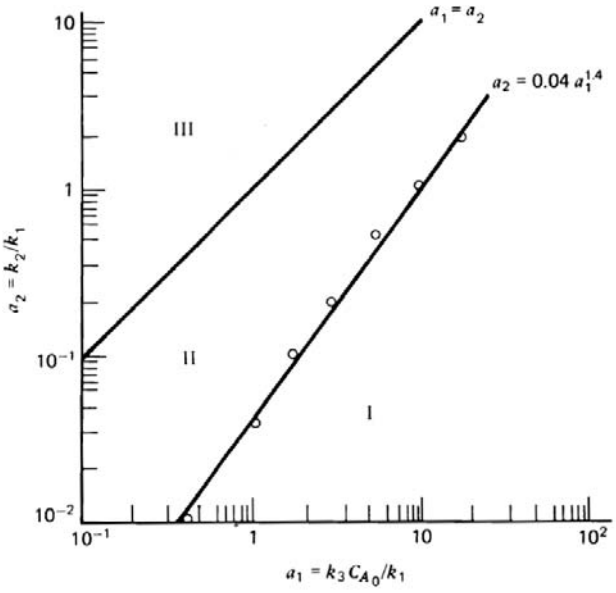

Figure 10.3.1-3

Comparison of yield and selectivity in plug flow and perfectly mixed reactors. Points correspond to pairs of values of a_1 and a_2 for which both types of reactor give the same maximum yield. The upper line corresponds to equal selectivity for both types of reactor (at zero conversion). From van de Vusse [1964].

optimize the intermediate mixing levels for complex reactions, including the one under discussion. An alternate procedure was utilized by Gillespie and Carberry [1966] and van de Vusse [1966] who considered a recycle reactor with a portion of the product stream from a plug flow reactor being returned to the entrance. For zero recycle one obviously has a plug flow reactor. For infinite recycle the system in some sense behaves as a perfectly mixed reactor because of the large feedback of material. Gillespie and Carberry [1966] showed that for certain values of a_1 and a_2, an intermediate recycle rate indeed provided the best performance.

Van de Vusse and Voetter [1961] also considered the parallel second-order reactions

$$A + B \xrightarrow{1} Q$$

$$A + A \xrightarrow{2} S$$

where Q is the desired product. Here, the best results would be obtained by keeping C_A low, throughout the reactor. The suggested way to do this was to have a plug flow reactor with an entrance feed of B and some A, together with side feed of A along the length of the reactor. The purpose was to always keep C_A low by continually converting it, but also provide sufficient A to convert the

amount of *B* fed to the reactor. A more practical system, of course, would be a series of stirred tank reactors with intermediate feeds of *A*.

If a specified product distribution has to be achieved, rather than just the maximization of a yield, the problem is naturally more complicated. Usually, numerical simulations with the reactor design equations are necessary, often combined with formal optimization procedures. A study of choice of reactor type, together with separation and recycle systems, was presented by Russell and Buzzelli [1969] for the important class of reactions

$$A + B \xrightarrow{1} P_1$$

$$P_1 + B \xrightarrow[\vdots]{2} P_2$$

$$P_{n-1} + B \xrightarrow{n} P_n$$

which are encountered in industrial processes such as the production of mono-, di-, and triethylene glycol from ethylene oxide and water; mono-, di-, and triethanolamine from ethylene oxide and ammonia; mono-, di-, and triglycol ethers from ethylene oxide and alcohols; mono-, di-, and trichlorobenzenes from benzene and chlorine; and methylchloride, di- and trichloromethane from methane and chlorine. In these cases, usually the lower members of the product spectrum, P_1 or P_2, are primarily desired and the proper reactor design is crucial to success of the operation. Except for a few general cases such as this, most cases must be handled on an individual basis by the above methods.

10.3.2 Polymerization in Perfectly Mixed Flow Reactors

One of the most important areas in which the concepts discussed in the previous section can be applied is the selection and design of polymerization reactors. The properties of polymers depend on their molecular weight distribution (MWD), and the design should account for this. The subject is a vast one, therefore only the basic concepts will be briefly discussed here. Several excellent reviews, covering various aspects of the area from a chemical reaction engineering viewpoint, in particular mathematical modelling, exist: Shinnar and Katz [1972], Keane [1972], Gerrens [1976], Laurence and Chiovetta [1983], Ray [1972], Min and Ray [1974], Tirrell et al. [1987], and Kiparissides [1996].

Performing polymerization reactions in perfectly mixed flow reactors leads to quite different results from those obtained in batch or plug flow reactors, as discussed in 1951 already by Denbigh [1951]. The key point concerns the relative lifetimes of the active propagating polymer species. If this is long relative to the mean holding time of the fluid in the reactor, the rules in Section

10.3.1 apply, and so the product distribution (the MWD) is narrow in a batch reactor (BR)/plug flow reactor (PFR) and broader in a perfectly mixed flow reactor (PMFR), just as in the earlier examples. The reason was the broader distribution of residence times in the PMFR. However, if the active propagating polymer lifetimes are much shorter than the mean holding time, the residence time of almost all the fluid elements is approaching infinity compared to the local reaction velocity. In this case, the constant availability of monomer tends to produce a more uniform product, and so the PMFR produces a narrower MWD than the BR/PFR. Figures 10.3.2-1a and 10.3.2-1b show results computed by Denbigh [1951] for the free radical polymerization considered in Section 1.6.2 of Chapter 1, illustrating the striking differences that may be obtained. Also, for the

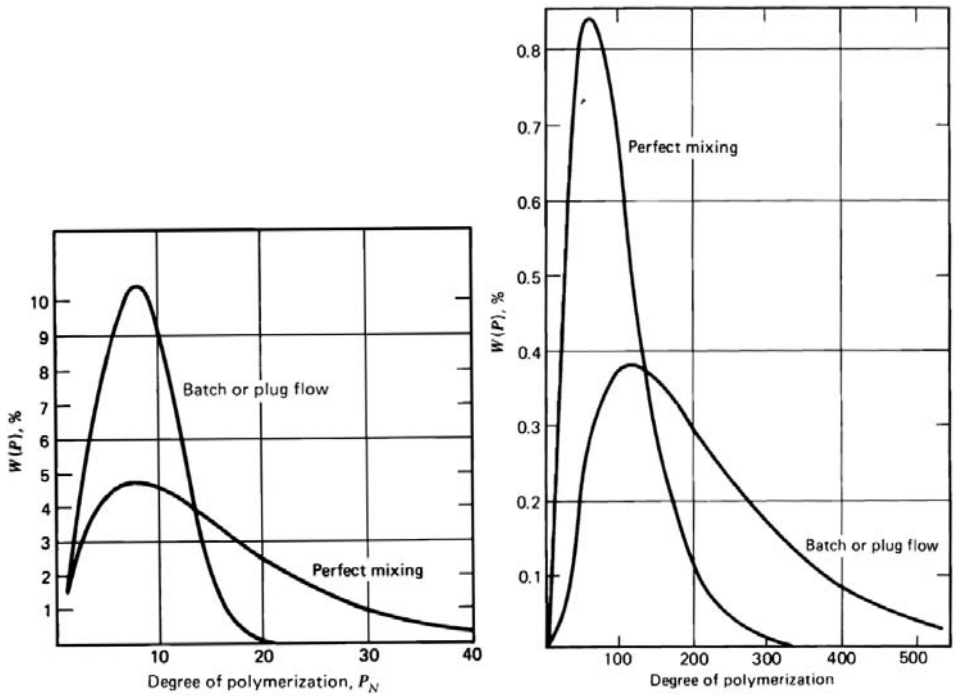

Figure 10.3.2-1a

Chain length distribution by weight when the lifetime of the propagating macroradical is long compared to the mean holding time in the reactor. After Denbigh [1951], from Levenspiel [1962].

Figure 10.3.2-1b

Chain length distribution by weight when the lifetime of the propagating macroradical is short compared to the mean holding time in the reactor. After Denbigh [1951], from Levenspiel [1962].

TABLE 10.3.2-1
MOLECULAR WEIGHT DISTRIBUTIONS RESULTING FROM POLYREACTIONS PREDICTED BY VARIOUS REACTOR MODELS[a]

Reactor / Reaction	BR or PFR	HCSTR	SCSTR
Monomer coupling with termination	(1.1)- Broader than Schulz-Flory	(1.2)- Schulz-Flory distribution	(1.3)-Broader than 1.1.
Monomer coupling without termination	(2.1)- Narrower than Schulz-Flory (Poisson)	(2.2)- Schulz-Flory distribution	(2.3)- Between (2.1) and (2.2)
Polymer coupling	(3.1)- Schulz-Flory distribution	(3.2)- Much broader than Schulz-Flory	(3.3)- Between (3.1) and (3.2)

[a]From Gerrens [1976]. BR = batch reactor; PFR = plug flow reactor; HCSTR = homogeneous continuous stirred tank reactor = perfectly mixed flow reactor of this chapter; SCSTR = segregated continuous stirred tank reactor.

copolymerization of two monomers, the uniform concentrations of a PMFR tend to produce a product of more uniform composition than a BR/PFR.

Monomer coupling with termination is encountered in free radical polymerization (Chapter 1), without termination in living polymerization, discussed in Chapter 8, and polymer coupling in polycondensation, encountered e.g., in the production of nylon.

SCSTR in Table 10.3.2-1 refers to a reactor model with "segregated flow", considered in more detail in Chapter 12. In this special state of mixing the fluid elements are randomly distributed in the reactor, like in HCSTR, but also retain their individual identities. This situation is considered to be characteristic for very viscous fluids [see Nauman, 1974]. In (1.1) and (1.2) the life time of the growing radical is much smaller than the average residence time in the reactor. In (2.1) and (2.2) it is long and equals the residence time. For the free radical polymerization considered in Section 1.6.2 of Chapter 1, Fig. 10.3.2-2 indicates how the MWD evolves with conversion in a HCSTR and gets narrower with increasing conversion.

The polymerization model used by Gerrens is very simple. A more complete description of the polymerization process would include steps like thermal initiation; chain transfer to monomer, solvent and polymer; diffusion control of propagation (glass effect) and of termination (Trommsdorff effect). As second steps in a series of consecutive reactions the chain transfer, or branching, steps, are very sensitive to mixing effects. They are very important for the polymer properties.

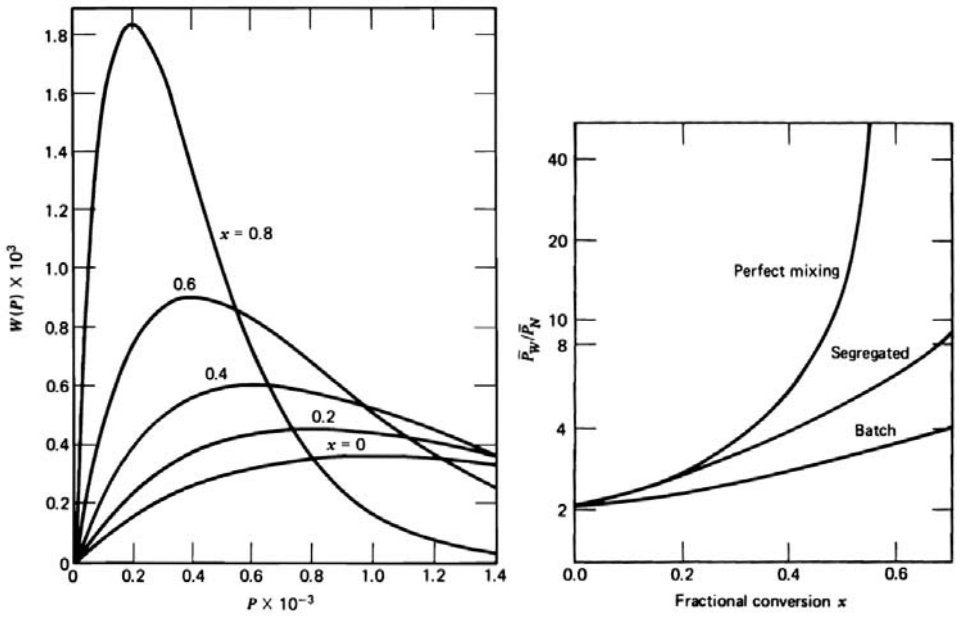

Figure 10.3.2-2

Weight distribution of polymer in HCSTR; parameter: conversion, x; number average degree of polymerization $\overline{P}_N$ at zero conversion = 1000. From Gerrens [1976].

Figure 10.3.2-3

Vinyl acetate polymerization. Evolution of polydispersity with fractional conversion in three reactor types for typical parameter values. From Nagasubramanian and Graessley [1970].

Nagasubramanian and Graessley [1970] compared MWD obtained in vinyl acetate polymerization — a rapid reaction — carried out in a batch reactor and in HCSTR and SCSTR. Branching was included in the model. Figure 10.3.2-3 shows that the polydispersity is higher or the MWD wider in a CSTR than in a BR/PFR, regardless of the degree of segregation of the liquid elements—the opposite of what is shown in Fig. 10.3.2-1b. For typical parameter values the residence time distribution of the fluid elements becomes the predominant factor in this case.

10.4 STABILITY OF OPERATION AND TRANSIENT BEHAVIOR

10.4.1 Stability of Operation

The problem addressed in this section is the state arrived at by the reactor on a perturbation of the operating conditions. Do small perturbations necessarily lead to slight differences in operating conditions or can they lead to drastic changes?

Will the reactor necessarily return to its original steady state when the perturbation is removed? The answers depend on whether the original steady state is "stable" or not.

Considerable, but not complete, information on the stability of a steady state can be derived from the combined steady-state continuity and energy equations. Therefore, (10.2.2-1) is considered simultaneously with the steady-state form of (10.2.1-3):

$$x_A = \tau \frac{r_A}{C_{A0}} \tag{10.4.1-1}$$

$$T - T_0 = \frac{\tau}{\lambda} \frac{r_A}{C_{A0}} - Q_H(T) \tag{10.4.1.-2}$$

with

$$\tau = \frac{C_{A0} V}{F_{A0}} = \frac{V}{F_0^{'}}$$

$$\lambda = \frac{\rho_f c_p}{C_{A0}(-\Delta H)}$$

$$Q_H(T) = -\frac{Q}{\rho_f c_p F_0^{'}}$$

Equation (10.4.1-2) can be written

$$\frac{r_A(x_A, T)}{\lambda C_{A0}} = \frac{1}{\tau}\left[T - T_0 + Q_H(T)\right]$$

When $Q_H(T)$ is explicited in the following way,

$$Q_H(T) = \frac{UA_k}{\rho_p c_p F_0^{'}}\left(T - T_r\right)$$

with T_r the temperature of the heat exchanging fluid, (10.4.1-2) becomes

$$\frac{r_A(x_A, T)}{\lambda C_{A0}} = \left(\frac{1}{\tau} + \frac{UA_k}{\rho_f c_p V}\right)T - \left(\frac{T_0}{\tau} + \frac{UA_k}{\rho_f c_p V} T_r\right) \tag{10.4.1-3}$$

Equation (10.4.1-3) is a nonlinear algebraic equation, to be solved for T, given values for all the parameters. The equation has been arranged in such a way that the left-hand side represents the rate of heat generated per total heat capacity of

the reactor, $Q_G(T)$, and the right-hand side represents the rate of heat removal by flow and heat exchange, $Q_H(T)$. The heat balance just states, then, that at a steady-state operating point, $Q_G(T) = Q_H(T)$.

The two relationships are plotted in Fig. 10.4.1-1 versus the reactor temperature for an exothermic irreversible reaction. The *S* shape of Q_G results from the Arrhenius dependence of the rate coefficient, whereas from (10.4.1-3) it follows that Q_H leads to an (essentially) straight line. When τ is kept constant, a variation in T_0 does not affect Q_G; but in the first quadrant, the Q_H lines are shifted to the right as T_0 is increased. For a value T_{0_1}, only one intersection of Q_G and Q_H is observed, namely, point 1. For a range of T_0 values between T_{0_2} and T_{0_4}, three intersections are observed; therefore three steady states are possible for one and the same operating condition.

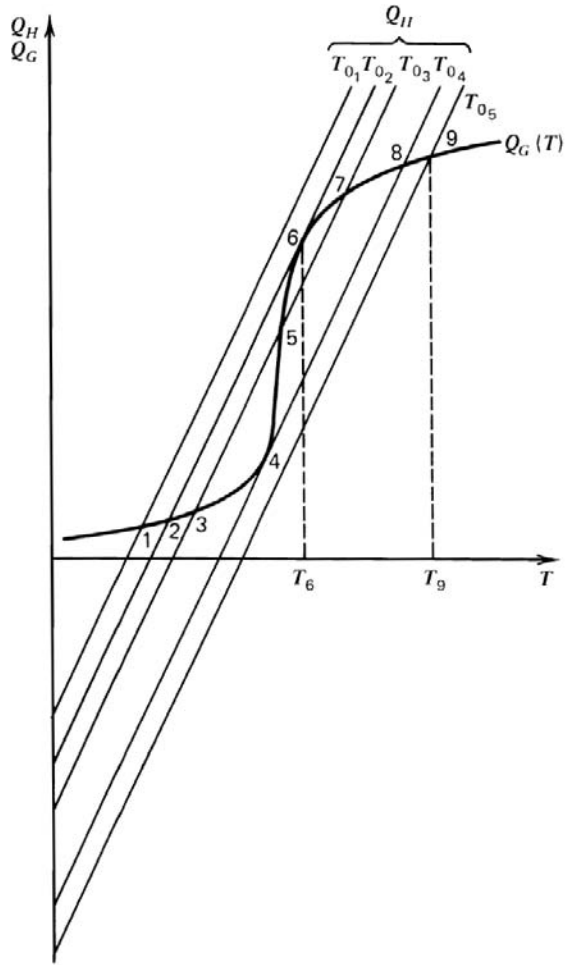

Figure 10.4.1-1

Shift of heat removal line Q_H with increasing feed temperature T_0 and resulting shift of intersection with heat generation curve, Q_G.

This multiplicity of steady states is caused by the highly nonlinear nature of the heat generation expression and by the internal thermal feedback associated with complete mixing. Note that the phenomenon is not limited to completely mixed reactors but can also occur with plug flow reactors with external recycle, as discussed by van Heerden [1953] and, a long time before, by Liljenroth [1918] (see Chapter 11).

Of the three possible steady states 3, 5, and 7, the middle one is unstable, while 3 and 7 are naturally stable. Van Heerden explained this in terms of the shapes of Q_G and Q_H at these points. A small increase in temperature from T_5 leads to a more important increase of Q_G than of Q_H, since the slope of Q_G at 5 is much larger than that of Q_H. Consequently, the reactor temperature increases to a value T_7, corresponding with the higher intersection and a higher conversion. A slight decrease in reactor temperature would again have a larger effect on Q_G than on Q_H, and the reactor would continue to cool until T_3 is reached, corresponding to a low conversion. Point 5, therefore, corresponds to an unstable steady state and would not be maintained without automatic control. By the same reasoning, based on the local slopes of Q_G and Q_H, it can be shown that the conditions corresponding to points 3 and 7 are naturally stable.

If T_0 is slowly increased from T_{0_1} to T_{0_3}, the reactor will behave as indicated by the so-called lower branch of the *S* curve. But as T_0 slightly exceeds T_{0_4}, the reactor conditions jump to values corresponding to point 8, on the upper branch of the Q_G curve. The reactor is said to ignite. Any further increase in T_0 leads to a gradual increase in T along the upper branch. Upon reducing T_0 from T_{0_5} to T_{0_2}, for example, the temperature slowly decreases, but any further decrease in T_0 leads to an intersection 2 on the lower branch. The reactor is said to be quenched. Further decreasing T_0 now leads to a gradual decrease in T. The hysteresis of reactor conditions upon increasing and decreasing one of the operating parameters, in this case T_0, is typical for the occurrence of multiple steady states. It is illustrated in Fig. 10.4.1-2.

An experimental illustration of the above theoretical derivations was provided by Vejtassa and Schmitz [1970] by means of the exothermic reaction between sodium thiosulfate and hydrogen peroxide in an adiabatic flow reactor with complete mixing.

For an adiabatic reactor (10.4.1-1) and (10.4.1-2) can be combined to give

$$x_A = \lambda(T - T_0)$$

This relationship between conversion and temperature can be used to express the

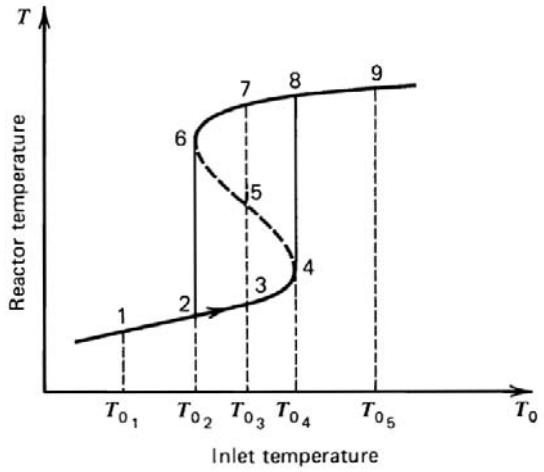

Figure 10.4.1-2

Hysteresis of steady reactor temperature T upon variation of feed temperature T_0.

rate of reaction solely in terms of the temperature, so that (10.4.1-3) becomes

$$\frac{1}{\lambda C_{A0}} r_A(T) = \frac{1}{\tau}(T - T_0)$$

The heat generation curve shown in Fig. 10.4.1-3 was derived from adiabatic batch reactor data. For given inlet concentration this curve depends only on the reactor temperature. Each point on the curve corresponds to a given conversion and holding time, therefore reactor temperature. The increasing part results from the increase of the reaction rate with temperature, while the decreasing part reflects the depletion of reactants. The curve drops to zero as the complete adiabatic temperature rise is achieved; that is, the reaction rate drops to zero as the limiting reactant, hydrogen peroxide, is completely consumed. Heat is only removed through the exit stream. The heat removal is a function of $T - T_0$, with T_0 a constant. For each value of T, and therefore of τ, a different straight line is obtained. The steady state requires $Q_H = Q_G$, and Fig. 10.4.1-3 illustrates how three steady states are possible with this reaction between holding times of 6.8 and 17.8 s. Figure 10.4.1-4 shows the hysteresis observed in the steady state when the holding time is progressively increased and decreased.

Multiplicity of steady states was also observed by Schmidt et al. [1984] who studied the solution polymerization of methylmethacrylate in a continuous stirred tank with complete mixing. With endothermic reactions the straight lines $Q_H(T)$ have negative slopes, and only one intersection is possible.

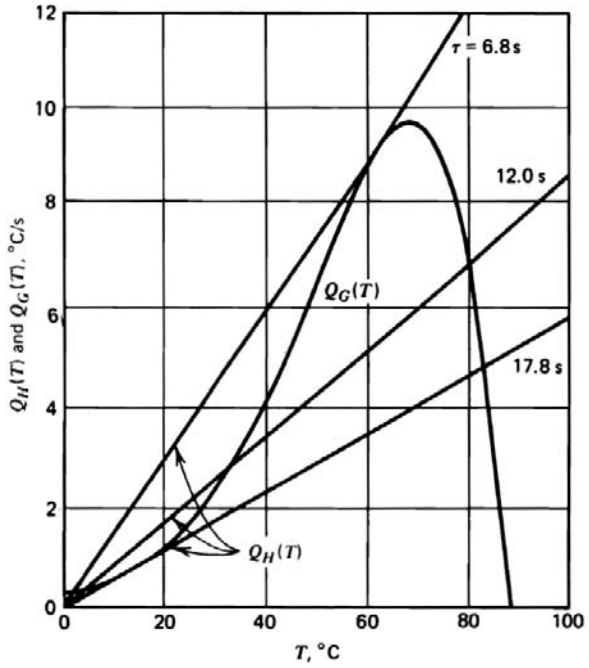

Figure 10.4.1-3

Heat generation and removal functions versus reactor temperature for a feed mixture of 0.8-*M* $Na_2S_2O_3$ and 1.2-*M* H_2O_2 at 0°C. From Vejtassa and Schmitz [1970].

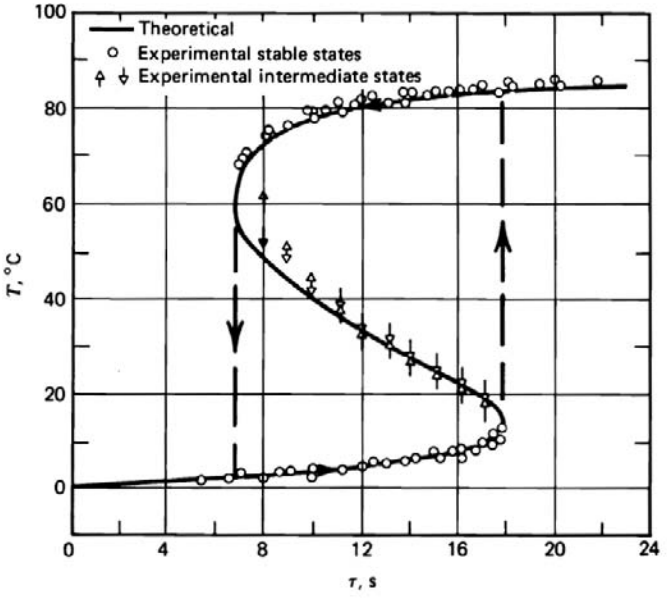

Figure 10.4.1-4

Steady-state hysteresis results. From Vejtassa and Schmitz [1970].

Reversible exothermic reactions have an ultimate decrease in rate with temperature, and so the heat generation curve turns down (as in Fig. 10.4.1-3); therefore, the qualitative features remain the same. The heat generation curve for complex reactions can have more than one "hump", and thus more than three steady states are possible for given operating condition. The humps also tend to be smaller, leading to more readily obtained transitions between steady states [Westerterp, 1969]. Also, other types of multiple steady states and instabilities can occur. For example, with certain forms of rate expressions highly nonlinear in concentration, just the mass balance (10.4.1-1) may have more than one solution, as discussed in Perlmutter [1972].

These considerations can be cast in analytical form, following the reasoning of van Heerden [1953] given above. The slopes of the heat removal and generation rates in (10.4.1-3) are found as follows:

$$\frac{dQ_H}{dT} = \frac{d}{dT}\left\{\frac{1}{\tau}[T - T_0 + Q_H(T)]\right\} = \frac{1}{\tau}\left(1 + \frac{dQ_H}{dT}\right) \qquad (10.4.1\text{-}4)$$

$$\frac{dQ_G}{dT} = \frac{d}{dT}\left[\frac{1}{\lambda C_{A0}} r_A(x_A, T)\right] \qquad (10.4.1\text{-}5)$$

Now,

$$\frac{dr_A}{dT} = \frac{\partial r_A}{\partial x_A}\frac{dx_A}{dT} + \frac{\partial r_A}{\partial T}$$

$$= \frac{\partial r_A}{\partial x_A} \cdot \frac{\tau}{C_{A0}}\frac{dr_A}{dT} + \frac{\partial r_A}{\partial T}$$

where the last line utilized the mass balance (10.4.1-1). The total change of the heat generation rate with temperature is

$$\frac{dQ_G}{dT} = \frac{\dfrac{1}{\lambda C_{A0}}\dfrac{\partial r_A}{dT}}{1 - \dfrac{\tau}{C_{A0}}\dfrac{\partial r_A}{\partial x_A}} \qquad (10.4.1\text{-}6)$$

Then, the reactor *can* be stable if the heat removal slope is greater than the heat generation slope at the steady-state operating point, that is, when

$$\frac{dQ_H}{dT} > \frac{dQ_G}{dT}$$

leading to

$$\left(1-\frac{\tau}{C_{A0}}\frac{\partial r_A}{\partial x_A}\right)\left(1+\frac{dQ_H}{dT}\right)>\frac{\tau}{\lambda C_{A0}}\frac{\partial r_A}{\partial T} \qquad (10.4.1\text{-}7)$$

For the case of a first-order irreversible reaction in a reactor with simple heat exchange, from (10.4.1-3) with (10.4.1-1), this criterion becomes

$$(1+k\tau)\left(1+\frac{UA_k}{\rho_f c_p F_0'}\right)>\frac{1}{\lambda}\frac{E}{RT^2}\frac{k\tau}{1+k\tau} \qquad (10.4.1\text{-}8)$$

Equation (10.4.1-7) is a necessary but not sufficient condition for stability. In other words, if the criterion is satisfied, the reactor may be stable; if it is violated, the reactor will be unstable. (Aris [1965] prefers to use the reverse inequality as a sufficient condition for instability.) The reason is that in deriving (10.4.1-6), it was implicitly assumed that only the special perturbations in conversion and temperature related by the steady-state heat generation curve were allowed. To be a general criterion giving both necessary and sufficient conditions, arbitrary perturbations in both conversion and temperature must be considered. Van Heerden's reasoning actually implied a sense of time ("tends to move ..."). Therefore, the proper criteria can only be clarified and deduced by considering the complete transient mass and energy balances.

10.4.2 Transient Behavior

The transient mass and energy balances are given by (10.2.1-2) and (10.2.1-4):

$$\tau\frac{dx_A}{dt}=-x_A+\tau\frac{r_A}{C_{A0}} \qquad (10.4.2\text{-}1)$$

$$\tau\frac{dT}{dt}=T_0-T+\frac{\tau}{\lambda}\frac{r_A}{C_{A0}}-Q_H(T) \qquad (10.4.2\text{-}2)$$

Analytical solution of this system of differential equations is not possible. Therefore, Aris and Amundson [1958] linearized it by a Taylor expansion, about the steady-state operating points. Consider the small perturbations

$$x=x_A-x_{A,s}$$

$$y=T-T_s$$

where the subscript *s* refers to a steady-state solution. Then, subtracting equations (10.4.1-1) and (10.4.1-2) from equations (10.4.2-1) and (10.4.2-2) gives

$$\tau \frac{dx}{dt} = -x + \frac{\tau}{C_{A0}}(r_A - r_{A,s}) \tag{10.4.2-3}$$

$$\tau \frac{dy}{dt} = -y + \frac{\tau}{\lambda C_{A0}}(r_A - r_{A,s}) - [Q_H(T) - Q_H(T_s)] \tag{10.4.2-4}$$

Expanding r_A and $Q_H(T)$ in Taylor series and neglecting second-order terms leads to

$$r_A = r_{A,s} + \left(\frac{\partial r_A}{\partial x_A}\right)_s x + \left(\frac{\partial r_A}{\partial T}\right)_s y$$

$$Q_H(T) = Q_H(T_s) + \left(\frac{dQ_H}{dT}\right)_s y$$

Substituting into (10.4.2-3) and (10.4.2-4) yields

$$\tau \frac{dx}{dt} = -\left[1 - \frac{\tau}{C_{A0}}\left(\frac{\partial r_A}{\partial x_A}\right)_s\right]x + \left[\frac{\tau}{C_{A0}}\left(\frac{\partial r_A}{\partial T}\right)_s\right]y \tag{10.4.2-5}$$

$$\tau \frac{dy}{dt} = \left[\frac{\tau}{\lambda C_{A0}}\left(\frac{\partial r_A}{\partial x_A}\right)_s\right]x - \left[1 - \frac{\tau}{\lambda C_{A0}}\left(\frac{\partial r_A}{\partial T}\right)_s + \left(\frac{dQ_H}{dT}\right)_s\right]y \tag{10.4.2-6}$$

These equations, (10.4.2-5) and (10.4.2-6), are linear differential equations whose solutions are combinations of exponentials of the form $\exp[mt/\tau]$, where the values of m are solutions of the characteristic equation

$$m^2 + a_1 m + a_0 = 0 \tag{10.4.2-7}$$

where

$$a_1 = \left[1 - \frac{\tau}{C_{A0}}\left(\frac{\partial r_A}{\partial x_A}\right)_s\right] + \left[1 + \left(\frac{dQ_H}{dT}\right)_s\right] - \left[\frac{\tau}{\lambda C_{A0}}\left(\frac{\partial r_A}{\partial T}\right)_s\right]$$

$$a_0 = \left[1 - \frac{\tau}{C_{A0}}\left(\frac{\partial r_A}{\partial x_A}\right)_s\right]\left[1 + \left(\frac{dQ_H}{dT}\right)_s\right] - \left[\frac{\tau}{\lambda C_{A0}}\left(\frac{\partial r_A}{\partial T}\right)_s\right]$$

The solutions will only go to zero as $t \to \infty$ when the real parts of the roots are negative [e.g., see Himmelblau and Bischoff, 1968]. The solution of (10.4.2-7) is

$$m = \frac{1}{2}(-a_1 \pm \sqrt{a_1^2 - 4a_0})$$

This stability condition is always met when

$$a_1 > 0 \tag{10.4.2-8}$$

and

$$a_0 > 0 \tag{10.4.2-9}$$

If $a_0 < 0$, at least one of the roots will be positive, and the solution will diverge for $t \to \infty$. If $a_1 = 0$ and $a_0 > 0$, the roots will be purely imaginary numbers, with oscillatory solutions for x and y. Thus, the necessary and sufficient conditions for stability (i.e., x_A and T return to the steady state after removal of the perturbation or x and $y \to 0$ as $t \to \infty$) are equations (10.4.2-8) and (10.4.2-9). In terms of the physical variables those equations can be written as follows:

$$\left[1-\frac{\tau}{C_{A0}}\left(\frac{\partial r_A}{\partial x_A}\right)_s\right]+\left[1+\left(\frac{dQ_H}{dT}\right)_s\right]>\left[\frac{\tau}{\lambda C_{A0}}\left(\frac{\partial r_A}{\partial T}\right)_s\right] \tag{10.4.2-10}$$

and

$$\left[1-\frac{\tau}{C_{A0}}\left(\frac{\partial r_A}{\partial x_A}\right)_s\right]\left[1+\left(\frac{dQ_H}{dT}\right)_s\right]>\left[\frac{\tau}{\lambda C_{A0}}\left(\frac{\partial r_A}{\partial T}\right)_s\right] \tag{10.4.2-11}$$

Comparing (10.4.2-11) with (10.4.1-7) reveals that they are identical, and the above discussion shows that the "slope" criterion, $a_0 > 0$, is indeed a necessary condition for stability. Also, the condition $a_0 > 0$ is not sufficient, for if $a_1 = 0$, the oscillations are not stable, in that x_A and T do not return to their steady-state values. Thus, the second criterion, (10.4.2-10), is related to oscillatory behavior—a discussion is given by Gilles and Hofmann [1961].

For the case of a first-order irreversible reaction with simple heat exchange, the second ("dynamic") criterion (10.4.2-10) becomes

$$(1+k\tau)+\left(1+\frac{UA_k}{\rho_f c_p F_0'}\right)>\frac{1}{\lambda}\frac{E}{RT^2}\frac{k\tau}{1+k\tau} \tag{10.4.2-12}$$

For an adiabatic reactor, in which $Q_H \equiv 0$, the "slope" criterion (10.4.2-11) implies the other equation (10.4.2-10). In that case the slope criterion is both necessary and sufficient.

EXAMPLE 10.4.2.A

TEMPERATURE OSCILLATIONS IN A MIXED REACTOR FOR THE VAPOR-PHASE CHLORINATION OF METHYL CHLORIDE

The reaction

$$CH_3Cl \xrightarrow{Cl_2} CH_2Cl_2 \xrightarrow{Cl_2} CHCl_3 \xrightarrow{Cl_2} CCl_4$$

was studied by Bush [1969]. First, the steady-state heat generation and removal rates were determined as shown in Fig. 10.4.2.A-1.

The necessary "slope" criterion is satisfied over the entire range of conditions:

$$\frac{dQ_H}{dT} > \frac{dQ_G}{dT}$$

so that there may be a unique steady-state reactor temperature for a given bath temperature T_r.

It was found, however, that the reactor showed oscillatory behavior in certain ranges [see Bush, 1972]. Therefore, the second "dynamic" criterion, (10.4.2-10) was also checked with relationships similar to (10.4.2-12), but also accounting for some of the additional complexities in the real (gas phase) experimental system. The results are shown in Fig. 10.4.2.A-2, where the left-hand side (LHS) and right-hand side (RHS) of the criterion are plotted. A central region exists where the criterion is violated.

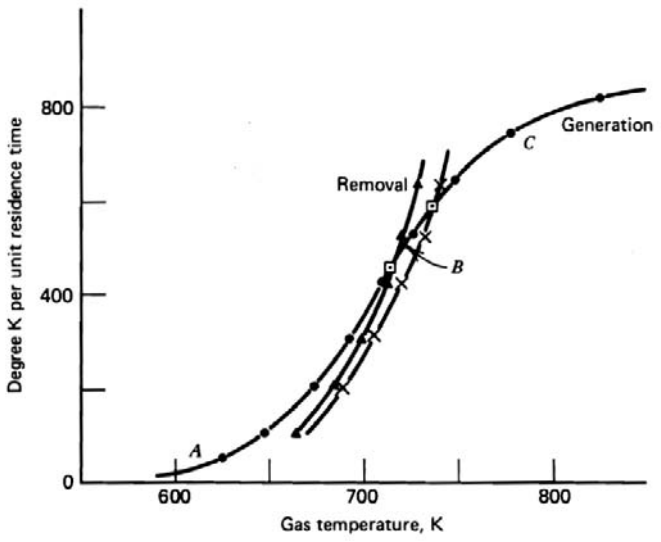

Figure 10.4.2.A-1

Steady-state temperature: ●, heat evolution; ×, heat removal for T_r = 400°C; ▲, heat removal for T_r = 390°C; □, steady-state temperatures T_s. From Bush [1969].

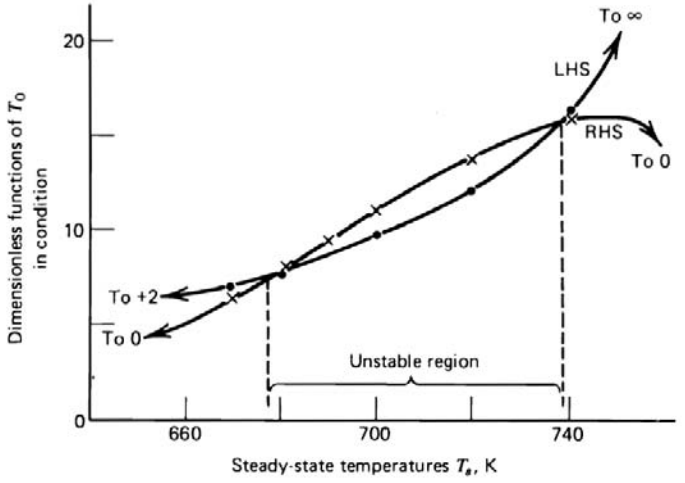

Figure 10.4.2.A-2

Stable and unstable reaction temperatures: ●, LHS; ×, RHS. From Bush [1969].

If a control device acts upon the reactor temperature e.g., by modifying the flow rate of the heat exchanging fluid, Q_H in (10.4.2-2) has to be adapted into

$$Q_H + [\beta + \mu(T - T_s)]$$

and the corresponding term in the linearized equation (10.4.2-6) is changed into

$$\left(\frac{dQ_H}{dT}\right)_s \rightarrow \left(\frac{dQ_H}{dT}\right)_s + \mu$$

This adapted derivative has to be substituted into the two criteria, (10.4.2-10) and (10.4.2-11). This will increase the value of the LHS and make it easier to satisfy the criteria. An inherently unstable reactor can be made stable by proper control. Real life control problems require more detail, however.

All of the above conclusions were based on the linearized equations for small perturbations about the steady state. A theorem of differential equations states that if the linearized calculations show stability, then the nonlinear equations will also be stable for sufficiently small perturbations. For larger excursions, the linearizations are no longer valid, and the only recourse is to (numerically) solve the complete equations. Uppal, Ray, and Poore [1974] performed extensive calculations and laid the basis for a detailed mathematical classification of the many various behavior patterns possible; refer to the original work for the extremely complex results. The evolution of multiple steady states when the mean holding time is varied leads to even more bizarre possible behavior [see Uppal et al., 1976]. Further aspects can be found in Aris [1965],

Perlmutter [1972], and Denn [1975], and in reviews of Schmitz [1975], Razón and Schmitz [1987], and Morbidelli et al. [1987]. Balakotaiah and Luss [1982, 1983, 1984] presented penetrating analyses of multiplicity encountered with parallel and consecutive reactions using singularity theory. The fundamentals of multiplicity of steady states and oscillatory behavior have been studied extensively by Prigogine and his co-workers, also in living organisms [Babloyantz, 1986].

PROBLEMS

10.1 Kermode and Stevens [1965] studied the reaction of ammonia and formaldehyde to make hexamine:

$$\underset{\text{(A)}}{4NH_3} + \underset{\text{(B)}}{6HCHO} \rightarrow (CH_2)_6N_4 + 6H_2O$$

The continuous flow reactor was a 490-cm^3 baffled stainless steel tank stirred at 1800 rpm, with several precautions to ensure almost perfect mixing. The overall reaction had a rate

$$r_A = kC_AC_B^2 \quad \text{mol } A/\text{l s}$$

with $k = 1.42 \times 10^3 \exp(-3090/T)$. The reactants were fed in streams of 1.50 cm^3/s, with the ammonia concentration 4.06 mol/l and the formaldehyde concentration 6.32 mol/l. The temperature in the reactor was 36°C. Calculate C_A and C_B, the concentrations in the reactor and in the effluent.

10.2 A perfectly mixed flow reactor is to be used to carry out the reaction $A \rightarrow R$. The rate is given by

$$r_A = kC_A \quad \text{kmol/m}^3\text{ s}$$

with

$$k = 4 \times 10^6 \exp\left[-\frac{8000}{T\,(\text{K})}\right] \quad \text{s}^{-1}$$

Other physicochemical data are

ΔH = -167,480 kJ ρc_p = 4,187 kJ/m^3°C
M_A = 100 kg/kmol C_{A0} = 1 kmol/m^3

At a temperature of 100°C and a desired production rate of 0.4 kg/s, determine **(a)** the reactor volume required at a conversion of 70 percent; **(b)** the heat exchange requirement.

10.3 The first-order reversible reaction

$$A \underset{2}{\overset{1}{\rightleftharpoons}} R$$

is carried out in a constant-volume perfectly mixed flow reactor. The feed contains only A, at a concentration of C_{A0}, and all initial concentrations are zero.

(a) Show that the concentration of A is given by

$$\frac{C_A}{C_{A0}} = \frac{1+k_2\tau}{1+k_1\tau+k_2\tau} - \frac{k_2}{k_1+k_2}e^{-t/\tau} - \frac{k_1 e^{-(1+k_1\tau+k_2\tau)t/\tau}}{(k_1+k_2)(1+k_1\tau+k_2\tau)}$$

where $\tau = V/F'$ = mean residence time.

(b) Find C_A/C_{A0} at steady state, and also show that for very rapid reactions, $(k_1,k_2) \to \infty$, the equilibrium concentration is

$$\frac{C_A}{C_{A0}} = \frac{1}{1+K} \qquad K \equiv \frac{k_1}{k_2}$$

(c) For very rapid reactions, $(k_1,k_2) \to \infty$, show that, in general,

$$\frac{C_A}{C_{A0}} = \frac{1}{1+K} - \frac{1}{1+K}e^{-t/\tau}$$

and explain how this can be physically interpreted as the final steady-state equilibrium minus the equilibrium "washout".

10.4 For a first-order reaction, the conversion to be expected in a series of n stirred tanks can be formed from Fig. 10.2.2-1. Alternatively, at given conversion level, and for a given rate coefficient and mean residence time, $k\tau$, the total volume required to carry out the reaction can be determined.

(a) With this basis, plot $V_{\text{total}}/V_{\text{plug flow}}$ versus the fraction of unreacted reactant, $1 - x_A$, for various values of n = 1, 2, 5, 10, 40. Study the effect of utilizing several stirred tank reactors in series compared to a plug flow reactor.

(b) Add further lines of constant values of the dimensionless group $k\tau_{\text{total}}$ to the plot — these are convenient for reactor design calculations.

10.5 **(a)** For the reversible consecutive reactions

$$A \underset{2}{\overset{1}{\rightleftharpoons}} R \underset{4}{\overset{3}{\rightleftharpoons}} S$$

taking place in a steady-state, constant-volume perfectly mixed reactor, show that the concentration of *R*, when the feed contains only *A* at concentration C_{A0}, is

$$\frac{C_R}{C_{A0}} = \frac{\dfrac{k_1\tau}{1+k_1\tau}\left(1+\dfrac{k_2\tau}{K_b}\right)}{\left(\dfrac{k_1\tau}{1+k_1\tau}\dfrac{1}{K_a}+1\right)\left(1+\dfrac{k_2\tau}{K_b}\right)+k_2\tau}$$

where

$K_a = k_1/k_2$ = equilibrium constant for the first reaction

$K_b = k_3/k_4$

(b) For both reactions irreversible, show that the results of part (a) reduce to the equation given in Section 10.3.

(c) If the first reaction is very rapid, it is always close to its equilibrium as *R* is reacting further to *S*. Explain how this can be represented by $k_1 \to \infty$ but K_a = finite, and find the expression for C_R/C_{A0} by appropriately reducing the result of part (a). This is similar to a rate-determining step situation, and is more simply derived by taking the first reaction to always be in instantaneous equilibrium, $C_A \approx C_R/K_a$. Show that a new derivation of the mass balances with this basis leads to the same result as above. Note that this is a useful technique in more complex situations of this type, when the general expression may not be possible to derive.

10.6 Consider the startup of a perfectly mixed flow reactor containing a suspended solid catalyst. For a first-order reaction, $r_A = kC_A$, and assuming constant volume, show that the outlet concentration of reactant *A* is

$$\frac{C_A(t)}{C_{A0}} = \frac{1}{\left[1+\frac{(1-\varepsilon)V}{F'}k\right]} + \left\{\frac{C_A(0)}{C_{A0}} - \frac{1}{\left[1+\frac{(1-\varepsilon)V}{F'}k\right]}\right\} \times \exp\left\{-\left[1+\frac{(1-\varepsilon)V}{F'}k\right]\left(\frac{F'}{\varepsilon V}t\right)\right\}$$

where

$C_A(0)$ = initial concentration

C_{Ai} = feed concentration

ε = void fraction, not occupied by solids

εV = fluid volume

Note that the steady-state ($t \rightarrow \infty$) result depends only on the group $(1 - \varepsilon)\, Vk/F'$, the *solid catalyst* inverse space velocity-rate coefficient group, but the transient effects also require knowledge of $(F'/\varepsilon V)^{-1}$, or the *fluid* mean residence time.

10.7 In a process to make compound *R*, the following reactions occur:

$$A + B \xrightarrow{1} 2R$$

$$A + A \xrightarrow{2} 2S$$

(a) Based on the text, explain why the optimum chemical composition would be high *B* and low *A* concentrations.

(b) An idealized reactor configuration to achieve this is reactor with side stream feeds of *A*, as shown below:

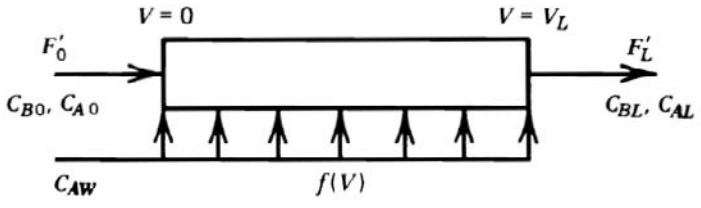

where $f(V)$ (in m^3 side feed/h m^3 reactor volume) is the distribution of side feed additions along the reactor length (volume) to be determined. Assuming the reactor to operate with plug flow, derive the following mass balances:

Total:

$$\frac{dF'}{dV} = f(V)$$

A:

$$\frac{d}{dV}(F'C_A) = C_{AW} f(V) - k_1 C_A C_B - k_2 C_A^2$$

B:

$$\frac{d}{dV}(F'C_B) = -k_1 C_A C_B$$

(c) As an appropriate optimal design, the condition will be used that the side feed be adjusted to maintain C_A = constant (i.e., $C_A = C_{A0} = C_{AL}$). Also, a high conversion of *A* is desired, and to simplify the calculations, it will be assumed that the side feed concentration is high, $C_{AW} >> C_A = C_{A0} = C_{AL}$. For these special conditions, show that the three mass balances become

$$F' \cong \text{ constant } = F_0'$$

$$0 = C_{AW} f(V) - k_1 C_{AL} C_B - k_2 C_{AL}^2$$

$$F' \frac{dC_B}{dV} = -k_1 C_{AL} C_B$$

(d) Using the simplified balances, determine the total reactor volume required as a function of F_0', C_{Al}, C_{B0}, and C_{BL}.

(e) Show that to maintain the above condition of constant C_A, the side feed distribution as a function of reactor length, has to satisfy

$$f(V) = \frac{C_{AL}}{C_{AW}} \left(k_2 C_{AL} + k_1 C_{B_0} e^{-k_1 C_{AL} V / F_0'} \right)$$

(f) As a final condition, equal stoichiometric feeds of *A* and *B* are to be used:

$$F_0' C_{B0} = F_0' C_{A0} + C_{AW} \int_0^{V_L} f(V) dV$$

Show for this case that the relationship between the outlet levels of *A* and *B* is

$$C_{AL} = \frac{C_{BL}}{1 - \dfrac{k_2}{k_1} \ln \dfrac{C_{BL}}{C_{B0}}}$$

(g) A useful measure is the weight yield of the desired *R*:

$$Y \equiv \frac{\text{total } R \text{ formed}}{\text{total } A \text{ fed}}$$

For $k_2/k_1 = 1$, compare the yield as a function of conversion with that found in a single perfectly mixed reactor and with a single plug flow reactor without side feeds.

Note:
This problem was first solved by van de Vusse and Voetter [1961], who also considered more general cases and a true mathematically optimal profile, *f*(*V*). These latter results were rather close to the approximately optimal basis of C_A = constant. Finally, such an ideal scheme might be implemented in practice by using a series of stirred tank reactors with intermediate feed additions of *A*.

10.8 A perfectly mixed reactor is to be used for the hydrogenation of olefins and will be operated isothermally. The reactor is 10 m^3 in size, and the feed rate is 0.2 m^3/s, with a concentration of C_{A0} = 13 $kmol/m^3$. For the conditions in the reactor, the rate expression is

$$r_A = \frac{C_A}{(1 + C_A)^2} \frac{\text{kmol}}{\text{m}^3 \cdot \text{s}}$$

It is suspected that this nonlinear rate form, which has a maximum value, may cause certain regions of unstable operation with multiple steady states.

(a) From the reactor mass balance (10.2.2-2), determine if this is the case by plotting r_A and $(1/\tau)(C_{A0} - C_A)$ on the same graph.

(b) To what concentration(s) should the feed be changed to avoid this problem?

Note:
This problem was investigated by Matsuura and Kato [*Chem. Eng. Sci.*, 22, 17 (1967)], and general stability criteria are provided by Luss [*Chem. Eng. Sci.*, 26, 1713 (1970)].

10.9 Using the expressions for the necessary and sufficient conditions for stability of a stirred tank chemical reactor as derived in Section 10.4,

(a) Show that for a single endothermic reaction the steady state is always stable.

(b) Show that for an adiabatic reactor the slope condition

$$\left[1-\frac{\tau}{C_{A0}}\left(\frac{\partial r_A}{\partial x_A}\right)_s\right]\left[1+\left(\frac{dQ_H}{dT}\right)_s\right]>\left[\frac{\tau}{\lambda C_{A0}}\left(\frac{\partial r_A}{\partial T}\right)_s\right]$$

is sufficient, as well as necessary.

(c) If the reactor is controlled on concentration,

$$Q_H(x, y) = Q_H(y) + vx$$

show that it is not always possible to get control of an unstable steady state. Note here that $Q_H = Q_H(x, y)$, and be careful of the criteria that you use.

10.10 Show that recycling the effluent of a perfectly mixed reactor has no effect on the conversion.

10.11 Consider two perfectly mixed reactors in series. For a given total volume, determine optimal distribution of the subvolumes for **(a)** first-order reaction, **(b)** second-order reaction.

REFERENCES

Aris, R., *Introduction to the Analysis of Chemical Reactors*, Prentice-Hall, Englewood Cliffs, N.J. (1965).

Aris, R., and Amundson, N.R., *Chem. Eng. Sci.*, 7, 121 (1958).

Babloyantz, A., *Molecules, Dynamics and Life*, Wiley, NY (1986).

Baccaro, G.P., Gaitonde, N.Y., and Douglas, J.M., *AIChE J.*, 16, 249 (1970).

Bailey, J.E., *Chem. Eng. Commun.*, 1, 111 (1973).

Balakotaiah, V., and Luss, D., *Chem. Eng. Sci.*, 37, 433 (1982); 38, 1709 (1983); 39, 865 (1984).

Bischoff, K.B., *Can. J. Chem. Eng.*, 44, 281 (1966).

Bush, S.F., *Proc. Roy. Soc.*, A309, 1 (1969).

Bush, S.F., in *Proc. 1st Int. Symp. Chem. React. Eng. Amer. Soc. Adv. Chem.*, Ser. No. 109, p. 610, Washington, D.C. (1972).

Chang, M., and Schmitz, R.A., *Chem. Eng. Sci.*, 30, 21 (1975).

Denbigh, K.G., *Trans. Farad. Soc.*, 40, 352 (1944); 43, 648 (1947); *J. Appl. Chem.*, 1, 227 (1951).

Denn, M.M., *Stability of Reaction and Transport Processes*, Prentice-Hall, Englewood Cliffs, N.J. (1975).

Gerrens, H., in *Proc. 4th Int. Symp. Chem. Reac. Eng.*, 585-614, Dechema (1976).

Gilles, E. D., and Hofmann, H., *Chem. Eng. Sci.*, 15, 328 (1961).

Gillespie, B.M., and Carberry, J.J., *Chem. Eng. Sci.*, 21, 472 (1966).

Himmelblau, D.M., and Bischoff, K.B., *Process Analysis and Simulation*, Wiley, New York (1968).

Keane, T.R., in *Proc. 2nd Int. Symp. React. Eng.*, Elsevier, Amsterdam (1972).

Kermode, R.I., and Stevens, W.F., *Can. J. Chem. Eng.*, 43, 68 (1965).

Kiparissides C., *Chem. Eng. Sci.*, 31, 1637 (1996).

Kramers, H., and Westerterp, K.R., *Elements of Chemical Reactor Design and Operation*, Academic Press, New York (1963).
Laurence R.L., and Chiovetta, M.G., in *Proc. of Berlin Workshop on Polymer Reactor Engineering*, K.H. Reichert, Carl Hanser Verlag, Munich (1983).
Levenspiel, O., *Chemical Reaction Engineering*, 1st ed., Wiley, New York (1962).
Levenspiel, O., *Chemical Reaction Engineering*, 2nd ed., Wiley, New York (1972).
Liljenroth, F.G., *Chem. Metal. Eng.*, 19, 287 (1918).
Luss, D., *Chem. Eng. Sci.*, 20, 17 (1965).
Min, K.W., and Ray, W.H.J., *Macromolec. Sci.-Rev. Macromolec. Chem.*, C11, 177 (1974).
Morbidelli, M., Varma, A., and Ans, R., in *Chemical Reaction and Reactor Engineering*, ed. by J.J. Carberry and A. Varma, M. Dekker, New York (1987).
Nagasubramanian, K., and Graessley, W.W., *Chem. Eng. Sci.*, 25, 1549, 1559 (1970).
Nauman, E.B., *J. Macromolec. Sci.-Rev. Macromolec. Chem.*, C10, 75 (1974).
Paynter, J.D., and Haskins, D.E., *Chem. Eng. Sci.*, 25, 1415 (1970).
Perlmutter, D.D., *Stability of Chemical Reactors*, Prentice-Hall, Englewood Cliffs, N.J. (1972).
Ray, W.H., *Can. J. Chem. Eng.*, 47, 503 (1969).
Ray, W.H., *J. Macromolec. Sci.-Rev. Macromolec. Chem.*, C8, 1 (1972).
Razón, L.F., and Schmitz, R.A., in *Plenary Papers, 9th Intl. Symp., Chem. Eng. Sci.*, 42, 1005 (1987).
Russell, T.W.F., and Buzzelli, D.T., *Ind. Eng. Chem. Proc. Des. Dev.*, 8, 2 (1969).
Schmidt, A.D., Clinch, A.B., and Ray, W.H. *Chem. Eng. Sci.*, 39, 419 (1984).
Schmitz, R.A., in *Proc. 3rd Int. Symp. Chem. React. Eng. Rev.*, ed. H.M. Hulburt, Am. Chem. Soc. Adv. Chem. Ser. 148, Washington, D.C. (1975).
Schoenemann, K., *Dechema Monographien*, 21, 203 (1952).
Shinnar, R., and Katz, S., in *Proc. 1st Int. Symp.*, Am. Chem. Soc. Adv. Chem. Ser. 109, Washington, D.C. (1972).
Tirrell, M., Galvan, R., and Laurence, R.L., *Chemical Reaction and Reactor Engineering*, ed. by J.J. Carberry and A. Varma, Marcel Dekker, New York (1987).
Uppal, A., Ray, W.H., and Poore, A.B., *Chem. Eng. Sci.*, 29, 967 (1974).
Uppal, A., Ray, W.H., and Poore, A.B., *Chem. Eng. Sci.*, 31, 205 (1976).
van de Vusse, J.G., *Chem. Eng. Sci.*, 19, 994 (1964).
van de Vusse, J.G., *Chem. Eng. Sci.*, 21, 611 (1966).
van de Vusse, J.G., and Voetter, H., *Chem. Eng. Sci.*, 14, 90 (1961).
van Heerden, C., *Ind. Eng. Chem.*, 45, 1245 (1953).
Vejtassa, S.A., and Schmitz, R.A., *AIChE J.*, 16, 410 (1970).
Wei, J., *Can. J. Chem. Eng.*, 44, 31 (1966).
Westerterp, K.R., *Chem. Eng. Sci.*, 17, 423 (1969).

Get Chapter 11

Fixed Bed Catalytic Reactors

PART ONE
INTRODUCTION

11.1 THE IMPORTANCE AND SCALE OF FIXED BED CATALYTIC PROCESSES

The discovery of solid catalysts and their application to chemical processes in the early years of the 20th century has led to a breakthrough of the chemical industry. Since then, this industry has diversified and grown in a spectacular way through the development of new or the rejuvenation of established processes, mostly based on the use of solid catalysts.

The major part of these catalytic processes is carried out in fixed bed reactors. Some of the main fixed bed catalytic processes are listed in Table 11.1-1. Except for the catalytic cracking of gasoil, which is carried out in a fluidized bed to enable the continuous regeneration of the catalyst, the main solid catalyzed processes of today's chemical and petroleum refining industries appear in this table. It should be added that there are also fluidized bed alternatives for phthalic anhydride and ethylene dichloride synthesis. Furthermore, Table 11.1-1 is limited to fixed bed processes with only one fluid phase; trickle bed processes (e.g., encountered in the hydrotreatment and hydrocracking of heavier petroleum fractions) are not included in the present chapter. Finally, important processes

TABLE 11.1-1
MAIN FIXED BED CATALYTIC PROCESSES[a]

Basic Chemical Industry	Petrochemical Industry	Petroleum Refining
Steam reforming	Ethylene oxide	Catalytic reforming
{ primary	Ethylene dichloride	Isomerization
{ secondary	Vinylacetate	Polymerization
Water-gas-shift		
CO-methanation	Butadiene	(Hydro)desulfurization
Ammonia }	Maleic anhydride	Hydrocracking
Sulfuric }	Phthalic anhydride	
acid } synthesis		
Methanol }	Cyclohexane	
Oxo }	Styrene	
	Hydrodealkylation	

[a]From Froment [1974].

such as ammonia oxidation for nitric acid production or hydrogen cyanide synthesis, in which the catalyst is used in the form of a few layers of gauze, are also omitted from Table 11.1-1.

Today's fixed bed reactors are mainly large-capacity units. Between 1950 and 1970 the capacity of phthalic anhydride synthesis reactors increased from 10,000 to 300,000 T/year and that of ammonia synthesis reactors from 50,000 to 500,000 T/year. Such a spectacular rise in reactor capacity is evidently tied to the growing market demand, but its realization undoubtedly also reflects progress in both technological and fundamental areas, pressed by the booming construction activity of the sixties and early seventies. Saturated markets and the construction of production units in newly industrialized countries have slowed down this capacity increase in the eighties. The present decade saw new spectacular developments. The utilization of remote natural gas and the associated transport problems has provided a new impetus to the development and construction of giant reactors for its conversion near the production sites: methanol and ammonia synthesis reactors with a capacity of 1,600,000 T/year are now in use.

11.2 FACTORS OF PROGRESS: TECHNOLOGICAL INNOVATIONS AND INCREASED FUNDAMENTAL INSIGHT

Among the many technological innovations of recent years are the following examples:

- The introduction of better materials of construction (e.g., in steam reforming) where the use of centrifugal cast 25% Cr/20% Ni steel tubes has permitted increasing the operating temperature and consequently the throughput.
- Better design of reactor internals (e.g., in phthalic anhydride synthesis), improving the rate and uniformity of heat removal by molten salts.
- More adequate shop techniques and increased shipping clearance, permitting the construction of multitubular reactors of large diameters containing up to 20,000 tubes.
- Modification of auxiliary equipment (e.g., the introduction of centrifugal compressors) boosted the capacity of well-established processes such as ammonia and methanol synthesis.
- Modification of flow pattern (e.g., the use of radial flow reactors in catalytic reforming and ammonia synthesis) to reduce the pressure drop and thus enhance the recycle compressor capacity.

- The use of small catalyst particles in regions where heat transfer matters and larger particles in other zones to limit the pressure drop, as in primary steam reformers.
- The design of improved control schemes.

Examples of progress that may be termed fundamental are:

- The development of new catalysts or the modification of existing ones. Major recent achievements concerning fixed bed processes were the addition of rhenium and other rare metals to platinum/Al_2O_3 catalysts for catalytic reforming, to increase stability; the formulation of a stable low-pressure methanol synthesis catalyst; the introduction of a low-temperature CO-shift catalyst, permitting operation under thermodynamically more favorable conditions; and a V_2O_5 catalyst allowing high throughputs at relatively low temperatures in phthalic anhydride synthesis.
- Advances in fundamental data. Intensive research has led to more extensive and more reliable physicochemical data; heat transfer in packed beds has been studied more carefully. Large companies are now well aware of the importance of reliable kinetic data as a basis for design and kinetic studies have benefited from more systematic methods for the design of experiments and improved methods for analysis of the data.
- The use of reactor models as a basis for design, associated with the ever-increasing possibilities of computers. This is an aspect that will be dealt with extensively further in this chapter. To place this aspect in the right perspective, earlier stages of design in which decisions are taken on the basis of sound judgment and semiquantitative considerations will be discussed first.

11.3 FACTORS INVOLVED IN THE PRELIMINARY DESIGN OF FIXED BED REACTORS

When a reactor has to be scaled up from its bench scale version, a certain number of questions arise as to its ultimate type and operation. In general, several alternatives are possible. These may be retained up to a certain degree of progress of the project, but a choice will have to be made in as early a stage as possible on the basis of qualitative or semiquantitative considerations before considerable effort is invested into the detailed design.

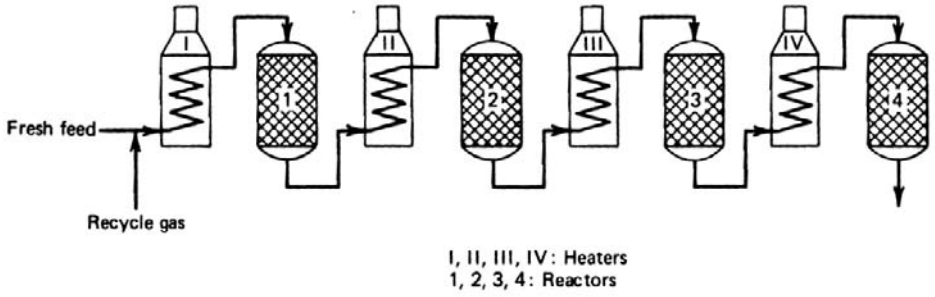

Figure 11.3-1

Multibed adiabatic reactor for catalytic reforming. After Smith [1959], from Froment [1974].

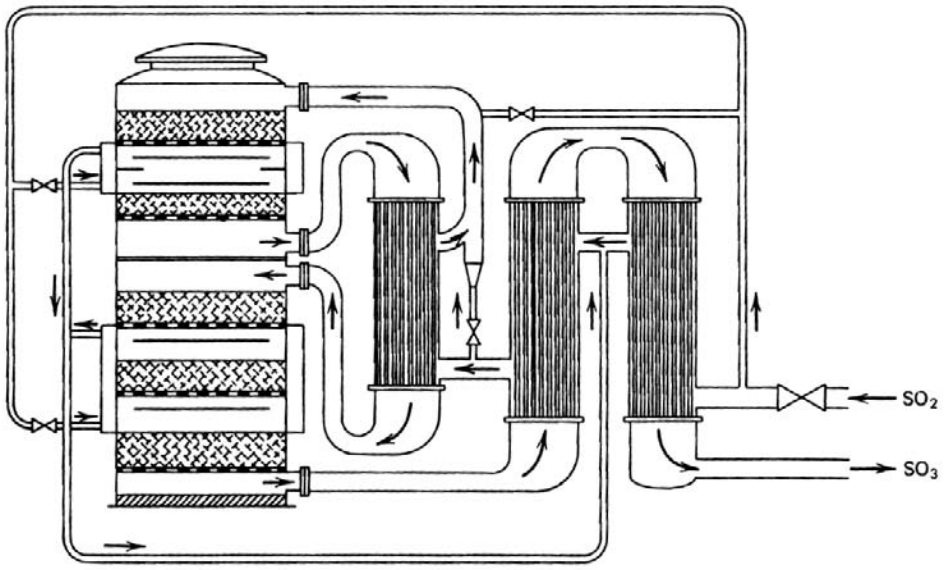

Figure 11.3-2

Multibed adiabatic reactor for SO_3 synthesis. After Winnacker and Kuechler [1970], from Froment [1974].

The first and most elementary type of reactor to be considered is the adiabatic reactor. In this case the reactor is simply a vessel of relatively large diameter. Such a simple solution is not always applicable, however. Indeed, if the reaction is very endothermic, the temperature drop may be such as to extinguish the reaction before the desired conversion is attained — this would be the case with catalytic reforming of naphtha or with ethylbenzene dehydrogenation into styrene. Strongly exothermic reactions lead to a temperature rise that may be prohibitive for several reasons: for its unfavorable influence on the equilibrium

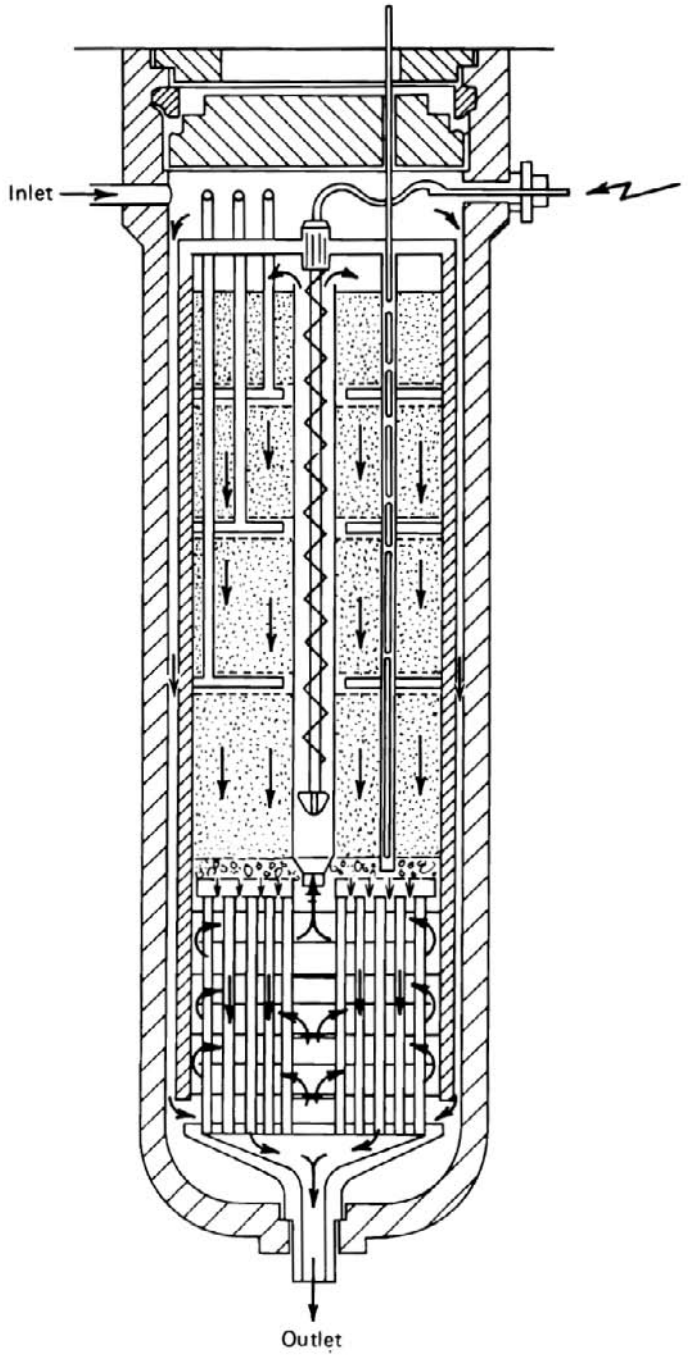

Figure 11.3-3

Multibed adiabatic reactor for NH_3 synthesis. After Winnacker and Kuechler [1970], from Froment [1974].

conversion, as in ammonia, methanol, and SO_3 synthesis; or on the selectivity, as in maleic anhydride or ethylene oxide synthesis; or on the catalyst stability, or simply because it would lead to unsafe operation. A solution that can be applied to endothermic reactions, although it is not without drawbacks, is to dilute the reactant with a heat carrier. More often, however, the reactor is subdivided into several stages, with intermediate heat exchange. An example of such a multibed adiabatic reactor is shown in Figure 11.3-1 for an endothermic process-catalytic reforming of naphtha into gasoline.

The exothermic SO_3- and NH_3-synthesis are carried out in reactors of the type illustrated in Fig. 11.3-2 and Fig. 11.3-3, respectively. In ammonia- or SO_3-synthesis the intermediate cooling may be achieved by means of heat exchangers or by injection of cold feed. With SO_3 synthesis the heat exchangers are generally located outside the reactor. Special care has to be taken to provide homogeneous distribution over the bed underneath of the quench or the flow coming from an intermediate heat exchanger.

The temperature-composition relationships in such a multibed adiabatic reactor are illustrated in Fig. 11.3-4 for ammonia synthesis [Shipman and Hickman, 1968]. The Γ_e curve in this diagram represents the equilibrium relation between composition and temperature. The maximum ammonia content that could be obtained in a single adiabatic bed with inlet conditions corresponding to *A* would be 14 mole-% as indicated by point *B*', and this would theoretically require an infinite amount of catalyst. The five-bed quench converter corresponding to the reaction path *ABCDEFGHIJ* permits attaining a much higher ammonia content. The reaction path *ABCDEFGHIJ* evolves around the curves Γ_m, which represents the conversion-temperature relationship that ensures maximum reaction rate in each point of the reactor. Clearly, for each bed the question is how close the adiabatic outlet condition will be allowed to approach equilibrium and how far the reaction mixture will have to be cooled in the heat exchanger before proceeding to the next stage. This is a problem of optimization, requiring a more quantitative approach. For the specific case considered here, another possibility is to depart from the adiabatic stages in order to follow more closely the curve of optimum reaction rates, Γ_m. The continuous removal of excess heat implied by this is only possible in a multitubular reactor. One way of achieving this in ammonia synthesis is shown in Fig. 11.3-5. Use is made of the feed stream to remove the heat from the reaction section [Vancini, 1971]. How well the objective is met by a proposed design (i.e., how well the actual trajectory approximates the Γ_m curve) can only be found by a more quantitative approach involving modeling, discussed further in Parts 2 and 3 of this chapter. In modern reactors like that of Ammonia-Casale the continuous heat exchange is achieved by plate heat exchangers.

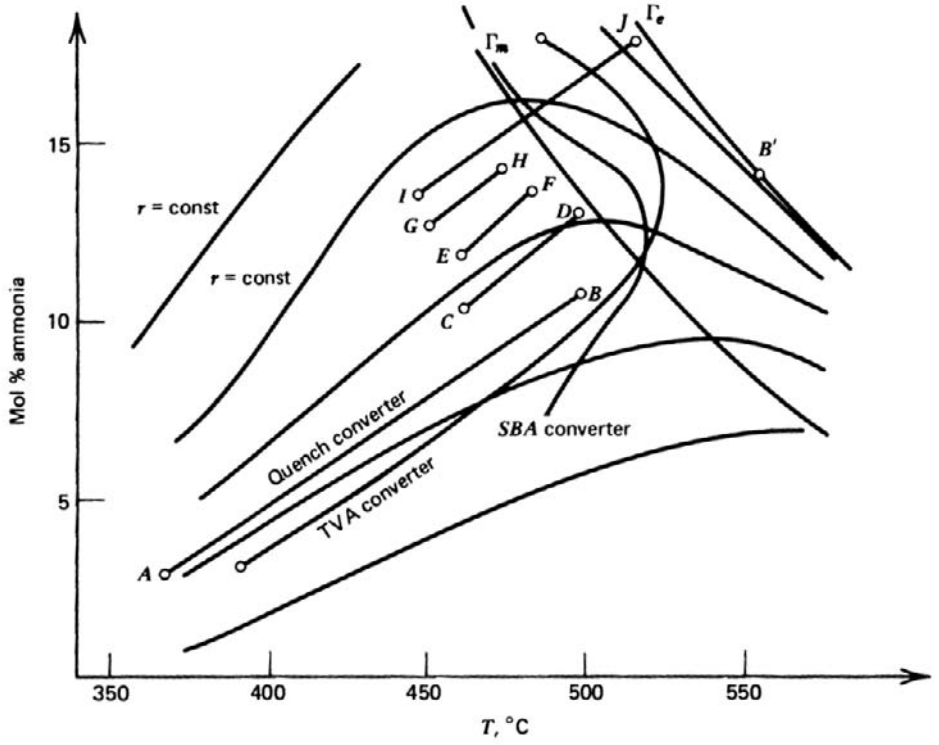

Figure 11.3-4

Mole percent ammonia versus temperature diagram. After Shipman and Hickman [1968].

With other very exothermic reactions, such as air oxidation of aromatic hydrocarbons, the number of beds would have to be uneconomically large to limit the temperature increase per bed, so that the multitubular reactor is definitely preferred. Cooling the reactor with the incoming reactant would be insufficient, however, and require too much heat exchanging surface. Such reactors are therefore cooled by means of circulating molten salts that in turn give off their heat to a boiler. The phthalic anhydride synthesis reactor shown in Fig. 11.3-6 [Suter, 1972] may contain up to 20,000 tubes of 2.5 cm inside diameter. The tube diameter has to be limited to such a small value to avoid excessive overtemperatures on the axis, a feature that is discussed later in this chapter. A different type of multitubular reactor has to be used in natural gas or naphtha steam reforming into hydrogen or synthesis gas, an endothermic reaction (Fig. 11.3-7). In this case the gases are gradually heated from 500° to 850°C. To obtain the highest possible capacity for a given amount of catalyst, heat fluxes of 75.6 kJ/m² s are applied to tubes of 10 cm inner diameter. The tubes, 10 m long, are suspended in two rows in a furnace that may contain as many as 300 tubes.

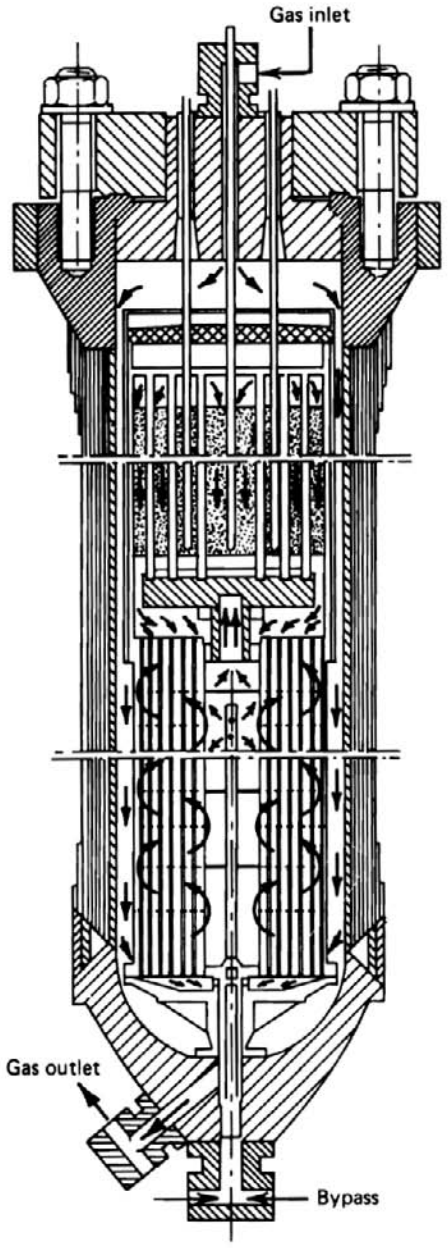

Figure 11.3-5
Ammonia synthesis reactor with tubular heat exchanger. From Vancini [1971].

In several cases effluent gases have to be recycled (e.g., in catalytic reforming — hydrogen and light hydrocarbons; in ammonia synthesis — the non-condensed fraction of the effluent, because of equilibrium limitations on the conversion per pass). To limit the cost of recycling and get a maximum capacity

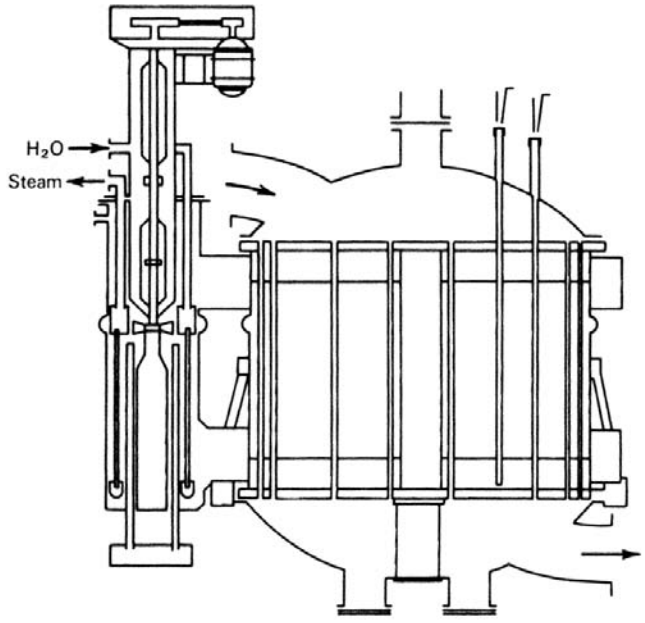

Figure 11.3-6

Multitubular reactor for phthalic anhydride synthesis by *o*-xylene oxidation. After Suter [1972], from Froment [1974].

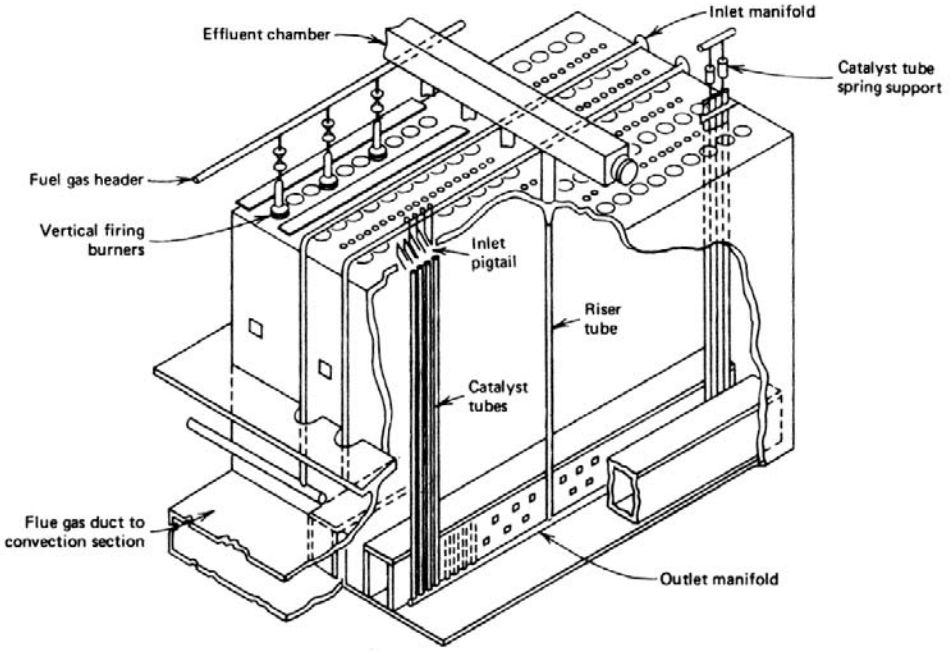

Figure 11.3-7

Multitubular natural gas steam reformer with furnace. From Froment [1974], after "High Performance Process Furnaces," M. W. Kellogg Co.

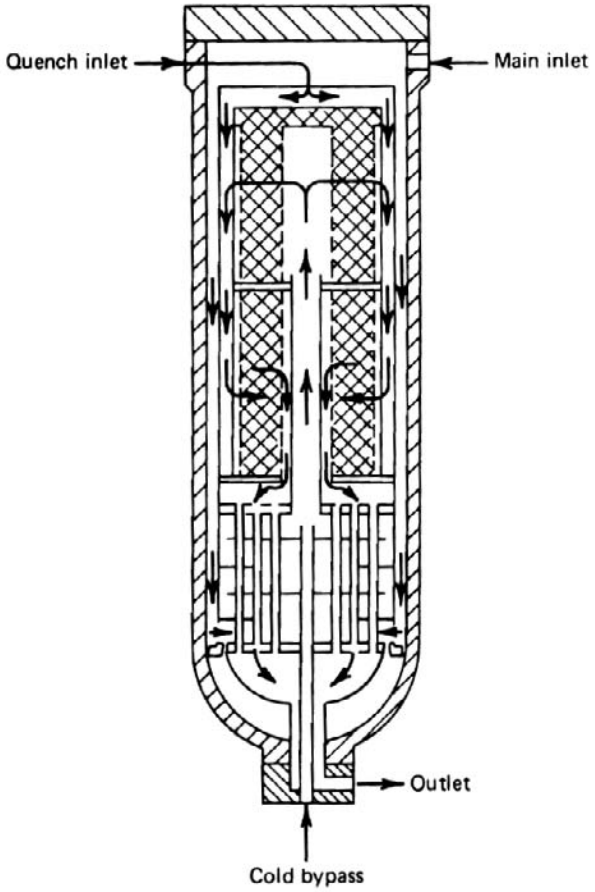

Figure 11.3-8

Ammonia synthesis reactors.

(a) Radial H. Topsøe converter. After Finneran et al. [1972], from Froment [1974].

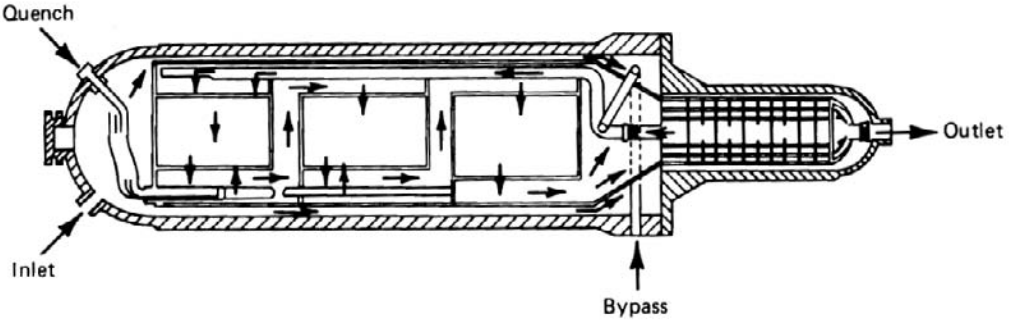

(b) Horizontal multibed Kellogg reactor. After Finneran et al. [1972], from Froment [1974].

out of the centrifugal recycle compressor, the pressure drop over the catalyst bed has to be kept as low as possible. This requires limiting the bed depth, which means, in conventional reactors at least, that the diameter would have to be increased. This is no longer possible for the giant ammonia synthesis converters, so that other solutions had to be sought. Figure 11.3-8 shows two ways of increasing the flow area without increasing the bed depth [Finneran et al., 1972]. Radial flow has been applied for quite a number of years already in catalytic naphtha reforming. Clearly, in all the decisions related to the above discussion, the following elements had to be considered all the time: technology in all its various aspects, the rate of reaction, reaction scheme, equilibrium, catalyst composition and properties, heat transfer, and pressure drop, with constant reference to safety, reliability, and economics.

The same factors will, of course, have to be considered in the next stage of design, only more quantitatively and in a way accounting for their interaction. This stage requires some degree of mathematical modeling of the reactor.

11.4 MODELING OF FIXED BED REACTORS

In this chapter it is not possible to concentrate on specific cases and processes. Instead, general models and principles involved in the design and analysis of any type of fixed bed reactor, no matter what the process, will be discussed.

The development of chemical reaction engineering as a recognized discipline and the increasing possibilities of computers have led to extensive exploration of reactor design and performance, both in the steady and nonsteady state. Models now range from the very simple ones that could be handled before 1960 to some very sophisticated ones aiming at a more representative description of the geometry and phenomena.

Reactor design and analysis groups are continuously confronted with the degree of sophistication that is required and can be justified. This is a question that cannot be answered in a general manner. The required degree of sophistication depends in the first place on the process, that is, on the reaction scheme and on its sensitivity to perturbations in the operating conditions. Of equal importance is the degree of accuracy with which the kinetic and transport parameters are known. Figure 11.4-1 shows the problems that have to be faced in fixed bed reactor modeling and design. It relates the aspects on microscale, already dealt with in Chapters 2 and 3, to the macroscale, to be dealt with in the present chapter. The modeling of the macroscale, that is, the reactor, is mainly determined by the hydrodynamics. Is plug flow a sufficient approximation or not?

A given reactor can be modeled in various ways. To establish a better insight into the models, a classification is presented in Table 11.4-1 [Froment, 1972a, b]. In this table the models have been grouped in two broad categories: pseudohomogeneous and heterogeneous. Pseudohomogeneous models do not account explicitly for the presence of catalyst, in contrast with heterogeneous models, which consist of separate conservation equations for fluid and catalyst. Within each category the models are classified in an order of growing complexity. The basic model, used in most of the studies until now, is the pseudohomogeneous one-dimensional model, which only considers transport by plug flow in the axial direction (Section 11.5). Some type of mixing in the axial direction may be superposed on the plug flow so as to account for nonideal flow conditions (Section 11.6). If radial gradients have to be accounted for, the model becomes two-dimensional (Section 11.7). The basic model of the heterogeneous category considers only transport by plug flow again, but distinguishes between conditions in the fluid and on the solid (Section 11.8). The next step toward complexity is to take the gradients inside the catalyst into account (Section 11.9). Finally, the most comprehensive models — the two-dimensional heterogeneous models — are discussed in Section 11.10. In the following sections the specific features of these models and their adequacy with respect to industrial practice are discussed.

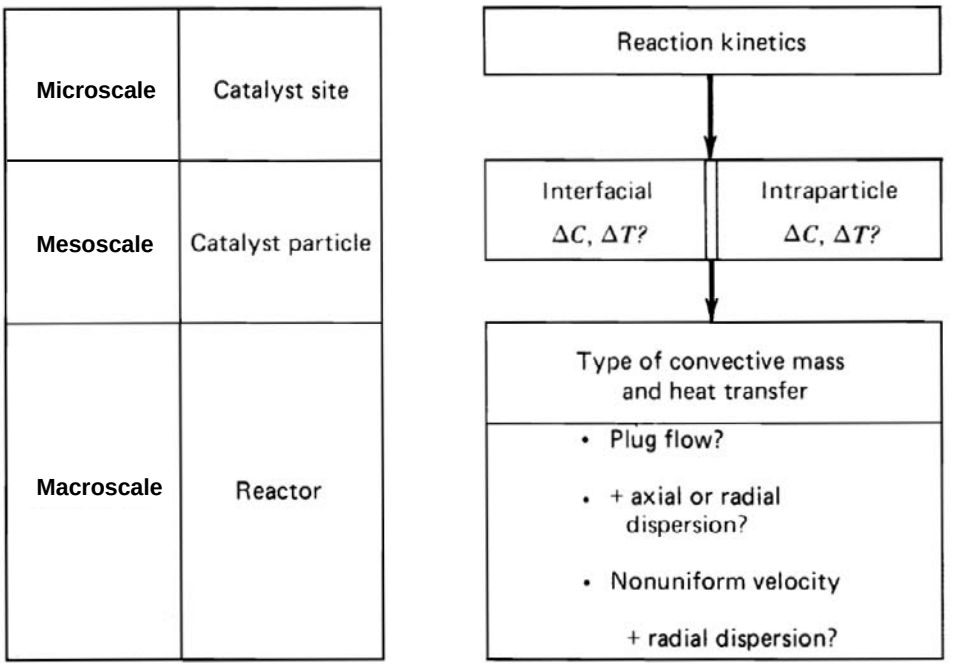

Figure 11.4-1
Aspects to be dealt with in the modeling of fixed bed reactors.

TABLE 11.4-1
CLASSIFICATION OF FIXED BED REACTOR MODELS

	A-Pseudohomogeneous Models $T = T_s$; $C = C_s$		**B-Heterogeneous Models** $T \neq T_s$; $C \neq C_s$	
One-dimensional	I Sec. 11.5	basic, ideal	I Sec. 11.8	+ interfacial gradients
	II Sec. 11.6	+ axial mixing	II Sec. 11.9	+ intraparticle gradients
Two-dimensional	III Sec. 11.7	+ radial mixing	III Sec. 11.10	+ radial mixing

PART TWO
PSEUDOHOMOGENEOUS MODELS

11.5 THE BASIC ONE-DIMENSIONAL MODEL

11.5.1 Model Equations

The basic or ideal model assumes that concentration and temperature gradients only occur in the axial direction. The only transport mechanism operating in this direction is the overall flow itself, and this is considered to be of the plug flow type. For the steady state and a single reaction carried out in a cylindrical tube, the conservation equations may be written:

$$-\frac{d(u_s C_A)}{dz} = r_A \rho_B \tag{11.5.1-1}$$

$$u_s \rho_g c_p \frac{dT}{dz} = (-\Delta H) r_A \rho_B - 4\frac{U}{d_t}(T - T_r) \tag{11.5.1-2}$$

$$-\frac{dp_t}{dz} = f\frac{\rho_g u_s^2}{d_p} \tag{11.5.1-3}$$

with the following initial conditions: at $z = 0$, $C_A = C_{A0}$, $T = T_0$, $p_t = p_{t0}$. In (11.5.1-3), d_p is the equivalent particle diameter, to be defined further in this section. In specific cases, u_s, ρ_g, and c_p may be considered to be constant. The

integration of this system of ordinary differential equations by means of a Runge-Kutta or other method is a straightforward matter. The purpose of this integration can be the simulation of an existing reactor or the design of a new reactor. Important questions that can be asked in the latter case are: What is the bed or tube length required to reach a given conversion? What will the tube diameter have to be? Or the wall temperature? Before considering such problems, however, some features of the system of the differential equations (11.5.1-1), (11.5.1-2), and (11.5.1-3) will be discussed.

Equation (11.5.1-1) is obtained from a material balance on a reference component, say, *A*, over an elementary cross section of the tubular reactor containing an amount of catalyst *dW*. As previously mentioned, rate equations for heterogeneously catalyzed reactions are generally referred to unit catalyst weight, rather than reactor volume, to eliminate the bed density. Obviously, different packing densities between the laboratory reactor in which kinetic data were determined and the industrial reactor, calculated on the basis of these data, would lead to different results.

When use is made of conversion, the material balance for *A* over an elementary weight of catalyst may be written

$$r_A dW = F_{A0} dx_A \tag{11.5.1-4}$$

where F_{A0} is the molar feed rate of *A*, or

$$r_A \rho_B \Omega dz = F_{A0} dx_A \tag{11.5.1-5}$$

from which (11.5.1-1) is easily obtained. *U* in (11.5.1-1) is an overall heat transfer coefficient defined by

$$\frac{1}{U} = \frac{1}{\alpha_i} + \frac{d}{\lambda}\frac{A_b}{A_m} + \frac{1}{\alpha_u}\frac{A_b}{A_u} \tag{11.5.1-6}$$

where

α_i = heat transfer coefficient on the bed side (kJ/m²s°C)
α_u = heat transfer coefficient, heat transfer medium side (kJ/m²s°C)
A_b = heat exchanging surface, bed side (m²)
λ = heat conductivity of the wall (kJ/m s °C)
A_u = heat exchanging surface, heat transfer medium side (m²)
A_m = log mean of A_b and A_u (m²)

In general, the thickness of the wall, *d*, is small, so that the ratio of surfaces is close to one. α_u is found from classical correlations in books on heat transfer.

α_i may be based on Leva's correlation [1949], for heating up the reaction mixture:

$$\frac{\alpha_i d_t}{\lambda_g} = 0.813\left(\frac{d_p G}{\mu}\right)^{0.9} e^{-6d_p/d_t}$$

for cooling (11.5.1-7)

$$\frac{\alpha_i d_t}{\lambda_g} = 3.50\left(\frac{d_p G}{\mu}\right)^{0.7} e^{-4.6d_p/d_t}$$

where

d_t = tube diameter (m)
d_p = equivalent particle diameter (m)

Further correlations of this type were published by Maeda [1952] and Verschoor and Schuit [1950].

De Wasch and Froment, on the other hand, found a linear relation between the Nusselt and Reynolds numbers [1972]:

$$\frac{\alpha_i d_p}{\lambda_g} = \frac{\alpha_i^0 d_p}{\lambda_g} + 0.033\left(\frac{c_p \mu}{\lambda_g}\right)\left(\frac{d_p G}{\mu}\right) \qquad (11.5.1\text{-}8)$$

The influence of the tube diameter and of the catalyst properties enter the correlation through α_i^0, the so-called static contribution. With the units given above:

$$\alpha_i^0 = \frac{10.21\lambda_e^0}{d_t^{4/3}}$$

where λ_e^0 is the static contribution to the effective thermal conductivity of the bed and will be discussed in detail in Section 11.10.

The friction factor f now remains to be specified. The pressure drop equation, (11.5.1-3), requires special attention. It differs from the Fanning equation, in which the right-hand side is multiplied by 2. When a friction factor is substituted into (11.5.1-3), special care has to be taken to check from which type of pressure drop relation f was derived. Further, the units have to be handled with care. Equation (11.5.1-3) is written for S.I. units, with p_t in Pa = N/m². With other units, the right-hand side has to be multiplied by a conversion factor. When engineering units are used for p_t (kg force/m² = N × 9.81), the right-hand side has to be divided by g (m²/s).

The most popular pressure drop equation for flow through packed beds is that of Ergun [1952]. Ergun considered the packed bed to consist of a bundle of

nonconnecting parallel channels with hydraulic radius R_h (ratio of void fraction, ε, to surface of solid per m³ bed, a_v):

$$R_h = \frac{\varepsilon}{a_v}$$

The equivalent particle diameter d_p is the diameter of a sphere with the same surface area per unit volume as the actual particle, S_v:

$$S_v = \frac{a_v}{1-\varepsilon}$$

so that

$$d_p = \frac{6(1-\varepsilon)}{a_v} \qquad (11.5.1\text{-}9)$$

The Hagen-Poiseuille equation, expressing the pressure drop for laminar flow in an empty conduit, when written in the form of (11.5.1-3), leads to a friction factor

$$f = \frac{(1-\varepsilon)^2}{\varepsilon^3}\frac{36}{(d_p G/\mu)} \qquad (11.5.1\text{-}10)$$

Since the channels in a packed bed are not straight, a correlation factor of $25/6$ had to be introduced by Ergun to fit the experimental data, so that (11.5.1-10) becomes

$$f = \frac{(1-\varepsilon)^2}{\varepsilon^3}\frac{150}{(d_p G/\mu)} \qquad (11.5.1\text{-}11)$$

The Burke and Plummer equation for highly turbulent flow in a channel, written in the form of (11.5.1-3), leads to a friction factor

$$f = 1.75\frac{1-\varepsilon}{\varepsilon^3} \qquad (11.5.1\text{-}12)$$

Adding both contributions Ergun proposed,

$$f = \frac{1-\varepsilon}{\varepsilon^3}\left[a + \frac{b(1-\varepsilon)}{\mathrm{Re}}\right] \qquad (11.5.1\text{-}13)$$

with $a = 1.75$ and $b = 150$.

Handley and Heggs [1968] derived a value of 1.24 for a and 368 for b. McDonald et al. [1979] proposed $a = 1.8$ for smooth particles and 4.0 for rough particles and $b = 180$.

Hicks [1970] reviewed several pressure drop equations and concluded that the Ergun equation is limited to $\mathrm{Re}/(1-\varepsilon) < 500$ and Handley and Hegg's equation to $1000 < \mathrm{Re}/(1-\varepsilon) < 5000$. He proposed an equation for spheres that can be written

$$f = 6.8\frac{(1-\varepsilon)^{1.2}}{\varepsilon^3}\mathrm{Re}^{-0.2} \tag{11.5.1-14}$$

and which fits Ergun's and Handley and Hegg's data and the results of Wentz and Thodos obtained at very high Reynolds numbers [1963]. This implies that a and b are not true constants, in agreement with Tallmadge [1970], who proposed $a = 1.75$ and $b = 4.2\ \mathrm{Re}^{5/6}$.

At d_t/d_p values below 5, a and b drastically change. From velocity measurements by Bey and Eigenberger [1997] and radial void fraction profiles of de Klerk [2003], Castillo-Araiza and Lopez-Isunda derived values of 270 for a and 2.5 for b.

For hollow rings the equivalent particle diameter as defined by (11.5.1-9) is not sufficiently accurate. Reichelt and Blasz [1957] proposed

$$d_p = 6\frac{V(\text{cylinder})}{S(\text{external cylinder})}E^m$$

where

$$E = \frac{V(\text{particle})\ S(\text{external cylinder})}{S(\text{particle})\ V(\text{external cylinder})} \tag{11.5.1-15}$$

and

$$m = \frac{d_e/d_i}{\left(\varepsilon\dfrac{d_e^2}{d_i^2}\right)^{0.4} + 0.010\left(\varepsilon\dfrac{d_e^2}{d_i^2}\right)^{0.75}}$$

where d_e and d_i are the external and internal diameters of the hollow cylinder, respectively.

The void fraction in packed beds of spheres has been correlated by Haughey and Beveridge [1969] in the following way:

$$\varepsilon = 0.38 + 0.073\left[1 + \frac{(d_t/d_p - 2)^2}{(d_t/d_p)^2}\right] \tag{11.5.1-16}$$

but whenever convenient, it is preferable to determine ε experimentally.

EXAMPLE 11.5.1.A
CALCULATION OF PRESSURE DROP IN PACKED BEDS

A tube with a length 2.5 m and an internal diameter 0.025 m is packed with alumina cylinders with a diameter and height 0.003 m. The void fraction of the bed is $\varepsilon = 0.38$. Air flows through the tube at 372°C with a superficial mass flow velocity of 1.3 kg/m² s. Calculate the pressure drop in the bed. Viscosity of air at 372°C = 0.031 cps = 0.1116 kg/m² h = 3.1 × 10^{-5} kg/m² s; specific mass of air at 372°C = 0.9487 kg/m³.

Solution

1. Ergun equation, (11.5.1-13):

$\rho_g u_s = 1.3$ kg/m² s $\qquad u_s = 1.37\ \mathrm{m_g^3/m_r^2\,s}$

$$d_p = \sqrt{1.5} \times 0.003 = 0.0037\,\mathrm{m}$$

$$\mathrm{Re} = \frac{d_p \rho_g u_s}{\mu} = \frac{0.0037 \times 1.3}{3.1 \times 10^{-5}} = 155$$

$$f = \frac{0.62}{(0.38)^3}\left(1.75 + \frac{150 \times 0.62}{155}\right) = 26.53$$

$$-\Delta p_t = 26.53 \times \frac{0.9487 \times (1.37)^2}{0.0037} \times 2.5 = 31918\,\mathrm{N/m^2} = 0.319\,\mathrm{bar}$$

2. McDonald et al.'s modification of (11.5.1-13):

$$f = 28.47; \qquad -\Delta p_t = 34253\ \mathrm{N/m^2} = 0.342\ \mathrm{bar}$$

3. Hicks equation, (11.5.1-14):

$$f = 25.45; \qquad -\Delta p_t = 0.306\ \mathrm{bar}$$

■

11.5.2 Design of a Fixed Bed Reactor According to the One-Dimensional Pseudohomogeneous Model

This design example is suggested from hydrocarbon oxidation processes such as benzene oxidation into maleic anhydride or the synthesis of phthalic anhydride from *o*-xylene. These strongly exothermic processes are carried out in multi-tubular reactors cooled by molten salt that is circulating around the tubes and that exchanges heat to an internal or external boiler. The length of the tubes is 3 m and their internal diameter is 2.54 cm. One reactor may contain 2500 tubes in parallel and even 10,000 or more in the latest versions. In German processes the

catalyst is V_2O_5 on promoted silica gel, and the operating temperature range is 335° to 415°C. The particle diameter is 3 mm, and the bulk density is 1300 kg/m³. The hydrocarbon is vaporized and mixed with air before entering the reactor. Its concentration is kept below 1 mole-%, in order to stay under the explosion limit.

The operating pressure is nearly atmospheric. The phthalic anhydride production from such a reactor with 2500 tubes is 1650 tons/yr. It follows that with this catalyst a typical mass flow velocity of the gas mixture is 4684 kg/m^2 h. With a mean fluid density of 1293 kg/m^3, this leads to a superficial fluid velocity of 3600 m/h. A typical heat of reaction is 1,285,409 kJ/kmol, and the specific heat is 0.992 kJ/kg K. In this example the kinetic equation for the hydrocarbon conversion will be considered in first approximation to be pseudo-first order, due to the large excess of oxygen:

$$r_A = k p_B^0 p_A$$

where p_B^0 = 0.211 bar represents the partial pressure of oxygen. Let k be given by

$$\ln k = 19.837 - \frac{13{,}636}{T}$$

More complex rate equations for this type of reaction will be used in a later example given in Section 11.7.5.

The continuity equation for the hydrocarbon, in terms of partial pressures and the energy equation, may be written, for constant density,

$$u_s \frac{dp_A}{dz} + \frac{M_m p_t \rho_B}{\rho_g} k p_B^0 p_A = 0 \qquad (11.5.2\text{-}1)$$

$$u_s \rho_g c_p \frac{dT}{dz} - (-\Delta H)\rho_B k p_B^0 p_A + \frac{4U}{d_t}(T - T_r) = 0 \qquad (11.5.2\text{-}2)$$

with

$$p_A = p_0 \qquad \text{at } z = 0$$

$$T = T_0 = T_r \qquad \text{at } z = 0$$

The total pressure is considered to be constant and equal to 1 bar. The overall heat transfer coefficient U may be calculated from the correlations given above to be 0.096 kJ/m² s. T_r is chosen to be 352°C.

The figures reveal a “hot spot” in the bed, which is typical for strongly exothermic processes. The magnitude of this hot spot depends, of course, on the heat effect of the reaction, the rate of reaction, the heat transfer coefficient, and

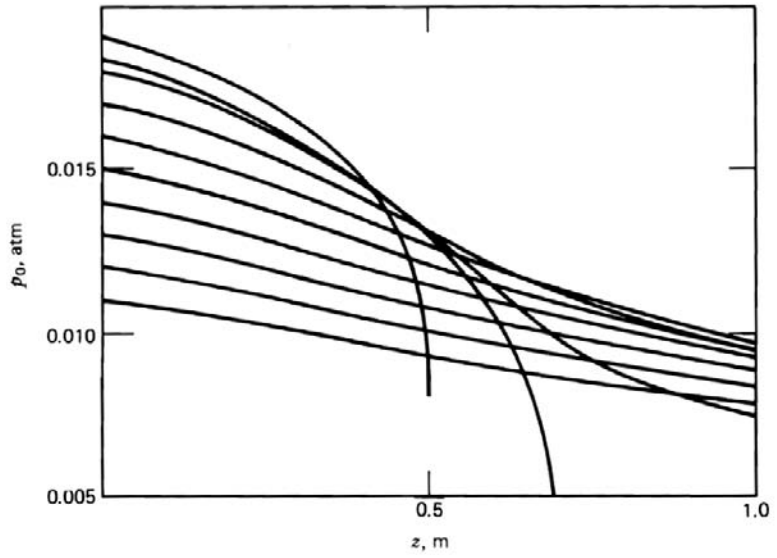

Figure 11.5.2-1

Partial pressure profiles in the reactor illustrating the sensitivity with respect to the inlet partial pressure. From Van Welsenaere and Froment [1970].

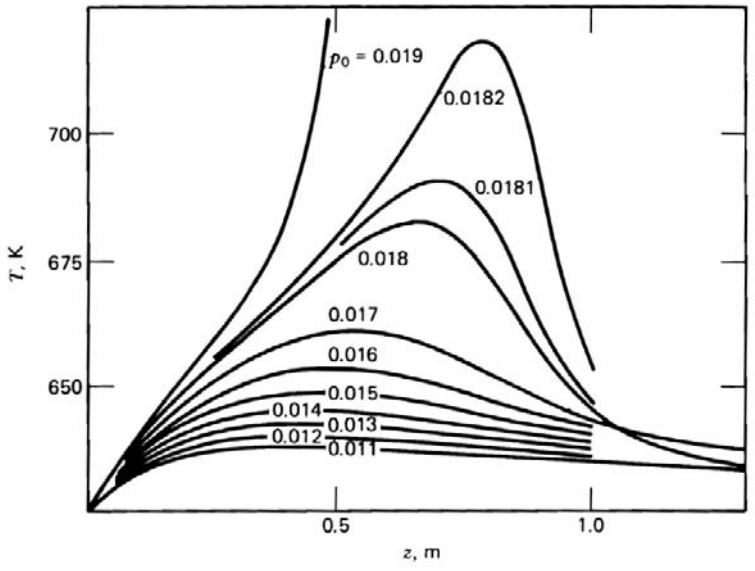

Figure 11.5.2-2

Temperature profiles corresponding to partial pressure profiles of Fig. 11.5.2-1. From Van Welsenaere and Froment [1970].

transfer areas as shown by Bilous and Amundson [1956]. Its location depends on the flow velocity. It is also observed that the profiles become sensitive to the parameters from certain values onward. If the partial pressure of the hydrocarbon

were 0.018 bar, an increase of 0.0002 bar would raise the hot spot temperature beyond permissible limits. Such a phenomenon is called runaway. Note that for the upper part of the curves with p_{A0} = 0.0181, 0.0182, and 0.019 (Figs. 11.5.2-1 and 11.5.2-2), the model used here is no longer entirely adequate: heat and mass transfer effects would have to be taken into account. There is no doubt, however, as to the validity of the lower part, indicating excessive sensitivity in this region.

11.5.3 Runaway Criteria

In the above example it was shown how hot spots develop in fixed bed reactors for exothermic reactions. An important problem associated with this is how to limit the hot spot in the reactor and how to avoid excessive sensitivity to variations in the parameters. Several approaches have been attempted to derive simple criteria that would permit a selection of operating conditions and reactor dimensions prior to any calculation on the computer. The results are represented in Fig. 11.5.3-1. In this figure the abscissa is $S = \beta\gamma$, that is, the product of the dimensionless adiabatic temperature rise,

$$\frac{T_{ad} - T_0}{T_0} = \frac{(-\Delta H)\, p_{A0}}{M_m p_t c_p T_0} = \frac{(-\Delta H) C_{A0}}{\rho_g c_p T_0}$$

and the dimensionless activation energy E/RT_0, for the common situation where $T_r = T_0$, two groups characterizing the reaction properties and the operating conditions. The ordinate N/S is the ratio of the rate of heat transfer per unit reactor volume at $f_r = 1$, where

$$f_r = \left(\frac{E}{RT_r^2} \right) (T - T_r)$$

to the rate of heat generation per unit volume at $f_r = 0$ and zero conversion (i.e., at the reactor inlet). In the original derivation,

$$N = \frac{4}{d_t} \frac{U}{M_m c_p k_{B0}}$$

where k_{B0}, as defined by Barkelew, has units: s^{-1} kmol/ m_r^3 . With the rate form of Section 11.5.2,

$$N = \frac{4U}{d_t c_p M_m} \frac{1}{\rho_B k_0 p_B^0 p_t}$$

Also,

$$\frac{N}{S} = \frac{4U(T - T_r)}{d_t} \frac{1}{k_{B0} C_{A0} (-\Delta H)} \frac{RT_r^2}{E(T - T_r)}$$

as stated above in physical terms. Further details are given in Example 11.5.3.A. Curves 1, 2, 3, and 4 in Fig 11.5.3-1 define a band that bounds two regions. If the operating conditions are such that they lead to a point in the diagram above the curves, the reactor is insensitive to small fluctuations; but if it is situated under the curves, runaway is likely.

Barkelew [1959] arrived at curve 1 by inspecting a very large number of numerical integrations of the system [(11.5.1-1) to (11.5.1-3)] for a wide variation of the parameter values, but used a simplified temperature dependence of the reaction rate. Dente and Collina [1964] came to essentially the same curve with less effort by taking advantage of the observation that in drastic conditions the temperature profile through the reactor has two inflection points before the maximum, which coincide in critical situations. Hlavacek et al. [1969] and Van Welsenaere and Froment [1970] independently utilized two properties of the *T-z* curve to derive criteria without any of the integrations involved in the approach of Barkelew and with the Arrhenius temperature dependence for the rate coefficient. From an inspection of the temperature and partial pressure profiles in

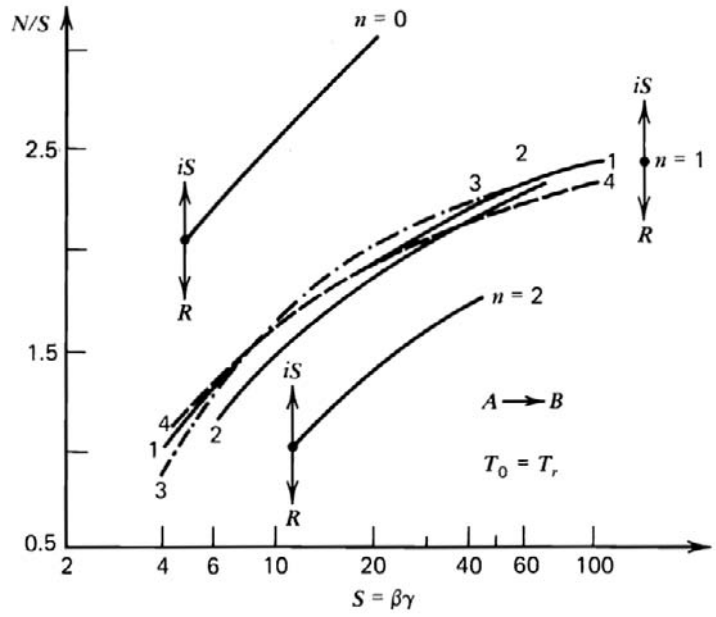

Figure 11.5.3-1

Runaway diagram. Curve 1, Barkelew [1959]; curve 2, Dente and Collina [1964]; curve 3, Hlavacek et al. [1969]; curve 4, Van Welsenaere and Froment [1979]. Curves $n = 0$ and $n = 2$ from Morbidelli and Varma [1982].

the reactor they concluded that extreme parametric sensitivity and runaway is possible (1) when the hot spot exceeds a certain value and (2) when the temperature profile develops inflection points before the maximum, as noticed already by Dente and Collina [1964]. Van Welsenaere and Froment transposed the peak temperature and the conditions at the inflection points into the *p-T* phase plane, a diagram often used in the study of the dynamic behavior of a reactor.

In Fig. 11.5.3-2 the locus of the partial pressure and temperature in the maximum of the temperature profile and the locus of the inflection points before the hot spot are shown as p_m and $(p_i)_1$, respectively. Two criteria were derived from this. The first criterion is based on the observation that extreme sensitivity is found for trajectories — the *p-T* relationships in the reactor — intersecting the maxima curve p_m beyond its maximum. Therefore, the trajectory going through the maximum of the p_m curve is considered as critical. This is a criterion for runaway based on an intrinsic property of the system, not on an arbitrarily limited temperature increase. The second criterion states that runaway will occur when a trajectory intersects $(p_i)_1$, which is the locus of inflection points arising before the maximum. Therefore, the critical trajectory is tangent to the $(p_i)_1$ curve. A more convenient version of this criterion is based on an approximation for this locus represented by p_s in Fig. 11.5.3-2. Representation of the trajectories in the *p-T* plane requires numerical integration, but the critical points involved in

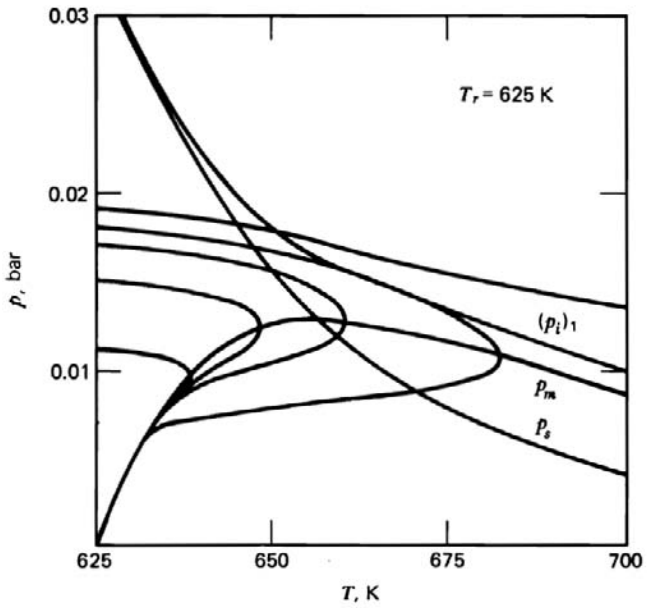

Figure 11.5.3-2

The *p-T* phase plane, showing trajectories, maxima curve, loci of inflextion points, and the "simplified" curve p_s. From Van Welsenaere and Froment [1970].

the criteria — the maximum of the maxima curve and the point of tangency of the critical trajectory with p_s — are easily located by means of elementary formulas. Two simple extrapolations from these points to the reactor inlet conditions lead to upper and lower limits for the inlet partial pressures.

The formulas used in the first criterion are easily derived. Considering again the case of a pseudo-first-order reaction treated under Section 11.5.2 and dividing (11.5.2-2) by (11.5.2-1) leads to

$$\frac{dT}{dp} = -\frac{B}{A} + \frac{C}{A}\frac{T - T_r}{p\exp\left(-\frac{E}{RT} + b\right)} \qquad (11.5.3\text{-}1)$$

where

$$A = \frac{M_m p_t \rho_B}{\rho_g} p_B^0 \qquad B = \frac{(-\Delta H)\rho_B}{c_p \rho_g} p_B^0 \qquad C = \frac{4U}{c_p d_t \rho_g}$$

Trajectories in the *p*-*T* diagram may be obtained from this equation by numerical integration. The locus of the *p* and *T* values in the maximum of the temperature profile in the reactor is obtained by setting *dT/dz* = 0 in (11.5.2-2) or *dT/dp* = 0 in (11.5.3-1). This leads to

$$p_m = \frac{T_m - T_r}{\frac{B}{C}\exp\left(-\frac{E}{RT_m} + b\right)} \qquad (11.5.3\text{-}2)$$

This curve is called the maxima curve. It can be seen from Fig. 11.5.3-2 that it has a maximum. The temperature corresponding to this maximum, T_M, is obtained by differentiating (11.5.3-2) with respect to T_m and setting the result equal to zero:

$$T_M = \frac{1}{2}\left[\frac{E}{R} - \sqrt{\frac{E}{R}\left(\frac{E}{R} - 4T_r\right)}\right]$$

or, in dimensionless form,

$$f_M = \frac{E}{RT_M^2}(T_M - T_r) = 1 \qquad (11.5.3\text{-}3)$$

Note the slightly different definition of f_M in this formula, compared to that of f_r used in conjunction with Fig. 11.5.3-1.

What remains to be done is to find the inlet conditions leading to the critical situations. Rigorously, this requires numerical back integration. Approximate values for the critical inlet conditions may be obtained by simple

extrapolations, however. Two ways of extrapolation were retained to define an upper and a lower limit for the approximated critical inlet conditions. The lower limit is based on the property of the trajectories to start in the *p*-*T* plane with an adiabatic slope for $T_0 = T_r$ and to bend under this line, due to heat exchange through the wall. Therefore, an adiabatic line starting from a point on a critical trajectory leads to a lower limit for the critical inlet conditions. Indeed, the critical trajectory through the critical point starts from inlet partial pressures that are higher than those of the adiabatic lines. This extrapolation defines a lower limit for p_0, which is entirely safe. The upper limit is based on the observation that tangents to the trajectories taken at a given T between T_r and T_M all intersect the ordinate at T_r at values for p that are higher than those intersected by the trajectories themselves. The intercepts of these tangents are determined by two opposing effects: the higher the trajectory is situated the smaller the value of the slope of the tangent. One of the trajectories will therefore lead to a minimum intercept on the ordinate through T_r. The corresponding inlet partial pressure, which is higher than that of the critical trajectory, will be the best possible approximation and is considered as an upper limit for the inlet partial pressure. The value of the abscissa at which the tangents are drawn is the critical temperature (T_M for the first criterion). This extrapolation defines an upper limit above which runaway will certain occur. The following formulas are easily derived:

From the first criterion:

Lower limit,

$$p_0^l = \frac{A}{B}\left(T_m - T_r\right)\left(1 + Q^2\right)$$

or

$$\frac{\Delta T_{ad}}{\Delta T} = 1 + Q^2$$

where

$$Q = \frac{1}{\sqrt{\dfrac{A}{C}\exp\left(-\dfrac{E}{RT_M} + b\right)}} \qquad (11.5.3\text{-}4)$$

Upper limit,

$$p_0^u = \frac{A}{B}\left(T_M - T_r\right)\left(1 + Q\right)^2$$

or

$$\frac{\Delta T_{ad}}{\Delta T} = \left(1 + Q\right)^2 \qquad (11.5.3\text{-}5)$$

A very accurate approximation of the true critical value is given by the mean

$$\frac{\Delta T_{ad}}{\Delta T} = 1 + Q + Q^2 \qquad (11.5.3\text{-}6)$$

which is represented in Fig. 11.5.3-1 as curve 4.

From the second criterion, Van Welsenaere and Froment [1970] derived the following formulas:

Lower limit,

$$\frac{\Delta T_{ad}}{\Delta T} = 1 + \frac{Q^2}{f_c}$$

where

$$f_c = \frac{E}{RT_c^2}\left(T_c - T_r\right)$$

and T_c is the critical temperature derived from the second criterion

Upper limit,

$$\frac{\Delta T_{ad}}{\Delta T} = \left(1 + Q\right)^2$$

Mean,

$$\frac{\Delta T_{ad}}{\Delta T} = 1 + Q + \frac{Q^2}{2}\left(1 + \frac{1}{f_c}\right) \qquad (11.5.3\text{-}7)$$

These formulas lead to values that are in close agreement with those based on the first criterion.

As previously mentioned, the methods discussed here are helpful in first stages of design to set limits on the operating conditions, but cannot answer questions related to the length of the reactor — these require integration of the set of equations (11.5.2-1) and (11.5.2-2). Also, Fig. 11.5.3-1 is limited to single reactions, except if some meaningful lumping could be applied to the reaction system, a topic studied by Luss and Hutchinson [1971] and Golikeri et al. [1972].

The runaway limits determined by Morbidelli and Varma [1982] are based on the occurrence of an inflection point in the temperature profile before the hot spot. They used the method of isoclines, which requires the numerical integration of a differential equation. The method is also applicable to reaction orders different from 1, as shown in Fig. 11.5.3-1. The runaway region becomes more important as the order decreases. Tjahjadi et al. [1987] developed a new approach, applicable to more complex reactions, for example, the radical polymerization of ethylene in a tubular reactor. Hosten and Froment [1986]

extended the Van Welsenaere and Froment approach to co-currently cooled tubular reactors in which the wall temperature varies with distance. Again, the runaway limits could be determined through very simple calculations. Parameter sensitivity in the presence of transport limitations was investigated by Rayadyaksha et al. [1975]. It will be dealt with in Section 11.9 of this chapter.

Finally, it should be added that the phenomenon of parametric sensitivity, dealt with in this section, is essentially different from the instability encountered in Chapter 10. The tubular reactor with plug flow without recycle as considered here is intrinsically stable in the strict sense (except if kinetic instability would occur). On removal of the perturbation, the reactor will return to its original state. The hysteresis phenomenon encountered in Chapter 10 is not possible in the present case: all intermediate steady states are possible.

EXAMPLE 11.5.3.A
APPLICATION OF THE FIRST RUNAWAY CRITERION OF VAN WELSENAERE AND FROMENT

The reaction and operating variables are those considered in Section 11.5.2, so that $A = 6150$, $B = 257 \times 10^6$, and $E/R = 13{,}636$.

Calculation of the permissible inlet partial pressure for a given wall and inlet temperature and given tube radius

Let $T_R = T_0 = 635$ K and $R_t = 0.0125$ m. According to the first criterion, the critical temperature is T_M, the maximum of the maxima curve, and $f_M = (E / RT_M^2)(T_M - T_r) = 1$, from which $T_M = 667.69$ K so that, to avoid runaway, the maximum ΔT in the reactor is 32.7°C. From (11.5.3-4) it follows that $Q = 2.9203$. Once Q is known, ΔT_{ad} can be calculated, and from $\Delta T_{ad} = (B / A)p_0$ the inlet partial pressure p_0 is obtained. The results are given in Table 11.5.3.A-1, where use has been made of equations (11.5.3-4), (11.5.3-5), and (11.5.3-6), respectively, for calculating ΔT_{ad}.

If $T_r = T_0 = 625$ K and $d_t/2 = 0.0125$ m, T_M is 656.6 K and ΔT has to be limited to 31.6 K. Then, $Q = 3.4675$. The corresponding p_0 values are given in Table 11.5.3.A-2. Numerical back integration from the critical point onward leads to a critical inlet value for p_0 of 0.01651 bar, which is in excellent agreement with the mean.

Calculation of the critical radius

Given $p_0 = 0.0127$ bar and $T_r = T_0 = 625$ K. What would be the radius leading to critical conditions? From (11.5.3-3), T_M is found to be 656.6 K, so that $\Delta T = 31.6$ K. ΔT_{ad} amounts to 521.09 K. From (11.5.3-4) it follows that $Q = 3.4675$.

TABLE 11.5.3.A-1

	ΔT_{ad}		p_0 (bar)
Lower limit	$\Delta T\left(1+Q^2\right)$	= 310°C	0.0075
Upper limit	$\Delta T\left(1+Q\right)^2$	= 504°C	0.012
Mean	$\Delta T\left(1+Q+Q^2\right)$	= 407°C	0.00978

TABLE 11.5.3.A-2

	ΔT_{ad}		p_0 (bar)
Lower limit	$\Delta T\left(1+Q^2\right)$	= 411.5°C	0.01371
Upper limit	$\Delta T\left(1+Q\right)^2$	= 521.1°C	0.02002
Mean	$\Delta T\left(1+Q+Q^2\right)$	= 466.3°C	0.01687

From

$$C = Q^2 A \exp\left(-\frac{E}{RT} + b\right)$$

the radius R_t is found to be 0.0175 m.

Subcritical conditions

Given a radius R_t =0.0125 m and p_0 = 0.0076 bar, determine the wall temperature that limits the hot spot to 675 K. For this maximum to be critical, the wall temperature would have to be, from (11.5.3-3), 641 K. The lower limit for the inlet partial pressure would be, from (11.5.3-4), 0.0086 bar; the upper limit, from (11.5.3-5), 0.0136 bar. Therefore, the maximum is definitely subcritical. With p = 0.0075 bar, it follows from B/A $p_0 = \Delta T_{ad}$ = 312.6 K. Q is found to be 3.094. Equation (11.5.3-6) then leads to $\Delta T = 22.9$ K, so that T_r = 652.2 K. A numerical integration starting from p_0 = 0.0076 bar and $T_0 = T_r$ = 652.2 K yields a maximum temperature of 677 K.

Figure 11.5.3-1 also permits a check on the criticality of the conditions. Therefore, we require the numerical values of the groups:

$$S = \frac{\left(-\Delta H\right)p_{A0}}{c_p M_m p_t}\left(\frac{E}{RT_r^2}\right) \quad \text{and} \quad N = \frac{4h}{k_B\left(T_r\right)d_t c_p}$$

where Barkelew's symbols and units were used in the group N. Thus, $k_B(T_r)$ is Barkelew's rate constant. Take care when translating this formula into the groups used here. Indeed, Barkelew expressed the rate as follows:

$$r = k_B C$$

where C = mole fraction of key reacting component A and k_B has the dimensions mol fluid/cm^3 bed s.

Van Welsenaere and Froment [1970] used a pseudo-first-order rate law:

$$r = k_F \rho_B^0 p_A$$

with r in kmol A/kg cat. h. It follows that

$$k_B = \frac{k_F p_t p_B^0 \rho_B}{3.6 \times 10^6}$$

so that, with the symbols and units used here, N becomes

$$N = \frac{4U}{3.6 \times 10^6 d_t c_p M} \frac{3.6 \times 10^6}{p_t p_B^0 \rho_B} \frac{1}{k_F(T_r)} = \frac{C}{A} \frac{1}{\exp\left(-\frac{a}{T_r} + b\right)}$$

Furthermore,

$$S = \frac{B}{A} p_0 \frac{E}{RT_r^2} = \frac{\Delta T_{ad}}{T_r} \frac{E}{RT_r} = \beta\gamma$$

For $d_t/2 = 0.0125$ m; $p_0 = 0.0076$ bar, and $T_r = 652.2$ K it has been calculated that $(B/A)p_0 = \Delta T_{ad} = 312.6$ K so that

$$S = \beta\gamma = 312.6 \times \frac{13{,}636}{(652.2)^2} = 10$$

Since

$$C = \frac{4U}{d_t c_p \rho_g} = \frac{2 \times 82.7}{0.0125 \times 0.323} = 41{,}000$$

and

$$A = \frac{M p_t p_B^0 \rho_B}{\rho_g} = \frac{29.48 \times 1 \times 0.208 \times 1300}{1.293} = 6{,}150$$

$$\frac{N}{S} = \frac{C}{A} \frac{1}{\exp\left(-\frac{a}{T_r} + b\right)} \frac{1}{\beta\gamma} = \frac{41{,}000}{6{,}150 \times 0.348} \times \frac{1}{10} = 1.92$$

The point (1.92; 10) falls well above curves 1, 2, 4, and 5 in Fig. 11.5.3-1, so that the reactor is insensitive. ■

11.5.4 The Multibed Adiabatic Reactor

In discussing the preliminary design of fixed bed reactors in Section 11.3, it was mentioned that adiabatic operation is frequently considered in industrial operation because of the simplicity of construction of the reactor. It was also mentioned why straight adiabatic operation may not always be feasible and examples of multibed adiabatic reactors were given. With such reactors the question is how the beds should be sized. Should they be designed to have equal $\Delta T'$s or is there some optimum in the $\Delta T'$s, therefore in the number of beds and catalyst distribution? In Section 11.3 this problem was already discussed in a qualitative way. It is taken up in detail on the basis of an example drawn from SO_2 oxidation, an exothermic reversible reaction. To simplify somewhat, it will be assumed that no internal gradients occur inside the catalyst so that the effectiveness factor is 1.

A very convenient diagram for visualizing the problem of optimizing a multibed adiabatic reactor is the conversion-versus-temperature plot, already encountered in Section 11.3, and drawn in Fig 11.5.4-1 for the SO_2 oxidation based on the rate equation of Collina, Corbetta, and Cappelli [1971] with an

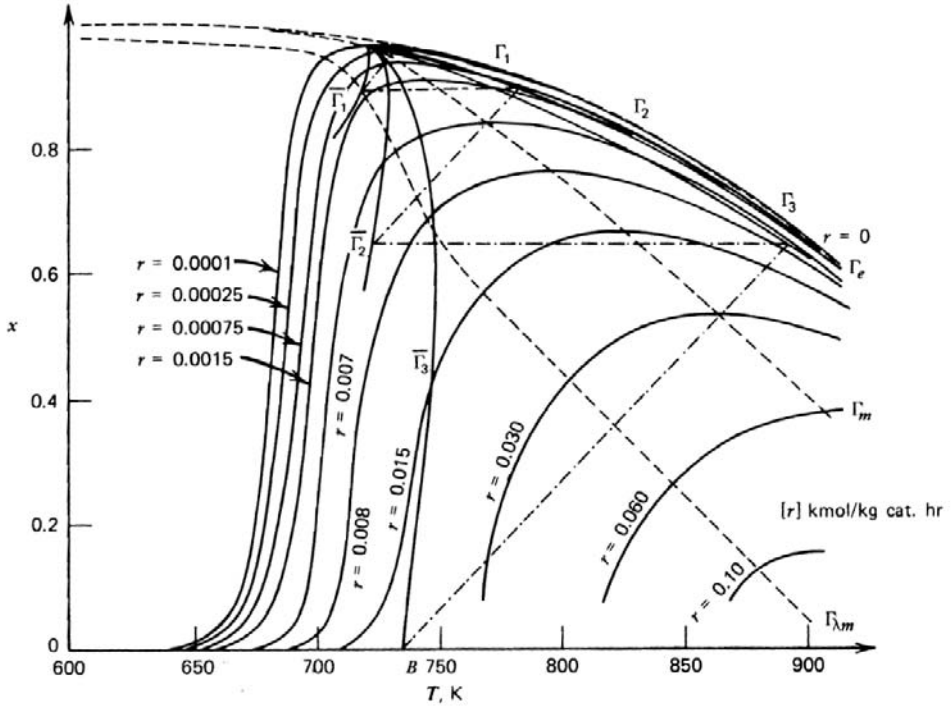

Figure 11.5.4-1

Conversion-versus-temperature plot for SO_2 oxidation.

effectiveness factor of 1. (For further reading on this subject see Livbjerg and Villadsen [1972] and Calderbank [1952, 1953]). This equation is based on the Hougen-Watson concept and on the observation that the reaction between adsorbed SO_2 and oxygen from the gas phase is the rate-controlling step:

$$r = \frac{k_1 p_{o_2} p_{so_2} \left(1 - \dfrac{p_{so_3}}{p_{so_2} \cdot p_{o_2}^{1/2} K_p} \right)}{22.414 \left(1 + K_2 p_{so_2} + K_3 p_{so_3} \right)^2} \qquad (11.5.4\text{-}1)$$

where

r = kmol SO_2/kg cat. h

k_1 = $\exp(12.160 - 5473/T)$

K_2 = $\exp(-9.953 + 8619/T)$

K_3 = $\exp(-71.745 + 52596/T)$

K_p = $\exp(11300/T - 10.68)$

The coefficients k_1, K_2 and K_3 were determined by nonlinear regression on 59 experiments carried out in a temperature range of 420° to 590°C. The partial pressures are converted into conversions by means of the following formulas. For 1 mol SO_2 fed per hour, the molar flow rates in a section where the conversion is x are given in the left-hand column. The partial pressures are given in the right-hand column:

mol SO_2	$1 - x$	$\dfrac{1-x}{\left(1 + a + b\right) - \frac{1}{2}x} p_t$
a mol O_2	$a - \frac{1}{2}x$	$\dfrac{a - \frac{1}{2}x}{\left(1 + a + b\right) - \frac{1}{2}x} p_t$
b mol N_2	b	
SO_3	x	$\dfrac{x}{\left(1 + a + b\right) - \frac{1}{2}x} p_t$
Total molar flow		$\left(1 + a + b\right) - \frac{1}{2}x$

Figure 11.5.4-1 contains curves of equal reaction rate ("rate contours") $r(x, T)$ = constant. These are obtained by finding the root of $r(x, T) - C = 0$ for a given temperature value. The shape of these contours is intuitively clear: at a constant conversion, the rate first increases with temperature but then decreases as the influence of the equilibrium is more strongly felt. The figure also contains the Γ_e

curve. This is the locus of equilibria conditions. The Γ_m curve is the locus of the points in which the rate is maximum, by the appropriate selection of the temperature (i.e., $\partial r / \partial T = 0$). This locus is found by determining the root of $\partial r(x,T) / \partial T = 0$ for given values of the temperature. The curve $\Gamma_{\lambda m}$, also shown, is the locus of the points in which the rate is maximum when the reaction is carried out adiabatically. This locus is found by determining along the adiabatic line, starting from the inlet temperature and by means of a search method, the position where the rate is maximum. The $\Gamma_{\lambda m}$ curve is also the locus of the contact points between the adiabatic lines, which are straight lines with a slope

$$\lambda = \frac{\dot{m} c_p}{F_{A0}(-\Delta H)}$$

and the rate contours.

The figure has been calculated for the following feed composition: 7.8 mole-% SO_2; 10.8 mole-% O_2; 81.4 mole-% inerts, atmospheric pressure, a feed temperature of 37°C, a mean specific heat of 0.925 kJ/kg K and a $(-\Delta H)$ of 89,600 kJ/kmol. Cooling by means of a heat exchanger is represented by a parallel to the abscissa in this diagram.

If only the amount of catalyst is considered in an optimization of the reactor, the curve Γ_m would have to be followed. If, in addition, it is attempted to achieve this by adiabatic operation, the curve $\Gamma_{\lambda m}$ would have to be followed as closely as possible. This is achieved by the zigzag line shown in the figure and corresponding to multibed adiabatic operation. The more beds there are, the better $\Gamma_{\lambda m}$ is approximated. However, when the cost of equipment, supervision, control, and the like is also taken into account, there is an optimum in the number of beds. Accounting in the optimization for the profit resulting from the conversion will, of course, also affect the location of the optimal zigzag line. The choice of the inlet temperature to a bed and the conversion in it determine the amount of catalyst required in that bed and also the heat exchanger. With N beds, $2N$ decisions have to be taken. The simultaneous variation of $2N$ variables to find the optimum policy leads to an enormous amount of computation, which rapidly becomes prohibitive, even for fast computers. There are methods for systematizing the search for the optimum and for reducing the amount of computation. A technique that is very well suited for stagewise processes is the technique of "dynamic programming," which allows one to reduce a $2N$-dimensional problem to a sequence of two-dimensional problems. The method introduced by Bellman [1957] has been discussed in detail in books by Aris [1960] and by Roberts [1964]. Only a brief discussion, oriented toward direct application, is given here.

The calculations do not necessarily proceed according to the direction of the process flow. This is only so for a final-value problem (i.e., when the conditions at the exit of the reactor are fixed). For an "initial-value" problem, whereby the inlet conditions are fixed, the direction of computation for the optimization is opposite to that of the process stream. In what follows, an initial-value problem is treated.

First, consider the last bed. No matter what the policy is before this bed, the complete policy cannot be optimal when the last bed is not operating optimally, whatever its feed. The specifications of the feed of the last bed are not known yet. Therefore, the optimal policy of the last bed has to be calculated for a whole set of possible inlet conditions.

Next, consider the last two beds. There exists an optimal policy for the subsystem comprising the two beds as a whole. In this optimal policy the first of the two (considered in the direction of the process flow) does not necessarily operate in the conditions which would be optimal if it were alone. The second has to be optimal for the feed coming from the first, however, or the combined policy would not be optimal. Therefore,

$$\begin{bmatrix}\text{maximum profit}\\ \text{from two beds}\end{bmatrix} = \text{maximum of}\left[\left(\begin{matrix}\text{profit of}\\ \text{first bed}\end{matrix}\right) + \left(\begin{matrix}\text{maximum profit}\\ \text{of second bed}\\ \text{with feed}\\ \text{from first}\end{matrix}\right)\right] \quad (11.5.4\text{-}2)$$

To find this maximum it suffices to choose the conditions in the first of the two beds, since the optimal policy of the second has been calculated already. Equation (11.5.4-2) is Bellman's "optimum principle." Consider now the last three beds. These can be decomposed into a first bed (in the direction of process flow) and a pseudo-stage consisting of the last two beds, for which the optimal policy has already been calculated for a series of inlet conditions. The procedure is continued in the same way towards the inlet of the multibed reactor.

Finally, all stages are done again in the direction of the process stream to determine "the" optimal policy, corresponding to the given feed to the whole reactor, among all available data. Dynamic programming is a so-called imbedding technique. Optimal policies are computed for all possible feed conditions of which ultimately only one is retained — that corresponding to the given feed conditions. Nevertheless, dynamic programming permits an enormous saving in computation time, because the conditions are only varied step by step (i.e., sequentially and not simultaneously over the N stages).

The optimization procedure is illustrated here for an exothermic, reversible reaction. The cooling between the beds is realized by means of heat exchangers. With N stages, $2N$ decisions have to be taken: N inlet temperatures to

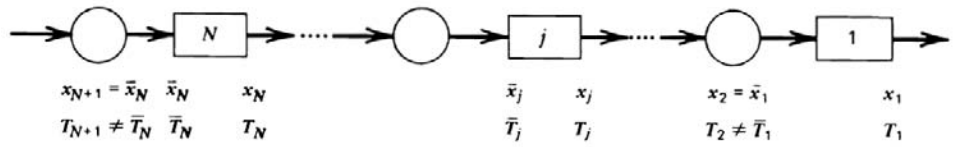

Figure 11.5.4-2

Definition of symbols used in multibed adiabatic reactor optimization by dynamic programming.

the beds and N conversions at the exit of the beds. The beds are numbered in the direction of the computations, that is, opposite to the process flow, since the case considered is an initial-value problem. The symbols are shown in Fig. 11.5.4-2; x_{N+1} and T_{N+1} are given. The conversion is not affected by the heat exchanger, so that $\bar{x}_j = x_{j+1}$. The choice of the inlet temperature to bed j together with the exit temperature of bed $j + 1$ determines the heat exchanger between $j + 1$ and j; the choice of x_j determines the amount of catalyst in j. These decisions have to be optimal with respect to a certain objective or profit function. Such a profit function contains the profit resulting from the conversion of A (e.g., SO_2) into the product P (e.g., SO_3), but also the costs (catalyst, construction, control, and the like). If the costs were not taken into account, it would follow from the computations that the conversions should proceed to the equilibrium values, and this would require an infinite amount of catalyst. Let α represent the profit resulting from the conversion of 1 kmol of A into P. (e.g., U.S. \$/kmol). Per stage, the value of the reaction mixture increases by an amount (in \$/h)

$$\alpha F_{A0}\left(x_j - \bar{x}_j\right)$$

where F_{A0} is the molar feed rate of A (kmol/h).

The only negative item considered in this example is the cost of the catalyst. The cost of cooling is not considered here. For a detailed example taking this into account, see Lee and Aris [1963]. For a given purchase price and life, the cost of 1 kg of the catalyst can be expressed per hour, say, β /h. If the conversion in bed j requires W_j kg catalyst, then the cost of this stage is βW_j and the net profit is

$$\alpha F_{A0}\left(x_j - \bar{x}_j\right) - \beta W_j$$

Summing up over all the beds, the total profit P_N becomes

$$P_N = \sum_1^N \left[\alpha F_{A0}\left(x_j - \bar{x}_j\right) - \beta W_j\right]$$

or

$$P_N = \alpha F_{A0} \sum_1^N \left[\left(x_j - \bar{x}_j \right) - \nu \frac{W_j}{F_{A0}} \right] = \alpha F_{A0} \sum_1^N p_j \qquad (11.5.4\text{-}3)$$

where

$$\nu = \frac{\beta}{\alpha} \qquad \text{and} \qquad p_j = \left(x_j - \bar{x}_j \right) - \nu \frac{W_j}{F_{A0}}$$

Because αF_{A0} is a fixed amount, it suffices to optimize the quantity in the square brackets: the maximum profit is obtained subsequently by multiplying by αF_{A0}.

The problem is now to optimize (11.5.4-3), that is, to find

$$\text{Max} \sum_1^N p_j = g_N(N+1)$$

by the proper choice of $\bar{T}_N, x_N; \bar{T}_{N-1}, ..., \bar{T}_1, x_1$. For the bed numbered 1:

$$g_1(x_2) = \text{Max}\, p_1 = \text{Max}\left(x_1 - x_2 - \nu \frac{W_1}{F_{A0}} \right) = \text{Max} \int_{x_2}^{x_1} \left(1 - \frac{\nu}{r_1} \right) dx \qquad (11.5.4\text{-}4)$$

Therefore, $\bar{T}_1$ and x_1 have to be chosen such that

$$\frac{\partial p_1}{\partial x_1} = 1 - \frac{\nu}{r_1} = 0 \qquad (11.5.4\text{-}5)$$

and

$$\frac{\partial p_1}{\partial \bar{T}_1} = \nu \int_{x_2}^{x_1} \frac{1}{r_1^2} \frac{\partial r_1}{\partial \bar{T}_1} dx = 0 \qquad (11.5.4\text{-}6)$$

Equation (11.5.4-5) means that the reaction has to be stopped when the rate has reached a value of ν. Beyond that point, the increase in cost outweighs the increase in profit resulting from the conversion. It is clear that this point is situated on that part of the adiabatic reaction path that is beyond $\Gamma_{\lambda m}$ and Γ_m. The part of the rate contour that has a value ν and that is to the right of Γ_m is represented by Γ_1.

The second condition in (11.5.4-6) is satisfied only when $\partial r / \partial \bar{T}_1$, the partial derivative of the rate with respect to the temperature, is partly positive and partly negative. Substituting into this partial derivative, the relation between x and T along an adiabatic reaction path starting from Γ_1 [condition (11.5.4-5)] turns $\partial r / \partial \bar{T}_1 = f_1(x, T_1)$ into a function $\partial p / \partial \bar{T}_1 = f_2(\bar{T}_1)$. The root of this equation is easily found by a one-dimensional search procedure and is the optimum inlet temperature leading to the exit conditions represented by the point chosen on Γ_1. This procedure is repeated for a certain number of points on Γ_1 to

obtain the locus of optimum inlet conditions for bed 1, represented by $\overline{\Gamma}_1$ in Fig. 11.5.4-1. It follows from (11.5.4-6) that Γ_1 and $\overline{\Gamma}_1$ intersect on Γ_m, not on $\Gamma_{\lambda m}$.

Consider now two steps, the last two of the multibed adiabatic reactor. From Bellman's maximum principle it follows that the optimal policy of bed 1 is preserved. This time, x_2 and $\overline{T}_2$ have to be chosen in an optimal way to arrive at

$$g_2(x_3) = \mathrm{Max}\left(p_2 + p_1\right) = \mathrm{Max}\left[\int_{x_3}^{x_2}\left(1-\frac{v}{r_2}\right)dx + g_1(x_2)\right]$$

To do so, the following conditions have to be fulfilled:

$$\frac{\partial}{\partial x_2}\left(p_2 + p_1\right) = 0 \tag{11.5.4-7}$$

$$\frac{\partial}{\partial \overline{T}_2}\left(p_2 + p_1\right) = 0 \tag{11.5.4-8}$$

where x_2 is the upper limit of the integral but appears also in $g_1(x_2)$, so that it is necessary to calculate dg_1/dx_2. Since $g_1 = f(x_2, x_1, \overline{T}_1)$,

$$\frac{dg_1}{dx_2} = -\left[1-\frac{v}{r_1(x_2,\overline{T}_1)}\right] + \left[1-\frac{v}{r_1(x_1,\overline{T}_1)}\right]\frac{dx_1}{dx_2} + \left[\int_{x_2}^{x_1}\frac{v}{r_1^2}\frac{\partial r_1}{\partial \overline{T}_1}dx\right]\frac{dT}{dx_2}$$

whereby dT/dx_2 has to be taken along an adiabatic path, so that

$$T = \overline{T}_1 + \frac{1}{\lambda}\left(x - x_2\right)$$

It follows that

$$\frac{dT}{dx_2} = \frac{d\overline{T}_1}{dx_2} - \frac{1}{\lambda}$$

Stage 1 has been determined in such a way that the parts between the brackets of the last two terms are zero, and since neither dx_1/dx_2 nor dT/dx_2 are infinite,

$$\frac{dg_1}{dx_2} = -\left[1-\frac{v}{r_1(x_2,\overline{T}_1)}\right]$$

and

$$\frac{\partial}{\partial x_2}\left(p_2 + p_1\right) = \left[1-\frac{v}{r_2(x_2)}\right] - \left[1-\frac{v}{r_1(x_2)}\right] = 0$$

The optimal policy, therefore, requires that

$$r_2(x_2, T_2) = r_1(x_2, \bar{T}_1) \tag{11.5.4-9}$$

which means that the rate at the exit of bed 2 must equal that at the inlet of bed 1. This determines the heat exchanger: it should change the temperature in such a way that (11.5.4-9) is fulfilled. Figure 11.5.4-3 illustrates how the curve representing optimal exit conditions for bed 2 (i.e., Γ_2) may be obtained from curve $\bar{\Gamma}_1$ — the heat exchanger does not modify the conversion.

The second condition, (11.5.4-7), leads to

$$\frac{\partial}{\partial \bar{T}_2}(p_2 + p_1) = \frac{\partial p_2}{\partial \bar{T}_2} = v \int_{x_3}^{x_2} \frac{1}{r_2^2} \frac{\partial r}{\partial \bar{T}_2} dx = 0 \tag{11.5.4-10}$$

Equation (11.5.4-10) is completely analogous to (11.5.4-6), and the locus of optimal inlet temperatures to bed 2, represented by $\bar{\Gamma}_2$, is derived from Γ_2 in the same way as $\bar{\Gamma}_1$ is from Γ_1. The procedure outlined above may be continued for further beds. Figure 11.5.4-1 shows Γ and $\bar{\Gamma}$ curves for a three-bed SO_2 oxidation reactor. For a given feed at 310K and zero conversion, the optimal policy is determined as shown: first preheat to *B*, then perform the adiabatic reaction in bed 3 until curve Γ_3, and so on.

The above discussion was based on a graphical representation. In reality, the computations are performed on a computer and the $x_j, T_j, \bar{x}_j$, and $\bar{T}_j$ values are stored. The above has been applied to a three-bed adiabatic reactor for SO_2 oxidation, using Collina, Corbetta, and Cappelli's [1971] rate equation. The pressure is considered constant. There are no ΔT and Δp over the film surrounding the catalyst. Also, to simplify the treatment, the effectiveness factor is considered to be 1 in this illustrative example. The objective function to be optimized consists of two parts:

1. The profit resulting from the conversion.
2. The cost of the catalyst and the reactor, *v*.

From an example treated by Lee and Aris [1963], α = 2.5$/kmol SO_2 converted, β = 0.00037 $/kg cat. h. The amount of gas fed was 55,000 kg/h.

The feed composition is that already mentioned in (10.5.4-1). The results are represented graphically in Fig. 11.5.4-1. This figure shows, besides the reaction contours and Γ_e, Γ_m, and $\Gamma_{\lambda m}$ curves, the Γ and $\bar{\Gamma}$ curves and the optimum reaction path. Note that (11.5.4-6) and (11.5.4-10) require the reaction path to lie on both sides of Γ_m, but not necessarily on both sides of $\Gamma_{\lambda m}$. The latter may differ significantly from Γ_m for rate contours of the type encountered

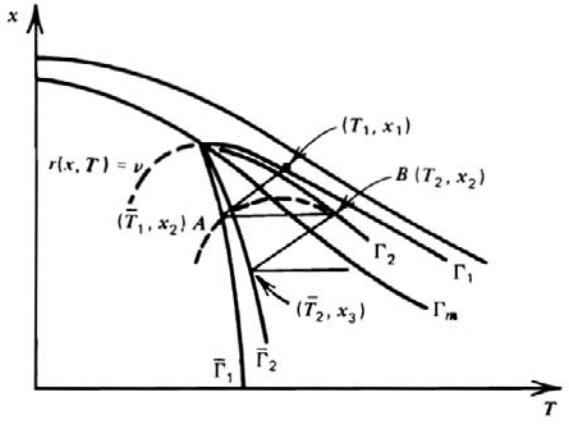

Figure 11.5.4-3

Optimal reaction paths in a multibed adiabatic reactor according to dynamic programming.

TABLE 11.5.4-1

Bed	$\bar{x}_j$	x_j	$\bar{T}_j$ (K)	T_j (K)	**Profit** ($/kg gas)	**Total profit** ($/kg gas)	**Catalyst Weight** (kg)
1	0.	0.65	734.2	891.2	0.00405	0.00405	3248
2	0.65	0.90	723.3	783.3	0.00152	0.00557	7819
3	0.90	0.96	718.5	733.6	0.00029	0.00586	14.427

Optimal three-bed reactor for SO_3 synthesis. Rate equation from Collina et al. [1971].

with the rate equations considered here. Table 11.5.4-1 contains the weights of catalyst in each bed for both rate equations. Note the large conversion in the first bed obtained with relatively little catalyst and the large amount of catalyst required in the third bed. In practice, intermediate cooling is also realized by cold shot cooling. The optimization of such a reactor has been discussed in detail by Lee and Aris [1963]. Further work on the optimization of SO_2 oxidation has been published by Paynter et al. [1971] and by Burkhardt [1968].

11.5.5 Fixed Bed Reactors with Heat Exchange Between the Feed and Effluent or Between the Feed and Reacting Gas. "Autothermal Operation"

In industrial operation it is necessary, for economic reasons, to recover as much as possible the heat produced by exothermic reactions. One obvious way of doing this, mentioned earlier in Section 11.3, is to preheat the feed by means of the reacting fluid and/or the effluent. When the heat of reaction is sufficient to raise

the temperature of the feed to such a value that the desired conversion is achieved in the reactor without further addition of heat, the operation is called "autothermal." Some of the most important industrial reactions such as ammonia and methanol synthesis, SO_2 oxidation, and phthalic anhydride synthesis, the water gas shift reaction can be carried out in an autothermal way. Coupling the reactor with a heat exchanger for the feed and the reacting fluid or the effluent leads to some special features that require detailed discussion.

Consider, as an example, a large-size ammonia synthesis process. In such a process, producing 5000 T/day of ammonia in a single converter, the feed is preheated by the effluent in a heat exchanger. In the catalyst bed itself, the reaction is carried out adiabatically. For reasons discussed in Section 11.3, the reactor is subdivided into several beds with intermediate cold shot cooling. The principles are discussed first on a simplified scheme consisting of only one adiabatic bed with given amount of catalyst and one heat exchanger with given exchange surface, as shown in Fig. 11.5.5-1.

Consider a single reaction and let the pressure drop over the reactor be small so that a mean value may be used with sufficient accuracy. Then, the continuity equation for the key component and the energy equations for the reactor and the heat exchanger, respectively, may be written (in the steady state)

$$\frac{dx}{dz} = \frac{\pi d_t^2}{4F_{A0}} \rho_B r_A \tag{11.5.5-1}$$

$$\frac{dT}{dz} = \frac{\pi d_t^2}{4} \frac{\rho_B (-\Delta H) r_A}{\dot{m} c_p} \tag{11.5.5-2}$$

$$\frac{dT_1}{dz'} = \frac{U \pi d_t}{(\dot{m} c_p)_1} (T_2 - T_1) \tag{11.5.5-3}$$

$$(\dot{m} c_p)_1 dT_1 = -(\dot{m} c_p)_2 dT_2$$

with the following boundary conditions:

In the reactor,

$$x(z = 0) = x_i$$

$$T(z = 0) = T_1(Z' = L)$$

In the heat exchanger, with reference to the complete system inlet and outlet temperatures,

$$T_1(z' = 0) = T_i$$

$$T_2(z'=0) = T_e \qquad \text{unknown}$$

or with reference to the reactor inlet and outlet temperatures,

$$T_1(z'=Z'=L) = T(z=0)$$

$$T_2(z'=Z'=L) = T(z=Z) \qquad \text{unknown}$$

where L is the length of the heat exchanger.

For the situation represented in Fig. 11.5.5-1, $(\dot{m}\,c_p)_1 = (\dot{m}\,c_p)_2$. It is seen how the reactor and heat exchanger are coupled through the boundary or initial conditions. Even more, the problem is a so-called two-point boundary value problem. Indeed, the inlet temperature to the reactor, $T(0)$, is not known, since $T_1(Z'=L)$ depends on the outlet temperature of the reactor. For the heat exchanger, $T_1(0) = T_i$ is given, but not $T_2(0)$, that depends on the reactor outlet temperature. Solving the problem, therefore, involves trial and error. One procedure assumes a value for $T(0) = T_1(L)$ and simultaneously integrates the differential equations describing the reactor, (11.5.5-1) and (11.5.5-2), yielding $T(Z) = T_2(z'=L)$. Then, the heat exchanger (11.5.5-3) may be integrated, yielding $T_1(0)$. This value has to be compared with the given inlet temperature T_i. If it corresponds, the assumed

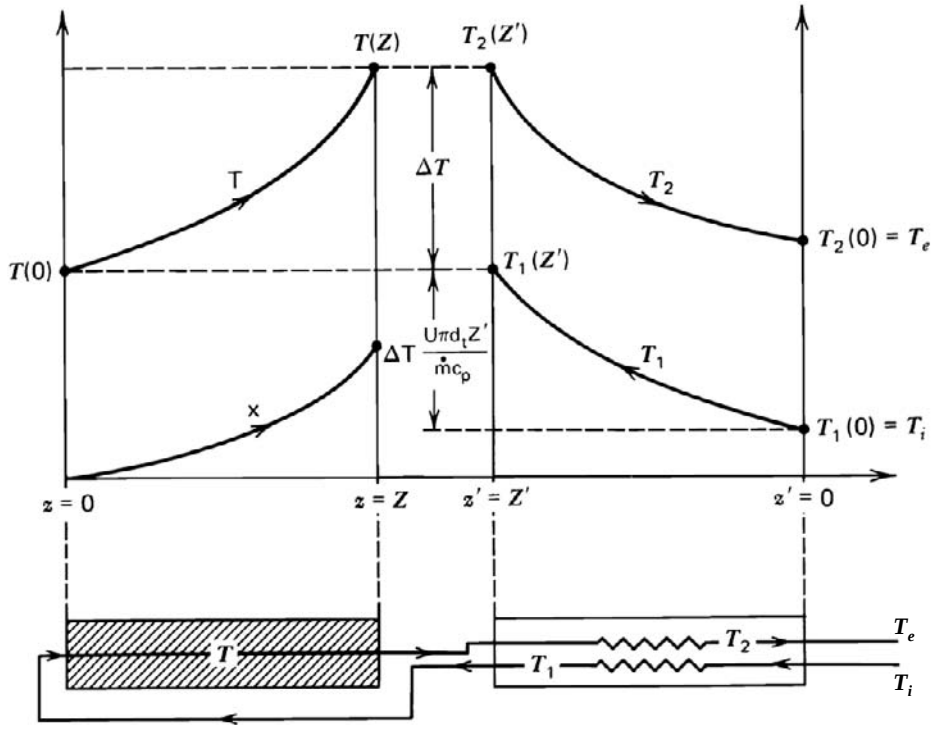

Figure 11.5.5-1

Single adiabatic bed with preheat of reactants by means of effluent.

value of $T(0)$ is correct and the calculated values are the final ones, if not $T(0)$ has to be improved. Problems of this type will be encountered later; but for a better insight, the one under discussion will be approached in a somewhat less formal way along the lines set by Van Heerden [1953] by decomposing it into two parts. First, consider the adiabatic reactor. In the formal procedure described above, the integration of (11.5.5-1) and (11.5.5-2) was performed for various values of $T(0)$. What are, then, the possible outlet conditions for the reactor? Integration of the ratio of (11.5.5-1) and (11.5.5-2) from the inlet to the outlet leads to

$$\Delta x = \frac{\dot{m} c_p}{F_{A0}\left(-\Delta H\right)} \Delta T = \lambda \Delta T = \lambda \left[T(Z) - T(0)\right] \qquad (11.5.5\text{-}4)$$

and integration of (11.5.5-1) leads to

$$\frac{W}{F_{A0}} = \int_{x(0)}^{x(Z)} \frac{dx}{r_A}$$

Let the reaction be reversible, $A \rightleftarrows B$, and first order in both directions, so that the rate can be written

$$r_A = k\left(p_A - \frac{p_B}{K} \right)$$

or

$$r_A = k p_t \left[\left(1 - x\right) - \frac{x}{K} \right]$$

or

$$r_A = A_0 p_t \left[\exp\left(-\frac{E}{RT} \right) \right] \left[\left(1 - x\right) - \frac{x}{K} \right]$$

in which T is to be substituted by $T(0) + \Delta x / \lambda$. This means that, for a given reaction [given A_0, E, K, c_p, $(-\Delta H)$, feed conversion $x(0)$, feed rate F_{A0}, and a given amount of catalyst, W],

$$x(Z) - x(0) = f\left[T(0)\right] \quad \text{and also} \quad T(Z) = g\left[T(0)\right] \qquad (11.5.5\text{-}5)$$

The shape of this relationship between the outlet and inlet conditions is shown in Fig. 11.5.5-2 as curve (a). The rising, sigmoidal-shaped part of curve (a) stems from the Arrhenius temperature dependence of the rate, the descending part from the unfavorable influence of the equilibrium. With such a bell-shaped curve there

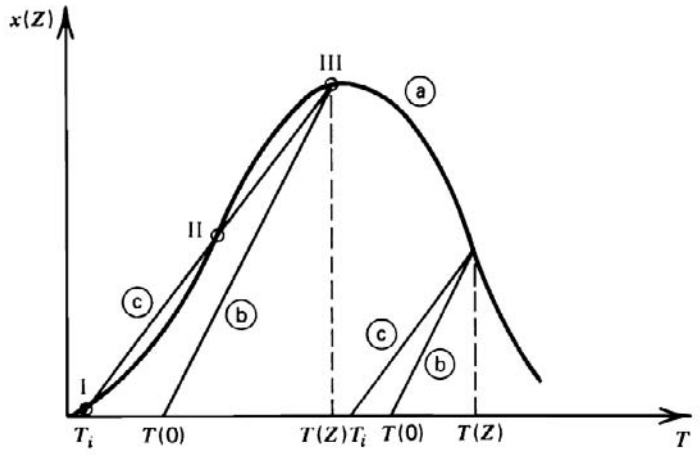

Figure 11.5.5-2

Possible steady-state operating points in reactor heat exchanger system, for two inlet temperatures T_i.

is an optimum region for $T(0)$ if a maximum conversion is to be reached. The location of curve (a) obviously depends on the factors that determine the kinetics of the reaction: total pressure, the reactant concentrations (in ammonia synthesis, the presence of inerts and catalyst activity). Curve (a) can also be considered as a measure of the amount of heat produced by the reaction.

In this diagram of possible outlet conditions for various inlet conditions, the adiabatic reaction path corresponding to given $x(0)$ and $T(0)$ is represented by the straight line (b) having a slope λ and ending in a point of (a). Curve (a) and the line (b) have only one point in common.

The second step in the formal procedure is to calculate the temperatures in the heat exchanger and to check whether or not the assumed $T(0)$ leads to $T_1(0) = T_i$. The coupling with a heat exchanger will obviously impose a restriction on the $T(0)$.

Simplifying somewhat and considering the difference $T_2 - T_1 = \Delta T$ to be constant over the total length of the heat exchanger, L, the equation for the heat exchanger (11.5.5-3) becomes, after integration,

$$\frac{\int_{T}^{T(0)} dT_1}{\Delta T} = \frac{U\pi d_t}{\dot{m}c_p} L$$

or

$$T(0) - T_i = \frac{U\pi d_t}{\dot{m}c_p} L\Delta T \qquad (11.5.5\text{-}6)$$

adding $T(Z)$ to both sides and transferring $T(0)$ to the RHS,

$$T(Z) - T_i = \Delta T\left(1 + \frac{U\pi d_t}{\dot{m}c_p}L\right)$$

since

$$\Delta T = T_e - T_i = T_2 - T_1 = T(Z) - T(0)$$

Now, $\Delta T = T(Z) - T(0)$ is the adiabatic temperature rise in the reactor, which is given by (11.5.5-4). So, combining the reactor and the heat exchanger leads to

$$x(Z) - x(0) = \frac{\lambda\left[T(Z) - T_i\right]}{1 + \dfrac{U\pi d_t}{\dot{m}c_p}L} \qquad (11.5.5\text{-}7)$$

which reduces to (11.5.5-4) when $L = 0$ [i.e., when there is no heat exchanger, since T_i then equals $T(0)$].

Equation (11.5.5-7) is represented in the $x - T$ diagram by a straight line (c), starting from T_i, with a slope

$$\frac{\lambda}{1 + \dfrac{U\pi d_t}{\dot{m}c_p}L}$$

smaller than λ, and ending on a point of (a). Line (c) may be considered to be representative of the amount of heat exchanged.

The steady state of the complete unit — reactor and heat exchanger — has to satisfy both (11.5.5-5) and (11.5.5-7). But it is easily seen that, depending on the location of T_i and on the slope, the straight line (c) can have up to three intersections with (a) (i.e., three steady-state operating conditions are possible for the system reactor + heat exchanger, whereas the reactor by itself in Fig. 11.5.5-2 has a unique steady state). The multiplicity of steady states in the complete system is a consequence of the thermal feedback between the feed and the effluent in the heat exchanger.

The operating point represented by I in Fig. 11.5.5-2 is of no practical interest: the conversion achieved under these conditions is far too low. The operating point corresponding to II is a naturally unstable point (i.e., extremely sensitive to perturbations in the operating conditions). Indeed, for these conditions the slightest increase in $T(Z)$ has a much larger effect on the heat produced than on the heat exchanged [curve (a) has a much larger slope than line (c)] and the operating point will shift to III. The reverse would happen for a

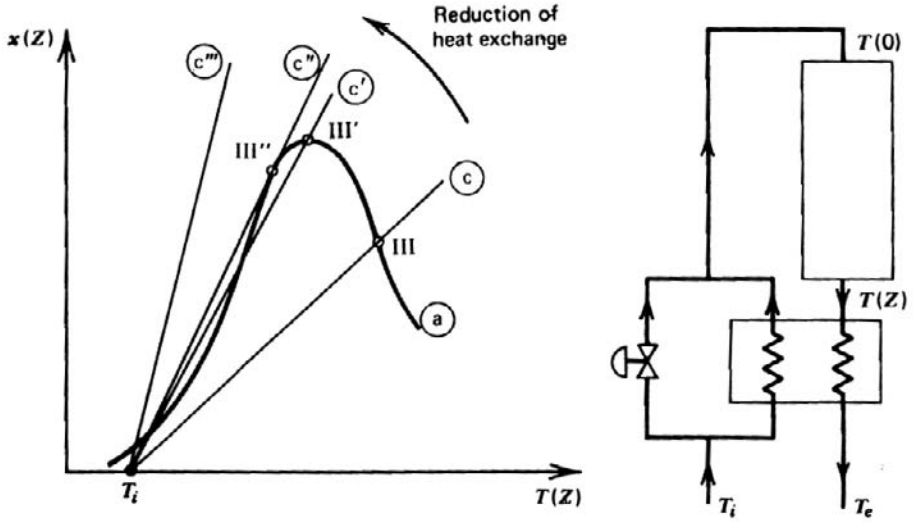

Figure 11.5.5-3

Modification of the location of the steady-state operating conditions as the amount of heat exchanged is reduced.

decrease in $T(Z)$: the operating point would shift to I and the reaction would practically extinguish. By the same reasoning it can be shown that III represents intrinsically stable operating conditions.

The conditions represented by III in Fig. 11.5.5-3 are not optimal, however, since the point is way beyond the maximum of (a), which means that the rate is considerably influenced already by the equilibrium. Operation in III", corresponding to the straight line (c") in Fig. 11.5.5-3, tangent to curve (a), would lead to an extremely sensitive reactor which would easily extinguish.

Obviously, with a heat-exchanging line (c'''), no intersection with (a) is possible, except at very low conversion, which is of no practical interest. The sensitivity of an ammonia synthesis reactor is well known to its operators. Thus, point III' is chosen as a reasonable compromise.

Increasing the slope of (c) to obtain a straight line (c') requires $T(Z)$ and therefore $T(0)$ to be lowered. At the design stage, this can be achieved by reducing the heat-exchange surface, therefore L in (11.5.5-7). For an existing reactor and given T_i this can also be achieved by the use of a bypass, so that less feed is preheated in the heat exchanger. This is effectively done in ammonia synthesis. Equation (11.5.5-7) is not valid any more in this situation, because ΔT no longer equals $T(Z) - T(0)$ in the heat exchanger, but rather $T(Z) - T_{1e}$, where T_{1e} is the exit temperature of the fraction of the feed flowing through the heat exchanger. The equation below is easily derived, completely along the lines followed in the former situation:

$$x(Z) - x(0) = \lambda \left(1 - \frac{\dfrac{U\pi d_t}{\dot{m}_h C_p} L \dfrac{\dot{m}_h}{\dot{m}_r}}{1 + \dfrac{Ud_t}{\dot{m}_h C_p} L} \right) \left[T(Z) - T_i \right] \qquad (11.5.5\text{-}8)$$

where $\dot{m}_r$ is the mass flow rate through the reactor and $\dot{m}_h$ is the mass flow rate through the heat exchanger. When $\dot{m}_h / \dot{m}_r$ equals 1, (11.5.5-8) reduces to (11.5.5-7). When this ratio is smaller than unity, the slope of Δx versus $T(Z) - T_i$ becomes larger than that in the case represented by (11.5.5-7). For the same T_i it follows that in the present situation, $T(Z)$ and $T(0)$ will be lower than in the former.

The bypass illustrated in Fig. 11.5.5-3 is important also for compensating for a decrease in catalyst activity. Initially the catalyst is very active; but due to poisons, temperature variations, and other operational problems inducing structural changes, the activity gradually decreases. Such a situation is represented in Fig. 11.5.5-4. A decrease in activity of the catalyst has to be compensated for by higher operating temperatures in the reactor, which means, for given T_i, that the heat-exchanging surface would have to be reduced. This is achieved by decreasing the amount of feed going through the bypass, reducing the slope in (11.5.5-8) to a value close to that encountered in the former situation, reflected by (11.5.5-7). It can be seen from Fig. 11.5.5-4 how $T(0)$ and $T(Z)$ correspondingly increase, so that the desired conversion is maintained.

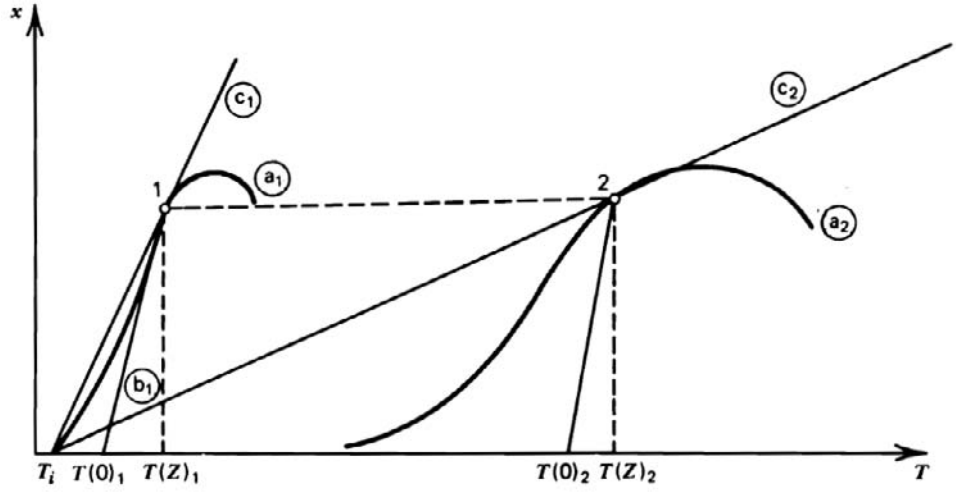

Figure 11.5.5-4
Influence of catalyst activity on operating conditions.

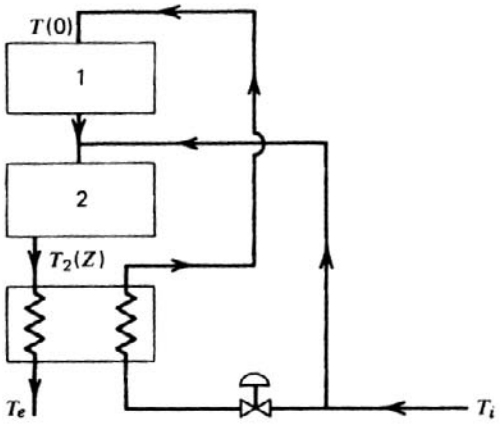

Figure 11.5.5-5
Schematic representation of two-stage adiabatic reactor.

It is stressed again that the occurrence of multiple steady states is due to the feedback of heat. Tubular reactors that are not coupled with a heat exchanger generally do not exhibit this feature — except in very particular situations, as will be shown later. This does not mean that perturbations in the operating conditions cannot give rise to drastic changes in the conversion and temperature profiles, but this is then caused by parametric sensitivity, a feature already discussed in Section 11.5.2.

The preceding discussion is illustrated quantitatively by the results of a simulation study by Shah [1967], who numerically integrated the system of differential equations describing an ammonia synthesis reactor of the type represented schematically in Fig. 11.5.5-5 and including an intermediate quench by means of cold feed. Figure 11.5.5-6 shows the hydrogen conversion and outlet temperature as a function of the percentage of the feed being preheated. When the fraction of the feed being preheated exceeds 0.7, two exit conditions are possible: for instance, when all the feed is preheated, 18.5 percent and 15.5 percent for the conversion and 547°C and 487°C for the temperature. If the amount of "cold split" becomes too important, no solution is found (i.e., no autothermal operation is possible).

The same situation is reflected in Fig. 11.5.5-7, which shows the effect of inlet temperature on the exit conditions; again two steady states are found. Also, when the inlet temperature is decreased below 107°C, the reactor is extinguished. It also follows from Fig. 11.5.5-7 that the maximum conversion is obtained close to the conditions leading to extinction, as shown already in the preceding discussion. The simulation also predicts that the reactor would extinguish when the pressure is decreased from 240 bar to 160 bar or the inerts

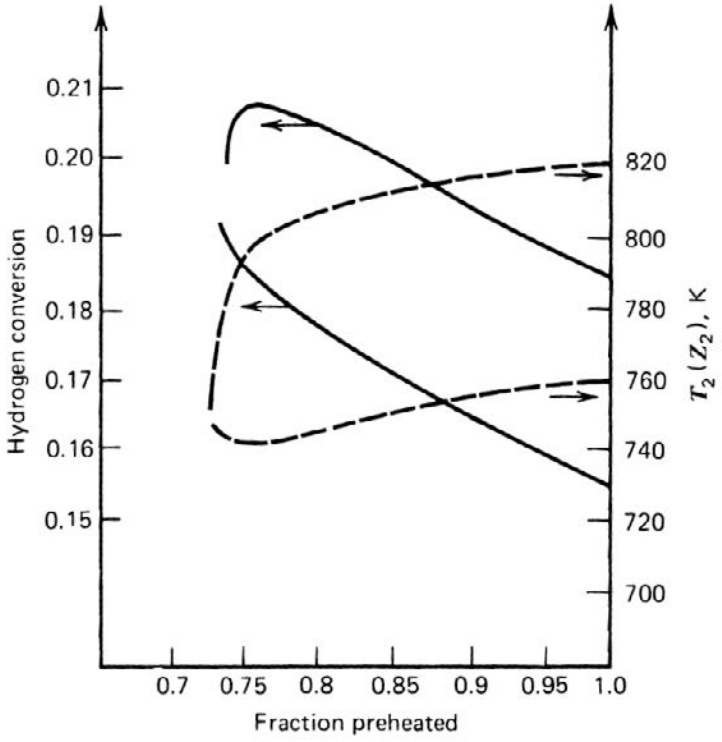

Figure 11.5.5-6

Two-stage adiabatic reactor. Hydrogen conversion as a function of fraction of feed being preheated. From Shah [1967].

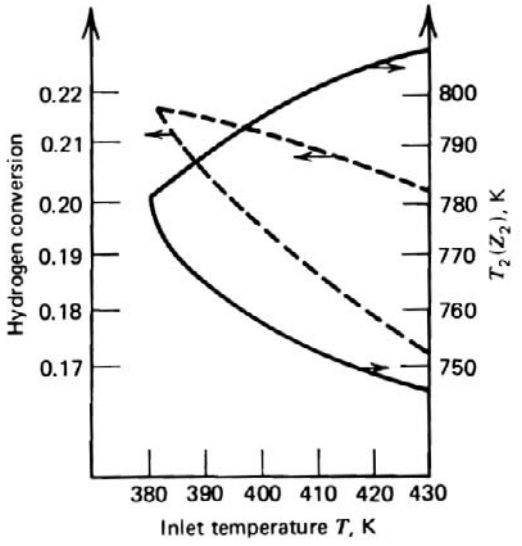

Figure 11.5.5-7

Two-stage adiabatic reactor. Hydrogen conversion versus inlet temperature. From Shah [1967].

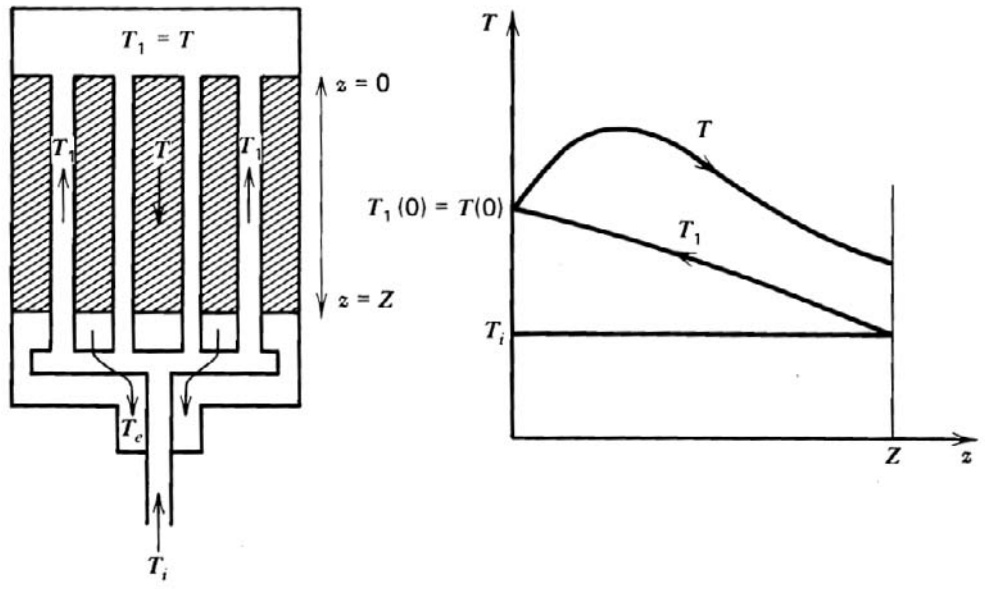

Figure 11.5.5-8
Multitubular reactor with internal heat exchanger.

content increased from 9 percent to 18 percent. Therefore, the inlet temperature T_i should be kept sufficiently above the blowout temperature (20°C to 25°C) to avoid the possibility that an increase in inerts content or in the feed rate may cause instability. The question of which steady state will be attained depends on the initial conditions and cannot be answered by steady-state calculations — transients have to be considered.

The scheme illustrated by Fig. 11.5.5-5 is not the only one possible for autothermal operation. Another possibility is the multitubular arrangement with internal heat exchanger, represented schematically in Fig. 11.5.5-8, together with the temperature profiles in the catalyst bed and in the heat exchanger tubes. For constant total pressure, the simulation of such a reactor with built-in heat exchanger requires the simultaneous integration of the continuity equation(s) for the key component(s) and of two energy equations, one for the effluent gas in the tubes and one for the reacting gas in the catalyst bed.

The steady-state continuity equation for the key component may be written

$$\frac{dx}{dz} = r_A \rho_B \frac{\Omega}{F_{A0}}$$

Provided the heat capacities of the feed and the reacting gas are constant, the energy equation may be written

$$\frac{dT_1}{dz} = -\frac{UA_k}{\dot{m}c_p}(T - T_1)$$

for the reacting gas in the catalyst bed

$$\frac{dT}{dz} = \frac{(-\Delta H)\rho_B r_A}{u_s \rho_g c_p} - \frac{UA_k}{\dot{m}c_p}(T - T_1)$$

The boundary or initial conditions are

$$\begin{aligned} T &= T_1 \quad \text{at} \quad z = 0 \\ T_1 &= T_i \qquad\quad z = Z \\ x &= x_i \qquad\quad z = 0 \end{aligned}$$

Again, this is a two-point boundary value problem and again three steady states are possible, the outer two of which are stable, at least to small perturbations, the intermediate being unstable. A figure completely analogous to Fig. 11.5.5-2 may be constructed, with two types of curves: the first, bell-shaped for reversible reactions, which is a measure of the heat generated; and the second, a straight line, which is a measure of the heat exchanged. Again, for a certain range of operating variables, more than one intersection is possible.

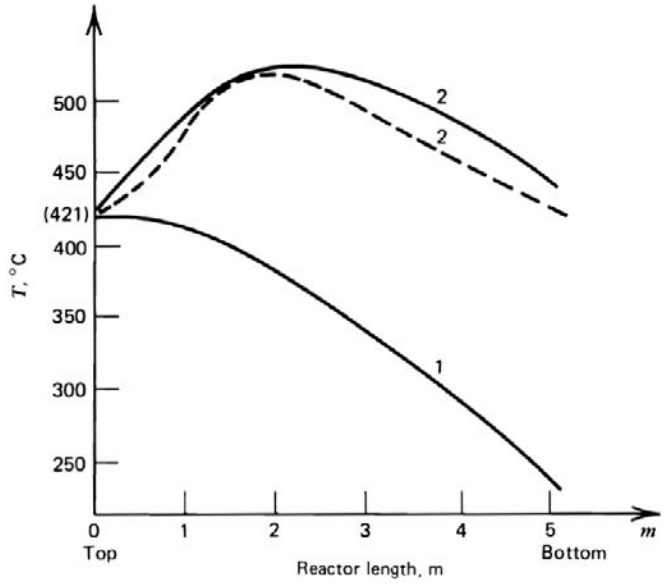

Figure 11.5.5-9

Temperature profiles inside TVA ammonia synthesis reactor. 1, Gas in heat exchanger tubes; 2, gas in catalyst bed; full curve 2, simulated; dashed curve 2, plant data. From Baddour et al. [1965].

The NEC (Nitrogen Engineering Co.) and TVA (Tennessee Valley Authority) ammonia synthesis reactors are practical realizations of the above principles. Figure 11.3-5 of Section 11.3 schematically represents a TVA reactor. The corresponding temperature profiles inside the tubes and in the catalyst bed section, calculated by Baddour, Brian, Logeais, and Eymery [1965] are shown in Fig. 11.5.5-9. Reactor dimensions for the TVA converters simulated by Baddour et al. [1965] and also by Murase, Roberts and Converse [1970] are

Catalyst Bed:

total catalyst volume = 4.07 m^3
reactor length = 5.18 m
reactor basket diameter = 1.1 m
reactor basket cross-sectional area = 0.95 m^2
catalyst bed cross-sectional area = 0.78m^2

Cooling Tubes:

number = 84
tube outside diameter = 50.8 mm
tube inside diameter = 38.1 mm
tube heat exchange area (outer) = 69.4 m^2
tube heat exchange area (inner) = 52.0 m^2

Typical operating conditions are as follows:

production capacity = 120 T NH_3/day
H_2 mole fraction in feed = 0.65
N_2 mole fraction in feed = 0.219
NH_3 mole fraction in feed = 0.052
inert = 0.079
mass flow rate = 26,400 kg/h
space velocity = 13,800 h^{-1}
pressure = 290 bar
top temperature = 421°C

The rate equation used in these simulations is that proposed by Temkin and Pyzhev [1960]

$$r_A \rho_B = f\left(k_1 \frac{p_{N_2} p_{H_2}^{1.5}}{p_{NH_3}} - k_2 \frac{p_{NH_3}}{p_{H_2}^{1.5}} \right)$$

where r_A is the rate of reaction of nitrogen (kmol/kg cat. h), f is the catalyst activity (1, at zero process time), and

$$k_1 = 1.79 \times 10^4 \exp\left(-\frac{87{,}090}{RT}\right) \qquad k_2 = 2.57 \times 10^{16} \exp\left(-\frac{198{,}464}{RT}\right)$$

$$-\Delta H = 111{,}370 \text{ kJ/kmol } N_2 \text{ reacted}$$

Baddour et al. [1965] retained the above model equations after checking for the influence of heat and mass transfer effects. The maximum temperature difference between gas and catalyst was computed to be 2.3°C at the top of the reactor, where the rate is a maximum. The difference at the outlet is 0.4°C. This confirms previous calculations by Kjaer [1958]. The inclusion of axial dispersion, which will be discussed in a later section, altered the steady-state temperature profile by less than 0.5°C. Internal transport effects would only have to be accounted for with particles having a diameter larger than 6 mm, which are used in some high-capacity modern converters to keep the pressure drop low. Dyson and Simon [1968] have published expressions for the effectiveness factor as a function of the pressure, temperature, and conversion, using Nielsen's experimental data for the true rate of reaction [1964]. At 300 bar and 480°C, the effectiveness factor would be 0.44 at a conversion of 10 percent and 0.80 at a conversion of 50 percent.

Figure 11.5.5-10 shows the relationship between the inlet temperature and the top temperature for the TVA reactor simulated by Baddour et al. for the conditions given above. The curve given corresponds to a space velocity of 13,800 m^3/m^3 cat. h. The space velocity, often used in the technical literature, is the total volumetric feed rate under normal conditions, F'_0 (Nm^3/h), per unit catalyst volume (m^3), that is, $\rho_B F'_0 / W$. It is related to the inverse of the space time, W/F_{A0} used in this text (with W in kg cat. and F_{A0} in kmol A/h). It is seen that, for the nominal space velocity of 13,800 (m^3/m^3 cat. h) and inlet temperatures between 224° and 274°C, two top temperatures correspond to one inlet temperature. Below 224°C no autothermal operation is possible. This is the blowout temperature. By the same reasoning used in relation with Fig. 11.5.5-2, it can be seen that points on the left branch of the curve correspond to the unstable, those on the right branch to the upper stable steady state. The lower steady state is not shown. The optimum top temperature (425°C), leading to a maximum conversion for the given amount of catalyst, is marked with a cross. The difference between the optimum operating top temperature and the blowout temperature is only 5°C, so that severe control of perturbations is required. Baddour et al. [1965] also studied the dynamic behavior, starting from the

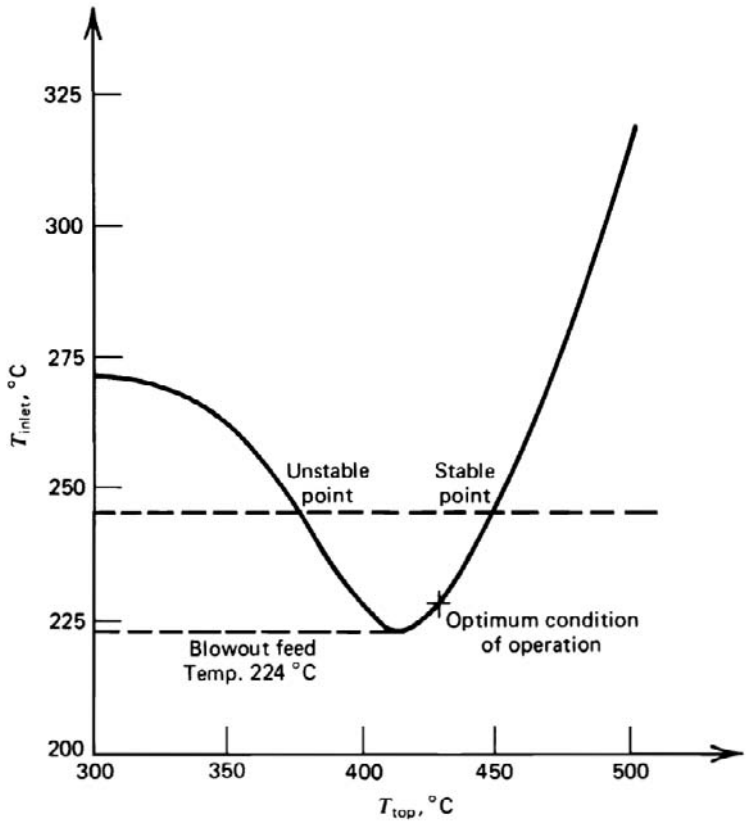

Figure 11.5.5-10

TVA ammonia synthesis reactor. Relationship between inlet and top temperatures. From Baddour et al. [1965].

transient continuity and energy equations. The dynamic behavior was shown to be linear for perturbations in the inlet temperature smaller than 5°C, around the conditions of maximum production. Use of approximate transfer functions was very successful in the description of the dynamic behavior.

In the preceding section, Section 11.5.4, on multibed adiabatic reactors, the optimization of the reactor was discussed in detail, and, for example, one way of doing this rigorously according to dynamic programming was worked out. The multitubular reactor with feed-effluent heat exchange considered in this section has also been the object of optimization, first by sound judgment, more recently by a more systematic and rigorous approach. Again, the problem is best illustrated by means of an *x*-*T* diagram or a mole-%-*T* diagram like that of Fig. 11.3-4 of Section 11.3, which shows the mole-%-*T* diagram of a TVA reactor compared with that of a five-bed quench converter of the same capacity (1968). Murase et al. [1970] optimized the profit of the countercurrent TVA NH3-synthesis converter by optimizing the temperature profile. This was done by

means of Pontryagin's maximum principle [1969], which is the method best suited to systems with continuous variables. The countercurrent flow in the reactor-heat exchanger systems tends to lower the temperature in the first catalyst layers. It follows from Murase's calculation that in the TVA reactor this effect would have to be enhanced. The production of the TVA reactor could have been increased by 5.4 percent if it could have been designed with a continuously varying heat transfer coefficient along the bed. In practice, this is not so simple: it means that, without changing their number, the tubes would have to be finned in the top zone. It would then be almost impossible to pack the catalyst homogeneously. The SBA reactor, (b) in Fig. 11.5.5-11, which also has countercurrent flow, has a much larger number of tubes (900 for a production of 200 tons NH_3/day) so that the temperature in the first layers is more optimized. However, this large exchange surface would also lower too much the temperature towards the end of the bed and lower the reaction rate too much, in spite of the more favorable equilibrium. The remedy is, then, to decrease the heat exchange in the second half of the catalyst bed. SBA chose to do this by shielding the tubes with concentric tubes. The trajectory for such a 200 tons/day reactor is also shown in Fig. 11.3-4 of Section 11.3.

There are also cocurrent flow-type reactors as shown in Fig. 11.5.5-11(a). They permit a closer approach to the curve of maximum rate, at the expense of a more complicated construction involving a set of concentric tubes in which the gas is given the desired flow direction. In case (a) the main feed enters at the top, flows along the reactor wall to protect this from the heat produced in the catalyst bed and the relatively high temperature in the internal heat exchanger. The main feed then flows around the tubes of this heat exchanger, together with cold "by-pass" feed (see Fig. 11.5.5-3 and related text) before entering the inner pipe of a set of 2 concentric pipes immersed in the catalyst bed. The flow in the inner pipe is upwards, that in the space between inner and outer pipe downwards — that is, in countercurrent with the reacting gases in the catalyst bed. The latter is reached through the central pipe of the bed. The gases leaving the bed flow through the pipes of the internal heat exchanger, preheating the feed, before exiting the reactor at the bottom [Fodor, 1971].

In modern Casale reactors (Casale Group, Lugano, Switzerland), plate heat exchangers are inserted in the catalyst bed. The coolant can be either the synthesis gas to be preheated or water for steam generation. The flow in these exchangers is radial, in co- or countercurrent with the gas. The reactor may contain 185 m^3 of catalyst.

Autothermal reactors can run away either because of parametric sensitivity, already encountered in the simple tubular reactor without feedback,

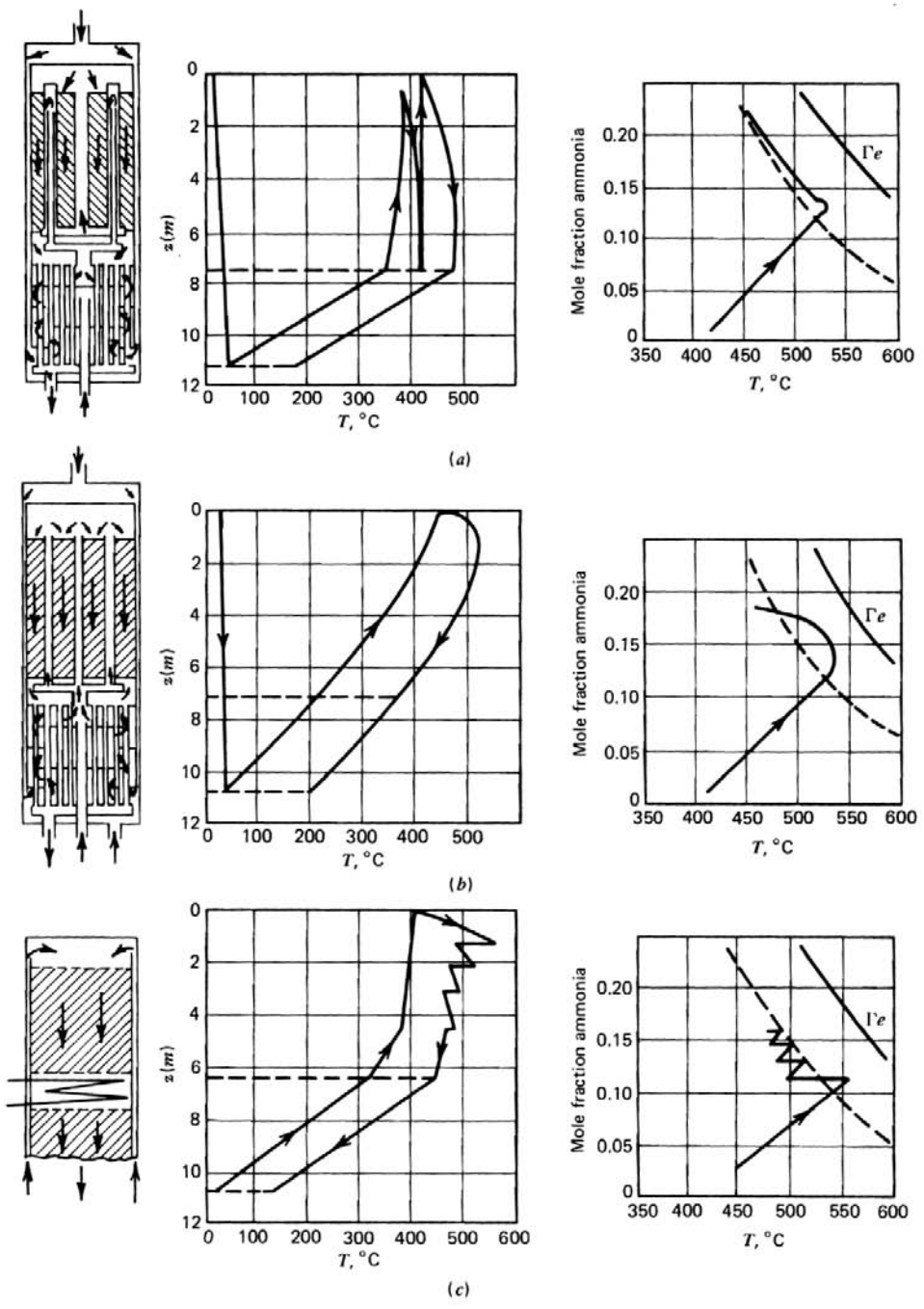

Figure 11.5.5-11

Operating diagrams for various types of ammonia synthesis reactors. (a) Multitubular reactor with cocurrent flow. (b) Multitubular reactor with countercurrent flow. (c) Multibed adiabatic reactor. From Fodor [1971].

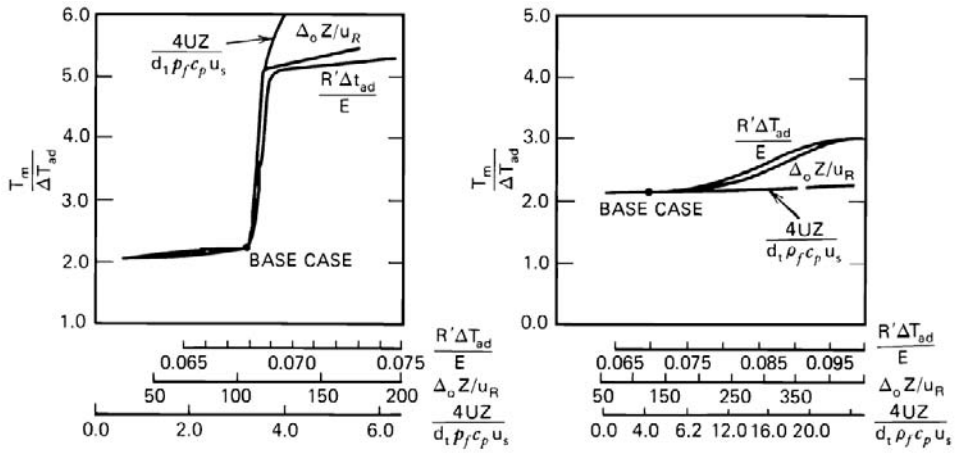

Figure 11.5.5-12

Parametric sensitivity in autothermal reactors. (a) Countercurrent flow, (b) Cocurrent flow. After Degnan and Wei [1979].

or because of instability *sensu strictu*, associated with the existence of multiple steady states. Inoue [1978] derived the following criteria: There is no risk of instability with an *n*th-order irreversible reaction when $\beta\gamma < 8$ and for first-order reversible reactions when $\beta\gamma < 8\kappa$, where $\kappa = (1 + K)/K$, $\beta = (-\Delta H) \times C_{A0} / \rho_g c_p T_0$ is the dimensionless adiabatic temperature rise and $\gamma = E/RT_0$ is the dimensionless activation energy.

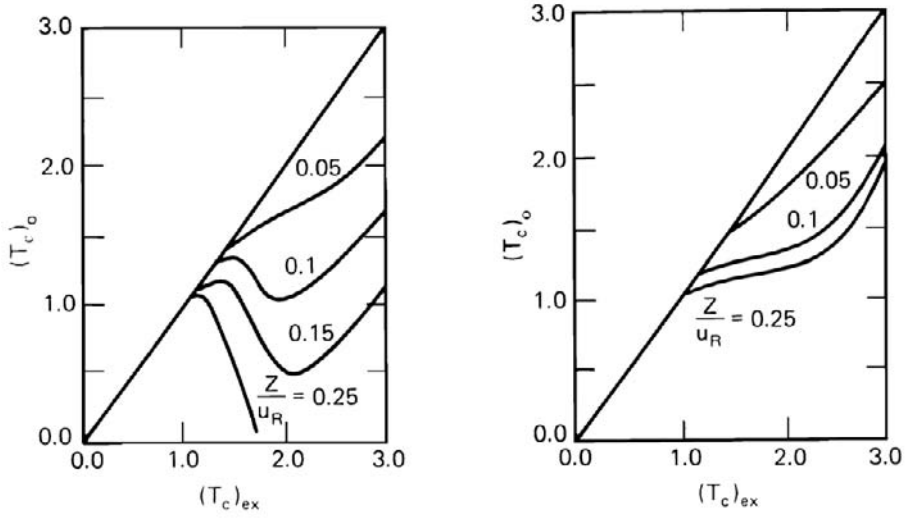

Figure 11.5.5-13

Autothermal reactors. Relationship between coolant inlet temperature and reactor top temperature. (a) Countercurrent flow, (b) Cocurrent flow. After Degnan and Wei [1979].

The optimal operating conditions for autothermal reactors are close to the blowoff conditions, beyond which an external heat supply is required. For first-order reactions, Ampaya and Rinker [1977] related the difference between the critical feed temperature leading to blowoff and the critical bed inlet temperature to the operating and design parameters.

A comparison of the sensitivity of the cocurrent and countercurrent operation of autothermal reactors was published by Degnan and Wei [1979]. The parameters shown in the abcissa of Figs. 11.5.5-12 and 11.5.5-13 were varied around base case values for which the reactor shows extreme parametric sensitivity. The cocurrent reactor is far less sensitive and unconditionally stable.

11.5.6 Nonsteady-State Behavior of Fixed Bed Catalytic Reactors Due to Catalyst Deactivation

In Chapter 5, rate equations were set up for several types of catalyst deactivation. In this section the consequences of catalyst deactivation on fixed bed reactor performance is discussed. Clearly, when the catalyst deactivates in a point in the reactor, the conversion in that point is affected. Consequently, the conversion profile and the temperature profile will be modified with time; in other words, the reactor is operating in nonsteady-state conditions. The way the profiles are shifted and the rate at which this happens depend on the mechanism of deactivation. This shift is well known in industrial practice. In an ammonia synthesis reactor, for example, the hot spot is known to migrate slowly through the reactor, due to sintering of the catalyst: If the first layers the feed contacts are becoming less active, more catalyst will be required to reach a given conversion and the hot spot moves down the bed. If no precautions are taken, this would mean a decrease in production of the reactor. What is done in this case is to oversize the reactor so that sufficient catalyst is available to compensate for loss in activity until it has to be replaced for other, more imperative reasons, such as excessive pressure drop due to powder formation. Another way to compensate for loss in activity is to increase the inlet temperature, as already discussed. Another example is catalytic reforming of naphtha, where the catalyst is deactivated by coke deposition. In this case the deactivation is compensated for by increasing the operating temperature so that the conversion, measured here by the octane number of the reformate, is kept constant. There is a limit to this temperature increase, of course, since it causes a higher production of light gases (i.e., decreases the selectivity) so that the coke has to be burnt off and the catalyst regenerated. It is clear that it is important to predict the behavior of reactors subject to deactivation. This requires setting up a mathematical model. This model consists of the set of continuity and energy equations already derived, but

considering the transient nature of the process and the variable catalyst activity, reflected in a rate equation that contains a deactivation function.

The following example deals with the effect of fouling by coke deposition in an isothermal reactor. The continuity equation for the reactant *A* may be written in terms of mole fractions, assuming that both the density and the number of moles remain constant [see Froment and Bischoff, 1961]:

$$\frac{\partial y_A}{\partial t} + \frac{M_m F_T}{\varepsilon \rho_g \Omega} \frac{\partial y_A}{\partial z} = -\frac{M_m \rho_B}{\varepsilon \rho_g} r_A \qquad (11.5.6\text{-}1)$$

When the following dimensionless variables are introduced,

$$z' = \frac{z}{d_p} \qquad t' = \frac{M_m F_t}{\varepsilon \rho_g \Omega d_p} t$$

(11.5.6-1) becomes

$$\frac{\partial y_A}{\partial t'} + \frac{\partial y_A}{\partial z'} = -\frac{\Omega \rho_B d_p}{F_t} r_A \qquad (11.5.6\text{-}2)$$

The continuity equation for the catalyst coking compound is

$$\frac{\partial C_C}{\partial t} = r_C \qquad (11.5.6\text{-}3)$$

In this equation C_C is really written in terms of the amount of carbon per unit weight of catalyst, since the amount of carbonaceous compound is usually measured as carbon. When the dimensionless variables defined above are introduced, (11.5.6-3) becomes

$$\frac{\partial C_C}{\partial t} = \frac{\varepsilon \rho_g \Omega d_p}{M_m F_t} r_C \qquad (11.5.6\text{-}4)$$

The rate terms r_A and r_C remain to be specified. If it is assumed, for simplicity, that both the main reaction and the coke deposition are of first order, r_A and r_C may be written as follows:

For a parallel coking mechanism:

$$r_A = k_A p_t y_A + \frac{k_c p_t y_A}{\psi_A M_A}$$

$$r_C = k_C p_t y_A$$

with k_c in units of kg coke/kg cat. h·bar and the conversion factor ψ_A in kg coke/kg *A*.

For a consecutive coking mechanism:

$$r_A = k_A p_t y_A$$

$$r_C = k_C p_t (1 - y_A)$$

Next the deactivation function has to be introduced. Let this function be of the exponential type;

$$k_A = k_A^0 e^{-\alpha_A C_C}$$

$$k_C = k_C^0 e^{-\alpha_C C_C}$$

To permit analytical integration of the system, (11.5.6-2) through (11.5.6-4), Froment and Bischoff considered $\alpha_C = 0$, that is, the amount of coke already deposited influences the rate of the main reaction, but not that of the parallel reaction leading to coke, because it is of a thermal origin, rather than catalytic. Integrating the set of equations with suitable boundary conditions leads to the results represented in Figs. 11.5.6-1 and 11.5.6-2. In these figures,

$$a = \frac{\Omega \rho_B d_p p_t}{F_t} k_A^0$$

$$b = \frac{\Omega \rho_g \varepsilon d_p p_t}{F_t} k_C^0$$

$$\chi = t' - z'$$

For all practical cases, $\chi \cong t'$.

It is clear from Fig. 11.5.6-1 that the mole fraction of the reactant *A* increases with time at a given bed depth, in other words, the conversion decreases. From Fig. 11.5.6-2 it is seen that the carbon is not deposited uniformly along the bed, but according to a descending profile. This is intuitively clear; when the carbonaceous compound is deposited by a reaction parallel to the main, its rate of formation is maximum at the inlet of the reactor, where the mole fraction of the reactant is maximum.

Froment and Bischoff also treated consecutive coking along the lines given above and obtained the diagrams of Figs. 11.5.6-3 and 11.5.6-4. The difference with the parallel coking case is striking, particularly in the carbon content of the catalyst, which again is not uniform but increases with bed length.

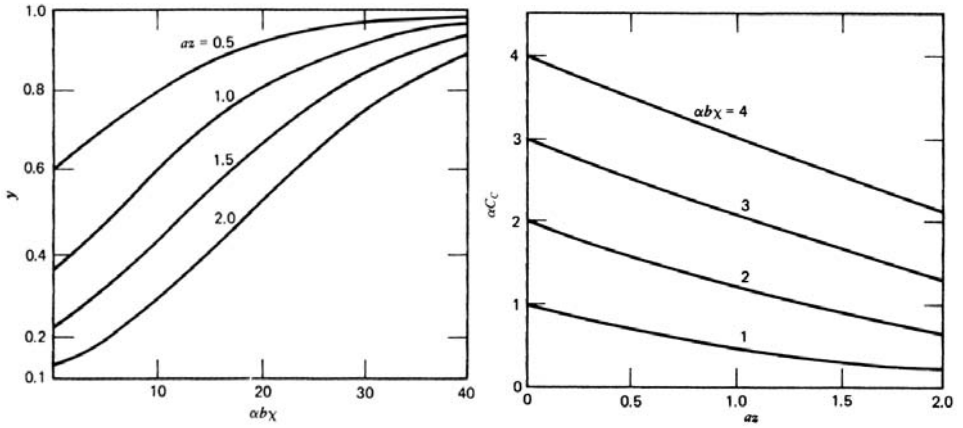

Figure 11.5.6-1

Reactant mole fraction versus time group for parallel coking and exponential activity function. From Froment and Bischoff [1961].

Figure 11.5.6-2

Coke profiles for parallel coking with exponential activity function. From Froment and Bischoff [1961].

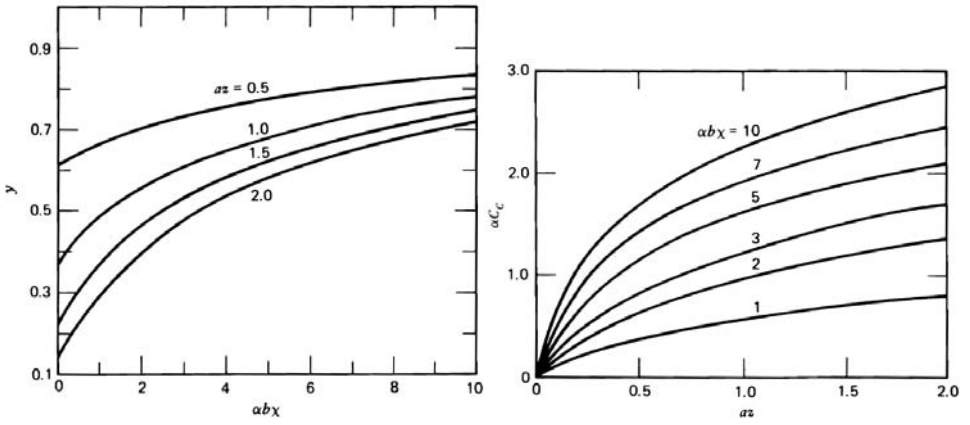

Figure 11.5.6-3

Reactant mole fraction versus time group for consecutive coking with exponential deactivation function. From Froment and Bischoff [1961].

Figure 11.5.6-4

Coke profiles for consecutive coking with exponential deactivation function. From Froment and Bischoff [1961].

It follows from the preceding that equations that try to relate the activity of the bed with time (Voorhies formula) can only be approximate. The Voorhies formula can at best be valid only for a *given* bed length. By plotting the *average* carbon content of the bed versus time in a double-logarithmic plot — the way Voorhies and others did (Chapter 5) — Froment and Bischoff obtained a power

of 1 for the Voorhies formula with the parallel coking mechanism with exponential activity function. For consecutive coking, they obtained a power of 1 at low process times and 0.5 at higher process times. The same is true for a parallel fouling mechanism with a hyperbolic activity function. These values are in the same range as those of the experimental studies quoted in Chapter 5. In their study of the dehydrogenation of butene into butadiene, Dumez and Froment [1976] observed coke formation from both butene (parallel mechanism) and butadiene (consecutive mechanism), whereas hydrogen inhibited the coking. The power in the Voorhies relation decreased from 0.55 to 0.35. In the catalytic cracking of light East Texas gasoil, Eberly et al. [1966] found a power varying from 0.77 to 0.55 as process time increased.

It further follows from Froment and Bischoff's study that, for a given bed length, both the point and the average carbon content increase with increasing space time (or decrease with space velocity) for the consecutive reaction mechanism, but decrease for the parallel mechanism (increase in terms of space velocity). Eberly's data [1966] also indicate that the power in the Voorhies relation depends on the space time or on the liquid hourly space velocity. Another consequence of this analysis is shown in Fig. 11.5.6-5 for a parallel reaction. In the absence of coking, and for isothermal conditions, the maximum rate of reaction $A \rightarrow R$ is always at the reactor entrance. This is not necessarily true when the catalyst is coked according to a parallel mechanism. In that case the inlet is deactivated to a greater extent than other portions of the reactor so that a ridge develops in the rate surface. A maximum is developed that travels down the bed as time progresses. If the operation is not isothermal this activity wave will be reflected in a temperature wave traveling through the bed and complicating the control of the reactor. Such a behavior was observed by Menon and Sreeramamurthy [1967, 1972] in their study of hydrogen sulfide air oxidation into water and sulfur on a charcoal catalyst. The sulfur progressively covers the catalyst surface, thus deactivating the catalyst. An activity profile results, which is revealed by a temperature peak traveling through the bed.

In the case of an ascending carbon profile, which is obtained when the carbonaceous deposit results from a consecutive mechanism, the rate is continuously decreasing with time in all points of the reactor, except at $z = 0$, where coke is not deposited yet. A gradually decreasing part of the reactor will then be effective in the conversion to the main product.

Descending coke profiles were observed experimentally by Van Zoonen in the hydroisomerization of olefins [1965]. Hughes et al. [1987] observed a decreasing coke profile when xylenes reacted over a silica/alumina bead catalyst around 460°C. The profile was measured by a noninvasive technique: neutron beam attenuation coupled with a BF_3 counter.

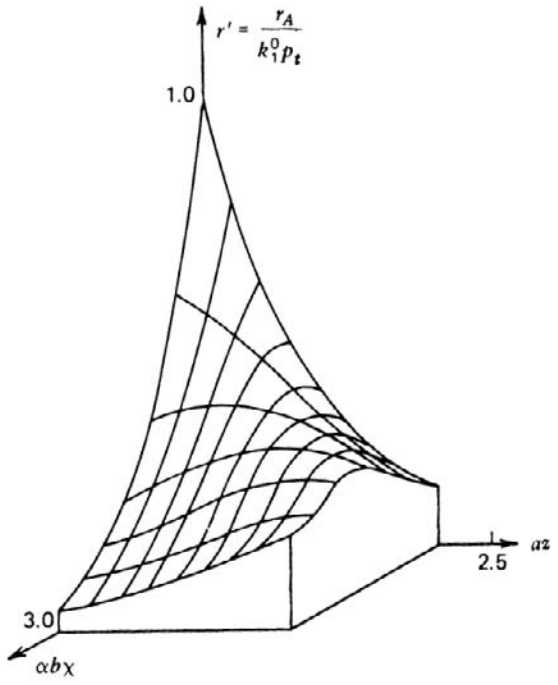

Figure 11.5.6-5

Rate surface for parallel reaction mechanism with exponential deactivation function. From Froment and Bischoff [1961].

In butene dehydrogenation into butadiene on a chromium/aluminum oxide catalyst at 595°C, Dumez and Froment [1976] measured nearly uniform coke contents in the integral reactor. It was shown, by experiments on a electrobalance, that coke originated from both butene and butadiene, whereas hydrogen inhibited its formation. The absence of a pronounced coke profile results from a balance between the three phenomena. In the isothermal isomerization of *n*-pentane under hydrogen pressure on a platina/alumina reforming catalyst, DePauw and Froment [1975] observed ascending coke profiles. The coke content of the catalyst was not zero at the inlet of the reactor, however, so that a parallel-consecutive coking mechanism — confirmed by independent measurements on an electrobalance — was adopted. In addition, some hydrocracking had to be accounted for, so that the following set of continuity equations was considered:

For *n*-pentane, in terms of partial pressures:

$$\frac{\partial p_A}{\partial t} + \frac{M_m F_t}{\Omega \rho_g} \frac{\partial p_A}{\partial z} = -\frac{M_m p_t \rho_B}{\Omega \rho_g} r_A$$

For the lumped hydrocracking products (methane, ethane, propane, butane):

$$\frac{\partial p_D}{\partial t} + \frac{M_m F_t}{\Omega \rho_g}\frac{\partial p_D}{\partial z} = -\frac{M_m p_t \rho_B}{\Omega \rho_g} r_D$$

For the coke:

$$\frac{\partial C_C}{\partial t} = r_C$$

The rate of isomerization r_I was found to be controlled by the surface reaction of *n*-pentene on Al_2O_3 instead of the adsorption on *n*-pentene on these sites, as found by Hosten and Froment for a slightly different catalyst and with continuous chlorine injection (see Chapter 2):

$$r_I = \frac{\left(k^I\right)\left(p_A - \dfrac{p_B}{K}\right)}{p_{H_2} + K^I_{AB}\left(p_A + p_B\right) + K^I_D p_D}$$

in which the adsorption equilibrium constants of *n*-pentene and isopentene are taken to be identical, so that $K^I_{AB} = K^I_A = K^I_B$. The total rate of disappearance of *n*-pentane is given by

$$r_A = r_I + 0.5 r_D$$

since two moles of hydrocracked products are formed from one mole of pentane and since the rate of coke formation r_C is small compared with r_I and r_D. Hydrocracking was shown to originate from both *n*-pentene and isopentene. The rate of hydrocracking was found to be given by

$$r_D = \frac{k^D\left(p_A + 0.714\, p_B\right)}{\left(1 + K^D_{AB}\dfrac{p_A + p_B}{p_{H_2}} + K^D_D \dfrac{p_D}{p_{H_2}}\right)^2}$$

The coke also originated from *n*-pentene and isopentene and its rate of formation was described by

$$r_C = \frac{k^p_C p_A}{p^2_{H_2}} + \frac{k^c_C p_B}{p^2_{H_2}}$$

Each rate coefficient in the above equations contains the corresponding deactivation function. This was shown, by experiments on an electrobalance, to be of the exponential type. Furthermore, it was shown that coking and hydrocracking occurred on the same sites, so that

$$\phi_C = \phi_D = e^{-\alpha_D C_C} \qquad \text{whereas} \qquad \phi_I = e^{-\alpha_I C_C}$$

and

$$k^I = \left(k^I\right)^0 \phi_I \qquad k^D = \left(k^D\right)^0 \phi_D \qquad k_C = \left(k_C\right)^0 \phi_C$$

The rate constants, the adsorption equilibrium constants, and the deactivation parameters α_I and α_D were determined from the measurement of p_A and p_D as a function of time and position (i.e., W/F_{A0}) in the bed, through a special sampling device. In addition, the coke profile was measured at the end of the run. The parameters were found to be statistically significant, and the rate coefficients satisfied the Arrhenius temperature dependence.

Figures 11.5.6-6, 11.5.6-7, and 11.5.6-8 compare experimental data with results obtained from a simulation on the basis of the above equations and the best set of parameters. The agreement is quite satisfactory, and the approach appears to be valuable despite the empirical nature of the deactivation functions which do not explicitly reflect the mechanism of the deactivation.

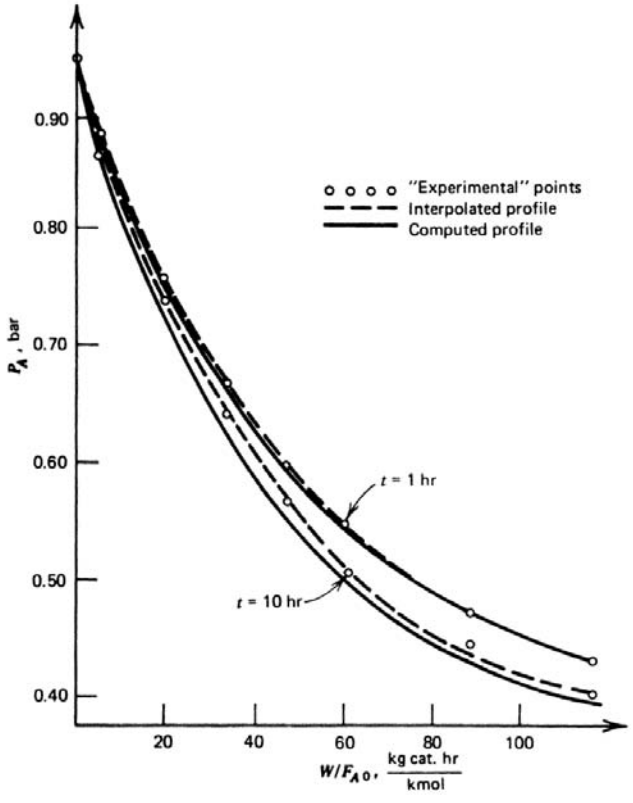

Figure 11.5.6-6

Pentane isomerization. Partial pressure profiles of *n*-pentane versus W/F_{A0}. From DePauw and Froment (1975).

Beeckman and Froment [1979, 1980] and Nam and Froment [1987] formulated the deactivation by coke formation in terms of site coverage, coke growth, and pore blockage. Mechanistic kinetic equations were derived for the rate of change of the coke content with time. An illustration of the application of such equations to deactivation in a fixed bed reactor is given by Froment [1980]. The trends illustrated here on the basis of empirical models are not essentially modified.

An important aspect of coking is its influence on the selectivity. As the product distribution or the selectivity depends on the ratios of the various rate coefficients, it is evident that the selectivity may also be affected by changes in catalyst activity, when the different reactions are not influenced in the same way by the coke deposition. Froment and Bischoff [1962] worked out the theory for such a situation. Figure 11.5.6-9 shows the results for coupled parallel reactions with parallel coking.

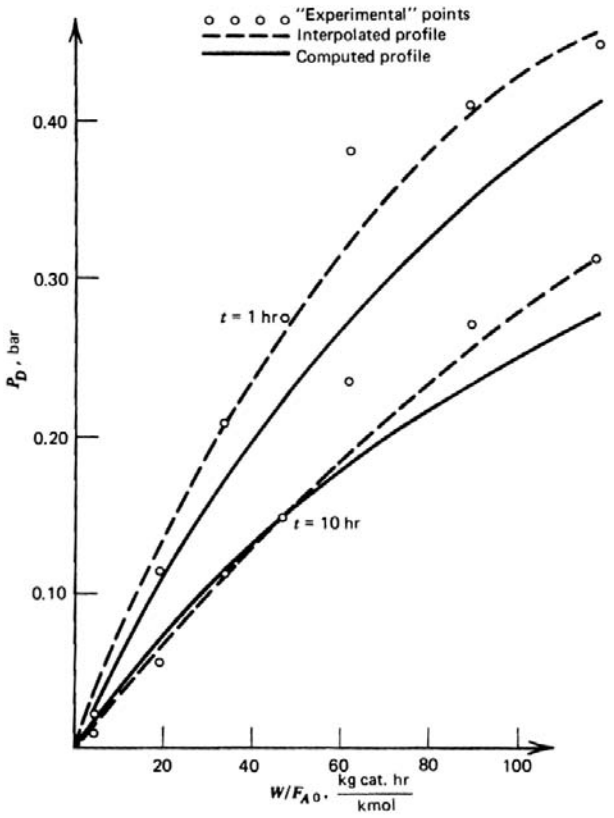

Figure 11.5.6-7

Pentane isomerization. Partial pressure profiles of lumped hydrocracked products versus W/F_{A0}. From DePauw and Froment [1975].

The selectivity for the isomerization of *n*-pentane varied with the coke content of the catalyst. Because the hydrocracking is more affected by the coke content of the catalyst, the isomerization selectivity increases under those conditions. Ultimately, however, the decrease in the isomerization rate would become too important. To compensate for this, before regeneration of the catalyst is resorted to, the temperature could be increased. Thereby, hydrocracking and coking would be more promoted than the isomerization and the selectivity would seriously decrease. In the catalytic cracking of gasoil on silica/alumina catalysts, on the other hand, the selectivity for gasoline was found to be independent of the coke content of the catalyst, but this is probably due to the large number of reactions of various types contributing to the coke formation [see Weekman and Nace, 1970].

Considerable attention has been given to the problem of maintaining the conversion of a reactor constant by adapting the temperature level. Butt [1972] has studied this problem for simple and for bifunctional catalysts, such as used in reforming. Optimization techniques have been applied to this problem by Jackson [1967]; Chou, Ray, and Aris [1967]; and Ogunye and Ray [1970].

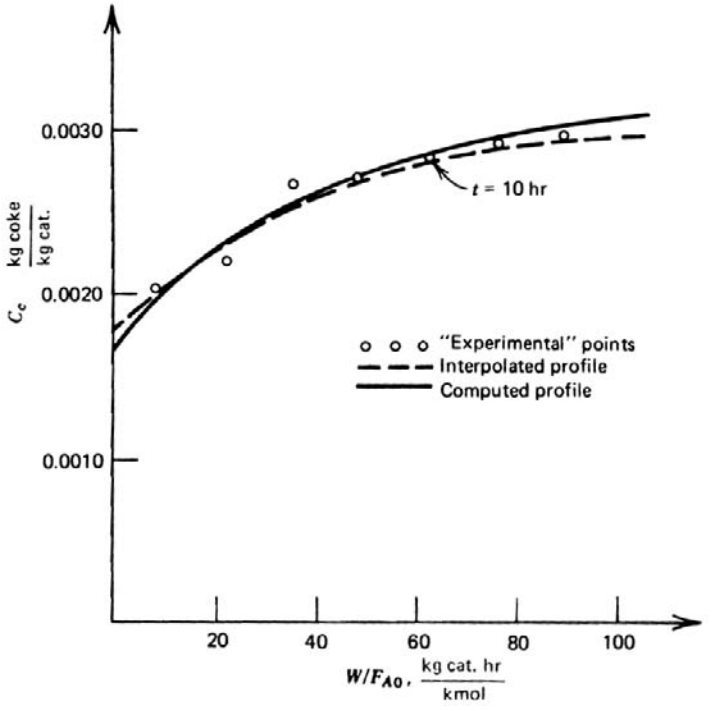

Figure 11.5.6-8

Pentane isomerization. Coke profiles after 10 h, from DePauw and Froment [1975].

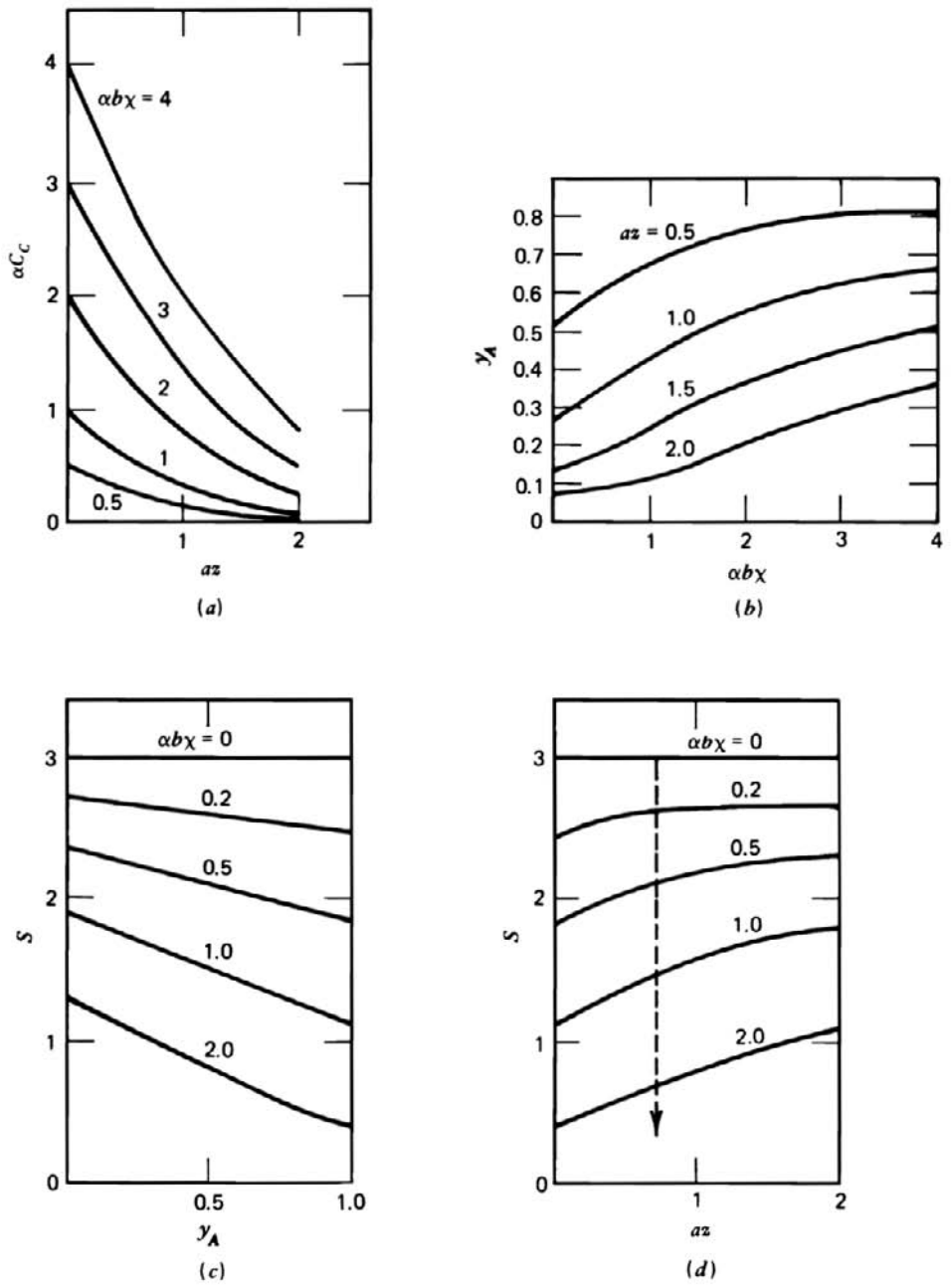

Figure 11.5.6-9

Influence of coking on selectivity. Coupled parallel reaction scheme. (a) Coke profiles. (b) Mole fraction of reactant versus process time group. (c) Selectivity versus mole fraction of reactant. (d) Selectivity versus dimensionless position. From Froment and Bischoff [1962].

11.6 ONE-DIMENSIONAL MODELWITH AXIAL MIXING

In Section 11.5 the one-dimensional pseudohomogeneous model was discussed in considerable detail. Several aspects such as runaway, optimization, and transient behavior due to catalyst coking, which are, in fact, entirely general, were analyzed under this model. There is sound justification for doing so. Most of the practical reactor design work so far has been based on this model, sometimes because it was considered sufficiently representative, more often because it was more convenient. Yet, several assumptions involved in the model are subject to criticism. It may be argued that the flow in a packed bed reactor deviates from the ideal pattern because of radial variations in flow velocity and mixing effects due to the presence of packing. Furthermore, it is an oversimplification also to assume that the temperature is uniform in a cross section. The first objection led to a development that will be discussed in the present section, the second to a model discussed in Section 11.7.

Mixing in the axial direction, which is due to the turbulence and the presence of packing, is accounted for by superposing an "effective" transport mechanism on the overall transport by plug flow. The flux due to this mechanism is described by a formula analogous to Fick's law for mass transfer or Fourier's law for heat transfer by conduction. The proportionality constants are "effective" diffusivities and conductivities. Because of the assumptions involved in their derivation, they implicitly contain the effect of the velocity profile. This whole field has been reviewed and organized by Levenspiel and Bischoff [1963]. The principal experimental results concerning the effective diffusivity in axial direction, D_{eA}, are shown in Fig. 11.6-1. From an extensive review of experimental and theoretical results, Gunn [1987] derived correlations for D_{ea} in

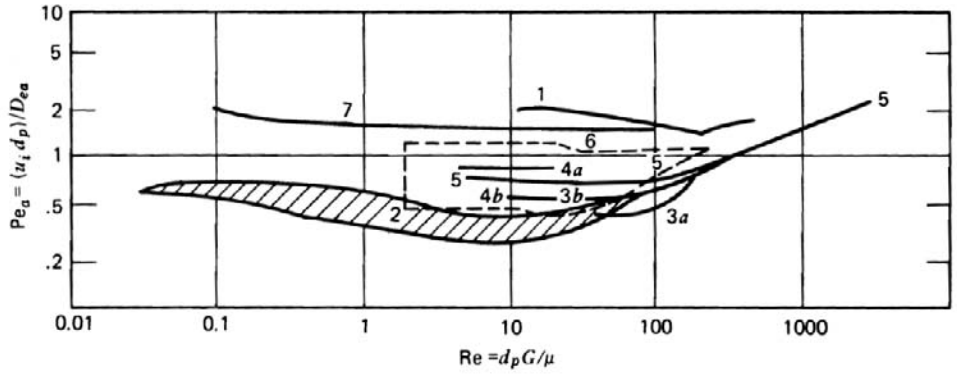

Figure 11.6-1

Peclet number for axial effective diffusion, based on particle diameter, versus Reynolds number. 1, McHenry and Wilhelm [1957]; 2, Ebach and White [1958]; 3, Carberry and Bretton [1958]; 4, Strang and Geankoplis [1958]; 5, Cairns and Prausnitz [1959]; 6, Hiby [1962], without wall effect, Hiby [1962]. From Froment [1967].

fixed beds of spheres and cylinders, both solid and hollow. For design purposes, Pe_a, based on d_p, may be considered to lie between 1 and 2. Little information is available on λ_{ea}. Yagi, Kunii, and Wakao [1960] determined λ_{ea} experimentally, while Bischoff [1963] derived it from the analogy between heat and mass transfer in packed beds.

Accounting for axial mixing, the steady-state continuity equation for a component *A* may be written

$$\varepsilon D_{ea} \frac{d^2 C_A}{dz^2} - u_s \frac{dC_A}{dz} - r_A \rho_B = 0 \qquad (11.6\text{-}1)$$

and the energy equation

$$\lambda_{ea} \frac{d^2 T}{dz^2} - \rho_g u_s c_P \frac{dT}{dz} + (-\Delta H) r_A \rho_B - \frac{4U}{d_t}(T - T_r) = 0 \qquad (11.6\text{-}2)$$

Axial mixing smoothens axial gradients of concentration and temperature so that it decreases the conversion obtained in a given reactor, in principle, at least.

The boundary conditions have given rise to extensive discussion [Danckwerts, 1953; Wehner and Wilhelm, 1956; Pearson, 1959; Bischoff, 1961; Van Cauwenberghe, 1966]. Those generally used are

$$u_s (C_{A0} - C_A) = -\varepsilon D_{ea} \frac{dC_A}{dz} \qquad \text{for } z = 0$$

$$\rho_g u_s c_p (T_0 - T) = -\lambda_{ea} \frac{dT}{dz}$$

$$\frac{dC_A}{dz} = \frac{dT}{dz} = 0 \qquad \text{for } z = L$$

This leads to a two-point boundary value problem requiring trial and error in the integration. It has been shown several times that for the flow velocities used in industrial practice, the effect of axial dispersion of heat and mass on conversion is negligible when the bed depth exceeds about 50 particle diameters [Carberry and Wendel, 1963]. The following more accurate criteria were derived by Young and Finlayson [1973]. When the rate is monotonically decreasing in the bed, the critical position where the importance of axial mixing has to be assessed is the bed inlet. Axial dispersion is negligible when

$$\frac{r_{A0}\rho_B d_p}{u_s C_0} << \mathrm{Pe}_{ma}$$

$$\frac{(-\Delta H) r_{A0}\rho_B d_p}{(T_0 - T_w) u_s \rho_g c_p} << \mathrm{Pe}_{ha} \qquad (11.6\text{-}3)$$

When the rate is maximum at some intermediate position, because of a hot spot for example, axial dispersion may be neglected when

$$\max\left|\frac{dx}{d(z/d_p)}\right| << \mathrm{Pe}_{ma}$$

$$\max\left|\frac{dT}{d(z/d_p)}\right| << \mathrm{Pe}_{ha} \qquad (11.6\text{-}4)$$

These are not a priori criteria, but the gradients can be approximated from a simulation based upon the one-dimensional basic pseudohomogeneous model. It takes very steep gradients not to satisfy (11.6-4).

In spite of this, the model has received great attention, more particularly the adiabatic version. The reason is that the introduction of axial mixing terms into the basic equations leads to an entirely new feature, that is, the possibility of more than one steady-state profile through the reactor [Raymond and Amundson, 1964].

Indeed, for *a certain range of operating conditions*, three steady-state profiles are possible with the same feed conditions, as is shown in Fig. 11.6-2. The outer two of these steady state profiles are stable, at least to small perturbations, whereas the middle one is unstable. Which steady-state profile will be predicted by steady-state computations depends on the initial guesses of C_A and T involved in the integration of this two-point boundary value problem. Physically, this means that the steady state actually experienced depends on the initial profile in the reactor. For all situations where the initial values are different from the feed conditions, transient equations have to be considered to make sure that the correct steady-state profile is predicted. To avoid those transient computations when they are unnecessary, it is useful to know a priori if more than one steady-state profile is possible. From Fig. 11.6-2 it is seen that a necessary and sufficient condition for uniqueness of the steady-state profile in an adiabatic reactor is that the curve $T_0 = f[T(L)]$ has no hump.

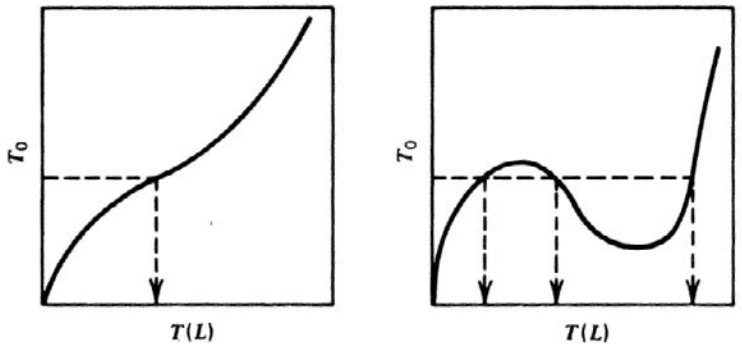

Figure 11.6-2

Relationships between T and $T(L)$, which lead to a unique and to three steady-state profiles, respectively. After Raymond and Amundson [1964].

Mathematically, this means that the equation

$$\frac{d^2T}{dz'^2} - \mathrm{Pe}_a' \frac{dT}{dz'} + f(T) = 0$$

where

$$z' = \frac{z}{L} \qquad \mathrm{Pe}_a' = \frac{u_i L}{D_{ea}}$$

and

$$f(T) = \frac{k_0 L^2}{\varepsilon D_{ea}} \rho_B (T_{ad} - T) \exp \frac{E}{RT_0} \left(1 - \frac{T_0}{T}\right)$$

has no bifurcation point, whatever the length of the reactor. This led Luss and Amundson [1967] to the following conditions:

$$\mathrm{Sup}\left[f'(T) - \frac{\mathrm{Pe}_a'^2}{4} \right] \le 0 \qquad (11.6\text{-}5)$$

$$T_0 \le T \le T_{ad}$$

which can be satisfied by diluting the reaction mixture. Another way of realizing a unique profile is to limit the length of the adiabatic reactor so that

$$\mathrm{Sup}\left[f'(T) - \frac{\mathrm{Pe}_a'^2}{4} \right] \le \mu_1$$

$$T_0 \le T \le T_{ad} \qquad (11.6\text{-}6)$$

where μ_1 is the smallest positive eigenvalue of

$$\Delta v + \mu v = 0 \tag{11.6-7}$$

and where $v(z)$ is the difference between two solutions $T_1(z)$ and $T_2(z)$. Uniqueness is guaranteed only if the only solution of (11.6-7) is $v(z) = 0$.

When applied to a first-order irreversible reaction carried out in an adiabatic reactor, these conditions lead to (11.6-8) and (11.6-9), respectively:

$$\frac{k_0 L^2}{\varepsilon D_{ea}} \rho_B \left[\frac{E}{R} \left(\frac{T_{ad} - T_0}{T_p^2} \right) - 1 \right] \exp\left[\frac{E}{RT_0} \left(1 - \frac{T_0}{T_p} \right) \right] - \frac{u_i^2 L^2}{4 D_{ea}^2} \leq 0 \tag{11.6-8}$$

or

$$< \mu_1 \tag{11.6-9}$$

where $T_{ad} - T_0 = [(-\Delta H)/(\rho_g c_p)]C_{A0}$ is the adiabatic temperature rise and T_p is the value for T for which $f'(T)$ assumes its supremum. A sufficient, but not necessary, condition for (11.6-8) is that

$$\frac{E}{RT_0} \frac{T_{ad} - T_0}{T_0} << 1 \tag{11.6-10}$$

or that

$$\gamma\beta \leq 1$$

Luss [1968] later refined these conditions and arrived at

$$(T - T_0) \frac{d \ln f(T)}{dT} \leq 1 \tag{11.6-11}$$

The magnitude of the axial effective diffusivity determines which of the two conditions, (11.6-5) or (11.6-11), is stronger. For a first-order irreversible reaction carried out in an adiabatic reactor, (11.6-11) leads to

$$\frac{E}{RT_0} \frac{T_{ad} - T_0}{T_0} \leq 4 \frac{T_{ad}}{T_0} \quad \text{or} \quad \gamma\beta \leq 4 \frac{T_{ad}}{T_0} \tag{11.6-12}$$

which is far less conservative than (11.6-10), based on (11.6-6). Hlavacek and Hofmann [1970] derived the following form, which is identical to the Luss criterion, (11.6-12):

$$\frac{E}{RT_0} \frac{T_{ad} - T_0}{T_0} < \frac{4}{1 - \dfrac{4RT_0}{E}}$$

Hlavacek and Hofmann also defined necessary and sufficient conditions for multiplicity for a simplified rate law of the type Barkelew used (described in

Section 11.5.3) and equality of the Peclet numbers for heat and mass transfer. The necessary and sufficient conditions for multiplicity, which have to be fulfilled simultaneously, are:

1. The group $(E/RT_0)\ [(-\Delta H)C_{A0}/(\rho_g c_p T_0)] = \gamma\beta$ has to exceed a certain value.
2. The group $Lk_0/u_i = \mathrm{Da}$ has to lie within a given interval.
3. The Peclet number based on reactor length $u_i L/D_{ea} = \mathrm{Pe}_a$ has to be lower than a certain value.

For instance, when $\beta\gamma = 8$ and the order of the reaction is 1, multiplicity only occurs in a narrow strip of the Pe–Da plane: for Pe = 0 (complete mixing!) bounded by $0.008 < \mathrm{Da} < 0.06$; for Pe = 50 bounded by $0.128 < \mathrm{Da} < 0.132$; and reduced to a point for Pe = 106 when Da = 0.1394.

Hlavacek and Hofmann calculated that the adiabatic temperature rise is sufficiently high in ammonia, methanol, and oxo-synthesis and in ethylene, naphthalene, and *o*-xylene oxidation. None of the reactions is carried out in adiabatic reactors, however, although multibed adiabatic reactors are sometimes used. According to Beskov (mentioned in Hlavacek and Hofmann [1970]), in methanol synthesis the effect of axial mixing would have to be taken into account when $\mathrm{Pe}'_a < 30$. In industrial methanol synthesis reactors, Pe'_a is of the order of 600 and more. In ethylene oxidation, Pe'_a would have to be smaller than 200 for axial effective transport to be of some importance; but in industrial practice, Pe'_a exceeds 2500. Baddour et al. [1965] in their simulation of the TVA ammonia synthesis converter found that the axial diffusion of heat altered the steady-state temperature profile by less that 0.6°C. Therefore, the length of industrial fixed bed reactors removes the need for reactor models including axial diffusion and the risks involved with multiple steady states, except perhaps for very shallow beds. In practice, shallow catalytic beds are only encountered in the first stage of multibed adiabatic reactors. One may question if very shallow beds can be described by effective transport models, in any event. The question remains if shallow beds really exhibit multiple steady states. The answer to this question requires a completely different approach, based on better knowledge of the hydrodynamics of shallow beds.

In summary, in our opinion there is no real need for further detailed study of the axial transport model. There are several other effects, more important than axial mixing, that have to be accounted for.

11.7 TWO-DIMENSIONAL PSEUDOHOMOGENEOUS MODELS

11.7.1 The Effective Transport Concept

The one-dimensional models discussed thus far neglect the resistance to heat and mass transfer in the radial direction and therefore predict uniform temperatures and conversions in a cross section. This is obviously a serious simplification when reactions with a pronounced heat effect are involved. For such cases there is a need for a model that predicts the detailed temperature and conversion pattern in the reactor, so that the design would be directed toward avoiding detrimental overtemperatures in the axis. This then leads to two-dimensional models.

The model discussed here uses the effective transport concept, this time to formulate the flux of heat or mass in the radial direction. This flux is superposed on the transport by overall convection, which is of the plug flow type. Since the effective diffusivity is mainly determined by the flow characteristics, packed beds are not isotropic for effective diffusion, so that the radial component is different from the axial mentioned in Section 11.6.2. Experimental results concerning D_{er} are shown in Fig. 11.7.1-1. Gunn [1987] recently presented accurate correlations for D_{er}. For practical purposes Pe_{mr} may be considered to lie between 8 and 10 [Bernard and Wilhelm, 1950; Dorweiler and Fahien, 1959; Fahien and Smith, 1955]. When the effective conductivity λ_{er} is determined from heat transfer experiments in packed beds, it is observed that λ_{er} decreases

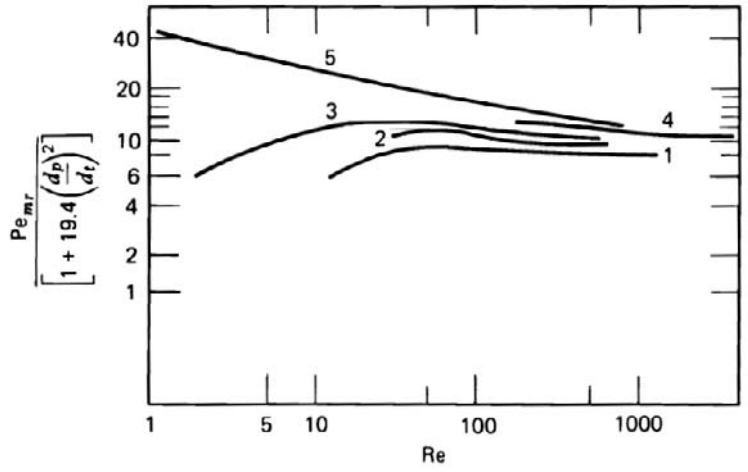

Figure 11.7.1-1

Peclet number for radial effective diffusion, based on particle diameter, versus Reynolds number. 1, Fahien and Smith [1955]; 2 Bernard and Wilhelm [1950]; 3, Dorweiler and Fahien [1959] ; 4, PLautz and Johnstone [1955] ; 5, Hiby [1962].

strongly in the vicinity of the wall. It is as if a supplementary resistance is experienced near the wall, which is probably due to variations in the packing density and flow velocity. Two alternatives are possible: either use a mean λ_{er} or consider λ_{er} to be constant in the central core and introduce a new coefficient accounting for the heat transfer near the wall, α_w, defined by

$$\alpha_w (T_R - T_w) = -\lambda_{er} \left(\frac{\partial T}{\partial r} \right)_w \qquad (11.7.1\text{-}1)$$

When it is important to predict point values of the temperature with the greatest possible accuracy, the second approach is preferred, so that two parameters are involved to account for heat transfer in the radial direction. Figures 11.7.1-2 and 11.7.1-3 show some experimental results for λ_{er} and α_w.

The data for α_w are very scattered. De Wasch and Froment [1972] published data recognized to have the high degree of precision required for the accurate prediction of severe situations in reactors. The correlations for air are of the form

$$\lambda_{er} = \lambda_{er}^0 + \frac{0.0105}{3600\left[1 + 46\left(\frac{d_p}{d_t}\right)^2\right]} \mathrm{Re} \qquad (11.7.1\text{-}2)$$

$$\alpha_w = \alpha_w^0 + \frac{0.0481 d_t}{3600 d_p} \mathrm{Re} \qquad (11.7.1\text{-}3)$$

where λ_{er}^0 and α_w^0 (in kJ/m^2 s °C) are static contributions depending on the type and size of the catalyst. The correlation for α_w is of an entirely different form from those published before, but confirms Yagi and Kunii's theoretical predictions [1960].

Since both solid and fluid are involved in heat transfer, λ_{er} is usually based on the total cross section and therefore on the superficial velocity, in contrast with D_{er}. This is reflected in (11.7.2-1). Yagi and Kunii [1957, 1960] and Kunii and Smith [1960] and later Schlünder [1971] have set up models for calculating λ_{er} and α_w. In these models the flux by effective conduction is considered to consist of two contributions, the first dynamic (i.e., dependent on the flow conditions) and the second static, so that

$$\lambda_{er} = \lambda_{er}^0 + \lambda_{er}^t$$

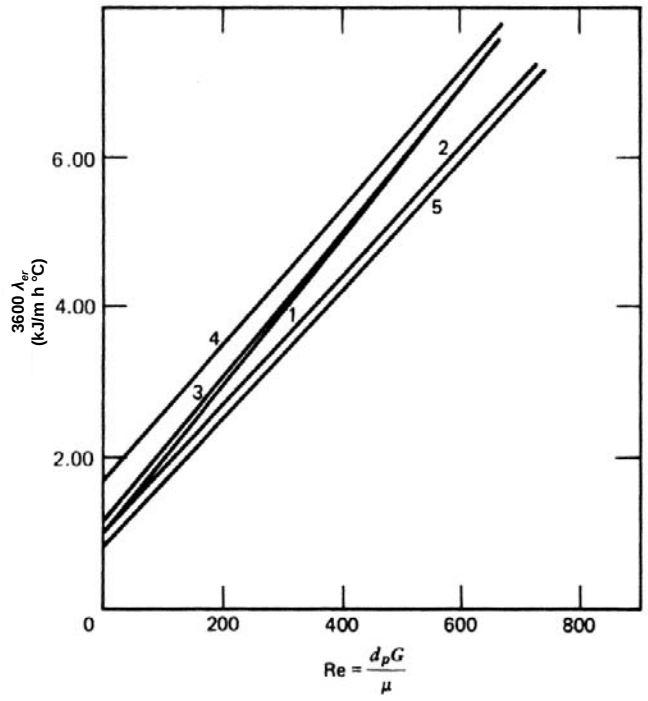

Figure 11.7.1-2

Effective radial thermal conductivity versus Reynolds number. 1, Coberly and Marshall [1951]; 2, Campbell and Huntington [1952]; 3, Calderbank and Pogorsky [1957]; 4, Kwong and Smith [1957]; 5, Kunii and Smith [1960].

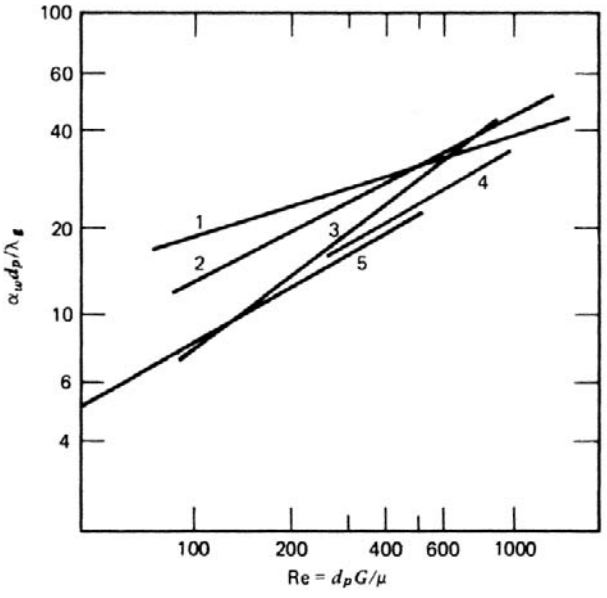

Figure 11.7.1-3

Nusselt number for wall heat transfer coefficient versus Reynolds number. 1, Coberly and Marshall [1951]; 2, Hanratty (cylinders) [1954]; 3, Hanratty (spheres) [1954]; 4, Yagi and Wakao [1959]; 5, Yagi and Kunii [1960].

THE STATIC CONTRIBUTION

In the absence of flow, the following mechanisms contribute to the effective conduction, according to Yagi and Kunii [1957] and Kunii and Smith [1960]:

1. Transport through the fluid in the voids.
   a) By conduction.
   b) By radiation between neighboring voids.

2. Transport in which the solid phase is involved.
   a) Conduction through the contact surface between particles.
   b) Conduction in the stagnating film in the vicinity of the contact surface.
   c) Radiation from particle to particle.
   d) Conduction through the particles.

Except in high vacuum, the contribution 2(a) may be neglected. Figure 11.7.1-4 represents this model by means of an electrical network. By expressing each of these contributions by means of the basic formulas for heat transfer and combining them in the appropriate way, depending on whether they operate in series or parallel, the following equation is obtained:

$$\frac{\lambda_{er}^0}{\lambda_g} = \varepsilon\left(1+\beta\frac{d_p\alpha_{rv}}{\lambda_g}\right)+\frac{\beta(1-\varepsilon)}{\dfrac{1}{\dfrac{1}{\phi}+\dfrac{\alpha_{rs}d_p}{\lambda_g}}+\gamma\dfrac{\lambda_g}{\lambda_s}} \qquad (11.7.1\text{-}4)$$

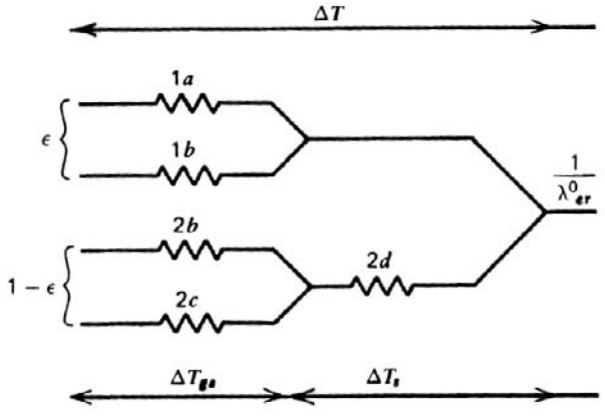

Figure 11.7.1-4
Model for heat transfer in packed bed according to Yagi and Kunii [1960].

where

λ_g, λ_s = conductivities of fluid and solid, respectively

ε = void fraction

α_{rv} = radiation coefficient from void to void, used when the expression for heat transfer by radiation is based on a temperature difference $T_1 - T_2$, in view of combining it with transport by convection or conduction:

$$\alpha_{rv} = \frac{0.227 \cdot 10^{-3}}{1 + \dfrac{\varepsilon}{2(1-\varepsilon)} \dfrac{1-p}{p}} \left(\frac{T + 273}{100} \right)^3$$

where p is the emissivity of the solid and T is in °C and α_{rv} in kJ/m²sK.
α_{rs} = radiation coefficient for the solid, also in kJ/m^2 s K

$$\alpha_{rs} = 0.227 \cdot 10^{-3} \frac{p}{2 - p} \left(\frac{T + 273}{100} \right)^3$$

β = a coefficient that depends on the particle geometry and the packing density, comprised between 0.9 and 1.0

$\gamma = \dfrac{2}{3}$ and ϕ depends on the packing density.

ϕ may be calculated when ϕ_1 and ϕ_2 are known. ϕ_1 is the value of ϕ for the loosest possible packing ($\varepsilon = 0.476$); ϕ_2 is the value of ϕ for the densest packing ($\varepsilon = 0.260$). ϕ_1 and ϕ_2 may be calculated from the knowledge of λ_s/λ_g. These functions are plotted in Fig. 11.7.1-5. When ε is comprised between its two extreme values, ϕ is calculated according to

$$\phi = \phi_2 + (\phi_1 - \phi_2) \frac{\varepsilon - 0.260}{0.476 - 0.260}$$

Zehner and Schlünder [1972] arrived at the following formula for the static contribution:

$$\frac{\lambda_{er}^0}{\lambda_g} = \left(1 - \sqrt{1-\varepsilon}\right) \left(1 + \varepsilon \frac{\alpha_{rs} d_p}{\lambda_g} \right) + \frac{2\sqrt{1-\varepsilon}}{1 + \left(\dfrac{\alpha_{rs} d_p}{\lambda_g} - B \right) \dfrac{\lambda_g}{\lambda_s}} \theta$$

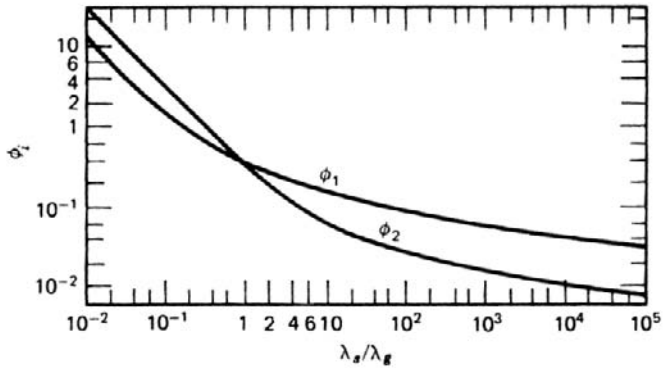

Figure 11.7.1-5

Curves ϕ_1 and ϕ_2 versus ratio of solid to gas conductivity, λ_s / λ_g. After Kunii and Smith [1960].

with

$$\theta = \frac{\left[1+\left(\frac{\alpha_{rs} d_p}{\lambda_g}-1\right)\frac{\lambda_g}{\lambda_s}\right]B}{\left[1+\left(\frac{\alpha_{rs} d_p}{\lambda_g}-B\right)\frac{\lambda_g}{\lambda_s}\right]^2}\ln\frac{1+\frac{\alpha_{rs} d_p}{\lambda_s}}{B\frac{\lambda_g}{\lambda_s}}$$

$$-\frac{B-1}{1+\left(\frac{\alpha_{rs} d_p}{\lambda_g}-B\right)\frac{\lambda_g}{\lambda_s}}+\frac{B+1}{2B}\left(\frac{\alpha_{rs} d_p}{\lambda_g}-B\right)$$

where $B = b[(1-\varepsilon)/\varepsilon]^{10/9}$ with b = 1.25 for spheres and 2.5 for cylinders and Raschig rings.

THE DYNAMIC CONTRIBUTION

This contribution arises exclusively from the transport in the fluid and corresponds to the mixing described by the effective diffusion in radial direction, D_{er}. When the analogy between heat and mass transfer is complete, the following relation may be written:

$$\lambda_{er}^t = \varepsilon \rho_g c_p D_{er}$$

from which

$$\frac{\lambda_{er}^t}{\lambda_g} = \Psi \,\mathrm{Pr}\,\mathrm{Re} \quad \text{with} \quad \Psi = \frac{1}{Pe_{mr}}$$

For Pe_{mr} = 10, Ψ = 0.1. Yagi and Kunii [1957] have derived Ψ from experimental data on λ_{er} and obtained a value of Ψ for spherical and cylindrical packing between 0.10 and 0.14.

De Wasch and Froment [1972] obtained the following equation:

$$\Psi = \frac{0.14}{1 + 46\left(\frac{d_p}{d_t}\right)^2}$$

The wall heat transfer coefficient can be predicted by a model that is analogous to that outlined for λ_{er} [Yagi and Kunii, 1960; and Yagi and Wakao, 1959]. It should be stressed here that α_w is intrinsically different from the "global" coefficients discussed in Section 11.5.1. The latter are obtained when the experimental heat transfer data are analyzed on the basis of a one-dimensional model that does not consider radial gradients in the core of the bed. This comes down to localizing the resistance to heat transfer in radial direction completely in the film along the wall. Dixon and Cresswell [1979] and Dixon [1985] extensively discussed heat transfer in packed beds. Further results, also for low d_t/d_p, are presented by Gunn et al. [1987].

11.7.2 Continuity and Energy Equations

The continuity equation for the key reacting component *A* and the energy equation can now be written as follows, for a single reaction and steady state:

$$\begin{cases} (D_{er})_s\left(\dfrac{\partial^2 C}{\partial r^2} + \dfrac{1}{r}\dfrac{\partial C}{\partial r}\right) - u_s \dfrac{\partial C}{\partial z} - \rho_B r_A = 0 \\ \lambda_{er}\left(\dfrac{\partial^2 T}{\partial r^2} + \dfrac{1}{r}\dfrac{\partial T}{\partial r}\right) - u_s \rho_g c_p \dfrac{\partial T}{\partial z} + \rho_B(-\Delta H) r_A = 0 \end{cases} \tag{11.7.2-1}$$

with boundary conditions

$$C = C_0$$

$$T = T_0 \qquad \text{at} \quad z = 0 \qquad 0 \le r \le R_t$$

$$\frac{\partial C}{\partial r} = 0 \qquad \text{at} \quad r = 0 \quad \text{and} \quad r = R_t$$

$$\frac{\partial T}{\partial r} = 0 \qquad \text{at} \quad r = 0 \qquad \text{all } z$$

$$\frac{\partial T}{\partial r} = -\frac{\alpha_w}{\lambda_{er}}(T_R - T_w) \qquad \text{at} \quad r = R_t$$

$(D_{er})_s$ is based upon the superficial flow velocity, like λ_{er}. It equals εD_{er}, with D_{er} based upon the interstitial flow velocity u_i.

Note that the term accounting for effective transport in the axial direction has been neglected in this model, for the reasons already given in Section 11.6. This system of nonlinear second-order partial differential equations was integrated by Froment [1961, 1967] using a Crank-Nicholson procedure, to simulate a multitubular fixed bed reactor for a reaction involving yield problems.

Mihail and Iordache [1976] compared the performance of some numerical techniques for integrating the system (11.7.1-1): Liu's average explicit scheme with a five-point grid [1970], the Crank-Nicholson implicit scheme [Froment, 1962, 1967], and orthogonal collocation [Finlayson, 1971]. The reactor was an *o*-xylene oxidation reactor and the reaction scheme that of Froment [1967], discussed in the next section. The computation time was of the same order of magnitude with the Crank-Nicholson and Liu's scheme, but orthogonal collocation only required two thirds of this time. Liu's explicit scheme was very sensitive to step size and led to problems of stability and convergence for severe operating conditions leading to important hot spots.

11.7.3 Design or Simulation of a Fixed Bed Reactor for Catalytic Hydrocarbon Oxidation

In this example the design or simulation of a multitubular reactor for a catalytic hydrocarbon oxidation is discussed [Froment, 1967]. The case considered here is of a rather complex nature, that is,

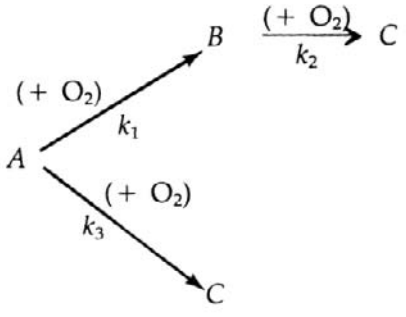

This reaction model is fairly representative of the gas-phase air oxidation of *o*-xylene into phthalic anhydride on V_2O_5 catalysts; *A* represents *o*-xylene, *B* phthalic anhydride, and *C* the final oxidation products CO and CO_2 lumped together. The process conditions were already described in Section 11.5.2. The purpose of this example is mainly to check whether or not radial temperature

gradients occur in such a reactor. For a better approximation of reality, a reaction model is chosen that is closer to the true model than the one used in Section 11.5.2. In addition, it illustrates a yield problem, such as is often encountered in industrial practice.

Due to the very large excess of oxygen, the rate equations will be considered to be of the pseudo-first-order type, so that, at atmospheric pressure,

$$r_A = (k_1 + k_3) y_{A0} y_0 (1 - x_A)$$

$$r_B = y_{A0} y_0 [k_1 (1 - x_A) - k_2 x_B]$$

$$r_C = y_{A0} y_0 [k_2 x_B + k_3 (1 - x_A)]$$

where y_0 represents the mole fraction of oxygen, x_A is the total conversion of *o*-xylene, and x_B is the conversion of *o*-xylene into phthalic anhydride. When x_C represents the conversion into CO and CO_2, then $x_A = x_B + x_C$. The rate coefficients are given by the following expressions:

$$\ln k_1 = -\frac{13{,}588}{T' + T_0} + 19.837$$

$$\ln k_2 = -\frac{15{,}803}{T' + T_0} + 20.86$$

$$\ln k_3 = -\frac{14{,}394}{T' + T_0} + 18.97$$

where T_0 is the inlet temperature to the reactor and $T' = T - T_0$.

A more detailed reaction scheme and more realistic kinetic model accounting for the interaction of the species with the catalyst and the reoxidation of the latter by the oxygen of the feed was derived by Papageorgiou and Froment [1995]. Its application is reported in Section 11.10.

Using the reduced temperature T' and the following dimensionless variables,

$$z' = \frac{z}{d_p} \qquad r' = \frac{r}{d_p} \qquad R_t' = \frac{R_t}{d_p}$$

the steady-state continuity and energy equations may be written, in cylindrical coordinates and in terms of conversion,

$$\frac{\partial x_B}{\partial z'} = a_1 \left(\frac{\partial^2 x_B}{\partial r'^2} + \frac{1}{r'} \frac{\partial x_B}{\partial r'} \right) + b_1 r_B$$

$$\frac{\partial x_C}{\partial z'} = a_1\left(\frac{\partial^2 x_C}{\partial r'^2} + \frac{1}{r'}\frac{\partial x_C}{\partial r'}\right) + b_1 r_C$$

$$\frac{\partial T'}{\partial z'} = a_2\left(\frac{\partial^2 T'}{\partial r'^2} + \frac{1}{r'}\frac{\partial T'}{\partial r'}\right) + b_2 r_B + b_3 r_C$$

The constants in these equations have the following meaning:

$$a_1 = \frac{(D_{er})_s}{u_i d_p} = \frac{1}{Pe_{mr}} \qquad b_1 = \frac{\rho_B d_p M_m}{G N_{A0}}$$

$$a_2 = \frac{\lambda_{er}}{G c_p d_p} = \frac{1}{Pe_{hr}} \qquad b_2 = \frac{\rho_B d_p (-\Delta H_1)}{G c_p}$$

$$b_3 = \frac{\rho_B d_p (-\Delta H_3)}{G c_p}$$

The boundary conditions are those of the previous section and are the same for x_C as for x_B, of course.

Bulk mean values are obtained from

$$\langle \zeta \rangle = 2\int_0^1 \zeta \frac{r}{R_t} d\left(\frac{r}{R_t}\right)$$

The following typical data were used in the computations: y_{A0} = 0.00924, corresponding to 44 g/m^3; $-\Delta H_1$ = 1.285×10^6 kJ/kmol, and $-\Delta H_3$ = 4.564×10^6 kJ/kmol. All the other data were already given in Section 11.5.2. From Kunii and Smith's correlation [1960] it follows that at Re = 121, λ_{er} = 0.78×10^{-3} kJ/m s K; and from Yagi and Kunii's equation [1960], α_w = 0.156 kJ/m² s K, so that Pe$_{hr}$ = 5.25, whereas Pe$_{mr}$ = 10. In all cases the feed inlet temperature equaled that of the salt bath.

Figure 11.7.3-1 shows the results obtained for an inlet temperature of 357°C. The bulk mean conversion and temperature profile is shown. The conversion to phthalic anhydride tends to a maximum, typical for consecutive reaction systems, but which is not shown on the figure. Also typical for exothermic processes, as we have seen already, is the hot spot, where T'_m equals about 30°C. Even for this case, which is not particularly drastic, and with a small tube diameter of only 2.54 cm, the radial temperature gradients are severe, as seen from Fig. 11.7.3-2. The temperature in the axis is well above the mean.

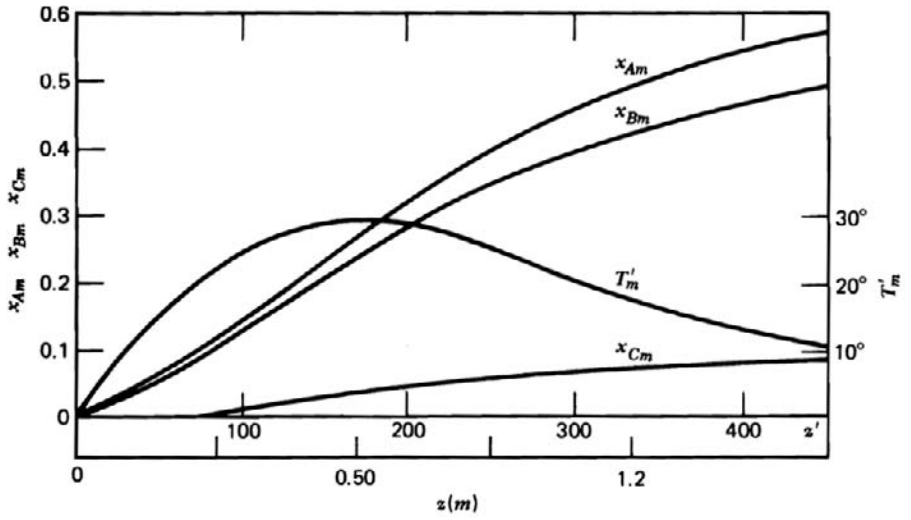

Figure 11.7.3-1

Radial mean conversions and temperature profile in multitubular *o*-xylene oxidation reactor. From Froment [1967].

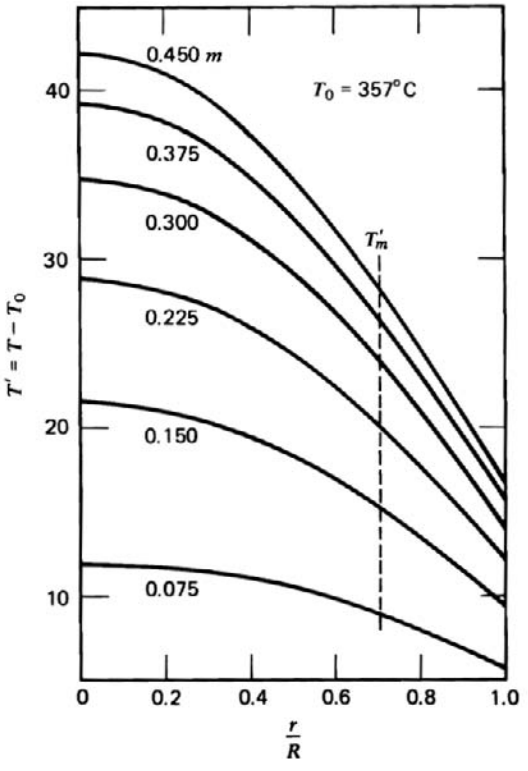

Figure 11.7.3-2

o-xylene oxidation. Radial temperature profiles at various bed depths. From Froment [1967].

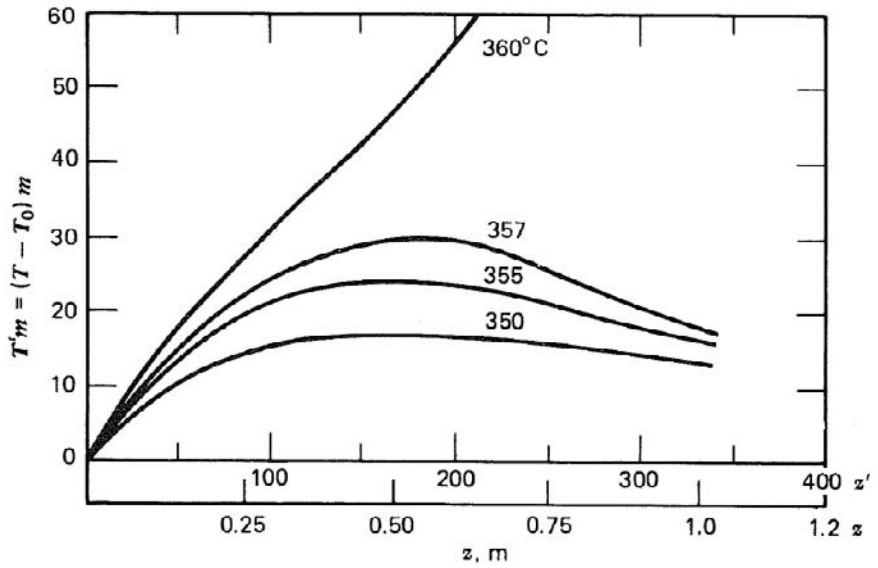

Figure 11.7.3-3

o-xylene oxidation parametric sensitivity. Influence of inlet temperature. From Froment [1967].

It follows from Froment [1967] and from calculations by Carberry and White [1969] that the computed results are not very sensitive with respect to Pe_{mr}, but very sensitive with respect to λ_{er} and α_w. Beek [1962] and Kjaer [1958] have also discussed features of this model.

From the computed radial mean profiles, which are cut off at $z = 1.5$ m in Fig. 11.7.3-1, it follows that a length of 3 m is insufficient to reach the maximum in phthalic anhydride concentrations. What happens when the inlet temperature is raised by only 3°C to overcome this is shown in Fig. 11.7.3-3. This is another example of parametric sensitivity. Hot spots even less dramatic than that corresponding to $T_0 = 360$°C may be detrimental for the catalyst. Even if it were not, important hot spots would be unacceptable for reasons of selectivity. Indeed, the kinetic equations are such that the side reactions are favored by increasing the temperature. The effect of the hot spot on the yield is shown in Fig. 11.7.3-4, in which the yield is plotted as a function of total conversion for several inlet temperatures. A few percent more in yield, due to judicious design and operation, are important in high-tonnage productions.

As illustrated in Section 11.5.2, the inlet temperature is not the only parameter determining the runaway temperature. The influence of the hydrocarbon inlet concentration is shown in Fig. 11.7.3-5, which summarizes Fig. 11.7.3-3 obtained with 44 g/m^3 and two more diagrams like this, but with 38 and 32 g/m^3. Figure 11.7.3-5 shows how the runaway limit temperature rises

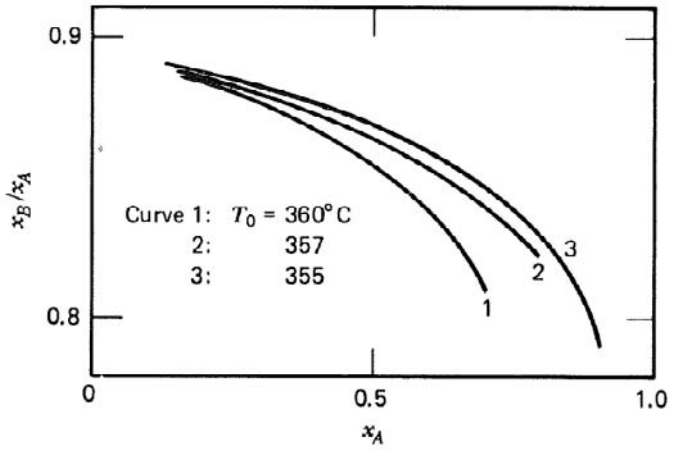

Figure 11.7.3-4

o-xylene oxidation. Effect of hot spot on phthalic anhydride yield. From Froment [1967].

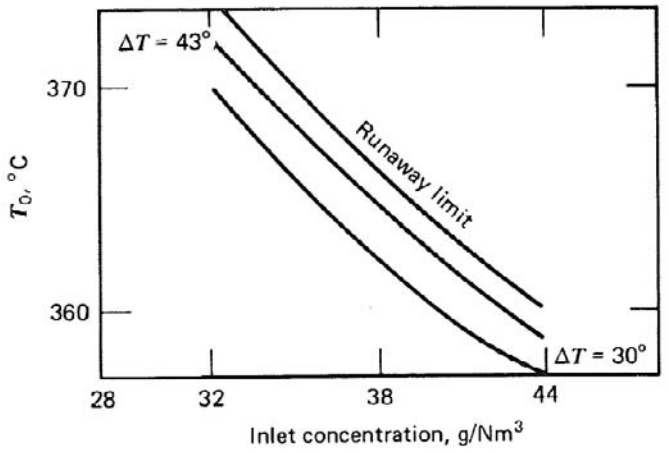

Figure 11.7.3-5

o-xylene oxidation. Influence of hydrocarbon inlet concentration on critical inlet temperature. From Froment [1967].

with decreasing hydrocarbon inlet concentration, but it is important to note that no noticeable gain in safety margin is obtained by lowering the inlet concentration. Moreover, such a measure would decrease the production capacity and unfavorably influence the economics of the plant. Yet, as designed, the risk of operating the reactor is too large; a safety margin of 3°C is unthinkable. With the given length of 3 m, there seems to be only one way out, that is, to realize an entirely different type of temperature profile, showing no pronounced hot spot, but leading all together to a higher average temperature. An appropriate dilution of the catalyst with inert packing in the front section of the bed would enable

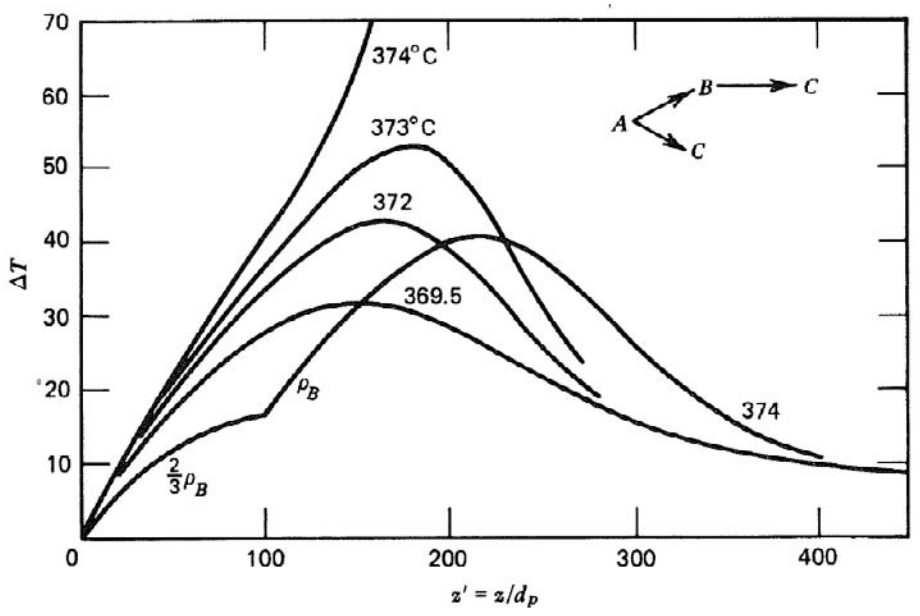

Figure 11.7.3-6
o-xylene oxidation. Effect of diluting the catalyst bed with inert material.

this. This is shown in Fig. 11.7.3-6. The dilution of the catalyst in an optimal way has been discussed by Calderbrank et al. [1968], by Adler at al. [1972], and by Narsimhan [1976].

11.7.4 An Equivalent One-Dimensional Model

The question arises how well the results predicted by the one-dimensional model of Section 11.5.1 correspond with those of the model discussed here. For such a comparison to be valid and only reflect the effect of the model itself, the heat transfer coefficient α_i of the one-dimensional model has to be derived from λ_{er} and α_w according to

$$\frac{1}{\alpha_i} = \frac{1}{\alpha_w} + \frac{R_t}{4\lambda_{er}} \qquad (11.7.4\text{-}1)$$

as derived by Froment [1962, 1967]. Slightly different but analogous relationships were obtained by Crider and Foss [1965], Marek et al. [1969], and Hlavacek [1970].

Equation (11.7.4-1) was derived with the purpose of matching as closely as possible the radially averaged temperature profile of the two-dimensional model in a purely heat transfer situation, that is, without chemical reaction. This is why this model is called “equivalent one-dimensional model”.

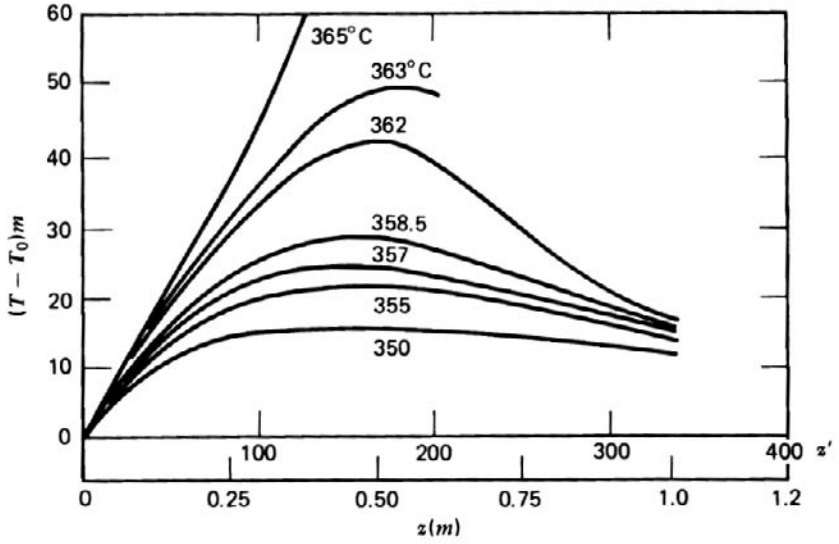

Figure 11.7.4-1

o-xylene oxidation. Predictions of equivalent one-dimensional model for influence of inlet temperature. From Froment [1967].

Figures 11.7.4-1 and 11.7.3-3 permit a comparison of the predictions based on the two models. The two-dimensional model predicts runaway at an inlet temperature of less than 360°C, the equivalent one-dimensional model at 365°C. The discrepancy between the predictions of both models grows as the conditions become more severe. Indeed, the condition (11.7.4-1) is incomplete insofar as it only considers heat transfer.

The possibilities of present-day computers are such that there is no longer any reason for not using the two-dimensional model for steady-state calculations, provided that the required physical and chemical parameters are sufficiently accurate. The one-dimensional model will continue to be used for on-line computations and for process control studies.

11.7.5 A Two-Dimensional Model Accounting for Radial Variations in the Bed Structure

Assuming plug flow in reactors with low d_t/d_p ratio, as encountered in multitubular reactors with fixed bed, is not very realistic. The void fraction in a cross section of the bed has been shown to vary from the wall to the central axis [Benenati and Brosilow, 1962] and this induces a radial variation in flow velocity [Schwartz and Smith, 1953; Cairns and Prausnitz, 1959; Schertz and Bischoff, 1969; Mickley et al., 1965; Lerou and Froment, 1977; McGreavy et al., 1986]. Govindarao and Froment [1986] and Delmas and Froment [1988] derived

correlations for the radial variation of the void fraction from geometrical considerations and these were applied. Fig. 11.7.5-1 shows the radial void fraction profile in packed beds of spheres for 3 tube to particle diameter ratios calculated by Papageorgiou and Froment [1995]. As this ratio is increased the variation of the porosity covers a decreasing fraction of the cross section of the bed. To account for the effect of the void fraction profile on the flow velocity distribution in a fixed bed reactor for *o*-xylene air oxidation into phthalic anhydride they constructed a reactor model including the Reynolds averaged Navier-Stokes equations for the momentum of the fluid and the correlation of Ergun [1952] for both viscous and kinetic energy losses. The equations consider flow in axial and radial direction and assume angular symmetry.

$$\rho_f\left(u_z\frac{\partial u_z}{\partial z}+u_r\frac{\partial u_z}{\partial r}\right)-\mu\left[\frac{\partial^2 u_z}{\partial z^2}+\frac{1}{r}\frac{\partial}{\partial r}\left(r\frac{\partial u_z}{\partial r}\right)\right]+\frac{\partial p}{\partial z}+\phi u_z=0 \qquad (11.7.5\text{-}1)$$

$$\rho_f\left(u_z\frac{\partial u_r}{\partial z}+u_r\frac{\partial u_r}{\partial r}\right)-\mu\left[\frac{\partial^2 u_r}{\partial z^2}+\frac{\partial}{\partial r}\left(\frac{1}{r}\frac{\partial}{\partial r}(r\,u_r)\right)\right]+\frac{\partial p}{\partial r}+\phi u_r=0$$

where ϕ is given by the correlation of Ergun [1952]:

$$\phi=150\frac{(1-\varepsilon)^2}{\varepsilon^3 d_p^2}\mu+1.75\frac{(1-\varepsilon)}{\varepsilon^3 d_p}\rho_f|\boldsymbol{u}| \qquad (11.7.5\text{-}2)$$

The flow velocity components in this and the following equations are superficial, but these are related to the local void fraction and the interstitial velocity through $u_s = \varepsilon\, u_i$.

To eliminate the unknown local pressure field, the set is rewritten according to the stream function and vorticity formulation [Bird et al., 1960; Patankar, 1980]. This development is explained in detail in the original paper.

The continuity equations for the various species and the energy equation need to be added to the equations given above. These are of course also two-dimensional and account for the non uniform velocity profile.

$$u_z\frac{\partial C_i}{\partial z}+u_r\frac{\partial C_i}{\partial r}=\frac{1}{r}\frac{\partial}{\partial r}\left(rD_{ers}\frac{\partial C_i}{\partial r}\right)+\rho_s(1-\varepsilon)R_i \qquad (11.7.5\text{-}3)$$

$$\rho_f c_p\left[u_z\frac{\partial T}{\partial z}+u_r\frac{\partial T}{\partial r}\right]=\frac{1}{r}\frac{\partial}{\partial r}\left(r\lambda_{er}\frac{\partial T}{\partial r}\right)+\rho_s(1-\varepsilon)\sum\left(-\Delta H_i R_i\right)$$

with the following boundary conditions:

$$\begin{aligned}
&\text{at} \quad z = 0: && C_i = C_{0i}, && T = T_0 \\
&\text{at} \quad r = 0: && \frac{\partial C_i}{\partial r} = 0, && \frac{\partial T}{\partial r} = 0 \\
&\text{at} \quad r = R_t: && \frac{\partial C_i}{\partial r} = 0, && T = T_w.
\end{aligned}$$

No distinction is made between the fluid and solid phase — there are no diffusion limitations neither at the fluid-solid interface nor inside the thin catalytic layer of V_2O_5/TiO_2 on the alumina particle, but the effect of the bed void fraction and, therefore, of the flow velocity profile, is accounted for also in $D_{er}(r)$ and $\lambda_{er}(r)$ [see Section 11.7.1]. The boundary condition at the wall for the energy equation does not contain a wall heat transfer coefficient any more, in contrast with the model of Section 11.7.2. Indeed, α_w was mainly introduced in the sixties in an attempt to compensate for the use of a uniform radial velocity in the correlations for λ_{er}. The reaction rates in (11.7.5-3) are those of a detailed kinetic model of the air oxidation of *o*-xylene, going way beyond the simple model used in Section 11.7.3. It considers the reduction of the V_2O_5-TiO_2 catalytic layer that acts as a donor of oxygen for the oxidations and its reoxidation by air [Papageorgiou et al., 1994]. Fig. 11.7.5-2 shows radial flow velocity profiles for a particle based Reynolds number of 175, typical for this process. The velocity is highest where the void fraction is highest. The radial profiles of temperature and *o*-xylene conversion are shown in Fig. 11.7.5-3. Notice the humps in the conversion profile. Humps of this type were observed by de Wasch and Froment [1972] in their study of radial heat transfer in packed beds. An axial conversion profile is shown in Fig. 11.10-1.

The simulation results shown here were obtained with a radial void profile constant over the whole bed length, but the model was also applied to variable radial void profiles. More recently Chigada and Mann [2008] used a model with a 2-dimensional network of voids to assess wall flow patterns for d_t/d_p ratios as low as 1.32. For these large void fractions there is a considerable radial flow component and its local value is strongly influenced by the neighboring voids.

The model presented here is a significant step forward in the simulation of fixed bed catalytic reactors. It is an early computational fluid dynamics (CFD) model of the continuum type. In recent years supercomputers have led to an increased application of CFD to studies of heat transfer in packed beds. In modeling the fluid flow in the voids confined by the catalyst particles, Nijemeisland and Dixon [2004] investigated the possibility of deriving values for the heat transfer coefficient between the bed and the wall in terms of the local properties of the flow field, but found no statistically valid correlation. They

concluded that these values are related to larger scale flow patterns in the bed, which is not surprising when the lessons of the application of the present model are kept in mind: the structure of the bed determines the gross flow pattern and that contribution to the heat transfer with the wall overweighs that of the local eddies. Reactor models are computationally very demanding when complex kinetic schemes are involved. Only recently, Dixon et al. [2007] applied CFD to a steam reforming reactor using the kinetic scheme of Example 11.9.1.A, but no comparison is made with simple model predictions.

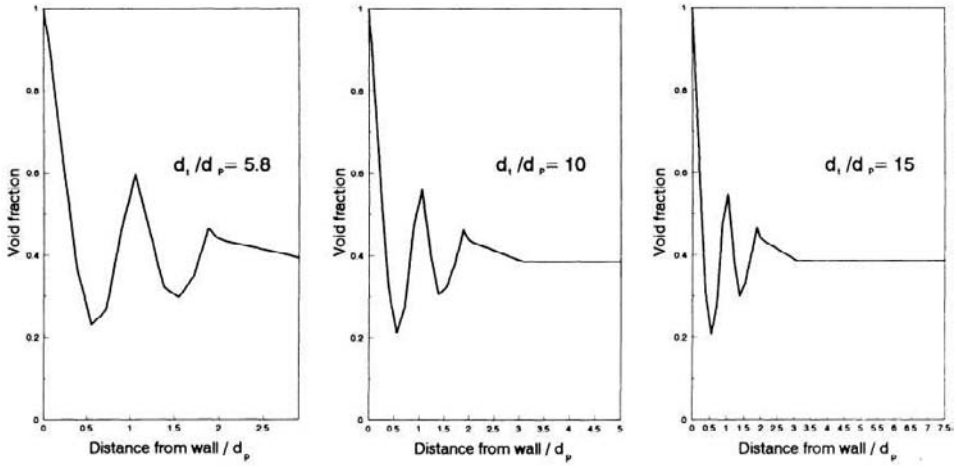

Figure 11.7.5-1

Void fraction profiles in a packed bed for various ratios of d_t/d_p. From Papageorgiou and Froment [1995].

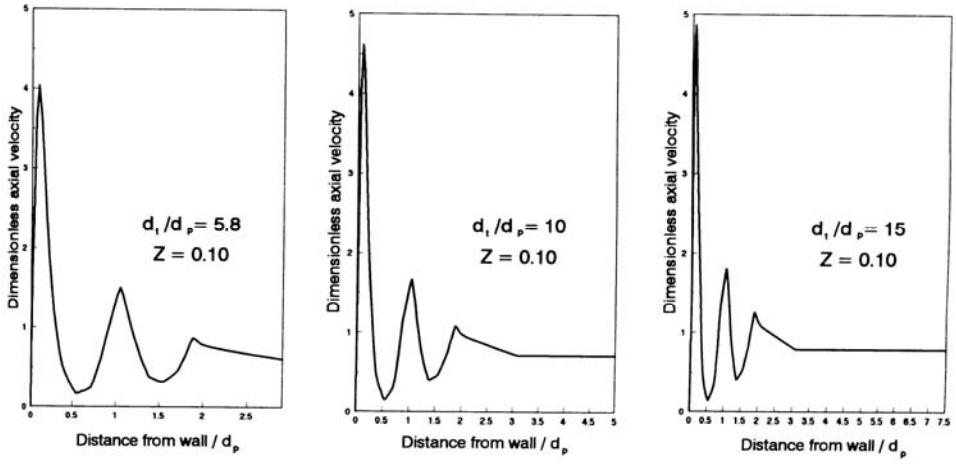

Figure 11.7.5-2

Radial profiles of the dimensionless axial velocity. Effect of tube-to-particle diameter ratio at Z = z/L = 10 for Re_p = 175. From Papageorgiou and Froment [1995].

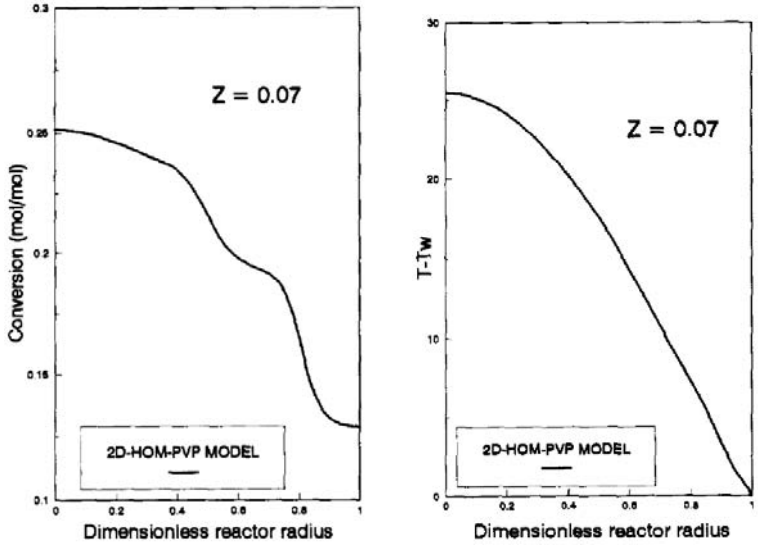

Figure 11.7.5-3

Two-dimensional homogeneous model with porosity and void fraction profile (2D-HOM-PVP). Radial conversion (a) and temperature (b) profiles at a given distance in the bed and for $Re_p = 175$. $Z = z/L = 0.07$ [Papageorgiou and Froment, 1995].

The present model is easily extended to 3 dimensions by including the angular dependency. For the usual reactors, fed uniformly over the inlet cross-section of the bed, this is not really required, however.

11.7.6 Two-Dimensional Cell Models

The discussion of the tubular reactor with radial mixing has been based on a continuum model leading to a system of differential equations, with mixing effects expressed in terms of effective diffusion and conduction. There exists a different approach that considers the bed to consist of a two-dimensional network of perfectly mixed cells with two outlets to the subsequent row of cells. Alternative rows are offset half a stage to allow for radial mixing. In the steady state, a pair of algebraic equations must be solved for each cell. This model was proposed by Deans and Lapidus [1960] and applied by McGuire and Lapidus [1965] to non-steady-state cases. Agnew and Potter [1966] used it to set up runaway diagrams of the Barkelew type. In fact, the model is not completely analogous to the one discussed above, since it considers heat to be transferred only through the fluid. It is clear already from the correlations for λ_{er} given above that this is a serious simplification, as will be illustrated in Section 11.10. More elaborate cell modes, with a coupling between the particles to account for

conduction or radiation, are possible [Amundson, 1970; and Kunii and Furusawa, 1972], but the computational problems then become overwhelming. The effective transport concept keeps the problem within tractable limits.

The equivalence between the predictions of continuum and cell models has been studied extensively for both one- and two-dimensional cases [Aris and Amundson, 1957; Olbrich et al., 1966; Sundaresan et al., 1980; and Varma, 1980]. It should not be forgotten that cell models were developed for mathematical convenience. They may seem closer to reality but are still far away from true hydrodynamic models. The cell size, for example, is chosen so as to match the results of residence time distribution experiments. To achieve this, the cell size in the radial direction has to be 0.9 d_p. Recently, Klingman and Lee [1987] described mass and heat dispersion in a packed bed in terms of flow through an axially repeating series of cells, either filled with packing or void. The fluid moves through the voids in plug flow. Dispersion is achieved by repeated splitting and merging of the fluid plugs.

Clearly, no model will ever represent the reactor behavior in an absolutely rigorous and exact way. The equations contain a number of parameters, some of which are "effective" in the sense that they lump the effects of phenomena that would otherwise have to be expressed by means of additional equations, to be solved simultaneously in the reactor simulation. Admittedly, further improvement and extension of existing correlations is required for severe reaction conditions or unusual reactor configurations. Indeed, for convenience, these parameters were generally obtained from purely physical experiments. Under reaction conditions, different gradients may develop which may eventually cause the parameter values to be less accurate, even when the underlying description of the phenomena is correct. This is still no justification for an arbitrary tuning of the parameters on the basis of experimental testing of the reactor model, because this may lead to inconsistencies and violation of their physicochemical background.

PART THREE
HETEROGENEOUS MODELS

For very rapid reactions with an important heat effect, it may be necessary to distinguish between conditions in the fluid and on the catalyst surface (Section 11.8) or even inside the catalyst (Section 11.9). As in Part Two, the reactor models may be of the one- or two-dimensional type.

11.8 ONE-DIMENSIONAL MODEL ACCOUNTING FOR INTERFACIAL GRADIENTS

11.8.1 Model Equations

The steady-state equations are, for a single reaction carried out in a cylindrical tube and with the restrictions already mentioned in Section 11.5.1 for the basic case,

For the fluid phase:

$$-u_s \frac{dC}{dz} = k_g a_v (C - C_s^s) \tag{11.8.1-1}$$

$$u_s \rho_g c_p \frac{dT}{dz} = h_f a_v (T_s^s - T) - 4\frac{U}{d_t}(T - T_r) \tag{11.8.1-2}$$

For a cross section of the bed including solid and fluid:

$$\rho_B r_A = k_g a_v (C - C_s^s) \tag{11.8.1-3}$$

$$(-\Delta H)\rho_B r_A = h_f a_v (T_s^s - T) \tag{11.8.1-4}$$

with boundary conditions

$$C = C_0 \qquad \text{at} \qquad z = 0$$

$$T = T_0$$

In this set of equations and in those to follow in this chapter, C stands for the concentration of a reactant A. Figure 3.2.1-1 and 3.2.2-1 of Chapter 3 show many of the correlations available to date for k_g and h_f [Froment, 1972]. Except perhaps for the most stringent conditions, these parameters are now defined with sufficient precision. The most likely interfacial gradient to occur is the temperature gradient.

The distinction between conditions in the fluid and on the solid leads to an essential difference with respect to the basic one-dimensional model, that is, the problem of stability, which is associated with multiple steady states. This aspect was studied first independently by Wicke [1961] and by Liu and Amundson [1963]. They compared the heat produced in the catalyst, which is a sigmoidal curve when plotted as a function of the particle temperature, with the heat removed by the fluid through the film surrounding the particle, which leads to a straight line. The steady state for the particle is given by the intersection of both lines. It can be seen from Fig. 11.8.1-1 that for a certain range of gas and particle temperatures, three intersections, therefore three steady states, are

possible. From a comparison of the slopes of the sigmoidal curve and the straight line in these three points, it follows, as in Section 10.4, that the middle steady state is unstable to any perturbation, while the upper and lower steady states are stable, but not necessarily to large ones. It follows that, when multiple steady states are possible, the steady states in which the particle actually operates also depends on its initial temperatures. Upon heating, solid temperatures in the range $(T_s)_1$-$(T_s)_2$ do not correspond to a stable steady state for T_s, and upon cooling in the range $(T_s)_3$-$(T_s)_4$ also do not. The hysteresis between heating and cooling is shown in Fig. 11.8.1-2.

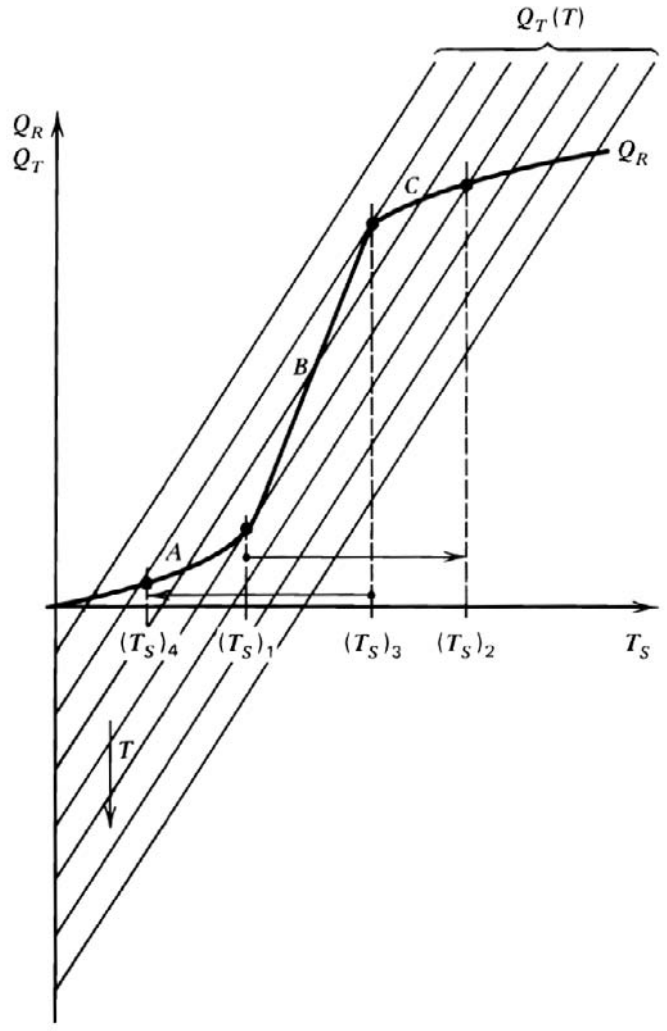

Figure 11.8.1-1
Heat generation and heat transfer rates for various catalyst temperatures.

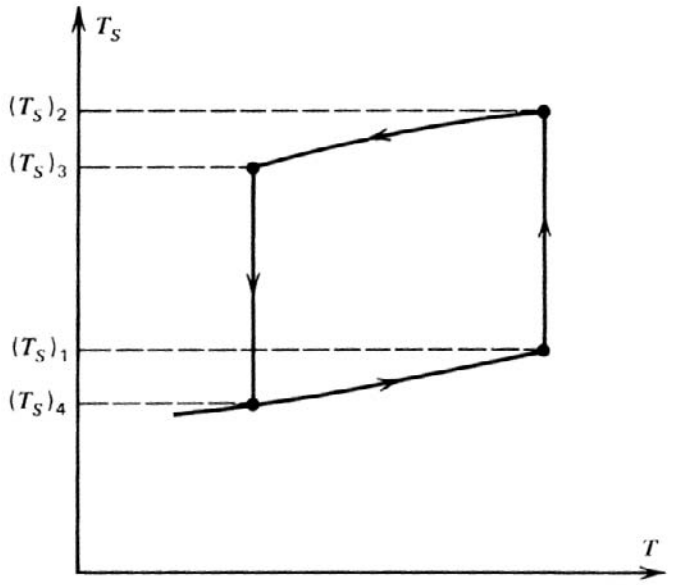

Figure 11.8.1-2

Hysteresis in catalyst temperature on variations in bulk gas temperature for the case of multiple steady states.

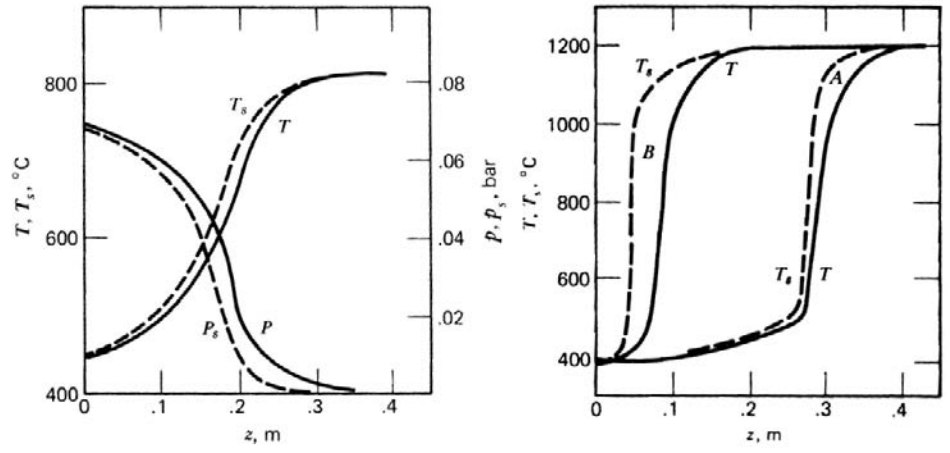

Figure 11.8.1-3

One-dimensional heterogeneous model with interfacial gradients. Unique steady-state case; $P_0 = 0.007$ atm, $T_0 = 449$°C. After Liu and Amundson [1963], from Froment [1972; 1974].

Figure 11.8.1-4

One-dimensional heterogeneous model with interfacial gradients. Nonunique steady-state case; $P_0 = 0.15$ atm, $T_0 = 393$°C. Initial T_S: A $\leq$ 393°C, B = 560°C. After Liu and Amundson [1963], from Froment [1972; 1974].

When this is now extended from a particle to an adiabatic reactor it follows that the concentration and temperature profiles are not determined solely

by the feed conditions but also by the initial solid temperature profile. If this is not equal to the fluid feed temperature, transients are involved. The design calculations would then have to be based on the system equations (11.8.1-1) through (11.8.1-4) completed with nonsteady-state terms. Figures 11.8.1-3 and 11.8.1-4 illustrate this for an adiabatic reactor [Liu and Amundson, 1963]. Figure 11.8.1-3 shows a situation with a unique steady-state profile. In Fig. 11.8.1-4 the gas is first heated up along the lower steady state and then jumps to the upper steady state as soon as the gas temperature exceeds 480°C. The higher the initial temperature profile, the earlier the profile jumps from the lower to the higher steady state. From a comparison with the unique steady-state case of Fig. 11.8.1-3 it follows that the shift from one steady state to another leads to temperature profiles that are much steeper. The reactor of Fig. 11.8.1-4 may be unstable while the reactor of Fig. 11.8.1-3 is stable, which does not exclude parametric sensitivity and runaway, as discussed under Section 11.5.3, however.

Are these multiple steady states possible in practical situations? From an inspection of Figs. 11.8.1-3 and 11.8.1-4 it is clear that the conditions chosen for the reaction are rather drastic. It would be interesting to determine the limits on the operating conditions and reaction parameters within which multiple steady states could be experienced. These limits will probably be extremely narrow, so that the phenomena discussed here would be limited to very special reactions or to very localized situations in a reactor, which would probably have little effect on its overall behavior. Indeed, in industrial fixed bed reactors, the flow velocity is generally so high that the temperature and concentration drop over the film surrounding the particle is small, at least in the steady state.

A criterion for detecting the onset of interphase temperature gradients has been proposed by Mears [1971a, b]. If the observed rate is to deviate less than 5 percent from the true chemical rate, the criterion requires

$$\frac{(-\Delta H) r_A \rho_B d_p}{2 h_f T} < 0.15 \frac{RT}{E}$$

Baddour et al. [1965] in their simulation of the TVA ammonia synthesis converter, already discussed in Section 11.5.5, found that in steady-state operation the temperature difference between the gas and the solid at the top, where the rate of reaction is a maximum, amounts to only 2.3°C and decreases as the gas proceeds down the reactor to a value of 0.4°C at the outlet. In the simulation of a methanol reactor, the difference between gas and solid temperature is of the order of 1°C. This may not be so with highly exothermic and fast reactions involving a component of the catalyst as encountered in the reoxidation of Fe and Ni catalysts used in ammonia synthesis and steam

reforming plants or involving material deposited on the catalyst, coke, for example.

Note that the model discussed here does not provide any explicit axial coupling in the solid phase. Consequently, heat is transferred in the axial direction only through the fluid. Eigenberger [1972a, b] added heat transfer through the solid to the model and this was found to significantly modify the behavior. The backward flow of heat prevents some parts of the reactor from being in the lower steady state and others from being in the high steady state, which could be the case if there were no coupling. If the reactor is in the high steady state at the exit, it will be so at the inlet, too, so that the temperature peak is right at the entrance. He also showed the influence of the boundary conditions to be quite significant.

Furthermore, the model also localizes the heat transfer to the wall entirely in the fluid phase. A model distinguishing between heat transfer in the gas phase and solid phase, in particular, at the wall, is discussed in Section 11.10. This requires a reconsideration of h_f as introduced in Chapter 3 and which is really a conglomerate reflecting the effect of several mechanisms. The latter are discussed by Balakrishnan and Pei [1979].

11.8.2 Simulation of the Transient Behavior of a Reactor

The system of equations for the transient state is easily derived from (11.8.1-1) to (11.8.1-4). The following equations are obtained for a single reaction with constant density:

For the fluid phase:

$$\frac{u_s \rho_g}{M_m p_t}\frac{\partial p}{\partial z} + \frac{\varepsilon \rho_g}{M_m p_t}\frac{\partial p}{\partial t} = k_g a_v (p_s^s - p) \qquad (11.8.2\text{-}1)$$

$$u_s \rho_g c_p \frac{\partial T}{\partial z} + \varepsilon \rho_g c_p \frac{\partial T}{\partial t} = h_f a_v (T_s^s - T) - 4\frac{U}{d_t}(T - T_r) \qquad (11.8.2\text{-}2)$$

For the bed cross section:

$$\rho_B r_A = k_g a_v (p - p_s^s) - \frac{C_t}{p_t}\varepsilon_s (1-\varepsilon)\frac{\partial p_s^s}{\partial t} \qquad (11.8.2\text{-}3)$$

$$(-\Delta H)\rho_B r_A = h_f a_v (T_s^s - T) + c_{ps}\rho_B \frac{\partial T_s^s}{\partial t} \qquad (11.8.2\text{-}4)$$

with boundary conditions

$$t = 0 \qquad z \geq 0 \qquad T = T_s = T_r$$
$$p = p_s = 0$$

$$t > 0 \qquad z = 0 \qquad T = T_0$$
$$p = p_0$$

The example considered here is again the hydrocarbon oxidation process with its simplified kinetic scheme used in Section 11.5.2. Suppose the reactor is at a temperature of 362°C and let the gas enter the bed at 362°C. How long will it take to reach the steady state after startup and what will the difference between gas and solid temperatures be? The integration is performed numerically along the characteristics.

The results are shown in Fig. 11.8.2-1. The fluid-phase temperature approaches the steady state within 1° to 2°C already after 0.11 h. The steady-state profiles are attained, within the accuracy of the computations, after 0.20 h. The difference in temperature between the gas and solid is really very small and of the order of 1°C. Yet, this is a very exothermic reaction, and the operating conditions used in these calculations are realistic.

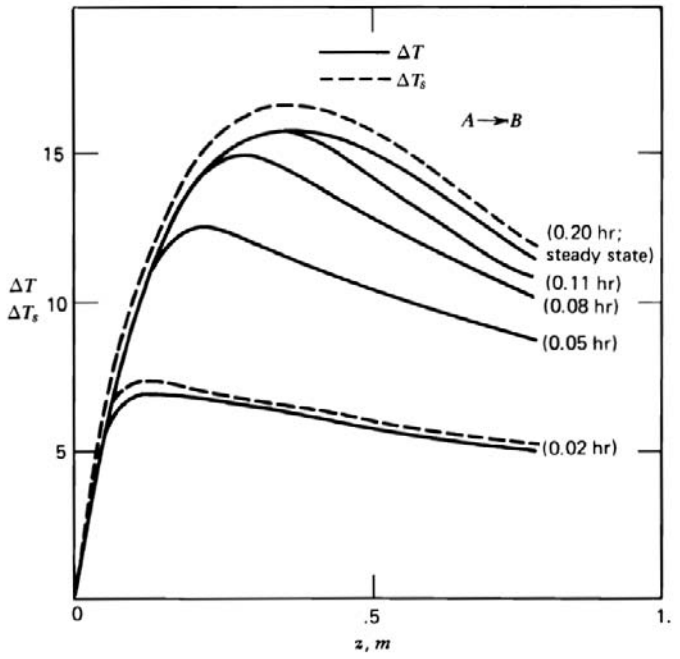

Figure 11.8.2-1

One-dimensional heterogeneous model with interfacial gradients. Startup of reactor, transient temperature profiles. ΔT = temperature increase of gas phase above feed value; ΔT_s = increase of solid temperature above initial value.

The calculations reported here assume that the catalyst instantaneously adapts its coverage and structure to the operating conditions, which is not necessarily true, however.

Commercial processes are generally operated in the steady state but Boreskov and Matros [1983] showed that SO_3-synthesis could benefit energetically from the essentially unsteady state reversed flow operation. In this process the feed is fed at a temperature below that of the adiabatic fixed catalytic bed and is gradually heated until the exothermic synthesis takes off. A temperature profile in the form of a plateau develops that travels through the bed towards the exit. Before the plateau reaches the exit and the heat content of the bed would be transported out of the reactor the flow direction is reversed and the feed is heated at the other end of the bed. This mode of operation has been applied at an industrial scale in Russia. Blanks et al. [1990] and De Groote et al. [1996] have investigated the potential of this mode of operation for synthesis gas production by catalytic partial oxidation of natural gas, Vanden Bussche and Froment [1996] for methanol synthesis. Kolios and Eigenberger [1999] studied the endothermic styrene production from ethylbenzene in reversed flow. In that case the heat required by the process is provided by the combustion of recycled hydrogen in a burner located in the center of the bed.

EXAMPLE 11.8.2.A
A GAS-SOLID REACTION IN A FIXED BED REACTOR

In Chapter 4 some gas-solid processes were mentioned and rate equations were derived that permit a quantitative description of the progression with time of the reaction inside the solid. When the solid particles are packed and form a fixed bed reactor, the approach discussed in the present section can be followed to model this reactor. Obviously, the model has to distinguish between the fluid and solid phase — it is “heterogeneous”. Furthermore, nonsteady-state equations have to be set up to account for the inherently transient character of the operation, not only in the solid but also in the fluid phase. Indeed, since the fluid phase is depleted in reactant, the reaction is confined to a zone that gradually moves through the reactor as the solid reactant is converted. The example that will be worked out in what follows concerns the reaction between an oxygen-containing gas phase on one hand and hydrogen and nickel contained in a steam-reforming catalyst on the other hand. The rate equation used does not explicitly consider the presence of intraparticle gradients. This is the reason why the example is dealt with in this section.

A secondary reformer is an adiabatic reactor which is a part of an ammonia-synthesis gas production line. In this reactor the mixture of CH_4, CO, CO_2, H_2, and steam coming from the primary reformer is mixed with air in a burner to add the required amount of nitrogen and achieve the ratio H_2/N_2 required for ammonia synthesis. Some H_2 is burnt and the gases reach a temperature of the order of 1200°C before flowing through the bed for further reforming of CH_4. The secondary reformer is packed with a NiO on Al_2O_3 catalyst operating in the reduced state. When the reactor has to be opened for inspection or repair, the catalyst, which is very pyrophoric, has to be reoxidized. This has to be done in a controlled way to avoid an excessive temperature rise. First, the reactor is cooled by means of a flow of steam. At about 250°C, the steam is switched off to avoid any condensation which would damage the catalyst, and further cooling is achieved by means of a flow of nitrogen containing only a very small fraction of oxygen. The oxygen content is gradually increased as the temperature decreases.

In this example the temperature in an adiabatic bed during reoxidation is investigated by means of simulation. This requires the combination of a rate equation for the gas-solid reaction and of the model equations for the reactor. The first reaction to consider in the present case is the reaction between the oxygen of the gas phase and the hydrogen adsorbed on the catalyst. It is this hydrogen that is mainly responsible for the pyrophoric character of such a catalyst. The reaction between the oxygen and the adsorbed hydrogen will be considered to be infinitely fast. It causes a temperature rise that may initiate the oxidation of the nickel of the catalyst.

Viville [1975] studied the rate of the latter process on an electrobalance. Hatcher, Viville, and Froment [1978] described its rate by a heterogeneous gas-solid model with a Hougen-Watson expression for the reaction rate

$$r_{Ni} = -\frac{dC_{Ni}}{dt} = \frac{kK_A pC_{Ni}^2}{1 + K_A p} \text{ (mol Ni/cm}^3 \text{ cat. s)} \qquad (11.8.2.\text{A-a})$$

where C_{Ni} is the nickel concentration of the catalyst (mol Ni/cm^3 cat.) and p_A is the oxygen partial pressure. The temperature dependences of the reaction rate coefficient k and of the oxygen adsorption coefficient K_A are given by the following Arrhenius relations:

$$k = 21.7e^{-3520/T}$$

$$K_A = 0.305e^{3070/T}$$

From the stoichiometry, $r_{O2} = \frac{1}{2} r_{Ni}$.

The reactor model chosen is one-dimensional and heterogeneous with interfacial gradients. Intraparticle gradients, if they occur, are accounted for implicitly through the fit of the experimental data by means of (11.8.2.A-a). The operation is adiabatic. Furthermore, as already mentioned, the operation is of a nonsteady-state nature, because the oxidation takes place in a zone that gradually moves through the reactor.

Continuity equation for oxygen in the gas phase:

$$\frac{G}{M_m p_t a_v k_g}\left[\frac{\partial p_A}{\partial z} + \frac{\varepsilon \rho_g}{G}\frac{\partial p_A}{\partial t}\right] = (p_A)_s - p_A \qquad (11.8.2.A\text{-b})$$

where k_g is in kmol/m^2 bar h.

Energy equation for the gas phase:

$$\frac{G c_p}{a_v h_f}\left[\frac{\partial T}{\partial z} + \frac{\varepsilon \rho_g}{G}\frac{\partial T}{\partial t}\right] = T_s - T \qquad (11.8.2.A\text{-c})$$

Continuity equation for O_2 in the solid phase:

$$k_g\left[p_A - (p_A)_s\right] = \frac{d_p}{6}\rho_s\left[\frac{1}{2} r_{H_2} + \frac{1}{2} r_{Ni}\right] \qquad (11.8.2.A\text{-d})$$

Since the rate of hydrogen oxidation is instantaneous and the phenomenon is mass transfer-limited, the adsorbed oxygen concentration is essentially zero as long as there is hydrogen on the surface, so that

$$k_g p_A = \frac{d_p}{12}\rho_S \frac{\partial C_{H_2}}{\partial t} \qquad (11.8.2.A\text{-e})$$

where C_{H_2} is the concentration of adsorbed hydrogen in kmol/kg cat. Also, once the hydrogen is used up,

$$k_g\left[p_A - (p_A)_s\right] = -\frac{d_p}{12}\rho_s \frac{\partial c_{Ni}}{\partial t} \qquad (11.8.2.A\text{-f})$$

The energy equation for the solid phase is written

$$h_f (T_s - T) + \frac{1}{6} d_p c_{p_s} \rho_s \frac{\partial T_s}{\partial t} = \frac{d_p}{6}\rho_s\left[(-\Delta H_{Ni}) r_{Ni} + (-\Delta H_{H_2}) r_{H_2}\right] \qquad (11.8.2.A\text{-g})$$

The initial and boundary conditions are

$$\text{at} \quad t = 0 \qquad z \geq 0 \qquad \begin{aligned} T_s &= T = T_0 \\ p_s &= p = 0 \\ C_{Ni} &= C_{Ni_0} \end{aligned}$$

$$\text{at} \quad t \geq 0 \qquad z = 0 \qquad p = p_0 \text{ and } T = T_0$$

The following conditions are typical for industrial operation:

G	=	1342.8 kg/m^2 h	vol-% oxygen at the inlet: 5%
M_m	=	28.2 kg/kmol	C_p = 1.05 kJ/kg K
p_t	=	1.52 bar	T_0 = 250°C
ρ_B	=	950 kg/m^3	ρ_s = 1515 kg/m^3 cat.
a_v	=	352.5 m^2/m^3	d_p = 0.014 m
C_{ps}	=	1.01 kJ/kg K	
C_{Ni0}	=	0.00624 kmol/kg cat	
C_{H2}	=	0.00093 kmol/kg cat.	

From the j_D and j_H correlations, k_g is calculated to be 0.00381 kmol/m² s bar and h_f = 0.0974 kJ/m² s K.

Figure 11.8.2.A-1 shows the hydrogen and nickel concentration profiles through the reactor as a function of time. Note the steep hydrogen profile, caused by the infinitely fast reaction between hydrogen and oxygen, which raises the temperature to such values where the nickel also reacts rapidly. The temperature peaks travel through the bed with time, as shown in Fig. 11.8.2.A-2. The simulation illustrates the combined effect of too high an oxygen content and too low a flow velocity, leading to temperatures exceeding 1400°C and weakening of the catalyst from a bed depth between 1.2 and 1.3 m onward. This value has to be compared with 1.46 m, observed in an actual case.

Figure 11.8.2.A-3 illustrates that the difference between gas and solid temperatures can reach 100°C. Clearly, a reactor model accounting for interfacial gradients is required here. Note from Fig. 11.8.2.A-3 how the solid temperature exceeds the gas temperature at positions already passed by the thermal wave and how the difference rapidly increases on the rear slope of the wave. Near the peak of the wave, the difference becomes smaller. In front of the wave, the temperature of the gas exceeds that of the catalyst. It is also observed that after a certain time the wave travels at a nearly constant rate.

Analogous equations are used to simulate the regeneration of coked catalysts, and similar waves are obtained [Olson et al., 1968; and Hughes et al., 1987].

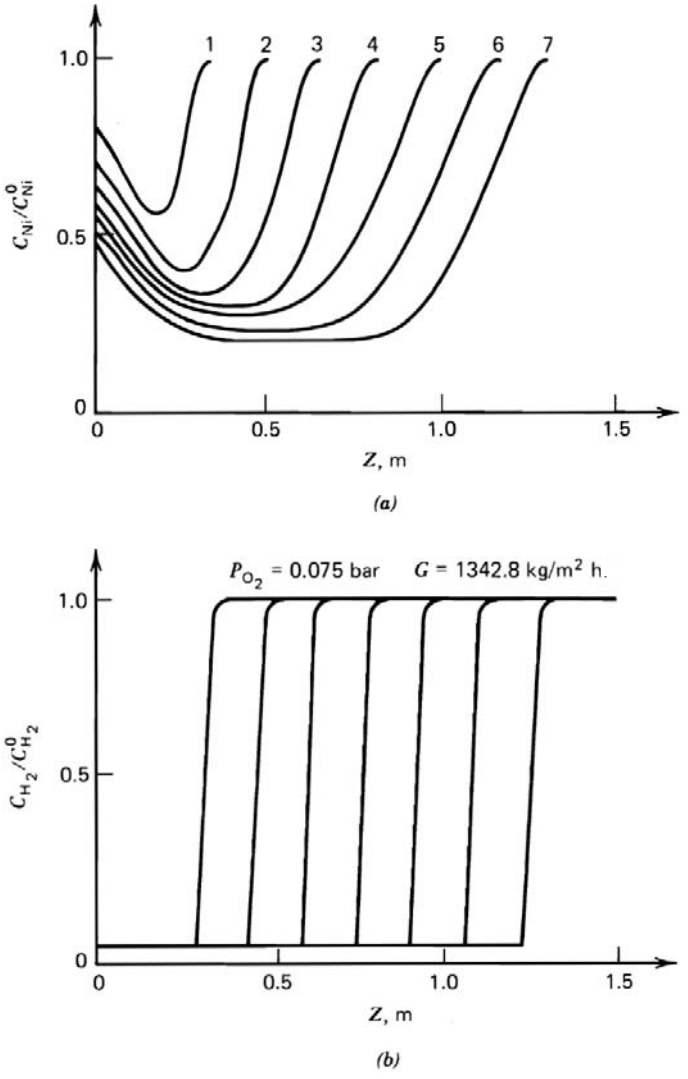

Figure 11.8.2.A-1

Reoxidation of secondary steam reforming catalyst bed. Profiles of (a) nickel and (b) hydrogen concentrations as a function of time. After Hatcher et al. [1978].

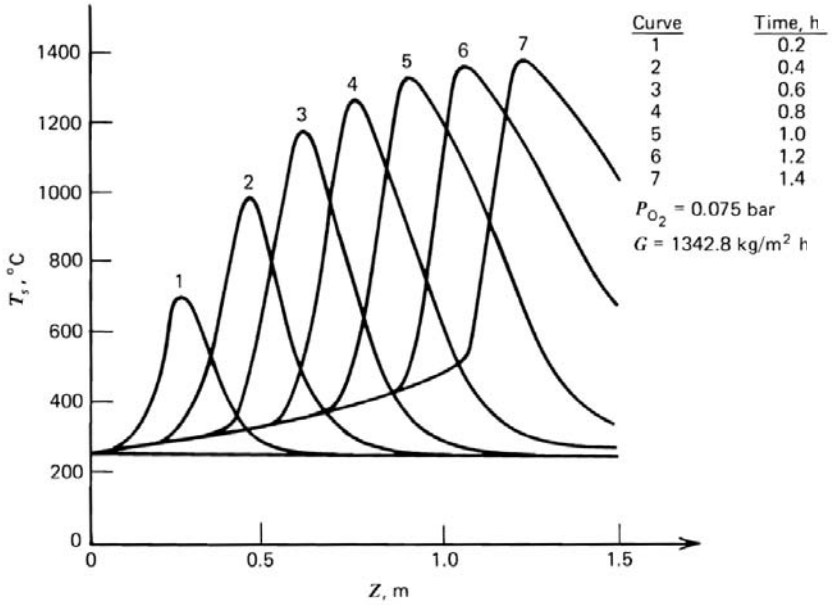

Figure 11.8.2.A-2

Reoxidation of secondary steam reforming catalyst bed. Solid temperature profiles. After Hatcher et al. [1978].

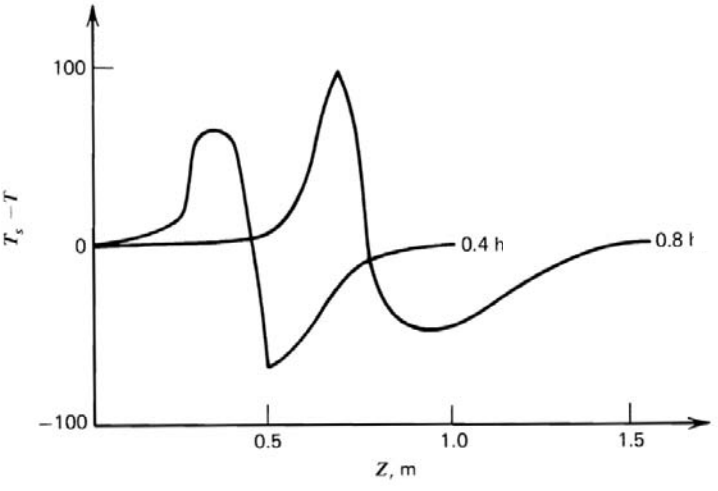

Figure 11.8.2.A-3

Reoxidation of secondary steam reforming catalyst bed. Differences in solid and gas temperatures. After Hatcher et al. [1978].

■

11.9 ONE-DIMENSIONAL MODEL ACCOUNTING FOR INTERFACIAL AND INTRAPARTICLE GRADIENTS

11.9.1 Model Equations

When the resistance to mass and heat transfer inside the catalyst particle is important, the rate of reaction is not uniform throughout the particle. The set of equations (11.8.1-1) through (11.8.1-4) of Section 11.8.1 then no longer adequately describes the situation. It has to be completed with equations describing the concentration and temperature gradients inside the particle, so that the complete set may be written

For the fluid phase:

$$-u_s \frac{dC}{dz} = k_g a_v (C - C_s^s) \qquad (11.9.1\text{-}1)$$

$$u_s \rho_g c_p \frac{dT}{dz} = h_f a_v (T_s^s - T) - \frac{4U}{d_t}(T - T_r) \qquad (11.9.1\text{-}2)$$

For the solid phase:

$$\frac{D_e}{\xi'^2}\frac{d}{d\xi'}\left(\xi'^2 \frac{dC_s}{d\xi'}\right) - \rho_s r_A(C_s, T_s) = 0 \qquad (11.9.1\text{-}3)$$

$$\frac{\lambda_e}{\xi'^2}\frac{d}{d\xi'}\left(\xi'^2 \frac{dT_s}{d\xi'}\right) + \rho_s(-\Delta H) r_A(C_s, T_s) = 0 \qquad (11.9.1\text{-}4)^1$$

with boundary conditions

$$\begin{aligned} C &= C_0 \\ T &= T_0 \end{aligned} \quad \text{at} \quad z = 0 \qquad (11.9.1\text{-}5)$$

$$\frac{dC_s}{d\xi'} = \frac{dT_s}{d\xi'} = 0 \quad \text{at} \quad \xi' = 0 \qquad (11.9.1\text{-}6)$$

$$k_g (C_s^s - C) = -D_e \frac{dC_s}{d\xi'} \quad \text{at} \quad \xi' = \frac{d_p}{2} \qquad (11.9.1\text{-}7)$$

$$h_f (T_s^s - T) = -\lambda_e \frac{dT_s}{d\xi'} \quad \text{at} \quad \xi' = \frac{d_p}{2} \qquad (11.9.1\text{-}8)$$

[1] The signs in (11.9.1-3) and (11.9.1-4) are those obtained when the rate is defined for first order as $r_A = kC_A$. Many books define $r_A = -kC_A$. See Chapter 1 for use of the stoichiometric coefficients.

Note that a single particle is considered, not the bed cross section, when intraparticle profiles are to be dealt with. Indeed, the shape of the particle also determines the profile. Numerical values for D_e and λ_e are given in Satterfield's book [1970] and in Weisz and Hicks' classical paper on this subject [1962], discussed in Chapter 3.

The system of second-order, nonlinear differential equations, (11.9.1-1) through (11.9.1-8), has to be integrated in each node of the computational grid used in the integration of the fluid field equations, (11.9.1-1) and (11.9.1-2). This is feasible on present-day computers but still extremely lengthy. Analytical solution is only possible for isothermal situations inside the particle and first-order irreversible reactions. Fortunately, even with strongly exothermic reactions the particle is practically isothermal: the main resistance inside the pellet is to mass transfer, and the main resistance in the film surrounding the particle is to heat transfer [Weisz and Hicks, 1962; and Carberry, 1961]. When gradients occur inside the catalyst particle, use is often made of the effectiveness factor η introduced in Chapter 3. In its classical sense, η is a factor that multiplies the reaction rate at the particle surface conditions to yield the rate that is actually experienced when the conditions inside the particle are different. The use of the effectiveness factor reduces the system (11.9.1-1) through (11.9.1-4) to (11.8.1-1) through (11.8.1-2), with boundary conditions (11.9.1-5) and the following algebraic equations:

$$k_g a_v (C - C_s^s) = \eta \rho_B r_A (C_s^s, T_s^s) \qquad (11.9.1\text{-}9)$$

$$h_f a_v (T_s^s - T) = \eta \rho_B (-\Delta H) r_A (C_s^s, T_s^s) \qquad (11.9.1\text{-}10)$$

with

$$\eta = f(C_s^s, T_s^s)$$

Note that (11.9.1-9) and (11.9.1-10) differ from (11.8.1-3) and (11.8.1-4) only by the factor η.

The effectiveness factor depends on the local conditions, which are introduced through the modulus ϕ, and therefore has to be computed in each node of the grid. With a first-order reaction and an isothermal spherical particle, the following relationship between η and the determining variables may be obtained by analytical integration of (11.9.1-3)

$$\eta = \left(\frac{3}{\phi''^2} \right) [\phi''(\coth \phi'') - 1] \qquad (11.9.1\text{-}11)$$

where ϕ'', the modulus, which contains these variables is related to the ratio of the reaction rate at surface conditions to the mass transfer rate toward the inside:

$$\phi'' = \frac{d_p}{2}\sqrt{\frac{k(T_s^s)\rho_s}{D_e}}$$

When an analytical solution is not available for η, there is no gain in the use of η from the reactor design and computational viewpoint. The only advantage of η, then, is its possibility of characterizing the situation inside the particle by means of a single number. For single reactions with an order different from 1 but isothermal conditions, advantage can be taken of approximate expressions for η (e.g., through the use of the generalized modulus [Bischoff, 1967], which avoids the numerical integration of (11.9.1-3) and only requires the evaluation of an integral in each point of the grid.

The effectiveness factor η is generally expressed as a function of the surface conditions C_s^s and T_s^s. It is also possible to refer to bulk fluid conditions in case these are different from those prevailing at the particle surface. With this version of the effectiveness factor, represented by η_G, the rate r_A has to be expressed as a function of fluid conditions (C, T), and η_G enters into (11.9.1-9) and (11.9.1-10). The equivalent of (11.9.1-11), then, is for isothermal conditions in both the film and the particle [McGreavy and Cresswell, 1969]

$$\eta_G = \frac{3Sh'}{\phi''^2}\left[\frac{\phi''\cosh\phi'' - \sinh\phi''}{\phi''\cosh\phi'' + (Sh'-1)\sinh\phi''}\right] \qquad (11.9.1\text{-}12)$$

where

$$Sh' = \frac{k_g R}{D_e}$$

is also called the Biot number for mass transfer and (11.9.1-12) is the spherical analog of (3.9-4).

$$\phi'' = \frac{d_p}{2}\sqrt{\frac{k(T)\rho_s}{D_e}}$$

Kehoe and Butt [1972] provide some experimental tests of these relations. The use of η_G reduces the system equations (11.9.1-1) - (11.9.1-4) to

$$-u_s\frac{dC}{dz} = \eta_G\rho_B r_A(C,T)$$

$$u_s\rho_g c_p\frac{dT}{dz} = \eta_G\rho_B r_A(C,T) - 4\frac{U}{d_t}(T - T_r)$$

with

$$\eta_G = f(C,T)$$

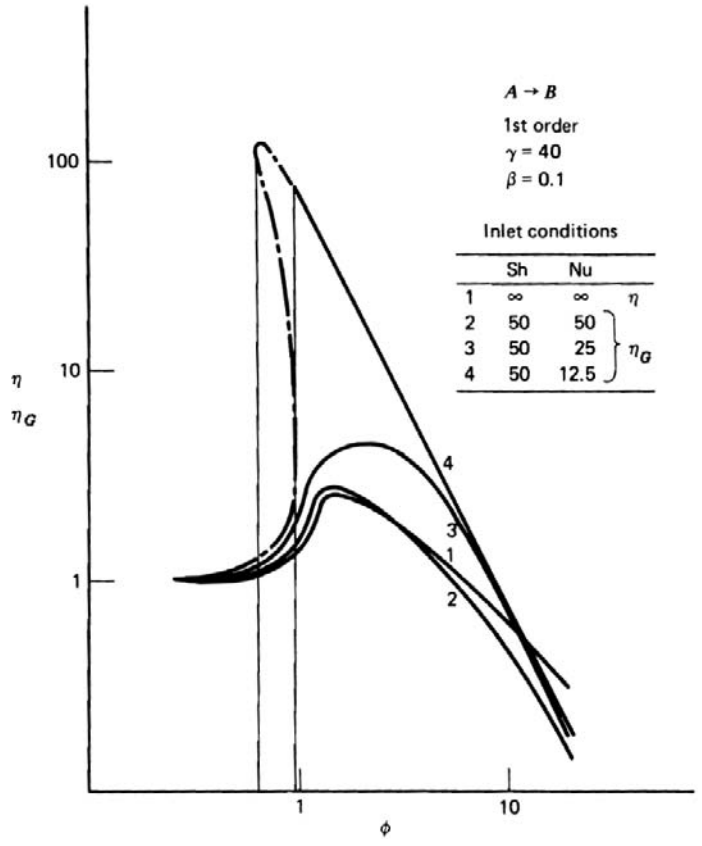

Figure 11.9.1-1

Effectiveness factor diagram for nonisothermal situations. After McGreavy and Cresswell [1969]. From Froment [1972, 1974].

Figure 11.9.1-1 shows the relation between the effectiveness factors η and η_G and the modulus ϕ [Kehoe and Butt, 1972; and McGreavy and Cresswell, 1969]. This relation can only be obtained by numerical integration of the set, (11.9.1-1) through (11.9.1-8), except for the cases already mentioned. With isothermal situations, η tends to a limit of 1 as ϕ decreases; with nonisothermal situations, however, η or η_G may exceed 1. Curve 1 corresponds to the η concept, curves 2, 3, and 4 to η_G. The dotted part of curve 4 corresponds to a region of conditions within which multiple steady states inside the catalyst are possible. But it should be stressed that the range of parameters leading to this situation is very narrow. Again, this may be extended to the reactor, which will then have nonunique profiles. The steady state actually experienced may depend on the initial conditions, so that transients have to be computed. To avoid these when they are unnecessary, considerable effort has recently gone into defining criteria for the uniqueness of the steady state of a particle. We illustrate these for a first-order irreversible reaction treated

numerically by Drott and Aris [1969] with β = 0.1 and γ = 50. It should be noted that β = 0.1 is an extremely high value. Normal values for γ are 20 and 30. According to Luss and Amundson's criterion [1967] for uniqueness $\beta\gamma << 1$ or Luss' less conservative criterion $\beta\gamma \leq 4(1+\beta)$ [1968], multiplicity is possible, because $\beta\gamma$ = 5. Multiplicity may still be avoided by the appropriate choice of the modulus, that is, the size of the particle. According to Weisz and Hicks [1962], ϕ'' should be smaller than 0.1; according to Luss and Amundson, it should be smaller than 0.4218. But from Fig. 11.9.1-1 it follows that multiplicity can only occur for a certain interval of ϕ'' values. Luss [1971] gives approximate values for the bounds on ϕ''. In this example 0.4191 and 0.4655 are values for the lower bound and 0.4965 for the upper bound. The values computed by Drott and Aris are 0.4707 and 0.4899, respectively. Once more, this confirms that multiplicity is possible only for extremely exothermic reactions and in an extremely narrow region of ϕ''.

McGreavy and Thornton [1970] included the film surrounding the particle into their analysis of the multiplicity of solutions. With gradients over the film, multiplicity is possible even when the particle is isothermal, of course. As mentioned in Chapter 3, Luss [1976] came to the following criterion for uniqueness for a first-order reaction:

$$\beta\gamma < 4\left(\frac{Nu'}{Sh'} + \beta\right)$$

while Kehoe and Butt obtained, for an *n*th-order reaction,

$$\beta\gamma < 4(n+1)\left(\frac{Nu'}{Sh'} + \beta\right)$$

Even with an isothermal particle and without including the film, multiplicity is theoretically possible when the rate increases with conversion as may occur for some type of Hougen-Watson rate equations and some particular parameter values. According to Luss, the sufficient condition for uniqueness of the concentration profile in the particle is

$$(C_s - C_s^s)\frac{d\ln f(C_s)}{dC_s} \leq 1$$

where $f(C_s)$ is the rate equation. Luss and Lee [1971] developed a method for obtaining stability regions for the various steady states, based on the knowledge of the steady-state profiles. It thus becomes possible to predict towards which steady state a particle will tend starting from given initial conditions.

This whole field of uniqueness and stability has been reviewed by Aris [1969] and by Luss [1987]. As previously mentioned, the possibility of multiple steady states seriously complicates the design of the reactor. Indeed, transient computations have to be performed to make sure that the correct steady-state profile throughout the reactor is predicted. Another way would be to check the possibility of multiple steady states on the effectiveness factor chart for every point in the reactor. This would, in principle, require an enormous set of such charts, because β and γ vary throughout the reactor.

McGreavy and Thornton [1970] reformulated the problem to allow a single graph to be used for the whole reactor and to reduce the effectiveness factor curve to a single point in the new chart. For this purpose they introduced a new parameter

$$\theta = \frac{d_p}{2}\sqrt{\frac{A_0}{D_e}}$$

replacing the Thiele modulus and based on the frequency factor A_0 rather than the rate coefficient itself. Another convenient group is

$$\frac{\beta}{\gamma Nu'} = \frac{(-\Delta H)CD_e R}{d_p h_f E}$$

For a given reactor this group depends only on the reactant concentration in the fluid. It is, therefore, an implicit function of axial position. Taking advantage of the fact that the particle is generally isothermal, a relatively simple formula for the bounds on the *fluid* temperature within which multiple steady states may occur can be derived. It is represented graphically in Fig. 11.9.1-2. With a reactant concentration corresponding to a $\beta/\gamma Nu$ value of 8×10^{-5}, for example, multiple steady states are possible when the gas temperature is between 265° and 320°C. The diagram of Fig. 11.9.1-2 is essentially a *C*-*T* phase plane and allows a trajectory through the reactor to be plotted. When a trajectory intersects the nonunique region, multiple profiles are possible. The figure shows a trajectory for adiabatic conditions that just intersects the zone. In the corresponding reactor zone, the temperature may jump to the higher steady state; but as the region is very narrow, it is possible that instabilities will be damped. As soon as the conditions are no longer adiabatic, only unique profiles are possible in the example considered. Since McGreavy and Thornton really used a two-dimensional model for the reactor in the nonadiabatic case, the figure shows longitudinal profiles in the axis and at the wall. The parameter values used appear to be realistic, although rather drastic. McGreavy and Adderley [1973, 1974] and, in a more detailed way, Rajadhyasha et al. [1975] studied the

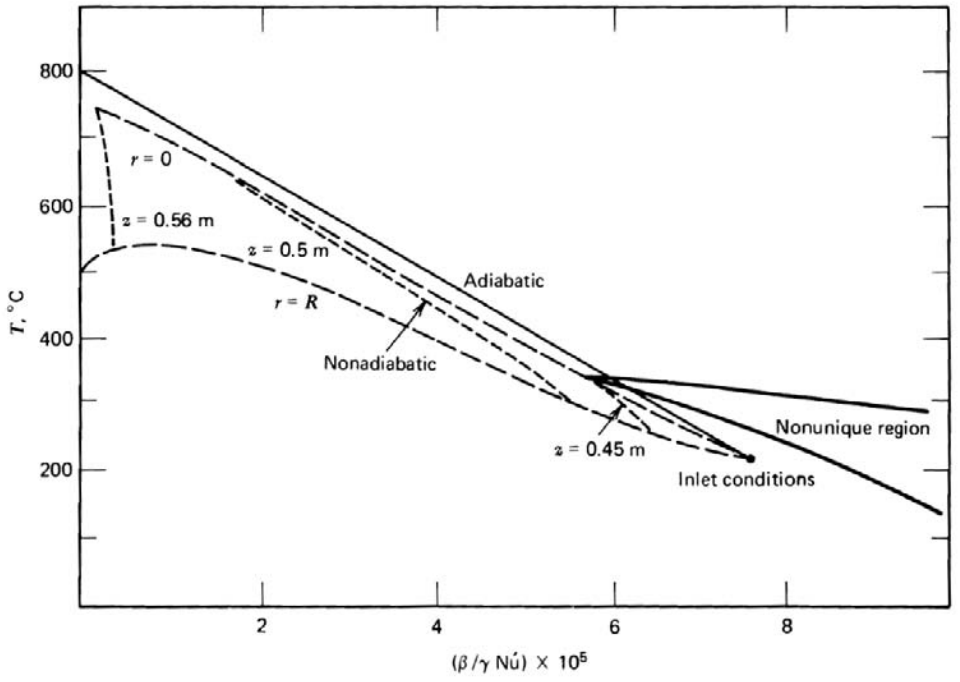

Figure 11.9.1-2

Tubular reactor with interfacial and intraparticle gradients. *C-T* phase plane and region of multiple steady states. After McGreavy and Thornton [1970]. From Froment [1972; 1974].

parametric sensitivity and instability of reactors with concentration gradients inside the particle and interfacial temperature gradients by extending the treatment of Van Welsenaere and Froment, outlined and applied in Section 11.5.3. A runaway line is easily derived for such a model and represented in the *p-T* phase plane. For a given coolant temperature, McGreavy and Adderley obtained the critical inlet partial pressure by adiabatic extrapolation toward the ordinate from the intersection of the maxima curve and the runaway line onward. This prediction is rather conservative, however. McGreavy and Adderley also present an estimate of the critical inlet partial pressure that would lead to runaway caused not by parametric sensitivity but by the occurrence of multiple steady states. This involves an adiabatic extrapolation from the intersection of the runaway line and the lower bound of the nonunique region, shown in Fig. 11.9.1-2, onward. Rajadhyasha et al. [1975] derived upper and lower limits for the critical inlet partial pressure. The average of these values was an excellent approximation for the numerical solution, as experienced by Van Welsenaere and Froment with the pseudohomogeneous model.

EXAMPLE 11.9.1.A
SIMULATION OF A PRIMARY STEAM REFORMER

Steam reforming of natural gas (or eventually naphtha) on nickel/alumina is the main process for the production of synthesis gas, H_2 + CO, or hydrogen. Figure 11.3-7 shows a steam reforming furnace. The natural gas and steam are fed around 500°C and 30 bar to a number of parallel tubes, usually 10 to 12 m long and having an internal diameter of 0.10 m. The exit temperature is of the order of 775°C. Details of the configuration and catalyst and operating conditions are given in Table 11.9.1.A-1. The overall reaction scheme is represented in Fig. 11.9.1.A-1 [Xu and Froment, 1989].

Xu and Froment [1989] determined the intrinsic kinetics through an extensive experimental program carried out in a tubular reactor. The steam reforming proper was studied on crushed catalyst with a particle diameter between 0.17 and 0.25 × 10^{-3} m, molar ratios of H_2O/CH_4 between 1 and 5, and H_2/CH_4 of 1.25. The total pressure was varied between 3 and 15 bar, the temperature between 500° and 575°C. The water gas shift (or, for convenience, its reverse) and the methanation were studied on the same catalyst with molar feed ratios of H_2/CO_2 between 0.5 and 1.0, temperatures between 300° and 400°C, and pressures between 3 and 10 bar. A total of some 280 runs were carried out. The detailed reaction scheme is given in Fig. 11.9.1.A-2. From this scheme, Hougen-Watson-type equations were derived using the approach presented in Section 2.3 of Chapter 2 for single reactions and after discrimination among some 22 rival models, each comprising three rate equations.

TABLE 11.9.1.A-1
INPUT DATA FOR THE SIMULATION OF A COMMERCIAL STEAM REFORMER

T_o: 793.15 K	Total tube length: 12 m
p_{to}: 29 bar	Heated tube length: 11.12 m
135.0 Nm^3/h natural gas	Dimensions of catalyst ring
399.17 Nm^3/h steam	d_{pe} = 0.0173 m
Natural gas composition (vol-%)	d_{pi} = 0.0084 m
CH_4: 81.4	H = 0.010 m
N_2: 14.1	ρ_s = 2355.2 kg/m^3
C_2H_6: 2.8	Thickness of active layer: 0.002 m
CO_2: 1.0	Equivalent CH_4 feed: 5.168 kmol/h
C_3H_8: 0.4	Molar ratio
C_4H_{10}: 0.1	H_2O/CH_4: 3.358
C_5H_{12}: 0.2	CO_2/CH_4: 0.056
Internal tube diameter: 0.1016 m	H_2/CH_4: 0.122
External tube diameter: 0.1322 m	N_2/CH_4: 0.164

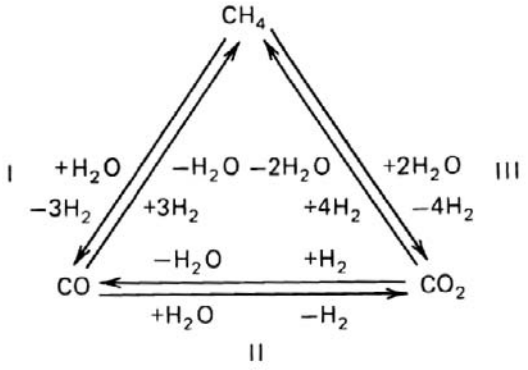

Figure 11.9.1.A-1

Overall reaction scheme. From Xu and Froment [1989].

The retained rate equations are given below, together with the conservation equations (11.9.1.A-a) through (11.9.1.A-d).

The Arrhenius and Van't Hoff plots for the rate and adsorption coefficients are shown in Fig. 11.9.1.A-3. The pre-exponential factors, activation energies, and enthalpy changes are given in Table 11.9.1.A-2.

From the work of De Deken et al. [1982] it was already clear that the reactions are strongly diffusion-controlled. This was confirmed by the present work, so that the reactor simulation required a one-dimensional heterogeneous model. It was also confirmed that interfacial gradients are negligible [De Deken

H_2O	+ l	=	O-l	+ H_2	(1)	
CH_4	+ l	=	CH_4-l		(2)	
CH_4-l	+ l	=	CH_3-l	+ H-l	(3)	
CH_3-l	+ l	=	CH_2-l	+ H-l	(4)	
CH_2-l	+ O-l	=	CH_2O-l	+ l	(21)	
CH_2O-l	+ l	=	CHO-l	+ H-l	(22)	
CHO-l	+ l	=	CO-l	+ H-l	(23) r.d.s.; r_1	
CO-l	+ O-l	=	CO_2-l	+ l	(8) r.d.s.; r_2	
CHO-l	+ O-l	=	CO_2-l	+ H-l	(25) r.d.s.; r_3	
CO-l		=	CO	+ l	(7)	
CO_2-l		=	CO_2	+ l	(10)	
2H-l		=	l	+ H_2-l	(1-bis)	
H_2-l		=	H_2	+ l	(1-ter)	

Figure 11.9.1.A-2

Detailed reaction scheme and rate-determining steps. From Xu and Froment [1989].

et al., 1982], so that model B-II of Table 11.4-1 was used. The tortuosity factor τ entering in the effective diffusivities, as discussed in Chapter 3, was determined in the presence of reaction on the basis of reverse water-gas shift experiments. A value of 3.54 was obtained. The equations are:

Continuity equations for CH_4 and CO_2:

$$\frac{dx_{CH_4}}{dz} = \Omega \frac{\rho_B \eta_{CH_4} R_{CH_4}}{F^0_{CH_4}} \qquad (11.9.1.A\text{-a})$$

$$\frac{dx_{CO_2}}{dz} = \Omega \frac{\rho_B \eta_{CO_2} R_{CO_2}}{F^0_{CH_4}} \qquad (11.9.1.A\text{-b})$$

where x_{CH_4} is the total conversion of methane and x_{CO_2} the conversion of methane into CO_2, which is also a molar yield of CO_2 out of CH_4.

Energy equation:

$$\frac{dT}{dz} = \frac{1}{c_p \rho_g u_s}\left[\rho_B(\sum(-\Delta H_i) r_i \eta_i) - 4\frac{U}{d_{ti}}(T - T_r)\right] \qquad (11.9.1.A\text{-c})$$

Momentum equation:

$$-\frac{dp_t}{dz} = \frac{f\rho_g u_s^2}{d_p} \qquad (11.9.1.A\text{-d})$$

with

$$x_{CH_4} = x_{CO_2} = 0 \qquad T = T_0 \qquad p_t = (p_t)_0 \qquad \text{at } z = 0$$

The intrinsic rate equations are:

For reaction I of Fig. 11.9.1.A-1 (rate of transformation of CH_4 into CO):

$$r_1 = \frac{\dfrac{k_1}{p_{H_2}^{2.5}}\left(p_{CH_4} p_{H_2O} - \dfrac{p_{H_2}^3 p_{CO}}{K_1}\right)}{(DEN)^2}$$

For reaction II (water-gas shift, rate of transformation of CO into CO_2):

$$r_2 = \frac{\dfrac{k_2}{p_{H_2}}\left(p_{CO} p_{H_2O} - \dfrac{p_{H_2} p_{CO_2}}{K_2}\right)}{(DEN)^2}$$

For reaction III (rate of transformation of CH_4 into CO_2):

$$r_3 = \frac{\dfrac{k_3}{p_{H_2}^{3.5}}\left(p_{CH_4}\,p_{H_2O}^2 - \dfrac{p_{H_2}^4\,p_{CO_2}}{K_3}\right)}{(DEN)^2}$$

$$DEN = 1 + K_{CO}\,p_{CO} + K_{H_2}\,p_{H_2} + K_{CH_4}\,p_{CH_4} + \left(\frac{K_{H_2O}\,p_{H_2O}}{p_{H_2}}\right)$$

Reaction rates for the formation of CO and CO_2 and for the disappearance of methane in steam reforming are obtained from

$$R_{CO} = r_1 - r_2$$
$$R_{CO_2} = r_2 + r_3$$
$$R_{CH_4} = r_1 + r_3$$

The heat transfer coefficient U is calculated from

$$\frac{1}{U} = \frac{d_{ti}}{2\lambda_{st}}\ln\left(\frac{d_{te}}{d_{ti}}\right) + \frac{1}{\alpha_i}$$

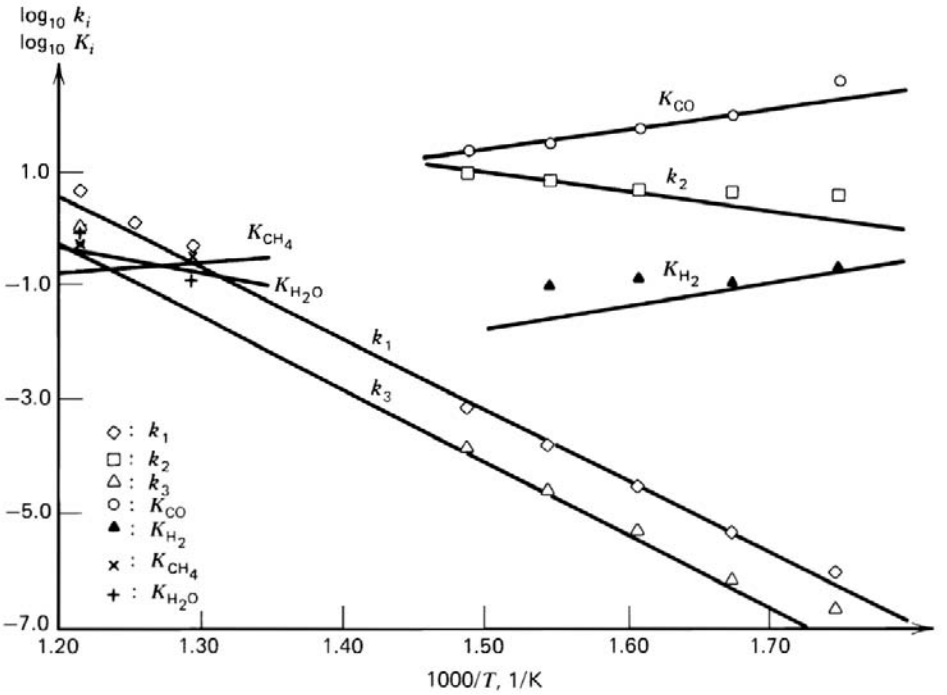

Figure 11.9.1.A-3

Arrhenius diagram for rate coefficients and Van't Hoff diagram for adsorption coefficients. From Xu and Froment [1989].

TABLE 11.9.1.A-2
PRE-EXPONENTIAL FACTORS, ACTIVATION ENERGIES, AND ENTHALPY CHANGES

$A(k_1)$	$A(k_2)$	$A(k_3)$	$A(K_{CO})$	$A(k_{H_2})$	$A(K_{CH_4})$	$A(K_{H_2O})$
4.225×10^{15}	1.955×10^{6}	1.020×10^{15}	8.23×10^{-5}	6.12×10^{-9}	6.65×10^{-4}	1.77×10^{5}

Activation Energy (kJ/mol)

E_1	E_2	E_3
240.1	67.13	243.9

Enthalpy Change (kJ/mol) of Reactions I to III

948 K			298 K		
ΔH_1^0	ΔH_2^0	ΔH_3^0	ΔH_1^0	ΔH_2^0	ΔH_3^0
224.0	−37.3	187.5	206.1	−41.15	164.9

To predict as closely as possible by means of the above one-dimensional model the cross-sectional averaged conversions and temperatures that would be calculated by a two-dimensional model, α_i is related to the heat transfer parameters of the two-dimensional model by means of the following formula (see Section 11.7.4: An Equivalent One-Dimensional Model):

$$\alpha_i = \frac{8\lambda_{er}\alpha_w}{8\lambda_{er} + \alpha_w d_{t,i}}$$

where

$$\alpha_w = \alpha_w^0 + 0.033\,\mathrm{Re}\,\mathrm{Pr}\frac{\lambda_g}{d_p}$$
$$\lambda_{er} = \lambda_{er}^0 + 0.14\lambda_g\,\mathrm{Re}\,\mathrm{Pr}$$

with α_w^0 calculated from [de Wasch and Froment, 1972]

$$\alpha_w^0 = \frac{10.21}{d_{t,i}^{4/3}}\lambda_{er}^0$$

and λ_{er}^0 calculated from the relationship introduced by Kunii and Smith [1960].

The friction factor f in (11.9.1.A-d) is that of Ergun [1952]; the equivalent diameter of the catalyst rings is calculated according to Brauer [1957]; and the porosity of the bed is calculated according to Reichelt and Blasz [1971].

Equations (11.9.1.A-a), (11.9.1.A-b), and (11.9.1.A-c) contain the effectiveness factors η_{CH_4} and η_{CO_2}. To obtain these, the partial pressure profiles inside the particle have to be calculated in each axial position *z*.

Since the partial pressure gradients are limited to a very thin layer near the surface, planar geometry was used. The continuity equations for CH_4 and CO_2 then become

$$D_{e,CH_4}\frac{d^2 p_{s,CH_4}}{d\xi^2} = 10^{-5} RT \cdot R_p^2 \cdot R_{CH_4}(\mathrm{P}_s)\rho_s \qquad \text{(11.9.1.A-e)}$$

$$D_{e,CO_2}\frac{d^2 p_{s,CO_2}}{d\xi^2} = 10^{-5} RT \cdot R_p^2 \cdot R_{CO_2}(\mathrm{P}_s)\rho_s \qquad \text{(11.9.1.A-f)}$$

with boundary conditions

$$\frac{dp_{s,CH_4}}{d\xi} = \frac{dp_{s,CO_2}}{d\xi} = 0 \qquad \text{at } \xi = 0$$

$$p_{s,CH_4} = p_{CH_4} \qquad p_{s,CO_2} = p_{CO_2} \qquad \text{at } \xi = 1$$

The concentrations of the non-key components H_2, CO, and H_2O are related to those of CH_4 and CO_2 through the rate equations; for H_2, for example,

rate of formation of H_2 = $3r_1 + r_2 + 4r_3$
= 3 (rate of disappearance of CH_4)
+ rate of formation of CO_2

In each point inside the porous catalyst, these rates can be eliminated through (11.9.1.A-e) and (11.9.1.A-f), so that

$$D_{e,H_2}\frac{d^2 p_{s,H_2}}{d\xi^2} = 3D_{e,CH_4}\frac{d^2 p_{s,CH_4}}{d\xi^2} - D_{e,CO_2}\frac{d^2 p_{s,CO_2}}{d\xi^2}$$

Integrating twice and accounting for the boundary conditions at $\xi = 1$ leads to an algebraic equation which is coupled with (11.9.1.A-e) and (11.9.1.A-f):

$$D_{e,H_2}(p_{s,H_2} - p_{H_2}) = 3D_{e,CH_4}(p_{CH_4} - p_{s,CH_4}) - D_{e,CO_2}(p_{CO_2} - p_{s,CO_2})$$

Spline orthogonal collocation was used to calculate the concentration profiles. The two splines in which the concentration gradients occur have a total thickness of 0.08 mm. The spline point was positioned at the dimensionless coordinate of 0.7, with 14 collocation points in the outer spline and 8 in the inner spline.

The effectiveness factors η_i were calculated from

$$\eta_i = \frac{\int_0^V r_i(\mathrm{P}_s)\rho_s \frac{dv}{V}}{r_i(\mathrm{P}_s^s)\rho_s}$$

The industrial catalyst is ring-shaped, with active layers at the external and internal surfaces of 2 mm. The slab upon which the calculation of the effectiveness factor was based was chosen to contain the same amount of active material, therefore the same volume, as the active part of the ring. This active volume-equivalent slab has an external surface per unit volume (a_v or $a_m\,\rho_s$) which is easily calculated to be 1.071 times that of the active part of the ring, for the dimensions given in Table 11.9.1.A-2. Therefore, the η calculated on the basis of the active volume-equivalent slab has to be divided by this factor to obtain the value for the industrial ring-shaped catalyst. The temperature of the external reactor wall is generated from a coupled simulation of the fire box and the reactor. A zone model, developed by Plehiers and Froment [1989], for the simulation of the temperature distribution in an ethylene furnace, was adapted to the reformer furnace simulation. The results of the simulation are shown in Figs. 11.9.1.A-4 through 11.9.1.A-8.

The evolution of the total conversion of methane and of the conversion of methane into CO_2 is shown in Fig. 11.9.1.A-4, together with the process gas temperature, total pressure, and wall temperature profiles. The temperature drop

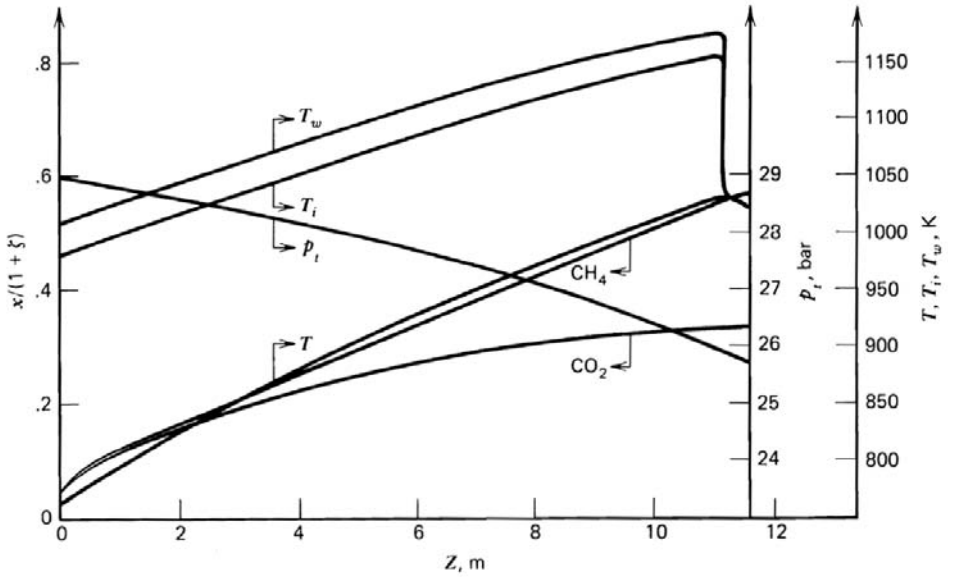

Figure 11.9.1.A-4

Evolution of the total conversion of methane and of its conversion into CO_2, of the total pressure, and process gas external and internal tube skin temperatures in a commercial steam reformer. From Xu and Froment [1989].

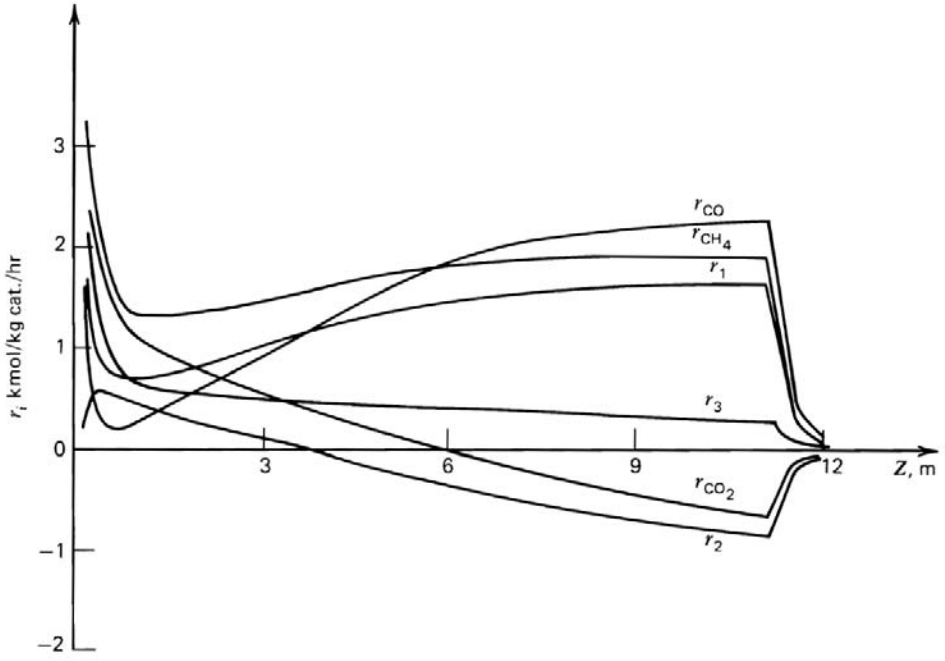

Figure 11.9.1.A-5

Evolution of intrinsic reaction rates in a commercial steam reformer. From Xu and Froment [1989].

over the film surrounding the catalyst particle is negligible, as already shown by De Deken et al. [1982]. Beyond 11.12 m, in the nonfired zone of the tube, the temperature is considered to drop adiabatically. The profiles of the intrinsic rates in the reactor are shown in Fig. 11.9.1.A-5. The intrinsic rate r_2 changes from positive to negative at a reactor length of about 5 m.

The approach to equilibrium of the reactions, defined by

$$V(i) = \frac{\left(\prod_j p_j^{\nu_j}\right)_i}{K_i}$$

is shown in Fig 11.9.1.A-6. Already beyond 3 m, reaction II comes very close to equilibrium. For reactions I and III, the approach to equilibrium exceeds 70 percent in the second half of the reactor. It only slowly increases to 80 percent because the rising process gas temperature shifts the equilibrium of these reactions further to the right. The conversion in a steam reformer is mainly limited by the heat flux supplied per unit weight of catalyst.

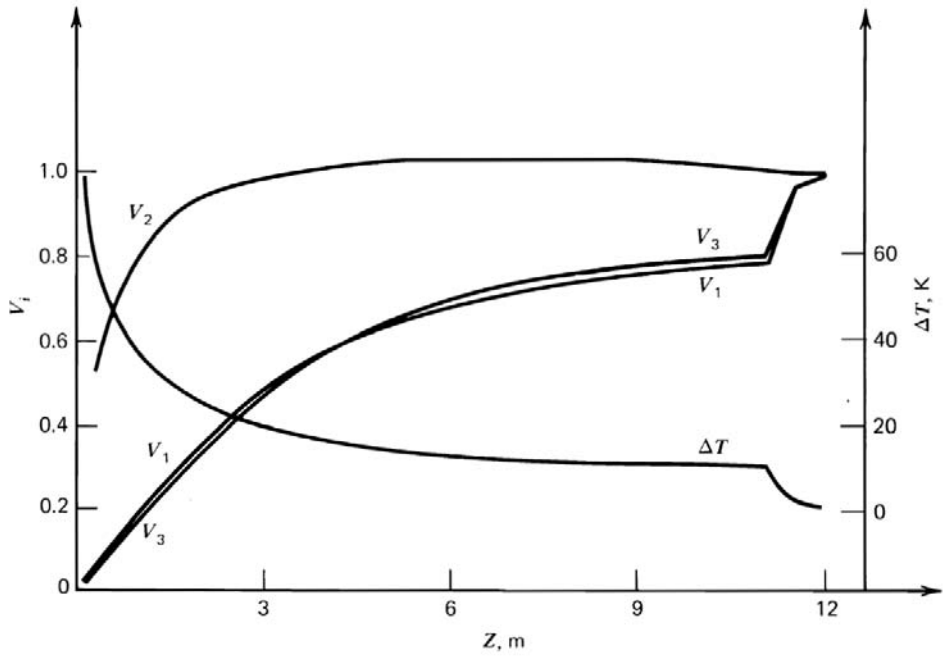

Figure 11.9.1.A-6

Approach to equilibrium in a commercial steam reformer, V_1: $CH_4 + H_2O \rightleftarrows CO + 3H_2$; V_2: $CO + H_2O \rightleftarrows CO_2 + H_2$; V_3: $CH_4 + 2H_2O \rightleftarrows CO_2 + 4H_2$. From Xu and Froment [1989].

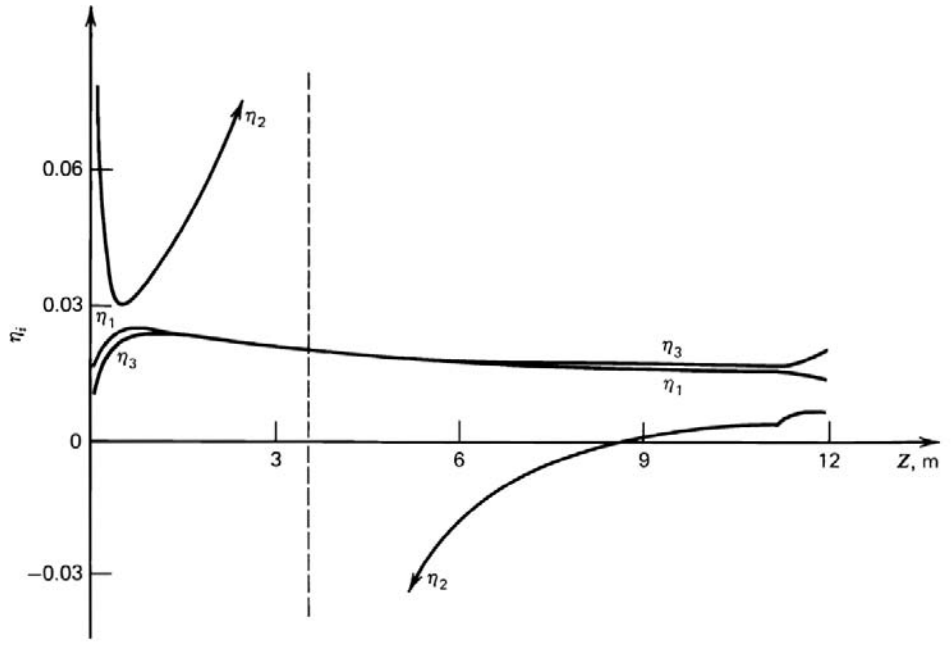

Figure 11.9.1.A-7

Evolution of effectiveness factors in a commercial steam reformer. From Xu and Froment [1989].

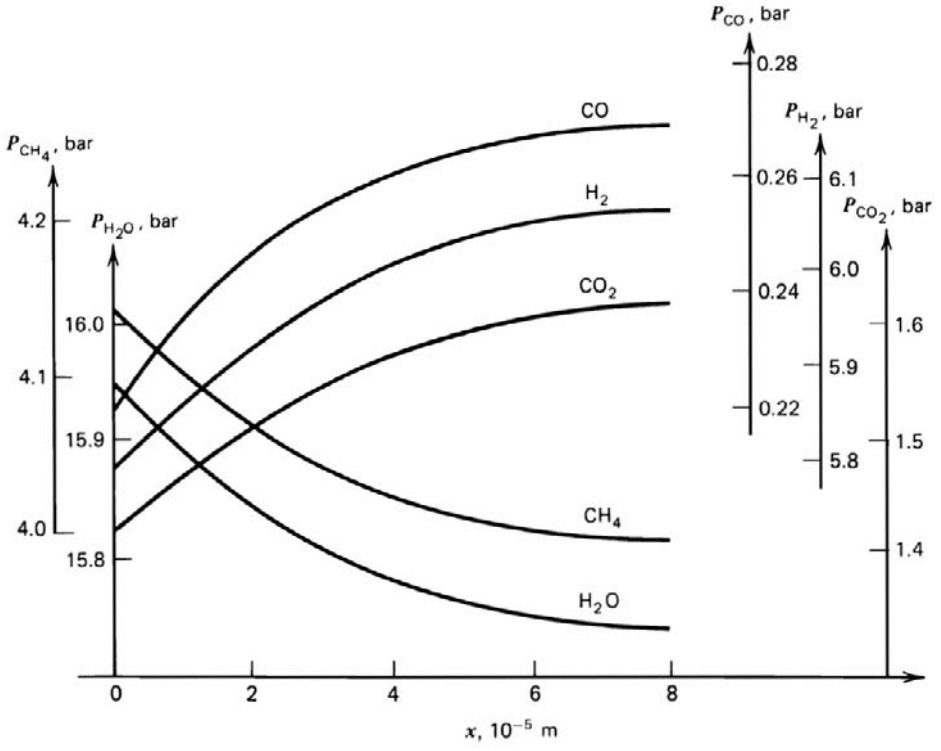

Figure 11.9.1.A-8

Partial pressure profile in the catalyst pellet at $Z = 7.00$ m from the inlet in a commercial steam reformer tube. From Xu and Froment [1989].

Figure 11.9.1.A-6 also shows ΔT, the local difference between the actual process gas temperature and the temperature that would be reached if the process gas were at equilibrium. This ΔT is often used to characterize the operation of an industrial reformer. Its value is about 10°C at the exit of the heated part of the tube.

The evolution of the various effectiveness factors is shown in Fig. 11.9.1.A-7. The effectiveness factor of reaction II shows a discontinuity at a reactor length of 3.4 m because the direction of reaction II changes from positive to negative on the catalyst surface, while there is no such tendency yet inside the catalyst particle. The η_2 value switches back from negative to positive values only at a reactor length of 9 m, meaning that the overall effect of the reaction inside the catalyst pellet reverses from the formation of CO_2 and H_2 out of CO and H_2O to the formation of CO and H_2O out of CO_2 and H_2.

The effectiveness factors of reactions I and III both decrease through the reactor, despite the decrease in the rate of reaction III. When the reaction is near equilibrium, the reaction rate is even more sensitive with respect to changes in

concentration, since the rate of the reverse reaction increases with a similar value as the reduction in rate of the forward reaction. The values of the effectiveness factors η_1 and η_3 obtained in the present study are close to those calculated by De Deken et al. [1982] for a different catalyst. These low effectiveness factors also explain why many authors obtained activation energies for steam reforming of approximately half the intrinsic values. The partial pressures of the components at the catalyst surface are very close to equilibrium values at reactor lengths exceeding 6 m. In spite of this, the reaction rates do not drop to very small values, because of the temperature rise which shifts the equilibrium to the right. The partial pressure profiles in the catalyst pellet at a reactor length of 4.00 m are shown in Fig. 11.9.1.A-8.

Further simulations of steam reforming units are reported by Grevskott et al. [2001]. ■

EXAMPLE 11.9.1.B

SIMULATION OF AN INDUSTRIAL REACTOR FOR 1-BUTENE DEHYDROGENATION INTO BUTADIENE

This is an example, taken from Dumez and Froment [1976], combining reactor simulation on the basis of a slightly simplified version of the model considered in this section but accounting for transients resulting from startup and from catalyst deactivation due to coke deposition.

The 1-butene dehydrogenation process considered here is carried out at temperatures of about 600°C in an adiabatic reactor and under reduced pressure

TABLE 11.9.1.B-1
CHARACTERISTICS OF AN INDUSTRIAL REACTOR FOR 1-BUTENE DEHYDROGENATION

Length	0.8 m
Cross section	1 m^2
Catalyst and inert particle diameter	0.0046 m
Amount of catalyst	800 kg
Catalyst bulk density	400 kg of cat./m^3 of diluted bed
Inert bulk density	900 kg of solid/m^3 of diluted bed
Catalyst geometrical surface area	274 m^2/m^3 of diluted bed
Inert surface area	411 m^2/m^3 of diluted bed
Total pressure	0.245 bar
Inlet butene pressure	0.245 bar
Molar flow rate	15 kmol/m^2 h
Feed temperature	600°C
Initial bed temperature	600°C

to minimize coke formation. The reaction is strongly endothermic, and the catalyst bed is diluted with inert particles providing a heat reservoir that reduces to a certain extent the temperature drop resulting from the endothermicity. Because of catalyst deactivation by coking, the time on stream is generally limited to about 15 min. Before regeneration the reactor has to be purged. The heat given off by the regeneration restores the original temperature level in the reactor. After purging the bed, the butene may be fed again and a new cycle starts. The characteristics of a typical reactor and its operating conditions are given in Table 11.9.1.B-1.

Since the amount of butene and butadiene lost in coking reactions cannot be neglected (and since there are three independent reactions), three continuity equations have to be written for the fluid-phase components. Also, since the flow velocity is high, the interfacial concentration and temperature gradients were neglected so that the fluxes at the catalyst surface are directly linked to the variations in the bulk gas-phase composition and enthalpy.

The continuity and energy equations are as follows:

For the fluid phase:

$$\frac{\partial(u_s C_B)}{\partial z} + \varepsilon \frac{\partial C_B}{\partial t} = -a_k D_{eB} \left(\frac{\partial C_{B,k}}{\partial \xi'} \right)_{d_p/2} \qquad (11.9.1.B\text{-a})$$

$$\frac{\partial(u_s C_H)}{\partial z} + \varepsilon \frac{\partial C_H}{\partial t} = -a_k D_{eH} \left(\frac{\partial C_{H,k}}{\partial \xi'} \right)_{d_p/2} \qquad (11.9.1.B\text{-b})$$

$$\frac{\partial(u_s C_D)}{\partial z} + \varepsilon \frac{\partial C_D}{\partial t} = -a_k D_{eD} \left(\frac{\partial C_{D,k}}{\partial \xi'} \right)_{d_p/2} \qquad (11.9.1.B\text{-c})$$

$$u_s \rho_g c_p \frac{\partial T}{\partial z} + \varepsilon \rho_g c_p \frac{\partial T}{\partial t} = \left[a_k h_k (T_i - T_k) + a_i h_i (T - T_i) \right] \qquad (11.9.1.B\text{-d})$$

in which the subscripts *k* and *i* refer to catalyst and inert material, respectively.

For the solid phase:

$$\rho_{B,k} c_{pk} \frac{\partial T_k}{\partial t} = a_k h_k (T - T_k) + a_{ik} h_{ik} (T_i - T_k) + a_k (-\Delta H) D_{eH} \left(\frac{\partial C_{H,k}}{\partial \xi'} \right)_{d_p/2} \qquad (11.9.1.B\text{-e})$$

$$\rho_{B,i} c_{pi} \frac{\partial T_i}{\partial t} = a_i h_i (T - T_i) - a_{ik} h_{ik} (T_i - T_k) \qquad (11.9.1.B\text{-f})$$

Inside the catalyst particles:

$$\frac{\partial^2 C_{B,k}}{\partial \xi'^2} + \frac{2}{\xi'} \frac{\partial C_{B,k}}{\partial \xi'} - \frac{\varepsilon_s}{D_{eB}} \frac{\partial C_{B,k}}{\partial t} = \frac{\rho_k}{D_{eB}} \left(r_H + \frac{r_{CB}}{\Psi_{CB} M_B} \right) \qquad (11.9.1.B\text{-g})$$

$$\frac{\partial^2 C_{H,k}}{\partial \xi'^2} + \frac{2}{\xi'} \frac{\partial C_{H,k}}{\partial \xi'} - \frac{\varepsilon_s}{D_{eH}} \frac{\partial C_{H,k}}{\partial t} = -\frac{\rho_k}{D_{eH}} r_H \qquad (11.9.1.B\text{-h})$$

$$\frac{\partial^2 C_{D,k}}{\partial \xi'^2} + \frac{2}{\xi'} \frac{\partial C_{D,k}}{\partial \xi'} - \frac{\varepsilon_s}{D_{eD}} \frac{\partial C_{D,k}}{\partial t} = -\frac{\rho_k}{D_{eD}} \left(r_H - \frac{r_{CD}}{\Psi_{CD} M_D} \right) \qquad (11.9.1.B\text{-i})$$

$$\frac{\partial C_c}{\partial t} = r_{CB} + r_{CD} \qquad (11.9.1.B\text{-j})$$

The pressure drop equation for turbulent flow is taken from Leva [1948; 1949].

The boundary conditions are

$z =$ 0 all t: $C_B = C_B^0$ $C_H = C_H^0$ $C_D = C_D^0$ $u_s = u_s^0$

$t =$ 0 all z: $T_k = T_k^0$ $T_i = T_i^0$

$\xi' =$ $d_p/2$ all z and t: $(C_{B,k})_R = C_B$

$(C_{H,k})_R = C_H$

$(C_{D,k})_R = C_D$

$\xi' =$ 0 all z and t: $\left(\frac{\partial C_{B,k}}{\partial \xi'} \right)_{\xi'=0} = \left(\frac{\partial C_{H,k}}{\partial \xi'} \right)_{\xi'=0} = \left(\frac{\partial C_{D,k}}{\partial \xi'} \right)_{\xi'=0} = 0$

$t =$ 0 all z and ξ: $C_C = 0$

The continuity and energy equations for the fluid phase in the reactor contain nonsteady-state terms. However, since the interstitial flow velocity is 4 m/s and since the bed length is only 0.8 m, the second terms on the left-hand side of (11.9.1.B-a)–(11.9.1.B-d) can be neglected. The products ($u_s C_B$), ($u_s C_H$), … are kept under the differential in these equations to account for the important change in number of moles in the gas phase owing to the dehydrogenation and to a certain extent to the coking. The right-hand side in (11.9.1.B-d) expresses the amount of heat exchanged between the gas and the solid particles, both catalytic and inert. The second term in the right-hand side of (11.9.1.B-e) and (11.9.1.B-f)

expresses the amount of heat exchanged between the catalyst and the inert particles by conduction and radiation. Of course, the nonsteady-state terms have to be kept in (11.9.1.B-e) and (11.9.1.B-f). In the particle equations, (11.9.1.B-g), (11.9.1.B-h) and (11.9.1.B-i), again the nonsteady-state terms can be neglected. No energy equation is written for the catalyst particle, which may be considered as isothermal for the reasons explained in Chapter 3.

The rate equations were determined by Dumez and Froment by means of sequentially designed experimental programs for model discrimination and parameter estimation, discussed and illustrated in Chapter 2. The following equations were obtained:

- For the rate of formation of hydrogen in the absence of coking, r_H^0,

$$r_H^0 = \frac{1.826 \times 10^7 \exp(-14{,}714/T)\left(p_B - \dfrac{p_H p_D}{K}\right)}{(1 + 18727\, p_B + 3.593\, p_H + 38028\, p_D)^2} \qquad \text{(11.9.1.B-k)}$$

- For the rate of disappearance of butene into butadiene and coke on fresh catalyst, r_B^0,

$$r_B^0 = r_H^0 + \frac{r_{CB}^0}{\Psi_{CB} M_B} \qquad \text{(11.9.1.B-l)}$$

  where r_{CB}^0 is the rate of coke formation from butene on fresh catalyst. Since r_B^0 is in kmol butene/kg cat. h and r_{CB}^0 in kg coke/kg cat. h, the conversion factor Ψ_{CB}, expressed in kg coke/kg butene, is required; M_B is the molecular weight of butene.

- For the net rate of production of butadiene, which also reacts further into coke,

$$r_D^0 = r_H^0 - \frac{r_{CD}^0}{\Psi_{CD} M_D} \qquad \text{(11.9.1.B-m)}$$

  where Ψ_{CD} is the corresponding conversion factor and M_D is the molecular weight of butadiene.

The influence of coke on the rate of these reactions is accounted for by exponential deactivation functions based on the coke content, as advocated in Chapter 5:

$$r_H = r_H^0 \exp(-42.12 C_c)$$

$$r_{CB} = r_{CB}^{0} \exp(-45.53 C_c) \qquad \text{(11.9.1.B-n)}$$

$$r_{CD} = r_{CD}^{0} \exp(-45.53 C_c)$$

The form of the deactivation function and the numerical value of the deactivation parameter were determined by means of an electrobalance. The deactivation constant is essentially identical for the three reactions in this case. The total rate of coke formation, $r_C = r_{CB} + r_{CD}$, has been given in Chapter 5 as (5.3.3.A-i) of Example 5.3.3.A.

The effective diffusivities for transport inside the catalyst were determined from experiments with particle radii varying from 0.35 mm to 2.3 mm. For butene, for example, the effective diffusivity contains the tortuosity, the internal void fraction, and the molecular and Knudsen diffusivity:

$$\frac{1}{D_{eB}} = \frac{\tau}{\varepsilon_s}\left(\frac{1}{D_{B,m}} + \frac{1}{D_{K,B}}\right) \qquad \text{(11.9.1.B-o)}$$

The molecular diffusivities were calculated from a weighted average of the binary diffusion resistances which, in turn, were estimated from the formula of Fuller et al. The calculation of the Knudsen diffusivities requires information about the pore size. The catalyst had a bimodal pore distribution. Furthermore, via electron microscopy it was found that the catalyst consisted of crystallites of about 5 μ, separated by voids of about 1 μ. Consequently, the maximum length of the micropores with average diameter 70 Å cannot exceed 5 μ. It is easily calculated that this is too short to develop any significant concentration gradients. Therefore, only the macropores with a pore volume of 0.155 cm^3/g and with average pore diameter of 10000 Å were considered in the evaluation of the Knudsen diffusivity.

The only unknown parameter left in (11.9.1.B-o) is the tortuosity factor τ. This factor was determined from a comparison between the experimental rate at zero coke content, measured in a differential reactor and the surface fluxes. The latter were calculated using Fick's law and for a given τ from the concentration profiles obtained by numerical integration of the system (11.9.1.B-g)–(11.9.1.B-j). A value of $\tau = 5$ led to the best fit of all six experiments. This is the generally accepted value for the tortuosity factor in a catalyst of the type used in this work. It was also possible to calculate an effectiveness factor from these results. A value of 0.20 was obtained for a particle radius of 2.3 mm at 550°C. The Bischoff general modulus approach, presented in Chapter 3, leads to a value of 0.28. Finally, the heat transfer coefficients were calculated from the j_H correlation of Handley and Heggs, mentioned in Chapter 3.

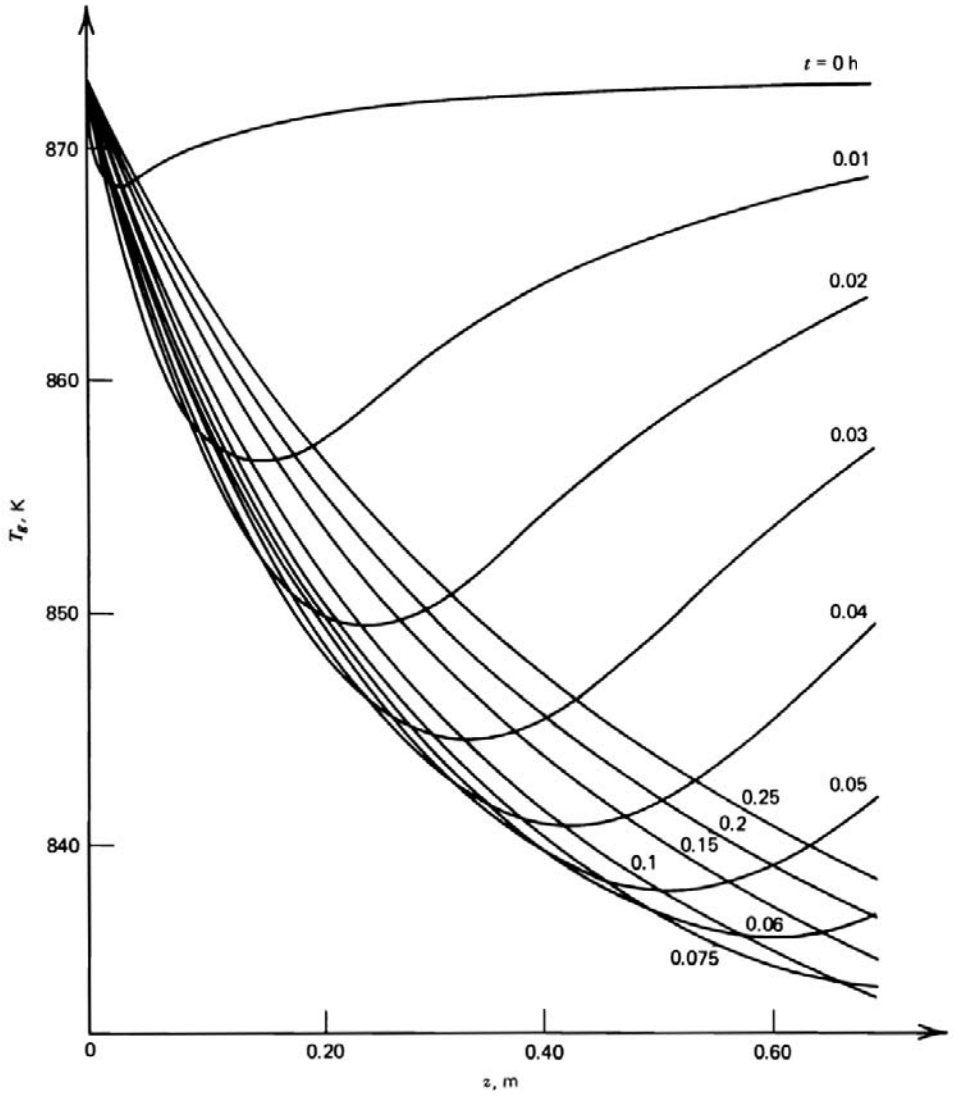

Figure 11.9.1.B-1

Gas temperature profiles in 1-butene dehydrogenation reactor. From Dumez and Froment [1976].

With all this information the design calculations can now be performed. The particle equations were solved by means of collocation, the continuity equations for the fluid phase by means of a Runge-Kutta-Merson routine, and the energy equations in a semianalytical manner. The results for one particular operation are shown in Figs. 11.9.1.B-1, 11.9.1.B-2 and 11.9.1.B-3. In Fig. 11.9.1.B-1 the temperature is seen to drop rapidly below the initial value, due to the endothermic nature of the reaction. A temperature wave rapidly travels through the reactor as the reaction gradually extends to increasing depths. In the

presence of coking, no true steady state is reached, however. The temperature profile is slowly translated upward, because of the decrease in reaction rate caused by the catalyst deactivation. The corresponding coke profiles are shown in Fig. 11.9.1.B-2.

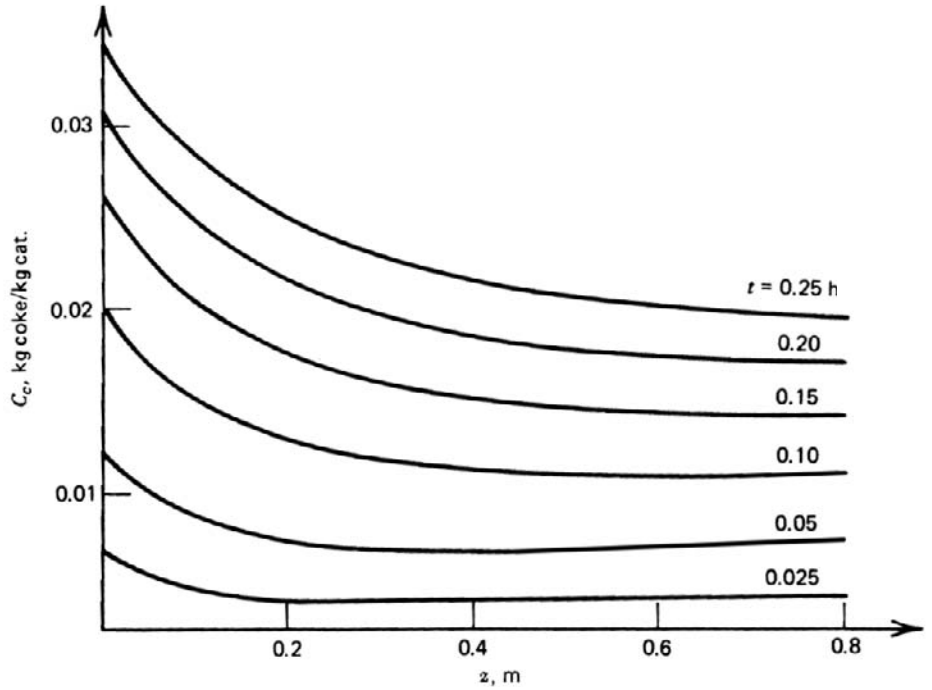

Figure 11.9.1.B-2

Coke content profiles in 1-butene dehydrogenation reactor. From Dumez and Froment [1976].

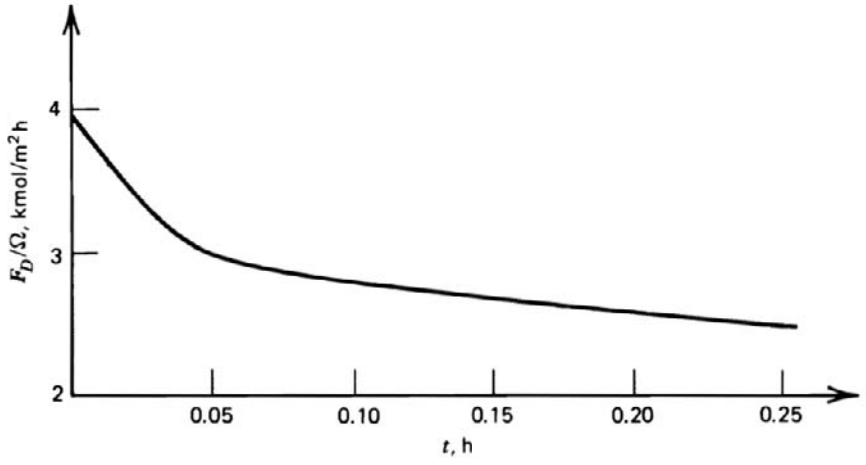

Figure 11.9.1.B-3

Butadiene flow rate at the reactor outlet. From Dumez and Froment [1976].

The profile is decreasing, mainly because of the higher temperature at the inlet and of the inhibition of the coke formation due to the hydrogen concentration near the outlet. Figure 11.9.1.B-3 illustrates the butadiene flow rate at the outlet as a function of time. The rapid initial decrease corresponds to the initial temperature drop. Beyond this initial period the decrease in production is much slower. The catalyst is deactivated by the coking; but as the dehydrogenation rate is lowered, the bed temperature slowly rises, thus favoring the butadiene production. Further aspects of the problem and an optimization of the on-stream time can be found in Dumez and Froment [1976]. ■

EXAMPLE 11.9.1.C

INFLUENCE OF INTERNAL DIFFUSION LIMITATIONS IN CATALYTIC REFORMING

Catalytic reforming is one of the main operations of petroleum refining. It aims at boosting the research octane number of a straight run naphtha from 50-60 to 90-100 and processes it with a large molar ratio hydrogen/hydrocarbons in a 3- or 4-bed adiabatic reactor on bifunctional Pt/Re-alumina or Pt/Sn-alumina catalysts. The process is globally endothermic and the flow leaving a bed is reheated before entering into the next. The naphthenes are dehydrogenated into aromatics while the *n*-paraffins isomerize into *i*-paraffins and also undergo dehydrocyclization into aromatics. Sotelo-Boyas and Froment [2009] simulated a three bed adiabatic reforming reactor with radial flow, linking the possibility of internal diffusion limitations to the various reactions. Interphase gradients were negligible, given the high flow velocities. The naphtha feed contained some 200 components in the range C_5-C_{12}. The reactions catalyzed by the acid alumina were written in terms of elementary steps of carbenium ion chemistry, as explained in Chapter 2. The dehydrogenations of the naphthenes and paraffins, catalyzed by the metal function, were expressed on the molecular level. The reaction network was generated by computer, using the Boolean matrix approach illustrated in Chapter 2. The number of independent rate parameters of the acid catalyzed steps was reduced through the single event concept to 21, that for the reactions on the metal function to 24 (16 rate parameters and 8 adsorption equilibrium constants) by accounting for the nature of the C-atoms surrounding the double bond. These parameters were derived from a detailed data base obtained by 24 experiments carried out in the pressure range 5 to 9 bar and temperature range 400-500°C in an isothermal fixed bed reactor with plug flow and filled with catalyst crushed to $0.5\text{-}0.7 \times 10^{-3}$ m, to avoid internal diffusion limitations. At 500°C the number of component responses per experiment was 56.

The reactor model is very similar to that presented in Example 11.9.1.B but the pressure drop is calculated from the Ergun equation and there is no solid diluent. Two versions were considered: a homogeneous and a heterogeneous, accounting for diffusion limitations in the catalyst particles with diameter 3.2×10^{-3} m. The diffusion fluxes were expressed by the Stefan-Maxwell equations for multicomponent mixtures or by the Wilke approximation. The flux equations were integrated by means of orthogonal collocation, mentioned in Chapter 3. The set of fluid field equations was stiff and was integrated using Gear's routine. The number of continuity equations per phase (fluid or solid) amounted to 69, representing the variation along the beds of 69 pure components and Groups of Isomers (GOI) with equilibrium among their members. Fig. 11.9.1.C-1 shows the effect of the diffusion limitations for just one of the reactions, the dehydrogenation of the feed component *n*-octane, in terms of its effectiveness factor profile through the beds. This factor is much smaller than one and increases towards the exit of each bed because the lower temperatures there affect more the reaction rates than the diffusion rates. The increase is strongest in the first bed in which the fast endothermic dehydrogenations are prevailing. Fig. 11.9.1.C-2 illustrates the difference between the simulations with and without diffusion limitations for the total yield of the aromatics, naphthenes, C_5+ *n*-paraffins and C_5+ *i*-paraffins. These quantities are calculated from the yields of the individual components. The yield of naphthenes (kg naphthenes in the flow per 100 kg naphtha fed) is lower in the homogeneous case than in the heterogeneous case because they are converted faster in the absence of diffusion limitations. The opposite is true for the formation of aromatics which has an

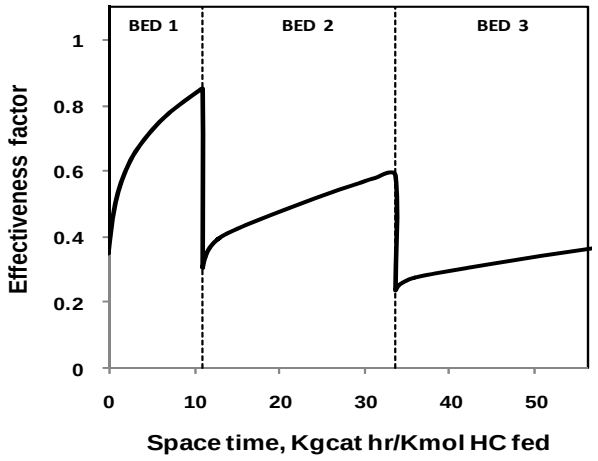

Figure 11.9.1.C-1

Profiles of the effectiveness factor for the conversion of *n*-octane in a 3-bed adiabatic catalytic reformer with radial flow. Sotelo-Boyas and Froment [2009].

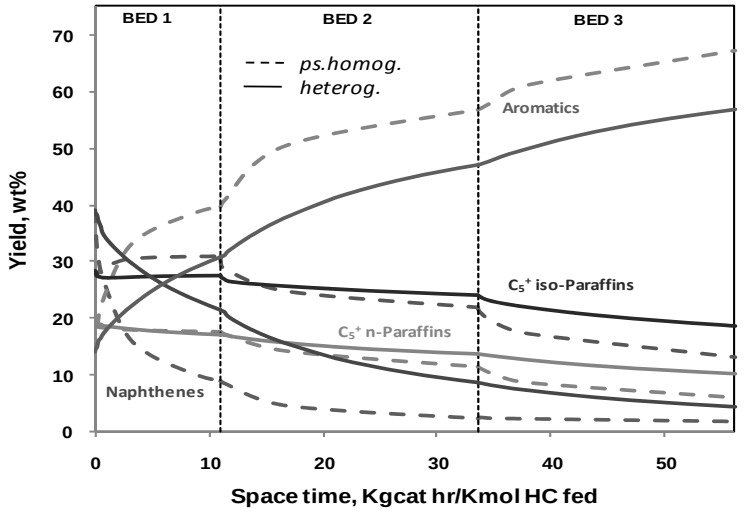

Figure 11.9.1.C-2

Yield profiles in catalytic reformer with radial flow for various fractions. Dashed curve: pseudo-homogeneous model; Full curve: heterogeneous model. Sotelo-Boyas and Froment [2009].

effectiveness factor exceeding one. These two figures suffice to illustrate the necessity of accounting for these limitations to achieve accurate simulations and predictions for real processes. An approach based on "effective" rates, implicitly combining reaction and diffusion, is not recommended. With the levels of modeling and the computational means presently available there is no reason any more to resort to this approach.

■

11.10 TWO-DIMENSIONAL HETEROGENEOUS MODELS

In Section 11.7.5 a pseudo-homogeneous model was presented and applied that accounts for radial variations in the structure of a packed bed. The model can easily be extended to account for inter- and intraparticle gradients of concentration and, if required, also for temperature gradients. Such a two-dimensional heterogeneous model needs to distinguish between the fluid phase and the solid phase as a whole — not just a particle — to correctly account for the heat transfer in radial direction. That requires a distinction between the effective radial conductivity λ^f_{er} for the fluid phase and that for the gas phase, λ^s_{er} [de Wasch and Froment, 1971]. This concept of λ^f_{er} and λ^s_{er} was introduced as far back as 1950 by Singer and Wilhelm [1950] but strangely enough all subsequent work made use of the global λ_{er} concept discussed in Section 11.7. The preceding

considerations led de Wasch and Froment [1971] and Papageorgiou and Froment [1995] to the following mathematical model:

For the fluid phase:

$$u_z \frac{\partial C_{fi}}{\partial z} + u_r \frac{\partial C_{fi}}{\partial r} = \frac{1}{r}\frac{\partial}{\partial r}\left(r D_{ers} \frac{\partial C_{fi}}{\partial r} \right) + k_g a_v (C_{si}^s - C_{fi})$$

$$\rho_f c_p \left[u_z \frac{\partial T_f}{\partial z} + u_r \frac{\partial T_f}{\partial r} \right] = \frac{1}{r}\frac{\partial}{\partial r}\left(r \lambda_{er}^f \frac{\partial T_f}{\partial r} \right) + h_f a_v (T_s^s - T_f)$$

For the solid phase:

$$k_g a_v (C_{si}^s - C_{fi}) = \rho_s (1-\varepsilon) \eta_i R_i$$

$$h_f a_v (T_s^s - T_f) = \frac{1}{r}\frac{\partial}{\partial r}\left(r \lambda_{er}^s \frac{\partial T_s}{\partial r} \right) + \rho_s (1-\varepsilon) \sum (-\Delta H_i \eta_i R_i)$$

with the boundary conditions:

at $z = 0$: $\quad C_{fi} = C_{0i}$, $T_f = T_0$

at $r = 0$: $\quad \frac{\partial C_{fi}}{\partial r} = \frac{\partial C_{si}}{\partial r} = 0$, $\frac{\partial T_f}{\partial r} = \frac{\partial T_s}{\partial r} = 0$

at $r = R_t$: $\quad \frac{\partial C_{fi}}{\partial r} = \frac{\partial C_{si}}{\partial r} = 0$, $T_f = T_s = T_w$.

These equations have to be solved simultaneously with the Reynolds averaged Navier-Stokes equations and the Ergun-equation given in Section 11.7.5 to account for the radial void profile and generate both axial and radial flow velocity components, u_r and u_z. In these equations it is assumed that the heat transfer through the fluid and solid phase occur in parallel [de Wasch and Froment, 1971; Dixon and Cresswell, 1979; Dixon, 1985]. λ^f_{er} and λ^s_{er} can be calculated from the correlations of de Wasch and Froment [1972] and Zehner and Schlünder [1972]. The internal diffusion limitations appear in those equations by means of the effectiveness factor η, which is obtained by numerical integration of the diffusion and reaction equations inside the particles, as discussed in Chapter 3.

Papageorgiou and Froment applied this model to the phthalic anhydride synthesis, discussed under Section 11.7.5. The Figs. 11.10-1(a) and (b) show the radial conversion and temperature profiles at a given axial distance in the

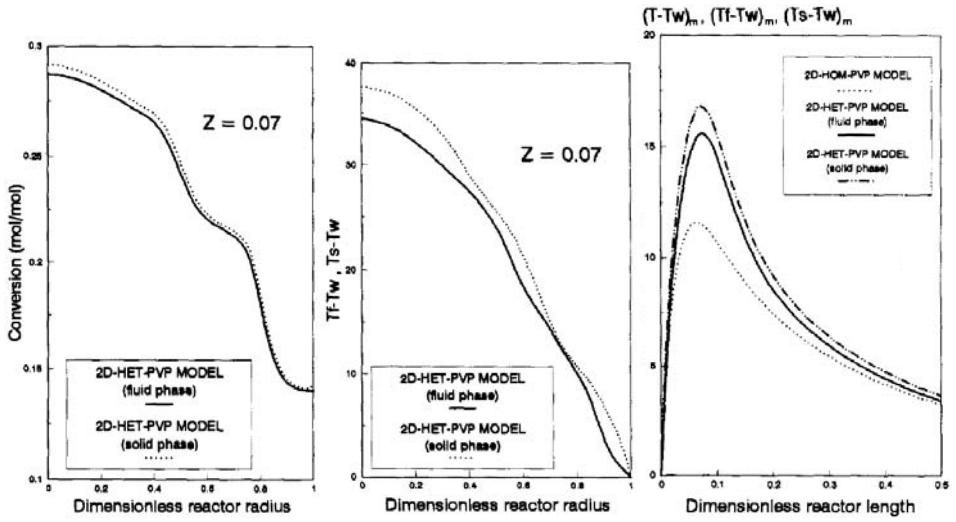

Figures 11.10-1

Radial conversion (a) and temperature (b) profiles in two-dimensional heterogeneous model with porosity and velocity profiles. (c) Comparison of radially averaged axial temperature profiles for 2D pseudo-homogeneous and heterogeneous models. $d_t/d_p = 5.8$; $Re_p = 175$ [Papageorgiou and Froment, 1995].

reactor. The difference between the gas and solid temperature is only 2-3°C, even for this very exothermic process. This is generally so in industrial reactors because of the high flow velocity. Fig. 11.10-1(c) compares the radially averaged axial temperature profile of the 2D heterogeneous model with that of the 2D pseudo-homogeneous model of Section 11.7.5. The difference between the two simulations is significant.

The results shown here reflect accurately controlled operating conditions. An increase in the feed temperature or in the temperature of the salt bath cooling system may lead to much more pronounced profiles and differences between the two models discussed here. The model predictions are very sensitive to the heat transfer parameters and the validity of some among these may be limited to relatively narrow operating conditions. The detailed CFD models could contribute in the future to checking and improving existing heat and mass transfer correlations derived in the sixties and seventies on the basis of simple plug flow models. Given the irregular boundaries between fluid and solid and the location of the heat source or sink inside the solid the task is extremely complicated.

PROBLEMS

11.1 **(a)** The kinetics of the catalytic reaction $A \rightleftarrows R + S$ are given by

$$r = \frac{dx}{d\dfrac{W}{F_{A0}}} = \frac{kK_A[\rho_A - \rho_R(p_s / K)]}{(1 + K_A p_A + K_R + K_s p_s)^2}$$

The reaction is carried out isothermally in a packed bed reactor with plug flow at 275°C. The feed contains 0.155 mole water per mole reactant. Water is not adsorbed on the catalyst and acts purely as an inert diluent. Given the following data,

F_{t0} =	4.2 kmol/h (total flow rate)		
ρ_b =	1500 kg/m³		
d_t =	0.05 m	k =	4.3593 [kmol/kg cat. h]
p_t =	3 bar	K_A =	0.43039 [bar $^{-1}$]
K =	0.589 [bar]	$K_R + K_s$ =	2.8951 [bar^{-1}]

calculate the length of the reactor required to reach an exit conversion of (i) 40 percent, (ii) 70 percent.

(b) Suppose the reaction is carried out under the same conditions in a multitubular reactor. The tube length is 3 m. The total feed per tube is 4 kmol/h. An annual production of 20,000 metric tons of product is required. The molecular weight of the product is 44. One year on stream is equivalent to 8000 h. Determine the number of tubes required to meet the production.

11.2 Discuss whether the following is correct or wrong:

(a) The relationship conversion versus reactor length is linear for a zero-order reaction without heat effect carried out in an adiabatic reactor.

(b) In an adiabatic reactor the relationship of temperature versus conversion is a straight line for first-order reactions only.

(c) Optimization of a multibed adiabatic reactor turns out to be roughly equivalent with distributing the catalyst in equal amounts over the different beds.

11.3 **(a)** Consider an isothermal fixed bed reactor with axial mixing superposed on plug flow conditions in which an irreversible first-order reaction takes place. Show that, for a given set of operating variables, the effect of axial diffusion decreases with increasing reactor length.

(b) Given the values

u_s	= 0.01 m/s	d_p	= 0.004 m
ε	= 0.4	ρ_b	= 1200 kg/m³
Pe_a	= 2	k	= 1×10^{-5} m³/kg cat. s

Compute the C_A profiles in tubular reactors with axial mixing as a function of total length and compare with the plug flow profile.

(c) Verify for this case if a bed depth of $50d_p$ is sufficient for eliminating axial mixing effects.

(d) On what basis has the $50d_p$ rule been established?

(e) Explain why the concentration profiles under axial mixing conditions never converge to the plug profile, not even in the limiting case $L \to \infty$.

11.4 Calculate the heat transfer parameters of the two-dimensional pseudohomogeneous models for the design of the reactor for hydrocarbon oxidation of Section 11.7.3, using the correlations given in Section 11.7.1. Compare the value λ_{er}^0 calculated from the expressions given by (a) Kunii and Smith, (b) Zehner and Schundler. Determine their sensitivity with respect to the solid conductivity. Additional data:

λ_s =	1.163×10^{-3} kJ/m s K
λ_g =	4.99×10^{-5} kJ/m s K
p =	0.8
β =	0.95
d_p =	0.003 m
d_t =	0.0254 m
T_m =	382°C
ε =	0.38

11.5 Check whether multiple steady states can occur in the case of the hydrocarbon oxidation of Section 11.7.3, but considering only the reaction $A \to B$. Required data:

$-\Delta H$	=	1,285,350 kJ/kmol
λ_s	=	1.163×10^{-3} kJ/m s K
T_f	=	655 K
E	=	1113,044 kJ/kmol
R	=	8.3144 kmol K
C_f	=	0.4145×10^{-3} kmol/m^3
D_e	=	5×10^{-4} m^2/h

11.6[2] A tubular, fixed bed catalytic reactor is to be used for a highly exothermic reaction, and the preliminary design must consider the possibility of a hot spot. The following parameters have been selected in the initial design estimates:

$\beta = \frac{\Delta T_{ad}}{T_{ref}} = \frac{600}{400} = 1.5$	dimensionless adiabatic temperature rise
$\gamma = \frac{E}{RT_{\mathrm{Re}\,f}} = \frac{3200}{2 \times 400} = 40$	dimensionless activation energy
$\frac{k_B C_{A0} V}{F_{A0}} = 3$	reaction rate group or the number of reactor units
$\frac{UA}{F' \rho C_p} = 22.5$	number of heat transfer units

(a) Will there be an excessive hot spot for the set of parameters given in the preliminary design?

(b) An obvious (if expensive) way to overcome a hot spot problem is to add diluents to the reactor feed. What must the dilution be to achieve a design 10 percent safer than the hot spot minimum dilution?

(c) Indicate how the two parameters of the hot spot analysis are altered by the following design choices:

- Decrease inlet (reference) temperature by 10 K.
- Decrease the tube diameter by 20 percent.
- Increase the reactor length by 20 percent.
- Change the catalyst to lower the activation energy by 40 percent.

(d) The reactor designed in part (b) is expected to undergo two changes during extended operation: the catalyst activity will decrease by 30 percent and the heat transfer coefficient will decrease by 20 percent. The loss in catalyst activity will be compensated by raising the reactor temperature enough to keep k_B constant. Investigate the probability of developing a hot spot in the reactor under the revised conditions.

11.7 Fixed Bed Reactor for Styrene Production

(a) *Introduction*

Styrene is produced by catalytic dehydrogenation of ethylbenzene on an iron catalyst. The reaction is endothermic and reversible and takes place

[2] This problem was contributed by Prof. J. H. Olson, University of Delaware.

with an increase in the number of mole. Consequently, styrene conversion is favored by high temperatures, low pressures, and dilution of the feed by means of an inert component, such as benzene or, more generally, steam. The steam also serves as a heat carrier, reducing the temperature drop in adiabatic operation.

(b) *Reactor*

Operating conditions

Molar feed rates:

Ethylbenzene:	707	kmol/h
Styrene:	7.104	kmol/h
Benzene:	0.293	kmol/h
Toluene:	4.968	kmol/h
Steam:	7777	kmol/h

Inlet temperature of the mixture: $T_0 = 620°C$

Inlet pressure: 2.37 bar

Reactor dimensions

Inner diameter: 7 m

$(W / F_{EB}^{0})_{\text{total}}$ = 62 kg cat. h/kmol

Additional data

Catalyst equivalent diameter: $d_p = 0.0055$ m

Catalyst internal void fraction: $\varepsilon_s = 0.4$

Tortuosity of the catalyst: $\tau = 3$

Catalyst density: $\rho_s = 2500$ kg/m^3 cat.

Void fraction of the bed: $\varepsilon_B = 0.4312$

Bulk density of the catalyst bed: $\rho_B = 1422$ kg/m³

(c) *Kinetics*

The main reaction is:

$$C_6H_5 - CH_2 - CH_3 \rightleftarrows C_6H_5 - CH = CH_2 + H_2 \qquad (1)$$

3 parallel reactions occur:

$$C_6H_5 - CH_2 - CH_3 \rightarrow C_6H_6 + C_2H_4 \qquad (2)$$

$$C_6H_5 - CH_2 - CH_3 + H_2 \rightarrow C_6H_5 - CH_3 + CH_4 \qquad (3)$$

$$C_6H_5 - CH = CH_2 + 2H_2 \rightarrow C_6H_5 - CH_3 + CH_4 \qquad (4)$$

Reactions (1), (2), and (3) were assumed to be both catalytic and thermal. Reaction (4) was assumed to be catalytic. Only the main reaction (1) was assumed to be reversible.

The following rate expressions were proposed for the above catalytic (r_{cj}) and thermal (r_{tj}) reactions [Lee, W.J., Froment, G.F., *Ind. Eng. Chem. Res.*, 47, 9183 (2008)]:

$$r_{c1} = \frac{k_1 K_{EB}\left[p_{EB} - \dfrac{p_{ST}\, p_{H2}}{K_{eq}} \right]}{\left(1 + K_{EB}\, p_{EB} + K_{H2}\, p_{H2} + K_{ST}\, p_{ST}\right)^2}$$

$$r_{c2} = \frac{k_2 K_{EB}\, p_{EB}}{\left(1 + K_{EB}\, p_{EB} + K_{H2}\, p_{H2} + K_{ST}\, p_{ST}\right)^2}$$

$$r_{c3} = \frac{k_3 K_{EB}\, p_{EB} K_{H2}\, p_{H2}}{\left(1 + K_{EB}\, p_{EB} + K_{H2}\, p_{H2} + K_{ST}\, p_{ST}\right)^2}$$

$$r_{c4} = \frac{k_4 K_{ST}\, p_{ST} K_{H2}\, p_{H2}}{\left(1 + K_{EB}\, p_{EB} + K_{H2}\, p_{H2} + K_{ST}\, p_{ST}\right)^2}$$

$$r_{t1} = k_{t1}\left(p_{EB} - \frac{p_{ST}\, p_{H2}}{K_{eq}} \right)$$

$$r_{t2} = k_{t2}\, p_{EB}$$

$$r_{t3} = k_{t3}\, p_{EB}$$

where

$$k_i = A_i \exp\left(-\frac{E_i}{RT} \right)$$

$$k_{ti} = A_{ti} \exp\left(-\frac{E_{ti}}{RT} \right)$$

$$K_j = A_j \exp\left(-\frac{\Delta H_j}{RT} \right)$$

for i = 1, 2, 3, 4 and j = *EB*, *ST*, *H*2.

The rate parameters are given in Table 1, the thermodynamic parameters in Table 2.

TABLE 1

RATE PARAMETERS

i	$A_i[\frac{kmol}{kgcat \cdot hr}]$	$E_i[\frac{kJ}{mol}]$	$A_{ti}[\frac{kmol}{m_f^3 \cdot hr \cdot bar}]$	$E_{ti}[\frac{kJ}{mol}]$
1	$4.594 \cdot 10^9$	174.38	$2.2215 \cdot 10^{16}$	272.30
2	$1.060 \cdot 10^{15}$	296.29	$2.4217 \cdot 10^{20}$	352.79
3	$1.246 \cdot 10^{26}$	474.76	$3.8224 \cdot 10^{17}$	313.06
4	$8.024 \cdot 10^{10}$	213.78	/	/

TABLE 2

THERMODYNAMIC PARAMETERS

j	$A_j[\frac{1}{bar}]$	$\Delta H_j[\frac{kJ}{mol}]$
EB	$1.014 \cdot 10^{-5}$	-102.22
ST	$2.678 \cdot 10^{-5}$	-104.56
$H2$	$4.519 \cdot 10^{-7}$	-117.95

The following relation is used for the calculation of K_{eq}:

$$K = \exp\left(-\frac{\Delta G^{\circ}}{RT}\right)$$

and

$$K_{eq} = K \cdot (\mathrm{P}^{\circ})^{\delta}$$

where P° is the standard state pressure (1 bar) and $\delta = \sum_i \alpha_i$, with α_i the stoichiometric coefficients.

(d) *Physicochemical data*

$$\Delta G^{\circ} = \Delta H^{\circ} - T\Delta S^{\circ}$$

with

$$\Delta H^{\circ} = \Delta H^{\circ}_{298.15} + \int_{298.15}^{T} \Delta C_p^{\circ} \mathrm{d}T$$

$$\Delta S^{\circ} = \Delta S^{\circ}_{298.15} + \int_{298.15}^{T} \Delta C_p^{\circ} \frac{\mathrm{d}T}{T}$$

The heat capacities are calculated in the form of cubic functions of *T*.

$$C_{pj} = a_j + b_j T + c_j T^2 + d_j T^3$$

The coefficients are given in Table 3 [Reid, R.C., Prausnitz, J.M., and Sherwood, T.K., *The Properties of Gases and Liquids*, 3rd ed., McGraw Hill, New York (1977)].

TABLE 3
COEFFICIENTS IN THE CUBIC HEAT CAPACITY EQUATION AND STANDARD HEATS AND GIBBS FREE ENERGIES OF FORMATION

j	EB	ST	$H2$
$a_j[\frac{kJ}{kmol \cdot K}]$	-43.1	-28.25	27.14
$b_j[\frac{kJ}{kmol \cdot K^2}]$	$707.2 \cdot 10^{-3}$	$615.9 \cdot 10^{-3}$	$9.274 \cdot 10^{-3}$
$c_j[\frac{kJ}{kmol \cdot K^3}]$	$-48.11 \cdot 10^{-5}$	$-40.23 \cdot 10^{-5}$	$-1.381 \cdot 10^{-5}$
$d_j[\frac{kJ}{kmol \cdot K^4}]$	$130.1 \cdot 10^{-9}$	$99.35 \cdot 10^{-9}$	$7.645 \cdot 10^{-9}$
$\Delta H^\circ_{f,j}[\frac{kJ}{kmol}]$	$0.2981 \cdot 10^5$	$1.475 \cdot 10^5$	-
$\Delta G^\circ_{f,j}[\frac{kJ}{kmol}]$	$1.307 \cdot 10^5$	$2.139 \cdot 10^5$	-

The mixture viscosity can be calculated using Wilke's approximation. The viscosities of ethylbenzene, styrene, benzene, and toluene can be calculated using the corresponding-states method of Thodos [Perry, R.H., Green, D.W., *Perry's Chemical Engineers' Handbook*, 7th ed., McGraw-Hill (1997)]. The viscosities of hydrogen and steam can be calculated using the Chapman-Enskog equation.

The inert steam being largely present, Wilke's equation can be used for the calculation of the diffusion coefficients of the different species in the gas mixture. The binary diffusion coefficients can be calculated from the atomic diffusion volumes, according to:

$$D_{AB} = \frac{0.00143 T^{1.75}}{P M_{AB}^{1/2} [(\sum v)_A^{1/3} + (\sum v)_B^{1/3}]}$$

(e) *Reactor model*

The reactor is assumed to be adiabatic with plug flow. Axial dispersion can be ignored. Mass transfer limitations inside the catalyst pellet are to be accounted for by calculating the effectiveness factors. Heat transfer limitations inside the catalyst pellet can be neglected. The catalyst activity is assumed to be constant. Use the conversion of ethylbenzene and the

conversions of ethylbenzene to the different products in the set of continuity equations. Use the Ergun equation to describe the pressure drop.

(f) *Simulation*
Simulate the profiles of conversion into styrene, benzene, and toluene, and the temperature and pressure profiles in the reactor.

11.8 Determine the units of the rate coefficients k_1, k_2, k_3, and of the adsorption coefficients in the rate equations of Example 11.9.1.A, Table 11.9.1.A-2.

11.9 **(a)** Repeat the calculation of the primary methane steam reformer presented in Example 11.9.1.A. Assume constant effectiveness factors based on the calculations shown in Figure 11.9.1.A-7.
(b) Repeat the calculation as in (a), but using the 2-dimensional reactor model of Section 11.10. Verify the radial temperature uniformity in the reactor.

REFERENCES

Adler, R., Nagel, G., Hertwig, K., and Henkel, D. K., *Chem. Technol.*, 24, 600 (1972).
Agnew, J.B., and Potter, O.E., *Trans. Inst. Chem. Eng.*, (London), 44, T216 (1966).
Ampaya, J.P., and Rinker, R.G., *Chem. Eng. Sci.*, 32, 1327 (1977); *Ind. Eng. Chem. Proc. Des. Dev.*, 16, 63 (1977).
Amundson, N.R., *Ber. Bunsen Gesellschaft*, 74, 90 (1970).
Aris, R., *The Optimal Design of Chemical Reactors*, Academic Press, New York (1960).
Aris, R., *Chem. Eng. Sci.*, 46, 343 (1969).
Aris, R., and Amundson, N.R., *AIChE J.*, 3, 280 (1957).
Baddour, R.F., Brian, P.L., Logeais, B.A., and Eymery, J.P., *Chem. Eng. Sci.*, 20, 281 (1965).
Balakrishnan, A.R., and Pei, P.C.T., *Int. Eng. Chem. Proc. Des. Dev.*, 18, 31 (1979a); 18, 40 (1979b); 18, 47 (1979c).
Barkelew, C.H., *Chem. Eng. Prog. Symp. Ser.*, 55(25), 38 (1959).
Beeckman, J.W., and Froment, G.F., *Ind. Eng. Chem. Fundam.*, 18, 245 (1979a); 21, 243 (1982b).
Beeckman, J.W., and Froment, G.F., *Chem. Eng. Sci.*, 35, 805 (1980).
Beek, J., *Adv. Chem. Eng.*, 3, 249 (1962).
Bellman, R., *Dynamic Programming*, Princeton University Press, Princeton, N.J. (1957).
Benenati, R.F., and Brosilow, G.B., *AIChE J.*, 8, 359 (1962).
Bernard, R.A., and Wilhelm, R.H., *Chem. Eng. Prog.*, 46, 233 (1950).
Bey, O., and Eigenberger, G., *Chem. Eng. Sci.*, 52, 1365 (1997).
Bilous, O., and Amundson, N.R., *AIChE J.*, 2, 117 (1956).
Bird, R.B., Stewart, W.E., and Lightfoot, E.N., *Transport Phenomena*, Wiley, Int. Ed., New York (1960); 2nd Ed. (2002).
Bischoff, K.B., *Chem. Eng. Sci.*, 16, 731 (1961).
Bischoff, K.B., *Can. J. Chem. Eng.*, 40, 161 (1963).
Bischoff, K.B., *Chem. Eng. Sci.*, 22, 525 (1967).
Blanks, R.F., Wittrig, T.S., and Peterson, D.A., *Chem. Eng. Sci.*, 45, 2407-2413 (1990).
Boreskov, G.K., and Matros, Yu.Sh., *Catal. Rev. Sci. Engng.*, 25(4), 551-590 (1983).
Brauer, M., *Chem. Ing. Techn.*, 29, 785 (1957).
Burkhardt, D.B., *Chem. Eng. Prog.*, 64 No. 11, 66 (1968).

Butt, J.B., *Chemical Reaction Engineering*, Advances in Chemistry Series, 109, A.C.S., Washington, D.C. (1972).
Cairns, E.J., and Prausnitz, J.M., *Ind. Eng. Chem.*, 51, 1441 (1959).
Calderbank, P.H., and Pogorsky, L.A., *Trans. Inst. Chem. Eng.*, (London), 35, 195 (1957).
Calderbank, P.H., *J. Appl. Chem.*, 2, 482 (1952).
Calderbank, P.H., *Chem. Eng. Prog.*, 49, 585 (1953).
Calderbank, P.H., Caldwell, A, and Ross, G., in *Proc. 4th Eur. Symp. Chem. React. Eng.*, Pergamon Press, New York (1968).
Campbell, T.M. and Huntington, R.L., *Petrol. Refiner*, 31, 123 (1952).
Cappelli, A., Collina, A., and Dente, M., *Ind. Eng. Chem. Proc. Des. Dev.*, 11, 184 (1972).
Cappelli, A., and Dente, M., *Chim. Ind. Milan*, 47, 1068 (1965).
Carberry, J.J., *AIChE J.*, 7, 350 (1961).
Carberry, J.J. and Bretton, R.H., *AIChE J.*, 4,367 (1958).
Carberry, J.J. and Wendel, M., *AIChE J.*, 9, 132 (1963).
Carberry, J.J. and White, D., *Ind. Eng. Chem.*, 61, 27 (1969).
Castillo-Araiza, C.O., and Lopez-Isunda, F., *Int. J. Chem. React. Eng.*, 6, A1 (2008).
Chigada, P.I., and Mann, R., *Int. J. Chem. React. Eng.*, 6, A84 (2008).
Chou, A., Ray, H.W., and Aris, R., *Trans. Inst. Chem. Eng.*, 45, 153 (1967).
Clayton, J.O., and Giaucque, W.F., *J. Am. Chem. Soc.*, 54, 2610 (1932).
Coberly, C.A., and Marshall, W.R., *Chem. Eng. Prog.*, 47, 141 (1951).
Collina, A., Corbetta, D., and Cappelli, A., in *Proc. Eur. Symp.* "*Use of Computers in the Design of Chemical Plants*", Firenze (1971).
Crider, J.E., and Foss, A.S., *AIChE J.*, 11, 1012 (1965).
Danckwerts, P.V., *Chem. Eng. Sci.*, 2, 1 (1953).
Deans, H.A., and Lapidus, L., *AIChE J.*, 6, 656 (1960).
De Deken, J.C., Devos, E.F., and Froment, G.F., in A.C.S. Symp. Series-196-"Chemical Reaction Engineering" (1982).
Degnan, T.F., and Wei, J., *AIChE J.*, 25, 338 (1979).
De Groote, A., Froment, G.F., and Kobylinski, T.H., *Can. J. Chem. Eng.*, 74, 735-742 (1996).
de Klerk, A., *AIChE J.*, 49, 2022 (2003).
Delmas, H., and Froment, G.F., *Chem. Eng. Sci.*, 43, 2281 (1988).
Dente, M., Biardi, G., and Ranzi, E., in *Proc. 5th Eur. Symp. Chem. React. Eng.*, Amsterdam, 1972, Elsevier, Amsterdam (1972).
Dente, M., and Collina, A., *Chim. et Industrie*, 46, 752 (1964).
De Pauw, R., and Froment, G.F., *Chem. Eng. Sci.*, 30, 789 (1975).
de Wasch, A.P., and Froment, G.F., *Chem. Eng. Sci.*, 26, 629 (1971); *Chem. Eng. Sci.*, 27, 567 (1972).
Dickinson, N.L., Finneran, J.A., and Solomon, E., *Eur. Chem. News*, "Large Plants", Sept. 29 (1967).
Dixon, A.G., *AIChE J.*, 31, 826 (1985).
Dixon, A.G., and Cresswell, D.L., *AIChE J.*, 25, 663 (1979).
Dixon, A.G., Taskin, M.E., Stitt, E.H., et al., *Chem. Eng. Sci.*, 62, 4963 (2007).
Dixon, A.G., Taskin, M.E., Nijemeisland, M., et al., *Chem. Eng. Sci.*, 63, 2219 (2008).
Dorweiler, V.P., and Fahien, R.W., *AIChE J.*, 5, 139 (1959).
Drott, D.W., and Aris, R., *Chem. Eng. Sci.*, 24, 541 (1969).
Dumez, F.J., and Froment, G.F., *Ind. Eng. Chem. Proc. Des. Dev.*, 15, 291 (1976).
Dyson, D.C., and Simon, J.M., *Ind. Eng. Chem. Fundam.*, 7, 605 (1968).
Ebach, E.A., and White, R.R., *AIChE J.*, 4, 161 (1958).
Eberly, E.A., Kimberlin, C.N., Miller, W.H., and Drushel, H.V., *Ind. Eng. Chem. Proc. Des. Dev.*, 5, 193 (1966).
Eigenberger, G., *Chem. Eng. Sci.*, 27, 1909 (1972a); 27, 1917 (1972b).
Ergun, S., *Chem. Eng. Prog.*, 48(2), 89 (1952).
Eschenbrenner, G.P., and Wagner, G.A., *Chem. Eng. Prog.*, 68, No.1, 62 (1972).
Fahien, R.W., and Smith, J.M., *AIChE J.*, 1, 25 (1955).
Finlayson, B.A., *Chem. Eng. Sci.*, 28, 1081 (1971).
Finneran, J.A., Buividas, L.J., and Walen, N., *Hydrocarbon Processing*, 51(4), 127 (1972).

Fodor, L., *Génie Chimique*, 104, 1002 (1971).
Froment, G. F., *Chem. Eng. Sci.*, 7, 29 (1962).
Froment, G.F., *Ind. Eng. Chem.*, 59(2), 18 (1967).
Froment, G.F., *Periodica Polytechnica*, (Budapest), 15, 219 (1971).
Froment, G.F., *Chemical Reaction Engineering*, Advances in Chemistry Series 109, A.C.S., Washington, D.C. (1972a).
Froment, G.F., in *Proc. 5th Eur. Symp. Chem. React. Eng.*, Amsterdam, 1972, Elsevier, New York (1972b).
Froment, G.F., *Chem. Ing. Tech.*, 46, 374 (1974).
Froment, G.F., in *Catalyst Deactivation*, ed. by B. Delmon and G.F. Froment, Elsevier, Amsterdam (1980).
Froment, G.F., and Bischoff, K.B., *Chem. Eng. Sci.*, 16, 189 (1961).
Froment, G.F., and Bischoff, K.B., *Chem. Eng. Sci.*, 17, 105 (1962).
Golikeri, S.V., and Luss, D., *AIChE J.*, 18, 277 (1972).
Govindarao, V.H., and Froment, G.F., *Chem. Eng. Sci.*, 41, 533 (1986).
Grevskott, S., Rustan, T., Hillestad, M., Edwin, E., and Olsvik, O., *Chem. Eng. Sci.*, 56, 597 (2001).
Gunn, D.J., *Chem. Eng. Sci.*, 42, 363 (1987).
Gunn, D.J., Ahmad, M.M., and Sabri, M.N., *Chem. Eng. Sci.*, 12, 2163 (1987).
Handley, D., and Heggs, P.J., *Trans. Inst. Chem. Eng.*, 46, T251 (1968).
Hanratty, T.J., *Chem. Eng. Sci.*, 3, 209 (1954).
Hatcher, W., Viville, L., and Froment, G.F., *Ind. Eng. Chem. Proc. Des. Dev.*, 17, 491 (1978).
Haughey, D.T., and Beveridge, S.G., *Can. J. Chem. Eng.*, 47, 130 (1969).
Hiby, J.W., *Interaction Between Fluids and Particles*, Institution of Chemical Engineers, London (1962).
Hicks, R.E., *Ind. Eng. Chem. Fundam.*, 9, 500 (1970).
High Performance Process Furnaces, M.W. Kellogg Co., New York.
Hlavacek, V., *Ind. Eng. Chem.*, 62, 8 (1970).
Hlavacek, V., and Hofmann, H., *Chem. Eng. Sci.*, 25, 173, 187 (1970).
Hlavacek, V., Marek, M., and John, T.M., *Coll. Czechoslov. Chem. Comm.*, 34, 3868 (1969).
Hosten, L.H., and Froment, G.F., *Chem. Eng. Sci.*, 41, 1073 (1986).
Hughes, R., Dakessian, V., and Brito-Alayon, A., in *Reactions and Reaction Engineering*, ed. by R.A. Mashelkar and R. Kumar, Indian Academy of Sciences, Bangalore, India (1987).
Hutchinson, P., and Luss, D., *Chem. Eng. J.*, 1, 129 (1970).
Inoue, H., *Chem. Eng. J. Japan*, 11, 40 (1978).
Jackson, R., *Trans. Inst. Chem. Eng.*, 45, 160 (1967).
Kehoe, J.P.G., and Butt, J.B., *Proc. 5th Eur. Symp. Chem. React. Eng.*, Amsterdam, 1972, Elsevier, Amsterdam (1972).
Kjaer, J., *Measurement and Calculation of Temperature and Conversion in Fixed Bed Catalytic Reactors*, Gjellerup, Copenhagen (1958).
Klingman, K.J., and Lee, H.H., *AIChE J.*, 33, 366 (1987).
Kolios, G., and Eigenberger, G., *Chem. Eng. Sci.*, 54, 2637 (1999).
Kunii, D., and Furusawa, T., *Chem. Eng. J.*, 4, 268 (1972).
Kunii, D., and Smith, J.M., *AIChE J.*, 6, 71 (1960).
Kwong, S.S., and Smith, J.M., *Ind. Eng. Chem.*, 49, 894 (1957).
Lee, K.Y., and Aris, R., *Ind. Eng. Chem. Proc. Des. Dev.*, 2, 300 (1963).
Lerou, J., and Froment, G.F., *Chem. Eng. Sci.*, 32, 853 (1977).
Leva, M., *Ind. Eng. Chem.*, 40, 747 (1948).
Leva, M., *Chem. Eng.*, 56, 115 (1949).
Levenspiel, O., and Bischoff, K.B., *Adv. Chem. Eng.*, 4, 95 (1963).
Liu, S.L., *AIChE J.*, 16, 501 (1970).
Liu, S.L., and Amundson, N.R., *Ind. Eng. Chem. Fundam.*, 1, 200 (1962); 2, 12 (1963).
Livbjerg, H., and Villadsen, J., *Chem. Eng. Sci.*, 27, 21 (1972).
Luss, D., *Chem. Eng. Sci.*, 23, 1249 (1968).
Luss, D., *Chem. Eng. Sci.*, 26, 1713 (1971).
Luss, D., in *Proc. 4th Int. Symp. Chem. React. Eng.*, Heidelberg (1976).

Luss, D., in *Chemical Reaction and Reactor Engineering*, ed. by J.J. Carberry and A. Varma, Marcel Dekker, New York (1987).
Luss, D., and Amundson, N.R., *Chem. Eng. Sci.*, 22, 253 (1967).
Luss, D., and Hutchinson, P., *Chem. Eng. J.*, 2, 172 (1971).
Luss, D., and Lee, J.C., *Chem. Eng. Sci.*, 23, 1237 (1968); 26, 1433 (1971).
Maeda, S., *Techn. Dep. Tohoku Univ.*, 16, 1 (1952).
Marek, M., Hlavacek, V., and John, M.T., *Coll. Czechosl. Chem. Comm.*, 34, 3664 (1969).
McDonald, I.F., El-Sayed, M.S., Mow, K., and Dullien, F.A.L., *Ind. Eng. Chem. Fundam.*, 18, 199 (1979).
McGreavy, C., and Adderley, C.I., *Chem. Eng. Sci.*, 28, 577 (1973).
McGreavy, C., and Adderley, C.I., *Adv. Chem. Ser.*, 133, 519 (1974).
McGreavy, C., and Cresswell, D. L., *Can. J. Chem. Eng.*, 47, 583 (1969).
McGreavy, C., and Thornton, J.M., *Can. J. Chem. Eng.*, 48, 187 (1970).
McGreavy, E.A., Foumeny and Javed, K.H., *Chem. Engng. Sci.*, 41, 787 (1986).
McGuire, M., and Lapidus, L., *AIChE J.*, 11, 85 (1965).
McHenry, K.W., and Wilhelm, R.H., *AIChE J.*, 3, 83 (1957).
Mears, D.E., *J. Catal.*, 20, 127 (1971a).
Mears, D.E., *Ind. Eng. Chem. Proc. Des. Dev.*, 10, 541 (1971b).
Menon, P.G., and Sreeramamurthy, R., *J. Catal.*, 8, 95 (1967).
Menon, P.G., Sreeramamurthy, R., and Murti, P.S., *Chem. Eng. Sci.*, 27, 641 (1972).
Mickley, H.S., Smith, K.A., and Korchack, E.I., *Chem. Eng. Sci.*, 20, 237 (1965).
Mihail, R., and Iordache, C., *Chem. Eng. Sci.*, 31, 83 (1976).
Morbidelli, M., and Varma, A, *AIChE J.*, 28, 705 (1982).
Murase, A., Roberts, H.L., and Converse, A.O., *Ind. Eng. Chem. Proc. Des. Dev.*, 9, 503 (1970).
Nam, In-Sik, and Froment, G.F., *J. Catal.*, 108, 271 (1987).
Narsimhan, G., *Ind. Eng. Chem. Proc. Des. Dev.*, 15, 302 (1976).
Natta, G., Mazzanti, G., and Pasquon, I., *Chim. Ind., Milan*, 37, 1015 (1955).
Nielsen, A, *J. Catal.*, 3, 68 (1964).
Nielsen, A, *Catalysis Reviews*, Vol. 4, Marcel Dekker, New York (1971).
Nijemeisland, M., and Dixon, A.G., *AIChE J.*, 50, 906 (2004).
Ogunye, A.F., and Ray, M.W., *AIChE J.*, 17, 43 (1970).
Olbrich, W.E., Agnew, J.B., and Potter, O.E., *Trans. Inst. Chem. Eng.*, 44, T207 (1966).
Olson, K.E., Luss, D., and Amundson, N.R., *Ind. Eng. Chem. Proc. Des. Dev.*, 7, 96 (1968).
Papageorgiou, J.N., Abello, M.C., and Froment, G.F., *Appl. Cat. A: General*, 120, 17 (1994).
Papageorgiou, J.N., and Froment, G.F., *Chem. Eng. Sci.*, 50, 3043 (1995).
Papageorgiou, J.N., Abello, M.C., and Froment, G.F., *Appl. Cat.*, 124, 165 (1995).
Patankar, S.V., *Numerical heat transfer and fluid flow*, Hemisphere, Washington, D.C. (1980).
Paynter, J.D., Dranoff, J.S., and Bankoff, S.G., *Ind. Eng. Chem. Proc. Des. Dev.*, 10, 244 (1971).
Pearson, J.R.A., *Chem. Eng. Sci.*, 10, 28 (1959).
Petersen, E.E., *Chemical Reaction Analysis*, Prentice-Hall, Englewood Cliffs, N.J. (1965).
Plautz, D.A., and Johnstone, H.F., *AIChE J.*, 1, 193 (1955).
Plehiers P.M., and Froment, G.F., *Chem. Eng. Technol.*, 12, 20 (1989).
Pontryagin, L.S., Boltryanski, V.G., Gamkrelidze, R.V., and Mishenko, E.F., *Mathematische Theorie Optimaler Prozesse*, Holdenburg Verlag, München (1969).
Rajadhyaskha, R.A., Vasudeva, K., and Doraiswamy, L.K., *Chem. Eng. Sci.*, 30, 1399 (1975).
Ray, W.H., in *Proc. 5th Eur. Symp. Chem. React. Eng.*, Amsterdam 1972, Elsevier, New York (1972).
Raymond, L.R., and Amundson, N.R., *Can. J. Chem. Eng.*, 42, 173 (1964).
Reichelt, W., *Chem. Eng. Techn.*, 44, 1068 (1972).
Reichelt, W., and Blasz, E., *Chem. Ing. Techn.*, 43, 949 (1971).
Roberts, S.M., *Dynamic Programming in Chemical Engineering and Process Control*, Academic Press, New York (1964).

Satterfield, C.N., *Mass Transfer in Heterogeneous Catalysis*, M.I.T. Press, Cambridge, Mass. (1970).
Schertz, W.W., and Bischoff, K.B., *AIChE J.*, 15, 597 (1969).
Schlünder, E.U., *Chem. Eng. Technol.*, 43, 651 (1971).
Schwartz, C.S., and Smith, J.M., *Ind. Eng. Chem.*, 45, 1209 (1953).
Shah, M.J., *Ind. Eng. Chem.*, 59(1), 72 (1967).
Shipman, L.M., and Hickman, J.B., *Chem. Eng. Prog.*, 64(5), 59 (1968).
Singer, E., and Wilhelm, R.H., *Chem. Eng. Prog.*, 46, 343 (1950).
Smith, R.B., *Chem. Eng. Prog.*, 55(6), 76 (1959).
Sotelo-Boyas, R., and Froment, G.F., *Ind. Eng. Chem. Res.*, 48(3), 1107-1119 (2009).
Strang, D.A., and Geankoplis, C.I., *Ind. Eng. Chem.*, 50, 1305 (1958).
Sundaresan, S., Amundson, N.R, and Aris, R., *AIChE J.*, 26, 529 (1980).
Suter, H., *Phthalsäureanhydrid*, Steinkopf Verlag, Darmstadt (1972).
Temkin, M.I., and Pyzhev, V., *Acta Physicochim.* (*USSR*), 12,327 (1960).
Tallmadge, J.A., *AIChE J.*, 16, 1092 (1970).
Taskin, M.E., Dixon, A.G., and Stitt, E.H., *Int. J. Chem. React. Eng.*, 5, A41 (2007).
Tjahjadi, M., Gupta, S.K., Morbidelli, M., and Varma, A., *Chem. Eng. Sci.*, 42, 2385 (1987).
Valstar, J., "A Study of the Fixed Bed Reactor with Application to the Synthesis of Vinylacetate," Ph.D. Thesis, Delft University, The Netherlands (1969).
Van Cauwenberghe, A.R., *Chem. Eng. Sci.*, 21, 203 (1966).
Vancini, C.A., *Synthesis of Ammonia*, Macmillan, London (1971).
Vanden Bussche, K.M., and Froment, G.F., *Can. J. Chem. Eng.*, 74, 729-733 (1996).
Van Heerden, C., *Ind. Eng. Chem.*, 45, 1242 (1953).
Van Welsenaere, R.J., and Froment, G.F., *Chem. Eng. Sci.*, 25, 1503 (1970).
Van Zoonen, D.D., in *Proc. III Int. Congr. Catal.*, North-Holland Publishing, Amsterdam (1965).
Varma, A, *Ind. Eng. Chem. Fundam.*, 19, 316 (1980).
Verschoor, H., and Schuit, G., *Appl. Sci. Res.*, A2, 97 (1950).
Viville, L., "De oxydatie, reductie en pyrofoor karakter van ijzer-nikkel katalysatoren," Ph.D. Thesis, Rijksuniversiteit Ghent, Belgium (1975).
Weekman, V.W., and Nace, D.M., *AIChE J.*, 16, 397 (1970).
Wehner, J.F., and Wilhelm, R.H., *Chem. Eng. Sci.*, 6, 89 (1956).
Weisz, P.B., and Hicks, J.S., *Chem. Eng. Sci.*, 17, 265 (1962).
Wentz, C.A., and Thodos, G., *AIChE J.*, 9, 81 (1963).
Wicke, E., *Alta Tecn. Chim.*, Acad. Naz. Lincei, Roma (1961).
Winnacker, K., and Kuechler, L., *Chemische Technologie*, C. Hanser Verlag, München (1970).
Yagi, S., and Kunii, D., *AIChE J.*, 3, 373 (1957).
Yagi, S., and Kunii, D., *AIChE J.*, 6, 97 (1960).
Yagi, S., Kunii, D., and Wakao, N., *AIChE J.*, 6, 543 (1960).
Yagi, S., and Wakao, N., *Chem. Eng. Sci.*, 5, 79 (1959).
Xu, J., and Froment, G.F., *AIChE J.*, 35, 88 (1989); and 35, 97 (1989).
Young, L.C., and Finlayson, B.A., *Ind. Eng. Chem. Fundam.*, 12, 412 (1973).
Zehner, P., and Schlünder, E.U., *Chem. Eng. Technol.*, 42, 333 (1970); 44, 1303 (1972).

Chapter 12

Complex Flow Patterns

12.1 INTRODUCTION

Flow and the related mixing are important phenomena in reactors. The idealized flow patterns of plug flow and complete mixing were dealt with in Chapters 9 and 10, respectively. The flow pattern is often more complex because of the reactor geometry and turbulence. Corners and baffles can lead to stagnant regions. Non-uniform flow distributions and bypassing of fluid can occur. Furthermore, reactants or reactants and the catalyst are often separately fed to the reactor. Mixing in the inlet section of the reactor may then become an important issue.

Mixing occurs over a wide range of scales, from the reactor scale down to the molecular scale. The calculation of all phenomena occurring over such a wide range of scales is computationally not tractable and not necessarily required, but the increase in computer power over the last 30 years has drastically shifted the (range of) scales of phenomena amenable to calculation.

After introducing the concepts of macro- and micro-mixing, the importance of flow / mixing patterns in reactors is discussed. Next, an overview of the methods for describing complex flow patterns is given and the relation between the different methods is explained. Focusing on statistically stationary flow, each method is then presented and discussed in more detail in the remaining sections of this chapter.

This chapter considers single-phase flow only. Some extensions of the methods to gas-solid and multi-phase flow are presented in Chapters 13 and 14.

12.2 MACRO- AND MICRO-MIXING IN REACTORS

The evaluation of mixing limitations is essentially based on a comparison of the reaction rate and mixing time scales. These are intrinsically local properties and are not necessarily uniform over the whole reactor.

In the process industries the flow is mostly turbulent and the observed rates of heat transfer, mass transfer and reaction may be strongly affected or even determined by the turbulence. Macro-mixing covers the range of scales from the reactor scale down to the scale of the largest turbulent eddies, whereas micro-mixing covers the range of scales from the largest down to the smallest turbulent eddies. Micro-mixing is due to the decay of the turbulent eddies, determined by the decay time τ_Y. At scales smaller than that of the smallest turbulent eddies, molecular diffusion becomes responsible for the dissipation and mixing, down to the molecular scale.

The reactor time scale, τ(reactor), which is the largest macro-mixing time scale, τ(macro-mixing), and typically of the order of seconds, can be the mean residence time in the reactor, τ(residence), but in a reactor equipped with an impeller, the recirculation time, τ(recirculation), rather than the mean residence time, should be used. The recirculation time can be defined as the mean time between successive encounters of a given fluid element with the impeller. Typically $\tau_Y < \tau$(recirculation) < τ(residence).

A distinction between turbulent eddies in the velocity field and species concentration field has to be made. For the velocity field, the turbulence integral scale and the Kolmogorov scale characterize respectively the largest and the smallest turbulent eddies. Typical corresponding time scales are between 10^{-1} and 1 s, respectively between 10^{-4} and 10^{-3} s. At high Reynolds numbers, the decay at the turbulence integral scale is seen to be typically much slower than the decay at the Kolmogorov scale, and, hence, determines the overall decay time of the turbulent eddies in the velocity field, τ_u. The latter can then be modeled in terms of the turbulent kinetic energy, k, and the turbulence dissipation rate, ε:

$$\tau_u = \tau_I = \frac{k}{\varepsilon} = \frac{1}{2}\frac{\left\langle u_i' u_i' \right\rangle}{\varepsilon} \tag{12.2-1}$$

The calculation of k and ε is discussed in Sections 12.4 and 12.5. The correlation $\left\langle u_i' u_i' \right\rangle$ in (12.2-1), in which u_i' is the fluctuating velocity resulting from the turbulence, will be formally introduced in Section 12.3.

For the species concentration field, the scalar integral scale and the Batchelor scale characterize respectively the largest and the smallest eddies. In most cases, the scalar integral scale is approximately equal to the turbulence integral scale. The Batchelor length scale, on the other hand, is related to the Kolmogorov length scale via the Schmidt number, $Sc = \mu/\rho D$:

$$\sigma_B = Sc^{-1/2}\sigma_K \tag{12.2-2}$$

For gases, $Sc \approx 1$, for liquids, $Sc >> 1$. This implies that in turbulent flow of liquids, the species concentration field contains smaller scale structures than the velocity field. Similar to the decay time of the turbulent eddies in the velocity field, τ_u, (12.2-1), the decay time of the eddies in the species concentration field, the previously introduced micro-mixing time, τ_Y, can be modeled in terms of the correlation of the species mass fraction fluctuations, the so-called scalar (co-) variance, $\left\langle Y'Y' \right\rangle$, and its dissipation rate, the so-called scalar dissipation rate, ε_Y:

$$\tau\ (\text{micro-mixing}) \equiv \tau_Y = \frac{1}{2}\frac{\left\langle Y'Y' \right\rangle}{\varepsilon_Y} \tag{12.2-3}$$

$\left\langle Y'Y' \right\rangle$ is formally defined in Section 12.3, whereas the calculation of ε_Y is discussed in Sections 12.4 and 12.5.

Based on scale-similarity, Spalding [1971] suggested τ_u and τ_Y to be proportional:

$$\tau\ (\text{micro-mixing}) \equiv \tau_Y = \frac{\tau_u}{C_Y} = \frac{\tau_I}{C_Y} \tag{12.2-4}$$

with C_Y an empirical constant for which a value of 2.0 was proposed [see also Hinze, 1959]. For Schmidt numbers much larger than 1, a somewhat more general expression for the micro-mixing time at high Reynolds numbers was derived by Fox [2003].

The reaction time scales can be calculated from the finite eigenvalues of the Jacobian matrix of the intrinsic reaction rates:

$$\boldsymbol{\tau}\ (\text{reaction}) = \left|\boldsymbol{\lambda}_{\boldsymbol{reac}}\right|^{-1} \tag{12.2-5}$$

with:

$$\left|\boldsymbol{\lambda}_{reac}\right| = \text{eigenval}\left[\boldsymbol{J}(\boldsymbol{C})\right] \tag{12.2-6a}$$

and

$$\boldsymbol{J}(\boldsymbol{C}) = \frac{\partial \boldsymbol{r}(\boldsymbol{C})}{\partial \boldsymbol{C}} \tag{12.2-6b}$$

The reaction time scales depend on the values of the kinetic and equilibrium constants in the rate equations and, hence, on the local temperature values. For non-linear reaction kinetics, the reaction time scales also depend on the local concentrations. For complex reaction rate expressions, $\boldsymbol{J}(\boldsymbol{C})$ and the reaction time scales have to be numerically evaluated. The reaction time scales are also affected by the local temperature values.

It should be pointed out here that, as defined in Chapter 1, the reaction rate is a point value, related to the molecular scale. At larger scales, like those considered in the description of reactors, macro- or reactor-scale, averaged reaction rates may have to be calculated. The "reaction rate" on the macro-scale will be called macro-scale averaged reaction rate and is the average of the various reaction rate point values in a macro-scale element. The "reaction rate" on the reactor-scale will be called reactor-scale averaged reaction rate and is the average of the various macro-scale averaged reaction rate values in the reactor. In the averaged reaction rates, micro- / macro-mixing limitations may have to be accounted for. As will be shown in Section 12.3, micro-mixing can also significantly affect macro-mixing (so-called turbulent transport). In general, the calculation of micro-mixing effects requires information on the turbulence and its dissipation rate.

Based on a comparison of the time scales of the reactions and that of the mixing, different situations, each requiring an appropriate level of sophistication of the simulation model, can be encountered. If τ(reaction) >> τ(macro-mixing), the reactor is well macro-mixed. Macro-mixing limitations on the reactor-scale averaged reaction rates and the extent to which macro-mixing is affected by micro-mixing do not need to be accounted for. In practice, macro-mixing limitations can be reduced by equipping the reactor with an impeller. The reactor time scale is then reduced from the mean residence time to the recirculation time. If τ(reaction) >> τ(micro-mixing), the reactor is well micro-mixed. Micro-mixing limitations on the macro- and reactor-scale averaged reaction rates do not need to be accounted for. τ(reaction) >> τ(macro-mixing) and τ(reaction) >> τ(micro-mixing) allows a completely mixed type reactor description (Chapter 10). In case τ(reaction) $\leq \tau_B$, micro-mixing not only affects, but determines the macro-scale averaged reaction rates. The intrinsic reaction kinetics does not have to be accounted for, because the reactions are considered to reach local equilibrium.

Mixing limitations on the reaction rates can be quantified in terms of the Damköhler number(s):

$$Da_j = \frac{\tau(\text{mixing})}{\tau^j(\text{reaction})} \tag{12.2-7}$$

where *j* relates to the reaction.

In a Lagrangian framework, macro- and micro-mixing can be similarly defined starting from the concept of a fluid element [Danckwerts, 1958]. Macro-mixing is then described by the mean motion of fluid elements in the reactor. Micro-mixing can be regarded as mixing on scales below the fluid element scale or resulting from interactions between fluid elements due to deviations from their mean flow path (turbulent transport).

12.3 MODELS EXPLICITLY ACCOUNTING FOR MIXING

Data on the reactor behavior are most often only available at the reactor scale. This is no reason for modeling the reactor as a black box, however. Macro- and micro-scale phenomena affect the reactor scale behavior and the appropriate mixing details should be accounted for.

Methods accounting for mixing are most easily illustrated for steady state or stationary reactor operation, as in Fig. 12.3-1. Because of its stochastic nature, turbulent flow is in fact only *statistically* stationary. The random behavior of the variables results in rapid fluctuations of their values around mean or so-called Reynolds-averaged, "steady state" values. Nevertheless, turbulent flow is governed by deterministic equations, the Navier-Stokes equations, whose terms have been explained in Chapter 7 and in which a transient term is included to account for the fluctuations around the statistically steady state values.

The continuity equation for a species *A* is:

$$\frac{\partial C_A}{\partial t} + \frac{\partial C_A u_j}{\partial z_j} = \frac{\partial}{\partial z_j} D_{Am} \frac{\partial C_A}{\partial z_j} + r_A(\boldsymbol{C}) \tag{12.3-1a}$$

The Einstein notation is used throughout this chapter and a single reaction of *A* is considered. In (12.3-1a), the species concentrations are expressed in terms of molar concentrations, ***C***. An alternative form in terms of the species mass fractions, ***Y***, is:

$$\frac{\partial \rho Y_A}{\partial t} + \frac{\partial \rho Y_A u_j}{\partial z_j} = \frac{\partial}{\partial z_j} \rho D_{Am} \frac{\partial Y_A}{\partial z_j} + \rho \tilde{r}_A(\boldsymbol{Y}) \tag{12.3-1b}$$

In this form, the fluid density, ρ, appears.

The conservation of mass is expressed by means of the total continuity equation:

$$\frac{\partial \rho}{\partial t} + \frac{\partial \rho u_j}{\partial z_j} = 0 \tag{12.3-2}$$

The conservation of momentum is expressed as momentum continuity equation:

$$\frac{\partial \rho u_i}{\partial t} + \frac{\partial \rho u_i u_j}{\partial z_j} = -\frac{\partial P}{\partial z_i} + \frac{\partial \tau_{ji}}{\partial z_j} + \rho g_i \quad \text{for: } i = 1, 2, 3 \tag{12.3-3}$$

with the shear stress tensor τ_{ji} defined by:

$$\tau_{ji} = \mu\left(\frac{\partial u_i}{\partial z_j} + \frac{\partial u_j}{\partial z_i} - \frac{2}{3}\delta_{ij}\frac{\partial u_l}{\partial z_l}\right) \tag{12.3-4}$$

δ_{ij} is the delta operator.

The conservation of energy, expressed by means of the total energy continuity equation, is:

$$\frac{\partial \rho E}{\partial t} + \frac{\partial}{\partial z_j}\left[u_j\left(\rho E + P\right)\right] = \frac{\partial}{\partial z_j}\lambda_m \frac{\partial T}{\partial z_j} + \frac{\partial}{\partial z_j}\left[u_i \tau_{ji}\right] + \rho u_i g_i \tag{12.3-5a}$$

where the total energy E consists of internal and kinetic energy. The transport of energy by molecular diffusion and radiation are not considered in (12.3-5a). As shown in Chapter 7, the total energy continuity equation can be transformed to explicit the heat of reaction:

$$\begin{aligned} &\rho\left[\left(\frac{\partial e_{kin}}{\partial t}\right) + \left(c_p \frac{\partial T}{\partial t}\right)\right] + \rho u_j\left[\left(\frac{\partial e_{kin}}{\partial z_j}\right) + \left(c_p \frac{\partial T}{\partial z_j}\right)\right] \\ &= \frac{\partial}{\partial z_j}\lambda_m \frac{\partial T}{\partial z_j} + \frac{\partial}{\partial z_j}\left[u_i \tau_{ji}\right] + \rho u_i g_i + \sum_k \left(-\Delta H_k\right) r_k \end{aligned} \tag{12.3-5b}$$

where e_{kin} is the specific kinetic energy in (J/kg) and c_p is the specific heat at constant pressure in (J/kg K).

Direct Numerical Simulations (DNS) (Fig. 12.3-1: A): The Navier-Stokes equations are solved as such, yielding the full details of micro- and macro-mixing. The reaction rates in (12.3-1a), (12.3-1b), and (12.3-5b) are point values, as defined in Chapter 1. DNS requires a time-accurate calculation of the statistically stationary behavior and extremely fine temporal and spatial meshes.

Therefore, DNS is computationally not tractable for industrial scale reactors and will not be discussed in further detail here.

Micro-Probability Density Function (PDF) methods (Fig. 12.3-1: B): Because of the stochastic nature of turbulence, it is appropriate to deal with any flow or reaction property as a random variable and use a statistical description for the micro-mixing. The stationary statistical behavior of the variables at the micro-scales can be represented by a Probability Density Function, the micro-PDF, f, which is essentially independent of time. The latter can be a posteriori calculated from DNS data. A computationally less expensive method considers the direct calculation of f. In its most general form and in a Eulerian framework, the micro-PDF is a multi-point joint-PDF, f_N, describing the probability of finding simultaneously given values for all the variables in all points of the vessel. In a Lagrangian framework, a multi-fluid-element joint-PDF would be considered. The multi-point joint-PDF is high-dimensional and its calculation is computationally not tractable in practical cases. Instead, the lower-dimensional local, that is, one-point joint-PDFs are calculated from a micro-PDF transport equation. The latter can be derived from the Navier-Stokes equations. Both joint composition and joint velocity-composition PDFs can be considered. Fig. 12.3-1 shows a one-point one-variable (velocity component u) micro-PDF. In the particular case of a well macro-mixed reactor, f is not local and independent of the spatial coordinates $\boldsymbol{z}$ (see Example 12.6.1.A). By using a *one-point* joint-PDF description, closure problems are introduced in the PDF transport equation. The turbulence dissipation rates, for example, which contain essential information on the decay time of the turbulent eddies or fluctuations [see equations (12.2-1) and (12.2-3)-(12.2-4)], have to be calculated from additional transport equations or models. Micro-PDF methods are discussed in detail in Section 12.4.

Methods in between DNS and micro-PDF, not shown in Fig. 12.3-1, are the so-called Large- and Very-Large-Eddy Simulations (LES / VLES). In those, only the low-frequency, i.e., largest, energy containing turbulent eddies are directly calculated [Pope, 2000]. To do so, a filter frequency is introduced and filtered Navier-Stokes equations are solved that are able to capture phenomena with a frequency up to the filter frequency. The effects of the higher frequencies, i.e., smaller, turbulent eddies, that are not explicitly calculated can then, for example, be taken into account by a Filtered micro-PDF (Filtered Density Function or FDF) method [Colucci et al., 1998; Jaberi et al., 1999; Gicquel et al., 2002]. Similar to DNS, (V)LES requires essentially a time-accurate calculation of the statistically stationary behavior, although naturally larger temporal and spatial meshes can be used. Presently, (V)LES is computationally not tractable for the calculation of industrial scale reactors.

Micro-PDF moment methods (Fig. 12.3-1: C): Micro-PDF methods require a Monte-Carlo type approach and are computationally demanding. Micro-PDF moment methods have been developed which do not calculate the micro-PDF, *f*, but a limited number of moments of *f* (mean, (co-)variances / correlations, ...) or a limited number of functions of given moments of *f* (turbulent kinetic energy, ...). Not accounting for a given higher-order moment of *f* leads to a closure problem. The latter is often challenging and limits the general applicability of micro-PDF moment methods for calculating macro-scale averaged reaction rates. Sometimes a parametric or functional form of *f* is assumed, allowing its complete description from a limited number of moments. Similar to *f*, the moments of *f* are essentially local and independent of time. Computational Fluid Dynamics (CFD) methods solve Reynolds-Averaged Navier-Stokes (RANS) equations for the macro-scale averaged or mean values of the variables (first-order moments of *f* — in Fig. 12.3-1, $<u_{micro}> \equiv u_{macro}$). This essentially implies the calculation of the macro-mixing. The RANS equations contain higher-order moments resulting from the non-linear convection and reaction rates. They express the effects of micro-mixing on macro-mixing, that is, turbulent transport, and on the macro-scale averaged reaction rates. This can be seen as follows. Formally, the instantaneous local value of the variable $\phi(\mathbf{z},t)$ can be decomposed in the mean local value $\langle\phi(\mathbf{z},t)\rangle \equiv \langle\phi\rangle(\mathbf{z})$, that is, on the macro-scale, and a deviation or fluctuation $\phi'(\mathbf{z},t)$ which is a micro-scale random component:

$$\phi(\mathbf{z},t) = \langle\phi(\mathbf{z},t)\rangle + \phi'(\mathbf{z},t)$$

$$\equiv \phi_{macro}(\mathbf{z}) + \phi'(\mathbf{z},t)$$

$$= \text{mean} + \text{deviation},$$

where the mean < > is taken over all micro-scales and $\langle\phi'\rangle = 0$. The macro-scale behavior of a non-linear term, e.g., $\phi_1\phi_2$, is described by $\langle\phi_1\phi_2\rangle$. Decomposing the variables ϕ_1 and ϕ_2 into their mean and random components and formally averaging results in:

$$\langle\phi_1\phi_2\rangle = \left\langle\left(\langle\phi_1\rangle + \phi_1'\right)\left(\langle\phi_2\rangle + \phi_2'\right)\right\rangle$$

$$= \langle\phi_1\rangle\langle\phi_2\rangle + \langle\phi_1\rangle\langle\phi_2'\rangle + \langle\phi_1'\rangle\langle\phi_2\rangle + \langle\phi_1'\phi_2'\rangle$$

$$= \langle\phi_1\rangle\langle\phi_2\rangle + \langle\phi_1'\phi_2'\rangle$$

$$= \text{first-} + \text{second-order moments of } f,$$

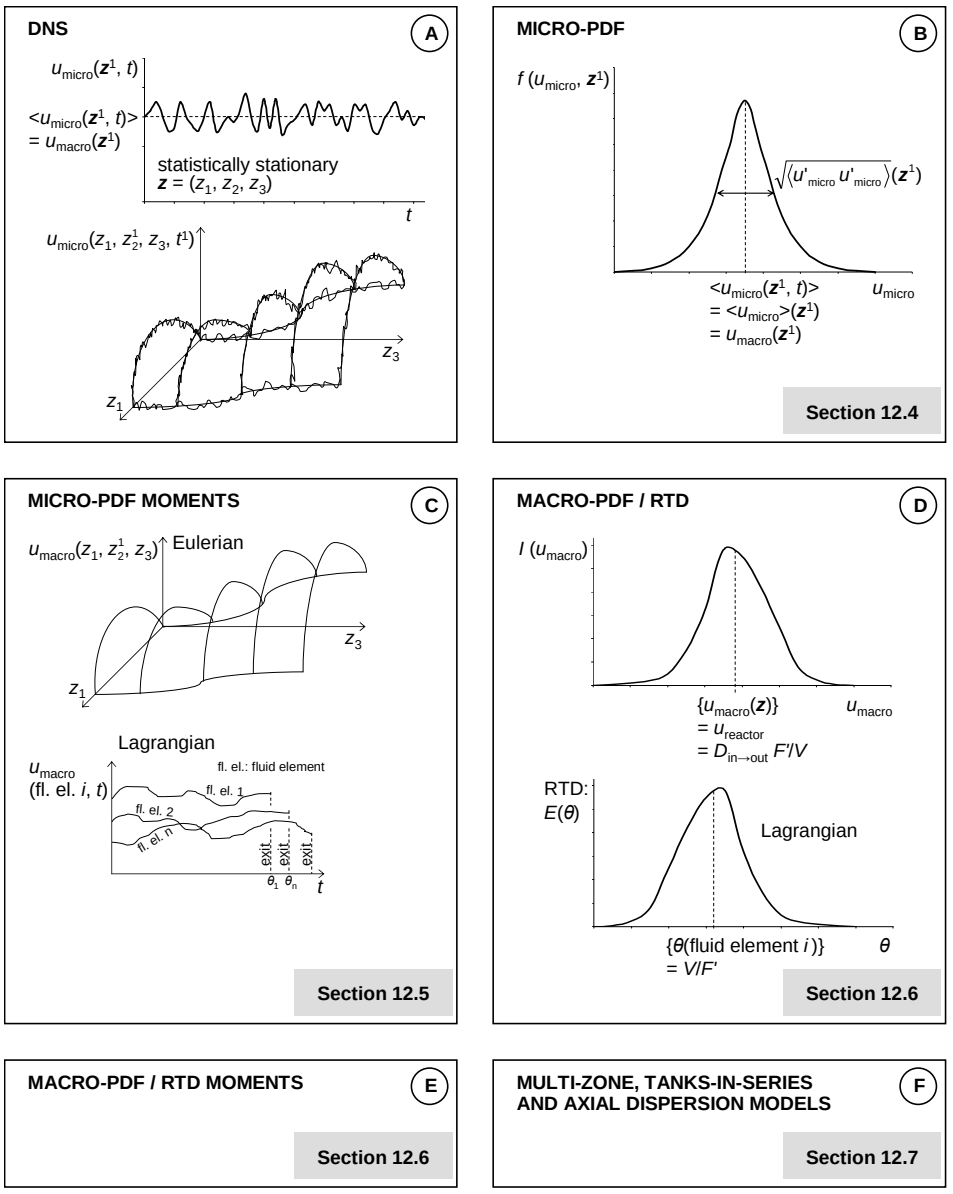

Figure 12.3-1

Major methods used to account for mixing in reactors. Illustrations on statistically stationary field of a velocity component. DNS: Direct Numerical Simulation; PDF: Probability Density Function; *I*: Internal distribution function; RTD: Residence Time Distribution; <>: macro-scale averaged; {}: reactor-scale averaged.

as $\langle \phi_1' \rangle$ and $\langle \phi_2' \rangle$ are zero. The correlation $\langle \phi_1' \phi_2' \rangle$ then expresses the impact of micro-scale phenomena on the macro-scale behavior of $\langle \phi_1 \phi_2 \rangle$.

The velocity correlations, $\langle u_i' u_j' \rangle$, are the so-called Reynolds-stresses and describe turbulent momentum transport. The velocity-concentration

correlations, $\langle u_i' Y_A' \rangle$, are the scalar fluxes and describe turbulent species transport. Concentration correlations, e.g., $\langle Y_A' Y_B' \rangle$, result from non-linear reaction rates. A given higher-order moment of *f* can then be calculated from an additional transport equation or described in terms of other calculated moments of *f* via a so-called closure model. Micro-PDF moment methods are presented in detail in Section 12.5.

Macro-PDF and RTD methods (Fig. 12.3-1: D): Micro-PDF moment methods can be computationally demanding. In such case, the statistical description of macro-mixing using a macro-PDF can be considered. A macro-PDF, *I*, can be defined by sampling in space over all the macro-scales, that is, over the entire reactor volume. The reactor-scale averaged value is noted {}. A macro-PDF method implies that no local details on macro-mixing are available. Rigorously accounting for micro-mixing effects using a macro-PDF method is challenging, because specific information on micro-mixing is not captured by *I*. The difference between a micro- and a macro-PDF should also be stressed. The calculation of a macro-PDF is challenging, but measurements (at the reactor scale) are possible and this explains the popularity of macro-PDF methods. Of course, a macro-PDF can also be a posteriori calculated from CFD data. The most frequently used macro-PDFs are the so-called Internal Age Distribution, $I(\alpha)$, and related Residence Time Distribution (RTD), $E(\theta)$. Their use is discussed in detail in Section 12.6. As illustrated in Fig. 12.3-1, $I(\alpha)$ and $E(\theta)$ are directly related to the macro-PDF of the velocity.

Macro-PDF and RTD moment methods (Fig. 12.3-1: E): The macro-PDF or RTD can be characterized by its moments. These can be directly calculated or measured. The knowledge of a sufficient number of moments allows the a posteriori reconstruction of the macro-PDF or RTD. Some details and an example of the application of macro-PDF moment methods are given in Section 12.6.

Summarizing, both for micro- and macro-mixing, a statistical description by means of a micro- or macro-PDF can be chosen. Furthermore, a limited number of moments can be considered instead of the full PDF.

Multi-zone, Tanks-in-Series, and Axial dispersion models (Fig. 12.3-1: F): Other, less fundamental approaches accounting for mixing limitations in reactors are described in Section 12.7. They are based on simplified descriptions of the mixing pattern, e.g., a 1D axial dispersion approach, or on the decomposition of the complex flow reactor into multiple interconnected regions or zones, each of these being described by a different idealized mixing pattern. Such semi-empirical models contain model parameters which have to be determined, experimentally or a posteriori from PDF, CFD, or RTD data.

A detailed discussion of the various methods is given in the next sections. It focuses on statistically stationary flow. The methods can be combined, but this should be done with care and the resulting accuracy and computational effort should be kept in mind.

Extensions to statistically non-stationary flow, where rapid variations in time of the values of the variables (random components) are superposed on slower variations in time of the mean components, i.e., of the macro-scale behavior, are rather straightforward.

12.4 MICRO-PROBABILITY DENSITY FUNCTION METHODS

These are also called Population Balance Equation (PBE) methods. The random nature of turbulence and related micro-mixing lends itself well to a statistical description. The general probabilistic approach [Katz and Shinnar, 1969; Zvirin and Shinnar, 1976] does not aim at predicting the value of the random variables, but determines the probabilities of the random variables adopting specified values, the Probability Density Function (PDF, here micro-PDF). Mixing in a reactor is then essentially described via the evolution of the PDF of the reactor. In Section 12.4.1, a general framework in terms of PDF transport equations or population balances is derived. Section 12.4.2 considers more specific models for describing turbulent flow and reaction, using the distribution of either the composition or the composition-velocity space.

The present chapter focuses on single-phase flow, but extensions to multi-phase flow or monitoring other variables, such as the coke content and / or activity level of catalyst pellets, concentrations within coalescing droplets, changing pore sizes in a reacting solid, biochemical properties of growing cells, sizes of growing crystals, are possible. Some of these extensions are dealt with in Chapters 13 and 14.

12.4.1 Micro-PDF Transport Equations

In the Lagrangian framework derivation of a population balance equation or PDF transport equation, a number of particles or fluid elements is considered. The external coordinates of a particle are the spatial location $\boldsymbol{z}$ and the time t. The internal coordinates $\boldsymbol{\varphi}$ are volume or mass, composition, velocity, temperature, ... — the so-called phase space. The velocity $\boldsymbol{v}$ is usually written separately from the other internal coordinates $\tilde{\boldsymbol{\varphi}}$, with $\boldsymbol{\varphi} = (\boldsymbol{v}, \tilde{\boldsymbol{\varphi}})$. The distribution of the particles can be defined by a number density function (NDF), n, or a single-particle joint probability density function (PDF), f_1, also noted f. By definition, $f_\gamma(\boldsymbol{\varphi}, \boldsymbol{z}, t)d\boldsymbol{\varphi}d\boldsymbol{z}$ is the probability of finding particles at a spatial location ($\boldsymbol{z} \leq \boldsymbol{s} < \boldsymbol{z} + d\boldsymbol{z}$) at time t

with properties in the ranges ($\boldsymbol{\varphi} \le \boldsymbol{\gamma} < \boldsymbol{\varphi} + d\boldsymbol{\varphi}$). The NDF follows from the single-particle joint-PDF:

$$n_{\boldsymbol{\gamma}}(\boldsymbol{\varphi};\mathbf{z},t) = N \cdot f_{\boldsymbol{\gamma}}(\boldsymbol{\varphi};\mathbf{z},t) \tag{12.4.1-1}$$

where N is the total number of particles in the sample space. Other types of distribution functions can be defined, e.g., mass fraction based.

The Eulerian analogy of the Lagrangian single-particle joint-PDF is the one-point joint-PDF. For the one-point joint velocity-composition PDF, $f_{\boldsymbol{u},\boldsymbol{Y}}$, used in Section 12.4.2, $f_{\boldsymbol{u},\boldsymbol{Y}}(\boldsymbol{v}, \boldsymbol{\psi}; \mathbf{z}, t)d\boldsymbol{v}d\boldsymbol{\psi}$ is the probability of having a given velocity ($\boldsymbol{v} \le \boldsymbol{u}(\mathbf{z}, t) < \boldsymbol{v} + d\boldsymbol{v}$) and composition ($\boldsymbol{\psi} \le \boldsymbol{Y}(\mathbf{z}, t) < \boldsymbol{\psi} + d\boldsymbol{\psi}$) at position $\mathbf{z}$ and time t. The $\boldsymbol{\psi}$-space is the sample space of the random variable $\boldsymbol{Y}$ and the $\boldsymbol{v}$-space is the sample space for the random variable $\boldsymbol{u}$. Sample spaces can be unbounded or bounded. The composition sample space is typically bounded. For a statistically stationary flow, as was assumed in Fig. 12.3-1 and will be focused on in what follows, $f_{\boldsymbol{u},\boldsymbol{Y}}(\boldsymbol{v}, \boldsymbol{\psi}; \mathbf{z})$.

By definition, the random variables $\boldsymbol{u}$ and $\boldsymbol{Y}$ are independent if their joint-PDF is the product of their so-called marginal PDFs:

$$f_{\boldsymbol{u},\boldsymbol{Y}}(\boldsymbol{v},\boldsymbol{\psi};\mathbf{z}) = f_{\boldsymbol{u}}(\boldsymbol{v};\mathbf{z})\, f_{\boldsymbol{Y}}(\boldsymbol{\psi};\mathbf{z}) \tag{12.4.1-2}$$

For a function $Q(\boldsymbol{u},\boldsymbol{Y})$, the mean or expectation in point $\mathbf{z}$, $\langle Q(\boldsymbol{u},\boldsymbol{Y})\rangle(\mathbf{z})$, can be obtained from the first-order moment

$$\langle Q(\boldsymbol{u},\boldsymbol{Y})\rangle(\mathbf{z}) = \int_{-\infty}^{\infty}\int_{-\infty}^{\infty} Q(\boldsymbol{v},\boldsymbol{\psi})\, f_{\boldsymbol{u},\boldsymbol{Y}}(\boldsymbol{v},\boldsymbol{\psi};\mathbf{z})\, d\boldsymbol{v}d\boldsymbol{\psi} \tag{12.4.1-3}$$

It reflects the macro-scale behavior of Q. In statistically stationary flow (Fig. 12.3-1), time averaging can be applied for the calculation of the mean, for example:

$$\langle Y_A(\mathbf{z},t)\rangle_{\Delta t} = \frac{1}{\Delta t}\int_{t}^{t+\Delta t} Y_A(\mathbf{z},\tau)\, d\tau\,, \tag{12.4.1-4}$$

where Δt is a specified time interval to be chosen sufficiently large for (12.4.1-4) to approach the mean. As described in Section 12.3 in the context of Reynolds-averaging, the instantaneous local value of a random variable can then be decomposed in terms of its mean and a fluctuation, for example:

$$Y_A = \langle Y_A \rangle + Y_A' \tag{12.4.1-5}$$

A covariance or correlation $\langle u_i' Y_A' \rangle$ in point $\mathbf{z}$ can be formally defined as the second-order moment

$$\left\langle u_i' Y_A' \right\rangle(\boldsymbol{z}) = \int_{-\infty}^{\infty}\int_{-\infty}^{\infty} \left(v_i - \langle u_i \rangle(\boldsymbol{z})\right)\left(\psi_A - \langle Y_A \rangle(\boldsymbol{z})\right) f_{\boldsymbol{u},\boldsymbol{Y}}(\boldsymbol{v},\boldsymbol{\psi};\boldsymbol{z})\, d\boldsymbol{v}\, d\boldsymbol{\psi} \tag{12.4.1-6}$$

The definition of the variances and covariances,

$$\left\langle u_i' u_i' \right\rangle \text{ and } \left\langle Y_A' Y_A' \right\rangle, \text{ respectively } \left\langle u_i' u_j' \right\rangle \text{ and } \left\langle Y_A' Y_B' \right\rangle$$

is, of course, similar. Independent random variables are uncorrelated and the corresponding correlation term vanishes.

Conditional PDFs express the probability of variables having certain values, provided that other variables have fixed given values. For example, $f_{\boldsymbol{u}|\boldsymbol{Y}}(\boldsymbol{v}|\boldsymbol{\psi};\boldsymbol{z})$ is defined as the probability that in a point $\boldsymbol{z}$, $(\boldsymbol{v} \le \boldsymbol{u}(\boldsymbol{z}) < \boldsymbol{v} + d\boldsymbol{v})$, given that $(\boldsymbol{Y}(\boldsymbol{z}) = \boldsymbol{\psi})$. From its definition, it follows that:

$$f_{\boldsymbol{u}|\boldsymbol{Y}}(\boldsymbol{v}|\boldsymbol{\psi};\boldsymbol{z}) = f_{\boldsymbol{u},\boldsymbol{Y}}(\boldsymbol{v},\boldsymbol{\psi};\boldsymbol{z}) / f_{\boldsymbol{Y}}(\boldsymbol{\psi};\boldsymbol{z}) \tag{12.4.1-7}$$

Using conditional PDFs, conditional expectations or means can be defined, in a way similar to (12.4.1-3).

In what follows, the notation for the single-particle or one-point joint-PDF will often be abbreviated. For the one-point joint velocity-composition PDF:

$$f_{\boldsymbol{u},\boldsymbol{Y}}(\boldsymbol{v},\boldsymbol{\psi};\boldsymbol{z}) \equiv f(\boldsymbol{v},\boldsymbol{\psi}) \tag{12.4.1-8}$$

or, sometimes, simply *f*.

The evolution of a general single-particle joint-PDF $f(\boldsymbol{\varphi};\boldsymbol{z})$ depends on interactions between particles, so that $f(\boldsymbol{\varphi};\boldsymbol{z})$ is not sufficient to fully describe its own evolution (similar reasoning for the Eulerian framework single-point joint-PDF, the evolution of which depends on interactions with other points). Information is needed on the probability of having specific encounters between particles. Encounters between two particles are, for example, determined by the two-particle joint-PDF or pair density function, f_2. By definition, $f_2(\boldsymbol{\varphi}^{(1)},\boldsymbol{\varphi}^{(2)};\boldsymbol{z}^{(1)},\boldsymbol{z}^{(2)})\, d\boldsymbol{\varphi}^{(1)}\, d\boldsymbol{\varphi}^{(2)}\, d\boldsymbol{z}^{(1)}\, d\boldsymbol{z}^{(2)}$ is the probability of finding a particle at position $(\boldsymbol{z}^{(1)} \le \boldsymbol{s}^{(1)} < \boldsymbol{z}^{(1)} + d\boldsymbol{z}^{(1)})$ with properties in the ranges $(\boldsymbol{\varphi}^{(1)} \le \boldsymbol{\gamma}^{(1)} < \boldsymbol{\varphi}^{(1)} + d\boldsymbol{\varphi}^{(1)})$ and another particle at position $(\boldsymbol{z}^{(2)} \le \boldsymbol{s}^{(2)} < \boldsymbol{z}^{(2)} + d\boldsymbol{z}^{(2)})$ with properties in the ranges $(\boldsymbol{\varphi}^{(2)} \le \boldsymbol{\gamma}^{(2)} < \boldsymbol{\varphi}^{(2)} + d\boldsymbol{\varphi}^{(2)})$. In general, the multi-particle joint-PDF, f_N, is required to completely define the system evolution. $f_N(\boldsymbol{\varphi}^{(1)},\boldsymbol{\varphi}^{(2)},...,\boldsymbol{\varphi}^{(N)};\boldsymbol{z}^{(1)},\boldsymbol{z}^{(2)},...,\boldsymbol{z}^{(N)})$ is the logical extension of the two-particle joint-PDF to *N* particles. In a Eulerian framework, f_N represents the *N*-point joint-PDF. The evolution of the multi-particle joint-PDF

is described by the multi-particle joint-PDF transport equation derived by Liouville. For statistically stationary flow:

$$\sum_{n=1}^{N} \frac{\partial}{\partial z_i^{(n)}} \left(v_i^{(n)} f_N \right) + \sum_{n=1}^{N} \frac{\partial}{\partial v_i^{(n)}} \left[\left(A_i^{p^{(n)}} + A_i^{(n)} \right) f_N \right] + \sum_{n=1}^{N} \frac{\partial}{\partial \tilde{\varphi}_A^{(n)}} \left(G_A^{(n)} f_N \right) = B_N - D_N \tag{12.4.1-9}$$

The first term in (12.4.1-9) represents physical transport. The second and third terms account for the continuous evolution of the particle internal coordinates, the second of the velocity, the third of the other particle internal coordinates. $A_i^{p^{(n)}}$, $A_i^{(n)}$ and $G_A^{(n)}$ represent the rate of change in the phase space of the properties, $A_i^{p^{(n)}}$ and $A_i^{(n)}$ of the *i*-component of the velocity of the n^{th} particle, $v_i^{(n)}$, and $G_A^{(n)}$ of the property $\tilde{\varphi}_A^{(n)}$. Discontinuous changes in the particle internal coordinates are due to collisions and are described by the source terms ($B_N - D_N$), *B* represents "birth" and *D* "destruction" processes.

The multi-particle joint-PDF transport equation (12.4.1-9) is closed. The calculation and use of the high dimensional multi-particle joint-PDF, f_N, is computationally not tractable. In practice, the low(er)-dimensional single-particle joint-PDF, *f*, is used instead:

$$f^{(n)}\left(\boldsymbol{\varphi}^{(n)}; \boldsymbol{z}^{(n)}\right) d\boldsymbol{\varphi}^{(n)}\, d\boldsymbol{z}^{(n)} = \int_{\neq n} f_N \left(\boldsymbol{\varphi}^{(1)}, ..., \boldsymbol{\varphi}^{(N)}; \boldsymbol{z}^{(1)}, ..., \boldsymbol{z}^{(N)}\right) d\boldsymbol{\varphi}^{(1)} ... d\boldsymbol{\varphi}^{(N)}\, d\boldsymbol{z}^{(1)} ... d\boldsymbol{z}^{(N)}$$

with (n), an n^{th} particle (12.4.1-10)

and its evolution calculated from a transport equation derived by Boltzmann. It can be obtained by formally integrating the multi-particle joint-PDF transport equation (12.4.1-9) using (12.4.1-10). The phenomena captured by and explicitly requiring the multi-particle joint-PDF cause a closure problem in the single-particle joint-PDF transport equation and have to be modeled [Ramkrishna et al., 1973, 1974, 1976]. For statistically stationary flow, the single-particle joint-PDF transport equation or population balance equation has the following form [see, e.g., Randolph and Larson, 1971 or Himmelblau and Bischoff, 1986]:

$$\frac{\partial}{\partial z_i} \left(v_i f \right) + \frac{\partial}{\partial v_i} \left[\left(\left\langle A_i^p \middle| \boldsymbol{\varphi} \right\rangle + \left\langle A_i \middle| \boldsymbol{\varphi} \right\rangle \right) f \right] + \frac{\partial}{\partial \tilde{\varphi}_A} \left(\left\langle G_A \middle| \boldsymbol{\varphi} \right\rangle f \right) = \left(B \middle| \boldsymbol{\varphi} \right) - \left(D \middle| \boldsymbol{\varphi} \right) \tag{12.4.1-11}$$

The transport equation for the NDF (12.4.1-1) is similar to (12.4.1-11) and obtained by summation of all the single-particle joint-PDF transport equations (12.4.1-11). In (12.4.1-11), the first term represents convection, the second the conditional acceleration, and the third the single-particle state conditional continuous changes in the internal coordinates other than the velocity. The rate of continuous changes of property $\widetilde{\varphi}_A$ in the phase space of $\boldsymbol{\varphi}$ is represented by $\langle G_A|\boldsymbol{\varphi}\rangle$. Discrete changes in the internal coordinates due to collisions are described by the conditional source terms $((B-D)|\boldsymbol{\varphi})$ on the right hand side of (12.4.1-11).

Equation (12.4.1-11) seems to be adequate for a variety of problems. It is very similar to the Boltzmann equation of kinetic theory, where *f* represents the distribution function of molecular velocities. Closure models are required for all the conditional terms in (12.4.1-11). They depend on the specific physical phenomena and reactions involved.

The integration of the single-particle joint-PDF transport equation (12.4.1-11) is tedious. Computer requirements for standard CFD techniques rise exponentially with the dimensionality of the joint-PDF. Therefore, micro-PDF methods commonly use a Monte-Carlo approach [Spielman and Levenspiel, 1965; Kattan and Adler, 1967, 1972; Pope, 1981]. A deterministic system is constructed with stochastic particles whose joint-PDF evolves in the same way as the joint-PDF of fluid particles. The trajectories of the so-called conditional particles define a formal solution of the joint-PDF transport equation (12.4.1-11). Ramkrishna [2000] presents details on the computational methods.

12.4.2 Micro-PDF Methods for Turbulent Flow and Reactions

The description is based on the previously defined single-particle (Lagrangian) or one-point (Eulerian) joint velocity-composition (micro-)PDF, $f(\boldsymbol{v},\boldsymbol{\psi})$. As mentioned in Section 12.4.1, in the one-point description no information on the local velocity and scalar (species concentrations, temperature, ...) gradients and on the frequency or length scale of the fluctuations is included and the related terms require closure models. The scalar dissipation rate model has to relate the micro-mixing time to the turbulence field (see (12.2-3)), either directly or via a transport equation for the turbulence dissipation rate ε. A major advantage is that the reaction rate is a point value and its behavior and mean are described exactly by a one-point PDF, even for arbitrarily complex and nonlinear reaction kinetics.

The one-point joint velocity-composition PDF transport equation expresses the evolution of the PDF by transport in real space, in velocity space, and in composition space and can be derived from the Navier-Stokes equations

(12.3-1)-(12.3-5) [Pope, 2000; Fox, 2003]. For inhomogeneous, variable-density flow, the natural dependent variable is the mass density function *mdf*:

$$mdf(\boldsymbol{v},\boldsymbol{\psi}) = \rho(\boldsymbol{\psi}) f(\boldsymbol{v},\boldsymbol{\psi}) = \langle \rho \rangle \tilde{f}(\boldsymbol{v},\boldsymbol{\psi}), \tag{12.4.2-1}$$

and the Favre-averaged PDF, $\tilde{f}(\boldsymbol{v},\boldsymbol{\psi})$, defined by (12.4.2-1) is to be used. The transport of $f(\boldsymbol{v},\boldsymbol{\psi})$ in real space results from the fluctuating velocity $\boldsymbol{v}$, whereas the transport in velocity and composition space results from conditional acceleration and reaction / diffusion. For statistically stationary flow:

$$\begin{aligned} \frac{\partial \rho(\boldsymbol{\psi}) v_i f(\boldsymbol{v},\boldsymbol{\psi})}{\partial z_i} = & -\frac{\partial}{\partial v_i}\left[\left\langle A_i \middle| \boldsymbol{v},\boldsymbol{\psi} \right\rangle \rho(\boldsymbol{\psi}) f(\boldsymbol{v},\boldsymbol{\psi})\right] \\ & -\frac{\partial}{\partial \psi_A}\left[\left\langle \Theta_A \middle| \boldsymbol{v},\boldsymbol{\psi} \right\rangle \rho(\boldsymbol{\psi}) f(\boldsymbol{v},\boldsymbol{\psi})\right] \end{aligned} \tag{12.4.2-2}$$

in which

$$\rho(\boldsymbol{\psi})\left\langle A_i \middle| \boldsymbol{v},\boldsymbol{\psi} \right\rangle = \left\langle \left(\frac{\partial \tau_{ji}}{\partial z_j} - \frac{\partial P}{\partial z_i} \right) \middle| \boldsymbol{v},\boldsymbol{\psi} \right\rangle + \rho(\boldsymbol{\psi}) g_i \tag{12.4.2-3}$$

is the conditional acceleration term, with τ_{ji} given by (12.3-4), and

$$\rho(\boldsymbol{\psi})\left\langle \Theta_A \middle| \boldsymbol{v},\boldsymbol{\psi} \right\rangle = \left\langle \left(\frac{\partial}{\partial z_j} \rho(\boldsymbol{\psi}) D_{Am} \frac{\partial Y_A}{\partial z_j} \right) \middle| \boldsymbol{v},\boldsymbol{\psi} \right\rangle + \rho(\boldsymbol{\psi}) \tilde{r}_A(\boldsymbol{\psi}) \tag{12.4.2-4}$$

the conditional diffusion / reaction term.

The PDF transport equation (12.4.2-2) is deterministic. Convection appears in closed form. The conditional acceleration term (12.4.2-3) and the conditional diffusion / reaction term (12.4.2-4) are unclosed. In the conditional acceleration term (12.4.2-3), only the first term in the right hand side is actually unclosed. The effects of gravity are dealt with in an exact way. In the conditional diffusion / reaction term (12.4.2-4), the turbulent mixing term is unclosed, but the reaction rate appears in closed form whatever the complexity and nonlinearity of the reaction kinetics. The remaining part of this section focuses on closure models.

The conditional acceleration term can be decomposed into:

$$\rho(\boldsymbol{\psi})\left\langle A_i \middle| \boldsymbol{v},\boldsymbol{\psi} \right\rangle = \rho(\boldsymbol{\psi})\left\langle A_i' \middle| \boldsymbol{v},\boldsymbol{\psi} \right\rangle + \frac{\partial \langle \tau_{ji} \rangle}{\partial z_j} - \frac{\partial \langle P \rangle}{\partial z_i} + \rho(\boldsymbol{\psi}) g_i \tag{12.4.2-5}$$

with:

$$\rho(\boldsymbol{\psi})\left\langle A_i^{'}\middle|\boldsymbol{v},\boldsymbol{\psi}\right\rangle = \left\langle\left(\frac{\partial \tau_{ji}^{'}}{\partial z_j}\right)\middle|\boldsymbol{v},\boldsymbol{\psi}\right\rangle - \left\langle\left(\frac{\partial P'}{\partial z_i}\right)\middle|\boldsymbol{v},\boldsymbol{\psi}\right\rangle \qquad (12.4.2\text{-}6)$$

Applying this decomposition, the effects of the mean pressure gradient and the mean shear stress also appear in closed form in the PDF transport equation (12.4.2-2).

At high Reynolds numbers, the fluctuating pressure field term dominates the fluctuating shear stress term in (12.4.2-6). It results from interactions between the turbulence and the mean velocity gradients, the so-called rapid-pressure contribution, and from the turbulence proper, the so-called slow-pressure contribution. To simulate the rapid-pressure related process, Pope [1985] proposed a linear deterministic model:

$$\left\langle\left(\frac{\partial P'^{rapid}}{\partial z_i}\right)\middle|\boldsymbol{v},\boldsymbol{\psi}\right\rangle = -2\rho\frac{\partial\langle u_l\rangle}{\partial z_m}B_{mli}\left(\boldsymbol{v}-\langle\boldsymbol{u}\rangle\right) \qquad (12.4.2\text{-}7)$$

where the tensor $\boldsymbol{B}$ is linear with respect to the velocity and a non-dimensional tensor $\boldsymbol{C}$ which is a function of the Reynolds stresses:

$$B_{mli}\left(\boldsymbol{v}-\langle\boldsymbol{u}\rangle\right) = \left(v_q - \langle u_q\rangle\right)C_{qmli} \qquad (12.4.2\text{-}8)$$

To simulate the slow-pressure phenomena, a stochastic mixing and reorientation model can be used. It describes the dissipation and the observed tendency of the Reynolds stresses to become isotropic. The stochastic mixing model is similar to that used for the scalar dissipation, whereas the reorientation process is described in analogy with collisions between Maxwellian molecules, i.e., conserving both momentum and energy. Pope [1985] developed an alternative model for the conditional acceleration term, based on the generalized Langevin model.

The modeling of the conditional diffusion / reaction term (12.4.2-4) starts from:

$$\begin{aligned}\rho(\boldsymbol{\psi})\left\langle\Theta_A\middle|\boldsymbol{v},\boldsymbol{\psi}\right\rangle = &\left\langle\left(\frac{\partial}{\partial z_j}\rho(\boldsymbol{\psi})D_{Am}\frac{\partial Y_A^{'}}{\partial z_j}\right)\middle|\boldsymbol{v},\boldsymbol{\psi}\right\rangle \\ &+\frac{\partial}{\partial z_j}\rho(\boldsymbol{\psi})D_{Am}\frac{\partial\langle Y_A\rangle}{\partial z_j}+\rho(\boldsymbol{\psi})\tilde{r}_A(\boldsymbol{\psi})\end{aligned} \qquad (12.4.2\text{-}9)$$

As the reaction rate appears in closed form in (12.4.2-9), only a closure model for the conditional diffusion is required. The approaches proposed for closing the conditional acceleration term cannot be used, due to the absence in (12.4.2-9) of

a fluctuating pressure field term which dominates the conditional acceleration (12.4.2-6) at high Reynolds numbers. Furthermore, compositions are usually bounded, i.e., they must remain in an allowable region of composition space. As a result, the concentration fields of the reacting species are non-Gaussian. To describe inert-species micro-mixing, Curl [1963] proposed a model in which two fluid elements with different compositions coalesce and mix upon their encounter before dispersing with identical compositions. A key factor in the coalescence-dispersion model is the frequency of encounters between fluid elements, given by the micro-mixing frequency τ^{-1}(micro-mixing) (12.2-4). The major drawback of the coalescence-dispersion model is the discontinuous behavior of the species concentration field during each mixing event. Villermaux and Devillon [1972] and Dopazo [1975] proposed a deterministic model for closing the conditional diffusion term, the so-called interaction by exchange with the mean (IEM) model, based on linear relaxation of a species concentration towards its mean:

$$\left\langle \left(\frac{\partial}{\partial z_j} D_{Am} \frac{\partial Y_A'}{\partial z_j} \right) \middle| \boldsymbol{\psi} \right\rangle = -\frac{1}{2\tau_Y} \left(\psi_A - \langle Y_A \rangle \right) \qquad (12.4.2\text{-}10)$$

The decay time of the species concentration fluctuations τ_Y (or micro-mixing time, see (12.2-3)) is mostly modeled using the scale-similarity (12.2-4) and (12.2-1). When applying (12.4.2-10) with (12.4.2-2), all species are assumed to mix at the same rate. Extensions of the IEM model accounting for differences in the mixing rate are based on a stochastic description of mixing using a Fokker-Planck equation [Fox, 1999; Fox, 2003]. Furthermore, Fox [1996] showed that the constraint of uncorrelated velocity and species concentration gradients requires the use of a velocity-conditioned VCIEM model, rather than the IEM model:

$$\left\langle \left(\frac{\partial}{\partial z_j} D_{Am} \frac{\partial Y_A'}{\partial z_j} \right) \middle| \boldsymbol{v}, \boldsymbol{\psi} \right\rangle = -\frac{1}{2\tau_Y} \left(\psi_A - \langle Y_A | \boldsymbol{v} \rangle \right) \qquad (12.4.2\text{-}11)$$

The IEM model, (12.4.2-10), does not account for changes in the shape of the PDF during decay. This is of less importance in inhomogeneous species concentration fields, more frequently encountered in practice, where the turbulent species transport often dominates the PDF shape. The qualitatively incorrect behavior of (12.4.2-10) is due to the absence of any information regarding the shape of the PDF, $f(\boldsymbol{v}, \boldsymbol{\psi})$. Indeed, in (12.4.2-10), only the mean $\langle Y_A \rangle$ is used. More advanced models containing information on the shape of $f(\boldsymbol{v}, \boldsymbol{\psi})$ have been proposed by Pope [1976], Janicka et al. [1979], and Dopazo [1979], but for flow with many species, the numerical solution of the resulting nonlinear and

integral nature PDF equation is computationally not tractable. Stochastic models that are computationally less demanding and allow obtaining the same result by simulating the scalar dissipation have been developed by Pope [1982, 1985]. Stochastic mixing models have to reflect the physics of mixing on the molecular scale and the relation between velocity and composition gradients. The composition of a fluid element or particle is changed by molecular exchange with neighboring fluid elements and the correlation between the velocities of interacting fluid elements has to be accounted for. One way of doing this is to bias the amount of mixing according to the difference in velocity between two particles [Pope, 1985].

Due to composition and enthalpy variations when reaction occurs, the density can vary significantly. Using the one-point joint velocity-composition PDF transport equation (12.4.2-2), the terms related to convection, gravity, and the mean pressure gradient, as well as the reaction rates, appear in closed form, irrespective of variations of the density in composition space. Some effects of the variable density on the conditional expectations (12.4.2-3) and (12.4.2-4) should be considered, however.

The behavior of $f(\boldsymbol{v},\boldsymbol{\psi})$ near the wall should be appropriately described. Boundary conditions to be imposed at walls have been developed by Dreeben and Pope [1997a, 1997b, 1998]. Details can also be found in Pope [2000] and Fox [2003].

A somewhat less computationally demanding approach for calculating the composition field is based on the one-point joint composition PDF, $f(\boldsymbol{\psi})$, instead of the one-point joint velocity-composition PDF, $f(\boldsymbol{v},\boldsymbol{\psi})$. With this approach, information on the turbulent flow / velocity field must be provided by appropriate flow, turbulence, scalar-flux and micro-mixing models. The reaction rate can still be exactly dealt with. A one-point joint composition PDF transport equation similar to the one-point joint velocity-composition PDF transport equation, (12.4.2-2), can be derived. For statistically stationary flow:

$$\frac{\partial \rho(\boldsymbol{\psi}) v_i f(\boldsymbol{\psi})}{\partial z_i} + \frac{\partial}{\partial z_i}\left[\rho(\boldsymbol{\psi})\langle u_i' | \boldsymbol{\psi}\rangle f(\boldsymbol{\psi})\right] = -\frac{\partial}{\partial \psi_A}\left[\langle \Theta_A | \boldsymbol{\psi}\rangle \rho(\boldsymbol{\psi}) f(\boldsymbol{\psi})\right] \tag{12.4.2-12}$$

The conditional diffusion / reaction term can be closed with the previously presented models. An additional unclosed term appears,

$$\frac{\partial}{\partial z_i}\left[\rho(\boldsymbol{\psi})\langle u_i' | \boldsymbol{\psi}\rangle f(\boldsymbol{\psi})\right]$$

which is the turbulent scalar flux or the scalar-conditioned velocity, commonly modeled using a gradient-diffusion assumption:

$$\frac{\partial}{\partial z_i}\left[\rho(\boldsymbol{\psi})\left\langle u_i'|\boldsymbol{\psi}\right\rangle f(\boldsymbol{\psi})\right] = -\frac{\partial}{\partial z_i}\left(\rho(\boldsymbol{\psi}) D_t \frac{\partial f(\boldsymbol{\psi})}{\partial z_i}\right) \qquad (12.4.2\text{-}13)$$

The turbulent viscosity μ_t required to calculate the turbulent diffusivity D_t is to be calculated from a CFD turbulence model, as described in Section 12.5. The applicability of (12.4.2-13) to variable-density flows is questionable, however.

12.5 MICRO-PDF MOMENT METHODS: COMPUTATIONAL FLUID DYNAMICS

The integration of the transport equation, (12.4.2-2), for the one-point joint velocity-composition micro-PDF, *f*, is tedious. Also, comparison with measured data is usually only possible at the level of certain moments of *f*. An approach often tried to reduce the computation, is to derive and solve the transport equations for a limited number of moments of *f*. In what follows, *f* will be simply referred to as the micro-PDF. Micro-PDF moment methods are also called Computational Fluid Dynamics (CFD) methods and have been extensively developed over the last decades [Anderson, 1995; Hirsch, 2007].

The transport equations for moments of the micro-PDF can be derived starting from the Navier-Stokes equations or also from the micro-PDF transport equation and involves formal integration or Reynolds-averaging over all turbulence or micro-mixing scales. Closure problems occur with higher-order moments of the micro-PDF. Additional closure problems may occur with the boundary conditions. CFD usually focuses on the calculation of the first- and second-order moments of the micro-PDF, as defined in (12.4.1-3) and (12.4.1-6). The corresponding dissipation rates, that is, of turbulence, turbulent species transport, and concentration correlations, are also calculated. Often, only some functions of a limited number of second-order moments of the micro-PDF are calculated, as for example the turbulent kinetic energy *k*. The calculation of higher-order moments of the micro-PDF is computationally demanding so that these are usually modeled in terms of the first- and second-order moments. This is often challenging and the resulting accuracy is sometimes questionable, in particular for complex reaction kinetics. An overview of the present section on CFD is given in Figure 12.5-1.

CFD starts from the Reynolds-Averaged Navier-Stokes (RANS) equations for the calculation of the macro-scale behavior expressed by the macro-scale averaged, also called Reynolds-averaged or mean variables — the

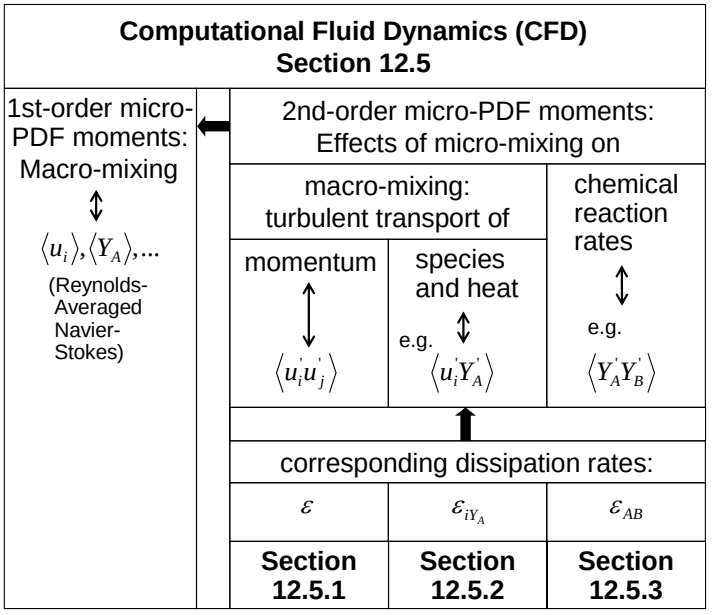

Figure 12.5-1

Computational Fluid Dynamics (CFD): Section overview. Micro-PDF: one-point joint velocity-composition micro-PDF.

first-order moments of the micro-PDF. The second- and eventually higher-order moments of the micro-PDF that appear in the RANS equations reflect and allow accounting for the influence of micro-mixing on the macro-scale behavior, i.e., on macro-mixing and the macro-scale averaged reaction rates.

In variable-density flow, density-based Favre-averaging is frequently applied [Favre, 1965]. The Favre-averaged velocity is defined as:

$$\langle \tilde{u}_i \rangle = \frac{\langle \rho u_i \rangle}{\langle \rho \rangle}, \tag{12.5-1}$$

implying:

$$\langle \tilde{u}_i' \rangle \neq 0 \tag{12.5-2}$$

Similarly, a Favre-averaged species mass fraction is defined by:

$$\langle \tilde{Y}_A \rangle = \frac{\langle \rho Y_A \rangle}{\langle \rho \rangle} \tag{12.5-3}$$

In what follows, no distinction is made between Reynolds- and Favre-averaging.

For statistically stationary flow, formally Reynolds-averaging the Navier-Stokes equations yields for the continuity equation for a species *A*:

$$\frac{\partial\langle C_A\rangle\langle u_j\rangle}{\partial z_j}+\frac{\partial\langle u_j' C_A'\rangle}{\partial z_j}=\frac{\partial}{\partial z_j}D_{Am}\frac{\partial\langle C_A\rangle}{\partial z_j}+\langle r_A(\boldsymbol{C})\rangle \qquad (12.5\text{-}4a)$$

The species concentrations are expressed in terms of their molar concentrations $\boldsymbol{C_A}$. Alternatively, using species mass fractions $\boldsymbol{Y}$:

$$\frac{\partial\rho\langle Y_A\rangle\langle u_j\rangle}{\partial z_j}+\frac{\partial\rho\langle u_j' Y_A'\rangle}{\partial z_j}=\frac{\partial}{\partial z_j}\rho D_{Am}\frac{\partial\langle Y_A\rangle}{\partial z_j}+\rho\langle\tilde{r}_A(\boldsymbol{Y})\rangle \qquad (12.5\text{-}4b)$$

The total mass continuity equation becomes:

$$\frac{\partial\rho\langle u_j\rangle}{\partial z_j}=0 \qquad (12.5\text{-}5)$$

The momentum continuity equation becomes:

$$\frac{\partial\rho\langle u_i\rangle\langle u_j\rangle}{\partial z_j}=-\frac{\partial\langle P\rangle}{\partial z_i}+\frac{\partial\langle\tau_{ji}\rangle}{\partial z_j}+\rho g_i-\frac{\partial\rho\langle u_i' u_j'\rangle}{\partial z_j} \quad \text{for: } i=1,2,3 \qquad (12.5\text{-}6)$$

with the stress tensor defined by (12.3-4).

The Reynolds-averaged total energy continuity equation is:

$$\begin{aligned}&\frac{\partial}{\partial z_j}\left[\langle u_j\rangle\left(\rho\langle E\rangle+\langle P\rangle\right)\right]=\frac{\partial}{\partial z_j}\lambda_m\frac{\partial\langle T\rangle}{\partial z_j}+\frac{\partial}{\partial z_j}\left[\langle u_i\rangle\langle\tau_{ji}\rangle\right]\\&-\frac{\partial\rho\langle E'u_j'\rangle}{\partial z_j}-\frac{\partial\langle P'u_j'\rangle}{\partial z_j}+\frac{\partial\langle u_i'\tau_{ij}'\rangle}{\partial z_j}+\rho\langle u_i\rangle g_i\end{aligned} \qquad (12.5\text{-}7a)$$

or:

$$\begin{aligned}&\rho\langle u_j\rangle\left[\left(\frac{\partial\langle e_{kin}\rangle}{\partial z_j}\right)+\left(c_p\frac{\partial\langle T\rangle}{\partial z_j}\right)\right]\\&=\frac{\partial}{\partial z_j}\lambda_m\frac{\partial\langle T\rangle}{\partial z_j}+\frac{\partial}{\partial z_j}\left[\langle u_i\rangle\langle\tau_{ji}\rangle\right]-\rho\left\langle u_j'\frac{\partial e_{kin}'}{\partial z_j}\right\rangle-\rho\left\langle u_j' c_p\frac{\partial T'}{\partial z_j}\right\rangle\\&+\frac{\partial\langle u_i'\tau_{ij}'\rangle}{\partial z_j}+\rho\langle u_i\rangle g_i+\sum_k(-\Delta H_k)\langle r_k\rangle\end{aligned} \qquad (12.5\text{-}7b)$$

in which the heat of reaction explicitly appears.

As already mentioned in Section 12.3, the unclosed correlation terms that appear in the RANS equations are the Reynolds-stresses

$$\left\langle u_i' u_j' \right\rangle$$

representing turbulent momentum transport, the scalar fluxes

$$\left\langle u_j' Y_A' \right\rangle$$

representing turbulent species transport, another scalar flux

$$\left(\rho \left\langle E' u_j' \right\rangle + \left\langle P' u_j' \right\rangle\right)$$

representing turbulent enthalpy or heat transport, and eventually the species concentration correlation terms

$$\left\langle Y_A' Y_B' \right\rangle$$

resulting from the macro-scale averaged reaction rates $\left\langle \tilde{r}_A(\boldsymbol{Y}) \right\rangle$. Their calculation is discussed in the next sub-sections. Higher-order moments of the micro-PDF may also occur, depending on the complexity of the reaction kinetics.

In solving the RANS equations, particular attention should be paid to the modeling of the boundary conditions at the wall. The mean velocity field has to satisfy the no-slip condition. The near-wall region is characterized by steep gradients in the mean velocity field. Resolving the near-wall behavior requires low-Reynolds turbulence models and sufficient grid refinement. The near-wall region can be subdivided into three layers. These are, from the wall onwards: (i) the viscous sublayer in which the flow is almost laminar, (ii) a buffer layer or blending region where the effects of molecular viscosity and turbulence are equally important, and (iii) the fully-turbulent layer. Wall functions can be used to bridge the viscosity-affected inner region, that is, the viscous sublayer and the buffer layer. Wall functions are popular, due to their robustness and reasonable accuracy although the hypotheses underlying the wall functions have to be verified for each particular case. The value of the wall shear stress τ_w can be calculated from the well known logarithmic law [Hinze, 1959; Schlichting, 1979]:

$$\frac{\langle u \rangle}{u_\tau} = \frac{1}{\kappa} \ln\left[\frac{y_1 u_\tau}{\nu} E\right] \quad \text{with:} \quad \tau_w = u_\tau^2 \, \rho_g \tag{12.5-8}$$

y_1 is the distance to the wall, E is an empirical constant and κ is the von Karman constant. The logarithmic law is valid for values of $y^+ = y_1 u_\tau / \nu$ around 50.

Approaches for calculating the near-wall behavior of the turbulence and related correlation terms are discussed in Section 12.5.1.

12.5.1 Turbulent Momentum Transport. Modeling of the Reynolds-Stresses

In the RANS-approach, turbulence or turbulent momentum transport models are required to calculate the Reynolds-stresses. This can be done starting from additional transport equations, the so-called Reynolds-stress models. Alternatively, the Reynolds-stresses can be modeled in terms of the mean values of the variables and the turbulent kinetic energy, the so-called turbulent viscosity based models. In either way, the turbulence dissipation rate has to be calculated also, as it contains essential information on the overall decay time of the velocity fluctuations. In what follows, the more popular models based on the turbulent viscosity are focused on. A detailed description of the Reynolds-stress models is given in Annex 12.5.1.A which can be downloaded from the Wiley web-page.

Turbulent viscosity based models start from the Boussinesq hypothesis [1877] relating the Reynolds stresses to the mean velocity gradients, the turbulent kinetic energy k and the turbulent viscosity μ_t:

$$-\rho\left\langle u_i' u_j' \right\rangle = -\frac{2}{3}\left(\rho k + \mu_t \frac{\partial \langle u_i \rangle}{\partial z_i} \right)\delta_{ij} + \mu_t \left(\frac{\partial \langle u_i \rangle}{\partial z_j} + \frac{\partial \langle u_j \rangle}{\partial z_i} \right) \qquad (12.5.1\text{-}1)$$

The turbulent kinetic energy k is defined as:

$$k = \frac{1}{2}\left\langle u_i' u_i' \right\rangle \qquad (12.5.1\text{-}2)$$

and can be calculated by taking the trace of the Reynolds stress tensor.

Using (12.5.1-1), the Reynolds-averaged momentum equation for statistically stationary flow, (12.5-6), reduces to:

$$\frac{\partial \rho \langle u_i \rangle \langle u_j \rangle}{\partial z_j} = -\frac{\partial}{\partial z_i}\left(\langle P \rangle + \frac{2}{3}\rho k \right) + \frac{\partial \langle \tau_{ji} \rangle_{eff}}{\partial z_j} + \rho g_i \qquad (12.5.1\text{-}3)$$

for: $i = 1, 2, 3$

with

$$\langle \tau_{ji} \rangle_{eff} = \mu_{eff}\left(\frac{\partial \langle u_i \rangle}{\partial z_j} + \frac{\partial \langle u_j \rangle}{\partial z_i} - \frac{2}{3}\delta_{ij}\frac{\partial \langle u_l \rangle}{\partial z_l} \right) \qquad (12.5.1\text{-}4)$$

The isotropic stress term, $2\rho k\delta_{ij}/3$, is combined with the mean pressure to form a modified or effective mean pressure. The effective viscosity μ_{eff} is the sum of the molecular and turbulent viscosities:

$$\mu_{eff} = \mu + \mu_t \tag{12.5.1-5}$$

which are independent of each other.

The calculation of the six components of the Reynolds stress tensor, that is, six second-order moments of the micro-PDF, $f(\boldsymbol{v},\boldsymbol{\psi})$, is reduced to the calculation of k and the modeling of the turbulent viscosity μ_t. As seen from (12.5.1-2), k is a function of a limited number of second-order moments of the micro-PDF. Turbulent viscosity based closure models for the Reynolds-stresses can be used at relatively low computational effort. In the two-equation model approach, the turbulent viscosity is expressed in terms of the turbulent kinetic energy, k, and the turbulence dissipation rate, ε, according to:

$$\mu_t = C_\mu \rho \frac{k^2}{\varepsilon} \tag{12.5.1-6}$$

Two additional transport equations, respectively for k and for ε, are then to be solved [Jones and Launder, 1972; Launder and Spalding, 1972; Launder and Sharma, 1974].

The transport equation for the turbulent kinetic energy is obtained by summing up the diagonal elements of the Reynolds stresses:

$$\begin{aligned} &\frac{\partial \rho k \langle u_i \rangle}{\partial z_i} + \frac{1}{2}\frac{\partial \rho \langle u_j' u_j' u_i' \rangle}{\partial z_i} + \frac{\partial \langle u_i' P \rangle}{\partial z_i} \\ &= \mathrm{P}_k + \frac{\partial}{\partial z_i}\mu\frac{\partial k}{\partial z_i} + \frac{\partial}{\partial z_i}\mu\frac{\partial \langle u_i' u_j' \rangle}{\partial z_j} + B_k - \rho\varepsilon \end{aligned} \tag{12.5.1-7}$$

in which:

$$\mathrm{P}_k = -\rho \langle u_i' u_j' \rangle \frac{\partial \langle u_i \rangle}{\partial z_j} \tag{12.5.1-8}$$

represents the turbulent kinetic energy production; B_k represents the buoyancy production of turbulent kinetic energy, i.e., due to gravity, defined similar to (12.5.1.A-8) (Annex 12.5.1.A: web-page access).

The turbulent kinetic energy transport equation (12.5.1-7) contains unclosed terms that need to be modeled. A standard closure model is:

$$\frac{1}{2}\frac{\partial\rho\left\langle u_j' u_j' u_i'\right\rangle}{\partial z_i}+\frac{\partial\left\langle u_i' P\right\rangle}{\partial z_i}-\frac{\partial}{\partial z_i}\mu\frac{\partial k}{\partial z_i}-\frac{\partial}{\partial z_i}\mu\frac{\partial\left\langle u_i' u_j'\right\rangle}{\partial z_j}=-\frac{\partial}{\partial z_i}\left(\frac{\mu_t}{\sigma_k}\frac{\partial k}{\partial z_i}\right) \tag{12.5.1-9}$$

It allows the turbulent kinetic energy transport equation (12.5.1-7) to be reduced to:

$$\frac{\partial\rho k\left\langle u_i\right\rangle}{\partial z_i}=\frac{\partial}{\partial z_i}\left[\left(\mu+\frac{\mu_t}{\sigma_k}\right)\frac{\partial k}{\partial z_i}\right]+\mathrm{P}_k+B_k-\rho\varepsilon \tag{12.5.1-10}$$

σ_k is the model parameter [Jones and Launder, 1972; Launder and Spalding, 1972; Launder and Sharma, 1974]. At high Reynolds numbers, the contribution of molecular viscosity can be neglected.

Turbulence due to gravity can be modeled as:

$$B_k=\beta g_i\frac{\mu_t}{\mathrm{Pr}_t}\frac{\partial T}{\partial z_i} \tag{12.5.1-11}$$

The turbulent Prandtl number Pr_t is defined as

$$\mathrm{Pr}_t=\frac{\mu_t c_P}{\lambda_t} \tag{12.5.1-12}$$

and

$$\beta=-\frac{1}{\rho}\left(\frac{\partial\rho}{\partial T}\right)_P \tag{12.5.1-13}$$

is the thermal expansion coefficient.
For ideal gases:

$$B_k=-g_i\frac{\mu_t}{\rho\,\mathrm{Pr}_t}\frac{\partial\rho}{\partial z_i} \tag{12.5.1-14}$$

A remaining unclosed term in (12.5.1-7) or (12.5.1-10) is the turbulence dissipation rate ε. A transport equation for the latter can be rigorously derived, but it is difficult to close. An alternative semi-empirical transport equation is commonly used. It is derived in analogy with the turbulent kinetic energy transport equation and takes the form:

$$\frac{\partial\rho\varepsilon\left\langle u_i\right\rangle}{\partial z_i}=\frac{\partial}{\partial z_i}\left[\left(\mu+\frac{\mu_t}{\sigma_\varepsilon}\right)\frac{\partial\varepsilon}{\partial z_i}\right]+C_{\varepsilon 1}\frac{\varepsilon}{k}\left(\mathrm{P}_k+C_{\varepsilon 3}B_k\right)-C_{\varepsilon 2}\rho\frac{\varepsilon^2}{k} \tag{12.5.1-15}$$

σ_ε, $C_{\varepsilon 1}$, and $C_{\varepsilon 2}$ are the model parameters to be determined from experimental data [Jones and Launder, 1972; Launder and Spalding, 1972; Launder and Sharma, 1974].

Near the wall, the k-ε model cannot be applied in the viscous sub-layer. Wall functions are needed for the logarithmic layer [Launder and Spalding, 1972]. The turbulence variables near the solid wall are then calculated from:

$$k_{wall} = \frac{u_\tau^2}{\sqrt{C_\mu}} \tag{12.5.1-16}$$

$$\varepsilon_{wall} = \frac{u_\tau^4}{50\kappa\nu} = \frac{u_\tau^3}{\kappa y_1} \tag{12.5.1-17}$$

u_τ is obtained from (12.5-8). For many flow conditions, the physical basis of the wall functions is uncertain and their accuracy insufficient. Alternate approaches exist in which the k-ε transport equations are solved in near-wall grid points, taking into account additional terms reflecting the effects of the wall.

The performance of the standard k-ε model has been found to be acceptable for flow with small mean streamline curvature and mean pressure gradient. The renormalization group (RNG) method based k-ε turbulence model allows to account for the effects of swirl or rotation [Yakhot and Orszag, 1986; Smith and Reynolds, 1992; Orszag et al., 1996; Smith and Woodruff, 1998]. The realizable k-ε model [Shih et al., 1995] uses a different eddy-viscosity formula and a turbulence dissipation rate transport equation based on the dynamic equation of the mean-square vorticity fluctuation. It offers substantially improved performance for rotating homogeneous shear flow, free flow, including jets and mixing layers, channel and boundary layer flow, and separated flow. Wilcox [1993] developed a k-ω model which solves an equation for the turbulence frequency $\omega = \varepsilon / k$ instead of the ε-equation. A significant advantage of the k-ω model with respect to the k-ε model is that it can be applied well into the viscous sub-layer, facilitating the wall treatment. The performance of the k-ω model was shown to be superior to that of the k-ε model for a variety of flows. The accuracy of different turbulence models has been extensively compared in the literature, see for example Bradshaw et al. [1996] and Menter [1994]. Turbulent viscosity based models may perform reasonably well in a number of cases, but for complex flow Reynolds-stress models (Annex 12.5.1.A) have been demonstrated to be superior.

12.5.2 Turbulent Transport of Species and Heat. Modeling of the Scalar Flux

In the RANS-approach, models for turbulent species and heat transport are required to calculate the scalar fluxes $\left\langle u_i' Y_A' \right\rangle$, $\left\langle u_i' E' \right\rangle$ and $\left\langle u_i' P' \right\rangle$, appearing in (12.5-4b) and (12.5-7a). Similar to the Reynolds-stresses, the scalar fluxes can be calculated from additional transport equations, the so-called scalar flux models. Alternatively, the scalar fluxes can be modeled in terms of the mean values of the variables and the turbulent diffusivity / conductivity. In many practical cases, the scalar-flux dissipation rate can be shown to be negligible. In what follows, the more frequently used models based on the turbulent diffusivity / conductivity are focused on. Details on the scalar flux models can be found in Annex 12.5.2.A, available via the Wiley web-page.

Turbulent diffusivity based closure models for the scalar fluxes describing turbulent transport of species relate the scalar flux to the mean species concentration gradient according to Reynolds' analogy between turbulent momentum and mass transport. The standard gradient-diffusion model can be written:

$$\left\langle u_i' Y_A' \right\rangle = -D_t \frac{\partial \left\langle Y_A \right\rangle}{\partial z_i} \tag{12.5.2-1}$$

with:

$$D_t = \frac{\mu_t}{\rho Sc_t} \tag{12.5.2-2}$$

The turbulent diffusivity, D_t, is assumed to be proportional to the turbulent viscosity. Sc_t is the turbulent Schmidt number with a typical value of 0.7. Equation (12.5.2-1) assumes that the scalar flux and the mean species concentration gradient are aligned, in contrast with the scalar flux model (Annex 12.5.2.A). This is strictly valid only for isotropic turbulence. Nevertheless, (12.5.2-1) is frequently applied in CFD codes.

Accounting for (12.5.2-1), the Reynolds-averaged species continuity equation for statistically stationary flow, (12.5-4b), reduces to:

$$\frac{\partial \rho \left\langle Y_A \right\rangle \left\langle u_j \right\rangle}{\partial z_j} = \frac{\partial}{\partial z_j} \rho D_{A\_eff} \frac{\partial \left\langle Y_A \right\rangle}{\partial z_j} + \rho \left\langle \tilde{r}_A (\boldsymbol{Y}) \right\rangle \tag{12.5.2-3}$$

The effective diffusivity is the sum of the molecular and turbulent diffusivities:

$$D_{eff} = D_m + D_t \tag{12.5.2-4}$$

The turbulent diffusivity is independent of the molecular diffusivity and, in general, several orders of magnitude larger.

Turbulent heat transfer is commonly modeled using Reynolds' analogy to turbulent momentum transfer. Equation (12.5-7a) then becomes:

$$\frac{\partial}{\partial z_j}\left[\langle u_j\rangle\left(\rho\langle E\rangle+\langle P\rangle\right)\right] = \frac{\partial}{\partial z_j}\lambda_{eff}\frac{\partial\langle T\rangle}{\partial z_j}+\frac{\partial}{\partial z_j}\left[\langle u_i\rangle\langle\tau_{ji}\rangle_{eff}\right]+\rho\langle u_i\rangle g_i \tag{12.5.2-5}$$

with $<\tau_{ji}>_{eff}$ defined as in (12.5.1-4).

The effective conductivity λ_{eff} is the sum of the molecular and the turbulent conductivity:

$$\lambda_{eff} = \lambda_m + \lambda_t\,, \tag{12.5.2-6}$$

with:

$$\lambda_t = \frac{c_P\,\mu_t}{\mathrm{Pr}_t} \tag{12.5.2-7}$$

Pr_t is the turbulent Prandtl number with a typical value of 0.85.

In the thermal conduction sublayer near solid walls, a linear law can be used. In the turbulent near-wall region, Reynolds' analogy between momentum and energy transport allows to derive a logarithmic law for the mean temperature, similar to (12.5-8). In general, the thickness of the thermal conduction layer differs from the thickness of the viscous sublayer and depends on the physico-chemical properties of the fluid. The thermal sublayer thickness can be estimated from the intersection between the linear law and the logarithmic law.

12.5.3 Macro-Scale Averaged Reaction Rates

Defining the macro-scale averaged reaction rate in (12.5-4b) is straightforward only in some special cases, i.e., for zero- or first-order reactions carried out under isothermal conditions or for slow reactions, when only the mean species concentrations have to be considered. For non-linear reaction rates and relatively fast reactions, the effect of micro-mixing on the macro-scale averaged reaction rates has to be accounted for. As shown in Section 12.4, this can be done starting from the one-point joint (velocity-) composition micro-PDF. Computationally less demanding micro-PDF moment methods have been considered. Second-order micro-PDF moment methods calculate the scalar variances, $\left\langle Y_A^{'}Y_A^{'}\right\rangle$, and covariances, $\left\langle Y_A^{'}Y_B^{'}\right\rangle$, from additional transport equations. For general, nonlinear

reaction rates, micro-PDF moment methods face, however, a variety of closure problems. Some details are given in Annex 12.5.3.A. The present section focuses on frequently used phenomenological models, i.e., the Eddy Dissipation Concept (EDC) and Eddy Break-Up (EBU) closure models. In general, the different methods require the (joint) scalar dissipation rate (Fig. 12.5-1). The latter contains essential information on the micro-mixing time (12.2-3), the decay time of the species concentration or other scalar fluctuations. At high Reynolds numbers, the scale similarity model (12.2-4) is often used in CFD calculations (Spalding, 1971; Béguier et al., 1978).

12.5.3.1 Models Based upon the Concept of Eddy Dissipation

The present and the next sections address phenomenological models accounting for the effects of micro-mixing on the macro-scale averaged reaction rates. These models do not start from the one-point joint velocity-composition micro-PDF, $f(\boldsymbol{v},\boldsymbol{\psi})$, and do not require micro-PDF moments other than first-order for the species concentration variables. They are in general less accurate, but computationally less demanding than micro-PDF or its moments based methods.

In the Eddy Dissipation Concept (EDC) model, a distinction is made between the large and small scale structures of the fluid. Reactions are assumed to occur in the small scale structures only. In these Batchelor scale structures, mixing down to the molecular level is fast compared to the rate of the reactions so that these are rate-determining. Micro-mixing determines the rate at which small scale structures are formed from large scale (scalar integral scale) structures. In the EDC model, micro-mixing effects are quantified by the mass fraction of the small scale structures, m^S, and the specific transfer rate from the large to the small scale structures, r_t, which is directly related to the micro-mixing rate. The mean mass fractions of the species, $\langle Y_A \rangle$, are related to the mass fractions of the species in the large scale structures, Y^L, and in the small scale structures, Y^S, as:

$$\langle Y_A \rangle = m^S \, Y_A^S + \left[1 - m^S\right] Y_A^L \qquad (12.5.3.1\text{-}1)$$

The reaction rates are calculated at the conditions in the small scale structures.

Applying a turbulent energy cascade model, Ertesvåg and Magnussen [2000] derived expressions for m^S and r_t in terms of the turbulent kinetic energy k and the turbulence dissipation rate ε :

$$m^S = 2.43\left(\frac{\varepsilon}{\nu}\right)^{0.5} \qquad (12.5.3.1\text{-}2)$$

$$r_t = 9.66\left(\frac{\nu\,\varepsilon}{k^2}\right)^{0.75} \qquad (12.5.3.1\text{-}3)$$

The latter can be calculated from a turbulence model, as explained in Section 12.5.1.

In statistically steady state, the species balance equation over the small scale structures expresses the species transfer rate between the large and the small scale structures compensating the reaction rate:

$$r_t\left[Y_A^S - Y_A^L\right] = \frac{r_A^S\,M_A}{\rho^S} \qquad (12.5.3.1\text{-}4)$$

where molar reaction rates are used, [kmol A/(m^3 small scale · s)]. Using (12.5.3.1-1), equation (12.5.3.1-4) can be rewritten as:

$$\frac{r_t}{[1-m^S]}\left[Y_A^S - \langle Y_A\rangle\right] = \frac{r_A^S\,M_A}{\rho^S} \qquad (12.5.3.1\text{-}5)$$

Generally, (12.5.3.1-5) is a non-linear algebraic equation in Y_A^S. The Reynolds-averaged species balance equations and the algebraic small scale structure balance equations (12.5.3.1-5) are to be solved simultaneously with m^S and r_t as an input from the turbulence model. The macro-scale averaged net reaction rates, in [kmol A/(m$_r^3$ s)], accounting for micro-mixing effects and required for the calculation of the Reynolds-averaged species balance equations (12.5-4b), are obtained from:

$$\langle r_A\rangle = \frac{m^S\langle\rho\rangle}{\rho^S}\,r_A^S \qquad (12.5.3.1\text{-}6)$$

A steady state energy balance equation over the small scale structures can be derived in a similar way. Assuming that radiative and diffusive heat transfer between the large and small scale structures can be neglected the result is:

$$\frac{r_t}{[1-m^S]}\left[\sum_A\left[Y_A^S\,h_A^S - \langle Y_A\rangle\langle h_A\rangle\right]\right] = 0 \qquad (12.5.3.1\text{-}7)$$

12.5.3.2 The Eddy Break-Up Model

The Eddy Break-Up (EBU) model considers either micro-mixing or the reactions to be rate-determining. The micro-mixing rate and the intrinsic reaction rate, i.e.,

assuming perfect micro-mixing, are calculated and the lowest of the two is taken to be the effective, that is, macro-scale averaged reaction rate:

$$r_{eff} = \min\left[r_A,\, r(\text{micro}-\text{mixing})\right] \qquad (12.5.3.2\text{-}1)$$

The original EBU model proposed by Spalding [1971] calculates the micro-mixing rate for a single second-order irreversible reaction from:

$$r(\text{micro}-\text{mixing}) = \rho C_{EBU} \frac{\varepsilon}{k} \sqrt{\left\langle Y_A^{'2} \right\rangle} \qquad (12.5.3.2\text{-}2)$$

where C_{EBU} is a model parameter and $Y_A^{'}$ is the fluctuating mass fraction of the species A (compare (12.5.3.2-2) to (12.2-1), (12.2-2) and (12.2-4)). The calculation of $\left\langle Y_A^{'2} \right\rangle$ is treated in Annex 12.5.3.A, but is not straightforward. Magnussen and Hjertager [1976] proposed an expression for the micro-mixing rate in terms of the mean species mass fractions, omitting the calculation of $\left\langle Y_A^{'2} \right\rangle$. A major limitation of the EBU model is that it can only be used with irreversible reactions. With reversible reactions, micro-mixing determined macro-scale averaged reaction rates can drive the reaction in a direction opposite to the one imposed by the reaction thermodynamics, that is, away from chemical equilibrium. For a more extensive discussion on the limitations of the EBU model, reference is made to Brink et al. [2000].

EXAMPLE 12.5.A

THREE DIMENSIONAL CFD SIMULATION OF FURNACE AND REACTOR TUBES FOR THE THERMAL CRACKING OF HYDROCARBONS

Detemmerman and Froment [1998] carried out a three dimensional coupled CFD simulation of furnaces and reactor tubes for the millisecond thermal cracking of propane into ethylene in the presence of steam, a process already discussed in Chapters 1 and 9.

A Kellogg thermal cracking furnace is shown in Fig. 12.5.A-1. It contains 160 straight reactor tubes on a single row in the center plane of the furnace. Each reactor tube is internally, helicoidally finned. After the radiation section, the process gas flows through an adiabatic connection, uniting four reactor tubes, before reaching the quenches. The radiation section of the furnace is heated by 40 burners, positioned in the bottom plate. These burners are rectangular boxes through which air flows, while the fuel gas, a mixture of methane and hydrogen, is fed through a rectangular slit in the center of the box. To limit the computational effort, the calculations focus on a furnace element containing one of the 40 flames, as illustrated in Fig. 12.5.A-1.

The coupled furnace-reactor simulation requires an accurate description of the heat transfer from the furnace to the reactor. The global radiative heat transfer from the furnace to the reactor was calculated by the zone method (Fig. 12.5.A-2, Left) proposed by Hottel and Sarofim [1967]. To take into account the local influence of radiative heat transfer, CFD simulations of the furnace were carried out using a radiative heat transfer model for short distances [De Marco and Lockwood, 1975]. Knowledge of the local flue gas composition is required to calculate the heat release by combustion in each flue gas volume element and the absorption coefficients for radiation. Coupled CFD simulations of the reactor tubes and furnace predict the process gas conversion and the product yields, as well as coke formation rates.

For the calculation of the global radiative heat transfer from the furnace to the reactor, the former is divided into isothermal surface and volume zones (Fig. 12.5.A-2). Because of the symmetry, only one fourth of the furnace has to

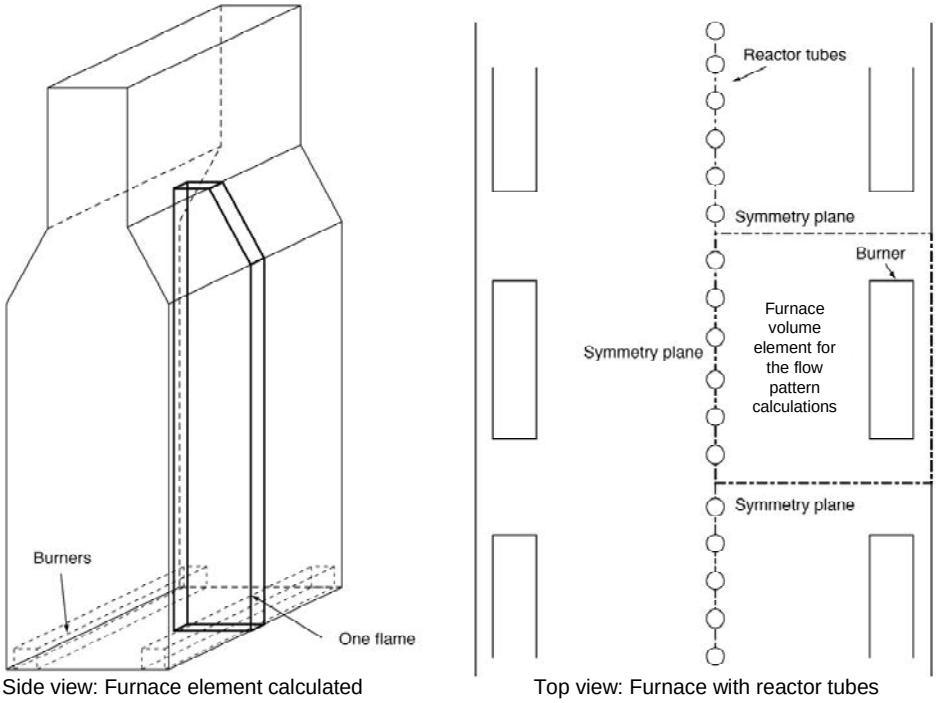

Side view: Furnace element calculated

Top view: Furnace with reactor tubes

Figure 12.5.A-1

Side and top view of a thermal cracking furnace with straight parallel reactor tubes.

be considered. It contains 40 gas volume zones, 68 furnace wall zones, and 400 reactor tube zones. An energy balance is constructed for each zone, accounting also for the heat exchange between the different zones. The total exchange area between two zones, which is the amount of radiative heat emitted by the first zone and absorbed by the second, divided by the black body emissive power, are calculated from the view factors in a diathermal medium, taking into account absorption of heat and reflection on the surface zones. The view factors are determined by means of a Monte-Carlo simulation method. Absorption by the flue gas is expressed via the band model of Edwards. Reflection of heat is incorporated via a matrix algorithm developed by Hottel [Hottel and Sarofim, 1967]. See Vercammen and Froment [1978, 1980], Rao et al. [1988] and Plehiers and Froment [1989] for details.

Both the simulation model for the detailed calculation of the flue gas pattern in the furnace and the process gas pattern in the cracking tubes are based on the Reynolds-Averaged Navier-Stokes mass, momentum, energy, and species balance equations described in Section 12.5. Turbulent momentum, species, and

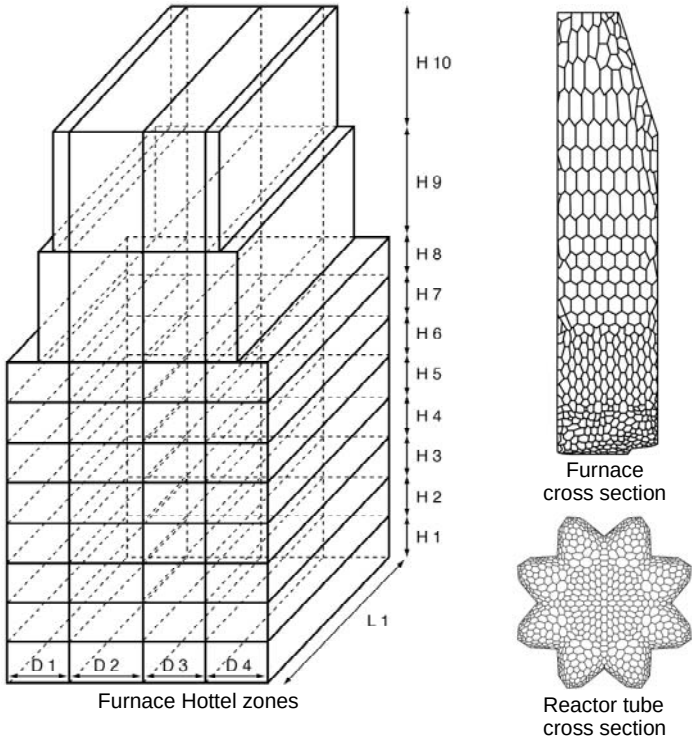

Figure 12.5.A-2

Left: Division of the furnace into Hottel zones for the furnace calculation. Right: Two-dimensional cross section of the non-structured furnace and reactor tube integration grids.

heat transport are accounted for through the turbulent viscosity, diffusivity, and conductivity models described in Sections 12.5.1 and 12.5.2. The standard k-ε model is used for the calculation of the turbulence properties.

A source term Q_{rad} is added to the right-hand-side of the energy balance equation (12.5-7), representing the radiation heat received per unit volume furnace. It is calculated from:

$$Q_{rad} = \int_{4\pi} \frac{\partial}{\partial z_j}\left(I\,\Omega_j\right) d\Omega \qquad \text{(12.5.A-a)}$$

where I is the radiation intensity. In the six flux model proposed by De Marco and Lockwood [1975], a generalized distribution for the radiation intensity

$$I = A_x \cdot \Omega_x + A_y \cdot \Omega_y + A_z \cdot \Omega_z + B_x \cdot \Omega_x^2 + B_y \cdot \Omega_y^2 + B_z \cdot \Omega_z^2 \qquad \text{(12.5.A-b)}$$

is substituted into the integro-differential intensity equation

$$\frac{\partial}{\partial z_j}\left(I\,\Omega_j\right) = -k_g I + k_g \frac{\sigma T^4}{\pi} \qquad \text{(12.5.A-c)}$$

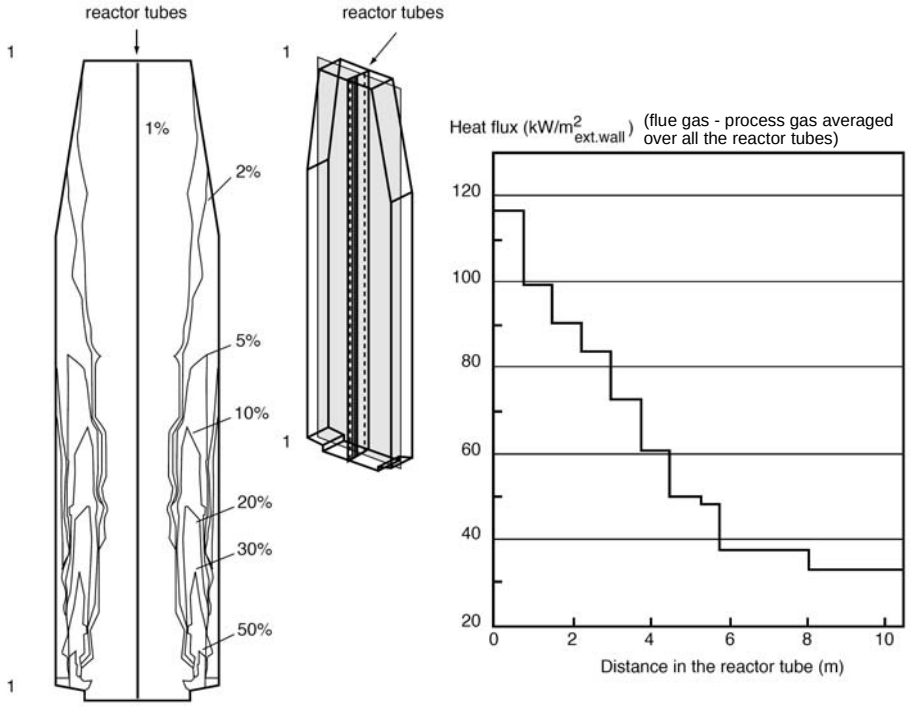

Figure 12.5.A-3

Left: Residual methane percentage in a two-dimensional cross section of the furnace. Right: Heat flux, flue gas - process gas averaged over all the reactor tubes.

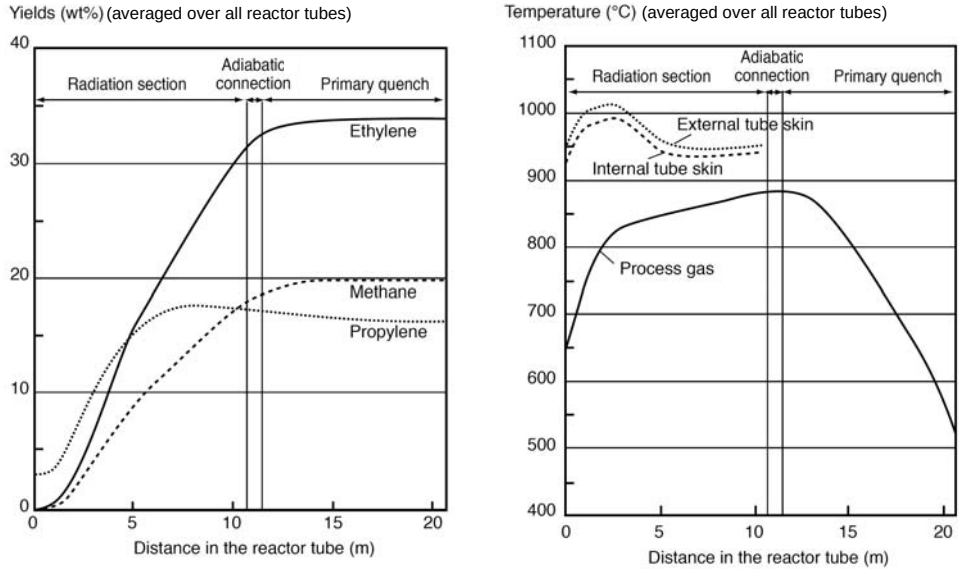

Figure 12.5.A-4

Methane, ethylene and propylene yields (Left) and temperature profiles (Right), averaged over all reactor tubes.

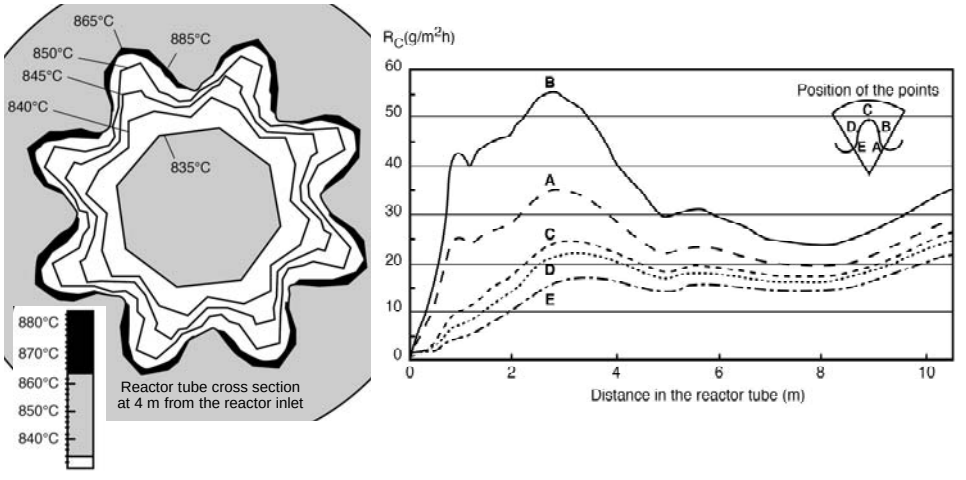

Figure 12.5.A-5

Left: Isotherms in a cross section of the reactor tube at 4 m from the reactor inlet. Right: Initial coking rate profiles for several points of a cross section of the reactor tube.

Equation (12.5.A-c) expresses that net changes in the radiation intensity result from flue gas absorption and emission. k_g is the radiation absorption coefficient [m^{-1}]. Equations for the coefficients A and B in (12.5.A-b) are obtained by integration of (12.5.A-c) over six segments of the total solid angle

4π. In solving the intensity equation, the tube skin and furnace wall temperatures are considered as fixed boundary conditions. After a coupled simulation of the furnace and reactor, improved tube skin and furnace wall temperatures are obtained by means of an iterative cycle.

For the combustion of the fuel gas in the furnace, the following reaction scheme was assumed:

$$CH_4 + \frac{3}{2}O_2 \overset{1}{\rightarrow} CO + 2H_2O$$

$$CO + \frac{1}{2}O_2 \overset{2}{\rightarrow} CO_2$$

$$H_2 + \frac{1}{2}O_2 \overset{3}{\rightarrow} H_2O$$

The kinetic equations were taken from Dryer and Glasman [1973]:

$$r_{1,k} = 10^{7.2} \exp\left[-\frac{202600}{RT}\right] C_{CH_4}^{0.7} C_{O_2}^{0.8}$$

$$r_{2,k} = 10^{8.6} \exp\left[-\frac{167500}{RT}\right] C_{CO} C_{H_2O}^{0.5} C_{O_2}^{0.25} \qquad \text{(12.5.A-d)}$$

$$r_{3,k} = +\infty$$

The rate of combustion of hydrogen was assumed to be infinite. Combustion reactions are relatively fast so that micro-mixing limitations have to be accounted for. The Eddy Break-Up model [Spalding, 1972], presented in Section 12.5.3.2, was applied. Using (12.2-4) with a value for C_Y of 4, the following mixing rates were obtained for the combustion reactions 1, 2, 3:

$$r_{1,m} = 4\rho \frac{\varepsilon}{k} \min\left(Y_{CH_4}, 0.33 Y_{O_2}\right)$$

$$r_{2,m} = 4\rho \frac{\varepsilon}{k} \min\left(Y_{CO}, 1.75 Y_{O_2}\right) \qquad \text{(12.5.A-e)}$$

$$r_{3,m} = 4\rho \frac{\varepsilon}{k} \min\left(Y_{H_2}, 0.13 Y_{O_2}\right)$$

Micro-mixing and combustion occur sequentially so that mixing and reaction times can be added up, leading to overall rates:

$$r_{1,t} = \left(\frac{1}{r_{1,k}} + \frac{M_{CH_4}}{r_{1,m}} \right)^{-1}$$

$$r_{2,t} = \left(\frac{1}{r_{2,k}} + \frac{M_{CO}}{r_{2,m}} \right)^{-1} \qquad \text{(12.5.A-f)}$$

$$r_{3,t} = \frac{r_{3,m}}{M_{H_2}}$$

The kinetics of the cracking reactions in the reactor tubes were expressed in terms of a radical reaction scheme, presented in Chapter 1 and already applied in Chapter 9. For the cracking of light hydrocarbons, 1200 elementary reaction steps between 128 species were considered, implying the solution of a stiff set of 128 continuity equations for the reacting species in addition to the total mass, momentum, and energy equations.

Fig. 12.5.A-3 (Left) shows the residual methane percentage in the flue gases. 50% of the methane is consumed directly above the burner, but a significant amount is burnt higher up in the furnace, resulting in the observed long flames. The heat flux from the furnace towards the process gas is also shown in Fig. 12.5.A-3 (Right). The heat fluxes have been averaged over all the reactor tubes. There are no significant differences among them. Figs. 12.5.A-4, Left and Right, show the methane, ethylene, and propylene yields through the reactor and the tube skin and process gas temperatures. Fig. 12.5.A-5 (Left) illustrates isotherms in a cross section of the reactor tube at 4 m from the reactor inlet. In the core of the tube, temperature gradients are eliminated by turbulent mixing, but steep temperature gradients occur in the valleys of the fins. From the process gas composition and the internal tube skin temperature, the initial coking rate can be calculated. Coke formation — inevitable in the thermal cracking of hydrocarbons — hampers the heat transfer and reduces the diameter, thus increasing the pressure drop over the reactor. Coke is formed on the wall, initially by catalytic mechanisms associated with the surface composition of the tube alloy. In a later stage, coke grows through addition of unsaturated components to radical positions in the macroradical coke [Froment, 1990]. Fig. 12.5.A-5 (Right) presents the circumferential distribution of the initial coking rate. The high coking rates inside the valleys of the fins cause a rapid filling of these valleys which is detrimental for the heat transfer. These results were in excellent agreement with the industrial observations. They illustrate to what extent present day modeling and computational means can contribute to an optimal operation of commercial chemical processes. ■

12.6 MACRO-PDF / RESIDENCE TIME DISTRIBUTION METHODS

12.6.1 Reactor Scale Balance and Species Continuity Equations

Determination of the spatial dependence of the (one-point joint velocity-composition) micro-PDF, *f*, or its moments is often difficult, and in many cases only the distribution of properties φ_A in the entire volume, that is, at the reactor scale, is desired. The volume integral or macro-average of (12.4.1-11) for statistically stationary flow is:

$$\frac{1}{V}\left(F_e'\psi_e - F_0'\psi_0\right) + \frac{\partial}{\partial \varphi_A}\left\{\left\langle G_A|\boldsymbol{\varphi}\right\rangle f\right\} = \left\{B|\boldsymbol{\varphi}\right\} - \left\{D|\boldsymbol{\varphi}\right\} \qquad (12.6.1\text{-}1)$$

The volume averaged distribution function or macro-PDF, *I*, also called the internal distribution function, is given by:

$$I_\gamma(\boldsymbol{\varphi}) \equiv \left\{f_\gamma(\boldsymbol{\varphi};\mathbf{z})\right\} \equiv \frac{1}{V}\int\int\int f_\gamma(\boldsymbol{\varphi};\mathbf{z})d\mathbf{z} \qquad (12.6.1\text{-}2)$$

and expresses the probability of finding (in the reactor) properties in the range $(\boldsymbol{\varphi} \le \boldsymbol{\gamma} < \boldsymbol{\varphi} + d\boldsymbol{\varphi})$.

The statistical description of the macro-scale behavior (12.6.1-2) involves averaging over all macro-scales, noted {}, and implies spatial sampling over the entire reactor volume *V*. This is different from the averaging introduced in Sections 12.4 and 12.5 which sampled only over all micro-scales. As a consequence, the macro-PDF, *I*, is not local, i.e., does not depend on the spatial coordinates $\mathbf{z}$, in contrast to the micro-PDF. Hence, extracting local information on mixing from a RTD is not possible. The first term on the left-hand side of (12.6.1-1) represents any flow into or out of the macroscopic volume. The derivation is similar to that used in Chapter 7 and is given in Himmelblau and Bischoff [1968].

By sampling over all micro- and macro-scales, the averages or integrals in (12.6.1-1) and (12.6.1-2) account for the combined effects of micro- and macro-mixing on the reactor-scale behavior. Only in particular cases, specific information on micro- or macro-mixing can be associated with or extracted from *I* (see Example 12.6.1.A). This will be shown to be of importance for the applicability of RTD to cases in which both flow and reaction occur (see Section 12.6.4). The solution of (12.6.1-1) requires closure models for $\left\{\left\langle G_A|\boldsymbol{\varphi}\right\rangle f\right\}$, $\left\{B|\boldsymbol{\varphi}\right\}$, and $\left\{D|\boldsymbol{\varphi}\right\}$, a challenging and often impossible task. An example of a micro-mixing closure model is given in Example 12.6.1.A. Instead of calculating the macro-PDF itself, a limited number of its moments can be calculated.

Equations for the macro-PDF moments have then to be derived, leading to additional closure problems. This is also illustrated in Example 12.6.1.A. An alternative to the calculation of I or its moments are measurements, which are relatively easy (see Example 12.6.2.B).

Frequently used macro-PDFs are the so-called Internal Age Distribution, $I(\alpha)$, and related Residence Time Distribution (RTD), $E(\theta)$, which are closely related to the macro-PDF of the velocity, $E(\boldsymbol{v})$. The characteristics and practical use of the RTD are discussed in more detail in the next sub-sections. RTD methods are commonly based on the response of the reactor to a tracer impulse or step given at the reactor inlet. This implies statistically non-stationary calculations, for which (12.6.1-1) can be extended to

$$\frac{1}{V}\frac{\partial(V\,I)}{\partial t}+\frac{1}{V}\left(F_e^{'}\psi_e-F_0^{'}\psi_0\right)+\frac{\partial}{\partial\varphi_A}\left\{\left\langle G_A|\boldsymbol{\varphi}\right\rangle f\right\}=\left\{B|\boldsymbol{\varphi}\right\}-\left\{D|\boldsymbol{\varphi}\right\} \quad (12.6.1\text{-}3)$$

and a time dependent macro-PDF, $I_{\boldsymbol{\gamma}}(\boldsymbol{\varphi};t)$, can be introduced.

EXAMPLE 12.6.1.A
POPULATION BALANCE MODEL FOR MICRO-MIXING IN A PERFECTLY MACRO-MIXED REACTOR: PDF MOMENT METHOD

If a flow system is visualized as consisting of a large number of fluid elements that collide, coalesce, and then reform into two new elements, a population balance model similar to that for immiscible droplet interaction can be formulated. The latter was devised by Curl [1963]; see also Rietema [1964] for a review of this complex area.

For a perfectly macromixed reactor, Evangelista, Katz, and Shinnar [1969] utilized (12.6.1-3) and $I_\gamma(\boldsymbol{\varphi};\,t)$, defined similarly to (12.6.1-2), for the volume averaged distribution of concentrations:

$$I\equiv I(C_A;t)=f(C_A;t) \quad (12.6.1.\text{A-a})$$

The latter equality results from perfect macro-mixing. In a perfectly macro-mixed reactor, information on the micro-PDF can be extracted from data at the reactor scale. With this choice of $\varphi_A\equiv C_A$,

$$-G_A=-\frac{dC_A}{dt}=r_A=\text{ reaction rate} \quad (12.6.1.\text{A-b})$$

For a constant-volume, (12.6.1-3) then becomes:

$$\frac{\partial f}{\partial t}+\frac{1}{\tau}(f-f_0)-\frac{\partial(r_A\,f)}{\partial C_A}=B-D \quad (12.6.1.\text{A-c})$$

with τ the mean residence time. Considering binary interactions between fluid elements only, the "birth" of a fluid element of concentration C_A occurs when two other fluid elements of concentrations $C_A^{'}$ and $C_A^{''}$ coalesce with concentrations such that $C_A = (C_A^{'} + C_A^{''})/2$. The "death" term means any collision with another fluid element resulting in a change of the original concentration. The net birth and death rates are given by

$$B - D = 2\beta \left[\begin{array}{l} \int\int f\left(C_A^{'}\right) f\left(C_A^{''}\right) \delta\left(\frac{\left(C_A^{'} + C_A^{''}\right)}{2} - C_A \right) dC_A^{'}\, dC_A^{''} \\ - f\left(C_A\right) \int f\left(C_A^{'}\right) dC_A^{'} \end{array} \right] \quad \text{(12.6.1.A-d)}$$

The first term in the brackets reflects the collisions of two elements producing a concentration C_A, the second term all the collisions of elements of concentration C_A; β is a measure of the agglomerative mixing of the fluid elements in the reactor, i.e., of the micro-mixing rate, and can be related to the turbulence (see Section 12.2).

The main variable of interest is the "mean" concentration $\langle C_A \rangle$, which is actually measured [the "expected value" of $f(C_A;t)$]. It is the first-order moment of the micro-PDF, *f*, defined as:

$$\langle C_A \rangle (t) \equiv \int C_A \, f\left(C_A;t\right) dC_A \quad \text{(12.6.1.A-e)}$$

The variance or second-order moment of the micro-PDF is also defined in the usual way:

$$\sigma_{C_A}^2 (t) = \int \left(C_A - \langle C_A \rangle\right)^2 f dC_A = \int C_A^2 f dC_A - \langle C_A \rangle^2 \quad \text{(12.6.1.A-f)}$$

To calculate the mean concentration, the population balance equations (12.6.1.A-c) and (12.6.1.A-d) are multiplied by C_A and integrated. The resulting equation for the first-order moment of the micro-PDF, $\langle C_A \rangle$ is:

$$\begin{aligned} &\frac{\partial \langle C_A \rangle}{\partial t} - \left[C_A \, r_A(C_A) f \Big|_{\text{limits}}^{\nearrow 0} - \int r_A(C_A) f \, dC_A \right] \\ &= \frac{1}{\tau} \left(\langle C_A \rangle_0 - \langle C_A \rangle \right) + 2\beta \left(\langle C_A \rangle - \langle C_A \rangle \right) \end{aligned} \quad \text{(12.6.1.A-g)}$$

where

$$\int C_A dC_A \int\int f\left(C_A^{'}\right) f\left(C_A^{''}\right) \delta\left(\frac{C_A^{'} + C_A^{''}}{2} - C_A \right) dC_A^{'}\, dC_A^{''} \quad \text{(12.6.1.A-h)}$$

$$= \int\int f\left(C_A^{'}\right) f\left(C_A^{''}\right) \int C_A \delta\left(\frac{C_A^{'} + C_A^{''}}{2} - C_A\right) dC_A \, dC_A^{'} \, dC_A^{''} \qquad (12.6.1.A\text{-h})$$

$$= \frac{1}{2}\int C_A^{'} f\left(C_A^{'}\right) dC_A^{'} \int f\left(C_A^{''}\right) dC_A^{''} + \frac{1}{2}\int f\left(C_A^{'}\right) dC_A^{'} \int C_A^{''} f\left(C_A^{''}\right) dC_A^{''}$$

$$= \frac{1}{2}\langle C_A \rangle (1) + \frac{1}{2}(1)\langle C_A \rangle = \langle C_A \rangle$$

has been used. The equation for the mean (measured) concentration becomes:

$$\frac{\partial \langle C_A \rangle}{\partial t} = -\int r_A(C_A) f \, dC_A + \frac{1}{\tau}\left(\langle C_A \rangle_0 - \langle C_A \rangle\right) \qquad (12.6.1.A\text{-i})$$

A similar procedure yields an equation for the second-order moment of the micro-PDF, *f*, or variance:

$$\frac{d\sigma_{C_A}^2}{dt} = -2\int \left(C_A - \langle C_A \rangle\right) r_A \, f \, dC_A + \frac{1}{\tau}\left[\sigma_{C_{A0}}^2 - \sigma_{C_A}^2 + \left(\langle C_{A0} \rangle - \langle C_A \rangle\right)^2\right] - \beta\sigma_{C_A}^2 \qquad (12.6.1.A\text{-j})$$

Equation (12.6.1.A-i) for $\langle C_A \rangle$ indicates that, for zero- or first-order reactions, the result is independent of β (i.e., the micro-mixing (β) has no effect). For a pure tracer experiment with no reaction, $r_A \equiv 0$, and for a step input in time, $f_0(C_A; t) = \delta(C_A - C_{A0})$, or $\langle C_{A0} \rangle = C_{A0}$:

$$\langle C_A \rangle(t)\big|_{step} = C_{A0}\left(1 - e^{-t/\tau}\right); \quad \langle C_A \rangle(0) = 0 \qquad (12.6.1.A\text{-k})$$

With $\sigma_{C_{A0}}^2 = \int C_A^2 \delta(C_A - C_{A0}) dC_A - \langle C_{A0} \rangle^2 = 0$, the variance becomes:

$$\sigma_{C_A}^2 = C_{A0}^2 e^{-(t/\tau)} \frac{e^{-(t/\tau)} - e^{-\beta\tau(t/\tau)}}{\beta\tau - 1} \qquad (12.6.1.A\text{-l})$$

Setting $\beta = \infty$ implies perfect micro-mixing. The corresponding results are shown in Fig. 12.6.1.A-1.

The variance about the mean is usually difficult to measure, but Evangelista et al. [1969] suggested that the time at maximum variance might be observable:

$$t_{\max} = \tau \ln\left(\frac{\beta\tau + 1}{2}\right) \Big/ (\beta\tau - 1) \qquad (12.6.1.A\text{-m})$$

which is one way to obtain values of β.

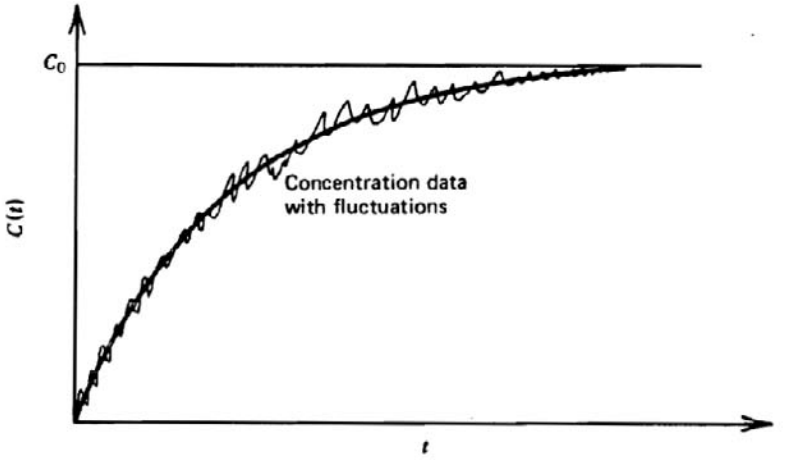

Figure 12.6.1.A-1

Concentration data, with micro-mixing fluctuations, in a perfectly macro-mixed flow vessel after a step input.

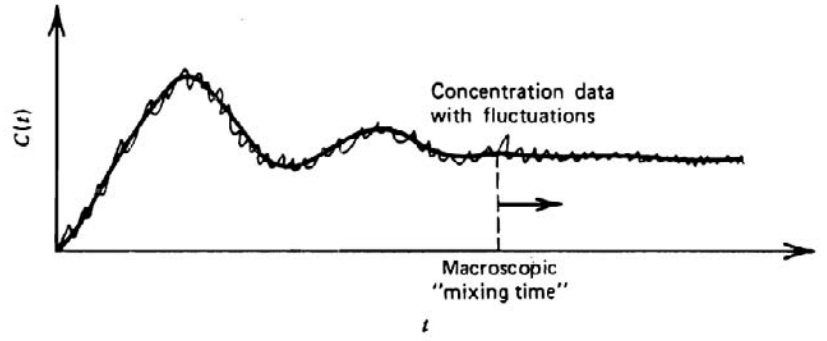

Figure 12.6.1.A-2

Concentration data, with micro-mixing fluctuations, in a batch vessel.

In a batch vessel, as $\tau \to \infty$ and in the absence of reaction, the equations are:

$$\frac{d\langle C_A \rangle}{dt} = 0 \;\Rightarrow\; \langle C_A \rangle = \text{const.} = \langle C_A \rangle(0) \qquad \text{(12.6.1.A-n)}$$

$$\frac{d\sigma^2_{C_A}}{dt} = -\beta\,\sigma^2_{C_A} \;\Rightarrow\; \sigma^2_{C_A} = \sigma^2_{C_A}(0)e^{-\tau t} \qquad \text{(12.6.1.A-o)}$$

In a perfectly macro-mixed batch vessel, the mean concentration is obviously constant and the variance of the fluctuations decreases exponentially with time. The latter is observed in turbulent regimes and is also predicted from isotropic, homogeneous turbulence theory (Fig. 12.6.1.A-2).

The above types of tracer experiments can be used to calculate the micro-mixing parameter β. Evangelista et al. [1969] describe typical values:

$$\beta \approx (0.1 - 0.5)\left(\frac{\varepsilon}{L^2}\right)^{1/3} \qquad (12.6.1.A\text{-p})$$

in which:

ε = power / mass of fluid ($\propto$ power / volume)
$\propto N^3 L^2$, geometrically similar vessels
N = impeller rpm
L = characteristic length

For large processing vessels, Evangelista et al. [1969] estimate:

$$\beta \approx 0.5\,s^{-1} \qquad (12.6.1.A\text{-q})$$

Such "scale-up" parameters are similar to what would be found from simpler dimensional arguments, but the theory also indicates how this information can be used to predict concentration fluctuations, i.e., micro-mixing. More rigorous turbulence theories, as presented in Sections 12.5.1-12.5.3 and in Section 12.4.2, or experiments can be used to provide more exact values of β for a specific situation.

Using the above derived relationships in the presence of reaction illustrates the principles discussed in this chapter. For a first-order reaction and isothermal conditions:

$$r_A = k\,C_A \qquad (12.6.1.A\text{-r})$$

(12.6.1.A-i) for $\langle C_A \rangle$ becomes:

$$\frac{\partial \langle C_A \rangle}{\partial t} = -k \langle C_A \rangle + \frac{1}{\tau}\left(\langle C_A \rangle_0 - \langle C_A \rangle\right) \qquad (12.6.1.A\text{-s})$$

which can be directly integrated, given the feed $\langle C_{A0} \rangle$. For a first-order reaction and isothermal conditions, the micro-mixing parameter β has no effect on the outlet conversion (see Sections 12.2 and 12.3). For a steady-state perfectly macro-mixed reactor and first-order reaction:

$$\frac{\langle C_A \rangle}{\langle C_{A0} \rangle} = \frac{1}{1 + k\,\tau} \qquad (12.6.1.A\text{-t})$$

as will be found from RTD theory (see (12.6.4.A-d)). There is a variance in the outlet concentration, caused by imperfect micro-mixing:

$$\left(\frac{\sigma_{C_A}}{\langle C_A \rangle}\right)^2 = \frac{(k\tau)^2}{2k\tau + \beta\tau + 1} \qquad (12.6.1.A\text{-u})$$

Again, $\beta = \infty$ implies perfect micro-mixing, resulting in $\sigma^2_{C_A} = 0$.

The case of a steady- or unsteady-state reactor with a non-linear reaction rate is more complicated. For example, with a second-order reaction and isothermal conditions:

$$r_A = k C_A^2 \qquad (12.6.1.A\text{-v})$$

and from (12.6.1.A-i):

$$k\int C_A^2 \, f \, dC_A = \frac{1}{\tau}\left(\langle C_{A0} \rangle - \langle C_A \rangle\right) \qquad (12.6.1.A\text{-w})$$

$$k\left(\sigma^2_{C_A} + \langle C_A \rangle^2\right) = \frac{1}{\tau}\left(\langle C_{A0} \rangle - \langle C_A \rangle\right) \qquad (12.6.1.A\text{-x})$$

For perfect micro-mixing, that is, with no fluctuations, $\sigma^2_{C_A} = 0$ and:

$$k\langle C_A \rangle^2 = \frac{1}{\tau}\left(\langle C_{A0} \rangle - \langle C_A \rangle\right) \qquad (12.6.1.A\text{-y})$$

With micro-mixing effects, the mean concentration $\langle C_A \rangle$ cannot be obtained without knowledge of $\sigma^2_{C_A}$. If the concentration fluctuations are symmetrical, implying the third central moment is zero, the variance is obtained from:

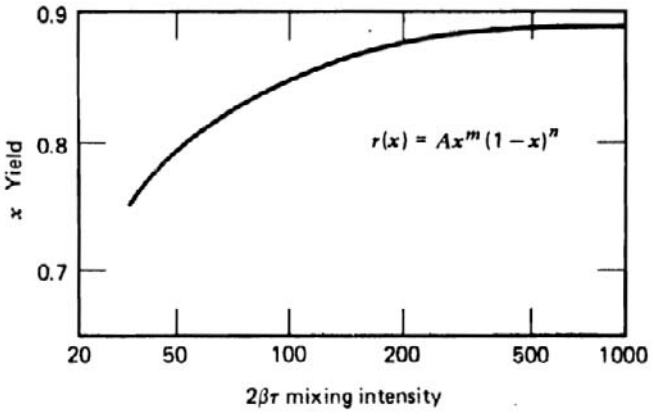

Figure 12.6.1.A-3

Adiabatic process: x = conversion to product; yield = averaged over contents of vessel. Asymptotic value = 0.897. From Evangelista et al. [1969].

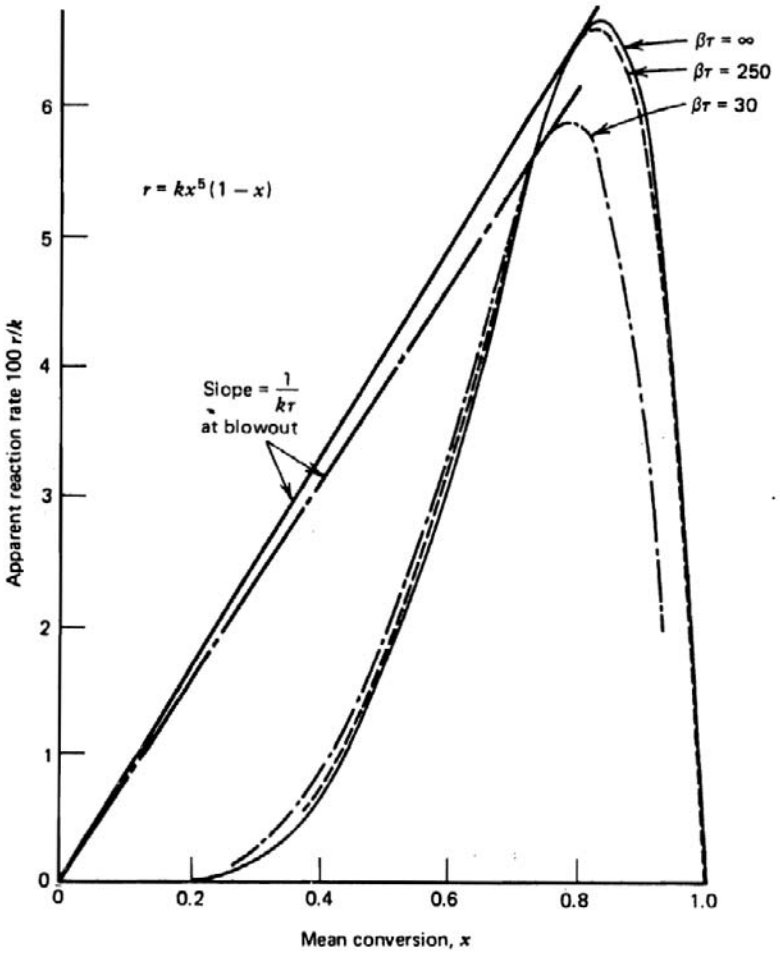

Figure 12.6.1.A-4

Effect of micro-mixing intensity on apparent or reactor-scale averaged reaction rate. From Evangelista et al. [1969b].

$$\left(4k\langle C_A\rangle\tau+\beta\tau+1\right)\left(\frac{\sigma_{C_A}}{\langle C_A\rangle}\right)^2=k\langle C_A\rangle\tau\left[\left(\frac{\sigma_{C_A}}{\langle C_A\rangle}\right)^2+1\right]^2 \qquad (12.6.1.A\text{-z})$$

In standard process vessels with low viscosity fluids, the approximate values of $\beta \approx 0.5\ s^{-1}$ are such that β is large compared to k — several orders of magnitude. For not too rapid reactions, micro-mixing is much faster than the reactions and micro-mixing effects are not very critical (Section 12.2). For viscous fluids with smaller β or very fast reactions with higher k, the value of β can be small relative to k, in which case the micro-mixing effects become important (Section 12.2).

Evangelista et al. [1969a, 1969b] illustrate the effects of micro-mixing for an adiabatic combustion process, for which the rate equation in terms of conversion of *A* is written:

$$r_A(x_A) = A x_A^m (1 - x_A)$$

(The x_A^m, for m = 5-20, is an approximation of the Arrhenius temperature dependence. The adiabatic temperature rise is expressed in terms of conversion from the mass and heat balances.) Fig. 12.6.1.A-3 shows how the conversion x_A decreases with imperfect micro-mixing (for A = 15, m = 5). It was also found that the variance divided by the conversion could range from about 20% to zero for very high mixing intensity ($\beta \to \infty$). Fig. 12.6.1.A-4 shows that the stability criteria could also be affected by the micro-mixing effects. The latter is even more true for highly exothermic reactions, if m = 15. ■

12.6.2 Age Distribution Functions

RTD methods are based on the concept of age distribution functions and make use of the experimentally measured or calculated residence time distribution of fluid elements in a reactor vessel (Figure 12.3-1, C and D). A Lagrangian perspective is taken and the age of a fluid element is defined as the time elapsed since it entered the reactor. In what follows, steady state operation of a vessel fed with a volumetric flow rate F' is considered. A residence time distribution (RTD) experiment can be performed with inert tracers, such that at an instant of time all fluid elements entering a reactor or process vessel are marked. The injection of an impulse of tracer into the vessel at time zero can be mathematically represented by means of the Dirac delta function or perfect unit impulse function:

$$\delta(\theta - \theta_0) \begin{matrix} = 0, \ \theta \neq \theta_0 \\ \neq 0, \ \theta = \theta_0 \end{matrix} \qquad (12.6.2\text{-}1)$$

where θ_0 is a specified value of θ at which the tracer is injected. Normalizing is expressed by:

$$\int_{-\infty}^{+\infty} \delta(\theta - \theta_0) d\theta = 1 \qquad (12.6.2\text{-}2)$$

When the vessel outlet stream of the marked fluid elements are monitored, several possibilities can be observed in between the extreme behaviors of plug flow and complete mixing. With plug flow, no marked fluid is observed until a time elapsed equal to the mean residence time of the vessel, at which point all the marked fluid elements leave the vessel. With complete mixing, the shape obtained reflects the instantaneous mixing of the tracer at time

zero giving a certain initial tracer concentration and its decay resulting from the continued inflow of non-tracer fluid. An intermediate behavior shows very little tracer fluid leaving the vessel directly from the inlet, most of the fluid elements spending about the mean residence time in the vessel, and a small number of fluid elements staying in the vessel for a long time. The residence time distribution or exit age distribution curve shows the fraction of fluid elements that has a certain residence time in the vessel as a function of the residence time [Danckwerts, 1953; Himmelblau and Bischoff, 1968]. $E(\theta)d\theta$ is the fraction of fluid leaving the vessel with a residence time (exit age) in the range $(\theta, \theta + d\theta)$. The RTD is properly normalized by stating that all the fluid elements have a finite residence time in the vessel:

$$\int_0^\infty E(\theta)d\theta = 1 \tag{12.6.2-3}$$

Equation (12.6.2-3) implies the absence of any permanent retention in the vessel. The fraction of fluid leaving the vessel with an age or residence time less than θ_1 is given by:

$$\int_0^{\theta_1} E(\theta)d\theta \tag{12.6.2-4}$$

The mean residence time τ is the centroid of the RTD and can be calculated from:

$$\tau = \int_0^\infty \theta\, E(\theta)d\theta = \frac{V}{F'} \tag{12.6.2-5}$$

where V is the vessel volume. Spaulding [1958] has shown that (12.6.2-5) holds for any arbitrary closed vessel, that is, a vessel without back diffusion at the flow boundaries.

It is often convenient to use a dimensionless time $\theta' = \theta / \tau$ and a corresponding version of the RTD, $E(\theta')$. The relationship between $E(\theta')$ and $E(\theta)$ follows from both distributions representing the same physical entity, i.e., the fraction of fluid leaving the vessel with age θ:

$$E(\theta)d\theta = E(\theta')d\theta' = E(\theta')\frac{d\theta}{\tau} \tag{12.6.2-6}$$

Hence:

$$E(\theta') = \tau\, E(\theta) \tag{12.6.2-7}$$

Equation (12.6.2-7) shows that the use of $E(\theta')$ is also consistent with the normalization (12.6.2-3).

A property of the Dirac delta function (12.6.2-1) that is often of use is the so-called filtering property:

$$\int_{-\infty}^{+\infty} \delta(\theta - \theta_0) f(\theta) d\theta = f(\theta_0) \qquad (12.6.2\text{-}8)$$

Next to the RTD, another age distribution of interest in some applications is the internal age distribution, *I*. $I(\alpha)d\alpha$ is the fraction of the fluid inside the vessel with age in the range $(\alpha, \alpha + d\alpha)$, where age is the length of time that a fluid element has been in the vessel. $I(\alpha)$ has properties similar to $E(\theta)$:

$$\int_0^{\infty} I(\alpha) d\alpha = 1 \qquad (12.6.2\text{-}9)$$

$$\int_0^{\alpha_1} I(\alpha) d\alpha = \text{fraction of fluid in vessel younger than age } \alpha_1 \qquad (12.6.2\text{-}10)$$

$$\tau_{\text{int}} = \int_0^{\infty} \alpha\, I(\alpha) d\alpha = \text{mean internal age} \qquad (12.6.2\text{-}11)$$

The interrelationship between $I(\alpha)$ and $E(\theta)$ follows from the fluid entering a vessel at a given time either leaving the vessel or staying inside [e.g., Himmelblau and Bischoff, 1968]:

$$\tau\, I(\alpha) = 1 - \int_0^{\alpha} E(\theta) d\theta \qquad (12.6.2\text{-}12)$$

or:

$$E(\theta) = -\tau \frac{dI(\theta)}{d\theta} \qquad (12.6.2\text{-}13)$$

Equation (12.6.2-12) is a special case of the general convolution result from linear systems theory, based on the fact that $E(\theta)$ is the impulse response of the flow system:

$$\text{OUTPUT}(\theta) = \int_0^{\theta} E(\theta_1)[\text{INPUT}(\theta - \theta_1)] d\theta_1 \qquad (12.6.2\text{-}14)$$

Equation (12.6.2-14) is valid for any input. Of particular interest is the output response to a step function input of tracer, $\text{INPUT}(\theta) = \text{U}(\theta)$. In the case of a unit step input, (12.6.2-14) gives:

$$\text{OUTPUT}(\theta) \text{ to unit step INPUT} = \int_0^{\theta} E(\theta_1)[1]d\theta_1 \quad (12.6.2\text{-}15)$$

Combining (12.6.2-12) and (12.6.2-15) shows that:

$$\text{OUTPUT}(\theta) \text{ to unit step INPUT} = 1 - \tau I(\theta) \quad (12.6.2\text{-}16)$$

Hence, step response tracer tests easily permit the determination of the internal age distribution function.

A comprehensive listing of various tracers and experimental tracer methods is provided by Wen and Fan [1975], including flow visualization techniques.

The fluid age distributions defined above for steady state flow systems can be extended to non-steady situations. Nauman [1969] illustrated this for vessels with time-varying inflow, outflow, and volume, related by:

$$\frac{dV}{dt} = F'_{IN}(t) - F'_{OUT}(t) \quad (12.6.2\text{-}17)$$

In such case, the RTD and the like will be a function of both the residence time and the "clock time", $E(\theta, t)$. Other more general situations are discussed in Himmelblau and Bischoff [1968] and by Chen [1971]. Recycle and a nonzero initial inventory of fluid have been considered by Chu and Fan [1963], see also Wen and Fan [1975].

EXAMPLE 12.6.2.A

RTD OF A PERFECTLY MIXED VESSEL

The transient tracer continuity equation for a completely mixed vessel in which M units of tracer are injected into the inlet stream at time zero is:

$$V\frac{dC}{d\theta} = M\,\delta(\theta) - F'C \quad (12.6.2.\text{A-a})$$

Assuming the initial tracer concentration, that is, before injection, to be zero, $C(0) = 0$, the solution of (12.6.2.A-a) is:

$$\begin{aligned} C(\theta) &= \exp[-(F'/V)\theta]\int_0^{\theta} \exp[+(F'/V)\theta_1]\frac{M}{V}\delta(\theta_1)d\theta_1 \\ &= \frac{M}{V}\exp[-(F'/V)\theta] \end{aligned} \quad (12.6.2.\text{A-b})$$

where the filtering property (12.6.2-8) has been used. The fractional tracer concentration in the outlet stream is, in dimensionless form:

$$\begin{aligned}\frac{C(\theta)}{(M/V)} &= \exp\left[-(F'/V)\theta\right] \\ &= \exp\left[-\theta/\tau\right] \\ &= \exp\left[-\theta'\right] \\ &= E(\theta')\end{aligned} \qquad \text{(12.6.2.A-c)}$$

For a completely mixed vessel, the RTD is exponential:

$$E(\theta') = \exp\left[-\theta'\right] \qquad \text{(12.6.2.A-d)}$$

or, applying (12.6.2-7):

$$E(\theta) = \frac{1}{\tau}\exp\left[-(\theta/\tau)\right] \qquad \text{(12.6.2.A-e)}$$

Using (12.6.2-12) and (12.6.2.A-e), the internal age distribution for the completely mixed vessel is found to be:

$$\tau\, I(\alpha) = 1 - \int_0^{\alpha} \frac{1}{\tau}\exp\left[-(\theta/\tau)\right] d\theta \qquad \text{(12.6.2.A-f)}$$

so that:

$$\begin{aligned}I(\alpha) &= \frac{1}{\tau}\exp\left[-(\alpha/\tau)\right] \\ &\equiv E(\theta)\end{aligned} \qquad \text{(12.6.2.A-g)}$$

Equation (12.6.2.A-g) expresses that in a completely mixed vessel, the internal and outlet conditions are identical, as mentioned already in Chapter 10.

■

EXAMPLE 12.6.2.B
EXPERIMENTAL DETERMINATION OF THE RTD

A pulse of tracer is injected in an arbitrary vessel. The outlet stream tracer concentration is measured in some arbitrary units. With *M* units of tracer injected

and in the absence of permanent retention of any tracer in the vessel, the overall tracer mass balance can be expressed as:

$$M = \int_0^\infty F' C(\theta) d\theta \qquad (12.6.2.B\text{-a})$$

and for constant F' :

$$M = F' \int_0^\infty C(\theta) d\theta \qquad (12.6.2.B\text{-b})$$

As was shown previously (12.6.2.A-c), the RTD in dimensionless form is given by:

$$E(\theta') = \frac{C(\theta)}{(M/V)} \qquad (12.6.2.B\text{-c})$$

Applying (12.6.2.B-b):

$$E(\theta') = \frac{V}{F'} \frac{C(\theta)}{\int_0^\infty C(\theta) d\theta} \qquad (12.6.2.B\text{-d})$$

or, via (12.6.2-5) and (12.6.2-7):

$$E(\theta) = \frac{C(\theta)}{\int_0^\infty C(\theta) d\theta} \qquad (12.6.2.B\text{-e})$$

Thus, the RTD $E(\theta)$ can be determined from the measured outlet concentrations in arbitrary units and without knowing the exact amount of tracer injected. In practice, it is recommended to also use the tracer mass balance (12.6.2.B-a) to check the quality of the experiment. Alternatively, from a known amount M of tracer injected and the integral of the outlet tracer concentration curve, the flow rate F' can be found via (12.6.2.B-b) (often used in physiology).

Combining (12.6.2-5) and (12.6.2.B-e) allows calculating the mean residence time in the vessel τ directly from the experimental data:

$$\tau = \frac{V}{F'} = \int_0^\infty \theta C(\theta) d\theta \Big/ \int_0^\infty C(\theta) d\theta \qquad (12.6.2.B\text{-f})$$

Equation (12.6.2.B-f) is often used in two-phase systems, for example, to determine the vessel volume for the flowing phase, V (usually called holdup then), which is difficult to measure by other techniques. Finally, it should be

noted that the dimensionless RTD, $E(\theta')$, can be obtained directly from experimental tracer data by combining (12.6.2-7), (12.6.2.B-e) and (12.6.2.B-f).

■

All of the age distribution formalism could be derived by starting from the single-particle joint-PDF transport equation (12.4.1-11) or the macroscopic population balance equation (12.6.1-3). Indeed, the only property of interest is the age, so that $\varphi_1 = \alpha$, the age. Now intervals of age are also intervals of clock time, so that $G_1 = d\alpha/dt = 1$ and (12.6.1-3) reduces to:

$$\frac{1}{V}\frac{\partial(V\{f\})}{\partial t} + \frac{\partial\{f\}}{\partial\alpha} = \frac{1}{V}\left(F_0' f_0 - F_e' f_e\right) \qquad (12.6.2\text{-}18)$$

where $G_1 = d\alpha/dt = 1$ was used. The correspondence with the previously defined functions in this section is:

$$\{f\} = \text{ internal age distribution } = I(\alpha)$$

$$f_e = \text{ exit age distribution } = E(\alpha)$$

$$f_0 = \text{ inlet age distribution } = \delta(\alpha)$$

so that

$$\frac{1}{V}\frac{\partial(V\,I)}{\partial t} + \frac{\partial I}{\partial\alpha} = \frac{1}{V}\left(F_0' f_0 - F_e' f_e\right) \qquad (12.6.2\text{-}19)$$

which reduces to many of the earlier results for special cases. More detailed examples of the use of this is given in Himmelblau and Bischoff [1968], Chen [1971], and Wen and Fan [1975]. A generalization of population balance methods to reactions with arbitrary RTD was given by Kattan and Adler [1972]. The phase space of the distribution functions was expanded to include the life expectation λ as well as the concentration of the individual fluid elements $\boldsymbol{C}$: $f(\boldsymbol{C}, \lambda; t)$.

12.6.3 Flow Patterns Derived from the RTD

An experimentally measured RTD of a steady state flow reactor reflects the spatial characteristics of the macro-flow and -mixing in the reactor, including eventual effects of micro-flow and -mixing phenomena on the macro-flow and -mixing. Hence, inspection of experimental RTD can be used to infer certain properties of the flow pattern. Local information on the macro- or micro-flow and mixing behavior inside the reactor can, however, not be revealed, due to the length scale over which RTD are defined (see (12.6.1-2)) and measurements are

carried out, i.e., the largest macro-scale, that is, the reactor scale. A typical and useful characteristic of the RTD curve is its width, a second-order moment of the RTD. For plug flow, the RTD is infinitely narrow (zero width), whereas for completely mixed flow, the RTD is rather wide. Thus, the width of the observed RTD can be used to position the characteristics of the flow in the spectrum between plug flow and complete mixing. This information can be used directly to decide whether a reactor has the proper flow design for a particular application.

Using the analogy with probability theory, a useful measure of the width of the RTD is the variance with respect to the mean residence time:

$$\sigma^2 = \int_0^\infty (\theta'-1)^2 E(\theta')d\theta' = \int_0^\infty (\theta')^2 E(\theta')d\theta' - 1 \qquad (12.6.3\text{-}1)$$

The dimensionless residence time θ' is used in (12.6.3-1), allowing to compare the widths of different RTD curves at the same location, i.e., $\theta = \tau$ or $\theta' = 1$. Higher statistical moments of the RTD can also be used in theory, but calculating them from the usually rather scattered tracer data turns out to be quite difficult in practice.

In addition to the use of statistical measures, other aspects of RTD curves are also of interest, in particular for the detection of certain malfunctions of a reactor. Malfunctions include significant bypassing of some of the fluid and/or regions of stagnant fluid, so-called "dead space". In the situation of bypassing of a significant portion of the fluid, in ideal form, two maxima in the $E(\theta)$ curve will be produced — one corresponding to the bypassing fluid and the second to the remainder. This maldistribution is often easier seen on the $I(\theta)$ curve, since a portion of the inventory very rapidly leaves the reactor, followed by the main portion of the fluid. In the converse situation of regions of fluid stagnancy, the $E(\theta)$ curve will have a very long tail.

Since bypassing and regions of fluid stagnancy cause respectively gross under- or over-conversion of part of the reactants, they are usually detrimental to the operation of the reactor. In addition, stagnant fluid experiences an order of magnitude greater severity in reaction conditions, often leading to undesired side reactions. If a reactor does not appear to be properly behaving, tracer tests can be used to verify if the problem concerns macro-mixing and the flow pattern. These troubleshooting applications of tracer tests can sometimes suggest improvements to be made to the reactor design, for example, addition or elimination of baffles, repacking, modification of the feed sparger, and others.

As explained in Section 12.3, the RTD can be calculated a posteriori from a PDF or CFD calculation, allowing comparison with an experimental RTD or avoiding the measurement of the RTD.

EXAMPLE 12.6.3.A

RTD FOR SERIES OF *N* COMPLETELY STIRRED TANKS

Consider flow through *n* completely stirred tanks of equal volume (V_t/n) in series. The flow rate *F'* is assumed to be constant. The transient mass balance of the *i*th tank in the series of *n* can be written:

$$\left(\frac{V_t}{n}\right)\frac{dC_i}{dt} = F'C_{i-1} - F'C_i \qquad \text{(12.6.3.A-a)}$$

M units of tracer are injected into the first tank at time zero:

$$t = 0 : C_{i=1} = \frac{M}{F'}\delta(t) \qquad C_{i\neq 1} = 0 \qquad \text{(12.6.3.A-b)}$$

The set of ordinary differential equations (12.6.3.A-a) can be solved successively or by Laplace transforms and gives:

$$E(\theta') = \frac{C(\theta)}{(M/V)} = \frac{(n)^n}{(n-1)!}(\theta')^{n-1}\exp[-n\theta'] \quad \text{for: } i = 1, 2, 3, ..., n \qquad \text{(12.6.3.A-c)}$$

The corresponding curves are shown in Fig. 12.6.3.A-1. It should be noted that the dimensionless time θ' in (12.6.3.A-c) is based on the total mean residence time in the *n* reactors.

It can be easily verified that:

$$\int_0^\infty E(\theta')d\theta' = \frac{(n)^n}{(n-1)!}\int_0^\infty (\theta')^{n-1}\exp[-n\theta']d\theta' = 1 \qquad \text{(12.6.3.A-d)}$$

and:

$$\int_0^\infty \theta' E(\theta')d\theta' = \frac{(n)^n}{(n-1)!}\int_0^\infty (\theta')^{n}\exp[-n\theta']d\theta' = 1 \qquad \text{(12.6.3.A-e)}$$

Furthermore,

$$\sigma^2 = \int_0^\infty (\theta')^2 E(\theta')d\theta' - 1 = \frac{(n+1)(n)}{n^2} - 1 = \frac{1}{n} \qquad \text{(12.6.3.A-f)}$$

so that the curve width or variance changes from $\sigma^2 = 1$ for $n = 1$ to $\sigma^2 = 0$ for $n \rightarrow \infty$. This indicates that the behavior of a number of stirred tanks in series ranges from complete mixing to plug flow. In Chapter 10, a similar behavior was also arrived at for a series of steady-state completely mixed reactors.

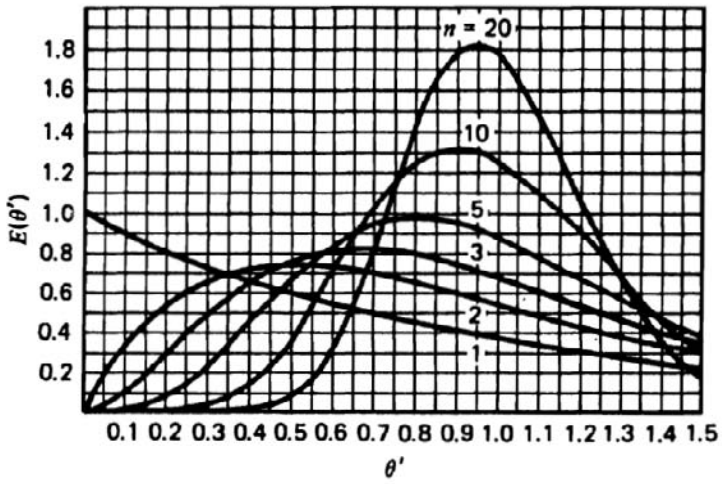

Figure 12.6.3.A-1
E curve for tanks-in-series model.

One practical implication of this is that if a plug flow pattern is desired for the reaction optimization, but stirring is essential for other reasons (e.g., a suspended slurry), a compromise design would call for a series of stirred tanks. This is often done in polymerization, where stirring is needed for heat transfer and/or to maintain an emulsion, but where a plug flow pattern might be desired for the molecular weight distribution. ■

12.6.4 Application of RTD to Reactors

The usual application of RTD to account for the effects of mixing on reactor behavior is based on considering the extents of reaction in a sufficient number of fluid elements pulsed in the reactor and then averaging over these fluid elements as they exit the reactor.

$$\left\langle C_A^{OUT} \right\rangle = \int_0^\infty C_A(\theta) E(\theta) d\theta \tag{12.6.4-1}$$

Taking a Lagrangian description, the concentration of a component *A* in a fluid element $C_A(\theta)$ is assumed to depend on the residence time of the fluid element in the reactor θ :

$$-\frac{dC_A}{d\theta} = r_A\left(C_A(\theta)\right) \tag{12.6.4-2}$$

with initial condition:

$$C_A\big|_{\theta=0} = C_{A0} \tag{12.6.4-3}$$

Equation (12.6.4-2) implies that the fluid elements are considered as small batch reactors moving independently. Neglecting interactions between fluid elements implies that the conversion of *A* in a fluid element depends only on the residence time of the fluid element in the vessel and not on its exact pathway through the vessel. This is strictly valid only for first order reactions and isothermal conditions. Non-linear processes also depend on the encounter of two different sets of fluid elements and, therefore, on both the residence time and the trajectory. Interactions between fluid elements can be associated with turbulent transport. Equation (12.6.4-2) considers the reaction conditions within each individual fluid element to be spatially uniform, assuming complete micro-mixing within each individual fluid element, and should rather be written:

$$-\frac{d\langle C_A\rangle}{d\theta} = \langle r_A(C_A(\theta))\rangle \qquad \text{(12.6.4-2b)}$$

For relatively fast non-linear reaction rates, $\langle r_A(C_A(\theta))\rangle \neq r_A(\langle C_A(\theta)\rangle)$, and the interaction between fluid elements and non-uniformities within the individual fluid elements should be accounted for. In using a segregated batch reactor type model for the fluid elements (12.6.4-2) and the RTD as in (12.6.4-1), the effects of micro-mixing on the macro-mixing and the macro-scale averaged reaction rates are not rigorously accounted for: micro-mixing between fluid elements is neglected, whereas micro-mixing within each individual fluid element is assumed to be complete. The latter may in particular affect the evaluation of the fluid element scale or macro-scale averaged reaction rates for higher-order, relatively fast reactions and/or non-isothermal conditions. Simply comparing complete segregation of the fluid elements as done in direct RTD application with the extreme case of no micro-mixing is incorrect.

Using (12.6.4-1) and (12.6.4-2), a mean outlet concentration of component *A* for any intrinsic reaction rate expression and experimentally measured RTD can be calculated.

As shown in Section 12.2 and illustrated in what follows, neglecting the effects of micro-mixing is of no importance for first order reactions carried out isothermally. For non-linear reaction rates or non-isothermal conditions, the effects of micro-mixing can be important (see Section 12.2 for evaluation criteria). In such case, micro-mixing should be rigorously accounted for, e.g., using the methods described in Sections 12.4 and 12.5.

EXAMPLE 12.6.4.A

FIRST ORDER REACTION(S) IN ISOTHERMAL COMPLETELY MIXED REACTORS, PLUG FLOW REACTORS, AND SERIES OF COMPLETELY STIRRED TANKS

For a first order reaction:

$$\frac{dC_A}{d\theta} = -k\,C_A \qquad (12.6.4.A\text{-a})$$

or:

$$C_A = C_{A0}\exp\left[-k\theta\right] \qquad (12.6.4.A\text{-b})$$

Substituting (12.6.4.A-b) into (12.6.4-1) gives:

$$\frac{\left\langle C_A^{OUT}\right\rangle}{C_{A0}} = \int_0^\infty \exp\left[-k\theta\right]E(\theta)d\theta \qquad (12.6.4.A\text{-c})$$

This equation links the mean exit concentration of *A*, $\left\langle C_A^{OUT}\right\rangle$, to the RTD.

For a completely mixed reactor, the use of the RTD (12.6.2.A-e) leads to:

$$\frac{\left\langle C_A^{OUT}\right\rangle}{C_{A0}} = \int_0^\infty \frac{1}{\tau}\exp\left[-\left[k+(1/\tau)\right]\theta\right]d\theta = \frac{1}{1+k\,\tau} \qquad (12.6.4.A\text{-d})$$

Equation (12.6.4.A-d) is identical to the expression derived in Chapter 10 where, instead of using the RTD, complete mixing was assumed, both at the macro- and micro-scale. For a first order reaction and isothermal conditions, the extent of micro-mixing is seen to have no influence on the average reactor exit. This will be further demonstrated and confirmed for other reactor types.

For a plug flow reactor RTD, (12.6.4.A-c) becomes:

$$\begin{aligned}\frac{\left\langle C_A^{OUT}\right\rangle}{C_{A0}} &= \int_0^\infty \exp\left[-k\theta\right]\delta(\theta-\tau)d\theta \\ &= \exp\left[-k\tau\right]\end{aligned} \qquad (12.6.4.A\text{-e})$$

Equation (12.6.4.A-e) is identical to the expression derived in Chapter 9, where the RTD was not used.

For a plug flow reactor followed by a completely mixed reactor, the RTD is shown in Figure 12.6.4.A-1. It can be represented mathematically by:

$$E(\theta) = \frac{1}{\tau(CSTR)}U(\theta-\tau(PF))\exp\left[-(\theta-\tau(PF))/\tau(CSTR)\right] \qquad (12.6.4.A\text{-f})$$

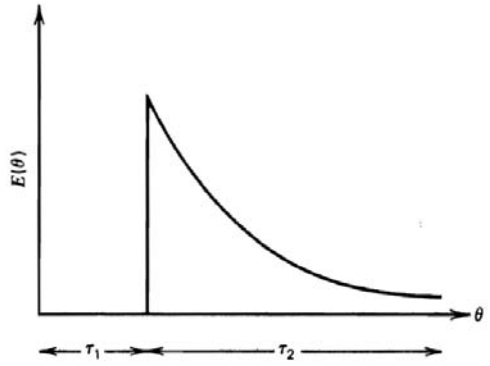

Figure 12.6.4.A-1
Residence time distribution curve.

where $\tau(CSTR)$ is the mean residence time in the completely mixed reactor and $\tau(PF)$ is the mean residence time in the plug flow reactor. For a first order reaction and isothermal conditions, accounting for the RTD through (12.6.4-1) or directly applying the completely mixed and plug flow reactor assumptions leads to (Chapters 9 and 10):

$$\begin{aligned} x_A &= 1 - \frac{\left\langle C_A^{OUT} \right\rangle}{C_{A0}} \\ &= 1 - \frac{\exp\left[-k\,\tau(PF)\right]}{1 + k\,\tau(CSTR)} \end{aligned} \tag{12.6.4.A-g}$$

The same RTD and x_A would be generated by the reverse configuration.

For n tanks in series, the use of the RTD (12.6.3.A-c), where τ is the mean total holding time in the n tanks, reduces (12.6.4.A-c) to:

$$\begin{aligned} \frac{\left\langle C_A^{OUT} \right\rangle}{C_{A0}} &= \frac{1}{\tau^n} \frac{(n)^n}{(n-1)!} \int_0^\infty \theta^{n-1} \exp\left[-\left[k + (n/\tau)\right]\theta\right] d\theta \\ &= \frac{1}{\left[1 + (k\,\tau/n)\right]^n} = \frac{1}{\left[1 + (k\,\tau_n)\right]^n} \end{aligned} \tag{12.6.4.A-h}$$

which corresponds to the expression derived via the assumption of complete mixing in Chapter 10. ■

Considering coupled first order reaction schemes, Wei [1966] found that "for a reactor with distribution of residence times, all reactions are slowed down

in comparison with those in a plug flow reactor, but the faster reactions are slowed down a great deal more than the slower ones. This logically follows from the reactor-scale and macro-scale averaged reaction rate of a faster reaction being more sensitive to macro-mixing, respectively micro-mixing limitations than that of a slower reaction (see Section 12.2). Consequently, the occurrence of distribution of residence times makes all reactor-scale (averaged) chemical reaction rates of the characteristic species nearly equal." The differences between the various reaction rates at the reactor scale are decreased, thereby lowering the selectivity. This effect is similar to the diffusion effects dealt with in Chapter 3.

EXAMPLE 12.6.4.B

SECOND ORDER BIMOLECULAR REACTION IN ISOTHERMAL COMPLETELY MIXED REACTORS AND IN A SUCCESSION OF ISOTHERMAL PLUG FLOW AND COMPLETELY MIXED REACTORS: COMPLETELY MACRO-MIXED VERSUS COMPLETELY MACRO- AND MICRO-MIXED

For a second order bimolecular reaction, based on the complete (macro- and micro-) mixing assumption (Chapter 10), the conversion of *A* is given by:

$$x_A = 1 - \frac{\left\langle C_A^{OUT} \right\rangle}{C_{A0}} = 1 - \frac{-1 + \sqrt{1 + 4k\,C_{A0}\,\tau}}{2k\,C_{A0}\,\tau} \qquad (12.6.4.B\text{-a})$$

Starting from the RTD of a completely mixed reactor (12.6.2.A-e) and applying (12.6.4-1) leads to [Metzner and Pigford, 1958]:

$$x_A = 1 - \frac{1}{\tau}\int_0^\infty \frac{\exp\left[-\theta/\tau\right]}{1 + k\,C_{A0}\,\theta}\,d\theta = 1 - \frac{\exp\left[1/k\,C_{A0}\,\tau\right]}{k\,C_{A0}\,\tau} E_1\left(\frac{1}{k\,C_{A0}\,\tau}\right) \qquad (12.6.4.B\text{-b})$$

where:

$$E_1(x) = \int_x^\infty \frac{\exp\left[-y\right]}{y}\,dy \qquad (12.6.4.B\text{-c})$$

is the exponential integral.

Clearly, for this second order reaction, the RTD assumption of complete segregation of the fluid elements in the reactor with complete micro-mixing within each individual fluid element affects the conversion of *A*. This is true for any non-linear reaction rate expression and / or non-isothermal conditions.

Considering the RTD curve shown in Fig. 12.6.4.A-1 and discussed in Example 12.6.4.A, for a second order reaction with $kC_{A0}\tau(PF) = 1$ and $\tau(CSTR)/\tau(PF) = 4$, the conversion of *A* is calculated from:

$$x_A = 1 - \frac{1}{\tau(CSTR)} \int_{\tau(PF)}^{\infty} \frac{\exp\left[-\left(\theta - \tau(PF)\right)/\tau(CSTR)\right]}{1 + k\,C_{A0}\,\theta} d\theta$$

$$= 1 - \frac{\exp\left[\tau(PF)/\tau(CSTR)\right]\exp\left[1/k\,C_{A0}\,\tau(CSTR)\right]}{k\,C_{A0}\,\tau(CSTR)} \qquad (12.6.4.B\text{-d})$$

$$\times E_1\left(\frac{\tau(PF)}{\tau(CSTR)} + \frac{1}{k\,C_{A0}\,\tau(CSTR)}\right)$$

and amounts to 76.9 %.

The RTD curve of Fig. 12.6.4.A-1 can be interpreted as resulting from a plug flow vessel followed by a completely mixed vessel. Applying the expressions derived in Chapters 9 and 10, a value of 75 % would be calculated from:

$$x_A = 1 + \frac{1}{2k\,C_{A0}\,\tau(CSTR)}\left[1 - \sqrt{1 + 4\left(\frac{k\,C_{A0}\,\tau(CSTR)}{1 + k\,C_{A0}\,\tau(PF)}\right)}\right] \qquad (12.6.4.B\text{-e})$$

The RTD could have been generated as well by the reverse reactor configuration, but in that case, the conversion would be given by:

$$x_A = 1 - \frac{-1 + \sqrt{1 + 4k\,C_{A0}\,\tau(CSTR)}}{2k\,C_{A0}\,\tau(CSTR) + k\,C_{A0}\,\tau(PF)[-1 + \sqrt{1 + 4k\,C_{A0}\,\tau(CSTR)}]} \qquad (12.6.4.B\text{-f})$$

and amounts to 72 %.

For this second order reaction, different conversions are obtained when assuming complete segregation of the fluid elements with complete micro-mixing within each individual fluid element or overall complete micro-mixing, illustrating the influence of micro-mixing on non-linear or non-isothermal reactions. ■

12.7 SEMI-EMPIRICAL MODELS FOR REACTORS WITH COMPLEX FLOW PATTERNS

12.7.1 Multi-Zone Models

To account to a certain extent for the effects of macro-mixing in the species balance equations, so-called multi-zone models have been developed. The reactor is divided in multiple, not necessarily geometrical, zones and, within each zone, an idealized mixing or flow pattern is assumed in the derivation of the species

balance equations. Macro-mixing is reflected in the transport rates F between the different zones and determined by the flow field in the reactor. The transport rates F have to be experimentally measured, or modeled and calculated.

Similar to RTD-based models (Section 12.6), multi-zone models do not explicitly account for the effects of micro-mixing. The latter may affect macro-mixing, that is, the transport rates between zones. Micro-mixing may also affect the averaged reaction rates at the scale of the zones or the macro-scale, as a result of non-uniformities within the individual zones. Micro-mixing effects can eventually be accounted for by the methods discussed in Sections 12.5 and 12.4.

Consider the case where there are two (or more) distinct regions or zones within the reactor that can basically be described by an axial dispersion type model in each of the zones considered. Transport balances can be written for each zone, per unit reactor volume. For statistically stationary flow:

$$u_1 \frac{\partial C_{A1}}{\partial z} = D_{a1} \frac{\partial^2 C_{A1}}{\partial z^2} - \frac{\Delta C}{V_1/V} + r_{A1} \qquad (12.7.1\text{-}1)$$

and

$$u_2 \frac{\partial C_{A2}}{\partial z} = D_{a2} \frac{\partial^2 C_{A2}}{\partial z^2} + \frac{\Delta C}{V_2/V} + r_{A2} \qquad (12.7.1\text{-}2)$$

where

u_i = velocity in zone i = $F_i^{'}/\Omega_i$

r_{Ai} = reaction rate per volume of zone i

ΔC = rate of mass (or heat) interchange (kg/m^{3}s)
= $k_{T1}C_{A1} - k_{T2}C_{A2}$
= $k_T a_v \left(C_{A1} - C_{A2}/K\right)$, for example (with K = equilibrium constant).

In (12.7.1-1) and (12.7.1-2), the symbol C_{Ai} could represent mass concentrations, or for heat transfer, $C_i = \rho_i c_{pi} T_i$. Also, the axial dispersion coefficients for heat transfer would be $D_{ai} = \lambda_{ai}/\rho_i c_{pi}$, and the transfer coefficient would be $k = h/\rho_1 c_{p1}$ (for zone 1 normally being the fluid, and then $K \equiv \rho_2 c_{p2}/\rho_1 c_{p1}$).

As written, the above equations are the standard equations for interfacial mass transfer used in Chapters 6 and 14 [see also Pavlica and Olson, 1970, and Miller and Bailey, 1973]. They are also the basis of the "cross flow" models for fluidized beds (see Chapter 13) or other multiphase reactors, and have been used for heat transfer studies.

For larger-scale mixing flow, for example, in real stirred tanks, other types of models are required. From the viewpoint of macro-mixing, the existence

of significant zones of bypassing or stagnant fluid are particularly important. A basic multi-zone model that can account for these features has been developed by Cholette et al. [1959, 1972] (see Fig. 12.7.1-1). The parameters bypassing fraction and dead (totally stagnant) fraction of the volume have been correlated for a wide range of operating variables. See Levenspiel [1972], Himmelblau and Bischoff [1968], and Wen and Fan [1975] for further aspects of these models.

A multi-zone model that more closely agrees with the observed mixing patterns in real stirred tanks was presented by van de Vusse [1962]. The basis is a zone of intense shear and mixing around the impeller followed by recirculating flows around the rest of the tank. These "signal flow" models have the general features shown in Fig. 12.7.1-2. Each of the elements can represent a flow zone with a certain amount of dispersion, or idealized tanks-in-series model. Compact mathematical methods for the solution of the mass balances for these types of models have been given by Gibilaro, Kropholler, and Spikins [1967]. Experimental determination of the model parameters was illustrated by Taniyama and Sato [1965], and an interesting example better explaining microbial reactions was given by Sinclair and Brown [1970].

A comprehensive review of these and other aspects of mixing and reactions was given by Olson and Stout [1966]. One conclusion was that the signal flow models are often overly sensitive to rather ill-defined parameters such as exact inflow conditions. Furthermore, these models cannot account for mass interchange between internal flow paths that undoubtedly occurs in stirred tanks. A similar model has been used by Khang and Levenspiel [1976] to predict mixing times in batch mixing vessels.

The scale-up of stirred tanks is often based on power input per unit volume — a survey of various applications is given by Connolly and Winter [1969]. A more detailed consideration accounting for reaction was published by

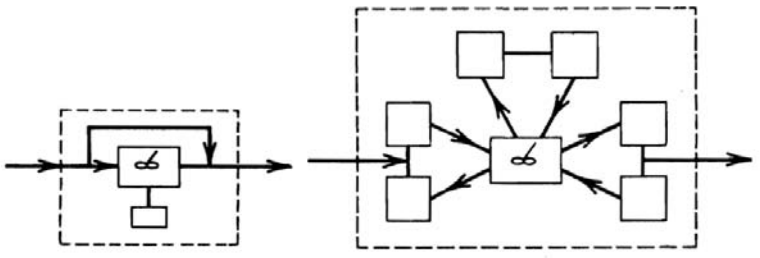

Figure 12.7.1-1
Model of real stirred tank with bypassing and dead space.

Figure 12.7.1-2
Signal flow model of real stirred tank.

Paul and Treybal [1971]. They found that "Power per unit volume is ... incapable of correlating the widely different local conditions within a stirred vessel." Instead, a criterion involving both the intrinsic reaction rate constants and a micro-time scale to account for micro-mixing effects (see Sections 12.2 and 12.3) was developed.

A multi-zone model similar to the finite volume methods used in Computational Fluid Dynamics (CFD, see Section 12.5) is based on geometrical zones and assumes uniform conditions within each zone, that is, completely mixed (CSTR) zones, while essentially allowing conditions to differ between zones. For statistically stationary flow, the species balance equations for species *A* in zone *i* of *N* can then be written as:

$$\sum_{j=0}^{N+1}\left(F_{j\to i}\,C_A^{(j)} - F_{i\to j}\,C_A^{(i)}\right) + \left\langle r_A\left(\boldsymbol{C}^{(i)}\right)\right\rangle = 0 \qquad i = 1, ..., N \qquad (12.7.1\text{-}3)$$

where zones (0) and (*N+1*) can be included in the summation to impose the inlet and outlet conditions. Hence, CFD models can be regarded as an extension of this type of multi-zone models to a more rigorous description of the transport rates between the zones based on the momentum equations. The assumption of uniform conditions within each zone implies complete micro-mixing within each zone. CSTR-based multi-zone models are the Eulerian framework analogy of the Lagrangian framework fluid element based models (see (12.6.4-1) and (12.6.4-2)). Calculating the time behavior of a number of batch reactors is replaced by calculating the behavior in space of a number of CSTRs. The effect of micro-mixing on macro-mixing (turbulent transport) appears in the transport rates *F* in (12.7.1-3) and corresponds to the interactions between fluid elements. Considerations on the uniformity within individual zones and within fluid elements are completely similar and concern the averaged reaction rate <*r*> at the scale of the zone in (12.7.1-3). The evaluation of the importance of micro-mixing effects was discussed in Section 12.2. Approaches to account for eventual micro-mixing effects were presented in Sections 12.4 and 12.5.

The transport rates *F* in (12.7.1-3) can be measured experimentally or calculated from CFD simulations (see Section 12.5). With respect to the latter, multi-zone models may offer some advantages compared to a fully CFD-based approach in case the scale of the non-uniformities in the species concentration field is larger than the scale of the non-uniformities in the velocity field. This allows a coarser grid for the species concentration field calculation than for the velocity field calculation, that is, less zones than CFD finite volumes, and significantly reduces the computational effort.

12.7.2 Axial Dispersion and Tanks-in-Series Models

The axial dispersion and tanks-in-series models are the two most common of models that have been developed as general semi-empirical correlations of mixing behavior, presumably bearing some relation to the actual flow pattern in the vessel. The model parameters have to be determined from experimental data and are then correlated as functions of fluid and flow properties and reactor configurations for use in design calculations.

The "axial dispersion" or "axial dispersed plug flow" model [Levenspiel and Bischoff, 1963] takes the form of a one-dimensional convection-diffusion equation, allowing to utilize all of the clasical mathematical solutions that are available [e.g. Carslaw and Jaeger, 1959, 1986; Crank, 1956].

For statistically stationary flow, the species continuity equation for the axial dispersion model is (Chapter 7):

$$u\frac{\partial C_A}{\partial z} = \frac{\partial}{\partial z} D_a \frac{\partial C_A}{\partial z} + r_A(\boldsymbol{C}) \qquad (12.7.2\text{-}1)$$

In (12.7.2-1), u is taken to be the mean (plug flow) velocity through the vessel, and D_a is an axial dispersion coefficient to be obtained by means of experiments. One important application is the modeling of fixed beds, as discussed in detail in Chapter 11, and then it is usually termed an "effective" transport model, with $D_a = D_{ea}$. The axial dispersion model has also been used to approximately describe a variety of other reactors.

One common approach to determine the model parameter D_a, is to perform a residence time distribution test on the reactor and to fit the value of D_a so that the model solution and the experimental output curve agree. For such a RTD analysis, a transient term, $\partial C_A/\partial t$, is to be included in equation (12.7.2-1). Fig. 12.7.2-1 shows the $E(\theta')$-θ' curves of the axial dispersion model for an impulse input with "closed" boundaries (here, $\theta' = \theta F'/V = \theta u/L$, with L = length of the reactor) [Carslaw and Jaeger, 1959, 1986].

The Peclet number is defined as:

$$Pe_a = u\,L/D_a \qquad (12.7.2\text{-}2)$$

The axial dispersion model can represent mixing behavior ranging from perfect mixing ($D_a \to \infty$) to plug flow ($D_a \to 0$). A thorough evaluation was given by Brenner [1962].

Other types of boundary conditions can also be used when solving (12.7.2-1). Many of the available solutions are given in Levenspiel and Bischoff [1963], Himmelblau and Bischoff [1968], and Wen and Fan [1975]. These

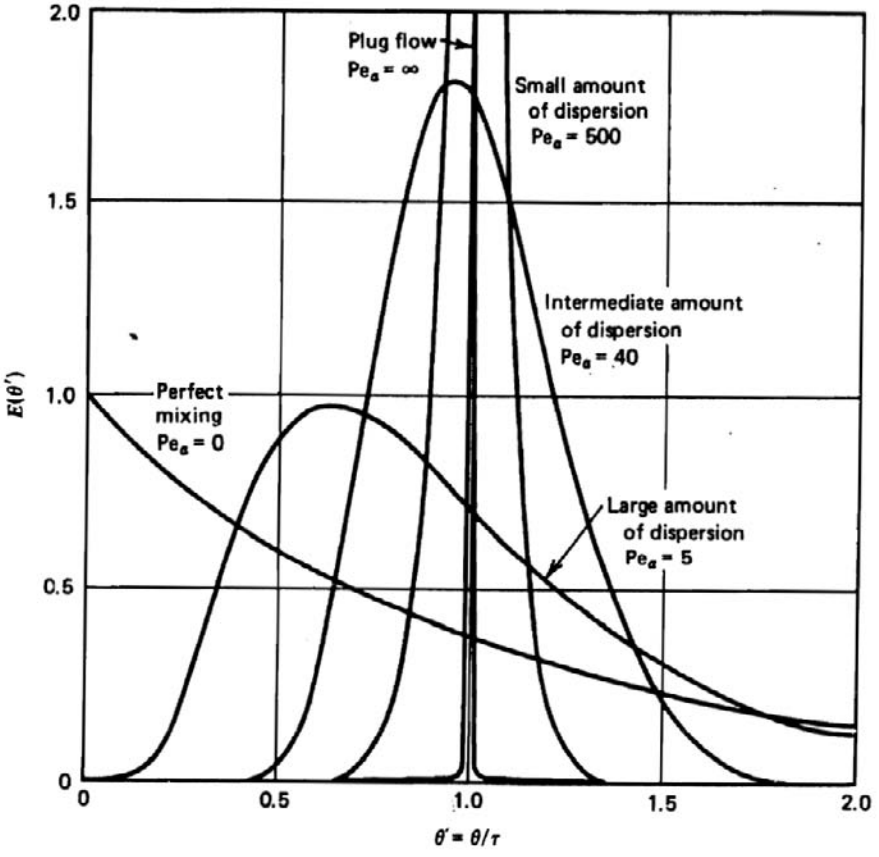

Figure 12.7.2-1

E curves in closed vessels for various extents of dispersion; $Pe_a = uL/D_a$. After Levenspiel [1972].

mathematical complexities should probably not be taken too literally, because the precise conditions at the boundaries of real equipment cannot usually be exactly defined, in any event. If the boundary condition details give significantly different results, caution about the axial dispersion model as being a faithful representation of the flow pattern in the vessel is recommended. These differences are only seen for large values of D_a (actually, small Pe_a), but the physical basis of the axial dispersion model is a diffusion-like situation, which would not be valid for large levels of mixing. For a diffusion-like model to be valid, the overall mixing should be the result of a large number of small random events.

As described in Sections 12.2 and 12.3, the moments of the impulse response can be used to characterize the RTD curve. This technique is also useful for estimating the model parameter D_a, although better techniques are described below. For a closed system it is found that

$$\mu = 1 \tag{12.7.2-3}$$

$$\sigma^2 = \frac{2}{Pe_a}\left[1 - \frac{1}{Pe_a}\left(1 - \exp\left[-Pe_a\right]\right)\right] \tag{12.7.2-4a}$$

$$\frac{2}{Pe_a} = 2\frac{D_a}{u\,L} \tag{12.7.2-4b}$$

The "width" of the axial dispersion model RTD is essentially inversely proportional to the Peclet number Pe_a or directly proportional to the axial dispersion coefficient D_a.

The "tanks-in-series" model is based on a series of perfectly mixed vessels, some features of which have been discussed in example 12.6.3.A. For the tanks-in-series model, Example 12.6.3.A gives

$$E(\theta') = \frac{(n)^n}{(n-1)!}(\theta')^{n-1}\exp\left[-n\theta'\right] \tag{12.7.2-5}$$

The model parameter need not strictly be an integer for curve-fitting purposes, and then (12.7.2-5) is interpreted as a gamma distribution, with mean equal to unity and variance

$$\sigma^2 = 1/n \tag{12.7.2-6}$$

There is no one exact way to compare the tanks-in-series and axial dispersion models, because the responses are never identical. In many ways, the two models are rather similar, although the mathematical details for the tanks-in-series model are much simpler than for the axial dispersion model. No theoretical justification such as Taylor diffusion is possible in general. The model parameter n, is strictly empirical, but a useful relationship can be obtained from equating the variances for the two models ((12.7.2-4a), (12.7.2-4b), (12.7.2-6)):

$$\sigma^2 = \frac{1}{n} = \frac{2}{Pe_a}\left[1 - \frac{1}{Pe_a}\left(1 - \exp\left[-Pe_a\right]\right)\right] \tag{12.7.2-7a}$$

or

$$n \cong \frac{Pe_a}{2} + \frac{1}{2} \qquad Pe_a > 2 \tag{12.7.2-7b}$$

which is similar to the relationship pointed out by Kramers and Alberda [1953]. This gives consistent results for plug flow, $D_a \to 0$ or $Pe_a \to \infty$ and $n \to \infty$, and also for perfect mixing, $D_a \to \infty$ or $Pe_a \to 0$ and $n \to 1$. This type of comparison

of the moments of the distribution curve of the two models has a wide applicability. It is based on the notion that two distributions must be similar if

(i) the "size" of the curve — the normalized form,
(ii) the "location" of the curve — the mean,
(iii) the "width" of the curve — the variance,

are equal. Finer details of the curves can also be matched through the use of higher moments, but, especially with experimental data, these higher moments are almost impossible to obtain. For the axial dispersion or tanks-in-series models that have only one (macro-)mixing parameter, the higher moments give no further information (beyond model consistency).

Even though the two models agree in many respects, one can devise situations where this is not true. For example, if a steady stream of tracer is injected into the reactor halfway to the exit, the axial dispersion model predicts "back mixing" because of the symmetrical nature of diffusion, but the tanks-in-series model obviously has no provision for backward transport of tracer. In situations where this phenomenon is important, the two models would *not* be similar at all. A closer similarity would be to modify the tanks-in-series model to include back flow streams [Roemer and Durbin, 1967; Klinkenberg, 1968, 1971]. A general analysis of systems with internal reflux using modified tanks-in-series models is presented by Shinnar and Naor [1967]. An interesting example of application to a real reactor with internal staged mixing characteristics that should be able to be represented by a modified tanks-in-series model is given by Lelli et al. [1972], including correlations of the parameters. Further details and comparisons with the axial dispersion model, are given in Seinfeld and Lapidus [1974]. With more complex flow and mixing situations, it is advisable to use more rigorous models, discussed earlier in this Chapter.

Once the model parameters are determined and correlated, the flow model can be used to predict the behavior of the reactor. With a first-order reaction occurring in a steady flow reactor with axial dispersion, the continuity equation for species *A* is:

$$D_a \frac{d^2 C_A}{dz^2} - u \frac{dC_A}{dz} - k C_A = 0 \qquad (12.7.2\text{-}8)$$

The proper boundary conditions have been extensively considered in the literature. For a "closed" reactor, consideration of flux balances at the entrance and exit provides what are usually termed the "Danckwerts boundary conditions" [1953]:*

$$C_{A0} = C_A\left(0^+\right) - \frac{D_a}{u}\frac{dC_A\left(0^+\right)}{dz} \tag{12.7.2-9}$$

$$\frac{dC_A\left(1^-\right)}{dz} = 0 \tag{12.7.2-10}$$

* As a matter of historic interest, these boundary conditions were utilized by Langmuir, *J. Am. Chem. Soc.*, 30, 1742 (1908).

[These boundary conditions can also be used to derive a solution for (12.7.2-1).] The same results are also found for other situations, as shown by Wehner and Wilhelm [1956] and Bischoff [1961]; transient cases are more complex — see Van Cauwenberghe [1966].

For specific reactors, the boundary conditions (12.7.2-9) and (12.7.2-10) may not be the most appropriate, since they imply that the local diffusion-like symmetrical "back dispersion" is valid at the boundaries [Beek and Miller, 1959]. In packed beds it is known from the work of Hiby [1962] that there is essentially no true "back mixing" and Wicke [1975] concluded that the only back transport would occur by molecular diffusion, which is usually small compared to other processes, and so the boundary conditions (12.7.2-9) would be replaced with

$$C_{A0} = C_A\left(0^+\right) \tag{12.7.2-9a}$$

The outlet boundary condition (12.7.2-10) is equivalent to a partially reflecting boundary, and taking the packed bed as a portion of a semi-infinite region may be preferable. This changes the boundary condition (12.7.2-10) into

$$C_A(\infty) \to 0 \tag{12.7.2-10a}$$

Again, there is a significant difference between the various solutions only when mixing is important — small Pe_a, in which case the axial dispersion model is not valid anyway. Other complicating situations are discussed in Young and Finlayson [1973], Zvirin and Shinnar [1976], Gill [1975], and Wen and Fan [1975].

With the Danckwerts boundary conditions, the solution of (12.7.2-8), (12.7.2-9), and (12.7.2-10) is

$$\frac{C_A}{C_{A0}} = \frac{4a\exp\left[\frac{1}{2}Pe_a\right]}{(1+a)^2\exp\left[(a/2)Pe_a\right] - (1-a)^2\exp\left[-(a/2)Pe_a\right]} \tag{12.7.2-11}$$

with

$$a \equiv \left(1 + \frac{4k\tau}{Pe_a}\right)^{1/2}$$

It is useful to compare this result for small deviations from plug flow — large Pe_a — by an expansion about the plug flow reactor conversion. The result is:

$$\frac{C_A}{(C_A)_{PF}} \cong 1 + \frac{(k\tau)^2}{Pe_a} \qquad (12.7.2\text{-}12a)$$

$$\cong 1 + \frac{D_a}{uL}\left[\ln\left(\frac{C_{A0}}{C_A}\right)\right]^2 \qquad (12.7.2\text{-}12b)$$

An alternate form is found by equating the actual and plug flow conversions:

$$\frac{k\tau}{(k\tau)_{PF}} \cong 1 + \frac{k\tau}{Pe_a} \qquad (12.7.2\text{-}13a)$$

$$\cong 1 + \frac{D_a}{uL}\ln\left(\frac{C_{A0}}{C_A}\right) \qquad (12.7.2\text{-}13b)$$

an expression already obtained by Langmuir [1908]. These results show that for a given plug flow conversion level, the reactor model with axial dispersion will produce essentially the same results for sufficiently large Pe_a.

For a given type of reactor, the axial dispersion coefficient is usually correlated using a characteristic local length l (e.g., the tube diameter, packing size):

$$Pe_a = \frac{uL}{D_a} = \left(\frac{ul}{D_a}\right)\left(\frac{L}{l}\right) = Pe_{l,a}\left(\frac{L}{l}\right) \qquad (12.7.2\text{-}14)$$

where $Pe_{l,a}$ is the *local* Peclet number for mass dispersion. Comparison of (12.7.2-14) with (12.7.2-12a) or (12.7.2-13a) indicates that axial dispersion effects may be neglected for reactors that are sufficiently long with respect to the characteristic dispersion length l. Mears [1976] has combined (12.7.2-13b) and (12.7.2-14) to provide a formal criterion:

$$\frac{L}{l} > \frac{1}{e}\frac{1}{Pe_{l,a}}\ln\frac{C_{A0}}{C_A} \qquad (12.7.2\text{-}15)$$

where e is the allowable error (e.g., 5 percent, $e = .05$). This criterion is generally satisfied for industrial reactors of the simple empty tube or packed bed types.

However, it may not be true for laboratory studies, especially in differential reactors, or for reactors with more complicated flow leading to large characteristic dispersion lengths. Results similar to (12.7.2-12a) for more complex rate forms, including adiabatic reactors, have been derived using formal perturbation techniques — see Turian [1973].

For reactors with finite wall heat transfer, Young and Finlayson [1973] pointed out that the ultimate conditions for a large reactor are determined by the heat exchange. In isothermal and adiabatic situations, the concentrations and temperatures are determined only by the reaction so that the difference between plug flow and axial dispersion model results always diminishes with increasing reactor length. But differences between the two models at the entrance may persist for reactors with wall heat transfer. They provide alternate criteria for the unimportance of axial dispersion (of both mass and heat) effects. Mears [1976] pointed out that these criteria were not general, and he provided alternate ones for equal feed and wall temperatures. These criteria are usually more stringent than (12.7.2-12a) or (12.7.2-15), but since their exact form is based on the precise boundary conditions at the reactor entrance, the uncertainties discussed below equation (12.7.2-9) should make one cautious in their implementation. For practical purposes, axial dispersion effects can usually be neglected in the common industrial and laboratory reactor if these are sufficiently long.

The radial dispersion characteristics can also be modeled with a diffusionlike equation. This is most often done for empty tubes or packed beds; the latter has been thoroughly covered in Chapter 11.

The conversion for the tanks-in-series model was presented in Chapter 10 and is close to the results from the axial dispersion model for $n \sim Pe_a/2 >> 1$. Two-dimensional networks of such compartments can be used to describe dispersion — this was briefly discussed in Chapter 11.

Even though the axial dispersion and tanks-in-series models discussed in this section can be used to handle a wide variety of nonideal flow situations, many reactors contain elements that do not satisfy the fundamental basis of a diffusionlike model and the development of consistent correlations for the dispersion coefficients might not be possible. In these situations, more fundamental models, as presented in the previous sections, need to be utilized.

PROBLEMS

12.1 **(a)** Starting from the Navier-Stokes equations (12.3-1)–(12.3-5), derive the Reynolds-averaged Navier-Stokes equations.

(b) Calculate the Reynolds-averaged reaction rate for a second-order reaction: $r = kC_AC_B$. Consider the extreme cases of no and complete micro-mixing.

12.2 Cold-shot cooling in a fixed bed ammonia synthesis reactor

Consider a fixed bed ammonia synthesis reactor with fresh feed quenching between the adiabatic beds. Consider in particular the quenching zone in between the first and the second bed. Assuming that the temperature and the composition of the gas mixture at the exit of the first bed are uniform, verify by means of a 3-dimensional simulation if such is still the case at the inlet of the second bed.

Simulation model:

Use the Reynolds-averaged Navier-Stokes equations as described in Section 12.5. Account for the effects of turbulence via the turbulent viscosity and conductivity, as described in Sections 12.5.1 and 12.5.2, and using the standard k-ε model and wall functions. The set of coupled partial differential equations can be solved with a CFD code. Verify the grid independency of the results.

Data:

Reactor inner diameter: 1.5 m
Operating pressure: 200 bar
Quenching zone height: 1 m
Cold-shot configuration:

- 5 axially aligned tubes, open at both ends
- diameter: 0.1 m
- height: 0.1 m
- distance of the top of the cold-shot tubes to the exit of the first bed: 0.1 m
- radial position: 1 central, 4 at 0.5 m from the center of the reactor

First bed mass flow rate: $500 \cdot 10^3$ t/y
Exit temperature first bed: 510°C
Total cold-shot mass flow rate: $127.02 \cdot 10^3$ t/y
Cold-shot temperature: 250°C
c_{pg} = 3500 J/kg K

As a first approximation, a constant gas density of 50 kg/m^3 can be assumed. Next, account for variations in the gas density.

Alternative configurations can be studied, for example, closing the bottom ends of the cold-shot tubes.

The importance of turbulence (and of its accurate modeling) can also be studied.

12.3 Consider the following flow system:

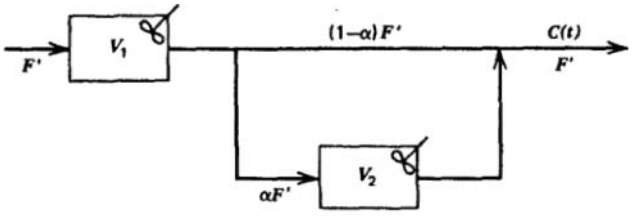

where a fraction α of the flow passes through the second tank V_2.

(a) For an impulse function input to tank V_1, derive the RTD for the complete system that would be measured at $C(t)$.

(b) Show that, for the special flow split,

$$\alpha = \frac{V_2}{V_1 + V_2}$$

The overall RTD becomes as for a *single, perfectly mixed region*!

Note that this example illustrates that overall perfect mixing, as measured by RTD, need not mean that the specific details of the flow system are a simple perfect mixer. Further discussion is provided by T. Fitzgerald, *Chem. Eng. Sci.*, 29, 1019 (1974).

12.4 Find the mean and variance for the RTD of Fig. 12.6.4.A-1.

12.5 Derive (12.6.4.B-d), (12.6.4.B-e), and (12.6.4.B-f). It might be helpful to first derive the first-order reaction results.

12.6 Given the reactor configurations

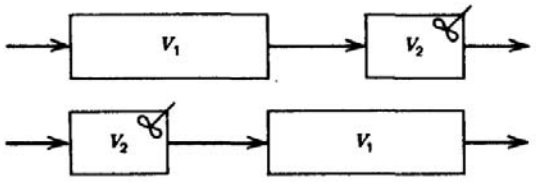

If the total volume $V = V_1 + V_2$ is imposed, what should be the ratio of the volumes V_1/V_2 in both cases to obtain the same exit conversion X_{Af} for a first-order reaction? For a second-order reaction?

12.7 Calculate the effect of recycle on the conversion in tubular reactors with plug flow.

12.8 Suppose a reactor system consists of many piston flow reactors in parallel:

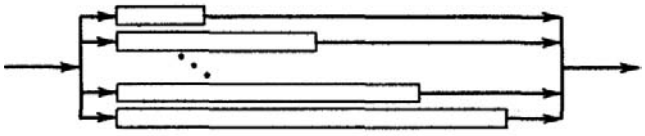

From Chapter 9 (or 1), the exit concentration in any one of them is, with a first-order reaction,

$$\frac{C_A(L)}{C_{A0}} = \exp[-\Omega kL / F']$$

(a) If the reactor lengths are arranged according to the gamma distribution,

$$f(L) = \left(\frac{\alpha+1}{\bar{L}}\right)^{\alpha+1} \frac{L^\alpha}{\Gamma(\alpha+1)} \exp\left[-\frac{(\alpha+1)L}{\bar{L}}\right]$$

where

$$\bar{L} = \text{mean length} = \int_0^\infty L f(L) dL \qquad \text{(check this)}$$

show that the total output of the system is given by

$$\frac{\bar{C}}{\bar{C}_{A0}} = \int_0^\infty \frac{C_A(L)}{C_{A0}} f(L) dL$$

$$= \left(1 + \frac{\bar{L}}{\alpha+1}\frac{\Omega k}{F'}\right)^{-(\alpha+1)}$$

(b) For the special case of $\alpha = 0$, the exponential distribution, the result of part (a) becomes

$$\frac{\bar{C}_A}{C_{A0}} = \left(1 + \frac{\bar{L}\Omega k}{F'}\right)^{-1}$$

which is the result for a single perfectly mixed reactor (Chapter 10). Discuss this result in view of reactor flow models.

12.9 Derive (12.7.2-11) and plot a few curves for various values of the parameters.

12.10 Show that for an axial dispersion flow system with variable density, area, velocity, and dispersion coefficients between two adjacent sections, equating total fluxes leads to the boundary condition

$$\left(\frac{C_1}{\rho_1}\right) - D_1 \frac{d}{dz}\left(\frac{C_1}{\rho_1}\right) = \left(\frac{C_2}{\rho_2}\right) - D_2 \frac{d}{dz}\left(\frac{C_2}{\rho_2}\right)$$

REFERENCES

Anderson, J.D., *Computational Fluid Dynamics*, McGraw-Hill, 1st ed. (1995).
Andersson, A.S., and White, E.T., *Chem. Eng. Sci.*, 26, 1203 (1971).
Aris, R., *Proc. Roy. Soc.*, A235, 67 (1956).
Arva, P., Kafarov, V.V., and Dorokhov, I.N., *Theor. Found. Chem. Eng.*, 3, 221 (1969).
Aubry, C., and Villermaux, J., *Chem. Eng. Sci.*, 30, 457 (1975).
Baldyga, J., *Chem. Eng. Sci.*, 44, 1175 (1989).
Baldyga, J., and Henczka, M., *Chem. Eng. J.*, 58, 161 (1995).
Baldyga, J., and Henczka, M., *Récent Progrès en Génie des Procédés*, 11, 341 (1997).
Bashi, H., and Gunn, D., *AIChE J.*, 23, 40 (1977).
Beek, J., and Miller, R.S., *Chem. Eng. Prog. Symp. Ser.*, 55, 25, 23 (1959).
Béguier, C., Dekeyser, I., and Launder, B.E., *Physics of Fluids*, 21, 307 (1978).
Berty, J.M.J., *Macromol. Sci. Chem.*, A8, 919 (1974). .
Bischoff, K.B., *Chem. Eng. Sci.*, 16, 131 (1961).
Bischoff, K.B., *Can. J. Chem. Eng.*, 41, 129 (1963).
Bischoff, K.B., and Coxson, P.G., *Sadhana-Proc. Indian Acad. Sci.*, 10, 299 (1987).
Boussinesq, J., "Théorie de l'Écoulement Tourbillant," Mem. Acad. Sci. Inst. Fr., 23, 46-50 (1877).
Böxkes, W., and Hofmann, H., *Chemie lng. Techn.*, 44, 882 (1972).
Bradshaw, P., Launder, B.E., and Lumley, J.L., *J. Fluids Eng. Trans. ASME*, 118, 243 (1996).
Brenner, H., *Chem. Eng. Sci.*, 17, 229 (1962).
Brink, A., Mueller, C., Kilpinen, P., and Hupa, M., *Combus. Flame*, 123, 275 (2000).
Brodkey, R.S., Ed., *Turbulence in Mixing Operations*, Academic Press, New York (1975).
Carberry, J.J., *Ind. Eng. Chem.*, 58(10), 40 (1966).
Carslaw, H.S., and Jaeger, J.C., *Conduction of Heat in Solids*, Oxford University Press, London (1959); 2nd Ed. (1986).
Chauhan, S.P., Bell, J.P., and Adler, R.J., *Chem. Eng. Sci.*, 27, 585 (1972).
Chen, M.S.K., *Chem. Eng. Sci.*, 26, 17 (1971).
Cholette, A. et al., *Can. J. Chem. Eng.*, 37, 105 (1959).
Cholette, A. et al., *Can. J. Chem. Eng.*, 50, 348 (1972).
Chu, L.C., and Fan, L.T., *Can. J. Chem. Eng.*, 41, 60 (1963).
Clements, W.C., *Chem. Eng. Sci.*, 24, 957 (1969).
Collucci, P.J., Jaberi, F.A., Givi, P., and Pope, S.B., *Phys. Fluids*, 10, 499 (1998).
Connolly, J.R., and Winter, R.L., *Chem. Eng. Prog.*, 65(8), 70 (1969).
Coulaloglou, C.A., and Tavlarides, L.L., *AIChE J.*, 22, 289 (1976).
Craft, T.J., and Launder, B.E., *AIAA J.*, 30, 2970 (1992).
Crank, J., *Mathematics of Diffusion*, Oxford University Press, London (1956).
Curl, R.L., *AIChE J.*, 9, 175 (1963).
Danckwerts, P.V., *Chem. Eng. Sci.*, 2, 1 (1953).
Danckwerts, P.V., *Chem. Eng. Sci.*, 8, 93 (1958).
Dayan, J., and Levenspiel, O., *Chem. Eng. Prog. Symp. Ser.*, 101, 66, 28 (1970).
De Marco, A.G., and Lockwood, F.C., *La Rivista dei Combustibili*, 29, 184 (1975).
Detemmerman, T., and Froment, G.F., *Rev. Inst. Fr. Pétr.*, 53, 181 (1998).
De Wasch, A.P., and Froment, G.F., *Chem. Eng. Sci.*, 26, 629 (1971).
Dopazo, C., *Physics of Fluids*, 18, 397 (1975).
Dopazo, C., *Physics of Fluids*, 22, 20 (1979).

Dreeben, T.D., and Pope, S.B., *Phys. Fluids*, 9, 154 (1997a).
Dreeben, T.D., and Pope, S.B., *Phys. Fluids*, 9, 2692 (1997b).
Dreeben, T.D., and Pope, S.B., *J. Fluid Mech.*, 357, 141 (1998).
Dryer, and Glassman, *Fourteenth Sym. (Int.) on Combustion*, The Combustion Institute, 987-1003 (1973).
Durbin, P.A., *Theor. Comput. Fluid Dyn.*, 3, 1 (1991).
Durbin, P.A., *J. Fluid Mech.*, 249, 465 (1993).
Ertesvåg, I.S., and Magnussen, B.F., *Combus. Sci. Technol.*, 159, 213 (2000).
Evangelista, J.J., Katz, S., and Shinnar, R., *AIChE J.*, 15, 843 (1969a).
Evangelista, J.J., Shinnar, R., and Katz, S., in *Proc. 12th Int. Symp. Comb.*, p. 901 (1969b).
Favre, A., *J. de Mécanique*, 4 (1965).
Fox, R.O., *Phys. Fluids*, 7, 1082 (1995).
Fox, R.O., *Phys. Fluids*, 8, 2678 (1996).
Fox, R.O., *Phys. Fluids*, 11, 1550 (1999).
Fox, R.O., *Computational Models for Turbulent Reacting Flows*, Cambridge University Press (2003).
Froment, G.F., *Reviews in Chem. Eng.*, 6, 294 (1990).
Gibilaro, L.G., Kropholler, H.W., and Spikins, D.J., *Chem. Eng. Sci.*, 22, 517 (1967).
Gicquel, L.Y.M., Givi, P., Jaberi, F.A., and Pope, S.B., *Phys. Fluids*, 14, 1196 (2002).
Gill, W.N., *Chem. Eng. Sci.*, 30, 1123 (1975).
Glasser, D., Katz, S., and Shinnar, R., *Ind. Eng. Chem. Fundam.*, 12, 165 (1973).
Glasser, D., Crowe, C.M., and Jackson, R., *Chem. Eng. Comm.*, 40, 41 (1986).
Goldstein, A.M., *Chem. Eng. Sci.*, 28, 1021 (1973).
Goto, S., and Matsubara, M., *Chem. Eng. Sci.*, 30, 61, 71 (1975).
Gray, J.B., *Mixing-Theory and Practice*, Vols. I and II, ed. by V.W. Uhl and J.B. Gray, Academic Press, New York (1966).
Günkel, A.E. and Weber, M.E., *AIChE J.*, 21, 931 (1975).
Gunn, D.J., *Chem. Eng. Sci.*, 25, 53 (1970).
Gwyn, J.E., and Colhart, J.D., *AIChE J.*, 15, 932 (1969).
Gwyn, J.E., Moser, J.H., and Parker, W.A., *Chem. Eng. Prog. Symp. Ser.*, No. 101, 66, 19 (1970).
Hanjalić, K., and Launder, B.E., *J. Fluid Mech.*, 52, 609 (1972).
Haworth, D.C., and Pope, S.B., *Phys. Fluids*, 29, 387 (1986).
Hiby, J.W., in *Interactions Between Fluids and Solids*, Inst. Chem. Eng., London, p. 312 (1962).
Himmelblau, D.M., and Bischoff, K.B., *Process Analysis and Simulation*, Wiley, New York (1968).
Hinze, J., *Turbulence: An Introduction to its Mechanism and Theory*, New York, McGraw-Hill (1959).
Hirsch, C., *Computation of Internal and External Flows: Fundamentals of Computational Fluid Dynamics*, Butterworth-Heinemann (2007).
Hochman, J.M., and Effron, E., *Ind. Eng. Chem. Fundam.*, 8, 63 (1969).
Hochman, J.M., and McCord, J.R., *Chem. Eng. Sci.*, 25, 97 (1970).
Hofmann, H., "Interaction of Fluid Flow and Chemical Kinetics in Homogeneous Reactions," presented at AIChE National Meeting, Houston, Texas (December 1963).
Hofmann, H., *Int. Chem. Eng.*, 17, 19 (1977).
Hosten, L.H., *Chem. Eng. Sci.*, 29, 2247 (1974).
Hosten, L.H., and Emig, G., *Chem. Eng. Sci.*, 30, 1357 (1975).
Hottel, H.C., and Sarofim, A.F., *Radiative Transfer*, McGraw-Hill, New York (1967).
Hougen, J.O., *Experiences and Experiments with Process Dynamics*, CEP Monograph Ser. No. 4, AIChE, 60 (1964).
Hull, D.E., and von Rosenberg, D.U., *Ind. Eng. Chem.*, 52, 989 (1960).
Hunt, B., *Int. J. Heat Mass Trans.*, 20, 393 (1977).
Jacob, S.M., *Ind. Eng. Chem. Proc. Des. Dev.*, 9, 635 (1970).
Jaberi, F.A., Collucci, P.J., James, S., Givi, P., and Pope, S.B., *J. Fluid Mech.*, 401, 85 (1999).
Janicka, J., Kolbe, W., and Kollmann, W., *J. Non-Equil. Thermodyn.*, 4, 47 (1979).
Jones, W.P., and Launder, B.E., *Int. J. Heat Mass Transfer*, 15, 301 (1972).

Jones, W.P., and Musonge, P., *Phys. Fluids*, 31, 3589 (1988).
Kattan, A., and Adler, R.J., *AIChE J.*, 13, 580 (1967).
Kattan, A., and Adler, R.J., *Chem. Eng. Sci.*, 27, 1013 (1972).
Katz, S., and Shinnar, R., *Ind. Eng. Chem.*, 61, No. 4, 60 (1969).
Khang, S.J., and Levenspiel, O., *Chem. Eng. Sci.*, 31, 569 (1976).
Klinkenberg, A., *Ind. Eng. Chem. Fundam.*, 5, 383 (1966).
Klinkenberg, A., *Chem. Eng. Sci.*, 23, 175 (1968).
Klinkenberg, A., *Chem. Eng. Sci.*, 26, 1133 (1971).
Koros, R.M., in *Proc. Fourth Int. Symp. Chem. React. Eng.*, Heidelberg, Fed. Rep. Germany, Dechema, Frankfurt, p. 372 (1976).
Kramers, H., and Alberda, G., *Chem. Eng. Sci.*, 2, 1731 (1953).
Kramers, H., and Westerterp, K.R., *Elements of Chemical Reactor Design and Operation*, Academic Press, New York (1963).
Langmuir, I., *J. Am. Chem. Soc.*, 30, 1742 (1908).
Launder, B.E., *Simulation and Modeling of Turbulent Flows*, Chap. 6, p. 243, Oxford University Press (1996).
Launder, B.E., and Spalding, D.B., *Mathematical Models of Turbulence*, London, Academic Press (1972).
Launder, B.E., Reece, G.J., and Rodi, W., *J. Fluid Mech.*, 68, 537 (1975).
Launder, B.E., and Sharma, B.I., *Lett. Heat Mass Transf.*, 1, 131 (1974).
Launder, B.E., and Shima, N., *AIAA J.*, 27, 1319 (1989).
Lelli, U., Magelli, F., and Sama, C., *Chem. Eng. Sci.*, 27, 1109 (1972).
Levenspiel, O., *Chemical Reaction Engineering*, 2nd ed., Wiley, New York (1972).
Levenspiel, O. and Bischoff, K.B., *Adv. Chem. Eng.*, Vol. 4, Academic Press, New York (1963).
Littman, H. and Barile, R.G., *Chem. Eng. Prog. Symp. Ser.*, No. 67, 62, 10 (1966).
Lumley, J.L., *Phys. Fluids*, 18, 750 (1975).
Magnussen, B.F., and Hjertager, B.H., In *Proceedings from the 16th Symposium (International) on Combustion*, The Combustion Institute, Pittsburgh, 719-729 (1976).
Mah, R.S.H., *Chem. Eng. Sci.*, 26, 201 (1971).
Mann, U., Crosby, E.J., and Rubinovitch, M., *Chem. Eng. Sci.*, 29, 761 (1974).
Matsuyama, H., and Miyauchi, T.J., *Chem. Eng. Japan*, 2, 80 (1969).
Mears, D.E., *Chem. Eng. Sci.*, 26, 1361 (1971).
Mears, D.E., *Ind. Eng. Chem. Fundam.*, 15, 20 (1976).
Mellor, G.L., and Herring, H.J., *AIAA J.*, 11, 590 (1973).
Menter, F., *AIAA J.*, 32, 1598 (1994).
Metzner, A.B., and Pigford, R.L., *Scaleup in Practice*, ed. by R. Fleming, Reinhold, New York, p. 16 (1958).
Michelsen, M.L., *Chem. Eng. J.*, 4, 171 (1972).
Miller, G.A., and Bailey, J.E., *AIChE J.*, 19, 876 (1973).
Mireur, J.P., and Bischoff, K.B., *AIChE J.*, 13, 839 (1967).
Mixon, F.O., Whitaker, D.R., and Orcutt, J.C., *AIChE J.*, 13, 21 (1967).
Murphree, E.V., Voorhies, A., and Mayer, F.X., *Ind. Eng. Chem. Proc. Des Dev.*, 3, 381 (1964).
Nagasubramanian, K., and Graessley, W.W., *Chem. Eng. Sci.*, 25, 1549 (1970).
Naot, D., Shavit, A., and Wolfshtein, M., *Israel J. Technol.*, 8, 259 (1970).
Nauman, E.B., *Chem. Eng. Sci.*, 24, 1461 (1969).
Nauman, E.B., *J. Macromol. Sci.-Rev. Macromol. Chem.*, c10, 75 (1973).
Nauman, E.B., *Chem. Eng. Sci.*, 30, 1135 (1975).
Nauman, E.B., *Chem. Eng. Sci.*, 32, 359 (1977).
Nauman, E.B., in *Scaleup of Chemical Processes*, ed. by A. Bisio and R.L. Kabel, Wiley, New York (1985).
Nauman, E.B. and Collinge, C.N., *Chem. Eng. Sci.*, 23, 1309, 1317 (1968).
Nienow, A.W., *Chem. Eng. Sci.*, 29, 1043 (1974).
Olson, J.H., and Stout, L.E., *Mixing Theory and Practice*, Vol. II, ed. by V.W. Uhl and J.B. Gray, Academic Press, New York (1966).
Orth, P., and Schügerl, K., *Chem. Eng. Sci.*, 27, 497 (1972).
Orszag, S.A., Staroselsky, I., Flannery, W.S., and Zhang, Y., *Simulation and Modeling of Turbulent Flows*, 4, 155 (1996).

Østergaard, K., and Michelsen, M.L., *Can. J. Chem. Eng.*, 47, 107 (1969).
Paul, E.L., and Treybal, R.E., *AIChE J.*, 17, 718 (1971).
Pavlica, R.T., and Olson, J.H., *Ind. Eng. Chem.*, 62(12), 45 (1970).
Petersen, E.E., *AIChE J.*, 6, 488 (1960).
Plehiers, P.M., and Froment, G.F., *Ind. Eng. Commun.*, 80, 81 (1989).
Pope, S.B., *Comb. Flame*, 27, 299 (1976).
Pope, S.B., *Combus. Sci. Technol.*, 25, 159 (1981).
Pope, S.B., *Combus. Sci. Technol.*, 28, 131 (1982).
Pope, S.B., *Progr. Energy Combus. Sci.*, 11, 119 (1985).
Pope, S.B., *Phys. Fluids*, 6, 973 (1994).
Pope, S.B., *Turbulent Flows*, Cambridge University Press (2000).
Popovic, M., and Deckwer, W.D., *Chem. Eng. J.*, 11, 67 (1976).
Pratt, D.T., in *Proc. Int. Symp. on Combustion*, The Combustion Institute, Pittsburgh, Pa., p. 1339 (1975).
Ramkrishna, D., Borwanker, J.D., and Shah, B.H., *Chem. Eng. Sci.*, 28, 1423 (1973).
Ramkrishna, D., Borwanker, J.D., and Shah, B.H., *Chem. Eng. Sci.*, 29, 1711 (1974).
Ramkrishna, D., Borwanker, J.D., and Shah, B.H., *Chem. Eng. Sci.*, 31, 435 (1976).
Ramkrishna, D., and Fredrickson, A.G., *Population Balances: Theory and Application to Particulate Systems in Engineering*, Academic Press (2000).
Randolph, A.D., and Larson, M.A., *Theory of Particulate Processes*, Academic Press, New York (1971).
Rao, M.V.R., Plehiers, P.M., and Froment, G.F., *Chem. Eng. Sci.*, 43, 1223 (1988).
Rietema, K., *Adv. Chem. Eng.*, 5, 237 (1964).
Rippin, D.W.T., *Chem. Eng. Sci.*, 22, 247 (1967).
Roemer, M.H., and Durbin, L.D., *Ind. Eng. Chem. Fundam.*, 6, 121 (1967).
Rotta, J.C., *Zeitschrift für Physik*, 129, 547 (1951).
Rudd, D.F., *Can. J. Chem. Eng.*, 40, 197 (1962).
Sanders, J.P.H., and Gökalp, I., *Phys. Fluids*, 10, 938 (1998).
Satterfield, C.N., *AIChE J.*, 21, 209 (1975).
Schechter, R.S., and Gidley, J.L., *AIChE J.*, 15, 339 (1969).
Schlichting, H., *Boundary-Layer Theory*, (7^{th} ed.), New York, McGraw-Hill (1979).
Schneider, P., and Smith, J.M., *AIChE J.*, 14, 762 (1968).
Seinfeld, J.H., and Lapidus, L., *Process Modeling, Estimation and Identification*, Prentice-Hall, Englewood Cliffs, N.J. (1974).
Shih, T.-H., Liou, W.W., Shabbir, A., Yang, Z., and Zhu, J., *Comput. Fluids*, 24, 227 (1995).
Shinnar, R., and Naor, P., *Chem. Eng. Sci.*, 22, 1369 (1967).
Shir, C.C., *J. Atmos. Sci.*, 30, 1327 (1973).
Sinclair, C.G., and Brown, D.E., *Biotech. Bioeng.*, 12, 1001 (1970).
Sinex, W.E., Schechter, R.S., and Silberberg, I.H., *Ind. Eng. Chem. Fundam.*, 11, 205 (1972).
Smith, L.M., and Reynolds, W.C., *Phys. Fluids*, A4, 364 (1992).
Smith, L.M., and Woodruff, S.L., *Annu. Rev. Fluid. Mech.*, 30, 275 (1998).
Spalding, D.B., *Chem. Eng. Sci.*, 26, 95 (1971).
Spalding, D.B., *Mixing and Chemical Reaction in Steady Confined Turbulent Flames*, Imperial College of Science and Technology, London, 649 (1972).
Spaulding, D.B., *Chem. Eng. Sci.*, 9, 74 (1958).
Speziale, C.G., Sarkar, S., and Gatski, T.B., *J. Fluid Mech.*, 227, 245 (1991).
Spielman, L.A., and Levenspiel, O., *Chem. Eng. Sci.*, 20, 247 (1965).
Swift, S.T., and Fogler, H.S., *Chem. Eng. Sci.*, 32, 339 (1977).
Taniyama, I., and Sato, T., *Kagaku Kogaku*, 29, 709 (1965).
Taylor, G.I., *Proc. Roy. Soc.*, A219, 186 (1953).
Truong, K.T., and Methot, J.C., *Can. J. Chem. Eng.*, 54, 572 (1976).
Turian, R.M., *Chem. Eng. Sci.*, 28, 2021 (1973).
Van Cauwenberghe, A.R., *Chem. Eng. Sci.*, 21, 203 (1966).
Van Deemter, J.J., in *Proc. Int. Symp. Fluidization*, Eindhoven, ed. by A.A.H. Drinkenberg, The Netherlands Universities Press, Amsterdam (1967).
van der Laan, E.T., *Chem. Eng. Sci.*, 7, 187 (1957).
van de Vusse, J.G., *Chem. Eng. Sci.*, 17, 507 (1962).
Vassilatos, G., and Toor, H.L., *AIChE J.*, 11, 666 (1965).

Vercammen, H.A.J., and Froment, G.F., in *Chemical Reaction Engineering*, V.W. Weekman and D. Luss, eds., *A.C.S. Symp. Ser.*, 65, 271-281 (1978).
Vercammen, H.A.J., and Froment, G.F., *Int. J. Heat Transf.*, 23, 329 (1980).
Villermaux, J., in *Chemical Reaction Engineering-Plenary Lectures*, ed. by J. Wei and C. Georgakis, A.C.S. Symp. Series, 226, Washington, D.C. (1983).
Villermaux, J., in *Chemical Reactor Design and Technology*, ed. by H. de Lasa, Martinus Nimnhoff Publ., Dordrecht (1986a).
Villermaux, J., in *Encyclopedia of Fluid Mechanics*, Gulf Publ. Comp., Houston (1986b).
Villermaux, J., and DeviIlon, J.C., in *Proc. Second Int. Symp. Chem. React. Eng.*, Elsevier, Amsterdam (1972).
Villermaux, J., and van Swaaij, W.P.M., *Chem. Eng. Sci.*, 24, 1097, 1083 (1969).
Villermaux, J., and Zoulalian, A, *Chem. Eng. Sci*., 24, 1513 (1969).
Wakao, N., *Chem. Eng. Sci.*, 31, 1115 (1976).
Weekman, V.W., *Ind. Eng. Chem. Proc. Des. Dev.*, 7, 90 (1968).
Wehner, J.F., and Wilhelm, R.H., *Chem. Eng. Sci.*, 6, 89 (1956).
Wei, J., *Can. J. Chem. Eng.*, 44, 31 (1966).
Weinstein, H., and Adler, R.J., *Chem. Eng. Sci.*, 22, 65 (1967).
Wen, C.Y., and Fan, L.T., *Models for Flow Systems and ChemicalReactors*, Marcel Dekker, New York (1975).
Wicke, E., *Chemie Ing. Techn.*, 47, 547 (1975).
Wilcox, D.C., *Turbulence Modeling for CFD*, California, DCW Industries Inc (1993).
Williams, J.A., Adler, R.J., and Zolner, W.J., *Ind. Eng. Chem. Fundam.*, 9, 193 (1970).
Yakhot, V., and Orszag, S.A., *J. Sci. Comput.*, 1, 3 (1986).
Young, L.C., and Finlayson, B.A., *Ind. Eng. Chem. Fundam.*, 12, 412 (1973).
Zoulalian, A., and Villermaux, J., in *Proc. 3rd Int. Symp. Chem. React. Eng., Adv. Chem. Ser.*, 133, A.C.S., Washington, D.C. (1974).
Zvirin, Y., and Shinnar, R., *Water Research*, 10, 765 (1976a).
Zvirin, Y., and Shinnar, R., *Int. J. Multiphase Flow*, 2, 495 (1976b).
Zwietering, T.N., *Chem. Eng. Sci.*, 11, 1 (1959).

Chapter 13

Fluidized Bed and Transport Reactors

13.1 INTRODUCTION

Although Winkler introduced the fluidized bed technique in the gasification of lignite as early as 1926, the real breakthrough of fluidized beds was associated with the catalytic cracking of gasoil into gasoline, first practiced in 1942 at the Baton Rouge refinery of Standard Oil of New Jersey, now Exxon. Before that, catalytic cracking was carried out in fixed bed reactors. Catalytic cracking deposits carbonaceous products on the catalyst, causing rapid deactivation of the latter. To maintain the production capacity, the coke had to be burned off. This regeneration required switching the reactor out of production. In order to eliminate the cycling, attempts were made to circulate the catalyst and burn off the coke in a separate vessel, the regenerator. The first approach was to use a moving catalyst bed: in the reactor the catalyst moved downward, against the fluid stream, in a very compact mass, into the regenerator. From the regenerator the catalyst was returned to the top of the reactor by a bucket conveyor. Later, the conveyor system was replaced by a gas lift. Finally, both the reactor and the regenerator were operated under transport conditions. The high velocities required for pneumatic transport caused considerable attrition of the catalyst. To lower the velocities, very fine solids had to be used. It was then found that the dense mixture of solids and gas behaved in many aspects like a fluid, and this makes the control of streams much more convenient. Since then, fluidized beds have been used in other fields where solids have to be handled, such as the roasting of ores and in catalytic reactors for highly exothermic reactions. The latter application is based upon another advantage: the high turbulence created in the fluid-solid mixture leads to much higher heat transfer coefficients than those which can be obtained in fixed beds. Therefore, fluidized bed reactors have also found use in exothermic processes requiring close temperature control such as the oxidation of naphthalene into phthalic anhydride, the ammoxidation of propylene into acrylonitrile, the oxychlorination of ethylene into ethylene dichloride — the first step of vinyl chloride manufacture, and the Union Carbide process for polymerization of ethylene. An important application is fluid bed combustion of coal, which permits using low-grade coals rich in mineral matter, less suited for conventional boilers. An additional advantage is the in situ capture of sulfur dioxide by means of injected limestone. Whereas in the above cases

only a minor fraction of the catalyst is entrained with the gas, so that the major part is confined in a dense bed, with a dilute section and cyclones above it, there are also processes in which the total amount of catalyst is entrained by the gas. The reactors then belong to the category of transport reactors. Examples are some of the Fischer-Tropsch reactors used in Sasol, South Africa, for the production of hydrocarbons from synthesis gas and modern catalytic cracking units called "riser" units.

The design and operation of fluidized bed and transport reactors is by no means an easy task, particularly when the circulation of solids is involved. The technology is much more complicated than that associated with fixed bed reactors. Before dealing with the conversion problem along the lines of the preceding chapters, some technological aspects will be discussed, without entering into great detail, however. Several books have been published on the subject [Davidson and Harrison, 1963, 1971; De Groot, 1967; Kunii and Levenspiel, 1969, 1991; Leva, 1960; Zenz and Othmer, 1960; Angelino et al., 1974; and Avidan, 1982].

To begin with, some technological aspects will be illustrated by means of a brief description of catalytic cracking.

13.2 TECHNOLOGICAL ASPECTS OF FLUIDIZED BED AND RISER REACTORS

13.2.1 Fluidized Bed Catalytic Cracking

Catalytic cracking of gasoil for the production of gasoline is carried out at temperatures of the order of 525°C. The catalyst containing 1 or 2 wt-% coke is regenerated with air around 580°C, reducing the coke content to 0.4 to 0.8 wt-%. An early type of the reactor-regenerator system is shown schematically in Fig. 13.2.1-1, with some typical operating characteristics listed in Table 13.2.1-1. The oil is fed at the bottom of the reactor through a perforated plate distributor and the gasoline and gases are taken off at the top.

The top of the fluidized bed has a more or less clearcut surface, but some solids are entrained and a certain freeboard is necessary to minimize this. To avoid catalyst loss and elutriation, the exit stream flows through a two-stage cyclone. The catalyst is fed back to the bed through pipes called "diplegs", which have a seal at their bottom for preventing leakage of bed fluid.

The catalyst is allowed to leave the reactor through a bottom standpipe. It is first stripped with steam to remove adsorbed hydrocarbons, and it then moves through the transfer line, under the influence of a static head, to the regenerator,

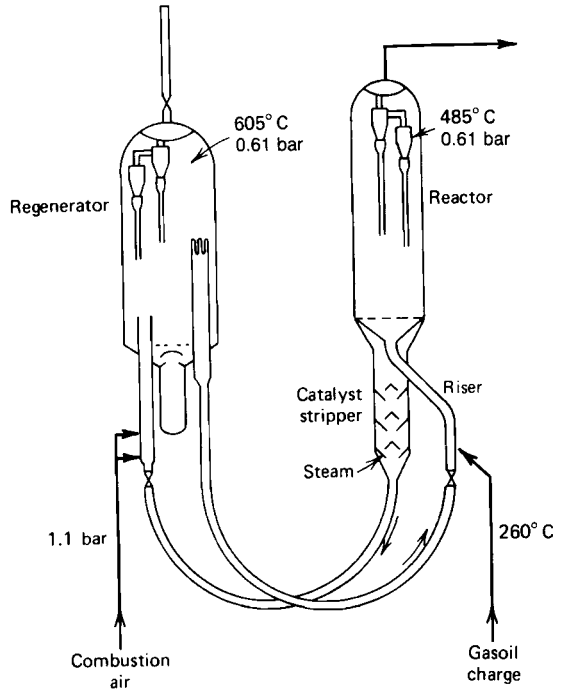

Figure 13.2.1-1

Reactor regeneration system for catalytic cracking of gasoil.

After Zenz and Othmer [1960].

TABLE 13.2.1-1

SOME TYPICAL OPERATING FIGURES FOR FLUID CATALYTIC CRACKERS. FROM ZENZ AND OTHMER [1960].

Medium size capacity: 15,000 barrels/day = 2390 m³ gasoil/day	
Catalyst: silica-alumina/zeolite catalyst or molecular sieves 20-80μm	
Total catalyst inventory:	250 tons
Amount in regenerator:	100 tons
Catalyst bulk densities (in kg/m³)	
Reactor and regenerator:	320-560
Stripper:	480-640
Standpipes:	560-720
Risers:	80-480
Diplegs:	240-560
Catalyst circulation rate:	24 tons/min
Catalyst flow rate to cyclones:	7 tons/min
Catalyst loss:	2 tons/day
Superficial velocity in reactor and regenerator:	0.5-1.3 m/s
Velocities in standpipes:	1.7 m/s
Risers:	7-10 m/s
Diplegs:	1.7 m/s

where the static pressure is lower. The lower static pressure in the riser leading to the regenerator is due to the aeration of the gas-solid mixture with air required for burning off the coke. More air for the regenerator is injected in the regenerator itself, through a distributor plate. The regenerator also has a two-stage cyclone to reduce the catalyst loss. The regenerated catalyst flows into a downcomer or standpipe and back to the reactor. The difference in static pressure required for this is realized by injection of the oil into the riser of the reactor. The oil rapidly evaporates in the pipe and reduces the catalyst bulk density. Slide valves in the lines permit additional adjustment of the flow rates.

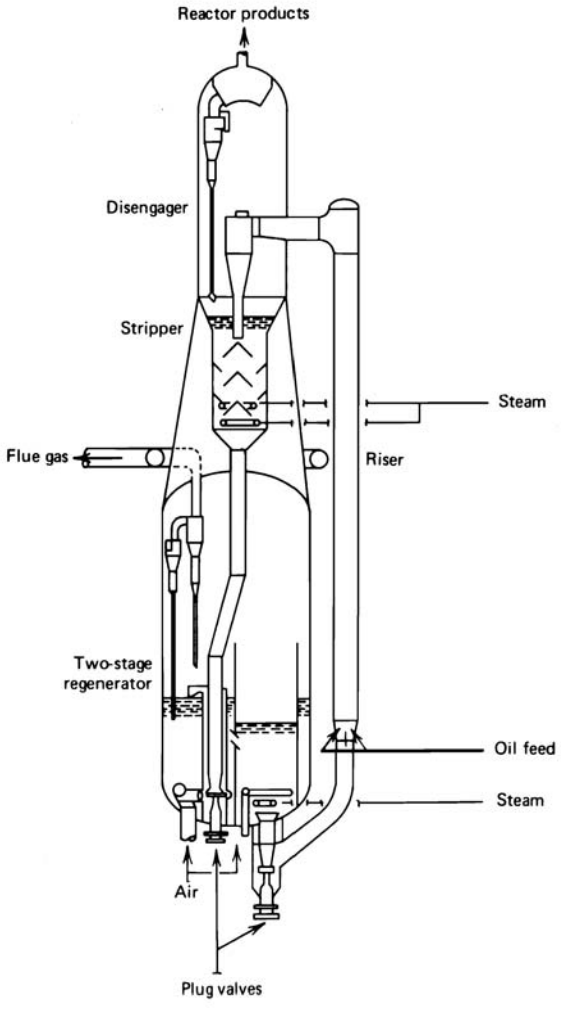

Figure 13.2.2-1

Kellogg Orthoflow model *F* converter with riser cracking and two-stage regeneration. From Murphy and Soudeck [1976].

The rate of circulation of the solids is dictated by the heat balance and activity level of the catalyst. The heat produced by the regeneration is carried to the reactor by the catalyst, and there it evaporates, heats, and cracks the oil. The transfer lines have to be designed in such a way that they are not eroded by the catalyst. The catalyst also has to withstand attrition.

13.2.2 Riser Catalytic Cracking

Modern technology is considerably different, particularly since the introduction, in the early sixties, of synthetic crystalline zeolite catalysts. These were so active that the cracking mainly or entirely took place in the riser, so that the reaction vessel caused overcracking into undesired light gases and coke. A recent version of a catalytic cracker is shown in Fig. 13.2.2-1. The catalyst is completely entrained in the riser-reactor, to reduce the contact time. The former reactor vessel is now essentially reduced to a vessel containing cyclones and a stripping section.

A more recent development is the fluidized bed with downflow of gas and solids for which the French Petroleum Institute built a large pilot plant. Talman et al. [1999] discussed modeling aspects of such an operation.

13.3 SOME FEATURES OF THE FLUIDIZATION AND TRANSPORT OF SOLIDS

There is a considerable difference in behavior between coarse particles with a size between 650 and 2600 μm, used in fluid bed combustion, and fine particles with a size between 60 and 100 μm, typically used in catalytic cracking. To begin with, the behavior of coarse particles will be discussed.

Consider a packed bed of coarse particles and the pressure drop over the total bed height as a function of the flow rate of a gas flowing through it. The pressure drop increases as shown in Fig. 13.3-1 along the line 1-2. From the velocity corresponding to point 3 onward, the pressure drop decreases slightly, due to resettling of the catalyst in the loosest arrangement. Beyond that point, the pressure drop remains practically constant. Upon decreasing the velocity, a certain hysteresis is found. The break in the curve, corresponding to point 4, is the point of minimum fluidization.

The point of minimum fluidization is easily observed. The voidage at minimum fluidization, which is an important value for design, is calculated from

$$\Delta p_t = L_{mf}(1-\varepsilon_{mf})(\rho_s - \rho_g)\,g \qquad (13.3\text{-}1)$$

In the absence of experimental data, it is possible to predict the minimum fluidization velocity by equating the pressure drop given by (13.3-1) and that calculated from a pressure drop equation for flow through a packed bed just before incipient fluidization. The resulting equation contains a shape factor and the void fraction at minimum fluidization, which may not be available. This ε_{mf} may be correlated with respect to the particle diameter. Finally, according to Leva [1960], this leads to

$$u_{mf} = 1.118 \times 10^{-13} \frac{d_p^{1.82}(\rho_s - \rho_g)^{0.94}}{\rho_g^{0.06}\mu^{0.88}} \tag{13.3-2}$$

with u_{mf} in m/s, d_p in μm, ρ in kg/m³, and μ in N s/m^2. As the fluid velocity is increased above u_{mf}, the bed expansion increases, but there are no really satisfactory general correlations in this range for predicting the void fraction or bed height.

When the velocity is further increased, the bed becomes less dense and finally the particles are blown out at the terminal or free-fall velocity. The velocity can be calculated by comparing the drag exerted on a spherical particle by the upflowing gas, F_D, and the gravity force, $(\pi d_p^3/6)(\rho_s - \rho_g)g$, so that

$$u_t = \sqrt{\frac{4gd_p(\rho_s - \rho_g)}{3\rho_g C_D}} \tag{13.3-3}$$

where C_D is the drag coefficient, a friction factor for flow around a submerged object. The drag coefficient depends upon the particle Reynolds number $\mathrm{Re}_p = d_p \rho_g u_t / \mu$.

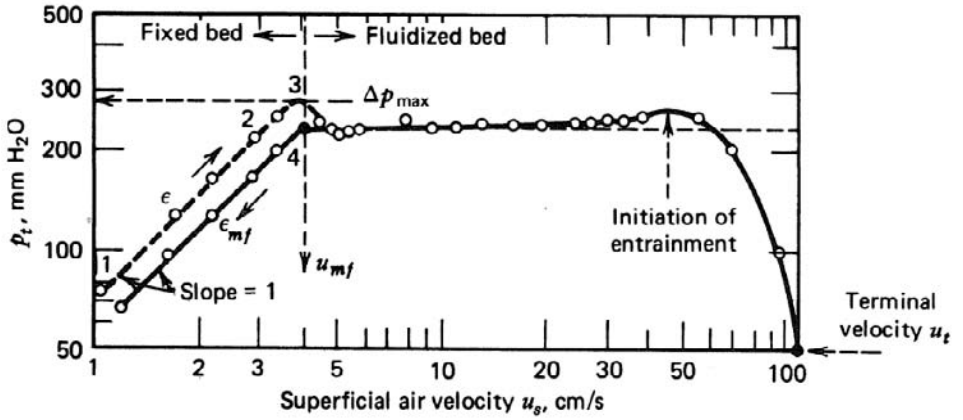

Figure 13.3-1

Pressure drop versus gas velocity for a bed of uniformly sized sand particles.
From Shirai [1958], after Kunii and Levenspiel [1969].

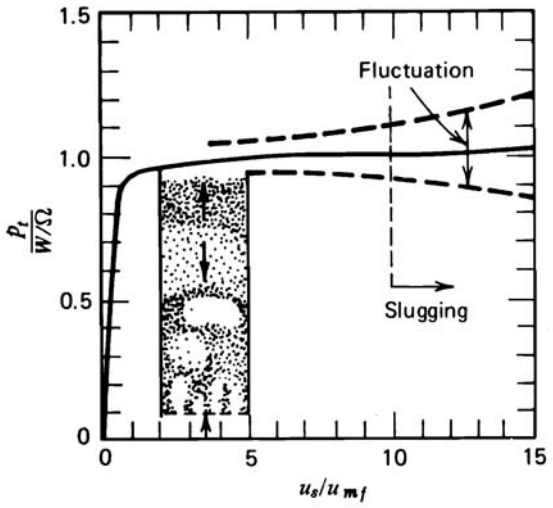

Figure 13.3-2

Pressure drop diagram for fluctuating and slugging fluidized beds. From Kunii and Levenspiel [1969].

For spheres and laminar flow ($Re_p < 0.4$), the drag coefficient is given by

$$C_D = \frac{24}{\mathrm{Re}_p} \tag{13.3-4}$$

so that Stokes' law is obtained for u_t (in m/s):

$$u_t = \frac{(\rho_s - \rho_g) g d_p^2}{18\mu} \tag{13.3-5}$$

For $1 < Re_p < 10^3$, the experimental results can be fitted by [Trambouze et al., 1984]

$$\ln C_D = -5.150 + \frac{69.43}{\ln \mathrm{Re}_p + 7.99} \tag{13.3-6}$$

For $Re_p > 10^3$, the drag coefficient C_D is 0.43 and Newton's law is obtained for u_t (in m/s):

$$u_t = \sqrt{\frac{3.1 d_p (\rho_s - \rho_g) g}{\rho_g}} \tag{13.3-7}$$

Pressure drop-versus-velocity diagrams do not always have the exact appearance of Fig. 13.3-1. Figure 13.3-2 shows such a diagram when slugging occurs, that is, when the bubble size equals the tube diameter. Slugging can be avoided by reducing the height/diameter ratio. Figure 13.3-3 is a diagram revealing channeling.

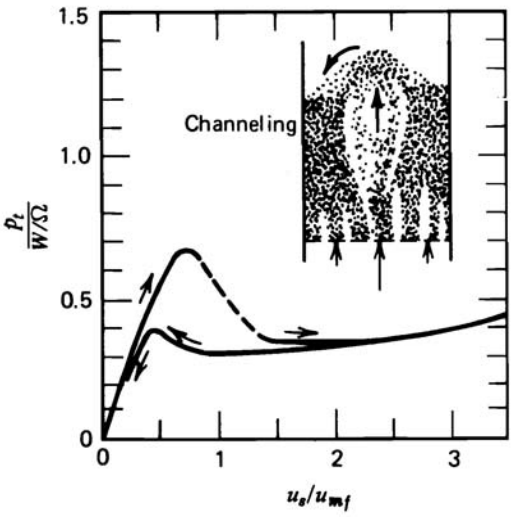

Figure 13.3-3
Pressure drop diagram for channeling fluidized beds. From Kunii and Levenspiel [1969].

This occurs when the fluid has preferential paths through the reactor and may be avoided by a better distributor and by increasing the height-to-diameter ratio. A rule of thumb says that the pressure drop over the distributor should be at least one tenth of the pressure drop over the bed.

A closer look at the bed permits a more detailed description, schematically represented in Fig. 13.3-4, in which the void fraction is plotted versus the relative superficial gas velocity. As soon as the minimum fluidization velocity is exceeded, bubbles appear in the bed. Beyond the bubbling regime, a turbulent regime is obtained in which the bubble life time is short, so that, overall, the bed looks more uniform. The terminal and blow-out velocities coincide. Beyond that velocity, the regime of fast fluidization is reached, with a net entrainment of solids. If the velocity is further increased, the transport regime is reached, with a very steep decline in the solid volume fraction.

With fine particles, such as those used in the FCC process, the diagram is modified, as shown by Fig. 13.3-5. Bubbles do not appear as minimum fluidization is reached. There is a range of velocities in which uniform expansion is observed. The bed is much more coherent than in the previous case, and the particles behave less individually. The turbulent regime sets in way beyond the terminal velocity of an individual particle. This is an interesting regime because the effect of the bubble short-circuiting is much less pronounced than in the bubbling regime, so that high conversions can be more readily obtained. It is encountered in acrylonitrile synthesis reactors, operating at a superficial gas velocity of 0.50 m/s, and in phthalic anhydride synthesis reactors (0.30 to 0.60 m/s). FCC regenerators operate at gas velocities as high as 0.60 m/s, yet the bed is more bubbling because of an additional factor, namely, a lack of fines. To

achieve smooth fluidization and really have turbulent conditions, 20 to 35 percent of fines with particle diameter below 40 μm are required. The ratio of highest to lowest operable gas velocity is much wider than with coarse particles. Carryover does not segregate the particles according to their size, as is observed with coarse particles; and when the gas flow is cut off, the bed is not immediately defluidized. The Kellogg-Fischer-Tropsch reactors at Sasol S.A. operate in the fast regime and modern catalytic cracking units in the riser flow regime, in which the solids flow rate is very high.

To operate a classical fluidized bed, that is, without net transport of catalyst, the solids have to be retained. The height at which the cyclone inlet is placed depends upon its size and efficiency. To determine this height, the designer requires information concerning the rate of entrainment and the size distribution of the solids in the entrained fraction as a function of height above the bed. The entrainment becomes approximately constant from a certain height above the bed meniscus onward, called "transport disengaging height". As far as the cyclone size is concerned, nothing is gained by placing the inlet higher than the transport disengaging height, which has been empirically correlated by Zenz and Weil [1958] for fluid cracking catalyst. The entrainment in g/cm^3 has been correlated by Lewis et al. [1959] as follows:

$$\frac{F}{\Omega u_s} = B \exp\left\{ -\left[\left(\frac{b}{u_s} \right)^2 + aH \right] \right\} \tag{13.3-8}$$

where $B = 0.02$ g/cm^3 and $b = 8.86 \times 10^4 \ \rho_s^{1/2} d_p$ cm/s.

Elutriation is the selective removal of fines by entrainment from a bed of particles with a distribution in particle size. Some work has been published on predicting rates of elutriation. The rate of elutriation of fines with particle diameter, d_p, is considered to be proportional to the fraction of the bed consisting of fines with diameter d_p so that

$$-\frac{1}{\Omega} \frac{dW(d_p)}{dt} = k_{\text{el}} \frac{W(d_p)}{W} \tag{13.3-9}$$

where W is the total weight of solids in the bed and $W(d_p)$ is the weight of the amount of catalyst with diameter d_p. The elutriation rate coefficient k_{el} has been correlated by Wen and Hashinger [1960] and by Yagi and Aochi [in Kunii and Levenspiel, 1969 - p. 315]. The cyclone design is a problem in itself, which is treated in detail in Zenz and Othmer [1960] and in standard handbooks on chemical engineering [e.g., Perry and Chilton, 1973].

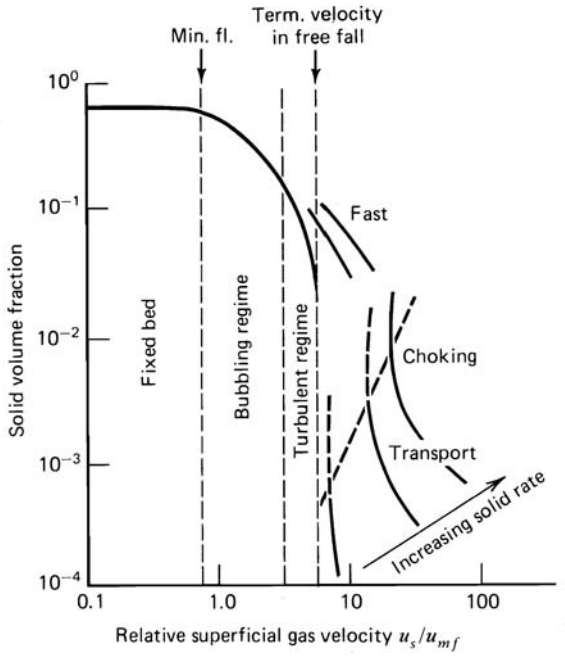

Figure 13.3-4

Fluidization regimes with coarse particles. After Squires et al. [1985].

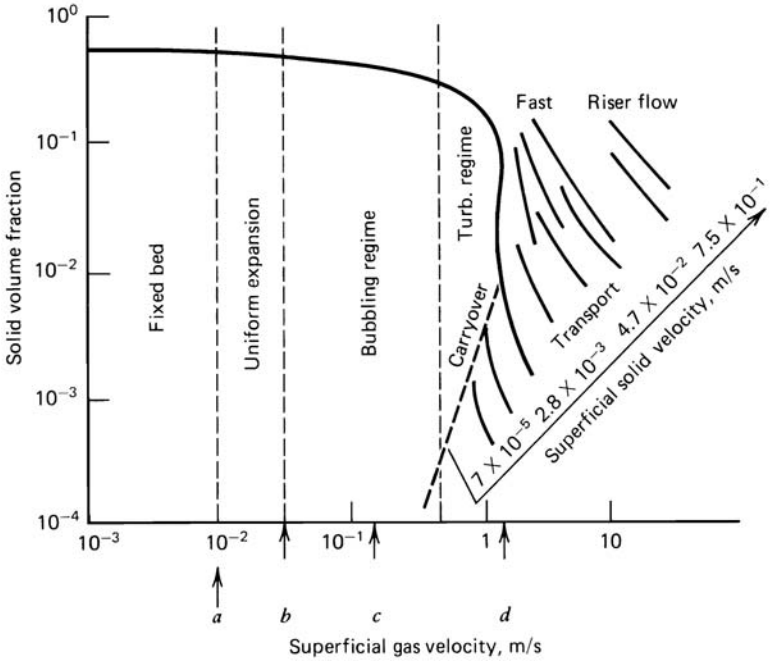

Figure 13.3-5

Fluidization regimes with fine particles. After Squires et al. [1985]. (a) Minimum buoyancy; (b) Minimum bubbling; (c) Terminal velocity; (d) Blowout velocity.

13.4 HEAT TRANSFER IN FLUIDIZED BEDS

In some cases it is necessary to exchange heat with the fluidized bed, for example, in the catalytic oxidation of naphthalene or propylene. Heat may be exchanged through the wall or through internal heat exchangers. The available data have been empirically correlated and are briefly mentioned here. Figure 13.4-1 shows the most complete correlation available for heat transfer between the bed and the wall, based on a pseudo-single-phase model [Wender and Cooper, 1958]. The diagram contains the usual groups involved in such correlations: on the abscissa the Reynolds number and on the ordinate the Nusselt number $\alpha d_p/\lambda_g$ multiplied by a group that accounts for the other variables involved. Further work on this problem has been reported by Fritz [1969].

Figure 13.4-2 shows the correlation for heat exchange between the bed and internal heat exchangers (where $\lambda_g/c_p\rho_g$ is in ft^2/h). In this figure C_R is a correction factor depending on the location of the heat exchanger with respect to the longitudinal axis of the bed, as shown in Fig. 13.4-3.

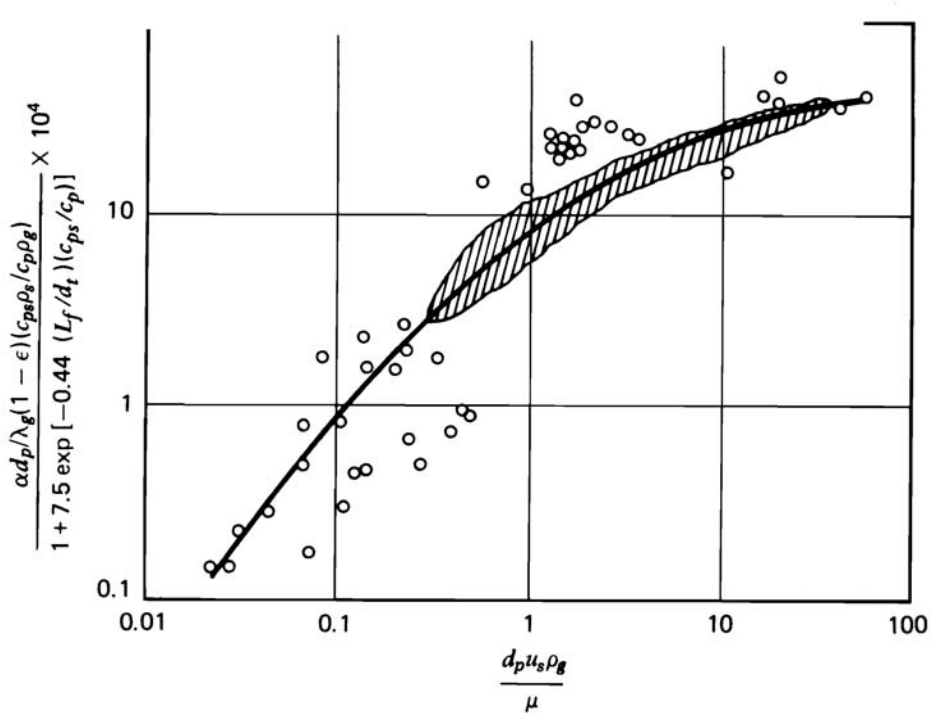

Figure 13.4-1

Correlation of fluid bed to external surface heat transfer coefficients. Wender and Cooper [1958]. From Zenz and Othmer [1960].

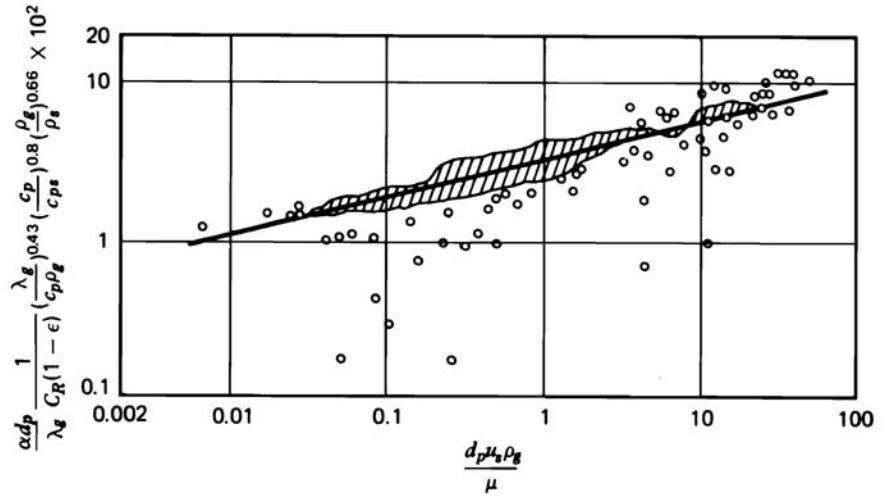

Figure 13.4-2

Correlation for fluid bed to internal surface heat transfer coefficients.
Wender and Cooper [1958]. From Zenz and Othmer [1960].

It follows from the above correlations that the heat transfer coefficient between a fluidized bed and a surface is high, often in the range of 0.232 to 0.697 kJ/m^{2}s K.

Finally, the temperature difference between the gas and the catalyst surface has to be calculated. The following correlation has been proposed for air:

$$\frac{\alpha d_p}{\lambda_g} = 0.017\left(\frac{d_p G}{\mu}\right)^{1.21} \tag{13.4-1}$$

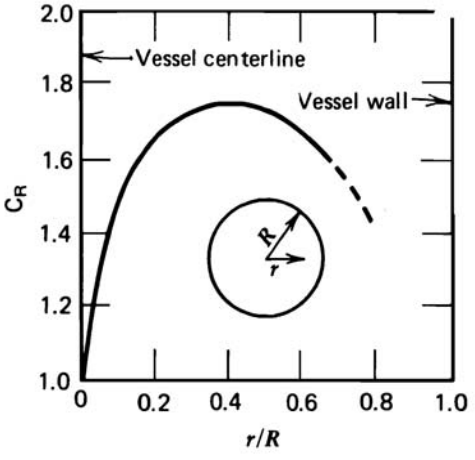

Figure 13.4.3

Correction factor for nonaxially located internal heat transfer surface. Based on data of Vreedenberg [1960], from Zenz and Othmer [1960].

It can be generalized somewhat more by introducing the Prandtl number. The correlation is based on a pseudo-single-phase model. It follows from the correlation that the gas approaches the temperature of the solid in the very first centimeters of the bed already. This is confirmed by a correlation of Balakrishnan and Pei [1975]:

$$j_H = 0.043\left[\frac{d_p g}{u_s^2}\frac{(\rho_s - \rho_g)(1-\varepsilon)^2}{\rho_g}\right]^{0.25} \qquad (13.4\text{-}2)$$

where ε is the void fraction of the fluidized bed.

13.5 MODELING OF FLUIDIZED BED REACTORS

13.5.1 Two-Phase Model

It was soon recognized that the simple plug flow and complete mixing models were inadequate for predicting conversion in fluidized beds. Around 1960, a model with effective axial diffusion superposed on the plug flow was tried, with little more success. Neither of these models can explain experimental conversion x-versus-W/F_0 curves below those for complete mixing. Such an observation can only be explained by assuming that a fraction of the gas bypasses the catalyst. This is quite logical, since an important fraction of the gas flows through the bed in the form of bubbles. The amount of catalyst in the bubbles is very small, and its contribution to the total conversion is usually negligible. Yet, in industrial reactors the fraction of gas flowing through the bed in the form of bubbles is so large that, to fit experimental data, one must conclude that this gas does not completely bypass the catalyst. Because of coalescence or bubble growth some interchange of gas was postulated between the bubble phase and the dense phase surrounding it, also called “emulsion phase”. These considerations led to the two-phase models, which have substantially clarified and refined the interchange phenomenon. Figure 13.5.1-1 schematically represents such a two-phase model. A fraction of the total flow rate through the bed is considered to be in the bubble phase, the rest in the emulsion phase. Between both phases there is a certain interchange of gas, or cross flow. At the outlet, both streams, with their respective conversions, are hypothetically mixed to give the exit stream, with its mean conversion or concentration. Since there is no reaction in the bubble phase and because of its high velocity, the flow through that phase is usually taken to be of the plug flow type. In the emulsion phase various degrees of deviation from

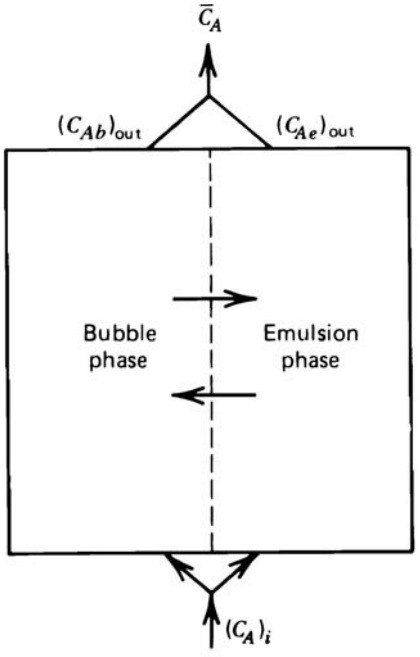

Figure 13.5.1-1
Two-phase model for fluidized bed.

plug flow can be postulated. The violent motion of the solid leads to mixing in the gas phase, which is generally described by an effective diffusivity model. Some authors have preferred complete mixing in that phase, based upon the observation that there is a definite pattern for the flow of solids: downward near the wall, upward in the central core.

Such a two-phase model, therefore, contains three parameters: the cross section of the bed taken by either the bubble or the emulsion phase, the interchange coefficient, and the axial effective diffusivity in the emulsion phase. The cross section or the volume fraction of the bed that is occupied by bubbles is easily derived from the observation that essentially all the gas flowing through the bed in excess of that required for minimum fluidization goes into the bubble phase. Based on this postulate, the fraction of the bed volume in the bubble phase can easily be derived from the bed heights and void fractions at minimum fluidization and the flow rate. The effective diffusivity of the gas in the emulsion phase, D_e, was determined by May [1959] from the residence time distribution of tagged solids in the bed, assuming the effective diffusivity of the gas to be equal to that of the solid. Knowing D_e, the interchange coefficient was determined by fitting gas residence time distribution measurements. Van Deemter [1961] combined the results of gas residence time distribution measurements and steady-state tracer experiments to obtain k_I and D_e. The model expressed mathematically in the following is one of the earliest and most complete, namely, that of May

[1959], discussed in detail by Van Deemter [1961] to make the determination of the parameters more convenient.

It is clear that for steady-state situations, only continuity equations have to be considered, since fluidized beds are essentially isothermal — the energy equation is not coupled with the continuity equation. For a single reaction, the equations are as follows.

Bubble phase:

$$f_b u_b \frac{dC_{Ab}}{dz} + k_I (C_{Ab} - C_{Ae}) + r_A \rho_b f_b = 0 \qquad (13.5.1\text{-}1)$$

where f_b is the fraction of the bed volume taken by bubbles and k_I is the interchange coefficient expressed in $m^3/(m^3$ total reactor volume) s. Note that the terms in (13.5.1-1) have dimensions kmol/(m^3 total reactor) s. May and Van Deemter neglect the term for reaction in the bubble phase.

Emulsion phase:

$$f_e u_e \frac{dC_{Ae}}{dz} - k_I (C_{Ab} - C_{Ae}) - f_e D_e \frac{d^2 C_{Ae}}{dz^2} + r_A \rho_e (1 - f_b) = 0 \qquad (13.5.1\text{-}2)$$

where f_e is the fraction of the bed volume taken by the emulsion gas (not by the emulsion phase, which also includes the catalyst) and u_e is the velocity of the emulsion gas, on an interstitial basis — the linear velocity u_{mf}/ε_{mf}.

The concentration $\overline{C}_A$ measured in the gas flow at the exit is given by

$$u_s \overline{C}_A = f_b u_b C_{Ab} + f_e u_e C_{Ae} \qquad (13.5.1\text{-}3)$$

where u_s is the superficial velocity based on the total bed cross section. The system (13.5.1-1) and (13.5.1-2) has to be integrated with the boundary conditions

$z = 0$, bubble phase	$C_{Ab} = (C_A)_i$
$z = 0$, emulsion	$-D_e \dfrac{dC_{Ae}}{dz} = u_e (C_{Ai} - C_{Ae})$
$z = L$	$\dfrac{dC_{Ae}}{dz} = 0$

Figure 13.5.1-2 shows some of the calculations of May for a first-order reaction according to this model and compared with idealized models. Curve 1 is for plug flow, curve 2 for complete mixing.

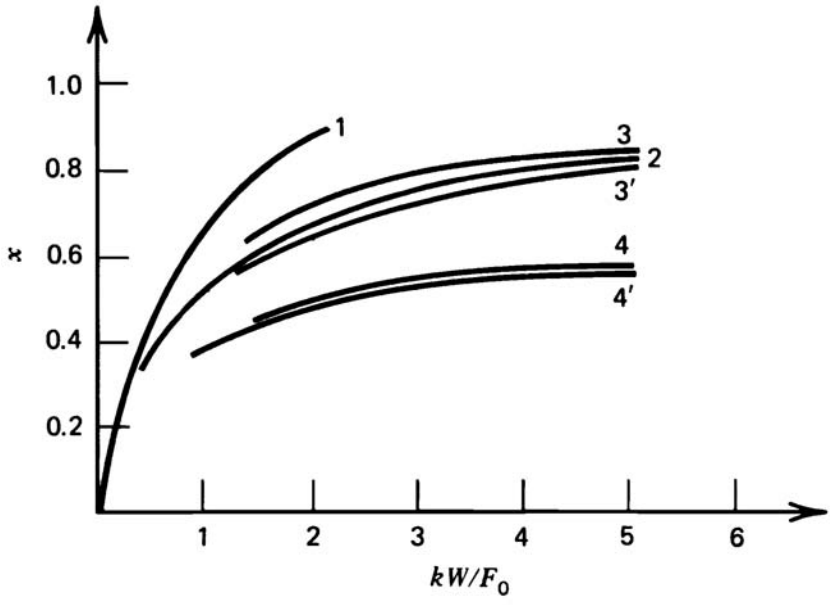

Figure 13.5.1-2

Conversion in a fluidized bed reactor. Curve 1, single-phase model with plug flow ($k_I = \infty$, $D_e = 0$); curve 2, single-phase model with complete mixing ($k_I = \infty$, $D_e = \infty$); curve 3, two-phase model ($k_I = 3$, $D_e = 0$); curve 3', two-phase model ($k_I = 3$, $D_e = \infty$); curve 4, two-phase model ($k_I = 1$, $D_e = 0$); curve 4', two-phase model ($k_I = 1$, $D_e = \infty$). After May [1959].

Curves 3, 3', 4 and 4' are obtained from the present model for a fixed value of the interchange coefficient, but curves 3 and 4 with $D_e = 0$ and curves 3' and 4' with $D_e = \infty$ (i.e., plug flow and complete mixing for the gas in the emulsion phase, respectively). The predicted curves can lie well below that for the ideal complete mixing model. The effect of D_e is rather small when the interchange coefficient has low values (curves 4 and 4'). The higher the values of k_I, the closer plug flow is approximated and the more important it is to know D_e accurately (curves 3 and 3').

Van Swaaij and Zuiderweg [1972] extensively tested the May-Van Deemter model as to its ability to scale up the Shell chlorine process (air oxidation of HCl into Cl_2). They investigated ozone decomposition on iron oxide deposited on sand or silica particles, in beds with diameters ranging from 0.1 to 0.6 m and heights ranging from 0.5 to 3.0 m. They derived the following correlation for k_I, in which u_s/k_I is the height of a transfer unit (in m):

$$\frac{u_s}{k_I} = \left(1.8 - \frac{1.06}{d_t^{1/4}}\right)\left(3.5 - \frac{2.5}{Z^{1.4}}\right) \qquad (13.5.1\text{-}4)$$

The correlation reveals a dependence on bed diameter and bed height. A correlation by Mireur and Bischoff [1967] yields values which are in good agreement with those of (13.5.1-4).

The effective diffusivity in the emulsion phase was correlated as follows by Baird and Rice [1975]:

$$D_e = 0.35(gu_s)^{1/3} d_t^{4/3} \tag{13.5.1-5}$$

where D_e is expressed in $\mathrm{m}_r^2/\mathrm{s}$.

Mireur and Bischoff [1967] derived the following correlation from their experiments in small-diameter beds:

$$\frac{u_s Z}{D_e \left(\frac{dt}{Z} \right)^{1.5}} = 0.33 \tag{13.5.1-6}$$

valid over a wide range of u_s/u_{mf}.

De Vries et al. [1972] measured a value of 1.5 m^2/s in a commercial reactor. The value calculated from Baird and Rice's correlation would be 1.25 m^2/s, which is in good agreement. For this situation (13.5.1-6) yields a value of only 0.35 $\mathrm{m}_r^2/\mathrm{s}$.

13.5.2 Bubble Velocity, Size, and Growth

The following equation was derived by Darton [1977] for d_b in the zone $0 < z < z_m$ between the distributor and the height z_m at which the maximum size is reached:

$$d_b = \frac{0.54}{g^{1/5}} (u_s - u_{mf})^{2/5} (z + 4\sqrt{A_0})^{4/5} \tag{13.5.2-1}$$

where A_0 is the orifice area of the plate, expressed in m^2, and d_b is expressed in m. For a porous plate distributor, Werther [1978] derived

$$d_b = 0.00853\left[1 + 27.2(u_s - u_{mf})\right]^{1/3} (1 + 6.84z)^{1.21} \tag{13.5.2-2}$$

The bubble rise velocity among a swarm of bubbles is given, according to Werther [1978], by the equation

$$u_{br} = \Psi \sqrt{d_b g} \tag{13.5.2-3}$$

where

$$\Psi = 0.64 \text{ when the bed diameter } d_t < 0.1 \text{ m}$$

$$= 1.6\, d_t^{0.4} \text{ when } 0.1 < d_t < 1.0 \text{ m}$$

$$= 1.6 \text{ when } d_t > 1.0 \text{ m}$$

whereas $\Psi = 0.711$, for a single bubble, according to the well-known Davis formula.

13.5.3 A Hydrodynamic Interpretation of the Interchange Coefficient k_I

Considerable efforts were made to predict the interchange coefficient from fundamentals. Using hydrodynamic theory, it has been possible to calculate the streamlines of gas and particles in the vicinity of a single bubble. The flow patterns depend strongly on the relative velocity of the bubble with respect to the emulsion gas. For all practical situations, the bubble rises faster than the emulsion gas, and Fig. 13.5.3-1 shows gas streamlines as calculated by Murray [1965] from the Davidson theory (on the left side of Fig 13.5.3-1). Bubble gas is seen to leave the bubble in the upper part and to enter again in the lower part. Yet the gas does not leave a sphere that surrounds the bubble. It is in this space between the two spheres, which has been given several names in the fluidization jargon but which we shall call the interchange zone, that the bubble gas comes into contact with the catalyst and that reaction occurs. The interchange zone decreases in importance as the relative bubble velocity u_{br} increases, so that the "contacting efficiency" of the bed decreases.

In reality, the bubble is not spherical, but more like that shown on the right-hand side of Fig. 13.5.3-1. Partridge and Rowe [1966] found experimentally that the wake occupies 25 percent of the spherical bubble volume. They also found that the ratio of the sum of the volumes of the bubble and the interchange zone to the volume of the bubble itself is given by $\alpha/(\alpha - 1)$, where $\alpha = u_b \varepsilon_{mf}/u_{mf}$ [Partridge and Rowe, 1966]. From this fundamental picture, the interchange coefficient has been derived in several ways.

Krishna [1981] tried to confirm values and trends for k_I starting from the model of Davidson and Harrison [1971] derived from hydrodynamic observations and theory. Davidson and Harrison expressed the interaction between the bubble phase and the emulsion in terms of two contributions: cross flow and diffusion. The total rate of gas transfer, Q (in m^3/s), is derived to be

$$Q = 1.19\,\pi d_b^2 u_{mf} + 0.91\,\pi d_b^{7/4} D_{be}^{1/2}\, g^{1/4}\, \frac{\varepsilon_{mf}}{1+\varepsilon_{mf}} \qquad (13.5.3\text{-}1)$$

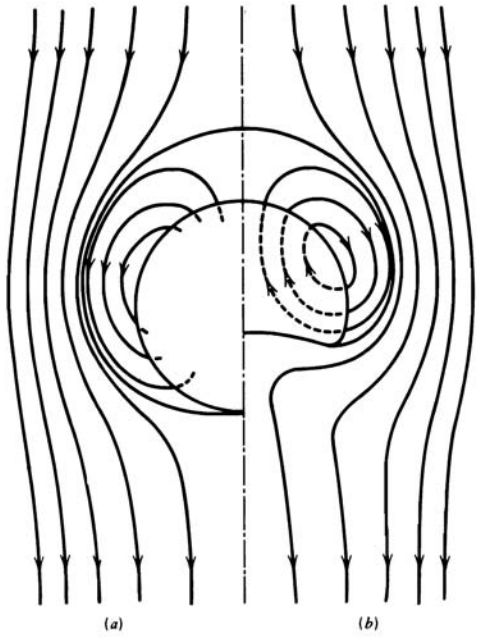

Figure 13.5.3-1

Gas streamlines for a real three-dimensional bubble when $\alpha = u_b/(u_{mf}/\varepsilon_{mf}) = 1.5$. (a) Murray streamlines for spherical bubble. (b) Streamlines for bubble with particle wake. From Partridge and Rowe [1966].

The first term in (13.5.3-1) is the flow term. It dominates in the range of flow rates encountered in commercial practice. The second term expresses the transfer by "effective" diffusion. The interchange coefficient k_I is related to Q by

$$Q = \frac{k_I}{f_b}\frac{\pi d_b^3}{6} \tag{13.5.3-2}$$

Since d_b varies with the bed height, k_I also depends on Z. It follows from (13.5.3-2) that k_I/f_b is independent of d_t, in contradiction with the van Swaaij-Zuiderweg correlation. One should keep in mind, however, that k_I derived from experiments is really an integral over the total bed height of point values, $\dot{k}_I$:

$$\frac{k_I}{f_b} = \frac{1}{Z}\int_0^Z \frac{\dot{k}_I}{f_b}\,dz \tag{13.5.3-3}$$

Krishna extensively confronted k_I values calculated from (13.5.3-1) and (13.5.3-2) with experimental data of De Groot [1967], De Vries et al. [1972] and van Swaaij and Zuiderweg [1972]. The results are shown in Fig. 13.5.3-2.

It was found that

$$\frac{k_I}{f_b} \sim (u_s - u_{mf})^{-0.4 \text{ to } -0.5}$$

$$\sim Z^{-0.8 \text{ to } -1} \qquad Z \le Z_m$$

$$\sim C_1 + \frac{C_2}{Z} \qquad Z > Z_m$$

where C_1 and C_2 are functions of the operating conditions. A couple of recommendations for the experimental determination of k_I can be extracted from the above results. First, k_I / f_b should be determined in beds with a sufficient diameter d_t, to avoid slugging. The bed height should exceed Z_m. For a tube diameter d_t between 0.5 to 1 m, the required height is of the order of 3 m. The flow velocity should exceed $5u_{mf}$.

Refinements are possible. Kunii and Levenspiel [1969, 1991] distinguish between transfer from the bubble to the interchange zone and from the latter to the emulsion phase, with the two steps purely in series. The corresponding mass transfer coefficients, based on unit bubble volume, are obtained respectively from

$$(k_{bi})_b = 4.5\frac{u_{mf}}{d_b} + 5.85\left(\frac{D_{bc}^{1/2} g^{1/4}}{d_b^{5/4}}\right) \tag{13.5.3-4}$$

with $(k_{bi})_b$ in $\text{m}_\text{g}^3/\text{m}_\text{b}^3\,\text{s}$, and from

$$(k_{ie})_b = 6.78\left(\frac{\varepsilon_{mf} D_{ce} u_b}{d_b^3}\right)^{1/2} \tag{13.5.3-5}$$

with the same units.

The coefficients may be combined by the rule of addition of resistances, since both steps are purely in series:

$$\frac{1}{(k_{be})_b} = \frac{1}{(k_{bi})_b} + \frac{1}{(k_{ie})_b} \tag{13.5.3-6}$$

The coefficient $(k_{be})_b$ is related to k_I by the equation

$$k_I = (k_{be})_b f_b \tag{13.5.3-7}$$

A diagram of Pyle [1972] shows differences between k_I calculated by the above and other models of the order of a factor of 5 to 10.

In line with the emphasis on fundamentals and bubble behavior, Partridge and Rowe wrote the continuity equation, (13.5.1-1), on a unit volume of bubble plus interchange zone, rather than on the bubble phase alone. Their model equations are as follows:

Bubble plus interchange phase or "cloud":

$$u_c \frac{dC_{Ac}}{dz} + (k_{ce})_c (C_{Ac} - C_{Ae}) + r_A \rho_e \frac{V_i}{V_c} = 0 \qquad (13.5.3\text{-}8)$$

The terms in this equation have the dimensions kmol/m_c^3s. The reaction rate term takes into account that the reaction in the ensemble of bubble and interchange zone really only takes place in the interchange zone, which has a volume V_i and in which one assumes that the catalyst bulk density is the same as that in the emulsion phase, ρ_e.

According to Partridge and Rowe's experimental correlation, V_i/V_c = 1.17(0.17 + α). Also, $\rho_e = \rho_B/(1 - f_b)$ when the fraction of the total volume occupied by the bubble plus interchange zone simply equals that taken by the

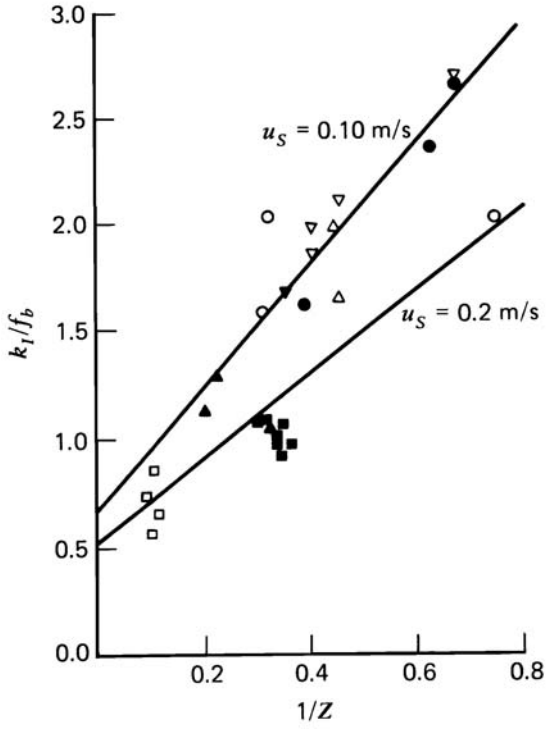

Figure 13.5.3-2

Variation of k_1/f_b with bed height. Comparison of model predictions and experimental results. After Krishna [1981].

bubble, and the amount of catalyst in the bubble phase is neglected.

Emulsion phase:

$$(u_e)_s \frac{dC_{Ae}}{dz} + (k_{ce})_c (C_{Ae} - C_{Ac}) \frac{f_b}{1 - f_b} + r_A \rho_e = 0 \qquad (13.5.3\text{-}9)$$

In this equation the transport by effective diffusion has been neglected. The fraction of the bed taken by the cloud phase is approximated by the fraction taken by the bubble phase, f_b, whereas $(u_e)_s$ is a superficial velocity based on the emulsion phase cross section. The terms are expressed per unit volume of emulsion phase. Since bubbles grow as they move through the bed, Partridge and Rowe let d_c, which determines $(k_{ce})_c$, vary with bed height according to an experimental correlation.

Kunii and Levenspiel [1969] have concentrated their attention on beds operated well above minimum fluidization, which is the usual industrial practice. In such beds there are definite gross mixing patterns for the solid: downward near the wall, upward in the central core. This has a marked effect on the gas flow in the emulsion phase, which is also forced downward near the wall. Kunii and Levenspiel showed that when u/u_{mf} exceeds 6 to 11, there is practically no net gas flow through the emulsion phase. Since Kunii and Levenspiel distinguish between the bubble itself and the interchange zone, (13.5.1-1) is written in this case

$$u_b \frac{dC_{Ab}}{dz} + (k_{bi})_b (C_{Ab} - C_{Ai}) + k C_{Ab} \rho_b = 0 \qquad (13.5.3\text{-}10)$$

The terms in (13.5.3-10) have the dimension kmol/m_b^3 s. The very small amount of reaction in the bubble itself is accounted for. First-order reaction is assumed. The rate coefficient k has dimensions [m^3 gas/kg cat. s] (see symbol list).

The continuity equation for the component A in the emulsion phase, as compared to (13.5.3-9), now becomes

$$(k_{ie})_b (C_{Ai} - C_{Ae}) = k C_{Ae} \rho_e \frac{1 - f_b}{f_b} \qquad (13.5.3\text{-}11)$$

provided there is no net flow and the transport by effective diffusion is neglected. Both equations are linked by the equation for the interchange zone:

$$(k_{bi})_b (C_{Ab} - C_{Ai}) = k C_{Ai} \rho_i \frac{V_i}{V_b} + (k_{ie})_b (C_{Ai} - C_{Ae}) \qquad (13.5.3\text{-}12)$$

In (13.5.3-11) and (13.5.3-12) the terms are expressed as unit volume of bubble phase. In (13.5.3-6) the interchange zone is calculated according to Partridge and Rowe's correlation; Kunii and Levenspiel include the wake in this zone. There is no evidence, however, that the bubble gas enters the wake. Eliminating C_{Ac} and C_{Ae} from (13.5.3-10), (13.5.3-11), and (13.5.3-12) leads to

$$-u_b \frac{dC_{Ab}}{dz} = k\left[\rho_b + \cfrac{1}{\cfrac{k}{(k_{bi})_b} + \cfrac{1}{\rho_i \cfrac{V_i}{V_b} + \cfrac{1}{\cfrac{k}{(k_{ie})_b} + \cfrac{1}{\rho_e \cfrac{(1-f_b)}{f_b}}}}}\right] C_{Ab} \tag{13.5.3-13}$$

The right-hand side of (13.5.3-13) could also be obtained directly by the proper combination of resistances, since only first-order processes are dealt with.

Equation (13.5.3-13) can also be written in a more concise way:

$$-u_b \frac{dC_{Ab}}{dz} = K_r C_{Ab} \tag{13.5.3-14}$$

Integration between $z = 0$ and $z = Z_f$ leads to the expression for the concentration of A in the exit stream:

$$\frac{\overline{C}_A}{C_{Ai}} = \exp\left(-\frac{K_r Z_f}{u_b}\right) \tag{13.5.3-15}$$

Pyle [1972] has compared several of these models, as is shown in Fig. 13.5.3-3. Johnsson et al. [1987] compared various bubbling bed models for the simulation of an industrial phthalic anhydride synthesis reactor. Simulation models have been extended to account for the flow of gas in the form of jets in the grid region [Behie and Kehoe, 1973; Grace and de Lasa, 1978]. The flow of solids in the freeboard region above the bed and prior to the cyclones was also studied [George and Grace, 1978].

The scaling up from one bed size to another was based by Horio et al. [1986] on the following similarity conditions, derived from their bubbling bed model. For identical bubble fraction, size distribution, and splitting frequency, the following condition has to be satisfied:

$$\frac{(u_s - u_{mf})_{\mathrm{II}}}{(u_s - u_{mf})_{\mathrm{I}}} = \sqrt{m}$$

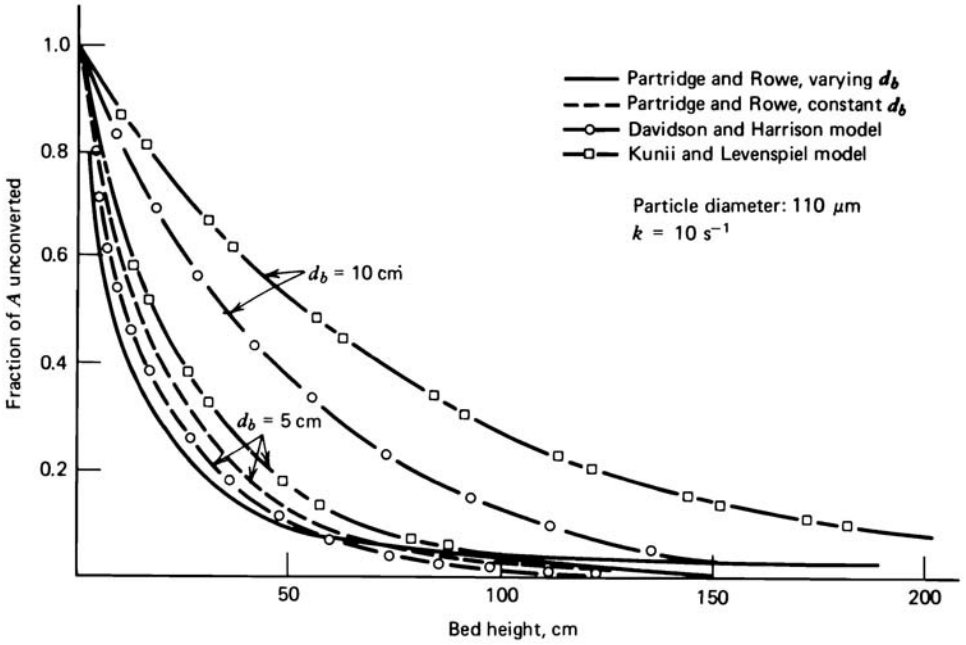

Figure 13.5.3-3

Comparison of models for fluidized bed reactors. From Pyle [1972].

where

$$m = \frac{Z_{\text{II}}}{Z_{\text{I}}} = \frac{(d_t)_{\text{II}}}{(d_t)_{\text{I}}} = \frac{(\text{orifice diameter})_{\text{II}}}{(\text{orifice diameter})_{\text{I}}}$$

so that all lengths are scaled up in the same ratio. For the geometrical similarity of the flow field around the bubble, the condition

$$\frac{(u_{mf})_{\text{II}}}{(u_{mf})_{\text{I}}} = \sqrt{m}$$

has to be satisfied.

13.5.4 One-Phase Model

The preceding mostly relates to bubbling beds. It is not clear at this stage whether or not the correlations given and even the model itself could be successfully applied to the turbulent regime in which the lifetime of the bubbles is shorter. It has been conjectured that a one-phase model with effective diffusion superimposed upon plug flow might be more appropriate [Avidan, 1982]. The model would then reduce to an equation like that derived in Chapter 11 on fixed bed reactors (one-dimensional pseudohomogeneous model with axial mixing, Section

11.6). Thompson et al. [1999] have presented a general model, valid for bubbling and turbulent fluidized beds that merges the two limiting models (two-phase and one-phase with axial dispersion) by allowing key parameters to vary continuously with the superficial velocity.

13.6 MODELING OF A TRANSPORT OR RISER REACTOR

Figures 13.3-4 and 13.3-5 illustrate that at high gas flow rates all solids are entrained and that the solids fraction is of the order of 1 percent only. Operation in the transport regime is of interest for very fast reactions subject to rapid deactivation and for very exothermic reactions.

One problem arising in the modeling of transport reactors is the slip, which is the difference between the interstitial velocity of the solid and the gas:

$$u_{sl} = u_t = u_{i,g} - u_{i,p} \tag{13.6-1}$$

The slip velocity is generally taken to equal the terminal velocity of the solid, u_t, which was discussed in Section 13.3. Substituting $u_{i,g}$ in (13.6-1) by $u_{s,g}/\varepsilon$ and $u_{i,p}$ by $u_{s,p}/(1-\varepsilon)$ leads to the following expression for the void fraction ε:

$$\varepsilon = \frac{(u_t + u_{s,g} + u_{s,p}) - \sqrt{(u_t + u_{s,g} + u_{s,p})^2 - 4u_{s,g}u_t}}{2u_t} \tag{13.6-2}$$

Figure 13.6-1 shows the slip ratio $u_{s,g}/u_{s,p}$ [Whittington et al., 1972]. Since the velocities are very high in transport reactors for fine solids, the slip ratio is close to 1. Both gas and solid are considered to move in plug flow. Because both phases have practically identical residence times, the catalyst activity can no longer be considered as being uniform: as the solid moves through the reactor, coke is progressively deposited on it, affecting the solid activity and the selectivities of the various reactions.

The continuity equation for a reacting component of the gas phase can be written

$$u_{s,g}\frac{dC_i}{dz} = \left[\sum_j \alpha_{ij} r_j \phi_j\right] \rho_s [1 - \varepsilon(z)] \tag{13.6-3}$$

with $\varepsilon(z)$ given by (13.6-2) and ϕ_j is the deactivation function for the main reaction j. The continuity equation for coke can be written

$$\frac{\dot{m}_s}{\Omega}\frac{dC_C}{dz} = \sum_l r_{C_l} \rho_s [1 - \varepsilon(z)] \phi_C \tag{13.6-4}$$

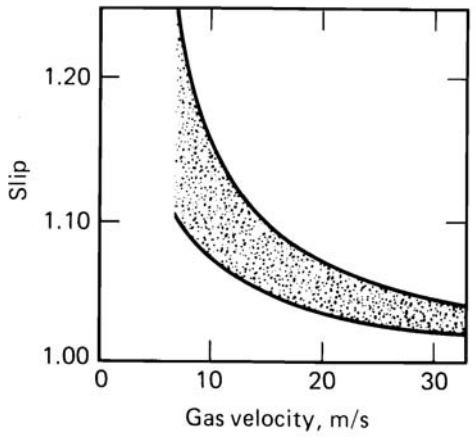

Figure 13.6-1
Slip ratio in a riser reactor versus the superficial gas velocity. From Whittington [1972].

with ϕ_C the deactivation function for the coking reactions.

The energy equation for adiabatic operation can be written

$$\frac{\dot{m}_{VGO}c_{p_{VGO}} + \dot{m}_s c_{p_s}}{\Omega}\frac{dT}{dz} = \left[\sum_i \sum_j r_{ij}(-\Delta H_{ij})\varphi_C\right]\rho_s[1-\varepsilon(z)] \qquad (13.6\text{-}5)$$

with the boundary conditions: at $z = 0$: $C_i = (C_i)_0$; $C_C = (C_C)_0$; $T = T_0$. Further, φ_C is the appropriate deactivation function, depending upon the type of reaction.

As written here, the equations do not account for vaporization. They assume immediate and perfect contact of gas and solid. Also, the reactor is considered to be adiabatic.

13.7 FLUIDIZED BED REACTOR MODELS CONSIDERING DETAILED FLOW PATTERNS

Considering the flow patterns in a more representative way than in the preceding sections inevitably leads to a three-dimensional model, requiring a rigorous calculation of the gas and solid phase velocities based upon the Navier-Stokes momentum equations. This type of approach has already been presented in Chapter 12 dealing with the modeling of single phase complex flow patterns in reactors and is extended here to a two phase situation. It yields a so-called Eulerian-Eulerian model and is written in terms of the true gas and solid phase, unlike the models presented until now in this chapter that started from a bubble and an emulsion phase. Each phase is a continuum moving at its own velocity but fully penetrates the other and interacts with it through the transfer of mass, heat and momentum [Anderson and Jackson, 1967; Ishii, 1975; Jackson, 2000].

As in Chapter 12, the Einstein notation is used.

Continuity equations for a species *A* in the gas phase:

$$\frac{\partial\left(\varepsilon_g C_{Ag}\right)}{\partial t}+\frac{\partial}{\partial z_j}\left(\varepsilon_g C_{Ag} u_{j,g}\right)-\frac{\partial}{\partial z_j}\left(\varepsilon_g D_{Am}\frac{\partial C_{Ag}}{\partial z_j}\right) \tag{13.7-1}$$

$$= k_{g_A} a_m \varepsilon_s \rho_s \left(C^s_{As} - C_{Ag}\right) \equiv k_{g_A} a_v \left(C^s_{As} - C_{Ag}\right)$$

Each term in this equation has the dimension [kmol A/m^3_r s]. As in Section 12.3, in statistically stationary flow, fluctuations of the variables around the averaged or mean values can be described by the transient term in this and the following equations. The second term represents the transport of the species by convection in the three dimensions z_j, the third that by molecular diffusion, and the fourth term is the interfacial transfer from the solid to the gas phase. The superscript *s* in the fourth term refers to surface conditions of the solid.

Continuity equation for a species *A* in the solid phase:

$$\frac{\partial\left(\varepsilon_s \varepsilon^s_g \overline{C}_{As}\right)}{\partial t}+\frac{\partial}{\partial z_j}\left(\varepsilon_s \varepsilon^s_g \overline{C}_{As} u_{j,s}\right)= \tag{13.7-2}$$

$$k_{g_A} a_v \left(C_{Ag} - C^s_{As}\right)+\varepsilon_s \rho_s \sum_k \alpha_{Ak} \eta_k r_k(\boldsymbol{C}^s_s, T_s)\phi_k$$

ε^s_g is the solid phase void fraction, that is, the fraction of the volume of a particle taken by pores. The internal diffusion limitation is not explicited in terms of equations, but its effect on the reaction rates is summarized in η_k, like in equation (11.9.1-9) of Chapter 11, and particle volume averaged concentrations, $\overline{C}_{As}$, are used in the transient and convection terms. ϕ_k is the deactivation function of reaction *k*, expressed in terms of the deactivating agent, not in terms of time, as explained in Chapter 5. Each term has the dimension [kmol A/m^3_r s].

Values for the interphase mass transfer coefficient k_{gA} can be calculated from j_D-correlations (see Chapter 3). Specific correlations for fluidized beds can be found in Perry [1984].

The solution of the continuity equations for the species requires the knowledge of the local gas and solids volume fractions ε_g and ε_s, pressures P and P_s, temperatures T_g and T_s, and velocities $\boldsymbol{u}_g$ and $\boldsymbol{u}_s$. These can be calculated from the total continuity equations and the momentum and energy equations. In the absence of accumulation of species on the solid:

Gas phase total continuity equation:

$$\frac{\partial}{\partial t}\left(\varepsilon_g \rho_g\right)+\frac{\partial}{\partial z_j}\left(\varepsilon_g \rho_g u_{j,g}\right)=0 \tag{13.7-3}$$

Solid phase total continuity equation:

$$\frac{\partial}{\partial t}\left(\varepsilon_s \rho_s\right)+\frac{\partial}{\partial z_j}\left(\varepsilon_s \rho_s u_{j,s}\right)=0 \tag{13.7-4}$$

In these equations each term has dimensions [kg total gas respectively solid/ m_r^3 s].

Gas phase momentum equations:

$$\begin{aligned}&\frac{\partial}{\partial t}\left(\varepsilon_g \rho_g u_{i,g}\right)+\frac{\partial}{\partial z_j}\left(\varepsilon_g \rho_g u_{i,g} u_{j,g}\right)\\&=-\varepsilon_g \frac{\partial P}{\partial z_i}+\varepsilon_g \frac{\partial \tau_{ji}^g}{\partial z_j}-\beta\left(u_{i,g}-u_{i,s}\right)+\varepsilon_g \rho_g g_i\end{aligned} \tag{13.7-5}$$

where i = 1, 2, 3. Each term has dimensions [kg gas/ m_r^2 s^2]. In these equations pressure and shear stress gradients are accounted for, as well as interphase momentum transfer by drag and the effect of gravity that can cause the so-called slip between the two phases.

Solid phase momentum equations:

$$\begin{aligned}&\frac{\partial}{\partial t}\left(\varepsilon_s \rho_s u_{i,s}\right)+\frac{\partial}{\partial z_j}\left(\varepsilon_s \rho_s u_{i,s} u_{j,s}\right)\\&=-\varepsilon_s \frac{\partial P}{\partial z_i}+\varepsilon_s \frac{\partial \tau_{ji}^g}{\partial z_j}-\frac{\partial P_s}{\partial z_i}+\frac{\partial \tau_{ji}^s}{\partial z_j}+\beta\left(u_{i,g}-u_{i,s}\right)+\varepsilon_s \rho_s g_i\end{aligned} \tag{13.7-6}$$

where i = 1, 2, 3.

The gas phase shear stress tensor τ_{ji}^g is defined by (12.3-2):

$$\tau_{ji}^g=\mu_g\left(\frac{\partial u_{i,g}}{\partial z_j}+\frac{\partial u_{j,g}}{\partial z_i}\right)-\left(\frac{2}{3}\mu_g-\xi_g\right)\left(\delta_{ij}\frac{\partial u_{l,g}}{\partial z_l}\right) \tag{13.7-7}$$

The solid phase shear stress tensor τ_{ji}^s is defined by:

$$\tau_{ji}^s=\mu_s\left(\frac{\partial u_{i,s}}{\partial z_j}+\frac{\partial u_{j,s}}{\partial z_i}\right)-\left(\frac{2}{3}\mu_s-\xi_s\right)\left(\delta_{ij}\frac{\partial u_{l,s}}{\partial z_l}\right) \tag{13.7-8}$$

The solid phase stress is usually written in a Newtonian form and introduces a solid phase pressure P_s, a solid phase bulk viscosity ξ_s, and a solid phase shear viscosity μ_s. These can be modeled on an empirical basis [Tsuo and Gidaspow, 1990; Sun and Gidaspow, 1999] or starting from the Kinetic Theory of Granular Flow (KTGF) [Haff, 1983; Savage, 1983; Jenkins and Savage, 1983; Lun et al., 1984; Koch, 1990; Gidaspow, 1994] and that is based upon instantaneous particle-particle collisions, that can be inelastic, unlike those between gas molecules. In the KTGF a granular temperature Θ, different from the physical temperature of the solid phase, is introduced. It quantifies the deviations of the individual particles from their mean motion and is proportional to the kinetic energy of their random motion:

$$\Theta = \frac{1}{3}\left\langle u_p^{'2} \right\rangle$$

Deviations from the particle mean motion are at the origin of particle-particle collisions and of the resulting solid phase pressure and viscosity. From the KTGF the following equation is derived for Θ:

$$\begin{aligned} &\frac{3}{2}\left[\frac{\partial}{\partial t}\left(\varepsilon_s \rho_s \Theta\right) + \frac{\partial}{\partial z_j}\left(\varepsilon_s \rho_s u_{j,s} \Theta\right)\right] - \frac{\partial}{\partial z_j}\left(\kappa \frac{\partial \Theta}{\partial z_j}\right) \\ &= \left(-P_s \delta_{ji} + \tau_{ji}^s\right)\left(\frac{\partial}{\partial z_j} u_{i,s}\right) - \gamma + \beta\left(q_{gs} - 3\Theta\right) \end{aligned} \tag{13.7-9}$$

It has to be integrated simultaneously with the other continuity equations. The third term describes conduction associated with granular temperature gradients, characterized by a conductivity κ. The first term on the right hand side represents the granular temperature build up by the solid phase pressure and shear stress, depending upon the gradients in the solid phase velocity field, the second term, γ, the granular temperature dissipation by inelastic particle-particle collisions and the third term, $\beta(q_{gs} - 3\Theta)$, interphase transfer of pseudothermal energy.

Knowing Θ, the solid phase pressure and the solid phase bulk and shear viscosities can be calculated from formulae derived by Lun et al. [1984]. The granular temperature conductivity, κ, has also been formulated by Lun et al. [1984]. γ has been modeled in terms of Θ by Jenkins and Savage [1983]. For dense regimes, the interphase momentum transfer coefficient, β, can be calculated from the Ergun equation already encountered in Chapter 11 on fixed bed reactors [Gidaspow, 1994]. For dilute regimes, a correlation has been proposed by Wen and Yu [1966].

Gas phase energy equation:

$$\frac{\partial}{\partial t}\left(\varepsilon_g \rho_g E_g\right)+\frac{\partial}{\partial z_j}\left(\varepsilon_g \rho_g E_g u_{j,g}\right)-\frac{\partial}{\partial z_j}\left(\varepsilon_g \lambda_g \frac{\partial T_g}{\partial z_j}\right)$$

$$=-\varepsilon_g \frac{\partial}{\partial z_j}\left(P u_{j,g}\right)+\varepsilon_g \frac{\partial}{\partial z_j}\left(u_{i,g}\tau_{ji}^{g}\right)-\frac{\beta}{2}\left(u_{k,g}u_{k,g}-u_{l,g}u_{l,g}\right)$$

$$+\frac{\beta}{2}\left(3\Theta-q_{gs}\right)+h_f a_V\left(T_s-T_g\right)+\varepsilon_g \rho_g g_j u_{j,g} \qquad (13.7\text{-}10)$$

Solid phase energy equation:

$$\frac{\partial}{\partial t}\left(\varepsilon_s \rho_s E_s\right)+\frac{\partial}{\partial z_j}\left(\varepsilon_s \rho_s E_s u_{j,s}\right)-\frac{\partial}{\partial z_j}\left(\varepsilon_s \lambda_s \frac{\partial T_s}{\partial z_j}\right)-\frac{\partial}{\partial z_j}\left(\kappa \frac{\partial \Theta}{\partial z_j}\right)$$

$$=-\varepsilon_s \frac{\partial}{\partial z_j}\left(P u_{j,s}\right)+\varepsilon_s \frac{\partial}{\partial z_j}\left(u_{i,s}\tau_{ji}^{g}\right)-\frac{\partial}{\partial z_j}\left(P_s u_{j,s}\right)+\frac{\partial}{\partial z_j}\left(u_{i,s}\tau_{ji}^{s}\right)$$

$$+\frac{\beta}{2}\left(u_{k,g}u_{k,g}-u_{l,s}u_{l,s}\right)-\frac{\beta}{2}\left(3\Theta-q_{gs}\right)-h_f a_V\left(T_s-T\right)+\varepsilon_s \rho_s g_j u_{j,s} \qquad (13.7\text{-}11)$$

Each term in these two equations has the dimension [kJ/ m_r^3 s]. *E* includes kinetic, internal and potential energy and for the solid phase a contribution from the granular temperature. The third term on the left hand side describes conduction resulting from gradients in the physical temperature. For the solid phase a fourth term on the left hand side describes conduction resulting from gradients in the granular temperature. On the right hand side work by pressure and by shear stresses is accounted for, along with interphase kinetic energy transfer by drag, interphase transfer of pseudothermal energy, interphase heat transfer by convection, and work by gravity. An alternative form of the solid phase energy equation, (13.7-11), in which the heat of reaction explicitly appears can also be used (see Chapters 7 and 12).

The set of partial differential equations (13.7-1) to (13.7-11) has to be integrated accounting for the appropriate boundary conditions. For the gas phase equations, these have already been encountered in Chapter 12. For the solid phase, the value of the specific shear stress and of the flux of pseudothermal energy, $-\varepsilon_s \kappa \partial\Theta / \partial z_w$, at the wall have to be specified. Equations were proposed by Johnson and Jackson [1987] and by Sinclair and Jackson [1989].

In solving the model equations for the flow of gas and solids based upon the Navier-Stokes equations, a major challenge is the formation of micro- and

meso-scale non-uniformities, i.e., complex multi-scale structures such as clusters and bubbles. Their calculation requires transient simulations with an extremely fine spatial and temporal mesh [Agrawal et al., 2001; De Wilde, 2005; De Wilde, 2007]. These Direct Numerical Simulations (DNS) are computationally still too demanding for industrial scale reactor simulations and a type of statistical description has to be accepted, already described in Chapter 12 on single phase complex flow patterns. If the statistically stationary or macro-scale behavior is judged to be adequate, a Reynolds (or Favre) Averaged Navier-Stokes (RANS) model can be taken [Hrenya and Sinclair, 1997], but the averaging of dynamic phenomena like bubbling or clustering then leads to closure problems. The dynamic behavior can be accounted for by means of a micro- and meso-probability density function, PDF. More promising than Reynolds/Favre averaging is the Large Eddy Simulation (LES) approach. The spatial and temporal mesh sizes are chosen and set a so-called filter frequency. The phenomena with lower frequency (macro- and meso-scale) and their dynamics are then calculated. The phenomena with a frequency higher than the filter frequency (micro-scale) can be accounted for using a statistical description by means of a filtered micro-probability density function, FPDF. Then, along the lines discussed in Chapter 12, either the evolution of the (F)PDF itself is calculated from a (F)PDF transport equation or the evolution of a limited number of moments of the (F)PDF is calculated from (F)PDF moment transport equations or from algebraic closure models. (F)PDF moment transport equations can be solved using conventional CFD methods.

Van Wachem et al. [1999] compared the results of simulations based upon this approach in the absence of reaction with experimental data on pressure- and voidage fluctuations obtained in a laboratory scale fluidized bed. The agreement was quite reasonable and they concluded that Eulerian CFD simulations could be useful in scaling up the influence of vessel diameter and height.

13.8 CATALYTIC CRACKING OF VACUUM GAS OIL

13.8.1 Kinetic Models for the Catalytic Cracking of Vacuum Gas Oil

Because of the complexity of the feedstock and its very incomplete analysis the kinetic modeling of processes of heavy oil conversion like catalytic cracking has been traditionally based upon strongly simplified reaction schemes, written in terms of “lumps”, i.e., fractions defined partly by their global chemical composition and partly by their boiling range. In the sixties, Weekman and co-workers [1968a; 1968b; 1979] based the simulation of the catalytic cracking of

vacuum gas oil (VGO) on a 3-lump reaction scheme consisting of gas oil, gasoline and dry gas + coke.

In the seventies Jacob et al. [1976] developed a 10 lump model represented in Fig. 13.8.1-1 and involving 20 reactions. In this figure *G* represents gasoline, and *C* represents coke and C_1-C_4 represent gases. The subscript *l* relates to fractions boiling between 221°C and 343°C, and the subscript *h* relates to heavier fractions. The symbols *P* and *N* stand for wt-% of paraffin and naphthenic molecules, respectively; *Ar* for wt-% carbon atoms among aromatic rings and *As* for wt-% of aromatic substituent groups.

The rates of the various reactions are given by

$$\mathbf{r} = \mathbf{K'}\,\mathbf{C} \tag{13.8.1-1}$$

where **r** represents the vector of net rates of formation of the various lumps (kmol/kg cat. s), **K'** is the matrix of pseudo-rate coefficients (m^3 gas/kg cat. s), and **C** is the vector of molar concentrations of the various lumps.

The matrix **K** is shown in Fig. 13.8.1-2, and the activation energies are listed in Table 13.8.1-1.

The weight yields of gases lumped in *C* are calculated from

$$\text{wt}-\%\ i = [\mathbf{b}_1(t)G + \mathbf{b}_2(t)C][\sum_j 100\mathbf{a}_1(i,j)(w_j)_0] \tag{13.8.1-2}$$

where *i* stands for methane, ethane, ethylene, propane, propylene, butane, isobutane, butenes, pentane, isopentane and pentenes; *G* and *C* stand for the wt yields of gasoline and coke + gas, respectively; $\mathbf{b}_1$ and $\mathbf{b}_2$ are the vectors of the correlation coefficients with the gasoline and coke + gas yields, respectively; and $\mathbf{a}_1$ is the matrix of the correlation coefficients with respect to the feed composition $(w_j)_0$.

The strong adsorption of the heavy aromatics Ar_h is accounted for by multiplying the elements of **K** by a function

$$g(Ar_h) = \frac{1}{1 + K_{Ar_h} C_{Ar_h}} \tag{13.8.1-3}$$

To account for deactivation of the catalyst by basic nitrogen compounds, the rate coefficients are multiplied by the function

$$f(N) = \frac{1}{1 + (K_N C_N / W)} \tag{13.8.1-4}$$

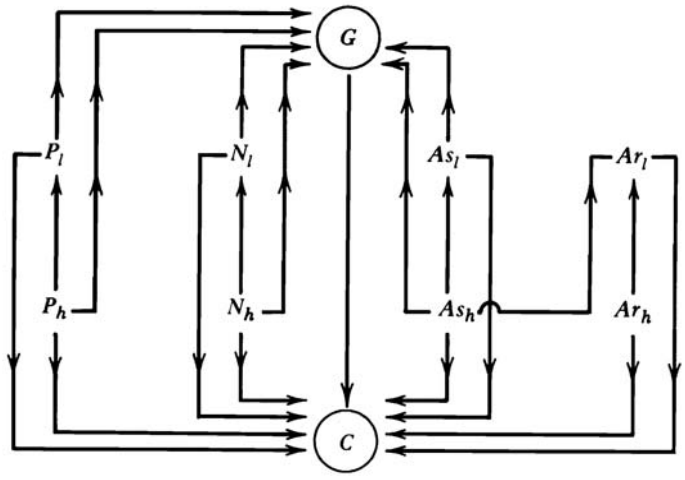

Figure 13.8.1-1

Mobil's ten-lump model for catalytic cracking of gasoil. From Jacob et al. [1976], Weekman [1979], Froment [1986].

where W is the mass of catalyst in contact with the hydrocarbons. According to Jacob et al. [1976], the coke content of the catalyst, C_C, varies with time according to

$$C_C = 2.43 \times 10^{-3} t_c^{0.2} \tag{13.8.1-5}$$

From this, a deactivation function with respect to the coke content can be determined:

$$\phi(C_C) = \frac{1}{1 + 69.47(100 C_C)^{3.8}} \tag{13.8.1-6}$$

	P_h	N_h	As_h	Ar_h	P_l	N_l	As_l	Ar_l	G	C
P_h	0	0	0	0	5.75	0	0	0	15.28	2.181
N_h		0	0	0	0	6.25	0	0	23.53	4.131
As_h			0	0	0	0	5.278	13.89	17.50	9.50
Ar_h				0	0	0	0	1.628	0	4.064
P_l					0	0	0	0	6.625	2.622
N_l						0	0	0	18.37	2.272
As_l							0	0	5.139	1.008
Ar_l								0	0	0.277
G									0	1.222
C									0	0

Figure 13.8.1-2

Matrix **K** of the reaction rate coefficients k_{ij} for the formation of j out of i at 482°C (in $10^{-3}\ \mathrm{m_g^3/kg\ cat.s}$). From Jacob et al. [1976].

TABLE 13.8.1-1
ACTIVATION ENERGIES FOR THE VARIOUS REACTIONS[a]

Reaction	**Activation Energy (kJ/kmol)**
1. Gasoline formation reactions from P_h, N_h, P_l, N_l	23045
2. Gasoline formation reactions from As_h, and As_l	60755
3. *C* lump formation reactions from P_h, N_h, P_l, N_l	35615
4. *C* lump formation reactions from As_h, Ar_h, As_l, Ar_l	73325
5. Formation of *C* lump from gasoline	83800
6. *LFO* formation reactions from P_h, N_h, As_h, Ar_h	33939

[a]From Jacob et al. [1976].

In the late eighties the characterization of the feedstock and the reaction scheme shifted to more detail, i.e., individual molecules. Liguras and Allen [1989] selected a large number of pseudo components, most of which were lumps in their own way. Klein et al. [1991] generated these pseudo components from analytical characteristics using Monte-Carlo simulation. In their "Structure Oriented Lumping" Quann and Jaffe [1992; 1996] constructed a large number of molecules from typical structures present in VGO and expressed the chemical transformations in terms of these molecules. Retaining lumps in the reaction scheme inevitably leads to rate parameters depending on the feedstock composition, so that additional experimental work is required for each new feedstock.

In Chapter 2 attention was drawn already on the Single Event Kinetics approach (SEK), also developed from the late eighties onwards [Baltanas et al., 1989; Vynckier and Froment, 1991; Froment, 2005]. In the SEK approach the network is developed in terms of the elementary steps of the process. The reaction network becomes gigantic and has to be developed by computer, but the number of types of elementary steps is very limited. Within such a type the number of independent frequency factors of the rate coefficients is reduced to only one when the transition state theory is applied to account for the effect of structure, while the activation energies are related to that of a reference step with known rate parameters. Moustafa and Froment [2003] applied the SEK approach to the catalytic cracking of VGO and also expressed the rate of coke formation in terms of the SEK concept. The total number of independent rate parameters was reduced to only 39. These parameters can be determined from an experimental program starting with judiciously chosen key components, representative for the various families of hydrocarbons and from typical VGO's. The results of the application of this model to the catalytic cracking in a riser reactor are given in Section 13.8.2.3.

13.8.2 Simulation of the Catalytic Cracking of Vacuum Gas Oil

13.8.2.1 Fluidized Bed Reactor. Two-Phase Model with Ten Lump Reaction Scheme

The two-phase model of Section 13.5.1 is used, neglecting reaction in the bubble phase, and axial diffusion in the emulsion phase. In the bubble phase (plug flow),

$$\frac{dc_{ib}}{dz} = -\frac{k_I (c_{ib} - c_{ie})}{u_b f_b} \qquad (13.8.2.1\text{-}1)$$

In the emulsion phase (plug flow),

$$\frac{dC_{ie}}{dz} = \frac{k_I}{u_e f_e}(C_{ib} - C_{ie}) + \frac{1}{u_e f_e}\left(\sum_j \frac{k'_{ij} c_{je}}{1 + K_{Ar_h} C_{Ar_h}}\right)\rho_s \phi (1 - f_b - f_e) \qquad (13.8.2.1\text{-}2)$$

The boundary conditions are:

$$\text{at } z = 0: \quad C_{ib} = (C_i)_0$$

$$C_{ie} = (C_i)_0$$

Since the catalyst is assumed to be completely mixed, the coke content is uniform over the whole bed. It is calculated from

$$\dot{m}_s C_C = \dot{m}_s (C_C)_0 + \int_0^z \left(\sum_j \frac{k'_{10,j} C_{je}}{1 + K_{Ar_h} C_{Ar_h}}\right)\rho_s \beta \phi M_C (1 - f_b - f_e)\Omega \, dz \qquad (13.8.2.1\text{-}3)$$

where $\dot{m}_s$ is the feed rate of catalyst (kg/h), β is the coke fraction of the *C* lump, and M_C is the molecular weight of the coke. The conversions of gasoil into gasoline and coke are calculated from

$$x_G = \frac{F_G}{F_{GO}^0} \quad \text{and} \quad x_C = \frac{F_C}{F_{GO}^0}$$

and the conversion of the heavy fuel oil fraction by

$$x_{HFO} = \sum_{i=1}^{4} \frac{(y_i)_0 (F_{i0} - F_i)}{\sum_{i=1}^{4} (y_i)_0 F_i}$$

TABLE 13.8.2.1-1
GASOIL COMPOSITION AND MOLECULAR WEIGHT OF LUMPS

	wt %	**M.W.**		**wt %**	**M.W.**
P_h	17	339	P_l	14	226
N_h	20	339	N_l	9	226
As_h	24	339	As_l	2	226
Ar_h	12	339	Ar_l	2	226
G	0	114	G	0	114
C	0	34	C	0	34

The sum of the weight yields of the gasoline lump and *C*-lump is represented by η_{GC}.

The following information is required for the simulation:

Reactor geometry: d_t = 8.41 m; Z = 7.00 m

Percentage of grid cross section taken by openings: 1.29%

Diameter of holes: 4.45×10^{-2} m

Catalyst: Average diameter $\bar{d}_p = 8.0 \times 10^{-5}$ m;

Solid density ρ_s = 1500 kg cat./m^3 cat.;

Uniform coke content of catalyst in reactor, $(C_C)_0$ = 1.0 wt-%

Bed void fraction at minimum fluidization, ε_{mf} = 0.55

Flow rates: $\dot{m}_s$ = 2000 tons/h; $\dot{m}_{GO}$ = 200 tons/h; W/$\dot{m}_{GO}$ = 0.77 h

Reactor temperature: 775 K

Viscosity of gasoil: 1.078×10^{-5} kg/m s, or Pa s

The composition of the gasoil is given in Table 13.8.2.1-1.

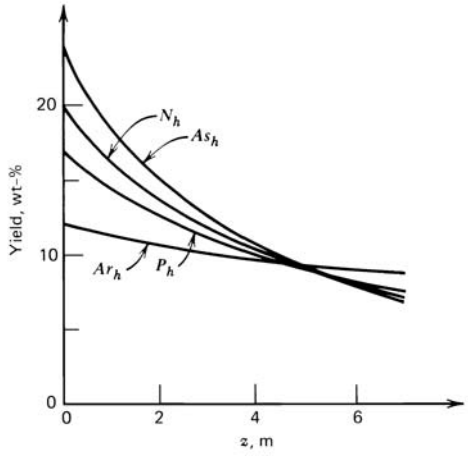

Figure 13.8.2.1-1

Yields of HFO lump versus bed height. From Schockaert [1988].

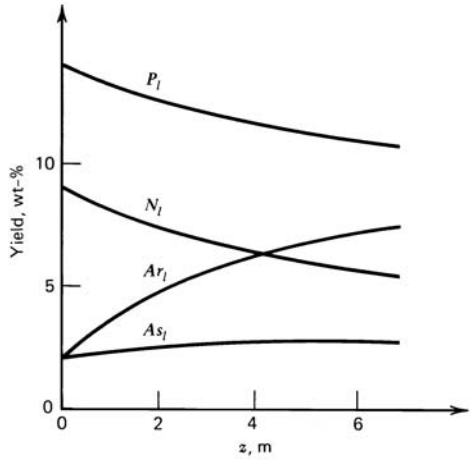

Figure 13.8.2.1-2

Yields of LFO lump versus bed weight. From Schockaert [1988].

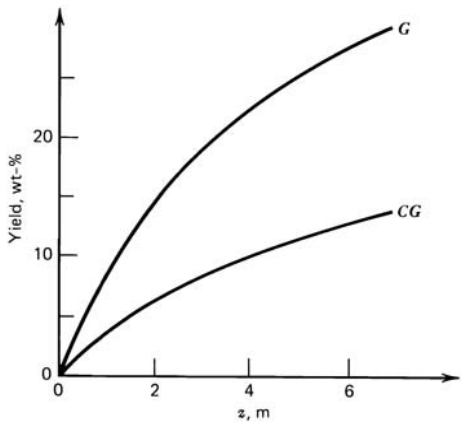

Figure 13.8.2.1-3

Gasoline and (coke + gas) yield versus bed height. From Schockaert [1988].

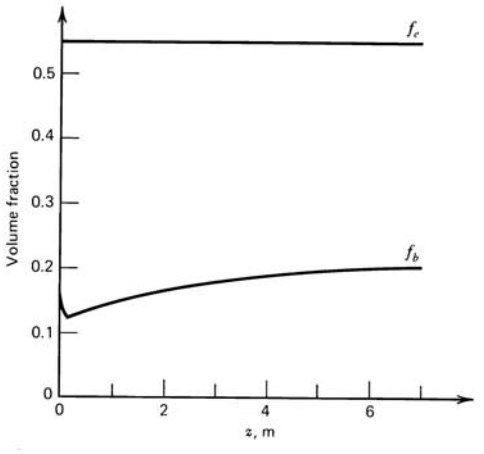

Figure 13.8.2.1-4

Fraction of bed taken by the bubble phase and fraction taken by the emsulsion gas versus bed height. From Schockaert [1988].

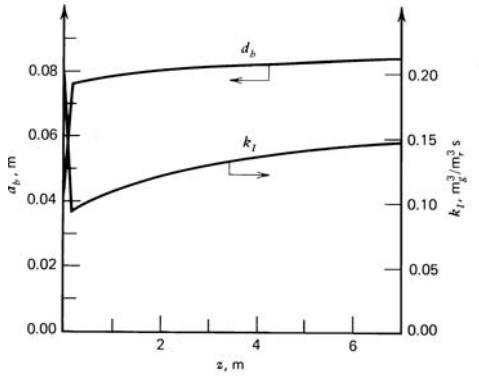

Figure 13.8.2.1-5

Bubble diameter and interchange coefficient versus bed height. From Schockaert [1988].

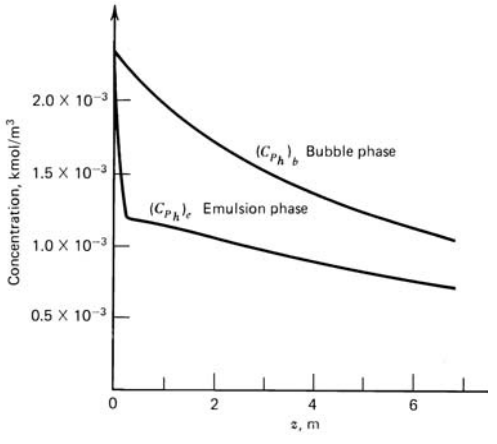

Figure 13.8.2.1-6

Molar concentration of the heavy paraffin lump in the emulsion phase and in the bubble phase versus bed height. From Schockaert [1988].

The simulation results are shown in Figs. 13.8.2.1-1 through 13.8.2.1-6 [Schockaert, 1988].

The catalytic cracking of residual oil was dealt with by Takatsuka and co-workers [1987]. They used a six-lump model and modeled the reactor as a sequence of continuous stirred tank reactors.

13.8.2.2 Fluidized Bed Reactor. Reynolds-Averaged Navier-Stokes Model with Ten Lump Reaction Scheme

(Waldo Rosales Trujillo is greatly acknowledged for his help with the calculations)

A part of the bottom section of a fluidized bed catalytic cracker was simulated in 2D using the Eulerian-Eulerian gas-solid flow model presented in Section 13.7 and the 10-lump kinetic model of Jacob et al. [1976] introduced in Section 13.8.1. The simulations aimed at illustrating to what extent a model of this type is capable of describing the details and dynamics of the complex gas-solid flow and species fields.

The simulation domain was 0.4 m wide and 1.0 m high. The gas oil, with composition shown in Table 13.8.2.1-1, is injected uniformly through the bottom. The catalyst is injected via lateral inlets at the bottom. Its coke content is 1 wt-%. Gas and catalyst exit via the top. The other operating conditions and the catalyst properties are similar to those used in Section 13.8.2.1.

The calculation of the details and dynamics of the fluctuations around the statistically stationary state, resulting from the formation of meso-scale structures

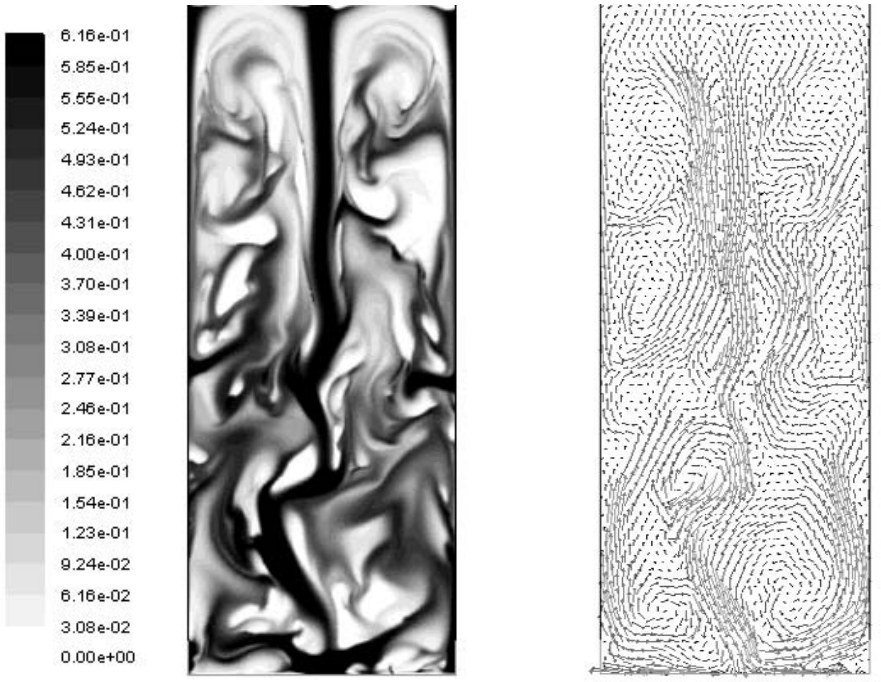

Figure 13.8.2.2-1

2D Eulerian-Eulerian simulation of fluid catalytic cracking of gas oil. Snapshot of fluctuations around the statistically stationary flow field. (a) Solids volume fraction profile and (b) solids velocity field.

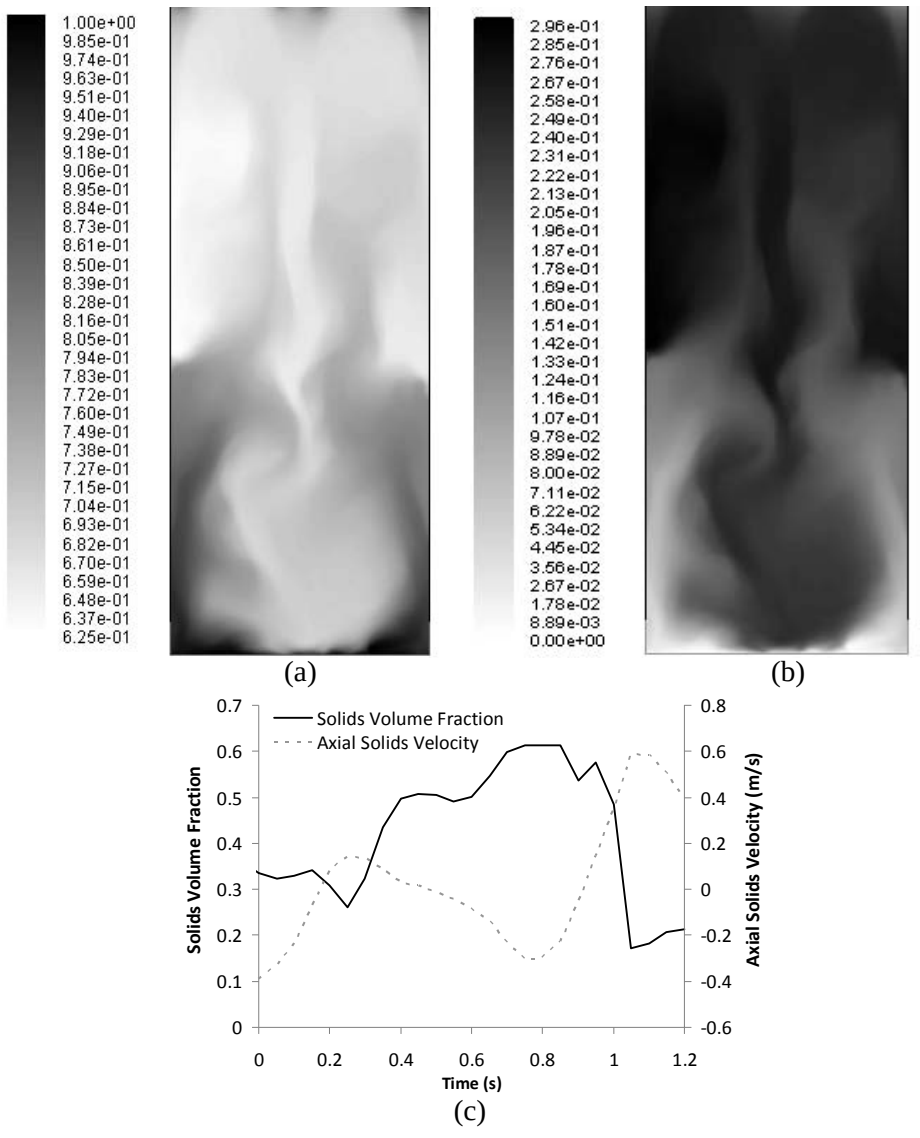

Figure 13.8.2.2-2

2D Eulerian-Eulerian simulation of fluid catalytic cracking of gas oil. Snapshot of fluctuations around the statistically stationary species field. Mass fraction in the gas phase: (a) gasoil fraction of the feed, (b) gasoline fraction in the product. (c) Transient calculation of the meso-scale fluctuations around a statistically stationary state: solids volume fraction and axial velocity at 0.1 m from the wall and 0.25 m from the bottom.

such as bubbles, requires extremely fine spatial and temporal grids. About 408,000 volume elements were used and the grid size at the bottom of the domain — in the vicinity of the inlets — was only 0.01 mm. The time steps were as small as 10^{-6} s.

Figures 13.8.2.2-1(a) and (b) show instantaneous profiles of the solids volume fraction and of the solids velocity field, while Figures 13.8.2.2-2(a) and

(b) show instantaneous profiles of the corresponding gas phase mass fraction fields of the gasoil fraction of the feed and the gasoline fraction in the product. Meso-scale structures develop. At their boundaries, steep gradients in the flow and species concentration fields are observed. The magnitude of the solids volume fraction and axial velocity fluctuations is shown in Fig. 13.8.2.2-2(c). The difference with the predictions of the classical two-phase model used in Section 13.8.2.1 is relatively large. It should be added that it was not attempted to correlate the parameter values of both models.

Theologos et al. [1997] used the Eulerian-Eulerian gas-solid flow model and the 10-lump kinetic model of Jacob et al. [1976] to carry out 3D simulations of FCC riser reactors. Extensions of the flow model to account for the details of the feed atomization were studied by Theologos et al. [1999] and by Simonin and co-workers [Saulnier et al., 2005].

13.8.2.3 Riser Reactor. Plug Flow Model with Slip with Reaction Scheme based upon Elementary Steps. Single Event Kinetics

This is an example of application of the detailed single event kinetic model described in Chapter 2 and mentioned in Sec 13.8.1 to the catalytic cracking of a heavy petroleum fraction, a Lagomedia VGO. This approach requires a VGO characterization that goes way beyond what is usually practiced, like ASTM boiling range, API gravity, UOP K-factor, Conradson carbon number, aniline point and so on. Table 13.8.2.3-1 is an analysis by Sheppard et al. [1998] of the chemical composition of a Lagomedio VGO with a boiling range between 310 and 510°C. Even this characterization is not sufficient. It does not distinguish between *n*- and *i*-paraffins and only their global sum is given. Naphthenes and aromatics are split per number of rings by means of high-resolution mass spectroscopy, but not per C-number, so that the latter distributions, in particular the location of their maximum, have to be estimated from the global contents of Table 13.8.2.3-1. Additional insight, like boiling points and ranges, is helpful in this. Fig. 13.8.2.3-1 shows the C-number distribution curves developed for the various hydrocarbon families of this Lagomedio VGO using a Gaussian distribution function

$$x_{ij} = \frac{\alpha_j}{\sqrt{2\pi}\sigma_j} \exp\left[-0.5 \left(\frac{n_C(i) - \mu_j}{\sigma_j} \right)^2 \right] \qquad (13.8.2.3\text{-}1)$$

x_{ij} is the mass fraction of a component with carbon number n_C. The Gaussian distribution function contains only 2 parameters: μ, the mean and σ, the variance. It was shown to be very adequate in the fit of observed C-number distributions of hydrocarbon families in petroleum fractions [Moustafa and Froment, 2003].

TABLE 13.8.2.3-1
CHEMICAL COMPOSITION OF LAGOMEDIO VGO [SHEPPARD ET AL., 1998].

Hydrocarbon	Formula	Content (wt%)	Hydrocarbon	Formula	**Content** (wt%)
Paraffins	C_nH_{2n+2}	11.0	Naphthalenes	C_nH_{2n-12}	2.8
1-ring Naphthenes	C_nH_{2n}	15.2	Naphtho-cycloparaffins/Biphenyls	C_nH_{2n-14}	10.1
2-ring Naphthenes	C_nH_{2n-2}	11.0	Tri-aromatics	C_nH_{2n-18}	9.4
3-ring Naphthenes	C_nH_{2n-4}	6.5	Tetra-aromatics	C_nH_{2n-24}	3.2
4-ring Naphthenes	C_nH_{2n-6}	2.8	Thiophenes	$C_nH_{2n-4}S$	0.6
5-ring Naphthenes	C_nH_{2n-8}	0.2	Benzothiophenes	$C_nH_{2n-10}S$	8.3
Alkylbenzenes	C_nH_{2n-6}	4.0	Dibenzothiophenes	$C_nH_{2n-16}S$	9.3
Benzo-cycloparaffins	C_nH_{2n-8}	5.5			

These feedstock characterizations were the starting point for the development of the reaction network using Boolean relation matrices and characteristic vectors. Components of a hydrocarbon family which are known to be at equilibrium were grouped so as to limit the number of continuity equations to be integrated in reactor simulations.

It should be added here that very recently approaches have been developed for the “molecular reconstruction” of heavy petroleum fractions starting from the global analyses as normally practiced by refinery research laboratories [Hudebise and Verstraete, 2004]. This composition is suited for the single event approach.

The riser reactor was modeled using a one-dimensional heterogeneous model with plug flow and slip between the gas and solid phase, described in Section 13.6. The steady state continuity and energy equations for the components and Groups of Isomers (GOI) and for the coke content of the catalyst can be written as in (13.6-3)-(13.6-5). The number of continuity equations amounts to 670. The r_j are the rate equations for the “global” reactions between the 670 components and lumps, constructed from the rates of the elementary steps in which these components and lumps, *i*, are involved, including coke formation. φ_C is the appropriate deactivation function, depending upon the type of elementary step. The number of independent rate parameters, including those for the coking steps amounted to 39.

The height of the reactor was 50m, the diameter 1.24m. The catalyst was a RE-Y-zeolite. The pressure was essentially atmospheric. The liquid feed rate was 218,900 kg/h, the catalyst to oil ratio 8.5.

The evolution of the gasoline-, LPG-, LCO-, HFO- and coke-yields along the riser are shown in Fig. 13.8.2.3-2a for a bottom temperature of the riser of 823 K. The adiabatic temperature decrease is of the order of 25 K. The profiles

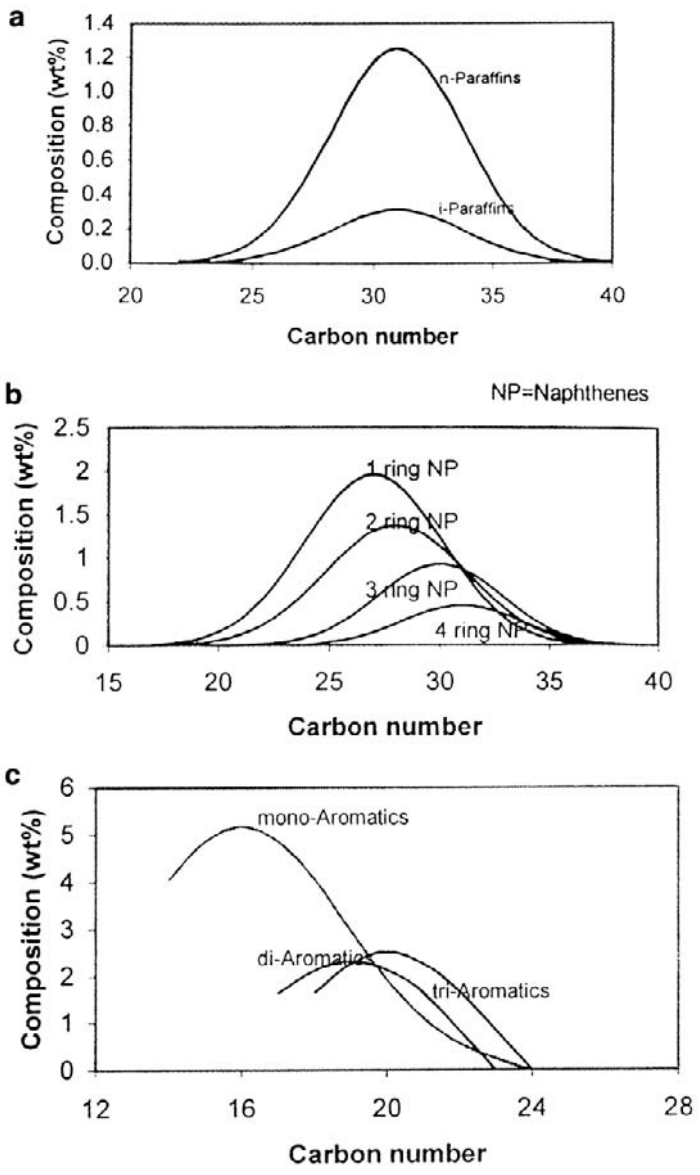

Figure 13.8.2.3-1

Predicted feed distribution for Lagomedio VGO. From Moustafa and Froment [2003].

and exit values of the yields of commercial fractions are in good agreement with the industrial trends and values. Fig. 13.8.2.3-2b shows the evolution of the yields of the hydrocarbon families making up the gasoline fraction. The normal paraffin content is very low and the olefins content high, in agreement with results of commercial catalytic cracking. This information can be further detailed down to the individual components level, if desired. The exit conversion defined as [100-(LCO - wt %yield)–(HFO - wt %yield)] amounts to 67.04. Increasing the

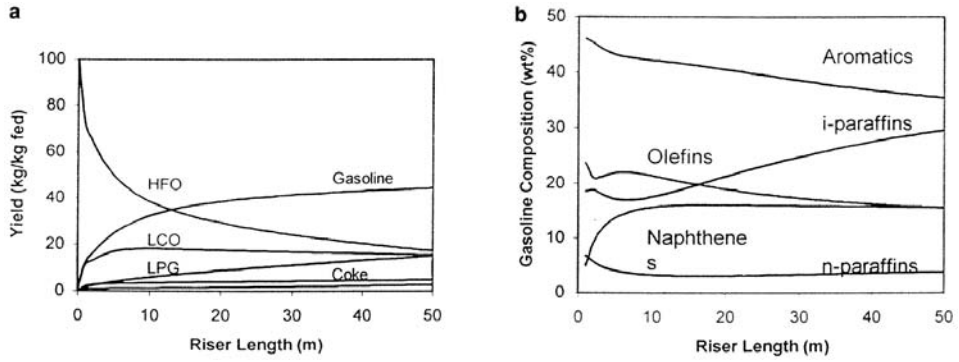

Figure 13.8.2.3-2

a. Evolution along the riser of the yields of gasoline, LPG, light cycle oil (LCO), heavy fuel oil (HFO), fuel gas and coke from Lagomedio VGO feed, T_f = 823 K.

b. Evolution of gasoline composition along the riser. Lagomedio VGO feed, T_f = 823 K. From Moustafa and Froment [2003].

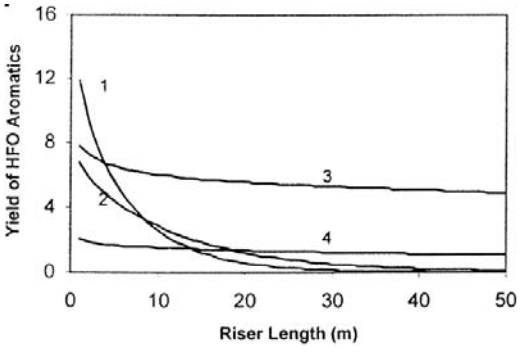

Figure 13.8.2.3-3

Yields of HFO aromatics (1-mono-ring Ar; 2-di-ring; 3-tri-ring; 4-Tetra-ring). Lagomedia feed. T_f = 823 K. From Moustafa and Froment [2003].

bottom temperature of the riser to 843 K and to 876 K increases the conversion to 70.62 and to 76.10, while the corresponding gasoline yields are 45.05 and 45.39 wt%. The gasoline yield clearly levels off, while the LPG yield rises to 17.58 and 22.02, indicating what is called over-cracking.

Coke formation is an important phenomenon in catalytic cracking. To quantitatively deal with the deactivation, coke first has to be defined. Coke is considered to be an aromatic carbenium ion with a size and structure preventing its desorption, so that it is permanently covering and deactivating the active sites on which it is formed. In the case of the catalytic cracking of VGO, coke would consist of five or more aromatic rings with a total number of C-atoms exceeding

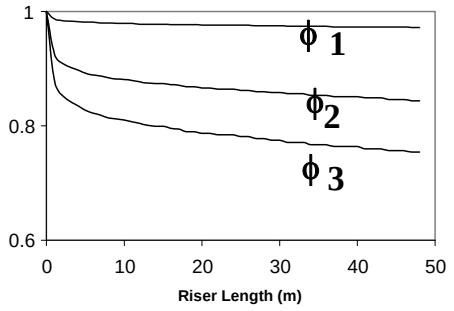

$\exp(-\alpha_1 C_c)$	$\exp(-\alpha_2 C_c)$	$\exp(-\alpha_3 C_c)$
Protonation	Alkylation	Deprotonation
Protolytic scission		Methyl shift
Hydride transfer		PCP branching
		Cyclization
		β-scission

Figure 13.8.2.3-4

Deactivation functions. Definition and evolution along the riser. From Moustafa and Froment [2003].

40. The effect of coke formation is accounted for by multiplying the rates of the elementary steps by a deactivation function. Three deactivation functions were introduced: one for the monomolecular reactions, one for the bimolecular reactions and one for the alkylation, the main step in the formation of coke. The exponential deactivation functions shown in Fig. 13.8.2.3-4 are an approximation of the effect of site coverage and pore blockage. The figure also shows the evolution of the deactivation functions along the riser. These level off from a certain conversion onwards, like the coking yield given in Fig. 13.8.2.3-2a, which is a well known feature. For the selected operating conditions coke is mainly formed in the bottom half of the riser. That may be a consequence of the temperature drop, of the evolution of the composition or of the deactivation effect of coke on its own formation.

13.8.3 Kinetic Models for the Regeneration of a Coked Cracking Catalyst

The catalyst is regenerated by burning off the coke by means of air. Coke has been observed to have an H/C ratio of 2, so that the combustion is represented by

$$CH_2 + O_2 \xrightarrow{k_1} CO + H_2O$$

$$CH_2 + 1.5O_2 \xrightarrow{k_2} CO_2 + H_2O$$

The rates of the reactions are expressed as follows:

$$r_1 = k_1 C_C y_{O_2} p_t \tag{13.8.3-1}$$

with $k_1 = k_C/(1 + \sigma)$ and σ = molar ratio CO_2/CO

$$r_2 = k_2 C_C y_{O_2} p_t \tag{13.8.3-2}$$

with $k_2 = k_C\sigma/(1 + \sigma)$, so that

$$r_C = (k_1 + k_2) C_{CM} y_{O_2} p_t \tag{13.8.3-3}$$

$$r_{O_2} = (k_1 + 1.5k_2) C_{CM} y_{O_2} p_t \tag{13.8.3-4}$$

with C_{CM} the molar coke content of the catalyst, in kmol coke/kg cat.

The rate coefficient k_C is that determined by Hano [1975], and σ is taken from Arthur [1951]:

$$\sigma = 0.000953 \ \exp\left(\frac{5585}{T}\right)$$

13.8.4 Simulation of the Regenerator of a Catalytic Cracking Unit

The two-phase model of Section 13.5.1 is used, again with plug flow in bubble and emulsion phases. The continuity equations for the components in the bubble phase are identical, (13.8.2.1-1), while those for the components in the emulsion phase are written

$$\frac{dC_{ie}}{dz} = \frac{k_I}{u_e f_e}(C_{ib} - C_{ie}) + \frac{r_i \rho_s (1 - f_b - f_e)}{u_e f_e} \tag{13.8.4-1}$$

The gas mass flow rate varies according to

$$\frac{d\dot{m}_g}{dz} = r_c \rho_s (1 - f_b - f_e) M_C \Omega \tag{13.8.4-2}$$

At $z = 0$, $\dot{m}_g = \dot{m}_A$, where $\dot{m}_A$ is the air flow rate (in kg/h).

Since the catalyst is completely mixed, the uniform coke content is calculated from

$$\dot{m}_s C_C = \dot{m}_s (C_C)_0 - \int_0^L r_C \rho_s M_C (1 - f_b - f_e) \Omega \, dz \tag{13.8.4-3}$$

with $(C_C)_0$ the coke content of the catalyst entering the reactor (kg coke/kg cat.) and M_C the molecular weight of coke.

The uniform reactor temperature is calculated from the enthalpy balance on the reactor, which is operated adiabatically:

$$(\dot{m}_s c_{ps} + \dot{m}_g c_{pg})T = \dot{m}_s c_{ps} T_{s0} + \dot{m}_A c_{pA} T_{A0} - \int_0^Z (\Delta H)_T r_C \rho_S f_S \Omega \, dz \quad (13.8.4\text{-}4)$$

where

$$\Delta H_T = (\Delta H)_1 + \frac{\sigma}{1+\sigma}(\Delta H)_2$$

$(\Delta H)_1$ is the enthalpy change for the reaction yielding CO, $(\Delta H)_2$ the enthalpy change for the reaction yielding CO_2 (in kJ/kmol).

The continuity equations (13.8.2.1-1), (13.8.4-1), (13.8.4-2), and (13.8.4-4) are integrated by a Runge-Kutta routine. The uniform temperature and coke content are calculated in an iterative way, starting from assumed values of T and C_C.

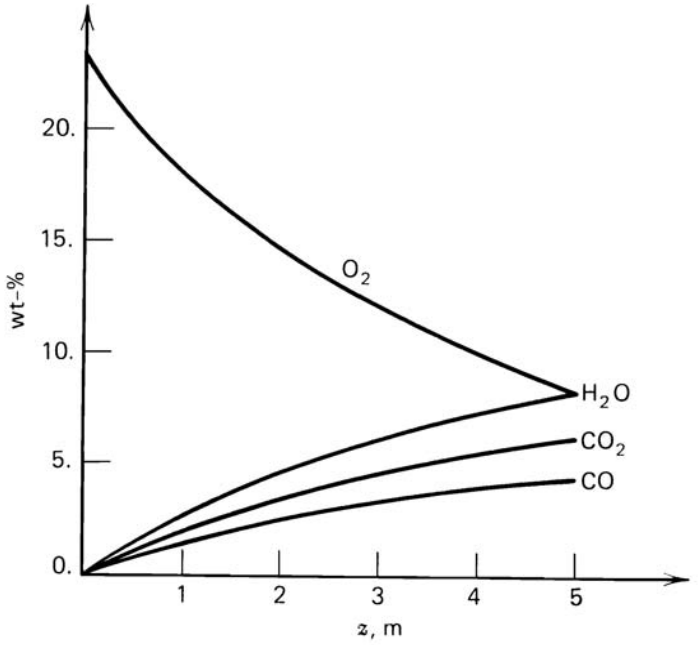

Figure 13.8.4-1
Gas-phase composition, excluding nitrogen, versus bed height.

Reactor geometry [Errazu et al., 1979]: d_t = 14.0 m; Z = 5.00 m; d_0 = 1.29×10^{-2} m

Catalyst: $\bar{d}_p$ = 8.0×10^{-5} m; ρ_s = 1500 kg cat./m^3 cat.; ε_{mf} = 0.55; $(C_C)_0$ = 1 wt-%

Flow rates: $\dot{m}_s$ = 2000 tons/h; $\dot{m}_A$ = 190 tons/h

Inlet temperatures: $(T_s)_0$ = 755 K; T_{A0} = 298 K

The uniform regenerator temperature is calculated to be 890.5 K, and the uniform coke content 0.5 wt-%. The gas phase composition, excluding nitrogen, versus bed height is shown in Fig. 13.8.4-1 [Schockaert, 1988]. The superficial gas velocity varies from 0.86 to 0.93 $m^3_g / m^2_r s$, the bubble diameter from 0.04 to 0.12 m, the interchange coefficient from 1.080 to 0.206 $m^3_g / m^2_r s$, f_b from 0.30 to 0.25, whereas f_e is 0.55.

13.8.5 Coupled Simulation of a Fluidized Bed (or Riser) Catalytic Cracker and Regenerator

A catalytic cracking unit is operated in an autothermal way. The heat required to vaporize and crack the feed is provided by the heat content of the catalyst returning from the regenerator. The average residence time of the catalyst in the reactor has to be such that the coke content suffices to satisfy this condition.

Figure 13.8.5-1 schematically represents the conditions in various locations in the combined unit, assuming no heat losses in the pipes.

The enthalpy balance for the fluidized bed reactor at the uniform temperature T_R is written

$$(\dot{m}_s c_{ps} + \dot{m}_{GO} c_{pg}) T_R = \dot{m}_s c_{ps} T_{RG} + \dot{m}_{GO} c_{pGO} T_{GO} + \int_0^Z \left(\sum_{i=1}^{10} \sum_{j=1}^{i-1} \frac{k'_{ij} C_{je}}{1 + K_{Ar_h} C_{Ar_h}} \right) \rho_s (-\Delta H)_{ij} \, f_s \Phi \Omega \, dz \tag{13.8.5-1}$$

The enthalpy balance for the regenerator is written

$$\left(\dot{m}_s c_{ps} + \dot{m}_g c_{pg}\right) T_{RG} = \dot{m}_s c_{ps} T_R + \dot{m}_A c_{pA} T_{A0} + \int_0^Z r_C \rho_s \left(-\Delta H\right)_T \, f_s \Omega \, dz \tag{13.8.5-2}$$

The coke content in the reactor is calculated from the mass balance

$$\dot{m}_s \left(C_C\right)_R = \dot{m}_s \left(C_C\right)_{RG} + \int_0^Z \sum_j \frac{k'_{10,j} C_{je}}{1 + K_{Ar_h} C_{Ar_h}} \rho_s M_C \Phi \beta \, f_s \Omega \, dz \tag{13.8.5-3}$$

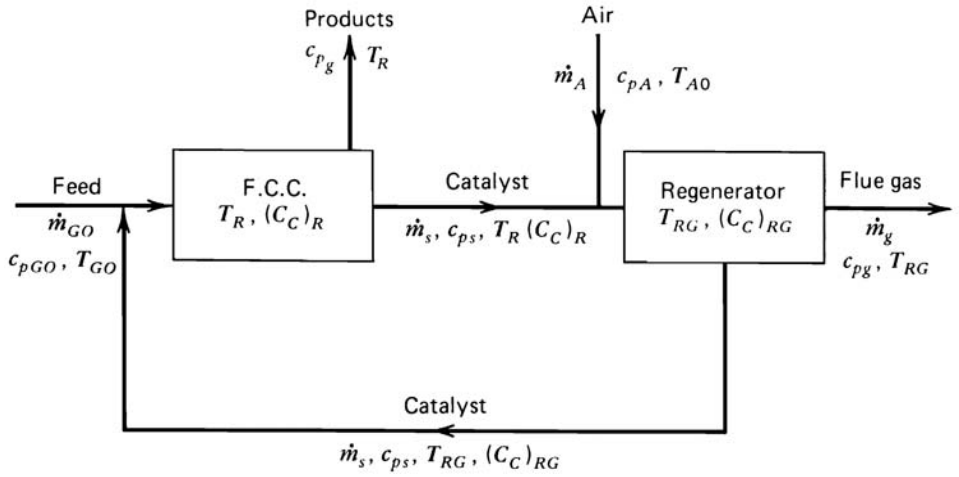

Figure 13.8.5-1
Conditions in various locations in a combined unit FCC and regenerator.

and that in the regenerator is calculated from

$$\dot{m}_s\left(C_C\right)_{RG} = \dot{m}_s\left(C_C\right)_R - \int_0^Z r_C \rho_s M_C f_s \Omega \, dz \qquad (13.8.5\text{-}4)$$

The calculations are iterative, starting from assumed values for $(C_C)_{RG}$ and for T_{RG}, the catalyst temperature and coke content in the regenerator and also at the inlet of the reactor. First, the fluidized bed reactor is calculated by means of the continuity equations, (13.8.2.1-1) and (13.8.2.1-2), and the $(C_C)_R$ and T_R from the balances, (13.8.5-1) and (13.8.5-3), which requires iteration in itself. Then, with $(C_C)_R$ and T_R obtained in this way, the regenerator values are calculated. This leads to new values for $(C_C)_{RG}$ and T_{RG}. A new cycle is then started, until convergence is reached. In a typical case, four iterations were required for convergence with an initial T_{RG} 13 K off and an initial $(C_C)_{RG}$ 0.15 wt-% off.

The results presented separately for the FCC reactor and the regenerator in Sections 13.8.2 and 13.8.4, respectively, were, in fact, obtained from their simultaneous simulation along the lines given here.

PROBLEMS

13.1 A 0.1-m column is loaded with 5 kg of sand. The size distribution is as follows:

$d_p \times 10^2$ (cm)	Weight Fraction X
7.8 and larger	0.2
6.5	0.25
5.2	0.4
3.9	0.1
2.6 and smaller	0.04

The density of the sand was measured by displacement methods to be 2,600 kg/m^3. The sand is to be fluidized with air at 100°C. Atmospheric pressure is 772 mm Hg. Estimate the minimum fluidization velocity. Calculate the composite particle diameter by means of

$$d_p = \frac{1}{\sum \frac{x_i}{d_{pi}}}$$

13.2 Tigrel and Pyle [1971] used the following expression for the catalyst deactivation function in a fluidized bed:

$$\Phi = \left(2\lambda_R \theta + \frac{1}{\Phi_0^2} \right)^{-1/2}$$

where $\theta = t/\bar{t}_R$, $\bar{t}_R = W_R/F_S$, $\lambda_R = k_R^0 \exp\left[-\left(E'/RT\right)\right]\bar{t}_R$, and Φ_0 is the value of the deactivation function for the catalyst entering the fluidized bed. When the particles are perfectly mixed, the average of Φ in the reactor, $\overline{\Phi}$, is given by

$$\overline{\Phi} = \exp\left(\frac{1}{2\lambda_R \Phi_0^2} \right) \operatorname{erfc}\left(\frac{1}{\Phi_0 \sqrt{2\lambda_R}} \right) \sqrt{\frac{\pi}{2\lambda_R}}$$

and the rate of catalytic cracking of gas oil, for example, is represented by

$$r = k_C^2 \overline{\Phi}$$

where c is the gas oil concentration.

Tigrel and Pyle adopted a two-phase model for the fluidized bed, assuming perfect mixing of gas in the emulsion phase and plug flow in the bubble phase and a transfer of gas between bubble and emulsion phases.

Considering a mean bubble size, derive the following expression for the fraction of feed component *A* unconverted at the top of the bed:

$$y_T = \frac{\exp(-Z)}{1-\gamma} + \frac{\left(1-\beta e^{-Z}-\gamma\right)^2}{2(1-\gamma)k^*\overline{\Phi}}\left(-1+\sqrt{1+\frac{4k^*\overline{\Phi}}{1-\beta e^{-Z}-\gamma}}\right)$$

where

$$\beta = 1-\frac{u_{mf}}{u} \qquad \gamma = \frac{u_s}{u} \qquad k^* = \frac{kH}{u} \qquad Z = \frac{KH}{u_a V}$$

and

u = superficial gas velocity (cm/s)
u_a = absolute bubble-rising velocity (cm/s)
u_s = downward velocity of catalyst particle (cm/s)
K = transversal mass transfer coefficient (cm^3/s)
H = total bed height (cm)
V = bubble volume (cm^3)

Plot the conversion as a function of the fluid velocity for solids velocities of 1.0, 3.0, and 10 cm/s for a mean bubble diameter of 30 cm, a value of $\Phi_0 = 0.9$, and a reactor height of 9 m.

13.3 Modeling of an Acrylonitrile Reactor [after Kunii and Levenspiel, 1969]. Design a fluidized bed reactor for the production of acrylonitrile by ammoxidation of propylene, with air as the oxidizing agent. The required production of acrylonitrile is 40,400 tons/year (count on approximately 8000 h or 340 days). The process achieves a 78 percent conversion of propylene at 400°C and atmospheric pressure. The rate constant of the reaction considered as a first-order process is k = 1.44 m^3/kg cat. h at 400°C. The volume fraction of propylene in the feed is 0.24. The catalyst used has a mean particle diameter d_p = 51 μ and the following size distribution:

d_p (m): 5×10^{-6} 15 25 35 45 55 65 75 85 95 105 115×10^{-6}

$p(d_p)$ (m^{-1}): 6×10^{-2} 22 46 76 118 170 200 152 99 63 36 12×10^{-2}

The solid density is 2500 kg/m^3; the specific heat 0.837 kJ/kg°C; the void fraction ε of the packed bed is 0.5. At the minimum fluidization

velocity u_{mf} = 7.2 m/h, the void fraction ε_{mf} is 0.6. Gas properties: ρ_g = 1 kg/m^3; c_p = 1.047 kJ/kg°C; μ = 0.144 kg/h m; D_e = 0.14 m^2/h.

Removing the heat of reaction necessitates an internal heat exchanger. This exchanger will also help to limit the bubble diameter. Take vertical tubes of 0.06 m outer diameter on a 0.14-m triangular pitch. This limits the effective diameter of the bubbles to 0.1 m. Note that this is a very crude way of determining the (average) bubble diameter, which is the main variable in the Kunii and Levenspiel model. Select the superficial velocity of the feed to be 1800 m/h. Calculate the mass transfer coefficients from (13.5.3-4) and (13.5.3-5) and use (13.5.3-13) to calculate the bed height.

13.4 Simulation of the Cracking of Gasoil in a Riser Reactor

Use the one-dimensional plug flow model with slip between the phases described in Section 13.6 and the 10-lump kinetic model presented in Section 13.8.1 and applied in Sections 13.8.2.1 and 13.8.2.2.

The following information required for the simulation, is based upon a paper by Shah et al. [Shah, Y.T., Huling, G.P., and Paraskos, J.A., *Ind. Eng. Chem. Proc. Des. Dev.*, 16, 1 (1977)].

Reactor geometry: d_t = 0.85 m; Z = 30 m

Catalyst: $\bar{d}_p = 8.0 \times 10^{-5}$ m; ρ_s = 1500 kg cat./m³ cat.; c_{ps} = 1.003 kJ/kg K

Coke content of catalyst entering the riser: 0.15 wt-%

Flow rates: $\dot{m}_s$ = 980 tons/h; $\dot{m}_{GO}$ = 49 tons/h

Reactor inlet temperature: 770 K

The gasoil has the same composition as that already given in Table 13.8.2.1-1.

13.5 Simulation of a circulating fluidized bed riser reactor for the gasification of biomass (synthesis gas production).

Reaction mechanism and kinetics

The reaction mechanism accounts for pyrolysis of biomass and tar, gas-phase combustion, the water gas shift reaction, and combustion and gasification of char [Di Blasi, C., *Chem. Eng. Sci.*, 55, 2931 (2000)].

The biomass pyrolysis is described by the following global reaction [Di Blasi, C., *Chem. Eng. Sci.*, 55, 2931 (2000); Sheth, P.N., and Babu, B., *Proc. Nat. Conf. Env. Cons.* (NCEC-2006), pp. 453-458 (2006)]:

$$Biomass \xrightarrow{k_{p1}} w_C^{p1} Char + w_G^{p1} Gas^{p1} + w_T^{p1} Tar \qquad (p1)$$

The weight fractions of char, gases, and tar produced, as well as the composition of the gases produced depend on the type of biomass used. For 0.5-1.0 cm wood chips, Di Blasi et al. [Di Blasi, C., Signorelli, G., Di Russo, C., and Rea, G., *Ind. Eng. Chem. Res.*, 38, 2216 (1999)] experimentally found $w_C^{p1} = 0.33$, $w_G^{p1} = 0.48$, and $w_T^{p1} = 0.19$, and a gas composition corresponding to 3.1 wt% CH_4, 15.6 wt% CO, 27.1 wt% CO_2, 52.1 wt% H_2O, and 2.1 wt% H_2. Tar (liquid at ambient conditions and as such also referred to as liquids) groups the carbonaceous components of high molecular mass. Their stoichiometric composition can be represented by $CH_{1.522}O_{0.0228}$ [Bryden, K.M., and Ragland, K.W., *Energy Fuels*, 10, 269 (1996)] and their mean molecular mass is taken 95 kg/kmol [Corella, J., Aznar, M.P., Delgado, J., and Aldea, E., *Ind. Eng. Chem. Res.*, 30, 2252 (1991)]. At the temperatures in the reactor, the tar can be considered to be gaseous. The char produced has the same size as the biomass particles, but a lower density. The heat required for the biomass pyrolysis can be provided by the combustion of the pyrolysis gases and the tar, as described hereafter.

Tar can undergo so-called secondary pyrolysis, described by:

$$Tar \xrightarrow{k_{p2}} Gas^{p2} \qquad (p2)$$

The composition of the gases produced is fixed and to be determined experimentally. Starting from wood, the gases resulting from the secondary pyrolysis were measured to typically contain 20.0 wt% CH_4, 50.0 wt% CO, and 30 wt% CO_2 [Di Blasi, C., Signorelli, G., Di Russo, C., and Rea, G., *Ind. Eng. Chem. Res.*, 38, 2216 (1999)]. The secondary pyrolysis is slightly exothermic.

The following gas phase reactions account for the combustion of tar, CH_4, CO, and H_2 [Di Blasi, C., *Chem. Eng. Sci.*, 55, 2931 (2000)]:

$$Tar\left(CH_{1.522}O_{0.0228}\right) + 0.867\,O_2 \xrightarrow{k_{c1}} CO + 0.761\,H_2O \qquad (c1)$$

$$CH_4 + 1.5\,O_2 \xrightarrow{k_{c2}} CO + 2\,H_2O \qquad (c2)$$

$$2\,CO + O_2 \xrightarrow{k_{c3}} 2\,CO_2 \qquad (c3)$$

$$2\,H_2 + O_2 \xrightarrow{k_{c4}} 2\,H_2O \qquad (c4)$$

The combustion reactions are highly exothermic and can provide the heat required for the primary pyrolysis.

The water gas shift reaction is also to be accounted for:

$$CO + H_2O \overset{k_{wg}}{\Leftrightarrow} CO_2 + H_2 \qquad (wg)$$

Finally, the combustion of char and the gasification of char by CO_2, H_2, and H_2O are described by:

$$C + O_2 \overset{k_{c5}}{\rightarrow} CO_2 \qquad (c5)$$

$$C + CO_2 \overset{k_{g1}}{\rightarrow} 2CO \qquad (g1)$$

$$C + 2H_2 \overset{k_{g2}}{\rightarrow} CH_4 \qquad (g2)$$

$$C + H_2O \overset{k_{g3}}{\rightarrow} CO + H_2 \qquad (g3)$$

The char combustion is exothermic, whereas the char gasification reactions are endothermic.

The reaction kinetics found in the literature is summarized in Table 1. Because of the different types of solids involved (biomass, char), all reaction rates are expressed per m_r^3. Values for the pre-exponential factors and the activation energies are given in Table 2. The combustion of hydrogen is considered infinitely fast.

A fraction of the char leaving the reactor can be recycled.

Reactor model

For the simulation of the circulating fluidized bed riser the one-dimensional plug flow model with slip between the gas and solid phases as described in Section 13.6 can be used.

When calculating the primary pyrolysis and the char combustion and gasification reaction rates, the variation of the particle size (char) by the combustion and gasification reactions is to be accounted for.

The biomass pyrolysis, reaction (*p*1), is relatively slow and gas-solid mass transfer limitations can be neglected.

TABLE 1
REACTION RATE EQUATIONS

Reaction	**Rate equation**	**Units**	**Ref.**
(*p*1)	$r_{p1} = k_{p1}(a_v)_B \varepsilon_{sB} \rho_B$	$[kg_B/m_r^3 s]$	[1]
(*p*2)	$r_{p2} = k_{p2}\, \varepsilon\, C_{TAR}$	$[kmol/m_r^3 s]$	[2]
(*c*1)	$r_{c1} = k_{c1}\, \varepsilon\, T_g C_{TAR}^{0.5} C_{O2}$		[3]
(*c*2)	$r_{c2} = k_{c2}\, \varepsilon\, T_g C_{CH4}^{0.5} C_{O2}$		[3]
(*c*3)	$r_{c3} = k_{c3}\, \varepsilon\, C_{CO} C_{O2}^{0.25} C_{H2O}$		[3]
(*c*4)	$r_{c4} = k_{c4}\, \varepsilon\, C_{H2} C_{O2}$		[3]
(*wg*)	$r_{wg} = k_{wg}\, \varepsilon (C_{CO} C_{H2O} - C_{CO2} C_{H2} / K_{wg})$		[4; 5]
(*c*5)	$\tilde{r}_{c5} = k_{c5}(a_v)_C \varepsilon_{sC} C_{O2}$		[6]
(*g*1)	$\tilde{r}_{g1} = k_{g1}(a_v)_C \varepsilon_{sC} C_{CO2}$		[7]
(*g*2)	$\tilde{r}_{g2} = k_{g2}(a_v)_C \varepsilon_{sC} C_{H2}$		[7]
(*g*3)	$\tilde{r}_{g3} = k_{g3}(a_v)_C \varepsilon_{sC} C_{H2O}$		[7]

$$k_{p1} = A_{p11} \exp(T_s / B_{p11}) + A_{p12} \exp(T_s / B_{p12});$$

$$k_j = A_j \exp(-E_j / RT_s) \quad \text{for } j\text{: } (c5), (g1), (g2), (g3);$$

$$k_j = A_j \exp(-E_j / RT) \quad \text{for } j\text{: } (p2), (c1), (c2), (c3), (c4), (wg);$$

$$\varepsilon_s = 1 - \varepsilon = \varepsilon_{sB} + \varepsilon_{sC} + \varepsilon_{s\_Inert}.$$

References:

[1] Sheth, P.N., and Babu, B., *Proc. Nat. Conf. Env. Cons.* (NCEC-2006), pp. 453-458 (2006).
[2] Lede, J., *Ind. Eng. Chem. Res.*, 39, 893 (2000).
[3] Bryden, K.M., and Ragland, K.W., *Energy Fuels*, 10, 269 (1996).
[4] Biba, V., Malecha, J., Macak, J., and Klose, E., *Ind. Eng. Chem. Proc. Des. Dev.*, 17, 92 (1978).
[5] Yoon, H., Wei, J., and Denn, M.M., *AIChE J.*, 24, 885 (1978).
[6] Kashiwagi, T., and Nambu, H., *Comb. Flame*, 88, 345 (1992).
[7] Groeneveld, M.J., and van Swaaij, W.P.M., *Chem. Eng. Sci.*, 35, 307 (1980).

TABLE 2
THERMODYNAMIC AND KINETIC DATA (REFERENCES: SEE TABLE 1)

Reaction	Kinetic and Thermodynamic data	Units	Ref.
(*p*1)	$A_{p11} = 1.1183 \cdot 10^{-10}$, $A_{p12} = 8.10156 \cdot 10^{-10}$ $B_{p11} = 68.4868$, $B_{p12} = 104.5661$ $-\Delta H_{p1} = -418 \cdot 10^{3}$	[m/s] [1/K] [J/kg biomass]	[1]
(*p*2)	$A_{p2} = 5.9 \cdot 10^{7}$ $E_{p2} = 123.5 \cdot 10^{6}$ $-\Delta H_{p2} = 42 \cdot 10^{3}$	[1/s] [J/kmol] [J/kg TAR]	[2]
(*c*1)	$A_{c1} = 9.2 \cdot 10^{6}$ $E_{c1} = 80.235 \cdot 10^{6}$	[kmol/m_r^3s] [J/kmol]	[3]
(*c*2)	$A_{c2} = 9.2 \cdot 10^{6}$ $E_{c2} = 80.235 \cdot 10^{6}$	[kmol/m_r^3s] [J/kmol]	[3]
(*c*3)	$A_{c3} = 1.3 \cdot 10^{11}$ $E_{c3} = 125.590 \cdot 10^{6}$	[kmol/m_r^3s] [J/kmol]	[3]
(*c*4)	$A_{c4} = 1 \cdot 10^{11}$ $E_{c4} = 83.144 \cdot 10^{6}$	[kmol/m_r^3s] [J/kmol]	[3]
(*wg*)	$A_{wg} = 2.78$ $E_{wg} = 12.58 \cdot 10^{6}$ $A_E = 0.0265$ $E_E = 32.9 \cdot 10^{6}$	[mol/m_r^3s] [J/kmol] [-] [J/kmol]	[4], [5]
(*c*5)	$A_{c5} = 5.67 \cdot 10^{9}$ $E_{c5} = 160 \cdot 10^{6}$	[kmol/m_r^3s] [J/kmol]	[6]
(*g*1)	$A_{g1} = 1 \cdot 10^{7}$ $E_{g1} = 218 \cdot 10^{6}$	[kmol/m_r^3s] [J/kmol]	[7]
(*g*2)	$A_{g2} = 1 \cdot 10^{5}$ $E_{g2} = 218 \cdot 10^{6}$	[kmol/m_r^3s] [J/kmol]	[7]
(*g*3)	$A_{g3} = 1 \cdot 10^{5}$ $E_{g3} = 218 \cdot 10^{6}$	[kmol/m_r^3s] [J/kmol]	[7]

Gas-solid mass transfer limitations encountered in the combustion and gasification of char — reactions (*c*5) and (*g*1)-(*g*3) — can be accounted for as described in Chapter 3. For r_{c5}, for example:

$$r_{c5} = (a_v)_C \varepsilon_{sC} \frac{1}{(1/k_m) + (1/k_{c5})} C_{O2} \qquad \text{(a)}$$

The gas-solid mass transfer coefficient, k_m, can be calculated according to [Gupta, A.S., and Thodos, G., *AIChE J.*, 9, 751 (1963)]:

$$k_m = 2.06\, u_g\, \mathrm{Re}^{-0.575}\, \mathrm{Sc}^{-2/3} \qquad \text{(b)}$$

where Re is the particle diameter based Reynolds number. The particles used in the simulations are considered small enough to allow neglecting intra-particle diffusion limitations.

The gas-solid heat transfer can be modeled as:

$$Q_{gs} = \varepsilon_s a_v h_{gs} \left(T_g - T_s\right) \qquad \text{(c)}$$

with [Gupta, A.S., and Thodos, G., *AIChE J.*, 9, 751 (1963)]:

$$h_{gs} = 2.06 \rho_g c_{p,g} u_g\, \mathrm{Re}^{-0.575}\, \mathrm{Pr}^{-2/3} \qquad \text{(d)}$$

Data

The circulating fluidized bed riser is 12 m tall and operated adiabatically. Consider the gasification of 650 μm biomass particles, assumed ash free. The moisture content of the biomass fed is 10 wt% on a dry basis. The moisture evaporation is assumed to be infinitely fast. The biomass is fed at room temperature (300 K), whereas the air fed is preheated to 600 K. The air is considered to be composed of oxygen (21 %) and nitrogen (79 %). Atmospheric pressure operation is considered. The air inlet velocity is 2.5 m/s. A fraction of the char leaving the reactor is adiabatically recycled.

The reactor temperature can be controlled by adjusting the feed air to dry biomass weight ratio and the char recycle. In general, high-temperature biomass gasification allows reducing the production of char and liquids, but faces the ash melting problem (ash melting temperature ≈ 900 - 1100 K). Consider simulations with two different inlet air to dry biomass weight ratios, 0.5 and 1.0 respectively, corresponding to outlet temperatures close to and well above the ash melting temperature. (For example, for a reactor outlet temperature of 1350.5 K, the inlet air to dry biomass weight ratio is 1.0, the char-to-biomass mass flow ratio at the bottom of the reactor is ≈ 0.6 with 90% of the char leaving the reactor being recycled adiabatically.)

Additional data:

- diffusivity = $2.0 \cdot 10^{-5}$ m^2/s

- viscosity = $5.3 \cdot 10^{-5}$ Pa s
- conductivity = 0.17 W / m K

Solution method

Solve the set of species continuity and energy equations using a fourth-order Runge-Kutta routine.

REFERENCES

Agrawal, K., Loezos, P.N., Syamlal, M., and Sundaresan, S., *J. Fluid Mech.*, 445, 151 (2001).

Anderson, T., and Jackson, R., *Ind. Eng. Chem. Fundam.*, 6, 527 (1967).

Angelino, H., Couderc, J.P., Gibert, H., and Laguerie, C., Eds., *Fluidization and Its Applications, Proc. Int. Symp., Sté Chimie Industrielle,* Paris (1974).

Arthur, J.P., *Trans. Farad. Soc.*, 47, 164 (1951).

Avidan, A., *Proceedings Joint Meeting CIESC-AICHE*, Chemical Industry Press, Beijing, China (1982).

Baird, H.M.I., and Rice, G., *Chem. Eng. J.*, 9, 171 (1975).

Balakrishnan, A.R., and Pei, D.C.T., *Can. J. Chem. Eng.*, 53, 231 (1975).

Baltanas, M.A., Van Raemdonck, K.K., Froment, G.F., and Mohedas, S.R., *Ind. Eng. Chem. Res.*, 28, 899 (1989).

Behie, L.A., and Kehoe, P., *AIChE J.*, 19, 1070 (1973).

Chavarie, C., and Grace, J.R., *Chem. Eng. Sci.*, 31, 741 (1976).

Chiba, T., and Kobayashi, T., *Proc. Int. Conf. Fluid.*, Toulouse (1973), p. 468.

Christensen, G., Apelia, M.R., Hickey, K.J., Jaffe S.B., *Chem. Eng. Sci.*, 54, 27 (1999).

Darton, R.C., *Trans. Inst. Chem. Engrs.*, 55, 274 (1977).

Davidson, J.F., and Harrisson, D., *Fluidized Particles*, Cambridge University Press, Cambridge (1963).

Davidson, J.F., and Harrisson, D., Eds., *Fluidization*, Academic Press, New York (1971).

De Groot, J.H., in *Proc. Int. Symp. on Fluidization*, Netherlands University Press, Eindhoven (1967), p. 348.

De Vries, R.J., van Swaaij, W.P.M., Mantovani, C., and Heijkoop, A., in *Proc. 5th Eur./2nd Int. Symp. Chem. React. Eng.*, Elsevier, Amsterdam (1972), p. B-9-59.

De Wilde, J., *Phys. Fluids*, 17, 113304 (2005).

De Wilde, J., *Phys. Fluids*, 19, 058103 (2007).

Ergun, S., *Chem. Eng. Prog.*, 48, 89 (1952).

Errazu, A.F., de Lasa, H.I., and Sarti, F., *Can. J. Chem. Eng.*, 57, 191 (1979).

Falk, L., Schaer, E., *Chem. Eng. Sci.*, 56, 2445 (2001).

Fritz, W., *Chem. Ing. Techn.*, 41, 435 (1969).

Froment, G.F., *Appl. Catal.*, 22, 3 (1986).

Froment, G.F., In *Concepts and Design of Chemical Reactors*, Eds. S. Whitaker and A.E. Cassano, Gordon and Breach Science Publishers, Chapter 5, 213 (1986).

Froment, G.F., *Catalysis Reviews*, 1, 83 (2005).

George, S.I., and Grace, J.R., *AIChE Symp. Ser.*, 74, 176 (1978).

Gidaspow, D., *Multiphase Flow and Fluidization: Continuum and Kinetic Theory Descriptions*, Academic Press (1994).

Grace, J.R., and de Lasa, H., *AIChE J.*, 24, 364 (1978).

Haff, P.K., *J. Fluid Mech.*, 134, 401 (1983).

Hano, T., Nakashio, F. and Kusoniki, K., *J. Chem. Eng. Japan*, 8, 127 (1975).

Horio, M., Nonaka, A., Sawa, Y., and Muchi, G. I., *AIChE J.*, 32, 1466 (1986).

Hrenya, C.M., and Sinclair, J.L., *AIChE J.*, 43, 853 (1997).

Hudebine, D., and Verstraete, J.J., *Chem. Eng. Sci.*, 59(22-23), 4755 (2004).

Ishii, M., Thermo-Fluid Dynamic Theory of Two-Phase Flow, *Direction des Etudes et Recherches d'Electricité de France*, Eyrolles, Paris (1975).

Jackson, R., *The Dynamics of Fluidized Particles*, Cambridge University Press (2000).

Jacob, S.M., Gross, B., Voltz, S.E., and Weekman, V.W.Jr., *AIChE J.*, 22, 701 (1976).

Jenkins, J.T., and Savage, S.B., *J. Fluid Mech.*, 130, 187, (1983).
Johnsson, J.E., Grace, J.R., and Graham, J.J., *AIChE J.*, 33, 614 (1987).
Johnson, P.C., and Jackson, R., *J. Fluid Mech.*, 176, 67 (1987).
Klein, M.T., Neurock, M., Nigam, A., and Libanati, C., *in Chemical Reactions in Complex Mixtures –The Mobil Workshop*, Sapre, A.V. and Krambeck, F.J., Eds., 126-142, Van Nostrand Reinhold, New York (1991).
Koch, D.L., *Physics of Fluids A-Fluid Dynamics*, 2, 1711 (1990).
Krishna, R., in *Multiphase Chemical Reactors*, ed. by A. Rodriguez, J. M. Calo, and N. Sweed, Sijthoff and Noordhoff, The Netherlands (1981).
Kunii, D. and Levenspiel, O., *Fluidization Engineering*, Wiley, New York (1969); 2nd ed. A Butterworth-Heinemann Title (1991).
Leva, M., *Fluidization*, McGraw-Hill, New York (1960).
Lewis, W.K., Gilliland, E.R., and Glass, W., *AIChE J.*, 5, 419 (1959).
Liguras, D.K., and Allen, D.T., *Ind. Eng. Chem. Res.*, 28, 674 (1989).
Lun, C.K.K., Savage, S.B., Jeffrey, D.J., and Chepurniy, N., *J. Fluid Mech.*, 140, 223 (1984).
May, M.G., *Chem. Eng. Prog.*, 55, 49 (1959).
Mireur, J.P., and Bischoff, K.B., *AIChE J.*, 13, 839 (1967).
Moustafa, T.M., and Froment, G.F., *Ind. Eng. Chem. Res.*, 42, 14 (2003).
Murphy, J.F., and Soudek, M., in *Proc. Third Int. Symp. Large Chemical Plants*, p.81, Uitg. Sprugt., Van Mantgen en De Dees b.v., Leiden (1976).
Murray, J.D., *J. Fluid Mech.*, 21, 465 (1965); 22, 57 (1965).
Nace, D.M., Voltz, S.E., and Weekman, V.W., *Ind. Eng. Chem. Proc. Des. Dev.*, 10, 530 (1971).
Osberg, G. L. and Charlesworth, D. H., *Chem. Eng. Progr.*, 47, 566 (1951).
Partridge, B. A. and Rowe, P. N., *Trans. Inst. Chem. Eng.*, 44, T335 (1966); 44, T349 (1966).
Perry, R.H., and Chilton, C.H., *Chemical Engineers Handbook*, 5th ed., McGraw-Hill, New York (1973).
Perry, R.H., and Green, D., *Perry's Chemical Engineers' Handbook*, Sixth Edition, Mcgraw-Hill (1984).
Petersen, E.E., *AIChE J.*, 6, 488 (1960).
Pyle, D.L., in *Proc. 1st Int. Symp. Chem. React. Eng.*, Washington, D.C. (1970), *Advances in Chem. Series*, 109, 106, A.C.S, Washington, D.C. (1972).
Quann, R.J., and Jaffe, S.B., *Ind. Eng. Chem. Res.*, 31, 2483 (1992).
Quann, R.J., and Jaffe, S.B., *Chem. Eng. Sci.*, 31, 1615 (1996).
Saulnier, C., Simonin, O., Védrine, D., and Donnat, L., in *Proceedings of the 8th International Conference on Circulating Fluidized Beds*, Hangzhou, China, 328 (2005).
Savage, S.B., in *Theory of Dispersed Multiphase Flow*, Ed. R.E. Meyer, Academic Press, New York (1983).
Schockaert, T., Ph. D. Thesis, Rijksuniversiteit Gent (1988).
Shah, Y.T., Huling, G.P. and Paraskos, J.A., *Ind. Eng. Chem. Proc. Des. Dev.*, 16, 1 (1977).
Sheppard, C.M., Green, J.B., and Vanderveen, J.W., *Energy Fuels*, 12, 320 (1998).
Shirai, L., *Fluidized Beds* (in *Japanese Kagaku Gyntsusha*), Kanazawa (1958) (quoted in Kunii and Levenspiel (1969)).
Sinclair, J.L., and Jackson, R., *AIChE J.*, 35, 1473 (1989).
Squires, A. M., Kwauk, M., and Avidan, A. A., Science, 230 (4732), p.1329 (1985).
Sun, B., and Gidaspow, D., *Ind. Eng. Chem. Res.*, 38, 787 (1999).
Takatsuka, T., Sato, S., Morimoto, Y., and Hashimoto, H., *Int. Chem. Eng.*, 27, 107 (1987).
Talman, J.A., Geier, R., and Reh, L., *Chem. Eng. Sci.*, 54, 2123 (1999).
Theologos, K.N., Nikou, I.D., Lygeros, A.I., and Markatos, N.C., *AIChE J.*, 43, 486 (1997).
Theologos, K.N., Lygeros, A.I., and Markatos, N.C., *Chem. Eng. Sci.*, 54, 5617 (1999).
Thompson, M.L., Bi, H., and Grace, J.R., *Chem. Eng. Sci.*, 54, 2175 (1999).
Tigrel, A.Z., and Pyle, D.L., *Chem. Eng. Sci.*, 26, 133 (1971).
Trambouze, P., Van Landeghem, H., and Waucquier, J.P., *Les Réacteurs Chimiques*, Eds.Technip, Paris (1984).

Tsuo, Y.P., and Gidaspow, D., *AIChE J.*, 36, 885 (1990).
Van Deemter, J.J., *Chem. Eng. Sci.*, 13, 143 (1961).
van Swaaij, W.P.M., and Zuiderweg, F.J., *Proc. 5th Eur./2nd Int. Symp. Chem. React. Eng.*, Elsevier, Amsterdam (1972), pp. B-9-25.
van Wachem, B.G.M., Schouten, J.C., Krishna, R., and van den Bleeck, C.M., *Chem. Eng. Sci.*, 54, 2141 (1999).
Vreedenberg, H.A., *Chem. Eng. Sci.*, 11, 274 (1960).
Vynckier, E., and Froment, G.F., In *Kinetic and Thermodynamic Lumping of Multicomponent Mixtures*, Eds. G. Astarita and S.I. Sandler, Elsevier Publishers B.V., Amsterdam, 131 (1991).
Weekman, V.W., *Ind. Eng. Chem. Proc. Des. Dev.*, 7, 90 (1968a).
Weekman, V.W., *Ind. Eng. Chem. Proc. Des. Dev.*, 7, 252 (1968b).
Weekman, V.W.Jr., *AIChE Monograph Series 11*, Vol. 75 (1979).
Wen, C.Y., and Hashinger, R.F., *AIChE J.*, 6, 220 (1960).
Wen, C.Y., and Yu, Y.H., *Chem. Eng. Prog. Symp. Ser.*, 62, 100 (1966).
Wender, L., and Cooper, G.T., *AIChE J.*, 4, 15 (1958).
Werther, J., *Chem. Ing. Techn.*, 50, 850 (1978).
Whittington, E.L., Murphy, J.R., and Lutz, I.H., *Oil & Gas Journal*, Oct. 30, 49, (1972).
Yates, J.G., *The Chemical Engineer*, p. 671, November (1975).
Zenz, F.A., and Othmer, D.F., *Fluidization and Fluid-Particle Systems*, Reinhold, New York (1960).
Zenz, F.A., and Weil, N.A., *AIChE J.*, 4, 472 (1958).

Chapter 14

Multiphase Flow Reactors

14.1 TYPES OF MULTIPHASE FLOW REACTORS

Reactions between components of a gas and a liquid, the kinetics of which were discussed in Chapter 6, are carried out in a variety of equipment, often having confusing names. The variety stems from a number of conditions that have to be fulfilled simultaneously: efficient contact between gas and liquid — and eventually a solid catalyst, limitation of pressure drop, ease of removal of heat, and low cost of construction and operation. Depending on whether the main mass transfer resistance is located in the gas or in the liquid, multiphase reactors or absorbers are operated either with a dispersed gas phase and continuous liquid phase or vice versa. Whether cocurrent or countercurrent flow of gas and liquid is used depends on the availability of driving forces for mass and heat transfer and reaction.

Table 14.1 classifies various types of equipment for gas-liquid reactions. It is based on geometric aspects, the presence or absence of a solid catalyst, and the flow directions. Before discussing model equations and specific design aspects, the various types of reactors of Table 14.1 will be briefly characterized in a qualitative way.

14.1.1 Packed Columns

Packed columns are frequently encountered in industry. Their construction is simple, and they can be easily adapted by replacing the packing. They permit rather large variations in flow rates, and the pressure drop is relatively low. The packing is often staged to avoid maldistribution of the fluid. Sometimes, staging is required to provide intermediate heat exchange, either in external heat exchangers or by means of direct cooling by liquid injection. Packed columns for gas purification, often called “absorbers”, always operate with counter-current flow. Typical examples are the absorption of carbon dioxide and hydrogen sulfide by ethanolamines, potassium carbonate or sodium hydroxide in steam reforming or thermal cracker effluents, and the absorption of ammonia by sulfuric acid.

When the packing is also a catalyst, both countercurrent and cocurrent flows are applied. In the latter case both upflow and downflow operations are encountered. With upflow operation the contacting between gas and liquid is superior, but the pressure drop is higher and there are restrictions on flow rates and packing diameter because of flooding. The downflow cocurrent column packed with catalyst may operate in two distinct flow regimes: “the trickle flow” regime when the gas phase is continuous and the liquid phase is dispersed, or

TABLE 14.1
CLASSIFICATION OF MULTIPHASE FLOW REACTORS

	Column				
Locus of Reaction	**Packed**	**Plate**	**Empty**	**Stirred Vessel**	**Miscellaneous**
Fluid phase only	Countercurrent flow "Absorber"	Countercurrent Flow "Absorber"	Countercurrent Flow "Spray tower" Cocurrent or countercurrent "Bubble column	"Absorber" or "Reactor	Venturi Static mixers Falling film, etc.
Solid catalyst	Countercurrent Cocurrent downward "Trickle bed reactor" "Packed bubble reactor" Cocurrent upward		Cocurrent or Countercurrent "Bubble reactor"	"Slurry Reactor"	

the “bubble flow” regime when the gas phase is dispersed and the liquid phase is continuous. For a given gas flow rate, both regimes may lead to pulsed flow when the liquid flow rate is increased.

Trickle bed reactors have grown rapidly in importance because of their application in hydrodesulfurization of naphtha, kerosene, gasoil, and heavier petroleum fractions; in hydrocracking of heavy gasoil and atmospheric residues; in hydrotreating of lube oils; and in hydrogenation processes. In trickle bed operation the flow rates are much lower than those in absorbers. To avoid effectiveness factors in the reaction that are too low, the catalyst size must be much smaller than that of the packing used in absorbers, which also means that the overall void fraction is much smaller.

The fixed bed is preferred to a slurry-type operation when the gas flow rate is relatively low because it leads to a gas and liquid flow pattern that better approximates plug flow. Only for high gas flow rates would an operation with suspended catalyst be preferred — when the catalyst size permits it — to avoid the pulsed flow regime that might be encountered in fixed bed operation.

14.1.2 Plate Columns

Plate columns are only used in processes that do not require a solid catalyst and for which relatively long contact times are needed. Because the liquid flow is evenly distributed over the complete height of the column, large diameters can be used. The interfacial area per unit volume of the gas-liquid mixture is larger than in packed columns; but, on the other hand, plate columns only have gas-liquid mixtures on the plates themselves. Whether there is more interfacial area per unit total volume of column in the plate column depends on the plate spacing, which is determined by the presence or absence of downcomers, foaming, entrainment, and so on.

A very important industrial example of a plate column reactor is the so-called absorber in nitric acid production, in which NO, dissolved in dilute acid, is transformed into nitric acid by means of air oxygen.

14.1.3 Empty Columns

Empty columns are characterized by the absence of materials or devices for the continuous dispersion of the phases, which does not mean that internal heat exchangers are excluded. In fact, the insertion of heat exchangers in such reactors easily permits a continuous and efficient temperature control.

In spray towers the liquid is the dispersed phase and the interfacial area is large. This type of column is used for fast reactions requiring only very short

contact times. Although a large volume is needed, the investment cost is low. The pressure drop is also low.

Bubble columns, in which the liquid is the continuous phase, are used for slow reactions. Drawbacks with respect to packed columns are the higher pressure drop and the important degree of axial and radial mixing of both the gas and the liquid, which may be detrimental for the selectivity in complex reactions. On the other hand, they may be used when the fluids carry solid impurities that would plug packed columns. In fact, many bubble column processes involve a finely divided solid catalyst that is kept in suspension, such as the Rheinpreussen Fischer-Tropsch synthesis, described by Kölbel [1971], or the former I.G. Farben coal hydrogenation process or vegetable oil hardening processes. Several oxidations are carried out in bubble columns: the production of acetaldehyde from ethylene, of acetic acid from C_4 fractions, of vinyl chloride from ethylene by oxychlorination, and of cyclohexanone from cyclohexanol.

14.1.4 Stirred Vessel Reactors

Stirred vessel reactors are preferentially used for reactions involving rather large ratios of liquid to gas for rather exothermic reactions, because the agitation improves the heat transfer and internal heat exchangers are easily built in. They also permit achieving high interfacial areas. The agitation is favorable also when a finely divided catalyst (e.g., Raney nickel) has to be kept in suspension. The reactor is then of the "slurry" type. There are examples, however, of nonstirred operation (e.g., when the reaction has to be carried out under very high pressure and shaft leakage may be a problem). There are many examples of hydrogenations, oxidations, and chlorinations that are carried out in stirred tank reactors, either batch, semibatch, or continuous.

14.1.5 Miscellaneous Reactors

Table 14.1 also mentions some less common types, used for very specific tasks. Venturi reactors are used, for instance, in antipollution devices to wash out small amounts of remaining SO_2 by means of caustic. Their advantage resides in their low pressure drop, since the Venturi exhausts the gas into the liquid.

Falling film or wetted wall reactors can be used for very exothermic reactions. Furthermore, the limited and well-defined interfacial area permits excellent control of very rapid reactions.

14.2 DESIGN MODELS FOR MULTIPHASE FLOW REACTORS

In this section general models that could be used for the design or simulation of any of the reactors or absorbers of the classification of Table 14.1 are derived and their solution briefly described. The models are mostly based on plug flow or complete mixing of one or both phases, but effective diffusion and two zone models are also presented. More specific models are discussed in later sections. When the liquid flow rate L, the gas flow rate F, the inlet and outlet partial pressures of the reacting component A of the gas phase, $(p_A)_{\text{in}}$ and $(p_A)_{\text{out}}$, respectively, and the inlet concentration of the reacting component B of the liquid phase are given, the problem consists of finding the outlet concentration of B, written $(C_B)_{\text{out}}$, and the volume V of the reactor. This is the kind of problem commonly encountered in absorbers. In reactors, on the other hand, conditions are often imposed on the liquid components — in hydrodesulfurization, for example, but also in hydrogenations, oxidations, or chlorinations — and L, F, $(C_B)_{\text{in}}$, $(C_B)_{\text{out}}$, and $(p_A)_{\text{in}}$ would be given or imposed through certain constraints such as flooding rates, for example, to be discussed in later sections. The unknowns would then be $(p_A)_{\text{out}}$ and the volume V. The situation mainly thought of in the next three sections, Sections 14.2.1, 14.2.2, and 14.2.3, is that of a gas-liquid reaction, without solid catalyst. Sections 14.2.4 and 14.2.5 deal with catalytic reactors. To keep the notation simple, only single reactions are considered in this section.

14.2.1 Gas and Liquid Phases Completely Mixed

This is the simplest situation from the computational point of view, since the concentrations of A and B are uniform and no differential equations are involved. The continuity equation for the gas-phase component A may be written

$$\frac{F}{p_t}\left[\left(p_{A_b}\right)_{\text{in}} - \left(p_{A_b}\right)_{\text{out}}\right] = N_A\Big|_{y=0} A_v V\left(1-\varepsilon_G\right) \qquad (14.2.1\text{-}1)$$

where F is the total flow rate, ε_G the gas holdup, and V the total reactor volume (i.e., including liquid and gas). N_A depends, of course, on the order of the reaction. In Chapter 6 various cases were discussed and the corresponding N_A derived. Analytical solutions are possible only for (pseudo) first-order and instantaneous second-order reactions, whereas only approximate solutions were given for other orders. N_A could even be a tabulated function of the gas and liquid composition. In this section the functional form of N_A will not be specified. Recall from Chapter 6 that N_A depends on C_{Ai}, C_A, and C_B. The interfacial concentration may be calculated from p_{Ab} when the gas-phase transfer coefficient

is known or N_A can be referred directly to p_A as in (6.3.2-5). Two more relations are required, however, to calculate V: $(C_A)_{out}$ and $(C_B)_{out}$ or $(p_A)_{out}$ and $(C_A)_{out}$.

Since A is distributed over two phases, a second continuity equation for A, this time for the liquid phase, is required. This can be written, for the bulk of the liquid,

$$N_{A|y=yL} A_v V(1-\varepsilon_G) = (1 - A_v y_L) V (1-\varepsilon_G) r_A + L\left(C_{A_b}\right)_{out} \quad (14.2.1\text{-}2)$$

where $r_A = r_A(C_A, C_B, T)$ is the rate of reaction based on A. Further, an equation relating the partial pressure of A in the gas phase to the concentration of the reacting component of the liquid phase, B, is required. Since both phases are completely mixed, this relation is nothing but a material balance over the reactor:

$$\frac{F}{p_t}\left[\left(p_{A_b}\right)_{in} - \left(p_{A_b}\right)_{out}\right] = \frac{a}{b} L\left[\left(C_{B_b}\right)_{in} - \left(C_{B_b}\right)_{out}\right] + L\left(C_{A_b}\right)_{out} \quad (14.2.1\text{-}3)$$

whereby, because of complete mixing, $(C_{Ab})_{out} = C_{Ab}$ and $(C_{Bb})_{out} = C_{Bb}$.

When the reaction is completed in the film, $C_A = 0$ and one of the above equations drops out, leaving the two equations (14.2.1-1) and (14.2.1-3).

When the reaction is very slow and takes place entirely in the bulk, the mass transfer and reaction are purely in series. As mentioned in Chapter 6, N_A in (14.2.1-1) and (14.2.1-2), then, equals $k_L(C_{Ai} - C_A)$. But since C_A again differs from zero, the complete system, (14.2.1-1), (14.2.1-2), and (14.2.1-3), has to be solved. An example of application of these design equations is given in a later section on stirred tank gas-liquid reactors.

14.2.2 Gas and Liquid Phase in Plug Flow

This is a situation more likely to be approximated in a packed tower. The continuity equation for A in a differential tower volume may then be written

$$-\frac{F}{p_t}\frac{dp_{A_b}}{dV} = N_A\Big|_{y=0} a_v' \quad (14.2.2\text{-}1)$$

where a_v' is the gas-liquid interfacial area per cubic meter reactor volume. Note that a_v' is usually not the geometric surface area of the packing and has to be determined from experiments. This is why (14.2.2-1) has not been written in terms of A_v, used in (14.2.1-1) and which is simply the geometric gas-liquid interface. Correlations for a_v' are given in a later section.

The continuity equation for A in the bulk liquid now becomes

$$N_A\Big|_{y=y_L} a_v' = (1 - A_v y_L)\varepsilon_L r_A + L\frac{dC_{A_b}}{dV} \qquad (14.2.2\text{-}2)$$

Note that this equation is nothing but (6.3.1-5). The relationship between p_A and C_B is derived from a balance on A over the top or bottom section of the column, depending upon the nature of the problem: absorber or reactor design. In the first case, for example, when $(p_A)_{\text{out}}$ and $(C_B)_{\text{in}}$ are given and for countercurrent operation, a balance on the upper part of the column may be written when the liquid feed does not contain any A:

$$\frac{F}{p_t}\left[p_{A_b} - \left(p_{A_b}\right)_{out}\right] = \frac{a}{b}L\left[\left(C_{B_b}\right)_{in} - C_{B_b}\right] + LC_{A_b} \qquad (14.2.2\text{-}3)$$

Again, when the reaction is completed in the film, $C_{Ab} = 0$ and (14.2.1-2) and (14.2.1-3) are correspondingly simplified.

Examples of application of this model will be given later.

14.2.3 Gas Phase in Plug Flow. Liquid Phase Completely Mixed

The continuity equation for A in the gas phase is again (14.2.2-1), of course:

$$-\frac{F}{p_t}\frac{dp_{A_b}}{dV} = N_A\Big|_{y=0} a_v' \qquad (14.2.3\text{-}1)$$

The continuity equation for A in the bulk liquid when $(C_{Ab})_{\text{in}} = 0$ now takes the form

$$\int_0^V N_A\Big|_{y=y_L} a_v' dV = (1 - A_v y_L)V(1 - \varepsilon_G)r_A + L\left(C_{A_b}\right)_{\text{out}} \qquad (14.2.3\text{-}2)$$

The overall mass balance relating gas and liquid phase compositions becomes

$$\frac{F}{p_t}\left[\left(p_{A_b}\right)_{\text{in}} - \left(p_{A_b}\right)_{\text{out}}\right] = \frac{a}{b}L\left[\left(C_{B_b}\right)_{\text{in}} - \left(C_{B_b}\right)_{\text{out}}\right] + L\left(C_{A_b}\right)_{\text{out}} \qquad (14.2.3\text{-}3)$$

Note that there is no way of setting up (14.2.3-2) on an incremental volume, since the liquid is completely mixed.

14.2.4 An Effective Diffusion Model

Effective diffusion models have also been used to account for intermediate degrees of mixing in the axial direction — see Pavlica and Olson [1970] for a comprehensive survey. An example of such a model is developed here for the case of a reaction catalyzed by a solid and no reaction in the liquid.

Steady-state continuity equation for *A* in the gas phase:

$$(\varepsilon - \varepsilon_L) D_{eG} \frac{d^2 C_{AG}}{dz^2} - (\varepsilon - \varepsilon_L) u_{iG} \frac{dC_{AG}}{dz} - K_L a_v' \left(\frac{p_A}{H} - C_{AL} \right) = 0 \qquad (14.2.4\text{-}1)$$

with $1/K_L = (1/k_L) + (1/Hk_G)$, an overall mass transfer coefficient in terms of the liquid concentration gradient, and where ε_L is the liquid holdup. The first term arises from the effective diffusion, the second from the plug flow, and the third from the transfer of *A* from the gas to the liquid phase.

Steady-state continuity equation for *A* in the liquid phase:

$$\varepsilon_L D_{eL} \frac{d^2 C_{AL}}{dz^2} - \varepsilon_L u_{iL} \frac{dC_{AL}}{dz} + K_L a_v' \left(\frac{p_A}{H} - C_{AL} \right) - k_l a_v'' \left(C_{AL} - C_{As}^s \right) = 0 \qquad (14.2.4\text{-}2)$$

The fourth term represents the transfer of *A* from the liquid to the catalyst surface, where a_v'' is the liquid-solid interfacial area per unit reactor volume (in $\mathrm{m}_i^2 / \mathrm{m}_r^3$).

Transfer from liquid to catalyst surface and reaction:

$$k_l a_v'' \left(C_{AL} - C_{As}^s \right) = r_A \rho_B \text{ with } r_A \text{ in kmol/kg cat. h} \qquad (14.2.4\text{-}3)$$

When internal catalyst pellet concentration gradients have to be accounted for, the right-hand side of (14.2.4-3) would have to be multiplied by η, the effectiveness factor, computed as described in Chapters 3 and 11. Accounting for temperature gradients in the axial direction would require an additional differential heat balance, analogous in structure to (14.2.4-2).

The axial effective diffusivity of *A* in the gas and liquid phases, D_{eG} and D_{eL}, have been determined for various modes of operation and will be reported in the sections related to specific design aspects. Although the Peclet numbers are lower than for a single-phase fixed bed reactor — which means that the effective diffusivities are higher — it would seem again that this effect is negligible compared with that of plug flow. Deviations from plug flow are mainly caused by insufficient contacting between the gas and liquid resulting from preferential paths in the packing or by stagnant zones. The effect of these phenomena cannot adequately be described by effective diffusion, and a more appropriate description could be given by a two-zone model.

14.2.5 A Two-Zone Model

The underlying idea for such a model is that only a fraction of the liquid flows in a more or less ordered way through the packing, while at each height there is a stagnant zone in which the liquid is well mixed and that exchanges mass with the flowing fraction.

The continuity equation for *A* in the gas phase is either the same as in (14.2.4-1) or is simplified by neglecting the effective diffusion term. The continuity equations for *A* in the liquid phases, neglecting effective diffusion, may be written

For the flowing fraction:

$$-\varepsilon_L^f u_{iL}^{'} \frac{dC_{AL}^f}{dz} - k_T\left(C_{AL}^f - C_{AL}^d\right) + K_L a_v^{'}\left(\frac{p_A}{H} - C_{AL}^f\right) - k_l a_v^{''}\left(C_{AL}^f - C_{As}^s\right) = 0 \tag{14.2.5-1}$$

where $u_{iL}^{'}$ is the interstitial velocity of the flowing fraction of the liquid; k_l is the mass transfer coefficient between the flowing fraction of the liquid and the solid, and k_T is the mass transfer coefficient between the zones containing flowing and stagnant liquids.

For the well-mixed liquid in the corresponding slice of stagnant liquid:

$$k_T\left(C_{AL}^d - C_{AL}^f\right) = k_l^{'}\left(C_{AL}^d - C_{As}^s\right) \tag{14.2.5-2}$$

Reaction on the catalyst:

$$k_l a_v^{''}\left(C_{AL}^f - C_{As}^s\right) + k_l^{'}\left(C_{AL}^d - C_{As}^s\right) = \eta r_A \rho_B \tag{14.2.5-3}$$

The transfer coefficient between the two zones, k_T, and that between the stagnant fluid and the solid, $k_l^{'}$ contain interfacial areas that are not well established presently.

14.2.6 Models Considering Detailed Flow Patterns

Models considering detailed flow patterns in multi-phase reactors are similar to those presented in Section 13.7 for fluidized bed reactors. The models are based on the Navier-Stokes equations for each of the moving phases. The different phases are assumed to be fully penetrating each other. Interphase mass, momentum, and energy transfer is accounted for. The methods accounting for the fluctuations in the flow field discussed in Chapter 12 for single phase flow can be extended to multi-phase flow. Application to the simulation of a bubble column reactor is illustrated in Example 14.3.6.A.

14.3 SPECIFIC DESIGN ASPECTS

14.3.1 Packed Absorbers

The design of a packed column absorber starts with the choice of a particle diameter. To avoid bypassing liquid along the wall, the ratio of column to particle diameter should exceed a value of 15 to 20. As a rule of thumb, it can be said that for gas flow rates of 15 m³/min the particle diameter should exceed 2.5 cm. When the gas flow rate exceeds 50 m³/min, the particle should have an equivalent diameter of 5 cm at least. Other technological aspects should not be overlooked. If the height of the column is too large with respect to the diameter, a redistribution of the liquid at one or more intermediate positions should be provided. Furthermore, enough space has to be maintained above the packing to enable the separation of entrained liquid droplets. Internals, liquid, and gas distributions are practical aspects of column design discussed by Zenz [1972]. Since in absorbers the liquid and the gas generally flow in countercurrent directions, there is a close interaction between the column diameter and the liquid and gas flow rates. If, for a given column diameter and liquid flow rate, the gas flow rate is too high, the liquid will be blown to the top of the column, which is then said to be flooded. Zenz [1972] derived the following relation for the maximum allowable gas and liquid flow rates above which flooding occurs:

$$\left(\frac{F'/\Omega}{10.86\sqrt{\rho_G/\rho_L}}\sqrt{\frac{a_v}{\varepsilon^3}\mu_L^{0.2}}\right)^{1/3}+\left(\frac{L/\Omega}{2323}\sqrt{\frac{a_v}{\varepsilon^3}\mu_L^{0.2}}\right)^{1/2}=18.91 \qquad (14.3.1\text{-}1)$$

In this equation, F' and L are the gas and liquid flow rates (in m³/h), ε is the void fraction of the packing, and μ_L is the viscosity of the liquid (in kg/m h). Leva [1953] and Lobo et al. [1945] have published the generalized dimensionless correlation for flooding rates shown in Fig. 14.3.1-1, in which μ_W represents the viscosity of water. A generalized pressure drop correlation for packed columns with countercurrent flow has been derived by Sherwood et al. [1938] and adapted by Lobo et al. [1945]; it is shown in Fig. 14.3.1-2. The flooding line in this diagram corresponds with that of Fig. 14.3.1-1; $\mathcal{P}$ is a so-called packing factor, the value of which is given in tabular material provided by the producers of packing material to replace a_v/ε^3, as used by Sherwood.

The interfacial area a_v' differs from the packing surface area a_v because the packing is not always completely wetted, so that a fraction of the surface is not active in the mass transfer, or because of the presence of stagnant pockets that are less effective than flowing streams. Shulman et al. [1955] have

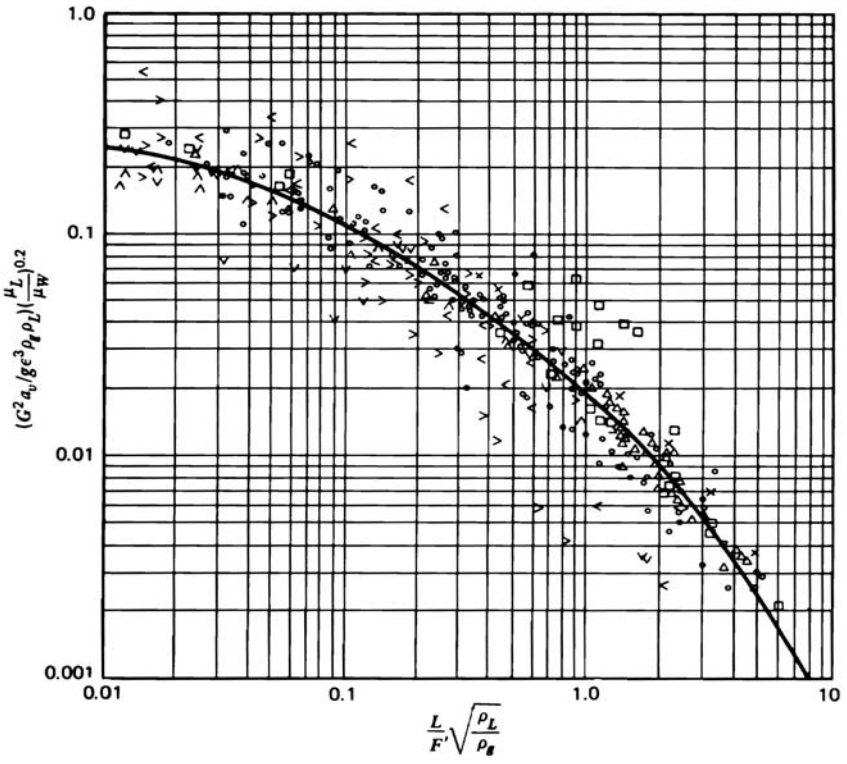

Figure 14.3.1-1

Generalized correlation for flooding rates in packed columns. After Lobo et al. [1945].

established correlations between $a_v^{'}$ and a_v for Rashig rings and Berl saddles for various values of the liquid and gas flow rates.

In a review of the subject, Laurent and Charpentier [1974] recommend the following equation by Onda et al. [1968]:

$$\frac{a_v^{'}}{a_v} = 1 - \exp\left[-1.45\left(\frac{\sigma_{L,c}}{\sigma_L}\right)^{0.75} \frac{\rho_L^{0.3} L^{0.4} g^{0.05}}{\Omega^{0.4} a_v^{0..35} \mu_L^{0.1} \sigma_L^{0.2}}\right] \qquad (14.3.1\text{-}2)$$

where $\sigma_{L,c}$ represents the critical surface tension above which the packing cannot be wetted. This correlation underestimates the interfacial area obtained with Pall rings by about 50 percent. The liquid holdup of the packing, ε_L, consists of the static holdup $\varepsilon_{S,L}$ and the operating holdup $\varepsilon_{O,L}$. The static holdup is the amount of liquid left in the column after the completely wetted packing is drained. The total holdup is the amount of liquid held in the tower under flow conditions. The operating holdup is the difference. The above amounts are divided by the total liquid holdup to yield fractions.

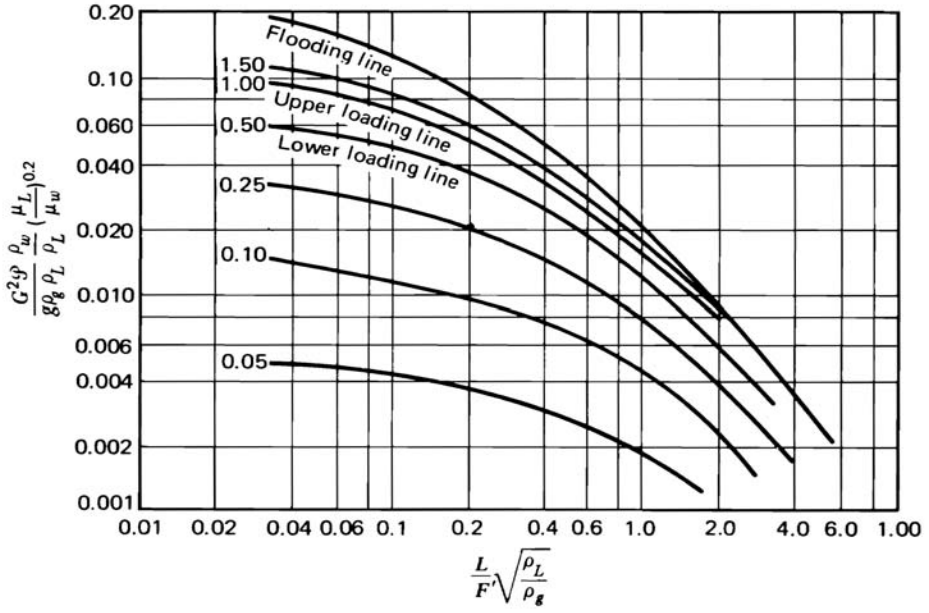

Figure 14.3.1-2

Generalized pressure drop correlation for packed columns with countercurrent flow. Parameter curves: pressure drop in inches water per foot. From Eckert [1970].

Shulman et al. [1955b; c] derived the following correlation for $\varepsilon_{S,L}$:

$$\varepsilon_{S,L} = C_1 \frac{\left(\mu_L / 3.6\right)^{C_2} \left(\sigma_L / 1.296 \times 10^4\right)^{C_3}}{\left(\rho_L / 16.018\right)^{0.37}} \tag{14.3.1-3}$$

The parameters C_1, C_2, and C_3 were determined for ceramic and graphitic Rashig rings and ceramic Berl saddles.

The operational holdup can be calculated from the dimensionless correlation of Buchanan [1967]:

$$\varepsilon_{O,L} = 2.2\left(\frac{\mathrm{Fr}_L}{\mathrm{Re}_L}\right)^{0.33} + 1.8\mathrm{Fr}_L^{0.5} \tag{14.3.1-4}$$

where $\mathrm{Fr}_L = \left(u_{sL}\right)^2 / g d_p$ and $\mathrm{Re}_L = u_{sL} d_p \rho_L / \mu_L$.

Many equations have been proposed for the mass transfer coefficients. For the liquid-side mass transfer coefficient of a component *A*, Laurent and Charpentier [1974] recommend Mohunta's equation [1969]:

$$k_L a_v^{'} = 0.0025\left(\frac{L^3 a_v^3 \mu_L}{\Omega^3 g^2 \rho_L}\right)^{1/4} \left(\frac{\mu_L}{\rho_L D_{AL}}\right)^{-1/2} \left(\frac{a_v \mu_L}{g\rho_L}\right)^{-2/3} \left(\frac{\mu_L}{g^2 \rho_L}\right)^{-1/9} \tag{14.3.1-5}$$

The range of validity of Onda's equation, (14.3.1-2), and of Mohunta's equation is as follows: liquid mass flow velocities $\rho_L L/\Omega$, 360-151, 200 kg/m² h; μ_L, 2.62-5.33 kg/m h; $Sc_L = \mu_L/\rho_L D_{AL}$, 142-1030; d_p, 0.006-0.05 m; column diameter, 0.06-0.5 m; ratio of column to packing diameter, 5-40.

Shulman et al. [1955b] correlated the data of several authors by means of the following equation:

$$\frac{k_L d_p}{D_{AL}} = 25.1\left(\frac{d_p \rho_L L}{\mu_L \Omega}\right)^{0.45}\left(\frac{\mu_L}{\rho_L D_{AL}}\right)^{0.5} \qquad (14.3.1\text{-}6)$$

Ramm [1953] mentions the following equation:

$$\frac{k_L d_p}{D_{AL}} = 0.02\left(\frac{d_p \rho_L L}{\mu_L \Omega}\right)^{0.67}\left(\frac{\mu_L}{\rho_L D_{AL}}\right)^{0.33}\left(\frac{g\rho_L 2d_p^3}{\mu_L^2}\right)^{0.33}\left(\frac{Z}{d_p}\right)^{-0.33} \qquad (14.3.1\text{-}7)$$

For the gas-side mass transfer coefficient of a component *A*, Laurent and Charpentier [1974] derived the correlation

$$\frac{k_G p_t \Omega}{F} = c\left(a_v d_p\right)^{-1.7}\left(\frac{d_p G}{\mu_G}\right)^{-0.3}\left(\frac{\mu_G}{\rho_g D_{AG}}\right)^{-0.5} \qquad (14.3.1\text{-}8)$$

where the constant *c* equals 2.3 when the equivalent packing diameter is smaller than 15 mm and 5.2 when it exceeds that value; k_G is expressed in kmol/m² bar h.

Ramm [1953] mentions

$$\frac{4k_G \varepsilon}{a_v D_{AG}}\frac{RTp_t}{p_{fA}} = 0.027\left(\frac{4G}{a_v \mu_G}\right)^{0.8}\left(\frac{\mu_G}{\rho_G D_{AG}}\right)^{0.33} \qquad (14.3.1\text{-}9)$$

with k_G in kmol/m² bar h. Semmelbauer [1967] derived the following correlation:

$$\mathrm{Sh}_G = a\,\mathrm{Re}_G^{0.59}\,\mathrm{Sc}_G^{0.33} \qquad \begin{aligned} &100 < \mathrm{Re}_G < 1000 \\ &0.01 < d_p < 0.05 \text{ m} \end{aligned} \qquad (14.3.1\text{-}10)$$

with a = 0.69 for Rashig rings and 0.86 for Berl saddles. Further, $\mathrm{Sh}_G = k_G RT d_p/D_G$.

The technical information sheets of the producers of packing material contain extremely important information, generally based upon large-scale reactors. Also, further correlations can be found in the book by Astarita et al. [1983].

EXAMPLE 14.3.1.A

THE SIMULATION OR DESIGN OF A PACKED BED ABSORPTION TOWER

Let a general single, irreversible reaction be written

$$a_A A(g) + \sum_{j=1}^{n_R} a_{R_j} R_j(l) \rightarrow \sum_{j=1}^{n_p} p_{P_j} P_j(l) \qquad (14.3.1.A\text{-a})$$

where A is the component of the gas phase which absorbs and reacts with the liquid phase components R_j to yield the products P_j.

Let the kinetic equation of the reaction occurring in the liquid phase be

$$r_A = kC_A^{m_A} \overset{m_R}{\underset{j=1}{\pi}} C_{R_j}^{m_{R_j}} \qquad (14.3.1.A\text{-b})$$

where r_A is the rate of reaction of A.

The concentration profiles in the liquid film and the uniform concentrations in the bulk at a given height in the column depend on a number of factors conveniently grouped into the Hatta number, as extended by Hikita and Asai [1966]:

$$\mathrm{Ha} = \frac{1}{k_{L,A}} \sqrt{\frac{2}{m_A + 1} a_A k_1 C_{A_i}^{m_A - 1} \prod_{j=1}^{n_R} (C_{R_j})_i^{m_{R_j}} D_A} \qquad (14.3.1.A\text{-c})$$

Hatta numbers smaller than 0.3 are encountered with very slow reactions. For moderately fast reactions, Ha is comprised between 0.3 and 3, whereas for very fast reactions, Ha exceeds 3. The most general case is that where the reaction takes place in both the film and the bulk, that is, when 0.3 < Ha < 3 and the reaction is only moderately fast.

The continuity equation for A in the gas phase, assumed to be in plug flow, may be written

$$\frac{F}{p_t - p_{A_b}} \frac{dp_{A_b}}{dz} = -N_A\big|_{y=0} a_v' \Omega \qquad (14.3.1.A\text{-d})$$

When the mole fraction of A in the gas phase is relatively high, the variation of the total molar flow has to be accounted for:

$$\frac{dF}{dz} = -N_A\big|_{y=0} a_v' \Omega \qquad (14.3.1.A\text{-e})$$

The interfacial flux $N_A|_{y=0}$ is a function of p_A, C_A, and C_{Rj}. The continuity equation for A in the bulk liquid phase, also assumed to be in plug flow, can be written

$$L\frac{dC_{A_b}}{dz} = -N_A\big|_{y=y_L} a_v' \Omega - (1 - A_v y_L)\varepsilon_L \Omega r_A \qquad (14.3.1.A\text{-f})$$

where C_A represents the concentration of A in the bulk of the liquid phase.

The rate of reaction of A contains the C_{Rj}. These liquid bulk concentrations are obtained from a mass balance over the top of the column:

$$\begin{aligned} L\left(C_{R_j}\right)_b = &\left[\left(C_{R_j}\right)_b(\text{in})L(\text{in})\right] \\ &-\frac{a_{R_j}}{a_A}\left[\frac{1}{p_t}\left(Fp_{A_b} - F(\text{out})p_{A_b}(\text{out})\right) - \left(LC_{A_b} - L(\text{in})C_{A_b}(\text{in})\right)\right] \end{aligned} \qquad (14.3.1.A\text{-g})$$

In this equation the second term inside the second square brackets of the R.H.S. represents the amount of A transferred from the gas phase that has not reacted yet. Analogous equations can be written for the product concentrations C_{Pj}.

The liquid flow rate may have to be updated in each increment used in the integration of the set of equations (14.3.1.A-d) through (14.3.1.A-f) according to

$$\begin{aligned} L(z+\Delta z) = L(z)\Bigg\{1 &+ \frac{M_A}{\rho_{L,A}}\left[C_{A_b}(z+\Delta z) - C_{A_b} z\right] \\ &+ \sum_{j=1}^{n_R}\left[\frac{M_{R_j}}{\rho_{L,R_j}}\left(\left(C_{R_j}\right)_b(z+\Delta z) - \left(C_{R_j}\right)_b(z)\right)\right] \\ &+ \sum_{j=1}^{n_R}\left[\frac{M_{P_j}}{\rho_{L,P_j}}\left(\left(C_{P_j}\right)_b(z+\Delta z) - \left(C_{P_j}\right)_b(z)\right)\right]\Bigg\} \end{aligned} \qquad (14.3.1.A\text{-h})$$

Equations (14.3.1.A-d) and (14.3.1.A-e) contain $N_A|_{y=0}$, and (14.3.1.A-f) contains $N_A|_{y=yL}$. These fluxes are obtained from

$$N_A\big|_{y=0} = k_{G,A}\left[p_{A_b} - p_{A_i}\right] = -D_A \left.\frac{dC_A}{dy}\right|_{y=0} \qquad (14.3.1.A\text{-i})$$

$$N_A\big|_{y=y_L} = -D_A \left.\frac{dC_A}{dy}\right|_{y=y_L} \qquad \text{(14.3.1.A-j)}$$

so that the concentration profile in the liquid film is required. For this purpose the following continuity equations for A and R_j (and also P_j when the reaction is reversible) have to be integrated:

$$D_A \frac{d^2 C_A}{dy^2} = r_A$$

$$D_{R_j} \frac{d^2 C_{R_j}}{dy^2} = \frac{a_{R_j}}{a_A} r_A \qquad \text{for } j = 1, \ldots, n_R \qquad \text{(14.3.1.A-k)}$$

with boundary conditions

$$\text{At } y = 0: \qquad C_A = (C_A)_i$$

$$C_{R_j} = \left(C_{R_j}\right)_i$$

$$\text{At } y = y_L: \qquad C_A = (C_A)_b \qquad \text{(14.3.1.A-l)}$$

$$C_{R_j} = \left(C_{R_j}\right)_b \quad \text{bulk values}$$

The concentrations of the liquid-phase reactants, C_{Rj}, and of the products, C_{Pj}, can be related to those of the absorbed component in the liquid film. Indeed, subtraction of the second equation of (14.3.1.A-k) from the first leads to

$$D_A \frac{d^2 C_A}{dy^2} - \frac{a_A}{a_{R_j}} D_{R_j} \frac{d^2 C_{R_j}}{dy^2} = 0 \qquad \text{(14.3.1.A-m)}$$

Integrating twice and accounting for the boundary conditions

$$\text{At } y = 0: \qquad \frac{dC_A}{dy} = -\frac{N_A\big|_{y=0}}{D_A}$$

$$\frac{dC_{R_j}}{dy} = 0 \qquad \text{(14.3.1.A-n)}$$

$$\text{At } y = y_L: \qquad C_A = C_{A_b}; C_{R_j} = \left(C_{R_j}\right)_b \quad \text{bulk values}$$

yields

$$C_{R_j} = \left(C_{R_j}\right)_b + \frac{a_{R_j}}{a_A}\frac{D_A}{D_{R_j}}\left(C_A - \left(C_A\right)_b\right) - \frac{a_{R_j}}{a_A}\frac{N_A\big|_{y=0}}{D_{R_j}}\left(y_L - y\right) \quad \text{(14.3.1.A-o)}$$

An analogous equation is derived in the same way for C_{P_j}.

The integration of the set of second-order differential equations (14.3.1.A-k) for the concentration profiles in the liquid film has to be carried out for each increment used in the integration in z of (14.3.1.A-d), and this is a very time-consuming task. This is why substantial efforts have been invested in deriving the analytical — but generally approximate — solutions for (14.3.1.A-k) discussed in Chapter 6.

Nonisobaric conditions are accounted for through the pressure drop correlation of Eckert, for example, represented in Fig. 14.3.1-2. Nonisothermal operation will be illustrated in Example 14.3.4.A.

De Leye and Froment [1986] developed a general method of solution of the above set of equations, valid for both the reactor and absorber problem, for the simulation of an existing column or the design of a new one. The program offers the possibility of calculating $N_A|_{y=0}$ and $N_A|_{y=yL}$ either by the numerical solution of the set of equations (14.3.1.A-k) or by means of the (approximate) analytical solution. Since the approach is based on the equations given above, it calculates the real height of the column, not the theoretical height, which has to be adapted afterwards through some measure of the efficiency.

The procedure is briefly outlined in what follows for an absorption accompanied by a moderately fast reaction, which is the most general case. The calculations start at the top of the column. For a design case the column diameter and the type and size of packing are chosen, accounting for minimum wetting rate and flooding correlations. When $(p_A)_b$(out) is not imposed a value for it is selected and $(p_A)_i$(out) is estimated. Equation (14.3.1.A-i) then permits $N_A|_{y=0}$ to be calculated. Numerical integration of (14.3.1.A-d) and (14.3.1.A-e) by means of a Runge-Kutta method permits $(p_A)_b(z + \Delta z)$ and $F(z + \Delta z)$ to be calculated. Then $(C_A)_b(z + \Delta z)$ is estimated. Equation (14.3.1.A-g) yields $(C_R)_b(z + \Delta z)$ and an analogous equation the concentration of the products. Numerical integration of (14.3.1.A-k) by means of a finite difference method with variable step size or by means of spline orthogonal collocation leads to $C_A(y)$ in the liquid film and to $N_A|_{y=yL}$. Alternatively, approximate analytical solutions may be used. Numerical integration of (14.3.1.A-f) then leads to $(C_A)_b(z + \Delta z)$, a value which is compared with the estimated value. If these values do not match, iteration is required.

Since $C_{R_j}(y)$ in the film can be calculated through (14.3.1.A-o), $(p_A)_i$ is obtained by means of Henry's law. This value is compared with its estimate, and the latter is iteratively improved. Finally, the liquid flow rate is adapted, using

(14.3.1.A-h) before the next increment in z is considered. The calculations are continued in the z-direction until $|(p_A)_b(z) - (p_A)_b(\text{in})|$ is smaller than a given value. The z at which this is achieved is the column height Z.

In the simulation case the total height is given and the calculated $(p_A)_b(\text{in})$ should match the given value.

The example given below deals with the absorption of CO_2 into a methanolamine (MEA)-solution. ■

EXAMPLE 14.3.1.B

THE ABSORPTION OF CO_2 INTO A MONOETHANOLAMINE (MEA) SOLUTION

The absorption in alkanolamine solutions (MEA, DEA, ADIP, DGA, etc.) is the commercially most important process for the removal of CO_2 from synthesis gas for ammonia and methanol production, for the production of hydrogen, in natural gas purification, coal liquefaction, and the like. In the present example a gas containing 13.55 mole-% of CO_2 is to be purified by absorption into an aqueous solution of 13.6 wt-% MEA. The column, filled with 0.05 m steel Pall rings, has a diameter of 1.05 m and is operating at a temperature of 315 K and a pressure of 14.3 bars. The inlet flow rates of gas and liquid are 497 kmol/h and 76.9 m³/h, respectively. Determine the packed column height necessary to reduce the mole fraction of CO_2 to 5×10^{-5} at the top of the column.

The absorption of CO_2 in a MEA solution is described by the following overall reaction:

$$CO_2 + 2RNH_2 \rightarrow RNHCOO^- + RNH_3^+$$

with kinetic equation

$$r = kC_{CO_2}C_{RNH_2}$$

At 315 K the reaction rate constant k equals 5.183×10^7 m³/kmol h [Hikita et al., 1977].

For the determination of the gas- and liquid-side mass transfer coefficients, the effective specific surface or interfacial area and the wetting rate of the packing, the pressure drop and flood condition, and the standard correlations incorporated in the program, shown in Table 14.3.1.B-1, are used.

For the determination of the viscosity of the solution and the diffusivity of MEA, experimental data of Thomas and Furzer [1962] are used. Densities of pure MEA and MEA solutions are found in the literature [Tseng and Thompson, 1964; Riddick and Bunger, 1970]. The diffusion coefficient of CO_2 in pure water [Thomas and Furzer, 1962] was corrected for the presence of MEA by using the

TABLE 14.3.1.B-1
LIST OF STANDARD CORRELATIONS FOR THE DETERMINATION OF k_G, k_L, a'_v, THE WETTING RATE, PRESSURE DROP, AND FLOODING POINT

Property	**Correlation Used**	
k_G	Laurent and Charpentier	[1974]
k_L	Onda et al.	[1968a]
$a_v^{'}$	Onda et al.	[1968b]
Wetting rate	Morris and Jackson	[1953]
Pressure drop	Eckert	[1970]
Flooding point	Eckert	[1970]

Stokes-Einstein relationship. Henry's law constant for CO_2 in H_2O equals 48.6 m³ bar/kmol at 315 K [Danckwerts and Sharma, 1966]. This coefficient is corrected for the ionic strength of the solution [Danckwerts, 1970; Danckwerts and Sharma, 1966]. The geometric specific surface of the packing equals 105 m²/m³. The calculated results are summarized in Table 14.3.1.B-2.

The calculated wetting rate largely exceeds the required minimum value of 0.08 m³/h m [Morris and Jackson, 1953]. The concentration and partial pressure profiles of the various components in the gas and liquid bulk along the columns are shown in Fig. 14.3.1.B-1.

The absorption of CO_2 in the MEA solution is accompanied by a very fast reaction. For the determination of the absorption flux, the approximate expression (6.3.2-5) [Hikita and Asai, 1966] was used. The example was recalculated, determining the absorption flux by numerical integration of the set of second-order differential equations of Example 14.3.1.A, (14.3.1.A-k). As shown in Table 14.3.1.B-3, the differences are negligible, while the amount of CPU time, using the rigorous model, has significantly increased.

Figure 14.3.1.B-2 shows the partial pressure and concentration profiles of CO_2 and MEA in the gas and liquid films at a number of heights in the column. Since CO_2 is not very soluble, the absorption of CO_2 in pure water is controlled by the resistance to mass transfer in the liquid film. In a MEA solution, on the other hand, the absorption is strongly enhanced by the very fast reaction, and gas film resistance to mass transfer becomes important. No depletion of the reactant MEA is observed at the top of the column, and the reaction is of pseudo-first order. At the bottom of the column the depletion of the MEA is almost complete in the liquid film.

TABLE 14.3.1.B-2
RESULTS OF THE DESIGN CALCULATIONS FOR THE CO_2 ABSORPTION COLUMN[a]

Flow Rates	**Top of Column**	**Bottom of Column**
L (m³/h)	76.9	79.8
F (kmol/h)	429.7	497.7
Gas-phase composition		
P_{CO_2} (bar)	0.715×10^{-3}	1.954
Liquid-phase composition		
C_{CO_2} (kmol/m³)	0.0	0.0
C_{RNH_2} (kmol/m³)	2.220	0.435
C_{RNHCOO^-} (kmol/m³)	0.0	0.825
$C_{RNH_3^+}$ (kmol/m³)	0.0	0.825
Ha (CO_2)	20.08	8.700
a_v' (m²/m³)	90.53	90.95
k_{G,CO_2} (kmol/m² h bar)	0.880	1.057
k_{L,CO_2} (m/h)	1.386	1.416
Percent of flooding	56	66
Calculated column height: 11 m		
Wetting rate: 0.85 m³/h m		
Pressure drop: 0.21×10^{-1} bar		
CPU time (Data General *MV* 6000): 30 s		

[a]From De Leye and Froment [1986a].

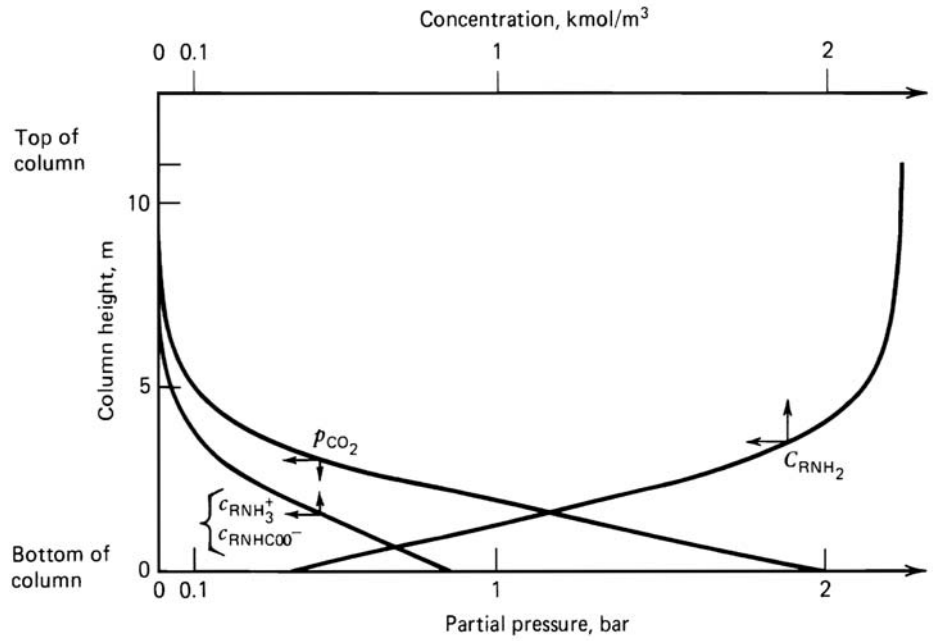

Figure 14.3.1.B-1

Concentration and partial pressure profiles along the column. From DeLeye and Froment [1986a].

TABLE 14.3.1.B-3
ABSORPTION OF CO_2 IN MEA. RESULTS OF APPROXIMATE AND EXACT MODELS [FROM DE LEYE AND FROMENT (1986a)]

Property	Approximate Model	Exact Model
Column height (m)	11	10.95
Bottom column		
L (m³/h)	79.80	79.80
F (kmol/h)	497.70	497.10
P_{CO_2} (bar)	1.954	1.939
C_{CO_2} (kmol/m³)	0.0	0.0
C_{RNH_2} (kmol/m³)	0.435	0.449
C_{RNHCOO^-} (kmol/m³)	0.852	0.845
$C_{RNH_3^+}$ (kmol/m³)	0.852	0.845
CPU time (s)	30	233

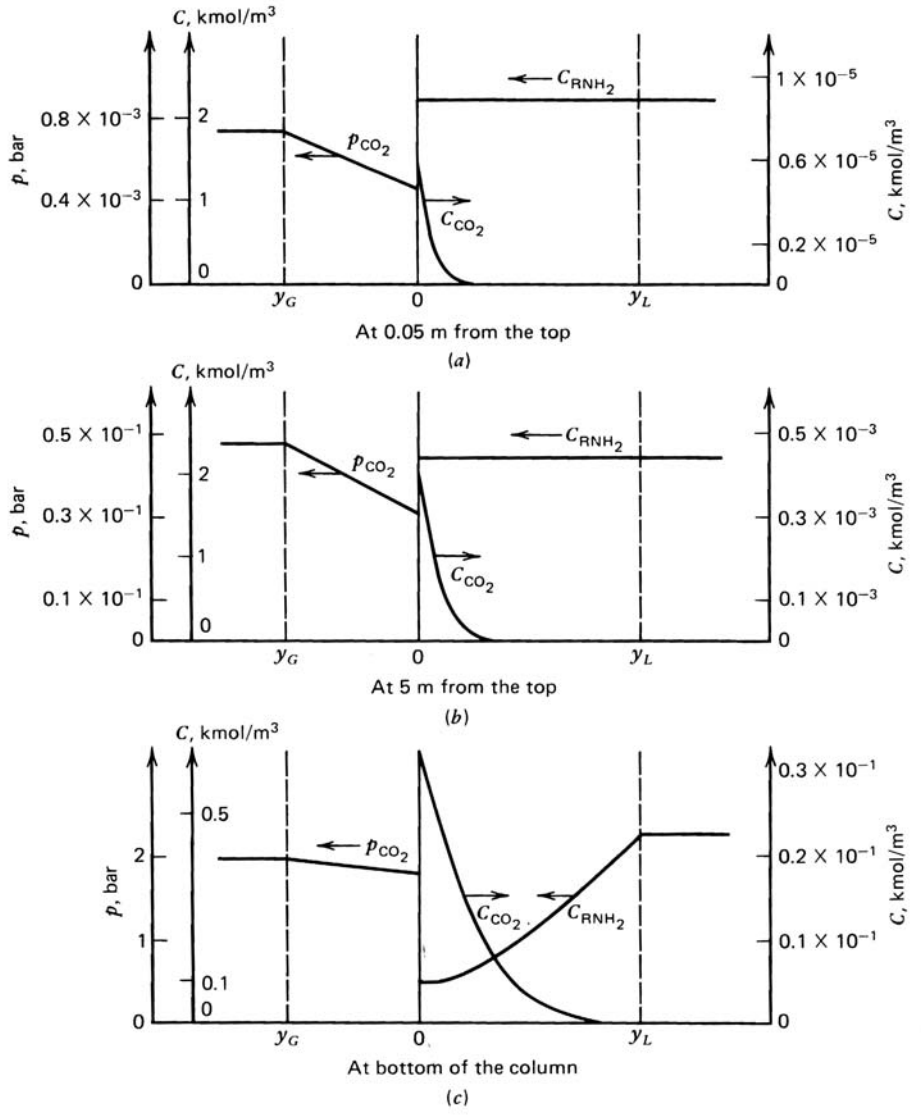

Figure 14.3.1.B-2

Partial pressure and concentration profiles in the gas and liquid films at various heights in the column. From DeLeye and Froment [1986a].

■

14.3.2 Two-Phase Fixed Bed Catalytic Reactors with Cocurrent Downflow. "Trickle" Bed Reactors and Packed Downflow Bubble Reactors

This section deals with problems that bear considerable relation to those dealt with in Chapter 11 on fixed bed catalytic reactors with a single fluid phase, the main difference being in the hydrodynamics, because of the existence of two

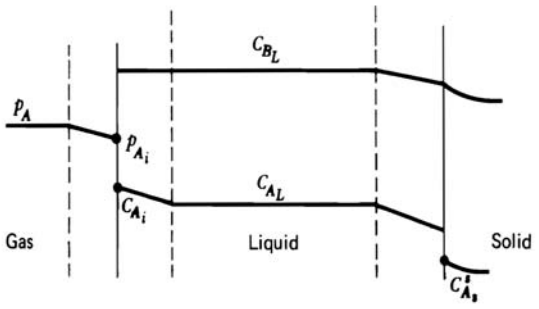

Figure 14.3.2-1
Concentration and partial pressure profiles in fluid phase and catalyst.

fluid phases. In addition, the mass and heat transfer phenomena are more complex, since resistances in the gas phase, the liquid phase, and the solid catalyst, where the reaction takes place, have to be considered. Figure 14.3.2-1 illustrates concentration and partial pressure profiles around a catalyst particle and defines the notation; *A* is the reacting component of the gas phase, *B* that of the liquid phase.

The advantage of downflow operation with respect to upflow lies in the fact that there is no limitation on the flow rates imposed by flooding limits. The flow rates are only limited by the available pressure head at the inlet. Furthermore, the liquid is much more evenly and thinly distributed than with upward flow. Depending on the respective flow rates of gas and liquid, different flow regimes may be obtained.

The trickle flow regime corresponds to rather low flow rates of gas and liquid; the gas phase is continuous and the liquid phase dispersed. Increasing the gas flow rate leads to pulsed flow. If, for a given liquid flow rate, the gas flow rate is increased too much, spray flow will be obtained, however. For higher liquid throughputs, the liquid phase may be continuous and the gas phase dispersed: this is called bubble flow. Increasing the gas flow rate will lead to dispersed bubble flow and then to pulsed flow.

Figure 14.3.2-2 represents the flow regimes encountered in downflow packed beds for foaming and nonfoaming liquids [Charpentier and Favier, 1975]. It extends diagrams presented by Sato et al. [1973] and by Hofmann [1975] which are limited to air and water. In Fig. 14.3.2-2,

$$\lambda = \left(\frac{\rho_G}{\rho_{air}} \frac{\rho_L}{\rho_{H_2O}} \right)^{0.5} \qquad \text{and} \qquad \psi = \frac{\sigma_{H_2O}}{\sigma_L} \left[\frac{\mu_L}{\mu_{H_2O}} \left(\frac{\rho_{H_2O}}{\rho_L} \right)^2 \right]^{0.33}$$

In actual situations, the transitions are not as sharply defined as indicated in Fig. 14.3.2-2.

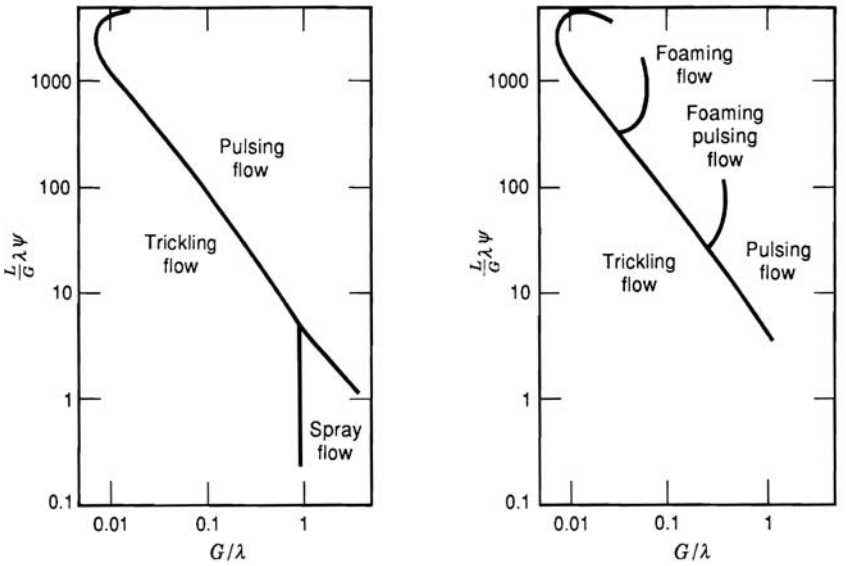

Figure 14.3.2-2

Flow regimes in downflow packed beds. Left: nonfoaming; right: foaming liquids. After Charpentier and Favier [1975].

In hydrodesulfurization, liquid flow rates range from 1 to 10 kg/m² s for heavy fractions, from 10 to 25 for naphtha, whereas hydrogen flow rates range from 470 Nm³/ton for heavy gasoil to 840 Nm³/ton for heavy residue. In hydrocracking, this ratio may be 1700.

Attempts have been made to predict the transition from trickle to pulsed flow on the basis of an analysis of flow in capillaries with constriction [Sicardi and Hofmann, 1980; Dimenstein and Ng, 1986]. Clearly, a single capillary or channel is a very incomplete representation of a packed bed, so that in the future networks of capillaries will have to be considered in such calculations.

There is relatively little information on the pressure drop in two-phase cocurrent downflow packed beds. Larkins et al. [1961] have proposed the following correlation for the two-phase frictional pressure drop:

$$\log\frac{\delta_2}{\delta_L+\delta_G}=\frac{0.416}{\left(\log\sqrt{\frac{\delta_L}{\delta_G}}\right)^2+0.666} \qquad (14.3.2\text{-}1)$$

where δ_2 is the two-phase frictional pressure drop. The measured pressure drop $\Delta p_{t2}/\Delta z$, in kilogram force per square meter cross section and unit length, is related to δ_2 by

$$\frac{\Delta p_{t2}}{\Delta z}=\delta_2-g\varepsilon_L\rho_L$$

where $g\varepsilon_L\rho_L$ represents the liquid head per unit height; δ_L and δ_G are the frictional pressure drops per unit length for liquid flow and gas flow only. It has been argued that the term $\varepsilon_L\rho_L$ should not be accounted for, since the liquid is supported by the packing; but in the experiments of Larkins et al. the difference between $\Delta p_{t2}/\Delta z$ and δ_2 was negligible anyway. Larkins et al. derived their equation from the concept of the "equivalent fluid," which considers the gas and the liquid to be quasi-homogeneous. This is strictly correct only when the gas and liquid flow rates u_{sG} and u_{sL} are identical.

Sweeney [1967] distinguished between the two phases. He assumed that the liquid flows uniformly over the packing surface, that both the liquid and the gas phase are continuous, and that the pressure drops through both phases are identical. He came to the following relation:

$$\left(\frac{\delta_L}{\delta_2}\right)^{1/3} + \left(\frac{\delta_G}{\delta_2}\right)^{1/3} = 1 \qquad (14.3.2\text{-}2)$$

The Larkins and Sweeney equations were developed for downward bubble flow. In trickle bed operation, the liquid and gas flow rates are not as high as in packed absorbers, so that there is much less interaction. Single-phase flow pressure drop equations could be used as a first approximation, with the void fraction reduced to account for the liquid holdup. Charpentier et al. [1969] recommend, on the basis of an energy balance instead of a force balance, to replace δ_2 in (14.3.2-1) and (14.3.2-2) by $(u_{sm}/\rho_L g)(\Delta p_{t2}/\Delta z) + u_{sL}\varepsilon_L + u_{sG}(1-\varepsilon)(\rho_g/\rho_L)$, where u_{sm} is the mean of the liquid and gas velocities [i.e., $u_{sL}\varepsilon + u_{sG}(1-\varepsilon)$]. Midoux et al. [1976] proposed the following correlation for δ_2/δ_L:

$$\left(\frac{\delta_2}{\delta_L}\right)^{0.5} = 1 + \left(\frac{\delta_L}{\delta_G}\right)^{-0.5} + 1.14\left(\frac{\delta_L}{\delta_G}\right)^{-0.27} \qquad (14.3.2\text{-}3)$$

for any type of flow with nonfoaming liquids and for trickle flow with foaming liquids only.

Rao and Drinkenburg [1983] proposed

$$\delta_2 = \left[\frac{\delta_{GW}}{\left(1-\varepsilon_L'/\varepsilon\right)^3}\right] - \rho_G g$$

where δ_{GW} is the pressure drop for the gas phase flowing over a prewetted, but not irrigated packed bed.

Biswas et al. [1988] developed a stratified flow model to predict the two phase pressure drop in trickle beds. The wetting of the packing depends on the

nature of the packing surface and on the surface tension of the liquid. For the wetting to be complete, an efficient liquid distribution at the top is required, while the column-to-particle diameter should exceed 20 to 25 to avoid liquid bypassing along the wall. Henry and Gilbert [1973] recommend that $d_p\rho_L L/\Omega\mu_L > 10$.

The liquid holdup (volume of liquid/volume of empty reactor) consists of liquid held in the pores of the catalyst and of that outside the catalyst particles, which is called external holdup. The latter is frequently divided into the free draining or dynamic holdup, ε_L' and the residual or static holdup. The static holdup has been related by Charpentier et al. [1968] to the Eötvös number $\delta_L g d^2{}_p/\sigma_L$; it varies between 0.02 and 0.05. Several correlations have been given for the dynamic or free draining holdup. They are

$$\varepsilon_L' = c\left(\frac{\rho_L d_p L}{\mu_L \Omega}\right)^{\alpha}\left(\frac{d_p^3 g \rho_L^2}{\mu_L^2}\right)^{\beta}\left(a_v d_p\right)^{\gamma} \qquad (14.3.2\text{-}4)$$

According to Otake and Okada [1953] for nonporous spherical packing c = 1.295, α = 0.676, β = −0.44, and γ = 1.0, whereas Satterfield et al. [1969] arrived at c = 1.0, α = 0.333, β = −0.33, and γ = 0. Note that the dynamic holdup is independent of the gas flow rate, but varies with the liquid flow rate. Goto and Smith [1975] observed agreement between their experimental data and Otake and Okada's correlation for large-particle diameters only and between their data and Satterfield et al.'s [1969] correlation for small-particle diameters only. Another correlation for ε_L' in the low-interaction regime has been published by Specchia and Baldi [1977]. The following external or total holdup equation is proposed by Midoux et al. [1976]:

$$\varepsilon_L = \frac{0.66\left(\dfrac{\delta_L}{\delta_G}\right)^{0.40}}{1 + 0.66\left(\dfrac{\delta_L}{\delta_G}\right)^{0.40}} \qquad (14.3.2\text{-}5)$$

for any type of flow with nonfoaming liquids and for trickle flow only with foaming liquids. The internal holdup, finally, depends on the porosity of the catalyst.

There are no effective interfacial area correlations in the literature for the specific cases discussed here. The correlation that comes closest to that required for trickle bed operation is that of Puranik and Vogelpohl [1974], which is for a continuous gas phase and a dispersed liquid phase, but in a countercurrent packed

column, well below the loading point. They derived the following correlation (for $\rho_L L/\Omega$ = 1.5 kg/m² s):

$$\frac{a_v'}{a_v} = 1.05 \ \ \mathrm{Re}_L^{0.04}\,\mathrm{We}^{0.135}\left(\frac{\sigma_{L,c}}{\sigma_L}\right)^{0.18} \tag{14.3.2-6}$$

where the Weber number We = $\rho_L L^2 d_p/\Omega^2\sigma_L$. It follows that, in the investigated range, a_v' is proportional to $L^{0.31}$. At higher flow rates, the equation of Onda et al. mentioned in the section on absorbers might be used — (14.3.1-2). Charpentier [1976] recommends the following from a literature survey of trickle bed results for spheres and pellets:

$$\frac{a_v'}{a_v} = c\left(\frac{\Delta p_{t2}}{\Delta z}\frac{\varepsilon}{a_v}\right)^{1.2} \tag{14.3.2-7}$$

with c = 0.81 or 5.23×10^4 when Δp_{t2} is expressed in kgf/m² or in bars.

The axial effective diffusivity for the liquid phase has been correlated by Elenkov and Kolev [1972] as follows:

$$\frac{u_{sL}}{D_{eL}a_v} = 0.068\left(\frac{4\rho_L L}{\Omega a_v \mu_L}\right)^{0.78}\left(\frac{g\rho_L^2}{a_v^3\mu_L^2}\right)^{-0.33} \tag{14.3.2-8}$$

Mears [1974] has given the minimum Z/d_p ratio required to hold the deviation from the reactor length as calculated on the basis of plug flow below 5 percent:

$$\frac{Z}{d_p} > \frac{20n}{\mathrm{Pe}_{aL}}\ln\frac{(C_A)_{\mathrm{in}}}{(C_A)_{\mathrm{out}}}$$

where n is the order of the reaction and $\mathrm{Pe}_{aL} = d_p u_{iL}/D_{eL}$. Hochman and Effron [1969] correlated the axial mixing in the gas phase in terms of the Peclet and Reynolds numbers for the gas and liquid phase, as follows:

$$Pe_{aG} = 1.8\,\mathrm{Re}_G^{-0.7}\,10^{-0.005\,\mathrm{Re}_L} \tag{14.3.2-9}$$

Deviations from plug flow in the gas phase are not ordinarily of concern in trickle bed operation.

As previously mentioned, the mass transfer from the gas to the active sites of the catalyst involves several steps. For trickle bed operation, in which the interaction between gas and liquid is limited, the values for k_G and k_L are of the same order of magnitude as those given for countercurrent operation in the previous section. Some specific results for cocurrent operation are available in

the literature. Reiss' correlation [1967] for $k_G a_v^{'}$ and $k_L a_v^{'}$ in air-ammonia and air-water systems are as follows:

$$k_G a_v^{'} = 2.0 + c_1 E_G^{0.66} \tag{14.3.2-10}$$

where E_G is an energy dissipation term for gas flow $= (\Delta p_{t2}/\Delta z) u_{sG}$. The constant c_1 equals 0.03 when E_G is expressed in N/m² s and 0.0665 when E_G is in W/m³. The mass transfer coefficient k_G is in m³/m² s.

$$k_L a_v^{'} = c_2 E_L^{0.5} \tag{14.3.2-11}$$

where E_L is an energy dissipation term for liquid flow $= (\Delta p_{t2}/\Delta z) u_{sL}$, in N/m² s ($c_2$ = 0.0055) or in W/m³ (c_2 = 0.017). k_L is in m³/m² s. Reiss' results were probably obtained in the pulse flow and spray flow regime. Charpentier [1976] extended the range of validity to low liquid and gas flow rates and proposed the following correlation:

$$k_L a_v^{'} = 0.0011 E_L \frac{D_{AL}}{2.4 \times 10^{-9}} \left(\mathrm{s}^{-1}\right) \tag{14.3.2-12}$$

where D_A is the diffusivity, in m²/s, in the liquid, assuming that the liquid viscosity does not differ too much from that of water; E_L is in W/m³.

The liquid-solid mass transfer coefficient may be obtained, in first approximation, from the j_D correlations for single-phase flow, mentioned in Chapters 3 and 11, although the gas phase exerts a certain influence, as shown by Mochizuki and Matsui [1974] for cocurrent upwards flow. Specific results for the situation considered here have been derived by Van Krevelen and Krekels [1948], who correlated their data as follows:

$$\mathrm{Sh} = 1.8\,\mathrm{Re}^{0.5}\,\mathrm{Sc}^{0.33} \tag{14.3.2-13}$$

with

$$\mathrm{Sh} = \frac{k_l}{a_v^{''} D_{AL}} \quad \text{and} \quad \mathrm{Re} = \frac{\rho_L L}{\Omega a_v^{''} \mu_L}$$

Also see Satterfield et al. [1978].

The resistance to mass transfer inside the catalyst particle is dealt with as outlined in Chapters 3 and 11. In trickle bed hydrodesulfurization, the gas film resistance is practically zero, since the gas phase is mainly hydrogen. The liquid side and liquid-solid side resistances are negligible with respect to that inside the catalyst, since hydrogen is very soluble in the liquid. The effectiveness factor is generally around 0.5 to 0.6. An additional complication arises when a fraction of the liquid feed is vaporized, such as in hydrodesulfurization of light petroleum

fractions (naphtha, kerosene) or in hydrocracking. In such a case the pores of the catalyst are filled with both liquid and vapor. The theory of the effectiveness factor for such a situation still has to be worked out.

Several approaches for the design of trickle bed reactors have been discussed by Satterfield [1975] and are briefly outlined below. With industrial hydrotreating operations in mind, suppose the gaseous reactant is present in great excess with respect to the reacting component of the liquid. Since hydrogen is very soluble in petroleum fractions and since the operation is carried out at high pressures (35 to 100 atm), the liquid may be considered to be saturated with hydrogen. If plug flow is assumed for the liquid, the continuity equation for a reacting component *B* of the liquid may be written

$$LC_{B0}dx = r_B dW$$

If the reaction were of first order, and if there were no diffusional limitations in the liquid film or in the catalyst particle,

$$r_B = kC_B$$

Integration then leads to

$$\ln\frac{C_{B0}}{C_B} = k\frac{W}{L}$$

When experiments are carried out in trickle bed reactors and first-order kinetics are assumed, a rate coefficient is derived, represented by k_{obs}, which is found to be different from the true rate coefficient *k*. It is found that when both *L* and *W* are doubled the conversion is also increased. This means, in the jargon of the trickle bed literature, that the contacting effectiveness is < 1. There may be several reasons for this. First, it may be argued that k_{obs} may include effects of diffusion in the liquid film and in the catalyst particles:

$$\frac{1}{k_{obs}} = \frac{1}{k\eta} + \frac{1}{k_L a_v'}$$

where $k_L a_v'$ is, of course, dependent on F' or L — according to correlations given above, to $L^{0.5}$ – $L^{1.0}$.

Furthermore, if the reaction is not truly first order, *k* values compared at different conversions will be different. When the species are adsorbed on the catalyst, first-order kinetics would be rather unlikely. Even if each species reacted according to first-order kinetics, the lumping of a spectrum of species with different reactivities into one pseudocomponent would lead to an overall order higher than 1.

Bondi [1971] related k_{obs} to k and the superficial liquid flow rate:

$$\frac{1}{k_{obs}} = \frac{1}{k} + \frac{A'}{\left(L\rho_L/\Omega\right)^b} \quad \text{where } 0.5 < b < 0.7$$

For hydrodesulfurization of a heavy gasoil, k_{obs}/k was found to be 0.12 to 0.2 at $L\rho_L/\Omega$ = 288 kg/m² h and 0.6 at $L\rho_L/\Omega$ = 1080 kg/m² h. The power would seem to drop at higher liquid velocities, however. According to Satterfield, the "contacting effectiveness" would become almost 1 at $L\rho_L/\Omega$ values of 1 to 5 kg/m² s. Henry and Gilbert [1973] associated the effect of the liquid flow rate with the free-draining holdup:

$$k_{\text{obs}} \sim k\varepsilon_L'$$

ε_L' varies at $L^{1/3}$ and Henry and Gilbert could indeed correlate their results in this way. There is, however, no theoretical justification for taking the rate to be proportional to the liquid free-draining holdup. Mears [1974] therefore proposed to consider the rate to be proportional to the external wetted area of the catalyst. Using the Puranik and Vogelpohl correlation, he derived the following relation:

$$\log_{10}\frac{C_{\text{in}}}{C_{\text{out}}} \sim \text{Z}^{0.32}\left(\text{LHSV}\right)^{-0.68} d_p^{0.18}\left(\frac{\mu_L}{\rho_L}\right)^{-0.05}\left(\frac{\sigma_{L,c}}{\sigma_L}\right)^{0.21}\eta_G \qquad (14.3.2\text{-}14)$$

where LHSV is the liquid hourly space velocity. This relation would be valid for $\rho_L L/\Omega$ < 54 kg/m² s. At higher flow rates, Onda's correlation (14.3.1-1) should be used for the wetted area.

Little is known on the effect of the gas flow rate on k_{obs}. The effect should be small if the liquid is saturated with the gas. According to Charpentier et al. [1968], an incerase in G decreases ε_L but favors the exchange between dynamic holdup and stagnant liquid.

Deviations from k could also be explained in terms of deviations from plug flow, because of axial mixing. This can be accounted for either directly through the residence time distribution or through an axial effective diffusivity model as discussed earlier in Chapter 11 for single-phase fixed beds. For trickle bed operation, Pe_{aL} is about 0.2 at a Re based on particle diameter of 10, whereas for single-phase operation $Pe_{aL} = 2$. For bench scale operation the minimum reactor length for absence of significant axial mixing could therefore be an order of magnitude greater than for single-phase fixed beds. But, again, for industrial reactors, axial mixing is completely negligible: Henry and Gilbert estimated the minimum length to be 30 cm when d_p = 1.6 mm, for a Reynolds

number of 10 and a conversion of 90 percent and 70 cm for 99 percent conversion.

More recent modeling mainly follows the approach outlined in Sections 14.2.4 and 14.2.5. Mills and Dudukovic [1983] applied a generalized dispersion model with partially wetted pellets. A review by Gianetto and Specchia [1992] and the text books of Ramachandran and Chaudhari [1983] and of Shah [1979] provide further insight into the modeling of trickle bed reactors.

Christensen et al. [1986] and Dimenstein and Ng [1986] revealed the possibility of multiple hydrodynamic states in the trickle regime, leading to nonunique pressure drop values for given operating conditions. A hysteresis is experienced with a lower branch followed when the liquid flow rate is gradually increased from zero and higher branch followed when it is gradually decreased back to zero.

EXAMPLE 14.3.2.A

TRICKLE BED HYDROCRACKING OF VACUUM GAS OIL

The hydrocracking of vacuum gas oil (VGO) into lighter and more valuable fractions is an important process of petroleum refining. It is carried out in a multistage reactor with adiabatic catalytic beds and hydrogen cold shot in between the beds — a “multibed adiabatic reactor”. It requires a high ratio of hydrogen to hydrocarbon because considerable hydrogenation is involved, to avoid the production of strongly unsaturated components that would deactivate the catalyst. That leads to a continuous gas phase and trickle flow conditions for the liquid, but both phases are considered to move in plug flow. The continuity equations for the gas and liquid phase components and groups of isomers at equilibrium (GOI) are written:

$$\frac{1}{\Omega}\frac{dF_{Sg}^{gas}}{dz} = -k_{O,Sg}a_v\left(\frac{C_{Sg}^{gas}}{K_{Sg}^{C,VLE}} - C_{Sg}^{liq}\right) \quad g = 1,2,.....N_{lumps} \qquad (14.3.2.A\text{-}1)$$

$$\frac{1}{\Omega}\frac{dF_{Sg}^{liq}}{dz} = k_{O,Sg}a_v\left(\frac{C_{Sg}^{gas}}{K_{Sg}^{C,VLE}} - C_{Sg}^{liq}\right) + R_{Sg,net}^{Form} \quad g = 1,2,.....N_{lumps} \qquad (14.3.2.A\text{-}2)$$

The particles are assumed to be completely wetted. The inter-phase mass transfer flux is described using the two film theory. In the above equations, the overall mass transfer coefficient is given by

$$\frac{1}{k_{O,Sg}} = \frac{1}{k_G K_{Sg}^{C,VLE}} + \frac{1}{k_L} \qquad (14.3.2.A\text{-}3)$$

The value of the liquid-side mass transfer coefficient $k_L a_v$ was calculated from the correlation of Sato et al. [1973] and the gas-side mass transfer coefficient $k_G a_v$ from Reiss' correlation [1967]. The gas-liquid interfacial area a_v was calculated according to Charpentier [1976]. $K_{Sg}^{C,VLE}$ is the *concentration* equilibrium partition coefficient relating the equilibrium concentrations of GOI S_g in the gas and liquid phases, $K_{Sg}^{C,VLE} = C_{Sg}^{gas} / C_{Sg}^{liq}$. This is expressed in terms of the *true* equilibrium partition coefficient K_{Sg}^{VLE} as

$$K_{Sg}^{C,VLE} = \left(\frac{y_{Sg}}{x_{Sg}}\right)\left(\frac{C_{total}^{gas}}{C_{total}^{liq}}\right) = K_{Sg}^{VLE}\left(\frac{C_{total}^{gas}}{C_{total}^{liq}}\right)$$

The values of K_{Sg}^{VLE} are calculated using the Peng-Robinson equation of state.
The liquid phase molar concentrations in (14.3.2.A-1) and (14.3.2.A-2) are calculated using the density of the liquid phase. The latter is obtained using the density of the various "Group of Isomers" (GOI) estimated by the Hankinson and Thomson (HBT) method and the liquid phase mole fractions of the GOI's. This approach efficiently accounts for the volume expansion of the hydrocarbon mixture along the reactor.

The liquid phase continuity equations for the components and GOI contain the rate equations expressed by Kumar and Froment [2007] in terms of the single-event approach, already presented in Section 2.4.4 "Hydrocracking" of Chapter 2. Their most advanced version of the simulation model characterizes the VGO-feed by 1266 components and GOI. The current methods used for the analysis of heavy petroleum fractions do not permit to reach such detail, but methods have been developed that reconstruct their composition at the molecular level starting from global analytical results such as carbon-, hydrogen-, and sulphur-content, specific gravity, mass spectrometry, distillation curve... [Hudebine and Verstraete, 2004; Martinis and Froment, 2009; Charon-Revellin et al., 2010].

A significant amount of heat is released in the hydrogenation of aromatics/ naphtheno-aromatics and in the hydrocracking reactions. The liquid phase temperature profile inside the reactor beds is obtained from

$$\frac{dT^{liq}}{dz} = \frac{\left(\sum_{g=1}^{N_{lumps}}\left(-\Delta H_{f,g}^{liq}\right)R_{Sg,net}^{Form} - \sum_{g=1}^{N_{lumps}}\frac{dF_{Sg}^{gas}}{dz}\lambda_{Sg}\right)}{\sum_{g=1}^{N_{lumps}}\left(F_{Sg}^{gas}C_{P,Sg}^{gas} + F_{Lg}^{liq}C_{P,Sg}^{liq}\right)} \qquad (14.3.2.A\text{-}4)$$

In the numerator of (14.3.2.A-4), the first term represents the total heat of reaction, calculated using the heats of formation of individual GOI's / pure

components obtained from the Benson's group contribution method. The second term accounts for the heat consumed in the vaporization of hydrocarbons. The heat transfer resistance between the gas and liquid phase was assumed to be negligible. The temperature of the solid phase is obtained from

$$T^{solid} = T^{liq} + \frac{\sum_{g=1}^{N_{lumps}} \left(-\Delta H_{f,g}^{liq}\right) R_{Sg,net}^{Form}}{a_{LS}\, h_{LS}} \qquad (14.3.2.A\text{-}5)$$

Figure 14.3.2.A-1(a) shows the temperature profiles in the 3 adiabatic beds and the effect of the cold shot cooling between the beds for bed inlet temperatures of 350 and 370°C. The temperature increase in each bed was limited to 15°C, to avoid degradation of products into carbonaceous residues and the associated catalyst deactivation. With this limit on the ΔT the larger amount that is converted at the higher T of 370°C requires 4 beds, instead of 3 at 350°C. Figure 14.3.2.A-1(b) shows the evolution of the H_2 flux in the gas and liquid phase, again for 350 and 370°C. Figure 14.3.2.A-2 presents some results of the simulation at bed inlet temperatures of 350°C, a total pressure of 150 bar and a molar ratio H_2/VGO of 15. The first diagram shows the yield profiles along the reactor of the commercial fractions LPG, light naphtha, heavy naphtha, kerosene, residue. The single event kinetic model goes way beyond these fractions and also permits the prediction of the yields of the hydrocarbon classes, paraffins, naphthenes, aromatics, naphtheno-aromatics …, of the subclasses *n*-paraffins, *i*-paraffins … and even of the individual components.

Such detailed predictions are only possible with the single event approach discussed in Section 2.4 of Chapter 2. They provide a deep insight into

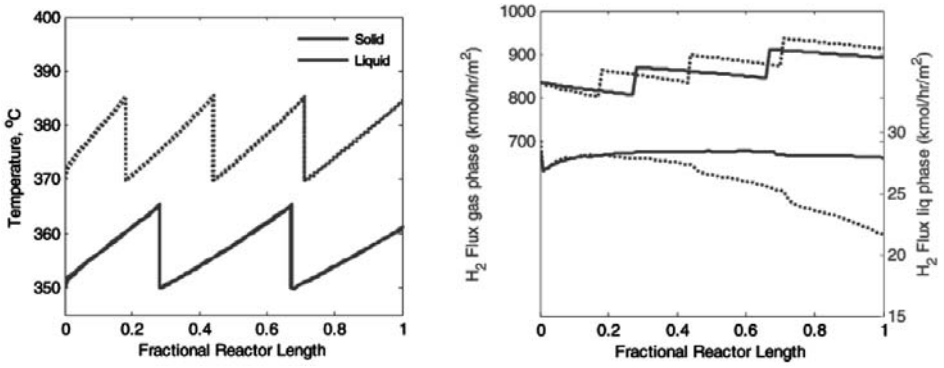

(a) (b)

Figure 14.3.2.A-1

VGO hydrocracking at 150 bar; molar H_2/VGO = 15. From Kumar and Froment [2007].

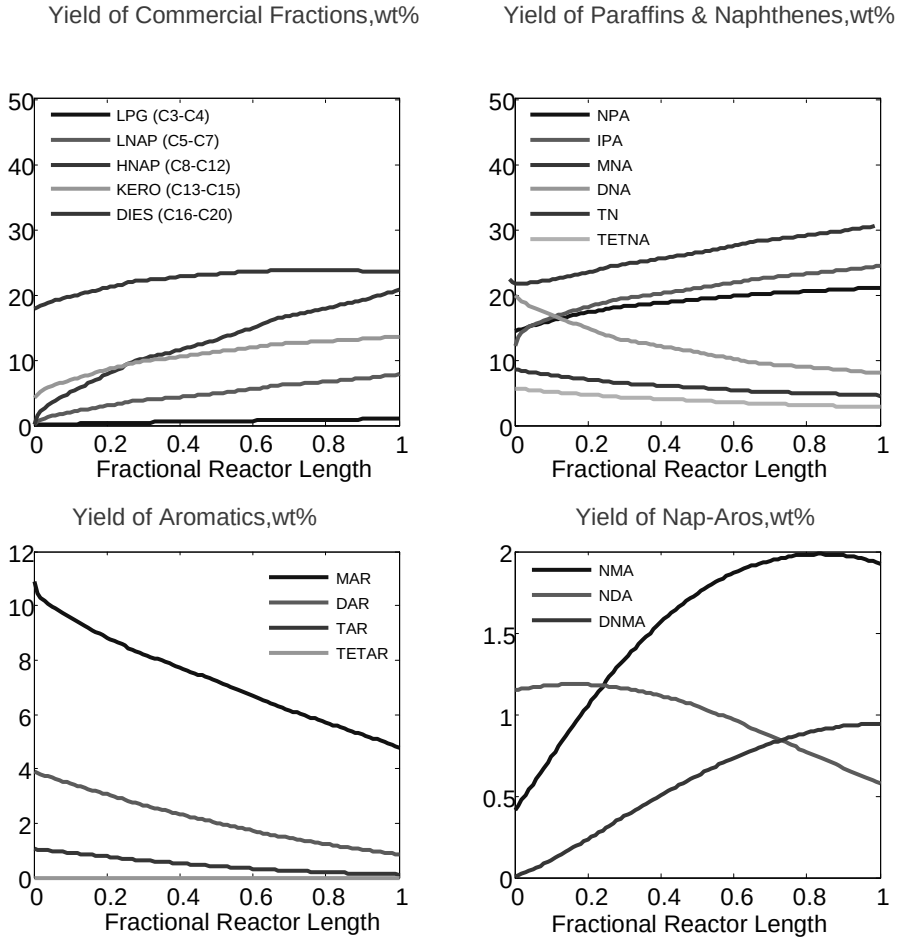

Figure 14.3.2.A-2

VGO hydrocracking. 350°C; 150 bar; molar H_2/VGO = 15. From Kumar and Froment [2007].

the influence of the feed composition, operating conditions and catalyst properties on the hydrocracking process and are of great importance for guiding and optimizing the operation.

14.3.3 Two-Phase Fixed Bed Catalytic Reactors with Cocurrent Upflow. Upflow Packed Bubble Reactors

Generally, the flow rates in these reactors are such that the gas phase is dispersed and the liquid phase continuous. In the bubble flow regime, the bubbles rise at a slightly higher velocity than the liquid. As the gas flow velocity is increased, pulse flow is obtained. For certain ranges of u_{sL} and u_{sG}, the spray flow regime, with continuous gas phase and a liquid mist, may be experienced. The regimes shown in Fig. 14.3.2-2 are also encountered here, the only difference being that

pulsing is initiated at slightly lower gas velocities and persists to slightly higher gas velocities for upward flow, at a given liquid rate, than for downflow.

The pressure drop for upward flow is the sum of the liquid head and of the friction of gas and liquid, between each other and with the packing and wall. Heilman [1969] derived the following semiempirical correlation for air and water and for various packing material and shapes:

$$\frac{\Delta p_{t2}}{\Delta z} = g\varepsilon_L\rho_L - (1-0.25u_{sL})\left(\frac{u_{sG}}{u_{iG}}\cdot\frac{0.85g\varepsilon_L\rho_L}{\varepsilon-\varepsilon_G^0} - \alpha g\varepsilon_G\rho_g\right)$$

$$+\left(0.292+\frac{4.16}{\mathrm{Re}_L}\right)\frac{\Omega(1-\varepsilon)}{\varepsilon^3}\rho_L u_{sL}^2 \qquad (14.3.3\text{-}1)$$

(u_{sG} up to 0.03 m/s; u_{sL} up to 0.04 m/s). Again, $\Delta p_{t2}/\Delta z$ is in kgf/m²/m. The first term on the right represents the liquid head, the second the bubble friction, the third the liquid friction; ρ_g is the gas density at the top of the column; u_{sL} and u_{sG} are superficial liquid and gas velocities; u_{iG} is the interstitial gas velocity; and ε_G^0 is the gas holdup at zero gas flow rate. α accounts for the roughness of the catalyst and varies between 300 and 700.

The following correlation for the gas holdup ε_G was also derived by Heilman:

$$\varepsilon_G = 0.01\left[0.012d_r + 8\left(\frac{\varepsilon}{d_p}\right) - 2 + 4.45u_{sG}^{0.66} + 11\left(\frac{\mu_L}{\mu_W}-1\right)^{1.25}\right]\left(\frac{\sigma_W}{\sigma_L}\right)^{1.8} \qquad (14.3.3\text{-}2)$$

This formula is valid only for ε_G < 0.45 and for constant total pressure. Therefore, high columns would have to be divided into sections before the above formulas could be applied to them. The rising velocity of the bubbles has been correlated as follows by Heilman:

$$u_G = \left(24.5-8\frac{\mu_L}{\mu_W}\right) + (2.2+1.32d_p)u_{sG} \quad \text{(in cm/s)}$$

No general correlation is available for the interfacial area. From Saada's measurements [1972] it would seem that a_v' varies approximately as $u_{sG}^{0.5}$, regardless of packing size and type, column diameter, or liquid superficial velocity.

Since the liquid flow rates are generally rather low, it may be necessary to account for axial mixing in the liquid phase. This is done in terms of axial

effective diffusion. The axial effective diffusivity for the liquid phase is given by Böxkes [1969]:

$$\frac{D_{eL}}{\nu_L} = 3.63\times 10^3\,\mathrm{Re}_L^{0.07}\,\mathrm{Re}_G^{0.13}\left(\frac{Z}{d_r}\right)^{0.63}(1-\varepsilon)^{3.6} \qquad (14.3.3\text{-}3)$$

For the gas phase Böxkes found

$$\frac{D_{eG}}{\nu_G} = 6.02\times 10^2\,\mathrm{Re}_L^{0.15}\,\mathrm{Re}_G^{0.55} \qquad (14.3.3\text{-}4)$$

in which Re_L and Re_G are based on interstitial velocities. The mass transfer coefficients for gas-liquid transfer and liquid-solid transfer have not been investigated in detail. The correlations for the gas-liquid transfer coefficient may be different from those derived from countercurrent packed absorbers.

Mochizuki and Matsui [1974] correlated the liquid-solid transfer coefficient for $\mathrm{Re}_L > 10$ as follows:

$$\frac{\mathrm{Sh}}{\mathrm{Sh}'} = 1 + 4\frac{\mathrm{Re}_G^{0.55}}{\mathrm{Re}_L^{0.7}} \qquad (14.3.3\text{-}5)$$

with $\mathrm{Sh}' = 0.75\mathrm{Re}^{0.5}\mathrm{Sc}^{0.33}$; Sh' is the Sherwood number for single-phase flow. The Reynolds numbers are based on interstitial velocities.

Dudukovic et al. [1999] thoroughly reviewed the state of the art of our understanding of the phenomena occurring in slurry bubble columns and ebullated beds, but also in packed beds with two-phase flow.

Chen et al. [1999] derived correlations for gas holdup, turbulent eddy diffusivity, and liquid recirculation velocity from measurements in a bubble column with a diameter of 0.45 m.

14.3.4 Plate Columns

Technological details and operating characteristics of various types of plate columns are extensively discussed in textbooks on mass transfer [e.g., Treybal, 1955]. The results of extensive research on bubble tray design is reported in the *Bubble Tray Manual* of the American Institute of Chemical Engineers [1958]. Flooding and weeping limits are discussed in a review by Zenz [1972]. Most of the early correlations were written in terms of “theoretical” plates, assuming that equilibrium is reached between vapor and liquid. This is an approach that is progressively abandoned in favor of real plates, obtained when finite rates of transfer are accounted for. This is the approach followed here, not only because

more information on transfer rates has become available, but also because it is the only approach possible when absorption is accompanied by reaction.

In what follows, a few correlations for the main quantities that are of direct relevance to the problem considered here are presented.

CORRELATIONS FOR k_G, THE GAS PHASE MASS TRANSFER COEFFICIENT OF A TRANSFERRING COMPONENT *A*

Stichlmair [1978] has proposed the following correlation, applicable to any type of tray:

$$k_G RT = \sqrt{\frac{4}{\pi} D_{A,G} \frac{u_{sG}}{h_F \varepsilon_G}} \tag{14.3.4-1}$$

where u_{sG} is the superficial gas velocity (in m^3_g/m^3_L h), based on the total active surface of the tray (i.e., not just on the total cross section of the holes only), ε_G is the gas holdup of the froth, and h_F the froth height.

Asano and Fujita [1966] proposed for bubble caps

$$\frac{k_G RTb_0}{D_{A,G}} = 4.7\left(\frac{\mu_G}{\rho_g D_{A,G}}\right)^{0.5}\left(\frac{u_{Go} b_0 \rho_g}{\mu_G}\right)^{0.63}\left(\frac{h_s + h_0}{b_0}\right)^{-0.6} \tag{14.3.4-2}$$

where b_0 and h_0 are the width and free height of the openings in the caps, h_s is the submergence under operation, and u_{Go} is the velocity of the gas through the openings. For sieve trays they proposed

$$\frac{k_G RTd_h}{D_{A,G}} = 1.0\frac{d_h}{h_L}\left(\frac{\mu_G}{\rho_g D_{A,G}}\right)^{0.5}\left(\frac{u_{Gh} d_h \rho_g}{\mu_G}\right)^{0.75} \tag{14.3.4-3}$$

where d_h is the diameter of the holes, h_L is the height of the clear liquid, and u_G is the velocity of the gas through the holes.

CORRELATIONS FOR k_L

Stichlmair [1978] proposed the general correlation

$$k_L = \sqrt{\frac{4}{\pi} D_{A,L} \frac{u_{sG}}{h_F \varepsilon_G}} \tag{14.3.4-4}$$

whereas Asano and Fujita's correlation for bubble caps can be written

$$\frac{k_L b_0}{D_{A,L}} = 100\left(\frac{\mu_L}{D_{A,L}\rho_L}\right)^{1/2}\left(\frac{L' M_L}{\Omega \mu_L} d_t\right)^{1/2}\left(\frac{h_s + h_0}{b_0}\right)^{-1} \tag{14.3.4-5}$$

and for sieve trays,

$$\frac{k_L d_h}{D_{A,L}} = 100 \frac{d_h}{h_L} \left(\frac{\mu_L}{D_{A,L} \rho_L} \right)^{1/2} \left(\frac{L' M_L}{\Omega \mu_L} d_t \right)^{1/2} \qquad (14.3.4\text{-}6)$$

where Ω is the active cross section of the plate.

CORRELATIONS FOR A_v'

A distinction has to be made between the bubble regime, where the gas rises as a bubble through the continuous liquid phase, and the drop regime, where the gas is continuous and the liquid is dispersed. According to Stichlmair [1978], the transition from the first to the second regime occurs when

$$\Psi = \frac{u_{sG} \sqrt{\rho_g}}{2.5 \left[\left(\frac{\Omega h}{\Omega_p} \right)^2 \sigma_L \left(\rho_L - \rho_g \right) g \right]^{1/4}} > 0.7 \qquad (14.3.4\text{-}7)$$

with Ω_h the total cross section of the holes and Ω_p the active surface of the plate. In that case

$$A_v' = \frac{u_{sG} \sqrt{\rho_g}}{2\sigma_L^2} \left(1 - \Psi^{0.28} \right) \qquad (14.3.4\text{-}8)$$

whereas when $\Psi < 0.7$:

$$A_v' = A\Psi^{0.28} - 0.0357 \frac{u_{sG} \sqrt{\rho_g}}{\sigma_L \left(\frac{\Omega_h}{\Omega_p} \right)^2} \Psi - 1.847 A \Psi^2 \qquad (14.3.4\text{-}9)$$

with

$$A = 6 \left[\frac{\left(\rho_L - \rho_g \right) g}{6\sigma_L} \right]^{1/2}$$

CORRELATION FOR FROTH HEIGHT

Stichlmair [1978] derived

$$h_F = h_W + \frac{1.45}{g^{1/3}} \left(\frac{L' M_L}{\rho_L \varepsilon_L l_w} \right)^{2/3} + \frac{250}{2g(\rho_L - \rho_g)} \frac{\left(u_{sG} - u_b \right)^2 \rho_g}{\left(1 - \varepsilon_L \right)^2} \qquad (14.3.4\text{-}10)$$

where l_w and h_w are the weir length and height, respectively, and u_b is the bubble velocity, given by

$$u_b = 1.55\left[\frac{\sigma_L(\rho_L - \rho_g)g}{\rho_L^2}\right]^{1/4}\left(\frac{\rho_g}{\rho_L}\right)^{1/24} \qquad (14.3.4\text{-}11)$$

CORRELATION FOR THE LIQUID HOLDUP OF THE FROTH

According to Stichlmair [1978],

$$\begin{aligned}\varepsilon_L &= (1-\Psi)^{0.86} \quad \text{when} \quad \Psi > 0.7 \\ &= (1-\Psi)^{0.28} \quad \text{when} \quad \Psi < 0.7\end{aligned} \qquad (14.3.4\text{-}12)$$

EXAMPLE 14.3.4.A

THE SIMULATION OR DESIGN OF A PLATE COLUMN FOR ABSORPTION AND REACTION

In the model to be described, the gas is assumed to be in plug flow, whereas the liquid on the plate is completely mixed. It is an application of Section 14.2.3 to each plate of the column, but in addition nonisothermal and nonisobaric conditions are also accounted for. By way of example, the process consists of two parallel reactions of a gas-phase component with two components of the liquid phase. The stoichiometry is given by

$$a_1 A + r_1 R_1 \rightarrow P_1$$

$$a_2 A + r_2 R_2 \rightarrow P_2$$

The continuity equation for the absorbing component *A* of the gas phase on plate *k* is written, in terms of mol fractions,

$$\frac{F}{1-y_A}\frac{dy_A}{dz} = -N_A\big|_{y=0} A_v' \Omega_p \qquad (14.3.4.\text{A-a})$$

The variation of the total flow rate over plate *k* is accounted for through

$$\frac{dF}{dz} = -N_A\big|_{y=0} A_v' \Omega_p \qquad (14.3.4.\text{A-b})$$

whereas for nonabsorbing components, Fy_j = constant.

The boundary conditions are

$$\text{for } z = 0: \quad y_A = (y_{A,k})_{\text{in}} \quad \text{and} \quad F = (F_k)_{\text{in}} \qquad (14.3.4.\text{A-c})$$

$$\text{for } z = h_p: \quad y_A = \left(y_{A,k}\right)_{\text{out}} \quad \text{and} \quad F = \left(F_k\right)_{\text{out}}$$

where $(F_k)_{\text{in}}$ and $(y_{j,k})_{\text{in}}$ are, respectively, the gas flow rate and the mole fractions in the gas entering plate k. These are related to the quantities leaving plate $k + 1$ in the way illustrated in Fig. 14.3.4.A-1, in which side streams are also considered.

The gas flow rate to plate k is given by

$$\left(F_k\right)_{\text{in}} = F_{k+1} + V_{V,k+1} - V_{W,k+1} \tag{14.3.4.A-d}$$

and the mole fraction of A is given by

$$\left(y_{A,k}\right)_{\text{in}} = \frac{y_{A,k+1}\left(F_{k+1} - V_{W,k+1}\right) + y_{A,V,k+1}V_{V,k+1}}{\left(F_k\right)_{\text{in}}} \tag{14.3.4.A-e}$$

The mass balance for the absorbing component A in the liquid phase, which is completely mixed, depends on the corresponding Ha number.

For a moderately fast reaction ($0.3 < \text{Ha} < 3$), which is the most general case, the equation is written

$$\begin{aligned} &x_{A,k}\left(L_k' + W_{Wk}\right) - \left(x_{A,k-1}L_{k-1}' + x_{A,W,k}W_{V,k}\right) \\ &= \int_0^{h_r} N_A\Big|_{y=y_L} A_v'\Omega_p dh_F - \sum_{l=1}^{2}\left(1 - A_v y_L\right)\Omega_p h_F \varepsilon_L \left(r_A\right)_l \end{aligned} \tag{14.3.4.A-f}$$

where L' is the liquid molar flow rate and $(r_A)_l$ is the rate of reaction of A in

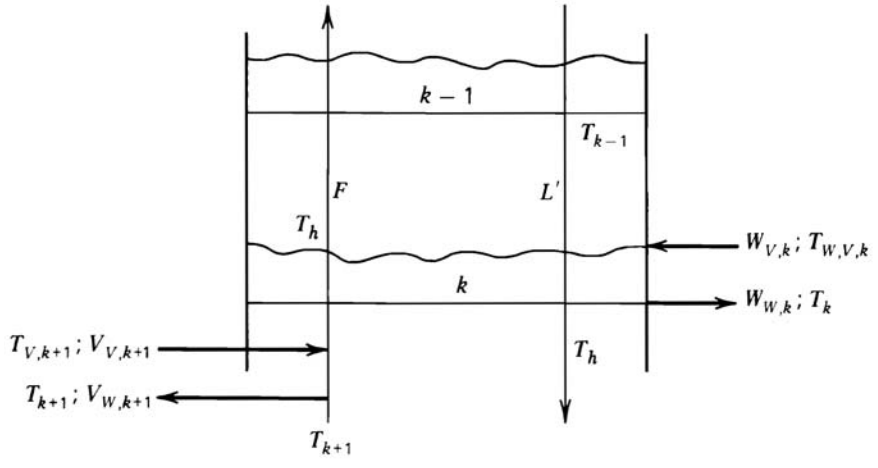

Figure 14.3.4.A-1
Definition of symbols and flows.

reaction *l*. An analogous equation can be written for the mole fractions of the reacting components of the liquid phase, R_1 and R_2, except that the second term in the R.H.S. has no summation sign.

Another way of relating the composition of the gas phase to that of the liquid phase is the following mass balance on plate *k*:

$$F_k\left(y_{A,k}\right)_{\text{in}} - F_k\left(y_{A,k}\right)_{\text{out}} = \sum_{j=l=1}^{2} \frac{r_j}{a_l}\Big(\Big(x_{R_{j,k-1}} L'_{k-1} + x_R W_{V,k}\Big) - x_{R_j}\left(L'_k + W_{W,k}\right)\Big) + \left(x_{A,k-1} L'_{k-1} + x_{A,W,k} W_{V,k}\right) - \left(x_{A,k} L'_k + x_{AW,k} W_{W,k}\right) \tag{14.3.4.A-g}$$

where the first term in the R.H.S. expresses the amount of *A* that reacted in terms of the change in the molar fractions of R_1 and R_2 and the second term expresses the amount of *A* that has not reacted on plate *k*.

The absorption fluxes of the various components are expressed by

$$N_A\big|_{y=0} = k_{G,A}\left(p_t\right)_k\left(y_A - H' x_{A,k}\right) \tag{14.3.4.A-h}$$

$$N_A\big|_{y=0} = -D_A C_k \frac{dx_A}{dy}\Big|_{y=0} \tag{14.3.4.A-i}$$

$$N_A\big|_{y=y_L} = -D_A C_k \frac{dx_A}{dy}\Big|_{y=y_L} \tag{14.3.4.A-j}$$

For the determination of the fluxes, the concentration profile of the absorbing component undergoing fast reactions in the liquid film has to be computed from the following set of second-order differential equations, describing the variation of the mole fraction of the component in the liquid film:

$$D_A \frac{d^2 x_A}{dy^2} = \frac{\sum_{l=1}^{2}\left(r_A\right)_l}{C_k} \tag{14.3.4.A-k}$$

and for the liquid phase reactants R_1 and R_2,

$$D_{R_1} \frac{d^2 x_{R_1}}{dy^2} = \frac{r_1}{a_1}\left(r_A\right)_1 \tag{14.3.4.A-l-a}$$

$$D_{R_2}\frac{d^2x_{R_2}}{dy^2}=\frac{r_2}{a_2}\left(r_A\right)_2 \qquad (14.3.4.A\text{-l-b})$$

with boundary conditions

$$\text{At } y=0: \quad \frac{dx_A}{dy}=\frac{N_A}{D_AC_k}\bigg|_{y=0}=k_{G,A}\left(p_t\right)_k\left(y_A-H'x_{A,k}\right)$$

$$\frac{dx_{R_1}}{dy}=\frac{dx_{R_2}}{dy}=0 \qquad (14.3.4.A\text{-m})$$

$$\text{At } y=y_L: \quad x_A=-\frac{N_A}{D_AC_k}\bigg|_{y=y_L}$$

$$x_{R_1}=x_{R_{1,k}} \qquad x_{R_2}=x_{R_{2,k}}$$

Subtraction of (14.3.4.A-l-a) or (14.3.4.A-l-b) from (14.3.4.A-k) and two integrations leads to relationships between A and R_1 and R_2, respectively so that only (14.3.4.A-k) has to be integrated over the film. As already mentioned in Chapter 6, approximate analytical solutions can be derived for specific cases.

An enthalpy balance is used for computing the temperature profile, since no reliable values for the heat transfer coefficient are available:

$$T_{k-1}L'_{k-1}\sum_{j=1}^{n_L}x_{j,k-1}c_{p_L,j}-T_k\left[F_k\sum_{j=1}^{n_G}y_{j,k}c_{p_G,j}+\left(W_{W_k}+L'_k\right)\sum_{j=1}^{n_L}x_{j,k}c_{P_L,j}\right]$$

$$+T_{k+1}\left[\left(F_{k+1}-V_{W,k+1}\right)\sum_{j=1}^{n_G}y_{j,k+1}c_{p_G,j}\right]+T_{V_{k+1}}V_{V_{k+1}}\sum_{j=1}^{n_G}y_{j,V_{k+1}}c_{p_G,j} \qquad (14.3.4.A\text{-n})$$

$$+T_{W_k}W_{V_k}\sum_{j=1}^{n_L}x_{j,W,k}c_{p_L,j}=Q_{c,k}-Q_{\text{abs}}-Q_{\text{react}}$$

where $Q_{c,k}$ represents the amount of heat removed from the plate by means of a cooling coil, Q_{abs} is the amount of heat produced by absorption, and Q_{react} is that produced by the reaction:

$$Q_{\text{abs}}=\left\{\begin{array}{r}\left[F_ky_{A,k}(\text{in})-F_ky_{A,k}(\text{out})\right]-\left(x_{A,k}L'_k+x_{A,k}W_{W,k}\right)\\ +\left(x_{A,k-1}L'_{k-1}+x_{AW,k}W_{V,k}\right)\end{array}\right\}\left(-\Delta H\right)_{\text{abs}} \qquad (14.3.4.A\text{-o})$$

where $(-\Delta H)_{abs}$ is the heat of absorption per kmol *A* absorbed.

$$Q_{\text{react}} = \sum_{j=1}^{2} \frac{1}{r_j} \left[x_{R_j,k-1} L'_{k-1} + x_{R_j,V,k} W_{V_k} - x_{R_j,k} \left(L'_k + W_{W_k} \right) \right] \left(-\Delta H_j \right) \quad (14.3.4.\text{A-p})$$

where $(-\Delta H)_j$ is the heat of reaction per mole R_j reacted.

The pressure drop over various types of plates can be calculated by means of correlations given, for example, in Perry and Chilton's *Chemical Engineers Handbook.*

De Leye and Froment [1986b] developed a general computer program for the design and simulation of plate absorbers. The calculations proceed per plate and yield, since they are based on the above equations, the true number of plates — i.e., not the theoretical number, which has to be adapted afterward for the plate efficiency. An example of the results of an application of the approach developed above is given in what follows.

■

EXAMPLE 14.3.4.B

THE ABSORPTION OF CO_2 IN AN AQUEOUS SOLUTION OF MONO- AND DIETHANOLAMINE (MEA AND DEA)

The CO_2-containing gas is fed at a rate of 497 kmol/h, a temperature of 313 K, and a pressure of 14.3 bar. The liquid feed rate is 3640 kmol/h, and its temperature 315 K. The gas and liquid compositions are given in Table 14.3.4.B-1. The column diameter is 1 m. The construction details of the sieve plate are given in Table 14.3.4.B-2.

TABLE 14.3.4.B-1
GAS AND LIQUID COMPOSITION

	Component	**Mole Fraction**
Gas	H_2	0.614
	N_2	0.001
	CO	0.213
	CO_2	0.1355
	CH_4	0.0365
Liquid	MEA	0.02335
	DEA	0.02335
	H_2O	0.95330

TABLE 14.3.4.B-2
CONSTRUCTION DETAILS OF SIEVE PLATE

Property	Value
Active surface (m²)	0.5012
Relative free surface	0.1
Weir length (m)	0.85
Weir height (m)	0.05
Diameter holes (m)	0.00476
Discharge coefficient C_D	0.74

Calculate the number of plates required to reduce the CO_2 mole fraction in the exit gas to 0.5×10^{-4}. Also compute the compositions, temperature, and pressure of the gas and liquid streams on each plate.

The absorption of CO_2 is accompanied by the two following reactions:

$$CO_2 + 2RNH_2 \rightarrow RNHCOO^- + RNH_3^+ \qquad (14.3.4.B\text{-a})$$

$$CO_2 + 2R_2NH \rightarrow R_2NCOO^- + R_2NH_2^+ \qquad (14.3.4.B\text{ -b})$$

for which Hikita et al. [1976] derived the following kinetic equations:

$$r_1 = k_1 C_{CO_2} C_{RNH_2}$$

$$r_2 = k_2 C_{CO_2} C^2_{R_2NH_2}$$

The reaction scheme (14.3.4.B-a)-(14.3.4.B-b) corresponds to that dealt with above in the general description of the design and simulation of plate columns. An estimate of the Ha number classifies them as very fast, but not instantaneous. In such a case the reactions take place entirely in the film, so that $x_{CO2,k}$, written $x_{A,k}$ in what follows, is set zero in (14.3.4.A-f) and (14.3.4.A-g). The viscosity of the solution and the diffusivity of CO_2 in the solution were calculated on the basis of experimental data of Thomas and Furzer [1962] and Shridar and Potter [1977]. Densities of ethanolamine solution were measured by Tseng and Thompson [1964] and Riddick and Bunger [1970].

The Henry coefficient of CO_2 in H_2O is given by Danckwerts and Sharma [1966]. It is further corrected to account for the ionic strength of the solution according to Danckwerts [1970].

The values of k_G, k_L, A_v', h_F, and ε_L on the various plates were all calculated from correlations given by Stichlmair [1978]. After a number of runs, it was found that 44 plates are required to reach the desired specifications. An initial estimate of the CO_2 mole fraction at the top of the column was 0.5×10^{-5},

TABLE 14.3.4.B-3
SIMULATION OF CO_2-ABSORPTION IN MONO- AND DI-ETHANOLAMINE IN A PLATE COLUMN. 2800 CPU SECONDS (DATA GENERAL MV6000).
FROM DE LEYE AND FROMENT [1986b].

	Top of Column	**Bottom of Column**
Flow rates		
L' (kmol/h)	3640	3640
F (kmol/h)	429.68	497.06
Gas phase composition (mol fr.)		
Y_{CO_2}	$0.47.10^{-4}$	0.1356
Liquid phase composition (mol fr.)		
x_{CO_2}	0.0	0.0
x_{RNH_2}	$2.335.10^{-1}$	$0.169.10^{-2}$
x_{R_2NH}	$2.335.10^{-1}$	$0.789.10^{-2}$
$x_{RNH_3^+}$	0.0	$0.108.10^{-1}$
$x_{R_2NH_2^+}$	0.0	$0.769.10^{-2}$
x_{RNHCOO^-}	0.0	$0.108.10^{-1}$
$x_{R_2NCOO^-}$	0.0	$0.769.10^{-2}$
p (bar)	13.99	14.29
T (K)	315	328.8
$A_v^{'}\ \left(m_i^2/m_f^3\right)$	427	450.8
k_{G,CO_2} (kmol/m² h bar)	0.506	0.473
k_{L,CO_2} (m/h)	0.351	0.364
h_F (m)	0.174	0.205
ε_L	0.352	0.283
$Ha_{CO_2-RNH_2}$	56.1	21.5
$Ha_{CO_2-R_2NH}$	31	16.2

whereas the temperature and pressure were supposed to be uniform and equal to the values given at the gas inlet. The calculations, the results of which are given in Table 14.3.4.B-3, confirm the classification “very fast, but not instantaneous” for the reactions—see the Hatta numbers at the top and the bottom of the column.

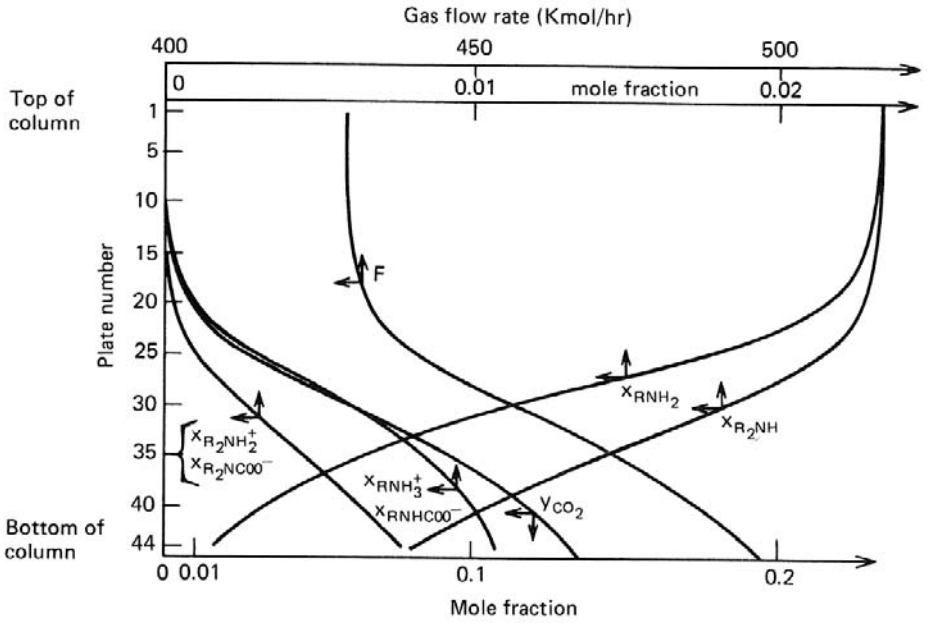

Figure 14.3.4.B-1

Mole fraction profiles of reactants and products and evolution of gas flow rate along the column. From DeLeye and Froment [1986b].

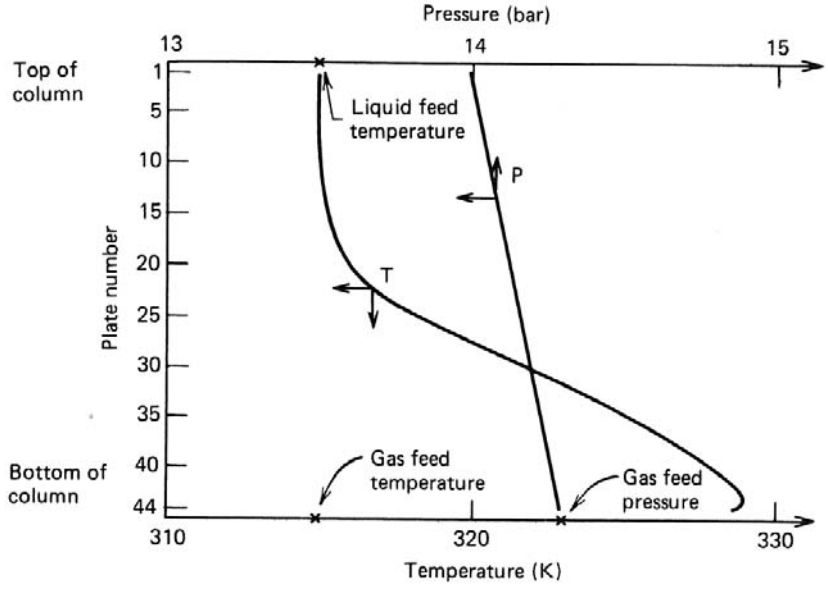

Figure 14.3.4.B-2

Evolution of temperature and pressure along the column. From DeLeye and Froment [1986b].

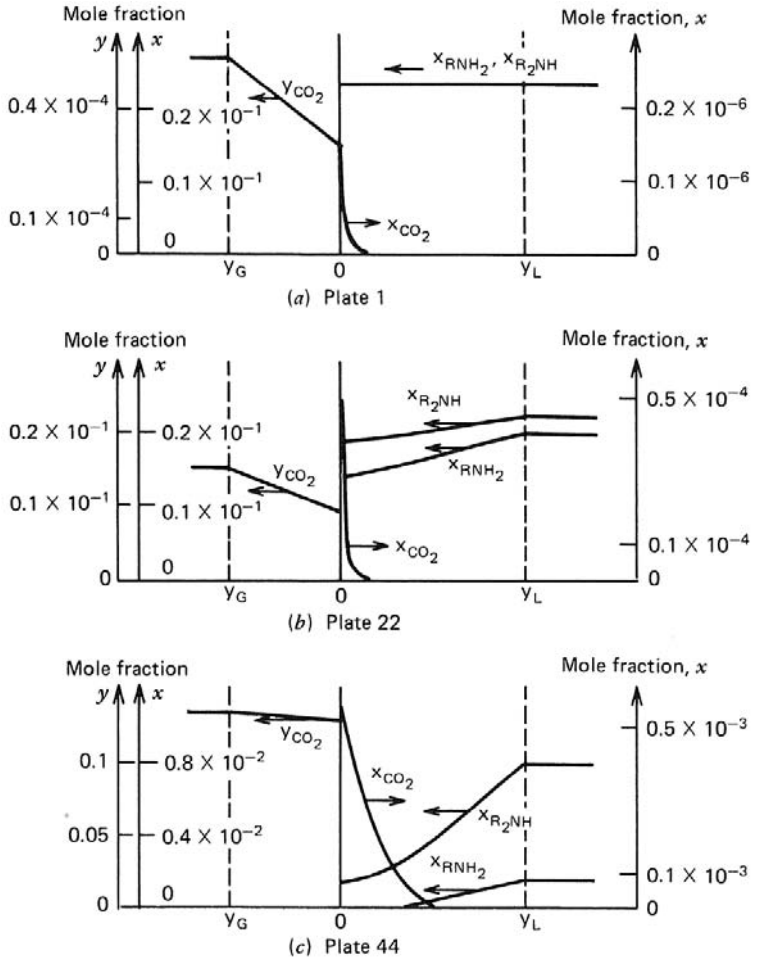

Figure 14.3.4.B-3

Profile of CO_2 mole fraction in the gas film and profiles of MEA and DEA mole fractions in the liquid film on plates 1, 22, and 44. From DeLeye and Froment [1986b].

Figure 14.3.4.B-1 shows the evolution of the various mole fractions and of the gas flow rate along the column, while Fig. 14.3.4.B-2 shows the temperature and pressure profiles (gas and liquid are assumed to have the same temperature). Figure 14.3.4.B-3 illustrates mole fraction profiles in the gas and liquid on plates 1, 22, and 44. It is clearly shown that CO_2 completely reacts in the film. At the top of the column, where the CO_2 has almost completely disappeared, the gas-phase mass transfer is rate-determining, as shown by the important drop in the CO_2 mole fraction over the film, whereas there is no depletion of MEA and DEA in the liquid film. The opposite is observed at the bottom of the column, where the CO_2 mole fraction is high.

■

14.3.5 Spray Towers

In gas-liquid spray towers the liquid is atomized and enters as a fine spray at the top and the gas is introduced at the bottom. The gas flow rate has to be kept sufficiently low to permit the liquid to fall. It is generally chosen in such a way that the liquid drops of mean diameter fall at 20 percent of their free-fall velocity, as calculated from Stokes' law. An efficient dispersion of the liquid requires the openings of the distributor to be small and the pressure high. Thereby a fraction of the drops hits the wall and flows down the wall as a film. Furthermore, a certain degree of coalescence of the drops is inevitable, so that the drop size, velocity, and therefore residence time vary strongly with position. A rigorous hydrodynamic analysis of such a situation is extremely complicated, so that only the overall behavior has been studied.

Mehta and Sharma [1970a; b] studied spray towers with a maximum diameter of 38 cm. For the interfacial area they found

$$A_v = \alpha \left(\frac{L \rho_L}{\Omega} \right)^{\beta} u_{sG}^{0.28} Z^{-0.38} \tag{14.3.5-1}$$

where u_{sG} is the superficial gas velocity, in cm/s, and Z is the effective height, in cm. The mass transfer rates are, of course, different from those encountered with single bubbles in rectilinear flow, and the following relation was obtained for k_G:

$$k_G = \gamma u_{sG}^{0.54} \tag{14.3.5-2}$$

In (14.3.5-1) and (14.3.5-2), α, β, and γ depend on the type of distributor (cone or shower) and the column diameter. With a shower, $\alpha = 2.46 \times 10^{-2}$, $\beta = 0.38$, and $\gamma = 1.02 \times 10^{-5}$. With a cone, α, β, and γ depend on the tower diameter, but average values may be 5×10^{-4}, 0.65, and 2×10^{-5}, respectively.

Liquid-liquid spray towers are less likely to find application as chemical reactors. In this case the dispersed phase flows upward and the continuous phase downward. Such towers have been thoroughly investigated by Letan and Kehat [1967; 1969a; b].

14.3.6 Bubble Reactors

Bubble reactors do not contain any packing and are fed by cocurrent or countercurrent gas and liquid streams. In general the chemical process requires a catalyst and this is fed continuously. Industrial bubble reactors are of the column type and generally contain an internal heat exchanger for controlling the temperature of the reaction mixture. The complex flow pattern of both phases achieves a reasonable mass transfer rate.

In recent years this type of reactor has been considered or selected for methanol synthesis [Tijm et al., 2001], Fischer-Tropsch synthesis [Krishna and Sie, 2000; Davis, 2002] and dimethylether synthesis [Fleisch et al., 2002, 2003; Fleisch and Sills, 2004; Ogawe et al., 2003].

The gas holdup in bubble columns has been measured by van Dierendonck [1970], who obtained the following correlation

$$\varepsilon = 1.2\left(\frac{\mu_L u_{sG}}{\sigma_L}\right)^{1/4}\left[\frac{u_{sG}}{\left(\frac{\sigma_L g}{\rho_L}\right)^{1/4}}\right]^{1/2} \qquad (14.3.6\text{-}1)$$

for $\varepsilon \leq 0.45$, $0.03 < u_{sG} < 0.4$ m/s, $0 \leq u_{sL} < 0.02$ m/s, $d_r > 0.15$ m, and $0.3 < Z/d_r < 3$. The correlation was also tested in industrial equipment for low-pressure polyethylene production, toluene oxidation, and cyclohexane oxidation, but was less reliable for the prediction of hydrogen holdup. The correlation leads to values of ε that agree with those of Towell et al. [1965], Calderbank and Moo-Young [1961], Yoshida and Miura [1963], and Reith [1968]. Further results were published by Letzel et al. [1999].

According to van Dierendonck, the bubble diameter is given by

$$\text{Eö}_b = \frac{d_b^2 \rho_L g}{\sigma_L} = c\left[\frac{u_{sG}}{\sqrt[4]{\frac{\sigma_L g}{\rho_L}}}\right]^{-(1/2)} \text{M}^{-(1/8)} \qquad (14.3.6\text{-}2)$$

where Eö_b is the Eötvös number, c = 6.25 for pure liquids and 2.1 for electrolytes, and $\text{M} = \sigma_L^3 \rho_L / \mu_L^4 g$. The bubble diameters calculated from this formula agree with those predicted by Yoshida and Miura [1963], Marucci and Nicodemo [1967], and Calderbank [1967]. The interfacial area is then obtained from

$$A_v' = \frac{6\varepsilon}{d_b} = 2\left[\frac{u_{sG}}{\sqrt[4]{\frac{\sigma_L g}{\rho_L}}}\right]\left(\frac{\rho_L g}{\sigma_L}\right)^{1/2} \qquad (14.3.6\text{-}3)$$

from which it can be seen that A_v' is independent of viscosity but varies linearly with the superficial gas velocity.

The mass transfer coefficient for the liquid phase is given by Calderbank [1967]:

$$k_L = 0.42 \sqrt[3]{\frac{\mu_L g}{\rho_L}} \sqrt{\frac{\rho_L D_{A_L}}{\mu_L}} \quad \text{for } d_b \geq 2 \text{ mm} \qquad (14.3.6\text{-}4)$$

so that k_L is independent of bubble size and velocity and depends only on the physical properties of the system. When d_b < 2 mm, van Dierendonck recommends

$$k_L = k_L(2 \text{ mm}) \times 500 d_b \text{ (in m/s)} \qquad (14.3.6\text{-}5)$$

The liquid flow pattern in a bubble column of 15 cm diameter was investigated by Kojura et al. [1974] at superficial liquid and gas velocities of the order of 1 cm/s. The liquid flow was found to be complicated and to vary continuously with time. The flow was mainly upward in the central part, but in other parts was both upward and downward, although mainly downward near the wall. Radial flow was present across the entire cross section as a result of the pumping effect of the wakes of bubble swarms: When the volume of liquid pumped per unit time by the wakes of the bubbles exceeds that of the liquid fed, downward flow has to occur, inducing radial flow. These observations confirm those of Towell and Ackerman [1972] who, in addition, expressed the mixing in terms of axial effective diffusivities for the liquid and gas phases. The authors add, however, that a more realistic model would have to contain a circulation pattern with a superimposed eddy diffusivity. The following dimensional correlations were derived from experiments in 16-in. and 42-in. bubble columns:

$$\text{Pe}_{aL} = \frac{u_{sL} Z}{(1-\varepsilon) D_{eL}} = \frac{u_{sL} Z}{73.5(1-\varepsilon) d_r^{1.5} u_{sG}^{0.5}} \qquad (14.3.6\text{-}6)$$

$$\text{Pe}_{aG} = \frac{u_{sG} Z}{\varepsilon D_{eG}} = \frac{Z}{19.7 \varepsilon d_r^2} \qquad (14.3.6\text{-}7)$$

Little effect of sparger type was observed, but the influence of the column diameter was very pronounced: the 42-in. column data were an order of magnitude higher than those of the 16-in. column. A draft tube increased the axial mixing at least two to threefold, while a horizontal disc and doughnut baffles reduced it by a factor of 3.

Typical Peclet numbers for the gas phase, based on the length as characteristic dimension, range from 2 to 15 and for the liquid phase from 0.10 to 0.16. The u_{sG} and u_{sL} are such that D_{eL} and D_{eG} are of the same magnitude. In fact, they are both high, so that the gas phase and the liquid phase are close to

complete mixing. The axial mixing characteristics of small laboratory reactors are vastly different from large-scale columns. The conditions in large reactors are close to complete mixing in both phases, whereas in small-diameter reactors they are almost invariably in plug flow with respect to the gas phase and can be either in plug flow or well mixed with respect to the liquid phase.

Scaling up of bubble columns is generally based on the requirement of keeping $k_L A_v^{'}$ constant. Since $k_L A_v^{'}$ is proportional to u_{sG}, this implies keeping the superficial gas velocity constant. Some design aspects of bubble reactors are illustrated in an example following the section on stirred vessel reactors.

EXAMPLE 14.3.6.A

SIMULATION OF A BUBBLE COLUMN REACTOR CONSIDERING DETAILED FLOW PATTERNS AND A FIRST-ORDER IRREVERSIBLE REACTION. COMPARISON WITH CONVENTIONAL DESIGN MODELS

As mentioned in Section 14.2.6, solving the Navier-Stokes equations allows accounting for the detailed flow patterns in multi-phase reactors. 3D simulations of a bubble column reactor in which a single first-order irreversible reaction $A \rightarrow B$ takes place were described by van Baten and Krishna [2004]. A 1 m diameter, 5 m high column was simulated. The superficial gas and liquid velocities at the inlet were respectively 0.04 m/s and 0.001 m/s. The inlet concentration of *A* was varied between 10 and 90%.

The model species, total mass, momentum, and energy continuity equations are similar to those presented in Section 13.7 on fluidized bed reactors. Constant values of the gas and liquid phase densities, viscosities, and diffusivities were assumed, as well as constant values of the interphase mass transfer coefficient and the reaction rate coefficient. The interphase momentum transfer was modelled in terms of the Eötvös number as in Clift et al. [1978]. The Reynolds-Averaged Navier-Stokes approach was taken and a standard Computational Fluid Dynamics solver was used. In the continuous liquid phase, turbulence, that is, fluctuations in the flow field at the micro-scale, was accounted for using a standard single phase k-ε model (see Chapter 12). Its applicability has been considered in detail by Sokolichin and Eigenberger [1999]. No turbulence model was used for the dispersed gas phase. Meso-scale fluctuations around the statistically stationary state occur and were explicitly calculated. This requires a transient simulation and sufficiently fine spatial and temporal grids.

The CFD simulation results were compared with conventional ideal flow reactor model predictions — combinations of plug flow and completely mixed

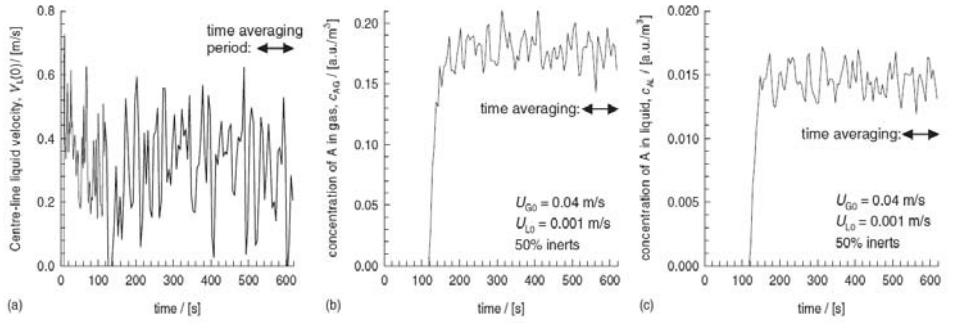

Figure 14.3.6.A-1

Transient calculation of the meso-scale fluctuations around a statistically stationary state. (a) Center-line liquid velocity; (b) concentration of *A* in the gas phase; (c) concentration of *A* in the liquid phase. Values at 4.5 m height at the center of the column. 50% inerts case. From van Baten and Krishna [2004].

reactor models as presented in Sections 14.2.1 – 14.2.3. To do so, the CFD data were a posteriori time averaged.

Figure 14.3.6.A-1 illustrates the transient calculation of the meso-scale fluctuations around a statistically stationary state and shows the a posteriori time-averaging period. Figure 14.3.6.A-2 shows radially averaged axial profiles of the concentration of *A* in the gas phase and in the liquid phase. The comparison with the conventional ideal flow models shows a behaviour typically between the extremes of plug flow and complete mixing, illustrating the importance of accounting for the details of the flow pattern.

An example of CFD simulation of a slurry bubble column reactor for the

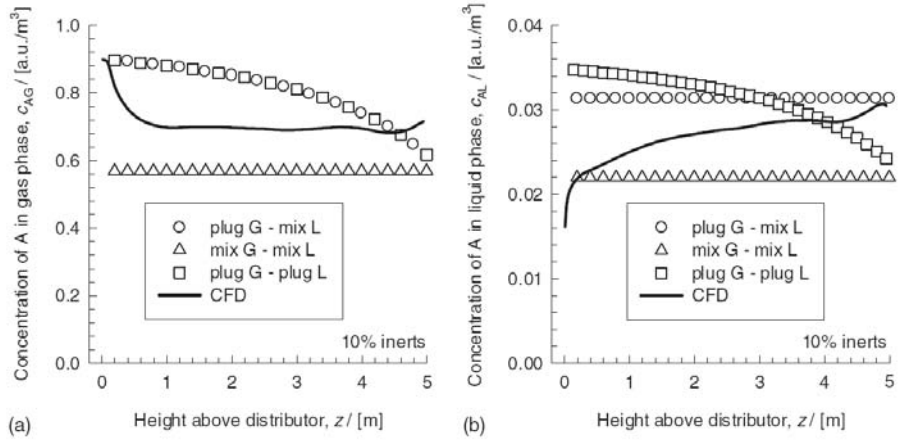

Figure 14.3.6.A-2

Radially averaged axial profiles of the concentration of *A* in (a) the gas phase and (b) the liquid phase. Comparison with conventional ideal flow models. 10% inerts case. From van Baten and Krishna [2004].

hydrodesulfurization of oil fractions was published by Matos et al. [2009]. Wang et al. [2006] simulated a 3000 T/year slurry bubble reactor for dimethyl ether synthesis combining CFD and the population balance method for the bubbles. They also published a review on this type of reactor [2007]. ■

14.3.7 Stirred Vessel Reactors

Agitated absorbers or reactors contain one or more stirrers mounted on a common shaft, depending on the height of the vessel. The influence of a stirrer extends to a height roughly equal to the vessel diameter. The stirrer diameter is generally taken to be one third of the vessel diameter. Stirred vessels also contain a certain number of vertical baffles, extending into the liquid for about one tenth of the tank diameter. Gas is distributed through some appropriate device into the liquid, underneath the lowest stirrer, but a certain amount of gas can also be aspirated into the liquid from the gas phase above the liquid level by means of a special stirrer. An example of such a gas-filled reactor is shown schematically in Fig. 14.3.7-1. This reactor, described by van Dierendonck and Nelemans [1972], is used for the hydrogenation of α-nitrocaprolactam into aminolactam, a step of the Dutch State Mines $_{L}$-lysine process. This is a semibatch reaction carried out at 20 to 30 bar and 85°C with a Raney nickel catalyst in a vessel with a volume of 9 m³. The gas phase was shown to be completely mixed.

Zwietering [1963] determined the maximum gas flow rate F'_{max} (in m³/h) that can be handled by a stirrer of given geometry rotating at a certain speed. The

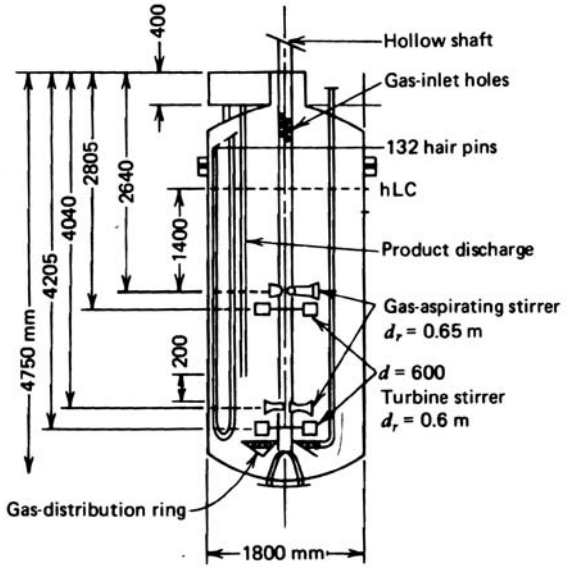

Figure 14.3.7-1
Stirred vessel for hydrogenation. From van Dierendonck and Nelemans [1972].

relation is as follows:

$$F'_{\max} = 16\frac{N^3 d_r^4}{g}\left(\frac{d_s}{d_r}\right)^{3.3} \tag{14.3.7-1}$$

According to van Dierendonck [1970; 1971], the bubble diameter can be obtained from the following relationships:

1. For pure liquids:

$$\text{Eö}_b = \frac{d_b^2(\rho_L - \rho_g)g}{\sigma_L} = 0.41 \tag{14.3.7-2}$$

and for stirred speeds $N > 25\,N_0^*$, where N_0^* is the characteristic speed for bubble aspiration and dispersion from the gas atmosphere above the liquid level. N_0^* is given by

$$\frac{N_0^* d_s^2}{\sqrt[4]{\frac{\sigma_L g}{\rho_L}}\,d_r} = 2\left(\frac{H_L - H_s}{d_r}\right)^{1/2} \tag{14.3.7-3}$$

where $H_L - H_s$ is the liquid height above the stirrer in the absence of gas flow.

2. For solutions of electrolytes and surface active agents:

$$\text{Eö}_b = \left[1.2 + 260\frac{\mu_L(N - N_0)d_s}{\sigma_L}\right]^{-2} \tag{14.3.7-4}$$

for $0 < (N - N_0)d_s < 1.5$ m/s, where N_0 is the minimum stirrer speed for efficient dispersion (i.e., the stirrer speed at which the bubble trajectories are markedly influenced).

N_0 is given by the following relationships:

1. For pure liquids:

$$\frac{N_0 d_s^2}{d_r\sqrt{g d_r}} = 0.07 \tag{14.3.7-5}$$

2. For solutions of electrolytes and surface-active agents:

$$\frac{N_0 d_s^2}{\sqrt[4]{\frac{\sigma_L g}{\rho_L}}\,d_r} = 1 \tag{14.3.7-6}$$

According to Calderbank [1967], in the case of pure liquids the bubble diameter is given by

$$d_b = 4.15\left[\frac{\sigma_L^{0.6}}{\left(\frac{P}{\varepsilon_L V}\right)^{0.4}\rho_L^{0.2}}\right]\varepsilon^{1/2} + 0.09 \quad \text{(in cm)} \qquad (14.3.7\text{-}7)$$

The gas holdup in pure liquids is obtained from [Calderbank, 1967]

$$\varepsilon_G = \left(\frac{\varepsilon u_{sG}}{u_b}\right)^{1/2} + 0.0216\left[\frac{(P/\varepsilon_L V)^{0.4}\rho_L^{0.2}}{\sigma_L^{0.6}}\right]\left(\frac{u_{sG}}{u_b}\right)^{1/2} \qquad (14.3.7\text{-}8)$$

where P is the power input, $P/\varepsilon_L V$ is the power input per unit liquid volume, and u_b is the free-rising velocity of the bubble, calculated from the Davies and Taylor equation [Davies and Taylor, 1950]

$$u_b = 0.711(gd_b)^{1/2}$$

For the holdup, van Dierendonck proposed

1. With pure liquids:

$$\varepsilon_G = 0.31\left(\frac{u_{sG}}{\sqrt[4]{\frac{\sigma_L g}{\rho_L}}}\right)^{2/3} + 0.45\frac{\left(N - N_0^*\right)d_s^2}{d_r\sqrt{gd_r}} \qquad (14.3.7\text{-}9)$$

provided $\varepsilon < 0.25$, $0 < u_{sG} < 0.05$ m/s, $Z/d_r = 1$, and $H_L - H_S = 0.5H_L$.

2. With solutions

$$\varepsilon_G = 0.075\frac{\left(N - N_0^*\right)d_s^2}{\sqrt[4]{\frac{\sigma_L g}{\rho_L}}d_r}\left(\frac{d_r}{H_L}\right) \qquad (14.3.7\text{-}10)$$

provided $\varepsilon \leq 0.3$, $0.003 < u_{sG} < 0.03$ m/s, $0.7 < H_L/d_r < 1.4$, and $H_L - H_S = 0.5H_L$. The interfacial area per unit dispersion volume is then easily derived from the relation $A_v' = 6(\varepsilon/d_b)$. Reith [1970] compared interfacial areas determined by different methods and found quite a discrepancy between the results.

With pure liquids, the mass transfer coefficient for the component *A* in the liquid is practically independent of the stirrer speed, since the bubble size is practically unaffected by the stirrer speed. Van Dierendonck proposed

$$k_L = 0.42\sqrt[3]{\frac{\mu_L g}{\rho_L}}\,\mathrm{Sc}^{-(1/2)} \quad (\text{in } \mathrm{m_L^3/m_i^2\,s}) \tag{14.3.7-11}$$

The bubble size does vary with the stirrer speed for solutions of electrolytes and surface-active agents. In that case, k_L is given by

$$\frac{1}{k_L} = \frac{1}{(k_L)_0}\left[1.2 + 260\frac{\mu_L}{\sigma_L}(N - N_0)d_s\right] \tag{14.3.7-12}$$

with

$$(k_L)_0 = 1.13\sqrt{\frac{D_{A_L} u_b}{d_{b0}}}$$

$$d_{b0} = 0.08\sqrt{\frac{\sigma_L}{\rho_L g}}$$

where $(k_L)_0$ is the mass transfer coefficient of *A* on the liquid side when $N = N_0$ (i.e., at zero stirring or at very low stirrer speed) and d_{b0} is the corresponding bubble diameter. The bubble rising velocity, u_b is calculated from

$$\begin{aligned} u_b &= \frac{1}{18}\frac{\rho_L g d_b^2}{\mu_L} \quad (\text{Stokes' law}) \text{ when } \mathrm{Re}_b < 1 \\ &= \frac{1}{4} d_b \sqrt[3]{\frac{(\rho_L - \rho_g)^2 g^2}{\rho_L \mu_L}} \quad \text{when } 30 < \mathrm{Re}_b < 10^3 \\ &= 1.76\sqrt{\frac{(\rho_L - \rho_g) g d_b}{\rho_L}} \quad \text{when } \mathrm{Re}_b > 10^3 \end{aligned} \tag{14.3.7-13}$$

Since the expression between the square brackets in the right-hand side of the equation for $1/k_L$ is nothing but $(\mathrm{Eö}_b)^{-(1/2)}$, it follows that k_L/d_b is a constant, at least when $0 < (N - N_0)d_s < 1.5$ m/s. Hughmark [1971] obtained the following correlation for $(k_L)_0$, for single bubbles, however:

$$\mathrm{Sh} = 2.0 + 0.061\left(\mathrm{Re}_b^{0.48}\,\mathrm{Sc}^{0.34}\,\frac{d_b g^{1/3}}{D_{A_L}^{2/3}}\right)^{1.61} \tag{14.3.7-14}$$

where

$$\mathrm{Sh} = \frac{k_L d_b}{D_{A_L}} \qquad \mathrm{Re}_b = \frac{d_b G}{\mu_G} \qquad \mathrm{Sc} = \frac{\mu_L}{\rho_L D_{A_L}}$$

The turbulence in the bubbles is usually very high, so that the mass transfer resistance in the gas phase may be neglected. For the usual stirrer speeds the mixing in the gas and the liquid phases is practically complete. The mixing time in the liquid phase is independent of the gas holdup and is given by [van Dierendonck, 1970]

$$Nt_m \left(\frac{d_s}{d_r} \right)^2 = 1.7 \qquad (14.3.7\text{-}15)$$

for $u_{sG} < 0.05$ m/s, $d_r < 1$ m, and $0.2 < d_s/d_r < 0.5$. The mixing time has to be smaller than the effective absorption time $\left(k_L A_v\right)^{-1}$ if the liquid phase is to be considered as completely mixed.

The power requirements are given by

$$P = c\rho_L N^3 d_s^5$$

with c a characteristic constant depending on the stirrer construction.

According to van Dierendonck [1970], scaling up has to be based on a constant value of the reduced effective stirring speed $(N - N_0)\, d_s^2 / d_r$, which ensures a constant value for the gas holdup ε. A second condition is to avoid overloading the stirrer; see (14.3.7-1). Therefore, u_{sG} should generally not exceed 0.03 m/s. According to Reith [1968], however, a safe design rule is to scale up on the basis of constant specific power input, to ensure constant specific interfacial area. Van Dierendonck discusses those two rules and refers to the design of a stirred vessel for the hydrogenation of α-nitrocaprolactam. The effective stirring speed criterion led to an industrial reactor with a volume of 6 m³, a stirrer diameter of 0.5 m, and 3.5 revolutions per second, whose performance was successful. The constant specific power input criterion would have led to a volume of 20 m³.

From the correlations given above, it is also evident that the liquid composition has an important effect on the interfacial area. All other conditions being equal, the area may be a factor 10 larger in electrolytes than in pure liquids. Evidently, the design and scaling up of stirred gas-liquid reactors still relies on model experiments involving the liquids actually used in the reaction.

EXAMPLE 14.3.7.A

DESIGN OF A LIQUID-PHASE *O*-XYLENE OXIDATION REACTOR

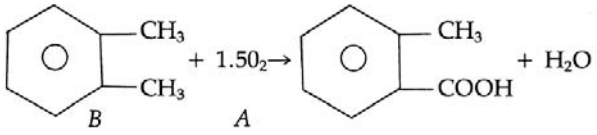

Continuous Stirred Tank Reactor

The liquid-phase oxidation of *o*-xylene into *o*-methylbenzoic acid by means of air is to be carried out in a continuous stirred tank reactor at 13.8 bar and 160°C. A yearly production of *o*-methylbenzoic acid of 30,000 tons is required. For reasons of selectivity, the *o*-xylene conversion per pass has to be limited to 16 percent. An excess of 25 percent with respect to the stoichiometric requirements is chosen for the oxygen feed rate. The rate equation is of pseudo-first order with respect to oxygen:

$$r_B = 2.4 \times 10^3 C_A$$

where r_B, in kmol/m³ h, is the rate of reaction of *o*-xylene and C_A, in kmol/m³, is the oxygen concentration. From the stoichiometry it follows that the rate based on oxygen consumption is given by $r_A = 1.5\, r_B$.

Calculate the reactor dimensions and the stirrer speed. The basic data for this example follows:

> For *o*-xylene: M = 106.16 kg/kmol, ρ_L = 750 kg/m³, $\sigma_L = 16.5 \times 10^{-3}$ kg/s², $\mu_L = 0.23 \times 10^{-3}$ kg/m s = 0.828 kg/m h, $D = 2.45 \times 10^{-6}$ m²/h.
> For oxygen: $D(O_2/\text{xylene}) = 5.2 \times 10^{-6}$ m²/h. Henry's constant H = 126.6 m³ bar/kmol.

The calculation of the reactor volume requires the oxygen mass transfer coefficient and the interfacial area to be known. This, in turn, necessitates knowledge of the stirrer speed. It was shown in Section 14.3.7, however, how the choice of the stirrer speed depends on the reactor dimensions and geometry, so that the design has an iterative character: a reactor diameter is chosen first; then the stirrer speed is derived from this; and finally the reactor volume required to achieve the desired conversion is calculated. The resulting reactor diameter is compared with the initially chosen value.

The model worked out in Section 14.2.1, with the gas and liquid phases completely mixed, is adopted here.

The initial choice of the reactor diameter can be oriented as follows, by way of example. Suppose the concentration of *A* in the liquid is in equilibrium

with that in the gas phase, that is, $(C_A)_{out} = (p_A)_{out}/H$. Consider the overall material balance for gas and liquid completely mixed, (14.2.1-2):

$$\frac{F}{p_t}\left[(p_A)_{in} - (p_A)_{out}\right] = \frac{a}{b} L\left[(C_B)_{in} - (C_B)_{out}\right] + L(C_A)_{out} \qquad (14.3.7.A\text{-a})$$

whereas a balance on B can be written

$$L\left[(C_B)_{in} - (C_B)_{out}\right] = r_B \cdot V(1-\varepsilon) \qquad (14.3.7.A\text{-b})$$

First determine the flow rates to be substitued into these equations.

Yearly production: 30×10^3 tons (for 8000 h)

Hourly production: 3750 kg/h = 27.5 kmol/h

o-Xylene feed rate (fresh + recycle): 27.5/0.16 = 172 kmol/h, from which $L = (172 \times 106.16)/750 = 24.4$ m³/h.

Oxygen consumption: 1.5 mol/mol xylene converted, so the total consumption is $27.5 \times 1.5 = 41.25$ kmol/h.

Oxygen feed rate (25 percent excess): $41.25 \times 1.25 = 51.5$ kmol/h.

Air feed rate at reaction conditions: $F' = (51.5/0.21) \times 22.4 \times (433/273) \times (1/13.6) = 640$ m³/h; also $F = 245$ kmol/h.

At this point, however, ε is not yet known. One way out is to drop the term $(1 - \varepsilon)$ from (14.3.7.A-b) for this first estimation. With $L = 24.4$ m³/h, $L[(C_B)_{in} - (C_B)_{out}] = 27.5$ kmol/h, $F' = 640$ m³/h, $p_t = 13.8$ bar, $(p_A)_{in} = 13.8 \times 0.21 = 2.9$ bar, (14.3.7.A-a) yields $(p_A)_{out} = 0.5547$ bar. Assuming equilibrium between the gas and liquid phases, $(C_A)_{out} = 4.37 \times 10^{-3}$ kmol/m³. Equation (14.3.7.A-b) then yields $V = 2.62$ m³. When the height equals the diameter, $d_r = 1.49$ m and the cross section $\Omega = 1.75$ m². Choose the stirrer diameter according to $d_s = d_r/3$, so that $d_s = 0.5$ m and the position of the stirrer $H_L - H_S = 1/2$ (liquid height without gas holdup).

The characteristic speed for bubble aspiration, N_0^* is obtained from (14.3.7-3):

$$N_0^* = 2\sqrt[4]{\frac{\sigma_L g}{\rho_L}}\frac{d_r}{d_s^2}\left(\frac{H_L - H_s}{H_L}\right)^{1/2}$$

$$= 2\sqrt[4]{\frac{16.5\times10^{-3}\times9.81}{750}} \times \frac{1.49}{(0.5)^2} \times \left(\frac{1}{2}\right)^{1/2} = 1.01 \text{ rev/s}$$

The minimum stirrer speed that can effectively disperse the gas flow rate is given by Zwietering's relationship, (14.3.7-1):

$$N_{\min} = \left[\frac{F'}{16} \frac{g\left(\frac{d_r}{d_s}\right)^{3.3}}{d_s^4} \right]^{1/3} = \left[\frac{640 \times 9.81 \times 3^{3.3}}{16 \times 3600 \times (0.5)^4} \right]^{1/3} = 4.028 \text{ rev/s}$$

Van Dierendonck advises taking the stirrer speed higher than either N_0^* or $N_{\min}$, so that a value of 4.1 rev/s will be chosen in this case.

According to van Dierendonck, for stirrer speeds > 2.5 N_0^* the Eötvös number equals 0.41, so that (14.3.7-2) yields for the bubble diameter

$$d_b = \sqrt{\frac{\text{Eö}_b \sigma_L}{g(\rho_L - \rho_g)}} = \sqrt{\frac{0.41 \times 16.5 \times 10^{-3}}{9.81 \times 737.8}} = 0.965 \times 10^{-3} \text{ m}$$

For pure liquids, (14.3.7-9) can be used to calculate the gas hold up

$$\varepsilon = 0.31 \left(\frac{u_{sG}}{\sqrt[4]{\frac{\sigma_L g}{\rho_L}}} \right)^{2/3} + 0.45 \frac{(N - N_0^*) d_s^2}{d_r \sqrt{g d_r}}$$

$$u_{sG} = \frac{640}{3600 \times 2.05} = 0.1016 \text{ m}_G^3 / \text{m}_r^2 \text{s}$$

so that

$$\varepsilon = 0.31 \left(\frac{0.1016}{0.121} \right)^{2/3} + 0.45 \frac{(4.1 - 1.01)(0.805)^2}{1.49\sqrt{9.81 \times 1.49}} = 0.336$$

The mass transfer coefficient follows from (14.3.7-11)

$$k_L = 0.42 \sqrt[3]{\frac{\mu_L g}{\rho_L}} \sqrt{\frac{D_{A_L} \rho_L}{\mu_L}} = 0.42 \sqrt[3]{\frac{0.23 \times 10^{-3} \times 9.81}{750}} \sqrt{\frac{5.2 \times 10^{-6} \times 750}{0.828}}$$

$$k_L = 1.485 \text{ m}_L^3 / \text{m}_i^2 \text{ h}$$

and the interfacial area from:

$$A_v' = \frac{6\varepsilon}{d_b} = A_v(1-\varepsilon) = \frac{6\times 0.336}{0.965\times 10^{-3}} = 2089 \ \ \mathrm{m}_i^2/\mathrm{m}_{L+G}^3$$

When the gas and liquid are completely mixed the three equations to be used are (14.2.1-1), (14.2.1-2), and (14.2.1-3):

$$\frac{F}{p_t}\left[(p_A)_{\text{in}} - (p_A)_{\text{out}}\right] = N_{A|_{y=0}} A_v V(1-\varepsilon) \qquad \text{(14.3.7.A-c)}$$

$$\frac{F}{p_t}\left[(p_A)_{\text{in}} - (p_A)_{\text{out}}\right] = \frac{a}{b} L\left[(C_B)_{\text{in}} - (C_B)_{\text{out}}\right] + L(C_A)_{\text{out}} \qquad \text{(14.3.7.A-d)}$$

$$N_{A|_{y=yL}} A_v V(1-\varepsilon) = r_A(1 - A_v y_L)V(1-\varepsilon) + L(C_A)_{\text{out}} \qquad \text{(14.3.7.A-e)}$$

For a pseudo-first-order irreversible reaction,

$$N_{A|_{y=0}} = \frac{k_L\gamma}{\sinh\gamma}(C_{Ai}\cosh\gamma - C_A)$$

which is (6.3.2-3), whereas $N_{A|_{y=yL}}$ is easily derived from (6.3.2-2):

$$N_{A|_{y=yL}} = \frac{k_L\gamma}{\sinh\gamma}(C_{Ai} - C_A\cosh\gamma)$$

Equations (14.3.7.A-c), (14.3.7.A-d), and (14.3.7.A-e) allow V, $(C_A)_{\text{out}}$, and $(p_A)_{\text{out}}$ to be determined. From (14.3.7.A-d), it follows that

$$(p_A)_{\text{out}} = 0.57 - 1.37(C_A)_{\text{out}} \qquad \text{(14.3.7.A-f)}$$

It is assumed that there is no partial pressure drop in the gas phase, so that in (14.3.7.A-c) and (14.3.7.A-e), $C_{Ai} = (p_A)_{\text{out}}/H$. Furthermore, $\gamma = \sqrt{kD_{AL}}/k_L = 9.2 \times 10^{-2}$, so that $\sinh\gamma = \gamma$ and $\cosh\gamma = 1$. Now, substituting (14.3.7.A-f) into (14.3.7.A-c) and (14.3.7.A-e) leads to

$$\frac{245}{13.8}\left[2.33 + 1.37(C_A)_{\text{out}}\right] = 1.485\left[\frac{0.576 - 1.37(C_A)_{out}}{126.6} - (C_A)_{\text{out}}\right]2089V$$

and

$$1.485\left[\frac{0.57 - 1.37(C_A)_{\text{out}}}{126.6} - (C_A)_{\text{out}}\right]2089V$$

$$= 1.5\times 2.4\times 10^3 (C_A)_{\text{out}} \times 0.664V + 24.4(C_A)_{\text{out}}$$

from which

$$(C_A)_{out} = \frac{0.7833V - 2.29}{1.35 + 173.9V} \qquad (14.3.7.A\text{-g})$$

and

$$(C_A)_{out} = \frac{14.145V}{5526V + 24.4} \qquad (14.3.7.A\text{-h})$$

From (14.3.7.A-g) and (14.3.7.A-h), a quadratic in V is obtained, leading to V = 6.776 m³. $(C_A)_{out}$ is found to be 2.56×10^{-3} kmol/m³ and $(p_A)_{out}$ = 0.573 bar. With the diameter = height of the dispersion, a value of 2.05 m is found for the diameter. These values are the initial values for a second iteration. The final result, corresponding to a reasonable convergence, V = 7.1 m³, d_r = 2.08 m, N = 2.7 rev/s, $(C_A)_{out} = 2.24 \times 10^{-3}$ kmol/m³, and $(p_A)_{out}$ = 0.574 bar.

Bubble Reactor

Suppose the *o*-xylene oxidation were carried out in a nonstirred vessel — a bubble reactor.

The model worked out in Section 14.2.3, with the gas phase in plug flow and the liquid phase completely mixed will be applied here.

First, an initial choice of cross section, liquid height and oxygen concentration has to be made.

Let d_r = 2 m so that Ω = 3.14 m² and $(C_A)_{out} = 2.04 \times 10^{-3}$, kmol/m³.

From the approximate relation

$$L\left[(C_B)_{in} - (C_B)_{out}\right] = r_B V(1-\varepsilon) \qquad (14.3.7.A\text{-i})$$

$$V(1-\varepsilon) = \frac{27.5}{2.4 \times 10^3 \times 2.04 \times 10^{-3}} = 5.616 \text{ m}^3$$

which is the volume of the liquid phase only. The superficial gas velocity would then be

$$u_{sG} = \frac{640}{3600 \times 3.14} = 0.0566 \text{ m/s}$$

The bubble diameter is calculated from (14.3.6-2),

$$d_b = \sqrt{\frac{\sigma_L}{\rho_L g} 6.25 \left(\frac{u_{sG}}{\sqrt[4]{\frac{\sigma_L g}{\rho_L}}} \right)^{-(1/2)} \left(\frac{\rho_L \sigma_L^3}{g \mu_L^4} \right)^{-(1/8)}}$$

$$d_b = 0.516\times10^{-3}u_{sG}^{-(1/4)} = 1.05\times10^{-3}\ \text{m}$$

and the gas hold up from (14.3.6-1),

$$\varepsilon = 1.2\left(\frac{\mu_L}{\sigma_L}\right)^{1/4}\left(\frac{\sigma_L g}{\rho_L}\right)^{-(1/8)} u_{sG}^{3/4}$$

$$\varepsilon = 1.18u_{sG}^{3/4} = 0.137$$

From (14.3.6-4) and (14.3.6-5),

$$k_L = 500d_b \times 0.42\sqrt[3]{\frac{\mu_L g}{\rho_L}}\left(\frac{D_{A_L}\rho_L}{\mu_L}\right)^{1/2}$$

$$= 0.207d_b \quad \text{m}_L^3/\text{m}_i^2\text{s}$$

$$= 2.17\times10^{-4} \quad \text{m}_L^3/\text{m}_i^2\text{s}$$

$$= 0.781 \quad \text{m}_L^3/\text{m}_i^2\text{h}$$

and from (14.3.6-3), the interfacial area is obtained:

$$A_v^{'} = A_v(1-\varepsilon) = \frac{6\varepsilon}{d_b} = \frac{6\times0.137}{1.05\times10^{-3}} = 782 \quad \text{m}_i^2/\text{m}_r^3$$

To calculate the reactor dimensions, (14.3.2-1), (14.2.3-2) and (14.2.3-3) are written

$$-\frac{F}{p_t}dp_A = N_{A|_{y=0}}A_v(1-\varepsilon)\Omega dz$$

$$\frac{F}{p_t}\left[(p_A)_{\text{in}} - (p_A)_{\text{out}}\right] = \frac{a}{b}L\left[(C_B)_{\text{in}} - (C_B)_{\text{out}}\right] + L(C_A)_{\text{out}}$$

$$\int_0^Z N_{A|_{y=y_L}}A_v\Omega(1-\varepsilon)dz = r_A(1-A_v y_L)V(1-\varepsilon) + L(C_A)_{\text{out}}$$

Equation (14.2.3-1) becomes, with N_A from (6.3.2-2) and in the absence of a Δp in the gas phase,

$$\int_{(p_A)_{\text{in}}}^{(p_A)_{\text{out}}} \frac{dp_A}{p_A - \dfrac{H(C_A)_{\text{out}}}{\cosh\gamma}} = \frac{k_L\gamma\cosh\gamma\, p_t A_v(1-\varepsilon)\Omega Z}{HF\sinh\gamma}$$

$(p_A)_{out}$ is not yet known, but may be calculated from (14.2.3-2):

$$(p_A)_{out} = (p_A)_{in} - \frac{p_t}{F}\left\{\frac{a}{b}L[(C_B)_{in} - (C_B)_{out}] + L(C_A)_{out}\right\}$$

so that

$$(p_A)_{out} = 2.90 - \frac{13.8}{245}\left(41.25 + 24.4 \times 2.04 \times 10^{-3}\right) = 0.577 \text{ bar}$$

Since

$$\gamma = \frac{\sqrt{kD_{A_L}}}{k_L} = \frac{\sqrt{1.5 \times 2.4 \times 10^3 \times 5.2 \times 10^{-6}}}{0.781} = 0.175$$

Z can now be calculated

$$Z = \frac{126.6 \times 245 \times 0.175}{0.781 \times 0.175 \times 1.01 \times 13.8 \times 782 \times 3.14} \ln \frac{2.90 - \dfrac{2.04 \times 10^{-3} \times 126.6}{1.01}}{0.577 - \dfrac{2.04 \times 10^{-3} \times 126.6}{1.01}}$$

$$= 2.43 \text{ m} \qquad (14.3.7.\text{A-j})$$

This is a first estimate for the height of the dispersion of gas + liquid. The total volume is 7.63 m³. A better estimate for $(C_A)_{out}$ is obtained from (14.3.7.A-i) in which ε can now be better approximated:

$$(C_A)_{out} = \frac{27.5}{2.4 \times 10^3 \times 3.14 \times 0.863 \times 2.43} = 1.74 \times 10^{-3} \text{ kmol/m}^3$$

A more accurate value for Z is now calculated from (14.3.7.A-j)

$$Z = 1.16 \ \ln \frac{2.86 - 0.215}{0.57 - 0.215} = 2.32 \text{ m}$$

A further estimate for $(C_A)_{out}$ is 1.82×10^{-3} kmol/m³, from which $Z = 2.35$ m. These values may be considered as final

The total volume gas and liquid is 7.38 m³—only slightly more than in the stirred case, whereas $(C_A)_{out}$ is even lower. This is easily explained on the basis of the model, which assumes plug flow for the gas in the nonstirred case, against complete mixing in the stirred case. Some design aspects of a continuous stirred tank for the liquid-phase oxidation of toluene into phenol have been discussed by van Dierendonck et al. [1974]. ■

It is appropriate to conclude this chapter with a reference to the very complete literature review and discussion by Dudukovic et al. [1999].

PROBLEMS

14.1 Calculate the pressure drop for a trickle bed reactor in which air and water flow down at room temperature through a packed bed of glass beads (0.2 cm diameter). The superficial gas and liquid velocities are 5 and 0.2 cm/s, respectively. The void fraction of the bed is 0.4. Use the correlations presented in Section 14.3.2 and compare the results.

14.2 Calculate the liquid holdup for the case considered in the previous problem.

14.3 Check by means of Fig. 14.3.2-2 in which regime the reactor described in Problem 1 operates.

14.4 Design of a packed column for carbon dioxide absorption. After Danckwerts and Sharma [1966].

Carbon dioxide is to be absorbed at 20.3 bar and 30°C from a gas stream of 900 kmol/h with the following molar properties: $N_2/H_2/CO_2$: 1/3/1.33 by means of a 2.5-molar monoethanolamine (MEA) solution:

$$CO_2 + 2R_2NH \rightarrow R_2NCOO^- + R_2N\,H_2^+$$

The CO_2 content is to be reduced to 2×10^{-3} percent. The amount of dissolved CO_2 in the MEA will be 0.15 and 0.40 mol CO_2/mol MEA at the top and bottom of the column, respectively. A column packed with $1\frac{1}{2}$ in Rashig rings will be used. The model is that of Section 14.2.2, which assumes the gas and the liquid to be in plug flow. Furthermore, since the reaction is very rapid, the bulk concentration of *A* may be taken to be zero. Choose a column diameter of 2.75 m, giving a gas mass flow rate of about half the flooding value calculated from Fig. 14.3.1-1.

14.5 Design of a packed bed absorber for the absorption of ammonia in sulfuric acid. After Ramm [1953].

The reaction may be considered to be instantaneous. The inlet partial pressure of ammonia in the gas entering the absorber at essentially atmospheric pressure is 0.051 bar, the exit partial pressure is to be 0.0101 bar. The total gas flow rate is 45 kmol/h. The liquid phase enters the column at the top and flows countercurrently with the gas at a rate of 9 m^3/h. The inlet concentration of sulfuric acid is 0.6 $kmol/m^3$. The

absorber operates isothermally at 25°C. Determine the exit concentration of sulfuric acid, the required interfacial area, and the height. Take k_G = 0.35 kmol/m² h bar, k_L = 0.005 m/h, and H = 76.33 m³ bar/kmol. (Remember that the reaction occurs in a plane located either in the liquid film or at the interphase.)

REFERENCES

Asano, K., and Fujita, S., *Kagaku Kogaku*, 4(2), 369 (1966).
Astarita, G., Savage, D.W., and Bisio, A, *Gas Treating with Chemical Solvents*, Wiley-Interscience, N.Y. (1983).
Biswas, J., Bhasku, G.V., and Greenfeld, P.F., *AIChE J.*, 34, 510 (1988).
Bondi, A, *Chem. Tech.*, 1, 185 (March 1971).
Böxkes, W., "Systemanalyse bei chemischen Reaktoren durchgeführt am Beispiel einer Zweiphasenaufstromkolonne," Ph.D. Thesis, Erlangen University, Germany (1969).
Bubble Tray Manual, *AIChE J.*, New York (1958).
Buchanan, J.E., *Ind. Eng. Chem. Fundam.*, 6, 400 (1967).
Calderbank, P.H., *The Chemical Engineer*, No. 212, CE209 (1967a).
Calderbank, P.H., in *Mixing, Theory and Practice*, Vol. II, ed. by V.W. Uhl and J.B. Gray, Academic Press, New York (1967b).
Calderbank, P.H., and Moo-Young, M.B., *Chem. Eng. Sci.*, 16, 39 (1961).
Charon-Revellin, N., Dulot, H., López-García, C., and Jose, J., Oil and Gas Science and Technology-Revue de l'Institut Français du Pétrole, (2010).
Charpentier, J.C., *Chem. Eng. J.*, 11, 161 (1976).
Charpentier, J.C., *Trans. Inst. Chem. Eng.*, 60, 131 (1982).
Charpentier, J.C., and Favier, M., *AIChE J.*, 21, 1213 (1975).
Charpentier, J.C., and Laurent, A., *AIChE J.*, 20, 1029 (1974).
Charpentier, J.C., Prost, C., and Le Goff, P., *Chem. Eng. Sci.*, 24, 1777 (1969).
Charpentier, J.C., Prost, C., Van Swaay, W., and Le Goff, P., *Chim. & Ind.-Gén. Chim.*, 99, 803 (1968).
Chen, J., Li, F., Degaleesan, S., Gupta, P., Al-Dahhan, M.H., Dudukovic, M.P., and Toseland, B.A., *Chem. Eng. Sci.*, 54, 2137 (1999).
Christensen, G., McGovern, S.J., and Sundaresan, S., *AIChE J.*, 32, 1677 (1986).
Clift, R., Grace, J.R., and Weber, M.E., *Bubbles, Drops and Particles*, Academic Press, San Diego, CA (1978).
Danckwerts, P.V., *Gas-Liquid Reactions*, McGraw Hill, New York (1970).
Danckwerts, P.V., and Gilham, A.J., *Trans. Inst. Chem. Eng.*, 44, T42 (1966).
Danckwerts, P.V., and Sharma, M.M., *The Chemical Engineer*, No. 202, CE244 (1966).
Davies, R.M., and Taylor, G.I., *Proc. R. Soc. London*, A200, 375 (1950).
Davis, B.H., Catal. Today, 78, 249 (2002).
De Leye, L., and Froment, G.F., *Computer & Chem. Eng.*, 10(5), 493 (1986a); 10(5), 505 (1986b).
Dimenstein, D.M., and Ng., K.M., *Chem. Eng. Comm.*, 41, 215 (1986).
Dudukovic, M.P., Larachi, F., and Mills, P.L., *Chem. Eng. Sci.*, 54, 1975 (1999).
Eckert, J.S., *Chem. Eng. Progr.*, 66(3), 39 (1970).
Elenkov, D., and Kolev, M., *Chem. Ing. Techn.*, 44, 845 (1972).
El-Hisnawi, A.A., Dudukovic, M.P., and Mills, P.L., *A.C.S. Symp. Ser.*, 196, 421 (1981).
Fleisch, T.H., Sills, R.A., and Briscoe, M.D., *J. Nat. Gas Chem.*, 11, 1 (2002); 12, 219 (2003).
Fleisch, T.H., and Sills, R.A., *Nat. Gas. Conv. VII*, 147, 31 (2004).
Gates, L.E., Morton, J.R., and Fondy, P.L., *Chem. Eng.*, 144, May 24 (1976).
Gianetto, A., Specchia, V., and Baldi, G., *AIChE J.*, 19, 916 (1973).
Gianetto, A., Specchia, V., *Chem. Eng. Sci.*, 47, 3197 (1992).
Goto, S., and Smith, J.M., *AIChE J.*, 21, 706 (1975).
Heilman, W., "Zur Hydrodynamik zweiphasig durchströmten Schüttschichten," Ph.D. Thesis, Erlangen University (1969).

Henry, H.C., and Gilbert, J.B., *Ind. Eng. Chem. Proc. Des. Dev.*, 12, 328 (1973).
Hicks, R.W., and Gates, L.E., *Chem. Eng.*, 141, July 19 (1976).
Hikita, H., and Asai, S., *Int. J. Chem. Eng.*, 4, 332 (1966).
Hikita, H., Asai, S., Ishikowa, H., and Honda, M., *Chem. Eng. J.*, 13, 7 (1977).
Hikita, H., Asai, S., and Takatsuka, H., *Chem. Eng. J.*, 11, 131 (1976).
Hochman, J.M., and Effron, E., *Ind. Eng. Chem. Fundam.*, 8, 63 (1969).
Hofmann, H., *Chem. Ing. Techn.*, 47, 823 (1975).
Hofmann, H., *Chem. Ing. Techn.*, 54, 865 (1982).
Hudebine, D., and Verstraete, J.J., Chem. Eng. Sci., 59, 4755-4763 (2004).
Hughmark, G.A., *AIChE J.*, 47, 1295 (1971).
Kirillov, V.A., and Orgakov, B.L., *Int. Chem. Eng.*, 20, 478 (1980).
Kojuna, E., Akehata, T., and Shirai, T., *Adv. Chem. Ser.*, 133, 131 (1974).
Kölbel, H., *Dechema Monographien*, 68, 35 (1971).
Koukolik, M., and Marek, J., in *Proc. 4th Eur. Symp. Chem. React. Eng.*, Brussels, 1968, Pergamon Press, Oxford (1971).
Krishna, R., and Sie, S.T., Fuel Proc. Techn., 64, 73 (2000).
Kumar, H., and Froment, G.F., *Ind. Eng. Chem. Res.*, 46, 18, 5881 (2007).
Larkins, R.P., White, R.R., and Jeffrey, D.W., *AIChE J.*, 7, 231 (1961).
Laurent, A., and Charpentier, J.C., *Chem. Eng.*, 8, 85 (1974).
Lee, E.S., *Quasilinearization and Invariant Imbedding*, Academic Press, New York (1968).
Letan, R., and Kehat, E., *AIChE J.*, 13, 443 (1967).
Letan, R., and Kehat, E., *AIChE J.*, 15, 3 (1969a).
Letan, R., and Kehat, E., *Brit. Chem. Eng.*, 14, 803 (1969b).
Letzel, H.M., Schouten, J.C., Krishna, R., and van den Bleeck, C., *Chem. Eng. Sci.*, 54, 2237 (1999).
Leva, M., *Tower Packings and Packed Tower Design*, U.A. Stoneware, Akron, Ohio (1953).
Lobo, W.E., Friend, L., Hashmall, F., and Zenz, F.A., *Trans. AIChE*, 41, 693 (1945).
Martinis, J., and Froment, G.F., PROMAX software, Bryan Research and Engineering, Bryan, Tx. (2009).
Marucci, G., and Nicodemo, L., *Chem. Eng. Sci.*, 22, 1257 (1967).
Matos, E.M., Guirardello, R., Mori, M., and Nunhez, J.R., *Comput. & Chem. Eng.*, 33, 1115 (2009).
Mears, D.E., *Adv. Chem. Ser.*, 133, 218 (1974).
Merchuk, J.C., *AIChE J.*, 21, 815 (1975).
Mehta, K.C., and Sharma, M.M., *Brit. Chem. Eng.*, 15, 1440 (1970a).
Mehta, K.C., and Sharma, M.M., *Brit. Chem. Eng.*, 15, 1556 (1970b).
Midoux, N., Favier, M., and Charpentier, J.C., *J. Chem. Eng. Japan*, 9(5), 350 (1976).
Mills, P.L., and Dudukovic, M.P., *A.C.S. Symp. Ser.*, 237, 37 (1983).
Mochizuki, S., and Matsui, S., *Chem. Eng. Sci.*, 29, 1328 (1974).
Mohunta, D.M., Vaidyanathan, A.S., and Laddha, G.S., *Indian Chem. Eng.*, 11, 39 (1969).
Morris, G.A., and Jackson, J., *Absorption Towers*, Butterworth, London (1953).
Nonhebel, G., *Gas Purification Process for Air Pollution Control*, Butterworth, London (1972).
Norman, W.S., *Distillation, Absorption and Cooling Towers*, Longmans Green, London (1961).
Ogawe, T., Inoue, P., Shikada, T., and Ohno, Y., *J. Nat. Gas Chem.*, 12, 219 (2003).
Onda, K., Sada, E., and Okumoto, Y., *J. Chem. Eng. Japan*, 1, 63 (1968a).
Onda, K., Takenchi, H. and Okumoto, Y., *J. Chem. Eng. Japan*, 1, 63 (1968b).
Otake, T., and Okada, K., *Chem. Eng. Japan*, 17, 176 (1953). .
Pavlica, R.T., and Olson, J.H., *Ind. Eng. Chem.*, 62(12), 45 (1970).
Puranik, S.S., and Vogelpohl, A., *Chem. Eng. Sci.*, 29, 501 (1974).
Ramachandran, P.A., and Chaudhari, R.V., *Three Phase Catalytic Reactors*, Gordon & Breach, London (1983).
Ramm, W.M., *Absorptionsprozesse in der Chemischen Technik*, VEB Verlag Berlin (1953).
Rao, V.G., and Drinkenburg, A.A.H., *Can. J. Chem. Eng.*, 61, 158 (1983).

Riddick, J.A., and Bunger, W.B., *Organic Solvents*, 3rd ed., Wiley-Interscience, New York (1970).
Reid, R.C., and Sherwood, T.K., *The Properties of Gases and Liquids*, McGrawHill, New York (1958).
Reiss, L.P., *Ind. Eng. Chem. Proc. Des. Dev.*, 6, 486 (1967).
Reith, T., "Physical Aspects of Bubble Dispersions in Liquids," Ph.D. Thesis, Delft University, The Netherlands (1968).
Reith, T., *Brit. Chem. Eng.*, 15, 1559 (1970).
Saada, M.Y., *Chem. Ind. Génie Chim.*, 105, 1415 (1972).
Sato, Y., Hirose, T., Takahashi, F., Toda, M., and Hashigushi, Y.J., *Chem. Eng. Japan*, 6, 315 (1973).
Satterfield, C.N., *AIChE J.*, 21, 209 (1975).
Satterfield, C.N., Pelossof, A.A., and Sherwood, T.K., *AIChE J.*, 15, 226 (1969).
Satterfield, C.N., van Eek, M.W., and Bliss, G.S., *AIChE J.*, 24, 709 (1978).
Semmelbauer, R., *Chem. Eng. Sci.*, 22, 1237 (1967).
Shah, Y.T., *Gas-Liquid-Solid Reactor Design*, McGraw-Hill, New York (1979).
Shah, Y.T., Kelkar, B.G., Godbole, S.P., and Deckwer, W.D., *AIChE J.*, 28, 353 (1982).
Sharma, M.M., and Gupta, R.K., *Trans. Inst. Chem. Eng.*, 45, T169 (1967).
Sharma, M.M., Mashelkar, R.A., and Mehta, V.D., *Brit. Chem. Eng.*, 1, 70 (1969).
Sherwood, T.K., Shipley, C.H., and Holloway, F.A., *Ind. Eng. Chem.*, 30, 765 (1938).
Shridar, T., and Potter, O.E., *AIChE J.*, 23(4), 590 (1977).
Shulman, H.L., Ulbrich, C.F., Proulx, A.Z., and Zimmerman, J.O., *AIChE J.*, 1, 253 (1955a).
Shulman, H.L., Ulbrich, C.F., and Wells, N., *AIChE J.*, 1, 247 (1955b).
Shulman, H.L., Ulbrich, C.F., Wells, N., and Proulx, A.Z., *AIChE J.*, 1, 259 (1955c).
Sicardi, S., and Hofmann, H., *Chem. Eng. J. & Biochem. Eng. J.*, 20, 251 (1980).
Sokolichin, A., and Eigenberger, G., *Chem. Eng. Sci.*, 54, 2273 (1999).
Specchia, V., and Baldi, G., *Chem. Eng. Sci.*, 32, 515 (1977).
Stichlmair, J., *Grundlagen der Dimensionierung des Gas-Flüssigkeiten Kontaktapparates, Bodenkolonne*, Verlag Chemie, Weinheim (1978).
Sweeney, D., *AIChE J.*, 13, 663 (1967).
Thomas, W.J., and Furzer, I.A., *Chem. Eng. Sci.*, 17, 115 (1962).
Tijm, P.J.A., Waller, F.J., and Brown, D.M., *Appl. Cat. A Gen.*, 221, 275 (2001).
Towell, G.D., and Ackerman, G.H., in *Proc. 2nd Int. 5th Eur. Symp. Chem. React. Eng.*, Elsevier, Amsterdam (1972).
Towell, G.D., Strand, C.P., and Ackerman, G.H., in *AIChE J., Inst. Chem. Eng. Symp., Symp. Ser. 10*, Trans. Inst. Chem. Eng., London (1965).
Treybal, R.E., *Mass Transfer Operations*, McGraw-Hill, New York (1955).
Tseng, Y.M., and Thompson, A.R., *J. Chem. Eng. Data*, 9(2), 265 (1964).
van Baten, J.M., and Krishna, R., *Chem. Eng. Technol.*, 27, 1302 (2004).
van Dierendonck, L.L., "Vergrotingsregels voor gasbelwassers," Ph.D. Thesis, Twente University, The Netherlands (1970).
van Dierendonck, L., de Jong, P., Van den Hoff, J., and Voncken, H., *Adv. Chem. Ser.*, 133, 432 (1974).
van Dierendonck, L.L., Fortuin, J.M.H., and Vandenbos, D., in *Proc. 4th Eur. Symp. Chem. React. Eng.*, Brussels, 1968, Pergamon Press, (1971).
van Dierendonck, L.L., and Nelemans, J., in *Proc. 2nd Int. 5th Eur. Symp. Chem. React. Eng.*, Elsevier, Amsterdam (1972). p. B6-45.
Van Krevelen, D.W., and Hoftijzer, P.J., *Chim. & Ind. Proc. 21 Congr. Ind. Chim.*, Brussels (1948).
Van Krevelen, D.W., and Krekels, J.T.C., *Rec. Trav. Chim. Pays-Bas*, 67, 512 (1948).
Wang, T.T., Wang, J.F., and Jin, Y.A., AIChE J., 52, 125 (2006).
Wang, T.T., Wang, J.F., and Jin, Y.A., Ind. Eng. Chem. Res., 46(18), 5824-5847 (2007).
Yoshida, F., and Miura, Y., *Ind. Eng. Chem. Proc. Des. Dev.*, 2, 263 (1963).
Zenz, F.A, *Chem. Eng.*, 13, 120 (Nov. 13, 1972).
Zwietering, T., *De Ingenieur*, 6, 60 (1963).

Author Index

S

T

U

V

Subject Index

D

E

U

V

W

X

Z